Peter Hawkes • Erwin Kasper

Principles of Electron Optics

Volume Two: Applied Geometrical Optics

Second Edition

Principles of Electron Optics

Volume Two: Applied Geometrical Optics

Principles of Electron Optics

Volume Two: Applied Geometrical Optics

Second Edition

Peter Hawkes

CEMES—CNRS, Toulouse, France

Erwin Kasper

Formerly Institute of Applied Physics, University of Tübingen, Germany

ELSEVIER

ACADEMIC PRESS

An imprint of Elsevier

Academic Press is an imprint of Elsevier
125 London Wall, London EC2Y 5AS, United Kingdom
525 B Street, Suite 1800, San Diego, CA 92101-4495, United States
50 Hampshire Street, 5th Floor, Cambridge, MA 02139, United States
The Boulevard, Langford Lane, Kidlington, Oxford OX5 1GB, United Kingdom

Notices
Knowledge and best practice in this field are constantly changing. As new research and experience broaden our understanding, changes in research methods, professional practices, or medical treatment may become necessary.

Practitioners and researchers must always rely on their own experience and knowledge in evaluating and using any information, methods, compounds, or experiments described herein. In using such information or methods they should be mindful of their own safety and the safety of others, including parties for whom they have a professional responsibility.

To the fullest extent of the law, neither the Publisher nor the authors, contributors, or editors, assume any liability for any injury and/or damage to persons or property as a matter of products liability, negligence or otherwise, or from any use or operation of any methods, products, instructions, or ideas contained in the material herein.

British Library Cataloguing-in-Publication Data
A catalogue record for this book is available from the British Library

Library of Congress Cataloging-in-Publication Data
A catalog record for this book is available from the Library of Congress

ISBN: 978-0-12-813369-9

For Information on all Academic Press publications
visit our website at https://www.elsevier.com/books-and-journals

Publisher: John Fedor
Acquisition Editor: Anita Koch
Editorial Project Manager: Brianna Garcia
Production Project Manager: Vijayaraj Purushothaman
Cover Designer: Christian Bilbow

Typeset by MPS Limited, Chennai, India

Preface to the Second Edition

In the quarter century since the first edition of the *Principles* appeared, many branches of electron optics have been developed considerably, often driven by the success of aberration correction in the 1990s. At the end of the 1980s, we echoed the general opinion that quadrupole—octopole correctors had been given their chance, notably in Darmstadt and Chicago, but had failed to reach their goal. But the germs of the revolution in aberration studies that began in the next decade were already present: the degree of correction attained in Scherzer's project was impressive and Harald Rose had outlined a promising corrector based on sextupoles in 1981. What was missing were the indispensable diagnostic tools and fast feedback control circuitry that would turn these complicated systems into working correctors. These became available in the 1990s and the various correctors that have emerged are now examined in detail here. A different type of aberration corrector based on electron mirrors has also gained importance, especially in the low-energy-electron microscope (LEEM) and the photoemission electron microscope (PEEM). The chapters on the optics of electron mirrors have therefore been expanded to include the work of Dirk Preikszas and the parallel studies of the Russian school.

The third-order geometrical aberrations of round lenses were very fully covered in the first edition but aberration integrals for the fifth-order aberrations were not included. Such formulae had been published by one of us but a much improved set of aberration integrals has subsequently been derived by Zhixiong Liu. These are reproduced in Chapter 24, The Geometrical Aberrations of Round Lenses. The chapter on parasitic aberration too has needed much revision. We have preferred to retain the simple explanations in the first edition and then add new material covering recent work on the subject.

Another topic that has been extensively studied is electron emission, especially in the hands of Kevin Jensen, Christopher Edgcombe and Richard Forbes. We have incorporated some of their work and included many references covering aspects not discussed here. In particular, we describe the recommendations of Forbes and Deane for reformulating the Fowler—Nordheim theory.

In some cases, we have felt justified in removing material. Thus computer algebra, which was not very familiar in 1989, is now in routine use and several packages are available to perform it.

In the wake of aberration correction, monochromators have gained in importance. With the correction of spherical aberration, some way of reducing the effect of chromatic aberration was needed in order to benefit fully from the potential improvement in resolution. Certainly, correctors of chromatic aberration were known and have been implemented in practice but they introduce a further degree of complexity into microscope design. The alternative, much preferred by commercial microscope manufacturers, is to reduce the energy spread of the beam emerging from the source. Monochromator optics has therefore been perfected and we give some account of this in Part X. The optics of Wien filters was covered very superficially in the first edition. A new Chapter (38, The Wien Filter) now provides a much fuller treatment. In the case of topics still in rapid development, we have included only short accounts and many references. Ultrafast electron microscopy and multiple-beam systems for high-throughput electron lithography and scanning electron microscopy are the main examples of these.

Some material is admittedly of antiquarian interest only! This is particularly true of the many field models examined at length in Chapters 35 and 36, Electrostatic Lenses and Magnetic Lenses. We have nevertheless decided to retain them for they were a valuable feature of electron optics in the precomputer years when the mathematical skills that produced them were essential and they are thus part of the history of our subject.

There are innumerable minor changes and additions, not worth mentioning here individually. One important addition is Section 47.7, in which an unpublished extension of brightness theory to include the effect of aberrations is presented. Many new references have been added and titles are now included in the lists of references.

In the Preface to the first edition, we claimed that *Principles* was the first attempt to cover the whole subject since Glaser's *Grundlagen der Elektronenoptik* appeared in 1952. A few substantial books on the subject have appeared since 1989, notably *Geometrical Charged-particle Optics* by Harald Rose and *Modern Map Methods in Particle Beam Physics* by Martin Berz as well the later volume by Berz, Kyoko Makino and Weishi Wan, *An Introduction to Beam Physics*, but none of these attempts the broad coverage of the present volumes. Nevertheless, they are essential complements to our text in that they deal with some subjects in greater detail or from a very different standpoint. Thus Rose, in a virtuoso performance, uses the eikonal theory systematically throughout and brings out clearly the importance of system symmetries, while Berz relies on the differential algebra that he has developed for charged-particle optics in several areas, notably accelerator optics as well as microscope optics. An introduction to this is included in Chapter 34, Numerical Calculation of Trajectories, Paraxial Properties and Aberrations.

Preface to the First Edition (Extracts)

The last attempt to cover systematically the whole of electron optics was made by the late Walter Glaser, whose *Grundlagen der Elektronenoptik* appeared in 1952; although a revised abridgement was published in the *Handbuch der Physik* 4 years later, we cannot but recognize that those volumes are closer to the birth of the subject, if we place this around 1930, than to the present day.

Furthermore, electron optics have been altered dramatically during these intervening decades by the proliferation of large fast computers. Analytic expressions for the aberration coefficients of superimposed deflection and round magnetic lens fields, for example, have been derived only recently, partly because the latest generation of microlithography devices required them but also because they could only be evaluated by numerical methods: the earlier practice of seeking models permitting hand calculation could never have served here. Again, computer calculations have shed considerable light on electron gun behaviour, as the length of Part IX testifies convincingly; in 1952, Glaser was able to condense his account of gun theory into four pages!

The growth of electron optics is not, however, solely due to the computer. Many systems that had not been thoroughly explored have now been analysed in detail and, in many cases, we have had to renounce the attempt to reproduce in detail new results, however interesting, to keep the number of pages within reasonable limits. This work should therefore be regarded as both a textbook and a source-book: the fundamentals of the subject are set out in detail, and there the student should find everything needed to master the basic ideas or to begin the analysis of some class of systems not yet explored; the principal electron optical components are likewise dealt within great detail. Where optical elements that are not quite so common are concerned, however, we have felt at liberty to direct the reader to original articles and reviews, or specialist texts, to leave space for topics of wider interest.

The following chapters are, moreover, limited to geometric optics: wave optics is to be covered in a companion volume. With the Schrödinger equation as starting point, we shall examine the propagation of electron waves in electrostatic and magnetic fields and study image formation and resolution in the principal electron optical instruments. This demands some discussion of electron specimen interactions. A chapter will be devoted to the four broad themes of image processing: discretization and coding; enhancement; restoration; and analysis, description and pattern recognition. In another, we shall give an account of the steadily growing field of electron holography. Finally, we shall return to the optics of electron sources in order to understand the concept of coherence and we shall show how the notions of brightness, partial coherence and various associated spectral functions are interconnected.

Students of electron optics have been fortunate in that many excellent textbooks on the subject have appeared over the years, the first when the subject was still young (Brüche and Scherzer, 1934; Myers, 1939; Klemperer, 1939; Picht, 1939); these were followed in the 1940s by the encyclopaedic Zworykin et al. (1945), Cosslett (1946) and Gabor (1945).

Many books on the subject appeared in the 1950s, of which the texts by Glaser already mentioned, Sturrock (1955), Grivet et al. (1955, 1958) and Kel'man and Yavor (1959) are the most important for our present purposes. Subsequently, however, the flow has shrunk to a trickle, new editions and short introductory texts dominating, with the exception of the multiauthor volumes edited by Septier (1967, 1980, 1983); conversely, monographs on limited topics have become more common. Although certainly 'standing on the shoulders of giants', the present volumes do differ considerably from their many predecessors in that the developments of the past 20 years are accorded ample space.

For whom is this work intended? A knowledge of physics and mathematics to first degree level is assumed, though many reminders and brief recapitulations are included. It would be a suitable background text for a postgraduate or final year course in electron optics, and much of the material has indeed been taught for some years in the University of Tübingen; a course in the University of Cambridge likewise covered many of the principles. Its real purpose is, however, to provide a self-contained, detailed and above all modern account of electron optics for anyone involved with particle beams of modest current density in the energy range up to a few mega-electronvolts. Such a reader will find all the basic equations with their derivations, recent ideas concerning aberration studies, extensive discussion of the numerical methods needed to calculate the properties of specific systems and guidance to the literature of all the topics covered.

Composition of volumes such as these puts us in debt to a host of colleagues: many have permitted us to reproduce their results; the librarians of our institutes and the Librarian and Staff of the Cambridge Scientific Periodicals Library have been unflagging in their pursuit of recondite and elusive early papers; Mrs Ströer has uncomplainingly word-processed hundreds of pages of mathematical and technical prose; Mrs Maczkiewicz and Mr Inial have taken great pains with the artwork as have Mrs Bret and her colleagues with the references; Academic Press and Prof. Dr K.-H. Herrmann, Director of the Institut für Angewandte Physik der Universität Tübingen, have generously supported this work; the Zentrum für Datenverarbeitung has provided the text-editing facilities needed for TEX. To all of these we are extremely grateful.

Acknowledgments

In the first edition, we expressed our gratitude to several colleagues and librarians who helped in various ways and to those who typed the text and prepared the illustrations. To them, it is a pleasure to add Madame Isabelle Labau (CEMES-CNRS), Frau Susanne Hempel and Frau Gabriele Thomas (University of Tübingen), Frau Katrin Quetting (Fritz-Haber-Institut der MPG, Berlin), and the ever-efficient personnel of the Technische Informationsbibliothek in Hannover.

Several colleagues pointed out errors or obscure passages in the first edition. We are most grateful to Erich Plies, the late Michal Lenc and Bohumila Lencová, the late Stella Yavor and her son Mikhail and Marijn Bronsgeest for their careful reading of the text. The advice of Shin Fujita, Dieter Kern and Tomáš Radlička has been much appreciated.

The expressions for aberration coefficients have been extended to include higher order aberrations of round lenses and those of electron mirrors. We are very grateful to Zhixiong Liu and Seitgerim Bimurzaev, who supplied lists of formulae that we could incorporate directly. We include a full account of the work of Dirk Preikszas on electron mirrors, who has been good enough to resuscitate his programs and provide aberration integrals for all the third-order geometrical aberrations (not hitherto published apart from the spherical aberration coefficient).

Peter Tiemeijer and Ondřej Shánĕl (FEI), Jaroslav Jiruše (Tescan) and Pieter Kruit (Delft University of Technology) have provided original drawings, not otherwise available, for which we thank them warmly.

PART VII

Instrumental Optics

Electrostatic Lenses

35.1 Introduction

We have derived a host of formulae for various characteristics of electrostatic lenses but have so far given no indication of the behaviour of these quantities in practice: their typical orders of magnitude and their dependence on the excitation and geometry of the lens. Our purpose in this chapter and its successor on magnetic lenses is to add some flesh to the bare bones so far presented. The literature on electrostatic lenses is so voluminous that we cannot attempt to provide formulae or tables or even graphs for all the designs that have been studied. The present chapter should therefore be regarded as a directory, indicating sources of further information, rather than a self-contained account. The subject has been surveyed by Lencová (1997, 2009).

As well as the many measurements of cardinal elements and aberration coefficients, there is a growing body of calculated data; in the earlier days, considerable efforts were made to find simple analytical expressions for the axial potential in each of the various types of lenses, with the aid of which the optical characteristics could be established and lens design curves plotted. In the best of all cases, these models even allowed the aberration integrals to be evaluated in closed form. Nowadays, it is not difficult to calculate the axial potential for any geometry of interest and these potential models have therefore lost much of their appeal for predicting the properties of any specific lens accurately. Conversely, they remain invaluable for acquiring an understanding of trends in lens behaviour, in particular of the variation of the numerous quantities of interest with geometry and electrode potential. We therefore give some account of the principal potential models and of the results they yield. They were superseded by such flexible interactive systems as CIELAS (Hill and Smith, 1980, 1981, for magnetic lenses) and ELOP-GELOP (van Oostrum, 1985) and these in turn have given way to the powerful and continually evolving program suites mentioned elsewhere in these books, Nevertheless, we feel that they will always have a role to play in establishing broad design principles and in providing a check on other numerical results.

The variety of electrostatic lenses is very wide, ranging from an opening in a single plate to the multielectrode accelerator structure that separates the low-voltage electron gun from the column of a high-voltage electron microscope. They may even consist of a conductive

Principles of Electron Optics: Applied Geometrical Optics.
DOI: http://dx.doi.org/10.1016/B978-0-12-813369-9.00035-X

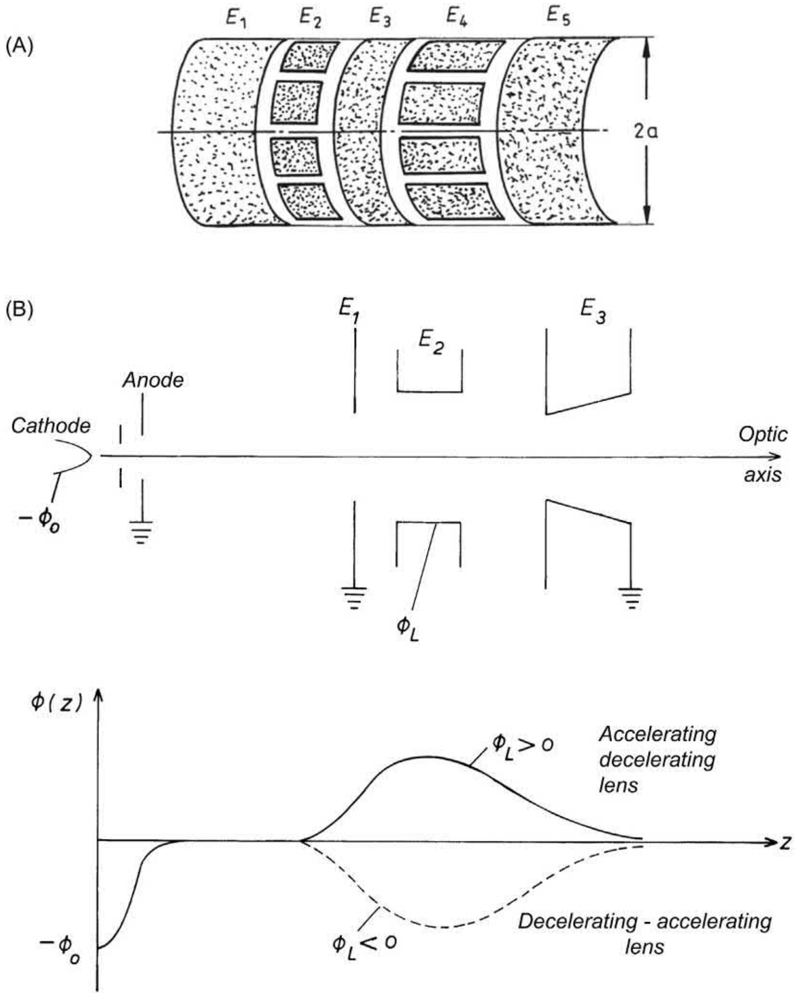

Figure 35.1

(A) Tube-wall electrodes. E_1, E_3 and E_5 produce round-lens fields while E_2 and E_4 create octopole distributions. (*After Tang (1991) Courtesy Wissenschaftliche Verlagsgesellschaft.*) (B) Potentials in a three-electrode einzel lens. The outer electrodes E_1 and E_3 may have different shapes but both are held at the same potential, commonly earth potential like the anode of the gun (or final electrode of any accelerating structure). The central electrode E_2 is held at some other potential ϕ_L, which may be positive, in which case the lens first accelerates electrons and then decelerates them, or negative, in which case the order is reversed.

coating on the wall of a cylindrical tube (Tang, 1991, Fig. 35.1A); round lenses and multipoles can be created in this way. The principal division is between lenses that cause an overall acceleration (or deceleration) of the electron beam and those that do not. The former may consist of any number of electrodes and only the simpler kinds lend themselves to systematic study; they have come to be known as *immersion lenses* by analogy with the light optical usage for lenses that have one face in air and the other immersed in a fluid, typically of high refractive index. A word of warning is needed here. We shall refrain from using the term 'immersion' when the object or emissive cathode is 'immersed' in an electrostatic field, but shall then speak of *cathode lenses*; the latter are, however, not infrequently referred to as immersion objectives, and they do undeniably have much in common with their optical counterparts.

Electrostatic lenses that do not impart any net acceleration to the beam can of course in principle consist of many electrodes but, in practice, the vast majority consist of three electrodes, the outer two at the same potential as that of the anode of the gun, the central one at some other potential. The variable parameters are thus this central potential, the separations between the electrodes and their shape and the radii of the openings in them. Such lenses are known as *einzel*[1] or *unipotential* lenses (Fig. 35.1B).

The field between the first outer electrode (E_1 in Fig. 35.1B) and the central electrode E_2 may be accelerating ($\phi_L > 0$) or decelerating ($\phi_L < 0$); in the latter case, the axial potential must not drop below the accelerating voltage of the gun, as the lens would then turn into a mirror, reflecting the electrons back towards the source. Mirrors are dealt with separately, in Sections 37.1 and 37.2. Lenses operating close to the lens-mirror transition are, however, of some interest as high-pass electron energy filters or monochromators; one can arrange that only the fastest electrons pass through the lens, the remainder being turned back at the potential barrier. A highly monochromatic beam can thus be extracted from a beam of electrons.

The practical properties of cylindrical lenses are not very different from those of round lenses; they are therefore included in Section 35.6.

35.2 Immersion Lenses

35.2.1 The Single Aperture

Electrons passing through a round opening in a plate that separates two regions of unequal electric field will be deviated. Such a structure is, however, different from all the lenses we shall consider below in that it is not the potential that is uniform outside the lens region but the electric field (Fig. 35.2). This is therefore a rare situation in which only the osculating

[1] It is usually said in English texts that the prefix 'einzel' indicates that a single voltage is required but this appears not to have been the original sense: "Die elektrische Einzellinse ist eine der Glaslinse entsprechende elektrische Elektronenlinse, die *einzeln* im Raum steht und zu deren beiden Seiten der Brechungsindex gleich ist" (from the glossary in Ramsauer, 1941).

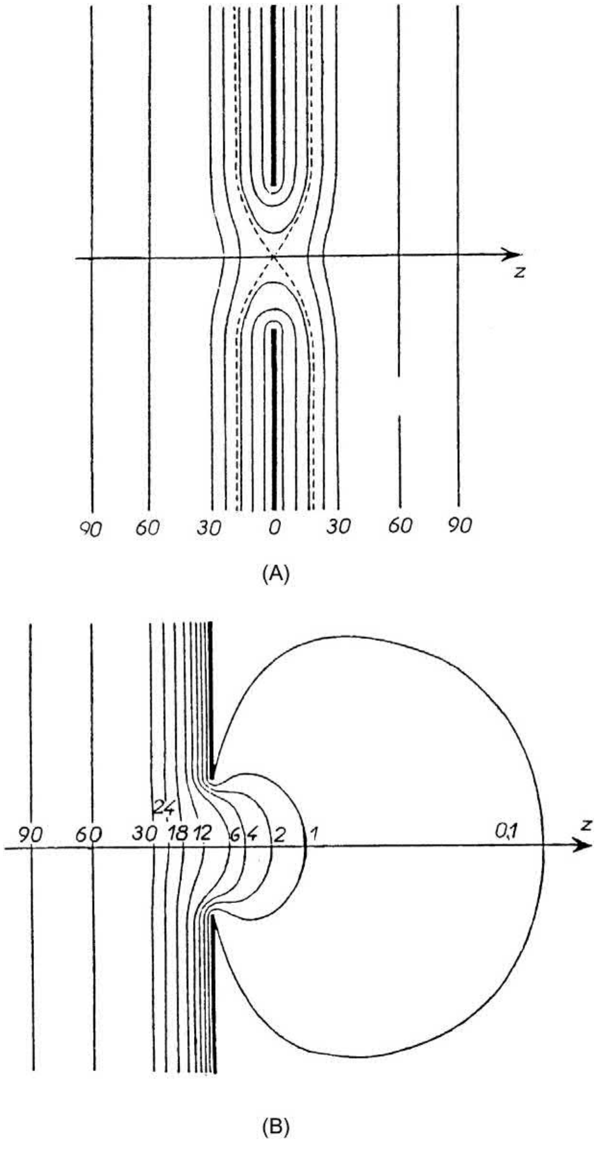

Figure 35.2
Equipotential surfaces around a single electrode with a circular opening. (A) Equal and opposite fields on either side of the electrode. The equipotential lines in the electrode plane intersect at an angle 2 arctan $\sqrt{2}$ or 109°28′. (B) The image space of the electrode is field-free.

cardinal elements have any meaning. However, the single aperture is of practical interest mainly as a means of focusing a beam on a target and is usually characterized by the high magnification or high demagnification cardinal elements and aberration coefficients, which are the same as the osculating quantities (Section 17.2).

The potential around a thin electrode in which a hole of radius R is pierced is given by

$$\Phi(r,z)=\phi_0-\frac{E_1+E_2}{2}z+\frac{E_1+E_2}{\pi}|z|\left(\arctan\mu+\frac{1}{\mu}\right) \tag{35.1a}$$

where

$$\mu=\left[\frac{z^2+r^2-R^2}{2R^2}+\frac{1}{2}\left\{\frac{4z^2}{R^2}+\left(\frac{z^2}{R^2}+\frac{r^2}{R^2}-1\right)^2\right\}^{1/2}\right]^{1/2} \tag{35.1b}$$

so that on the axis

$$\phi(z)=\phi_0-\frac{E_1+E_2}{2}z+\frac{E_1-E_2}{\pi}R\left(\frac{z}{R}\arctan\frac{z}{R}+1\right) \tag{35.2}$$

(Fry, 1932; Glaser and Henneberg, 1935; Ollendorff, 1955; Durand, 1966). This expression is equivalent to that given in Section 10.3.1. A rough estimate of the optical effect of the aperture may be obtained by supposing its effect to be concentrated in the plane of the aperture and neglecting the curvature of the emergent electron rays, incident parallel to the axis (Davisson and Calbick, 1931, 1932). Integrating (Gans, 1937) the paraxial equation

$$\left(\phi^{1/2}r'\right)'=-\frac{\phi''}{4\phi^{1/2}} \tag{35.3}$$

we deduce that

$$r'(+)-r'(-)=-\frac{\phi'(+)-\phi'(-)}{4\phi}r=\frac{E_2-E_1}{4\phi}r \tag{35.4}$$

For a beam incident parallel to the axis, therefore, $r'(-)=0$ and so $r'(+)=(E_2-E_1)r/4\phi$; the emergent beam would intersect the axis at F_i, $z_{Fi}=4\phi/(E_1-E_2)$. The aperture lens will thus be divergent if $E_1-E_2<0$, which may occur in different ways (cf. Hanszen and Lauer, 1967): if both fields are accelerating (E_1 and E_2 negative for electrons), then we require that $|E_1|>|E_2|$; if both are retarding, then $E_1<E_2$; while if $E_1<0$ and $E_2>0$, the lens is always divergent.

Unless $E_2=0$, the neglect of the emergent ray curvature renders this approximation very crude, however. Correction factors and calculations of spherical and chromatic aberration coefficients are to be found in Guckenberger and Heil (1972), see Fig. 35.3. The effect of finite electrode thickness is considered by MacNaughton (1952) and that of hole diameter by Hoeft (1959).

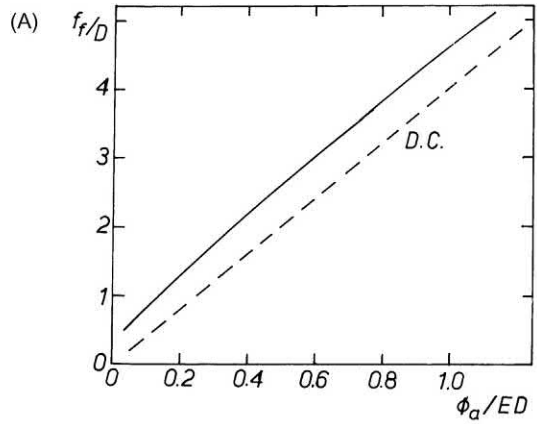

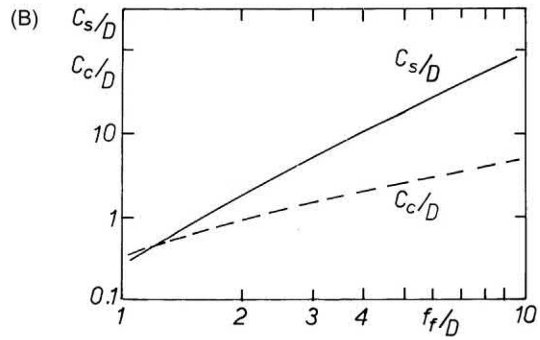

Figure 35.3
Electron optical properties of a single opening. (A) The focal length f_f as a function of ϕ_a/ED, where ϕ_a is the potential at the electrode, E the electric field on the target (image) side and D the diameter of the opening (the object space is field-free). The broken curve (D.C.) shows Davisson and Calbick's approximate value. Note that f_f is the 'fictitious' focal length, obtained by neglecting the effect of the uniform field E. (B) C_s/D and C_c/D as functions of f_f/D.
After Guckenberger and Heil (1972), Courtesy Institute of Physics.

The extreme situation in which electrons pass through a hole so small that they experience a force due to the image charge is examined by Birkhoff et al. (1980). A similar situation had been considered earlier by Hubert (1949), a tube replacing the perforated plate, as a means of overcoming spherical aberration (Chapter 41, Aberration Correction).

35.2.2 The Two-Electrode Lens

The electrodes of these lenses are typically cylinders or plates. They are invariably analysed on the assumption that the space on both sides of the lens is field-free; otherwise, allowance must be made for ray curvature outside the lens zone.

35.2.2.1 Adjacent cylinders

For cylinders of equal radius R separated by a gap S that is negligible in comparison with R, the potential distribution can be written down in closed form but the paraxial equations can be solved only numerically. The true potential proves to resemble a tanh function but the situation is scarcely improved and it is in general more satisfactory to compute the optical properties from the exact potential. Nevertheless, a very good idea of the optical behaviour of such a lens can be acquired by an ingenious manipulation of model potentials, devised by Grivet and Bernard (1951, 1952a,b); here, the true ϕ'/ϕ, or its representation in terms of hyperbolic functions, is replaced by a function that yields paraxial quantities and aberration coefficients in closed form.

When the gap between the cylinders is negligible ($S \ll R$) and the latter are held at potentials ϕ_1 and ϕ_2 (Fig. 35.4), the potential can be written

$$\Phi(r,z) = \frac{\phi_1+\phi_2}{2} + \frac{\phi_2-\phi_1}{\pi}\int_0^\infty \frac{I_0(tr)}{I_0(tR)}\frac{\sin tz}{t}dt \tag{35.5}$$

I_0 being the zero-order modified Bessel function, so that on the axis

$$\phi(z) = \frac{\phi_1+\phi_2}{2} + \frac{\phi_2-\phi_1}{\pi}F(z) \tag{35.6a}$$

where

$$F(z) = \int_0^\infty \frac{\sin tz}{I_0(tR)}\frac{dt}{t} \tag{35.6b}$$

(Gray, 1939; Durand, 1966). This distribution is very similar to a simple tanh function (Gray, 1939; Ollendorff, 1955)

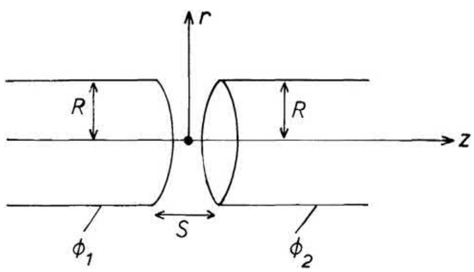

Figure 35.4
Symmetric two-cylinder lens.

$$\phi(z) = \frac{\phi_1 + \phi_2}{2}\left(1 + \frac{1-\gamma}{1+\gamma}\tanh \omega z\right) \tag{35.7}$$

where

$$\gamma := \frac{\phi_1}{\phi_2} \quad \text{and} \quad \omega := \frac{1}{\pi}\int_{-\infty}^{\infty} \frac{dt}{I_0(t)} = 1.318 \tag{35.8}$$

The function that occurs in the reduced paraxial equation (15.38) is ϕ'/ϕ and for Eq. (35.7)

$$\frac{\phi'}{\phi} = \frac{2(1-\gamma)\omega \exp 2\omega z}{(\exp 2\omega z + 1)(\exp 2\omega z + \gamma)} \tag{35.9}$$

which passes through a maximum value of -2ω tanh (ωz_m) at $z_m = \ln \gamma/4\omega$. This function is bell-shaped and is well represented by a function of the form

$$f(z) = \frac{T_m}{1 + (Z/a)^2} \tag{35.10a}$$

or

$$f(z) = T_m \operatorname{sech}(Z/b) \tag{35.10b}$$

where we have shifted the origin to the point z_m, $Z = z - z_m$, about which ϕ'/ϕ is symmetric. The constants a and b are chosen so that the areas under the curves for $(\phi'/\phi)^2$ are the same for the model field and for the tanh distribution. This requirement ensures that the focal lengths coincide in the weak-lens approximation (Section 17.4) and implies that

$$a = -\frac{1}{\pi\omega}\left(\frac{1+\gamma^{1/2}}{1-\gamma^{1/2}}\right)^2\left(\frac{1+\gamma}{1-\gamma}\ln\gamma + 2\right) \tag{35.11}$$

The first model (35.10a) has the great attraction that not only can the paraxial equation be solved in closed form but even the aberration integrals can be evaluated explicitly. We shall examine it in detail in Section 36.2; here we simply note that the cardinal elements are given by

$$\begin{aligned} f_i &= \frac{ak\gamma^{-1/4}}{\sin k\pi} \quad f_o = \frac{ak\gamma^{1/4}}{\sin k\pi} \\ z_{Fi} &= ak\cot(k\pi) - \frac{1}{2}\omega a^2 \tanh(\omega z_m) \\ z_{Fo} &= -ak\cot(k\pi) - \frac{1}{2}\omega a^2 \tanh(\omega z_m) \end{aligned} \tag{35.12}$$

where

$$k = \left(1 + \frac{3}{4}a^2\omega^2 \tanh^2 \omega z_m\right)^{1/2}$$
$$a = 0.483 \coth^2 (x/2)(x \coth x - 1) \quad x = -2z_m\omega \tag{35.13}$$

If we write $\gamma^{1/2} \approx 1 + \varepsilon$, then $k \approx 1 + 0.0675\varepsilon^2\gamma^{-1/2}$, $a \approx 0.644(1 + 0.1\varepsilon^2)$ and $f_o \approx 3.036\gamma^{3/4}/\varepsilon^2$. The agreement with measurement is very good.

35.2.2.2 Cylinders separated by a small gap

We now suppose that the gap S is not negligible but still much smaller than the radius R. The potential between the electrodes is modelled as a linear change from ϕ_1 to ϕ_2. The potential can now be written

$$\Phi(r, z) = \frac{\phi_1 + \phi_2}{2} + \frac{\phi_2 - \phi_1}{\pi S}\int_0^\infty \frac{I_0(tr)}{I_0(tR)}\frac{\sin(tz)}{t}\sin(tS/2)\frac{dt}{t} \tag{35.14}$$

and on the axis

$$\phi(z) = \frac{\phi_1 + \phi_2}{2} + \frac{\phi_2 - \phi_1}{\pi S}\int_0^\infty \frac{\sin(tz)\sin(tS/2)}{I_0(tR)}\frac{dt}{t^2} \tag{35.15}$$

which of course collapses to Eq. (35.6) as $S \to 0$. The integral in Eq. (35.15) can be expressed in terms of $F(z)$ (35.6b) thus:

$$\begin{aligned}\int_0^\infty \frac{\sin(tz)\sin(tS/2)}{I_0(tR)}\frac{dt}{t^2} &= \frac{1}{2}\int_0^\infty \frac{\cos t(z - S/2) - \cos t(z + S/2)}{t^2 I_0(tR)}dt \\ &= \frac{1}{2}\int_{z-S/2}^{z+S/2} d\zeta \int_0^\infty dt \frac{\sin t\zeta}{tI_0(tR)} \\ &= \frac{1}{2}\int_{z-S/2}^{z+S/2} F(\zeta)d\zeta\end{aligned} \tag{35.16}$$

If $F(\zeta)$ is replaced by a tanh function, the integral can be evaluated in closed form, giving

$$\phi(z) = \frac{\phi_1 + \phi_2}{2}\left\{1 + \frac{1-\gamma}{1+\gamma}\cdot\frac{1}{\omega S}\cdot\ln\frac{\cosh\omega(z + S/2)}{\cosh\omega(z - S/2)}\right\} \tag{35.17}$$

35.2.2.3 Two cylinders separated by an arbitrary distance

Several model potentials have been proposed to represent this general case; we mention most of these only briefly, lingering longer on the studies of Kanaya et al. (1972) and Kanaya and Baba (1977).

An early proposal was the distribution

$$\phi(z) = \phi_0 \exp\{(k \arctan(z/a)\} \tag{35.18}$$

(Hutter, 1945), for which

$$\frac{\phi'(z)}{\phi(z)} = \frac{k/a}{1 + (z/a)^2} \tag{35.19}$$

The reduced paraxial equation (15.38) can then be solved in terms of circular functions (see Section 36.2), and explicit formulae are found for the cardinal elements and aberration coefficients. We shall not pursue this model further, for its predictions are not especially reliable and, moreover, it conflicts with the requirements of electrostatics. Distributions such as Eq. (35.18) are of limited utility because they cannot be cast into the form $\phi(z) = \phi_0 + \sum_i \phi_L^{(i)} f_i(z)$, in which $\phi_L^{(i)}$ are electrode voltages and $f_i(z)$ are arbitrary functions (cf. Part II); this is explained in detail by Glaser (1952), who points out that any attempt to transfer magnetic field models to electrostatic lenses by setting ϕ'/ϕ proportional to B (15.39) is intrinsically unsatisfactory. The result, a potential of the form

$$\phi(z) = \phi_0 \exp\left\{ k \int_0^z B(\zeta) d\zeta \right\} \tag{35.20}$$

can never have the necessary linear dependence on the electrode potentials.

Despite this, the shape of $\phi(z)$ given by Eq. (35.18) is a fair representation of the true distribution and has been used to model the optics of an accelerator structure for a high-voltage microscope (Kanaya et al., 1965).

Another model, for which the paraxial equation is again soluble in terms of tabulated functions, is that proposed by Glaser and Robl (1951), which does not conflict with the laws of electrostatics:

$$\phi(z) = \phi_1 + (\phi_2 - \phi_1)\left\{1 - \frac{1}{\pi}\operatorname{arccot}\left(\frac{z}{a}\right)\right\} \tag{35.21}$$

A series of substitutions transforms the paraxial equation into an equation of the form

$$x'' + \frac{x'}{z} + \left(1 - \frac{1}{16z^2}\right)x = 0 \tag{35.22}$$

the solutions of which are $x(z) = J_{\pm 1/4}\,(z)$. For further details, see the original paper or Glaser (1952) or Ollendorff (1955), where the calculation is set out in great detail. It is interesting to note that Grinberg (1953) arrived at Eq. (35.21) as one of a family of potential models giving paraxial solutions in terms of Bessel functions by seeking those functions $\phi(z)$ for which the equation

$$v'' + \left\{ \frac{\phi'''}{2\phi'} - \frac{3}{4}\left(\frac{\phi''}{\phi'}\right)^2 + \left(\frac{1}{4} - \nu^2\right)\left(\frac{\phi'}{\phi}\right)^2 + \phi'^2 \right\} v = 0 \tag{35.23}$$

has the same form as the reduced equation (15.38), since Eq. (35.23) has the general solution

$$v(z) = \left(\frac{\phi}{\phi'}\right)^{1/2} J_\nu(\phi(z)) \tag{35.24}$$

(Kamke, 1977, §C.2.162, Eq. 14; Whittaker and Watson, 1927, Q7 at end of Chapter 17). The special case $\nu^2 = 1/16$ leads to a potential of the form (35.21) and to solutions in terms of $J_{\pm 1/4}(\phi)$, $\phi = A + B \arctan(Cz)$, where A, B and C are constants, in agreement with Glaser and Robl (1951). We note that the paper by Glaser and Robl (1951) also contains a detailed analysis of the model

$$\phi(z) = \phi_1 + \frac{\phi_2 - \phi_1}{2}\left(1 + \frac{z/a}{1 + |z/a|}\right) \tag{35.25}$$

None of these models is entirely satisfactory but we pause rather longer over two improved models due to Kanaya et al. (1972) and Kanaya and Baba (1977). In the first of these, the axial potential is represented by

$$\phi(z) = \phi_0 \exp\left[k \arctan\left\{\sinh(z/a)\right\}\right] \tag{35.26}$$

which can be matched very closely to calculated values. For this distribution,

$$\frac{\phi'(z)}{\phi(z)} = \frac{k}{a}\operatorname{sech}(z/a) \tag{35.27}$$

Setting $\phi(-\infty) \to \phi_1$ and $\phi(\infty) \to \phi_2$, we see that

$$k = \frac{1}{\pi}\ln\frac{\phi_2}{\phi_1} \quad \text{and} \quad \phi_0^2 = \phi_1\phi_2 = \phi^2(0) \tag{35.28}$$

The reduced paraxial equation takes the form

$$\left(1 - \mu^2\right)\frac{d^2 v}{d\mu^2} - 2\mu\frac{dv}{d\mu} + n(n+1)v = 0 \tag{35.29}$$

where

$$\mu = -\tanh(z/a), \quad n(n+1) = \frac{3}{16}k^2 \tag{35.30}$$

which is the same as that encountered for the Grivet–Lenz model for magnetic lenses (Section 36.2). We give more details of the analysis there; here we simply quote the results. Eq. (35.29) has as solutions the Legendre functions $P_n(\mu)$ and $Q_n(\mu)$. Sets of curves for the (real) cardinal elements and high-magnification spherical and chromatic aberration coefficients can then be plotted. The focal lengths agree with the experimental values obtained by Kanaya et al. (1965) and Bas et al. (1959). It finally remains to relate the characteristic length a to the gap (S) and the radius (R); Kanaya et al. use an approximate formula derived by Wang (1945) to obtain this relation.

A further improvement is the model introduced by Kanaya and Baba (1977) with the aid of which virtually all the optical properties of these bipotential lenses are analysed. The new model (yet again unrealistic in the sense explained earlier) has the form

$$\begin{aligned} \phi(\mu) &\coloneqq \phi_1 \exp(k_0 \arccos \mu) \\ -\frac{z}{a} &\eqqcolon \int_0^\mu (1-\lambda^2)^{-m} d\lambda \end{aligned} \tag{35.31}$$

The various models already mentioned correspond to different values of m: for $m = 3/2$, we have Eq. (35.18), for $m = 1$, (35.26) and for $m = 1/2$, ϕ'/ϕ is constant and hence $\phi(z)$ varies exponentially with z. For Eq. (35.31), we have in general

$$\frac{\phi'(z)}{\phi(z)} = \frac{k_0}{a}(1-\mu^2)^{m-1/2} \tag{35.32}$$

It is convenient to write

$$k = \sqrt{3}\frac{k_0}{4} = \left(\frac{\sqrt{3}}{4\pi}\right)\ln\left(\frac{\phi_2}{\phi_1}\right) \tag{35.33}$$

Fig. 35.5 shows $\phi(z)$ and $\phi'(z)/\phi(z)$ for a range of values of m. Substituting into the reduced paraxial equation, we obtain

$$(1-\mu^2)\frac{d^2 v}{d\mu^2} - 2m\mu\frac{dv}{d\mu} + k^2 v = 0 \tag{35.34}$$

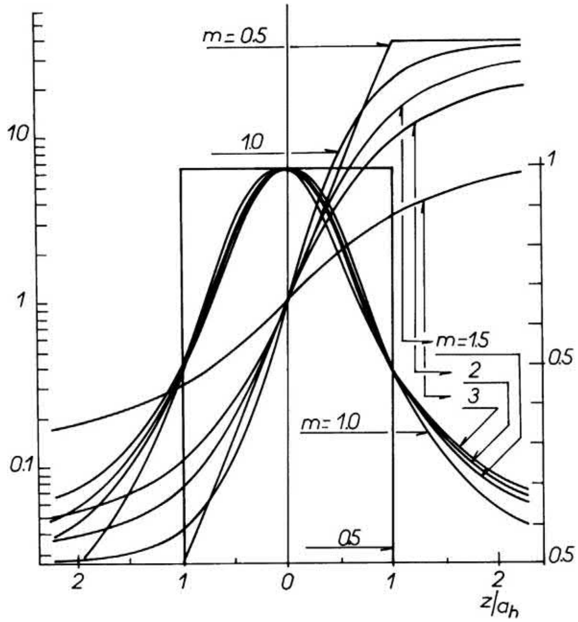

Figure 35.5
The potential distribution $\phi(z/a_h)$ as a function of z/a_h, for various values of the parameter m (left ordinate). The symmetric curves also included show $\phi'(z/a_h)/\phi(z/a_h)$, normalized to unity at $z = 0$ (right ordinate). *After Kanaya and Baba (1977), Courtesy Wissenschaftliche Verlagsgesellschaft.*

and setting $\mu =: 2\zeta - 1$,

$$\zeta(1-\zeta)\frac{d^2 v}{d\zeta^2} + m(1-2\zeta)\frac{dv}{d\zeta} + k^2 v = 0 \tag{35.35}$$

The general solutions of this equation may be written as hypergeometric functions:

$$v(\mu) = AF\left(\alpha,\ \beta,\ \gamma,\ \frac{1-\mu}{2}\right) + B\left(\frac{1-\mu}{2}\right)^{1-\gamma} F\left(\gamma-\alpha,\ \gamma-\beta,\ 2-\gamma,\ \frac{1-\mu}{2}\right) \tag{35.36}$$

where

$$\alpha + \beta + 1 = 2m, \quad \gamma = m, \quad \alpha\beta = -k^2 \tag{35.37}$$

or

$$\alpha, \beta = \frac{1}{2}(2m-1)(1 \pm \omega), \quad \omega = \left(1 + \frac{4k^2}{(2m-1)^2}\right)^{1/2} \tag{35.38}$$

The real foci must be found from the zeros of the appropriate hypergeometric function, and the real focal lengths can then be calculated from

$$\frac{f_i'}{a} = \frac{\gamma \exp\left\{\left(k/\sqrt{3}\right)\arccos \mu_i\right\}}{k^2 2^{m-1}\left(1-\mu_i\right)^m F\left(\gamma-\alpha,\ \gamma-\beta,\ \gamma+1,\ \dfrac{1-\mu_i}{2}\right)}$$
$$\frac{f_o'}{a} = \frac{f_i}{a}\exp\left\{\left(-2k/\sqrt{3}\right)\arccos \mu_i\right\} \tag{35.39}$$

in which μ_o and μ_i are the values of μ corresponding to the object and image foci. The asymptotic foci and focal lengths are given, for $m > 1$, by

$$\frac{z_{Fi}}{a} = -\frac{z_{Fo}}{a} = -\frac{\Gamma(\gamma-\alpha-\beta)\Gamma(\alpha)\Gamma(\beta)}{2^{2m-1}\Gamma(1-\gamma+\alpha+\beta)\Gamma(\gamma-\alpha)\Gamma(\gamma-\beta)} \tag{35.40a}$$

$$\frac{f_i}{a} = -\frac{\Gamma(\alpha)\Gamma(\beta)\exp\left(k\pi/\sqrt{3}\right)}{2^{2m-1}\Gamma^2(\gamma)} \tag{35.40b}$$

$$\frac{f_o}{a} = \frac{f_i}{a}\exp\left(-2k\pi/\sqrt{3}\right) \tag{35.40c}$$

or, for $m < 1$, by

$$\frac{z_{Fi}}{a} = -\frac{z_{Fo}}{a} = \frac{\sqrt{\pi}}{2}\frac{\Gamma(1-m)}{\Gamma\left(\dfrac{3-2m}{2}\right)} - \frac{\Gamma(\gamma-\alpha-\beta)\Gamma(\alpha)\Gamma(\beta)}{2^{2m-1}\Gamma(\gamma)\Gamma(\gamma-\alpha)\Gamma(\gamma-\beta)} \tag{35.40d}$$

Kanaya and Baba plot these quantities for a range of values of m as a function of the voltage ratio, measured by k; the minimum focal lengths are also plotted as a function of m. A convenient normalizing length is the half-width of the curve $\phi'(\mu)/\phi(\mu)$ for the appropriate value of m. Denoting this by a_h, we have

$$\frac{a_h}{a} =: \lambda = \int_0^{\arcsin \mu_h} (\cos\alpha)^{1-2m} d\alpha$$
$$\mu_h = \left\{1-\left(1/2\right)^{\frac{2}{(2m-1)}}\right\}^{1/2} \tag{35.41}$$

Kanaya and Baba find that

$$\left(\frac{f_i'}{a_h}\right)_{\min} = 1.52, \text{ for which } \frac{f_o'}{a_h} = 0.215 \text{ with } k = 1.08$$
$$\left(\frac{f_o'}{a_h}\right)_{\min} = 1.52, \text{ for which } \frac{f_i'}{a_h} = 0.215 \text{ with } k = -1.08 \tag{35.42}$$

with $\lambda = 1.754$ and $m = 0.58$ (the apparent contradiction here is explained by the different values of k and hence of m). For the same values of λ and m, the asymptotic focal lengths likewise pass through minima:

$$\left(\frac{f_i}{a_h}\right)_{\min} = \left(\frac{f_o}{a_h}\right)_{\min} = 2.952 \begin{cases} \dfrac{f_o}{a_h} = 0.243 \ \text{ for } \ k = 0.538 \\[2ex] \dfrac{f_i}{a_h} = 0.243 \ \text{ for } \ k = -0.538 \end{cases} \tag{35.43}$$

The minimum real focal lengths are of academic interest only, for it is unlikely that a real object would be placed between the electrodes, and these minimum values do in fact correspond to such an object position. For the same reason, the curves showing the spherical and chromatic aberration coefficients as a function of m plotted by Kanaya and Baba (1977, Fig. 4) are not of great practical use.

It still remains to relate the gap S and radius R to the quantity a occurring in Eq. (35.31). This can be done by matching the electric field midway between the electrodes to that obtained when it is assumed that the potential changes linearly across the gap. This requires Eqs (35.15) and (35.31)

$$\frac{\phi_1 - \phi_2}{S\pi} \int_0^\infty \frac{\cos(tz)\sin(tS/2)}{I_0(Rt)} \frac{dt}{t} = \frac{\sqrt{\phi_1\phi_2}\ln(\phi_2/\phi_1)}{a\pi} \tag{35.44}$$

in which we have used the boundary conditions $\phi(z \to -\infty, \mu = 1) = \phi_1$, $\phi(z \to \infty, \mu = -1) = \phi_2$ to establish that

$$k_0 = \frac{1}{\pi}\ln\left(\frac{\phi_2}{\phi_1}\right)$$

Eq. (35.44) may be rewritten

$$\frac{a}{S} = \frac{(\phi_1\phi_2)^{1/2}}{(\phi_1 - \phi_2)} \frac{\ln(\phi_2/\phi_1)}{T(S/D)} \qquad D = 2R \tag{35.45}$$

where

$$T(S/D) = \int_0^\infty \frac{\cos(2tz/D)\sin(tS/D)}{I_0(t)} \frac{dt}{t} \tag{35.46}$$

The function $T(S/D)$ is tabulated by Bertram (1942). Given the potential ratio ϕ_2/ϕ_1 and the gap-to-bore ratio S/D, a/S can be obtained; Kanaya and Baba plot $(\pi a/S)(\phi_1 - \phi_2)/(\phi_1\phi_2)^{1/2} \ln(\phi_2/\phi_1)$ as a function of S/D.

Several special cases are of interest. For $m = 1/2$, the potential varies exponentially with z; the paraxial solutions can be expressed in terms of Chebyshev polynomials in μ and hence as products of sinusoidal and exponential functions of z. Explicit formulae are given by Kanaya and Baba for the real and asymptotic cardinal elements and for the spherical and chromatic aberration coefficients. For $m = 0.58$, the real focal length is smallest but the specimen must be placed at the centre of the lens.

The case $m = 0.95$ accurately represents a lens consisting of a cylinder and an aperture in a plate, studied earlier by Kanaya et al. (1972) when analysing an accelerator. Curves for cardinal elements and the spherical and chromatic aberration coefficients are given, the latter for several finite values of the magnification as well as for $M \to \infty$.

For $m = 1$, we recover the model discussed earlier (35.26); explicit formulae can now be obtained for the cardinal elements:

$$\text{real focal lengths}\quad \begin{aligned} \frac{f_i'}{a} &= \frac{\exp\{k/\sqrt{3})\arccos\mu_i\}}{k^2(1-\mu_i)F\left(\dfrac{1-\omega}{2}, \dfrac{1+\omega}{2}, 2, \dfrac{1-\mu_i}{2}\right)} \\ \frac{f_o'}{a} &= \frac{\exp\{k/\sqrt{3})\arccos(-\mu_o)\}}{k^2(1+\mu_o)F\left(\dfrac{1-\omega}{2}, \dfrac{1+\omega}{2}, 2, \dfrac{1+\mu_o}{2}\right)} \end{aligned} \tag{35.47}$$

$$\begin{array}{l}\text{asymptotic}\\ \text{cardinal}\\ \text{elements}\end{array}\quad \begin{aligned} \frac{f_i}{a} &= -\frac{1}{2}\Gamma\left(\frac{1+\omega}{2}\right)\Gamma\left(\frac{1-\omega}{2}\right)\exp\left(\frac{k\pi}{\sqrt{3}}\right) \\ \frac{f_o}{a} &= -\frac{1}{2}\Gamma\left(\frac{1+\omega}{2}\right)\Gamma\left(\frac{1-\omega}{2}\right)\exp\left(-\frac{k\pi}{\sqrt{3}}\right) \\ \frac{z_{Fi}}{a} &= \frac{\pi}{2}\cot(\pi\nu) + \psi(\nu) + \gamma_e = -\frac{z_{Fo}}{a} \end{aligned} \tag{35.48}$$

where γ_e is Euler's constant, $\gamma_e = 0.577216$, $\psi(\nu) = (d/d\nu)\ln\Gamma(\nu+1)$, $\nu = (\omega - 1)/2$, $\omega = (1+4k^2)^{1/2}$ and $a_h/a = 1.3169$.

Finally, $m = 3/2$ corresponds to Eq. (35.18); in terms of the hypergeometric function, the cardinal elements take the following form:

$$\text{real focal lengths}\quad \begin{aligned} \frac{f_i'}{a} &= \frac{\exp\{k/\sqrt{3})\arccos\mu_i\}}{k^2\sqrt{2}(1-\mu_i)^{3/2}F\left(\dfrac{1-2\omega}{2}, \dfrac{1+2\omega}{2}, \dfrac{5}{2}, \dfrac{1-\mu_i}{2}\right)} \\ \frac{f_o'}{a} &= \frac{\exp\{k/\sqrt{3})\arccos(-\mu_o)\}}{k^2\sqrt{2}(1+\mu_o)^{3/2}F\left(\dfrac{1-2\omega}{2}, \dfrac{1+2\omega}{2}, \dfrac{5}{2}, \dfrac{1+\mu_o}{2}\right)} \end{aligned} \tag{35.49}$$

$$\begin{aligned} \text{asymptotic cardinal elements} \qquad & \frac{f_i}{a} = -\frac{1}{\pi}\Gamma(1+\omega)\Gamma(1-\omega)\exp\left(\frac{k\pi}{\sqrt{3}}\right) \\ & \frac{f_o}{a} = -\frac{1}{\pi}\Gamma(1+\omega)\Gamma(1-\omega)\exp\left(-\frac{k\pi}{\sqrt{3}}\right) \\ & \frac{z_{Fi}}{a} = -\frac{z_{Fo}}{a} = \frac{\pi^{1/2}\Gamma(1+\omega)\Gamma(1-\omega)}{2\Gamma\left(\frac{1-2\omega}{2}\right)\Gamma\left(\frac{1+2\omega}{2}\right)} \end{aligned} \tag{35.50}$$

35.2.2.4 Cylinders of different radius

This extra degree of complexity makes it difficult to establish universal curves analogous to those for cylinders of equal radius. An early study by Ehinger (1954a) suggested that the lens should be separated into two regions, the dividing line being the plane through the axial point at which the potential has its point of inflexion and hence $\partial E_z(0, z)/\partial z = 0$; close to the axis, $E_r \approx -\frac{1}{2}r\partial E_z/\partial z$ also vanishes. In each region, the potential is then represented by a function of the form (35.15); with the notation of Fig. 35.6, continuity of $\phi(z)$ implies that

$$\frac{z_1}{R_1} = \frac{z_2}{R_2}, \quad z_1 = \frac{R_1 S}{R_1 + R_2}, \quad z_2 = \frac{R_2 S}{R_1 + R_2} \text{ and } \phi_m = \frac{\phi_1 R_2 + \phi_2 R_1}{R_1 + R_2} \tag{35.51}$$

An extensive discussion using the tanh model is to be found in Ollendorff (1955, §IV.10).

An analytical expression for the potential in such a system has been obtained by Lebedev and Skalskaya (1960), who find (Fig. 35.7)

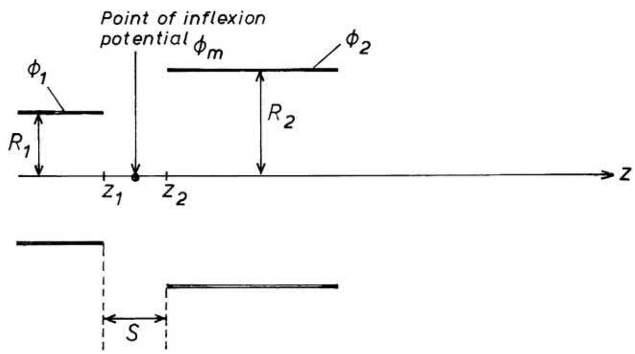

Figure 35.6
Unsymmetric two-cylinder lens.

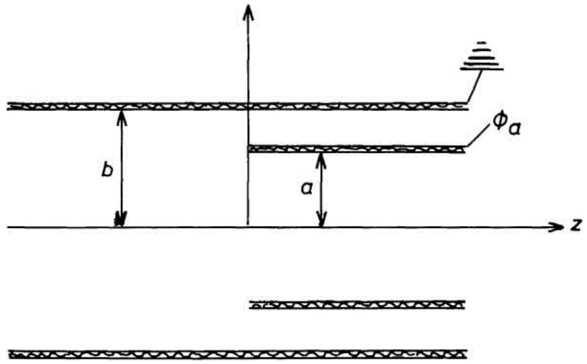

Figure 35.7
The unsymmetric two-cylinder lens geometry analysed by Lebedev and Skalskaya. Note that the larger cylinder encloses the smaller cylinder in the half-space $z > 0$.

$$
\begin{aligned}
\frac{\phi(z)}{\phi_a} &= 1 - \sum_{m=1}^{\infty} \frac{\exp\left(-\gamma_m z/a\right)}{\gamma_1 J_1\left(\gamma_m\right) K\left(\mathrm{i}\gamma_m/a\right)} \qquad 0 \le r \le a, \quad z > 0 \\
\frac{\phi(z)}{\phi_a} &= \frac{1}{\ln\left(b/a\right)} \sum_{m=1}^{\infty} \frac{K\left(\mathrm{i}\gamma_m/b\right)\exp\left(\gamma_m z/b\right)}{\gamma_m^2 J_1^2\left(\gamma_m\right)} J_0\left(\frac{\gamma_m a}{b}\right) \qquad 0 \le r \le b, \quad z < 0
\end{aligned}
\tag{35.52}
$$

in which the γ_m are the zeros of the zero-order Bessel function, $J_0(\gamma_m) = 0$. The zeros of

$$
J_0\left(\frac{a\delta}{b-a}\right) Y_0\left(\frac{b\delta}{b-a}\right) - J_0\left(\frac{b\delta}{b-a}\right) Y_0\left(\frac{a\delta}{b-a}\right) = 0
$$

are denoted by δ_m. The function K is conveniently written in terms of a new function $k(x)$:

$$
K\left(\mathrm{i}\gamma_m/a\right) = k\left(\frac{b-a}{a}\gamma_m\right), \quad K\left(\mathrm{i}\gamma_m/b\right) = k\left(\frac{b-a}{b}\gamma_m\right) \tag{35.53}
$$

where

$$
k(x) = \frac{P\left(\dfrac{bx}{b-a}\right)\exp\left\{-\dfrac{x}{\pi}\left(\pi S + \dfrac{1}{b-a}\right)\right\}}{P\left(\dfrac{ax}{b-a}\right)Q(x)} \tag{35.54a}
$$

and

$$
\begin{aligned}
P(x) &= \prod_1^{\infty}\left(1 + x/\gamma_m\right)\exp\left(-x/\gamma_m\right) \\
Q(x) &= \prod_1^{\infty}\left(1 + x/\delta_m\right)\exp\left(-x/\delta_m\right) \\
S &= \sum_1^{\infty}\left(1/\delta_m - 1/\gamma_m\right)
\end{aligned}
\tag{35.54b}
$$

Rapidly converging series for ln P, ln Q and ln S are given by Lebedev and Skalskaya, who plot $\phi(z)$ for several values of a/b. Numerical calculations based on this potential have been made by El-Kareh and El-Kareh (1970).

The potential in lenses consisting of two cylinders of different radius has been obtained by an analogue method (a resistance network) by Firestein and Vine (1963), who tabulate cardinal elements and spherical aberration coefficients for a range of values of potential and radius ratios. See also Gundert (1941). The effect of the lens geometry on the optical properties has been reconsidered by Al-Khashab and Ahmad (2012) and Al-Khashab and Al-Abdullah (2013a,b).

35.2.2.5 A unified representation

Ura (1998, 1999) has established a unified representation of the cardinal elements and spherical aberration coefficients of a range of bipotential lenses. Fig. 35.8A shows the eleven geometries examined. Model B-0 is the analytical model (35.7). The optical properties are normalized with respect to an 'effective diameter', D_e, defined by

$$D_e = D/\lambda$$

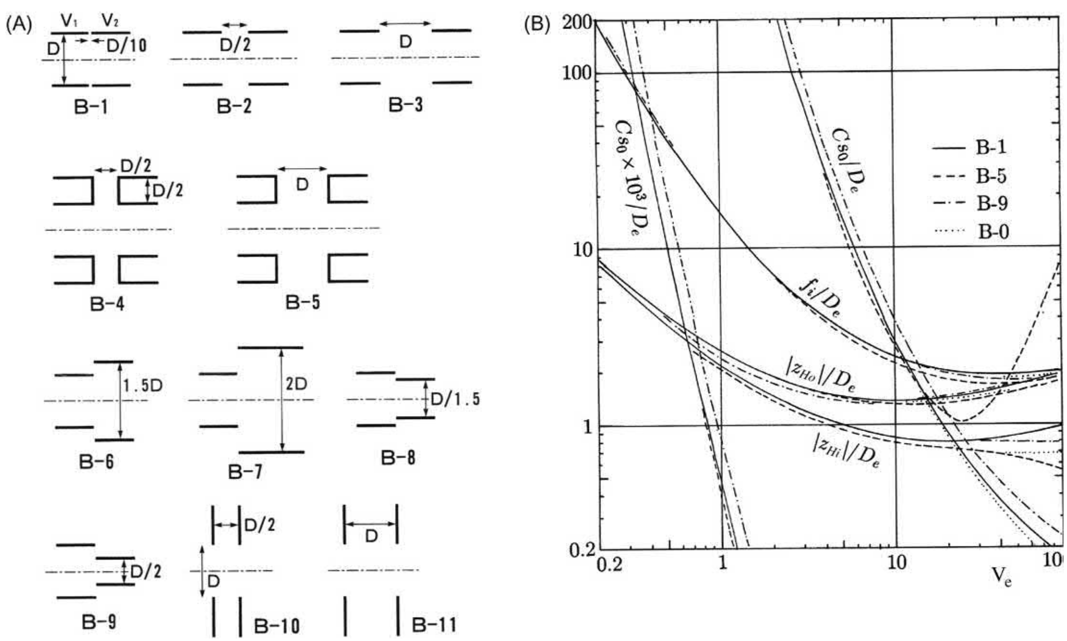

Figure 35.8
(A) The eleven bipotential lenses studied. (B) Unified presentation for the lenses B-1, B-5, B-9 and B-0; the curves for the other lenses are very similar. *After Ura (1999), Courtesy Japanese Society of Microscopy.*

and the lens excitation is now measured by V_e,

$$V_e = \mu\left(\frac{V_2}{V_1} - 1\right)$$

The scaling factors λ and μ are obtained by requiring that the curves for lenses B-2 to B-11 fit those for B-1 as closely as possible. Table 35.1 shows the appropriate values for this case and for einzel lenses (Section 35.3.1.7). The unified curves are reproduced in Fig. 35.8B. Ura also shows how well these results agree with the thin-lens approximation discussed at the end of Chapter 25 of Volume 1 and returns to this approximation in a later paper (Ura, 2003). An alternative normalization is also examined. The magnification dependence of the coefficients had been considered earlier (Ura, 1994).

35.2.3 Three or More Electrodes

The literature on such immersion lenses is distinctly less voluminous. It falls into two categories: numerical studies, few in number, of immersion lenses with three or more electrodes possessing some specific characteristic, such as the *zoom lenses* of Cross et al.

Table 35.1: Values of λ and μ for the various bipotential and einzel lens models. For the latter, R signifies retarding–accelerating and A, accelerating–retarding

Model	μ	λ
B-1	1	1
B-2	1	0.88
B-3	0.98	0.67
B-4	0.99	0.88
B-5	1	0.7
B-6	0.92	0.93
B-7	0.9	0.87
B-8	1.05	0.74
B-9	1.2	0.54
B-10	0.98	0.87
B-11	1	0.68
B-0	1	1
UR-1	1.05	1.1
UR-2	1.2	0.72
UR-3	1	1
UR-4	1.1	0.62
UR-0	0.84	0.52
UA-1	1.1	1.09
UA-2	1.08	0.92
UA-3	1	1
UA-4	1.1	0.64
UA-0	1	0.38

(1967) and the afocal five-electrode lens of Heddle (1971); and studies of accelerators in which the potential distribution is the same at each accelerating gap and the number of these gaps is large, typically 10 or more.

35.2.3.1 Zoom lenses

In studies involving low-energy electrons, it proves convenient to be able to vary the ratio of the final electron energy to that of the incident electrons without altering the positions of the conjugate planes. This condition can be satisfied with three-element immersion lenses, by suitably varying the two voltage ratios, ϕ_3/ϕ_1 and ϕ_2/ϕ_1. Such lenses have been studied by Cross et al. (1967), Imhof and Read (1968), Read (1970a) and Harting and Read (1976).

Although the conjugates remain fixed as the overall voltage ratio, ϕ_3/ϕ_1, is altered, the magnification will change; if two conditions are to be satisfied—fixed conjugates and constant magnification—an extra free parameter must be introduced. This can be achieved by adding a fourth electrode, so that by simultaneously adjusting ϕ_2/ϕ_1 and ϕ_3/ϕ_1 as ϕ_4/ϕ_1 is varied, both conditions can be satisfied. Four-cylinder systems have been studied as zoom lenses by Kurepa et al. (1974) and, as a special case of a method intended for complex systems in general, by Fink and Kisker (1980, cf. Kisker, 1982, where the ray-tracing method employed is described). They have also been analysed in some detail by Wannberg and Sköllermo (1977), who calculate all the aberration coefficients. The paraxial properties and spherical aberration coefficient of four-cylinder zoom lenses are presented by Martínez and Sancho (1983) and Martínez et al. (1983). Lenses with five or more elements are studied by Wilska et al. (1970), Heddle and Papadovassilakis (1984) and by Trager-Cowan et al. (1990a,b). Zoom-lens designs have been examined by Sise (2014, 2015) and Sise et al. (2007a,b, 2009) and by Isik (2016), who used artificial neural network theory.

35.2.3.2 Accelerators

Multielectrode structures for accelerating electrons to energies of a few hundred keV or a few MeV may be conveniently regarded as immersion lenses. Beyond this energy range, different methods prove more convenient; these are beyond the scope of this volume and we refer to such standard texts as Lapostolle and Septier (1970), Lawson (1977, 1988), Humphries (1986), Wiedemann (2015) and the work of Berz et al. (2015).

Although there are some earlier studies of accelerator optics (Bas et al., 1959; Bas, 1960; Taoka et al., 1967; Galejs and Rose, 1967; Fink and Kessler, 1963; Kessler, 1961; Koltay and Czeglédy, 1965; Mileikowsky and Paul, 1952; Timm, 1955), in particular Morikawa (1962a,b; 1963a,b,c) who obtained practical working formulae assuming that each gap acts as a thin lens, the most thorough analyses are those of Glikman et al. (1973a,b) and Glikman and Nurmanov (1976). These authors studied lenses with N electrodes of equal radius (R), separated by a negligible gap, for three electrode lengths: $R/2$, R and $2R$; $N = 2$, 3, 4, 8, 16 and 32. The voltages of adjoining electrodes are either such that the ratio

ϕ_{n+1}/ϕ_n is the same for every pair or such that the difference $\phi_{n+1} - \phi_n$ is constant. Both cardinal elements and the spherical aberration coefficient are calculated.

A selection of their results is reproduced in Fig. 35.9. In their later paper, Glikman and Nurmanov (1976) give approximate formulae for the cardinal elements:

Constant voltage ratio

$$\begin{aligned} z_{Fi} &= -z_{Fo} = L_e\left\{\frac{1}{2} + \frac{4}{\sqrt{3}\ln(\phi_N/\phi_1)}\cot\left(\frac{\sqrt{3}}{4}\ln\frac{\phi_N}{\phi_1}\right)\right\} \\ f_i &= -\frac{4(\phi_N/\phi_1)^{1/4}L_e}{\sqrt{3}\ln\left(\frac{\phi_N}{\phi_1}\right)\sin\left(\frac{\sqrt{3}}{4}\ln\frac{\phi_N}{\phi_1}\right)} \\ f_o &= \left(\frac{\phi_1}{\phi_N}\right)^{1/2} f_i \end{aligned} \tag{35.55}$$

Constant voltage difference

$$\begin{aligned} z_{Fo} &= -L_e\left[\frac{1}{2} + \frac{4}{3}\frac{3(\phi_N/\phi_1)^{1/2} - 1}{(\phi_N/\phi_1 - 1)\left\{(\phi_N/\phi_1)^{1/2} - 1\right\}}\right] \\ z_{Fi} &= -z_{Fo} + \frac{4}{3}L_e\frac{1 - (\phi_N/\phi_1)^{1/2}}{1 + (\phi_N/\phi_1)^{1/2}} \\ f_i &= -\frac{8}{3}L_e\frac{\phi_N/\phi_1}{(\phi_N/\phi_1 - 1)\left\{(\phi_N/\phi_1)^{1/2} - 1\right\}} \end{aligned} \tag{35.56}$$

For $N \geq 8$, the expressions for constant voltage ratio are accurate to within 6% (2% for $N = 32$); those for constant voltage difference are distinctly less useful. The effective length L_e is related to N as follows:

N	2	3	4	8	16	32
$(L_e - L)/R$	2.4	1.9	1.9	1.5	1.5	1.0

35.2.3.3 Other studies

Three-electrode immersion lenses are further studied by Adams and Read (1972b), Berger and Baril (1982), Bobykin et al. (1976), Heddle et al. (1982), Heddle and Kurepa (1970) and Saito et al. (1979), who examine the cardinal elements and spherical and chromatic aberration coefficients of an unusual geometry in which the first and third electrodes have

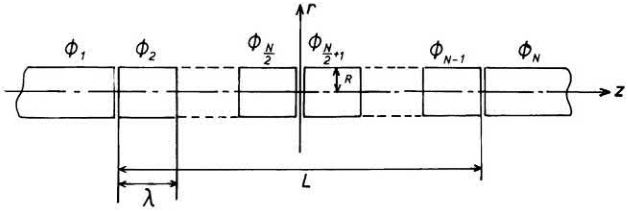

(A)

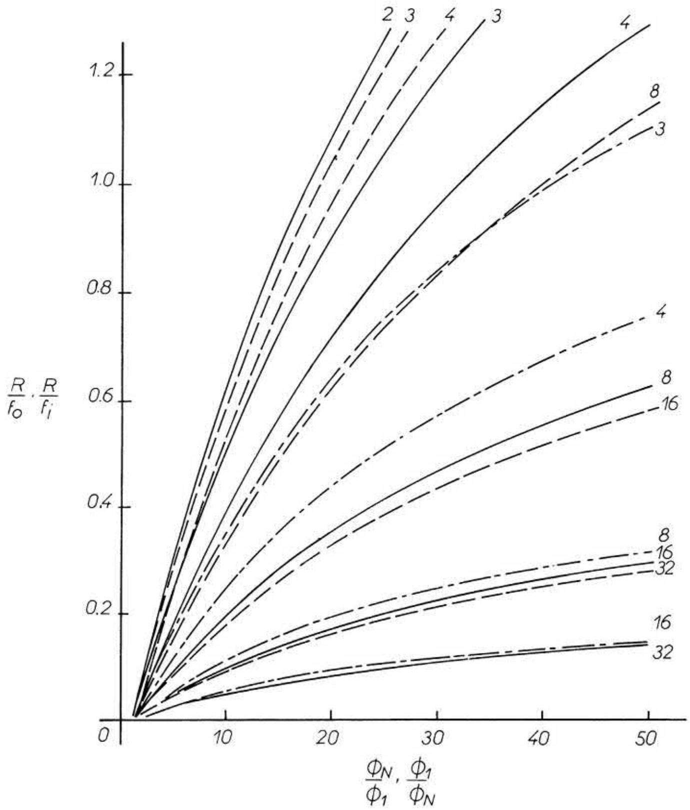

(B)

Figure 35.9

The optical properties of N-electrode accelerators. (A) Notation. (B)–(E) Constant voltage ratio. (B) Front focal length of an accelerating structure and rear focal length of a retarding structure. (C) Rear asymptotic focus of an accelerating structure and front asymptotic focus of a retarding structure. (D) and (E) Spherical aberration coefficient C_s (magnifying case, disc radius $= M\,C_s\alpha^3$) and B (demagnifying case, disc radius $= Br_a^3$). In (D), the lens is retarding for B and accelerating for C_s; in (E) the situation is reversed. (F)–(I) Constant voltage difference. (F) and (G) Real and virtual foci measured relative to the first (object foci) or last (image foci) gap. In (F) the front (image) foci correspond to an accelerating structure and the back (object) foci to a retarding structure; in (G) the opposite situation is shown. (H) The coefficient B for accelerating structures and C_s for retarding structures. (I) The coefficients C_s for accelerating structures and B for retarding structures. In all these, the parameter is N, the number of electrodes, and dashed curves correspond to $\lambda = 0.5R$, full curves to $\lambda = R$ and dot-dashed curves to $\lambda = 2R$. *After Glikman and Nurmanov (1976).*

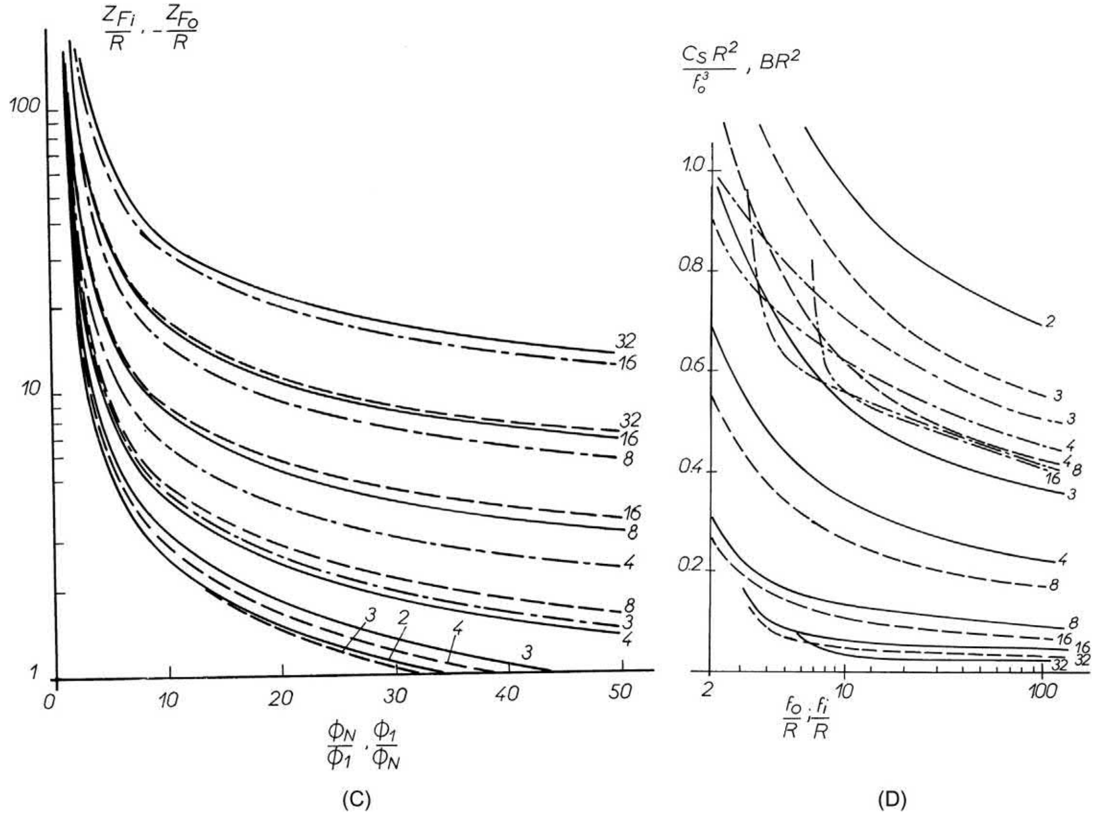

Figure 35.9
(Continued)

different radii and the central electrode contains a step from one radius to the other. An attempt to find general expressions for the focal length and coefficients of spherical and chromatic aberration has been made by Crewe (1991), who used the following model potential:

$$T := \frac{\phi'}{\phi} = \ln\phi_1(32z - 96z^2 + 64z^3) + \ln\phi_0(-10z + 42z^2 - 32z^3)$$

This was chosen to ensure that $T = 0$ at $z = 0$ and $z = 1$ and that $\phi(0) = 1$ and $\phi(1) = \phi_0$; $z = 0$ and $z = 1$ are the end-points of the lens. At the midpoint of the model lens, $\phi = \phi_1$. Crewe finds approximate expressions for the focal length and aberration coefficients, which agree with the exact values to within a factor 3 (except for few extreme cases).

Some five-electrode lenses are considered by Cross et al. (1967) and Heddle (1971) and a seven-electrode geometry by Chutjian (1979) and Boesten (1988). A method for the rapid calculation of trajectories in multielement lenses is described by Fink and Kisker (1980)

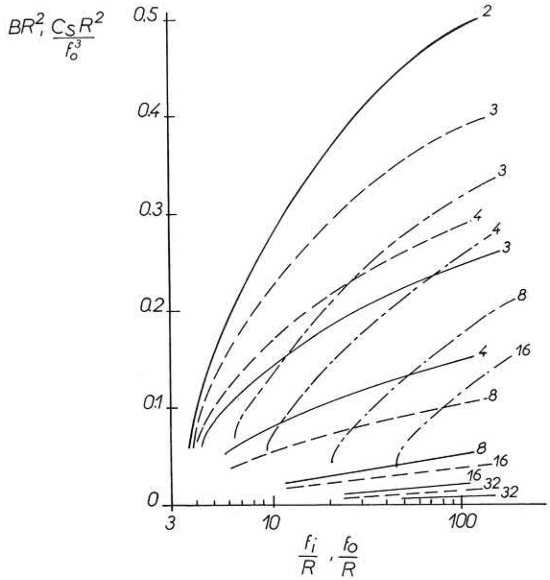

(E)

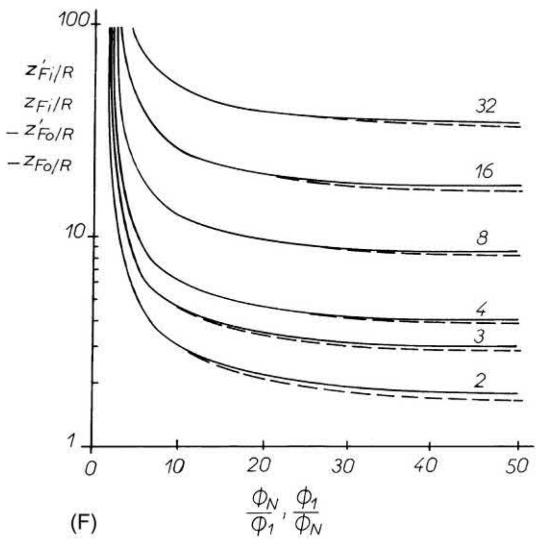

(F)

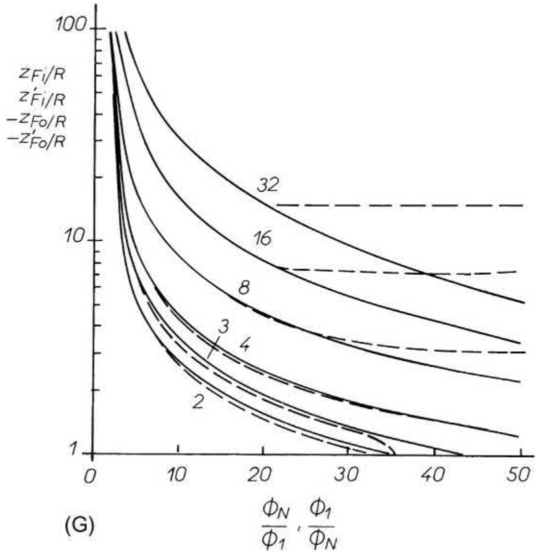

(G)

Figure 35.9
(Continued)

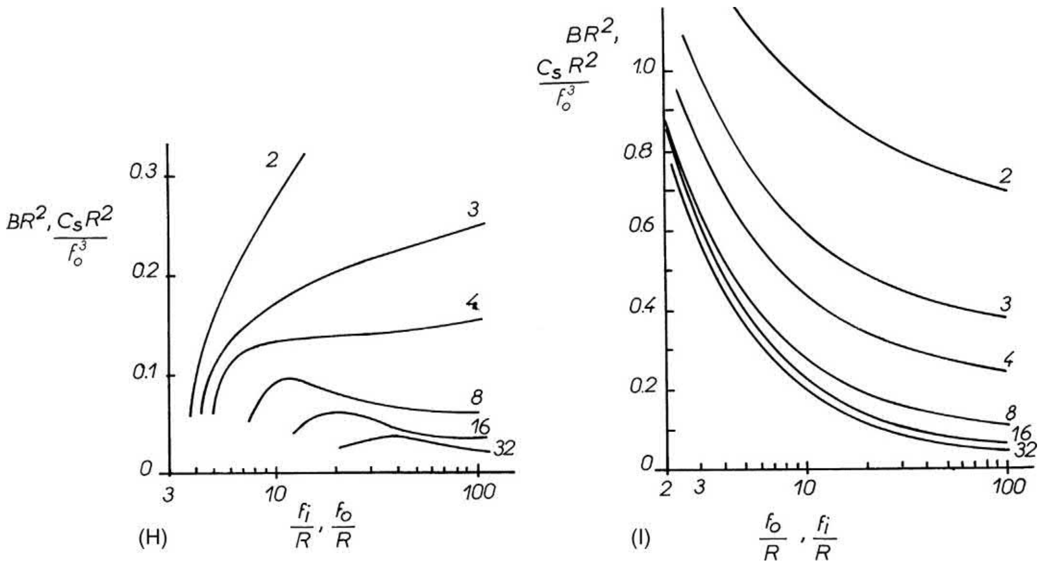

Figure 35.9
(Continued)

and applied to four-element zoom lenses. Ulu et al. (2007) have analysed the properties of a seven-element gun and Sise et al. (2005, 2007a,b) have studied numerous multielectrode designs. For related studies, see Chou et al. (1987), Bernius et al. (1988), Sellidj and Erskine (1990), Sakae et al. (1990), Ohye et al. (1993), Morita et al. (1995), Yavor et al. (1999), Escher et al. (2002), Colman and Legge (1994), Al-Khashab and Al-Shamma (2009a,b) and Zouros et al. (2015).

35.3 Einzel Lenses

The class of three-electrode lenses that have no overall accelerating or retarding effect on the electrons has been widely studied. Since the outer electrodes are tied to the nearest adjoining electrodes and are in practice almost invariably earthed, there is only one free potential, that of the central electrode; such lenses are commonly known as einzel ('single') or unipotential lenses.[2] Although there is no reason why electrostatic lenses consisting of four or more electrodes, the outer two earthed and the inner ones at arbitrary potentials, should not be built, there are very few such designs in the literature and systematic studies, even of highly symmetric arrangements (such as five-electrode lenses with both electrical and geometric symmetry about the midplane), are just as rare.

[2] A verbal distinction is sometimes made between lenses in which the voltage applied to the central electrode is variable and those in which it is the same as the cathode voltage. We shall regard the latter merely as a special case.

We first examine the principal potential models and then list the numerous sources of information on lenses of this type.

35.3.1 The Principal Potential Models

35.3.1.1 Regenstreif's model

The earliest model, to which later studies frequently refer, is that proposed by Regenstreif (1951), which is excellent for predicting the behaviour of such lenses, though as usual some caution is needed before using the absolute values of the various quantities. Regenstreif considers in detail three-plate lenses and, as an extension of this work, similar lenses in which the central electrode is thick. The potential is represented by a linear superposition of three potentials of the form (35.1, 35.2), each representing that of a plate with a circular opening, and the weights attached to each potential are chosen in such a way that $\phi_1 = \phi(-\infty) = \phi(\infty) = \phi_2$ for $R_1 > R_2 << S$. The axial potential thus has the general form

$$\phi(z) = A + B\left\{(z+S)\arctan\left(\frac{z+S}{R_2}\right) + (z-S)\arctan\left(\frac{z-S}{R_2}\right) - 2z\arctan\left(\frac{z}{R_1}\right)\right\} \quad (35.57)$$

with

$$A = \phi_1 - 2B\left\{R_1 + S\arctan\left(\frac{S}{R_2}\right)\right\} \quad (35.58a)$$

$$B = (\phi_1 - \phi_2)\Big/\left\{2R_1 + 2S\arctan\left(\frac{S}{R_1}\right) + R_2 + 2S\arctan\left(\frac{S}{R_2}\right) - 2S\arctan\left(\frac{2S}{R_2}\right)\right\} \quad (35.58b)$$

and if S/R_2 is large (≥ 3),

$$B \approx \frac{\phi_1 - \phi_2}{2R_1 + 2S\arctan(S/R_1)} \quad (35.58c)$$

In the latter case, the potential at the origin is given by

$$\phi(0) = \phi_1 + \frac{\phi_2 - \phi_1}{1 + (S/R_1)\arctan(S/R_1)} \quad (35.59)$$

showing the importance of the parameter S/R_1. The axial potential at the outer electrodes, where $z = S$, is given by

$$\phi(S) = \phi_1 + (\phi_2 - \phi_1)\left\{1 - \frac{R_2/2R_1}{1 + (S/R_1)\arctan(S/R_1)}\right\} \quad (35.60)$$

(again assuming that S/R_2 is large) so that $\phi(\pm S)$ is a function of $S/R_1 =: s$ and of R_2/R_1. Finally, we note that $\phi(0)/\phi(S)$, which occurs frequently in later formulae, is given by

$$\frac{\phi(0)}{\phi(S)} =: x = \frac{\phi_1 + \left(\phi_2 - \phi_1\right)(1+s\arctan s)^{-1}}{\phi_1 + \left(\phi_2 - \phi_1\right)\left\{1 - (1+s\arctan s)^{-1}R_2/2R_1\right\}} \tag{35.61}$$

and that

$$x\left(\phi_1 = 0\right) = \left(1+s\arctan s - R_2/2R_1\right)^{-1} \approx \frac{2R_1}{\pi(S-R_2)} \tag{35.62}$$

The derivation of (35.58) is unsatisfactory, as has been pointed out by Glaser (1952) and Lenz (1956), and the expressions for A and B given by Lenz are to be preferred since $\phi(z)$ then always tends to the correct value as $z \to \pm\infty$: these are

$$A = \phi_2 + \frac{2(\phi_2 - \phi_1)(R_1 - R_2)}{\pi S}, \quad B = \frac{\phi_1 - \phi_2}{\pi S},$$

Nevertheless, Regenstreif's model gives reasonable results within an error of roughly 8%.

It is not possible to solve the paraxial equation explicitly for Eq. (35.57) and Regenstreif therefore replaced this axial potential by three parabolic segments, joining at the points of inflexion of Eq. (35.57), which occur at $z = \pm 2S/3$ for $R_1 = 2R_2$ and are assumed to occur at this point for all other values of interest. Such a procedure has little attraction today when numerical ray tracing is so straightforward but his explicit formulae for the asymptotic cardinal elements remain useful for teaching purposes and we list them here for this reason. For a *thin* central electrode, Regenstreif finds

$$\begin{aligned} \frac{z_F}{S} - 1 &= -\frac{1}{\sqrt{6(1-x)}} \cdot \frac{\left(9\cosh^2 2\beta_o - 1\right)^{1/2}\sin\left\{2\alpha_o + \arctan\left(2\sqrt{2}\coth 2\beta_o\right)\right\}}{\left(3\cosh^2 2\beta_o - 2\right)\sin\left(2\alpha_o - \arctan\beta_1\right)} \\ \frac{1}{f} &= \beta\left(\frac{3}{2}\cosh^2\beta_o - 1\right)\sin\left(2\alpha_o - \arctan\beta_1\right) \end{aligned} \tag{35.63}$$

in which

$$\begin{aligned} n &:= \frac{3}{2}\frac{\phi(S)-\phi(0)}{S^2} & \beta_o &= \frac{1}{\sqrt{2}}\arcsin\left(\frac{\beta S}{3}\right) \\ \beta &= \left\{2n/\phi(S)\right\}^{1/2} & \alpha_o &= \frac{1}{\sqrt{2}}\operatorname{arcsinh}\left(\frac{2\alpha S}{3}\right) \\ \alpha &= \left\{n/\phi(0)\right\}^{1/2} & \beta_1 &= \frac{2\sqrt{2}\tanh\beta_o}{1 - 2\tanh^2\beta_o} \end{aligned} \tag{35.64}$$

When the central electrode is *thick*, Regenstreif models it by two plane thin electrodes held at the same potential ϕ_1. The cardinal elements are now given by

$$
\begin{aligned}
\frac{1}{f} &= \frac{1}{f_1} + \frac{1}{f_2} \\
\frac{1}{f_1} &= \frac{\beta}{\lambda\sqrt{2}}\left(\cosh^2\beta_o + \lambda^2\sinh^2\beta_o\right)\sin\left(2\alpha_o - \arctan\frac{2\lambda\tanh\beta_o}{1-\lambda^2\tanh^2\beta_o}\right) \\
\frac{1}{f_2} &= -\frac{\alpha\beta k_1 S}{\lambda}\cos^2\alpha_o\cosh^2\beta_o(\tan\alpha_o - \lambda\tanh\beta_o)^2
\end{aligned}
\tag{35.65}
$$

in which

$$
\begin{aligned}
\lambda &= \sqrt{\frac{k-k_1}{1-k}} \quad k_1 = \zeta_1/S \quad k = \zeta/S \\
\alpha_o &= \frac{1}{\sqrt{2}}\operatorname{arcsinh}\left\{\alpha S(k-k_1)\right\} \\
\beta_o &= \frac{1}{\sqrt{2}}\arcsin\left\{\beta S(1-k)\right\} \\
\alpha &= \frac{1}{S}\left(\frac{1-x}{(1-k_1)(k-k_1)x}\right)^{1/2} \\
\beta &= \frac{1}{S}\left(\frac{1-x}{(1-k_1)(1-k)}\right)^{1/2}
\end{aligned}
\tag{35.66}
$$

and the quantities ζ, ζ_1 denote the boundaries between the parabolic or linear segments of potential. Likewise,

$$
\begin{aligned}
\frac{z_F}{S} &= 1 + \frac{1}{\sqrt{2}\beta S}\frac{\sqrt{2}\alpha k_1 SI + J}{\sqrt{2}\alpha k_1 SM + N} \\
I &= \left(\sin^2\alpha_o - \lambda^2\cos^2\alpha_o\right)\sinh\left\{2\beta_o - \operatorname{arctanh}\left(\frac{2\lambda\tan\alpha_o}{\lambda^2+\tan^2\alpha_o}\right)\right\} \\
J &= \left\{4\lambda^2 + \left(\lambda^2+1\right)^2\sinh^2 2\beta_o\right\}^{1/2}\sin\left\{2\alpha_o + \arctan\left(\frac{2\lambda}{\lambda^2-1}\coth 2\beta_o\right)\right\} \\
M &= -\cos^2\alpha_0\cosh^2\beta_o(\tan\alpha_o - \lambda\tanh\beta_o)^2 \\
N &= \frac{\lambda\sqrt{2}}{\beta f_o}
\end{aligned}
\tag{35.67}
$$

If the approximations $\zeta_1 \approx z_1/2$, $\zeta \approx z_1 + 2(S - z_1)/3$, $k_1 \approx \nu/2$, $k \approx (2 + \nu)/3$ are made, with $\nu := z_1/S$, we have

$$\begin{aligned} &\lambda \approx \left(\frac{4-\nu}{2(1-\nu)}\right)^{1/2} \\ &\beta S = \left\{\frac{6(1-x)}{(2-\nu)(1-\nu)}\right\}^{1/2} \qquad \alpha_o = \frac{1}{\sqrt{2}}\operatorname{arcsinh}\left\{\frac{(4-\nu)(1-x)}{3(2-\nu)x}\right\} \\ &\beta_o = \frac{1}{\sqrt{2}}\arcsin\left\{\frac{(2-\nu)(1-x)}{3(2-\nu)}\right\} \quad \alpha S = \left\{\frac{12(1-x)}{(2-\nu)(4-\nu)x}\right\}^{1/2} \end{aligned} \tag{35.68}$$

and the cardinal elements become functions of $x = \phi(0)/\phi(S)$ and $\nu = z_1/S$.

We shall not pursue Regenstreif's work further, into the domain of aberrations; his results are expressed not in terms of the conventional aberration coefficients but in terms of (curved) principal surfaces and focal surfaces, as in some earlier experimental work (Heise and Rang, 1949; Heise, 1949) with which Regenstreif compares his results and finds good agreement. We note that Regenstreif also considers briefly lenses in which the central opening is first slightly elliptical, and second slightly misaligned (see Chapter 31 of Volume 1).

35.3.1.2 Schiske's model

A second model, which has been extensively studied (Schiske, 1953; Glaser and Schiske, 1954, 1955; Kanaya et al., 1966), is that generated by setting out from the paraxial equation (15.12) and transforming it as already mentioned briefly in Section 17.2. For generality, we retain magnetic and electrostatic terms, and substituting

$$z =: a \cot\psi \tag{35.69}$$

in Eq. (15.12), we obtain

$$\hat{\phi}^{1/2}\frac{d}{d\psi}\left(\hat{\phi}^{1/2}\frac{du}{d\psi}\right) + 2\hat{\phi}\cot\psi\frac{du}{d\psi} + \frac{1}{4}\left\{\left(\ddot{\phi} + 2\dot{\phi}\cot\psi\right)(1 + 2\varepsilon\phi) + \eta^2 a^2 B^2 \operatorname{cosec}^4\psi\right\}u = 0 \tag{35.70}$$

where

$$\dot{\phi} = d\phi/d\psi \tag{35.71}$$

Fig. 35.10 shows how z and ψ are related. We now set

$$r(\psi) := u \sin\psi \tag{35.72}$$

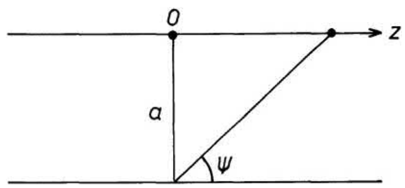

Figure 35.10
The transformation (35.69). As the z-axis is followed from very large positive values to zero and thence to large negative values, ψ advances from zero ($z \to \infty$) through $\pi/2$ ($z = 0$) towards $\pi(z \to -\infty)$.

whereupon Eq. (35.70) becomes

$$\hat{\phi}\frac{d}{d\psi}\left(\hat{\phi}^{1/2}\dot{r}\right) + \left\{\hat{\phi} + \frac{1}{4}\ddot{\phi}(1 + 2\varepsilon\phi) + \frac{1}{4}\eta^2 a^2 B^2 \operatorname{cosec}^4\psi\right\} r = 0 \tag{35.73}$$

Finally, we replace ψ by

$$\zeta := \hat{\phi}_0^{1/2}\int\frac{d\psi}{\hat{\phi}^{1/2}} \tag{35.74}$$

so that Eq. (35.73) becomes

$$\frac{d^2 r}{d\zeta^2} + \frac{1}{\hat{\phi}_0}\left\{\hat{\phi} + \frac{1}{4}\ddot{\phi}(1 + 2\varepsilon\phi) + \frac{1}{4}\eta^2 a^2 B^2 \operatorname{cosec}^4\psi\right\} r = 0 \tag{35.75}$$

This has solutions in terms of circular functions if the coefficient of $r(\zeta)$ is a constant, that is, if we consider fields $B(z)$ and potentials $\phi(z)$ for which

$$\frac{1}{4}\ddot{\phi}(1 + 2\varepsilon\phi) + \hat{\phi} + \frac{1}{4}\eta^2 a^2 B^2 \operatorname{cosec}^4\psi = \omega^2\hat{\phi}_0 \tag{35.76}$$

with a free parameter ω or, with $B(\psi) = B_0 \sin^2\psi$ and setting

$$k_m^2 := \frac{\eta^2 B_0^2 a^2}{4\hat{\phi}_0} \tag{35.77}$$

those for which

$$\ddot{\phi}(1 + 2\varepsilon\phi) + 4\hat{\phi} = 4\hat{\phi}_0\left(\omega^2 - k_m^2\right) \tag{35.78}$$

Solving for $\phi(\psi)$ and hence for $\phi(z)$ in the nonrelativistic case, we obtain

$$\begin{aligned}\phi(\psi) &= \left(\omega^2 - k_m^2\right)\phi_0 + C_1\cos 2\psi + C_2\sin 2\psi\\ &= \phi_0\left(1 - \kappa^2\sin^2\psi\right) + C_2\sin 2\psi\end{aligned} \tag{35.79}$$

in which we have used the boundary condition $\phi(\pi) = \phi_0$ and written

$$\kappa^2 = 2\left(1 - \omega^2 + k_m^2\right) \tag{35.80}$$

In terms of the original variable z, therefore,

$$\phi(z) = \phi_0\left(1 - \frac{k^2}{1 + \left(z/a\right)^2}\right) + \frac{2C_2}{a}\frac{z}{1 + \left(z/a\right)^2} \tag{35.81}$$

The choice $B(\psi) = B_0 \sin^2 \psi$ is known as Glaser's bell-shaped field and is examined in detail in Section 36.2.

The potential distribution (35.81) has the proper form $\phi(z) = \phi_0 + \phi_{\mathrm{L}} f(z)$. We now consider the symmetric case, $C_2 = 0$, and assume for simplicity that there is no superimposed magnetic field: $k_m = 0$, and so

$$\omega^2 = 1 - \frac{\kappa^2}{2} \tag{35.82}$$

Of course, ω^2 need not be less than unity but if $\omega^2 > 1$, clearly κ^2 becomes negative; we deal with the two ranges of ω^2 separately, writing

$$\overline{\kappa}^2 := -\kappa^2 = 2(\omega^2 - 1) \;\; \text{when} \;\; \omega^2 > 1 \tag{35.83}$$

From Eqs (35.74) and (35.79), we see that

$$\zeta = \int_0^{\psi} \frac{d\theta}{\left(1 - \kappa^2 \sin^2\theta\right)^{1/2}} = F(\psi, \kappa) \;\; \omega^2 < 1$$

or

$$\zeta = \int_0^{\psi} \frac{d\theta}{(1 + \overline{\kappa}^2 \sin^2\theta)^{1/2}} \quad \omega^2 > 1 \tag{35.84}$$

in which $F(\psi, \kappa)$ is an elliptic integral of the first kind; the inverse, $\psi = \psi\,(\zeta, \kappa)$, is known as the amplitude:

$$\psi = \mathrm{am}(\zeta, \kappa) \tag{35.85}$$

Eq. (35.75) now reduces to

$$\frac{d^2 r}{d\zeta^2} + \omega^2 r = 0 \tag{35.86}$$

with solutions of the form $\begin{smallmatrix}\cos\\ \sin\end{smallmatrix}(\omega\zeta)$ so that returning to the original paraxial equation, typical solutions are

$$\begin{aligned} u_1(z) &= \frac{\cos \omega F(\psi, \kappa)}{\sin \psi} \\ u_2(z) &= \frac{\sin \omega F(\psi, \kappa)}{\sin \psi} \end{aligned} \tag{35.87}$$

with $z = a \cot \psi$. Conjugate planes will thus occur at zeros of the sinusoidal function in $u_2(z)$; the planes corresponding to ψ_o and ψ_i will be conjugate if

$$\omega F\left(\psi_i, \kappa\right) = \omega F\left(\psi_o, \kappa\right) - n\pi \tag{35.88}$$

where n is an integer. Solving for ψ_i with the aid of (35.85),

$$\psi_i = \operatorname{am}\left(F(\psi_o, \kappa) - n\pi/\omega, \kappa\right) \tag{35.89}$$

and hence

$$z_i = a \cot \psi_i = \frac{\operatorname{cn}\left(F(\psi_o, \kappa) - n\pi/\omega\right)}{\operatorname{sn}\left(F(\psi_o, \kappa) - n\pi/\omega\right)} \tag{35.90}$$

where cn and sn denote the Jacobi elliptic functions $\operatorname{cn}(x) \coloneqq \cos(\operatorname{am} x)$, $\operatorname{sn}x \coloneqq \sin(\operatorname{am} x)$. Simple addition theorems are known for $\operatorname{cn}(a + b)$ and $\operatorname{sn}(a + b)$, from which we deduce that

$$\frac{z_i}{a} = \frac{z_o \operatorname{cn}\left(n\pi/\omega\right) + a h(z_o) \operatorname{dn}\left(n\pi/\omega\right)}{a \operatorname{cn}\left(n\pi/\omega\right) \operatorname{dn}\left(n\pi/\omega\right) - z_o h(z_o)} \tag{35.91}$$

where

$$h(z_o) = \left(\frac{a^2 + z_o^2 - \kappa^2 a^2}{a^2 + z_o^2}\right)^{1/2} \tag{35.92}$$

and

$$\operatorname{dn}(x) \coloneqq \left(1 - \kappa^2 \operatorname{sn}^2 x\right)^{1/2} \tag{35.93}$$

By considering the extreme cases $z_o \to -\infty$ and $z_i \to \infty$, the real foci are seen to occur for

$$\begin{aligned} &F\left(\psi'_{Fo}, \kappa\right) = n\pi/\omega \quad \text{or} \quad \psi'_{Fo} = \operatorname{am}\left(n\pi/\omega, \kappa\right) \\ &F\left(\psi'_{Fi}, \kappa\right) = F(\pi, \kappa) - n\pi/\omega \quad \text{or} \quad \psi'_{Fi} = \operatorname{am}\left(f(\pi, \kappa) - n\pi/\omega, \kappa\right) \end{aligned} \tag{35.94}$$

The osculating focal lengths (17.24) are found to be

$$\frac{\phi_o^{1/2}}{f_o} = \frac{\phi_i^{1/2}}{f_i} = \frac{\phi_0^{1/2}}{a}\left(\sin\psi_o\cos\psi_i\sqrt{1-\kappa^2\sin^2\psi_i} - \cos\psi_o\sin\psi_i\sqrt{1-\kappa^2\sin^2\psi_o}\right) \quad (35.95)$$

from which the ordinary real focal lengths may be written down immediately by letting $\psi_i \to 0$ for f_o' and $\psi_o \to \pi$ for f_i':

$$\begin{aligned}\frac{f_o'}{a} &= \left(\frac{\phi_{Fo}}{\phi_0}\right)^{1/2}\operatorname{cosec}\psi_{Fo} = \frac{\left(1-\kappa^2\sin^2\psi_{Fo}\right)^{1/2}}{\sin\psi_{Fo}}\\ \frac{f_i'}{a} &= \left(\frac{\phi_{Fi}}{\phi_0}\right)^{1/2}\operatorname{cosec}\psi_{Fi} = \frac{\left(1-\kappa^2\sin^2\psi_{Fi}\right)^{1/2}}{\sin\psi_{Fi}}\end{aligned} \quad (35.96)$$

and since $\psi_{Fo} = \pi - \psi_{Fi}$, $f_o' = f_i'$ as expected.

For the asymptotic cardinal elements, we find

$$\begin{aligned}\frac{z_{Fo}}{a} &= -\omega\cot(\omega F(\pi,\kappa))\\ \frac{a}{f} &= \frac{\sin(\omega F(\pi,\kappa))}{\omega}\end{aligned} \quad (35.97)$$

The spherical aberration coefficient corresponding to an object at $\psi = \psi_o$ and an image at $\psi = \psi_i$ is given by

$$\begin{aligned}\frac{C_s}{a} = \frac{\left(1-\kappa^2\sin^2\psi_o\right)^{3/2}}{2\sin^4\psi_o}&\left\{\frac{E_o - E_n}{\kappa^2(1-\kappa^2)} - \frac{n\pi}{\omega}\left(\frac{1}{\kappa^2} + \frac{8-\kappa^2}{16\omega^4}\right)\right.\\ &\left. - \frac{1}{2(1-\kappa^2)}\left(\frac{\sin 2\psi_o}{\left(1-\kappa^2\sin^2\psi_o\right)^{1/2}} - \frac{\sin 2\psi_n}{\left(1-\kappa^2\sin^2\psi_n\right)^{1/2}}\right)\right\}\end{aligned} \quad (35.98a)$$

the high-magnification expression for which is

$$\frac{C_s}{a} = \frac{1-\kappa^2\sin\psi_o}{\sin^4\psi_o}\left\{\frac{E_o}{\kappa^2(1-\kappa^2)} - \frac{n\pi}{\omega}\left(\frac{1}{\kappa^2} + \frac{8-\kappa^2}{16\omega^4}\right) - \frac{\sin 2\psi_o}{2(1-\kappa^2)\left(1-\kappa^2\sin^2\psi_o\right)^{1/2}}\right\} \quad (35.98b)$$

$$\approx \frac{1}{2\kappa^2}\left(\frac{f}{a}\right)^3 \quad 0 \le \kappa^2 \le 1 \quad (35.98c)$$

In these formulae, E denotes the elliptic integral of the second kind: $E_o = \int_0^{\psi_o} \left(1-\kappa^2\sin^2\phi\right)^{1/2} d\phi$ and likewise for E_n. For the chromatic aberrations,

$$\begin{aligned}\frac{C_c}{a} = \frac{\left(1-\kappa^2\sin^2\psi_o\right)^{1/2}}{\omega\sin^2\psi_o}\left\{\frac{\pi}{2\omega^2} + \frac{\omega(E_i - E_o)}{2(1-\kappa^2)}\right. \\ \left. + \frac{\omega\kappa^2}{4(1-\kappa^2)}\left(\frac{\sin 2\psi_o}{\left(1-\kappa^2\sin^2\psi_o\right)^{1/2}} - \frac{\sin 2\psi_i}{\left(1-\kappa^2\sin^2\psi_i\right)^{1/2}}\right)\right\}\end{aligned} \tag{35.99a}$$

$$\xrightarrow{M\to\infty} \frac{\left(1-\kappa^2\sin^2\psi_o\right)^{1/2}}{2\sin^2\psi_o}\left\{\frac{\pi}{\omega^3} - \frac{E_o}{1-\kappa^2} + \frac{\kappa^2\sin 2\psi_o}{2(1-\kappa^2)\left(1-\kappa^2\sin^2\psi_o\right)^{1/2}}\right\} \tag{35.99b}$$

$$\approx \frac{2f}{a}\frac{1+\kappa^2/4}{1-3\kappa^2/4} \tag{35.99c}$$

and

$$\begin{aligned}C_D(M\to\infty) = -\frac{\omega}{2\sin 2\omega k}\left\{\frac{E_o}{1-\kappa^2} - \frac{\pi}{\omega^3} - \frac{\kappa^2}{2(1-\kappa^2)}\frac{\sin 2\psi_o}{\left(1-\kappa^2\sin^2\psi_o\right)^{1/2}}\right\} \\ \approx \frac{32}{3\pi\kappa^2\left(1-\kappa^2/4\right)}\end{aligned} \tag{35.100}$$

The approximate formulae are accurate to within about 10% over the whole range of κ.

The meaning of the integer n, which occurs in all the real formulae but not in the asymptotic expressions, can be understood from the sinusoidal nature of the solutions (35.87). Consider a ray incident from object space parallel to the axis. Such a ray will, for low excitation, intersect the axis at $\psi = \psi_{Fi}$ and emerge with negative gradient. As the lens strength is increased, the point $\psi = \psi_{Fi}$ retreats towards the symmetry plane of the lens, reaching $\psi = \pi/2$ when $F(\pi, \kappa) - F(\pi/2, \kappa) = \pi/\omega$. Writing $F(\pi, \kappa) = 2\int_0^{\pi/2} (1-\kappa^2\sin^2\psi)^{-1/2} d\psi =: 2K$, this corresponds to $K = \pi/\omega$ or $\omega = \pi/K$. The same ray will now emerge parallel to the axis (the asymptotic focal length becomes infinite). As the excitation is increased further, the first point of intersection of the ray with the axis retreats into the region for which $\pi/2 < \psi < \pi$ and the ray now intersects the axis afresh in the region $\pi/2 > \psi > 0$: there are now two image foci (and of course two object foci).

For $K < \pi/\omega < 2K$, there is thus a single focus, for $2K/3 < \pi/\omega < K$, there are two, and in general, for $2K/(n+1) < \pi/\omega < 2K/n$, there are n intersections. Meanwhile, the modulus of the asymptotic focal length varies from its minimum value, $|f|/a = \omega$, to infinity in each interval.

In the case $\omega^2 > 1$, we write $\overline{\kappa}^2 = 2(\omega^2 - 1)$ and obtain (Kanaya et al., 1966) the following expressions:

$$\begin{aligned}\zeta &:= \int_0^{\psi} \frac{d\theta}{\left(1+\overline{\kappa}^2\sin^2\theta\right)^{1/2}} =: F'(\psi, \overline{\kappa}) \\ &= \frac{1}{\left(1+\overline{\kappa}^2\right)^{1/2}} \int_0^{\psi'} \frac{d\theta}{\left(1-\kappa'^2\sin^2\theta\right)^{1/2}} = \frac{1}{\left(1+\overline{\kappa}^2\right)^{1/2}} F(\psi', \kappa')\end{aligned} \tag{35.101}$$

in which

$$\kappa' = \overline{\kappa}/\left(1+\overline{\kappa}^2\right)^{1/2} \tag{35.102}$$

$$\psi' = \arctan\left\{\left(1+\overline{\kappa}^2\right)^{1/2}\tan\psi\right\} \tag{35.103}$$

The real focus and focal length are now given by

$$\begin{aligned}\psi'_{Fo} &= \mathrm{am}\left(\frac{\pi}{\omega}\left(1+\overline{\kappa}^2\right)^{1/2},\ \frac{\overline{\kappa}}{\left(1+\overline{\kappa}^2\right)^{1/2}}\right) \\ \frac{f'}{a} &= -\frac{\left(1+\overline{\kappa}^2\right)^{1/2}}{\mathrm{sn}\left(\frac{\pi}{\omega}\left(1+\overline{\kappa}^2\right)^{1/2},\ \frac{\overline{\kappa}}{\left(1+\overline{\kappa}^2\right)^{1/2}}\right)}\end{aligned} \tag{35.104}$$

and the asymptotic quantities by

$$\begin{aligned}\frac{z_{Fo}}{a} &= -\omega\cot\left\{\frac{\omega F(\pi, \kappa')}{\left(1+\overline{\kappa}^2\right)^{1/2}}\right\} \\ \frac{f}{a} &= \omega\operatorname{cosec}\left\{\frac{\omega F(\pi, \kappa')}{\left(1+\overline{\kappa}^2\right)^{1/2}}\right\}\end{aligned} \tag{35.105}$$

It only remains to relate a and κ^2 to the geometry and electrode voltage. Suitable formulae are to be found in Kanaya et al. (1966), for lenses of all practical configurations. Regenstreif's models are used to establish these approximate relations.

Finally, we mention that paraxial formulae corresponding to einzel lenses with a very thick central electrode, modelled by two bell-shaped curves with different half-widths, are also to be found in Kanaya et al. (1966).

35.3.1.3 The model of Kanaya and Baba

We continue with a brief account of the very flexible model proposed by Kanaya and Baba (1978),

$$\phi(z/a) = \phi(0)\exp\{K_0 \arctan(z/a)^m\} \tag{35.106}$$

Setting $\phi(z \to -\infty) = \phi_0$, we see that

$$K_0 = \frac{2}{\pi}\ln\left(\frac{\phi_0}{\phi(0)}\right) \tag{35.107}$$

Substituting Eq. (35.106) into the paraxial equation in reduced coordinates, we obtain

$$\mu(1-\mu)\frac{d^2 v}{d\mu^2} + \left(\frac{2m+1}{2m} - 2\mu\right)\frac{dv}{d\mu} + k^2 v = 0 \tag{35.108}$$

where

$$k := \frac{\sqrt{3}}{8}K_0 = \frac{\sqrt{3}}{4\pi}\ln\left(\frac{\phi_0}{\phi(0)}\right), \quad \mu := \frac{1}{1+(z/a)^m} \tag{35.109}$$

The differential equation (35.108) has solutions of the form

$$v = AF_1(\mu) + BF_2(\mu) \tag{35.110}$$

where $F_1(\mu)$ denotes the hypergeometric function,

$$F_1(\mu) = F(\alpha, \beta, \gamma, \mu) \tag{35.111a}$$

and

$$F_2 = \mu^{1-\gamma}F(\alpha-\gamma+1, \beta-\gamma+1, 2-\gamma, \mu) \tag{35.111b}$$

with

$$\omega^2 = m^2(1+4k^2), \quad \alpha, \beta = \frac{m \pm \omega}{2m}, \quad \gamma = \frac{2m+1}{2m} \tag{35.112}$$

The cardinal elements can be written down explicitly, with the aid of the rays $G(z)$ and $\overline{G}(z)$:

$$G(z) = \exp\left\{\frac{2k}{\sqrt{3}}\left(\frac{\pi}{2} - \arctan(z/a)^m\right)\right\}F_1(\mu) \tag{35.113a}$$

$$\overline{G}(z) = \exp\left\{\frac{2k}{\sqrt{3}}\left(\frac{\pi}{2} - \arctan(z/a)^m\right)\right\}(AF_1(\mu) + BF_2(\mu)) \tag{35.113b}$$

for $-\infty \le z/a \le 0$ and

$$G(z) = \exp\left\{\frac{2k}{\sqrt{3}}\left(\frac{\pi}{2} - \arctan(z/a)^m\right)\right\}(AF_1(\mu) + BF_2(\mu)) \tag{35.113c}$$

$$\overline{G}(z) = \exp\left\{\frac{2k}{\sqrt{3}}\left(\frac{\pi}{2} - \arctan\,(z/a)^m\right)\right\}F_1(\mu) \tag{35.113d}$$

for $0 \le z/a \le \infty$, in which

$$\begin{aligned} A &= -\frac{1}{2\sin^2(\pi/2m)}\left\{\cos\left(\frac{\pi}{m}\right) + 1 + 2\cos\left(\frac{\omega\pi}{m}\right)\right\} \\ B &= \frac{\Gamma^2(1/2m)\cos(\omega\pi/2m)}{m\sin\,(\pi/2m)\Gamma((m+1+\omega)/2m)\Gamma((m+1-\omega)/2m)} \end{aligned} \tag{35.114}$$

The real focal length is given by

$$\frac{f'}{a} = -\frac{F_1(\mu_{Fi})}{B}\exp\left\{-\frac{2k}{\sqrt{3}}\left(\frac{\pi}{2} - \arctan\,(z_{Fi}/a)^m\right)\right\} \tag{35.115}$$

and the asymptotic cardinal elements by

$$\begin{aligned} \frac{f}{a} &= -\frac{m\sin\,(\pi/2m)\Gamma((m+1+\omega)/2m)\Gamma((m+1-\omega)/2m)}{\Gamma^2(1/2m)\cos(\omega\pi/2m)} \\ \frac{z_{Fi}}{a} &= A\frac{f}{a} \end{aligned} \tag{35.116}$$

Kanaya and Baba plot the real and asymptotic cardinal elements as functions of k for various values of m. Their scaling factor is a_h, the half-width of $\phi(z)$, that is, the value of z for which

$$\frac{1}{2}\left(1 - \frac{\phi(0)}{\phi_0}\right) = 1 - \frac{\phi(a_h)}{\phi_0}$$

and hence

$$\frac{a_h}{a} := \lambda = \left[\tan\left\{\frac{\pi\ln(1+\phi_0/2\phi(0))}{2\ln(\phi_0/\phi(0))}\right\}\right]^{1/m} \tag{35.117}$$

The parameter m is a measure of the shape of the potential distributions. Fig. 35.11 shows a number of distributions, the value of k chosen to give the minimum asymptotic focal length.

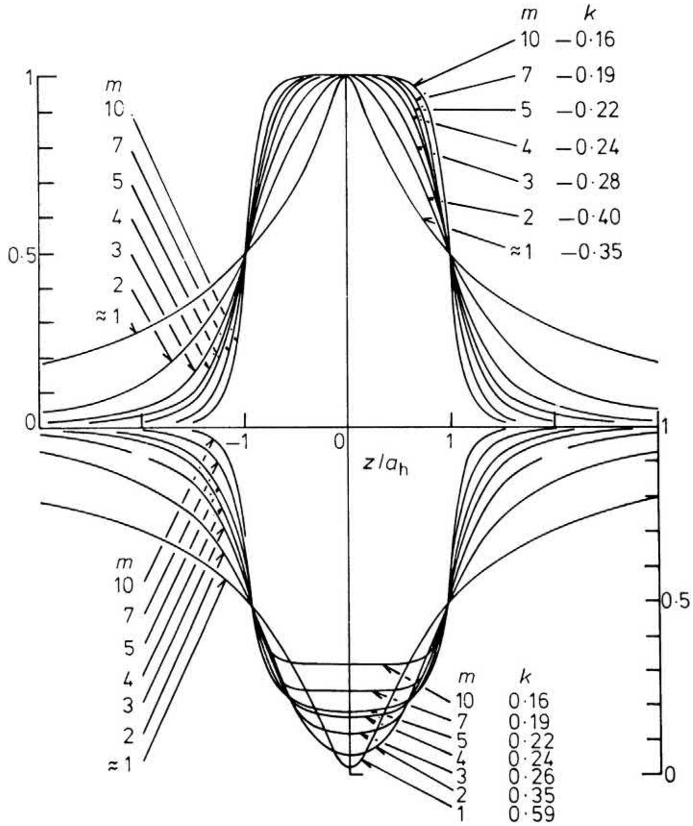

Figure 35.11

Potential distributions in three-electrode lenses characterized by different values of m, normalized to unity at $z = 0$ and to zero for large values of $|z|$. The excitations shown correspond to minimum asymptotic focal length. *After Kanaya and Baba (1978), Courtesy Institute of Physics.*

The spherical and chromatic aberration coefficients cannot be written in closed form. Kanaya and Baba plot the variation of these coefficients with excitation for various values of m and for both infinite and several finite magnifications.

35.3.1.4 The theory of Wendt

We now briefly recapitulate the work of Wendt (1951), who noticed an interesting pattern in the principal potential models. For a two-electrode lens consisting of two adjacent plates, the potential takes the form

$$\phi(z) = \kappa + \frac{z}{(1+z^2)^{1/2}} =: \kappa + s(z) \tag{35.118}$$

where κ is a constant and the hole radius is the unit of length. Inverting $s(z)$, we see that

$$\begin{aligned} z(s) &= \frac{s}{(1-s^2)^{1/2}} = \frac{1}{2}\left(\frac{1+s}{1-s}\right)^{1/2} - \frac{1}{2}\left(\frac{1-s}{1+s}\right)^{1/2} \\ z'(s) &= \frac{1}{(1-s^2)^{3/2}} \end{aligned} \tag{35.119}$$

For the tanh model, $\phi(z) = \kappa + \tanh z$, we have $s(z) = \tanh z$ and hence

$$\begin{aligned} z(s) &= \operatorname{arctanh} s = \frac{1}{2}\ln\left(\frac{1+s}{1-s}\right) \\ z'(s) &= \frac{1}{1-s^2} \end{aligned} \tag{35.120}$$

This led Wendt to enquire whether lenses corresponding to

$$z'(s) = \frac{1}{(1-s^2)^n} \tag{35.121}$$

have some special significance and he discusses the case $n = 5/4$, which gives funnel-shaped electrodes. Of more interest, however, is his study of einzel lenses. For

$$\phi(z) = \kappa - \frac{1}{1+z^2} =: \kappa - s \tag{35.122a}$$

we find

$$\begin{aligned} z(s) &= \left(\frac{1-s}{s}\right)^{1/2} \\ z'(s) &= -\frac{1}{2s^{3/2}(1-s)^{1/2}} \end{aligned} \tag{35.122b}$$

and for

$$\begin{aligned} \phi(z) &= \kappa - \operatorname{sech}^2 z =: \kappa - s \\ z(s) &= \operatorname{arccosh} s^{-1/2} = \ln\left\{\frac{1+(1-s)^{1/2}}{s^{1/2}}\right\} \\ z'(s) &= -\frac{1}{2s(1-s)^{1/2}} \end{aligned} \tag{35.123}$$

Wendt therefore examined the class of lenses for which

$$z'(s) = -\frac{1}{2s^n(1-s)^{1/2}} \tag{35.124}$$

For $n = 5/4$, a funnel-shaped lens is again obtained.

These relations between z and s can be used to transform the paraxial equations; for two-electrode immersion lenses (in the accelerating mode), we write

$$dz = \left(1-s^2\right)^n ds \tag{35.125}$$

giving

$$(s+\kappa)\left(s^2-1\right)u'' + \left(\frac{4n+1}{2}s^2 + 2n\kappa s - \frac{1}{2}\right)u' + \frac{ns}{2}u = 0 \tag{35.126}$$

the solutions of which can be expressed in terms of Riemann functions (see discussions of Heun's equation in texts on analysis). For einzel lenses, we write

$$dz = -\frac{ds}{2s^n(1-s)^{1/2}} \quad \left(1 \le n \le 3/2\right) \tag{35.127}$$

and find

$$s(s+\kappa)(s-1)u'' + \left\{(n+1)s^2 + \left(n+\frac{1}{2}\right)(\kappa-1)s - n\kappa\right\}u' + \left(\frac{2n+1}{8}s - \frac{n}{4}\right)u = 0 \tag{35.128}$$

which again has Riemann function solutions.

Wendt discusses in some detail cases in which these differential equations collapse to that satisfied by the hypergeometric function. He also examines the case

$$z'(s) = A(s-a)^n, \quad A, a, n \ \text{constants} \tag{35.129a}$$

for which

$$\phi(z) = a + \left\{\frac{n+1}{A}(z-B)\right\}^{1/(n+1)} \quad B \ \text{constant} \tag{35.129b}$$

Finally, he generalizes the two-electrode case to include two-tube lenses of different radius by writing

$$z = \frac{1}{2}\left\{\alpha \ln(1+s) - \beta \ln(1-s)\right\} \tag{35.130}$$

instead of Eq. (35.125), which again leads to a differential equation satisfied by Riemann functions.

35.3.1.5 Shimoyama's contribution

We continue this account of the various models with a reference to a paper that goes further than Grinberg (1953) in the methodical search for models; in this, Shimoyama (1982) sets out from the paraxial equation in the form

$$u'' + \frac{f'}{2f}u' + \frac{f''}{4f}u = 0, \tag{35.131}$$

with $f(z) = \phi(z)/a$ and a, a suitable scaling factor. He writes $\upsilon := f^{1/4}\,u$ and $y := \{g'(z)\}^{1/2}\upsilon$, where g is for the moment arbitrary. Writing $x = g(z)$, the paraxial equation becomes

$$\frac{d^2y}{dx^2} + Ny = 0 \tag{35.132}$$

where

$$N = \frac{3}{16}\left\{\frac{f'(z)}{f(z)g'(z)}\right\}^2 + \frac{3}{4}\frac{\{g''(z)\}^2}{\{g'(z)\}^4} - \frac{g'''(z)}{\{g'(z)\}^3} \tag{35.133}$$

Shimoyama enquires what potentials are obtained if

$$N = C_0 + C_1 x^{\sigma} + C_2 x^{-2}, \quad C_0, C_1, C_2 \quad \text{arbitrary} \quad \sigma \neq 0 \ \text{ or } \ -2 \tag{35.134}$$

for various forms of $g(z)$. We reproduce his table of axial potentials and their corresponding paraxial solutions (Table 35.2).

35.3.1.6 Crewe's model

Crewe (1991a,b) suggests that the approximate formulae

$$f = 1.06\frac{L}{\ln(\phi_1/\phi)}$$

$$C_s = \frac{20f^3}{L^2}$$

$$C_c = 2f$$

where L is a measure of the length of the lens and ϕ_1 is the central voltage, give useful estimates of the values of these quantities.

Table 35.2: Some examples of the axial potential distribution and the corresponding general solutions of the paraxial ray equation

$x=g(z)$	C_0	C_1	C_2	General Solution $y(x)$	Examples of $f(z)$
	0	0	$\frac{1}{4}+\nu^2$	$x^{1/2}\left[A_1\sin(\nu\log x)+A_2\cos(\nu\log x)\right]$	$\pm(a_0z+a_1)^{\pm1/\sqrt{m}}$, $\pm\left(\frac{a_1}{z+a_0}+a_2\right)^{1/\sqrt{m}}$, $(m>0)$ $a_0\exp\left[\frac{2}{\sqrt{\lvert m\rvert}}\tan^{-1}(a_1z+a_2)\right]$, $(m<0)$ $a_0\exp(a_1z)$, $a_0\exp\left(\frac{a_2}{z+a_1}\right)$, $(m=0)$ $m=3/4-4\nu^2n^2$
$\{f(z)\}^n$	0	0	$-\nu(\nu-1)$	$A_1x^{\nu}+A_2x^{-\nu+1}$ $(\nu\neq1/2)$ $x^{1/2}(A_1+A_2\log x)$ $(\nu=1/2)$	$\pm(a_0z+a_1)^{\pm1/\sqrt{m}}$, $\pm\left(\frac{a_1}{z+a_0}+a_2\right)^{1/\sqrt{m}}$, $m=3/4+(2\nu-1)^2n^2$
	β^2	0	$\frac{1}{4}-\nu^2$	$x^{1/2}[A_1J_\nu(\beta x)+A_2J_{-\nu}(\beta x)]$ $(\nu\neq\text{integer})$ $x^{1/2}[A_1J_\nu(\beta x)+A_2N_\nu(\beta x)]$ $(\nu=\text{integer})$	$\pm\left\{\frac{1}{\beta}\tan^{-1}(a_0z+a_1)+a_2\right\}^{1/n}$, $n^2=\frac{3}{4(1-4\nu^2)}$
	$-\beta^2$	0	$\frac{1}{4}-\nu^2$	$x^{1/2}\{A_1I_\nu(\beta x)+A_2I_{-\nu}(\beta x)\}$ $(\nu\neq\text{integer})$ $x^{1/2}\{A_1I_\nu(\beta x)+A_2K_\nu(\beta x)\}$ $(\nu=\text{integer})$	$\pm\left[\frac{1}{2\beta}\log\left\lvert\frac{z+a_1}{z+a_0}\right\rvert+a_2\right]^{1/n}$, $\pm\left[\frac{1}{2\beta}\log\lvert z+a_0\rvert+a_1\right]^{1/n}$, $n^2=3/4(1-4\nu^2)$
$\exp(\alpha z)$	β^2	0	$\frac{1}{4}$	$A_1J_0(\beta x)+A_2N_0(\beta x)$	$\exp\left(\pm\frac{4}{\sqrt{3}}\beta\exp(\alpha z)\right)$

35.3.1.7 Ura's unified representation

We have mentioned Ura's unified representation of the properties of bipotential lenses in Section 35.2.2. In the same paper (Ura, 1999), a similar representation was advanced for einzel lenses. The geometries examined are shown in Fig. 35.12A; UR-0 and UA-0 correspond to the analytical model (35.81 with $C_2 = 0$). The decelerating and accelerating situations are examined separately. We again have $D_e = D/\lambda$; for the effective potential,

$$V_e = k\left(\frac{V_2}{V_1} - 1\right) \quad \text{for} \quad \frac{V_2}{V_1} > 1$$

and

$$V_e = \frac{kx}{1 - kx}, \quad x := 1 - \frac{V_2}{V_1} \quad \text{for} \quad \frac{V_2}{V_1} < 1$$

The values of the factor k, extracted from the calculations of Renau and Heddle (1986a), are as follows: $k = 0.57$ (U-1), $k = 0.86$ (U-2), $k = 0.51$ (U-3) and $k = 0.73$ (U-4). The unified curves are reproduced in Figs 35.12B (decelerating−accelerating lens) and 35.12C (accelerating−decelerating lens). The thin-lens situation is again examined.

35.3.2 Measurements and Exact Calculations

We have already mentioned the limitations of the use of models. In this section, we draw attention to einzel lens data obtained either by measurement or by calculating both the potential distribution and the trajectories numerically (or occasionally by an analogue technique).

The first collection of einzel lens properties was published by Bruck and Romani (1944), who considered only the special case in which the central electrode is at cathode potential, but for several geometries; the potential was obtained by an analogue method (electrolytic tank) and the cardinal elements by calculation; approximate formulae gave the spherical and chromatic aberration coefficients. The properties of such lenses were then measured by Heise and Rang (1949) and Lippert and Pohlit (1952, 1953, 1954). Data for asymmetric einzel lenses are to be found in the work of Everitt and Hanszen (1956) and Hanszen (1958a,b; 1964), who collected all this together in a survey (Hanszen and Lauer, 1967) and of Fitzgerald et al. (2012b). Further tables or graphs, describing the variation of the cardinal elements and aberration coefficients with geometry and excitation, are to be found in the following: Adams and Read (1972a,b), Ahmad (1998, 1999, 2010), Ahmad and Juma (1999), Ahmad et al. (1998, 1999, 2002, 2007, 2010), Al-Mudarris et al. (2006), Aničin et al. (1976), Archard (1956), Ashley (1971, 1972), Berger and Baril (1982), Bonjour (1979a,b), Bruck and Romani (1944), Chanson (1946, 1947), Chanson et al. (1945), Ćirić et al. (1976a,b), Der-Shvarts and Makarova (1966, 1969, 1971), Ehinger (1954), Ehinger

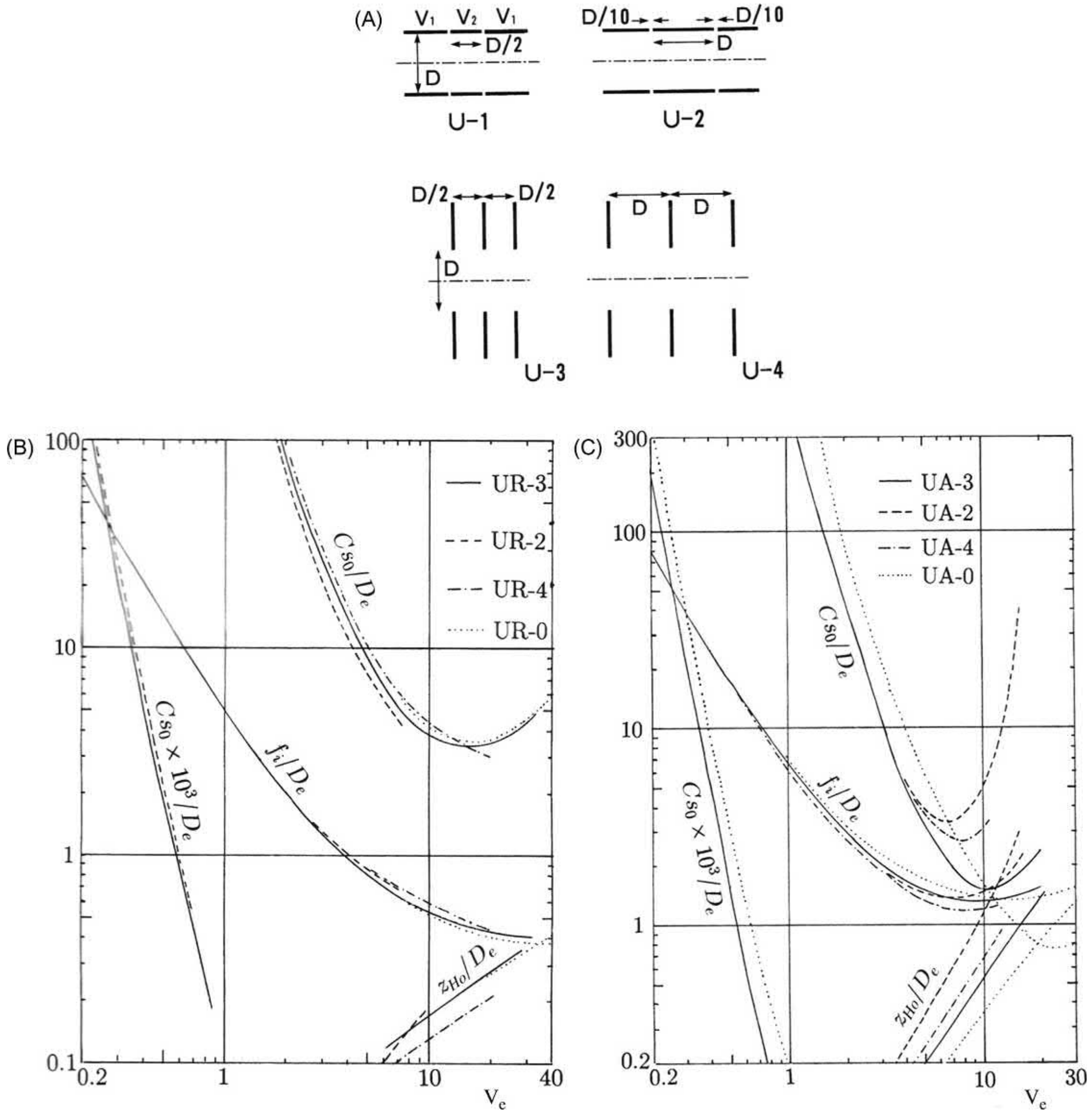

Figure 35.12

(A) The four einzel lens geometries. (B) Unified representation for the decelerating–accelerating configuration. (C) Unified representation for the accelerating–decelerating configuration.
After Ura (1999), Courtesy Japanese Society of Microscopy.

and Bernard (1954), El-Kareh and Sturans (1971a,b, 1972), Everitt and Hanszen (1956), Fert (1952), Gillespie and Brown (1997), Glaser and Schiske (1954, 1955), Glikman et al. (1974), Gobrecht (1941, 1942), Grivet (1950, 1951), Hamad et al. (2005), Hanszen (1958a, b, 1964), Hanszen and Lauer (1965/66), Heise (1949), Heise and Rang (1949), Jacob and

O'Sullivan (1973), Jasim et al. (2001, 2010), Johannson and Scherzer (1933), Juma et al. (2000, 2002), Kochanov (1963), Laplume (1947), Liebmann (1949), Lippert and Pohlit (1952, 1953), Mahl (1940, 1947), Mahl and Recknagel (1944), Parks (1971), Rang (1948), Read (1969b, 1978, 1979), Regenstreif (1949, 1950a–c, 1951), Rempfer (1985, 1999, examined below), Riddle (1978), Saito and Sovers (1977), Saito et al. (1973), Seeliger (1948), Septier and Ruytoor (1959a,b), Septier (1960), Shah and Jacob (1951), Shimizu and Kawakatsu (1974), Slodzian and Figueras (1978), Tsumagari et al. (1988), van der Merwe (1978a,b), Vine (1960), Werner (1971), Yamazaki (1973, 1977, 1979), Yaseen Al–Ali et al. (2002) and Yassin et al. (2012). In the papers by Rempfer, the conventional definitions of the aberration coefficients are not adopted and the notion of principal surfaces (rather than principal planes) is employed. Rempfer's claim that there are fewer independent terms in the polynomial form of the asymptotic spherical aberration coefficient than was believed is not justified. The relation that she believed to be generally true is correct only in the thin-lens approximation (Hawkes and Lencová, 2002). Nomura (1998, 1999) examines the properties of four- and five-electrode einzel lenses.

The paper by Glikman et al. (1974) is unusual in that the properties of multielectrode nonimmersion lenses are calculated. The authors state that the spherical aberration coefficient is 'almost always' least when the tube radii (all equal and denoted by R) and the length of each tube (λ) are the same, and examine this case in detail (a) for equal voltage ratio and (b) for equal voltage difference. For (a), the potential ϕ_k on the k-th electrode of an N-electrode lens (N odd) is given by

$$\phi_k = \phi_1 q^{k-1}, \quad k = 1, 2, \ldots (N+1)/2, \quad q \coloneqq \left(\frac{\phi_c}{\phi_1}\right)^{2/(N-1)} \tag{35.135}$$

where ϕ_c is the potential at the central electrode, $\phi_c = \phi_{(N+1)/2}$; for $k = (N+1)/2, \ldots N$, we have $\phi_{\mathrm{N}-k} = \phi_k$. For the case of equal voltage difference, (b), the potentials are given by

$$\phi_k = \phi_1 + (k-1)\Delta\phi, \quad \Delta\phi \coloneqq \frac{2(\phi_c - \phi_1)}{N-1} \tag{35.136}$$

for the first half of the lens and again, $\phi_{N-k} = \phi_k$, for the second half.

Glikman et al. also consider a third situation in which the axial potential is given by

$$\phi_k(z) = 1 \pm \frac{m^2}{1 + \left(z_k - L/2\right)^2/a^2} \quad k = 1, 2, \ldots N \tag{35.137}$$

where m and a are constants, L is the distance between the outer electrodes and $z_k \coloneqq -L/2 + (k-1)\lambda$. Thus z_k is the coordinate of the centre of the k-th electrode, measured from the gap between the first two electrodes. The spherical aberration proves to be smallest for $L/a = 4$ and Glikman et al. give details of this case only.

Another special case of interest is the 'hyperbolic lens', introduced by Rüdenberg (1948) and subsequently studied by Septier (1960), Septier and Ruytoor (1959a,b) and, as an energy filter, by Der-Shvarts and Belen'kii (1962). Rüdenberg had argued that a potential distribution of the form $\Phi(r, z) = p(z^2 - r^2/2)$ would be capable of producing a sharp image even for rays steeply inclined to the axis, since it would be free of spherical aberration. Such a field would require hyperbolic electrodes (Fig. 35.13A), which might in reality be constructed as shown in Fig. 35.13B and C. The perfect focusing property is lost when openings are made for the passage of the electrons but Septier's measurements suggest that the geometry is advantageous. A careful study of the potential distribution, cardinal elements and coefficients of spherical and chromatic aberration of two-dimensional hyperbolic lenses has been made by Yokota and Kishi (1970), Yokota and Nagami (1978) and Yokota et al. (1975). Fraser et al. (1971) considered an analogous geometry in connection with guns.

This work on hyperbolic lenses leads us to enquire what is the optimum shape for the electrodes of an einzel lens, with some well-defined condition for optimality (cf. Section 33.7). We have already mentioned the work of Septier and Ruytoor (1959a,b) and Septier (1960), who examined a range of geometries (Fig. 35.14) and showed the advantage of asymmetry, confirmed by Hanszen (1958a). More recently, Shimizu (1983) introduced a practical figure of merit for symmetric and asymmetric einzel lenses, which provides a useful guide to their relative performance, in particular as probe-forming lenses for ion microprobe devices. Adding the aberration disc diameters arising from spherical and chromatic aberration in quadrature gives a beam spread D of

$$D = \sqrt{D_s^2 + D_c^2} \qquad \begin{aligned} D_s &= \frac{1}{2} C_s \alpha^3 \\ D_c &= C_c \left(\Delta\phi/\phi\right)\alpha \end{aligned} \tag{35.138}$$

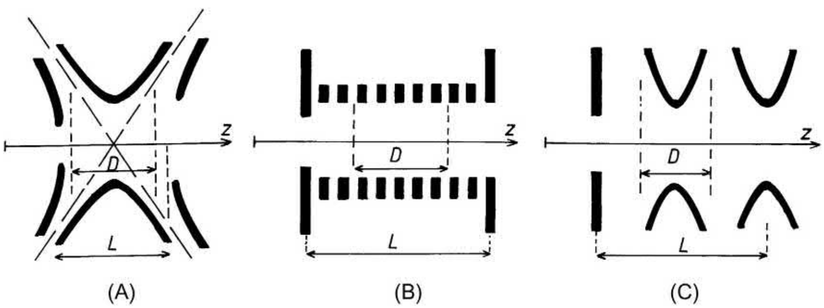

Figure 35.13

The hyperbolic lens. (A) Electrodes shaped to create a hyperbolic field directly. (B) By choosing the ring potentials suitably, a hyperbolic distribution can be synthesized. (C) The desired distribution is only crudely produced here. In each case, the distribution is hyperbolic in the zone D, which diminishes relative to the lens length L as we go from (A) to (C).

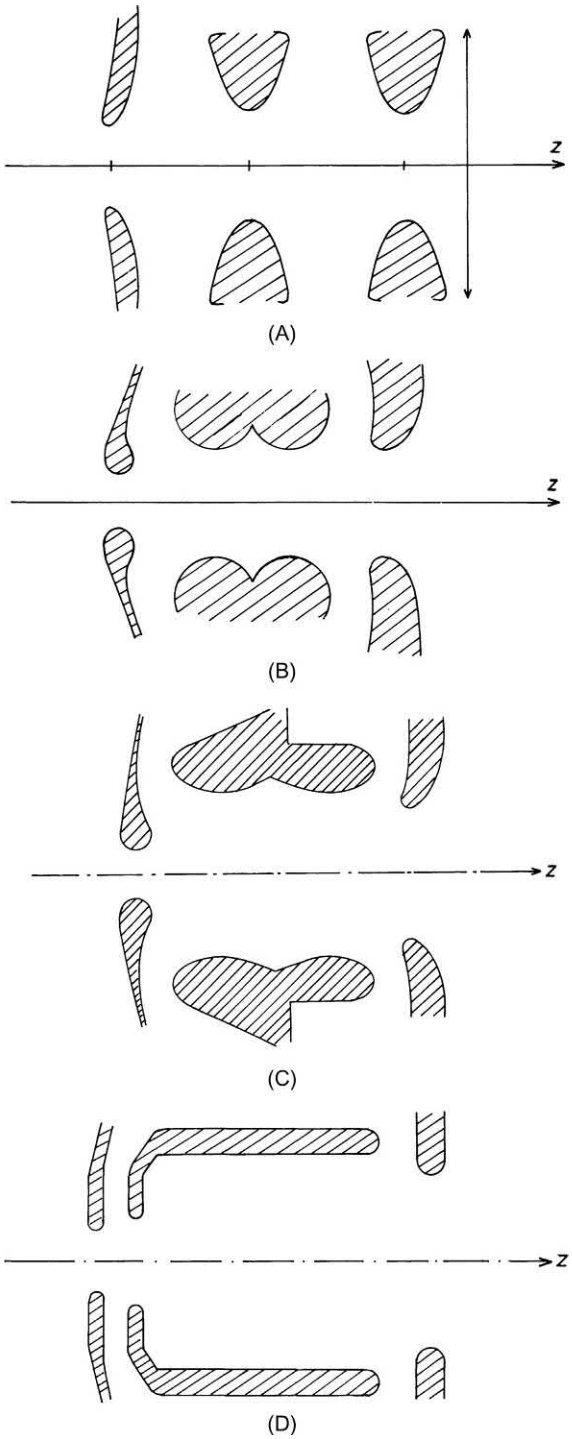

Figure 35.14

Einzel lens geometries studied by Septier and Ruytoor. The spherical aberration decreases sharply as we go from (A) to (D), all other conditions remaining unchanged.

After Septier and Ruytoor (1959b), Courtesy Académie des Sciences, Paris.

where α is the semiangle at the probe. Regarding the working distance w and the angle α as fixed constraints, we write

$$\frac{D}{w(\Delta\phi/\phi)\alpha} = \frac{C_c}{w}\left[\left\{\frac{\alpha^2 C_s/C_c}{2(\Delta\phi/\phi)}\right\}^2 + 1\right]^{1/2} \tag{35.139}$$

The free parameters on the right-hand side are C_c/w and C_s/C_c. For a lens such as that shown inset in Fig. 35.15A, where the aberration coefficients and focal length are plotted against lens strength, C_s/w and C_c/w vary with R/w as shown in Fig. 35.15B; Fig. 35.15C shows how C_c/w is related to C_s/C_c for minimum $D/w(\Delta\phi/\phi)\alpha$. The figure of merit D^* introduced by Shimizu is this minimum:

$$D^* := \left(\frac{D}{w(\Delta\phi/\phi)\alpha}\right)_{\min} \tag{35.140}$$

and is a different function of the predetermined quantity $2(\Delta\phi/\phi)/\alpha^2$ for each geometry. A convenient approximation is obtained by choosing C_s/C_c so that the effects of the two types of aberration are equal; this gives

$$(C_s/C_c)_{\mathrm{opt}} \approx 2(\Delta\phi/\phi)/\alpha^2 \tag{35.141}$$

and hence

$$D^* \approx \sqrt{2}C_c/w \tag{35.142}$$

Shimizu uses these ideas to compare four asymmetric lenses (Figs 35.16A and B); Fig. 35.16C and D show D^* for various geometries with the lens operating in the decelerating (C) and accelerating (D) modes. We note that D^* is distinctly smaller in the accelerating mode, a point emphasized by Slodzian and Figueras (1978) and confirmed by the various model calculations; in practice, though, it may not be convenient to provide the necessary voltage supply. The properties of asymmetric einzel lenses are also discussed by Read (2015).

The foregoing discussion tacitly demonstrates that most electrostatic lens optimization has been achieved by systematic investigation of rather few configurations, with a view to establishing the dependence of the optical properties on a small number of geometrical and electrical variables. A quite different approach, which would approach more closely to genuine optimization but for one major obstacle, is that of Szilágyi who, in a series of papers (Szilágyi, 1977, 1978a, 1983; Szilágyi et al., 1984), has developed procedures for revealing particularly advantageous electrostatic and magnetic lens distributions. The first two papers rely on a ‘dynamic programming’ search, described in more detail in

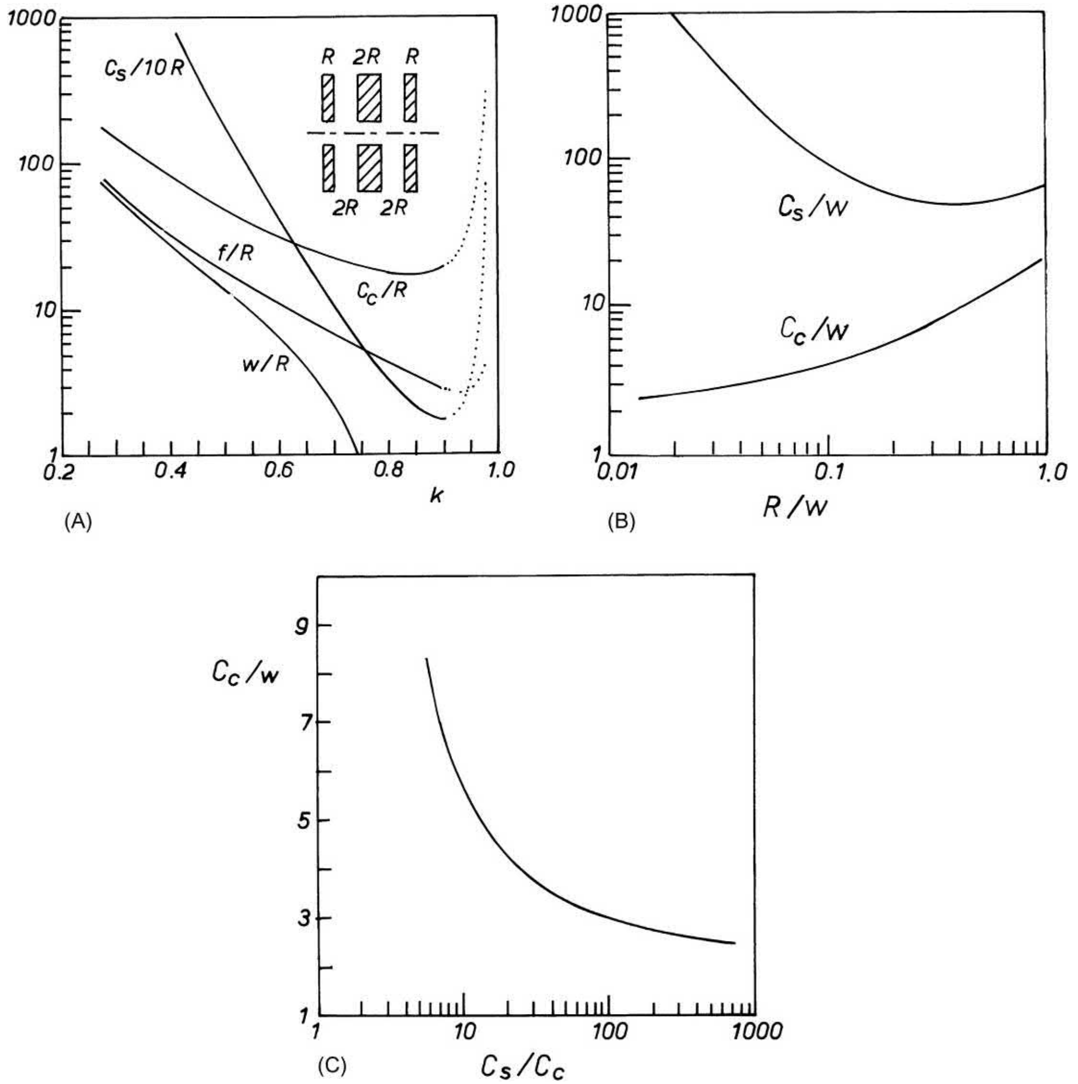

Figure 35.15

Einzel lenses and probe formation. (A) For the lens geometry shown, f/R, C_c/R, $C_s/10\,R$ and w/R are plotted as functions of lens strength k, defined by $k = 1 - \phi(0)/\phi_0$, where $\phi(0)$ is the potential in the centre of the lens and ϕ_0 is the potential at the outer electrodes. (B) C_s/w and C_c/w as functions of R/w. (C) C_c/w as a function of C_s/C_c for minimum D^*. *After Shimizu (1983), Courtesy Japanese Journal of Applied Physics.*

Section 36.4.3 on magnetic lenses. The axial electric field is approximated by a series of linear segments, so that Eq. (36.172) is replaced by

$$\phi(z) = a_0 + a_1 z + a_2 z^2/2 \tag{35.143}$$

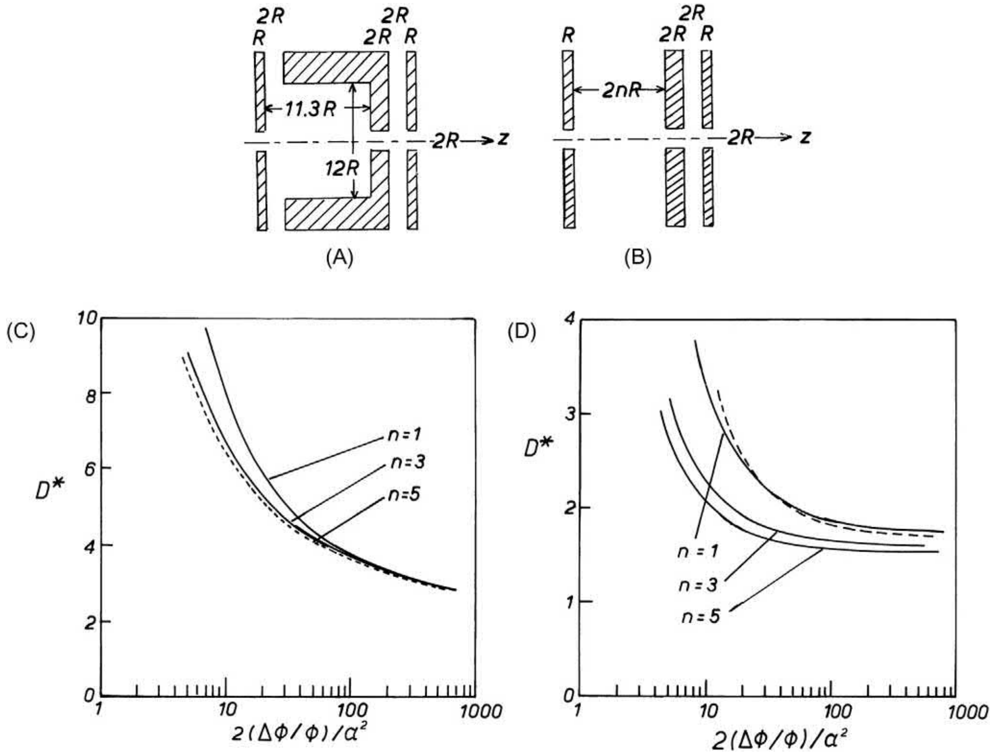

Figure 35.16

(A)–(B) Configurations analysed by Shimizu. (C) and (D) The figure of merit D^* as a function of $2(\Delta\phi/\phi)/\alpha^2$. In (C), the incident beam is first decelerated then accelerated while in (D) the order is reversed. Dotted curves correspond to 35.14A, full curves to 35.14B for various values of *n*. *After Shimizu (1983), Courtesy Japanese Journal of Applied Physics.*

but as in the magnetic case, the method suffers from the drawback, emphasized in Section 33.7, that it yields not a lens but an axial potential distribution. Many examples of searches for immersion lenses with minimum spherical aberration are to be found in Szilágyi (1978a). The dynamic programming is relatively slow and Szilágyi has subsequently returned to a simpler technique (Szilágyi, 1983; Szilágyi et al., 1984), of the type mentioned in Section 33.7. We note that his findings confirm that lenses in which the first part of the field has an accelerating action are advantageous, a result obtained by many earlier investigators. For some electrostatic lens designs of high quality, see Szilágyi (1984a,b, 1985, 1986, 1987a,b) and Szilágyi and Szép (1988) and for criticism of some of these designs, see Glatzel and Lenz (1988).

As a final example of the search for perfect image formation, we draw attention to Glaser's discussion (1948) of the electron optical equivalent of Maxwell's fish-eye lens (cf. Born and Wolf, Section 4.2.2; Ingarden, 1957; Luneberg, 1964, Section 28 and, for the more general Luneberg lens, Section 29; and also note [25] in Glaser, 1952).

35.3.3 Miniature Lenses

Miniature electrostatic lenses and columns have been the subject of numerous studies. Here we simply direct the reader to sources of information as the optics is not very different from that of larger lenses. Miniature columns based on permanent-magnet lenses are mentioned in Section 36.6.3. See Chang et al. (1990), Crewe et al. (1992, 1996), Feinerman et al. (1992, 1994a,b, 2002, 2004a,b), Perng et al. (1992), Kern and Chang (1994), Koops et al. (1995), Burstert et al. (1996), Feinerman and Crewe (1997, 2002), Bubeck et al. (1999), Muray et al. (2000, 2006, 2014), Khursheed (2001), Ambe et al. (2002), Schubert et al. (2002), Syms et al. (2003), Saini et al. (2005, 2006), Spallas et al. (2006, 2016), Rochow et al. (2008) and Sinno et al. (2010). An unusual miniature SEM and variable-pressure SEM project is associated with space exploration. Designs for such instruments to be landed on the moon and on Mars are described by Edmunson et al. (2016, 2017), Gaskin et al. (2009, 2010, 2012), Loyd (2015), Loyd and Gregory (2016), Loyd et al. (2017) and Thaisen et al. (2009).

35.4 Grid or Foil Lenses

The earliest grid lens is also one of the earliest electron lenses, for a 'screen lens' is considered by Knoll and Ruska (1932). This was an attempt to mimic the form of a glass lens with electron-transparent foils or gauze. Sporadic interest in electrostatic lenses in which one or more of the openings were covered by a grid was shown during the 1930s but these lenses were thoroughly studied only after it was realized that they offered a way of circumventing Scherzer's theorem: such lenses can be divergent, and their spherical aberration can be cancelled. Here, therefore, we describe their optical properties and indicate sources of detailed information; we shall return to their aberrations in Chapter 41, Aberration Correction. Grid lenses are special cases of lenses in which a stable cloud of space charge is somewhere maintained, and here we list formulae for the various aberration coefficients in the presence of space charge in general. We consider space charge distributions that can be represented by the series expansion

$$\begin{aligned}\rho(r,z) &= \varepsilon_0 \sum_{n=0}^{\infty} \frac{(-1)^n r^{2n}}{2^{2n}(n!)^2} \rho_{2n}(z) \\ &= \varepsilon_0 \rho_0(z) - \frac{\varepsilon_0}{4} r^2 \rho_2(z) + \cdots \end{aligned} \tag{35.144}$$

so that the electrostatic potential in a rotationally symmetric lens with space charge present becomes

$$\Phi(r,z) = \phi(z) - \frac{1}{4} r^2 \left(\phi'' + \rho_0\right) + \frac{1}{64} r^4 \left(\phi^{(4)} + \rho_o'' + \rho_2\right) \tag{35.145}$$

The spherical and chromatic aberration coefficients may be written in various equivalent forms. Hoch et al. (1976) use

$$C_s = \frac{1}{64}\int_{z_o}^{z_i}\left(\frac{\phi(z)}{\phi_o}\right)^{1/2}\left(\alpha_0 h^4 + \alpha_1 h^3 h' + \frac{16\rho_0}{\phi}h^2 h'^2\right)dz \tag{35.146}$$

in which

$$\begin{aligned}\alpha_0(z) &:= 5F'^2 - \frac{9}{2}F'F^2 + 3F^4 + \frac{8\eta^2 B'^2}{\phi} + \frac{16}{3}\frac{\eta^4 B^4}{\phi^2}\\ &\quad + \frac{32}{3}\frac{\eta^2 B^2}{\phi}\left(F' + F^2\right) - \frac{4\eta^2}{3}\frac{BB'F}{\phi}\\ &\quad + \rho_0\left(9F' + \frac{19}{2}F^2 + \frac{28}{3}\frac{\eta^2 B^2}{\phi} + \frac{4\rho_0}{\phi}\right) - 2\rho_2\\ \alpha_1(z) &= 4FF' + \frac{16\eta^2}{3}\frac{BB'}{\phi} + \frac{80}{3}\frac{\eta^2 B^2 F}{\phi} + 20F\rho_0\end{aligned} \tag{35.147}$$

and

$$F(z) := \phi'/\phi(z) \tag{35.148a}$$

so that

$$F'(z) = \phi''/\phi(z) - F^2(z) \tag{35.148b}$$

$$C_c = \int_{z_o}^{z_i}\left(\frac{\phi_o}{\phi(z)}\right)^{1/2}\left(\frac{3}{8}F^2 + \frac{\eta^2 B^2}{4\phi} + \frac{\rho_0}{4\phi}\right)h^2 dz$$

Typke (1968/69) gives the alternative expression

$$\begin{aligned}C_s = \frac{1}{16\phi_o^{1/2}}\int_{z_o}^{z_i}&\left\{\frac{5}{4}\left(\frac{\phi''}{\phi} + \frac{\phi' h'}{\phi h} - \frac{\phi'^2}{\phi^2}\right)^2 + \frac{\phi'^2}{\phi^2}\left(\frac{h'}{h} + \frac{7\phi'}{8\phi}\right)^2\right.\\ &+ \frac{1}{64}\frac{\phi'^4}{\phi^4} + \frac{2\eta^2}{\phi}\left(B' + B\frac{h'}{h} - \frac{5B\phi'}{4\phi}\right)^2 + \frac{2\eta^2 B^2}{\phi}\left(\frac{h'}{h} + \frac{\phi'}{4\phi}\right)^2\\ &+ \frac{\eta^4 B^4}{\phi^2} + \frac{\eta^2 B^2 \phi'^2}{16\phi^3} - \frac{\rho_2}{2\phi}\\ &\left. + \frac{\rho_0}{\phi}\left(\frac{9}{4}\frac{\phi''}{\phi} + \frac{\rho_0}{\phi} - \frac{\phi'^2}{16\phi^2} + \frac{5\phi' h'}{\phi h} + \frac{4h'^2}{h^2} + \frac{2\eta^2 B^2}{\phi}\right)\right\}\phi^{1/2}h^4 dz\end{aligned} \tag{35.149}$$

If the space charge is concentrated on a *plane* foil or gauze at $z = z_G$, we write

$$\rho(z, r) = \sigma(r)\delta(z - z_G) \tag{35.150}$$

whereupon the spherical aberration coefficient separates into two parts:

$$C_s =: C_s^{(G)} + C_s' \tag{35.151}$$

where

$$\begin{aligned} C_s^{(G)} &= \frac{h^4(z_G)}{32\left(\phi_o\phi_G\right)^{1/2}}\left[\phi''' - \left\{\frac{183}{128}\frac{\phi'^2}{\phi^2} + 2\left(\frac{5}{16}\frac{\phi'}{\phi} + 2\frac{h'}{h}\right)^2 + \frac{4\eta^2 B^2}{\phi}\right\}\phi\right]_{z_G^-}^{z_G^+} \\ C_s' &= \frac{1}{16\phi_o^{1/2}}\left(\int_{z_o}^{z_G^-} + \int_{z_G^+}^{z_i}\right) I dz \end{aligned} \tag{35.152}$$

and I is the integrand in Eq. (35.149).

If the gauze or foil is not plane but *spherical*, with radius R, concave towards the object, the coefficient $C_s =: C_s^{(1)} + C_s^{(2)}$ becomes (Hoch et al., 1976)

$$\begin{aligned} C_s^{(1)} = \int_{z_o}^{z_i}\left(\frac{\phi_o}{\phi}\right)^{1/2}\Bigg\{&\Bigg(5F'^2 - \frac{11}{2}F'F^2 + 3F^4 + \frac{8\eta^2 B'^2}{\phi} \\ &+ \frac{16\eta^4 B^4}{3\phi^2} + \frac{32\eta^2 B^2 F'}{3\phi} + \frac{4\eta^2 B^2 F^2}{\phi} - \frac{8BB'F}{3\phi}\Bigg)h^4 \\ &+ \left(4FF' + \frac{16\eta^2 BB'}{3\phi} + \frac{80\eta^2 B^2 F}{3\phi}\right)h^3 h'\Bigg\}dz \end{aligned} \tag{35.153a}$$

$$\begin{aligned} C_s^{(2)} = \frac{1}{64}\left(\frac{\phi_G}{\phi_o}\right)^{1/2}\Bigg[\Bigg\{&\frac{2\delta\phi'''}{\phi_G} - \Delta_1\phi'\left(\frac{2\Phi_{rr}}{\phi_G} - \frac{4\eta^2 B_G^2}{3\phi_G} + \frac{16}{R^2}\right) \\ &- \frac{2}{R}\Delta_2\phi' - 5\Delta_3\phi'\Bigg\}h_G^4 + \left(\frac{16\Delta_1\phi'}{R} - 8\Delta_2\phi'\right)h_G^3 h_G' - 16\Delta_1\phi' h_G^2 h_G'^2\Bigg] \end{aligned} \tag{35.153b}$$

The quantity $\delta\phi^{(n)}$ denotes the abrupt change in $\phi^{(n)}$ at the gauze:

$$\delta\phi^{(n)} := \phi^{(n)+} - \phi^{(n)-} \tag{35.154}$$

and

$$\Delta_n \phi' := \left\{ \left(\phi'^{+} \right)^n - \left(\phi'^{-} \right)^n \right\} / \phi_G^n, \quad n = 1, 2, 3 \tag{35.155}$$

Finally $\Phi_{rr} := \partial^2 \Phi / \partial r^2 |_{r=0}$.

For the chromatic aberration, Typke gives

$$C_c = \int_{z_o}^{z_i} \left(\frac{\phi_o}{\phi} \right)^{1/2} \left(\frac{3}{8} \frac{\phi'^2}{\phi^2} + \frac{\eta^2 B^2}{2\phi} \right) h^2 dz - \frac{h^2(z_G)\phi_o^{1/2}}{4\phi_G^{3/2}} \left[\phi' \right]_{z_G^-}^{z_G^+} \tag{35.156}$$

in agreement with Hoch et al. who give the last (integrated) term in the form $\int_{z_o}^{z_i} \left(\phi_o/\phi \right)^{1/2} \left(\rho_0/4\phi \right) h^2 dz$. When the foil is spherical, this last term becomes $-\left(\phi_o/\phi_a \right)^{1/2} h_G^2 \Delta_1 \phi'/4$.

A third set of formulae has been derived by Munro and Wittels (1977) for all the aberration coefficients of magnetic and/or electrostatic lenses containing plane foils. They find

$$\begin{aligned} C_s' &= F(w_h, w_h, w_h^*) \\ K' &= F\left(w_h, w_h, w_g^*\right) \\ F' &= F\left(w_h, w_g, w_g^*\right) + F\left(w_g, w_h, w_g^*\right) \\ A' &= F\left(w_g, w_g, w_h^*\right) \\ D' &= F\left(w_g, w_g, w_g^*\right) \end{aligned} \tag{35.157}$$

in which

$$\begin{aligned} F(w_1, w_2, w_3^*) = \frac{1}{\phi_o^{1/2}} \int_{z_o}^{z_i} \phi^{1/2} \Bigg\{ & \frac{1}{2} \left(\frac{\phi''}{2\phi} w_1 w_h^* + w_1' w_h^{*\prime} \right) \\ & \times \left(\frac{\phi''}{4\phi} w_2 w_3^* + w_2' w_3^{*\prime} \right) - \frac{\phi^{(4)}}{32\phi} w_h^* w_1 w_2' w_3^* \\ & + \frac{\mathrm{i}\eta}{\phi^{1/2}} \left(-\frac{1}{16} w_h^{*\prime} w_1 w_2 w_3^* + \frac{1}{8} w_h^* w_1 w_2' w_3^* - \frac{1}{16} w_h^* w_1 w_2 w_3^{*\prime} \right) B'' \Bigg\} dz \end{aligned} \tag{35.158}$$

and (see 15.7)

$$\begin{aligned} w_g &= g(z) \exp(\mathrm{i}\theta) \\ w_h &= h(z) \exp(\mathrm{i}\theta) \end{aligned}$$

We have added primes to the aberration coefficients $C_s' \ldots D'$ since Munro and Wittels define their coefficients in terms of the fixed coordinates $w = X + \mathrm{i}Y$. Likewise, chromatic aberration coefficients are given by

$$\begin{aligned} C_c' &= -\phi_o^{1/2} \int_{z_o}^{z_i} \frac{1}{2\phi^{1/2}} \left(\frac{\phi''}{4\phi} w_h w_h^* + w_h' w_h^{*\prime} \right) dz \\ C_D' &= -\phi_o^{1/2} \int_{z_o}^{z_i} \frac{1}{2\phi^{1/2}} \left(\frac{\phi''}{4\phi} w_g w_h^* + w_g' w_h^{*\prime} \right) dz \end{aligned} \tag{35.159}$$

Formulae for the third- and fifth-order spherical aberration coefficients are to be found in a series of Japanese papers (Hibino and Maruse, 1976; Hibino et al., 1978; Kuzuya et al., 1982; Hanai et al., 1982). In the first two papers, the conventional rotating coordinates are used and explicit expressions obtained for the third- and fifth-order spherical aberration coefficients of probe-forming lenses. In the third paper, where magnifying conditions are considered, the coefficients are recalculated in fixed coordinates, as in the paper by Munro and Wittels.

35.5 Conical Lenses and Coaxial Lenses

Two unconventional lens geometries have been studied in detail by the Saint-Petersburg group: coaxial lenses (Ovsyannikova and Fishkova, 1997, 1998, 1999a,b; Fishkova, 2009, 2010, 2013) and conical lenses (Baranova et al., 1989a,b, 1990; Yavor and Baranova, 1990).

Coaxial lenses consist of two or more coaxial cylinders held at different potentials. A conical beam passes between the inner and outer cylinders. Fig. 35.17A and B shows two of the geometries studied. Curves representing the electron optical properties of several such lenses are to be found in the references cited.[3]

Conical lenses consist of conical frusta (Fig. 35.18A) or a series of cones, each pierced by a single slit (Fig. 35.18B). In the first case, the conical beam passes between the two sets of conical surfaces and the potentials may be chosen to give einzel-like lenses or multielectrode lenses. In a meridional plane, the paraxial trajectory equation takes the form

$$y'' + \frac{\phi'}{2\phi} y' + \frac{1}{2\phi} \left(\phi'' + \frac{\phi'}{x} \right) y = \frac{\phi_\perp}{2\phi}$$

[3] These curves are readily available as the Russian journals are open access. The English translations can be found on SpringerLink from 1997 onwards.

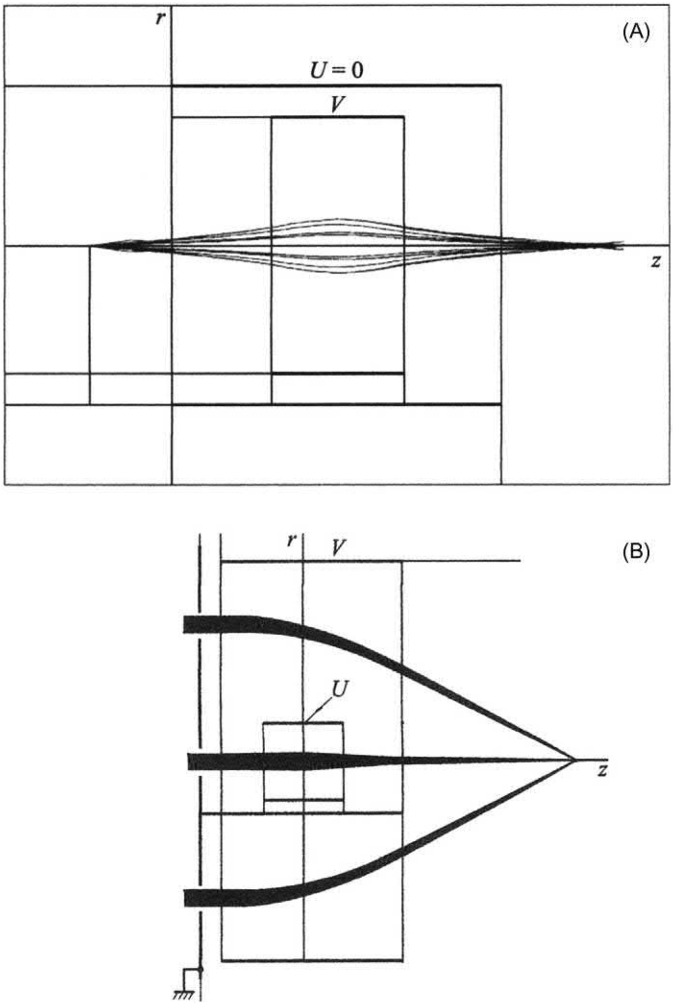

Figure 35.17
Two types of coaxial lens.

in which $\phi(x)$ is the potential distribution along the x-axis midway between the conical frusta; $\phi_{\perp}$ denotes the derivative of the potential with respect to y at the axis.

In the second configuration, the lens consists of a series of cones with the same cone-angle, displaced as shown. The lens action is provided by slits in the cones, which define an 'optic axis' perpendicular to the surfaces of the cones. For many details of the optical properties of these lenses, we refer to the works cited.

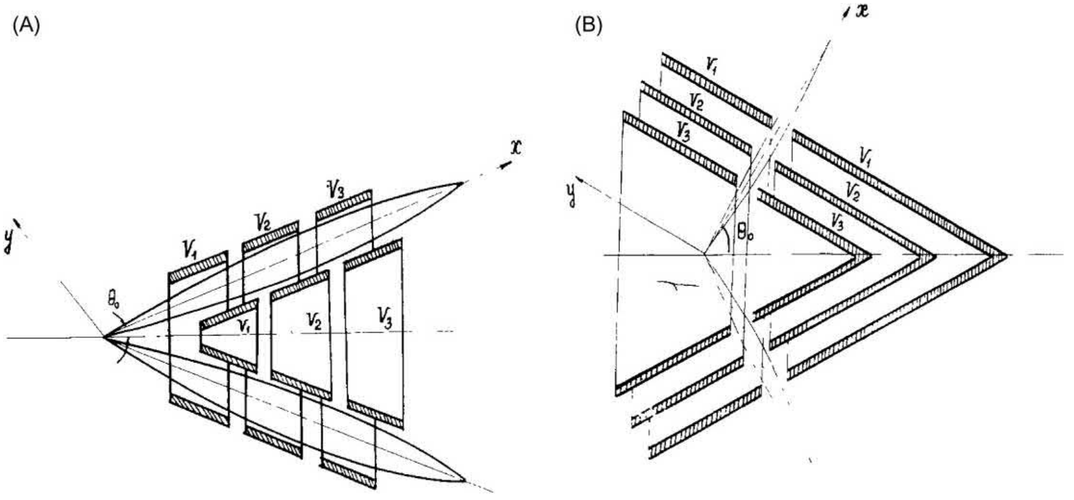

Figure 35.18
Conical lenses. (A) A set of conical frusta. (B) Parallel pierced cones. *After Yavor and Baranova (1990), Courtesy Elsevier.*

35.6 Cylindrical Lenses

There is no large body of information available on cylindrical lenses comparable with that listed above for round lenses, for the good reason that cylindrical lenses are used for very specific purposes and there is no dominant simple design to play the role of the symmetric einzel lens, for example. A family of devices that regularly use multielectrode electrostatic cylindrical lenses comprises electron bombardment ion sources (Fig. 35.19) for mass spectrometry. Here an electron beam arrives perpendicular to the ion optic axis and ionizes the gas to be analysed. The resulting ions are accelerated and focused by the sequence of electrodes leading to the spectrometer. Such lenses are also employed in beta-ray spectrometers.

It is easy to calculate the properties of such systems provided that the electrodes can be modelled by rectangular profiles or, as is commonly done, by planes. The Schwarz–Christoffel conformal transformation can then be used to derive sets of equations, which implicitly describe the potential distribution as a function of the geometric parameters of the system. Although these equations are nonlinear, methods of solving them have been available for many years (e.g., Durand, 1961; Wallington, 1970, 1971). Once the field is known, the optical properties are established either by solving the paraxial equations and evaluating the aberration integrals or, particularly if large angles are involved, by solving the exact equations of motion and drawing conclusions about the optics of the system from the results.

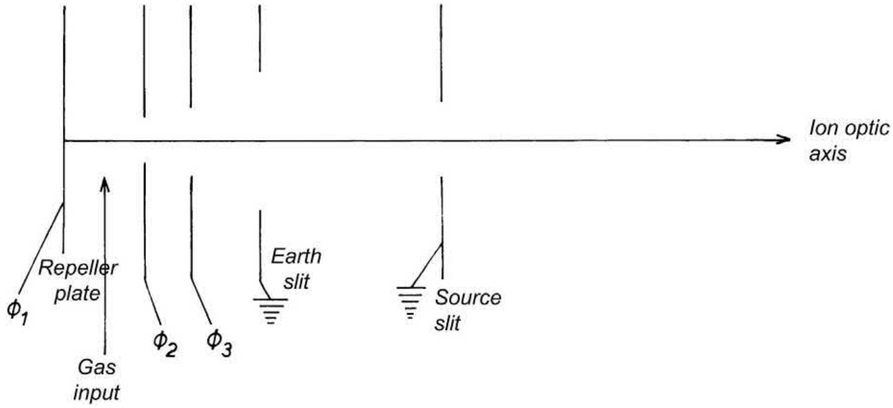

Figure 35.19
Very schematic representation of an electron bombardment ion source. The electron beam arrives perpendicular to the plane of the diagram in the same zone as the gas input.

Sets of curves showing the variation of the cardinal elements and some aberration coefficients are available for a few simple geometries: the symmetric three-electrode structure (Laudet, 1953; Archard, 1954; Yokota and Kishi, 1987; Yokota and Nagami, 1987); the two-electrode immersion lens (Glikman et al., 1967b), extended to a three-electrode immersion lens with equal plate separation in Glikman et al. (1967c) where the conditions for telescopic operation are given.

Detailed field calculations are to be found in Archard (1954), Laudet (1953) and in the work of Boerboom (1959, 1960a,b) and Wallington (1970, 1971, see Mulvey and Wallington, 1973). A model field based on the use of elliptic coordinates has been introduced by Grümm (1956b), a particular case of the family of fields (Grümm, 1956a) for which the equations of motion have explicit solutions. This field, $\phi(z) = \phi_o\{1 + k^2z/(1 + z^2)^{1/2}\}$, has paraxial solutions expressible in terms of circular and hyperbolic functions; see also Grümm and Spurny (1956, 1957).

For further information, see Glikman et al. (1967a), who show that electrostatic cylindrical lenses can never be divergent, Glikman and Yakushev (1967), who calculate the field of a general three-electrode cylindrical lens, Harting and Read (1976), who give detailed data on two two-electrode slit lenses and two three-electrode slit lenses, Hibi et al. (1967), who give the cardinal elements of five geometries, and Vukanić et al. (1976a,b) and Ćirić et al. (1976a, b), who analyse the fields and cardinal elements of a range of 'unipotential' cylindrical lenses. For a five-electrode design for use with an unusual energy analyser, see Kishi et al. (1987a,b).

The calculation of the parameters occurring in the Schwarz–Christoffel transformation has been reconsidered by Boerboom and Chen (1984), who have devised an accurate and rapidly converging iterative method for this purpose.

CHAPTER 36

Magnetic Lenses

36.1 Introduction

Like their electrostatic counterparts, magnetic lenses take a great many different physical forms, but optically, they fall into a few categories only. In the vast majority of cases, magnetic lenses are devices that produce a rather intense field within a small volume, and the superficial differences arise from the design and nature of the windings, yoke and polepieces employed to create this field. The traditional magnetic lens (Fig. 36.1A) produces a field distribution $B(z)$ by means of an iron yoke terminated by polepieces of higher permeability, enclosing a current-carrying coil. In a well-designed lens, the flux remains within the yoke or coil region, except between the polepieces. Such lenses are characterized by the gap, invariably denoted by S, and the bore diameter D, if the lens is symmetric, or the front and back bores, D_1 and D_2, otherwise. We emphasize that magnetic lenses are said to be *symmetric* if the field $B(z)$ is symmetric about a centre-plane; taking the latter as the origin, $B(-z) = B(z)$ in a symmetric lens. The lens may be physically far from symmetric, with the polepieces at one end for example (Fig. 36.1B). A lens is said to be unsymmetric only if $D_1 \neq D_2$ or if the shapes of the upper and lower polepieces are different (e.g., Fig. 36.40). The polepieces are usually made of one of the cobalt-iron alloys, such as Permendur or Vacoflux 48, as these have a particularly high saturation magnetization. For the remainder of the yoke, an unalloyed soft iron such as Hyperm O may be employed or a 48% nickel−iron alloy (Alloy 48 or Supran); the latter saturates at about 1.8 kT and exhibits less hysteresis than pure iron.

Not all lenses belong to this category, however, the exceptions being lenses with more than one gap, notably permanent magnet lenses, the various unconventional designs introduced by Mulvey and colleagues in which asymmetry is taken to extreme limits and side-gap lenses, and some superconducting designs. The advantages of exploiting the properties of superconductors in electron lens design were first recognized in the 1960s (Laberrigue and Levinson, 1964; Fernández-Morán, 1965, Boersch et al., 1966; Ozasa et al., 1966; Siegel et al., 1966; Kitamura et al., 1966) and numerous superconducting lens designs have since been studied (Hardy, 1973; Dietrich, 1976; Hawkes and Valdrè, 1977). In some of these, only the coil is superconducting, giving almost perfect current stability; in others, the entire lens is cooled and the high saturation magnetization of the rare earths holmium and dysprosium is exploited to produce a very strong lens without excessive saturation.

Principles of Electron Optics: Applied Geometrical Optics.
DOI: http://dx.doi.org/10.1016/B978-0-12-813369-9.00036-1

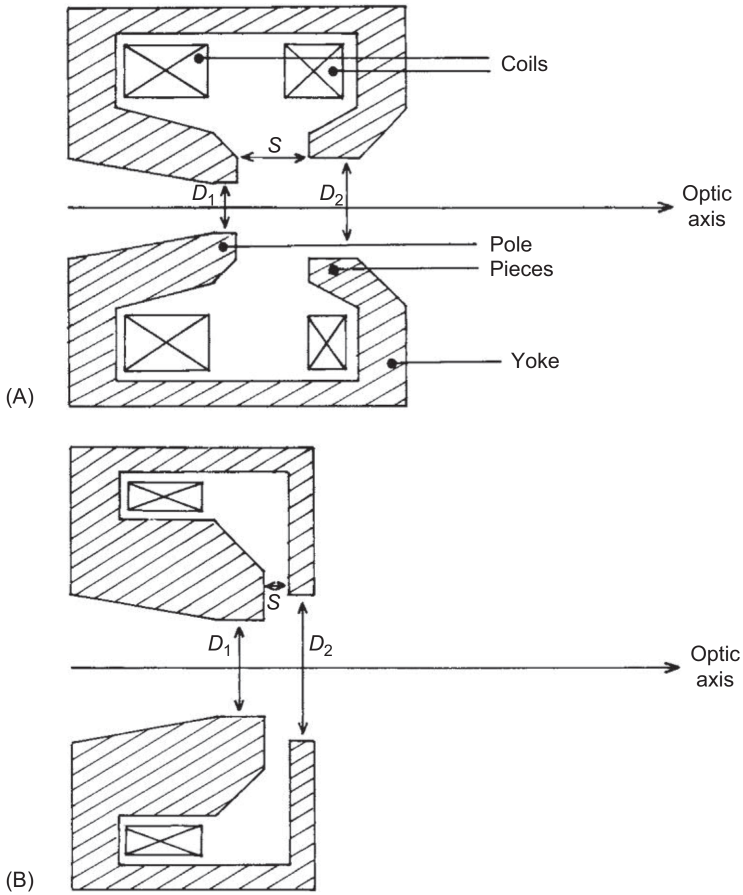

Figure 36.1
Cross-sections of typical magnetic lenses. Both are said to be symmetric if $D_1 = D_2$.

The interest of using high-temperature superconductors has been investigated by Adriaanse (1994) and Adriaanse et al. (1991a, b). In the 'shielding cryolens' introduced by Dietrich and colleagues (Dietrich et al., 1969; Weyl et al., 1972; Dietrich, 1976), the field, produced directly by the coil and not conveyed by yoke and polepieces, is confined within a small volume by superconducting cylinders, into which flux cannot penetrate by virtue of the Meissner−Ochsenfeld effect. Although these superconducting designs require a different technology from conventional lenses, they are optically indistinguishable. Only the shielding lens is accorded a special section, therefore (36.7.2), the others being covered in the appropriate paragraphs of Sections 36.2 and 36.3. The superconducting microscope project of Laberrigue was intended to reduce the dimensions of the huge high-voltage microscopes of the 1960s (Laberrigue and Levinson, 1964; Laberrigue and Séverin, 1967; Laberrigue et al., 1967, 1971, 1973, 1976; Génotel et al., 1967a,b, 1971; Séverin et al., 1971)

From these remarks, we see that magnetic lenses may be excited by windings, at room temperature or in the superconducting state, or the field may be created by employing a permanent magnet. In the former case, it is in practice almost invariably preferable to avoid magnetic saturation in the yoke and polepieces, though there may be good theoretical reasons for tolerating saturation. In the absence of saturation, the flux density at any point is proportional to the number of ampère-turns in the winding, which we denote by $J := IN$, where N is the number of turns in the coil and I the current flowing. (J has the dimensions of a current but excitations are always quoted in ampère-turns or A-t, to prevent misunderstanding.) As J is increased, saturation eventually sets in and the proportionality fails.

The various forms of the ray equation or the paraxial equation show clearly that the quantity characteristic of a magnetic lens is $\eta B/\hat{\phi}^{1/2}$, which has the dimensions of reciprocal length. If, therefore, L is some convenient length associated with the lens, $\eta BL/\hat{\phi}^{1/2}$ will be dimensionless. On scaling the lens dimensions uniformly, therefore, without changing $\eta BL/\hat{\phi}^{1/2}$, lens properties having the dimensions of length such as the focal length and the spherical and chromatic aberration coefficients will likewise scale as L. Thus f/L, C_s/L and C_c/L will be invariant under such a scale change.

From these general observations, we may anticipate that magnetic lens properties should be presented in terms of some function of $\eta BL/\hat{\phi}^{1/2}$ for different values of some other function of S and D (or D_1 and D_2). For some quantities, a single 'universal' curve represents this dependence for all conventional lenses operating in conservative conditions.

Another convenient notion is the *form factor*. If we set $B(z) =: B_0 f(z)$, where $f(z)$ rises to a maximum value of unity, and apply Ampère's circuital theorem (Fig. 36.2),

$$\int_{-\infty}^{\infty} B(z)dz = B_0 \int_{-\infty}^{\infty} f(z)dz = \mu_0 NI = \mu_0 J \tag{36.1}$$

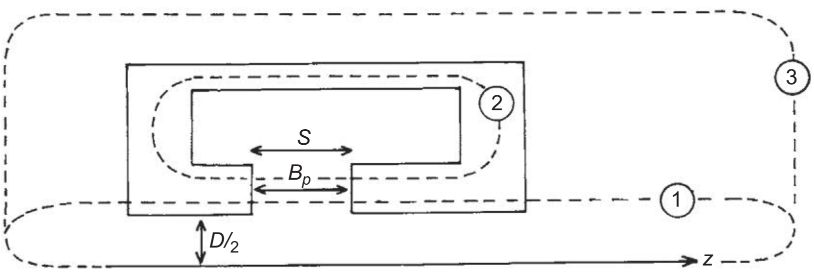

Figure 36.2
Ampère's circuital theorem. Integration around curve 3 yields Eq. (36.1). If the reluctance of the yoke is negligible, integration around circuits 1 and 2 tells us that $B_0 \int f(z)dz = SB_p = \mu_0 J$.

we have

$$B_0 = \frac{\mu_0 J}{AL}, \quad A := \frac{1}{L}\int_{-\infty}^{\infty} f(z)dz \tag{36.2}$$

The excitation parameter $\eta B_0 L/\hat{\phi}^{1/2}$ may thus be written

$$\frac{\eta B_0 L}{\hat{\phi}^{1/2}} = \frac{\eta \mu_0 J}{A\hat{\phi}^{1/2}} \tag{36.3}$$

The dimensionless quantity A is known as the *form factor* of the lens (Lenz, 1952) and provided that the lens remains unsaturated, $f(z)$ and hence A are characteristic of each lens geometry. As J is raised, the polepieces eventually saturate, $f(z)$ broadens and A changes; A may likewise be affected if the yoke is so badly designed that 'parasitic' lenses appear along the bore: some typical situations are illustrated in Fig. 36.3.

36.1.1 Modes of Operation

Magnetic lenses are of course employed both as objective or probe-forming lenses, in which case the real cardinal elements and aberration coefficients are required, and as projectors, condensers or other beam transport lenses, in which case it is the asymptotic

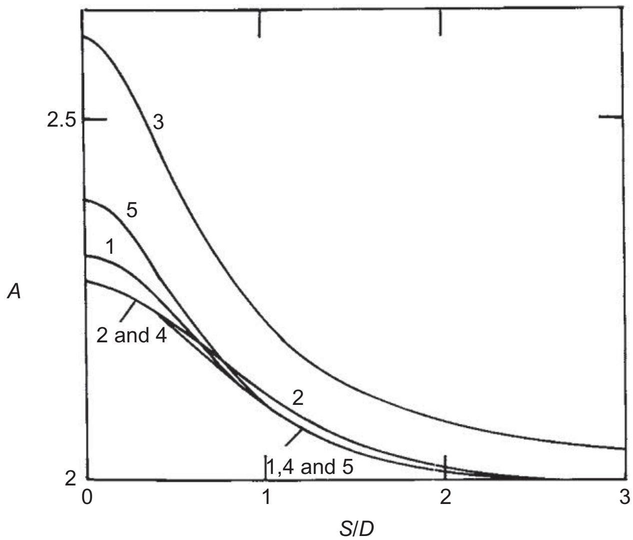

Figure 36.3
The form factor A as a function of S/D for various unsaturated lens models. 1. Exact calculation. 2. Lenz's model (see 36.84). 3. (36.87). 4. Convoluted Gray's model (36.84). 5. Convoluted Grivet–Lenz model (36.85). *After Lenz, 1982, Courtesy Springer Verlag.*

quantities that are needed. In the first case, it is nowadays usual to immerse the specimen or target deep within the field whenever high resolution is demanded and the lens is then fully characterized by two sets of real quantities, those belonging to the space before the specimen or target and those to the space beyond it. In such conditions, we speak of a *condenser−objective*. The reduction in C_s to be gained by placing the specimen in the centre-plane of an objective was pointed out as long ago as 1941 (Glaser, 1941a) but practical lenses operating in or close to this symmetric mode are often referred to as Ruska−Riecke condenser−objectives, after the scientists who first deliberately set out to exploit the predicted advantage (Riecke and Ruska, 1966; see Riecke, 1982); even before that, however, a number of microscopes had been operated with the specimen well within the field region. If the lens is still stronger, one of the object foci retreats even further towards image space for there are now two planes conjugate to an infinitely distant image (Fig. 36.4). In a *second-zone objective*, the specimen is placed at the focus in the second or positive half of the lens (Suzuki et al., 1968; Tochigi et al., 1969; Akashi et al., 1970). A special case of the latter is the telescopic-condenser mode (Francken, 1972; Francken and Heeres, 1973; Kamminga, 1976), in which the condenser part of the objective acts as a telescope.

36.1.2 Practical Design

There is a great deal more to designing a lens than just evaluating cardinal elements and aberration coefficients. The gap S and bore D must be of suitable sizes to accommodate the specimen-stage mechanism, the objective aperture holder and anticontamination equipment; provision for both top-entry and side-entry stages may be required, and here the top bore must be large enough to receive the former and the gap wide enough to allow the latter to be introduced and manœuvred. For metallurgists especially, the space around the specimen should be capable of housing all the appliances of their mini-laboratory, as Valdrè has explained (1975), which again reflects on the choice of the inner dimensions. The needs of environmental electron microscopy impose new demands on the specimen region.

Design of the polepieces too is a complex task: they normally have the form of truncated cones (Fig. 36.1A), and the choice of cone-angle and the length of the conical section are both important design parameters. The lens core, that is, the part of the yoke nearest to the optic axis, must likewise be designed in such a way that no flux leaks into the bore, where it would create a weak parasitic lens. Even the remainder of the yoke requires careful thought, to ensure that the amount of metal is sufficient but not excessive and to provide good magnetic contact between the different parts. We shall not discuss these topics here, but refer the reader to a very detailed account by Riecke (1982) and to the survey of Tsuno (2009). Fig. 36.5 shows a detailed drawing of a conventional electron microscope objective as a reminder of the complexity that results from the need to squeeze so many moving parts

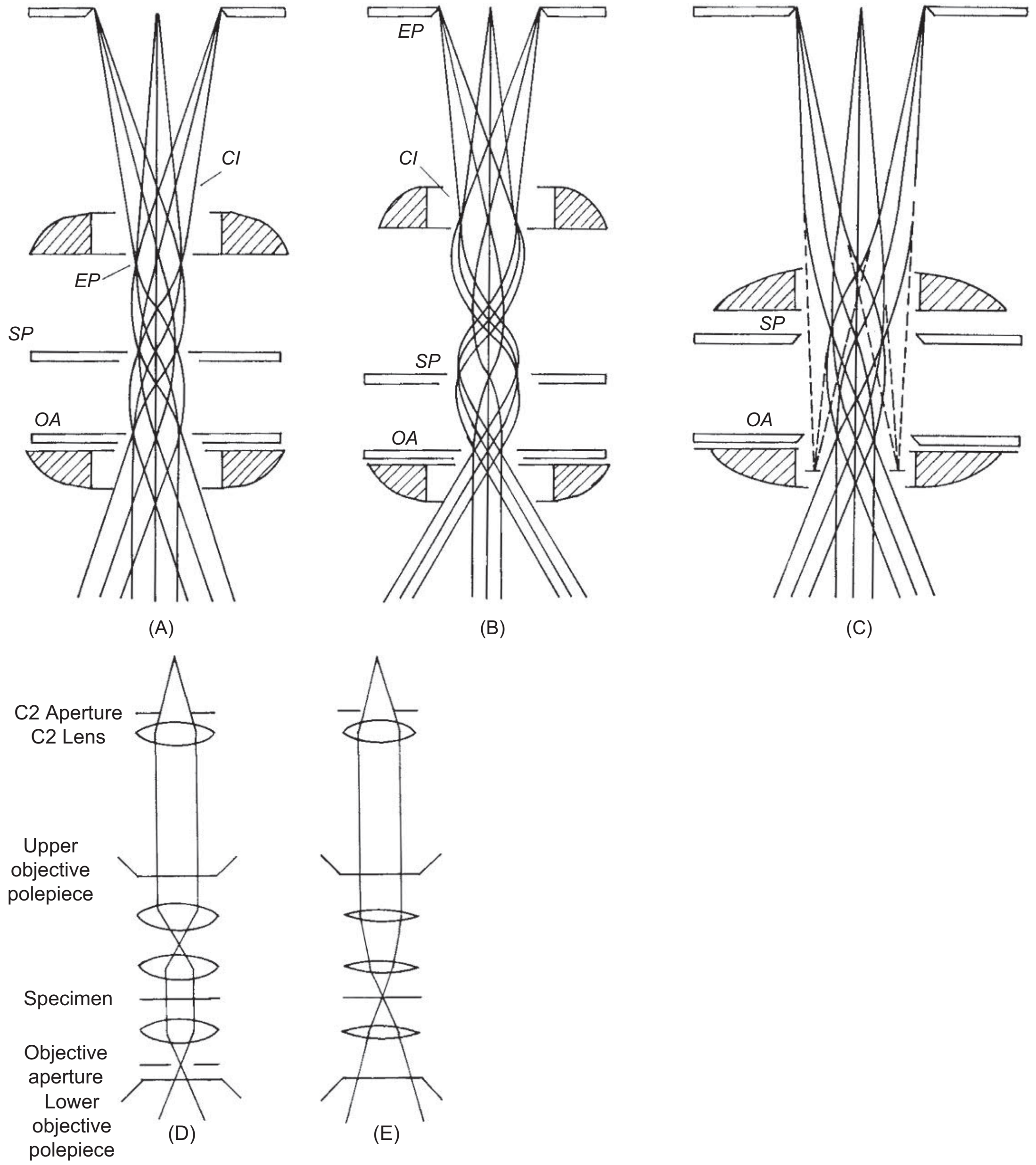

Figure 36.4

Lens operating modes. (A) Condenser—objective mode. (B) Second-zone mode. (C) Conventional mode. (D) and (E) Second-zone mode for fixed-beam operation and for STEM operation. *EP*: Entrance pupil; *SP*: specimen; *OA*: objective aperture; *CI*: crossover image. *After Riecke (1982), Courtesy Springer Verlag.*

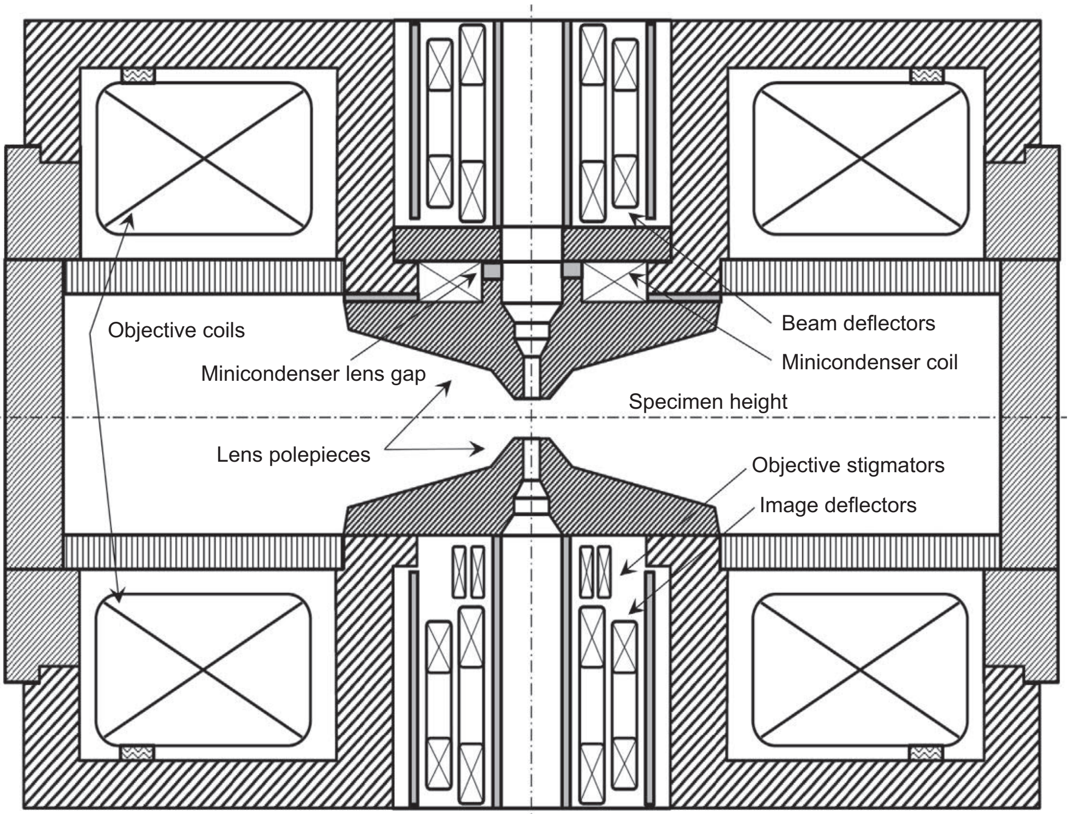

Figure 36.5
The objective lens area of the FEI Talos electron microscope. *Courtesy Dr Ondrej Shanel, FEI.*

into so small a volume, under vacuum conditions. Furthermore, every new development in electron microscopy brings new problems: in high-voltage microscope objectives, there is ample space but the lenses are so large that delicate movements must all be performed at the end of a control rod perhaps 1 m in length; in dedicated STEMs the constraints of ultra-high vacuum must be accepted; in analytical instruments, where many signals are generated − by X-rays, secondary electrons, back-scattered electrons, luminescence and beam-induced currents, and this list is not complete − space must be made available for all the corresponding detectors, and furthermore the magnetic circuit must leave a clear path between the specimen and each detector, often a very demanding requirement.

Such constraints, although continually being added to, are familiar, in the sense that lens designers are accustomed to them and satisfactory solutions are known and have been incorporated into commercial instruments, at least in most cases. There are, however, more egregious demands on lens design that have not yet found definitive solutions. An example is the type of lens that will be needed if three-dimensional reconstruction is to be automated as highly as it is in the field of X-rays (e.g., Hoppe and Typke, 1979; Hoppe and Hegerl, 1980); for an idea of the new difficulties that arise, see Typke et al. (1976, 1980), Plies and Typke (1978), Plies (1981) and Typke (1981).

36.1.3 Notation

We shall repeatedly encounter the paraxial equation of motion, so it is convenient to define standard forms of this equation. The fundamental expression is

$$u'' + \frac{\eta^2 B^2}{4\hat{\phi}} u = 0 \tag{36.4}$$

As before, we write

$$B(z) = B_0 f(z) \quad f(z) \le 1 \tag{36.5}$$

and introduce a length unit, L, whereupon Eq. (36.4) becomes

$$\frac{d^2u}{d\zeta^2} + k^2 f^2 u = 0, \quad k^2 := \frac{\eta^2 B_0^2 L^2}{4\hat{\phi}}, \ \zeta := z/L \tag{36.6}$$

This definition of k^2 is the same as that used by Glaser for his bell-shaped field (Section 36.2.1) if L is set equal to the half-width a. Alternatively, we may substitute $B_0 = \mu_0 J/AL$ (36.2), giving

$$\frac{d^2u}{d\zeta^2} + \frac{\pi^2 \kappa^2 f^2}{A^2} u = 0, \quad \kappa^2 := \frac{\eta^2 \mu_0^2 L^2}{4\pi^2 \hat{\varphi}} \tag{36.7}$$

The constant π^2 is introduced so that for the Glaser field, for which $AL = \pi a$, κ^2 and k^2 are the same (Lenz, 1950c).

36.2 Field Models

Magnetic lens design studies have followed much the same path as those for electrostatic lenses: first, heavy reliance on simple models of the axial field $B(z)$ supported by calculations based on analogue techniques for establishing $B(z)$, gradually supplanted by computer modelling, progressively more exact as sophisticated numerical techniques have become widely available.

In this section, we give some account of the principal models; we stress once again that these remain useful for studying lens behaviour as a function of the various parameters of the model but that they should always be supplemented and corrected by exact calculation whenever possible.

36.2.1 Symmetric Lenses: Glaser's Bell-Shaped Model

36.2.1.1 Paraxial properties

In 1941, Glaser (1941a) introduced the field model

$$B(z) = \frac{B_0}{1 + z^2/a^2} \tag{36.8}$$

This is a good enough approximation to the field in symmetric lenses to give an acceptable idea of the variation of the lens properties with B_0 and a, though it falls to negligible values far more slowly than real fields; it has the great attraction that all the optical properties – cardinal elements and aberration coefficients, real and asymptotic – can be expressed in closed form in terms of circular functions.

Substituting Eq. (36.8) in the paraxial equation (36.4) and replacing z by the angle ψ,

$$z =: a \cot \psi \tag{36.9}$$

(Fig. 35.10), we find

$$\frac{d^2u}{d\psi^2} + 2\cot\psi \frac{du}{d\psi} + \frac{\eta^2 B_0^2 a^2}{4\hat{\phi}} u = 0 \tag{36.10}$$

Writing

$$u(\psi) =: \frac{r(\psi)}{\sin \psi} \tag{36.11}$$

gives

$$\frac{d^2 r}{d\psi^2} + \left(1 + \frac{\eta^2 B_0^2 a^2}{4\hat{\phi}}\right) r = 0 \tag{36.12}$$

Setting

$$\omega^2 := 1 + \frac{\eta^2 B_0^2 a^2}{4\hat{\phi}} =: 1 + k^2 \tag{36.13}$$

the solutions are thus of the form

$$u_1 = \frac{\cos \omega\psi}{\sin \psi}, \quad u_2 = \frac{\sin \omega\psi}{\sin \psi} \tag{36.14}$$

The rays $G(z)$ and $\overline{G}(z)$ (16.1), which, we recall, satisfy the boundary conditions

$$\lim_{z \to -\infty} G(z) = 1, \quad \lim_{z \to \infty} \overline{G}(z) = 1$$

are thus

$$G(\psi) = -\frac{\sin \omega(\psi - \pi)}{\omega \sin \psi} \tag{36.15a}$$

$$\overline{G}(\psi) = \frac{\sin \omega\psi}{\omega \sin \psi} \tag{36.15b}$$

while the rays $g(z)$ and $h(z)$, satisfying $g(z_o) = h'(z_o) = 1$, $g'(z_o) = h(z_o) = 0$ (15.42), are

$$g(\psi) = \frac{\sin \psi_o}{\sin \psi} \frac{\sin \omega(\psi - \alpha)}{\sin \omega\left(\psi_o - \alpha\right)} \tag{36.16a}$$

where

$$\alpha = \psi_o - \frac{1}{\omega} \arctan\left(\omega \tan \psi_o\right) \tag{36.16b}$$

and

$$h(\psi) = -\frac{a \sin \omega\left(\psi - \psi_o\right)}{\omega \sin \psi_o \sin \psi} \tag{36.16c}$$

In systems with real apertures, the rays $s(z)$ and $t(z)$ are also needed, $s(z_o) = t(z_a) = 1$, $s(z_a) = t(z_o) = 0$. These are given by

$$s(\psi) = \frac{\sin\psi_o}{\sin \omega\left(\psi_a - \psi_o\right)} \frac{\sin \omega\left(\psi_a - \psi\right)}{\sin \psi} \tag{36.17a}$$

$$t(\psi) = \frac{\sin\psi_a}{\sin \omega\left(\psi_o - \psi_a\right)} \frac{\sin \omega\left(\psi_o - \psi\right)}{\sin \psi} \tag{36.17b}$$

From Eq. (36.16c), we see that the plane(s) conjugate to $z = z_o$ occur at

$$\psi_i = \psi_o - n\frac{\pi}{\omega} \tag{36.18}$$

For $\psi_0 = \pi$, there will be only one such plane, $\psi_i = \psi_o - \pi/\omega$, if ψ_i lies between $\psi = 0$ and $\psi = \pi/2$ and hence if ω lies between 1 and 2; this is commonly the case. For stronger lenses, there will be two (or more) planes conjugate to ψ_o. The magnification is given by $g(\psi_i)$ and from Eqs (36.16a) and (36.18) we see that

$$g\left(\psi_i\right) = M = (-1)^n \frac{\sin \psi_o}{\sin \psi_i} \tag{36.19}$$

From $G(\psi)$ and $\overline{G}(\psi)$, we can read off the real (high-magnification) foci:

$$\psi_{Fo} = \frac{n\pi}{\omega}, \quad \psi_{Fi} = \pi + \frac{n\pi}{\omega} \tag{36.20}$$

Likewise

$$\left.\frac{d\overline{G}}{dz}\right|_{z=z_{Fo}} = \frac{(-1)^n \sin(n\pi/\omega)}{a}$$
$$\left.\frac{dG}{dz}\right|_{z=z_{Fi}} = -\frac{(-1)^n \sin(n\pi/\omega)}{a}$$

so that the real focal length is

$$f' = (-1)^n\, a \operatorname{cosec}\,(n\pi/\omega) \tag{36.21}$$

But since $\psi_i = \psi_o - n\pi/\omega$ and $z = a \cot \psi$ we see that

$$\begin{aligned} z_o = a \cot \psi_o &= a \cot(\psi_i + n\pi/\omega) \\ &= a\, \frac{\cot \psi_i \cot(n\pi/\omega) - 1}{\cot \psi_i + \cot(n\pi/\omega)} \end{aligned}$$

or

$$\{z_o - a \cot(n\pi/\omega)\}\ \{z_i - a \cot(n\pi/\omega)\} = -a^2 \operatorname{cosec}^2(n\pi/\omega)$$

Thus

$$(z_o - z'_{Fo})(z_i - z'_{Fi}) = -f'^2 \tag{36.22}$$

where

$$z'_{Fo} = a \cot \psi_{Fo}, \qquad z'_{Fi} = a \cot \psi_{Fi} \tag{36.23}$$

Thus Glaser's bell-shaped field is a Newtonian field (Section 17.2), real image formation when neither conjugate is at infinity being characterized by fixed (not object-dependent) cardinal elements.

The asymptotic cardinal elements are obtained by calculating $\lim_{z\to\infty} G(z)$ or $\lim_{z\to-\infty} \overline{G}(z)$. We have

$$\lim_{z\to-\infty} \overline{G}(z) = z\overline{G}'(-\infty) + \lim_{z\to-\infty} (\overline{G} - \overline{G}'\, z)$$

But

$$\lim_{z\to-\infty}\left(\overline{G}-\overline{G}'\,z\right)=\frac{1}{\omega}\quad\lim_{\psi\to\pi}\left(\frac{\sin\omega\psi}{\sin\psi}+\omega\cos\psi\cos\omega\psi-\frac{\cos^2\psi}{\sin\psi}\sin\omega\psi\right)$$
$$=\frac{1}{\omega}\quad\lim_{\psi\to\pi}(\sin\psi\sin\omega\psi+\omega\cos\psi\cos\omega\psi)$$
$$=-\cos\omega\pi$$

and

$$\overline{G}'(-\infty)=-\frac{1}{a\omega}\sin\omega\pi \tag{36.24}$$

Hence (16.5−16.7)

$$f=a\omega\ \operatorname{cosec}\omega\pi \tag{36.25a}$$

$$z_{Fo}=-z_{Fi}=-a\omega\cot\omega\pi \tag{36.25b}$$

The rotation between real object and image is given by

$$\theta_{oi}=\frac{\eta}{2\hat{\phi}^{1/2}}\int_{z_o}^{z_i}B\ dz=\frac{n\pi\,k}{\omega} \tag{36.26}$$

When object and image are both asymptotic, the rotation is equal to $k\pi$.

36.2.1.2 Aberrations

All the aberration integrals can be evaluated in closed form (Glaser, 1941a; Glaser and Lammel, 1943; Kanaya, 1949a,b, 1951a,b,c,d, 1954, 1955). We reproduce the resulting formulae. Since the field is Newtonian, the real coefficients can be written partially as polynomials in reciprocal magnification as well as the asymptotic coefficients (Hawkes, 1968a,b, 1970, 1974) and we recast the formulae to bring out this dependence.

a. *Real aberrations, expressed in terms of object and aperture coordinates*[1]

$$\begin{aligned}C&=\frac{1}{4a^2}\frac{\sin^3\psi_a}{\sin\psi_o\sin^3\omega(\psi_o-\psi_a)}\left\{\pi k^2-\frac{4\omega^2-7}{4\omega^2-1}\omega^3\sin\frac{\pi}{\omega}\cos(\psi_o+\psi_i)\right\}\\&\underset{M\to\infty}{\rightarrow}\frac{1}{4a^2}\ \frac{\sin^3\psi_a}{\sin(\pi/\omega)\sin^3\omega\psi_a}\left(\pi k^2-\frac{\omega^3}{2}\frac{4\omega^2-7}{4\omega^2-1}\sin(2\pi/\omega)\right)\end{aligned} \tag{36.27−C}$$

[1] A few errors in the expressions given by Glaser (1952) have been detected (Jandeleit and Lenz, 1959); the formulae given here are of course the corrected expressions.

$$\begin{aligned}
A = {} & \frac{1}{4a^2}\frac{\sin\psi_o \sin\psi_{\tilde{a}}}{\sin^3 \omega\left(\psi_o - \psi_{\tilde{a}}\right)}\left[\pi k^2 \cos 2\omega\left(\psi_{\tilde{a}} - \psi_o\right)\right. \\
& - \frac{\omega^2}{4\omega^2 - 1}\sin\left(\pi/\omega\right)\left\{\omega\left(4\omega^2 - 7\right)\cos\left(\psi_o + \psi_i\right)\cos 2\omega\left(\psi_a - \psi_o\right)\right. \\
& \left.\left. - 3\sin\left(\psi_o + \psi_i\right)\sin 2\omega\left(\psi_o - \psi_a\right)\right\}\right] \\
& \underset{M\to\infty}{\rightarrow} \frac{1}{4a^2}\frac{\sin\left(\pi/\omega\right)\sin\psi_a}{\sin^3 \omega\psi_a}\left[\pi k^2 \cos 2\omega\psi_a\right. \\
& \left. - \frac{\omega^2}{4\omega^2 - 1}\sin\left(\pi/\omega\right)\left\{\omega\left(4\omega^2 - 7\right)\cos\left(\pi/\omega\right)\cos 2\omega\psi_a + 3\sin\left(\pi/\omega\right)\sin 2\omega\psi_a\right\}\right]
\end{aligned} \tag{36.27-A}$$

$$\begin{aligned}
\tilde{a} = {} & \frac{k}{2a^2}\frac{\sin\psi_o \sin\psi_a}{\sin^2 \omega\left(\psi_a - \psi_o\right)}\left[-\frac{\pi}{2\omega}\left(2\omega^2 - 1\right)\cos\omega\left(\psi_a - \psi_o\right)\right. \\
& + \frac{\omega}{k^2}\sin\left(\pi/\omega\right)\left\{\left(\omega^2 - 2\right)\omega\cos\left(\psi_o + \psi_i\right)\cos\omega\left(\psi_a - \psi_o\right)\right. \\
& \left.\left. + \sin\left(\psi_o + \psi_i\right)\sin\omega\left(\psi_a - \psi_o\right)\right\}\right]
\end{aligned} \tag{36.27-a}$$

$$\begin{aligned}
& \underset{M\to\infty}{\rightarrow} \frac{k}{2a^2}\frac{\sin\left(\pi/\omega\right)\sin\psi_a}{\sin^2 \omega\psi_a}\left[\frac{\pi}{2\omega}\left(2\omega^2 - 1\right)\cos\omega\psi_a\right. \\
& \left. - \frac{\omega}{k^2}\sin\left(\pi/\omega\right)\left\{\left(\omega^2 - 2\right)\omega\cos\left(\pi/\omega\right)\cos\omega\psi_a + \sin\left(\pi/\omega\right)\sin\omega\psi_a\right\}\right]
\end{aligned}$$

$$\begin{aligned}
2A - F = {} & \frac{\omega k^2}{a^2}\frac{\sin\psi_o \sin\psi_a}{\sin\omega\left(\psi_a - \psi_o\right)}\left\{\frac{\pi}{\omega} - \sin\left(\pi/\omega\right)\cos\left(\psi_o + \psi_i\right)\right\} \\
& \underset{M\to\infty}{\rightarrow} \frac{\omega k^2}{a^2}\frac{\sin\left(\pi/\omega\right)\sin\psi_a}{2\sin\omega\psi_a}\left(\sin\frac{2\pi}{\omega} - \frac{2\pi}{\omega}\right)
\end{aligned} \tag{36.27-Petzval}$$

$$D = \frac{k}{4a^2}\frac{\sin^2\psi_o}{\sin^3\,\omega(\psi_a-\psi_o)}\Big[\{\pi-\omega\,\sin(\pi/\omega)\,\cos(\psi_o+\psi_i)\}\,\cos\,\omega(\psi_a-\psi_o)$$

$$+\,\frac{\omega^2}{k^2}\,\frac{2\omega^2+1}{4\omega^2-1}\,\sin(\pi/\omega)\,\cos(\psi_o+\psi_i)\cos\,3\omega(\psi_a-\psi_o)$$

$$-\,\frac{3}{k^2}\,\frac{\omega^2}{4\omega^2-1}\,\sin(\pi/\omega)\sin(\psi_o+\psi_i)\sin\,3\omega(\psi_a-\psi_o)\Big] \tag{36.27-D}$$

$$\underset{M\to\infty}{\to}\frac{k^2}{8a^2}\frac{\sin^2(\pi/\omega)}{\sin^3\,\omega\psi_a}\Big\{(\omega\,\sin(2\pi/\omega)-2\pi)\,\cos\,\omega(\psi_a-\pi/\omega)$$

$$+\,\frac{\omega}{k^2}\frac{2\omega^2+1}{4\omega^2-1}\,\sin(2\pi/\omega)\,\cos\,3\omega\psi_a-\frac{6}{k^2}\frac{\omega^2}{4\omega^2-1}\,\sin^2(\pi/\omega)\,\sin\,3\omega\psi_a\Big\}$$

$$d = \frac{k}{4a^2}\frac{\sin^2\psi_o}{\sin^2\,\omega(\psi_o-\psi_a)}\Big[\frac{\pi}{2\omega}(2\omega^2-1)-\omega^2\sin(\pi/\omega)\cos(\psi_o+\psi_i)$$

$$+\,\frac{\omega}{k^2}\,\sin(\pi/\omega)\Big\{\omega\,\cos(\psi_o+\psi_i)\,\cos\,2\omega(\psi_o-\psi_a)$$

$$+\sin(\psi_o+\psi_i)\sin\,2\omega(\psi_o-\psi_a)\Big\}\Big] \tag{36.27-d}$$

$$\underset{M\to\infty}{\to}\frac{k}{8a^2}\frac{\sin^2(\pi/\omega)}{\sin^2\,\omega\psi_a}\Big\{\frac{\pi}{\omega}(2\omega^2-1)-\omega^2\,\sin(2\pi/\omega)$$

$$+\,\frac{\omega^2}{k^2}\,\sin(2\pi/\omega)\,\cos\,2\omega\psi_a-\frac{2\omega}{k^2}\,\sin^2(\pi/\omega)\,\sin\,2\omega\psi_a\Big\}$$

$$K = \frac{1}{4a^2}\frac{\sin^2\,\psi_a}{\sin^3\,\omega(\psi_a-\psi_o)}\Big[\pi\,k^2\,\cos\,\omega(\psi_a-\psi_o)$$

$$-\,\frac{\omega^2}{4\omega^2-1}\,\sin\,\pi\omega\Big\{(4\omega^2-7)\omega\,\cos(\psi_o+\psi_i)\,\cos\,\omega(\psi_a-\psi_o)$$

$$+\,3\,\sin(\psi_o+\psi_i)\sin\,\omega(\psi_a-\psi_o)\Big\}\Big] \tag{36.27-K}$$

$$\underset{M\to\infty}{\to}\frac{1}{4a^2}\frac{\sin^2\,\psi_a}{\sin^3\,\omega\psi_a}\Big[\pi\,k^2\,\cos\,\omega\psi_a-\frac{\omega^2}{4\omega^2-1}\,\sin(\pi/\omega)$$

$$\times\{(4\omega^2-7)\omega\,\cos(\pi/\omega)\,\cos\,\omega\psi_a+3\,\sin(\pi/\omega)\,\sin\,\omega\psi_a\}\Big]$$

$$\tilde{k} = \frac{k}{4a^2} \frac{\sin^2 \psi_a}{\sin^2 \omega(\psi_a - \psi_o)} \left\{ \frac{\pi}{2\omega}(2\omega^2 - 1) - \frac{\omega^2(\omega^2 - 2)}{k^2} \sin(\pi/\omega)\cos(\psi_o + \psi_i) \right\}$$
$$\underset{M \to \infty}{\to} \frac{k}{8a^2} \frac{\sin^2 \psi_a}{\sin^2 \omega\psi_a} \left\{ \frac{\pi}{\omega}(2\omega^2 - 1) - \frac{\omega^2(\omega^2 - 2)}{k^2} \sin(2\pi/\omega) \right\} \tag{36.27–k}$$

The anisotropic astigmatism and coma are here denoted by $\tilde{a}$ and $\tilde{k}$ to prevent confusion with a and k.

The coma-free aperture position is obtained by solving the equation $K = 0$, for which

$$\tan \omega(\psi_a - \psi_o) = \frac{1}{3} \left\{ \pi k^2 \frac{4\omega^2 - 1}{\omega^2} \operatorname{cosec}(\pi/\omega) - (4\omega^2 - 7)\,\omega \cos(\psi_o + \psi_i) \right\} \operatorname{cosec}(\psi_o + \psi_i) \tag{36.28}$$

This is easily shown to give the same result as (24.134).

A similar equation obtained by setting $A = 0$ yields two real aperture planes for which the isotropic astigmatism vanishes, but these never coincide with the solution of (36.28). Likewise, planes for which D and $\tilde{a}$ vanish can be found, whereas $\tilde{k}$ and d do not vanish for any aperture position.

For the chromatic aberrations, we find

$$C_C = \frac{\sin \psi_a}{\sin \psi_o} \frac{\pi k^2}{2\omega^2} \operatorname{cosec} \omega(\psi_a - \psi_o)$$
$$C_D = \frac{\pi k^2}{2\omega^2} \cot \omega(\psi_a - \psi_o) \tag{36.29}$$

b. *Real aberrations in terms of position and gradient in the object plane*

$$\frac{C_S}{a} = \left\{ \frac{\pi k^2}{4\omega^3} - \frac{4k^2 - 3}{4(4k^2 + 3)} \cos(2\psi_o - \pi/\omega) \sin(\pi/\omega) \right\} \operatorname{cosec}^4 \psi_o$$
$$=: C_4 m^4 + C_3 m^3 + C_2 m^2 + C_1 m + C_0 \tag{36.30a}$$
$$\underset{M \to \infty}{\to} \left\{ \frac{\pi k^2}{4\omega^3} - \frac{4k^2 - 3}{8(4k^2 + 3)} \sin(2\pi/\omega) \right\} \operatorname{cosec}^4(\pi/\omega)$$

The coefficients C_j are obtained by setting

$$\cot \psi_o = m \operatorname{cosec}(\pi/\omega) + \cot(\pi/\omega) \tag{36.31}$$

giving

$$C_4 = C_0 = \left\{\frac{\pi\, k^2}{4\omega^3} - \frac{4k^2-3}{8(4k^2+3)}\ \sin\left(2\pi/\omega\right)\right\}\mathrm{cosec}^{\,4}\left(\pi/\omega\right)$$

$$C_3 = C_1 = \left\{\frac{\pi\, k^2}{\omega^3}\ \cot\left(\pi/\omega\right) - \frac{4k^2-3}{4(4k^2+3)}\ \left(3+\cos\left(2\pi/\omega\right)\right)\right\}\mathrm{cosec}^{\,3}\left(\pi/\omega\right) \tag{36.30b}$$

$$C_2 = \left\{\frac{\pi\, k^2}{2\omega^3}\ \left(1+3\cot^2\left(\pi/\omega\right)\right) - \frac{3\left(4k^2-3\right)}{2(4k^2+3)}\ \cot\left(\pi/\omega\right)\right\}\mathrm{cosec}^{\,2}\left(\pi/\omega\right)$$

The coma can likewise be written exactly as a polynomial in m. Each of the other aberrations has a polynomial structure plus a term in $\sin\psi_o$ and $\cos\psi_o$. The results are as follows:

$$\begin{aligned} A &= \sum_0^2 A_j m^j + \overline{A}, \quad F = \sum_0^2 F_j m^j + \overline{F} \\ K &= \sum_0^3 K_j m^j, \quad D = D_1 m + D_o + \overline{D} \end{aligned} \tag{36.32}$$

where

$$\begin{aligned}
A_2 &= p/a\,\sin^2\left(\pi/\omega\right)\\
A_1 &= 2\left\{p\,\cos\left(\pi/\omega\right) - (q+r)\sin^2\left(\pi/\omega\right)\right\}/a\,\sin^2\left(\pi/\omega\right)\\
A_0 &= \left\{p\,\cot^2\left(\pi/\omega\right) - 2(q+r)\cos\left(\pi/\omega\right) - s\omega^2\right\}/a\\
\overline{A} &= \frac{4k^2+5}{4k^2+3}\frac{\omega^2 k^2}{2a}\ \sin\left(\pi/\omega\right)\,\cos\psi_o\,\cos\psi_i\\
F-2A &= k^2\left\{\pi - \omega\,\sin\left(\pi/\omega\right)\,\cos\left(\pi/\omega\right) + 2\omega\,\sin\psi_o\,\sin\left(\psi_o-\pi/\omega\right)\,\sin\left(\pi/\omega\right)\right\}/a\omega\\
K_3 &= -\,p\,\mathrm{cosec}^{\,3}\left(\pi/\omega\right)\\
K_2 &= -\,\left\{3p\,\cos\left(\pi/\omega\right) - (q+2r)\,\sin^2\left(\pi/\omega\right)\right\}\mathrm{cosec}^{\,3}\left(\pi/\omega\right)\\
K_1 &= -\,\left\{p\left(2\cos^2\left(\pi/\omega\right)+1\right) - r\,\sin\left(2\pi/\omega\right)\right\}\mathrm{cosec}^{\,3}\left(\pi/\omega\right)\\
K_0 &= -\,\left\{p\,\cos\left(\pi/\omega\right) + q\,\sin\left(\pi/\omega\right)\right\}\mathrm{cosec}^{\,3}\left(\pi/\omega\right)\\
D_1 &= -\,p/a^2\,\sin\left(\pi/\omega\right)\\
D_0 &= -\,p/a^2\,\tan\left(\pi/\omega\right) + (3q+2r)\,\sin\left(\pi/\omega\right)/a\\
\overline{D} &= -\frac{k^2}{a^2}\frac{2k^2+1}{4k^2+3}\ \sin^2\psi_o\,\cos\psi_o\,\sin\left(\psi_o-\pi/\omega\right)\,\sin\left(\pi/\omega\right)\\
&\quad -\frac{k^2}{a^2}p\,\sin\psi_o\,\cos\psi_o - \frac{5k^2\,\sin^2\psi_o\,\sin^2\left(\pi/\omega\right)}{4a^2(4k^2+3)}
\end{aligned} \tag{36.33}$$

and

$$
\begin{aligned}
p &\coloneqq \frac{2\pi\, k^2 - \dfrac{4k^2-3}{4k^2+3}\,\omega^3 \sin\left(\dfrac{2\pi}{\omega}\right)}{8\omega^3} \\
q &\coloneqq \frac{3\sin(\pi/\omega)}{4k^2+3} \\
r &\coloneqq \frac{4k^2+3}{4(4k^2-3)}\ \sin\left(\frac{\pi}{\omega}\right) \\
s &\coloneqq \frac{2\pi\, k^2 + \dfrac{4k^2-3}{4k^2+3}\,\omega^3 \sin\left(\dfrac{2\pi}{\omega}\right)}{8\omega^3}
\end{aligned} \tag{36.34}
$$

The anisotropic coefficients may be derived straightforwardly from the anisotropic members of (36.27) but their structure in reciprocal magnification is of little interest, as only the coma ($\tilde{k}$) has a pure polynomial form:

$$
\begin{aligned}
&\tilde{k} \eqqcolon k_2 m^2 + k_1 m + k_0 \\
&k_2 = k_0 = \frac{\pi\, k\left(2k^2+1\right)}{8\omega^3}\ \mathrm{cosec}^{\,2}(\pi/\omega) - \frac{k^2-1}{4k}\ \ \cot(\pi/\omega) \\
&k_1 = \frac{\pi\, k\left(2k^2+1\right)}{4\omega^3}\ \mathrm{cosec}\,(\pi/\omega)\cot(\pi/\omega)\,\frac{k^2-1}{2k}\ \mathrm{cosec}\,(\pi/\omega) \\
&\tilde{a} = -\frac{k\pi\left(2k^2+1\right)}{4a\omega^3}\cot\psi_o - \frac{\sin(\pi/\omega)\ \sin\left(2\psi_o - \pi/\omega\right)}{2ak} \\
&\quad + \frac{k^2-1}{2ak}\cot\psi_o \sin(\pi/\omega)\cos\left(2\psi_o - \pi/\omega\right) \\
&d = \frac{\pi k\left(2k^2+1\right)}{8a^2\omega^2}\ \left(1 + k^2\sin^2\psi_o\right) \\
&\quad + \frac{\sin(\pi/\omega)}{4a^2 k}\left[\sin 2\psi_o \sin\left(2\psi_o - \pi/\omega\right) - \left\{\left(k^2-1\right)\cos^2\psi_o + \omega^4\sin^2\psi_o\right\}\cos\left(2\psi_o - \pi/\omega\right)\right]
\end{aligned} \tag{36.35}
$$

For the real chromatic aberrations, we have

$$\frac{C_c}{a} = \frac{\pi k^2}{2\omega^3}\operatorname{cosec}^2\psi_o$$
$$= \frac{\pi k^2}{2\omega^3}\left(m^2\operatorname{cosec}^2(\pi/\omega) + 2m\operatorname{cosec}(\pi/\omega)\cot(\pi/\omega) + \operatorname{cosec}^2(\pi/\omega)\right)$$
$$\underset{M\to\infty}{\to} \frac{\pi k^2}{2\omega^3}\operatorname{cosec}^2(\pi/\omega)$$
$$\frac{C_D}{a} = \frac{\pi k^2}{2\omega^3}\cot\psi_o$$
$$= \frac{\pi k^2}{2\omega^3}\left(m\operatorname{cosec}(\pi/\omega) + \cot(\pi/\omega)\right) \qquad (36.36)$$
$$\underset{M\to\infty}{\to} \frac{\pi k^2}{2\omega^3}\cot(\pi/\omega)$$

(The anisotropic term is as usual equal to half the image rotation.)

A number of useful predictions concerning C_s may be drawn from Eq. (36.30a). The variation of the high-magnification value with k^2 (Fig. 36.6) indicates that C_s passes through a shallow minimum near $k^2 = 7$, where $C_s/a = 0.252$. For the value of k^2 corresponding to the shortest focal length, obtained by setting $\sin(\pi/\omega) = 1$ so that $\omega = 2$ or $k^2 = \omega^2 - 1 = 3$, we find $C_s/a = 0.294$. We can also enquire which object position gives the smallest value of C_s for each value of k^2 but the result is of little

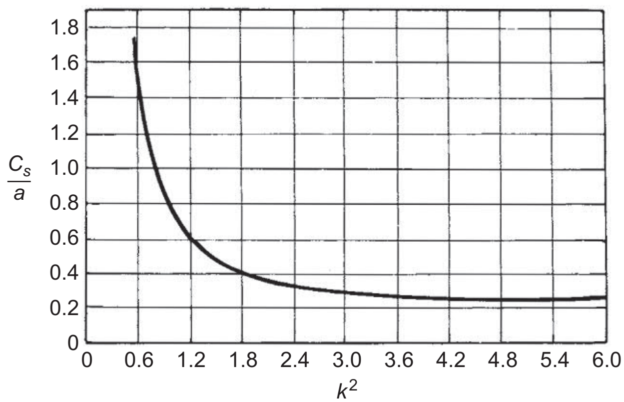

Figure 36.6
Variation of C_s/a with k^2 for Glaser's bell-shaped model. *After Glaser (1952), Courtesy Springer Verlag.*

interest since the corresponding minimum of C_s/a hardly varies with k^2. A more interesting question is the best choice of the half-width a; on substituting $a = 2\hat{\phi}^{1/2}k/B_0$ in Eq. (36.30a), we find that C_s is smallest for given $\hat{\phi}^{1/2}/B_0$ when $k^2 = 2.8$ or in practical units,

$$C_{s\ \min}/\mathrm{mm} = 3.4 \times 10^{-3} \frac{\left(\hat{\phi}/\mathrm{V}\right)^{1/2}}{B_0/\mathrm{T}} \tag{36.37}$$

for which

$$a_{\mathrm{opt}}/\mathrm{mm} = 1.13 \times 10^{-2} \frac{\left(\hat{\phi}/\mathrm{V}\right)^{1/2}}{B_0/\mathrm{T}} \tag{36.38}$$

and

$$\frac{C_{s\ \min}}{a_{\mathrm{opt}}} \approx 0.3 \tag{36.39}$$

The axial chromatic aberration, C_c, may be analysed in a similar fashion. For every value of k^2, C_c is smallest when the object is placed at the centre of the lens. For high magnification, C_c/a varies as shown in Fig. 36.7; it passes through a very shallow minimum around $k^2 = 4$, where $C_c/a = 0.577$. If we seek the half-width that gives the smallest C_c, we find

$$C_{c\ \min}/\mathrm{mm} = 5.85 \times 10^{-3} \frac{\left(\hat{\phi}/\mathrm{V}\right)^{1/2}}{B_0/\mathrm{T}} \tag{36.40}$$

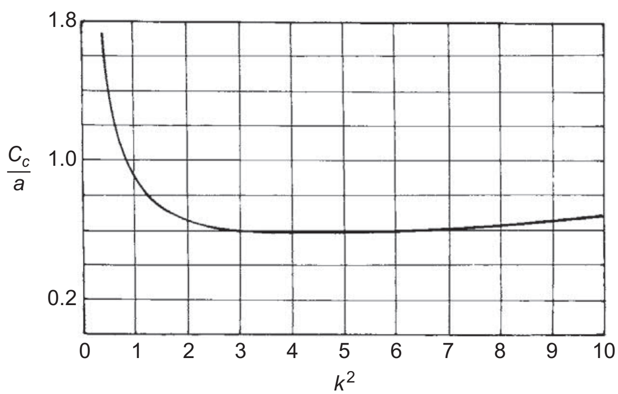

Figure 36.7
Variation of C_c/a with k^2 for Glaser's bell-shaped model. *After Glaser (1952), Courtesy Springer Verlag.*

at

$$a_{\text{opt}}/\text{mm} = 7.4 \times 10^{-3} \frac{\left(\hat{\phi}/\text{V}\right)^{1/2}}{B_0/\text{T}} \tag{36.41}$$

and

$$\frac{C_{c\ \min}}{a_{\text{opt}}} \approx 0.8 \tag{36.42}$$

c. *Asymptotic aberration coefficients*

Since the asymptotic coefficients may be expressed in many different ways, we simply list the fundamental integrals from which all the different forms can be built up with the aid of (25.28–25.31).

For the isotropic aberrations, we need $\int_{-\infty}^{\infty} \Lambda_m G^p \overline{G}^q\, dz$, $p + q = 4$, and $(\eta^2/\hat{\phi}) \int_{-\infty}^{\infty} B^2 dz$, where Λ_m is given by (25.32) and G and $\overline{G}$ by (36.15).

We find

$$\int_{-\infty}^{\infty} \Lambda_m G^4\, dz = \int_{-\infty}^{\infty} \Lambda_m \overline{G}^4\, dz = \frac{1}{8a^3\omega^2}\left(2k^2\,\pi - \frac{\sin 2\omega\pi}{\omega} + \frac{k^2}{4k^2+3}\,\frac{\sin 4\omega\pi}{\omega}\right) \tag{36.43}$$

$$\int_{-\infty}^{\infty} \Lambda_m G^3 \overline{G}\, dz = \int_{-\infty}^{\infty} \Lambda_m G \overline{G}^3\, dz = \frac{1}{32a^3\omega^2}\left(-8k^2\pi\cos\omega\pi + \frac{16k^2+15}{4k^2+3}\,\frac{\sin\omega\pi}{\omega} + \frac{3}{4k^2+3}\,\frac{\sin 3\omega\pi}{\omega}\right) \tag{36.44}$$

$$\int_{-\infty}^{\infty} \Lambda_m G^2 \overline{G}^2\, dz = \frac{1}{24a^3\omega^2}\left(2k^2\pi(2+\cos 2\omega\pi) - 3\frac{2k^2+3}{4k^2+3}\,\frac{\sin 2\omega\pi}{\omega}\right) \tag{36.45}$$

The following auxiliary quantity also occurs in some formulae:

$$\frac{\eta^2}{\hat{\phi}} \int_{-\infty}^{\infty} B^2\, dz = \frac{2\pi\, k^2}{a}$$

For the anisotropic coefficients, the integrals $\int_{-\infty}^{\infty} \Lambda_a G^p \overline{G}^q\, dz$, $p + q = 2$, are required, where Λ_a is defined by (25.32).

$$\int_{-\infty}^{\infty} \Lambda_a G^2\, dz = -\int_{-\infty}^{\infty} \Lambda_a \overline{G}^2\, dz = -\frac{1}{8a^2\omega^2 k}\left[\left\{\pi\, k^2\left(1+2k^2\right) + \left(2+k^2\right)\frac{\sin 2\omega\pi}{2\omega}\right\}\right] \tag{36.46a}$$

$$\int_{-\infty}^{\infty} \Lambda_a G\overline{G}\, dz = \frac{1}{8a^2\omega^2 k}\left\{\pi k^2\left(1+2k^2\right)\cos\omega\pi - \left(2+k^2\right)\frac{\sin\omega\pi}{\omega}\right\} \tag{36.46b}$$

Some high-magnification expressions are listed by Lenz (1956b, 1957).

36.3 Related Bell-Shaped Curves

Some attention has also been paid to the bell-shaped curves of the form

$$B(z) = \frac{B_0}{\left(1+z^2/a^2\right)^n} \tag{36.47}$$

(Glaser, 1941a; Svartholm, 1942; Glaser and Lenz, 1951) and in particular to the cases $n = 3/2$, the field of a single turn (Hutter, 1945; Lenz, 1952; Kanaya, 1955), $n = 2$ (Glaser, 1952; Lenz, 1952) and $n \to \infty$, for which the distribution becomes Gaussian with suitable weighting (Lenz, 1950c, 1952). In this model, a is no longer the half-width at half-height, a_h, which is now given by

$$a_h = a\left(2^{1/n}-1\right)^{1/2} \tag{36.48}$$

The form factor (36.2) is given by

$$\begin{aligned} A &= \frac{1}{L}\int_{-\infty}^{\infty}\frac{dz}{\left(1+z^2/a^2\right)^n} \\ &= \frac{1}{L}\int_{-\infty}^{\infty}\frac{dz}{\left\{1+\left(z^2/a_h^2\right)\left(2^{1/n}-1\right)\right\}^n} \\ &= \frac{a_h}{L}\frac{\Gamma\left(n-1/2\right)\Gamma\left(1/2\right)}{\left(2^{1/n}-1\right)^{1/2}\Gamma(n)} \end{aligned} \tag{36.49}$$

As n becomes very large, the field (36.47) goes over into a Gaussian distribution:

$$B(z) = B_0 \exp\left(-z^2/a^2\right) \tag{36.50}$$

for which the half-width is

$$a_h = a(\ln 2)^{1/2} \tag{36.51}$$

and

$$A = \frac{a_h}{L}\left(\frac{\pi}{\ln 2}\right)^{1/2} = 2.13 \quad \text{for} \quad a_h = L \tag{36.52}$$

(Lenz, 1952).

36.3.1 The Grivet–Lenz Model

Glaser's bell-shaped model has the drawback of falling to zero much more slowly than real fields, far from the lens centre. In 1951, Grivet and Lenz separately proposed a different model (Lenz, 1951; Grivet, 1951, 1952a,b), which tends exponentially to zero for large values of $|z|$ and should describe the field in unsaturated lenses with cylindrical bores satisfactorily. This *Grivet–Lenz model* has the form

$$B(z) = B_0 \operatorname{sech}\left(z/a\right) \tag{36.53}$$

and by writing

$$s = -\tanh\left(z/a\right) \tag{36.54}$$

the paraxial equation becomes

$$\left(1 - s^2\right)\frac{d^2u}{ds^2} - 2s\frac{du}{ds} + \nu(\nu + 1)u = 0 \tag{36.55}$$

where

$$\nu(\nu + 1) = \frac{\eta^2 a^2 B_0^2}{4\hat{\phi}} \tag{36.56}$$

or using (36.2)

$$\nu(\nu + 1) = \frac{\eta^2 \mu_o^2 J^2}{4\hat{\phi}\pi^2} \tag{36.57}$$

Eq. (36.55) is satisfied by the Legendre functions, P_ν and Q_ν, and has the general solution

$$u(s) = K_1 P_\nu(s) + K_2 Q_\nu(s) \tag{36.58}$$

The ray $G(z)$ is now

$$G(z) = P_\nu\left(-\tanh\frac{z}{a}\right) \tag{36.59}$$

from which the real focus and focal length may be obtained. As $z \to \infty$, we find that

$$G(z) \to -\frac{2z \sin \pi\nu}{a\pi} + \cos \pi\nu + \frac{2 \sin \pi\nu}{\pi}(\psi(\nu) + \tilde{\gamma}) \tag{36.60}$$

where $\psi(\nu) = (d/dv) \ln \Gamma(v+1)$ and $\tilde{\gamma} = 0.5772$ is Euler's constant. The asymptotic focal length and foci are therefore given by

$$\frac{a}{f} = \frac{2 \sin \pi\nu}{\pi} = 0.4413 \sin \pi\nu \tag{36.61}$$

and

$$\begin{aligned} \frac{z_{Fi}}{a} &= \frac{2 \sin \pi\nu \left\{\psi(\nu) + \tilde{\gamma}\right\} + \pi \cos \pi\nu}{2 \sin \pi\nu} \\ &= \psi(\nu) + \tilde{\gamma} + \frac{\pi}{2} \cot \pi\nu \end{aligned} \tag{36.62}$$

The Grivet–Lenz distribution is not a Newtonian field but the spherical aberration coefficient can be nevertheless written as a polynomial in object position to a very good approximation (Hawkes, 1970).

36.3.2 The Exponential Model

The other models that lead to a paraxial equation soluble in terms of tabulated functions are of less interest. We mention the exponential field (Rebsch, 1938; Glaser and Lenz, 1951; Worster, 1975) since this has been found useful for 'single-pole' lenses (Section 36.6.1; Marai and Mulvey, 1974; Mulvey, 1982). The field is here described by

$$B(z) = B_0 \exp\left(-z/a\right) \tag{36.63}$$

so that for a conventional lens, the field is useful only for objectives with the specimen well beyond the centre of the gap. Writing

$$a_h := a \ln 2 \quad \bar{u} := u/a_h \quad \zeta = z/a_h \tag{36.64}$$

and (36.6)

$$k^2 = \frac{\eta^2 B_0^2 a_h^2}{4\hat{\phi}}, \quad a_h = L \tag{36.65}$$

the paraxial equation becomes

$$\frac{d^2\bar{u}}{d\zeta^2} + k^2 \exp(-2\zeta \ln 2)\bar{u} = 0 \tag{36.66}$$

We substitute

$$\xi = \frac{k}{\ln 2}\exp(-\zeta \ln 2) \tag{36.67}$$

and obtain the equation satisfied by zero-order Bessel functions,

$$\frac{d^2\overline{u}}{d\xi^2} + \frac{1}{\xi}\frac{d\overline{u}}{d\xi} + \overline{u} = 0 \tag{36.68}$$

The G-ray takes the form

$$G(z) = J_0(\xi) = J_0\left(\frac{k}{\ln 2}\exp\left(-z \ln \frac{2}{a_h}\right)\right) \tag{36.69}$$

and the real image focus therefore occurs at the zero of J_0; for single imaging,

$$z'_{Fi} = \frac{a_h}{\ln 2}\ln\frac{k}{1.667} \tag{36.70}$$

The corresponding focal length is given by

$$\frac{a_h}{f'} = \xi_1 J_1(\xi_1)\ln 2 = 0.8653 \tag{36.71}$$

where $\xi_1 = 2.405$ is the first solution of $J_0(\xi) = 0$. The chromatic aberration coefficient is given by

$$\frac{C_c}{a_h} = \frac{1}{2\ln 2} = 0.72 \quad \text{or} \quad \frac{C_c}{a} = \frac{1}{2} \tag{36.72}$$

For this model, therefore, the high-magnification focal length and chromatic aberration coefficient are independent of the lens-strength parameter, k^2. The same is true of the spherical aberration coefficient:

$$\frac{C_s}{a_h} = \frac{1}{4\ln 2} = 0.36 \quad \text{or} \quad \frac{C_s}{a} = \frac{1}{4} \tag{36.73}$$

(These values of C_s and C_c were first calculated by Lenz and rediscovered by Worster (1975), whose value for C_s is wrong; for a strong lens with multiple foci, the values of C_s and C_c are the same at each focus.)

36.3.3 The Power Law Model

Gianola (1952) and Hänsel (1964) have pointed out that the paraxial equation can be solved in terms of Bessel functions if $B(z)$ has the form

$$B(z) = B_0/z^n \tag{36.74}$$

where n may be any positive or negative number, not necessarily an integer, except unity. As for the exponential field, this model is useful for lenses, such as strong probe-forming and objective lenses, in which only the decreasing ($n > 0$) or only the increasing ($n < 0$) part of the field is employed. The case $n = 3$ has been used by Alshwaikh and Mulvey (1977) to model single-polepiece lenses (Section 36.6.1).

Substituting

$$u(z) = z^{1/2}R(z) \tag{36.75}$$

in the paraxial equation, we obtain

$$R'' + \frac{R'}{z} + \frac{1}{4}\left(\frac{\eta^2 B_0^2}{\hat{\phi}\, z^{2n}} - \frac{1}{z^2}\right)R = 0 \tag{36.76}$$

By writing

$$\zeta = \frac{\eta B_0 z^{1-n}}{2\hat{\phi}^{1/2}(n-1)} \qquad n > 1 \tag{36.77}$$

or

$$\zeta = \frac{\eta B_0 z^{1-n}}{2\hat{\phi}^{1/2}(1-n)} \qquad n < 1$$

(36.76) becomes

$$\frac{d^2R}{d\zeta^2} + \frac{1}{\zeta}\frac{dR}{d\zeta} + \left(1 - \frac{\nu^2}{\zeta^2}\right)R = 0 \tag{36.78}$$

with

$$\nu^2 = 1/4(n-1)^2 \tag{36.79}$$

This is Bessel's differential equation and the paraxial imaging can be investigated in some detail using the properties of Bessel functions. For further details we refer to the original papers cited above, to Lenc (1992) and to Crewe and Kielpinski (1996), Crewe (2001, 2003) and Hawkes (2002), culminating in a discussion by Crewe (2004), who considers $n = 2$, 1, 0, -1, -2, -3 and -4 (cf. Hawkes, 2004); we note that for $n = -1$, the solution is not expressed in terms of Bessel functions. The case $n = 0$ (uniform field) was also considered separately by Crewe (1993, 1995). It can be shown that the real object focal length is equal to (for $n = 2$) or proportional to the coordinate of the real object focus: The chromatic aberration coefficient is proportional to the focal length, $C_c/f = 1/2(n-1)$, cf. Alamir (2004, 2011). The spherical aberration coefficient is also proportional to the focal length but the constant of proportionality is less simple (Lenc, 1992; Hawkes, 2002). Other aspects have been considered by Alamir (2003a,b,c, 2005, 2009a,b).

The linear case

$$B(z) = B_0 + B_1 z \tag{36.80}$$

has also been analysed, as it provides a method of modelling any field shape by linear segments; for details, see Szilágyi (1969, 1970).

36.3.4 The Convolutional Models

Models that are accurate for very small values of S/D can be extended to larger values by assuming that the magnetostatic potential, ψ, $\boldsymbol{H} = -\mathrm{grad}\,\psi$, varies linearly across the gap at the bore radius: $\psi\,(D/2, z) = -Jz/S$ for $|z| \le S/2$. $H(z)$ can then be obtained by convolving the field corresponding to $S/D \to 0$, $H^{(0)}$ say, with a rectangular function equal to $1/S$ in the gap and zero elsewhere (Lenz, 1982):

$$\begin{aligned} H(z) &= \frac{1}{S} \int_{-S/2}^{S/2} H^{(0)}(z-\zeta)d\zeta \\ &= \frac{1}{S}\left\{\psi^{(0)}\left(z - S/2\right) - \psi^{(0)}\left(z + S/2\right)\right\} \end{aligned} \tag{36.81}$$

Typical forms of $H^{(0)}$ and $\psi^{(0)}$ are Gray's model (1939, see Eqs 35.10 and 35.37),

$$\begin{aligned} H^{(0)}(z) &= \frac{\omega J}{D}\mathrm{sech}^2\left(\frac{2\omega z}{D}\right), \quad \omega = 1.318 \\ \psi^{(0)}(z) &= -\frac{J}{2}\tanh\left(\frac{2\omega z}{D}\right) \end{aligned} \tag{36.82}$$

and the Grivet−Lenz model,

$$\begin{aligned} H^{(0)}(z) &= \frac{2\alpha_1 J}{\pi D}\mathrm{sech}\left(\frac{2\alpha_1 z}{D}\right), \quad \alpha_1 = 2.405 \\ \psi^{(0)}(z) &= -\frac{2J}{\pi}\arctan\left(\tanh\left(\frac{\alpha_1 z}{D}\right)\right) \end{aligned} \tag{36.83}$$

Applying Eq. (36.81), the first of these yields

$$H(z) = \frac{J}{S}\,\frac{\sinh\left(2\omega\,S/D\right)}{\cosh\left(2\omega\,S/D\right)+\cosh\left(4\omega\,z/D\right)} \tag{36.84}$$

(Bertram, 1940), which is identical with a model proposed by Lenz (1950b) except that there, α_1 appears rather than 2ω; this was further examined by De (1962). For Eq. (36.83), we find

$$H(z) = \frac{2J}{\pi S}\arctan\left(\frac{\sinh\left(\alpha_1 S/D\right)}{\cosh\left(2\alpha_1 z/D\right)}\right) \tag{36.85}$$

Finally, if we apply the convolution formula (36.81) to the field of a single turn,

$$\begin{aligned} H^{(0)}(z) &= \frac{J\,R^2}{2(R^2+z^2)^{3/2}} \\ \psi^{(0)}(z) &= -\frac{J\,z}{2(R^2+z^2)^{1/2}} \end{aligned} \tag{36.86}$$

we obtain the 'equivalent solenoid lens',

$$H(z) = \frac{J}{2S}\left[\frac{z+S/2}{\left\{R^2+\left(z+S/2\right)^2\right\}^{1/2}} - \frac{z-S/2}{\left\{R^2+\left(z-S/2\right)^2\right\}^{1/2}}\right] \tag{36.87}$$

extensively studied by Durandeau (1956a,b, 1957). For the latter, $H(0) = J/(S^2 + 4R^2)^{1/2}$ and Durandeau finds that this is a good approximation for a lens (S, D) provided that $R = D/3$, at least in the range $0.5 \le S/D \le 2$. The characteristic length L, defined by

$$\begin{aligned} L &:= \left(S^2+4R^2\right)^{1/2} \\ &= \left(S^2+4D^2/9\right)^{1/2} \approx \left(S^2+0.45D^2\right)^{1/2} \end{aligned} \tag{36.88}$$

proves to be a very suitable scaling unit when presenting electron optical properties in a unified fashion. Durandeau finds that the field half-width a_h is quite well represented by

$$a_h = 0.485L \tag{36.89}$$

We may also apply Eq. (36.81) to the magnetic equivalent of (35.5), which corresponds to a lens for which

$$B\left(D/2,z\right) = \begin{cases} \mu_0 J/S & |z| < S/2 \\ 0 & |z| > S/2 \end{cases} \tag{36.90}$$

Setting

$$\psi^{(0)}(z) = \frac{J}{\pi}\int_0^\infty \frac{\sin(tz)}{tI_0(tD/2)}\,dt \tag{36.91}$$

we obtain

$$H(z) = \frac{2J}{\pi S}\int_0^\infty \frac{\sin(tS/D)\cos(2tz/D)}{tI_0(t)}\,dt \tag{36.92}$$

36.3.5 A Generalized Model

The range of field shapes in the above models is comparatively narrow, a fact that led Kanaya et al. (1976) to introduce a more flexible model that nevertheless allows many of the optical properties to be expressed analytically. In this, the magnetic flux is written

$$\begin{aligned} B(z/a) &= B_0\left(1-\mu^2\right)^{(2m-1)/2} \\ \frac{d\mu}{d(z/a)} &= -\left(1-\mu^2\right)^m \end{aligned} \tag{36.93}$$

This includes the Grivet–Lenz model (36.53), $m = 1$ and Glaser's bell-shaped field (36.8), $m = 3/2$. Various other models are closely represented by other values of m: thus the 3/2 power model (36.47 with $n = 3/2$) corresponds to $m = 1.1$, the Gaussian model (36.50) to $m = 0.84$ and the model (36.92) to the range $0.75 \le m \lesssim 1$.

The paraxial equation takes the form

$$\left(1-\mu^2\right)\frac{d^2u}{d\mu^2} - 2m\mu\frac{du}{d\mu} + k^2u = 0, \quad k = \frac{a\eta B_0}{2\hat{\phi}^{1/2}} \tag{36.94}$$

and setting

$$\mu =: 2\xi - 1 \tag{36.95}$$

gives

$$\xi(1-\xi)\frac{d^2u}{d\xi^2} + m(1-2\xi)\frac{du}{d\xi} + k^2u = 0 \tag{36.96}$$

which is a form of the differential equation satisfied by the hypergeometric function ${}_2F_1$, which we denote F:

$$u = AF(\alpha, \beta, m, \xi) + B\xi^{1-m}F(\alpha + 1 - m,\ \beta + 1 - m,\ 2 - m,\ \xi)$$
$$\alpha + \beta + 1 = 2m, \quad \alpha\beta = -k^2 \tag{36.97}$$

The real focal length and the asymptotic focal length and focal distance can be written down explicitly:

$$\frac{f'}{a} = \frac{2m}{\alpha\beta 2^m (1-\mu_i)^m F\big(m-\alpha,\ m-\beta,\ m+1,\ (1-\mu_i)/2\big)} \tag{36.98}$$

in which μ_i corresponds to the real image focus,

$$\frac{f}{a} = -\frac{\Gamma(\alpha)\Gamma(\beta)}{2^{2m-1}\Gamma^2(m)} \tag{36.99}$$

$$\frac{z_{Fi}}{a} = -\frac{\Gamma(m-\alpha-\beta)\Gamma(\alpha)\Gamma(\beta)}{2^{2m-1}\Gamma(1-m+\alpha+\beta)\Gamma(m-\alpha)\Gamma(m-\beta)} \quad m > 1 \tag{36.100a}$$

or

$$\frac{z_{Fi}}{a} = \frac{\pi^{1/2}}{2}\frac{\Gamma(1-m)}{\Gamma\big(3/2-m\big)} - \frac{\Gamma(m-\alpha-\beta)\Gamma(\alpha)\Gamma(\beta)}{2^{2m-1}\Gamma(m)\Gamma(m-\alpha)\Gamma(m-\beta)} \quad m < 1 \tag{36.100b}$$

We note that Eq. (36.97) implies

$$\alpha, \beta = \big(m - 1/2\big)(1 \pm \omega)$$
$$\omega := \left\{1 + \frac{4k^2}{(2m-1)^2}\right\}^{1/2} \tag{36.101}$$

Figs 36.8 and 36.9A show the field distribution and μ as a function of z/a for various values of m and the corresponding cardinal elements as functions of ω. It is also useful to measure the focal lengths in units of half-width, a_h; these are shown in Fig. 36.9B, in which

$$\alpha := a_h/a \tag{36.102}$$

is also plotted. Two other quantities are likewise shown there. The first is the form factor (36.2), $A = \mu_0 J/B_0 a_h$, $L = a_h$, and

$$A = 2.5/\alpha \tag{36.103}$$

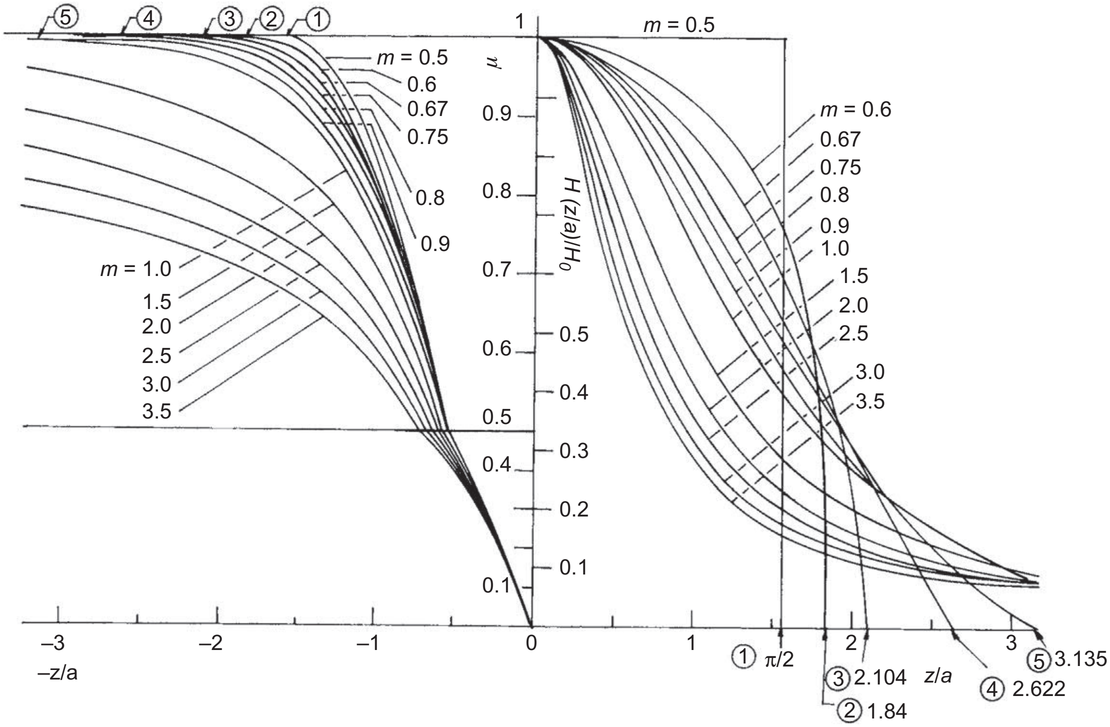

Figure 36.8

The field distribution analysed by Kanaya et al. expressed in terms of μ or $H(z/a)/H_0$. *After Kanaya et al. (1976), Courtesy Wissenschaftliche Verlagsgesellschaft.*

since $\int_{-\infty}^{\infty} Bdz/B_0 = \pi a$. The other is

$$\nu := \frac{B_0 \int\limits_{-\infty}^{\infty} B(z)dz}{\int\limits_{-\infty}^{\infty} B^2(z)dz} = \frac{\int\limits_{-\infty}^{\infty} f(z)dz}{\int\limits_{-\infty}^{\infty} f^2(z)dz} = \frac{\pi^{1/2}\Gamma(m+1/2)}{\Gamma(m)} \tag{36.104}$$

Much of the paper by Kanaya et al. (1976) is concerned with the case in which the real object focus lies at the centre of the lens, $z'_{Fo} = 0$ corresponding to $\mu = 0$. It can be shown that for this case, k and hence ω are related in a very simple way to m. For, consider the ray incident parallel to the axis in object space,

$$G(z) \propto F\big(\alpha, \beta, m, (1-\mu)/2\big), \quad \alpha, \beta = \big(m - 1/2\big)(1 \pm \omega) \tag{36.105}$$

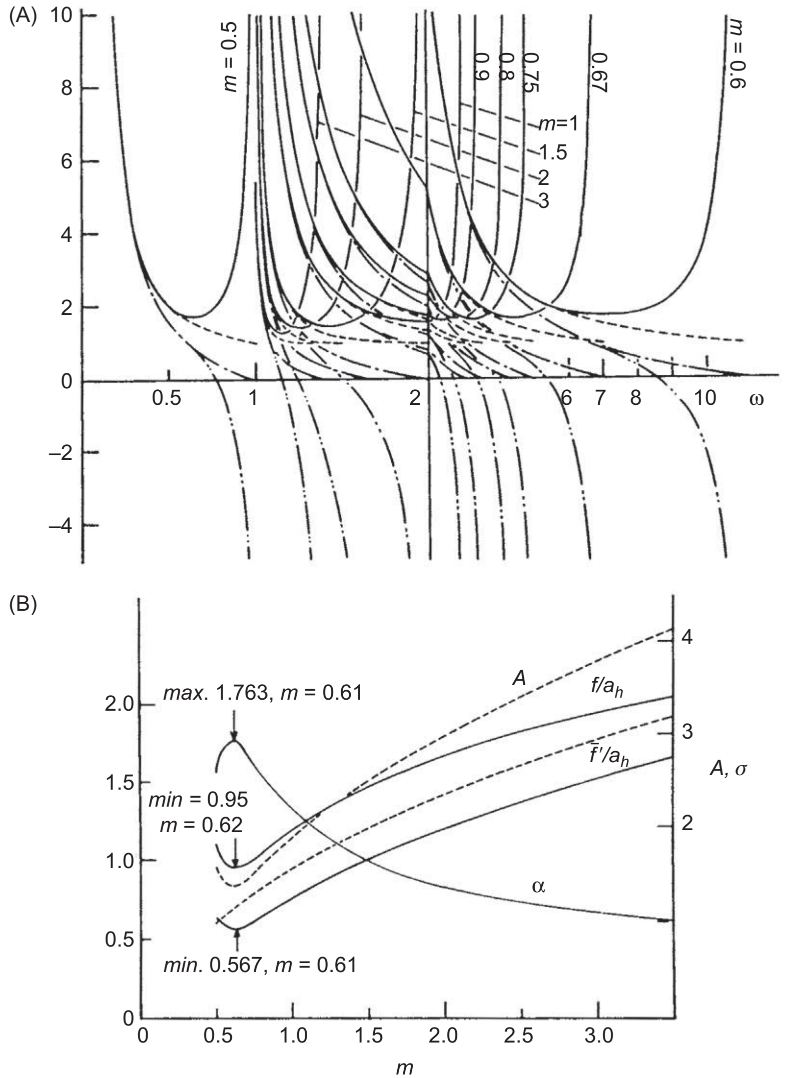

Figure 36.9

(A) Real and asymptotic cardinal elements as a function of the parameter ω for several values of *m*. Full line: f/a; ---:f'/a; --·: z'_{Fi}/a - · -: z_{Fi}/a. (B) Real and asymptotic focal lengths together with $A := J/H_0 a_h$, $\alpha = 2.5/A$ and $\sigma := H_0 \int_{-\infty}^{\infty} H(z)dz \,/\, \int_{-\infty}^{\infty} H^2(z)\, dz$ as a function of *m*.
After Kanaya et al. (1976), Courtesy Wissenschaftliche Verlagsgesellschaft.

If this ray is to intersect the axis at $\mu = 0$, then

$$F\left(\alpha, \beta, m,\ 1/2\right) = 0 \tag{36.106}$$

But from Eq. (36.97) we see that $m = (\alpha + \beta + 1)/2$, and for this case the hypergeometric function may be written as

$$\frac{\Gamma\left(\dfrac{\alpha+\beta+1}{2}\right)\Gamma\left(\dfrac{1}{2}\right)}{\Gamma\left(\dfrac{\alpha+1}{2}\right)\Gamma\left(\dfrac{\beta+1}{2}\right)}$$

or

$$\frac{\Gamma(m)\Gamma\left(1/2\right)}{\Gamma\left(\dfrac{2m+1+(2m-1)\omega}{4}\right)\Gamma\left(\dfrac{2m+1-(2m-1)\omega}{4}\right)}$$

The gamma function has simple poles when its argument is equal to a negative integer or zero and so Eq. (36.106) is satisfied if

$$2m + 1 - (2m-1)\omega = 0$$

or

$$\omega = \frac{2m+1}{2m-1} \tag{36.107a}$$

or again

$$k^2 = 2m \tag{36.107b}$$

For this case, Kanaya et al. find that C_s and C_c can be evaluated explicitly:

$$\begin{aligned}
\frac{C_s}{a_h} &= m\frac{2^{3(2m-1)}\Gamma^2(3m)}{2\alpha(6m+1)\Gamma(6m)}\left(\frac{34m-1}{3m-1} + 5\frac{2m-1}{3m-2}\right)\\
\frac{C_c}{a_h} &= m\frac{2^{2m-1}\Gamma^2(m)}{\alpha(2m+1)\Gamma(2m)}
\end{aligned} \tag{36.108}$$

As $m \to \infty$, $C_s/a_h \to 0.291$ but $C_s(m)$ does not pass through a minimum: there is no optimum value of m so far as C_s is concerned. C_s/a_h does, however, pass through a minimum at $m = 0.62$, the value for which the minimum projector focal length is also least: $(f/a_h)_{\min} = 0.95$ for $m = 0.62$. Unfortunately, the corresponding field shape is hardly realistic.

In the remainder of this paper, Kanaya et al. plot trajectories as a function of z and cardinal elements and the principal aberration coefficients as functions of excitation for numerous values of m: $m = 1/2$, the rectangular or top-hat field; $m = 0.62$; $m = 0.75$, corresponding to

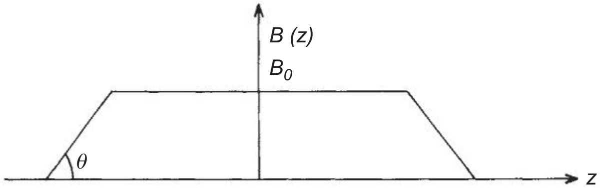

Figure 36.10
The trapezoidal model, which tends to the rectangular model as $\theta \to \pi/2$.

Eq. (36.92); $m = 0.84$, the Gaussian field; and $m = 2$, a broad field corresponding to a saturated lens. For the case $m = 1/2$, however, they obtain a finite value for C_s, which cannot be correct since for the rectangular model, $B'(z)$ reduces to a pair of δ-functions, and these are not square-integrable. (The behaviour of the rectangular model has indeed been an intermittent source of confusion. Thus Lenz (1950a), for example, wrote 'Eine Berechnung von $C_ö/d$ war für die Kastenkurve nicht möglich, da das Integral [for $C_s \equiv C_ö$] in diesem Fall über alle Grenzen wächst'[2] and confirmed this (Lenz, 1950d) by evaluating C_s for a trapezoidal field (Fig. 36.10). But in 1957, Durandeau stated 'Le calcul effectué pour un champ uniform aboutit aux resultats suivants: pour $\omega L > \pi/2$, $C_c = C_s$, pour $\omega L < \pi/2$, $C_c = C_s \sin^2 \omega L$. Les valeurs qui en résultent ne concordent pas avec les valeurs calculées...'.[3] The correct result is again stated by Tretner (1959: '...ist die Öffnungsfehlerkonstante gleich Unendlich ...'.[4]) and Hawkes (unpublished) has shown that for a rectangular field terminated by half-bells, $C_s \to \infty$ as the half-widths of the latter are reduced to zero. For more discussion, see Dodin and Nesvizhskii (1980)).

36.3.6 Unsymmetric Lenses

The only model that can be extended to unsymmetric lenses while allowing the trajectory equation to be solved explicitly is Glaser's bell-shaped field with different half-widths for $z < 0$ and $z > 0$ (Glaser, 1941a; Dosse, 1941a). Although this poses no problem so far as the paraxial quantities are concerned, care is needed when evaluating the aberration integrals because the second and higher order derivatives of $B(z)$ are discontinuous at the origin. For full details, we refer to the original articles or to Glaser (1952, Section 106). Fig. 36.11 shows C_s and C_c as functions of the excitation parameter $k^2 = \eta^2 B_0^2 a_i^2 / 4\hat{\phi}, B(z) = B_0/(1 + z^2/a_i^2)$ for $z > 0$. These curves are misleading, however, for the 'pinhole' lens (Liebmann, 1955a; Yanaka and Watanabe, 1966; Yada and Kimura, 1982), in which $D_1 \ll D_2$, has a rather low spherical aberration for given excitation since the condenser-side polepiece creates a 'mirror

[2] Calculation of $C_ö/d$ for the rectangular model is not possible since the integral [for $C_s \equiv C_ö$] increases beyond all bounds for this case.
[3] A calculation using the rectangular model leads to the following results: for $\omega L > \pi/2$, $C_c = C_s$, for $\omega L < \pi/2$, $C_c = C_s \sin^2 \omega L$. The resulting values do not agree with the calculated values.
[4] The spherical aberration constant becomes infinite.

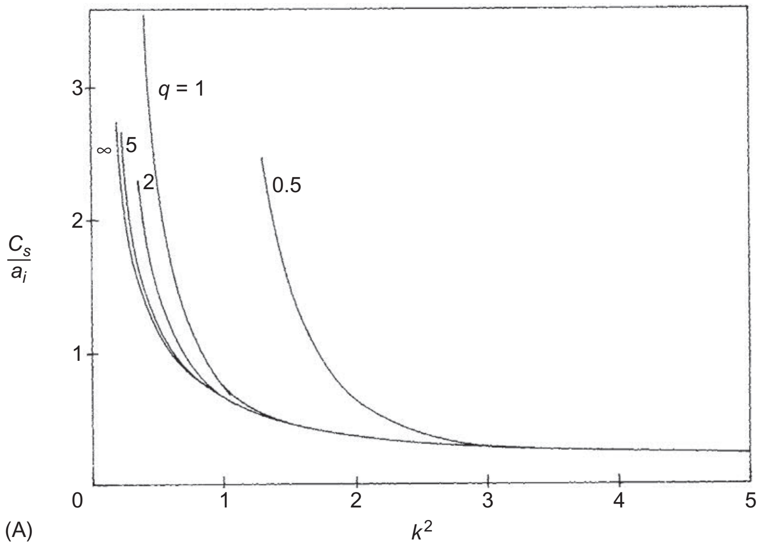

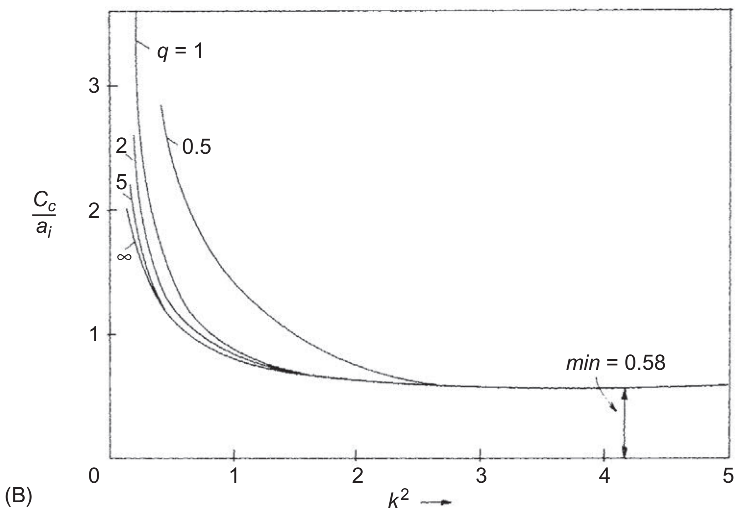

Figure 36.11

The asymmetric bell-shaped model. (A) C_s/a as a function of k^2. (B) C_c/a as a function of k^2. The parameter q is equal to a_o/a_i, where a_o and a_i are the object- and image-side values of a, and k^2 corresponds to a_i. *After Glaser (1952), Courtesy Springer Verlag.*

field'. Yada and Kawakatsu (1976) have tested such lenses experimentally in a methodical study of very asymmetric lenses, in which the cases $D_1 > D_2$ and $D_1 < D_2$ are both explored. When D_2 is smaller than D_1, they find that C_s decreases with D_2 for fixed D_1 and given excitation until a minimum is reached, beyond which C_s increases rapidly (Fig. 36.12A). When the bore D_1 is the smaller, C_s falls with excitation and the smaller the value of D_1, the more rapid is the initial decrease of C_s (Fig. 36.12B); among a number of extremely small

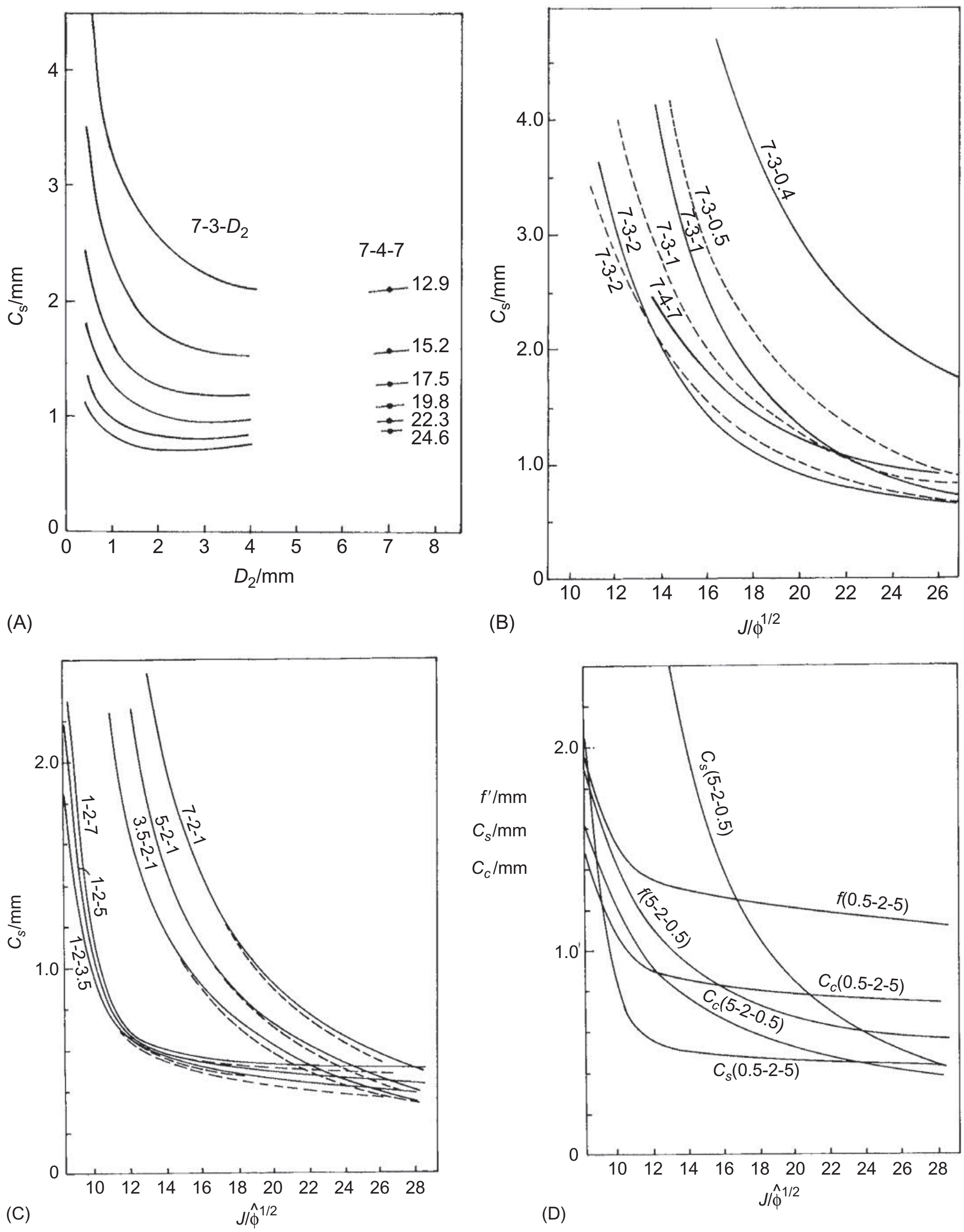

Figure 36.12

Measured and computed values of f', C_s and C_c for strongly asymmetric lenses, characterized by their values of D_1—S—D_2. (A) C_s as a function of D_2 for 7—3—D_2 lenses for various values of $J/\phi^{1/2}$ and also C_s for a 7—4—7 lens. (B) C_s as a function of excitation for several lenses for which $D_3 \leq D_1$. Full line: measured values; broken line: calculated values. (C) Computed values of C_s as a function of excitation with (full line) and without (broken line) saturation. (D) C_s, C_c and f'as a function of excitation, allowing for saturation, for several geometries at 100 kV. *After Yada and Kawakatsu (1976), Courtesy Japanese Society of Electron Microscopy.*

lenses studied, the geometry $D_1 = 1$ mm, $S = 1.5$ mm, $D_2 = 2$ mm gave the low value of $C_s \approx 0.3$ mm at 100 keV, $J/\hat{\phi}^{1/2} = 23.4$ A-t/V$^{1/2}$.

Various other models mentioned earlier in this section can be modified to represent asymmetric fields. Thus Eq. (36.87) (Durandeau, 1957) can be replaced by

$$B(z) = \frac{\mu_0 J}{2S}\left[\frac{z+S/2}{\left\{D_1^2/9+(z+S/2)^2\right\}^{1/2}} - \frac{z-S/2}{\left\{D_2^2/9+(z-S/2)^2\right\}^{1/2}}\right] \tag{36.109}$$

and (36.84) by

$$B(z) = \kappa\left[1+\tanh\left\{\frac{\alpha_1 S}{2D_1}\left(1+\frac{2z}{S}\right)\right\}\left\{1+\tanh\frac{\alpha_1 S}{2D_2}\left(1-\frac{2z}{S}\right)\right\}\right] \tag{36.110}$$

in which κ is chosen so that $\int_{-\infty}^{\infty} B\,dz = \mu_0 J$; the approximation

$$\kappa = \frac{\mu_0 J}{2S}\frac{1-\exp(-2\alpha_1 S/D)}{1+0.379\{(D_1-D_2)/(D_1+D_2)\}\exp(-\alpha_1 S/D)} \tag{36.111}$$

is accurate to within 0.6% for all values of S, D_1 and D_2. However, the simpler model (Lenz, 1982)

$$B(z) = \frac{\mu_0 J}{2S}\left[\tanh\left\{\frac{\alpha_1 S}{2D_1}\left(\frac{2z}{S}+1\right)\right\} - \tanh\left\{\frac{\alpha_1 S}{2D_2}\left(\frac{2z}{S}-1\right)\right\}\right] \tag{36.112}$$

is indistinguishable from Eq. (36.110) as Fig. 36.13 shows.

36.3.7 Hahn's Procedure

We have already mentioned the theory proposed by E. Hahn, in which the Cartesian coordinate z along the optic axis is replaced by a new variable ω, defined in terms of a pair of linearly independent solutions of the paraxial equations. The optic axis is thereby mapped into a finite range of ω, and in his fundamental paper, Hahn (1965a) gives a full study of the cardinal elements and aberration coefficients of magnetic and electrostatic lenses. It transpires that the Glaser bell-shaped field Eq. (36.8) is the simplest of the model fields to which this theory leads, though the theory is in no sense confined to this model. In a related paper (Hahn, 1965b), these ideas are applied to magnetic lenses explicitly, and in particular to the bell-shaped field and to the distribution (36.90) corresponding to a uniform field across the gap at the bore radius (the *Stufenfeld*). We now rehearse the main steps of Hahn's reasoning, though the theory seems to be of more use in the otherwise difficult situations that occur in mirrors and cathode lenses.

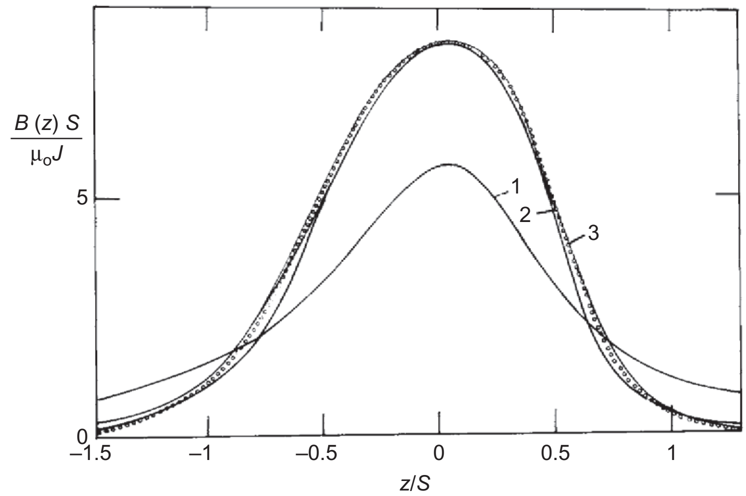

Figure 36.13
Comparison of field models for an asymmetric lens with $S/D = 1$, $D_2/D_1 = 1.5$, $D = (D_1 + D_2)/2$. 1: Glaser's bell-shaped model with different half-widths. 2: Durandeau's model (36.109). 3: Lenz's model (36.112). The dots are the result of an exact calculation. *After Lenz (1982), Courtesy Springer Verlag.*

We set out from the paraxial equation (36.4), which it is convenient to write as Eq. (36.6)

$$\frac{d^2u}{d\zeta^2} + k^2 f^2(\zeta)u = 0$$

$\zeta := z/L$, $\zeta_m := z_m/L$ and $B(\zeta)/B_m =: f(\zeta)$ where L is an arbitrary length and z_m is the plane in which $B(\zeta)$ reaches its maximum value. Let $p(\zeta)$ be a positive-definite quadratic form in two linearly independent solutions of (36.6), such that $p(\zeta_m) = 1$ and $p'(\zeta_m) = 0$. We now introduce the transformation upon which all Hahn's work reposes:

$$\omega(\zeta) := \frac{\mu L}{\hat{\phi}^{1/2}} \int_{-\infty} \frac{d\zeta}{p(\zeta)} - \frac{\pi}{2} \qquad (36.113)$$
$$\omega(\infty) := \pi/2$$

so that

$$\pi = \frac{\mu L}{\hat{\phi}^{1/2}} \int_{-\infty}^{\infty} \frac{d\zeta}{p(\zeta)} \qquad (36.114)$$

The value of the normalizing constant μ will be defined later. We also introduce a function $y(\zeta)$,

$$y^2 = 1/p \qquad (36.115)$$

and write

$$f(\zeta) =: H(\omega)\frac{d\omega}{d\zeta} = \frac{\mu L}{\hat{\phi}^{1/2}} H(\omega) y^2 \tag{36.116}$$

After some calculation, it can be shown that the paraxial equation implies that $y(\omega)$ must satisfy the equation

$$\frac{d^2y}{d\omega^2} + \left\{\frac{\lambda^2}{\mu^2} - k^2H^2(\omega)\right\} y = 0 \tag{36.117}$$

with the boundary conditions

$$y\big(-\pi/2\big) = y\big(\pi/2\big) = 0 \tag{36.118}$$

This is an eigenvalue equation; $y(\omega)$ and the eigenvalue $(\lambda/\mu)^2$ are uniquely determined by the conditions

$$y(\omega_m) = 1, \quad y(\omega) > 0 \quad \text{for } -\pi/2 < \omega < \pi/2 \tag{36.119}$$

We know that $f(\zeta_m) = 1$ and if we impose the condition $H(\omega_m) = 1$, Eq. (36.116) determines the normalization constant μ:

$$\mu L/\hat{\phi}^{1/2} = 1 \tag{36.120}$$

It remains to establish $p(\zeta)$ and λ. If $u_1(\zeta)$ and $u_2(\zeta)$ are two linearly independent solutions of (36.6) such that $u_1(\zeta_m) = \big[du_2/d\zeta\big]_{\zeta_m} = 0$ and $\big[du_1/d\zeta\big]_{\zeta_m} = u_2(\zeta_m) = 1$, then Eqs (36.113) and (36.120) yield

$$\begin{aligned} u_1(\zeta) &= \frac{\mu}{\lambda} p^{1/2} \sin\big\{\lambda(\omega - \omega_m)/\mu\big\} \\ u_2(\zeta) &= p^{1/2} \cos\big\{\lambda(\omega - \omega_m)/\mu\big\} \end{aligned} \tag{36.121}$$

from which we see that

$$p(\zeta) = u_2^2 - \frac{\lambda^2}{\mu^2} u_1^2 \tag{36.122}$$

We shall not reproduce the reasoning that gives λ but simply state the result. Writing

$$\frac{\lambda'\pi}{\mu'} := \int\limits_{-\infty}^{\infty} \frac{d\zeta}{u_1^2 + u_2^2}, \quad \lambda' := \hat{\phi}^{1/2}/L \tag{36.123}$$

it can be shown that for $\lambda'\mu'$ equal to an integer n, then $\lambda = n\mu$; if $n < \lambda'/\mu' < n+1$, then λ/μ likewise lies between n and $n+1$, and the exact value of λ must be found from a not unduly complicated transcendental equation.

Suppose now that $H(\omega) = 1$, the simplest possible hypothesis. Then

$$\frac{d^2y}{d\omega^2} + \left(k^2 - \lambda^2/\mu^2\right)y = 0 \tag{36.124}$$

and the conditions (36.118) will be satisfied only if

$$y(\omega) = \cos\omega, \quad \lambda/\mu = \left(1+k^2\right)^{1/2} \tag{36.125}$$

Hence

$$\zeta = \tan\omega \tag{36.126}$$

and so

$$p(\omega) = \sec^2\omega, \quad p(\zeta) = 1+\zeta^2 \tag{36.127}$$

and finally

$$f(\zeta) = \frac{1}{1+\zeta^2} \tag{36.128}$$

Thus $H(\omega) = 1$ corresponds to the Glaser bell-shaped field. More original is the field for which

$$f(z) = \begin{cases} \dfrac{1}{1-2T(S/D)}\left\{T\left(\dfrac{2z+S}{D}\right) - T\left(\dfrac{2z-S}{D}\right)\right\} & -\infty \le z \le -S/2 \\ \dfrac{1}{1-2T(S/D)}\left\{1 - T\left(\dfrac{2z+S}{D}\right) - T\left(\dfrac{2z-S}{D}\right)\right\} & -S/2 \le z \le S/2 \\ \dfrac{1}{1-2T(S/D)}\left\{T\left(\dfrac{2z-S}{D}\right) - T\left(\dfrac{2z+S}{D}\right)\right\} & S/2 \le z \le \infty \end{cases} \tag{36.129}$$

where

$$T(x) := \sum_{k=1}^{\infty} \frac{J_0\left(\lambda_k D/2\right)}{\lambda_k J_1(\lambda_k)} e^{-\lambda_k|x|} \tag{36.130}$$

corresponding to a uniform field at the gap. The function $H(\omega)$ must now be obtained numerically; some examples of $H(\omega)$ and $y(\omega)$ are reproduced in Fig. 36.14 for various values of *S/D*.

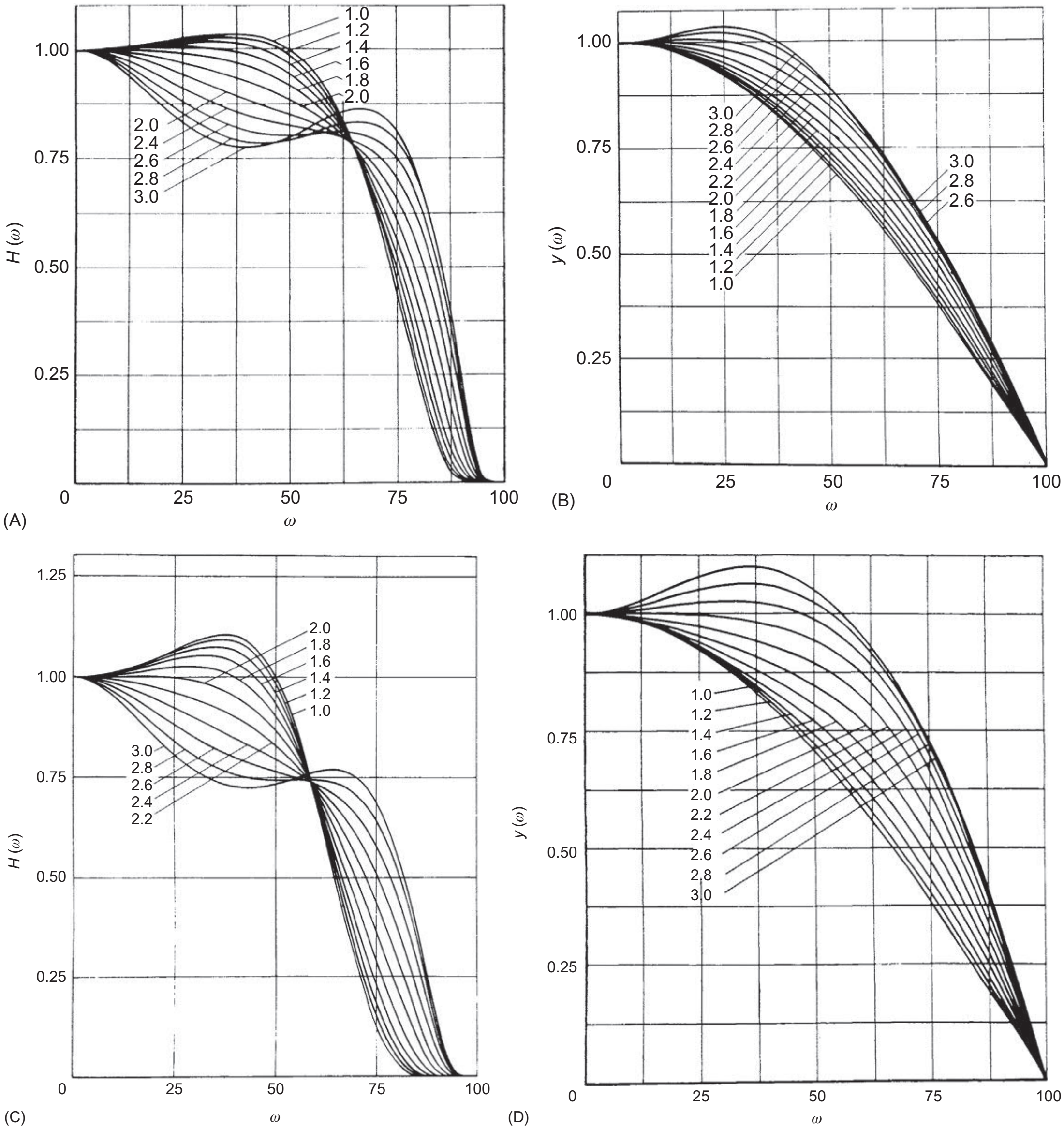

Figure 36.14

Hahn's procedure. (A) $H(\omega)$ and (B) $y(\omega)$ for the case $D = 0$. (C) $H(\omega)$ and (D) $y(\omega)$ for $S/D = 1$. (E) $H(\omega)$ and (F) $y(\omega)$ for $S/D = 2$. The parameter is $(1 + k^2)^{1/2}$. *After Hahn (1965b), Courtesy Deutscher Verlag der Wissenschaften.*

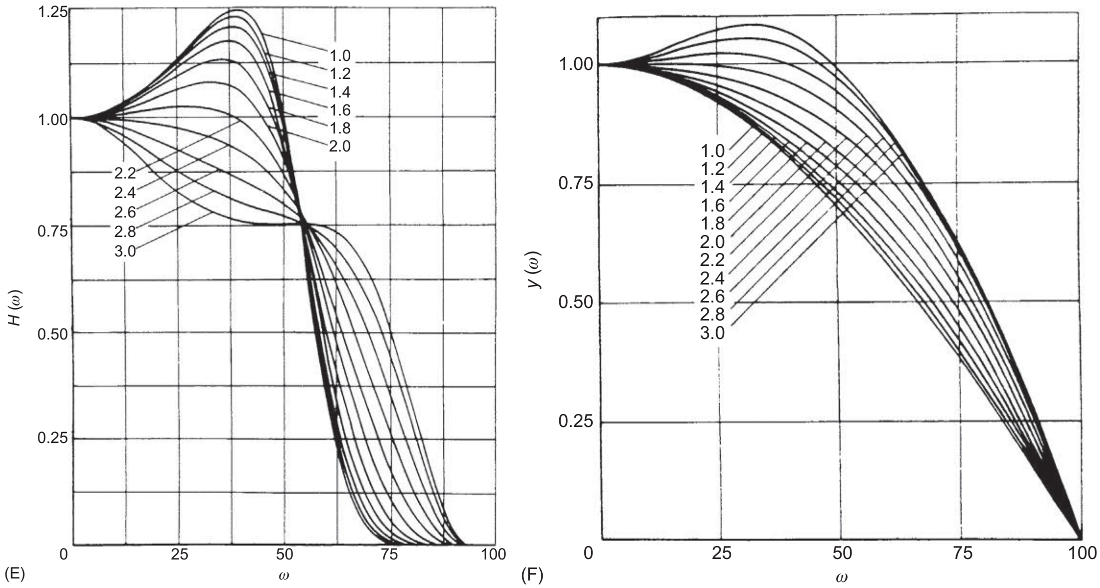

Figure 36.14
(Continued).

The asymptotic cardinal elements can be written down directly (Hahn, 1965a):

$$\frac{\mu}{\hat{\phi}^{1/2}} f = -\frac{(\lambda/\mu)\ \mathrm{cosec}\ (\lambda\pi/\mu)}{\dot{y}(-\pi/2)\dot{y}(\pi/2)}$$

and

$$\frac{\mu}{\hat{\phi}^{1/2}}(z_F - z^*) = \frac{(\lambda/\mu)\ \cot\ (\lambda\pi/\mu)}{\dot{y}^2(\pi/2)} \qquad (36.131)$$

in which $\dot{y}$ denotes $dy/d\omega$. For the bell-shaped field, $\dot{y}(-\pi/2) = -\dot{y}(\pi/2) = 1$, $\lambda/\mu = (1 + k^2)^{1/2}$ and $\mu L/\hat{\phi}^{1/2} = 1$. For other symmetric and normalized field functions $H(\omega)$, we need to know the three 'correction functions' $\lambda/\mu(1 + k^2)^{1/2}$, $\dot{y}^2(\pi/2)$ and z^*. Hahn has calculated these as functions of $(1 + k^2)^{1/2}$ for a range of values of S/D.

36.3.8 Other Models

In an attempt to find a unified representation of the many values of the spherical aberration coefficient, Crewe (1991) considered the parabolic lens, $B(z) = B_0(1 - 4z^2/L^2)$ and the cosine lens $B(z) = B_0\cos(\pi z/L)$ as well as the exponential and bell-shaped models. For the parabolic lens, L denotes the distance between the zeros of $B(z)$ and for the cosine model, $B(z)$ is zero outside the zone $|z| \leq L/2$. Crewe proposes

$$C_s = 5f\left(\frac{f}{L}\right)^2 + \rho_3 f\left(\frac{f}{L}\right) + \rho_4 f + \rho_5$$

where the factors ρ_i are shape factors.

36.4 Measurements and Universal Curves

36.4.1 Introduction

Useful as these various models may be for gaining a preliminary understanding of lens behaviour, the next stage in practical lens design must be the calculation or measurement of the characteristics of interest of real lenses. For methods of measuring these, we refer to the textbooks of Grivet (1972) and Klemperer and Barnett (1971) and to Kunath and Riecke (1965/66), Heinemann (1971) and Hanai et al. (1986). For lenses of conventional design, suffering from little or no saturation in the yoke and polepieces, a considerable body of calculated and measured data is now available and most of the details of the lens behaviour can be reliably predicted on the basis of this information. Nevertheless, it is always wise to recalculate the properties once a design has been selected if the lens is to be used in any but the most conservative mode of operation. This is particularly necessary in the case of strong objective or probe-forming lenses, in which the specimen or target is immersed deep within the lens, which must hence be characterized by two sets of optical properties: those of the part of the field preceding the specimen, which belongs to the condenser system in the image-forming mode or is the final demagnifying lens in the probe-forming mode; and those of the part of the field beyond the specimen, which is the objective lens in the first case or part of the intermediate-projector sequence in a transmission probe-forming instrument such as a STEM. Such a calculation is a wise precaution too if, as is usually the case, some parts of the magnetic circuit are close to saturation.

It is distinctly less easy to present unified information for lenses in which the polepieces have deliberately been allowed to saturate. In the absence of saturation, quite reliable universal curves can be obtained, but once saturation sets in, the situation is very different. We can make general remarks and a reasonable amount of accurate computed information has now been published but unless the lens of interest closely resembles one of those already studied, it is prudent to make a fresh calculation.

36.4.2 Unsaturated Lenses

Curves showing f'/D and z'_F/D for objective lenses and f/D for projectors as a function of $J^2/\hat{\phi}$ for a wide range of values of S/D, based on measured field distributions, were published as early as 1947 by van Ments and Le Poole (reproduced in Hawkes, 1982, Appendix I), but the first extensive sets of magnetic lens design curves did not appear until the early 1950s (Liebmann and Grad, 1950, 1951; Liebmann, 1955b); the latter relied on fields given by an analogue device (a resistance network, see Francken (1967) for an account of these). Their results were widely used until computers became available, whereupon more accurate values were established (see Mulvey and Wallington (1969, 1973) for much discussion of this). However, Liebmann's curves are important in that he established that 'universal' curves can be found for many of the optical properties. By scaling the focal lengths, focal distances and C_s with respect to $(S+D)$ or $\{S+(D_1+D_2)/2\}$, he managed to 'unify' the resulting curves with reasonable success.

Not long after, Durandeau and Fert (1957) and Dugas et al. (1961) published two detailed accounts of magnetic lens design, the first confined to symmetric lenses, the second covering both symmetric and unsymmetric geometries. Their design curves show the real and asymptotic focal lengths and focal distances as functions of J/J_0, where J_0 is the excitation corresponding to the minimum projector focal length, which is chosen as the unit of length. A separate curve relates this minimum focal length to J_0 and to S/D; this demonstrates that although scaling with respect to $S+D$, as adopted by Liebmann, gives a constant value of focal length for $D/S>1$, the scaling factor L (36.88) is better, giving a constant value of f/L for $0.5<D/S<\infty$, in which range it is equal to 0.5. In the same range, $J_0/\hat{\phi}^{1/2}$ is also constant and equal to 13.5 A-t/V$^{1/2}$. Durandeau and Fert (1957) also plot $C_c/f_{\min}$ and $C_s/f_{\min}$ for $D=S$ as functions of J/J_0 and mention that their results do not agree with those given by the rectangular model, $B(z)=\mu_0 J/L$, $|z|<L/2$, $B(z)=0$ otherwise. As explained earlier, this model cannot be used to calculate C_s. These curves are extended in Dugas et al. (1961) to cover a wider range of values of D/S for C_s and to include unsymmetric lenses, $D_1 \neq D_2$. Some of this work is surveyed by Fert and Durandeau (1967).

The real field distributions in unsymmetric lenses below saturation have been very thoroughly investigated by Juma and Yahya (1984). From among their many results, we mention their confirmation of Dugas's empirical formula for the maximum axial field, $B_m=\mu_0\, J/L$ where $L=\{S^2+0.45(D_1+D_2)^2/4\}^{1/2}$, for a wide range of asymmetry. We also give their expressions for the half-widths (a_1, a_2) of the two halves of the field distribution:

$$\frac{a_1}{a_2}=\left(\frac{D_1}{D_2}\right)^{0.55} \quad \text{for } s \geq D_1/D_2 \geq 0.5$$

$$\frac{a_1}{a_2}=1.3\frac{D_1}{D_2} \quad \text{for } \frac{D_1}{D_2}<0.5$$

Useful though these curves are, they can be misleading if not used with care for the lens must not be allowed to run into saturation. The necessary conditions that must be satisfied are clearly stated in Durandeau and Fert (1957) but a distinct improvement in the presentation of the lens properties was made in 1968 by Kamminga et al. (1968, 1968/69) and Brookes et al. (1968), who incorporated the maximum magnetic flux between the polepieces (not that on the axis, B_0). Writing

$$B_m \coloneqq \mu_0 J/S, \quad K \coloneqq J^2/\hat{\phi} \tag{36.132}$$

Kamminga et al. plot the objective cardinal elements, C_s and C_c, scaled with respect to D, as functions of S/D for various values of K. Setting

$$\frac{C_s}{D} =: g(K, S/D) \tag{36.133}$$

and replacing D by

$$D = \frac{\mu_0 \hat{\phi}^{1/2} K^{1/2}}{B_m (S/D)} \tag{36.134}$$

we find

$$C_s = \frac{\mu_0 \hat{\phi}^{1/2}}{B_m} g(K, S/D) \frac{K^{1/2}}{S/D} \tag{36.135}$$

and the resolution parameter (see Section 66.4 in Volume 3),

$$d \coloneqq \left(C_s \lambda^3\right)^{1/4} \tag{36.136}$$

becomes

$$d = \left\{ \frac{g(K, S/D) K^{1/2}}{\hat{\phi} B_m (S/D)} \right\}^{1/4} \tag{36.137}$$

For the highest resolution, therefore, $\hat{\phi}$ and B_m should be as high as is compatible with the physical limits while $g(K, S/D)K^{1/2}\, D/S$ should be as small as possible. It is therefore extremely convenient to display the function

$$\frac{C_s B_m}{\mu_0 \hat{\phi}^{1/2}} \equiv \frac{g(K, S/D) K^{1/2}}{S/D} \tag{36.138}$$

as a function of S/D for various values of K. This function is shown in Fig. 36.15A, while Fig. 36.15B shows contours of constant $\{g(K, S/D)K^{1/2}\, D/S\}^{1/4}$, to which d is proportional, in the $K - S/D$ plane. Having selected a suitable region of the latter, K and S/D can be chosen in such a way that C_c is also small and that the illumination is as it should be.

This presentation is superior to more conventional analyses in that the real field B_m occurs rather than the maximum axial field B_0. If the relation between these is taken into account,

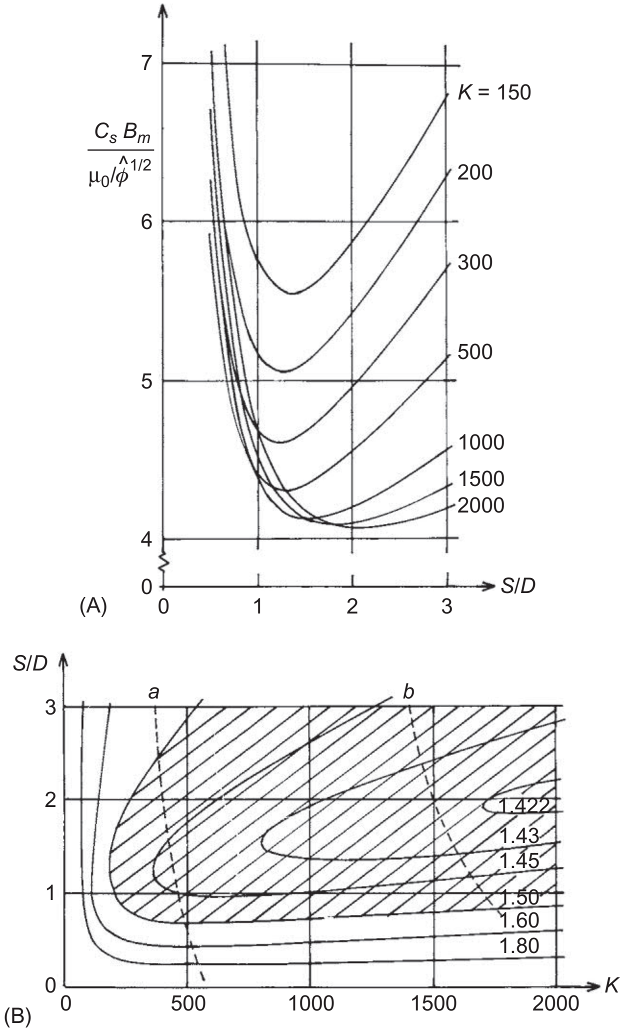

Figure 36.15

(A) The dependence of $C_sB_m/\mu_0\hat{\phi}^{1/2}$ on S/D for various values of $K := J^2/\hat{\phi}$. (B) Contours of constant $(C_sB_m/\mu_0\hat{\phi}^{1/2})^{1/4}$ in the S/D-K plane. In the shaded region, $(C_s\,B_m/\mu_0\hat{\phi})^{1/4} \leq 1.5$. The dotted lines a and b indicate values of S/D and K for which the illumination is correct. *After Kamminga et al. (1968/9), Courtesy Wissenschaftliche Verlagsgesellschaft.*

the results are of course the same. Kamminga et al. give the following values for this relation:

S/D	0.25	0.5	0.75	1	1.5	2	3
B_0/B_m	0.32	0.57	0.73	0.83	0.93	0.96	0.97

Similar information is presented graphically by Zelev (1982), who measured B_0 as a function of J/S for 11 different sets of values of S and D (or D_1 and D_2); the polepieces were for the most part of Permendur, though some examples of Permalloy are included. Curves showing B_0 as a function of S/D for various values of J/S, for Permendur and two varieties of Permalloy are also presented, together with graphs of the half-width of the field, a_h, plotted against S/D for values of S ranging from 1 to 10 mm. The latter are obtained from the extended bell-model (Section 36.3 and Glaser, 1952, Eq. 81.7):

$$\frac{a_h}{S} = \frac{1}{f_1(\nu)\tanh\left(\alpha S/2D\right)} \tag{36.139}$$

where α is the first zero of the zero-order Bessel function J_0 and $f_1(\nu) = \{\pi/(2^{1/2} - 1)\}^{1/2}\ \Gamma(n - 1/2)/\Gamma(n)$; n is defined in Section 36.3. The few measured values included by Zelev agree well with his analysis.

An alternative representation, which is also very convenient in practice, uses as abscissa not the absolute excitation but the ratio of J to J_0, where J_0 is the excitation for which the relative projector focal length, f/S, is smallest. Figs 36.16A–E form a most useful set of working curves for practical lens design, while Fig. 36.16F shows how the minimum values of $C_sB_m/\hat{\phi}^{1/2}$ and $C_cB_m/\hat{\phi}^{1/2}$ vary with S/D.

All these questions have been re-examined by Lenz (1982), who gives sets of curves for the various paraxial quantities as well as the chromatic and third-order geometric aberration coefficients. Here Durandeau's unit of length $L = (S^2 + 0.45D^2)^{1/2}$ is adopted as scaling factor, raised to an appropriate power (C_s/L, for example, but FL and AL for field curvature and astigmatism, and DL^2 for distortion). The abscissa is κ/κ_t, where κ is defined by Eq. (36.7) and κ_t is the value of κ for which the projector lens action is telescopic, or in other words the projector focal length becomes infinite. These curves are reproduced as Figs 36.17A–D.

Also during the 1960s, the values of the spherical aberration coefficient were established for finite magnification for a wide range of S/D by Der-Shvarts and Makarova (1966, with major corrections in 1976). These findings were subsequently extended to include the other geometric aberrations (Der-Shvarts and Makarova, 1972). The same authors have obtained convenient approximate formulae for the aberration coefficients as a function of magnification (Der-Shvarts and Makarova, 1967, 1972, 1973; Der-Shvarts, 1970, 1971); these expressions are analysed in some detail in Hawkes (1980b) and listed in Hawkes (1982) and are not reproduced here. The coefficients that appear in the polynomial expressions for the asymptotic aberration coefficients are considered by Heritage (1971, 1973), Maclachlan (1972) and Hawkes (1973).

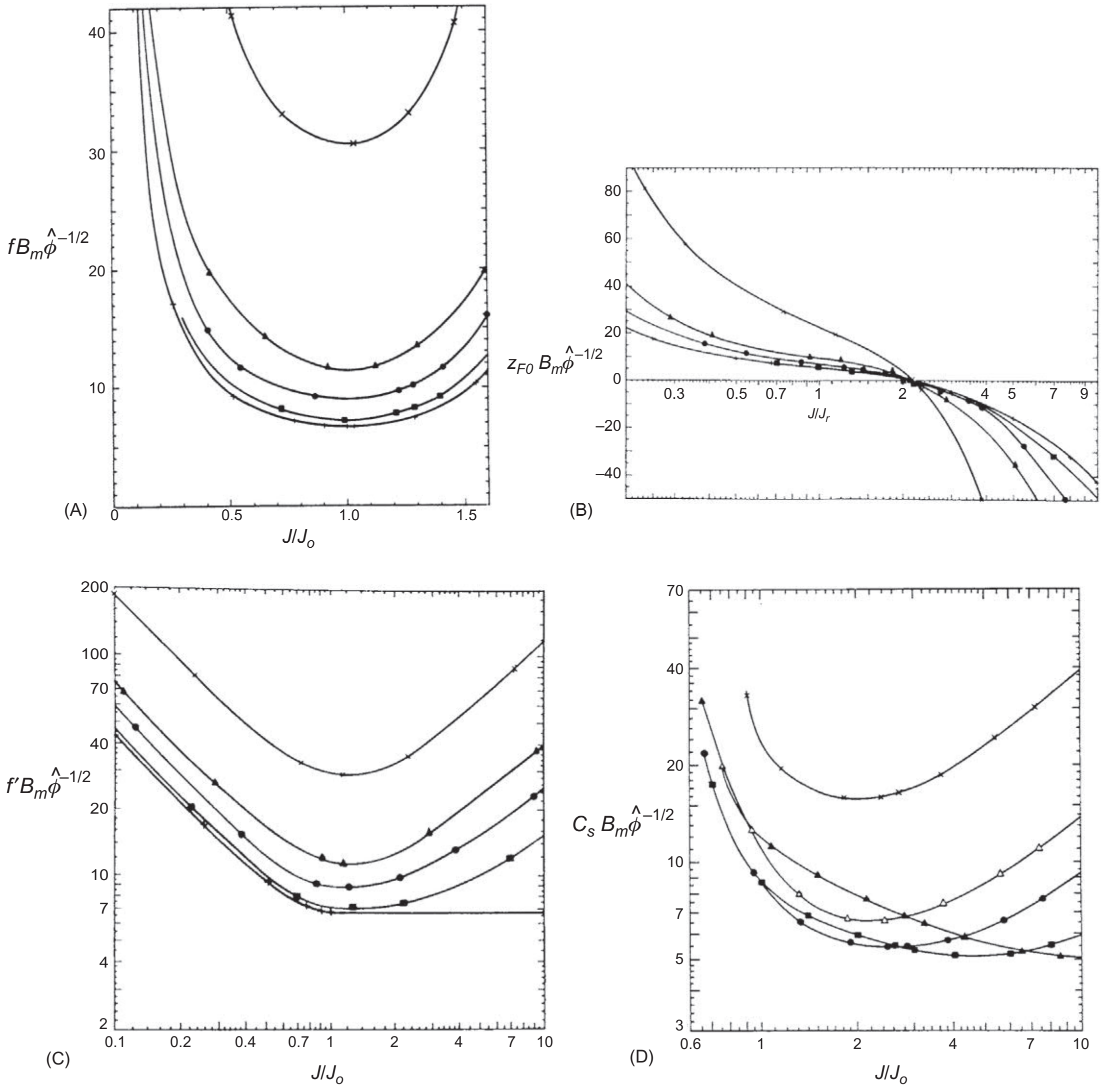

Figure 36.16

Magnetic lens properties. (A) Projector properties: $fB_m/\hat{\phi}^{1/2}$ as a function of J/J_0, where J_0 is the value of J corresponding to the minimum of f, for several values of S/D. (B)–(F) Objective properties. (B) $z'_{Fo}B_m/\hat{\phi}^{1/2}$ as a function of J/J_0. (C) $f'B_m/\hat{\phi}^{1/2}$ as a function of J/J_0. (D) $C_s\ B_m/\hat{\phi}^{1/2}$ as a function of J/J_0. (E) $C_cB_m/\hat{\phi}^{1/2}$ as a function of J/J_0. (F) Minimum values of $C_sB_m/\hat{\phi}^{1/2}$ and the resulting value of $C_cB_m/\hat{\phi}^{1/2}$ as functions of S/D; the appropriate value of $J/\hat{\phi}^{1/2}$ is also shown. $\times$: $S/D = 0.2$; Δ: 0.6; $\circ$: 1; $\square$: 2; $+$: ∞. The units are mm.mT.V$^{-1/2}$. *After Mulvey and Wallington (1973), Courtesy Institute of Physics.*

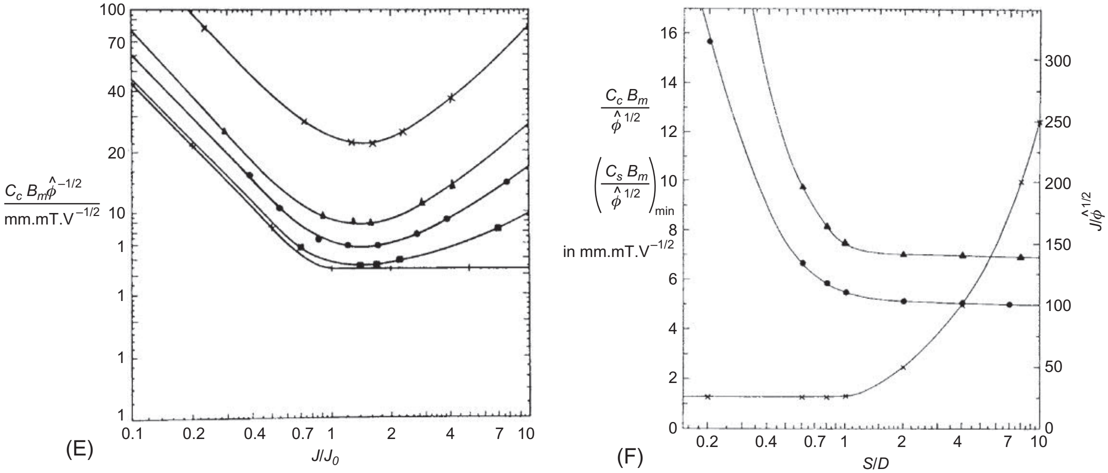

Figure 36.16
(Continued).

The fact that the optical properties vary rapidly with accelerating voltage has led first Lenz (1952) and later Schiske (1977) to examine the inverse problem, in which one seeks to obtain information about the field (or potential) distribution from the variation of the cardinal elements with accelerating voltage. The reader interested in the behaviour of these cardinal elements in the neighbourhood of the values of accelerating voltage corresponding to telescopic operation will find an analysis in Schiske's paper.

36.4.3 Saturated Lenses

Satisfactory studies of lenses in which saturation has become important had to wait for adequate computing power, although an early application of Southwell's relaxation method in electron optics was the calculation of the fields of saturated lenses by Hesse (1950). The work of Bauer (1968) showed that the latter merited much fuller investigation than they had yet been accorded and several studies followed soon after. Munro (1973, 1974, 1980) applied the finite-element method to various lenses at high excitation; the corresponding program formed one of a suite capable of analysing magnetic lenses with and without saturation and electrostatic lenses (Munro, 1975b). Kamminga (1976), using the same method, calculated the axial field for three values of S/D, $D = 2$ mm and five values of B_m: 2.32, π, 2π, 3π and 4π T (Figs 36.18A–C). The aberration coefficients are not published; instead, Kamminga plots the theoretical resolution (cf. 36.136), here defined by

$$d_{th} \coloneqq 0.43\left(C_s\lambda^3\right)^{1/4} \tag{36.140}$$

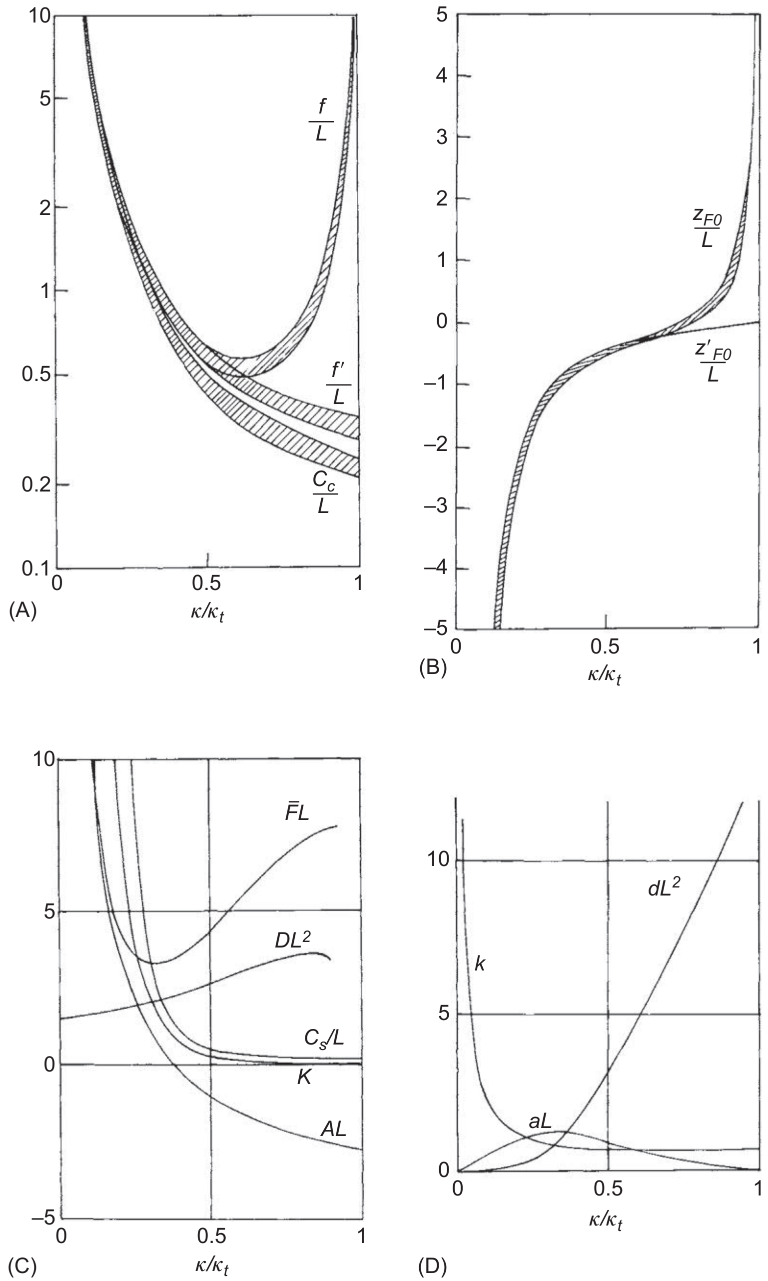

Figure 36.17

Unified representation of the properties of symmetric unsaturated magnetic lenses. (A) f/L, f'/L and C_c/L plotted against κ/κ_t. (B) z'_{Fo}/L and z_{Fo}/L plotted against κ/κ_t. (C) The real isotropic aberration coefficients C_s/L, K, $\bar{F}L$, AL and DL^2 plotted against κ/κ_t ($\bar{F} = F - A$). The magnification is high and $S/D < \sim 2$. (D) The real anisotropic aberration coefficients k, aL and dL^2 plotted against κ/κ_t. (E) The asymptotic isotropic aberration coefficients plotted against κ/κ_t. (F) The asymptotic anisotropic aberration coefficients plotted against κ/κ_t. *After Lenz (1982), Courtesy Springer Verlag.*

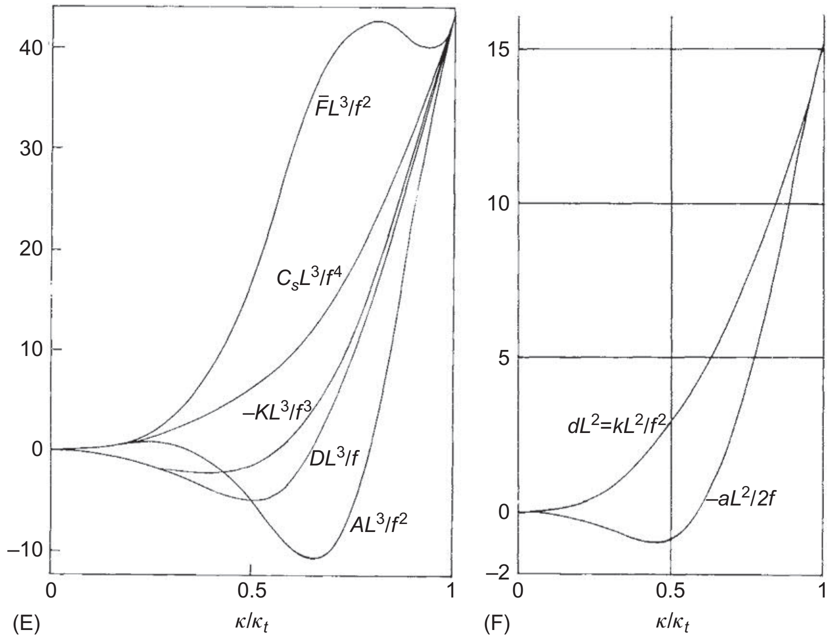

Figure 36.17
(Continued).

where the wavelength λ is given (Eq. 55.11 in Volume 3) by

$$\lambda = h/\left(2em_0\hat{\phi}\right)^{1/2} \tag{36.141}$$

or $\lambda/\text{Å} \approx 12.25/(\hat{\phi}/\text{V})^{1/2}$, and a stability criterion ST, defined by

$$ST = 10^{-5}\left(C_s\hat{\phi}^{-1/2}C_c^{-2}\right)^{1/2} \tag{36.142}$$

against S for $S/D = 0.6$, 1 and 2. The values of J and B_m are also plotted for the same range. Two situations are considered: the condenser−objective mode, in which, we recall, the entire lens operates as a telescope and the specimen is placed at the centre; and a telescopic-condenser mode (Francken and Heeres, 1973), in which the condenser part of the lens acts as a telescope and which requires even higher excitation. The results are reproduced as Figs 36.18D and E. Chen (1988) calculates the effect of saturation on C_s and C_c.

The fullest studies are those of Cleaver (1978, 1980, 1981). In the first of these, the paraxial properties and chromatic and spherical aberration coefficients and certain characteristic angles are presented for a series of symmetric lenses with Permendur polepieces, for all of

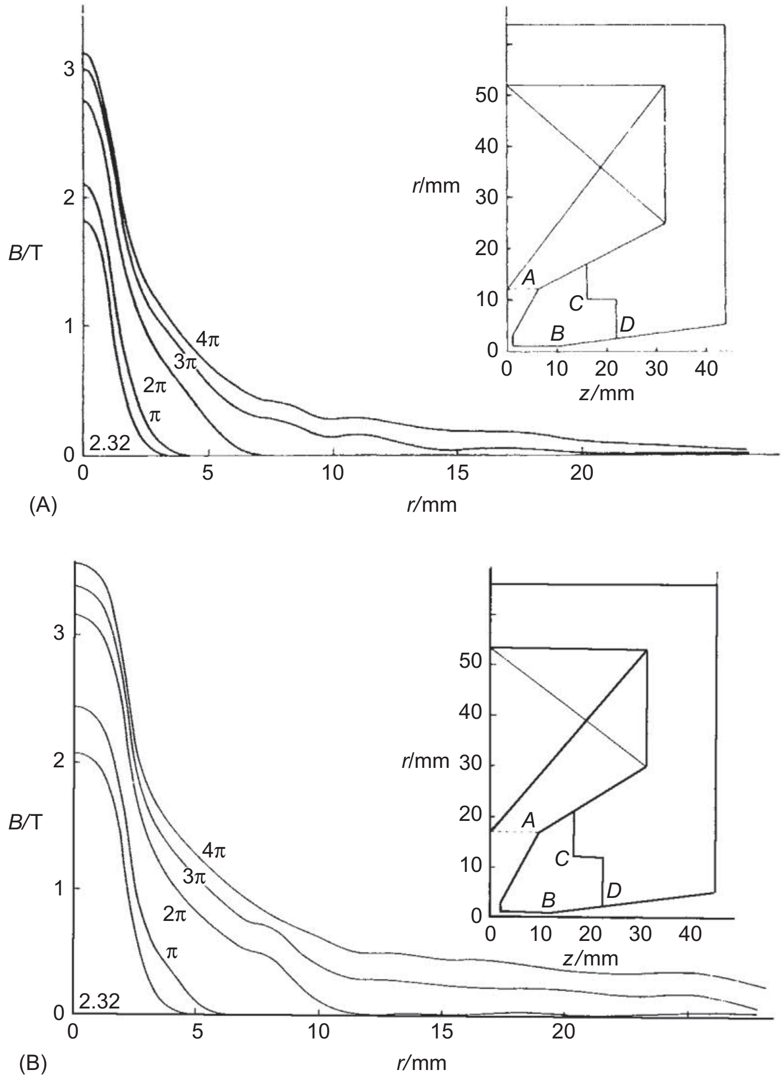

Figure 36.18

(A)–(C) The axial magnetic induction in three magnetic lenses with $D = 2$ mm and (A) $S/D = 1$, (B) $S/D = 2$, (C) $S/D = 0.6$. (D)–(E) d_{th}, ST, J and B_m as functions of S for $S/D = 0.6$ (dashed lines), $S/D = 1$ (dotted lines) and $S/D = 2$ (full line). (D) Corresponds to a condenser–objective operating at $\hat{\phi} = 2$ MV and (E) to a telescopic condenser–objective at the same accelerating voltage. *After Francken and Heeres (1973), Courtesy Wissenschaftliche Verlagsgesellschaft.*

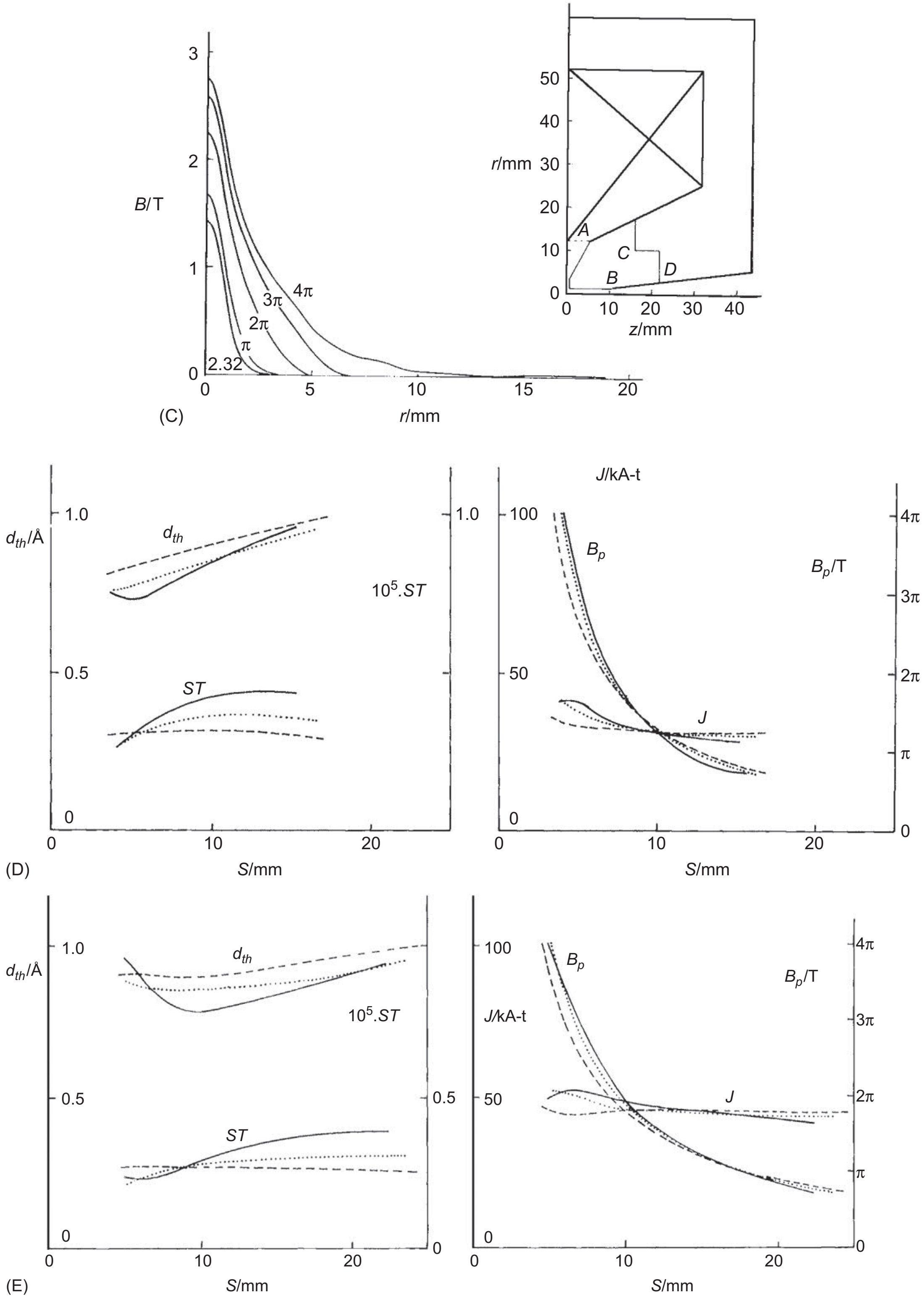

Figure 36.18
(Continued).

which $S = 10$ mm but 2.5 mm $< D <$ 10 mm. The excitation J is varied from 10 to 28 kA-t, except for the case $D = 5$ mm, for which values of J as high as 90 kA-t are considered. For lenses functioning in the condenser–objective mode (that is, with the specimen plane at the centre of the gap) and the image plane distant 20 cm from the specimen plane, Cleaver shows how C_s and C_c vary with $\hat{\phi}$ ($\hat{\phi}$ is used in preference to J since the magnetic circuit has a finite reluctance and it is convenient to compare lenses at the same value of $\hat{\phi}$). The position of the real back-focal plane is also plotted for various values of D.

If the specimen is not exactly at the centre of the lens, the relation between the various planes can be expressed by an empirical formula of the form

$$z_o \approx -k(J)\left\{\frac{1}{z_a + a(J)} + \frac{1}{z_i - a(J)}\right\} \tag{36.143}$$

in which the coefficients $k(J)$ and $a(J)$ are given graphically by Cleaver. For this situation, the aberration coefficients C_c and C_s, the position of the real and asymptotic back-focal planes and the principal angular quantities (see Fig. 36.19) are plotted in Fig. 36.20A–C. The relation between $J/\hat{\phi}^{1/2}$ and $\hat{\phi}$ for various object and image positions is shown in Fig. 36.20D. For a given value of S/D, it is also of interest to see how C_s and C_c vary with S at a given accelerating voltage; Fig. 36.20E shows this for $\hat{\phi} = 1$ MV and it can be seen that the minima of the two curves, though not sharp, occur for different values of S.

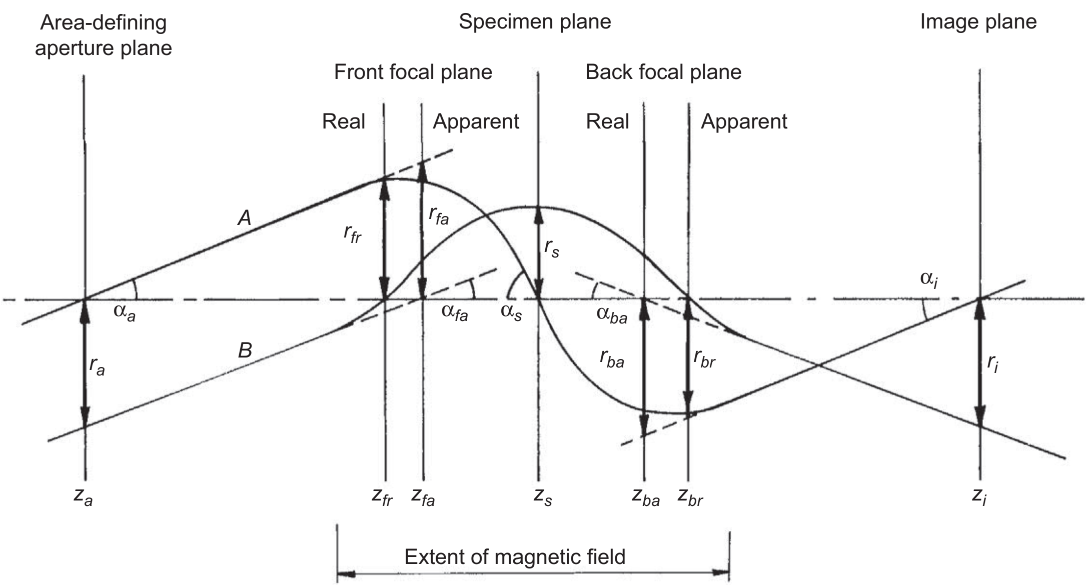

Figure 36.19
Notation used by Cleaver to characterize condenser–objective operation of a lens. *After Cleaver (1978, 1980), Courtesy Wissenschaftliche Verlagsgesellschaft.*

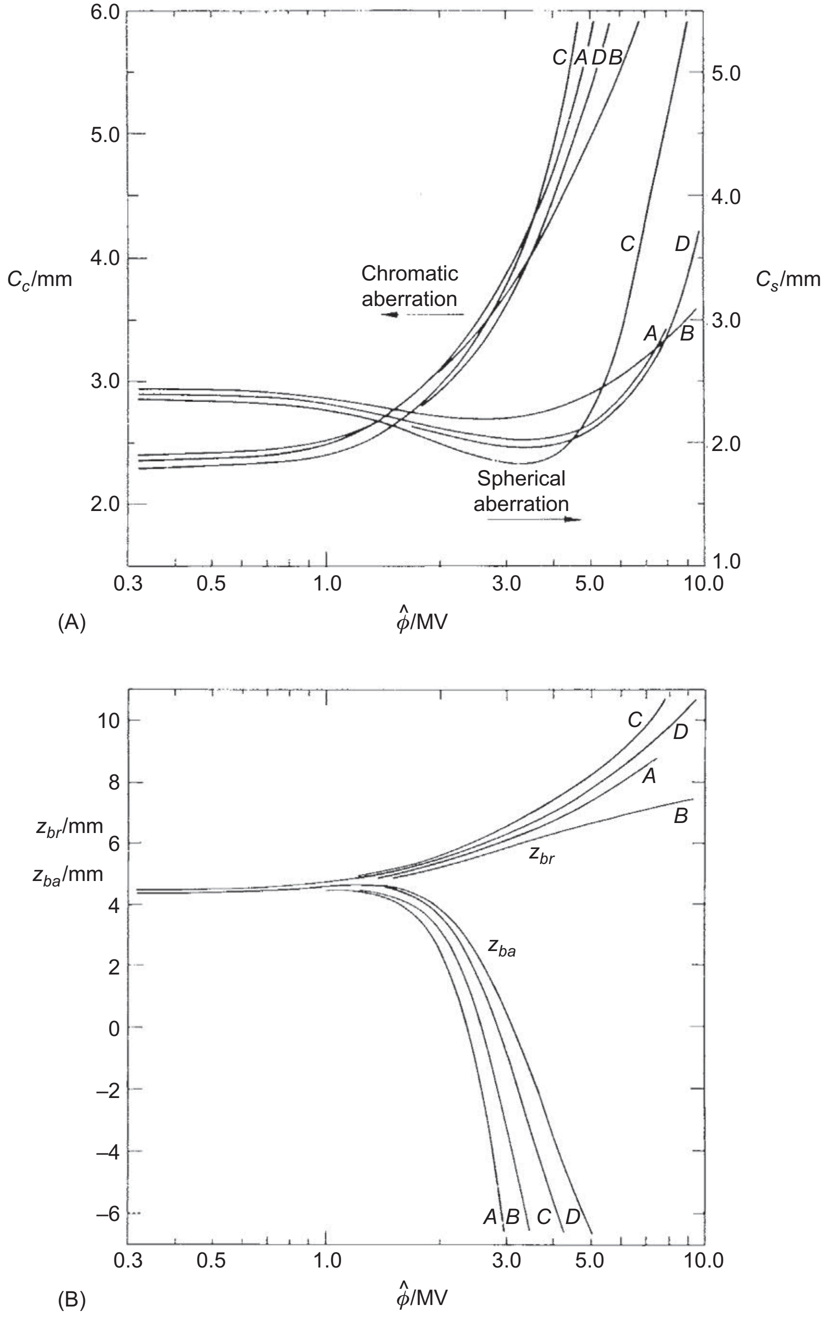

Figure 36.20

(A) C_s and C_c as functions of $\hat{\phi}$ for various object planes. $S = 10$ mm, $D = 5$ mm. (B) z_{br} and z_{ba} as functions of $\hat{\phi}$. $S = 10$ mm, $D = 5$ mm. (C) r_{br}, r_{ba} and r_{sb}, as functions of $\hat{\phi}$. $S = 10$ mm, $D = 5$ mm. (D) $J\hat{\phi}^{-1/2}$ as a function of $\hat{\phi}$. $S = 10$ mm, $D = 5$ mm. (E) C_s and C_c as functions of S for $\hat{\phi} = 1$ MV and $S/D = 2$. *After Cleaver (1978, 1980), Courtesy Wissenschaftliche Verlagsgesellschaft.*

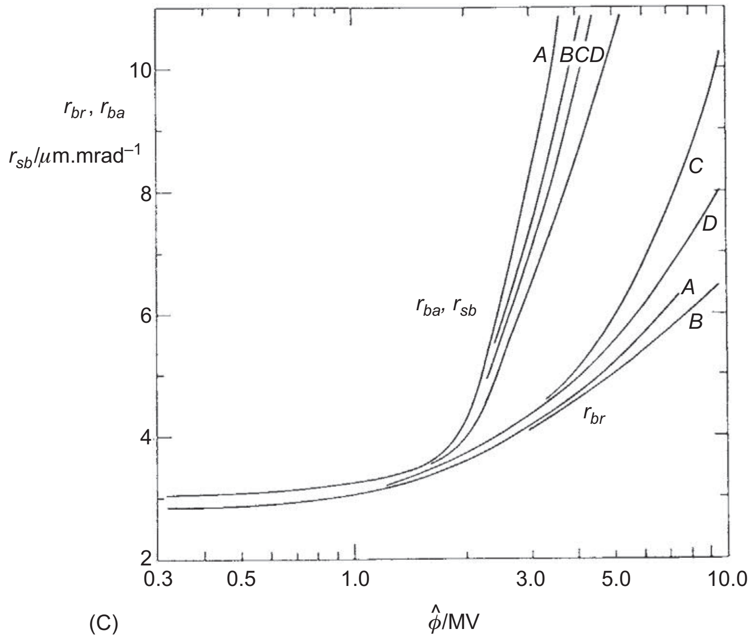

(C)

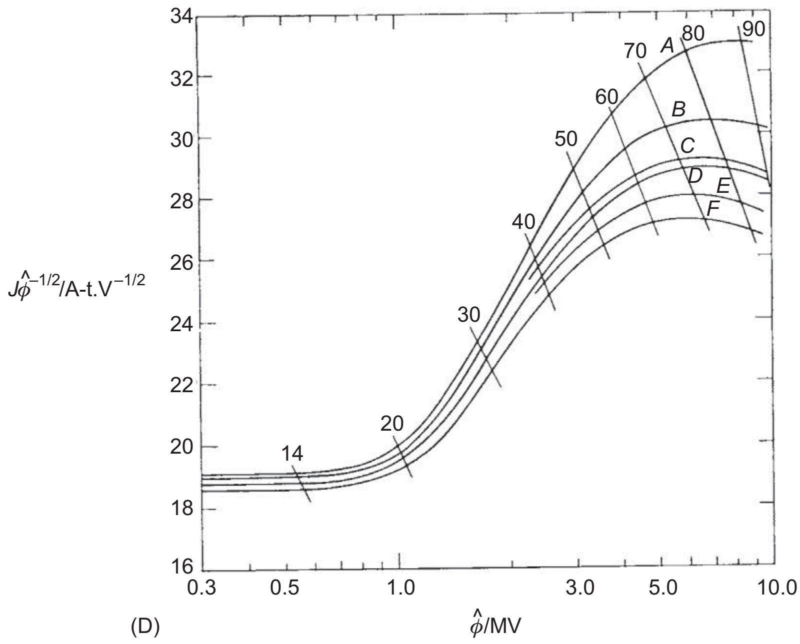

(D)

Figure 36.20
(Continued).

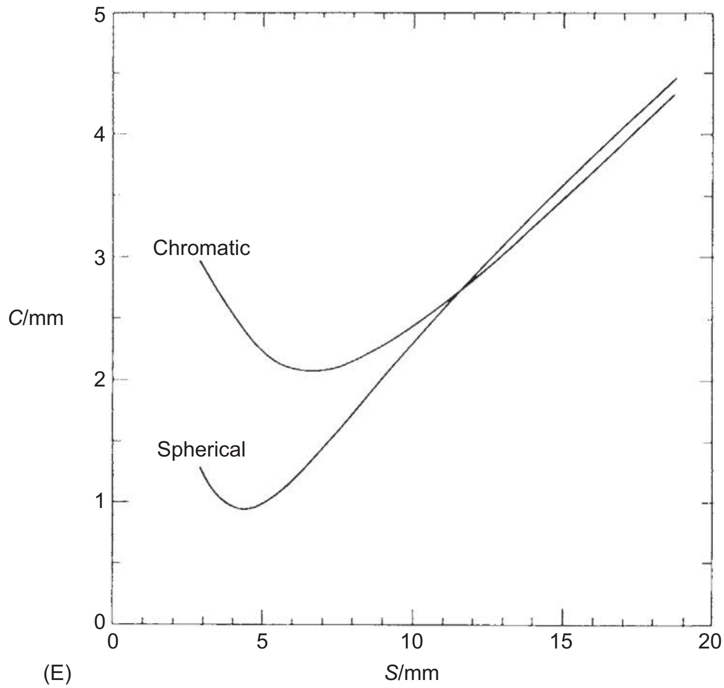

Figure 36.20
(Continued).

In his later papers, Cleaver (1980, 1981) has attempted to provide a unified treatment of lens behaviour from which the most suitable design for given operating conditions can be selected. The unification is obtained by establishing the curve relating C_s and $\hat{\phi}$ for each lens geometry considered, the excitation J and the specimen plane z_o being adjusted to minimize C_s; a similar curve can be established for C_c. The symmetric condenser–objective then corresponds to a point on this curve, with conventional operation on one side and second-zone operation on the other. Four asymmetric and four symmetric lenses are studied by Cleaver (Fig. 36.21); we first consider lens $S2$ (symmetric, $S = 5$, $D = 3$ mm) in detail and then extend the results to the remainder.

It is convenient to classify the operating modes in terms of the ratio of α_c/α_o; for conventional operation, in which the prefield is negligible, $\alpha_c/\alpha_o \approx 1$, for a condenser–objective $0 < \alpha_c/\alpha_o \ll 1$ and for the second-zone mode, $-1 < \alpha_c/\alpha_o < 0$ (Fig. 36.22A). The boundaries adopted by Cleaver are shown in Fig. 36.22B, where the bounds on the regions occupied by the conventional and second-zone modes have been determined by setting $\alpha_c/\alpha_o = \pm 0.2$.

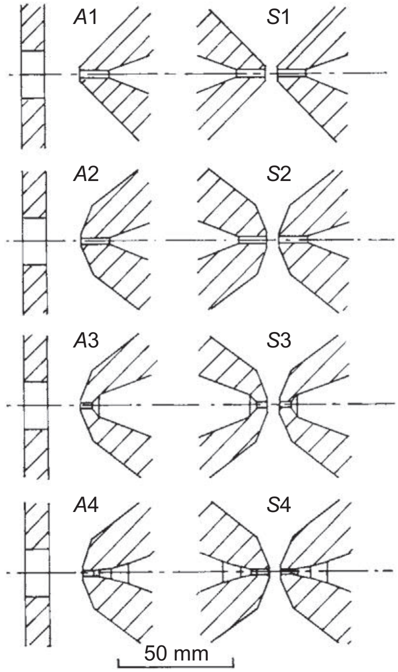

Figure 36.21
Lenses studied by Cleaver and considered in Figs 36.22–36.26. In the asymmetric lenses, $S = 15$ mm, $D_1 = 20$ mm and $D_2 = 3$ mm. Coordinate origin at face of small-bore polepiece. In the symmetric lenses, $S = 5$ mm, $D = 3$ mm and the coordinate origin is at the centre of the gap. The external cone semi-angles are initially 45° or 67°. *After Cleaver (1978, 1980), Courtesy Wissenschaftliche Verlagsgesellschaft.*

If now C_s and C_c are plotted against $\hat{\phi}$ for various values of z_o, families of curves are obtained (Fig. 36.23A and B), each of which proves to define an *envelope*, different parts of which correspond to the different operating modes. These envelopes are included in Fig. 36.22B; for a condenser–objective, for example, the best C_s value can be seen to be obtained for $\hat{\phi} = 1.7$ MV, whereas the best C_c value occurs at $\hat{\phi} = 0.56$ MV.

The effect of a scale change can easily be included, for if the lens size is increased by some factor k, then J, C_s and C_c will likewise increase as k provided that saturation remains constant, while $\hat{\phi}$ increases as k^2, to maintain equivalent trajectories. By using logarithmic plots for C_s and C_c against $\hat{\phi}$, the envelope curves can simply be translated, one step up for every two across.

These ideas are then applied to the family of lenses shown in Fig. 36.21. We cannot do justice to Cleaver's meticulous discussion here but we reproduce his figures which summarize his findings conveniently. Fig. 36.24A and B show the C_s and C_c envelopes and Fig. 36.25A shows how B_0 varies with J; Fig. 36.25B shows J as a function of $\hat{\phi}$ for

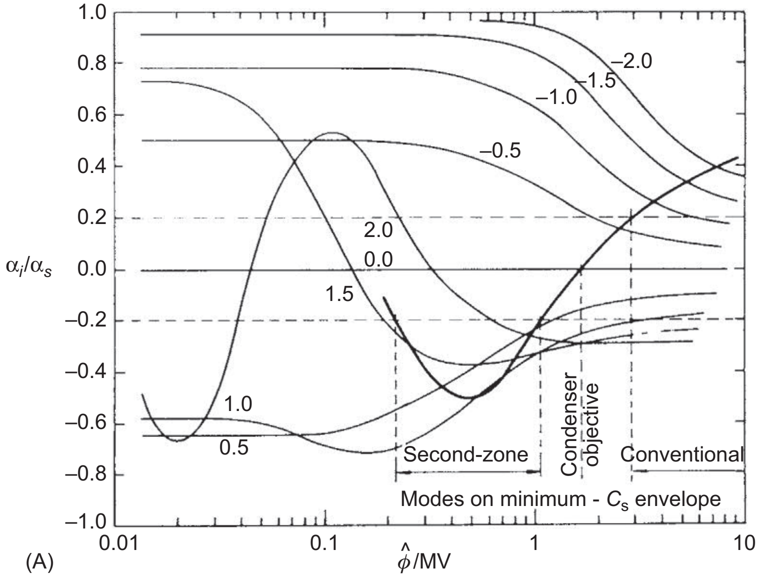

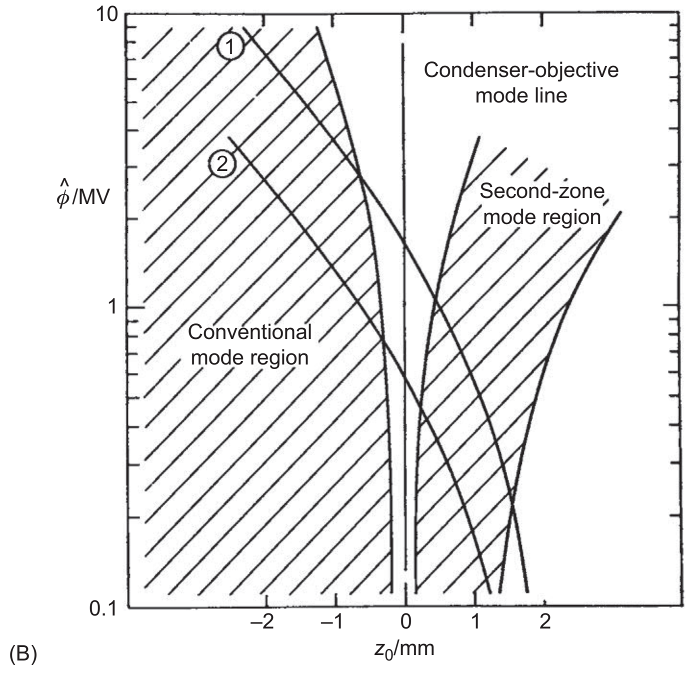

Figure 36.22

(A) Illumination-side angular magnification as a function of electron beam voltage and specimen height for lens S2. Positive specimen heights are on the image side, negative on the illumination side of the lens centre. Thin lines: fixed specimen heights, from −2.0 to +2.0 mm. Thick line: specimen height adjusted to minimize C_s. (B) Operating modes and minimum-aberration curves, for lens S2. 1: line corresponding to minimum-C_s envelope. 2: line corresponding to minimum-C_c envelope. *After Cleaver (1978, 1980), Courtesy Wissenschaftliche Verlagsgesellschaft.*

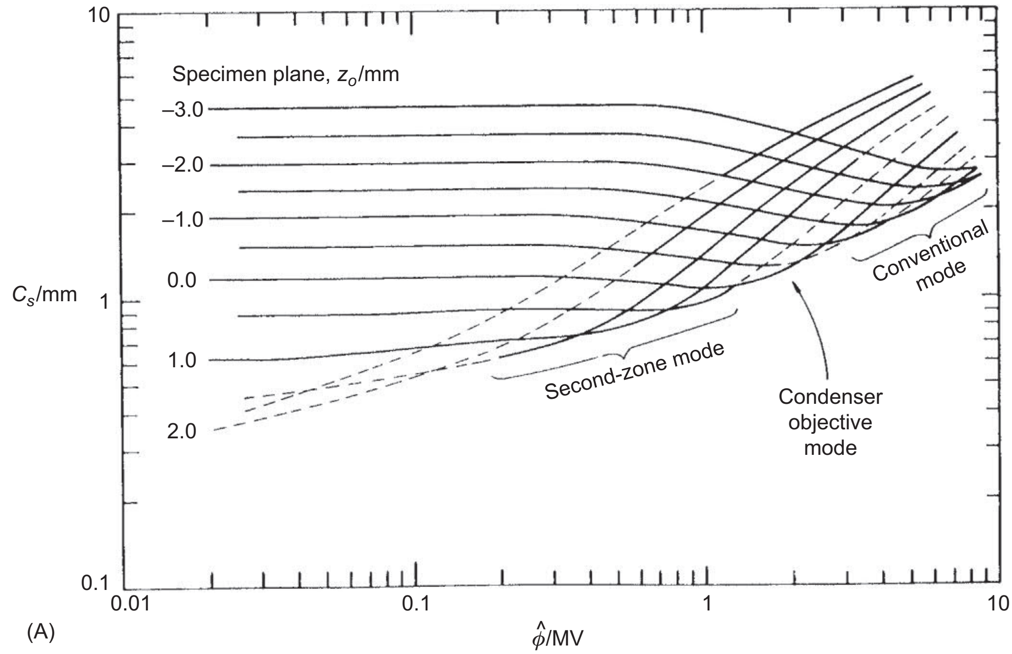

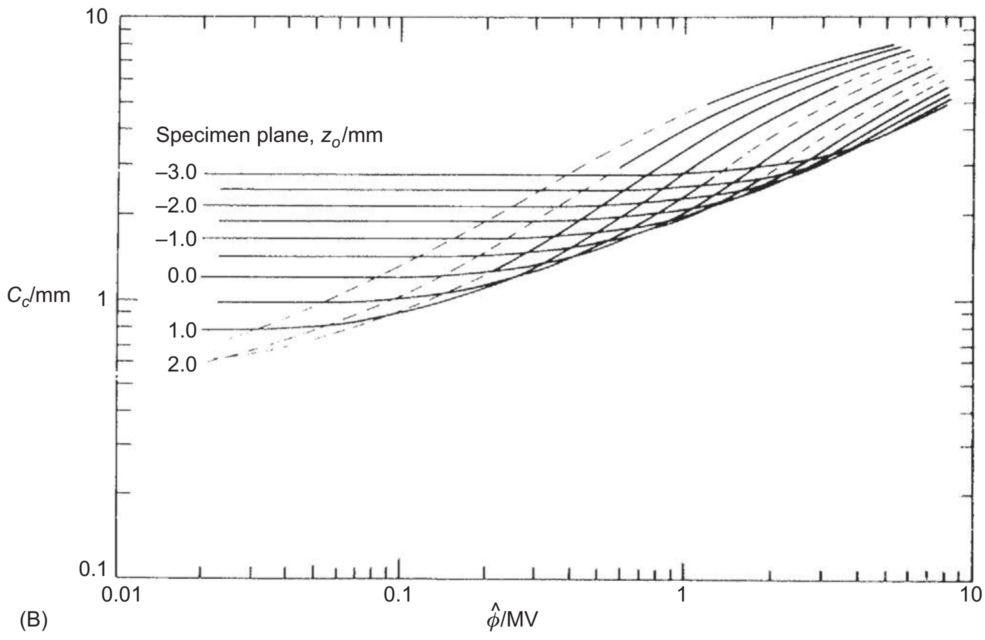

Figure 36.23

(A) Spherical aberration as a function of electron beam voltage and specimen height for lens S2. Solid lines: operation within a principal mode. Broken lines: operation not in a principal mode. (B) Chromatic aberration as a function of electron beam voltage and specimen height, for lens S2. *After Cleaver (1978, 1980), Courtesy Wissenschaftliche Verlagsgesellschaft.*

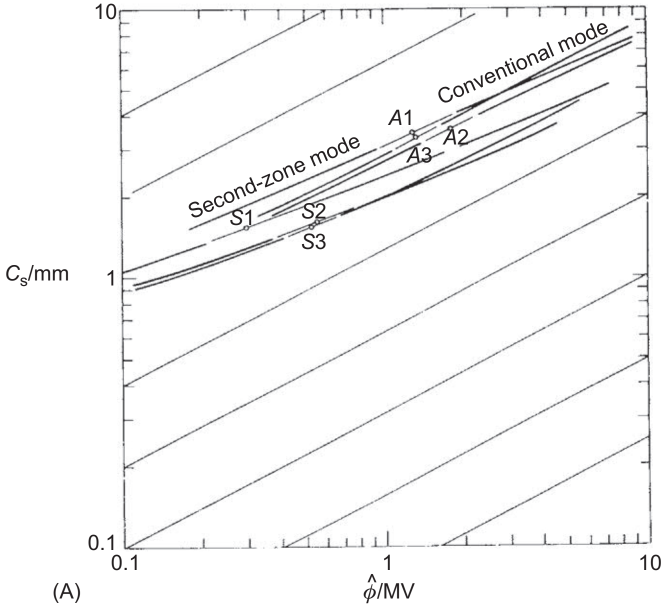

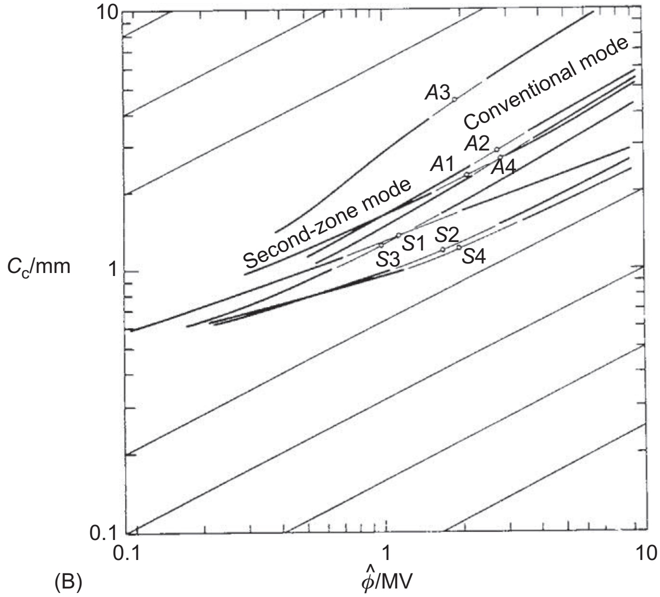

Figure 36.24

(A) Envelope curves for spherical aberration, for the main lens series. Circles: condenser—objective mode points. Thick lines: second-zone and conventional mode regions. (B) Envelope curves for chromatic aberration, for the main lens series. The curves for A4 and S4 are similar to those for A2 and S2. *After Cleaver (1978, 1980), Courtesy Wissenschaftliche Verlagsgesellschaft.*

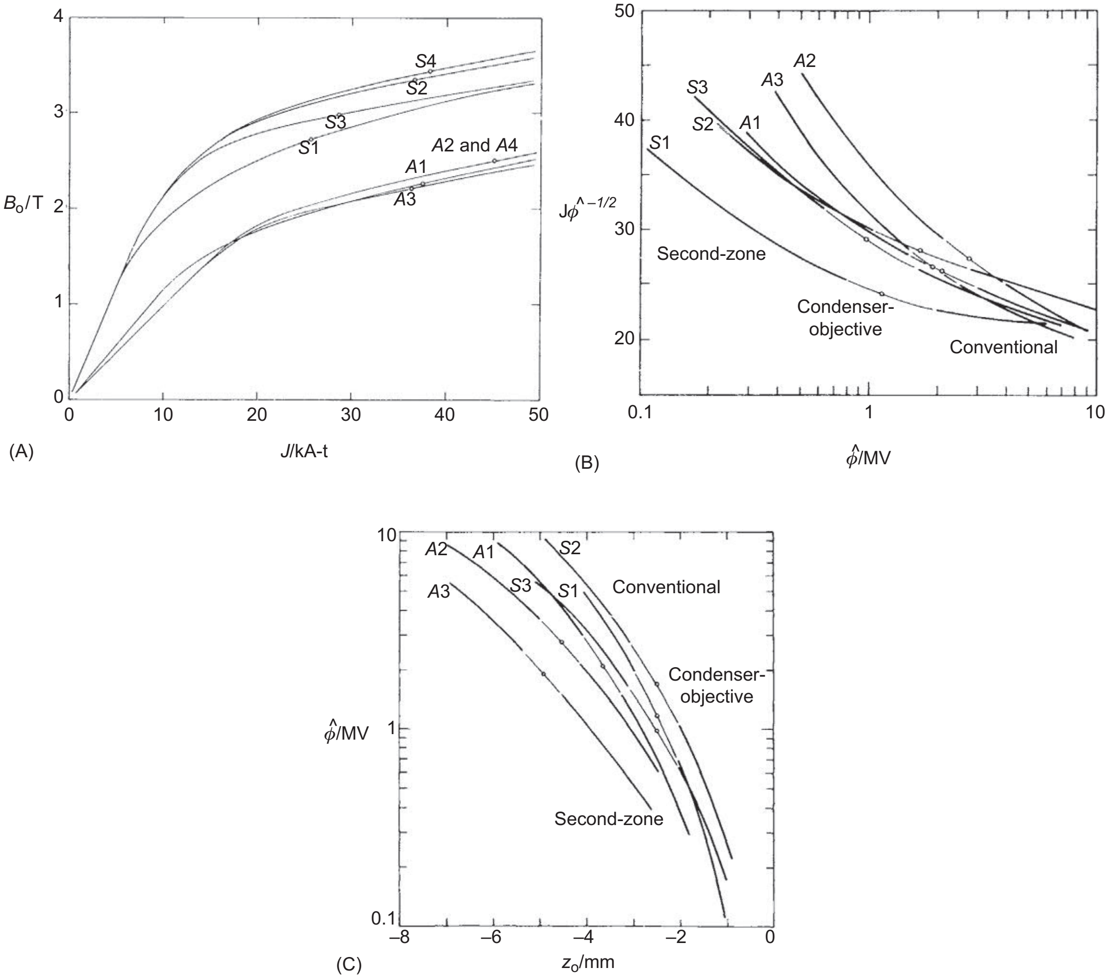

Figure 36.25

(A) Dependence of peak axial field on the polepiece shape. The circles indicate conditions corresponding to the condenser—objective points on the minimum-C_s envelope curves. (B) Excitation parameter in A-t.V$^{-1/2}$ as a function of electron beam voltage, for conditions corresponding to the minimum-C_s envelope curves. (C) Specimen height as a function of electron beam voltage, for conditions corresponding to the minimum-C_s envelope curves. The axial scale origin is in the plane of the image-side polepiece face. *After Cleaver (1978, 1980), Courtesy Wissenschaftliche Verlagsgesellschaft.*

minimum C_s, and the corresponding specimen position is plotted in Fig. 36.25C. For the same condition, Fig. 36.26A shows the magnification for fixed object-image distance (1 m), Fig. 36.26B the position of the back-focal plane and Fig. 36.26C the ray-height in this plane for a ray that intersects the axis at z_o and z_i. In Cleaver (1981), the off-axis aberrations are likewise studied in full detail.

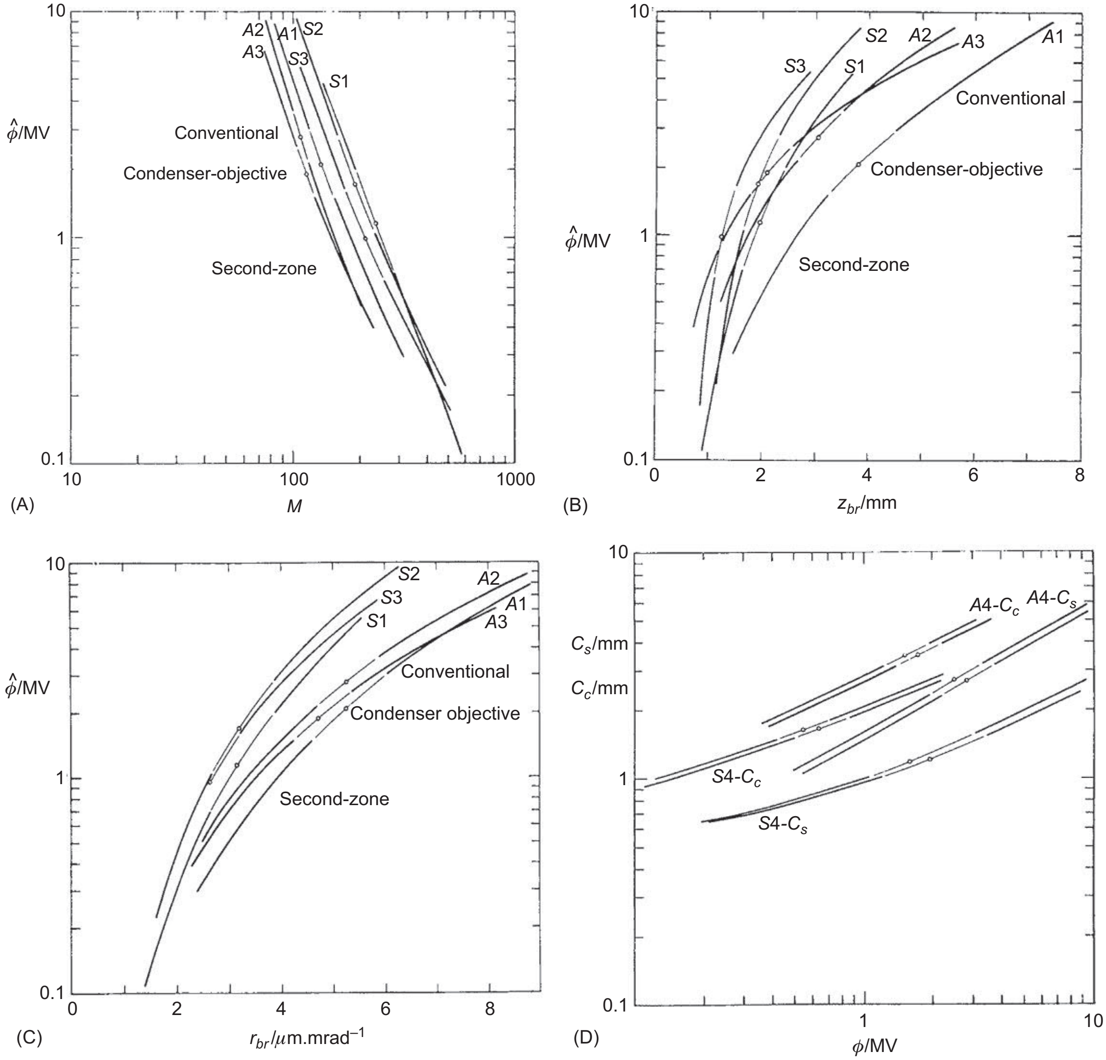

Figure 36.26

(A) Image magnification as a function of electron beam voltage for conditions corresponding to the minimum-C_s envelope curves. (B) Back-focal plane as a function of the electron beam voltage, for conditions corresponding to the minimum-C_s envelope curves. The coordinate origin is in the plane of the image-side polepiece face. (C) Radial distance at the back-focal plane for a ray cutting the axis at the specimen plane, for conditions corresponding to the minimum-C_s envelope curves. (D) Influence of polepiece material on lens aberrations. The curves are minimum-C_s and minimum-C_c envelopes for lenses A4 and S4; of each pair of curves that for Permendur is the lower and that for soft iron the upper. *After Cleaver (1981), Courtesy Wissenschaftliche Verlagsgesellschaft.*

Before leaving Cleaver's studies, we draw attention to his conclusions about the use of materials with lower saturation flux density than Permendur. Cleaver's curves (36.26) showing the C_s and C_c envelopes for one symmetric and one asymmetric lens for Permendur and for soft-iron polepieces are sufficiently close to encourage designers to accord such qualities as remanence, homogeneity and ease of machining at least as much importance as the $B-H$ curve.

The field distribution of asymmetric lenses, potential candidates for the objective of a very high resolution high-voltage microscope, has been studied by Tsuno and Honda (1983) close to the onset of saturation. The paraxial properties and principal aberration coefficients are shown, as well as the field distributions on the axis and throughout the lens region.

Superconducting lenses with conventional yokes (as opposed to shielding cryolenses, Section 36.6.2) are almost invariably operated with some degree of saturation; it was to circumvent the worst effects of this that holmium and dysprosium were introduced as polepiece materials since these rare-earth elements have a high saturation magnetization at low temperature. Lenses with rare-earth polepieces have been thoroughly studied by Bonjour and Septier (1967a,b, 1968; Bonjour, 1969, 1974; Septier, 1972); in their earlier designs, saturation was so high that the axial field exhibited wide sloping shoulders (this was partly due to the limited size of commercially available holmium ingots) but in their later proposals (Bonjour 1975a,b,c, 1976) this is largely corrected. Thus in the designs described in Bonjour (1975a–c) the field has the familiar bell-shape and the various aberration coefficients calculated are low for high-voltage operation; these designs are in principle capable of yielding resolutions below 0.2 nm at 3 MV. The cardinal elements and aberration coefficients of a similar experimental lens have been obtained from the measured axial field by Bonjour (1975b) and substantially confirm these predictions; the polepiece shape for the experimental lens allows more broadening of the axial field, however. A lens design in which the polepieces are saturated and the superconducting winding contributes substantially to the axial field has been proposed by Yin and Mulvey (1987). For further work on saturation, see Chen (1988), Hodkinson and Tahir (1995) and Lencová (2015).

36.5 Ultimate Lens Performance

36.5.1 Tretner's Analysis

The theorem of Scherzer (1936b) tells us that the spherical and chromatic aberration coefficients cannot change sign, and experiment and intuition combine to suggest that there must be limiting values of these quantities that cannot be surpassed in real lenses, in which physical considerations limit the maximum magnetic field. These limiting values were established by Tretner in a series of publications (1950, 1954, 1955, 1956) culminating in his survey of the *Existenzbereiche* of rotationally symmetric electron lenses (Tretner, 1959). His conclusions have been confirmed by later investigators in the sense that no lens has been found that does not fall within his domains (see, e.g., Mulvey and Wallington, 1973). The only claim that such a lens existed (Glaser, 1956a) proved to be a false alarm (Glaser, 1956b).

We follow Tretner in considering electrostatic and magnetic fields together. The problem to be solved may be stated as follows: what are the lower and upper bounds, if any, on the real spherical and chromatic aberration coefficients, C_s and C_c, when the object focal length f' for magnification M, the potential at object and image plane, ϕ_o and ϕ_i, the maximum potential ϕ_m and the maximum electric field, $|\phi'|_m$, the maximum magnetic flux density B_m or the maximum relative flux gradient, $|B'/B|_m$, are regarded as variables. In order to eliminate trivial solutions, the coefficients are normalized with respect to some convenient length; Tretner introduces three such lengths:

$$\left.\begin{aligned} L_1 &= \frac{2\phi_o^{1/2}}{\eta|B|_m} \\ L_2 &= \frac{1}{\left|B'/B\right|_m} \quad \text{for } M\to\infty \end{aligned}\right\} \quad \text{for magnetic lenses} \tag{36.144}$$

$$L_4 = \frac{\phi_o}{\left|\phi'\right|_m} \quad \text{for electrostatic lenses}$$

The fields must therefore satisfy

$$\begin{aligned} &-\frac{2\phi_o^{1/2}}{\eta L_1} \le B \le \frac{2\phi_o^{1/2}}{\eta L_1} \\ &-\frac{1}{L_2} \le \frac{B'}{B} \le \frac{1}{L_2} \\ &\text{or} \\ &-\frac{\phi_o}{L_4} \le \phi' \le \frac{\phi_o}{L_4} \end{aligned} \tag{36.145}$$

We shall not repeat here the ensuing variational calculus, fully set out in Tretner (1959), but reproduce the results in some detail.

36.5.1.1 Chromatic aberration, electrostatic case

The axial potential that gives the smallest value of C_c/L_4 is linear with abrupt changes in gradient (Fig. 36.27); at the object plane, the gradient changes from $\phi' = -|\phi'|_m$ to

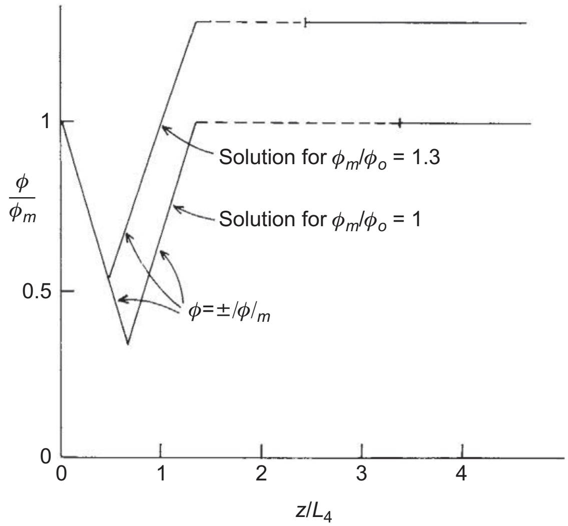

Figure 36.27
The axial potential in electrostatic lenses that gives the smallest chromatic aberration. *After Tretner (1959), Courtesy Wissenschaftliche Verlagsgesellschaft.*

$\phi' = |\phi'|_m$ and subsequently the potential abruptly becomes constant, $\phi = \phi_m$. The minimum value of C_c/L_4 is found by eliminating x and y between the equations

$$\left.\frac{C_c}{L_4}\right|_{\min} = 4\left\{\frac{6-2x^2-\sqrt{3}x}{\left(\sqrt{3}+x\right)^2} - Q(y)\left(1+\frac{1}{x^2}\right)\frac{\left(\sqrt{3}x+1\right)\left(x-\sqrt{3}\right)^3}{\left(\sqrt{3}x-1\right)\left(x+\sqrt{3}\right)^3}\right\}$$
$$\frac{\phi_m}{\phi_o} = \left(\frac{\sqrt{3}x-1}{\sqrt{3}y-1}\,\frac{y-\sqrt{3}}{x-\sqrt{3}}\,\frac{x+\sqrt{3}}{3x+\sqrt{3}}\right)^2 \tag{36.146}$$

where

$$Q(y) = 3y^2\,\frac{\sqrt{3}y-1}{\left(\sqrt{3}-y\right)^3}\left(\frac{\pi}{2}-\arctan y\right) \tag{36.147}$$

Tretner finds that for $\phi_m/\phi_o > 100$,

$$\left.\frac{C_c}{L_4}\right|_{\min} \to 1 + \frac{7.26}{\left(\phi_m/\phi_o\right)^{1/2}} - \frac{11.9}{\left(\phi_m/\phi_o\right)^{3/4}} \tag{36.148}$$

and that for $\phi_m/\phi_o < 100$, the following expression is a good approximation to the exact solution:

$$\left.\frac{C_c}{L_4}\right|_{\min} \approx \frac{2.8}{(\phi_m/\phi_o)^{1/6}} \tag{36.149}$$

C_c/L_4 has no finite upper limit. The electrostatic lens domain, for C_c/L_4, is shown in Fig. 36.28 in which the region occupied by the Glaser–Schiske field (Section 35.3.1b) is shown (retarding case only).

36.5.1.2 Spherical aberration, electrostatic case

The potential that gives the smallest value of C_s/L_4 is shown in Fig. 36.29; it consists of a straight zone, $\phi = \phi_o(1 - z/L_4)$ up to the point $z/L_4 = 0.484$, beyond which it gradually flattens out, tending asymptotically to $(4z/L_4)^{-1.15}$. The corresponding minimum is

$$\left.\frac{C_s}{L_4}\right|_{\min} = 0.23 \tag{36.150}$$

For comparison, Fig. 36.29 also shows the field model $\phi/\phi_o = 0.57 + 0.47\tanh(1.6-2.15z/L_4)$, for which $C_s/L_4|_{\min} \approx 1.2$.

$C_s/L_4|_{\max}$ is unbounded so that finally

$$\infty \geq C_s/L_4 \geq 0.23 \tag{36.151}$$

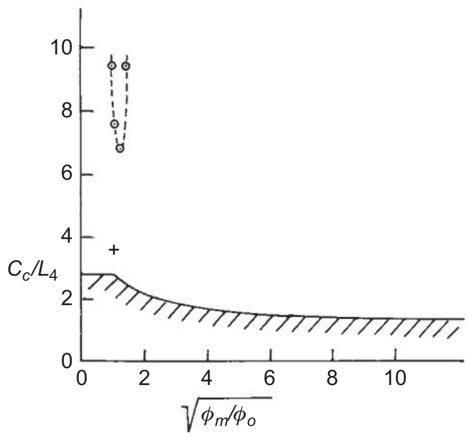

Figure 36.28

The limiting value of C_c/L_4 for electrostatic lenses as a function of $(\phi_m/\phi_0)^{1/2}$. The values for the Glaser–Schiske field (35.81 with $C = 0$) are shown as a broken curve. *After Tretner (1959), Courtesy Wissenschaftliche Verlagsgesellschaft.*

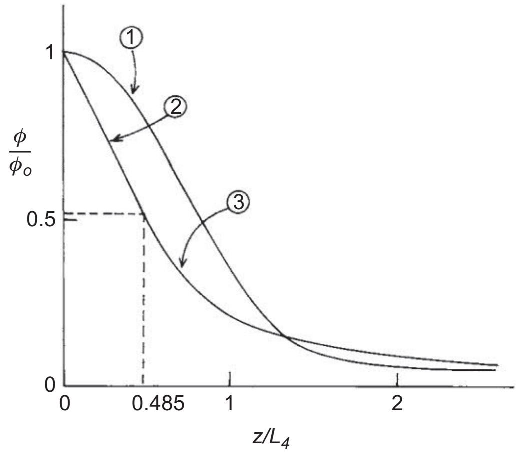

Figure 36.29

The potential in electrostatic lenses that gives the smallest spherical aberration. 1. Model field of Ramberg (1942). 2. Linear part of potential. 3. Nonlinear part of potential. *After Tretner (1959), Courtesy Wissenschaftliche Verlagsgesellschaft.*

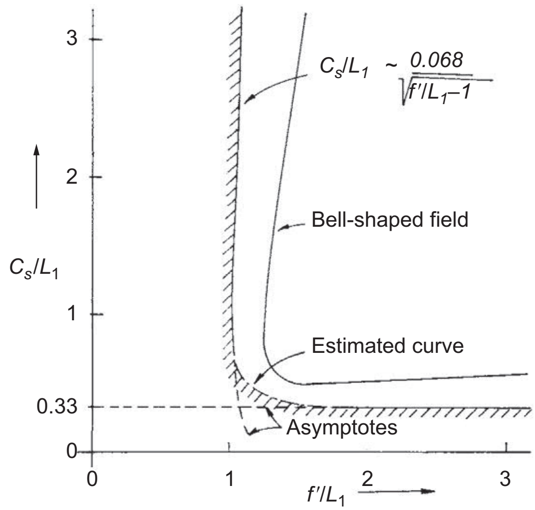

Figure 36.30

The lower limit of C_s/L_1 in magnetic lenses as a function of f'/L_1. Glaser's bell-shaped curve is included for comparison. *After Tretner (1959), Courtesy Wissenschaftliche Verlagsgesellschaft.*

36.5.1.3 Spherical aberration, magnetic case, L_1

The lower limit of C_s/L_1 is shown in Fig. 36.30; the curve has the approximate form

$$\left.\frac{C_s}{L_1}\right|_{\min} \approx \frac{0.068}{\left(f/L_1-1\right)^{1/2}} \tag{36.152}$$

along the vertical branch, and tends to

$$\left.\frac{C_s}{L_1}\right|_{\min} \to 0.33 \tag{36.153}$$

as $f/L_1 \to \infty$. It will be seen that the bell-shaped field comes close to this minimum value.

$C_s/L_1|_{\max}$ is unbounded and the corresponding magnetic lens domain is thus as shown in Fig. 36.30.

36.5.1.4 Spherical aberration, magnetic case, L_2

The optimum field is now the exponential distribution

$$B(z) = B_0 \exp\left(-z/L_2\right) \tag{36.154}$$

The coefficient C_s is described by

$$\left.\begin{aligned} \left.\frac{C_s}{L_2}\right|_{\min} &= 0.25 - 0.48\mu \\ \frac{f}{L_2} &= 0.8 + 0.15\mu \ln\left(1/\mu\right) \end{aligned}\right\} \quad 0 \le \mu \ll 1 \tag{36.155}$$

In the vicinity of the point corresponding to the shortest focal length,

$$f/L_2|_{\min} = 0.8, \quad \text{we have} \quad C_s/L_2 = 0.25 \tag{36.156}$$

(Rebsch, 1938; Lenz, 1951).

For large focal length,

$$\left.\frac{C_s}{L_2}\right|_{\min} = 0.239 \quad \text{for} \quad f/L_2 \gg 1 \tag{36.157}$$

The coefficient now does have an upper limit, which asymptotically tends to

$$\left.\frac{C_s}{L_2}\right|_{\max} \to 0.5\left(f/L_2\right)^2 \tag{36.158}$$

The magnetic lens domain for C_s/L_2 is thus as shown in Fig. 36.31; the 'corner' occurs at the point found by Rebsch already mentioned, where $C_s/L_2 = 0.25$ and $f/L_2 = 0.8$.

36.5.1.5 Chromatic aberration, magnetic case L_1

The lower limit of C_c/L_1 is given by

$$\left.\frac{C_c}{L_1}\right|_{\min} = \frac{\pi}{4} \tag{36.159}$$

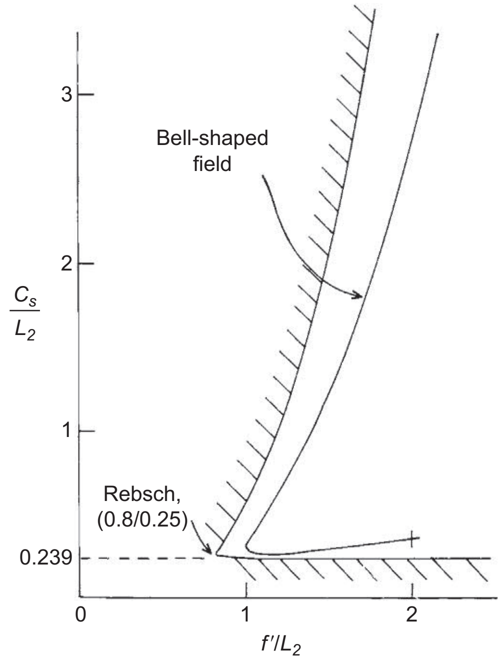

Figure 36.31
Limiting value of C_s/L_2 for magnetic lenses as a function of f'/L_2. Glaser's bell-shaped field is shown for comparison. The value found by Rebsch falls at the corner. *After Tretner (1959), Courtesy Wissenschaftliche Verlagsgesellschaft.*

for all focal lengths. For large values of f/L_1, it has an upper limit of the form

$$\left.\frac{C_c}{L_1}\right|_{max} \sim \frac{f}{L_1} - \frac{1}{6f/L_1} \tag{36.160}$$

In the vicinity of the point of shortest focal length,

$$f/L_1\big|_{min} = 1 \quad \text{and} \quad C_s/L_1\big|_{min} = \pi/4 \tag{36.161}$$

The domain is shown in Fig. 36.32.

36.5.1.6 Chromatic aberration, magnetic case L_2

As in case (e), the lower limit is simply

$$\left.\frac{C_c}{L_2}\right|_{min} = 0.5 \tag{36.162}$$

independent of focal length until the latter reaches its minimum value, $f/L_2|_{min} = 0.8$. Beyond this, the upper limit takes over, and when $f/L_2 \gg 1$,

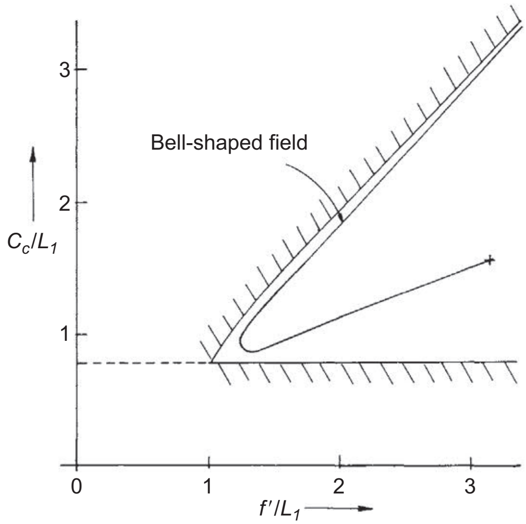

Figure 36.32
Limiting value of C_c/L_1 as a function of f'/L_1 for magnetic lenses. The bell-shaped lens is shown for comparison. *After Tretner (1959), Courtesy Wissenschaftliche Verlagsgesellschaft.*

$$\left.\frac{C_c}{L_2}\right|_{\max} \sim \frac{f}{L_2} - \frac{1}{8} \tag{36.163}$$

The domain is shown in Fig. 36.33.

36.5.2 Earlier Studies

As we have indicated in passing, Tretner's was not the first attempt to establish the smallest values of C_s and C_c. Thus in 1936, Scherzer had sought the weak einzel lens with the least spherical aberration by minimizing $\int_{-\infty}^{\infty} \phi''^2 dz$ keeping $\int_{-\infty}^{\infty} \phi'^2 dz$ and $\int_{-\infty}^{\infty} z^2 \phi'^2 dz$ (i.e., focal length and distance) constant; he found $\phi = \phi_0\{1 + A\exp(-Bz^2)\}$ and suggested an electrode configuration to produce it (Scherzer, 1936a). Rebsch and Schneider (1937) examined a number of fields to find the 'best corrected', in the sense that their measure G,

$$G := \frac{r_a^3 b}{r_i f l^2} \tag{36.164}$$

was least, where the 'lens-length' l is defined by

$$\left(\frac{l}{2}\right)^2 := \frac{\displaystyle\int z^2\left(\frac{3}{16}\frac{\phi'^2}{\phi^2} + \frac{\eta^2 B^2}{4\phi}\right)dz}{\displaystyle\int \left(\frac{3}{16}\frac{\phi'^2}{\phi^2} + \frac{\eta^2 B^2}{4\phi}\right)dz} \tag{36.165}$$

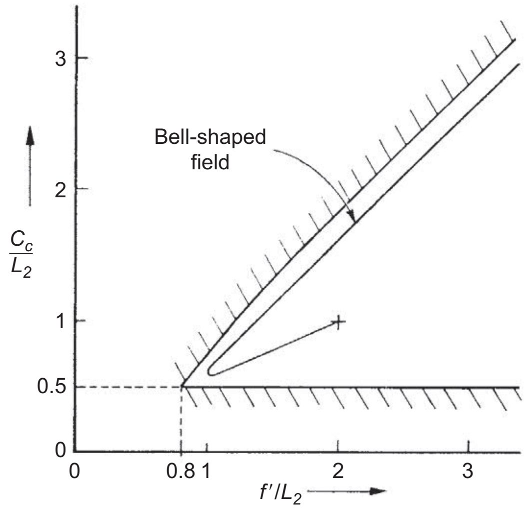

Figure 36.33
Limiting value of C_c/L_2 as a function of f'/L_2 for magnetic lenses. The bell-shaped lens is shown for comparison. *After Tretner (1959), Courtesy Wissenschaftliche Verlagsgesellschaft.*

r_a is the aperture radius and b is the image distance. Setting $(l/2)^2 = fh$, where h is the focal distance, they find

$$G_{el} = \frac{3}{5}\frac{\left(\int \phi'^2\, dz\right)^2}{\int z^2\phi'^2\, dz \int \phi''^2\, dz}$$
$$G_{\text{mag}} = \frac{1}{2}\frac{\left(\int B^2\, dz\right)^2}{\int z^2B^2\, dz \int B'^2\, dz} \tag{36.166}$$

For Scherzer's lens (1936a), $G = 0.267$; for a simple ring, $\phi = \phi_0(a^2 + z^2)^{-1/2}$, $G = 0.119$; for a ring inside a plate, $\phi = \phi_0/(a^2 + z^2)$, $G = 0.2$; for $\phi = \phi_0/(a^2 + z^2)^n$, $G = 2(2n + 3)(4n - 1)/15(4n + 1)(n + 1)$. They likewise investigated various magnetic fields: $B = B_0 \exp(-kz^2)$, for which $G = 2$; and a rotation-free lens, $B(z) = B_0 z \exp(-kz^2)$, $G = 0.222$. For a combined lens, they found

$$G_{comb} = G_{el}\frac{\left(1+\lambda^2 f_{el}/f_{\text{mag}}\right)^2}{\left(1+\lambda^2\, r_{i\,\text{mag}}/r_{i\,el}\right)\left\{1+\lambda^2\left(f_{el}/f_{\text{mag}}\right)\left(l^2_{\text{mag}}/l^2_{el}\right)\right\}} \tag{36.167}$$

where λ is the relative weight of the electrostatic and magnetic contributions ($\lambda = 0$, pure electrostatic and $\lambda \to \infty$, pure magnetic). The combined value of G always lies between G_{el} and G_{mag}.

Riedl (1937) and Gratsiatos (1937) obtained formulae for the aberration coefficients of weak electrostatic einzel lenses and magnetic lenses respectively. Rebsch (1938) and Scherzer (1941) calculated the minimum focal length and minimum spherical and chromatic aberrations of magnetic lenses; for $B(z) = B_0 \exp(z/a)$, $z < 0$, Rebsch found $C_s/a = 0.252$ and Lenz (1951) subsequently showed that the correct value is 0.25. For the same field, $C_c/a = 0.5$ while $a/f = \alpha_n J_1(\alpha_n)$, $J_0(\alpha_n) = 0$. Plass (1942) described electrodes capable of generating Scherzer's best weak symmetric lens (1936a) much less complicated than those proposed by Scherzer himself, and Ramberg (1942) studied the variation of C_s and C_c with lens strength for three electrostatic geometries (two einzel, one immersion) and one magnetic lens. In 1956, Schiske found

$$C_c \geq \frac{\pi}{2} \frac{\eta \hat{\phi}^{1/2}}{B_0} \left(1 + 1/M\right) \tag{36.168}$$

Meanwhile Glaser (1940a) had enquired what field is obtained by setting the integrand in the formula for C_s, in the form $\int f(B) h^4 \, dz$, equal to zero. This yields a differential equation for $B(z)$ but the resulting distribution is not suitable as an imaging field, being convex towards the axis (Rebsch, 1940; Recknagel, 1941; Glaser, 1940c). This field has, however, found a use in β-ray spectroscopy (Siegbahn, 1946) and can be represented by a field model closely related to Glaser's bell-shaped distribution, namely

$$B(z) = \pm \frac{B_0}{1 - z^2/a^2} \qquad (|z| \neq a) \tag{36.169}$$

studied by Sturrock (1951). This model was employed by Glaser (1956a,b), who found that even if the central region only is employed, and hence the fact that the field tends to infinity as $z \to \pm d$ disregarded, the minimum values of C_s/L_1 and C_s/L_2 are in accord with Tretner's rules; specifically, for fixed magnification (M) and $B_0/B_m \to 0$,

$$C_s = \frac{7}{4} L_1 \left(1 + M^{-2}\right) \quad \text{or} \quad \mathrm{C}_s = \frac{7}{2} L_2 \left(1 + M^{-2}\right)$$

while for high magnification and fixed B_0/B_m, we have $C_s = 7/L_1/4$ or $C_s = 7L_2/2$. See too Marton and Bol (1947). The magnetic lens with smallest spherical aberration was also calculated by Sugiura and Suzuki (1943), who arrived at a very asymmetrical design (cf. Suzuki et al., 1982). Recknagel (1941) applied Glaser's idea, of setting the C_s integrand equal to zero and solving for $\phi(z)$, to electrostatic lenses but the conclusions are similar.

The integral expression for the spherical aberration of a combined electrostatic and magnetic lens seems to indicate that there is nothing to be gained by superimposing an electrostatic field on that of a magnetic lens. The integral expression can be deceptive, however, for it is true that a combined lens is worse than either of the individual lens types only if the paraxial solutions are the same in all three cases, which is extremely unlikely. Yada (1986) has shown that, in fact, the spherical aberration coefficient of a magnetic lens can be appreciably reduced by adding a suitably designed electrostatic field (Fig. 36.34).

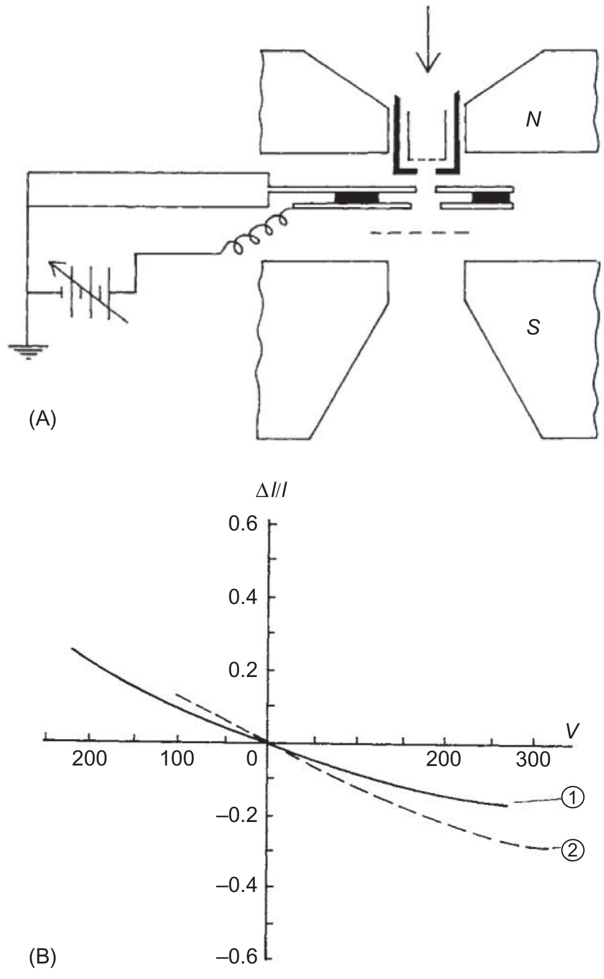

Figure 36.34

(A) Incorporation of an electrostatic lens within the field of a magnetic lens. (B) Variation of the spherical aberration coefficient, expressed in terms of the diffracted beam shift ($\Delta l/l$), with applied voltage (V). For positive voltages, the spherical aberration diminishes but the curves gradually flatten out. Curve 1: symmetric magnetic lens, $S/D = 4/7$; electrode separation 0.2 mm. Curve 2: asymmetric lens, $D_1 = 7$ mm, $D_2 = 2$ mm, $S = 3$ mm; electrode separation 0.1 mm. *After Yada (1996), Courtesy Japanese Society of Electron Microscopy.*

36.5.3 Optimization

Tretner's work had established limits on C_s and C_c in a systematic fashion but it was still not known which polepiece shapes and electrode configurations would approach these limits most closely, particularly if additional practical constraints – the need for a top-entry specimen stage, for example, or for negligible magnetic field at the specimen – were imposed. Some success in this direction has been achieved by Moses, using sophisticated variational calculus and by Szilágyi, using dynamic programming.

It must, however, be stressed that all these attempts at optimization yield a function $B(z)$, not a lens geometry. A more practical approach to lens design, which may not yield a strictly optimal design but reveals more about the intricate relation between lens geometry and optical performance and excellence, is that adopted by Hill and Smith (1980, 1982) and further developed by Tsuno and Smith (1985, 1986, 1987), who computed the field distribution and optical properties for a given geometry and varied the latter methodically until the desired characteristics were obtained; the procedure is interactive, geometry, trajectories and numerical values of the optical quantities being displayed on a screen as the search proceeds. A similar procedure is described by Tsuno and Harada (1983a) and there is related work by Gu and Chen (1984), Gu and Shan (1984) and Taylor and Smith (1986).

Calculus of variations. Moses applied techniques originally developed for quadrupoles (Moses, 1970, 1971a,b) to the design of magnetic round lenses having as little spherical aberration as possible and at the same time free of isotropic and anisotropic coma (Moses, 1972, 1973; Rose and Moses, 1973; Moses, 1974). Several fields, both round and cylindrical, were found that satisfy these conditions and create negligible magnetic field at the specimen. (The cylindrical lenses were also free of rotation.) Moses showed that it is advantageous to use an asymmetric field distribution, as already known from systematic lens studies, falling off slowly on the image side. Kodama (1982) enquired how these findings are modified if the bore radius of the polepieces is regarded as a variable.

Dynamic programming. A very different technique has been explored by Szilágyi (1977a), who has combined the search routines developed for 'dynamic programming' with a very simple electrostatic or magnetic lens model. The method generates vast numbers of field distributions corresponding to a minimum of some quantity, typically the spherical aberration coefficient. From among these, distributions can be selected that satisfy some practical constraint: that the magnification must take some preset value, for example. The function to be minimized, S, will be in the form of an integral between two values of z, which we now denote z_n and z_0. We divide the distance $z_n - z_0$ into n equal regions, so that $z_n - z_0 =: n\Delta z$ and write

$$S =: \Delta z \sum_{1}^{n} F_k \tag{36.170}$$

where

$$F_k \coloneqq \frac{1}{2}\left\{F(z_{k-1}) + F(z_k)\right\} \tag{36.171}$$

and S represents $\int_{z_o}^{z_n} F dz$ The field function $h(z) \coloneqq \eta B(z)/2\hat{\phi}^{1/2}$ is replaced by a sequence of linear segments

$$h(z) = H_0 + H_1\, z \tag{36.172}$$

for which the paraxial ray equation can be solved explicitly in terms of

Bessel functions (Szilágyi, 1969):

$$\begin{pmatrix} r_k \\ r'_k \end{pmatrix} =: \boldsymbol{r}\begin{pmatrix} r_{k-1} \\ r'_{k-1} \end{pmatrix} =: \frac{\pi\left\{H_0(H_0 + H_1\Delta z)\right\}^{1/2}}{2\sqrt{2}H_1}\boldsymbol{R}\begin{pmatrix} r_{k-1} \\ r'_{k-1} \end{pmatrix} \tag{36.173}$$

The elements of the 2×2 matrix $\boldsymbol{R}$ are as follows:

$$\begin{aligned}
R_{11} &= \pm H_0\left\{J_{3/4}(w_0)J_{1/4}(w) + J_{-3/4}(w_0)J_{-1/4}(w)\right\} \\
R_{12} &= J_{-1/4}(w_0)J_{1/4}(w) - J_{1/4}(w_0)J_{-1/4}(w) \\
R_{21} &= (H_0 + H_1\Delta z)H_0\left\{J_{3/4}(w_0)J_{-3/4}(w) - J_{-3/4}(w_0)J_{3/4}(w)\right\} \\
R_{22} &= \pm(H_0 + H_1\Delta z)\left\{J_{-1/4}(w_0)J_{-3/4}(w) + J_{1/4}(w_0)J_{3/4}(w)\right\}
\end{aligned} \tag{36.174}$$

with

$$w_0 = H_0^2/2|H_1|, \quad w = (H_0 + H_1\Delta z)^2/2|H_1| \tag{36.175}$$

Simpler expressions, listed by Szilágyi (1977a), are obtained for the special cases $H_0 = 0$ and $H_1 = 0$. In Eq. (36.174), the plus signs are to be used when H_1 is positive, the minus signs when it is negative.

Denoting the maximum value of $h(z)$ by h_m, we divide the total range over which the field can vary into steps Δh, so that

$$M\Delta h = h_m \tag{36.176}$$

The value of $h(z)$ at the point $z_k = k\Delta z$ is then characterized by a matrix element h_{ik} such that

$$h(z_k) = h_{ik} = i\Delta h \tag{36.177}$$

where i may take any integral value such that $-M \leq i \leq M$. It is to be emphasized that the suffices of h_{ik} characterize very different quantities: field (i) and distance along the optic axis (k). From Eq. (36.172) it is immediately clear that, for the axial zone between z_{k-1} and z_k,

$$H_o = h_{j,k-1} = j\Delta h \tag{36.178a}$$

$$H_1 = \frac{h_{ik} - h_{j,k-1}}{\Delta z} = (i-j)\frac{\Delta h}{\Delta z} \tag{36.178b}$$

As for i, $-M \leq j \leq M$.

The ray $r(z)$ can now be calculated across the kth axial zone, assuming that the preceding zones have already been evaluated, using the matrix $\boldsymbol{R}$. This will generate two new *arrays* of values, one for r and one for r', corresponding to the $(2M+1)$ values of i and j. Eq. (36.171) is then used to calculate the *array* of possible values of the integrand for the kth axial zone:

$$\begin{aligned}(F_k)_{ij} = {} & \frac{1}{2}F\left((r_{k-1})_{ij},\ \ (r'_{k-1})_{ij},\ \ j\Delta h,\ \ (i-j)\frac{\Delta h}{\Delta z}\right)\\ & + \frac{1}{2}F\left((r_k)_{ij},\ \ (r'_k)_{ij},\ \ i\Delta h,\ \ (i-j)\frac{\Delta h}{\Delta z}\right)\end{aligned} \tag{36.179}$$

If $G_{j,k-1}$ denotes the optimum field configuration for the first $k-1$ axial zones, therefore, we obtain G_{ik}, the optimum for the first k zones, by varying j until $(F_k)_{ij} + G_{j,k-1}$ is minimized:

$$G_{ik} = \min\left\{(F_k)_{ij} + G_{j,k-1}\right\} \tag{36.180}$$

Setting out from z_0, this process is performed iteratively until the endpoint z_n is reached. The result is a set of optimum values of H_0 and H_1 which may be represented graphically as line segments as we shall illustrate below. For each axial zone, $z_{k-1} \leq z \leq z_k$, an optimum pair (H_0, H_1) is associated with each initial value of h, $h = i\Delta h$, that is, with each value of h in the plane $z = z_{k-1}$. Fig. (36.35) shows the optimum linear field segments for $-4 \leq h/\Delta h \leq 4$ and $0 \leq z/\Delta z \leq 4$. We see that for each value of $z = k\Delta z$, a field line sets out from each value of $h = i\Delta h$. These are the optimum field segments for each axial zone as a function of the value of the field at the beginning of the axial zone in question.

Our choice from among these numerous optima is guided by boundary conditions — requirements on r_n and r'_n, for example — and by practical considerations. The field must not exhibit variations that cannot be produced to a reasonably good approximation by means of polepieces of acceptable shape.

This procedure has been applied to magnetic lenses (Szilágyi, 1977b) and electrostatic immersion lenses (Szilágyi, 1978a), in both cases with a view to minimizing the spherical aberration (see also Szilágyi, 1978b). The choice of M, n, and $\delta = \Delta h/\Delta z$ is important in obtaining the full range of possible solutions, as Szilágyi (1977b)

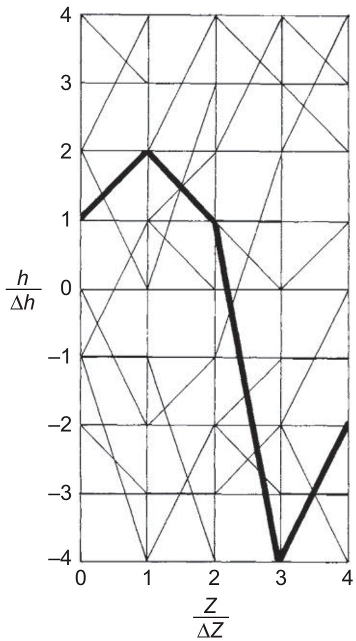

Figure 36.35
The pattern of branching lines shows how minimum values of the integral under consideration are generated for various values of the field as the distance advances step by step. The heavy line shows a relatively smooth, and hence physically realistic, distribution. *After Szilágyi (1977a), Courtesy Wissenschaftliche Verlagsgesellschaft.*

discusses and illustrates in considerable detail. Among the physically interesting special cases that emerge are the type of field found by Glaser by solving the differential equation obtained by setting the integrand of C_s equal to zero (Section 36.4.2) and a distribution with high field at the object, low field at the image and very small spherical aberration. The advantages of such condenser−objective operation have long been known but Szilágyi's approach might enable us to establish the optimum rate of fall-off of the field (though not how to create this in practice). Later work by this author is described in Szilágyi (1984a,b). Many other references are listed in Section 34.7 on optimization.

Calculus of variations reconsidered; direct search. Preikszas and Rose (1995) have re-examined the ways of searching for compound electrostatic−magnetic lenses with well-defined desirable properties. They first revisited the approach employed by Moses, mentioned above, based on the calculus of variations. A set of Euler equation was derived, forming a coupled set of nonlinear differential equations including two Lagrange multipliers. The difficulty of obtaining solutions of these is such that Preikszas and Rose dismissed this approach. Instead, they adopted a method of successive approximations that generates realistic field distributions known as 'direct search' or 'pattern search' (Hooke and Jeeves, 1961). The axial components of the electric field and magnetic induction. $E(z) = -\phi'(z)$ and $B(z)$, are expressed as linear combinations of analytic functions

$$E(z) = \sum_{0}^{N-1} E_n e_n(z), \quad B(z) = \sum_{0}^{N-1} B_n b_n(z)$$

The basis functions $b_n(z)$ are chosen to be the fields of circular currents situated at $z = nd$ and of radius $r = r_B$. For the electrostatic field[5], the basis functions are the fields generated by apertures of radius r_E:

$$b_n(z) = \frac{r_B^2 d}{2\left\{r_B^2 + (z - nd)^2\right\}^{3/2}}$$
$$e_n(z) = \frac{r_E^2 d}{2\left\{r_E^2 + (z - nd)^2\right\}^{3/2}}$$

The search then proceeds as follows. Each member of the set $\{E_n\}$ is varied and constrained in order to ensure that the potential satisfies the condition $\phi_e = \phi_0 + \sum_{0}^{N-1} E_n d$. For high magnification, the h-ray is required to emerge parallel to the optic axis and this is achieved by adjusting the values of B_n. Variations that reduce the total aberration are retained; when they do not, the sign of the variation is reversed and if this too is unsuccessful, the step-size of the variation is reduced. As in all iterative methods, the sequence is repeated until no further changes are obtained.

Preikszas and Rose then describe several lens designs obtained in this way and compare the properties of optimized compound lenses with those of purely electrostatic or purely magnetic lenses. In all cases, the radii are chosen to be $r_E = 1.5$ mm and $r_B = 2$ mm; the separation $d = 0.4$ mm.

The first case studied is a low-voltage immersion lens with a high value of ϕ_e/ϕ_0: $\phi_0 = 500$ V and $\phi_e = 10$ kV. Adding a magnetic field and requiring that the magnetic field at the object plane be low has little effect on the properties of the optimum lens apart from a reduction of C_s from 4.13 to 2.93 mm. If however a high magnetic field can be tolerated at the specimen, C_c can be reduced to 0.56 mm (from 1.63 mm) and C_s to 0.63 mm. The three situations are illustrated in Fig. 36.36A–C. Preikszas and Rose then enquire whether a magnetic lens can be improved by superimposing an electrostatic field. Whether or not the specimen can tolerate a high magnetic field, the addition of an electrostatic field has little effect. Figs 36.36D and E show the field-free case.

[5] The set $\tilde{e}_n = (z - nd)e_n$ would provide a closer match to the physical contraints.

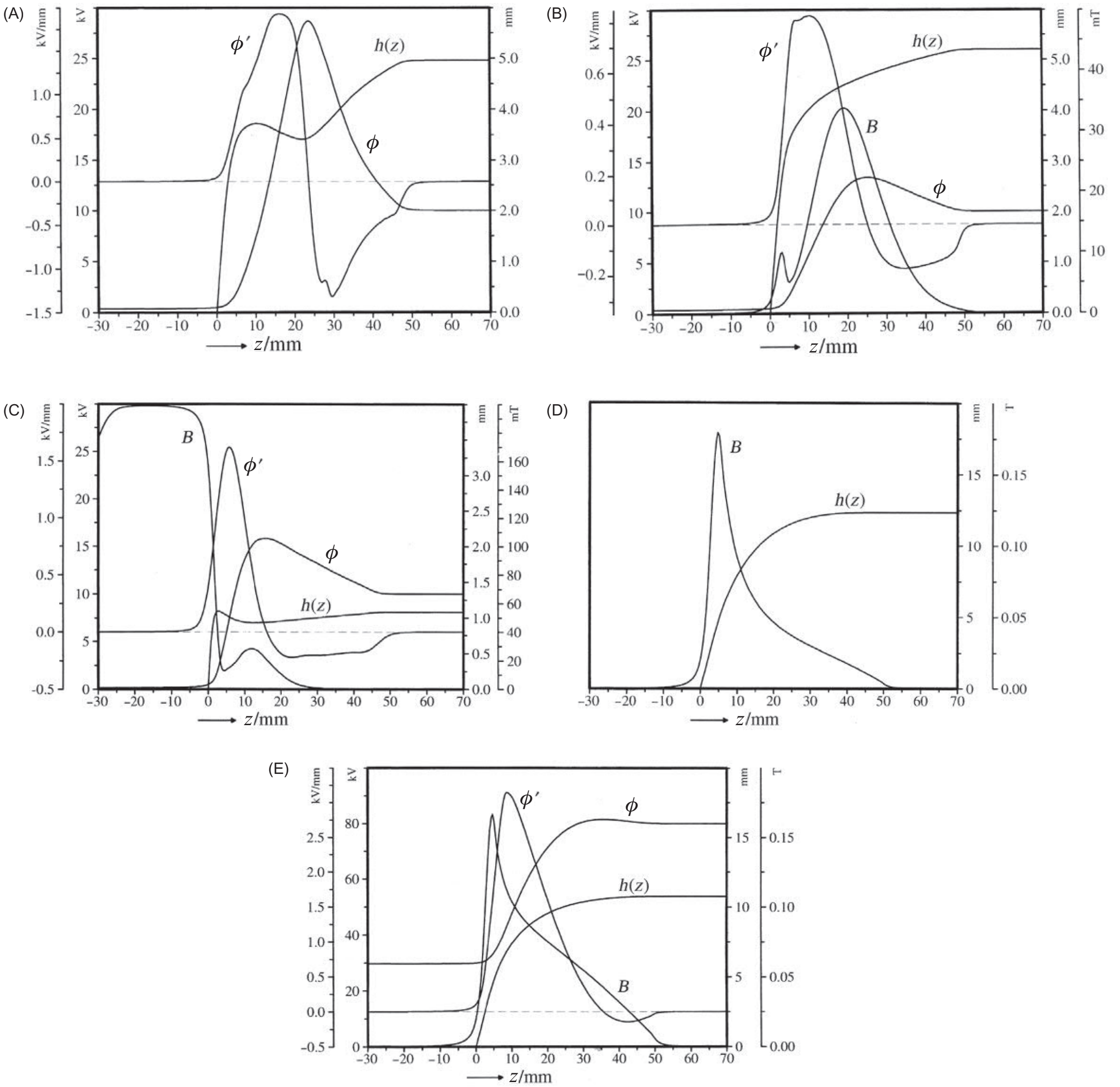

Figure 36.36

Field and potential distributions optimized by direct search (A) Optimum potential $\phi(z)$ and electric field $E(z) = -\phi'(z)$ of an immersion lens. The h-ray is also shown. (B) As (A) but with a magnetic field added, negligible field at the specimen. (C) As (B) but with a high field at the specimen. (D) Optimum induction $B(z)$ in a magnetic lens with negligible field at the specimen. (E) As (D) but with an electrostatic field added and again, negligible field at the specimen. *After Preikszas and Rose (1995), Courtesy Wissenschaftliche Verlagsgesellschaft*

36.6 Lenses of Unusual Geometry

36.6.1 Mini-Lenses, Pancake Lenses and Single-Polepiece Lenses

The traditional magnetic lens geometry, consisting of a pair of polepieces connected by an iron yoke enclosing a coil of approximately rectangular cross-section, has remained essentially unaltered since it was introduced by Ruska and von Borries in the early 1930s. Technologically, it has been vastly improved and modified to permit a host of important elements access to the gap region but its role remains the same: creation of a high, axially symmetric, magnetic field along a short stretch of the optic axis. A first departure from this design was the mini-lens (Le Poole, 1964; Fontijn et al., 1969; Cooke and Duncumb, 1969), consisting of a multi-layer wire-wound conical solenoid. Typically 5 cm long, the mean lens diameter is only a few millimetres and the current density between 50 and 100 A/mm^2. The resulting heat is carried away by a water-cooled copper jacket and there is no yoke: the lens field is the solenoid field.

The practical usefulness of such lenses (e.g., Troyon and Laberrigue, 1977; Podbrdský, 1980, 1982, 1983, 1984, 1987) led Mulvey and colleagues to consider a variety of lens designs in which the coil carried an unusually high current; original methods of dealing with the resulting heat were tested (Mulvey and Newman, 1972, 1973; Mulvey, 1974). Thus a boiling-water lens was subsequently tested by Crewe (1976), for use in a high-voltage instrument. The first practical results of these ideas were the various miniature lenses that emerged from Mulvey's laboratory (surveyed in Mulvey, 1982a,b, 1984); the doublet of Juma and Mulvey (1974, 1975, 1978) is free of overall rotation since the rotation due to one member cancels that of the other (see also Stabenow, 1935; Becker and Wallraff, 1940; Der-Shvarts and Rachkov, 1965; and Section 36.6.1).

Another extreme, high-current density design is the pancake lens, a thin helical coil resembling a gramophone record or 'vinyl' (Bassett and Mulvey, 1969a,b; Mulvey, 1971; Mulvey and Wallington, 1973; Mulvey and Newman, 1974). The axial field can be written explicitly:

$$B(z) = \frac{\mu_0 J}{2l}\left\{\cos\alpha_1 - \cos\alpha_2 + \ln\left(\frac{1+\cos\alpha_2}{1+\cos\alpha_1}\,\frac{D_2\cos\alpha_1}{D_1\cos\alpha_2}\right)\right\} \tag{36.181}$$

where the various parameters are defined in Fig. 36.37 and $l = (D_2 - D_1)/2$. Since

$$B(0) = \frac{\mu_0 J}{l}\left\{\ln\left(\frac{D_2}{D_1}\right)^{1/2}\right\}$$

the maximum flux density can be raised by increasing D_2/D_1 though in practice of course D_1 cannot be too small nor D_2 too big. As D_2/D_1 is increased, the full-width at half-height

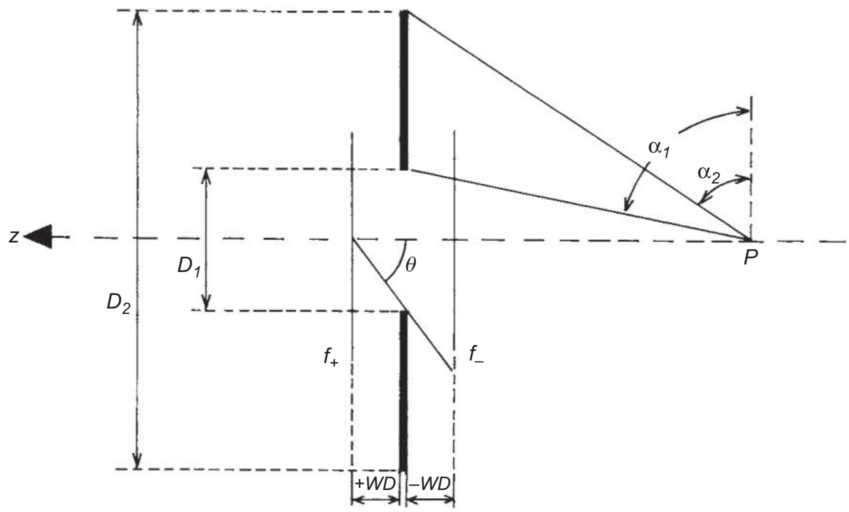

Figure 36.37
Notation used in connection with a thin helical coil (pancake lens). *After Mulvey (1982), Courtesy Springer Verlag.*

($2h$) decreases for constant excitation J, since $\int_{-\infty}^{\infty} Bdz$ must remain constant. Some typical figures are as follows:

D_2/D_1	5	10	25	100	200	1000	10^6
$\ln\{(D_2/D_1)^{1/2}\}$	0.80	1.15	1.60	2.30	2.65	3.45	12.9
$2h/D_m$	0.56	0.47	0.29	0.15	0.09		

D_m denotes $(D_2 + D_1)/2$. The spherical aberration of such lenses has been studied as a function of lens thickness (S) and the ratio D_2/D_1 by Marai (see Mulvey, 1982a). Provided that S/D_m is not greater than 0.1, the spherical aberration parameter (Eq. 36.138) $C_s B_{\max}/\hat{\phi}^{1/2}$ falls to about 3 mT/kV$^{1/2}$ for $D_2/D_1 = 20$ and changes little as D_2/D_1 is further increased; this is a very good value. Some further properties are illustrated in Fig. 36.38.

At comparatively high excitations, only half of the lens field will be used if the lens is acting as an objective or forming a probe, and it is therefore sensible to add an iron backing plate to the lens, in practice extended to provide some magnetic screening as shown in Fig. 36.39. From this idea sprang the family of iron-shrouded pancake lenses, which evolved into the snorkel lens and into a range of geometries known generically as single-polepiece lenses, for only one polepiece is near the optic axis. The exponential and power field models prove to represent the axial flux distribution in these lenses quite well (Marai and Mulvey, 1974; Alshwaikh and Mulvey, 1977; Al-Hilly and Mulvey, 1981), as the calculations of Mulvey and Nasr (1979, 1981), Nasr et al. (1981), Nasr (1982), Al-Khashab

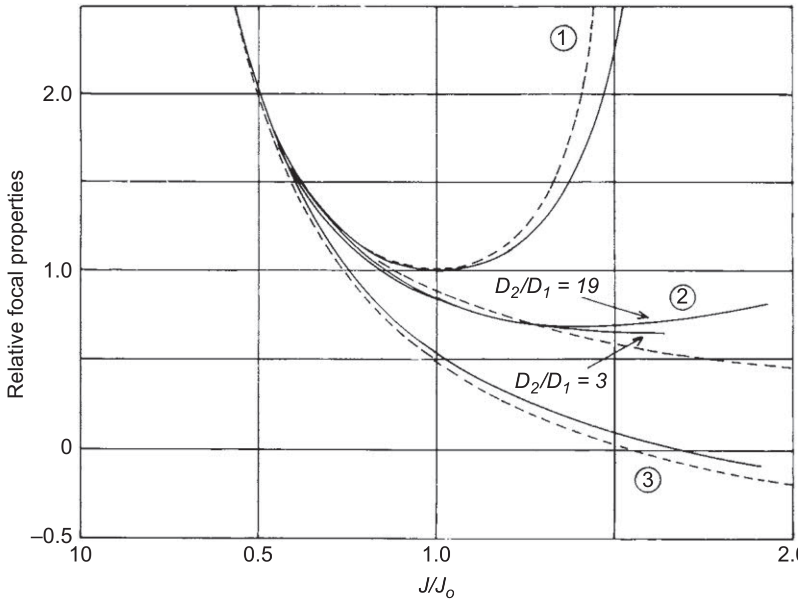

Figure 36.38
Focal properties of flat helical lenses (full curves) for various values of D_1/D_2. The broken curves correspond to long solenoids. 1: $f/f_{\min}$. 2: $f'/f_{\min}$. 3: $z'_{Fo}/f_{\min}$. *After Mulvey (1982), Courtesy Springer Verlag.*

(1983) and later Al-Khashab and Abbas (1991) show. For further calculations, see Lencová (1980), Lencová and Lenc (1982, 1984, 1986), Hill and Smith (1982) and Lenc and Lencová (1984). See also El-Shahat et al. (2014)

These lenses are of interest in instrument design for various reasons. They permit the projector lens system of electron microscopes to be improved in ways that are difficult if not impossible to implement with the bulkier traditional type of lens. The avoidance of image rotation and of spiral distortion is examined in Juma and Mulvey (1974, 1975, 1978), Lambrakis et al. (1977), El-Kamali and Mulvey (1977, 1979, 1980), Marai and Mulvey (1977), Al-Hilly and Mulvey (1981) and Alshwaikh (1982). The optical properties of single-polepieces lenses in general are explored in Marai and Mulvey (1975), Juma and Mulvey (1979, 1980), Juma and Alshwaikh (1979), Juma and Faisal (1981), Christofides and Mulvey (1980), Kordas (1982), Al-Nakeshli et al. (1983, 1984), Juma et al. (1983a,b), Alshwaikh (1983, 1984), Al-Nakeshli and Juma (1985), Juma (1986) and El-Shahat et al. (2014) and in the surveys of Mulvey (1971, 1972, 1974, 1976, 1978, 1980, 1982a,b, 1984, 1986). A single polepiece, with or without an axial bore, offers a possible means of superimposing a magnetic focusing field on the tip of a field-emission gun or of bringing such a field close to the anode (Cleaver, 1978/79, 1979; Stokes, 1980; Venables and Archer, 1980; cf. Troyon and Laberrigue, 1977; Troyon, 1980a,b; Shimoyama et al., 1982,

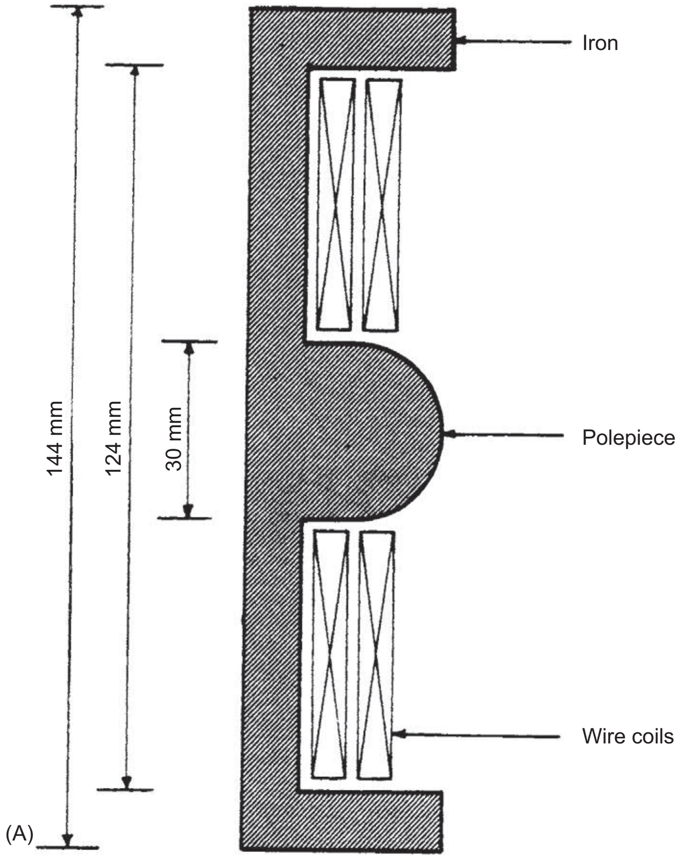

Figure 36.39
Single-polepiece lenses. (A) An unpierced design with spherical pole. (B) A lens with a bore and flat poleface. *After Mulvey and Wallington (1969), Courtesy Institute of Physics.*

1983). A scanning electron microscope incorporating a single-polepiece lens is described by Crewe and Kapp (2003).

The surveys of Mulvey (1982a,b, 1984, 1986) and Tsuno (2009) contain a wealth of additional details. Side-gap lenses, an extreme form of the single-polepiece arrangement, are mentioned in Section 36.7.6.

36.6.2 Laminated Lenses

In conventional magnetic lenses, the flux within the iron circuit is distributed far from uniformly; since the yoke must be designed to ensure that the regions in which the flux density is highest do not saturate, much of the yoke is far from saturation. In terms of weight and volume, this is a very wasteful situation and it is therefore interesting to enquire

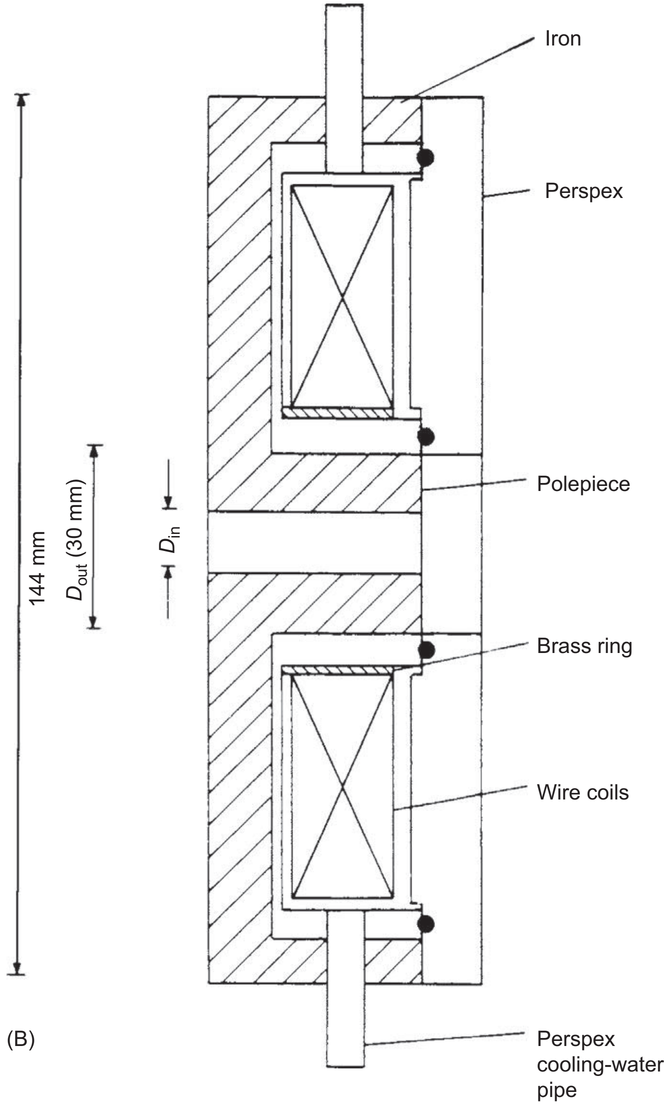

Figure 36.39
(Continued).

whether the yoke can be redesigned to ensure that the iron is everywhere quite near to saturation. This is the question that prompted Balladore and Murillo (Balladore and Murillo, 1977; Murillo, 1978; Balladore et al., 1977, 1981, 1984) to replace the homogeneous iron yoke by a set of laminated silicon-iron transformer stampings; this material is magnetically highly anisotropic, very permeable parallel to the surface of the yoke but of low permeability perpendicular to it. Thus if the magnetic flux is distributed uniformly over the whole cross-section of the yoke at the polepieces, it remains uniformly spread in the remainder of the circuit. The work is surveyed in Murillo et al. (1987ab).

36.7 Special Purpose Lenses

In this closing section, we examine a selection of lens types, indicating their properties and sources of further information. From the numerous candidates, we have selected (i) unsymmetrical round lenses; (ii) the shielding cryolens of Dietrich and colleagues (Dietrich et al., 1969; Weyl et al., 1972); (iii) permanent-magnet lenses; (iv) double-gap, and hence triple-polepiece projectors; (v) the objective specially designed for the observation of ferromagnetic specimens by Tsuno and Harada (1983b); (vi) probe-forming lenses for low-voltage scanning electron microscopes; (vii) the twin-lenses permitting hybrid operation of a transmission electron microscope as a conventional fixed-beam instrument or as a scanning device (STEM) employed in Philips/FEI microscopes; and (viii) multibeam lenses, the lotus-root lens. Other novel designs have been introduced by Tescan, notably the hybrid electrostatic–magnetic lens that provides wide-field optics in the MIRA3 and Brightbeam scanning electron microscopes (Sytar and Zavodny, 2017) and the very original triple-objective employed in a SEM and FIB–SEMs (Jiruše et al., 2016, 2017). These are illustrated in Section 36.7.6.

36.7.1 Unsymmetrical Round Lenses

Lenses in which the shapes of the upper and lower polepieces are different, whether or not the bore radii are equal, have been thoroughly investigated in the search for optimum

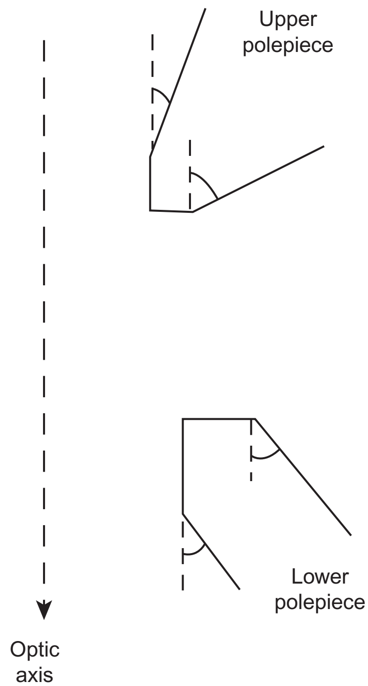

Figure 36.40
Dimensions and angles of lenses that are varied during optimization.

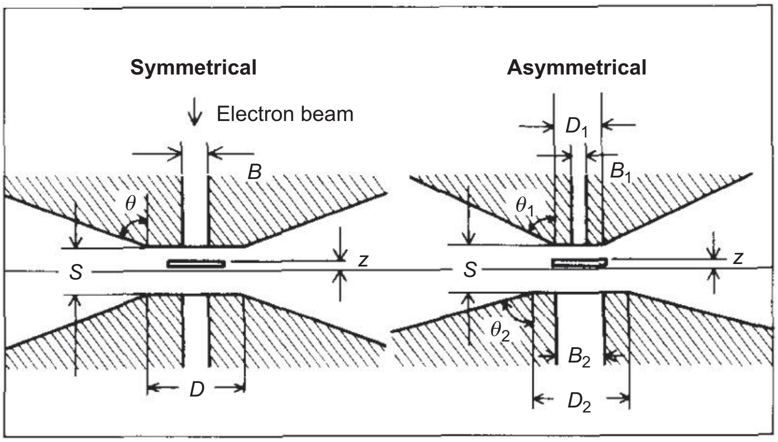

Figure 36.41
Symmetric and asymmetric models of polepieces. *After Tsuno (1993), Courtesy Elsevier.*

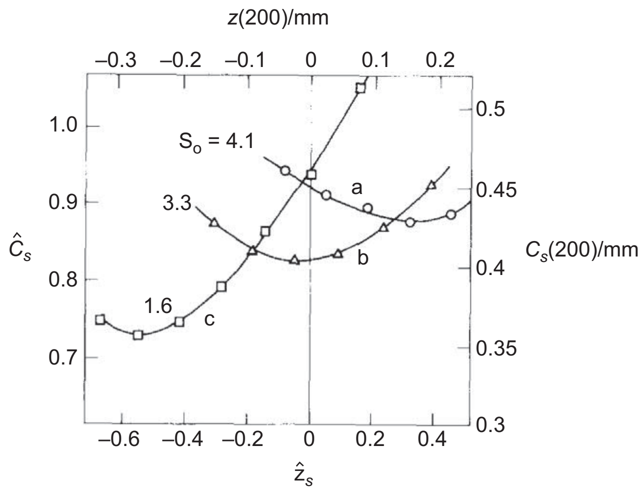

Figure 36.42
The reduced spherical aberration coefficient $\hat{C}_s$ as a function of reduced specimen height $\hat{z}_s$ for three values of the reduced gap $\hat{S}$ (symmetrical lens). (200) indicates the value for $\phi_0 = 200$ kV. *After Tsuno (1993), Courtesy Elsevier.*

performance. The numerous parameters that characterize the geometry are indicated in Fig 36.40. Kato and Tsuno (1990) have attempted to find an optimal design by means of the simplex procedure of Nelder and Mead (1965), which is a direct-search method. In earlier papers (Tsuno and Harada, 1983a,b; Tsuno and Honda, 1983; Tsuno et al., 1983), several such asymmetric designs had been explored. Here we first concentrate on a later study by Tsuno (1993), in which a symmetric and an asymmetric design are studied in detail, including the role of saturation in the yoke and in the polepieces (Fig. 36.41).

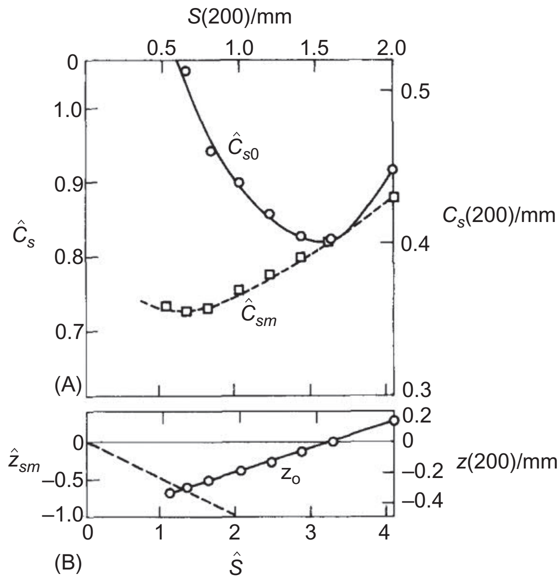

Figure 36.43
(A) The relation between $\hat{S}$ and $\hat{C}_s$ for two values of specimen height $\hat{z}_s = 0$ (specimen in the centre of the gap), denoted $\hat{C}_{s0}$, and $\hat{z}_{sm}$, the position for which $\hat{C}_s$ is smallest ($\hat{C}_{sm}$). (B) $\hat{z}_{sm}$as a function of $\hat{S}$ (symmetrical lens).

Symmetric lens. Fig. 36.42 shows the dependence of the reduced spherical aberration coefficient $\hat{C}_s = C_s/\hat{\phi}_0^{1/2}$ on the reduced specimen position $\hat{z}_s = z_s/\hat{\phi}_0^{1/2}$, where z_s is measured from the centre of the gap. These curves are extremely revealing since they show in what circumstances a condenser–objective or a second-zone lens is desirable and why. Fig. 36.43 shows the relation between the reduced gap, $\hat{S} = S/\phi_0^{1/2}$ and the values of $\hat{C}_s$ when the specimen is placed at the centre of the gap ($\hat{C}_{s0}$) and when it is placed in the plane for which it is smallest ($\hat{C}_{sm}$). These curves correspond to bore diameters $\hat{B} = \hat{D} = \hat{S}/2$ and $\theta = 70°$. Tsuno next illustrates the dependence of the aberration coefficient on $\hat{S}$ for a range of bore diameters (Fig. 36.44). Before turning to the asymmetric lens, Tsuno examines the important role of saturation; his findings are encapsulated in Figs 36.45A and B and 36.46.

Asymmetric lens. Fig. 36.42 shows that the smallest value of $\hat{C}_s$ is obtained with a symmetric lens when the specimen is placed not in the centre of the gap but close to the upper polepiece; there, however, the flux density is lower than in the centre of the lens and asymmetry is a way of remedying this. Fig. 36.47 shows the minimum value of $\hat{C}_s$ and the corresponding specimen plane $\hat{z}_s$ as functions of $\hat{S}$. The bores B_1 and B_2, the diameters of the pole faces D_1 and D_2 and the angles θ_1 and θ_2 are now such that $B_1 < B_2$, $D_1 < D_2$ and $\theta_1 < \theta_2$. The exact values of these were chosen to give the best values of $\hat{C}_s$. Tsuno found that the smallest value of $\hat{C}_s$, 0.63 μm/V$^{1/2}$, corresponded to $\hat{S} = 1.3$ μm/V$^{1/2}$. This minimum value (in μm/V$^{1/2}$) is related to the saturation flux density, B_s, by

$$\hat{C}_{sm,m} = 1.34/B_s$$

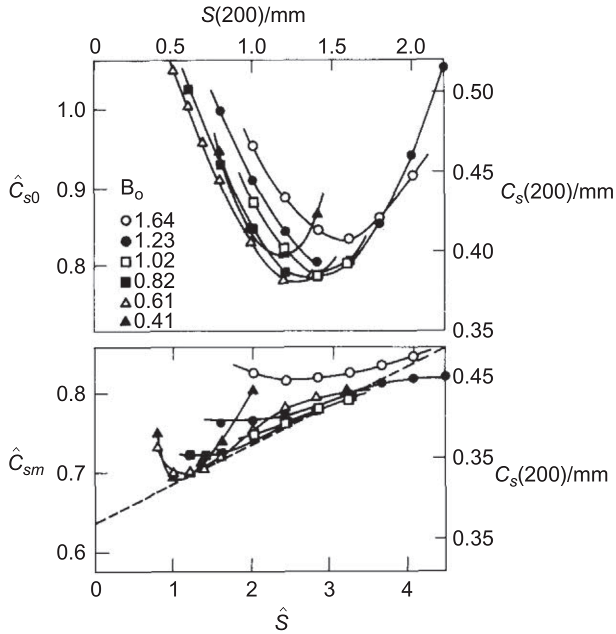

Figure 36.44

Dependence of $\hat{C}_{s0}$ (above) and $\hat{C}_{sm}$ (below) on $\hat{S}$ for various values of the reduced bore diameter (symmetrical lens). *After Tsuno (1993), Courtesy Elsevier.*

All these results are discussed critically in the paper cited; the figures also show the values of the various quantities for $\phi_0 = 200$ kV. Tsuno and Jefferson (1997, 1998) have made a study of the chromatic aberration coefficient, to which we refer for similar curves and punctilious discussion.

These are not the only features of magnetic lenses that can affect its imaging properties. Al-Khashab and colleagues in the University of Mosul have investigated the effect of several geometrical changes of the polepieces and neighbouring yoke and also of the coil geometry. Coil shape is studied by Al-Khashab and Al-Khashab (1988); polepiece angle by Al-Khashab and Al-Obeidy (2000) and Al-Khashab and Ahmad (2005); projector lens design is examined in detail by Al-Khashab (2010), Al-Khashab and Ahmad (2002, 2004, 2005) and Al-Khashab and Al-Hialey (2009); snout shape is considered by Al-Khashab and Al-Abdullah (2006); the Gemini lens configuration is studied by Al-Khashab and Hujazie (2011).

36.7.2 Superconducting Shielding Lenses or Cryolenses

Of the many proposals for the design of superconducting lenses (reviewed by Septier, 1972; Hardy, 1973; Bonjour, 1976; Dietrich, 1976, 1978; Hawkes and Valdrè, 1977;

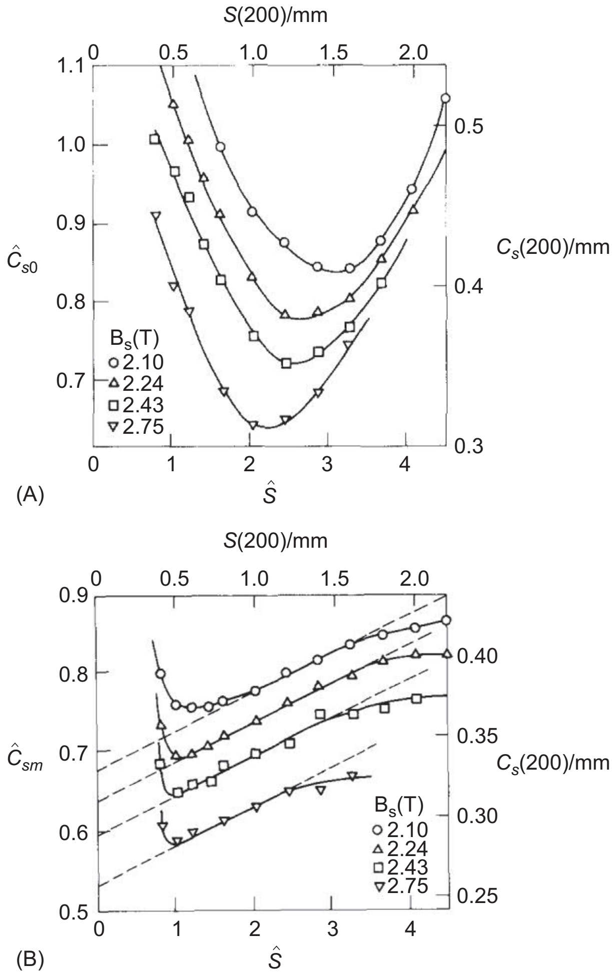

Figure 36.45

The effect of saturation. (A) $\hat{C}_{s0}$ as a function of $\hat{S}$ for four values of the saturation value of the magnetic flux density B_{sat}. of the polepieces. (B) Dependence of $\hat{C}_{sm}$ on $\hat{S}$ for four values of B_{sa} (symmetrical lens). *After Tsuno (1993), Courtesy Elsevier.*

Riecke, 1982), only the shielding lens introduced by Dietrich et al. (1969) survived, though the use of holmium or dysprosium as polepiece material in a lens of more traditional design was found promising (Bonjour, 1975a–c; see Section 36.3, saturated lenses). The shielding lens creates a high field within a small region of the optic axis by means of a superconducting coil enclosed within a metal shield also in the superconducting state. Magnetic flux cannot enter the latter and the coil field is therefore confined to the gap between the lips of the shield (Fig. 36.48). The evolution of this type of lens may be traced through the work of Dietrich and colleagues (Dietrich et al., 1970, 1972a,b, 1973, 1974,

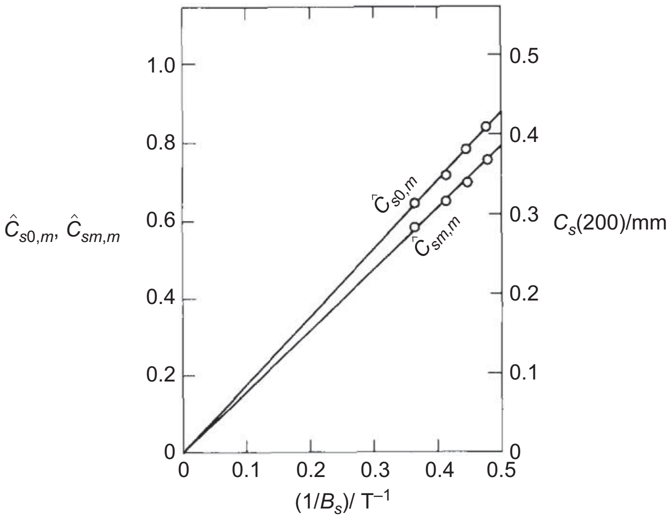

Figure 36.46

Dependence of the minimum values of $\hat{C}_{s0}$ and $\hat{C}_{sm}$, denoted $\hat{C}_{s0,m}$ and $\hat{C}_{sm,m}$ on $1/B_s$ (symmetrical lens). *After Tsuno (1993), Courtesy Elsevier.*

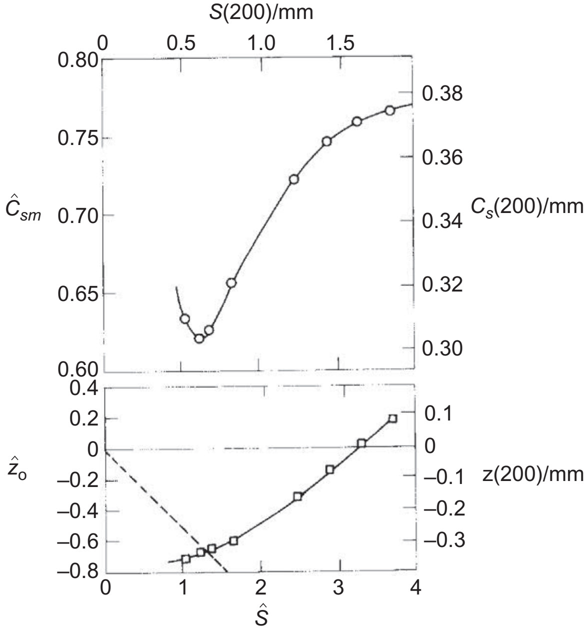

Figure 36.47

Dependence of $\hat{C}_{sm}$ and $\hat{z}_o$ on $\hat{S}$ for an asymmetric lens ($B_1 < B_2$, $D_1 < D_2$ and $G_1 < G_2$). The units are μm.$V^{-1/2}$. *After Tsuno (1993), Courtesy Elsevier.*

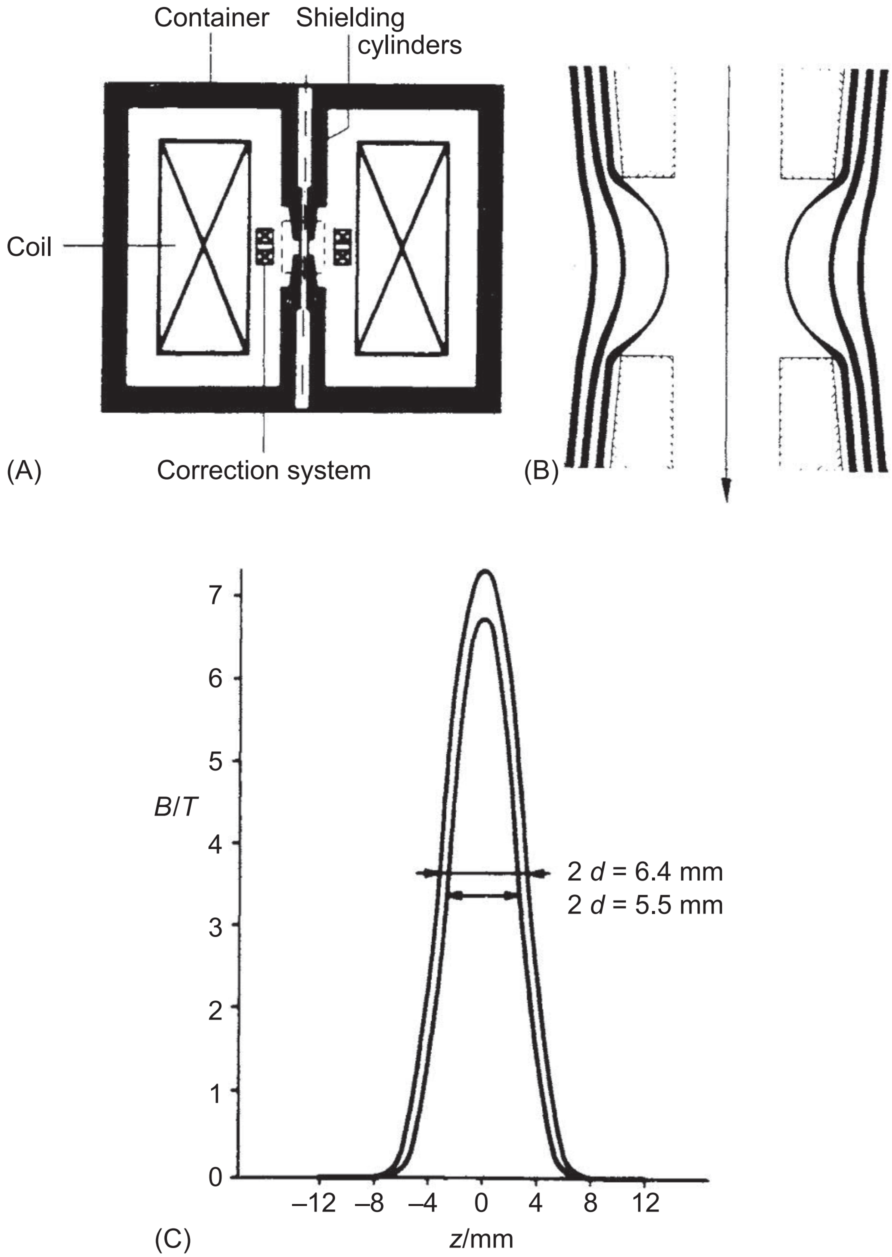

Figure 36.48

Superconducting lens of the shielding type, or cryolens. (A) Design. (B) Field distribution in the gap. (C) Axial field distribution with shielding cylinders made of a sintered niobium-tin material. For the maximum induction of $B_0 = 7.3$ T, it is found that $f' = 2$ mm, $C_c = 1.5$ mm and $C_s = 1.3$ mm at 1500 kV for condenser—objective operation. *After Lefranc et al. (1982), Courtesy North Holland Publishing Co.*

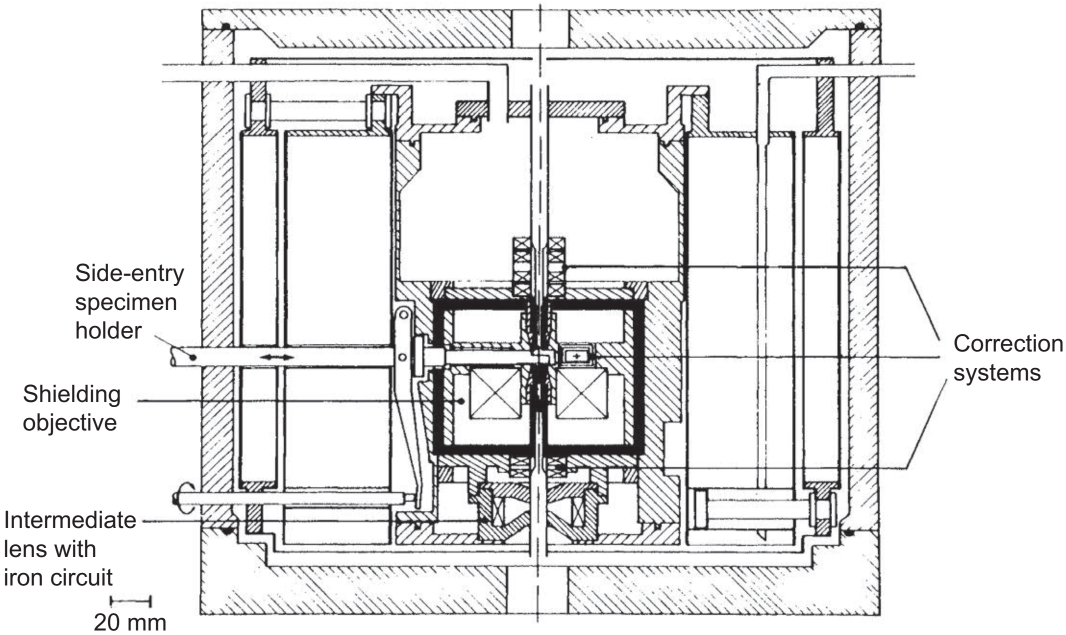

Figure 36.49
Detailed drawing of a cryolens with cryostat. *After Lefranc et al. (1982), Courtesy North Holland Publishing Co.*

1975, 1976, 1977, 1980; Weyl et al., 1972; Knapek, 1975, 1976; Lefranc and Nachtrieb, 1979; Lefranc and Müller, 1981; Lefranc et al., 1981, 1982); it has culminated in practical designs that could replace the normal objective in commercial microscopes for accelerating voltages up to 0.5 MV, and the extension to higher voltages presents no particular problem (Lefranc et al., 1982; Iwatsuki et al., 1986). Such an objective is shown with its cryostat in Fig. 36.49, where the focal length and principal aberration coefficients are also listed. A 400 kV microscope with a superconducting objective was tested up to 250 kV by Dietrich et al. (1977). After many improvements, this instrument (known as SULEIKA,[6] SUpraLEItende KryoApparat; Zemlin, 1992) was used by Baldwin et al. (1988) to obtain images of purple membrane at 2.8 Å resolution and by Henderson et al. (1986, 1990) who studied purple membrane and rhodopsin. A small weakness of SULEIKA was detected by Frank et al. (1993). A new instrument has been constructed (Zemlin et al., 1996, 1999) by incorporating a shielding lens in a Philips CM20 electron microscope with a field-emission gun (SOPHIE, Superconducting Objective in a PHIlips Electron microscope).

[6] Like speaker, not hiker (Max Beerbohm).

The narrow field distribution on the axis is essentially achieved by a subtraction, since currents flow on the surface of the shielding material to ensure that the boundary conditions governing the field at the interface are satisfied, and the observed field is the difference between these and the coil field. This has the practical consequence that any misalignment of the shielding cylinders causes a substantial parasitic aberration and that a considerable explosive force is exerted on the lens casing. It is, however, not difficult to correct the effects of any slight misalignment.

36.7.3 Permanent-Magnet Lenses

Much thought was given at one time to the design of electron microscopes using permanent-magnet lenses (von Borries et al., 1940, 1953, 1956a,b; von Borries, 1949, 1952; von Borries and Lenz, 1956; von Borries and Langner, 1956; Müller, 1956, 1957; Müller and Ruska, 1958, 1968; Müller et al., 1969; Ruska, 1951, 1952; Reisner, 1951; Reisner and Dornfeld, 1950; Reisner and Zollers, 1951; Kimura, 1956, 1959a,b, 1962; Kimura and Idei, 1957; Kimura and Kikuchi, 1958, 1959; Kimura and Katagiri, 1959) and sporadic proposals for such instruments continued to appear. A detailed account of the technical aspects of permanent-magnet lens design is to be found in Riecke (1982). Here we draw attention to a model that represents 'magnetic einzel lenses' as Lenz (1956a) styles them, quite satisfactorily, and to a more elaborate model devised by Baba and Kanaya (1979); neither model is confined to permanent-magnet lenses but it was these that prompted Lenz's study.

Since there is no current-carrying coil in a permanent-magnet lens, $\int_{-\infty}^{\infty} B(z)dz = 0$ and so $B(z)$ must have both positive and negative parts; the same is true of $E(z)$ (or $\phi'(z)$) in an einzel lens, where $\int_{\infty}^{\infty} E(z)dz = 0$, whence the name in the magnetic case. In the model introduced by Lenz, the field $B(z)$ is symmetric about the midplane of the lens and is represented by

$$B(z) = \frac{Cz}{1 + z^4/a^4} \tag{36.183}$$

The corresponding paraxial equation can be cast into the form satisfied by the hypergeometric function, namely

$$r(1-r)\frac{d^2u}{dr^2} + \left(\frac{5}{4} - 2r\right)\frac{du}{dr} + k^2u = 0 \tag{36.184}$$

where $r := 1/(1 + z^2/a^2)$ and $k := \eta aC/8\hat{\phi}^{1/2}$. The general solution is then

$$u = AF\left(\frac{2+w}{4}, \frac{2-w}{4}, \frac{5}{4}, \frac{1}{1+\zeta^4}\right) + B\left(1+\zeta^4\right)^{1/4} F\left(\frac{1+w}{4}, \frac{1-w}{4}, \frac{3}{4}, \frac{1}{1+\zeta^2}\right) \qquad (36.185)$$
$$w := 4\left(1+4k^2\right), \; \zeta = z/a$$

A more complicated expression is needed in the range $-1 \le \zeta \le 1$. The asymptotic focal length and focal distance can be written down explicitly:

$$\frac{f}{a} = -\frac{\Gamma\left((3+w)/4\right)\Gamma\left((3-w)/4\right)}{2\sqrt{2}\cos\left(w\pi/4\right)\Gamma\left(5/4\right)\Gamma\left(1/4\right)}$$
$$\frac{z_F}{a} = -\frac{\Gamma\left((3+w)/4\right)\Gamma\left((3-w)/4\right)\left(1+2\cos\left(w\pi/2\right)\right)}{2\sqrt{2}\Gamma\left(5/4\right)\Gamma\left(1/4\right)\cos\left(\left(w\pi/4\right)\right)} \qquad (36.186)$$

This model is extended by Baba and Kanaya (1979) to the more general form

$$B(z) = \frac{B_0 C\left|z/a\right|^{m-1}}{1+\left|z/a\right|^{2m}} \qquad (36.187)$$

which reduces to Eq. (36.183) for $m = 2$. The paraxial equation is again soluble in terms of the hypergeometric function. The real focal length is given by

$$\frac{f'}{a} = -\frac{1}{B}F\left(\frac{m+w}{2m}, \frac{m-w}{2m}, 1+1/2m, 1/\left(1+\zeta_{Fi}^{2m}\right)\right)$$

with

$$B := \frac{\Gamma^2\left(1/2m\right)\cos\left(w\pi/2m\right)}{m\sin\left(\pi/2m\right)\Gamma(p_1)\Gamma(p_2)} \qquad (36.188)$$

and

$$p_1 := \frac{m+1+w}{2m} \quad , \quad p_2 := \frac{m+1-w}{2m}$$

where ζ_{Fi} corresponds to the image focus. The asymptotic cardinal elements are given by

$$\begin{aligned}
\frac{f}{a} &= -\frac{m\sin(\pi/2m)\Gamma(p_1)\Gamma(p_2)}{\Gamma^2(1/2m)\cos(w\pi/2m)}\\
\frac{z_{Fi}}{a} &= -\frac{z_{Fo}}{a}\\
&= \frac{m\{\cos(\pi/m)+1+2\cos(w\pi/2m)\}\Gamma(p_1)\Gamma(p_2)}{2\sin(\pi/2m)\cos(w\pi/2m)\Gamma^2(1/2m)}\\
k &:= \frac{\eta aCB_0}{4m\hat{\phi}^{1/2}} \text{ and } w^2 := m^2(1+4k^2)
\end{aligned} \tag{36.189}$$

Fig. 36.50 shows $B(z)$ for various values of m and the various cardinal elements as functions of k^2 for values of m between 1.5 and 10. Lengths are measured in units of $a_{\max}$, the maximum half-width:

$$\alpha := \frac{a_{\max}}{a} = \left(\frac{m-1}{m+1}\right)^{1/2m} \tag{36.190}$$

Real and asymptotic aberration coefficients are likewise plotted for the case $m = 3$ and infinite magnification; the authors give formulae for all the coefficients, though the integrals cannot be evaluated in closed form.

Baba and Kanaya also give full formulae for a modified model that closely represents the field in lenses with $S/D \geq 3/4$, for which the basic model is inadequate. Here (36.187) represents the field in the zone $|z| \leq a_{\max}$ but outside this, the model discussed in Section 36.3.5 (36.93) is used:

$$\begin{aligned}
|z| \leq a_{\max}, \quad B(z) &= \frac{B_0 C\zeta^{m_1-1}}{1+\zeta^{2m_1}} \qquad \zeta := \alpha z/a_{\max} = z/a\\
|z| \geq a_{\max}, \quad B(z) &= B_0\left(1-\zeta^2\right)^{(2m_2-1)/2}
\end{aligned} \tag{36.191}$$

Two specific cases are discussed in detail, a lens described by $m = 3$ and a wide-gap lens, for which $m_1 = 2.78$ and $m_2 = 0.72$; the latter describes a design for which $S/D = 1.2$ and $T/D = 1.6$, where T is the thickness of the central polepiece. We refer to the original paper for details of these and draw attention to the sets of curves that form design charts for magnetic einzel lenses. For $(S+T)/D = 1$ and 2, the authors present the principal lens parameters as functions of $J/\hat{\phi}^{1/2}$ for several values of S/D and indicate the values of $J/\hat{\phi}^{1/2}$ for which the Finsterwalder condition is satisfied (24.135). Although Baba and Kanaya do not discuss the simultaneous elimination of isotropic and anisotropic distortion, their curves have much the same form as those of Tsuno and Harada (1981a,b; Section 36.7.1), though the different presentation of the results makes it difficult to compare the anisotropic coefficients.

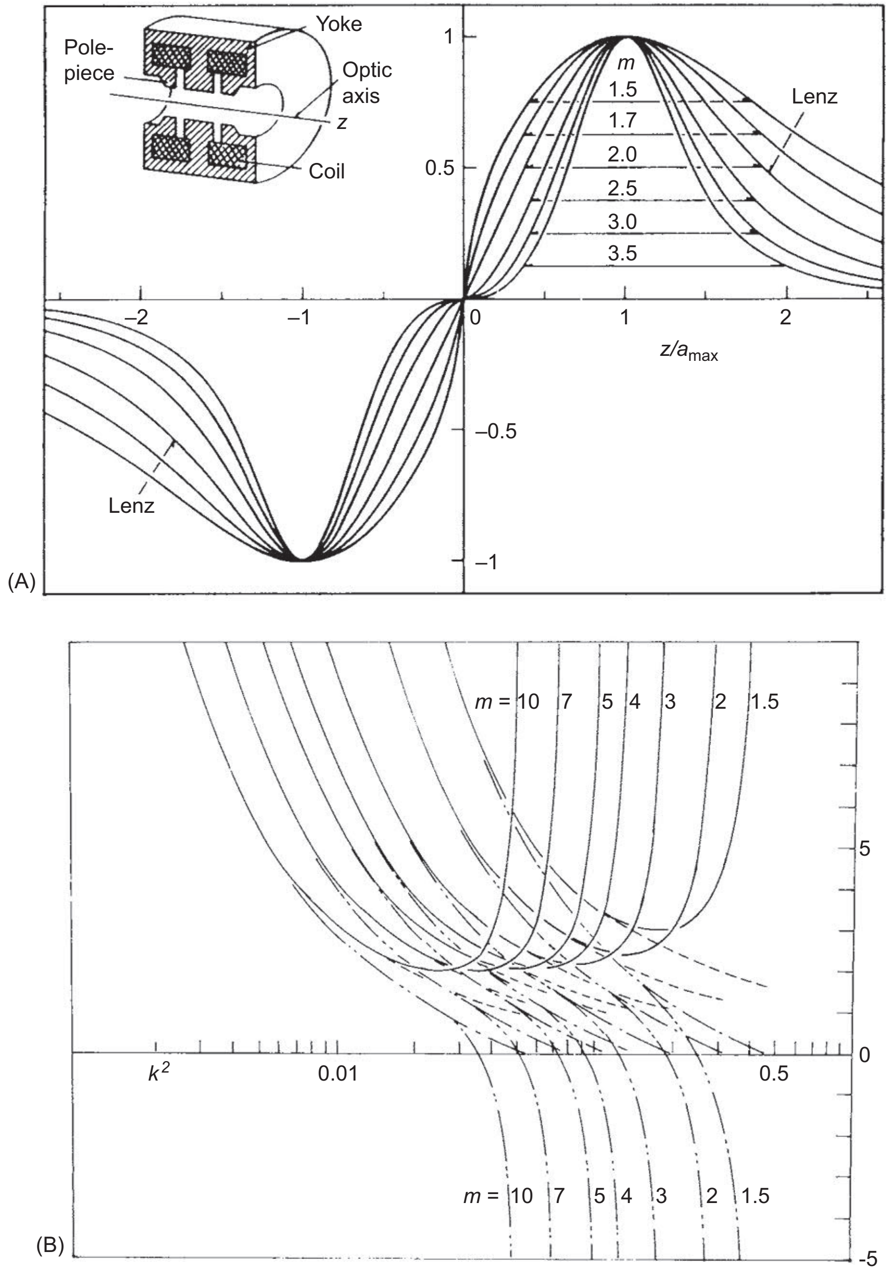

Figure 36.50

(A) Model fields for permanent-magnet lenses. The ordinate is normalized to unity. (B) Focal properties for various values of m. — f/a_{max}; - - - f'/a_{max}; — · — z'_{Fi}/a_{max}; — · · — z_{Fi}/a_{max}.
After Baba and Kanaya (1959), Courtesy Institute of Physics.

Attempts to construct miniature scanning electron microscopes have revived interest in permanent-magnet lenses. For detailed proposals and related material, see Tsuno and Nakayama (1976), Adamec et al. (1995), Khursheed (1998, 2000), Khursheed et al. (1997, 1998, 2001a,b, 2006), Buijsse (2003), Rochow et al. (2008), Nelliyan and Khursheed (2011), Chang and Chen (2016) and especially Khursheed (2001).

Delong and colleagues have been developing miniature transmission electron microscopes incorporating permanent-magnet lenses for many years, initially at the Institute of Scientific Instruments in Brno (Delong, 1992, 1993, 1994). Later, the company Delong Instruments was formed and a miniature low-voltage TEM was released, the LVEM-5. Like the prototype, this 5 kV instrument has a Schottky gun, followed by permanent-magnet condenser and objective lenses. The intermediate and projector lenses are electrostatic. Between these is a versatile unit consisting of three octopoles, capable of acting as a stigmator, assuring alignment and providing suitable fields for the scanning mode (Hlalil and Delong, 1994). A light microscope magnifies the very small fluorescent screen (Delong et al., 1998, 2000; Coufalová and Delong, 2000; Štěpán and Delong, 2000). The column was subsequently modified to allow scanning and scanning transmission imaging (Delong et al., 2002).

A new design has been introduced to permit imaging up to 25 kV without altering the basic conception, the LVEM-25 (Coufalová et al., 2015a,b, 2017; Sintorn et al., 2014).

36.7.4 Triple-Polepiece Projector Lenses

We have already mentioned the problem of distortion in the projector lenses of electron microscopes, which has been a perennial preoccupation of lens designers (Hillier, 1946; Mulvey and Jacob, 1949; Liebmann, 1952; Wegmann, 1953, 1954; De and Saha, 1954; Kynaston and Mulvey, 1962, 1963) and has more recently been investigated and to some extent solved by Mulvey and colleagues using first double-gap lenses and later single-polepiece lenses (see Section 36.6.1 and surveys by Mulvey, 1982, 1984). The work of Juma and Mulvey on double-gap lenses has been extended by Tsuno and Harada who investigated both experimentally and by computation symmetric and asymmetric double-gap designs (Tsuno and Harada, 1981a,b, 1982; Tsuno, 1984). For symmetric permanent-magnet lenses (Fig. 36.51A), they first measured the field and found that the full-width at half-height for one of the gaps, a, the gap, S, the thickness of the middle polepiece, T (here, 3 mm), and the distance from the centre of the latter to the field maximum, h, are related by

$$\begin{aligned} h &= 0.8S + 0.07T^2 \\ a &= \begin{cases} (S+4)^{1/2} & \text{for } T \geq D \\ S & \text{for } T < D \end{cases} \end{aligned} \tag{36.192}$$

For two particular geometries $S = 5$ mm and $S = 3$ mm, $D = T = 3$ mm, Fig. 36.51B shows the projector focal length and the isotropic (radial) and anisotropic (spiral) distortion as functions of $aB_0/\hat{\phi}^{1/2}$. For low magnification, $M = M_1$, f has a minimum at 8.8 mm for $aB_0/\hat{\phi}^{1/2} =$ 0.2 mm T/kV$^{1/2}$ and at higher magnification, $M = M_2$, f has a second minimum at 1.0 mm for an excitation of 0.6 mm T/kV$^{1/2}$. The isotropic distortion passes through zero when the focal length attains its first minimum, as already noted by Juma and Mulvey, but the anisotropic coefficient never vanishes. If T and S are altered, keeping $D = 3$ mm, the excitation at which the focal length is smallest and the radial distortion vanishes for low magnification is linearly related to T^2/S. For $h < 4.5$ mm, the minimum focal length is equal to $2h$. The anisotropic coefficient at minimum focal length increases linearly with T^2/S. The properties of triple-polepiece coil lenses are extensively illustrated in Tsuno and Harada (1981b).

Clearly, the anisotropic distortion does not vanish in this symmetrical design but examination of the sources of the contributions to the aberration integrals suggests that by rendering the lens asymmetric, it can be reduced to zero. This proves to be correct (Tsuno and Harada, 1981b) and Fig. 36.52A shows that there is a value of the ratio of the first and second gaps (S_1 and S_2) for which both distortions vanish simultaneously, namely $S_1/S_2 = 3.3$. A similar result is obtained if the first and last bores are different (Fig. 36.52B). Tsuno and Takaoka (1983) and Tsuno and Inoue (1984) have used the lens shown in Fig. 36.53A to observe magnetic specimens placed in a zone almost free of magnetic field.

A systematic study of double-polepiece lenses has been made by Kadhem (2015), which leads to several possible polepiece configurations with predetermined properties. The method employed is described by Kadhem and Al-Obaidi (2013); cf. Al-Jubori (2001) and Al-Obaidi (1995). See too Chandran and Biswas (2015).

36.7.5 Objective Lens With Low Magnetic Field at the Specimen Capable of Good Resolution

It is not easy to study ferromagnetic specimens at high resolution since the specimen plane must be situated in a region where the lens field is low. If the specimen is shielded from the field of the lens (Shirota et al., 1976; Chapman and Jakubovics, 1981), the resolution is poor. In an attempt to improve the situation, Tsuno and Taoka (1982, 1983) have studied asymmetric lenses in which the upper bore D_1 is very small close to the gap and the specimen is inserted into this upper bore through a hole cut in the polepiece (Fig. 36.54). Their paper describes their design strategy in detail and explains with admirable and rare clarity how they were led to their final design. Here we merely indicate the principal points of interest. Their various models all have a large lower bore (D_2) and small upper bore (D_1); it is found that for small C_s, the specimen should be as close to the face of the upper polepiece as possible (L small in Fig. 36.54) and that the diameter of the face of the upper polepiece (Δ_1) should be smaller than D_2: C_s decreases linearly with Δ_1/D_2. Although L must be small, it cannot be reduced indefinitely because the lens field at high excitation will be too high and the nearness to the gap of the hole through which the specimen holder passes creates excessive astigmatism. Conversely, the thickness (t) of the upper polepiece

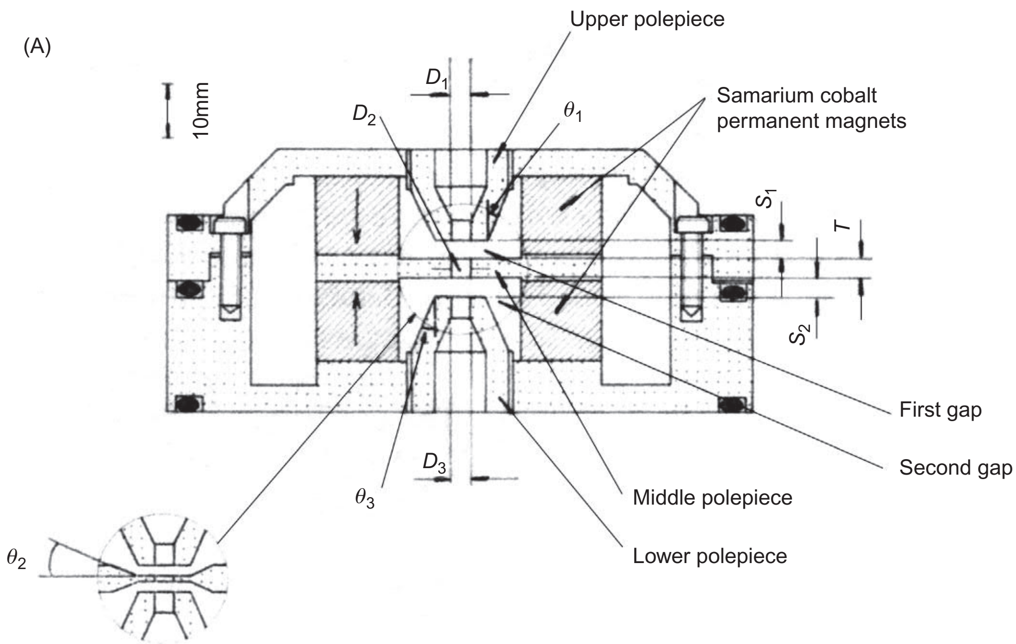

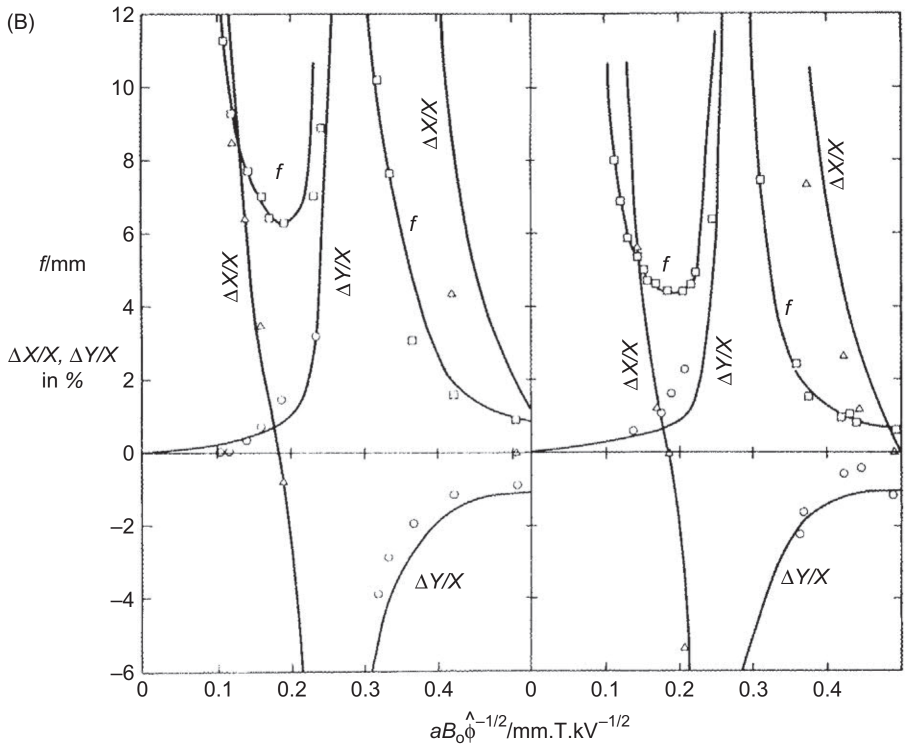

Figure 36.51

Symmetric double-gap lenses. (A) Geometry and notation. (B) Computed and measured values of the projector focal length and measures of the isotropic and anisotropic distortion coefficients for two lenses. Left: $S = D = T = 3$ mm. Right: $S = 5$ mm, $D = T = 3$ mm. In Figs 36.51 and 36.52, $\Delta X/X$ and $\Delta Y/X$ are measures of the isotropic and anisotropic distortion respectively. *After Tsuno and Harada (1981a), Courtesy Institute of Physics.*

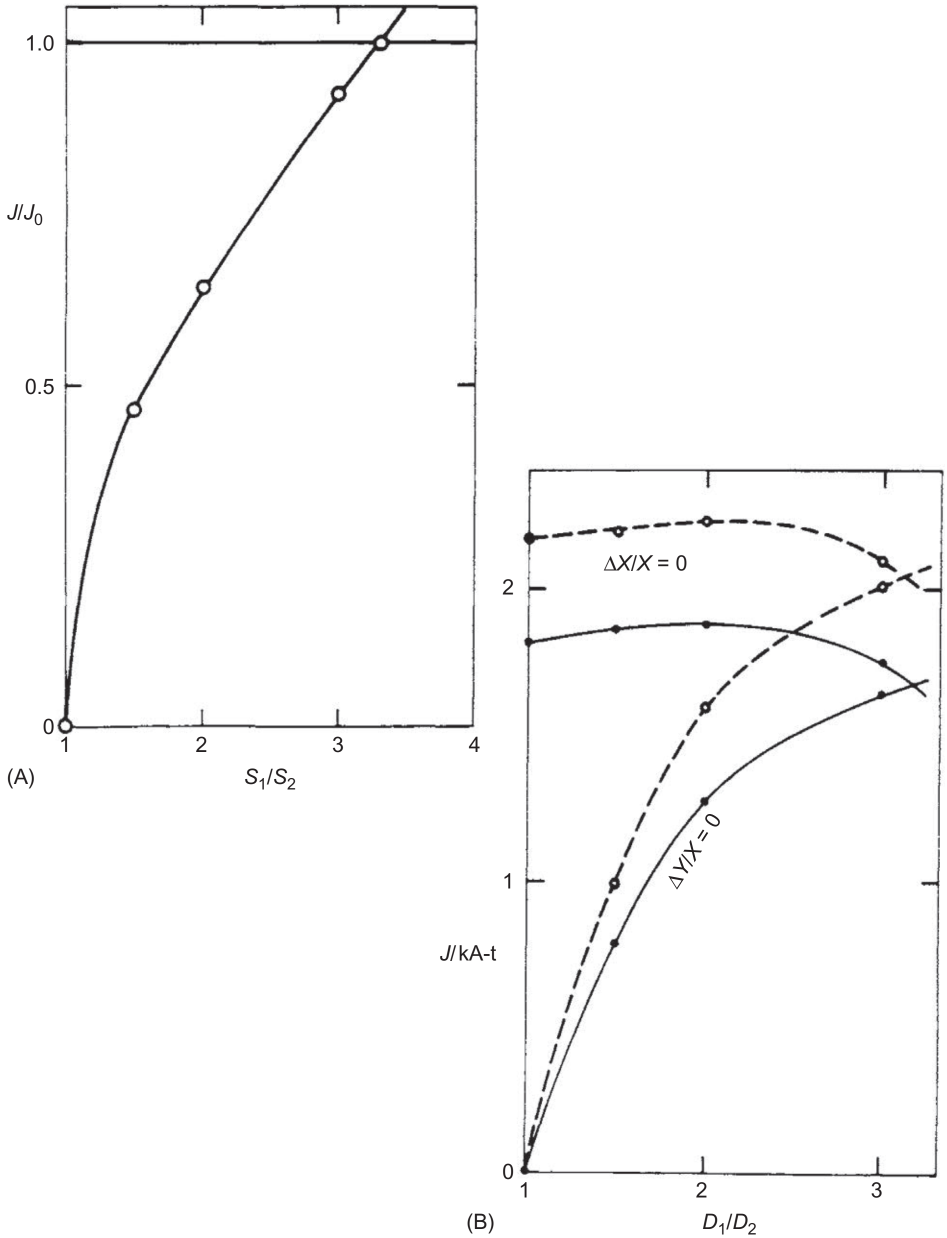

Figure 36.52
Unsymmetric double-gap lenses. (A) The ordinate is the ratio of the excitation at which the anisotropic distortion vanishes (J) to that at which the isotropic distortion vanishes (J_0) as a function of the ratio of the gap lengths S_1/S_2. Both coefficients vanish simultaneously for $J/J_0 = 1$. (B) Conditions in which both distortion coefficients vanish can also be found if $S_1 = S_2$ but $D_1 \neq D_3$. The ordinate shows the excitations required for vanishing isotropic and anisotropic distortions as a function of the bore ratio D_1/D_3. Full lines: central polepiece thickness = 2 mm; broken lines, 1 mm. *After Tsuno and Harada (1981b), Courtesy Institute of Physics.*

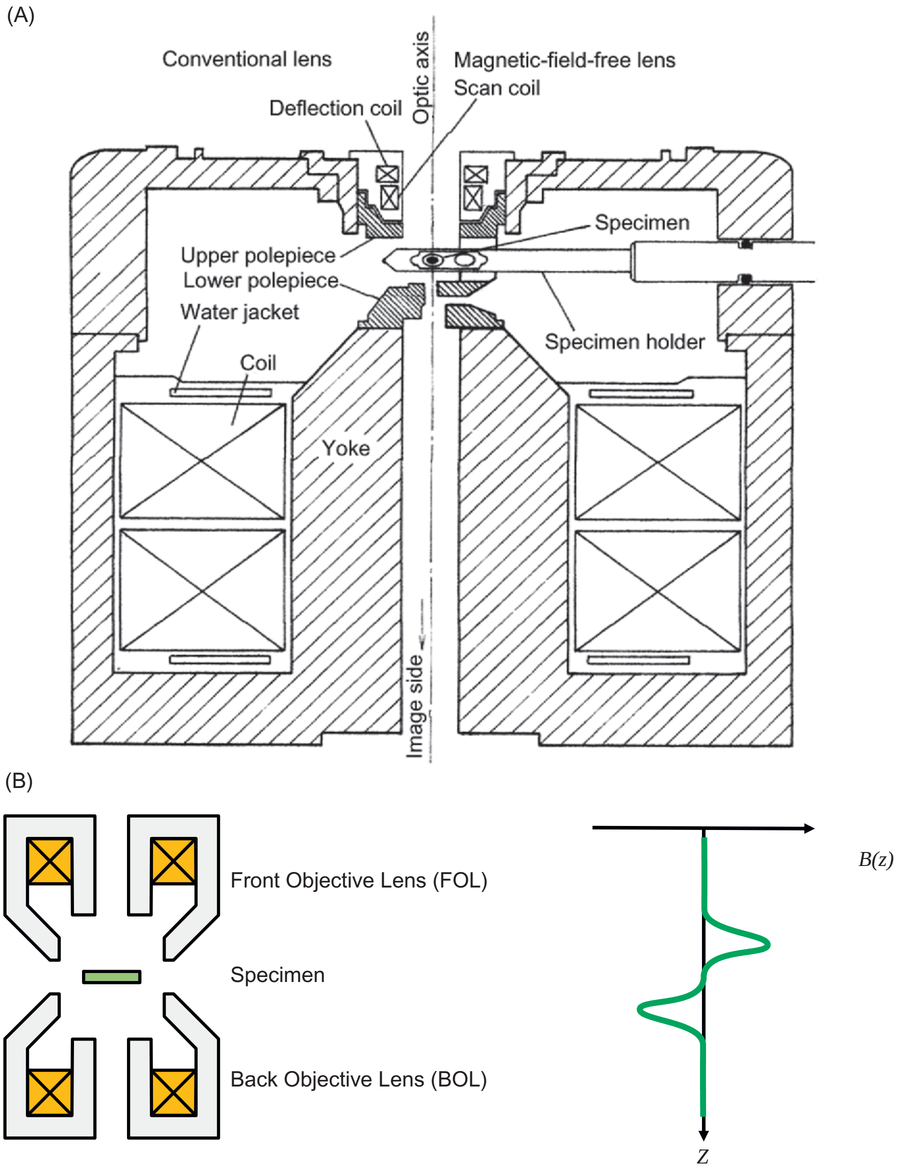

Figure 36.53
(A) Cross-sections of a conventional objective lens (left) and a double-polepiece objective for which there is no magnetic field at the specimen (right). (B) Pair of magnetic lenses for which the magnetic field at the specimen is cancelled. *After Tsuno and Taoka (1983), Courtesy the Japanese Society of Applied Physics* (A) *and Kohno et al. (2017a), Courtesy the authors* (B).

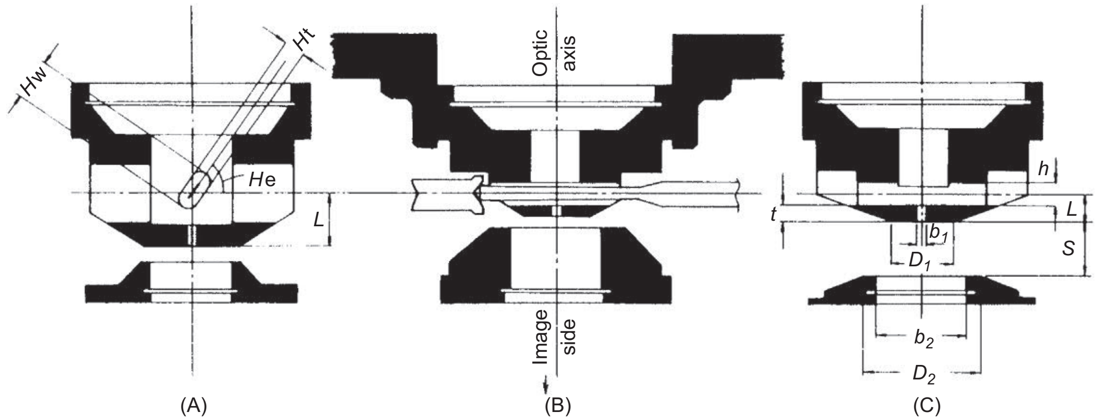

Figure 36.54
Magnetic lens designs in which the field at the object plane is very small. *After Tsuno and Taoka (1983), Courtesy Japanese Journal of Applied Physics.*

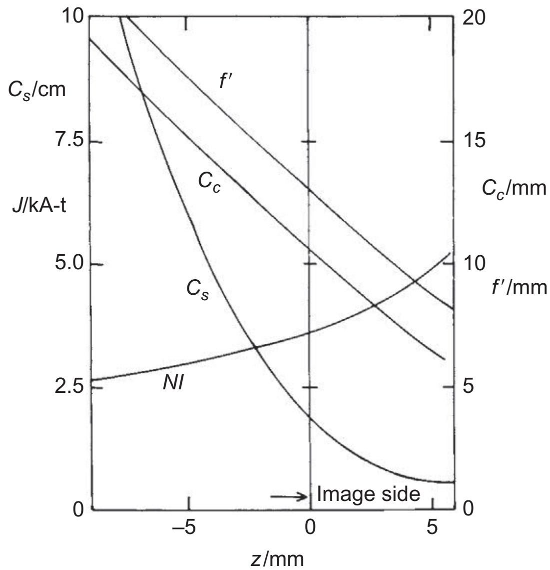

Figure 36.55
Optical properties of the design of Fig. 36.54C as a function of specimen position. *After Tsuno and Taoka (1983), Courtesy Japanese Journal of Applied Physics.*

before the bore is widened must be kept small as C_s is doubled by an increase of 1 mm (from 2.2 to 3.2 mm) in a typical design. The solution is to increase S, and Tsuno and Taoka arrive at a design in which $L = 6$ mm, $h = 5$ mm, $\Delta_1/D_2 = 0.7$, $S = 12$ mm, $t = 3.5$ mm, $f = 13$ mm, $C_s = 19$ mm, $C_c = 11$ mm and at 200 kV, $J = 3.6$ kA-t; the flux density at the specimen is only 0.35 mT (Fig. 36.55). The authors present a number of micrographs obtained with such a lens, indicating a resolution of 0.7 nm. For a slightly different solution, mentioned in Section 36.7.4, see Tsuno and Inoue (1984). A very different way of removing any magnetic field at the specimen is to enclose the latter between two oppositely wound lenses (Fig. 36.53B), as described by Kohno et al. (2017a,b). See also the work of Preikszas and Rose summarized in Section 36.5.3.

36.7.6 Probe-Forming Lenses for Low-Voltage Scanning Electron Microscopes

Tsuno (1999, 2009) has suggested a convenient classification for such lenses, shown schematically in Fig. 36.56: the in-lens geometry, where the specimen is inside the lens (e.g., Nakagawa et al., 1991); single-polepiece lenses (Section 36.5.1); side-gap (or radial-gap) lenses; conventional or 'axial-gap' lenses. The side-gap lenses, introduced by Tang and Song (1990) and used by Sato et al. (1993) are very unusual in that the gap is placed on the outer surface of the magnetic circuit (Fig. 36.57A). The resulting field is highly asymmetric but has a relatively small half-width. Tang and Song model the field, when the lens bore is small, by

$$B(z) = -\frac{\mu_0 NI}{\ln(r_b/r_a)}\left[\frac{r_b - r_a}{2r_a r_b}\left\{1 + \frac{2}{\pi}\left(\frac{zr_c}{z^2 + r_c^2} + \arctan\frac{|z|}{r_c}\right)\right\} + \frac{1}{(z^2+r_b^2)^{1/2}} - \frac{1}{(z^2+r_a^2)^{1/2}}\right] \text{ for } z<0$$

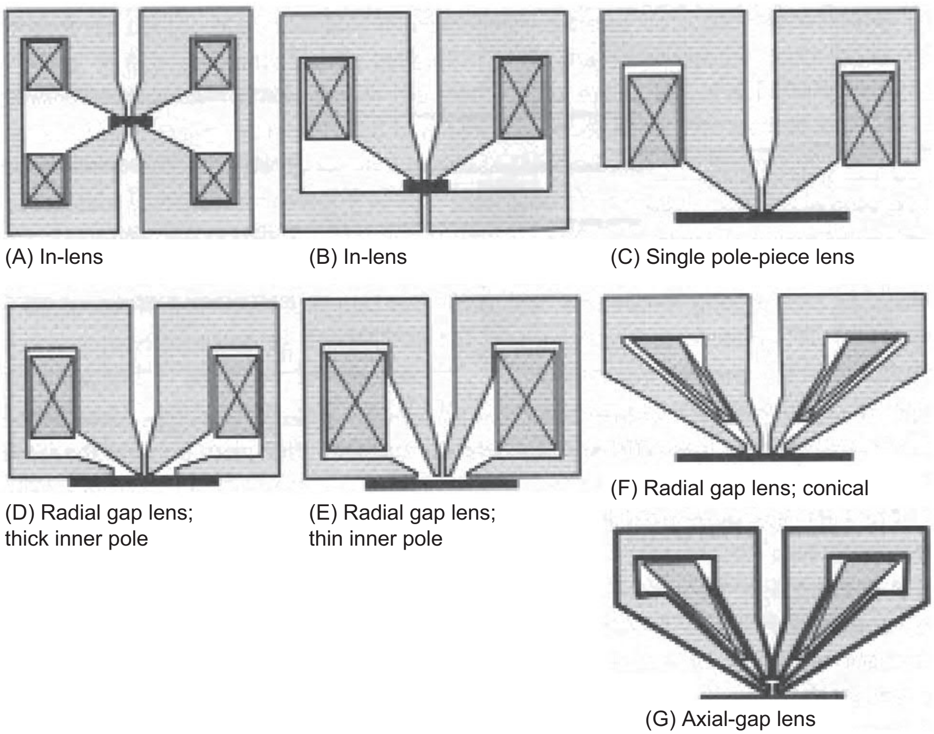

Figure 36.56
Various probe-forming lens geometries. *After Tsuno and Taoka (1983), Reproduced by permission of Taylor & Francis Group LLC, a division of Informa plc.*

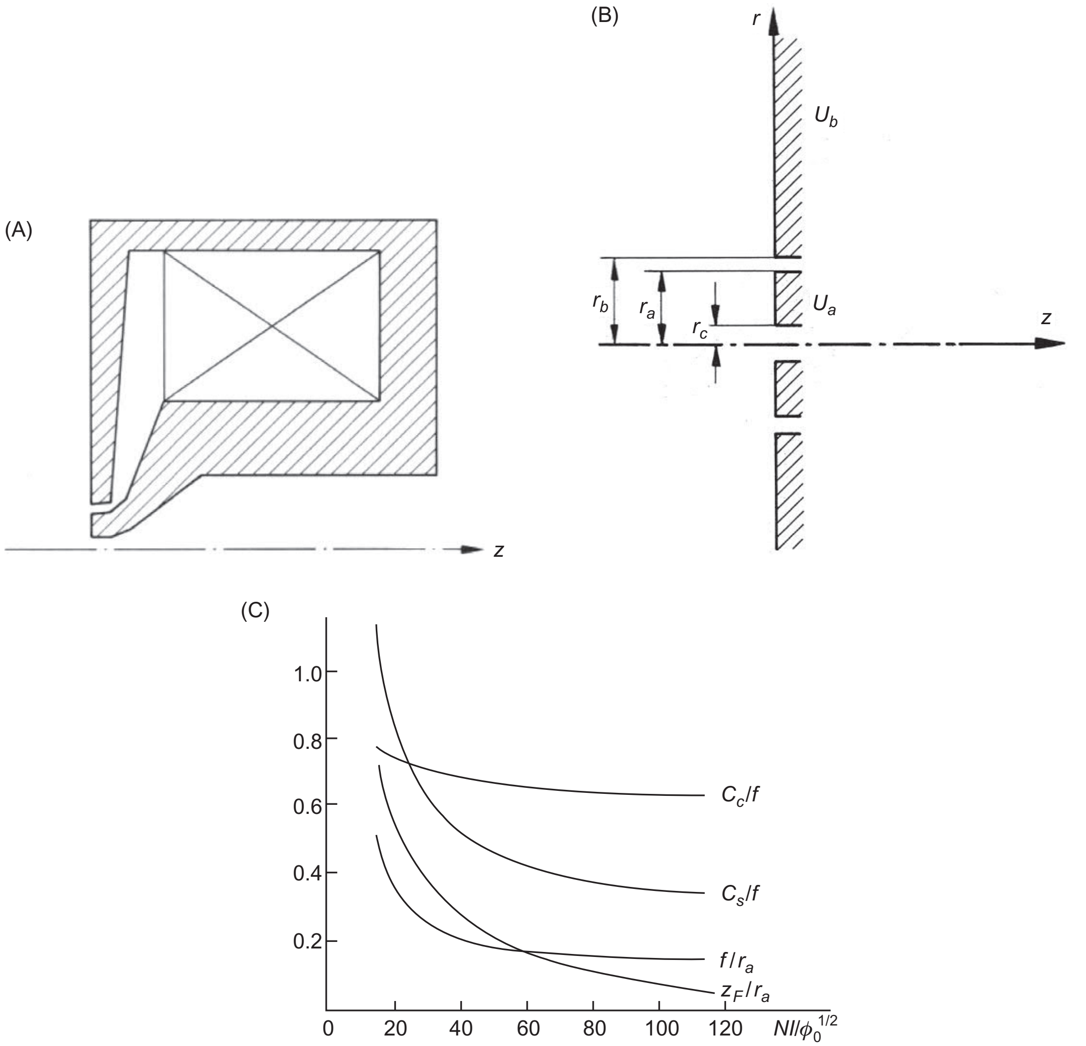

Figure 36.57

(A) A side-gap magnetic lens. (B) Notation. (C) Paraxial properties and aberration coefficients as functions of excitation. *After Tang and Song (1990), Courtesy Wissenschaftliche Verlagsgesellschaft.*

and

$$B(z) = -\frac{\mu_0 NI}{\ln(r_b/r_a)}\frac{r_b - r_a}{2r_a r_b}\left\{\frac{1}{2} - \frac{1}{\pi}\left(\frac{zr_c}{z^2 + r_c^2} + \arctan\frac{z}{r_c}\right)\right\} \quad \text{for} \quad z > 0$$

The notation is defined in Fig. 36.57B. The main optical properties are plotted as a function of $NI/\phi_0^{1/2}$ in Fig. 36.57C. Hybrid electrostatic–magnetic lenses have been studied thoroughly in this context by Tsuno et al. (1995, 1996), following earlier work by Frosien et al. (1989) and Müllerová and Lenc (1992). In the first paper (Tsuno et al., 1995), existing lens designs are examined critically, after which a family of new designs is analysed in detail. One such lens (Fig. 36.58) is re-examined in the later paper (Tsuno et al., 1996) and compared closely with a radial-gap lens. The aberration coefficients of the lens are computed and their dependence on lens geometry and on accelerating voltage is plotted.

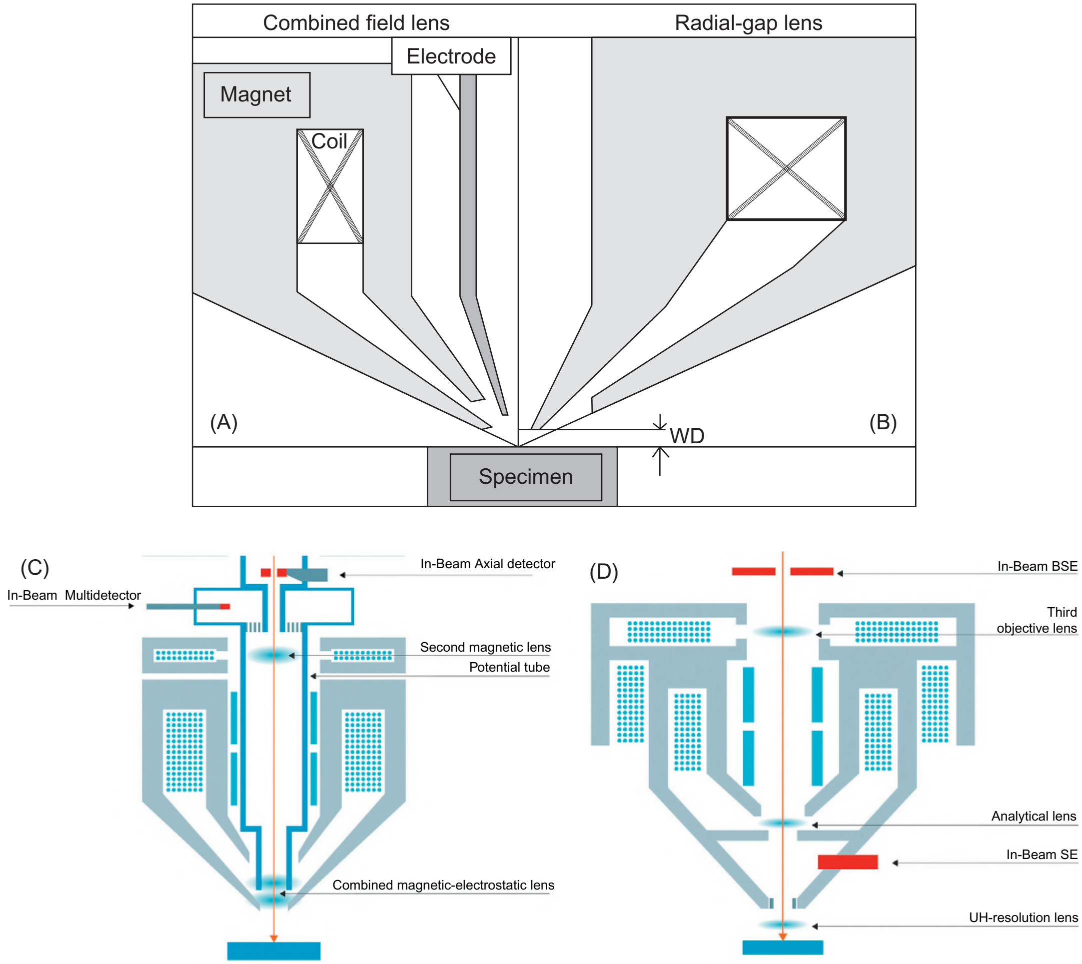

Figure 36.58
Hybrid electrostatic—magnetic lens (A) and radial-gap lens (B). (C) Hybrid lens employed in Tescan scanning electron microscopes. (D) Triple objective providing three operating modes. *After Tsuno et al. (1996), Courtesy Society of Photo-optical Instrumentation Engineers (A and B), and Courtesy Tescan (C and D).*

Inside the hybrid electrostatic–magnetic lens employed in the Tescan Brightbeam SEM is a tube held at high potential. The magnetic structure furnishes two magnetic lens fields, one above the scanning coils, the other close to the target (Fig. 36.58C). An even more extreme design is the Trilens, which combines three magnetic lenses in a single structure, The first lens, a traditional magnetic lens, offers a wide field of view; the central 'analytical' lens permits field-free studies in analytical work and the final lens close to the specimen is used when high-resolution is required. A battery of detectors completes the instrument.

For related work, see Shao and Lin (1989), Plies and Schweizer (1987), Chmelík et al. (1989), Nakagawa et al. (1991), Lenc (1992), Ximen et al. (1993), Miyokawa et al. (1995), Frank (2016) and especially Beck et al. (1995).

36.7.7 Hybrid TEM−STEM Operation: the Twin and Super-Twin Geometries

The scanning transmission mode has many attractions (Pennycook and Nellist, 2011) but it is often convenient to be able to examine the same specimen in both the conventional fixed-beam mode and in the scanning mode. Moreover, commercial realities have made it imperative to offer the two modes in a single instrument. The transfer from the types of illumination needed for conventional microscopy, typically illumination of a specimen area of variable size with a beam closely parallel to the axis at the specimen plane, to the formation of a fine probe at this same specimen plane, needed for STEM, makes severe demands on the optics of the condensers and objective. As an illustration of the response of lens designers to such problems, we briefly describe the twin-lens geometry adopted by the Philips company for this task (van der Mast et al., 1980; Thompson, 1983; Bormans and Hagemann, 1986; Otten, 1989; Otten et al., 1989). The problem to be solved was as follows: a good choice for a lens intended for both fixed-beam and scanning operation is clearly a symmetrical design with the specimen plane at the centre, the Ruska−Riecke condenser objective (Riecke and Ruska, 1966). In standard TEM operation, the strength of the second condenser (C2, Fig. 36.59A) should be chosen so that a parallel beam strikes the specimen, but the possible variation of the illuminating conditions is thereby somewhat restricted. The Ruska−Riecke arrangement is nevertheless an excellent way of providing the STEM probe (Fig. 36.59B). In order to circumvent the TEM problem, a small auxiliary lens is added just above the upper polepiece of the objective (Fig. 36.5), which very considerably increases the flexibility. Fig. 36.59C and D show two TEM illumination modes with the auxiliary lens in action, demonstrating that the C2 lens strength is now a free parameter because the combination of the new auxiliary lens and the objective prefield (that is, the part of the objective lens field above the specimen)

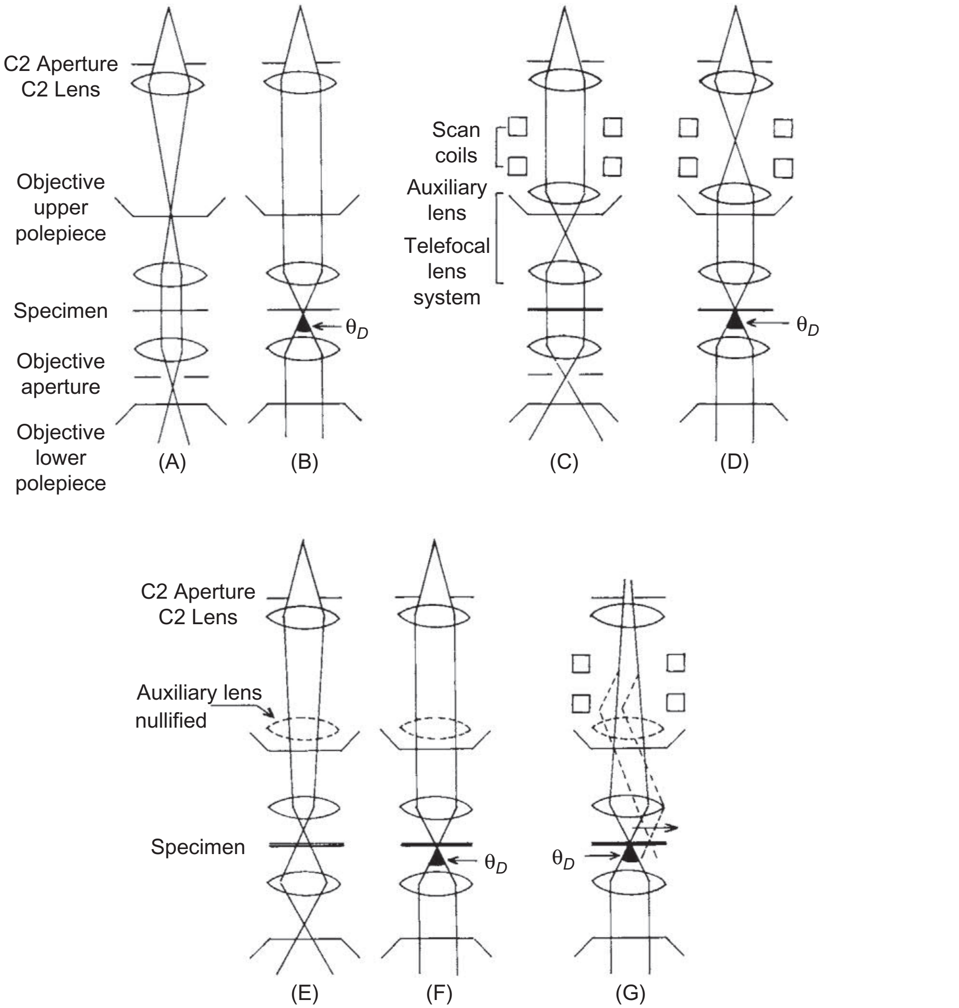

Figure 36.59

(A) and (B) Symmetric condenser—objective lens.
(A) To provide uniform illumination in the TEM mode, the second condensr C2 must focus the crossover image onto the front focal plane of the condenser part of the objective.
(B) By decreasing the strength of C2, the crossover image can be focused on the specimen, as required for STEM or convergent-beam operation.
(C)—(G) Twin-lens modes.
(C) TEM microprobe mode. Auxiliary lens on. A small specimen area is illuminated normally.
(D) TEM microprobe mode. Auxiliary lens on. Convergent-beam illumination at the specimen.
(E)—(G) Auxiliary lens disabled by reversing the lens current. (E) and (F) Alternative nanoprobe modes. (G) STEM mode. *Courtesy M.N. Thompson.*

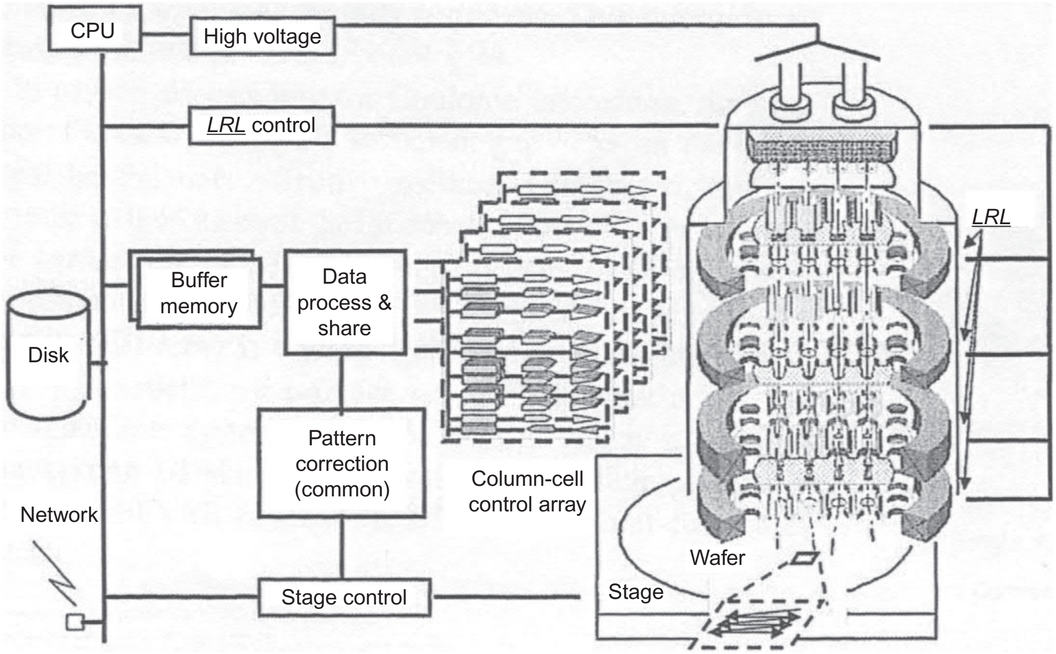

Figure 36.60
Four lotus-root lenses forming a multicolumn cell exposure unit. *Reproduced from Haraguchi et al. (2002) with the permission of the American Vacuum Society.*

acts as a telescope: an incident beam parallel to the axis emerges as a parallel beam, only its radius is changed. The other ray diagrams (Figs 36.59E–G) show modes of operation in which the effect of the auxiliary lens is removed, including standard STEM operation.[7]

36.7.8 The Lotus-Root Multibeam Lens

The use of a large number of sub-beams for electron lithography is mentioned in Section 50.6. A magnetic lens designed to separate the primary beam into sub-beams has been described by Haraguchi et al. (2002) and subsequent developments can be followed in Yasuda et al. (2004, 2008, 2009), Yamada et al. (2008) and Takizawa et al. (2011).

[7] The combination has been patented by the Philips company under the name of the Twin lens, subsequently improved to give the Super-twin lens.

Flat magnetic plates of very high permeability, each perforated with regularly placed circular holes, are inserted into the bore of a magnetic lens. These openings are aligned and form local magnetic lenses that guide the corresponding sub-beams towards the target. A four-plate version is shown in Fig. 36.60.

CHAPTER 37

Electron Mirrors, Low-Energy-Electron Microscopes and Photoemission Electron Microscopes, Cathode Lenses and Field-Emission Microscopy

This short chapter is to be regarded as no more than an indication of sources of further information about instruments incorporating an electron mirror, cathode lenses and emission microscopes. Although these are of importance in specific areas, mirrors and cathode lenses are not quite so widespread as the magnetic and electrostatic lenses examined earlier and the quadrupoles and deflectors that follow. In a final section, we mention the rapidly expanding subject of ultrafast electron microscopy, pioneered by Oleg Bostanjoglo some 30 years ago. As in low-energy-electron microscopy and photoemission electron microscopy, the electron beam is generated by bombarding a cathode.

There is a practical difference between mirrors in which the incident beam is nearly normal to the 'surface' of the mirror and this surface is approximately plane and mirrors in which the angle of incidence is large. In light optics, it is usual to treat these two situations together, but in particle optics, they require a different treatment because the optic axis in the first case is straight and the paraxial properties and aberrations are those of a system with a straight axis, often with rotational symmetry about this axis. In the second case, however, the optic axis is a curve in space and the optical properties are those of systems of lower symmetry, examined in Part X. Several kinds of energy analyser belong to this second category. In this chapter, we consider only the case of mirrors with a straight optic axis and hence near-normal incidence.

Electron mirrors are encountered in the electron mirror microscope and in certain types of energy analyser and filter lens. They are an essential part of modern low-energy-electron and photoemission electron microscopes, where they provide aberration correction.

37.1 The Electron Mirror Microscope

The mirror microscope is a device in which an electron beam approaches a nearly flat specimen surface normal to the latter but is reflected by a retarding electric field just before

Principles of Electron Optics: Applied Geometrical Optics.
DOI: http://dx.doi.org/10.1016/B978-0-12-813369-9.00037-3

reaching it. From the experimental point of view, it thus has the attraction that the beam electrons do not attack the specimen directly. The relief of the specimen surface and any local fields will perturb the uniformity of the retarding field that reverses the direction of motion of the beam, and the returning beam will therefore carry information about the local structure of the specimen surface and its electrical and magnetic character.

The properties of electron mirrors were first studied theoretically and experimentally in the 1930s by Henneberg and Recknagel (1935), Recknagel (1936), Hottenroth (1936), Nicoll (1938), Picht (1939) and Mahl and Pendzich (1943), who used Nicoll's two-tube arrangement as a projector. Many of the early studies of einzel lenses contain information about the mirror properties of these devices when the central electrode creates a high enough potential barrier to repel the electrons. The most detailed model study is that of Regenstreif (1951).

The 1950s and 1960s saw much activity in mirror microscope design, including the introduction of scanning into mirror microscopy, leading to the provision of a mirror attachment for a scanning electron microscope (Witzani and Hörl, 1976). The principal publications on instrumental development and image formation are those of Orthuber (1948), Bartz et al. (1954), Bartz and Weissenberg (1957), Mayer (1955, 1956, 1957a,b, 1959a,b, 1961, 1962), Mayer et al. (1962), Wiskott (1956), Spivak et al. (1955, 1959a,b, 1960, 1961, 1962, 1963, 1978, 1983), Bethge et al. (1960), Bok et al. (1964, 1971), Bok (1968, 1978), Forst and Wende (1964), Artamonov et al. (1966), Schwartze (1966, 1967), Barnett and Nixon (1967), Someya and Watanabe (1968a,b), Garrood and Nixon (1968), Sedov (1968a,b, 1970a,b), Luk'yanov et al. (1968, 1973, 1974), Artamonov and Komolov (1970a—c), Bethge and Heydenreich (1971, 1982, 1987), Witzani and Hörl (1981), Shern and Unertl (1987) and Foster et al. (2011). For a review describing mirror microscopes up to the mid-1990s, see Godehardt (1995). Kleinschmidt and Bostanjoglo (2000) have designed a high-speed mirror microscope (see also Bostanjoglo, 2002). Fig. 37.1 shows the Delft microscope (Bok, 1968, 1978; Bok et al., 1971). Rich sources of applications are the textbooks of Bethge and Heidenreich (1982, 1987) and many are included in Hawkes (2012). For more recent developments, see Nepijko and Sedov (1997), Schönhense et al. (2006) and Nepijko and Schönhense (2011).

37.2 Mirrors in Energy Analysis

The energy distribution of a beam of charged particles may be analysed by confronting the latter with a potential barrier, which can be raised to the point at which slower particles are reflected. By increasing the height of such a barrier, the energy distribution of the beam can be established. In early designs (Boersch, 1947, 1948, 1949, 1953), a grid covered the central opening of an einzel lens but this grid was subsequently dispensed with (Möllenstedt and Rang, 1951; Möllenstedt, 1955; Lippert, 1955a,b; Forst, 1966; Boersch and Miessner, 1962; Heinemann and Möllenstedt, 1967; Vertsner and Shchetnev, 1967; Stolz and Möllenstedt, 1971; Stolz, 1978/79, 1979). A five-electrode device was introduced by

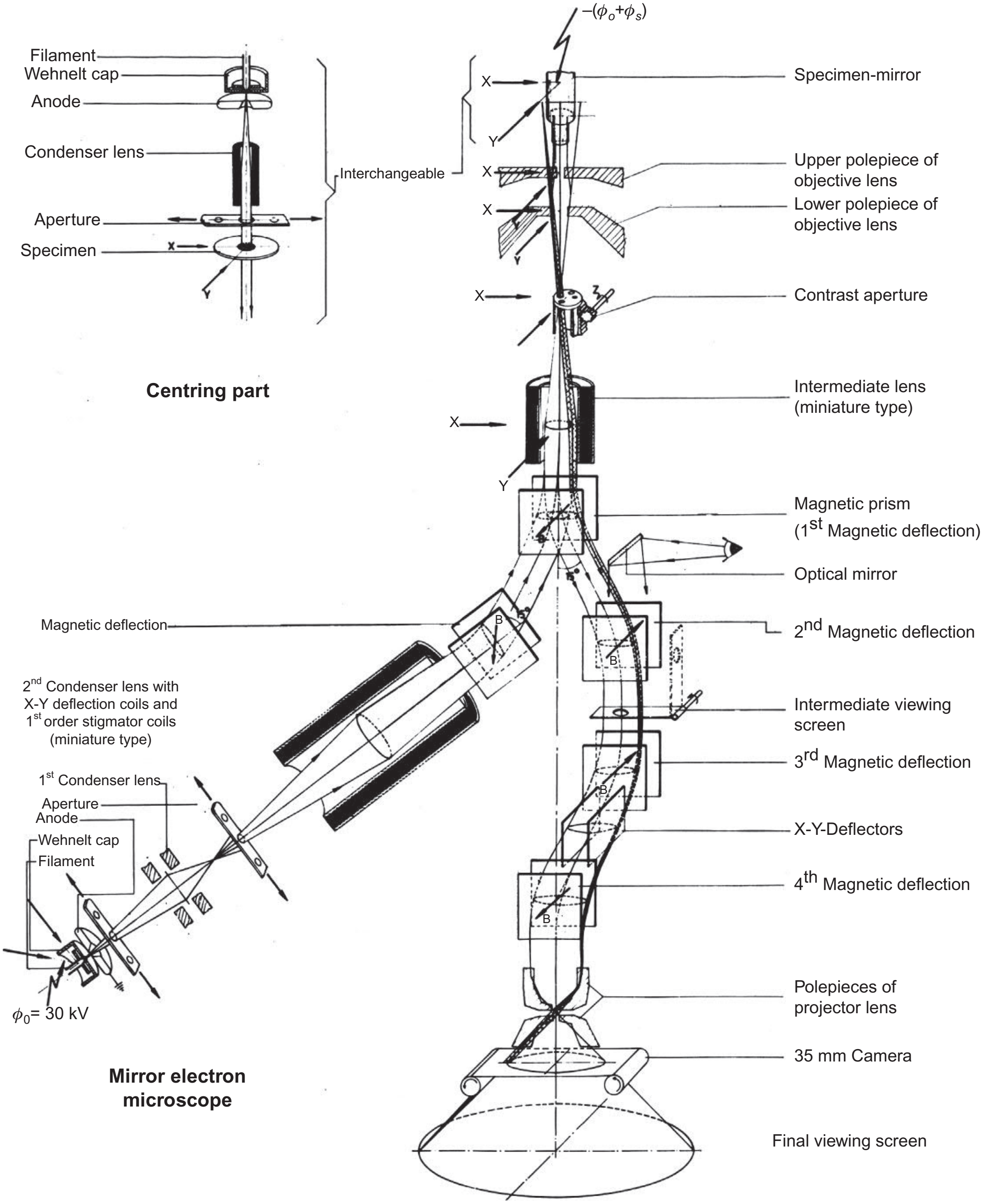

Figure 37.1
Ray diagram for the mirror electron microscope constructed by A.B. Bok in the Technische Hogeschool (now Universiteit) Delft. *Courtesy A.B. Bok.*

Simpson and Marton (1961) and used by Kessler and Linder (1964). Other designs are described by Brack (1962), Boersch and Schweda (1962), Hartl (1964, 1966) and Stenzel (1971). For further discussion, see Simpson (1961) and Steckelmacher (1973).

A very different form of device is the Castaing–Henry analyser (Fig. 18.1), first considered by Paras (1961) and developed by Castaing and Henry (1962, 1963, 1964), in which a magnetic prism (see Part X) is used to turn a beam through 90°; this beam is then reflected from an electrostatic mirror and returns to the prism, where it is turned through a further 90°. The beam thus emerges from the device travelling along the prolongation of the optic axis of the incident beam. Such a device has the interesting property of possessing two pairs of stigmatic conjugate planes, one real, the other virtual. Furthermore, the imagery between the virtual planes is achromatic (to first order). By arranging that the virtual planes are conjugate to the specimen plane of a transmission electron microscope and the real stigmatic planes to the back-focal plane, it is possible to form an energy-filtered image, that is, an image to which only electrons with energies within a certain narrow range contribute. For full details of the optics of this device and the various operating modes, we refer to Metherell (1971). Subsequently, interest in this device was revived (Ottensmeyer, 1984; Egle et al., 1984), and it has been incorporated into a commercial microscope, the Zeiss EM902.

The theory developed for cathode lenses is applicable, after making any necessary scale changes, to a number of very common devices in which electron emission is provoked by some incident radiation that would otherwise be difficult to detect or record; image converters and image intensifiers are typical examples.

37.3 Cathode Lenses, Low-Energy-Electron Microscopes and Photoemission Electron Microscopes

One of the many methods of studying surfaces is to provoke the emission of electrons or ions from the specimen surface and use these to furnish an image of the latter. The specimen surface may be approximately plane or only gently curved and quite large, in which case the electrons (or ions) are confined by a wehnelt electrode and accelerated by an anode, exactly as in a thermionic gun (see Part IX, where the roles of such electrodes are analysed in great detail); in this case, we speak of *cathode lenses*. At the other extreme, the emitter may be approximately spherical with a very small radius and the electrons fly out radially towards the detector, accelerated by suitably placed electrodes; this is the principle of the field-emission microscope. Numerous experimental and instrumental details are to be found in Grivet (1965) and Möllenstedt and Lenz (1963). An extremely full account of early work is given by Myers (1939).

The principle goes back to the early years of electron microscopy when Brüche (1932; Brüche and Johannson, 1932a,b) and Zworykin (1933) obtained images of surfaces bombarded with photons and electrons respectively. At the same date, Johannson analysed the optical properties of three- and four-electrode 'immersion objectives', the object forming the first electrode (Johannson, 1933, 1934). Other early contributions were made by Savchenko (1938, 1939), Sushkin (1941), Recknagel (1941, 1943) and Artsimovich (1944). Theoretical and experimental studies continued of the lens parameters in the two main families of lenses: those in which a simple electrode structure provided both focusing and acceleration, and those in which these two functions are separated. Of the earlier studies, we draw attention in particular to those of Septier (1952a,b, 1953a,b, 1954a,b), Möllenstedt and Düker (1953), Duchesne (1949, 1953), Kas'yankov (1953), Spivak and Dubinina (1953), Huguenin (1954, 1957), Prilezhaeva et al. (1955), Vorob'ev (1956), Wu (1956, 1957a,b), Fert and Simon (1956, 1957), Ximen (1957), Hahn (1958a,b, 1959), Soa (1959), Dubinina et al. (1959), Gardez (1959), Düker and Illenberger (1962) and Bonshtedt (1964).

More recently, the optical properties of cathode lenses have been extensively studied, particularly in Russia. We draw attention to the work of Zolina and Shapiro (1972) and Zolina and Flegontov (1978, 1982) on the aberrations of flat and curved cathodes; of Kel'man et al. (1973a−d, 1974) on the use of the transform discussed in Chapters 18 and 28; of Kulikov, Monastyrskii and Smirnov on various aspects of aberration theory (Kulikov, 1966, 1971, 1972, 1973, 1975; Kulikov et al., 1964, 1978; Monastyrskii, 1978, 1980; Monastyrskii and Kulikov, 1976, 1978; Smirnov et al., 1979); and of Dodin and Nesvizhskii (1981) who give a critical discussion of earlier attempts to establish aberration coefficients for cathode lenses. For connected accounts, see Yakushev and Sekunova (1986) and Yakushev (2013). Detailed calculations of the aberration coefficients have also been made by Zhou et al. (1983), Zhou (1984), Ximen (1957, 1981), Li and Ximen (1982) and Ximen et al. (1983, 1985). See too Bimurzaev and Yakushev (2004).

In practice, cathode lens optics is usually studied with the aid of a simple model, such as a uniform field between the cathode and anode and an aperture lens representing the anode itself (Müllerová and Lenc, 1992[1]; Lenc and Müllerová, 1992a, where the inadequacy of earlier estimates is pointed out; Müllerová and Frank, 2003). A magnetic lens may be added (Lenc and Müllerová, 1992b; Konvalina and Müllerová, 2011; Frank et al., 2011).

The instrument now universally known as a low-energy-electron microscope or LEEM is not, as its name suggests (since it is usually written low-energy electron microscope), a transmission or scanning electron microscope operating at a lower voltage than usual. A LEEM is an instrument in which a specimen is bombarded with electrons or ions and emits electrons at low energy, whence its name. These are accelerated by a cathode lens and conveyed to a recording medium of some kind. It is a close relative of the

[1] This article contains a review of many earlier instruments with numerous diagrams.

photoemission electron microscope (PEEM), where the electron emission is provoked by photons, ranging from ultraviolet light to x-rays. PEEM and LEEM operation are frequently combined in a single instrument, which may also permit mirror electron microscopy.

These instruments were gradually improved until it became clear that any further progress required correction of the aberrations of the cathode or 'immersion objective' lens. The history of these developments is presented at length with a very complete bibliography by Bauer in Chapters 1 and 3 of his *Surface Microscopy with Low Energy Electrons*[2] (Bauer, 2014; see also Bauer, 2008, 2018 and the book by Oura et al., 2003). An extremely complete classified bibliography of the earlier literature has been compiled by Pfefferkorn and Schur (1979). This is accompanied by a long study of the physics of emission microsocopy by Schwarzer (1979) and a short comment on the history of the subject by Pfefferkorm (1979). In the early 1990s, Skoczylas et al. (1991, 1994) built an electron optical bench as a prototype LEEM or PEEM or mirror electron microscope. Subsequent designs fall into three groups: PEEM instruments with a hyperbolic mirror and three deflection magnets (Könenkamp et al., 2008, 2010), which ensure that the incident and reflected beams are parallel; LEEMs with a four-magnet beam separator as incorporated in SMART, the SpectroMicroscope for All Relevant Techniques (Rose and Preikszas, 1982; Engel et al., 1996; Fink et al., 1997; Wichtendahl et al., 1998; Hartel et al., 1998, 2000, 2002) and PEEM3 (Feng et al., 2004, 2005, 2007; Wu et al., 2004, Feng and Scholl, 2008, 2018; Macdowell et al., 2007); and a LEEM in which the beam separation at the specimen is separated from that at the mirror (Tromp et al., 2010, 2013). Another design has been proposed by Tsuno et al. (2009). Yet another variant is the double-beam LEEM, in which a second incident beam is employed to prevent charging. This is the MAD−LEEM of Mankos (Mankos et al., 2007, 2008a,b, 2010, 2012, 2013; Mankos, 2011). In all of these, electron mirror action provides aberration correction; this is considered in Section 41.4.2, where figures illustrating these instruments are to be found. The aberrations of cathode lenses and their correction have been studied in depth by Tromp (2011, 2015a,b) and Tromp et al. (2012), using model field distributions. A spin-polarized LEEM with multiple sources is described by Wan et al. (2017). For scanning LEEM, see Müllerová and Frank (2003) and Müllerová et al. (2003) and on low-voltage scanning electron microscopes in general, Müllerová and Lenc (1992) and Müllerová et al. (1998). Other papers of interest are Blackburn (2008, PEEM), Osterburg and Khursheed (2008, PEEM), Tsuno et al. (1996, low-voltage scanning electron microscope), Tsuno et al. (1995, LEEM) and Müller et al. (1996b, PEEM−LEEM).

[2] This book is strongly recommended as all the topics mentioned only briefly here are covered at great length with numerous illustrations.

37.4 Field-Emission Microscopy

The study of a very small specimen by applying a high electric field and examining the resulting emission pattern was initiated by Müller (1936a,b, 1937a,b) and the development of the subject may be followed in the surveys written by Milyutin (1949), Müller (1951, 1953, 1960, 1975, 1976, 1978a,b), Good and Müller (1956), Dyke and Dolan (1956), Gomer (1961, 1994), Montagu-Pollock (1972) and Turner et al. (1972).

Both ion and electron emission are employed; further information may be found in Maly (1973), Müller and Tsong (1969, 1974), Müller (1975), Okano et al. (1976), Oshima et al. (1983) and Gibson and Thomas (1985). Müller's achievement is assessed by Drechsler (1978). The bibliography of emission microscopy, mirror electron microscopy, LEEM and PEEM compiled by Griffith et al. (1991) is useful for earlier work, Khursheed (2002) describes a time-of-flight (TOF) emission microscope.

37.5 Ultrafast Electron Microscopy

The possibility of illuminating the specimen for a very short time is attractive for several reasons. It would permit dynamic observation, whereby rapid changes in the specimen structure could be followed *in situ*; it might be possible to record an image of a fragile specimen before radiation damage altered the structure.

Considerable progress in the design and application of high-speed electron microscopes was made by Bostanjoglo, the leading pioneer in this area, in the Optisches Institut of the Berlin Technical University. This is described in detail in three long review articles (Bostanjoglo, 1989, 1999, 2002) and in Bostanjoglo et al. (2000), King et al. (2008) and Campbell et al. (2018) and is therefore mentioned only briefly here. The instrument was a photoemission electron microscope, the short electron pulses being generated by bombarding the emitter with very short laser pulses. In *short-time exposure imaging*, sets of three successive pulses, 7−20 ns long and separated by a time varying from 20 ns to 2 μs, were generated at the laser-pulsed photocathode. The peak current in the pulses was of the order of milliampères and the semi-angular aperture was 7 mrad. The instrument was used in the *pump−pulse mode*, in which changes in the specimen structure are provoked by a second laser pulse; the evolution of the specimen structure is followed by varying the time-difference between the gun pulse and the specimen pulse. Another early contribution was made by Hosokawa et al. (1978a,b). See too Fujioka and Ura (1983), Thong et al. (1987), Thong and Nixon (1990), Fehr et al. (1990).

Numerous attempts to perform ultrafast electron microscopy have been made subsequently and the subject is in rapid development. Thus Zewail has implemented a stroboscopic method, baptized *single-electron imaging*, in which a very small number of electrons reach the specimen at any one time and the image is built up by launching a sequence of such very short pulses (Zewail and Thomas, 2009; Zewail, 2010; Shorokhov and Zewail, 2016). The other projects mentioned below all use *single-shot imaging*, in which the entire image is created by a single pulse, like the image created by the continuous beam in a transmission electron microscope.

The problems to be overcome are set out very clearly by Browning et al. (2012b). In order to generate a usable image, each pulse must contain a sufficiently large number of electrons, typically 10^9, and at the same time the convergence angle at the specimen plane must be limited (or in the language of coherence (Section 66.2 and Part XVI), the spatial coherence must be as high as possible). At the same time, the energy spread of the electrons in the pulse must be very narrow, as in any electron source (high temporal coherence). From this, it emerges that the mean brightness must be 10^7 A cm^{-2} sr^{-1} at the very least and the beam current must be in the milliampère range. In order to reduce the energy spread in the electron pulses, van Oudheusden et al. (2007, 2010) have suggested passing the pulses through a radiofrequency cavity; the entry phase is chosen in such a way that slower electrons catch up the faster ones. (We recall that high-frequency fields have been investigated for aberration correction but at that date it was not possible to produce very short tight pulses, see Section 41.6.) Grzelakowski and Tromp (2013) suggest that a capacitor consisting of two concentric spheres (the α-spherical deflector analyser or α-SDA, Grzelakowski, 2012) could achieve the same end. Coulomb interactions are discussed by Cook and Kruit (2016).

The subject is evolving so rapidly that we conclude this short section with a brief account, certainly not exhaustive, of some current projects. The survey by King et al. (2008), which gives a good idea of the situation at that date, has been updated by Campbell et al. (2018). Time-resolved PEEM is surveyed by Siefermann and Neff (2017). See too Lee et al. (2017), Petruk et al. (2017) and Williams et al. (2017).

At the Lawrence Livermore National Laboratory, the dynamic transmission electron microscope (DTEM) is based on a modified JEOL instrument. See Armstrong et al. (2007), Reed et al. (2010), Lagrange et al. (2008, 2012b) and for broad surveys, Browning et al. (2012a,b) and LaGrange et al. (2012a).

At SLAC, the advantages of operating at high voltage (in the megavolt range) are being explored, first for electron diffraction (Weathersby et al., 2015) and subsequently for electron microscopy (Li and Musumeci, 2014; Piazza et al., 2014; Cesar et al., 2016; Musumeci et al., 2017; Musumeci and Li, 2018).

In Europe, Ropers and colleagues in the University of Göttingen have developed an ultrafast electron microscope in which the pulses are generated by localized photoemission from a Schottky emitter. The focused beam diameter can be as small as 9Å in diameter with an energy spread of 0.6 eV and a pulse length of 200 fs (Ropers et al., 2007; Gulde et al., 2014; Bormann et al., 2015; Feist et al., 2014, 2015, 2016, 2017; Storeck et al., 2017). Bücker et al. (2016a,b) in Strasbourg have constructed a pump–probe instrument and

Houdellier et al. (2016) in Toulouse have brought together a commercial femtosecond laser source and a modified Hitachi HT2000 electron microscope with a cold field emission gun. A high-voltage instrument (2−5 Mev) is in operation in Hamburg (Manz et al., 2015, 2016). Schelev et al. (2013) have made a thorough study of streak cameras, very relevant to this subject.

In Japan, Kuwahara and colleagues are developing a spin-polarized pulse-TEM (Kuwahara et al., 2011a,b, 2012a,b, 2013, 2014, 2016a,b).

At the beginning of this section, we mentioned that ultrafast electron microscopy might make it possible to outrun radiation damage in an electron microscope, by which we mean record the image before any damage has been inflicted. The subject is surveyed in depth by Egerton (2015), who draws attention to the numerous obstacles, of which Coulomb repulsion of the electrons tightly packed into pulses seems the most intractable, and by Spence (2017). An alternative configuration is proposed by Spence et al. (2015), who suggest that the use of hollow-cone illumination might offer a way round such difficulties.

The Wien Filter

The Wien filter is a device in which transverse electric and magnetic fields are present. In its basic but unrealistic form, the field distributions are such that the transverse forces on an electron of a given energy balance each other and the electron is not deflected; for all other energies, the electrons are deflected and can hence be removed from the beam. A Wien filter can be used as a monochromator or as an energy analyser or even as an aberration corrector.

We consider a system in which a rotationally symmetric electrostatic field, electrostatic and magnetic quadrupole, sextupole and octopole components and transverse fields characterized by F_1 for the electrostatic field and B_2 for the magnetic field (Eqs. 7.36−37, 7.46−48) may all be present. In the non-relativistic approximation, the paraxial equations of motion take the form

$$\begin{aligned} x'' + \frac{\phi'}{2\phi}x' + \left(\frac{\phi''}{4\phi} + \frac{F_1^2}{4\phi^2} - \frac{p_2}{2\phi} + \frac{\eta Q_2}{\phi^{1/2}}\right)x &= \frac{\eta B_2}{\phi^{1/2}} - \frac{F_1}{2\phi} \\ y'' + \frac{\phi'}{2\phi}y' + \left(\frac{\phi''}{4\phi} + \frac{p_2}{2\phi} - \frac{\eta Q_2}{\phi^{1/2}}\right)y &= 0 \end{aligned} \tag{38.1}$$

The deflection terms on the right-hand side of Eq. (38.1) vanish if

$$F_1 = 2\phi^{1/2}\eta B_2 \tag{38.2}$$

or

$$F_1 = \upsilon B_2 \tag{38.3}$$

where υ denotes the velocity (2.22)

$$\upsilon = 2\phi^{1/2}\eta \tag{38.4}$$

Eqs (38.2) and (38.3) are forms of the *Wien condition* (Wien, 1897/8, 1898). When this condition is satisfied, (38.1) simplify to

Principles of Electron Optics: Applied Geometrical Optics.
DOI: http://dx.doi.org/10.1016/B978-0-12-813369-9.00038-5

$$
\begin{aligned}
&x'' + \frac{\phi'}{2\phi}x' + \left(\frac{\phi''}{4\phi} + \frac{F_1^2}{4\phi^2} - \frac{p_2}{2\phi} + \frac{\eta Q_2}{\phi^{1/2}}\right)x = 0 \\
&y'' + \frac{\phi'}{2\phi}y' + \left(\frac{\phi''}{4\phi} + \frac{p_2}{2\phi} - \frac{\eta Q_2}{\phi^{1/2}}\right)y = 0
\end{aligned}
\tag{38.5}
$$

These bear a close resemblance to the paraxial equations of quadrupoles and, like them, the Wien filter does not have the same strength in the $x-z$ and $y-z$ planes. For the system to provide *stigmatic focusing*, another condition must be satisfied:

$$
\frac{F_1^2}{4\phi} - p_2 + 2\phi^{1/2}\eta Q_2 = 0 \tag{38.6}
$$

Inclusion of electrons with slightly different energies ($\Delta\phi$) from that of the reference particle adds a further term to Eq. (38.5):

$$
\begin{aligned}
&x'' + \frac{\phi'}{2\phi}x' + \left(\frac{\phi''}{4\phi} + \frac{F_1^2}{4\phi^2} - \frac{p_2}{2\phi} + \frac{\eta Q_2}{\phi^{1/2}}\right)x = \frac{F_1\kappa}{4\phi_0} \\
&y'' + \frac{\phi'}{2\phi}y' + \left(\frac{\phi''}{4\phi} + \frac{p_2}{2\phi} - \frac{\eta Q_2}{\phi^{1/2}}\right)y = 0
\end{aligned}
\tag{38.7}
$$

in which

$$
\kappa = \Delta\phi/\phi_0. \tag{38.8}
$$

The electrostatic potential ϕ is usually assumed to be constant within Wien filters so that finally, we have

$$
\begin{aligned}
&x'' + \left(\frac{F_1^2}{4\phi^2} - \frac{p_2}{2\phi} + \frac{\eta Q_2}{\phi^{1/2}}\right)x = \frac{F_1\kappa}{4\phi_0} + W_{2x} \\
&y'' + \left(\frac{p_2}{2\phi} - \frac{\eta Q_2}{\phi^{1/2}}\right)y = W_{2y}
\end{aligned}
\tag{38.9}
$$

W_{2x} and W_{2y} consist of terms of the next higher order in x, y and their derivatives, from which the primary geometrical aberrations will be derived. First however, we write down the paraxial solutions obtained from Eq. (38.9) after setting $W_{2x} = W_{2y} = 0$:

$$
\begin{aligned}
x^{(1)}(z) &= x_o g_x(z) + x_o' h_x(z) + \kappa x_\kappa(z) \\
y^{(1)}(z) &= y_o g_y(z) + y_o' h_y(z)
\end{aligned}
\tag{38.10}
$$

in which

$$x_\kappa(z) = h_x(z) \int_{z_o}^{z} \frac{F_1 g_x}{4\phi_0} d\zeta - g_x(z) \int_{z_o}^{z} \frac{F_1 h_x}{4\phi_0} d\zeta \tag{38.11}$$

Suppose now that the system forms a *stigmatic* image in some plane $z = z_i$ even though the stigmatic focusing condition may not be satisfied. On retaining the perturbation terms W_{2x} and W_{2y}, we have

$$\begin{aligned} x_i(z) &= x^{(1)}(z_i) + \Delta x(z_i) \\ y_i(z) &= y^{(1)}(z_i) + \Delta y(z_i) \end{aligned} \tag{38.12}$$

in which

$$\begin{aligned} \Delta x =& A_{11}x_o'^2 + A_{22}y_o'^2 + A_{33}x_o^2 + A_{44}y_o^2 + A_{13}x_o x_o' + A_{24}y_o y_o' \\ &+ C_{cx}x_o'\kappa + C_{tx}x_o\kappa + C_{c3}\kappa^2 \\ \Delta y =& B_{11}x_o y_o + B_{22}x_o' y_o' + B_{12}x_o y_o' + B_{21}x_o' y_o + C_{cy}y_o'\kappa + C_{ty}y_o\kappa \end{aligned} \tag{38.13}$$

The aberration coefficients as derived by Liu and Tang (1995) using the trajectory method, are as follows (referred back to the object plane):

$$A_{11} = -\int_{z_o}^{z_i} (Ah_x^2 + Ch_x'^2 + Dh_x h_x')h_x dz$$

$$A_{22} = -\int_{z_o}^{z_i} (Bh_y^2 - Ch_y'^2 - Dh_y h_y')h_x dz$$

$$A_{33} = -\int_{z_o}^{z_i} (Ag_x^2 + Cg_x'^2 + Dg_x g_x')h_x dz$$

$$A_{44} = -\int_{z_o}^{z_i} (Bg_y^2 - Cg_y'^2 - Dg_y g_y')h_x dz$$

$$A_{13} = -\int_{z_o}^{z_i} \left\{2Ag_x h_x + 2Cg_x' h_x' + D(g_x h_x)'\right\} h_x dz$$

$$A_{24} = -\int_{z_o}^{z_i} \left\{2Bg_y h_y - 2Cg_y' h_y' - D(g_y h_y)'\right\} h_x dz$$

$$B_{11} = -\int_{z_o}^{z_i} \left\{Gg_x g_y + 2Cg_x' g_y' + D(g_x g_y)'\right\} h_y dz$$

$$
\begin{aligned}
B_{21} &= -\int_{z_o}^{z_i} \left\{ G g_y h_x + 2C g_y' h_x' + D (g_y h_x)' \right\} h_y dz \\
B_{12} &= -\int_{z_o}^{z_i} \left\{ G g_x h_y + 2C g_x' h_y' + D (g_x h_y)' \right\} h_y dz \\
B_{22} &= -\int_{z_o}^{z_i} \left\{ G h_x h_y + 2C h_x' h_y' + D (h_x h_y)' \right\} h_y dz \\
C_{cx} &= -\int_{z_o}^{z_i} (E+F) h_x^2 dz \\
C_{tx} &= -\int_{z_o}^{z_i} (E+F) g_x h_x dz \\
C_{c3} &= \int_{z_o}^{z_i} E h_x dz \\
C_{cy} &= -\int_{z_o}^{z_i} H h_y^2 dz \\
C_{ty} &= -\int_{z_o}^{z_i} H g_y h_y dz
\end{aligned}
\tag{38.14}
$$

where

$$
\begin{aligned}
A &= \frac{5F_1 p_2}{8\phi_0^2} - \frac{\eta F_1 Q_2}{2\phi_0^{1/2}} - \frac{5F_1^3}{16\phi_0^3} - \frac{\eta B_2''}{4\phi_0^{1/2}} - \frac{p_3}{4\phi_0} + \frac{\eta Q_3}{2\phi_0^{1/2}} \\
B &= -\frac{F_1 p_2}{8\phi_0^2} + \frac{\eta B_2''}{4\phi_0^{1/2}} + \frac{p_3}{4\phi_0} - \frac{\eta Q_3}{2\phi_0^{1/2}} \quad C = \frac{F_1}{4\phi_0} \\
D &= \frac{F_1'}{2\phi_0} \quad E = \frac{5F_1^2}{16\phi_0^2} \quad F = \frac{\eta Q_2}{2\phi_0^{1/2}} - \frac{p_2}{2\phi_0} + \frac{5F_1^2}{16\phi_0^2} \\
G &= \frac{F_1''}{4\phi_0} + \frac{p_3}{2\phi_0} - \frac{\eta Q_3}{\phi_0^{1/2}} + \frac{\eta F_1 Q_2}{2\phi_0^{3/2}} - \frac{F_1 p_2}{2\phi_0^2} \\
H &= \frac{p_2}{2\phi_0} - \frac{\eta Q_2}{2\phi_0^{1/2}}
\end{aligned}
\tag{38.15}
$$

Liu and Tang also give the terms of third rank to be added to the right-hand side of Eq. (38.9). They analyse a device consisting of four Wien filters in series, and show that all second-rank aberrations can be eliminated by exploiting the symmetry of the configuration (Fig. 38.1); the g-ray is symmetric about the midplane of the quadruplet and antisymmetric about the midplanes of the first and last Wien doublets while the reverse is true of the h-ray. Numerous Wien quadruplets have been investigated by Plies and Bärtle, one of which is particularly attractive as a monochromator (Plies and Bärtle, 2003). Here, the focusing sequence is CNNC in one section and NCCN in the other, where C denotes 'converging' and N, 'neutral'; the axial and field rays are shown in Fig. 38.2.

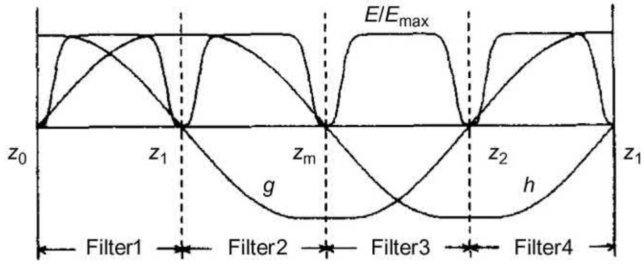

Figure 38.1
The quadruplet of Wien filters studied by Liu and Tang for aberration correction. *After Liu and Tang (1995), Courtesy Elsevier.*

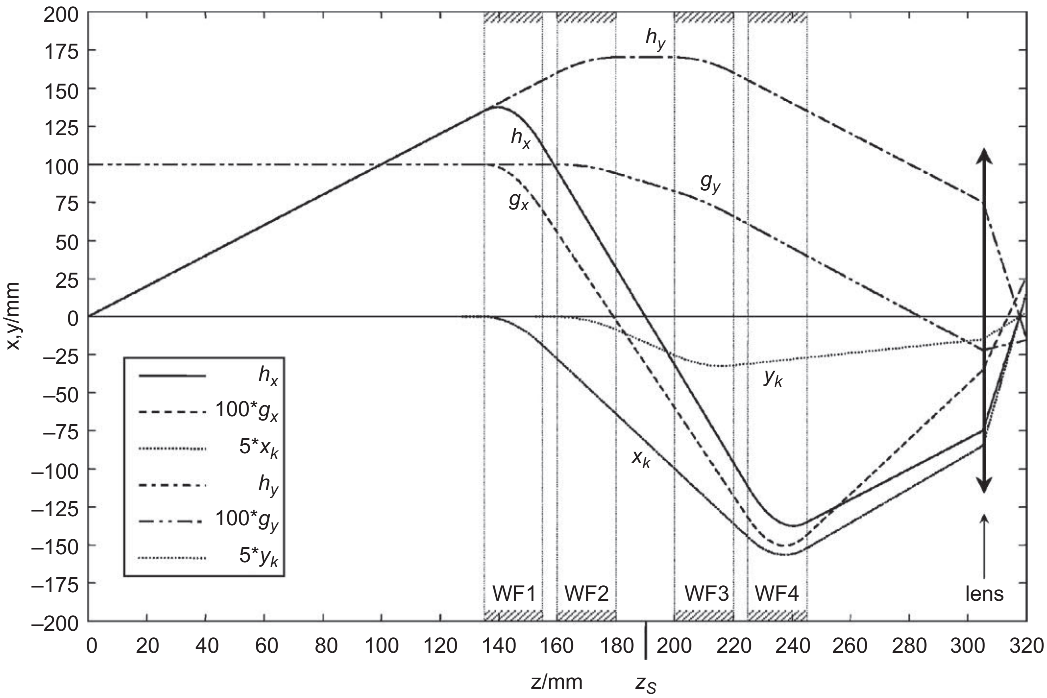

Figure 38.2
The Plies–Bärtle quadruplet intended for use as a monochromator. *After Plies and Bärtle (2003), Courtesy Cambridge University Press.*

A very general theory of systems that include Wien filters was developed by Plies and Typke (1978) and this was used by Rose (1987, 1990) to study the aberration coefficients of Wien filters by the eikonal method. Although the aberration coefficients are not given explicitly by Rose, they can be deduced easily from any of his forms of the eikonal function. Formulae from which all derivatives of the field functions and the paraxial solutions have been eliminated are listed below. Note that these are not immediately comparable with Eq. (38.14) as not only is a certain amount of partial integration needed to make them identical but the stigmatic focusing condition must also be imposed on Eq. (38.14).

$$\begin{aligned}
A_{11} &= 3\int(K_1+K_2)h^3dz\\
A_{22} &= \int(K_2-3K_1)h^3dz\\
A_{33} &= 3\int(K_1+K_2)g^2hdz\\
A_{44} &= \int(K_2-3K_1)g^2hdz\\
A_{13} &= 6\int(K_1+K_2)gh^2dz\\
A_{24} &= 2\int(K_2-3K_1)gh^2dz\\
B_{22} &= 2\int(K_2-3K_1)h^3dz\\
B_{11} &= 2\int(K_2-3K_1)g^2hdz\\
B_{12} &= 2\int(K_2-3K_1)gh^2dz\\
B_{21} &= 2\int(K_2-3K_1)gh^2dz\\
C_{cx} &= 2\int 3\{(K_1+K_2)h^2w_\kappa+(K_3+K_4)h^2\}dz\\
C_{cy} &= 2\int(K_2-3K_1)h^2w_\kappa+(K_4-K_3)h^2\}dz\\
C_{tx} &= 2\int 3\{(K_1+K_2)ghw_\kappa+(K_3+K_4)gh\}dz\\
C_{ty} &= 2\int(K_2-3K_1)ghw_\kappa+(K_4-K_3)gh\}dz
\end{aligned} \tag{38.16}$$

in which

$$\begin{aligned}
K_1 &= \frac{2\eta\phi^{1/2}Q_3-p_3}{12\phi}+\frac{F_1p_2}{16\phi^2}-\frac{F_1^3}{64\phi^3}\\
K_2 &= \frac{F_1}{16\phi}\left(\frac{p_2}{\phi}-\frac{F_1^2}{\phi^2}\right)\\
K_3 &= \frac{1}{8}\left(\frac{p_2}{\phi}-\frac{F_1^2}{\phi^2}\right)\\
K_4 &= \frac{F_1^2}{8\phi^2}+\frac{1}{16}\left(3\frac{\phi'^2}{\phi^2}+\frac{2\eta^2B^2}{\phi}\right)
\end{aligned} \tag{38.17}$$

In his first paper, Rose (1987b) lists the conditions for which the geometrical terms (second-order aberrations) vanish. The residual chromatic aberrations are then analysed and practical designs proposed. In his second long paper on the general subject of Wien filters, Rose (1990a) enquires whether the design parameters can be selected in such a way that the device acts as a corrector of spherical and chromatic aberration. Electrostatic and magnetic round lens terms are retained here, because the device is intended for use as a corrector but these fields do not overlap those of the Wien filter. Rose goes on to establish the conditions in which the filter is nondispersive and free of second-rank aberrations. Finally, he investigates the third-rank aberrations; the integrand of the next higher order contribution to the eikonal function is given and the aberration integrals for the aperture aberrations are listed and evaluated in the sharp cut-off (SCOFF) approximation, in which the fields are assumed to fall abruptly to zero and there are no fringing fields. Rose proposes a possible corrector design, which was exploited in the low-voltage transmission electron microscope of Delong and Štěpán (2006).

A contribution by Scheinfein (1989) gives all the second-rank aberration coefficients in the SCOFF approximation and also estimates the contributions to these coefficients arising from the fringing fields.

The extensive work of Ioanoviciu, Tsuno and Martínez, much of which antedates the papers cited above, is considered last because the SCOFF approximation is employed throughout. Ioanoviciu (1973) considers the model fields that correspond to a cylindrical condenser and a (magnetic) wedge field. The 'refractive index' is expanded for these fields and second-rank aberration coefficients are listed explicitly, including approximate formulae for the fringing fields. Among the many publications of Tsuno, we draw attention to his important paper of 1991, an extension of and improvement on the earlier studies of Tsuno et al. (1988a−c, 1990). In real Wien filters, the Wien condition is most unlikely to be satisfied exactly and this is recognized explicitly here; see also Tsuno (1992, 1993). The paraxial equations and second-rank aberrations are calculated without assuming that the Wien and stigmatic focusing conditions are satisfied. The SCOFF approximation is adopted and the contribution from the fringing fields is also estimated. Later, Tsuno and Martínez, who had published papers on the numerical analysis of Wien filters (Martínez and Tsuno, 2002, 2004a,b, Tsuno and Martínez, 2002, 2004a,b), made very full studies with Ioanoviciu of Wien filters (Ioanoviciu et al., 2004; Tsuno et al., 2003, 2005) and we now recapitulate these in some detail. Wien filters are the subject of a volume by Tsuno and Ioanoviciu (2013) and are examined in an earlier review by Ioanoviciu (1989).

We shall adopt a compact notation, well-suited to the SCOFF approximation. The cyclotron radius R,

$$R = \frac{\phi_0^{1/2}}{\eta B_2} \tag{38.18}$$

is used systematically as unit of length:

$$u = x/R, \quad \upsilon = y/R, \quad w = z/R \tag{38.19}$$

and the various field components are scaled with respect to the basic deflection functions, F_1 and B_2:

$$\begin{aligned} e_2 &= -p_2R/2F_1 \\ b_2 &= -Q_2R/2B_2 \\ e_3 &= p_3R^2/6F_1 \\ b_3 &= Q_3R^2/6B_2 \\ e_4 &= -p_4R^3/24F_1 \\ b_4 &= -Q_4R^3/24B_2 \end{aligned} \tag{38.20}$$

The equations of motion Eq. (38.9) take the form

$$\begin{aligned} u'' + k^2u &= F_{r1} + F_{r2} + F_{r3} \\ \upsilon'' + p^2\upsilon &= F_{\upsilon 2} + F_{\upsilon 3} \end{aligned} \tag{38.21}$$

in which

$$\begin{aligned} k^2 &= 2e_2 - 2b_2 + 1 \\ F_{r1} &= \kappa/2 \\ F_{r2} &= r_1u^2 + 2uu'' + u'^2/2 + r_2u\kappa - u''\kappa - \kappa^2/8 + r_3\upsilon^2 - \upsilon'^2/2 \\ F_{r3} &= r_4u^3 + r_5uu'' + r_6uu'^2 + r_7u^2\kappa \\ &\quad + r_8u\kappa^2 + \kappa^3/16 + 3u'^2\kappa/4 + r_9u\upsilon^2 \\ &\quad + r_{10}u\upsilon'^2 + r_{11}u'\upsilon\upsilon' + u'\upsilon'\upsilon'' \\ &\quad + r_{11}u''\upsilon^2 - u''\upsilon'^2 + r_{12}\upsilon^2\kappa + 3\upsilon'^2\kappa/4 \end{aligned} \tag{38.22}$$

and

$$\begin{aligned} r_1 &= -3e_3 + 3b_3 - 2b_2 - e_2 - 1/2 \\ r_2 &= b_2 + 1/2 \\ r_3 &= e_2 + 3e_3 - 3b_3 \\ r_4 &= -4e_4 + 4b_4 - 3b_3 - e_3 - b_2 - e_2 - 2b_2e_2 - 1/2 \\ r_5 &= 2e_2 \\ r_6 &= -2e_2 + 3b_2 - 3/2 \\ r_7 &= 3b_3/3 + b_2 + e_2/2 + 3/4 \\ r_8 &= -b_2/4 - 3/8 \\ r_9 &= 12e_4 - 12b_4 + 3b_3 + 3e_3 + 2e_2b_2 + e_2 \\ r_{10} &= 3b_2 - 4e_2 - 3/2 \\ r_{11} &= -2e_2 \\ r_{12} &= -3b_3/2 - e_2/2 \end{aligned} \tag{38.23}$$

Similarly,

$$
\begin{aligned}
p^2 &= -2e_2 + 2b_2 \\
F_{\upsilon 2} &= -h_2 \upsilon \kappa - \upsilon'' \kappa + h_1 u \upsilon + 2u\upsilon'' + u'\upsilon' \\
F_{\upsilon 3} &= h_2 \upsilon^3 + h_3 \upsilon \upsilon'^2 + h_4 \upsilon'' \upsilon^2 + h_5 \upsilon \kappa^2 + h_6 u \upsilon \kappa \\
&\quad + h_7 u^2 \upsilon - h_4 u^2 \upsilon'' - h_4 u u' \upsilon' + h_8 u'^2 \upsilon - u'^2 \upsilon'' + u' u'' \upsilon'
\end{aligned}
\tag{38.24}
$$

with

$$
\begin{aligned}
h_1 &= 6e_3 - 6b_3 + 2b_2 \\
h_2 &= -4e_4 + 4b_4 - 2b_2 e_2 \\
h_3 &= 2e_2 - 3b_2 \\
h_4 &= -2e_2 \\
h_5 &= b_2/4 \\
h_6 &= -3b_3 - b_2 \\
h_7 &= 12e_4 - 12b_4 + 2b_2 e_2 + b_2 + 6b_3 \\
h_8 &= 4e_2 - 3b_2
\end{aligned}
\tag{38.25}
$$

In the SCOFF approximation, we have

$$
F_{r2} = m_0 + m_1 \cos kw + m_2 \sin kw + m_3 \cos^2(kw) + m_4 \sin kw \cos kw \tag{38.26}
$$

and

$$
\begin{aligned}
\Delta u &= p_0 + p_1 \cos kw + p_2 \sin kw + p_3 w \cos kw + p_4 w \sin kw + p_5 \cos^2 kw + p_6 \sin kw \cos kw \\
\Delta \upsilon &= q_0 + q_1 \cos kw + q_2 \sin kw + q_3 w \cos kw + q_4 w \sin kw + q_5 \cos^2 kw + q_6 \sin kw \cos kw
\end{aligned}
\tag{38.27}
$$

in which

$$
\begin{aligned}
p_0 &= (m_0 + 2m_3/3)/k^2 \\
p_1 &= -(m_0 + m_3/3)/k^2 \\
p_2 &= (m_2/2 + m_4/3)/k^2 \\
p_3 &= -m_2/2k \\
p_4 &= m_1/2k \\
p_5 &= -m_3/3k^2 \\
p_6 &= -m_4/3k^2
\end{aligned}
\tag{38.28}
$$

where

$$\begin{aligned}
m_0 &= (u_o-\kappa)^2/4 + 2\alpha^2(r_1-1) - \upsilon_o^2/4 + 2\beta^2 r_3 + \kappa^2(r_1+r_2-1/8)\\
m_1 &= \kappa(u_o-\kappa)(2r_1+r_2-1/2)\\
m_2 &= \alpha\kappa(2r_1+r_2-1/2)/k\\
m_3 &= (r_1-5/4)\{(u_o-\kappa)^2-2\alpha^2\} + (r_3+1/4)(\upsilon_o^2-2\beta^2)\\
m_4 &= \{\alpha(u_o-\kappa)(2r_1-5/2) + \upsilon_o\beta(2r_3+1/2)\}/k
\end{aligned} \tag{38.29}$$

and

$$\begin{aligned}
q_0 &= (n_0+2n_3/3)/k^2\\
q_1 &= -(n_0+n_3/3)/k^2\\
q_2 &= (n_2/2+n_4/3)/k^2\\
q_3 &= -n_2/2k\\
q_4 &= n_1/2k\\
q_5 &= -n_3/3k^2\\
q_6 &= -n_4/3k^2
\end{aligned} \tag{38.30}$$

where

$$\begin{aligned}
n_0 &= (u_o-\kappa)\upsilon_o/2 + 2\alpha\beta(h_1-1)\\
n_1 &= \upsilon_o\kappa(h_1-b_2-1/2)\\
n_2 &= \beta\kappa(h_1-b_2-1/2)/k\\
n_3 &= (h_1-3/2)\{(u_o-\kappa)\upsilon_o-2\alpha\beta\}\\
n_4 &= (h_1-3/2)\{(u_o-\kappa)\beta+\alpha\upsilon_o\}/k
\end{aligned} \tag{38.31}$$

and α, β denote u_o', υ_o'.

For stigmatic focusing, we must have

$$e_2 - b_2 = -1/4 \tag{38.32}$$

which implies

$$k = 1/\sqrt{2} \tag{38.33}$$

For $kw = 2\pi$, where there is no energy dispersion, we have

$$\begin{aligned}
\Delta u &= p_0 + p_1 + 2\pi p_2/k + p_5\\
\Delta\upsilon &= q_0 + q_1 + 2\pi q_3/k + q_5
\end{aligned} \tag{38.34}$$

But $p_0 + p_1 + p_5$ and $q_0 + q_1 + q_5$ vanish and hence all the second-rank aberrations vanish at $w = 2\pi/k$ or $z = 2\pi R/k$ if p_3 and q_3 also vanish, which implies that m_2 and n_2 must be zero. If we require that only the geometrical aberrations vanish, then it is sufficient to set

$$p_3 = q_3 \tag{38.35a}$$

or

$$12(e_3 - b_3) + 4b_2 + 2e_2 + 1/2 = 0 \tag{38.35b}$$

This is the *second-order geometric-aberration-free condition*. Stigmatic focusing requires that

$$e_2 = -\frac{m+2}{8}, \quad b_2 = -\frac{m}{8} \tag{38.36}$$

(where m is arbitrary) whereupon condition (38.35b) becomes

$$e_3 - b_3 = \frac{m}{16}. \tag{38.37}$$

Returning to the expressions (38.34) for Δu and Δv, we find

$$\begin{aligned} \Delta u(z = 2\pi R/k) &= -\frac{\alpha\kappa}{8k^2}(m-2) \\ \Delta v(z = 2\pi R/k) &= -\frac{\beta\kappa}{8k^2}(m-2) \end{aligned} \tag{38.38}$$

and so the second-order terms all vanish for

$$m = 2 \tag{38.39a}$$

which implies

$$b_3 - e_3 = -1/8, \quad b_2 = -1/4, \quad e_2 = -1/2. \tag{38.39b}$$

Note that this is not the same as the value proposed by Rose (1987), which corresponds to $m = 6$ ($e_2 = -1$, $b_2 = -3/4$, $e_3 - b_3 = 3/8$).

In their later paper (Tsuno et al., 2005), expressions for the third-rank aberrations are given for two planes: the first focus $z = z_i^{(1)}$, at which $z = \pi R$, and the second focus $z = z_i^{(2)}$, at which $z = 2\pi R$. There will be both second- and third-rank aberrations at the first plane

$z = z_i^{(1)}$ but only third-rank aberrations at the second plane, $z = z_i^{(2)}$. The results are as follows:

$$\begin{aligned}
u(z_i^{(1)}) = {} & -u_0 + 2\kappa + A_{uu}u_0^2 + A_{ud}u_0\kappa + A_{aa}\alpha^2 \\
& + A_{ad}\alpha\kappa + A_{dd}\kappa^2 + A_{\upsilon\upsilon}\upsilon_0^2 + A_{bb}\beta^2 \\
& + A_{uuu}u_0^3 + A_{uua}u_0^2\alpha + A_{uud}u_0^2\kappa + A_{uaa}u_0\alpha^2 \\
& + A_{uad}u_0\alpha\kappa + A_{udd}u_0\kappa^2 + A_{u\upsilon\upsilon}u_0\upsilon_0^2 \\
& + A_{u\upsilon b}u_0\upsilon_0\beta + A_{ubb}u_0\beta^2 + A_{aaa}\alpha^3 + A_{aad}\alpha^2\kappa \\
& + A_{add}\alpha\kappa^2 + A_{a\upsilon\upsilon}\alpha\upsilon_0^2 + A_{a\upsilon b}\alpha\upsilon_0\beta \\
& + A_{abb}\alpha\beta^2 + A_{ddd}\kappa^3 + A_{d\upsilon\upsilon}\kappa\upsilon_0^2 + A_{d\upsilon b}\kappa\upsilon_0\beta + A_{dbb}\kappa\beta^2.
\end{aligned} \tag{38.40}$$

$$\begin{aligned}
\upsilon(z_i^{(1)}) = {} & -\upsilon_0 + A_{\upsilon u}\upsilon_0 u_0 + A_{\upsilon d}\upsilon_0\kappa + A_{ba}\beta\alpha + A_{bd}\beta\kappa \\
& + A_{\upsilon\upsilon\upsilon}\upsilon_0^3 + A_{\upsilon\upsilon b}\upsilon_0^2\beta + A_{\upsilon bb}\upsilon_0\beta^2 + A_{\upsilon dd}\upsilon_0\kappa^2 \\
& + A_{\upsilon du}\upsilon_0\kappa u_0 + A_{\upsilon da}\upsilon_0\kappa\alpha + A_{\upsilon uu}\upsilon_0 u_0^2 + A_{\upsilon ua}\upsilon_0 u_0\alpha \\
& + A_{\upsilon aa}\upsilon_0\alpha^2 + A_{bbb}\beta^3 + A_{bdd}\beta\kappa^2 + A_{bdu}\beta\kappa u_0 \\
& + A_{bda}\beta\kappa\alpha + A_{buu}\beta u_0^2 + A_{bua}\beta u_0\alpha + A_{baa}\beta\alpha^2.
\end{aligned}$$

$$\begin{aligned}
u(z_i^{(2)}) = {} & u_0 - 2A_{ad}\alpha\kappa + A_{2uua}u_0^2\alpha + A_{2uud}u_0^2\kappa \\
& + A_{2uad}u_0\alpha\kappa + A_{2udd}u_0\kappa^2 + A_{2u\upsilon b}u_0\upsilon_0\beta \\
& + A_{2aaa}\alpha^3 + A_{2aad}\alpha^2\kappa + A_{2add}\alpha\kappa^2 + A_{2a\upsilon\upsilon}\alpha\upsilon_0^2 \\
& + A_{2abb}\alpha\beta^2 + A_{2ddd}\kappa^3 + A_{2d\upsilon\upsilon}\kappa\upsilon_0^2 \\
& + A_{2d\upsilon b}\kappa\upsilon_0\beta + A_{2dbb}\kappa\beta^2.
\end{aligned} \tag{38.41}$$

$$\begin{aligned}
\upsilon(z_i^{(2)}) = {} & \upsilon_0 - 2A_{bd}\beta\kappa + A_{2\upsilon\upsilon b}\upsilon_0^2\beta + A_{2\upsilon dd}\upsilon_0\kappa^2 \\
& + A_{2\upsilon du}\upsilon_0\kappa u_0 + A_{2\upsilon da}\upsilon_0\kappa\alpha + A_{2\upsilon ua}\upsilon_0 u_0\alpha + A_{2bbb}\beta^3 \\
& + A_{2bdd}\beta\kappa^2 + A_{2bdu}\beta\kappa u_0 + A_{2bda}\beta\kappa\alpha + A_{2buu}\beta u_0^2 \\
& + A_{2baa}\beta\alpha^2.
\end{aligned}$$

in which

i. π-filter, x-direction

$$
\begin{aligned}
A_{uu} &= (m-4)/4 \\
A_{ud} &= -(m-4)/2 \\
A_{aa} &= m-6 \\
A_{ad} &= \pi k(m-2)/2 \\
A_{dd} &= (m-1)/2 \\
A_{vv} &= (m-12)/12 \\
A_{bb} &= (m-6)/3 \\
A_{uuu} &= -(m-4)^2/16 \\
A_{uua} &= -3(\pi/k)(b_{31}+t_1) + \pi\left(9m^2-64m+64\right)/(256k) \\
A_{uud} &= -2(7b_{31}+8t_1) + \left(3m^2-20m+40\right)/16 \\
A_{uaa} &= (m-12)(m-6)/4 \\
A_{uad} &= 6(\pi/k)(b_{31}+t_1) + \pi\left(7m^2-96m+192\right)/(128k) \\
A_{udd} &= \pi^2(m-2)^2/32 + 4(7b_{31}+8t_1) - \left(2m^2-9m+12\right)/8 \\
A_{uvv} &= \left(-5m^2+72m-144\right)/144 \\
A_{uvb} &= 3(\pi/k)(b_{31}+2t_1) + 3\pi m^2/(128k) \\
A_{ubb} &= -(m-6)(m+12)/36 \\
A_{aaa} &= -6(\pi/k)(b_{31}+t_1) + \pi\left(9m^2-64m+64\right)/(128k) \\
A_{aad} &= -8(7b_{31}+8t_1) + \left(m^2+8m-60\right)/4 \\
A_{add} &= -3(\pi/k)(4b_{31}+t_1) - \pi\left(11m^2-240m+480\right)/(256k) \\
A_{avv} &= (3\pi/2k)(b_{31}+2t_1) + \pi\left(25m^2-192m+192\right)/(768k) \\
A_{avb} &= m(m-6)/6 \\
A_{abb} &= 9(\pi/k)(b_{31}+2t_1) + \pi\left(43m^2-192m+192\right)/(384k) \\
A_{ddd} &= -\left(\pi^2/32\right)(m-2)^2 - 8(3b_{31}+4t_1) + \left(m^2-2m+2\right)/8 \\
A_{dvv} &= 2(b_{31}+8t_1) + \left(17m^2-36m+72\right)/144 \\
A_{dvb} &= -3(\pi/k)(b_{31}+2t_1) + \pi m(7m-32)/(384k) \\
A_{dbb} &= 8(3b_{31}+8t_1) + \left(19m^2-24m-36\right)/36
\end{aligned}
\tag{38.42a}
$$

ii. π-filter, y-direction

$$
\begin{aligned}
A_{vd} &= -m/6 \\
A_{vu} &= m/6 \\
A_{ba} &= 2(m-6)/3 \\
A_{bd} &= \pi k(m-2)/2 \\
A_{vvv} &= -m(m-12)/144 \\
A_{vvb} &= -3(\pi/k)t_1 - \pi(13m^2+192m-192)/(768k) \\
A_{vbb} &= m(m-6)/36 \\
A_{vdd} &= \pi^2/32(m-2)^2 - 4(3b_{31}+8t_1) - m(16m-3)/72 \\
A_{vdu} &= 4(3b_{31}+8t_1) + m(17m-12)/72 \\
A_{vda} &= -(3\pi/k)(b_{31}+2t_1) + \pi(7m^2-224m+384)/(384k) \\
A_{vuu} &= -\mathrm{m}(5m-12)/144 \\
A_{vua} &= 3(\pi/k)(b_{31}+2t_1) + 3\pi m^2/(128k) \\
A_{vaa} &= -(m-6)(m+24)/36 \\
A_{bbb} &= -6(\pi/k)t_1 - \pi(13m^2+192m-192)/(384k) \\
A_{bdd} &= 3(\pi/k)(3b_{31}/2+5t_1) + \pi(101m^2+208m-672)/(768k) \\
A_{bdu} &= -3(\pi/k)(b_{31}+2t_1) - \pi(9m^2+32m-192)/(384k) \\
A_{bdu} &= 8(6b_{31}+16t_1) + (5m^2+8m-60)/6 \\
A_{buu} &= (3\pi/2k)(b_{31}+2t_1) + \pi(25m^2-192m+192)/(768k) \\
A_{bua} &= (m-12)(m-6)/6 \\
A_{baa} &= 9(\pi/k)(b_{31}+2t_1) + \pi(43m^2-192m+192)/(384k)
\end{aligned}
\tag{38.42b}
$$

iii. 2π-filter, x-direction

$$
\begin{aligned}
A_{2uua} &= (3\pi/k)(b_{31}+b_{32}+t_1+t_2) + (\pi/k)(-9m^2/128+m/2-1/2) \\
A_{2uud} &= 2\{7(b_{31}-b_{32}) + 8(t_1-t_2)\} \\
A_{2uad} &= (\pi m/k)(9m/64-1) - (\pi/k)\{6(b_{31}+b_{32}+t_1+t_2)-1\} \\
A_{2udd} &= -(2\pi/8)(m-2)^2 - 4\{7(b_{31}-b_{32})+8(t_1-t_2)\} \\
A_{2uvb} &= -3\pi m^2/(64k) - (3\pi/k)\{b_{31}+b_{32}+2(t_1+t_2)\} \\
A_{2aaa} &= (6\pi/k)(b_{31}+b_{32}+t_1+t_2) + (\pi/k)(-9m^2/64+m-1) \\
A_{2aad} &= 8\{7(b_{31}-b_{32})+8(t_1-t_2)\} \\
A_{2add} &= (3\pi/k)\{4(b_{31}+b_{32})+5(t_1+t_2)\} + (\pi/k)(-21m^2/128+5m/8-1/4) \\
A_{2avv} &= \pi m/(2k)(-25m/192+1) - (\pi/k)\{(3/2)(b_{31}+b_{32})+3(t_1+t_2)+1/2\} \\
A_{2abb} &= -(9\pi/k)(b_{31}+b_{32}+2(t_1+t_2)) + \pi/k(-43m^2/192+m-1) \\
A_{2ddd} &= 8\{3(b_{31}-b_{32})+4(t_1-t_2)\} + \pi^2(m-2)^2/8 \\
A_{2dvv} &= -2\{b_{31}-b_{32}+8(t_1-t_2)\} \\
A_{2dvb} &= 3\pi m^2/(64k) + (3\pi/k)\{b_{31}+b_{32}+2(t_1+t_2)\} \\
A_{2dbb} &= -8\{3(b_{31}-b_{32})+8(t_1-t_2)\}
\end{aligned}
\tag{38.43a}
$$

iv. 2π-filter, y-direction

$$
\begin{aligned}
A_{2vvb} &= \pi m/(2k)\big(13m/192+1\big)+\big(\pi/k\big)\big\{3(t_1+t_2)-1/2\big\}\\
A_{2vdd} &= 4\big\{3(b_{31}-b_{32})+8(t_1-t_2)\big\}-\pi^2(m-2)^2/8\\
A_{2vdu} &= -4\big\{3(b_{31}-b_{32})+8(t_1-t_2)\big\}\\
A_{2vda} &= 3\pi m^2/(64k)+\big(3\pi/k\big)\big\{b_{31}+b_{32}+2(t_1+t_2)\big\}\\
A_{2vua} &= -3\pi m^2/(64k)-\big(3\pi/k\big)\big\{b_{31}+b_{32}+2(t_1+t_2)\big\}\\
A_{2bbb} &= 6\pi/k(t_1+t_2)+\pi/k\big(13m^2/192+m-1\big)\\
A_{2bdd} &= -\big(3\pi/k\big)\big\{3(b_{31}+b_{32})/2+5(t_1+t_2)\big\}+\big(\pi/k\big)\big(-133m^2/384+5m/8-1/4\big)\\
A_{2bdu} &= \big(\pi m/k\big)\big(25m/192-1\big)+\big(3\pi/k\big)\big\{b_{31}+b_{32}+2(t_1+t_2)+1/3\big\}\\
A_{2bda} &= -16\big\{3(b_{31}-b_{32})+8(t_1-t_2)\big\}\\
A_{2buu} &= \pi m/(2k)\big(1-25m/192\big)-3\pi/(2k)\big\{b_{31}+b_{32}+2(t_1+t_2)+1/3\big\}\\
A_{2baa} &= -\big(9\pi/k\big)\big\{b_{31}+b_{32}+2(t_1+t_2)\big\}+\pi/k\big(-43m^2/192+m-1\big)
\end{aligned}
\tag{38.43b}
$$

We recall that $k=1/\sqrt{2}$.

The field component b_3 is selected as an independent parameter and e_3 has been replaced by $b_3+m/16$ (38.37). The sextupole and octopole components of the π-filter and the second half of the 2π-filter are shown separately; thus, b_{31} denotes b_3 of the π-filter and b_{32} denotes b_3 of the second half of the 2π-filter and likewise for the other terms. For the octopole components e_4 and b_4, we have written

$$
\begin{aligned}
t_1 &= e_{41}-b_{41}\\
t_2 &= e_{42}-b_{42}\\
t &= t_1+t_2
\end{aligned}
\tag{38.44}
$$

It is interesting to see that some coefficients vanish when $b_{31}=b_{32}$ and $t_1=t_2$, while other coefficients are cancelled when $b_{31}=-b_{32}$ or $t_1=-t_2$.

These results can be exploited to find configurations with particularly desirable properties. For full discussion, the reader is referred to the original papers; here, we simply point out some highlights. Consider the third-order axial aberration (analogous to spherical aberration) at the plane $z=z_i^{(2)}$; for this to vanish, we require

$$A_{2aaa}=A_{2bbb}=0 \tag{38.45a}$$

for which

$$b_3=b_{31}+b_{32}=5m^2/144 \tag{38.45b}$$

and

$$t=t_1+t_2=-\frac{13m^2/192+m-1}{6} \tag{38.45c}$$

Ioanoviciu et al. plot the corresponding aberration figures for five values of the free parameter m: -2 (magnetic quadrupole only), 0 (electrostatic quadrupole only), 2 (all second-rank aberrations absent at $z = z_i^{(2)}$), 4 (no particular properties) and 6 (second-order aberrations all vanish at $z = z_i^{(1)}$).

To obtain a round beam, we need

$$A_{2aaa} = A_{2bbb} \tag{38.46}$$

which gives the conditions (38.45b, c) and to this we add

$$A_{2aaa} = A_{2abb} \quad (\equiv A_{2baa}) \tag{38.47a}$$

which ensures that the beam has the same radius in the planes midway between the x- and y-axes. This yields

$$t = t_1 + t_2 = -\frac{29}{1152} m^2 \tag{38.47b}$$

For what value of m does A_{2bbb} vanish? For this,

$$m^2 - 12m + 12 = 0 \tag{38.48a}$$

and so

$$m = 6 \pm 2\sqrt{6} \tag{38.48b}$$

Tsuno et al. point out that the Wien filter can be used as an aberration corrector, since negative values of the chromatic and aperture aberration coefficients are easily obtained; their design appears to be preferable to the earlier arrangements proposed by Mentink et al. (1999) and Steffen et al. (2000).

For other work on Wien filters, see Ioanoviciu (1973, 1974), Ioanoviciu and Cuna (1974), Smith and Munro (1986), Tang (1986a,b), Hurd (1987), Kato and Tsuno (1990), Tsuno (1994), Sakurai et al. (1995), and Tsuno and Rouse (1996), Martínez and Tsuno (2007), Horáček et al. (2008), as well as the earlier work of Andersen (1967) and Andersen and Le Poole (1970). We also remind the reader of the work of Plies and Bärtle on the design of monochromators based on Wien filters, already mentioned earlier. Numerous Wien quadruplets were studied and a most interesting configuration emerged, the properties of which are described in (Plies and Bärtle, 2003). The history of the Wien filter is retraced by Plies et al. (2011). The whole subject has been reconsidered in depth by Tsuno and Ioanoviciu (2013).

Quadrupole Lenses

39.1 Introduction

For particle energies in the range of tens or hundreds of kilovolts up to a few megavolts, quadrupole lenses are used, if at all, as components in an aberration-correcting unit or as devices that produce a line focus. It is mainly at higher energies, where rotationally symmetric lenses are too weak, that their strong focusing ability is exploited to provide the principal focusing field. As well as in particle accelerators, they are to be found in high-energy ion microprobe devices, intended for elemental analysis.

In all these fields — aberration correction, accelerator optics and ion microprobe analysis — detailed reviews and textbooks are available (Strashkevich, 1959, 1966; Hawkes, 1966, 1970, 1980; Steffen, 1965; Banford, 1966; Septier, 1966; Yavor, 1968; Lawson, 1977; Wollnik, 1987; Grime and Watt, 1984; Watt and Grime, 1987; Humphries, 1986). This chapter is therefore confined to the principal models and geometries encountered in quadrupole studies, and to the most important combinations. Aberration correctors that use quadrupoles and octopoles are examined in Chapter 41, Aberration Correction.

Electrostatic and magnetic quadrupoles are comparatively open structures and it is intuitively obvious that the field function characterizing a quadrupole lens, $p_2(z)$ or $Q_2(z)$, will have a roughly bell-shaped distribution if the poles or electrodes are short; if, on the other hand, they extend far along the axis relative to the bore radius, we may expect the distribution to exhibit a rather flat central plateau terminated by bell-shaped end-fields, the half-width of which may even be negligible leaving us with a rectangular field distribution. The three principal models correspond to these various situations: in the bell-shaped field model, we write

$$q(z) = \frac{1}{\left(1+z^2/d^2\right)^2} \tag{39.1}$$

In the rectangular field model,

$$q(z) = \begin{cases} 1 & |z| < L/2 \\ 0 & |z| > L/2 \end{cases} \tag{39.2}$$

where $q(z)$ is defined in Eq. (29.26). A hybrid model in which these are combined has likewise been used. These models have the double advantage of possessing analytical solutions in terms

Principles of Electron Optics: Applied Geometrical Optics.
DOI: http://dx.doi.org/10.1016/B978-0-12-813369-9.00039-7

of circular and hyperbolic functions, permitting evaluation of the aberration integrals in closed form, and of representing the true field distribution rather accurately. This is fortunate, for the task of computing the field distribution is distinctly more laborious in a quadrupole than in a round lens.

If a line focus is to be formed, a single quadrupole may be sufficient or a doublet may be used to give a measure of flexibility. If a probe is required or stigmatic imaging between a pair of planes, even a doublet is normally much too restrictive and the simplest practical system is the quadruplet and in particular, the antisymmetric or 'Russian' quadruplet, so named because it was introduced by the Leningrad group led by S. Ya. Yavor, who have contributed extensively to quadrupole studies.

For correction of round lens spherical and chromatic aberration, the situation is even more complicated, for the quadrupole fields must be combined with octopole fields, and to achieve simultaneous correction of all the resolution-limiting aberrations, elements with other symmetries are also needed (see Chapter 41, Aberration Correction). In the present section, we give some indication of the variation of the optical characteristics of individual quadrupoles and the more common systems, referring for details to Hawkes (1966, 1970) and Yavor (1968). Although some efforts have been made to classify and analyse the parasitic aberrations of quadrupoles, the results are of limited practical use, a disappointing situation for it is highly desirable to have some reliable theoretical estimate of the constructional tolerances that must be respected in real systems. The solution, as we have emphasized in Chapter 33, The Aberrations of Deflection Systems, is exact ray-tracing, the results being presented as spot diagrams or 'scatter-plots', several examples of which are to be found in Grime and Watt (1984).

In the following sections, we first consider the two main models and then examine briefly the simpler quadrupole combinations. In connection with the latter, a few specialized terms have come into use, of which the most useful is 'regular': a quadrupole system is said to be *regular* if it produces a sharp undistorted paraxial image of an object for all positions of the object plane, just like a round lens. If the magnifications M_x and M_y are unequal, the system is said to be *anamorphotic*; when they are equal, it is *orthomorphic* or *distortion-free*. If the system produces point-to-point imagery only for isolated locations of the object plane, it may be called *pseudo-stigmatic*. (See also Scherzer, 1965 and the glossary at the end of Hawkes, 1970.)

39.2 The Rectangular and Bell-Shaped Models

For both of these models (39.1, 39.2), the paraxial equations (19.5, 6) are soluble in closed form in terms of circular and hyperbolic functions. Expressions for the cardinal elements can then be written down immediately. We list only the asymptotic quantities, which are those more often needed, but their real counterparts are easily found.

In the absence of any round-lens component, Eq. (19.5) take the form

$$\begin{aligned}\frac{d}{dz}\left(\hat{\phi}^{1/2}x'\right)-\frac{\gamma p_2-2\eta Q_2\hat{\phi}^{1/2}}{2\hat{\varphi}^{1/2}}x=0\\\frac{d}{dz}\left(\hat{\phi}^{1/2}y'\right)+\frac{\gamma p_2-2\eta Q_2\phi^{1/2}}{2\hat{\phi}^{1/2}}y=0\end{aligned}\tag{39.3}$$

and introducing the convenient notation of Eqs (29.26, 29.27), these become

$$\begin{aligned}x''+\beta^2qx=0\\y''-\beta^2qy=0\end{aligned}\tag{39.4}$$

It is immediately obvious that for the rectangular model (39.2), for which $q(z)$ is unity for $|z|<L/2$ and zero elsewhere, Eq. (39.4) have solutions in terms of sin βz, cos βz, sinh βz and cosh βz. Writing

$$\theta:=\beta L\tag{39.5}$$

the asymptotic cardinal elements are given by

$$\begin{aligned}&\frac{z_{Fi}^{(x)}}{L}=-\frac{z_{Fo}^{(x)}}{L}=\frac{\cot\theta}{\theta}+\frac{1}{2}\quad &&\frac{z_{Fi}^{(y)}}{L}=-\frac{z_{Fo}^{(y)}}{L}=-\frac{\coth\theta}{\theta}+\frac{1}{2}\\&\frac{f^{(x)}}{L}=\frac{1}{\theta\sin\theta} &&\frac{f^{(y)}}{L}=-\frac{1}{\theta\sinh\theta}\end{aligned}\tag{39.6}$$

The ‘effective length’ L, defined by $L:=\int_{-\infty}^{\infty}q(z)\ dz$, has been found experimentally to be related to the length l and radius a of quadrupoles of simple shape (cylindrical rods parallel to the axis, for example) by

$$L\approx l+1.1a\tag{39.7a}$$

(Grivet and Septier, 1958, 1960), which agrees well with the theoretical estimate of Reisman (1957),

$$L=l+(\pi-2)a\tag{39.7b}$$

The excitation parameter $\beta^2=\beta_M^2-\beta_E^2$ is related to the potential $\pm U$ on the electrodes or the excitation J (A−turn/pole) as follows:

$$\beta_E^2=\frac{\gamma U}{a^2\hat{\phi}_0}\quad\beta_M^2=\frac{\mu_0\eta J}{a^2\hat{\phi}_0^{1/2}}\tag{39.8}$$

Explicit formulae for the coefficients that occur in the aperture aberration, distortion and chromatic aberration polynomials in m_x and m_y are known and are set out in full in Hawkes (1970), where numerous tables of their values are to be found. Formulae for various aberration coefficients for this model are also to be found in Dymnikov et al. (1965a,b), Ovsyannikova and Yavor (1967), Fishkova et al. (1968), Ovsyannikova (1968), Lee-Whiting (1970) and Szilágyi et al. (1973, 1974); the long study by Smith (1970) should be used in conjunction with Lee-Whiting (1972).

For the bell-shaped model (39.1), the paraxial equation in the converging plane has exactly the same form as that for a round magnetic lens when the Glaser bell is used, and the solutions are hence identical. In the diverging plane, the solutions are obtained by replacing β by iβ. Writing

$$\omega_x^2 = 1 + \beta^2 d^2 \qquad \begin{aligned} \omega_y^2 &= 1 - \beta^2 d^2 \\ \sigma_y^2 &= \beta^2 d^2 - 1 \end{aligned} \tag{39.9}$$

we find that the asymptotic cardinal elements are given by

$$\frac{f_x}{d} = -\frac{\omega_x}{\sin \pi\omega_x} \qquad \begin{aligned} \frac{f_y}{d} &= -\frac{\omega_y}{\sin \pi\omega_y} \quad \left(\beta^2 d^2 < 1\right) \\ \frac{f_y}{d} &= -\frac{\sigma_y}{\sinh \pi\sigma_y} \quad \left(\beta^2 d^2 > 1\right) \end{aligned}$$

$$\begin{aligned} \frac{z_{Fi}^{(x)}}{d} &= -\frac{z_{Fo}^{(x)}}{d} = \omega_x \cot \pi\omega_x \\ \frac{z_{Fi}^{(y)}}{d} &= -\frac{z_{Fo}^{(y)}}{d} = \omega_y \cot \pi\omega_y \quad \left(\beta^2 d^2 < 1\right) \\ &= \sigma_y \coth \pi\sigma_y \quad \left(\beta^2 d^2 > 1\right) \end{aligned} \tag{39.10}$$

The excitations are related to U and J by the approximate formulae (Hardy, 1967):

$$\begin{aligned} \beta_E^2 &= \frac{\gamma U}{a^2 \hat{\phi}_0}\left(1 - \frac{a^2}{3d^2}\right) \\ \beta_M^2 &= \frac{\mu_0 \eta J}{a^2 \hat{\phi}_0^{1/2}}\left(1 - \frac{a^2}{3d^2}\right) \end{aligned} \tag{39.11}$$

For the short lenses for which this model is intended, $a \approx d$ so that $1 - a^2/3d^2 \approx 0.67$, in agreement with Deltrap's experimental findings (1964).

We note that for weak lenses, for which $\beta^2 d^2 \ll 1$,

$$\frac{f_x}{d} = -\frac{f_y}{d} \approx \frac{2}{\pi \beta^2 d^2}$$

For this model, $L = \int q(z)dz = \pi d/2$ so that

$$\frac{f_x}{L} = -\frac{f_y}{L} \approx \frac{1}{\beta^2 L^2}$$

in agreement with Eq. (39.6). This weak-lens approximation is frequently encountered in the accelerator literature.

The polynomial coefficients for the aberrations are known for the bell-shaped model (see Hawkes 1967a,b; Hawkes and Hardy, 1967; Hawkes and Cham, 1967). For other expressions and further studies, see Glaser (1955), Dymnikov et al. (1965a–d), Tanguy (1965a,b) and Szilágyi et al. (1973, 1974). Other models have been proposed, such as the asymmetric bell-shaped distribution, intended to represent quadrupoles in which the electrode surfaces are tilted in conical fashion towards the axis, and the triangular model; for details and references, we refer to Hawkes (1970). Of more interest is the bell-shaped model for an electrostatic round-lens potential superposed on a quadrupole distribution (Dušek, 1959; Schiske, 1966/67). In the paper by Schiske, the more general case in which a round magnetic field is also present but orthogonality is preserved is analysed.

Ura (1991) has shown that a unified representation of the cardinal elements and chromatic and aperture aberration coefficients of electrostatic quadrupoles can be found for the principal field models: rectangular, bell-shaped and a combination of these. The cardinal elements and aberration coefficients are scaled with respect to the minimum focal length in the converging plane and the excitation is scaled with respect to the value corresponding to the minimum focal length. Ura plots curves for the rectangular model and the bell-shaped model and suggests how the values for the combined model can be deduced from them.

39.3 Isolated Quadrupoles and Doublets

Isolated quadrupoles are capable of stigmatic but not distortion-free imagery (Junior and Antony-Spies, 1967), and both conjugates cannot of course be real.

With doublets, we meet the notion of the antisymmetric multiplet: a multiplet of an even number of quadrupoles is said to be *antisymmetric* if it is geometrically symmetric about a midplane but electrically antisymmetric. In the case of a doublet, this would mean that the two members have equal excitations (β^2) of opposite polarity (Fig. 39.1). We have seen that

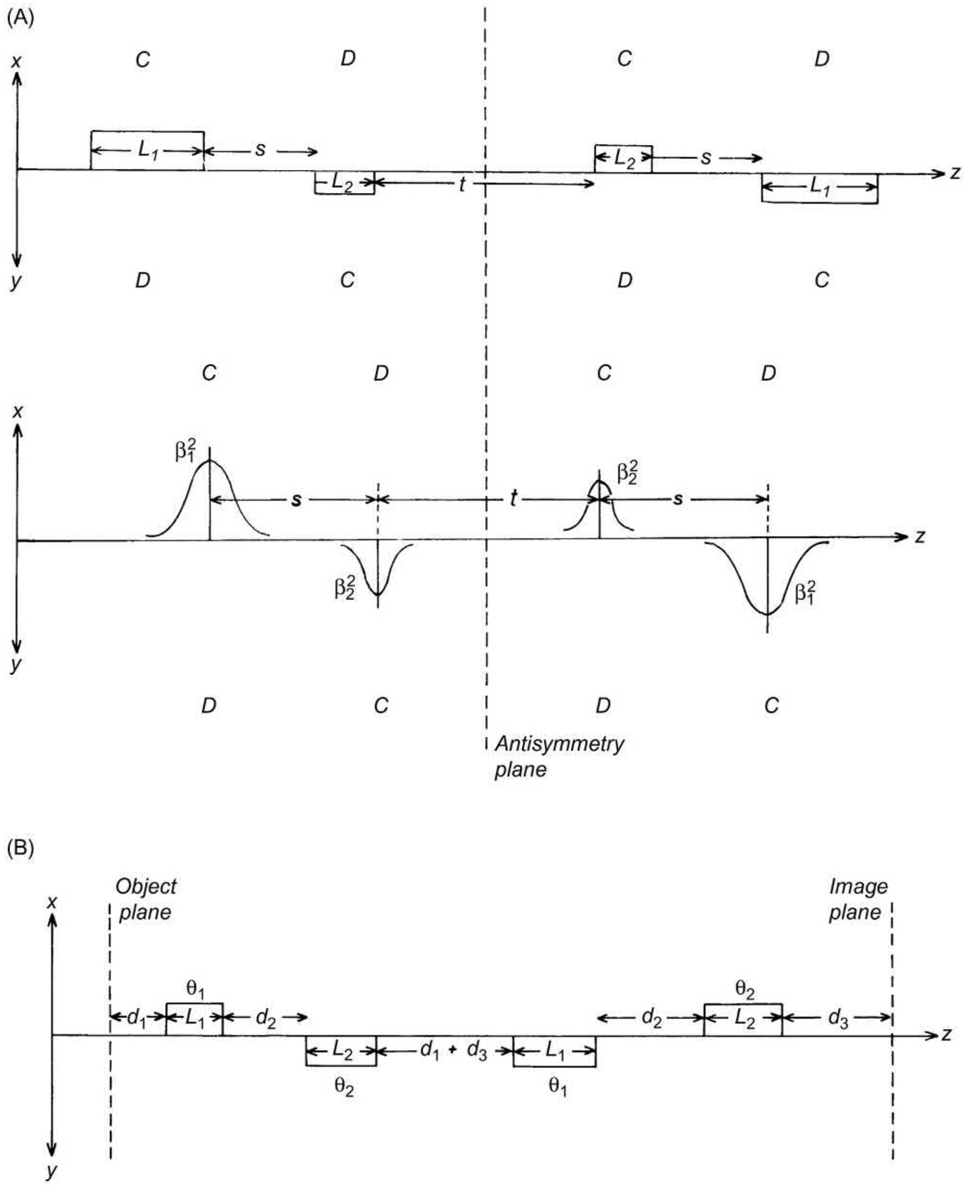

Figure 39.1

Quadrupole quadruplets. (A) Notation used when studying antisymmetric quadruplets by means of the rectangular and bell-shaped models. (B) Quadruplet consisting of two identical doublets rotated through 90° relative to each other. (C)–(G) Antisymmetric quadruplets. (C) Load characteristic for $L_1 = L_2$, $s = 0$; rectangular model. (D)–(G) Load characteristic for four configurations; bell-shaped model.

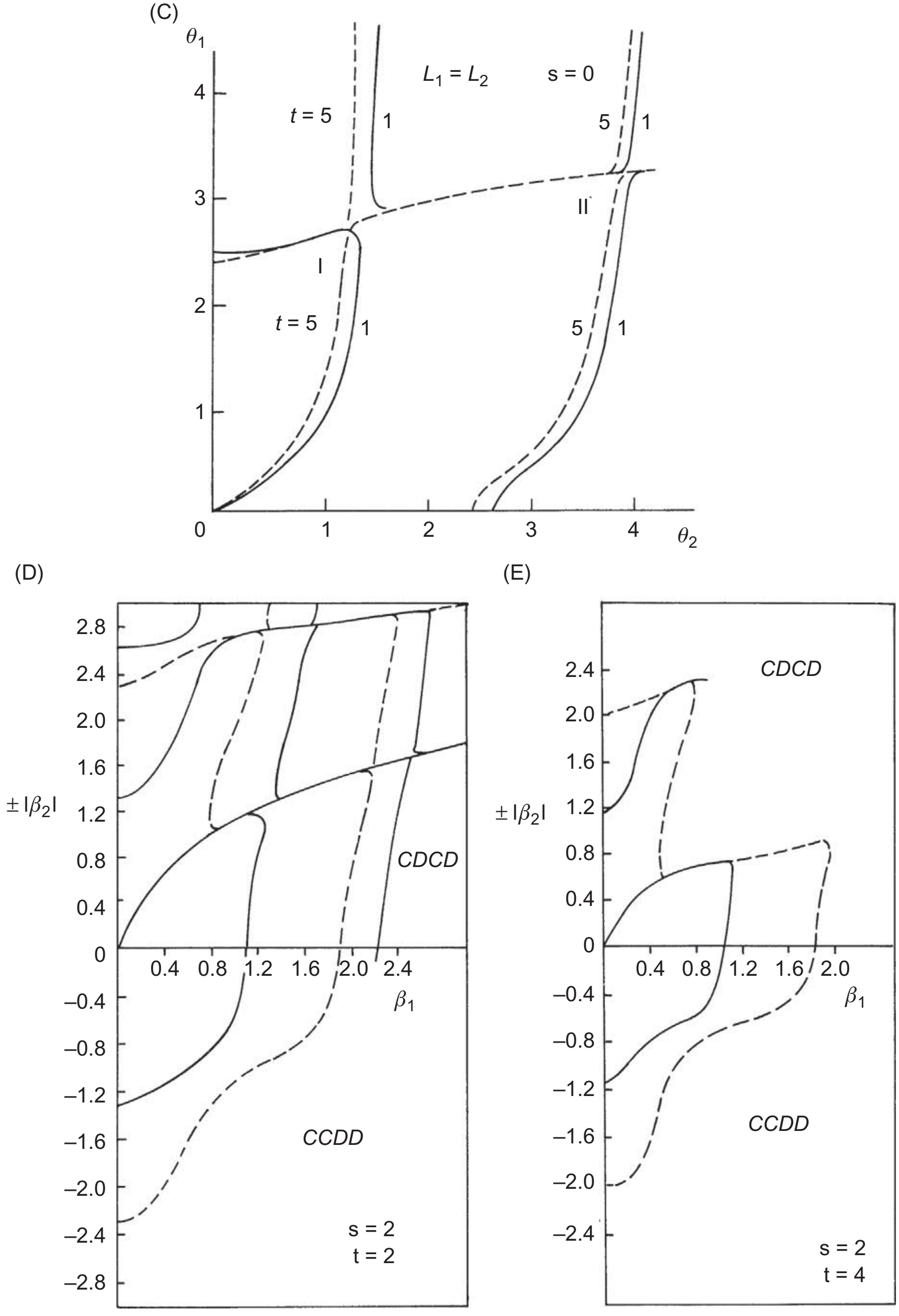

Figure 39.1
(Continued).

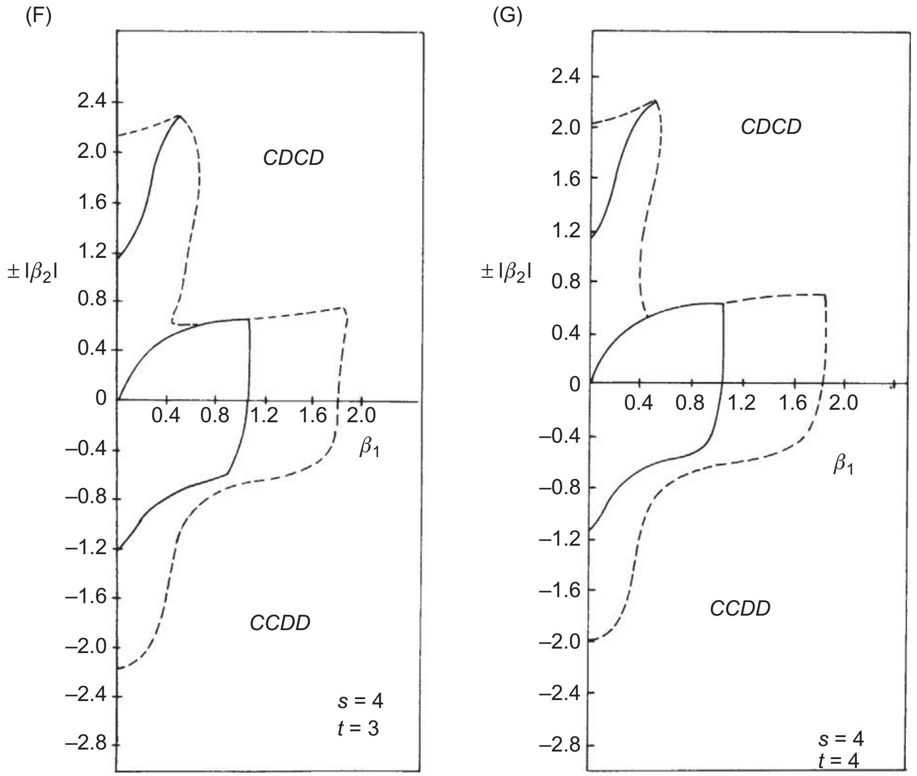

Figure 39.1
(Continued).

the focal lengths in the two principal sections are equal for antisymmetric multiplets and the system will therefore be regular if one other condition ($z_{Fi}^{(x)} = z_{Fi}^{(y)}$ for example) is satisfied. Since we have two free parameters, the distance D between the quadrupoles and their common excitation β^2, we can establish the curve $D = f(\beta^2)$ for which the system is regular (Glaser, 1955; Dušek, 1959; Dhuicq, 1961).

If the doublet is not antisymmetric, it is not possible to make it regular for a continuous range of the three free parameters (D, β_1^2 and β_2^2) since three conditions would now have to be satisfied ($f_x = f_y$, $z_{Fo}^{(x)} = z_{Fo}^{(y)}$, $z_{Fi}^{(x)} = z_{Fi}^{(y)}$). It is, on the other hand, relatively easy to make the doublet stigmatic but not orthomorphic for given separation and object distance; for references, see Hawkes (1966, 1970). Such an arrangement has been used by Crewe et al. (1967) to form a probe for a scanning microscope, though subsequently abandoned. Doublets have been employed to form line images in scanning and mirror instruments by Le Poole (1964), Bok et al. (1964) and Bok (1968).

39.4 Triplets

Triplets cannot of course be antisymmetric. The symmetric triplet has a considerable literature, mainly for use in particle accelerators, and has also been used to convert a virtual image into a real image with unit magnification. Foster (1968) considered employing a symmetric triplet in a lens spectrometer operating on the focal separation principle. Juma et al. (2007) have reconsidered the symmetric electrostatic triplet.

If all symmetry is abandoned, only one special case has been explored in detail, that in which the first two members of the triplet create a stigmatic image of a stigmatic object and the third member, a very strong quadrupole, converts this into a real image (Antony-Spies and Junior, 1967). Otherwise, the general case with numerous geometric and electrical degrees of freedom must be analysed. We have examined the conditions for regularity in some detail by setting two excitations (β_1 and β_2, say) and then calculating the third excitation and the two spacings for which the triplet is regular; the resulting curves (unpublished) varied so rapidly that any practical system of this kind would be acutely unstable and of negligible interest. In this context, see Ueda (1975), Ueda and Nagami (1975), Ueda et al. (1969, 1970, 1971, 1973) and Juma et al. (2007). The chromatic and aperture aberrations of stigmatic triplets have been studied by Baranova and Read (1998).

Crewe and Gorodezky (2006) noticed that a quadrupole triplet can be combined with a rotationally symmetric magnetic lens to create the flat ribbon-like beam that is required at the entrance to a high-energy synchrotron.

Finally, we note that a number of ion microanalysers used quadrupole triplets to form the probe; detailed accounts of the triplet systems employed at Harwell, Oxford, Bochum and Rossendorf are available (Cookson et al., 1972; Watt et al., 1981, 1982; Bischof et al., 1982; von Gersch et al., 1982) and are compared in Grime and Watt (1984) and Cookson (1979).

39.5 Quadruplets

Quadruplets have attracted much more attention than any other multiplet. The symmetric arrangement resembles a symmetric triplet in requiring only two independent excitations but has the central spacing as an additional degree of freedom. The antisymmetric arrangement has the attractive feature (common to all antisymmetric multiplets) that only one condition (typically $z_{Fo}^{(x)} = z_{Fo}^{(y)}$) need be satisfied for regularity. For a given geometry, therefore, the regularity condition will impose a functional relationship between the excitations β_1 and β_2. This function, $\beta_2 = f(\beta_1)$, is known as the *load characteristic* and as the geometry is altered, a family of such load characteristics will be generated. A number of possible quadruplet arrangements are illustrated in Fig. 39.1 and some load characteristics obtained using the rectangular model (Dymnikov et al., 1965a,b) and the bell-shaped model (Dymnikov et al., 1965c,d; Hawkes, 1970) are also reproduced there. The configuration of Fig. 39.1B, studied by Meads (see Hawkes, 1966), is automatically orthomorphic.

The fifth-order aberrations of three quadruplets have been studied by Baranova (2000): the basic antisymmetric quadruplet, with and without octopoles, and a 'mid-acceleration' quadruplet in which an acceleration potential is added to the central elements. The latter is advantageous at higher gradients where the fifth-order effects become appreciable.

At the time when replacement of the round objective or probe-forming lens in a microscope by a quadrupole multiplet corrected for spherical aberration seemed a real possibility, the antisymmetric quadruplet was the favourite candidate. The extensive literature is listed in Hawkes (1966, 1970) and Yavor (1968). The antisymmetric or Russian quadruplet has been employed in numerous ion microprobe devices (Grime and Watt, 1984).

39.6 Other Quadrupole Geometries

The quadrupoles discussed in the preceding sections were essentially 'pure' quadrupoles, possessing no round lens or octopole component. Other means of producing quadrupole fields in which the latter are accompanied by rotationally symmetric and octopole components have been examined, notably electrostatic designs with three, four or five electrodes in the form of arcs, crossed lenses, biplanar lenses, transaxial lenses and astigmatic tube lenses. Baranova and Read (1999) have made a thorough study of multiplets of electrostatic quadrupoles and octopoles consisting of two, three, four and five elements. An original feature is the inclusion of 'mid-acceleration', that is, addition of a (rotationally symmetric) accelerating potential to one or more of the inner electrodes. The aperture and chromatic aberration coefficients of the various configurations are critically compared.

39.6.1 Arc Lenses

Electrodes in the form of arcs, usually enclosed in a cylinder (Fig. 39.2) can be used to create combined round lens, quadrupole and octopole fields, and the choice of radius and arc-length governs the relative strengths of these. Their properties were analysed in some detail at one time (Szilágyi et al., 1968; Baranova et al., 1968, 1972; Koltay et al., 1972; Bosi, 1974; Ovsyannikova et al., 1972; Petrov et al., 1972, 1974; Petrov and Shpak, 1975) but interest in them has faded.

39.6.2 Crossed Lenses

Crossed lenses are sets of parallel plates, perpendicular to the optic axis, in which holes have been cut, as in some kinds of electrostatic round lens. Here, however, the holes are not

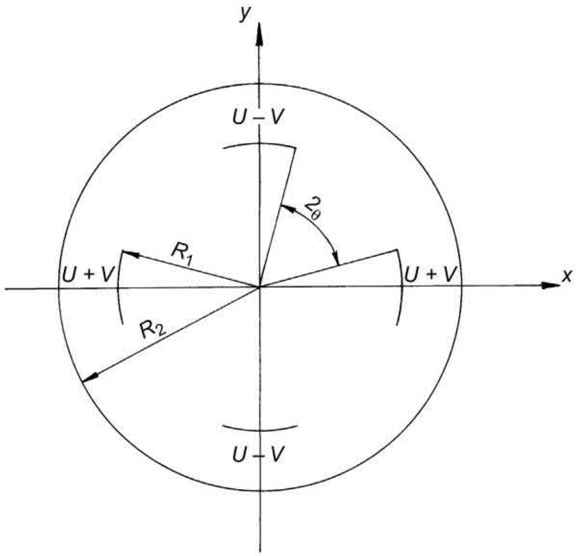

Figure 39.2
Arc lens, capable of generating round, quadrupole and octopole components.

circular but rectangular or more complicated in shape, always possessing planes of symmetry however. The sides of the rectangles (or the symmetry planes) in successive electrodes are parallel but there need in principle be no other restriction on the dimensions of the openings, though in practice some degree of symmetry is imposed on the electrode sequence (Fig. 39.3).

The first crossed lenses studied were symmetric three-electrode einzel lenses, in the sense that the outer electrodes were at the same potential as the final gun electrode and the central electrode at a different potential (Yavor, 1970; Petrov, 1976, 1977; Petrov and Yavor, 1975, 1976; Petrov et al., 1978; Baranova et al., 1978a,b, 1982). From the symmetry, it is clear that, except when the rectangles degenerate to squares, the triplet will act like a superposition of an electrostatic einzel lens, a symmetric quadrupole triplet and a symmetric octopole triplet. In view of the presence of all these fields, it is not surprising that combinations of rectangle dimensions and excitations can be found for which the aperture aberration coefficient in (angle)^3 in the converging plane vanishes (Petrov and Yavor, 1975, 1976). Subsequent work has been concerned with the aperture aberrations of doublets of such einzel lenses, consisting of five or six electrodes (in the former, the central electrode is common to both einzel lenses). For details we refer to Petrov (1977), Petrov et al. (1978), Baranova et al. (1978a,b, 1982, 1986, 1987b), Afanas'ev et al. (1979, 1980, 1981), Ovsyannikova and Shpak (1982) and the review article of Baranova and Yavor (1984a). An additional degree of complexity is introduced if the lens has an overall accelerating or decelerating effect, as discussed by Gritsyuk and Lachashvili (1979); another accelerating

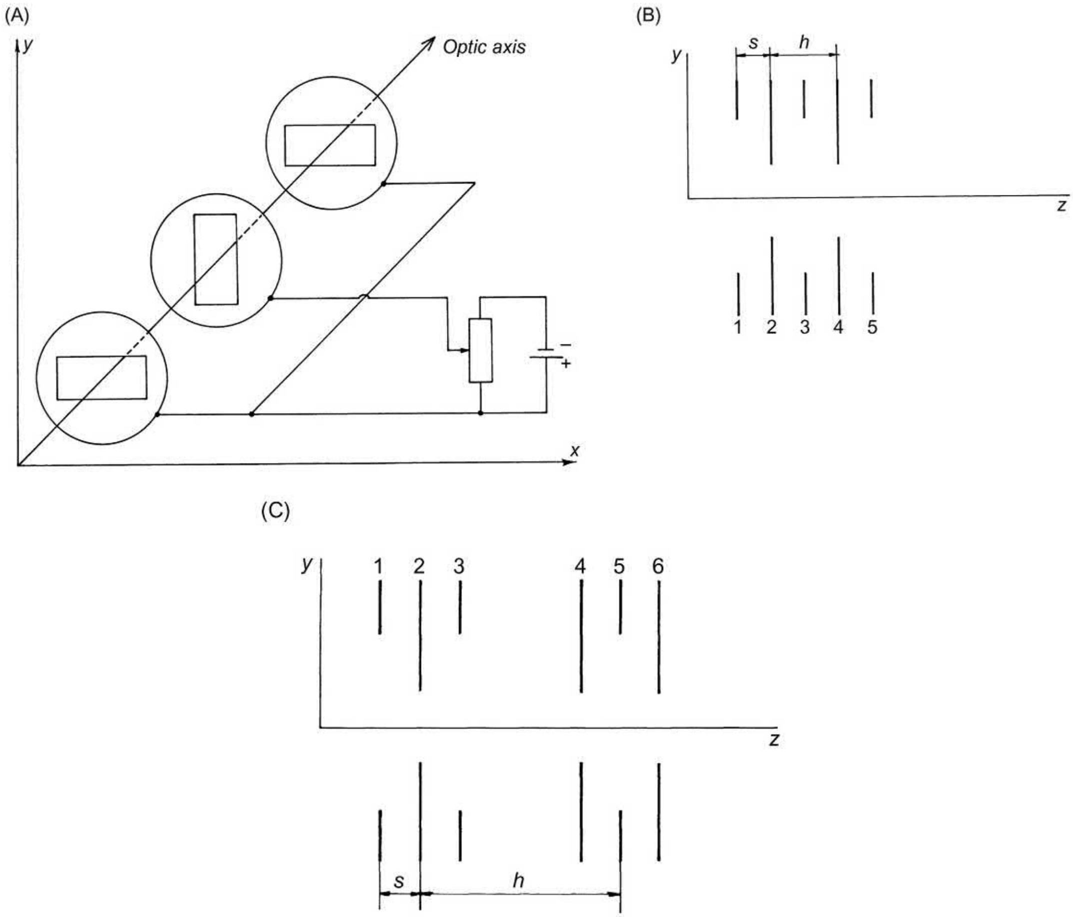

Figure 39.3
Crossed lenses. (A) A three-electrode crossed lens, excited like an einzel lens. (B) and (C) Crossed-lens doublets consisting of five or six electrodes.

quadrupole design is described by Fishkova et al. (1984). Baranova and Read (1994) study a four-electrode lens in which the apertures in the outer electrodes are square while those in the inner electrodes are rectangular. The chromatic and aperture aberrations are examined afresh by Baranova et al. (1993, 1996).

39.6.3 Biplanar Lenses

As their name suggests, these quadrupoles consist of a pair of parallel planes, each broken up into zones held at different potentials. A possible design is illustrated in Fig. 39.4. The field has been modelled by Afanas'ev (1982) and calculations of the focusing properties of such lenses and simple combinations of them are to be found in Afanas'ev and Sadykin

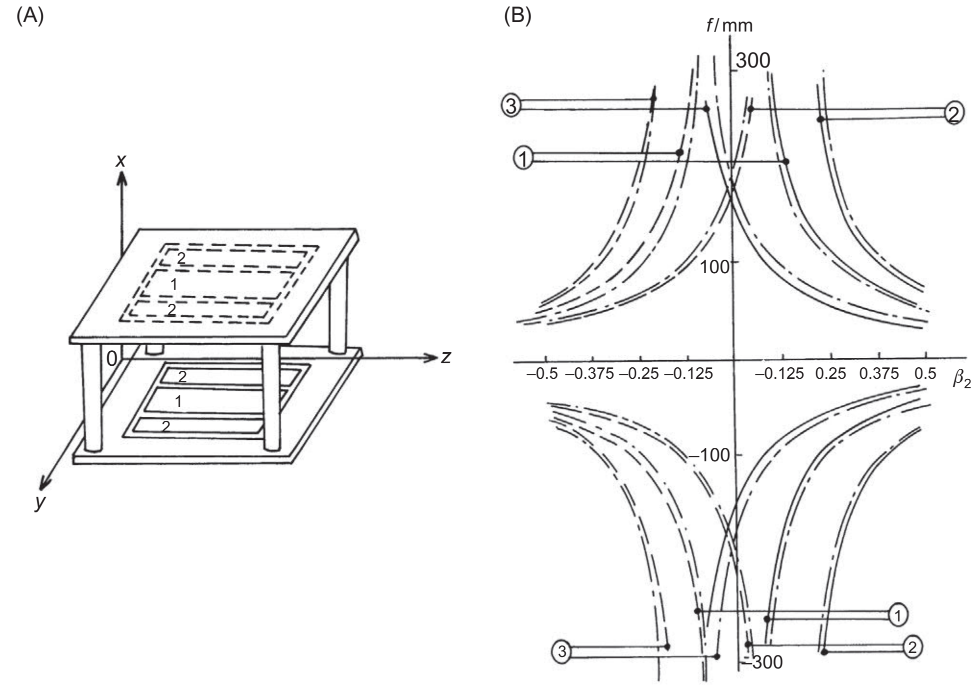

Figure 39.4

Biplanar lenses. (A) A single biplanar lens requiring two excitations, one applied to the pair of electrodes 1, the other to the four electrodes 2. (B) and (C) Variation of the focal lengths as a function of $\beta_2 = V_2/U$, where U is the accelerating voltage and $V_{1,2}$ are the potentials applied to electrodes 1, 2. Full curves correspond to focusing in the x–z plane, dashed curves, in the y–z plane. The various curves correspond to different values of $\beta_1 = V_1/U$. 1: $\beta_1 = 0$; 2: $\beta_1 = 1/16$; 3: $\beta_1 = -1/16$; 4: $\beta_1 = 1/8$; 5: $\beta_1 = -1/8$; 6: $\beta_1 = 1/4$; 7: $\beta_1 = -1/4$. (D) Variation of the focal lengths as a function of β_1 for $\beta_2 = 0$. (E) Variation of the principal spherical aberration coefficients with β_1 for fixed values of the focal length. Curves 1, 2, 3 correspond to focal lengths of 50, 100 and 125 mm in the y–z plane; curves 4, 5, 6 correspond to the same focal lengths in the x–z plane. (F) Variation of the focal lengths of a particular biplanar lens geometry, for which the quadrupole component of the lens action should be independent of V_2: $\pi b = 2x_0 \ln\{\coth(\pi a/4x_0)\}$ where $2x_0$ is the separation of the two planes, $2a$ is the width of the central electrode and $2b$ is the width of the lens. The focal length is plotted in the x–z plane (1–3) and in the y–z plane (4–6) for various fixed values of V_1 as a function of $\beta_2 = V_2/U$, where $V_{1,2}$ are again the potentials applied to electrodes 1, 2 and $U = 2.5$ kV is the accelerating voltage. 1: $V_1 = -585$ V; 2: $V_1 = -405$ V; 3: $V_1 = -295$ V; 4: $V_1 = 610$ V; 5: $V_1 = 410$ V; 6: $V_1 = 297$ V. (G) The principal spherical aberration coefficients in the x–z and y–z planes of the same lens (numbering as above).

(1982, 1983, 1984) and Afanas'ev et al. (1982). Among the various potential applications of such lenses mentioned by Afanas'ev (1982) are multichannel systems, since the lens can be extended periodically in the y-direction (Fig. 39.5) and could be made extremely small.

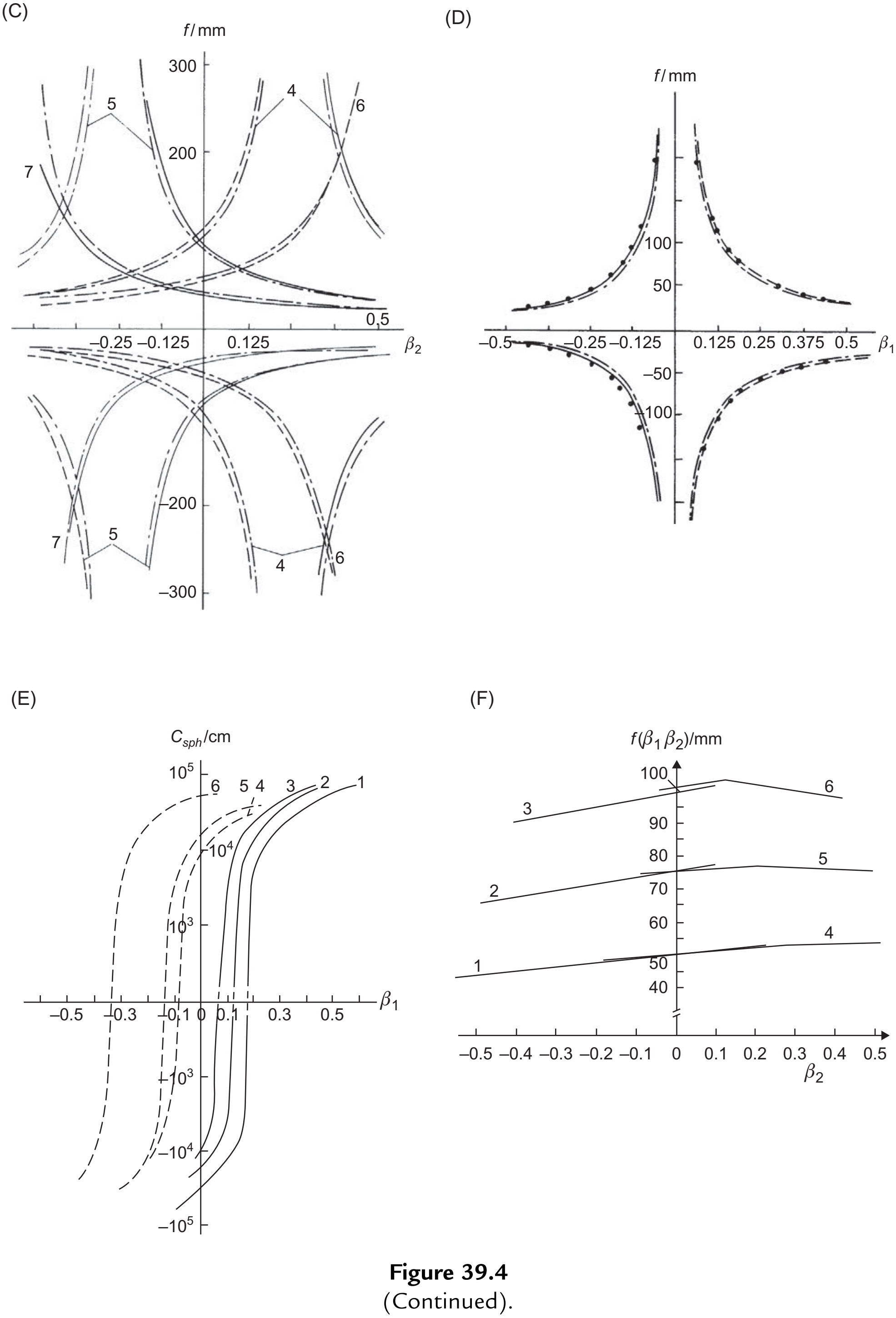

Figure 39.4
(Continued).

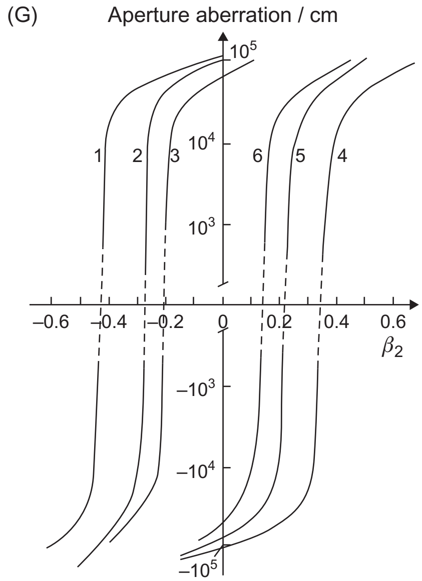

Figure 39.4
(Continued).

39.6.4 Astigmatic Tube Lenses

An old idea of Klemperer (1953, patented 1942–45) has been revived by Andreev, Glikman and Iskakova, who have explored the properties of two-tube astigmatic electrostatic lenses. These consist of two coaxial rotationally symmetric tubes, separated by a narrow gap that is not perpendicular to the common axis of the tubes but nevertheless leaves the system with quadrupole symmetry. In the case studied by Andreev et al. (1975a, b), the line of separation is defined by a third cylinder, or rather cylindrical arc, the axis of which is perpendicular to the lens axis (Fig. 39.6). The curve of intersection of this cylinder and a cylinder centred on the optic axis defines the gap. The paraxial properties and aberrations for various values of the voltage ratio and of the ratio of the radii of the cylinders are studied in the papers of Andreev et al. (1975a,b). In two later papers, Glikman and Iskakova (1976) tabulate object-independent parameters characterizing the aperture aberration coefficients for various geometries and excitations. For further studies, see Iskakova (1978) and Glikman and Iskakova (1982).

The analogous design in which the electrodes are not cylinders but square tubes is considered by Glikman and Sekunova (1981).

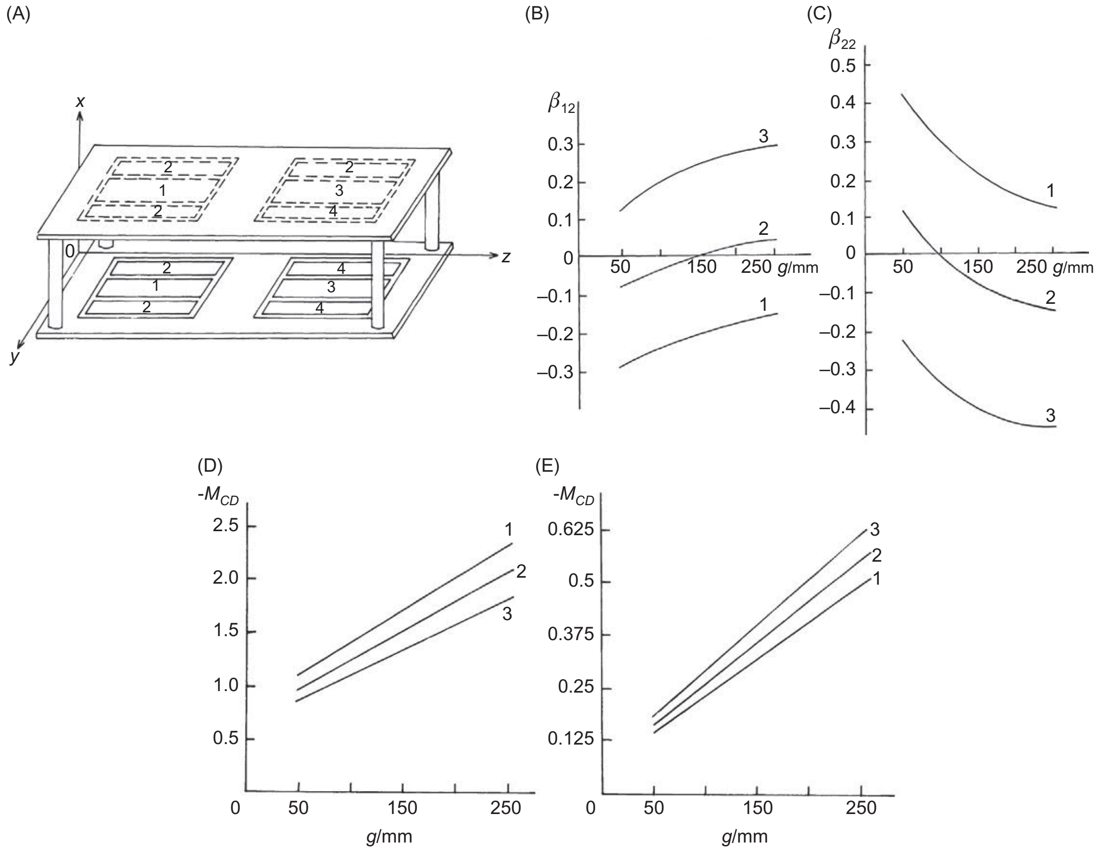

Figure 39.5

(A) A biplanar doublet. Electrodes with the same number have the same excitation. (B)–(C) Stigmatic focusing conditions. Electrodes 1 and 3 have equal and opposite excitations, the values of which are $\pm 0.1U$ (Curves 1), $\pm 0.2U$ (2) and $\pm 0.3U$ (3), where U denotes the accelerating voltage. For a fixed object distance (22 cm), the curves show the excitations (β_{12}) to be applied to electrodes 2 and those (β_{22}) to be applied to electrodes 4 to achieve stigmatic imaging at a distance g; β represents (applied voltage)/U. (D)–(E) show the corresponding magnifications.

39.6.5 Transaxial Lenses

These lenses, first explored many years ago by Strashkevich (1962), are so named because a rotationally symmetric field is present but the optic axis is no longer the symmetry axis. Instead, the particles travel approximately normal to the latter, as explained in Chapter 19, with the result that the system symmetry is lower: there are planes of symmetry but no longer an axis of symmetry, so that the optical properties are those of a quadrupole with round lens and octopole effects superimposed (Fig. 39.7). The optics of a number of configurations have been established; see Brodskii and Yavor

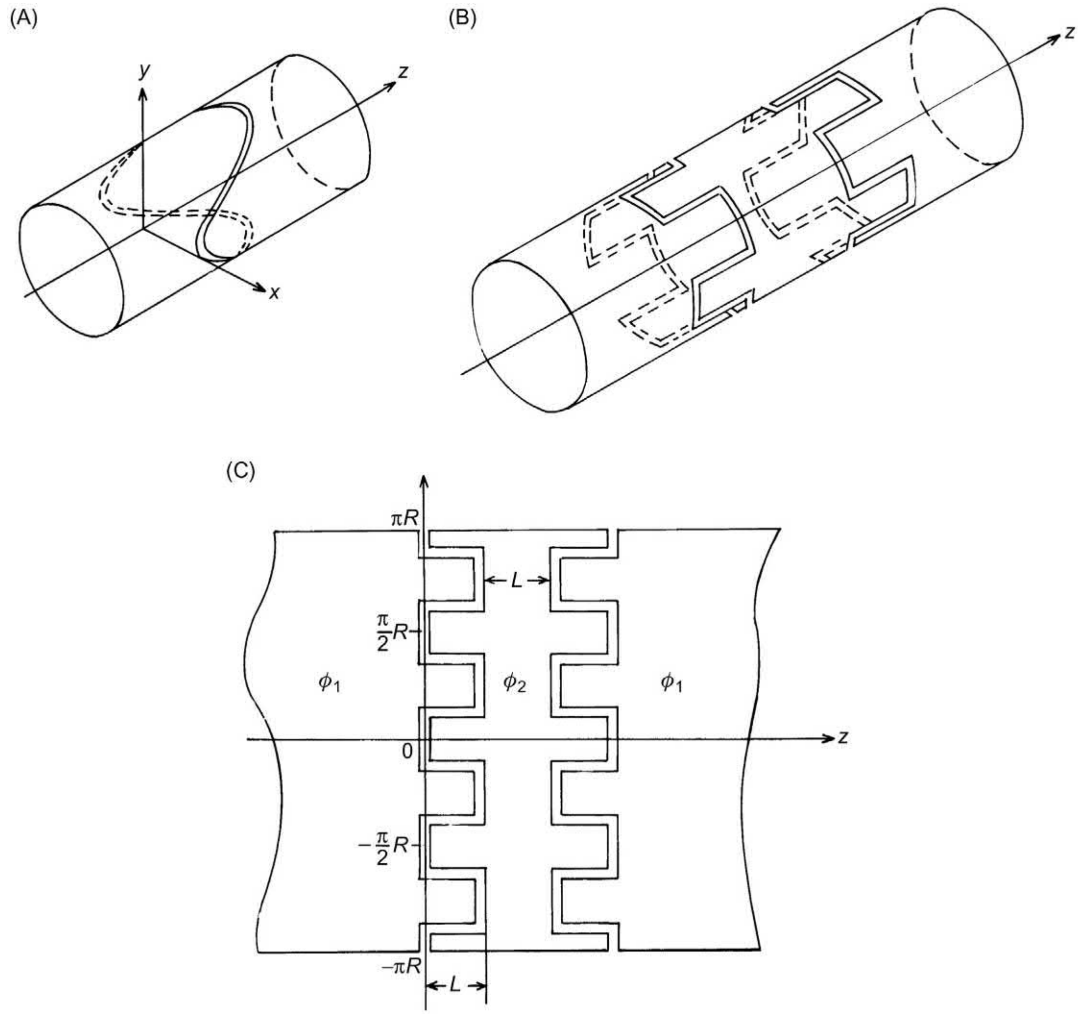

Figure 39.6
Astigmatic tube lenses. (A) A two-electrode structure. (B and C) A three-electrode structure excited like an einzel lens.

(1970, 1971), Karetskaya et al. (1970, 1971), Glikman et al. (1971) and the review by Baranova and Yavor (1984). A transaxial cathode lens is analysed by Ibraev and Sapargaliev (1981).

39.6.6 Radial Lenses

Two types of 'radial lenses' have been studied, one having a conical appearance, the other being more sphenoidal (Fig. 39.8A and B). Such devices were first considered as prisms

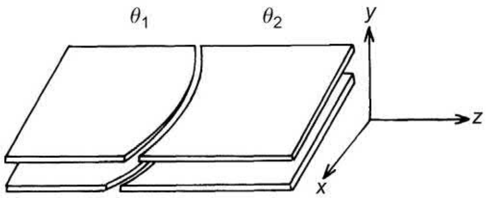

Figure 39.7
A transaxial lens.

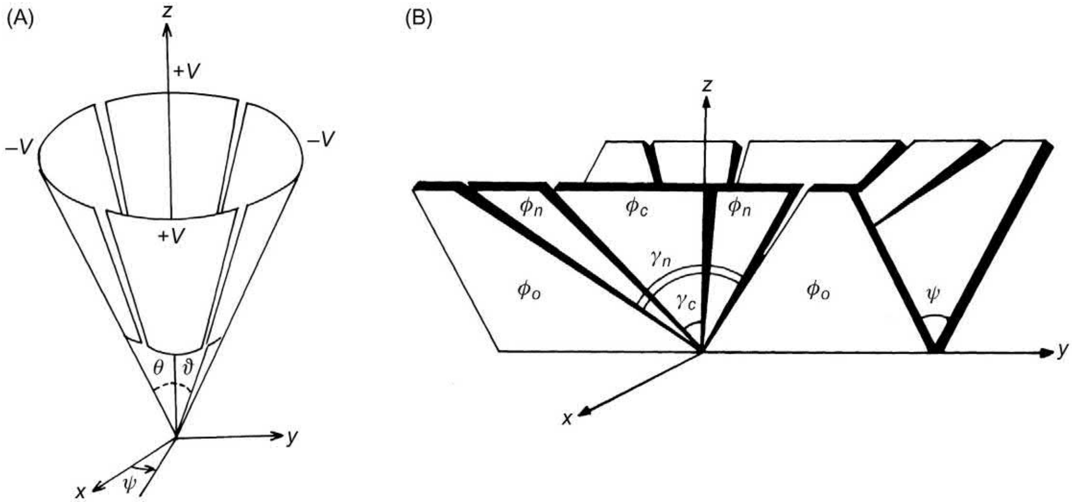

Figure 39.8
Radial lenses. (A) Conical design. (B) Sphenoidal design.

(Glikman et al., 1973a,b, 1976a,b, 1977a,b); their lens action was subsequently analysed by Yavor (1984), Baranova and Yavor (1984b) and Baranova et al. (1984, 1985a,b, 1986a−d, 1987a−c), who also considered using the radial design as a combined lens and deflector. The common feature of the potentials of such lenses, which may be electrostatic or magnetic, is that they are independent of the radial coordinate, measured from the apex of the cone or the edge of the wedge.

Deflection Systems

40.1 Introduction

In Chapters 32 and 33, Paraxial Properties of Deflection Systems and The Aberrations of Deflection Systems, we have already given some general information, which will not be repeated here. Hitherto, we have treated the different types of deflection units separately, but this is by no means always adequate since the design problems of individual elements can often be solved only in the context of the whole device in question and the design will depend strongly on the particular purposes of this and on the requirements imposed by the intended applications. A vast amount of technical knowledge has been accumulated into which we cannot go in much detail.

The traditional applications of electric deflectors consisting of pairs of condenser plates (Figs 32.1 and 32.5) are *cathode-ray tubes* (CRT), while magnetic hybrid deflectors (Fig. 32.4) are employed in the older types of *television tubes*. Magnetic double deflection systems (Fig. 40.1) are common in scanning electron microscopes (SEM) and scanning transmission electron microscopes (STEM). A common feature of all these devices is that the deflection units are clearly separated from the lens system. This is a major simplification as we can apply the analysis of Chapter 32, which refers to pure deflection systems. We shall therefore discuss these devices only very briefly.

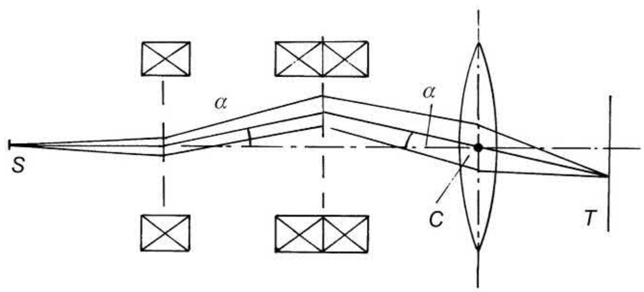

Figure 40.1
Schematic view of a prelens double deflection system in which a crossover. S is focused onto a target plane T. The deflection centre C remains fixed. The deflection angle α is exaggerated here.

Principles of Electron Optics: Applied Geometrical Optics.
DOI: http://dx.doi.org/10.1016/B978-0-12-813369-9.00040-3

In CRTs and old television tubes, the deflectors are located downstream from a weak electrostatic lens system, the purpose of which is to focus the beam to a small spot on the viewing screen. The most important aberrations are deflection distortions, which can be kept small by appropriate shaping of the condenser plates or the coils and the ferrite former (see Figs 32.1 and 32.2). In a CRT, additional post-acceleration is necessary in order to increase the sensitivities of the deflectors. This means that while passing through the latter, the beam velocity corresponds to a comparatively low acceleration voltage of a few kilovolts. This is then increased to about 25 kV immediately in front of the screen. The post-acceleration field is clearly separated from the deflecting fields, sometimes by a fine grid. The aberrations caused by the post-acceleration have been studied in great detail; we shall not repeat this here and refer to the corresponding publications (Lenz, 1979; Franzen, 1984).

In the SEM and STEM, a very small electron probe is formed by successive demagnifications of the crossover produced by an electron gun. In the SEM, the diameter of the final probe is rarely smaller than about 0.5 nm and essentially determines the resolution limit of the instrument. This small probe is now scanned in a raster pattern over the area of the specimen to be examined. The secondary and backscattered electrons are then collected by a suitable arrangement of detectors and converted into voltage signals, which are fed to a monitor. This technique, though very important, does not affect the design of the deflectors and will hence not be discussed here. The deflectors have to be designed in such a way that the aberrations caused by them do not degrade the probe diameter significantly. This is achieved in the arrangement shown in Fig. 40.1. The beam passes paraxially through the first deflector, which thus produces very little aberration. The second deflector is operated with the same excitation current but reversed in sign and with double the number of turns, so that the principal ray always intersects the optic axis at a fixed point C, the deflection centre. In the second deflector the off-axis distances become larger; they remain, however, so small that they are not critical. The deflection centre C is adjusted to coincide with the entrance nodal point of the lens; the direction of the principal ray hence remains unaltered by the lens and the beam stays close to the axis in the domain of strong lens field. The probe diameter is thus essentially determined by the spherical aberration and the axial chromatic aberration of the lens and by diffraction at the aperture. Moreover, some deflection aberrations can be corrected dynamically, as will be explained in connection with more sophisticated designs. Since the really severe design problems in the SEM and the STEM concern the electron gun and the lenses, but not the deflectors, the foregoing explanations should suffice.

A technology of great importance is *electron-beam lithography* (EBL), which has a long pre-history (e.g., Möllenstedt and Speidel, 1960). Here, the electron beam is used to write patterns on a silicon wafer. This causes chemical reactions on those parts of the wafer exposed to the beam, after which, by suitable processing not discussed here, materials are deposited in the exposed areas. The final result is the desired structure, typically a microcircuit for electronics. In order to compete with and surpass light optical lithography, the requirements for electron-beam lithography are extremely demanding, with the result that the devices that have been developed are highly sophisticated. Typical requirements are a stable resolution of 10 nm or better over an area of 1 mm × 1 mm and a reliable and high throughput of at least 20 wafers per hour and preferably many more.

Owing to the great technological importance of electron-beam lithography, there is an intense ever-growing activity in this field; we confine our attention to a few contributions. Good background reviews of the early years of the subject are given by Munro (1980b) and Koops (1980), who deal with the various technological problems in electron-beam lithography that must be solved simultaneously under the conditions of industrial production; Chapter 2 of the SPIE *Handbook of Microlithography*, *Micromaching and Microfabrication* (McCord and Rooks, 1997) gives clear accounts of many aspects of the subject as does the chapter by Lucas et al. in Greer et al. (2003). A long chapter is devoted to lithography using electrons in the book by Cui (2017). Among the more recent work we shall concentrate extensively on the achievements of the IBM laboratories in the USA, since these were very impressive; we shall also deal with the publications of Munro and Chu (Munro and Chu, 1982a,b; Chu and Munro, 1982a,b). We shall not consider mere projection systems without deflection, since such devices are not likely to prove to be important.

The ever more exacting demands on accuracy impose strong constraints on the design of every component of an electron-beam lithography machine. Here we are only concerned with the integrated system of lenses, deflectors and correctors. Fig. 40.2 shows schematically various arrangements, among which those with in-lens deflection produce least aberration. None of these simple arrangements is satisfactory, however, since the deflected principal ray does not land orthogonally on the target. In the case of a warped wafer this causes unacceptably large aberrations as is shown in an example given by Munro (see Fig. 40.3). The tolerance limit for the landing angle is about 5 mrad. An arrangement satisfying this additional constraint is the ‘variable-axis lens’ concept, proposed by Ohiwa et al. (1971), investigated theoretically by Goto and Soma (1977) and successfully developed and built by Pfeiffer and his coworkers at IBM. This concept is represented schematically in Fig. 40.4. The theoretical background of this scheme is so sophisticated that it is presented in a separate section (Section 40.3). Here our intention is only to point out the necessity for such complicated arrangements.

The subsequent presentation is ordered in the following way. In Section 40.2, we shall deal with some models for the numerical calculation of magnetic deflection fields. These models are quite useful, significantly reducing the amount of computation necessary, and with respect to the driving field they are indispensable. In Section 40.3 the theoretical background and the practical realization of the variable-axis lens concept are presented. In Section 40.4 we discuss some other advantageous configurations, essentially the

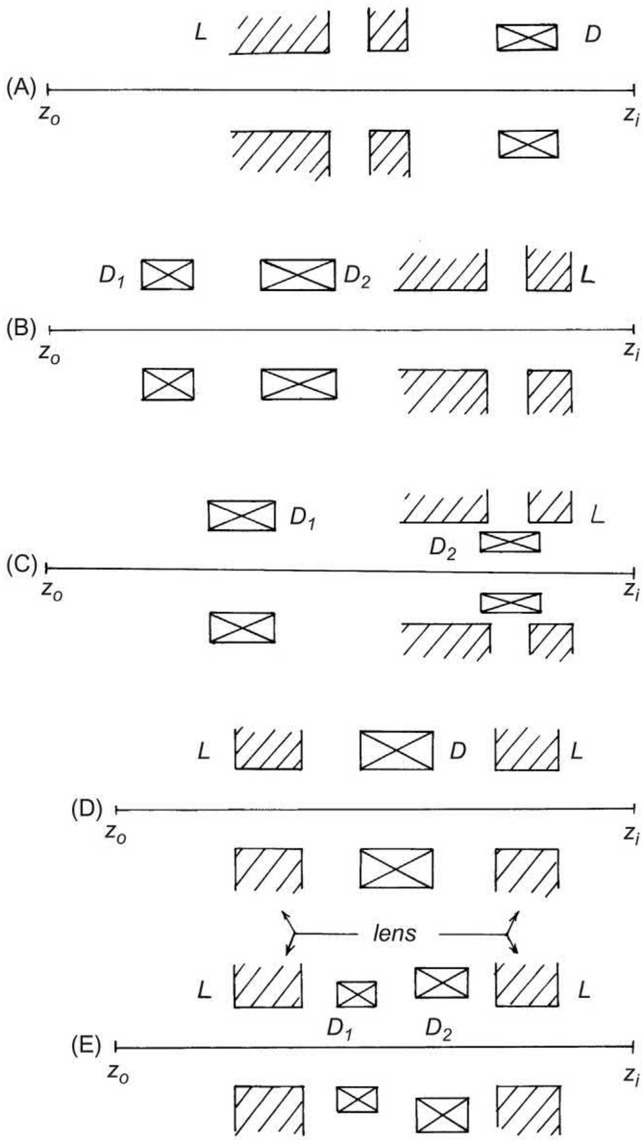

Figure 40.2
Various ways of combining a magnetic lens (L) and deflectors (D, D_1, D_2). Planes through $z = z_o$ and $z = z_i$ are conjugate. (A) Conventional postlens deflection; (B) prelens double deflection, with the yoke D_2 rotated if necessary; (C) double deflection with the yoke D_2 inside the lens; (D) in-lens single deflection; (E) in-lens double deflection. According to Munro (1980), configuration (C) gives the smallest aberrations, while (E) is the second best.

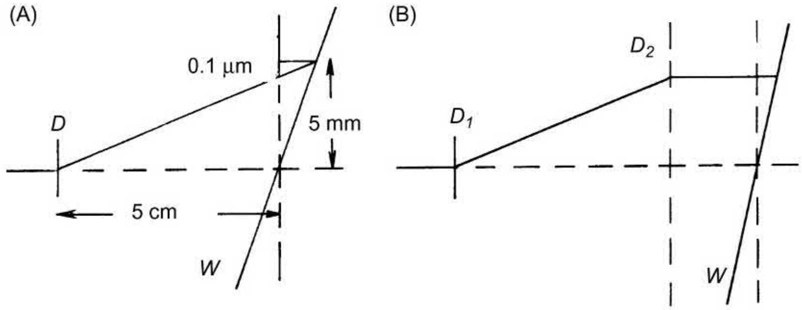

Figure 40.3
Error associated with warping of the wafer (W). (A) Arrangement in which the beam deflected at D is incident obliquely on W. There is a significant landing error. (B) The use of two deflectors at D_1 and D_2 renders the incident beam normal to the ideal wafer surface. The landing error is greatly reduced.

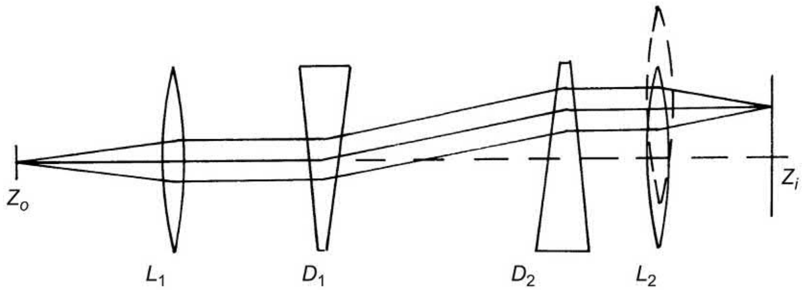

Figure 40.4
Optical analogue of the concept of a moving objective lens (L_2). When the deflectors D_1 and D_2 are suppressed, the beam is telescopic. When the deflectors are active, as shown here, the beam remains telescopic if the second lens is shifted laterally: the new position is indicated by the broken lens contour. In electron optics this shift is performed magnetically.

dual-channel systems investigated by Munro and Chu. A new aspect here is the consideration of impedance effects, which exclude magnetic deflectors at high scanning frequencies. Section 40.5 deals with different methods of enhancing the speed of exposure in electron-beam lithography machines. This is an essential aspect of the problem for the industrial application of this technique. It will be shown how the throughput of such machines can be made very high.

40.2 Field Models for Magnetic Deflection Systems

Although the electric or magnetic deflection fields in many practical devices have such a complicated structure that the field calculation obliges us to use the sophisticated numerical

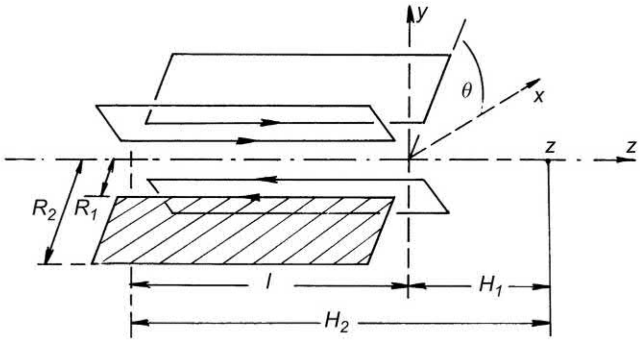

Figure 40.5
Perspective view of a toroidal coil system with four rectangular conducting loops showing the notation adopted. The hatched area indicates one of the four domains of integration considered in Section 40.2.3.

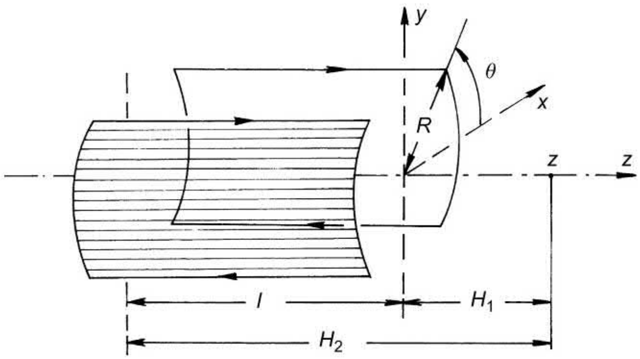

Figure 40.6
Perspective view of a pair of saddle coils, showing the notation used.

techniques outlined in Part II, there are some simple cases in which an analytic field model can be quite useful: for instance, the field calculations for toroidal and saddle coil systems having the simple geometric structures shown in Figs 40.5 and 40.6, respectively. These have been investigated in detail by Munro and Chu (1982a). The results of these calculations will be presented briefly later. A very full analysis has also been made by Hanssum (1984, 1985, 1986).

Moreover, the field $\boldsymbol{H}_0(\boldsymbol{r})$ of the coil system in the absence of any magnetic materials is important, being the driving field needed when the boundary-element method (BEM) is employed to compute the total field $\boldsymbol{H}(\boldsymbol{r})$. We shall therefore discuss here the determination of $\boldsymbol{H}_0(\boldsymbol{r})$ in a more general context, after which we shall outline some simple field models.

40.2.1 Field of a Closed Loop in Free Space

For reasons of simplicity we first consider a closed loop L which consists of N neighbouring thin wires, each conducting the electric current I, so that $J := NI$ is the number of ampère-turns. Though in some contexts the finite cross-section of the current distribution is of importance, we replace the latter by an infinitely thin wire, a line conductor. This simplification is justified if the distance of the reference point $\boldsymbol{r}$ from the line conductor is much larger than the diameter of the cross-section. The integral form of Biot–Savart's law now becomes

$$\boldsymbol{H}_0(\boldsymbol{r}) = J \int_L \frac{(\boldsymbol{r}' - \boldsymbol{r}) \times d\boldsymbol{r}'}{4\pi|\boldsymbol{r}' - \boldsymbol{r}|^3} \tag{40.1}$$

Apart from a very few special cases, this integration can be carried out only numerically. One such exceptional case is a straight wire of finite length (Fig. 40.7). Let $\boldsymbol{r}' = \boldsymbol{r}_j$ $(j = 1, 2)$ denote the two endpoints of the wire and $\boldsymbol{d}_j = \boldsymbol{r}_j - \boldsymbol{r}$ the vectors directed from the reference point $\boldsymbol{r}$ to these endpoints. The result of the elementary integration can then be brought into the following convenient form:

$$\boldsymbol{H}_{1,2}(\boldsymbol{r}) = \frac{J}{4\pi}\left(\frac{1}{d_1} + \frac{1}{d_2}\right)(\boldsymbol{d}_1 \times \boldsymbol{d}_2)F \tag{40.2a}$$

with $d_1 = |\boldsymbol{d}_1|$, $d_2 = |\boldsymbol{d}_2|$ and:

$$F = (d_1 d_2 + \boldsymbol{d}_1 \cdot \boldsymbol{d}_2)^{-1} \quad \text{for} \quad \boldsymbol{d}_1 \cdot \boldsymbol{d}_2 \geq 0, \tag{40.2b}$$

$$F = (d_1 d_2 - \boldsymbol{d}_1 \cdot \boldsymbol{d}_2)/(\boldsymbol{d}_1 \times \boldsymbol{d}_2)^2 \quad \text{for} \quad \boldsymbol{d}_1 \cdot \boldsymbol{d}_2 \leq 0 \tag{40.2c}$$

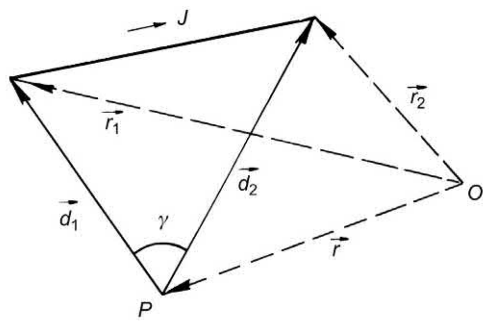

Figure 40.7
Notation used to discuss the magnetic field at an arbitrary reference point P. The straight conductor is shown as a thick line.

After some elementary trigonometric manipulations it is found that

$$\left|\boldsymbol{H}_{1,2}(\boldsymbol{r})\right| = \frac{J}{4\pi}\left(\frac{1}{d_1} + \frac{1}{d_2}\right)\tan\frac{\gamma}{2} \tag{40.3}$$

γ being the angle subtended at $\boldsymbol{r}$, as shown in Fig. 40.7. This makes Eq. (40.2) easier to interpret.

The magnetic field due to any closed polygonal loop with corners $\boldsymbol{r}_1, \boldsymbol{r}_2, \ldots \boldsymbol{r}_N$ and $\boldsymbol{r}_{N+1} = \boldsymbol{r}_1$ is now given by

$$\boldsymbol{H}_0(\boldsymbol{r}) = \sum_{j=1}^{N} \boldsymbol{H}_{j,j+1}(\boldsymbol{r}) \tag{40.4}$$

This procedure is very economic since, for each corner $\boldsymbol{r}_j$, the most time-consuming part of the calculation, the determination of the distance $d_j = |\boldsymbol{d}_j|$, has to be carried out only once. Hence for toroidal coil systems, built up entirely from polygonal loops (Fig. 40.5), this procedure is most favourable.

For curved parts of the loop the integration (40.1) is by no means elementary. Special formulae can be derived for circular arcs; the resulting expressions contain incomplete elliptic integrals of the first and second kinds. Since such expressions are rather inconvenient and since the integration loop may deviate from a circular arc, it can be favourable to approximate the true loop by a suitable polygon, so that (40.4) can still be used. For three points on a circular arc this approximation is shown in Fig. 40.8.

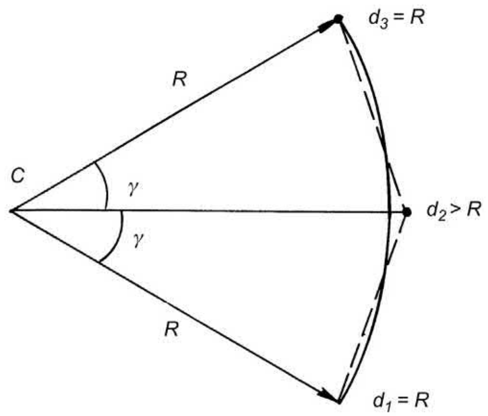

Figure 40.8
Replacement of a circular arc by a suitable polygon that produces the same magnetic field at the centre of curvature C. The semiangle γ is exaggerated for clarity.

It is convenient to assume constant azimuthal differences $\varphi_3 - \varphi_2 = \varphi_2 - \varphi_1 = \gamma$ relative to the centre of curvature C. Furthermore, it is advantageous to keep the endpoints $\boldsymbol{r}_1$ and $\boldsymbol{r}_3$ fixed, so that the polygon joins continuously to any straight or curved neighbouring line element. The point $\boldsymbol{r}_2$, however, need not necessarily be located on the circular arc; by a suitably chosen displacement, a part of the discretization error can be compensated. If we allow a radial shift of the point $\boldsymbol{r}_2$, the application of (40.3) to the field at the centre of curvature C of the arc results in

$$\left|\boldsymbol{H}_{1,3}\right| = \frac{J}{4\pi}\left(\frac{1}{d_1} + \frac{2}{d_2} + \frac{1}{d_3}\right)\tan\frac{\gamma}{2}$$

with $d_1 = d_3 = R$ (radius of curvature) and $d_2 > R$. On the other hand the exact value of the field strength is given by

$$\left|\boldsymbol{H}_{1,3}\right| = J\gamma/2\pi R$$

The two expressions for $|\boldsymbol{H}_{1,3}|$ are equal if

$$\frac{\gamma}{R} = \left(\frac{1}{R} + \frac{1}{d_2}\right)\tan\frac{\gamma}{2}$$

We hence obtain the condition

$$d_2 = R\frac{\tan\gamma/2}{\gamma - \tan\gamma/2} = R\left\{1 + \gamma^2/6 + O\left(\gamma^4\right)\right\} \tag{40.5}$$

Since the centre of curvature is usually located in the vicinity of the optic axis and since the paraxial field is the most important, this choice of the polygon is well suited to the requirements of electron optical design problems. Moreover, this approximation gives good results as long as the distance between the point ($\boldsymbol{r}$) of reference and the arc element is large compared with the lateral shift between arc and corresponding polygon.

40.2.2 Approximate Treatment of Ferrite Shields

We now consider a current-conducting loop in the vicinity of a ferrite yoke. For reasons of simplicity we start with a straight conducting wire parallel to the axis of a cylindrical tube; the cross-section through this configuration is shown in Fig. 40.9. We provisionally assume that the length in the axial direction is infinite so that the field is independent of the axial coordinate z. Though the permeability μ of the tube material is often very high, it is necessary to assume a *finite* value from the outset in order to avoid confusion.

The field calculation problem, specified in this way, can be solved by the familiar inversion method. This means that a second wire, the 'image conductor', is introduced which describes phenomenologically the influence of the shielding tube on the vacuum field.

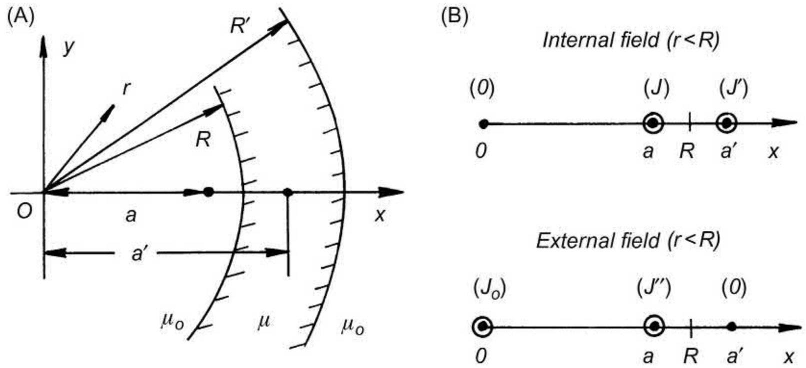

Figure 40.9
(A) Cross-section through part of a shielding tube and the notation employed. (B) Locations and strengths of the model currents needed for simulation of the magnetic fields; the symbols in parentheses represent the strengths of the currents flowing in the z-direction.

The off-axis distance of this second wire must be $a' = R^2/a$ (see Fig. 40.9). With an image current J' the vacuum field is then given by

$$\begin{aligned} H_x^V &= -Jy/D - J'y/D' \\ H_y^V &= J(x-a)/D + J'(x-a')/D' \end{aligned} \tag{40.6a}$$

with the denominators

$$D = 2\pi\{(x-a)^2 + y^2\}, \qquad D' = 2\pi\left\{(x-a')^2 + y^2\right\} \tag{40.6b}$$

The field in the tube wall is built up from that of two wires, one again chosen at the true singularity ($x = a,\ y = 0$), the other at the cylinder axis; this field is hence given by

$$\begin{aligned} H_x^M &= -J''y/D - J_0 y/D_0 \\ H_y^M &= J''(x-a)/D + J_0 x/D_0 \end{aligned} \tag{40.7a}$$

with

$$D_0 = 2\pi\left(x^2 + y^2\right) \tag{40.7b}$$

and J'' is the corresponding image current (see Fig. 40.9, lower part). In order to formulate and satisfy the boundary conditions at the inner tube surface, it is convenient to introduce polar coordinates and components:

$$\begin{aligned} x &= r\cos\varphi, \quad y = r\sin\varphi \\ H_r &= H_x\cos\varphi + H_y\sin\varphi \\ H_\varphi &= -H_x\sin\varphi + H_y\cos\varphi \end{aligned}$$

For $r = R$ we then find the special relations:

$$
\begin{aligned}
D &= 2\pi\left(R^2 - 2Ra\cos\varphi + a^2\right), \quad D' = DR^2/a^2 \\
D_0 &= 2\pi R^2 = DR\left(R + \frac{a^2}{R} - 2a\cos\varphi\right)^{-1} \\
H_\varphi^V &= D^{-1}\left\{J(R - a\cos\varphi) + J'\left(\frac{a^2}{R} - a\cos\varphi\right)\right\} \\
H_\varphi^M &= D^{-1}\left\{J''(R - a\cos\varphi)/D + J_0\left(R + \frac{a^2}{R} - 2a\cos\varphi\right)\right\} \\
H_r^V &= -D^{-1}(J + J')a\sin\varphi \\
H_r^M &= -D^{-1}J''a\sin\varphi
\end{aligned}
$$

The interface conditions

$$
H_\varphi^V = H_\varphi^M, \quad \mu_0 H_r^V = \mu H_r^M
$$

now lead to the linear relations

$$
\begin{gathered}
J + J'\frac{a^2}{R^2} = J'' + J_0\left(1 + \frac{a^2}{R^2}\right) \\
J + J' = J'' + 2J_0, \quad \mu_0(J + J') = \mu J''
\end{gathered}
$$

with the solution

$$
J' = J_0 = J\frac{\mu - \mu_0}{\mu + \mu_0}, \quad J'' = \frac{2\mu_0 J}{\mu + \mu_0} \tag{40.8}
$$

which turns out to be independent of R and a. It is easy to verify that Ampère's law is satisfied:

$$
J_0 + J'' = J = \int_0^{2\pi} RH_\varphi d\varphi
$$

So far we have tacitly assumed that the outer tube radius is infinite. Under certain realistic conditions, it is possible to give an approximate treatment of the case in which the outer radius R' is finite. These conditions are: (i) The wall thickness must be so large that $a' < (R + R')/2$ and that $R' - a$ is not much smaller than R'. (ii) The tube permeability must be very high: $\mu \gg \mu_0$.

Inspection of (40.8) shows that now $J' = J_0 = J$, $|J''| \ll |J|$. We can hence neglect the terms in J'' in (40.7a) and inside the tube wall we obtain the circular field of a current J flowing along the cylinder axis. For this field, having only an azimuthal component $H_\varphi = J/2\pi R'$, the continuity condition is automatically satisfied at the outer boundary. This implies that the finite outer radius R' has practically no influence on the field on the inner vacuum side.

In a similar way, the case of a wire outside a shielding tube can be treated. We shall not do this here, since this case is of little interest as we are mainly interested in the field in the vicinity of the optic axis ($r = 0$). We merely state briefly some results. In the outer vacuum domain, the field is strongly perturbed by the ferromagnetic cylinder; when the wall is thick, this field is essentially a superposition of the fields due to the wire itself, the 'image wire' conducting the same current J and an axial wire conducting the current $-J$. In the ferromagnetic tube the field is highly concentrated on the side that is closest to the wire, while in the inner vacuum part of the tube the field is strongly shielded. This shielding effect is well known and often exploited in practice.

We now apply these considerations to systems of saddle-coils and toroidal coils. On the inner vacuum side of the shielding tube, the total field is easily obtained. For each *inner* wire the corresponding 'mirror wire' of the inversion theorem is to be introduced and must conduct the same current J, while outer wires are to be omitted owing to the shielding effect. The required magnetic field is then simply the vacuum field of this configuration and can be calculated by the method of the previous section.

On the *outer* vacuum side of the yoke the outer conductors are likewise complemented by their mirror-lines and a common axial wire. The latter conducts the total oriented current of the coil system, which vanishes owing to the construction of the device. For the same reason the net contribution of all the inner parts of the windings vanishes, though the field of each inner wire is unscreened, if considered separately.

This approximation is sketched in Fig. 40.10. It is valid in domains far distant from the front planes of the yoke, but runs into difficulties in the vicinity of the latter, since there a clear separation between 'inner' and 'outer' vacuum side is impossible. Fortunately this problem is not too serious in electron optical applications. Here we are mainly interested in the paraxial field domain, where the 'inner' solution is to be employed, even in the fringe field zone. In the vicinity of the optic axis, the field contributions of the circular hoops of saddle coil systems are weak. We shall therefore introduce little error if we subject the hoops to the inversion procedure, that is, introduce 'image hoops' obtained by reflection at the front planes, which again gives closed loops; for toroidal coils a similar procedure cannot be justified. If the windings in saddle coils run very close to the ferrite surface, we can make the extreme simplification of shifting the model wires to the surface itself and doubling their currents.

The dependence of the shielding effect on the permeability has been investigated by Scherle (1983), who performed a rigorous field calculation by means of the boundary-element method, outlined in Part II. Fig. 40.11 shows the result for the axial deflection field strength in a saddle-coil system and Fig. 40.12 the corresponding results for a toroidal system with

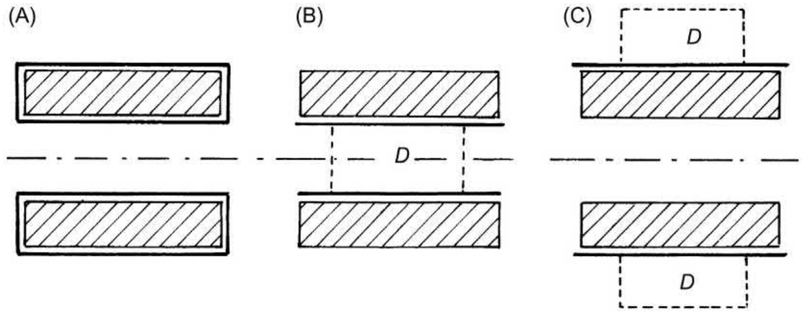

Figure 40.10
Schematic presentation of the domains D of application of the field model. (A) Complete real configuration of toroidal windings; (B) internal domain D and internal windings; (C) external domain D and external windings.

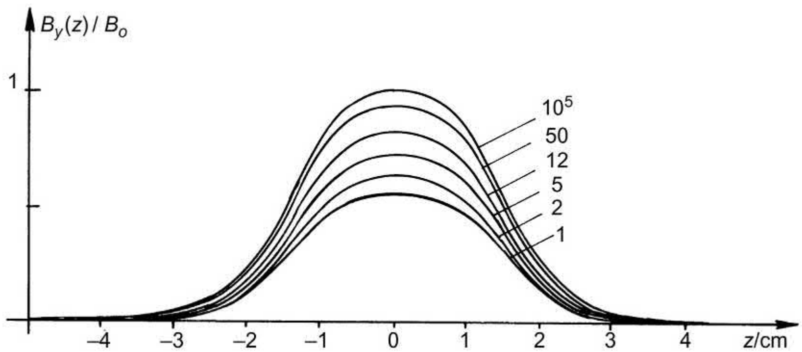

Figure 40.11
Normalized axial deflection field strength in a system of saddle coils for values of μ, the relative permeability of the shield material, ranging from 1 to 10^5.

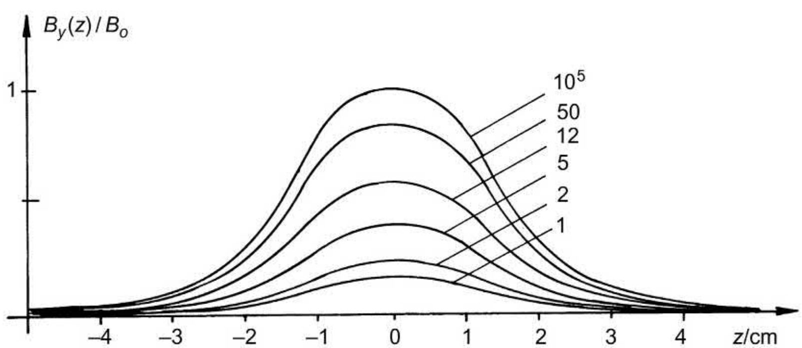

Figure 40.12
Normalized axial deflection field strength in a system of toroidal coils for the same range of values of μ as in Fig. 40.11. The enhancement of B_y with increasing μ is more pronounced than for saddle coils.

the same yoke geometry. The field strength in a saddle-coil system is almost doubled (error 10%) by an increase of the relative permeability from one to infinity. In toroidal systems the increase of the axial field strength as $\mu \to \infty$ is much stronger. This effect is due to the shielding of the outer parts of the windings.

40.2.3 The Axial Harmonics

In electron optical calculations, a power series expansion of the magnetic field in the form of (7.46–7.48) is needed, which can be evaluated if the axial distributions $B(z)$, $B_1(z)$, $B_2(z)$, $P_j(z)$, $Q_j(z)$ ($j = 2, 3, 4$), the axial harmonics, are known. Usually these are determined by a rigorous field calculation using the methods outlined in Part II. A suitable model for deflection systems in the absence of any magnetic material has been worked out by Munro and Chu (1982a). We shall not reproduce their derivation of the formulae here; we describe only briefly the basic ideas and the final results.

Munro and Chu have evaluated the integral representation (8.11) of the scalar magnetic potential for the configurations shown in Figs 40.5 and 40.6 (and also in Fig. 8.5). In toroidal systems the rectangular planar areas, confined by single windings, were chosen as domains of integration; in saddle-coil systems, the corresponding cylindrical areas were chosen. The integration was simplified by series expansion of the integrand with respect to the transverse coordinates of the reference point $\boldsymbol{r}$.

For conciseness, we consider only the pair of coils producing the magnetic deflection field in the x-direction; the other pair for the field component in the y-direction can be treated analogously. The scalar potential $\chi(\boldsymbol{r})$, given generally by Eq. (7.42), now specializes to

$$\mu_0\chi(r) = -B_1(z)\cos\varphi + \frac{r^3}{8}B_1''\cos\varphi - \frac{r^3}{6}P_3(z)\cos 3\varphi + O\left(r^5\right) \tag{40.9}$$

which differs from the expression in the paper of Munro and Chu only in the notation adopted and the sign. The coefficients in Eq. (40.9) are related to their coefficients d_1 and d_3 by $B_1 = \mu_0 d_1$, $P_3 = 6\mu_0 d_3$.

For a configuration consisting of single toroidal windings with the azimuths $\pm\theta$, $\pm(\pi - \theta)$ (see Fig. 40.5), these coefficients are given by

$$\begin{aligned} B_1(z) &= \frac{\mu_0 J}{\pi}\sin\theta\,(f_{22} - f_{21} - f_{12} + f_{11}) \\ P_3(z) &= \frac{\mu_0 J}{\pi}\sin 3\theta\,(g_{22} - g_{21} - g_{12} + g_{11}) \end{aligned} \tag{40.10}$$

where as usual $J \coloneqq NI$ and

$$f_{ij} \coloneqq \frac{\left(H_i^2 + R_j^2\right)^{1/2}}{H_i R_j}$$
$$g_{ij} \coloneqq \frac{8H_i^6 + 12H_i^4 R_j^2 + 3H_i^2 R_j^4 + 2R_j^6}{4H_i^3 H_j^3 \left(H_i^2 + R_j^2\right)^{3/2}} \tag{40.11}$$

with $H_i \coloneqq z \mp l/2$, l being the length of the coil system. For $H_1 = 0$ or $H_2 = 0$, (40.11) break down but the coefficients B_1 and P_3 can be cast in another form that remains finite.

For a pair of saddle coils with single windings and coaxial circular hoops of radius R the corresponding results are given by

$$B_1(z) = \frac{\mu_0 J}{\pi R} \sin\theta \left\{ \left(g_2^3 - 2g_2\right) - \left(g_1^3 - 2g_1\right) \right\}$$
$$P_3(z) = \frac{\mu_0 J}{4\pi R^3} \sin 3\theta \left\{ \left(5g_2^7 - 18g_2^5 + 25g_2^3 - 20g_2\right) - \left(5g_1^7 - 18g_1^5 + 25g_1^3 - 20g_1\right) \right\} \tag{40.12}$$

with the abbreviations $g_j \coloneqq H_j / \left(R^2 + H_j^2\right)^{1/2}$ $(j = 1, 2)$. For a pair of saddle coils with windings running very close to the surface of a cylindrical ferromagnetic shield, the influence of the latter can be considered approximately by doubling the values of the coefficients B_1 and P_3.

Inspection of (40.10) and (40.12) shows that for $\theta = 60°$ the third axial harmonic $P_3(z)$ vanishes. Since the corresponding term in the field strength causes mainly deflection aberrations, it seems to be favourable to choose $\theta = \pi/3$. A slightly different value, chosen so that different aberration terms compensate one another, may be still more favourable. This problem can be solved only by rigorous numerical calculations. Moreover, deflection systems with more than the minimum number of windings can be still better.

This question can be investigated in the following way. Following Munro (1980b), we expand the density $w(\theta) = dN/d\theta$ of the winding distributions (shown in Fig. 40.13) as a Fourier series with respect to θ:

$$w(\theta) = \frac{dN}{d\theta} = a_1 \sin\theta + a_3 \sin 3\theta + a_5 \sin 5\theta + \ldots \tag{40.13}$$

Suppose now that such a distribution consists of n groups of wires, each group characterized by the azimuth θ_i with $0 < \theta_i < 90°$ and the number N_i of turns. The Fourier coefficients are then given by

$$a_k = \frac{4}{\pi} \sum_{i=1}^{n} N_i \sin k\theta_i, \quad k = 1, 3, 5, \ldots \tag{40.14}$$

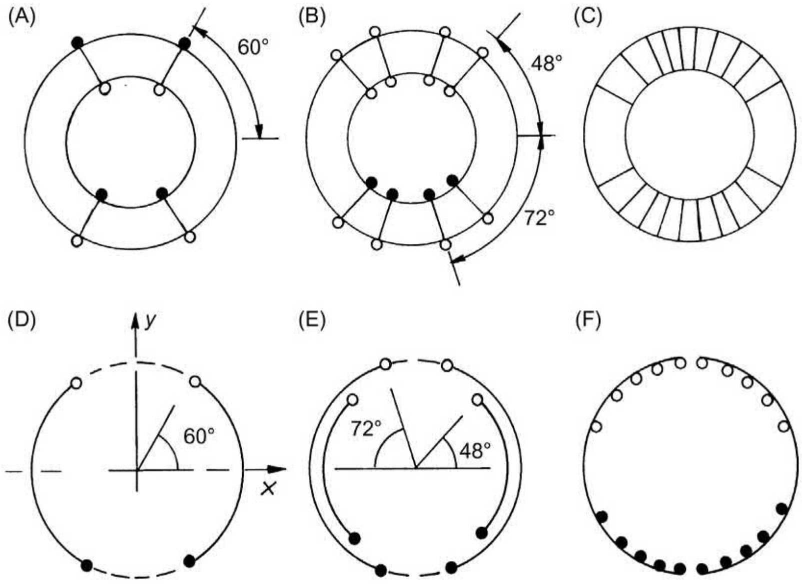

Figure 40.13
Front views of various types of deflection coil system, all producing a magnetic field in the horizontal (x) direction. (A)–(C) toroidal systems; (D)–(F) analogous saddle-coil systems. (A) and (D) have a single group of windings at 60° while (B) and (E) have two groups at 48° and 72°. In (C) and (F) there are many groups approximating a sinusoidal distribution.

The freedom in the choice of the n parameters (N_i, θ_i, $i = 1 \ldots n$) is to be used in such a manner that the device is simple and that $a_3 = a_5 = 0$. For example, $n = 2$, $N_1 = N_2$ leads to $\theta_1 = 48°$ $\theta_2 = 72°$. Returning to (40.10–40.12) with the corresponding abbreviations, we notice that the coefficients f and g depend only on the axial coordinate z and on the parameters l, R_1, R_2, R, which have the same value for all groups of windings. Hence Eqs. (40.10) and (40.12) can be further generalized by replacing $J \sin\theta$ by Ia_1 and $J \sin 3\theta$ by Ia_3.

40.3 The Variable-Axis Lens

As already mentioned in the introduction, it is necessary to deflect the beam in electron beam lithography devices into regions far from the axis in such a way that the principal ray is parallel to the optic axis at the target (normal incidence or 'vertical landing'). This is shown in Fig. 40.4. The requirements for the correction of electron optical aberrations are very exacting: a resolution of at least 10 nm at an off-axis distance of a few mm is necessary and can now be reached.

The aberrations could be kept very small if the beam remained on the lens axis throughout the whole lens field. Ohiwa et al. (1971) established the condition that must be satisfied if the lens axis is subjected to an effective lateral shift, as shown in Fig. 40.4. Goto and Soma (1977) later investigated this concept theoretically, calling it the 'moving objective lens' (MOL); Ohiwa (1978) described electron-beam scanning systems based on the moving objective lens scheme. Pfeiffer and his coworkers at IBM (e.g. Pfeiffer and Langner, 1981; Pfeiffer et al., 1981) developed a similar concept, which they named 'variable-axis lens' (VAL), and succeeded in demonstrating the practicability of this concept under industrial conditions (Pfeiffer, 2000; Pfeiffer and Stickel, 1995). We now briefly describe this MOL/VAL concept; our presentation is somewhat different from those given by Goto and Soma (1977) and Pfeiffer and Langner (1981).

40.3.1 Theoretical Considerations

We set out from the paraxial series expansion for the scalar magnetic potential in a round lens as a special case of (7.41), with $W \coloneqq \mu_0 \chi$:

$$\begin{aligned} W_L(\boldsymbol{r}) = &-\int B dz + \frac{1}{4}\left(x^2+y^2\right)B'(z) \\ &-\frac{1}{64}\left(x^2+y^2\right)^2 B'''(z) + O(6) \end{aligned} \tag{40.15}$$

We now assume that the optic axis is somehow shifted from $x=0$, $y=0$ to $x=x_o$, $y=y_o$ and hence introduce new variables u, υ by writing $u=x-x_o$, $\upsilon=y-y_o$; these are lateral coordinates relative to the new axis. Introducing these into Eq. (40.15), we are led to define the following rotational invariants:

$$\begin{aligned} &r^2 \coloneqq x^2+y^2, \quad w^2 := u^2+\upsilon^2, \quad r_o^2 \coloneqq x_o^2+y_o^2 \\ &c_1 \coloneqq x_o u + y_o \upsilon = r_o w \cos\alpha \\ &c_2 \coloneqq \left(x_o^2-y_o^2\right)\left(u^2-\upsilon^2\right) + 4x_o y_o u\upsilon = r_o^2 w^2 \cos 2\alpha \end{aligned} \tag{40.16}$$

$\alpha \coloneqq \arctan \upsilon/u - \arctan y_o/x_o$ being the difference in azimuths. We find

$$\begin{aligned} r^2 &= r_o^2 + w^2 + 2c_1 \\ r^4 &= r_o^4 + 4r_o^2 w^2 + w^4 + 4c_1\left(r_o^2+w^2\right) + 2c_2 \end{aligned}$$

and hence

$$\begin{aligned} W_L(\boldsymbol{r}) = &-\int B dz + \frac{c_1}{2}B' + \frac{B'}{4}\left(r_o^2+w^2\right) - \frac{c_1}{16}B'''\left(r_o^2+w^2\right) \\ &-\frac{1}{64}B'''\left(r_o^4+4r_o^2w^2+w^4+2c_2\right) \end{aligned} \tag{40.17}$$

Among the terms on the right-hand side is the group

$$\overline{W}_L := -\int B dz + \frac{B'}{4} w^2 - \frac{B'''}{64} w^4 \tag{40.18}$$

which describes the potential of a lens with shifted optic axis in the absence of any deflection aberrations. Our aim is to arrange that only these terms survive in $W_L(\boldsymbol{r})$ and we now try to eliminate the other terms by superimposing appropriate multipole fields.

The first term in c_1, which is linear in u and υ, can be eliminated by adding a suitable deflection potential W_D, the lowest order terms of which are given by

$$W_D = -uB_1(z) - \upsilon B_2(z) = -\frac{1}{2} x_o u B'(z) - \frac{1}{2} y_o \upsilon B'(z)$$

We notice immediately that the deflection field strengths B_1 and B_2 must satisfy

$$B_1(z) = \frac{x_o}{2} B'(z), \quad B_2(z) = \frac{y_o}{2} B'(z) \tag{40.19}$$

These are the MOL conditions proposed by Ohiwa et al. (1971). In order to satisfy them in practice, the currents producing these fields must be proportional to the shift coordinates, $I_x \propto x_o$, $I_y \propto y_o$, as is the case in double-deflection systems. The third-order terms of the deflection potential are given by

$$W_D = -\frac{1}{2}(x x_o + y y_o)\left\{B' - \frac{1}{8}\left(x^2 + y^2\right) B'''\right\} \tag{40.20}$$

The power series expansion in the vicinity of (x_o, y_o) gives

$$W_D = -\frac{1}{2}\left(r_o^2 + c_1\right) B' + \frac{1}{16}\left(r_o^4 + 2 r_o^2 w^2 + c_1\left(3 r_o^2 + w^2\right) + c_2\right) B'''$$

Superimposing this expression on (40.17) and recalling (40.18), we find

$$\begin{aligned} W_L + W_D = \overline{W}_L &- \frac{1}{4} B' r_o^2 + \frac{c_1}{8} B''' r_o^4 \\ &+ \frac{1}{64} B'''\left(3 r_o^4 + 4 r_o^2 w^2 + 2 c_2\right) \end{aligned} \tag{40.21}$$

Some of the remaining terms can be eliminated by the superposition of a suitable dynamic focusing field; this is a round magnetic field, the axial potential of which just compensates the second term on the right-hand side of Eq. (40.21):

$$W_F(r = 0) = \frac{1}{4} B' r_o^2 = -\int B_F dz$$

The axial focusing field strength is thus

$$B_F(z) = -\frac{1}{4}B''(z)r_o^2 \tag{40.22}$$

Since this field strength must be proportional to r_o^2, the paraxial series expansion for the potential is sufficient:

$$\begin{aligned} W_F &= -\int B_F dz + \frac{1}{4}B'_F\left(x^2 + y^2\right) \\ &= \frac{1}{4}B' r_o^2 - \frac{1}{16}B'''\left(r_o^4 + r_o^2 w^2 + 2c_1\right) \end{aligned} \tag{40.23}$$

Adding this to Eq. (40.21) and introducing the abbreviation

$$W_S := -\frac{1}{32}B'''c_2 = -\frac{B'''}{32}\left\{\left(x_o^2 - y_o^2\right)\left(u^2 - \upsilon^2\right) + 4x_o y_o u\upsilon\right\} \tag{40.24}$$

we now obtain

$$W_L + W_D + W_F + W_S = \overline{W}_L - \frac{1}{64}B'''r_o^4 \tag{40.25}$$

The term W_S, being quadratic in u and υ, can be generated approximately by a dynamic magnetic quadrupole-stigmator:

$$V_S = \frac{1}{2}\left(x^2 - y^2\right)P_2(z) + xyQ_2(z) \tag{40.26}$$

with the quadrupole strengths

$$\begin{aligned} P_2(z) &= -\frac{1}{16}B'''(z)\left(x_o^2 - y_o^2\right) \\ Q_2(z) &= -\frac{1}{8}B'''(z)x_o y_o \end{aligned} \tag{40.27}$$

Expanding (40.26) in the vicinity of (x_o, y_o), we obtain (40.24) plus some minor perturbation terms. We find

$$\overline{W}_L = W_L + W_D + W_F + W_S + W_P \tag{40.28}$$

where W_P denotes the resulting weak perturbations which are to be neglected or, if necessary, partially corrected. Eq. (40.28) means that, at least in theory, the lens axis can be shifted electronically by suitable arrangements of dynamic multipole fields. Here the word 'dynamic' means that the multipole strengths must be functions of the deflection signals $I_x \propto x_o$, $I_y \propto y_o$. The electrostatic analogue has been considered by Thomson (1996).

The theory has been re-examined by Zhao and Khursheed (1999a–c), who set out from a general form of the paraxial ray equation (32.4 without quadrupole terms):

$$w'' + \left(\frac{\phi'}{2\phi} - \mathrm{i}\hat{\eta}B\right)w' + \frac{1}{2}\left(\frac{\phi''}{2\phi} - \mathrm{i}\hat{\eta}B'\right)w = -\frac{F_T}{2\phi} - \mathrm{i}\hat{\eta}B_T \tag{40.29}$$

(As in Section 51, we write $\hat{\eta} = \eta/\phi^{1/2}$.) A ray is incident on an object plane at $w_0 = x_o + \mathrm{i}y_o$ at an angle $\theta \coloneqq w_o'$. If the combined effect of the focusing fields $\phi(z)$ and $B(z)$ and deflection fields F_T and B_T is such that this ray passes straight through them, it will be the new 'moved' optic axis, which we denote $w_1(z)$. For this, we have

$$w_1(z_o) = w_o, \quad w_1'(z_o) = \theta, \quad w_1'' = 0 \quad \text{for} \quad z_o \le z \le z_i$$

and so

$$w_1(z) = \theta(z - z_o) + w_o \tag{40.30}$$

Substituting this into (40.29) gives

$$\left(\frac{\phi'}{2\phi} - \mathrm{i}\hat{\eta}B\right)\theta + \frac{1}{2}\left(\frac{\phi''}{2\phi} - \mathrm{i}\hat{\eta}B'\right)\left\{\theta(z - z_o) + w_o\right\} = -\frac{F_T}{2\phi} - \mathrm{i}\hat{\eta}B_T \tag{40.31}$$

This very general condition reduces to the various moving objective lens configurations as special cases. If all electrostatic terms are omitted, we arrive at the 'swinging objective lens' described by Chen et al. (1983). By removing all magnetic terms, an analogous electrostatic swinging lens is obtained. If both sets of terms are present, a hybrid swinging lens results.

When the complex gradient θ is set equal to zero in (40.31), so that

$$\left(\frac{\phi''}{2\phi} - \mathrm{i}\hat{\eta}B'\right)w_o = -\frac{F_T}{\phi} - 2\mathrm{i}\hat{\eta}B_T \tag{40.32}$$

we recover the general moving objective lens condition. Zhao and Khursheed identify four configurations:

magnetic lens with magnetic deflectors:	$B_T = \frac{1}{2}B'(z)w_o$
electrostatic lens with electrostatic deflectors:	$F_T = -\frac{1}{2}\phi''(z)w_o$
magnetic lens with electrostatic deflectors:	$F_T = \mathrm{i}\eta\phi^{1/2}B'(z)w_o = i\hat{\eta}\phi B'(z)w_o$
electrostatic lens with magnetic deflectors:	$B_T = \frac{\mathrm{i}}{\eta\phi^{1/2}}\phi''(z)w_o = \frac{i}{\hat{\eta}}\frac{\phi''(z)}{\phi}w_o$

40.3.2 Practical Design

The theory outlined above gives us some idea of which types of field should be employed in a high-quality deflection system, but in this primitive form it cannot be put directly into practice. It is almost impossible to find forms of polepieces and of coil systems that produce accurately the required multipole fields proportional to $B'(z)$, B'' and B'''. Moreover, it is not necessary to satisfy these very severe conditions. It would be quite sufficient if the principal ray stayed in the vicinity of the shifted optic axis and the deflection aberrations were compensated globally. This can be achieved in realistic designs but the latter can be found only with the aid of the computer. Such designs have been developed by Pfeiffer and his coworkers, who were able to demonstrate experimentally the high resolution of the new devices. We cannot describe the details here, but only some of the results.

Fig. 40.14 shows schematically the entire VAL configuration, consisting of a telecentric lens system, a pre-lens double deflection system, an in-lens double deflection system, a dynamic stigmator and four dynamic focus coils. Fig. 40.15 shows the variable-axis field correction concept practically realized in the final lens with its in-lens deflectors.

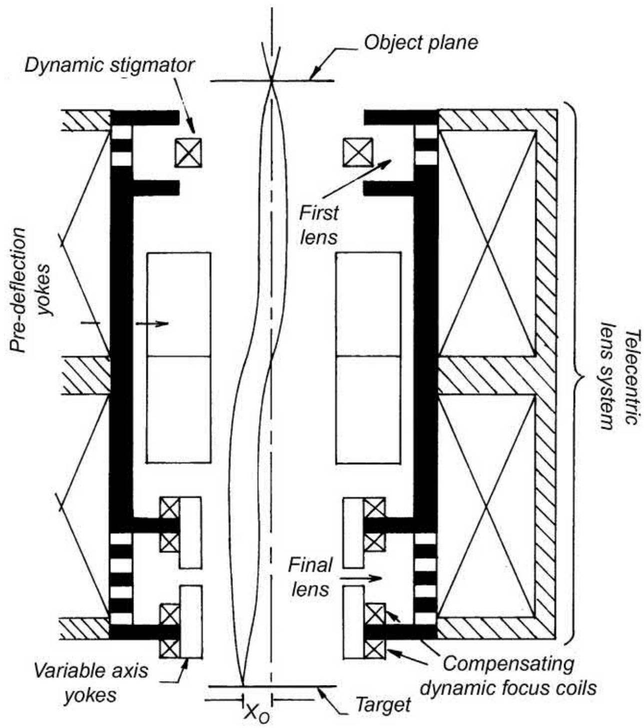

Figure 40.14
The elements of a variable-axis lens (VAL). *After Sturans and Pfeiffer (1984), Courtesy Academic Press.*

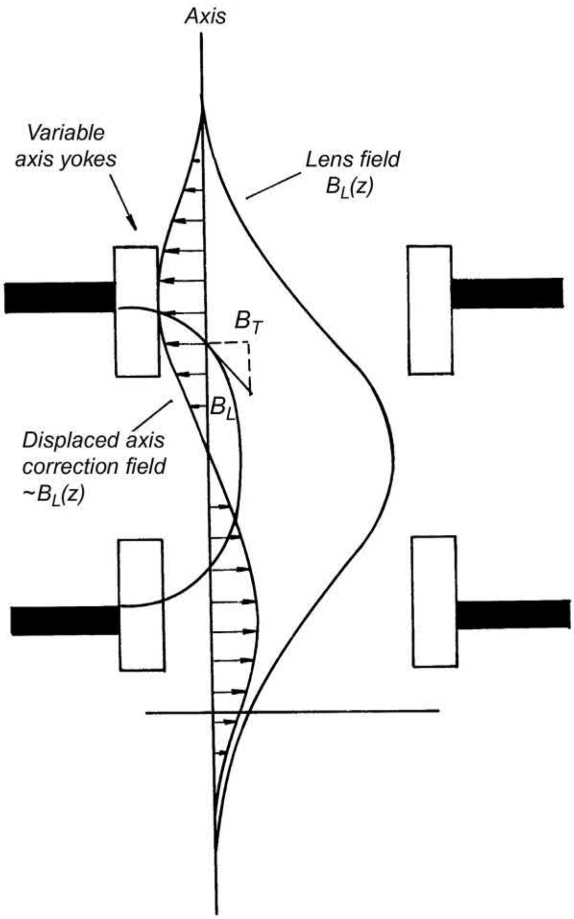

Figure 40.15
Field correction in the variable-axis design. *After Sturans and Pfeiffer (1984), Courtesy Academic Press.*

Fig. 40.16 demonstrates the importance of the dynamic focusing. Figs 40.17 and 40.18 show a later design, the 'variable axis immersion lens' (VAIL) configuration, built by Pfeiffer and his coworkers (Sturans and Pfeiffer, 1983; Kern et al., 1985; Pfeiffer, 1995). The lower half of the final lens, one field-correction yoke and two dynamic focus coils, can be eliminated by introducing a thick shielding plate into the symmetry plane; moreover, this arrangement eliminates stray fields from the target area. Fig. 40.19 illustrates the results of measurements of the transverse field compensation, which indicate that the idea of an electronically shifted lens axis can be realized to a certain degree of accuracy. Sturans and Pfeiffer (1983) measured a resolution limit of 0.2 μm over a 10 × 10 mm^2 field.

Ura (2016) has considered the role of the moving objective lens in a three-dimensionally imaging electron microscope.

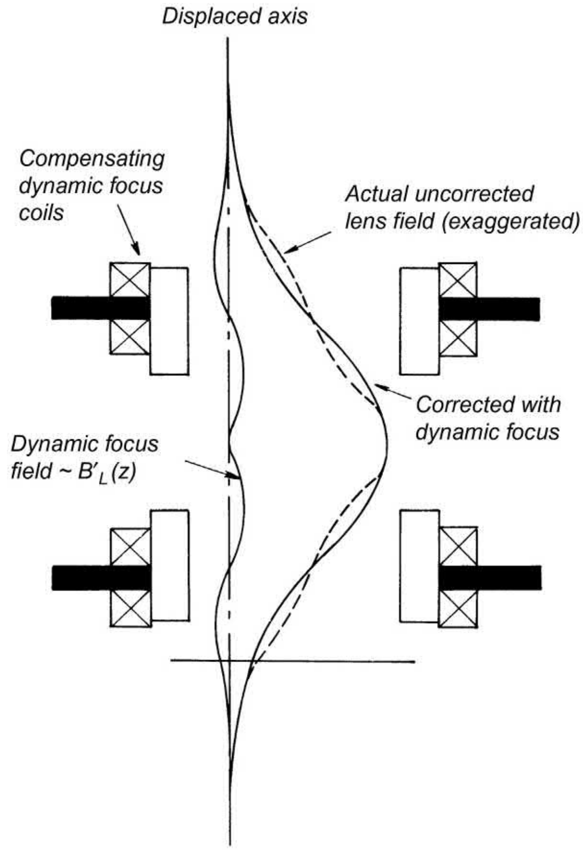

Figure 40.16
Dynamic focus correction in the variable-axis design. *After Sturans and Pfeiffer (1984), Courtesy Academic Press.*

40.4 Alternative Concepts

Any good design for an electron-beam lithography system must be such that the coma and the transverse chromatic aberration can be neglected, since these aberrations cannot be corrected. If astigmatism, curvature of field and distortion are corrected dynamically, which is always possible, there remain only the spherical and the axial chromatic aberrations of the lens system, but these can be kept small enough for practical purposes. The working distances between the final lens and the target must be kept very small in order to minimize the blurring of the writing spot due to electron–electron interactions.

The MOL/VAL concept is only one possible way of satisfying these requirements in electron-beam lithography devices. For non-specialists it has the advantage of being easy to understand. Other solutions may be of the same quality if the warping of the target is not

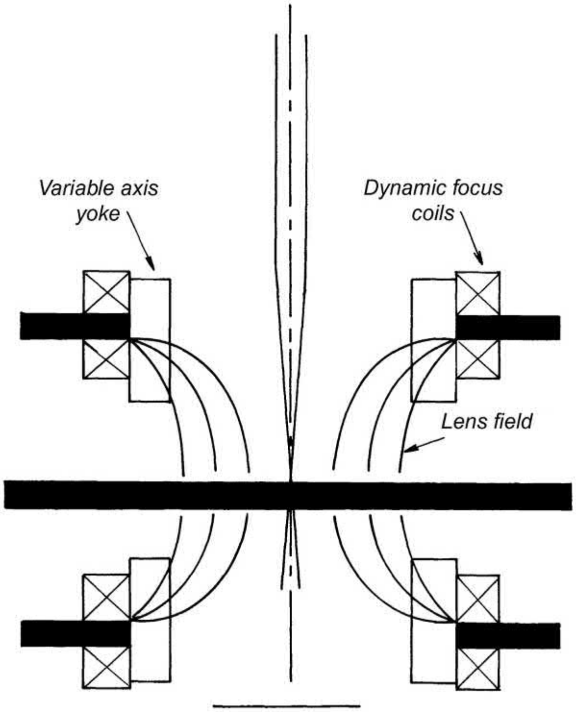

Figure 40.17
The immersion lens concept in the VAL system. *After Sturans and Pfeiffer (1984), Courtesy Academic Press.*

too great. There have been many proposals, all the result of computer-aided design (CAD) programs. It is customary to present the results in the form of tables listing the blurring radii resulting from the different types of aberrations and the total mean square radius. Some typical examples of designs studied by Kern (1984) are presented in Table 40.1. Here, four systems are compared: single in-lens deflection; double deflection; the MOL system with ideal predeflection, that is, assuming that all aberrations behind the first deflector vanish; and the real MOL system with all aberrations present. It emerges that for a $5 \times 5\ \mathrm{mm}^2$ field, the double-deflection system may be superior, especially in the absence of dynamic correction.

The data presented in such tables are easier to appreciate than to calculate, since they are the final output of complicated CAD routines, such as those dealt with in Chapter 33, The Aberrations of Deflection Systems. We cannot go into the details of such procedures here.

So far we have mostly considered purely magnetic systems. Although magnetic deflectors can be designed to produce very small aberrations, they are not quite satisfactory in every respect. Their essential drawback is the limitation of the scanning speed by inductance effects. Scherle (1983) found the upper limit of the scanning frequency of a sawtooth current-signal to be $5 \times 10^{-3} R/L$, R being the resistance and L the self-inductance of the

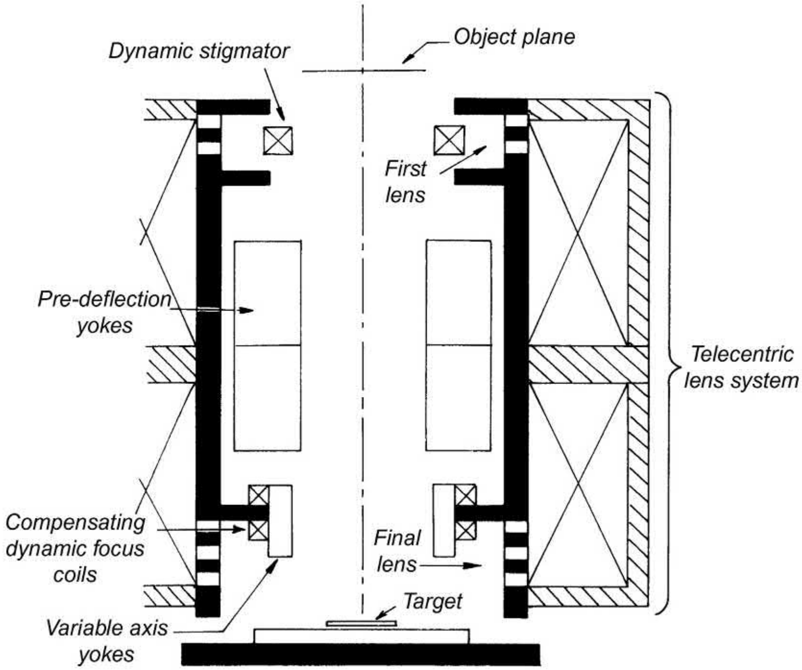

Figure 40.18
The elements of a variable-axis immersion lens (VAIL). *After Sturans and Pfeiffer (1984), Courtesy Academic Press.*

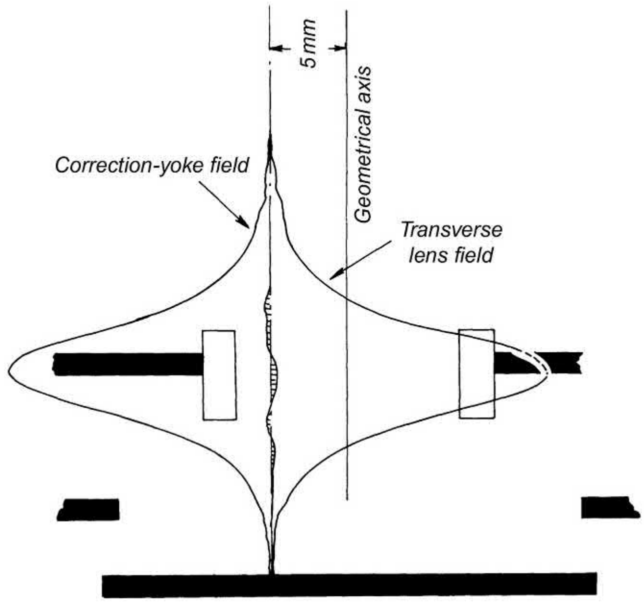

Figure 40.19
The compensating field effect in a VAIL as measured by a Hall probe. *After Sturans and Pfeiffer (1984), Courtesy Academic Press.*

Table 40.1: Typical values of the aberrations produced by different deflection systems

Beam voltage	25 kV			
Energy spread	2.5 eV			
Scan field	5×5 mm^2		10×10 mm^2	
Beam aperture	5 mrad			
	Single deflection	Double deflection	Real MOL ideal predeflection	Real MOL real predeflection
Spherical aberration	0.01	0.01	0.02	0.02
Axial chromatic aberration	0.04	0.03	0.05	0.05
Field curvature	1.68	0.56	10.15	9.11
Astigmatism	0.60	0.22	4.29	4.32
Coma	0.07	0.00	0.00	0.00
Transverse chromatic aberration	0.15	0.05	0.00	0.08
Landing angle	47	42	1.7	1.4
Total without dynamic correction	1.79	0.60	11.01	10.09
Total with dynamic correction	0.17	0.06	0.05	0.09

The units are μm, except for the landing angle (mrad).
After D. Kern, 1984.

coils. This relation has been confirmed experimentally. In order to decrease the self-inductance, saddle coils with very few windings and without ferromagnetic shields are favourable, but this does not suffice. Electric deflectors may be expected to be superior, since their very low impedance allows the scanning frequency to be very high.

The problem of designing electron-beam lithography machines with electric deflectors has been investigated in great detail by Munro and Chu. Their numerical analysis is published in four parts (Munro and Chu, 1982a,b; Chu and Munro, 1982a,b). Part I deals with the methods for computing magnetic deflection fields, while part II is concerned with electric deflection fields. Unfortunately, no simple analytic models for the latter are known, so that a rigorous field computation technique, such as the surface charge method or the finite-element method, is necessary but this is no great obstacle, particularly in view of the fact that extensive computing of trajectories and aberration coefficients is needed later. Part III presents a complete aberration theory for systems built up from round magnetic and electric lenses and magnetic and electric deflectors. This theory is highly complex: Munro and Chu found 27 relevant geometric aberrations of third order and three chromatic aberrations of first order. The authors renounced the use of the rotating frame. We shall not reexamine this theory here, some account of which is given in Chapter 33, The Aberrations of Deflection Systems.

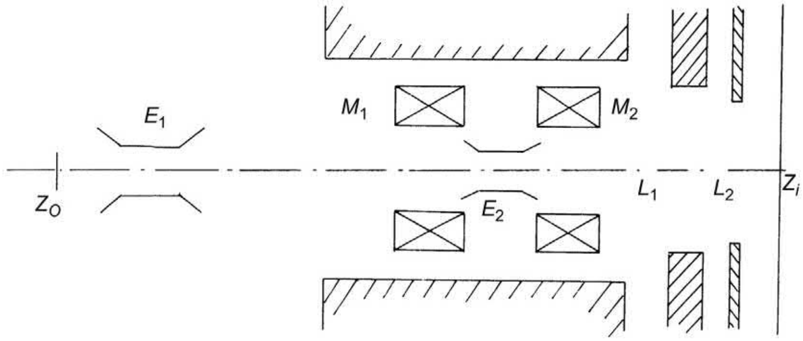

Figure 40.20

Principle of a focusing and dual-channel deflection system. $E_{1,2}$: electric deflectors; $M_{1,2}$: magnetic deflectors; L_1: magnetic round lens; L_2: round electrostatic retarding lens; z_o, z_i: axial object and image coordinates.

The arrangements investigated theoretically and numerically by Munro and Chu are represented schematically in Fig. 40.20. The underlying idea is that of a dual-channel deflection system. The magnetic deflectors are to perform the main beam deflections over fairly large angles and at low scanning speed, while the electric components are required to produce a superimposed high-speed deflection over small angles. Part IV of the series of papers deals with the development of an optimization routine, as outlined in Chapter 33, and with its application to dual-channel electron-beam lithography systems. Their program allowed axial shifts and rotations of deflectors, as well as alterations of the geometric scales and of the coil currents and electrode voltages, but no modification of the geometric shapes. The result of the optimization is that – with respect to aberrations – dual-channel systems can compete with MOL/VAL devices. Moreover, they are capable of high-speed deflections, whereas MOL/VAL devices are not. Another result of the investigations is that a retarding electric lens field between the final magnetic lens and the target may be favourable. Of course, the increased number of components renders the alignment of dual-channel systems more complicated.

40.5 Deflection Modes and Beam-Shaping Techniques

The traditional deflection mode is the raster scan in a TV-like fashion over the entire target area. This is the natural choice in all kinds of scanning microscopes, where information from each target image element (pixel) is needed though other scanning patterns may be advantageous if subsequent signal processing is envisaged. In this deflection mode eddy current errors are repeatable and can be compensated by introducing appropriate time delays.

In electron-beam lithography devices the raster scan is far from favourable, since all the time during which the beam is addressed to unexposed target areas and hence blanked out is wasted. The throughput is far lower than in light optical lithography devices as it is for all single-beam systems.

A first improvement is the vector scan technique (Speth et al., 1975), shown in Fig. 40.21. Here the beam is moved vectorially to the starting point of each pattern element, which is then exposed with a sequence of appropriate line scans. The blanking time between two subsequent patterns can be considerably reduced but great care is now necessary to eliminate eddy current errors and to minimize the beam settling times. Instead of writing in a zigzag line, a suitable framing scan may be favourable in order to obtain an intensity profile with a sharper edge, as is shown in Fig. 40.22.

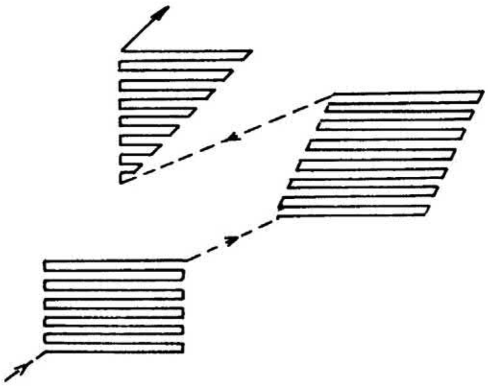

Figure 40.21
The vector scan technique.

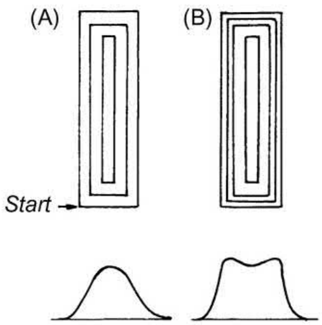

Figure 40.22
The framing scan technique. (A) Normal closure sequence and (B) modified closure sequence. The resulting electron density distributions are shown below.

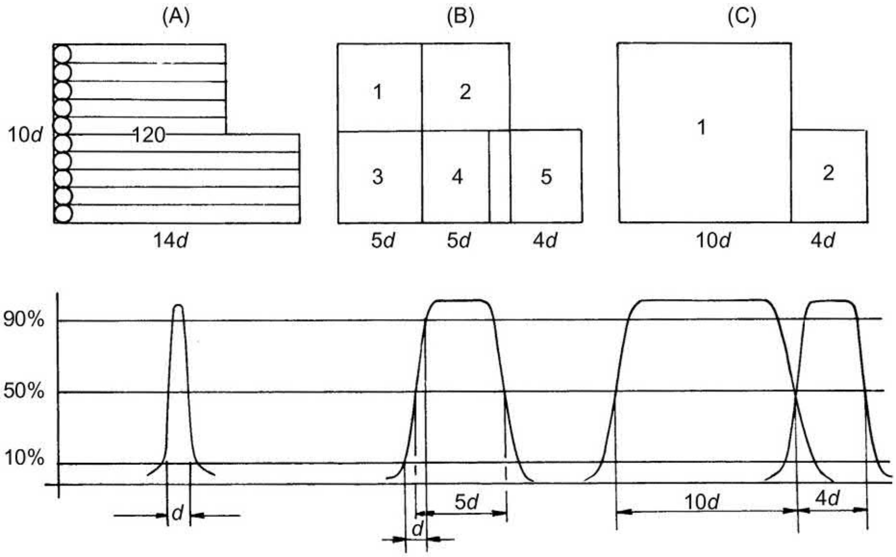

Figure 40.23
Variable spot shaping. The area illustrated requires 120 exposures to a standard round beam (A) but only five exposures to a fixed-shape beam (B) and two exposures to a variably shaped beam (C).

In spite of all these improvements, the electron-beam lithography technique was still inferior to its light optical rivals, in that the target is exposed sequentially, pixel after pixel, whereas in light optical projections the entire wafer used to be exposed at once. In order to overcome this disadvantage, Pfeiffer et al. developed beam-shaping techniques, by means of which larger zones of the target can be exposed simultaneously. A review of these procedures is given by Pfeiffer (1979, 1983). The fixed shaped-beam technique, in which only squares of constant side can be used, is too rigid in practice, as is obvious from Fig. 40.23: if the contour of the pattern to be produced does not fit onto a square-shaped grid, one can make double exposures of some areas, as is shown in one figure, but this causes overexposure and thus irregularities in the subsequent processing. For this reason only the *variable shaped-beam* technique which is shown on the right-hand side of Fig. 40.23 is satisfactory in practice. The sizes and the positions of the rectangular domains can be chosen in such a way that no irregular exposure occurs in the vicinity of inner boundaries and that the outer contour corresponds to 50% exposure.

The corresponding electron-beam lithography machine developed at IBM and named EL3 is presented schematically in a simplified manner in Fig. 40.24. The essential new components are the square-shaped apertures and an electric deflector. By appropriate deflections and filtering out of unnecessary parts of the beam, a variety of rectangular

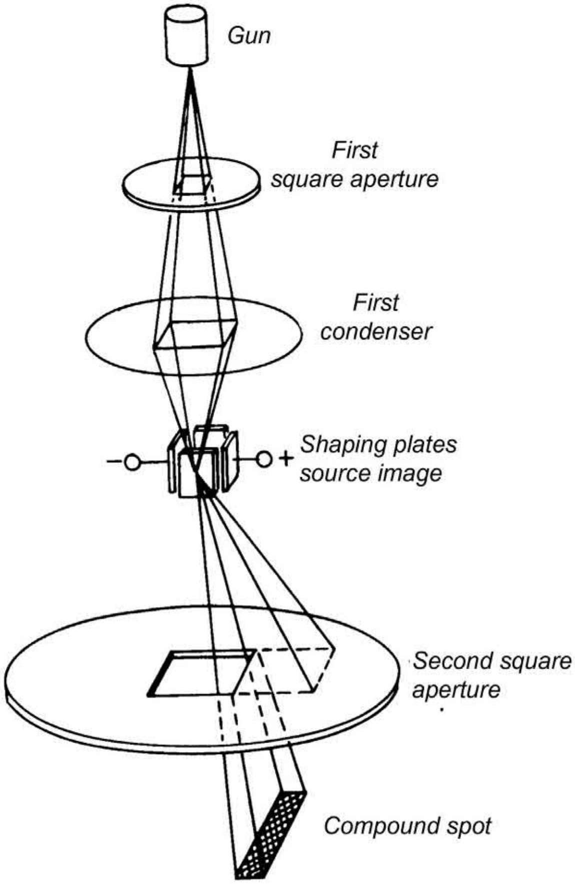

Figure 40.24
Dual-aperture shaping method. *After Pfeiffer (1979), Courtesy IEEE.*

compound spots can easily be obtained. In the EL3 configuration, the dual-channel principle is employed; below the second aperture, a lens combined with a magnetic deflector system is present, not shown in the figure. Fig. 40.25 shows EL3 in more detail.

A further development is electron-beam lithography by *cell projection*. A mask is brought into the beam, which contains various openings in the forms of different characters. Any required combination of characters can be written on the target if the deflectors shift the beam in the appropriate manner to the corresponding openings. This was implemented in the SCALPEL instrument (Bell Laboratories/Lucent Technologies); Here, a patterned mask was illuminated by a large square uniform electron beam; the mask moved across the beam,

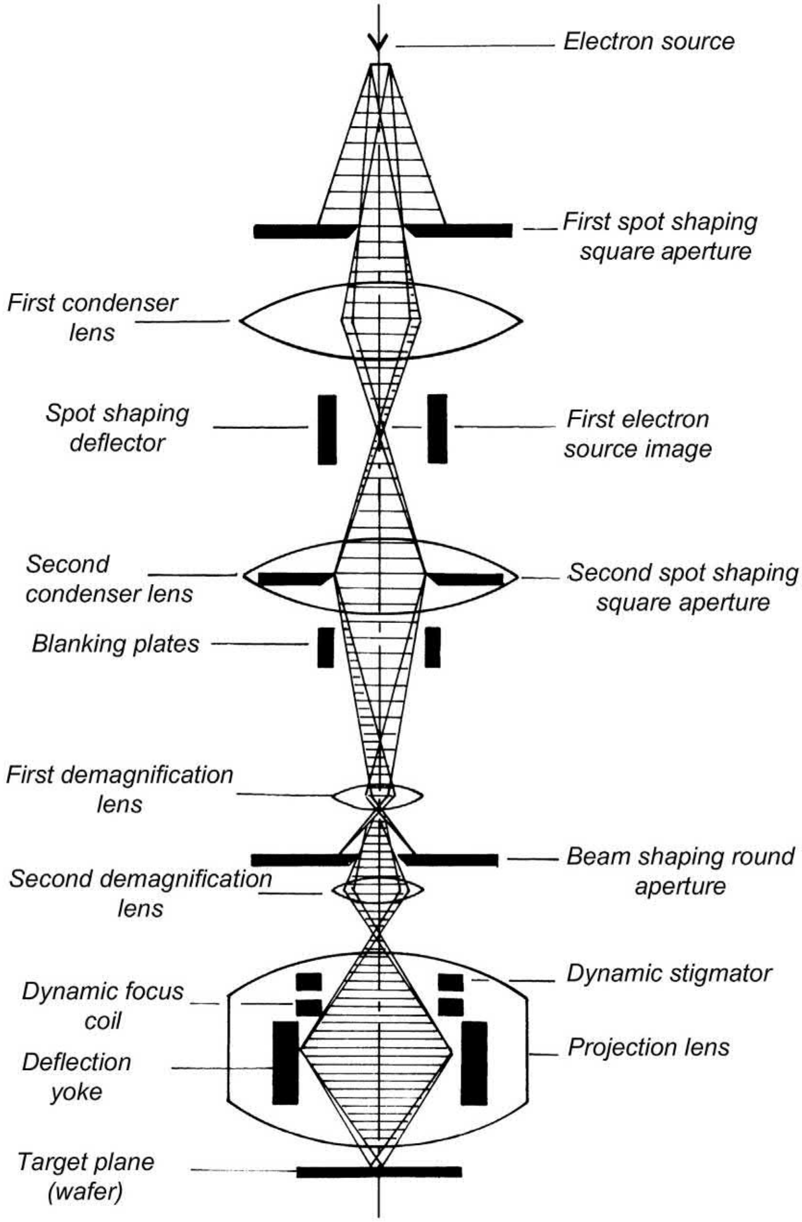

Figure 40.25
Linked-beam trace for variable-spot shaping. *After Pfeiffer (1979), Courtesy IEEE.*

causing the pattern to be projected onto a wafer, which moved in synchronism with the mask (Liddle et al., 1995; Waskiewicz et al., 1997). At IBM, a similar scheme was developed, (PREVAIL); the beam was now scanned over the mask (Pfeiffer and Stickel, 1995; Pfeiffer, 2000; Dhaliwal et al., 2001).

In order to avoid crossovers, where Coulomb forces spread the beam, Cheng and Tang (2000a,b, 2001) suggested that a combined electrostatic–magnetic lens with the cathode inside the magnetic field could be beneficial. This idea was pursued by Zhao et al. (2012b), who made a detailed study of the electron trajectories in the vicinity of curved optic axes coinciding with trajectories leaving the cathode. This is an unusual application of the general theory presented in Chapter 50, Complete Electron Guns. In a companion paper, Zhao et al. (2012a) had described a possible rotation-free design.

With all these technical refinements the throughput of electron-beam lithography machines was increased to such an extent that these devices could compete with light optical systems, at least for special purposes such as mask fabrication. They had the great advantage over the latter that their performance could be easily automated and controlled and directed by a computer, since the electronic deflection signals could be manipulated straightforwardly in various ways. Progress can be followed in the proceedings of the regular SPIE meetings specialized in this subject, in those of the Electron, Ion and Photon Beam Technology conferences (published in *J. Vac. Sci Technol. B*), the Micro- and Nanoengineering conferences (published in *Microelectronic Engineering*) and of the Japanese Microprocesses and Nanotechnology conferences (published in the *Japanese Journal of Applied Physics*). See surveys by Ura and Fujioka (1989), Levinson (2010), Tennant and Bleier (2011) and Suzuki (2018).

The present trend is towards multibeam devices, which are discussed in Section 50.6.

PART VIII

Aberration Correction and Beam Intensity Distribution (Caustics)

Aberration Correction

41.1 Introduction

The resolution of fixed-beam and scanning transmission electron microscopes is ultimately limited by the spherical and chromatic aberrations of the objective lens, which alone are unaffected by the distance of object points from the optic axis. For this reason, Scherzer's demonstration in 1936 that the corresponding integrands can be cast into the form of a sum of squared terms was received with dismay and even incredulity. By the same token, his proposals for correcting these aberrations by relaxing one or other of the assumptions on which the earlier proof reposed are at the heart of a large body of work on aberration correction. The various methods of correction lead us to consider electron optical elements that, with the exception of multipoles and mirrors, do not merit detailed analysis in their own right and we therefore discuss them together here. We shall examine correction of the other aberrations when first the primary spherical aberration and later the chromatic aberration have been eliminated.

We have seen that all the attempts, and in particular those of Glaser, to find a loophole in Scherzer's proof were finally shown to be vain by Tretner's work, which established lower limits on C_s and C_c for all realistic lens geometries and excitations. We recall too that the field distribution that resulted from Glaser's idea of setting the C_s integrand equal to zero to obtain a differential equation for the ideal $B(z)$, a model if over-optimistic example of lateral thinking, has proved useful in other domains, β-ray spectrometry in particular (Slätis and Siegbahn, 1949). A few authors continue to search for counter-examples to Scherzer's result (Garg, 1982, see Scherzer, 1982; Nomura, 2008, see Hawkes, 2009b).

The positive-definite form of the integrand correctly represents the real spherical aberration coefficient C_s provided that the lens is rotationally symmetric and produces a real image of a real object (this is implicit in the fact that we are considering the real coefficient), that the fields are static, that space charge is negligible, that $\phi(z)$ and $\phi'(z)/\phi(z)$ are continuous and that the lens is not replaced by a mirror. By relaxing any of these requirements, it might be possible to find a lens for which the spherical and chromatic aberration coefficients vanish and in 1947, Scherzer sketched a number of ways of achieving this. All have been pursued, some in greater detail than others, and we now know which methods finally proved successful.

Principles of Electron Optics: Applied Geometrical Optics.
DOI: http://dx.doi.org/10.1016/B978-0-12-813369-9.00041-5

We consider the various ways of correcting spherical and chromatic aberration in turn. The former was usually the more important in practice (except in the very early years) as the sources of electron-energy and lens-current spread could be contained and energy losses in the specimens used for high-resolution work are typically small. But once primary spherical aberration has been corrected, close attention must be paid to the chromatic aberration. The effect of this can be reduced either by means of a corrector element or by limiting the energy spread of the beam with a monochromator (see Section 52.9). A very different solution is to use a time-dependent field to invert the velocity distribution in the beam.

Departure from rotational symmetry leads us to systems involving quadrupoles and octopoles or sextupoles or all of these. The presence of space charge can in principle create an axial potential distribution for which C_s vanishes. The discontinuity caused by closing the bore of a lens with a gauze or a thin foil highly transparent to electrons can have the same effect. Electron mirrors can generate spherical aberration opposite in sign to that of rotationally symmetric lenses. Electrodes may be placed on the axis, giving more control over the potential distribution but obscuring the axial zone. Finally, the electron beam may be pulsed and the static lens replaced by a microwave cavity, which can be shown to act as a convergent or divergent lens with positive or negative spherical aberration, depending on the part of the high-frequency cycle encountered by the electrons.

Of all these approaches to aberration correction, only two survive today: the use of non-rotationally symmetric elements and the incorporation of electron mirrors, though there is renewed interest in the introduction of an axial electrode.

The history of aberration correction is traced in Hawkes (2009a) and in Rose (2008, 2009b).

41.2 Multipole Correctors

41.2.1 Quadrupoles and Octopoles

Systems of quadrupoles and octopoles can be designed to be free of spherical and chromatic aberrations either alone or in conjunction with round lenses. This can be deduced from the form of the aberration integrals listed in Chapter 29, The Aberrations of Quadrupole Lenses and Octopoles, and understood by recalling that isolated quadrupoles form line foci. We therefore expect that a quadrupole triplet with two intermediate line foci could be used as a corrector by placing an octopole at each line focus, thereby cancelling or over-correcting one aperture aberration coefficient at each, and a third octopole in some other plane to correct the remaining aperture aberration coefficient. This is not at all a practical configuration but the elementary principle, whereby quadrupoles destroy the rotational symmetry of the beam and three octopoles cancel or over-correct the three aperture aberration coefficients, remains valid in any such corrector. Clearly, alarmingly high demands will be made on the accuracy and performance of the quadrupole–octopole unit, since it is required to correct a lens already presumably of high quality by introducing rather large new aberrations and then correcting the total.

Systems based on cylindrical lenses and octopoles for correcting the spherical aberration of a round lens were proposed by Scherzer (1947), and an experimental system was built and investigated soon after by Seeliger (1948/49, 1949, 1951, 1953) and Möllenstedt (1954, 1956), cf. Scherzer (1949, 1950). Meanwhile Burfoot (1953) had found a theoretical answer to the problem of designing a corrected electrostatic lens with as few electrodes as possible. His four-electrode design assigns round-lens potentials to the first three electrodes, an octopole component to the second electrode and quadrupole components to all but the second electrode. The shapes required to generate the desired potentials were estimated by Burfoot, who found complicated profiles and very high tolerances; his estimates have not, unfortunately, been repeated with the vastly more powerful tools available today. The next advance came from Archard (1954a,b), who pointed out that the complicated arrangement of Seeliger could be simplified by replacing the cylindrical lenses by quadrupoles; in the following year, he suggested 'Two new simplified systems for the correction of spherical aberrations . . .' (Archard, 1955a). The first was essentially a quadrupole triplet; the four elements created successively a pure quadrupole field, an octopole field and two mixed quadrupole–octopole fields. The other system described was in essence the combination that for many years seemed the most likely to succeed: an antisymmetric quadrupole quadruplet, the second and third members of which produced octopole as well as quadrupole components, plus an additional octopole (located in Archard's design between the second and third elements) to give the necessary number of independent correctors. For subsequent work by this author, see Archard (1955b, 1958, 1960) and Archard et al. (1960). The early 1960s saw the design and construction of a corrector unit for a probe-forming lens by Deltrap (1964a,b); at that time, the advantages of antisymmetry, so obvious with hindsight, were not appreciated and Deltrap's designs seem unnecessarily complicated but, despite this, his telescopic system (the Archard–Deltrap telescopic corrector) acted as an important catalyst for later work. Fig. 41.1A shows the ray diagram in his experimental design, which consisted of four magnetic elements all capable of producing both quadrupole and octopole components, and Fig. 41.1B–E indicate the degree of correction attained.

Although most of the investigations of the 1960s were concentrated on spherical aberration (e.g., Dhuicq, 1968a,b; Dhuicq and Möller, 1970; Dhuicq and Septier, 1966a,b, 1968c; Septier, 1957, 1958, 1963; Septier and van Acker, 1960a,b; Thomson, 1966, 1967; and the many publications of the Leningrad group cited in Chapter 29) an important result was the finding by Kel'man and Yavor (1961) that a combined electrostatic–magnetic quadrupole

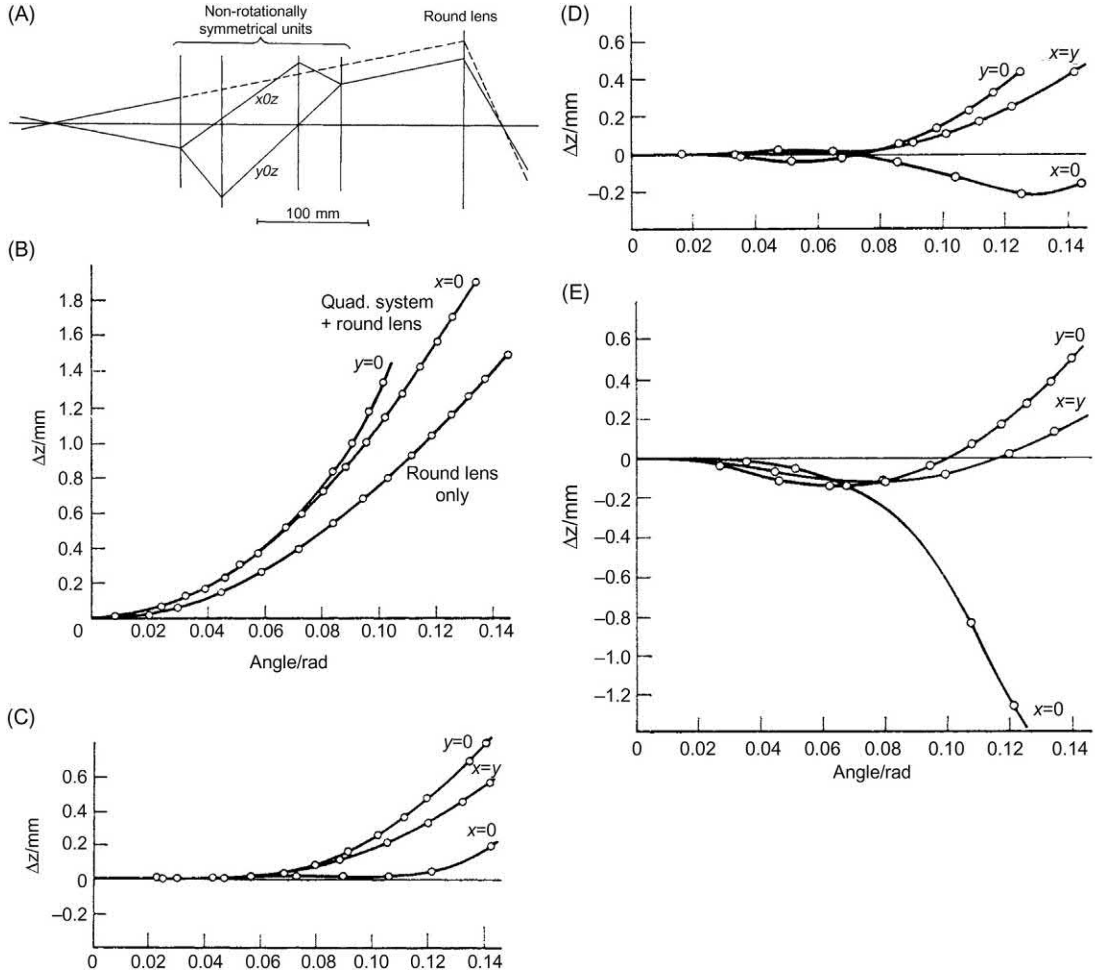

Figure 41.1
(A) Ray diagram in the correction unit investigated by Deltrap. (B) Longitudinal aberration as a function of angle for the round lens alone and for the combination of round lens and quadrupoles. (C)–(E) Various degrees of correction.

can be free of primary chromatic aberration for a suitable choice of excitation. This was later re-established by Septier (1963), generalized by Hawkes (1964, 1965b) and extensively studied experimentally by Hardy (1967).

A large body of information about quadrupoles was accumulated as the decade proceeded, which is briefly recapitulated in Chapters 19, 29 and 39 and in more detail in Hawkes (1966, 1970), Septier (1966), Strashkevich (1966) and Yavor (1968). A few determined attempts were made to design correctors, many based on the Russian quadruplet, which has a plane of geometric symmetry and electrical antisymmetry (Fig. 39.1A) and hence equal focal lengths in the initially converging and initially diverging planes (Dymnikov et al. 1963, 1964a,b, 1965a−d; Dymnikov and Yavor, 1963). Among the more thoroughgoing attempts to build such a corrector is that of Crewe, who tried to use a quadruplet to reduce the probe-size in a scanning transmission microscope (Crewe et al., 1968; Thomson, 1972; Beck and Crewe, 1974, 1976; Parker et al., 1976a,b; Beck, 1977, 2011; Crewe, 1978, 2009; Shao et al. 1988). Their efforts appear to have been frustrated by anisotropy in the magnetic circuit, despite the great care taken over all aspects of the construction, and by the unfortunate choice of polepiece material (mumetal).

It occurred to Scherzer and Typke (1967) to enquire whether a single octopole can be beneficial in conjunction with a round lens; they concluded that, under certain circumstances, such an arrangement could be advantageous.

The other major attempt to combine non-rotationally symmetric elements with a round lens to correct the resolution-limiting aberrations is the Darmstadt microscope (Scherzer, 1978). The aim of this long-term project was to build a microscope capable of a resolution of the order of 50 pm, for which it is necessary to correct the primary chromatic aberration and the third- and fifth-order spherical aberration and to correct or balance the coma and any threefold astigmatism (Fig. 41.2). The progress of the project may be followed through the papers of Reichenbach and Rose (1968/69), Rose (1970, 1971a), Bastian et al. (1971), Pöhner (1976, 1977), Bernhard and Koops (1977), Koops et al. (1977), Koops (1978a,b), Kuck (1979), Pejas (1978), Bernhard (1980), Fey (1980), Haider et al. (1982) and Hely (1982a,b). Many more informal details are to be found in the historical articles of Rose (2009b) and Marko and Rose (2010). The practical development of this complex system reached the point at which it was shown that the chromatic correction worked perfectly satisfactorily and that computer control of the very numerous components raised no great difficulties. Work on the project was, unfortunately, suspended with Scherzer's death in 1982 (Rose, 1983, 2009c). Looking back, it is apparent that the corrector would not have been usable in practice in the absence of the fast diagnostic and control tools that became available only in the 1990s. A cutaway illustration of the microscope is reproduced in Hawkes (2015).

Meanwhile, work continued on the design of new quadrupole lens types with a view to simplifying correction. The many papers on crossed lenses already cited in Chapter 29, The Aberrations of Quadrupole Lenses and Octopoles, are the main example (surveyed by Baranova and Yavor, 1984, 1986, 1989). A proposal by Okayama and Kawakatsu (1982) to use an electrostatic quadrupole terminated after a small gap by plates containing circular openings has the same object; the overlapping round and quadrupole fields create octopole components.

In the 1990s, three multipole-corrector projects were launched, two involving quadrupoles and octopoles, the third, sextupoles. The last is described in Section 41.2.2. In the European Molecular Biology Laboratory (EMBL) in Heidelberg, a four-element quadrupole−octopole

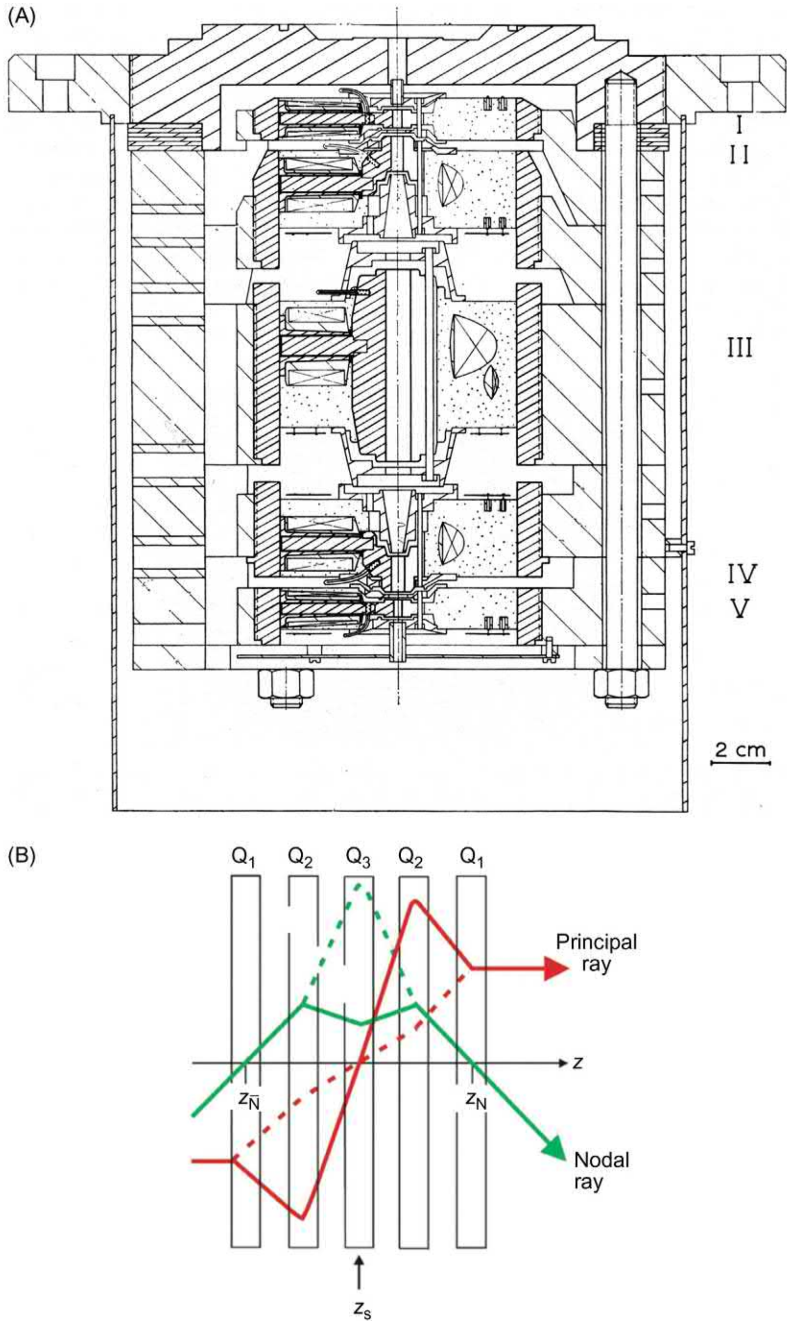

Figure 41.2

(A) Cross-section of the corrector of the Darmstadt microscope. Each of the five elements is a hybrid electrostatic–magnetic quadrupole. (B) Principal ray and nodal ray in the quintuplet. *After Hely (1982a), Courtesy Wissenschaftliche Verlagsgesellschaft* (A) and *after Rose (2009b), Courtesy Oxford University Press* (B).

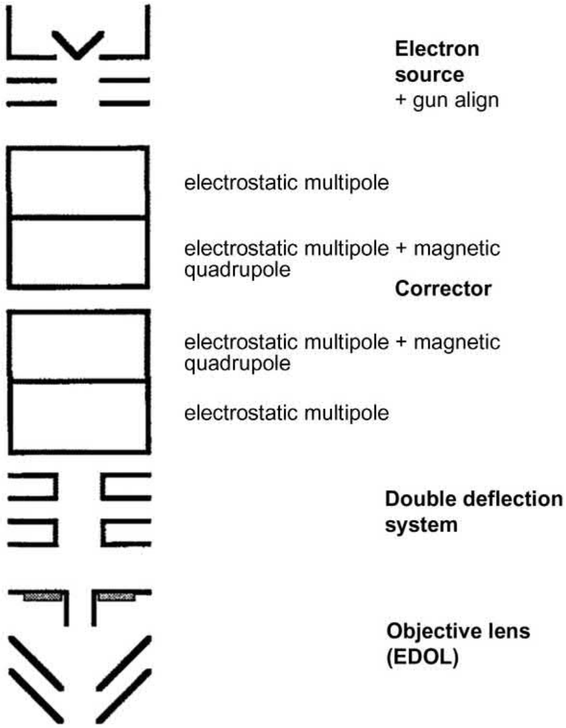

Figure 41.3
Incorporation of a quadrupole–octopole corrector in a low-voltage scanning electron microscope. *After Zach and Haider (1995), Courtesy Wissenschaftliche Verlagsgesellschaft.*

corrector was successful in improving the resolution of a scanning electron microscope from 5.6 nm to 1.8 nm (Fig. 41.3). Both spherical and chromatic aberration were corrected; the inner two quadrupoles of the quadruplet were mixed magnetic–electrostatic elements as in Hardy's studies (1967). The progress of this work can be followed in Zach and Rose (1987), Zach (1989a,b) and Zach and Haider (1994, 1995a,b). During the same period, a project to improve the resolution of a STEM by means of quadrupoles and octopoles was launched in the Cavendish Laboratory, Cambridge (Krivanek et al., 1996, 1997a,b). The six-element corrector (Fig. 41.4) was installed in a very early commercial STEM (a VG HB5, dating from 1974; see Wardell and Bovey, 2009, especially the Postscript) and in 1998, Krivanek et al. were able to show that the performance of the instrument had been improved, in the sense that fine fringes of graphitized carbon (002 planes) could be seen at a much smaller defocus than in the absence of the corrector (Krivanek et al., 1998, 1999a,b, 2000; Lupini et al., 2001). This encouraging result led Krivanek and colleagues (now established in Kirkland (WA) where Krivanek and Dellby had created the Nion company) to design an improved corrector consisting of four quadrupoles with octopoles (Fig. 41.5), with which a real gain in resolution was achieved (Batson et al., 2002; Batson, 2003a,b);

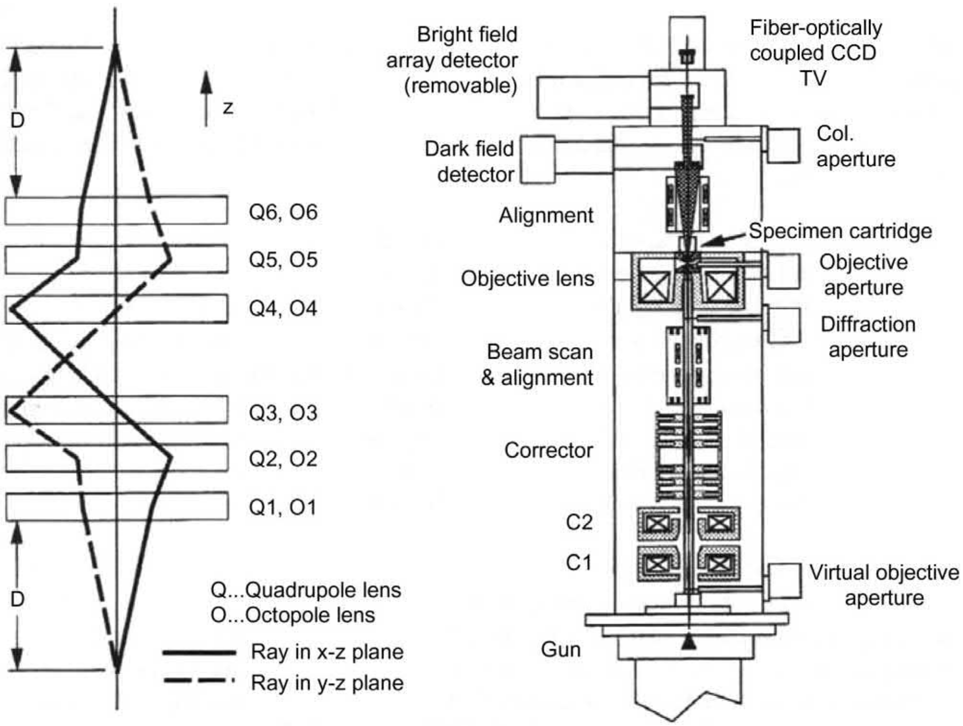

Figure 41.4
The first quadrupole−octopole corrector installed by Krivanek et al. in a VG STEM. *After Krivanek et al. (1996), Courtesy of the authors.*

this was confirmed by Nellist et al. (2003, 2004). Many such correctors were retrofitted to VG STEMs. It was becoming clear that any further improvement in resolution required correction of higher-order spherical aberration as well as certain other third-order aberrations and of course, the parasitic aberrations. For this, a new corrector was designed, composed of two quadrupole−octopole quintuplets (Fig. 41.6).

We shall see in Section 41.2.2 that, for several years, conventional transmission electron microscopes have been corrected by means of sextupole devices, inspired by the design of Rose (1990). In order to reach very high resolution, however, chromatic aberration had to be corrected as well as the geometric aberrations. The use of quadrupole−octopole correctors for conventional transmission electron microscopes was therefore revived.

It will prove convenient to examine the various quadrupole−octopole correctors chronologically, bringing out the optics of each. We shall concentrate on the physical principles whereby correction is achieved. These correctors are analysed in very great detail by Rose (2012) and we refer to his book and that of Erni (2010, 2015) and to the surveys of

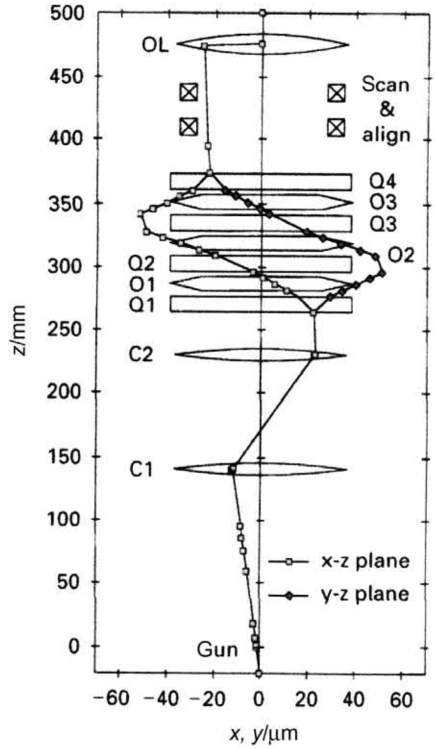

Figure 41.5
The structure of the Nion improved STEM aberration corrector. *After Krivanek et al. (1999), Courtesy Elsevier.*

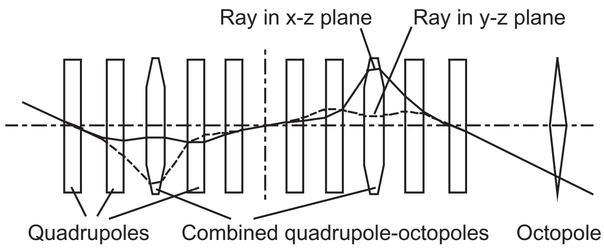

Figure 41.6
Quadrupole—octopole corrector consisting of two quadrupole—octopole quintuplets and a separate octopole. *After Krivanek et al. (2003), Courtesy Elsevier.*

Krivanek et al. (2008a,b, 2009a,b, 2015) and Hawkes and Krivanek (2018) for more ample information.

The Darmstadt corrector. Although this project could not be brought to a successful conclusion, very considerable progress was made. Rose (1971b) had shown that a symmetric telescopic quadrupole quintuplet can be made free of coma and free of the twofold chromatic aberration of simpler configurations. The various elements of the quintuplet and the axial and field rays in the $x-z$ and $y-z$ planes can be seen in Fig. 41.2B; the symmetry or antisymmetry of the individual elements about the midplane of the long central quadrupole is essential to eliminate the coma and the chromatic aberration. In a first stage, it was shown that the inner three mixed quadrupoles were able to provide chromatic correction (Kuck, 1979), after which the outer quadrupoles were added, as well as extra coils to combat the many parasitic aberrations (Bernhard, 1980). From this, it emerged that an unacceptably large fifth-order aberration was created by the central quadrupole−octopole element; this was reduced by replacing the central element by a dodecapole, which is capable of generating the desired fields with quadrupole and octopole symmetry free of the dodecapole component that was at the origin of the unwanted fifth-order aberration (Haider et al., 1982). Hely (1982a,b) gives a detailed description of the instrument with many diagrams. But after this, with Scherzer's death in 1982, the project was abandoned.

The Chicago corrector. We shall not say more than a few words about the Chicago STEM corrector, which consisted of a magnetic antisymmetric quadrupole−octopole quadruplet. It proved impossible to align the mechanical and electrical centres satisfactorily and this project too was abandoned. It is described in detail by Crewe (2009) and its progress can be followed in the long report reproduced there.

The Zach−Haider corrector for a low-voltage scanning electron microscope. At low voltages, the performance of a SEM is limited by chromatic aberration and a project was launched in the European Molecular Biology Laboratory in Heidelberg to design a suitable corrector, a quadrupole−octopole quadruplet incorporating two mixed quadrupoles to provide chromatic correction (Fig. 41.3). In the first design, the first and last quadrupole−octopoles were magnetic but this proved unsatisfactory, alignment could not be achieved. Zach therefore replaced them with electrostatic elements and the resolution of the SEM was appreciably improved (Zach, 1989a,b; Zach and Haider, 1994, 1995a,b). Such a corrector has been integrated into the JEOL JSM-7700F scanning electron microscope (Kazumori et al., 2004a,b: Uno et al., 2005; cf. Erdman and Bell, 2013). Hitachi too employ such a corrector (Kawasaki et al., 2009; Nakano et al., 2011; Hirose et al., 2011).

The Cambridge and Nion correctors. In 1994, funding was obtained for the construction of a quadrupole−octopole corrector for the scanning transmission electron microscope (Krivanek et al., 1996). The first design used a quadrupole sextuplet and differed in significant ways from its predecessors. In order to avoid the interactions between the quadrupole and octopole fields that had bedevilled the first model of the Zach−Haider corrector, the quadrupoles and octopoles were excited independently. By this date, computer technology had advanced to the stage at which misalignment could be rapidly diagnosed, notably with the aid of the Ronchigram (Section 41.2.4) and the appropriate currents could then be fed back to the alignment coils. We note in passing that this was probably the factor that made correction a reality in the 1990s. By 1997, Krivanek et al. had shown that their corrector could reduce the probe-size of the elderly VG HB5 STEM (a 1974 model) in which it had been installed and soon after, they showed that their test object, graphitized carbon, could be imaged at a much smaller defocus than in the absence of the corrector. This, coupled with the interest shown by Philip Batson at the IBM Watson Research Centre, encouraged Krivanek and his partner, Niklas Dellby, to construct an improved corrector. This was a quadruplet with three octopoles; installed in a VG HB501 STEM, it enabled Batson to attain a resolution better than 1 Å in 2001 (Batson et al., 2002; see Hawkes 2015 for historical details). These first correctors were installed in VG STEMs but this revealed weaknesses of these modified instruments, notably their sensitivity to mechanical and electrical perturbations. Nion therefore embarked on the design and construction of a new STEM, incorporating a corrector of many third- and fifth-order geometrical aberrations as well as several engineering improvements (Krivanek et al., 2008b; Dellby et al., 2011). The corrector now consisted of three quadrupole quadruplets and three quadrupole−octopole elements (Fig. 41.7). An additional quadrupole triplet coupled the corrector to the coma-free plane (24.134) of the probe-forming lens. If we denote the quadruplets by Q_4 and the quadrupole−octopole elements by QO, the sequence is Q_4−QO−Q_4−QO−Q_4−QO−Q_4; the first quadrupole of the fourth Q_4 is part of the preceding QO and the remaining three form the triplet. Two modes of operation have been studied: a 'symmetric' mode (Fig. 41.8A) in which the overall structure displays the mechanical symmetry and electrical antisymmetry of a Russian multiplet (Section 19.1) and an 'antisymmetric' mode (Fig. 41.8B). Both configurations are capable of eliminating third- and fifth-order geometrical aberrations with the result that geometrical aberrations of the next higher order become the limiting factors. For the symmetric mode, this is $C_{7,4}$

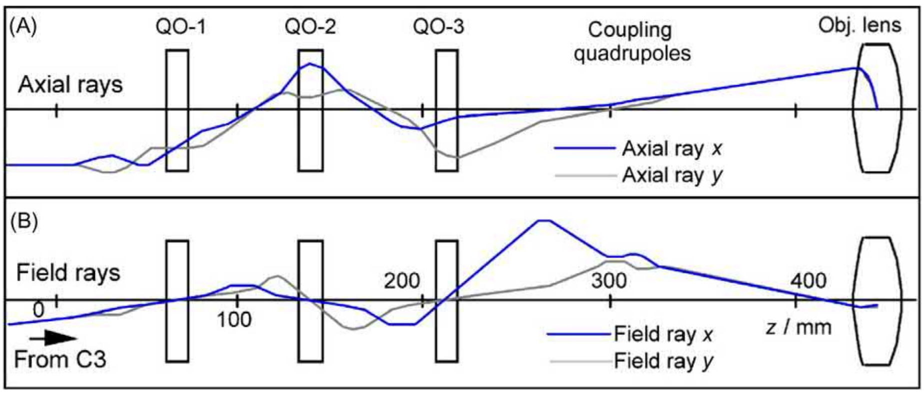

Figure 41.7
The sequence of elements in the Nion third-generation corrector, showing the three quadrupole−octopole units. Quadrupole quadruplets are situated before, between and after these. The first component of the final quadruplet is part of QO-3, the remainder thus forms a triplet between QO-3 and the probe-forming lens. *After Krivanek et al. (2008a), Courtesy Elsevier.*

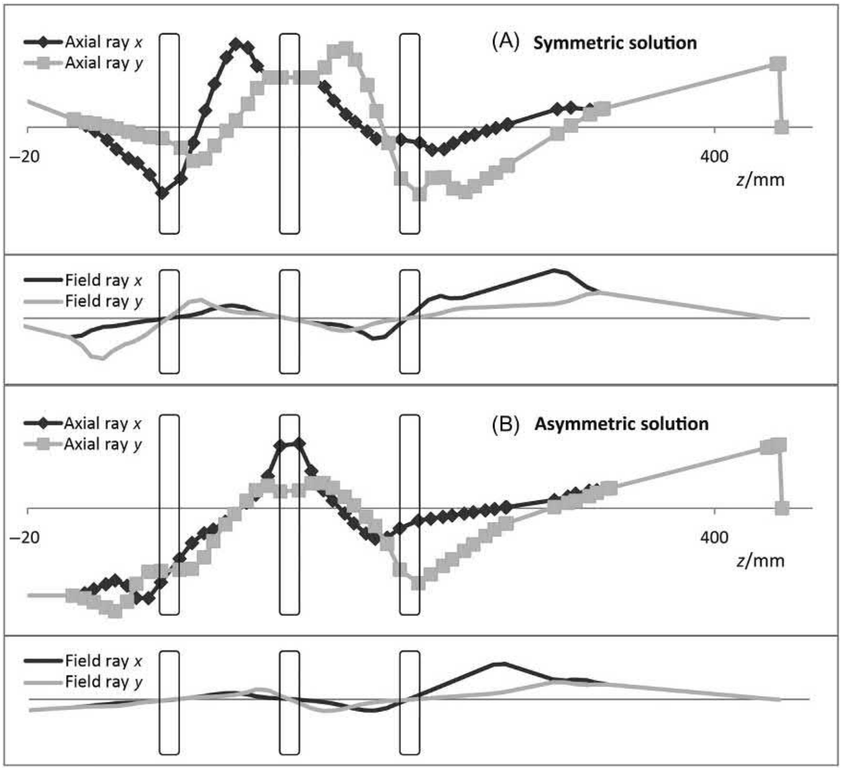

Figure 41.8
The two modes of operation of the corrector of Fig. 41.7. (A) Symmetric mode. (B) Asymmetric mode. *After Dellby et al. (2001), Courtesy Oxford University Press.*

(in Krivanek's notation, see Section 31.6) while for the antisymmetric mode, it is $C_{7,8}$. The antisymmetric configuration has the advantage that any chromatic aberration is smaller (see Dellby et al., 2008, for values of the various coefficients).

Chromatic correction in the conventional transmission electron microscope. If chromatic correction is not required, correctors based on sextupoles are preferable for conventional transmission electron microscopes (Section 41.2.2). When it is essential to cancel the chromatic aberration, however, quadrupoles cannot be avoided and sophisticated correctors have been designed for this purpose, for the Transmission Electron Aberration-corrected Microscope (TEAM) project (Kisielowski et al., 2008; Dahmen et al., 2009), for the PICO microscope in Jülich, for the Sub-ångström Low-voltage Electron Microscope (SALVE, Kaiser et al., 2009, 2011; Rose and Kaiser, 2012; Linck et al., 2016a,b; Müller et al., 2016) and for the Japanese CCC instrument (Sawada et al., 2011).

Two strategies are possible: either a hybrid quadrupole corrector is placed in tandem with a regular sextupole corrector or an elaborate quadrupole−octopole sequence is designed to

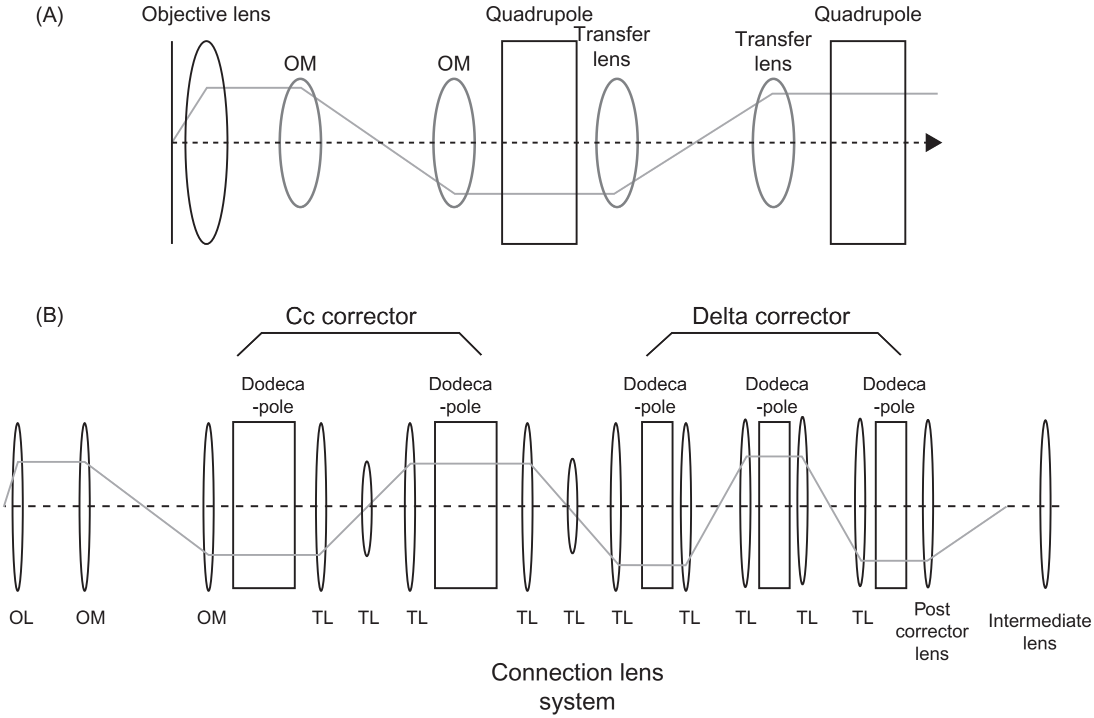

Figure 41.9

Chromatic and geometrical aberration correctors in tandem. (A) Chromatic correction provided by an antisymmetric quadrupole doublet with negative focal length. (B) The complete corrector.OL, objective lens; TL, transfer lens; OM, objective minilens. *After Sawada et al. (2011), Courtesy Elsevier.*

provide all the required types of correction. For a transmission electron microscope, off-axis geometrical aberrations must be corrected as well as the spherical aberration, with the result that many quadrupoles are necessary. The first solution is illustrated in Fig. 41.9B. All the correction elements consist of dodecapoles, which are capable of generating the quadrupole fields of the chromatic aberration corrector and the sextupoles of the geometric aberration corrector (Section 41.2.2). The chromatic correction is assured by means of an antisymmetric hybrid quadrupole doublet (Fig. 41.9A) and the geometric aberration corrector is the delta corrector described below.

If all the necessary correction is to be provided by quadrupoles and octopoles, complemented by other multipole fields to eliminate parasitic effects, the number of individual elements increases considerably. The device must not only be capable of cancelling the chromatic and spherical aberrations but must also be free of aberrations that are linear in the off-axis coordinates (comas). Furthermore, the remaining third-order geometrical aberrations, astigmatism and field curvature, which can usually be neglected, must not be large enough to contribute to coma of fifth order. (We recall that there are two

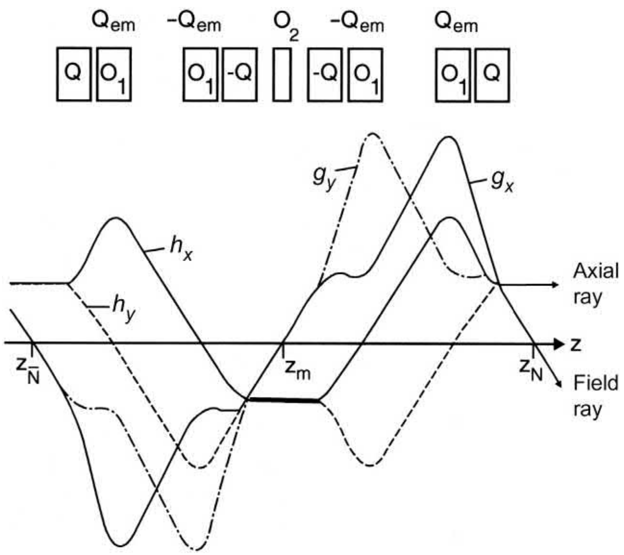

Figure 41.10
Achromatic semi-aplanat employing two symmetrically excited multipole quadruplets. The required fields are created by dodecapoles. *After Rose (2012), Courtesy Springer Verlag.*

contributions to fifth-order aberration coefficients, one coming from $M^{(5)}$, the other obtained by substituting the third-order solution in $M^{(2)}$.) Quadrupoles and octopoles have many more intrinsic aberrations than round lenses so it is clearly highly desirable to find configurations possessing symmetries for which these additional aberrations cancel out. Systems with this property are the doubly symmetric configurations. These are quadrupole multiplets consisting of two identical subunits. The quadrupoles that make up each subunit are symmetric about the midplanes of the subunit. The subunits may be excited symmetrically or antisymmetrically. In the first case, the excitations of the various quadrupoles are symmetric with respect to the centre-plane of the whole device; in the second case, the excitations are antisymmetric about this plane.

We have already seen that antisymmetric or Russian quadruplets have attractive features and by assembling two such quadruplets in tandem, we obtain the symmetric configuration (Fig. 41.10). The sequence is as follows

first quadruplet: $(\mathrm{Q}) - (\mathrm{QE} + \mathrm{QM} + \mathrm{O}_1) - (-\mathrm{QE} - \mathrm{QM} + \mathrm{O}_1) - (-\mathrm{Q})$

centre-plane: O_2

second quadruplet: $(-\mathrm{Q}) - (-\mathrm{QE} - \mathrm{QM} + \mathrm{O}_1) - (\mathrm{QE} + \mathrm{QM} + \mathrm{O}_1) - (\mathrm{Q})$

For clarity, we have written $\pm\mathrm{QE} \pm \mathrm{QM} + \mathrm{O}_1$ but in practice these are hybrid dodecapoles, capable of generating all the desired field components. The separation between the two quadruplets is chosen in such a way that the image principal plane (or nodal plane, the nodal and principal planes coincide here) of the first quadruplet and the object principal plane of the second quadruplet coincide. It can be shown that this arrangement satisfies all the desired conditions, in particular, cancellation of the chromatic and third-order aperture aberrations; the octopoles do not create any field aberrations.

The alternative antisymmetric configuration proposed by Rose consists of two quadrupole sextuplets. Here, the excitation of each sextuplet is symmetric about its midplane. Conversely, the excitations of the second sextuplet are the reverse of those of the first sextuplet: the whole device is thus antisymmetric, as in a Russian multiplet. Octopoles are placed in the midplanes of the sextuplets and a third octopole (with a different excitation) is placed outside the main structure. How can such a corrector be used in conjunction with an objective lens without introducing coma? In the solution found by Rose, two adaptor lenses, L_1 and L_2, enclose the twin-sextuplet device in such a way that the image focal plane of L_1 coincides with the object focal plane of the corrector element. Likewise, the object focal plane of L_2 coincides with the image principal (or nodal) plane of the corrector. And finally, the third octopole (O_2 in Fig. 41.11) is placed at the image focus of L_2 and suitably rotated. These two round lenses form a telescopic doublet. By replacing four of the quadrupoles with hybrid electrostatic–magnetic quadrupoles, chromatic correction is obtained as well as correction of the geometric aberrations; these hybrid quadrupoles replace the basic quadrupoles on either side of the octopoles O_1.

Examination of Fig. 41.11 suggests that each octopole O_1 can be combined with the adjacent mixed quadrupoles, thus reducing each sextuplet to a quintuplet. A slightly modified version of this double-quintuplet device is employed in the TEAM instrument;

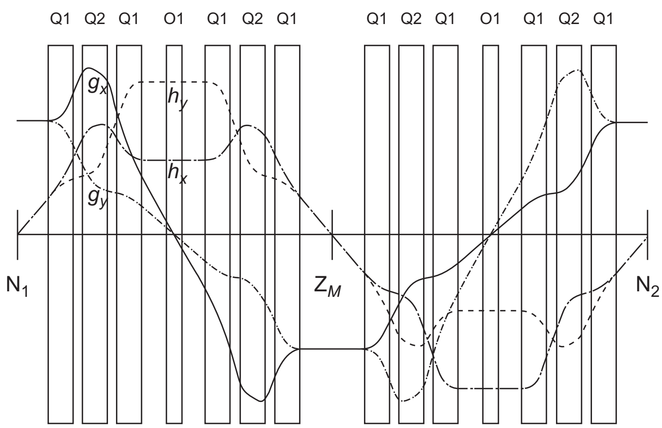

Figure 41.11
Telescopic doubly symmetric quadrupole–octopole corrector. An octopole is situated between each of the outer two symmetric quadrupole triplets. *After Rose (2012), Courtesy Springer Verlag.*

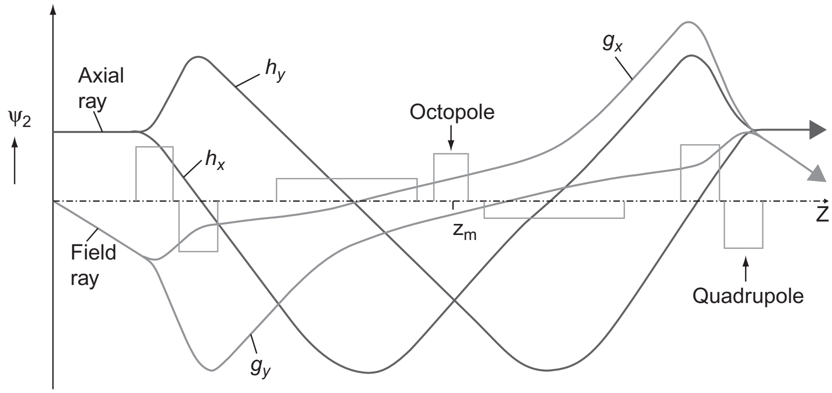

Figure 41.12
The configuration adopted for the SALVE microscope. The boxes indicate schematically the quadrupole strengths. *After Rose (2012), Courtesy Springer Verlag.*

here, a telescopic round-lens transfer doublet is introduced to couple the quintuplets. Anisotropic coma is eliminated by placing four skew octopoles symmetrically about the midplane of the corrector.

A simpler arrangement, also capable of correcting the spherical and chromatic aberrations, has been adopted for the SALVE project in the University of Ulm. A quadrupole doublet is now situated at each extremity of the device. Between these are two mixed quadrupoles and a central octopole. Two more octopoles are combined with the inner members of the quadrupole doublets (Fig. 41.12).

If we are willing to use still more quadrupoles and octopoles, a device that can correct *all* the primary geometrical and chromatic aberrations can be devised. This is Rose's *ultracorrector* (Rose, 2003, 2004). Four quadrupole quadruplets are required and thirteen octopoles. Fig. 41.13 shows how these are disposed. The fundamental rays are included in Fig. 41.13A and B. The rays shown in Fig. 41.13C are the fundamental pseudorays, defined by

$$u_\omega = \frac{1}{2}\left(t_x + t_y\right) \quad u_{\overline{\omega}} = \frac{1}{2}\left(t_x - t_y\right)$$
$$u_\eta = \frac{1}{2}\left(s_x + s_y\right) \quad u_{\overline{\eta}} = \frac{1}{2}\left(s_x - s_y\right)$$

These show the midplane symmetry: u_ω and $u_{\overline{\eta}}$ are symmetric about the midplane while $u_{\overline{\omega}}$ and u_η are antisymmetric. We refer to Rose's article for details of the correction procedure and in particular for the choice of geometry and excitations that enables correction to be attained systematically.

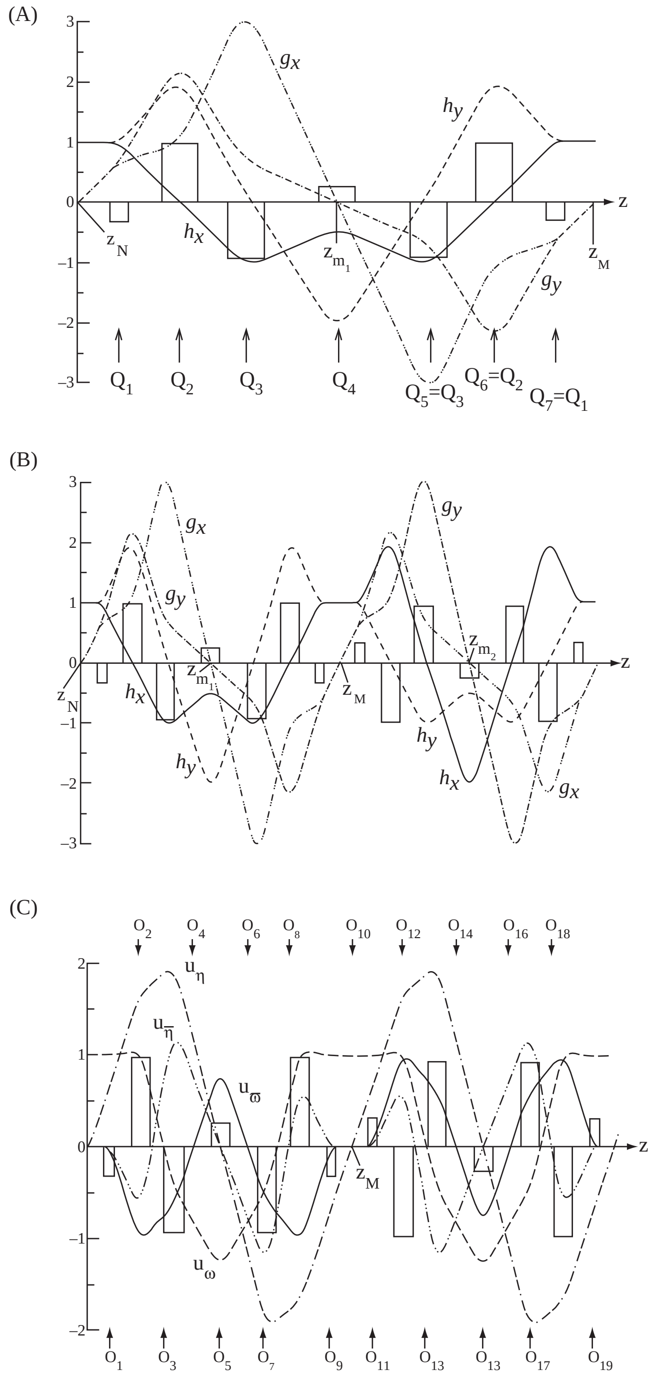

Figure 41.13

Rose's ultracorrector. (A) The positions and strengths of the quadrupoles in the first half of the device. (B) The complete ultracorrector. (C) The positions of the octopoles. The rays shown here are the fundamental pseudorays. *After Rose (2008), Courtesy Institute of Physics Publishing.*

Scherzer's all-electrostatic chromatic aberration corrector. Another of Scherzer's suggestions for aberration correction was inspired by the form of the chromatic aberration coefficients of combined electrostatic round lenses and quadrupoles. We have

$$\begin{aligned} C_{cx} &= -\int\left(\frac{\phi_0}{\phi}\right)^{1/2}\left(\frac{3}{8}\frac{\phi'^2}{\phi^2}-\frac{p_2}{2\phi}\right)h_x^2dz \\ C_{cy} &= -\int\left(\frac{\phi_0}{\phi}\right)^{1/2}\left(\frac{3}{8}\frac{\phi'^2}{\phi^2}+\frac{p_2}{2\phi}\right)h_y^2dz \end{aligned} \tag{41.1a}$$

which can be transformed into[1]

$$\begin{aligned} C_{cx} &= \frac{1}{2}\int\left(\frac{\phi_0}{\phi}\right)^{1/2}\left\{\left(\frac{h_x'}{h_x}-\frac{\phi'}{4\phi}\right)^2-\frac{\phi'^2}{8\phi^2}\right\}h_x^2dz \\ C_{cy} &= \frac{1}{2}\int\left(\frac{\phi_0}{\phi}\right)^{1/2}\left\{\left(\frac{h_y'}{h_y}-\frac{\phi'}{4\phi}\right)^2-\frac{\phi'^2}{8\phi^2}\right\}h_y^2dz \end{aligned} \tag{41.1b}$$

This transformation is best performed using Seman's procedure. The general form of the C_c integrand is obtained by considering the terms generated by

$$\left(\frac{d}{dz}\right)h^2\ \ \phi^{-1/2}$$

which are $hh'\phi^{-1/2}$ and $h^2\phi'\phi^{-3/2}$. Differentiating these and eliminating h'', we find

$$\begin{aligned} h'^2-\frac{hh'\phi'}{\phi}-\frac{h^2\phi''}{4\phi}\pm\frac{h^2p_2}{4\phi} &= 0 \\ 2\frac{hh'\phi'}{\phi}-\frac{3h^2\phi'^2}{2\phi^2}+\frac{h^2\phi''}{\phi} &= 0 \end{aligned}$$

(The plus sign corresponds to C_{cx} and the minus sign to C_{cy}; h denotes h_x in C_{cx} and h_y in C_{cy}.) These identically zero quantities are multiplied by arbitrary weights (λ and μ) and then added to the basic expressions for C_{cx} and $\mathrm{C_{cy}}$. The weights are chosen to eliminate terms in p_2 and ϕ'': $\lambda=-2$ and $\mu=-1/2$. From this, Eq. (41.1b) emerge.

We can ensure that both coefficients are negative by requiring that

$$\frac{h_x'}{h_x}=\frac{\phi'}{4\phi}$$

[1] Since $p_2(z)$ has been eliminated, the signs of the terms in C_{cx} and C_{cy} are the same.

or

$$h_x(z) = \left(\frac{\phi(z)}{\phi_0}\right)^{1/4} \tag{41.2}$$

and likewise for $h_y(z)$. From the paraxial equations

$$h_x'' + \frac{\phi'}{2\phi}h_x' + \frac{\phi'' - p_2}{4\phi}h_x = 0$$
$$h_y'' + \frac{\phi'}{2\phi}h_y' + \frac{\phi'' + p_2}{4\phi}h_y = 0$$

we deduce that $p_2(z)$ must take the form

$$p_2(z) = \frac{\phi''}{2} - \frac{\phi'^2}{16\phi} \tag{41.3}$$

as derived by Scherzer (1947). Such a field distribution can be created by means of a quadrupole triplet but although this will function as desired in one of the principal sections, it will have an unwanted focusing effect in the other. In order to obtain a true corrector, more quadrupoles must be added. Fig. 41.14 shows a suitable arrangement and the form of $p_2(z)$; the ideal form of $p_2(z)$ that would satisfy the Scherzer condition exactly is also shown. A second set of quadrupoles is needed to achieve correction in the other principal section; the polarity is the reverse of that in the first corrector. For a suitable separation between the two parts, the complete corrector does not introduce any chromatic distortion, coma or aberration with twofold symmetry (Weißbäcker and Rose, 2000, 2001a,b). Rose observes that such a corrector is more suitable for ions than for electrons.

41.2.2 Sextupole Optics and Sextupole Correctors

Correction of the spherical aberration of a round lens requires a device with an aperture aberration similar to that of the lens but of opposite sign. The fact that a sextupole has such an aberration has long been known (Hawkes, 1965a) but its consequent potential for aberration correction passed unnoticed until 1979 when Beck suggested that a sextupole doublet might make a good corrector (Beck, 1979, 2011). Crewe and Kopf (1980a,b) took up the suggestion and used a simple model to show that a triplet consisting of two identical sextupoles on either side of a weak round lens (Fig. 41.15) would make a suitable corrector for a high-quality probe-forming lens for a STEM. Further studies followed (Crewe, 1980, 1982, 1984; Shao, 1988a,b), all of which confirmed the earlier predictions, and Ximen and Crewe (1985) have enquired whether the other aberrations of such a corrector could be compensated satisfactorily. Ximen et al. (1985) have considered the correction in wave-optical terms and Ximen (1988) has obtained expressions for all the aberration coefficients of a system containing magnetic round lenses and sextupoles.

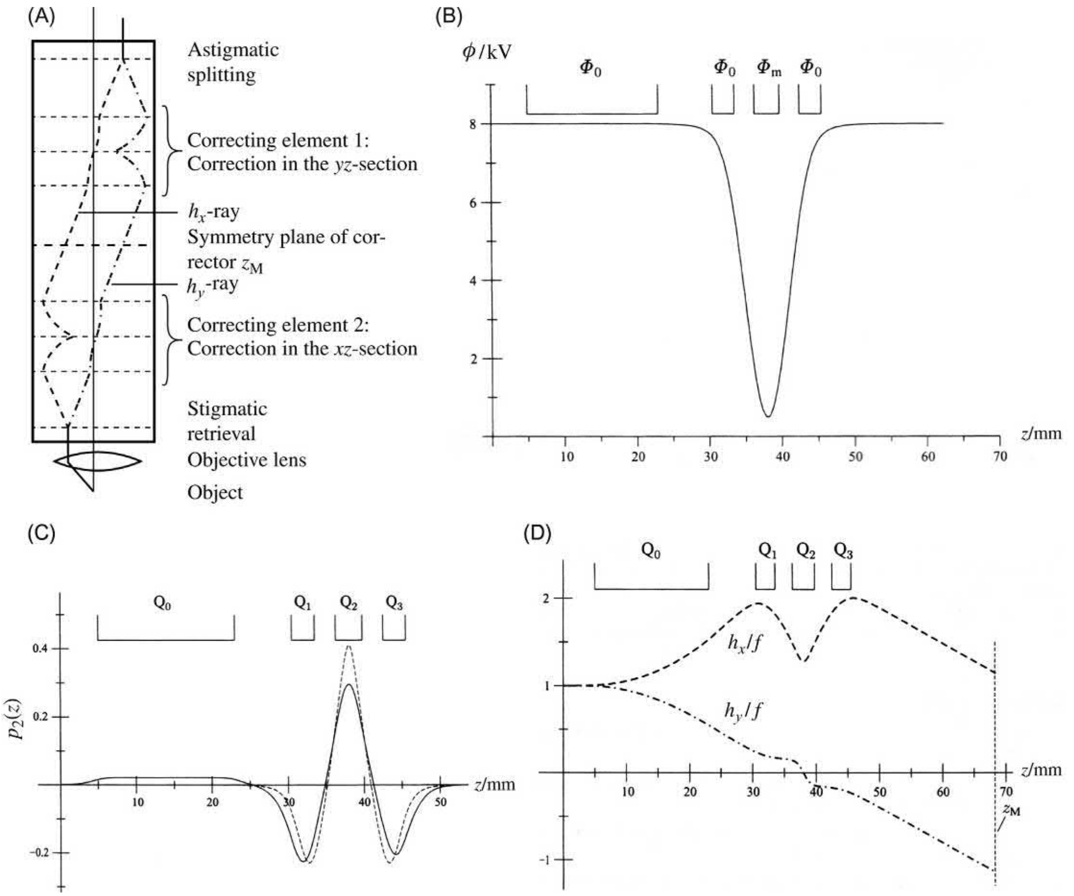

Figure 41.14

Scherzer's electrostatic corrector (ECO). (A) Fundamental rays in the entire corrector. (B) Axial potential $\phi(z)$ in one half of the corrector. (C) Real quadrupole distribution $p_2(z)$ (full line) and the ideal form of $p_2(z)$ (dotted line) in kV/mm^2. (D) Fundamental rays. *After Weißbäcker and Rose (2001), Courtesy Oxford University Press.*

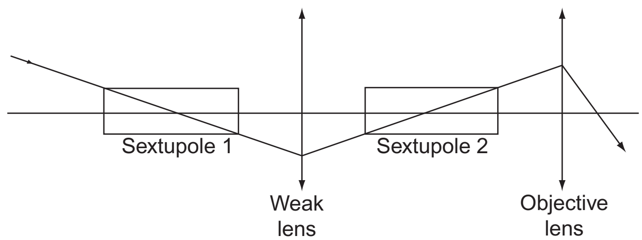

Figure 41.15

The sextupole corrector proposed by Crewe and Kopf. *After Crewe and Kopf (1980a), Courtesy Wissenschaftliche Verlagsgesellschaft.*

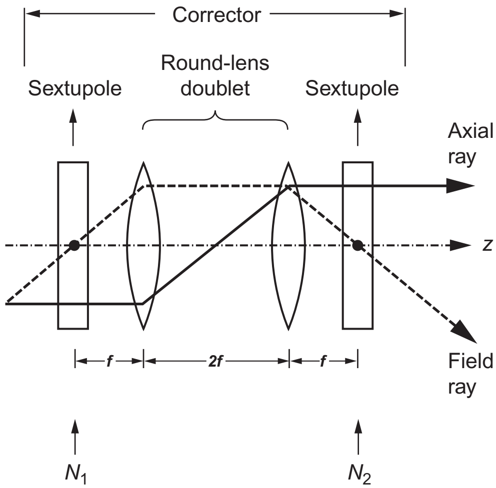

Figure 41.16
The basic element of a sextupole corrector. *After Rose (2002), Courtesy Springer Verlag.*

The aberrations of sextupole systems have also been extensively analysed by Rose (1981), for sextupole field components had been needed in an earlier project (Rose and Plies, 1973; Plies, 1973, 1974). On the basis of his aberration theory, Rose arrived at a system in which round lens fields separate two sextupoles and it is on his detailed proposal (Rose, 1990) that the later sextupole correctors are based. Similar designs emerge from the Lie algebra approach (Dragt and Forest, 1986). Funding for a project to incorporate a sextupole corrector based on Rose's design in a transmission electron microscope was obtained in 1992 by Max Haider, Harald Rose and Knut Urban (Haider, 1996; Uhlemann et al., 1996). The basic design is shown in Fig. 41.16. The first results were published in 1998 (though submitted to both *Nature* and *Science* in 1997) (Haider and Uhlemann, 1998; Haider and Zach, 1998; Haider et al., 1998a–c; Rose et al., 1998). The company CEOS (Corrected Electron Optical Systems), launched by Haider and Zach in 1996, supplied many such correctors. The development of the CEOS sextupole correctors is recorded in the following publications: Haider et al. (1994, 1995, 2008a–c, 2009), Haider (2000), Müller et al. (2008, 2010, 2011, 2012) and Haider and Uhlemann (2014). See Hawkes (2009a, 2015) and Rose (2008, 2009b) for many additional references and historical details.

We note that analyses of sextupoles in connection with ion optics had been made by Boerboom (1972), Taya and Matsuda (1971, 1972), Taya (1978) and Matsuo et al. (1982).

Sextupole optics. The function $M^{(3)}$ takes the form

$$M^{(3)} = -\frac{\gamma\hat{\phi}^{1/2}}{12}\frac{p_3 x(x^2 - 3y^2) + q_3 y(3x^2 - y^2)}{\hat{\phi}} - \frac{1}{6}\eta\left\{P_3 y(3x^2 - y^2) - Q_3 x(x^2 - 3y^2)\right\} \quad (41.4)$$

We shall be interested in systems consisting of a round magnetic lens followed (or preceded in the case of probe-forming lenses) by one or more sextupoles. We allow for this combination by writing the paraxial ray arriving at the sextupole as

$$w^{(1)} = u^{(1)}\exp(-\mathrm{i}\theta) \tag{41.5}$$

We shall need the 'sextupole function' $S(z)$, defined by

$$S(z) = -\mathrm{e}^{-3\mathrm{i}\theta}\frac{1}{6}\left\{\left(\frac{\hat{\phi}}{\hat{\phi}_0}\right)^{1/2}\frac{\gamma}{2}\frac{p_3+\mathrm{i}q_3}{\hat{\phi}}+\mathrm{i}\frac{\eta}{\hat{\phi}_0}(P_3+\mathrm{i}Q_3)\right\} \tag{41.6}$$

From Eq. (41.1), we find that the second-order effect of the sextupole is of the form

$$u^{(2)} = \overline{\omega}^2 u_{11} + \overline{\omega\rho} u_{12} + \overline{\rho}^2 u_{22} \tag{41.7}$$

where we have written

$$u(z) = x + \mathrm{i}y = \rho g(z) + \omega h(z) \tag{41.8}$$

We leave the exact forms of $g(z)$ and $h(z)$ undefined for the moment but we shall be associating them with rays satisfying the same conditions as the field ray $g(z)$ and the axial ray $h(z)$ in Chapter 15, Systems With an Axis of Rotational Symmetry, (15.6). We find

$$\begin{aligned} u_{11} &= 3(hS_1 - gS_0) \\ u_{12} &= 6(hS_2 - gS_1) \\ u_{22} &= 3(hS_3 - gS_2) \end{aligned} \tag{41.9}$$

in which

$$\begin{aligned} S_0 &= \int_{z_0}^{z} S(\zeta)\, h^3 d\zeta \\ S_1 &= \int_{z_0}^{z} S(\zeta) g\, h^2 d\zeta \\ S_2 &= \int_{z_0}^{z} S(\zeta)\, g^2 h d\zeta \\ S_3 &= \int_{z_0}^{z} S(\zeta)\, g^3 d\zeta \end{aligned} \tag{41.10}$$

Our objective is to use these expressions to help find sextupole combinations that have no second-order effect. They will thus be promising devices for correcting the spherical aberration of the round lens since only their third-order effects will be present, and we have seen that these are of the same nature as those of a round lens but not necessarily of the same sign. Clearly, S_1, S_2 and S_3 cannot all vanish in a single sextupole. In a doublet, however, we can arrange that the rays $h(z)$ and $g(z)$ exhibit symmetries that make it possible to cancel all three quantities. Suppose that one of these rays, $h(z)$, is symmetric about the central plane of the doublet and about the midplane of each individual sextupole and that the other ray, $g(z)$, is antisymmetric about these planes. Then terms linear in $h(z)$ will be the same in each sextupole while terms linear in $g(z)$ will make equal and opposite contributions. By introducing a round lens doublet between the two sextupoles, the integrals involving $h(z)$ will also cancel out, and we arrive at a configuration such as Fig. 41.16. The round (magnetic) lenses must have the same excitation but be wound in opposite directions to cancel the rotation.

Sextupole corrector design. We have thus found a sextupole arrangement free of quadratic effects. How can we use this to cancel some or even all of the third-order geometric aberrations of a round lens? We shall show that suitable sextupole systems can be found and that these become progressively more complex as the number of aberrations to be eliminated increases. Rose has analysed such systems with the aid of a simple model of the sextupole function $S(z)$ and we too adopt this strategy, following his reasoning closely (Rose, 2012, Chapter 9). The model is similar to the rectangular model for quadrupoles (39.2):

$$S(z) = \begin{cases} S_0 & \bar{z} - L/2 \leq z \leq \bar{z} + L/2 \\ 0 & \text{elsewhere} \end{cases} \tag{41.11}$$

where $z = \bar{z}$ is the centre of the sextupole. Provided that no round lens field overlaps the sextupole zone, the paraxial rays $g(z)$ and $h(z)$ are straight lines:

$$g(z) = \frac{z - z_N}{f_o} \qquad h(z) = f_o \tag{41.12}$$

where f_o is the focal length of the lens to be corrected and z_N is the (object) nodal plane of the corrector. The aberration coefficients of the sextupole (subscript S) are found to be as follows:

$$\begin{aligned} C_{3S} &= -6S_0^2 L^3 f_o^4 \\ F_{3S} &= -A_{3S} = \frac{3}{5} S_0^2 L^5 \end{aligned} \tag{41.13}$$

Coma and distortion both vanish. (We have included the subscript '3' as a reminder that these are of the same nature as the third-order aberrations of round lenses. The choice of symbols is also the same, C denoting spherical aberration, F field curvature and A astigmatism.)

From these formulae we see that a sextupole device can correct spherical aberration since the sign of C_{3S} is negative. The field curvature, however, has the same sign as that of a round lens and cannot be removed by this simple scheme.

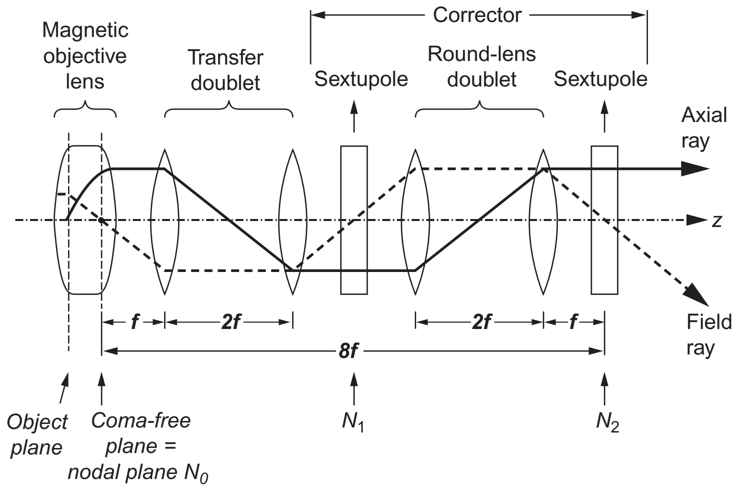

Figure 41.17

The basic element of Fig. 4.16 coupled to a round lens to form a semi-aplanat. *After Rose (2012), Courtesy Springer Verlag.*

The next important aberration is coma, being linear in the off-axis coordinate. The coma of a round lens can be avoided by arranging that the crossover at the source is conjugate to the coma-free point of the lens but the sextupoles introduce isotropic coma and also a threefold coma. Fortunately, these can be eliminated when the symmetries described earlier are respected. For this, the coma-free point of the round lens and the object nodal point of the corrector must coincide or be conjugates. The coma-free point is immersed in the lens and these points are therefore rendered conjugate by introducing further round lenses (a transfer doublet) between the round lens and the corrector. The resulting arrangement, known as a *semi-aplanat*, is shown in Fig. 41.17; the prefix 'semi' is a reminder that round lens coma has an isotropic and an anisotropic part and that the present system cannot correct the anisotropic part. Fortunately, this is often so small that it can be tolerated but we shall see below that it can be removed if necessary by increasing the complexity of the system.

The next aberrations that need consideration are field curvature and astigmatism. These too can be cancelled by increasing the number of sextupoles. A suitable configuration is shown in Fig. 41.18; we shall not reproduce the reasoning that leads to this arrangement, it is presented very clearly by Rose (2012, Section 9.2.5). Note that the orientation of the sextupoles S_1 and S_5 is not the same as that of S_2 and S_4 and that the polarity of S_2 and S_4 is the opposite of that of sextupoles $S_1 = S_5$ and S_3. We reproduce Rose's expressions for the aberration coefficients of this device (using the rectangular model) as they reveal that only the spherical aberration depends on the 'telescopic magnification' and hence on the position of the device relative to the round lens. The position of the corrector or *planator*, subscript P, can therefore be chosen to ensure that the spherical aberration is still corrected.

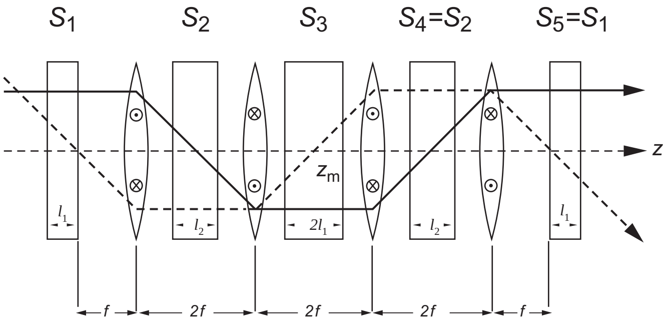

Figure 41.18
Sequence of sextupoles and round lenses for which third-order astigmatism and field curvature are cancelled. *After Rose (2012), Courtesy Springer Verlag.*

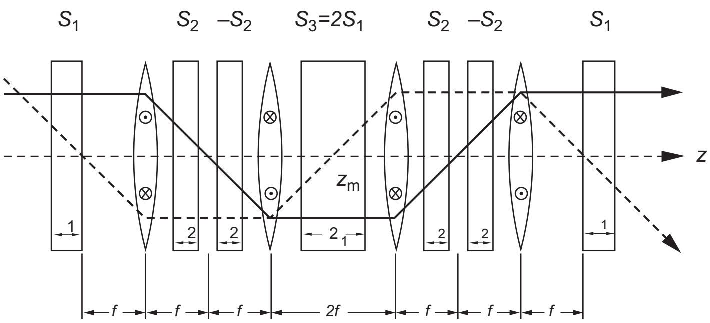

Figure 41.19
Sequence of sextupoles and round lenses for which third-order astigmatism, isotropic and anisotropic coma are cancelled. *After Rose (2012), Courtesy Springer Verlag.*

$$
\begin{aligned}
C_{3P} &= -3h^4(z_c)\left\{4L_1^3|S_1|^2 + \frac{1}{56}\frac{L_2^7}{f^4}|S_2|^2 + \frac{L_1L_2^3}{f}\Re(S_1S_2^*)\right\}\\
F_{3P} &= -\frac{24}{5}L_1^5|S_1|^2 + \frac{3}{5}L_2^5|S_2|^2 + 4\frac{L_1^3L_2^3}{f}\Re(S_1S_2^*)\\
A_{3P} &= -\frac{21}{5}L_1^5|S_1|^2 - \frac{3}{5}L_2^5|S_2|^2 - \frac{L_1^3L_2^3}{f}S_1S_2^* - 36L_1L_2f^3S_1^*S_2\\
K_{3P} &= D_{3P} = 0
\end{aligned}
\tag{41.14}
$$

The focal length f is defined in Fig. 41.18.

Finally we return to the coma. If it proves necessary to eliminate the anisotropic coma as well as the isotropic part, the symmetry that has proved so effective so far must be relaxed. A suitable arrangement is shown in Fig. 41.19. This consists of seven sextupoles in all.
The basic structure or skeleton consists of two pairs of sextupoles S_1 and the first half of S_3

followed by the second half of S_3 and $S_7 = S_1$. In between each pair of these sextupoles is placed a round-lens doublet, which itself encloses two more sextupoles, S_2 and $-S_2$. The latter breaks the overall symmetry as required. Rose finds

$$\begin{aligned}
C_{3S} &= -12 f_0^4 \left(|S_1|^2 L_1^3 + \frac{3}{7}\frac{L_2^7}{f^4} |S_2|^2 \right) \\
K_{3S} &= 3 L_1 L_2^2 f_0^2 f \left(12 S_1 S_2^* - S_1^* S_2 \frac{L_1^2 L_2^2}{f^4} \right) \\
A_{3S} &= -\frac{3}{5}\left(7|S_1|^2 L_1^5 - 18 |S_2|^2 L_2^5 \right) \\
F_{3S} &= -\frac{24}{5}\left(|S_1|^2 L_1^5 + 6 |S_2|^2 L_2^5 \right) \\
D_{3S} &= 12\mathrm{i}\Im(S_1^* S_2)\frac{L_1^3 L_2^2 f}{f_0^2}
\end{aligned} \tag{41.15}$$

The last terms in C_{3S} and K_{3S} will normally be negligible since f is at least double the length of a sextupole; S_1 can be chosen to be real. We therefore require that

$$C_s = -C_{3S} \text{ and } K = -K_{3S}$$

and hence that

$$S_1 = S_1^* \approx \frac{1}{2 f_0^2 L_1}\left(\frac{C_s}{3L_1}\right)^{1/2} \qquad S_2 = -\frac{K - ik}{6 L_2^2 f}\left(\frac{L_1}{3C_s}\right) \tag{41.16}$$

Since

$$\left|\frac{S_2}{S_1}\right| \approx \frac{|K|}{3C_s}\frac{f_0^2 L_1^2}{f L_2^2}$$

S_2 will be much weaker than S_1 so that correction of coma will fortunately not have much effect on the spherical aberration correction. Once coma has been corrected, it is no longer necessary to make the coma-free point of the lens and the nodal point of the corrector conjugate; this degree of freedom allows us to shift the image of the coma-free point ($z = z_K$) away from the nodal point ($z = z_N$) by a distance λ say. This creates a coma, $K = C_s \lambda / f_0^2$ and a fifth-order spherical aberration, $C_5 = 3K_3 C_s$. The coma can be cancelled and we thus have a means of varying the fifth-order spherical aberration.

Rose completes his account of sextupole correctors by showing that the round lens can be designed in such a way that the system is reasonably insensitive to energy variations.

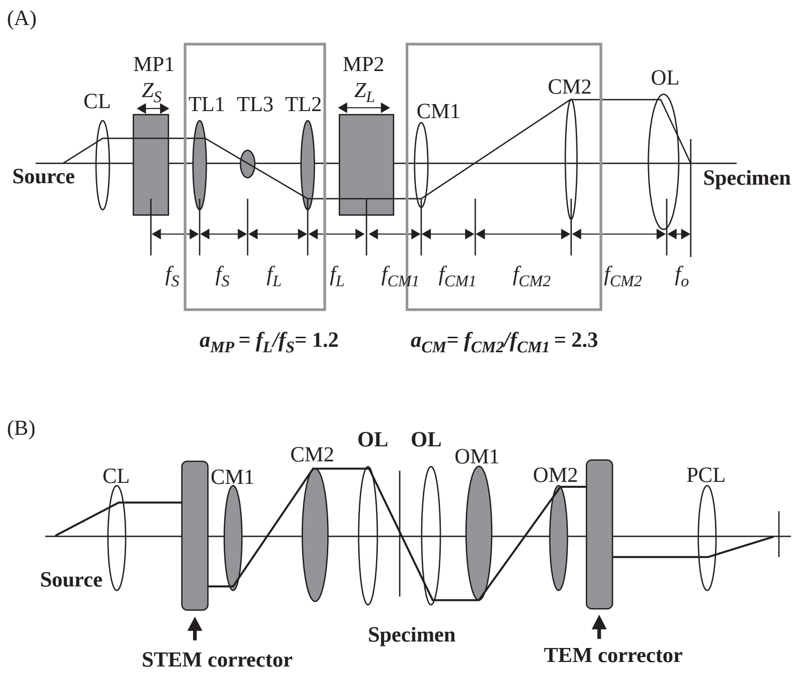

Figure 41.20

Modified corrector with lower symmetry (A). The elements of the corrector. (B) The corrector incorporated in a microscope, TEM and STEM modes. *After Hosokawa et al. (2013), Courtesy Oxford University Press.*

The asymmetric C_s corrector and the delta corrector. Once the roles of sextupoles in aberration correction and of the attendant symmetries have been understood, it is natural to enquire whether any unexplored variants on the basic design offer improvements. Hosokawa et al. (2006, 2013) and Sawada et al. (2009, 2010) have pursued this route. In a first extension, sextupole-based STEM and TEM correctors were considered in which the lengths and excitations of the multipole elements were different. Each multipole element is a dodecapole capable of generating the dominant sextupole field and supplementary dipole, quadrupole and octopole fields. Fig. 41.20A shows the corrector in detail and Fig. 41.20B depicts a configuration with STEM and TEM correction. The transfer lenses TL1 and TL2 now have different focal lengths (f_S and f_L in Fig. 41.20A). This asymmetry contributes to the demagnification of the source at the probe by a factor f_S/f_L and helps to reduce parasitic aberrations by a factor $(f_S/f_L)^{m-1}$, where m (>1) is the order of the corresponding aberration. Any increase in C_c is also limited.

If we denote the lengths of the correctors MP1 and MP2 by Z_S and Z_L, these quantities must satisfy the condition

$$Z_L = Z_S a^2$$

where

$$a := f_L / f_S$$

The excitations of MP1 and MP2, denoted by NI_S and NI_L, are related by

$$NI_L = NI_S / a^5$$

The correction power of MP1 is then defined by

$$C_{sc} = \frac{6f^4 Z_S^3 \mu_0^2 NI_S^2}{a^4 R^2 b^6 M^4}$$

in which $R = \hat{\phi}/\eta$, b is the bore radius of MP1 and M is the magnification between MP2 and the probe-forming (objective) lens OL.

The focal lengths of the round lenses that form the doublet between MP2 and the probe-forming lens are again different and the magnification between the image principal plane (or nodal plane) of the multipole and the coma-free plane of the probe-forming lens, $M = a_{cM}$, is greater than one. In consequence, the third-order correcting power of the corrector is reduced by a factor $1/a_{cM}^4$. This reduction is compensated by the smaller bore radius and higher excitation of MP2.

This corrector suffers from a sixfold astigmatism and to eliminate this, Sawada et al. (2010) designed a system consisting of three dodecapoles. This is the Delta (Dodecapole ELement Triple Aberration) corrector (Fig. 41.21). The azimuth of the sextupole field can be chosen by suitable excitation of the poles and Hosokawa et al. (2013) explain how to choose the relative azimuths in such a way that the magnitudes of the astigmatism and three-lobe aberration (R_5 in Table 31.1) are acceptable. See also Morishita (2017a) and Sasaki et al. (2017). An extremely careful study of certain higher-order aberrations, the sixth-order three-lobe aberration in particular, is to be found in Morishita et al. (2017b). By counterbalancing the fourth-order and sixth-order aberrations of this type, resolutions better than 100 pm were obtained at accelerating voltages as low as 15 and 60 kV.

Sextupole fields created by line currents. An n-fold symmetric set of line currents will generate the same magnetic field pattern as a $2n$-fold element (Nishi et al., 2014); this observation led Hoque et al. (2016) to design a spherical aberration corrector based on the arrangement shown in Fig. 41.17 but free of magnetic material. Problems of hysteresis and inhomogeneity would thus be avoided. Three line currents are disposed parallel to the optic axis with threefold symmetry (Fig. 41.22A). In reality, the circuit of each line current will be closed by bending it into a ring but the behaviour of the device can be modelled more easily and with reasonable accuracy by considering rectangular coils (Fig. 41.22B). Hoque et al. analyse the properties of the corrector analytically by making the following approximations: only the currents in the wires close to the optic axis (AB in Fig. 41.22B) are considered; the flux density is assumed to be zero beyond the ends of the wires; the magnetic potential inside

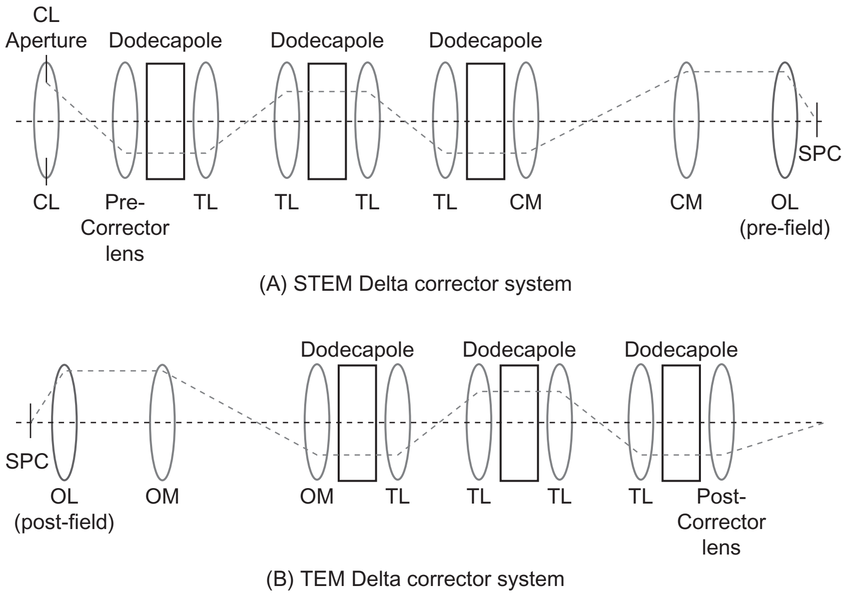

Figure 41.21
The Delta corrector. (A) STEM configuration. (B) TEM configuration. *After Sawada et al. (2011), Courtesy Elsevier.*

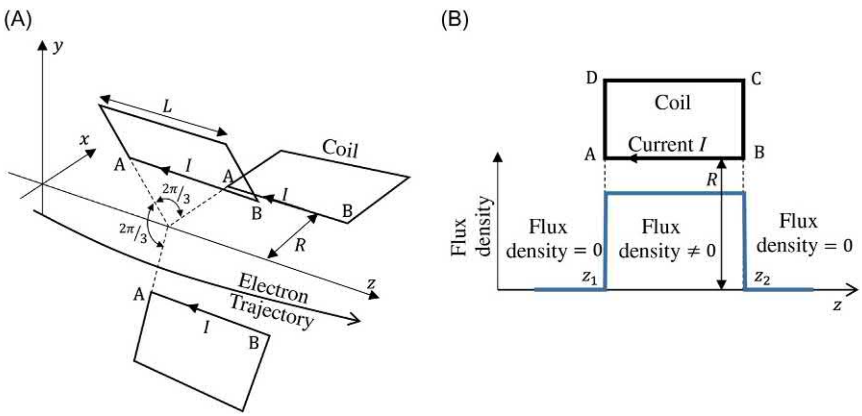

Figure 41.22
Sextupole fields created by line currents (A) Perspective view of the device. (B) Positions of the wires. *After Hoque et al. (2016), Courtesy Elsevier.*

the wire zone is assumed to be generated by infinitely long wires. (In their numerical calculation, this last assumption is not made as the Biot–Savart law is employed.) Fig. 41.23 shows the corrector of Fig. 41.17, line currents replacing the original sextupoles. Hoque et al. give approximate expressions for contribution of the line-current sextupole to the total spherical aberration and compare these with values furnished by the differential algebraic

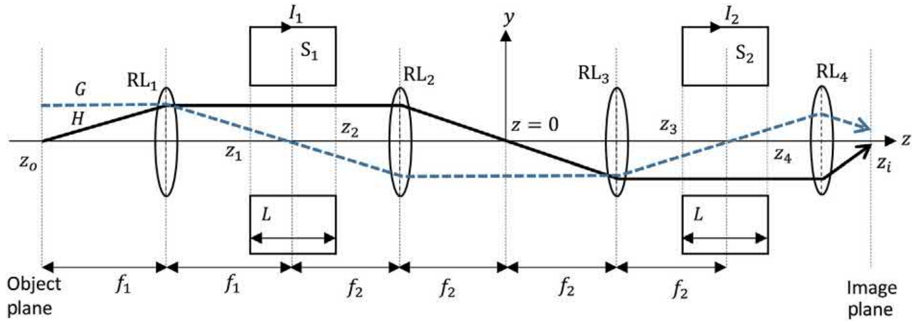

Figure 41.23

Ray diagram corresponding to the corrector of Fig. 41.20. *After Hoque et al. (2016), Courtesy Elsevier.*

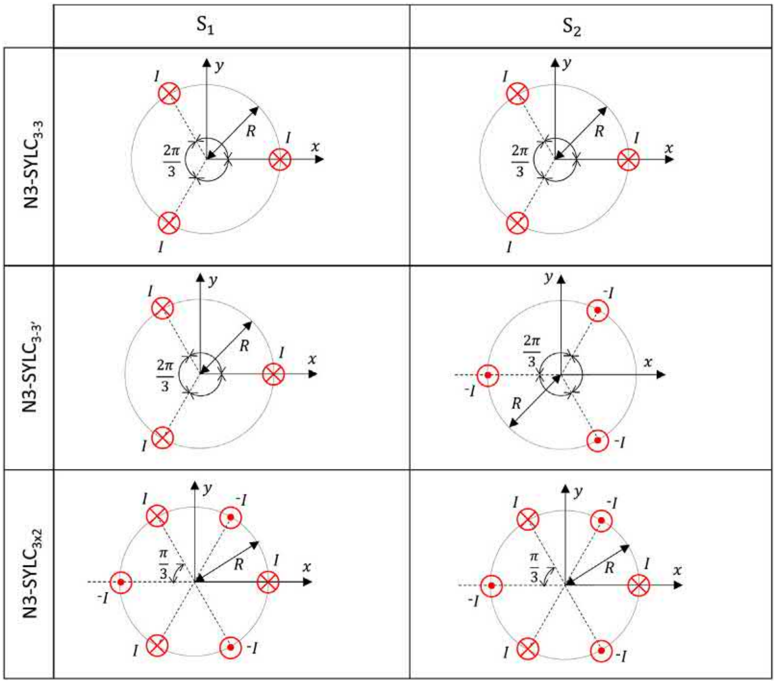

Figure 41.24

Generalizations of the corrector of Fig. 41.22. *After Hoque et al. (2016), Courtesy Elsevier.*

method (Section 34.8). They also consider more elaborate arrangements, notably a dodecapole with six line currents (Fig. 41.24). See also Nishi et al. (2017), Hoque et al. (2017a–c).

Sophisticated Pile of Apertures with NOnCircular Holes (SPANOCH). For miniature microscope columns or multicolumn arrays, the correctors described earlier are too bulky and complex. Janzen (2010, 2011) has suggested that the required fields (sextupole or quadrupole−octopole) should be created by means of apertures with polygonal boundaries (octagonal, hexagonal, square) or other shapes, see Fig. 41.25. Thus an all-electrostatic chromatic corrector (Eq. 41.3) has been studied, using three triplets of shaped apertures. A satisfactory configuration emerged from the calculations (Janzen et al., 2013).

41.2.3 Practical Designs

In the previous sections, the optical properties of the various multipole correctors were analysed. In this short section, we say a few words about the models that have been developed by the CEOS and Nion companies and the variants developed for certain Japanese projects. Many more details are to be found in the references, long lists of which are included in the survey by Hawkes (2015).

CEOS (Corrected Electron Optical Systems) has supplied sextupole correctors to the leading manufacturers of electron microscopes. At first, conventional transmission microscopes were privileged. Soon, however, modified models suitable for the STEM mode were introduced, notably for a JEOL microscope with two correctors, thus allowing both modes of operation in a corrected instrument. CEOS has also provided specialized correctors for the American TEAM project and the German SALVE, PICO and SATEM ventures.

For the conventional transmission electron microscope, the CETCOR corrector consists of a transfer doublet of round lenses to image the (inaccessible) coma-free plane of the lens to be corrected onto the first sextupole, as already shown in Fig. 41.17. A similar design (CESCOR) corrects the STEM mode. For the TEAM 0.5 microscope (without chromatic correction), the corrector (D-COR) cancelled fifth-order spherical aberration and sixfold astigmatism (as well as aberrations of lower order). Chromatic aberration was also corrected in the next instrument (TEAM 1).

The history of Nion divides into two periods. In the first, correctors were retrofitted to VG STEMs. Subsequently, a new STEM was developed, the UltraSTEM; this is equipped with an advanced quadrupole−octopole corrector, though in practice these elements are of course multipoles. It also incorporates the Nion monochromator, described in Section 52.9.6 (Krivanek et al., 2008a,b, 2009a,b; Batson, 2008; Dellby et al., 2011; Hawkes and Krivanek, 2018).

After early attempts to produce an in-house corrector (Maas et al., 2001; Mentink et al., 2003), FEI (Philips) adopted the CEOS correctors. An FEI microscope is at the heart of the American TEAM project, the aim of which was to make available a transmission microscope with a resolution of 0.5 Å. A first model (TEAM 0.5) included only C_s correction; it was followed by TEAM 1 in which C_c correction was included (Dahmen, 2009). An FEI microscope is likewise used in the PICO instrument (Ernst-Ruska-Centrum, Jülich), which has C_s and C_c correction as well as a monochromator.

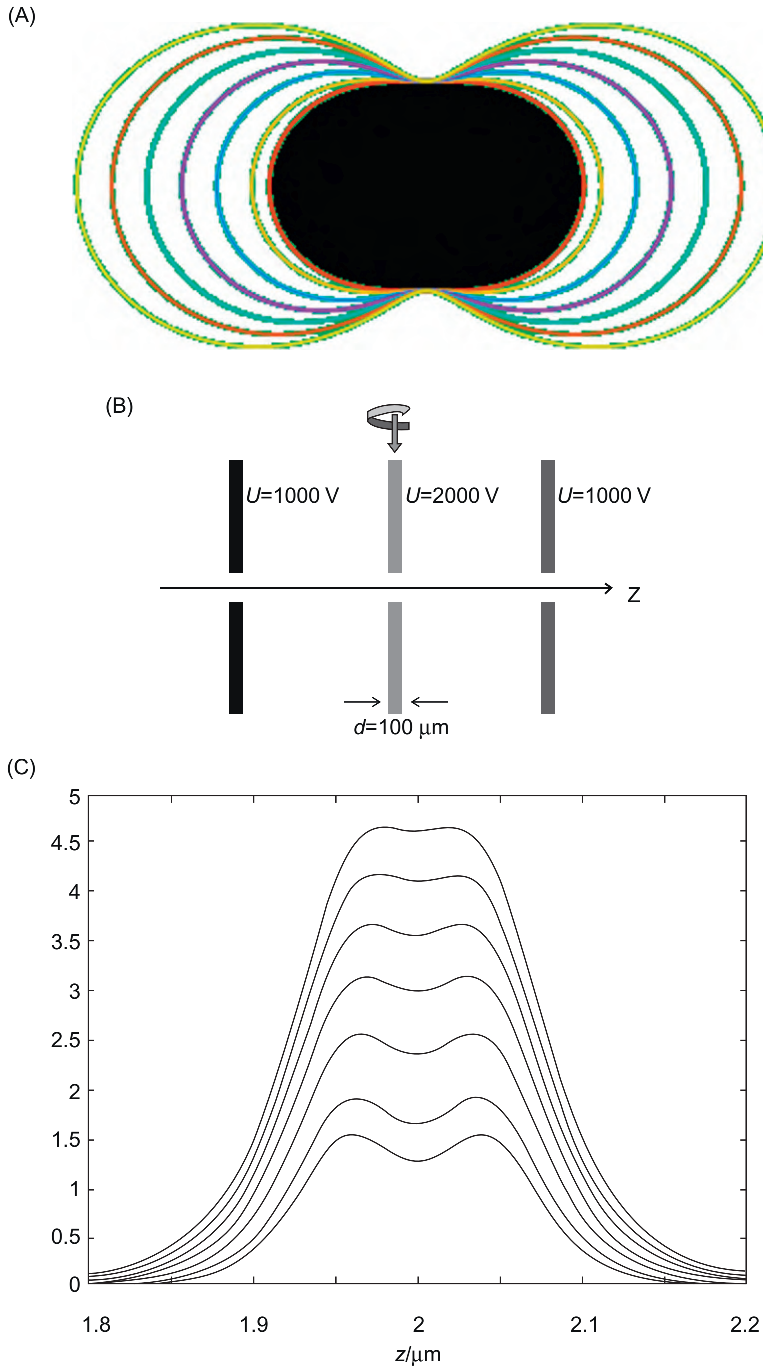

Figure 41.25

Apertures with which round lens, quadrupole and (weak) octopole fields can be created. (A) Aperture shapes with increasing eccentricity. (B) Position of the aperture in an einzel lens. (C) The quadrupole strength on the axis for each value of the eccentricity. From the centre outwards, the eccentricity in μm is 15, 20, 30, 40, 50, 60 and 70. *Courtesy Roland Janzen.*

In Japan, modified correctors have been introduced by JEOL for the R005 (Resolution 0.05 nm) and the Triple C (C_s correction, C_c correction, Carbon materials) projects. In the first stage, an asymmetric configuration was studied and this was followed by the delta corrector, with three dodecapole elements.

The SALVE project already mentioned was originally centred around a Zeiss Libra electron microscope. Zeiss, however, withdrew from the project and the new industrial partner is FEI. The SALVE III instrument is based on an FEI Themis electron microscope and CEOS correctors. See Kaiser et al. (2011), Linck et al. (2016a,b) and van Cappellen et al. (2017) for details.

41.2.4 Measurement of Aberrations

The long saga of aberration correction was brought to a successful conclusion largely thanks to the development of fast diagnostic tools allied to powerful control circuitry. Krivanek et al. (2015) gives a vivid idea of the resulting complexity. Several ways of measuring aberration coefficients are in use, of which the most common are based on the Zemlin tableau and on the far-field image obtained with a defocused probe, known as a Ronchigram. The methods of Meyer et al. (2004) and of Saxton (1995a,b, 2000, 2015; Saxton et al., 1994) are also valuable ways of obtaining some of the desired information.

Zemlin tableaux. In order to understand this method, we must anticipate Chapter 66 in which the notion of electron microscope transfer functions is introduced. The phase-contrast transfer function relates the spatial frequency spectrum or Fourier transform of the image of a weakly scattering specimen to the corresponding spectrum at the object. The spatial frequency spectrum of an amorphous specimen in the presence of third-order spherical aberration and defocus is governed by the function $\sin\dfrac{2\pi}{\lambda}W, \quad W = \dfrac{1}{4}C_s|\theta|^4 + \dfrac{1}{2}C_1|\theta|^2$ in which λ denotes the electron wavelength (55.11); C_1 denotes the defocus in the notation of Uhlemann and Haider (1998, see Section 31.6.2). The angle θ is here treated as a complex quantity, $\theta = \theta_x + i\theta_y$. For this ideal case, therefore, a series of concentric circles, the Thon rings (Fig. 66.6 in Volume 3), is seen, the dark rings corresponding to the zeros of the sine function. If other isoplanatic (axial) aberrations such as coma and astigmatism are present, additional terms will appear in the function $W(\theta)$. When first-order astigmatism is the only parasitic aberration present, $W(\theta)$ also contains a term in $\dfrac{1}{2}\Re(\theta^{*2}A_1)$. The circles become elliptical and the spatial frequency spectrum, or 'diffractogram', contains the information needed to deduce the defocus, the spherical aberration coefficient and the astigmatism.

By tilting the beam incident on the specimen and recording the diffractogram for a series of values of the tilt angle and azimuth, enough information can be retrieved to calculate all the parasitic aberration coefficients, as we now show.

Not all the terms in W affect the diffractogram. It is easy to see that only even terms will survive; we denote these by W_e. When the beam is tilted, the aberration function W becomes W_τ

$$W_\tau(\theta, \tau) := \frac{1}{2}W_e(\theta+\tau) + \frac{1}{2}W_e(-\theta+\tau) - W_e(\tau) \tag{41.17}$$

in which τ denotes the (complex) tilt angle. In this expression, there are terms proportional to $\theta\theta^*$ and to θ^{*2}, which we identified with defocus and astigmatism in the untilted formula. We call the new values of defocus and astigmatism after tilting the beam the *effective defocus* and *effective astigmatism*. They are related to the untilted coefficients as follows:

$$\begin{aligned}
C_1(\tau) &= C_1(0) + 4\Re(\tau B_2) + 2\tau\tau^* C_3 + 6\Re(\tau^2 S_3) \\
&\quad + 12\Re(\tau^2\tau^* B_4) + 8\Re(\tau^3 D_4) + 3(\tau\tau^*)^2 C_5 + \cdots \\
A_1(\tau) &= A_1(0) + 2\tau B_2^* + 2\tau^* A_2 + \tau^2 C_3 + 6\tau\tau^* S_3^* \\
&\quad + 3\tau^{*2} A_3 + 2\tau^3 B_4 + 6\tau^2\tau^* B_4^* + 12\tau\tau^{*2} D_4 \\
&\quad + 4\tau^{*3} A_4 + 2\tau^3\tau^* C_5 + 5\tau^{*4} A_5 + \cdots
\end{aligned} \tag{41.18}$$

From a set or tableau of diffractograms taken at different tilts, all the coefficients can be extracted. Off-axis aberration coefficients can also be obtained by generating Zemlin tableaux from zones not centred on the optic axis.

Such tableaux can also be used to measure aberrations in probe-forming instruments, though in practice Ronchigrams are preferred. This use of tableaux was first described by Zach in a patent application and a very full description is given in Uno et al. (2005), which we follow closely. The method employs two defocused images, above and below the Gaussian image plane. Each image is digitized and N radial line profiles are acquired at constant angular steps; the k-th line profile corresponds to the angle $\alpha = k\pi/N$. For each line profile, the width (σ), asymmetry (μ) and curvature (ρ) are recorded. These are defined by

$$\sigma = \left(\frac{\sum j^2 p_j}{\sum p_j}\right)^{1/2} \qquad \mu = \frac{\sum j p_j}{\sum p_j} \qquad \rho = \frac{\sigma^2}{\sum p_j^2}\sum_{j\neq 0}\frac{(p_j - p_0)p_j}{|j|} \tag{41.19}$$

where p_j, $j = 0, \pm 1, \pm 2, \cdots$ are the intensity values measured along the line profiles. $j = 0$ corresponding to the centre of the probe. The aberration coefficients of Eq. (41.18) up to third order are then extracted from the following formulae:

$$\begin{aligned}
C_1 &= \frac{1}{N}\sum(\sigma_{n,k} - \sigma_{0,k}) \\
A_1 &= \frac{2}{N}\sum(\sigma_{n,k} - \sigma_{0,k})\ \exp(2\mathrm{i}\alpha_k) \\
B_2 &= \frac{2}{N}\sum(\mu_{n,k} + \mu_{0,k})\ \exp(\mathrm{i}\alpha_k) \\
A_2 &= \frac{2}{N}\sum(\mu_{n,k} + \mu_{0,k})\ \exp(3\mathrm{i}\alpha_k) \\
C_3 &= C_s = \frac{1}{N}\sum(\rho_{n,k} - \rho_{0,k}) \\
S_3 &= \frac{2}{N}\sum(\rho_{n,k} - \rho_{0,k})\ \exp(2\mathrm{i}\alpha_k) \\
A_3 &= \frac{2}{N}\sum(\sigma_{n,k} - \sigma_{0,k})\ \exp(4\mathrm{i}\alpha_k)
\end{aligned} \tag{41.20}$$

We note that Uno et al. also describe a complete protocol for implementing aberration correction. Errors in the values of aberration coefficients obtained from Zemlin tableaux have been estimated by Lentzen et al. (2004).

Shadow images or Ronchigrams. If a small probe is brought to a focus close to a specimen, the aberrations of the probe-forming lens will affect the current distribution in the vicinity of the Gaussian focus and in turn, the distribution in the far-field downstream from the specimen. This observation has been used for many years to characterize the defects of glass lenses by obtaining the shadow image of a grating close to the focus of the lens (see Ronchi, 1964, where references to his pioneering work in the early 1920s are to be found). A similar method based on the shadow of a grid was used by Sakaki and Maruse (1954), Kanaya et al. (1959b), Kanaya and Kawakatsu (1960), Deltrap and Cosslett (1962), Deltrap (1964a,b) and Hardy (1967) to measure quadrupole aberrations and by Rempfer (1985) to measure those of einzel lenses.

Such shadow patterns have come into use for studying STEM imaging (Cowley, 1979a,b; Lin and Cowley, 1986) and the resemblance to Ronchi's work led Cowley to describe them as 'electron Ronchigrams' (Cowley, 1980). They are now used routinely to measure and then cancel aberrations in aberration-corrected STEMs. Here, we present the underlying theory and indicate how the results are used in practice. For very complete studies, see Lupini (2011), which includes much of his earlier work (Lupini, 2001) and Sawada (2015b). These are to some extent complementary; Sawada, for example, gives the mathematical details explicitly.

Fig. 41.26 shows an electron beam being focused by a lens from which it is clear that the shadow of the specimen will be distorted by the various aberrations of the lens. A ray characterized by $\boldsymbol{p_1} = (p_1, q_1)$ at the lens will strike the specimen at $\boldsymbol{x}_\mathrm{o} = (x_\mathrm{o}, y_\mathrm{o})$,

$$\boldsymbol{x}_o^{(1)} = \nabla W(\boldsymbol{p}_1) + \boldsymbol{R}_1 \tag{41.21a}$$

in which $\boldsymbol{R}_1$ denotes the probe position in the specimen plane. For a second ray,

$$\boldsymbol{x}_o^{(2)} = \nabla W(\boldsymbol{p}_2) + \boldsymbol{R}_2 \tag{41.21b}$$

so that

$$\boldsymbol{x}_o^{(2)} - \boldsymbol{x}_o^{(1)} = \nabla W(\boldsymbol{p}_2) - \nabla W(\boldsymbol{p}_1) + \boldsymbol{R}_2 - \boldsymbol{R}_1 \tag{41.22}$$

For rays for which the difference between $\boldsymbol{p}_1$ and $\boldsymbol{p}_2$ is very small, we write $\boldsymbol{p}_2 = \boldsymbol{p}_1 + \Delta\boldsymbol{p}$ and hence

$$\begin{aligned} \nabla W(\boldsymbol{p}_2) &= \nabla W(\boldsymbol{p}_1 + \Delta\boldsymbol{p}) \\ &= \nabla W(\boldsymbol{p}_1) + \Delta\boldsymbol{p}\cdot\nabla(\nabla W(\boldsymbol{p}_1)) \end{aligned} \tag{41.23}$$

Thus

$$\begin{aligned} \Delta\boldsymbol{x} \coloneqq \boldsymbol{x}_o^{(2)} - \boldsymbol{x}_o^{(1)} &= \Delta\boldsymbol{p}\cdot\nabla(\nabla W(\boldsymbol{p}_1)) + \Delta\boldsymbol{R} \\ &\eqqcolon H_p\Delta\boldsymbol{p} + \Delta\boldsymbol{R} \end{aligned} \tag{41.24}$$

and on expanding the derivatives, we obtain

$$H_{\boldsymbol{p}} = \begin{pmatrix} \dfrac{\partial^2 W}{\partial p^2} & \dfrac{\partial^2 W}{\partial p \partial q} \\[2ex] \dfrac{\partial^2 W}{\partial p \partial q} & \dfrac{\partial^2 W}{\partial q^2} \end{pmatrix}_{\boldsymbol{p}} \tag{41.25}$$

In the far field or shadow-image plane, we can identify the position coordinates with the angular quantities (p, q) and this in turn allows us to regard $\Delta\boldsymbol{p}$ as the magnification of $\Delta\boldsymbol{x}$. Inverting Eq. (41.24), we have

$$\Delta\boldsymbol{p} = H_p^{-1}(\Delta\boldsymbol{x} - \Delta\boldsymbol{R}) \tag{41.26a}$$

For a single object point, $\Delta\mathbf{x}_o = 0$, therefore,

$$\Delta\boldsymbol{p} = -H_{\boldsymbol{p}}^{-1}\Delta\boldsymbol{R} \tag{41.26b}$$

This is the basis of one of the ways of obtaining the aberration coefficients that appear in the Hessian matrix H_p. The shadow-image plane is divided into small patches, in each of which $\Delta\boldsymbol{p}$ is measured and $\Delta\boldsymbol{R}$ is known; the elements of H_p can hence be extracted (Fig. 41.26b). This is the method used to measure aberrations in the Nion instruments (Dellby et al., 2001; Krivanek et al., 1999a).

Kimoto and Ishizuka (2017) show that the low-order aberration coefficients can be extracted rapidly and conveniently from the Fourier transform of two Ronchigrams of a crystalline specimen. This has the advantage that it is not necessary to invert the matrix H_p

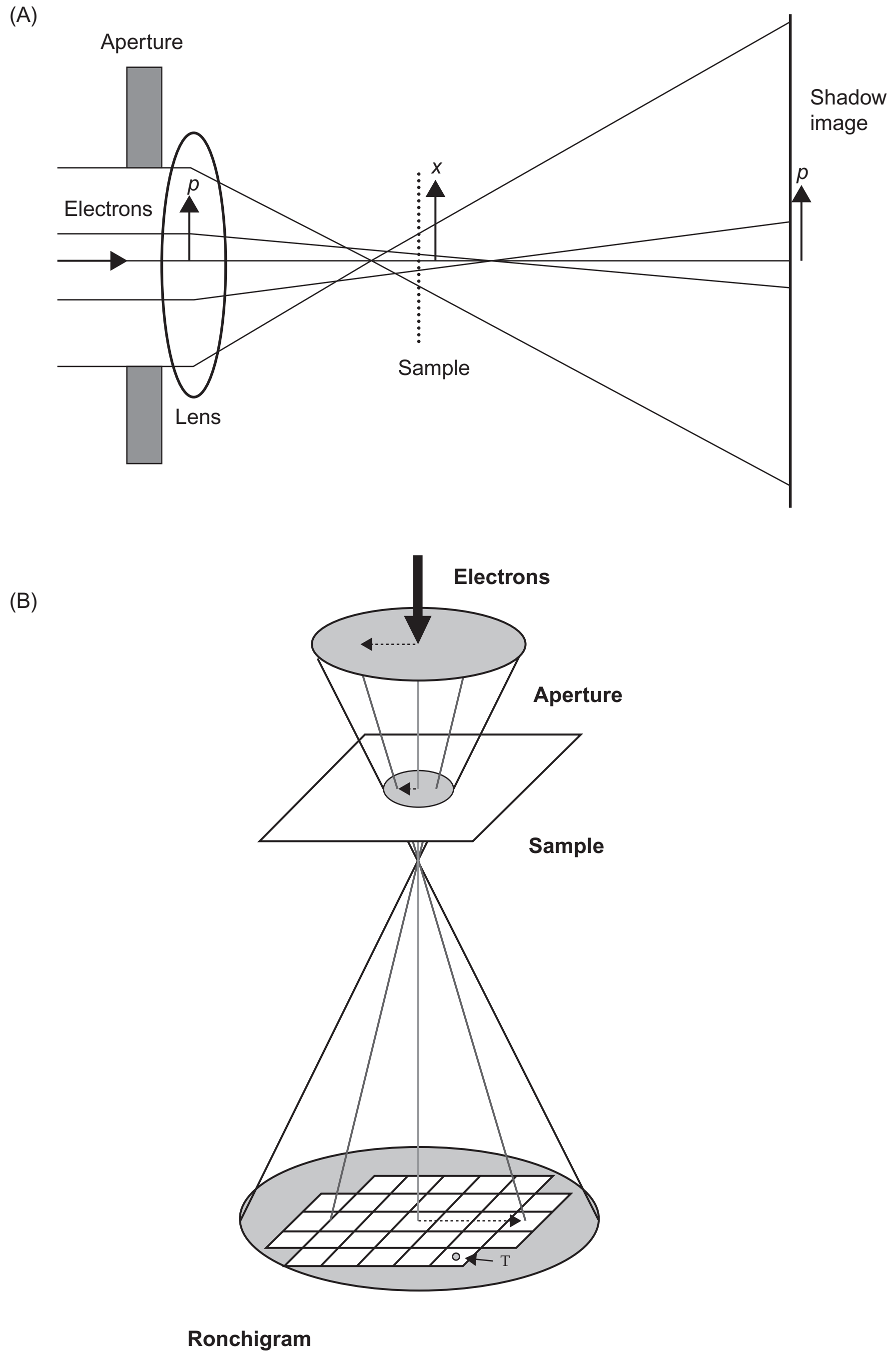

Figure 41.26
The Ronchigram. (A) Formation. (B) Division into small patches. *After Lupini (2001), Courtesy of the author.*

of Eq. (41.25). The theoretical basis of the method is given in full by Kimoto and Ishikawa together with examples. The method yields values of the defocus, axial (twofold) astigmatism, axial coma and threefold astigmatism.

Other methods. The method of Meyer et al. (2002, 2004) is based on focal series and has the attraction that the specimen can be crystalline. As in the case of a Zemlin tableau, tilt series are collected but here, a set of such series is recorded, one for each member of a focal series. Formulae from which the lower order axial aberration coefficients can be calculated are given explicitly by Meyer and are not reproduced here.

Saxton (1995a,b, 2015) exploits the shape and orientation of the patterns observed in diffractograms recorded under many different tilt arrangements. Image shift is examined separately. Explicit expressions are given in closed form for the axial aberration coefficients of the lowest orders; many different tilt patterns, classified by symmetry, are analysed in full detail. Saxton's earlier suggestion (2000) that the orientation of the diffractogram can be used to evaluate the aberration coefficients is likewise re-examined.

Lupini et al. (2016) have drawn attention to a way of using a pixelated detector in a STEM to measure aberration coefficients very rapidly. The scattering distribution is recorded for each position of the probe and the resulting four-dimensional data set yields an array of real-space images. By cross-correlating these, the gradient of the aberration function and hence the aberration coefficients can be obtained. The accuracy is excellent and the method is not limited to aberrations of the lowest order.

We note that other methods have been proposed by Koster and de Jonge (1991), Koster and de Ruijter (1992), Ishizuka (1994), Typke and Dierksen (1995), Stenkamp (1998), Steinecker and Mader (2000), Ramasse and Bleloch (2005), Mitsuishi et al. (2006), Akima and Yoshida (2014) and Sawada et al. (2017). A very ingenious method, in which two narrow beams are selected simultaneously by means of a plate contains two apertures, was devised by Nakagawa (1977). The pair of beams is scanned across a mesh (in a SEM) and the aberration coefficients are extracted from the resulting double image.

In the early years of the subject, Becker and Wallraff (1938) and Mahl and Recknagel (1944) devised methods of measuring aberrations. Seeliger (1948) obtained the third- and fifth-order spherical aberration coefficients by measuring the displacement of a beam incident on the lens at different angles of incidence. Table 41.1 illustrates his results.

41.3 Foil Lenses and Space Charge

41.3.1 Space Charge Clouds

The introduction of a space charge cloud into the path of a beam can in principle be beneficial: if the charge distribution is such that the density increases approximately

Table 41.1: Focal length and spherical aberration coefficients in mm of some electrostatic lenses

	Projector	Normal Objective	Unsymmetrical Objective		Objective with Thick Central Electrode	Unsymmetrical Objective	Immersion Objective
	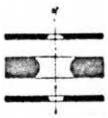	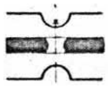	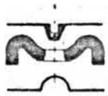	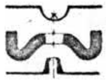	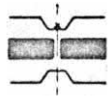	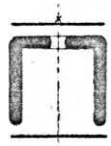	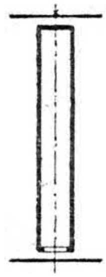
f	30	6.1	6.0	6.8	8.8	6.6	3.9
C_3	820	61.8	51.3	47.0	61.5	23.5	38.2
C_5	<2500	<180	<200	<200	5400	<200	<250

For the first four lenses, the central electrode is at cathode potential. For the last three, the potential is 80%, 95% and 95% of the cathode potential respectively. *After Seeliger (1948).*

quadratically with the off-axial distance, an electrostatic lens free of spherical aberration can be designed. The problem is to maintain such a cloud ‘stationary’, in order to avoid the frosted-glass effect to be expected if the medium is fluctuating, and of course to create the desired variation with radial distance. Various suggestions have been made, by Gabor (1945a,b, 1947) and Scherzer (1947), and experiments were later performed by Ash (1955), Ash and Gabor (1955) and by Haufe (1958). These were not sufficiently encouraging to attract any successors apart from an isolated study by Le Poole (1972); in the latter, slow electrons were injected at about 30° to the axis of a long magnetic lens in which they spiral down the field, creating a supposedly beneficial space charge potential. The technique did not, alas, live up to its inventor’s hopes.

The theory of space-charge lenses has also been examined in considerable detail. The chromatic aberration and the thin-lens approximation to C_s are studied by Sturrock (1955; see corrections by Typke, 1968/69) and expressions for all the geometric aberration coefficients were established shortly after by Yao (1957a,b, 1958). The expression for the spherical aberration coefficient in the presence of space charge obtained by Typke, (1968/69) was reproduced in (35.149). Correction of C_s by means of space charge was subsequently studied very thoroughly by Typke (1972a,b), who showed how the terms in ρ_0 and ρ_2 (7.54) in the space-charge contribution could be used to cancel the familiar round-lens term.

There has been little further work on space-charge correction of electron lenses, apart from a discussion by Meinel and Janssen (1985) of the homogeneous sphere of charge for which the spherical and chromatic aberration coefficients and focal length can be calculated exactly. In ion optics, however, the use of space charge has aroused interest (Wang, 1995a−c; Tang (1996); Tang et al., 1996a,b; Chao et al., 1997; Orloff, 1997).

41.3.2 Foil Lenses

Despite the danger that the insertion of a foil into the path of the beam may create problems comparable with those the corrector is intended to obviate, the associated methods of correcting spherical aberration attracted attention for many years. In the earlier studies, very thin foils were not available and it was thought preferable to use gauze, since scattering in the foil would have been too great. The advantages and disadvantages of placing a fine gauze across the path of the beam, thereby creating a discontinuity in $\phi'(z)$, were very thoroughly analysed by Bernard (1952, 1953), Seman (1952), Verster (1963), Rus (1965) and Barth (1967). The small holes in the gauze perturb the lens field (e.g. Bernard, Verster) but, as the calculations and preliminary experimental results of Rus (1965) showed, this perturbation can be tolerated if the gauze lens is designed to have negative spherical aberration and is used to cancel the positive spherical aberration of a conventional lens. The penetration of an electric field through a gauze has been calculated more recently by Williams et al. (1995) and Read et al. (1999). Barth (1967) demonstrated that the adverse effects of the holes in the gauze can be reduced by the use of several gauzes. Dekkers and Le Poole (1968) then had the idea of using a superconducting coil carrying a persistent current; this idea was very thoroughly explored by Dekkers (1969), who found that the foil thickness necessary to carry sufficient persistent current for correction was probably excessive. Conversely, a superconducting zone plate, designed so that the persistent current improved the shape of the phase-contrast transfer function (Eqs 65.30 and 65.6 of Volume 3) in the open rings, seemed very promising. The difficulties associated with both foils and zone plates might be avoidable by using superconducting gauze. Dekkers' work concludes with an account of his measurements of the aberrations of a lens equipped with current-carrying superconducting gauze: for different currents, he was able to obtain overcorrection and undercorrection.

Since the beginning of the century, there has been a revival of interest in electron phase plates, which may be physical films in the path of the beam (Zernike or Hilbert phase plates) or local fields (Boersch phase plates, Boersch, 1947). We mention them here, though their proper place is in Volume 3, because it is now realized that, since an aberration corrector alters the phase of the beam, it can be thought of as a 'phase plate' (Typke, 2010; Clark et al., 2013). Readers interested in this aspect of aberration correctors are referred to Danev and Nagayama (2001, 2011), Danev et al. (2001, 2009), Nagayama (2005), Schultheiss et al. (2006, 2010), Gamm et al. (2010), Dries et al. (2011, 2016), Edgcombe (2012, 2017a,b), Edgcombe and Loudon (2012), Edgcombe et al. (2012), Perry-Houts et al. (2012), Verbeeck et al. (2012), Guzzinati et al. (2015) and Minoda et al. (2015, 2017). Another way of employing a gauze for aberration correction has arisen in connection with multibeam scanning electron microscopes (Section 50.6). In these, an electron beam is rendered parallel by a condenser lens or collimator before falling on a perforated plate that creates many sub-beams (van Bruggen et al, 2006a,b). These authors show that this perforated plate could play the role of a gauze and hence help to correct the aberrations of the collimator. The papers of Sannomiya et al. (2014), Linck et al. (2014, 2017), Shiloh et al. (2016) and Tavabi et al. (2016) are of interest in this connection.

Typke's study of space charge mentioned in Section 41.3.1 naturally led him to study gauze and foil lenses (1972a,b). Some results and the design analysed are shown in Fig. 41.27. A paper by Hoch et al. (1976) supplements this work, in that the primary spherical aberration and paraxial chromatic aberration of electrostatic foil lenses with curved foils are calculated numerically. Fig. 41.28 shows the axial potential distribution and its first three derivatives in the vicinity of plane and curved foils; the radius of curvature of the curved foil is -1.875 mm in their example; the bore diameter of the inner electrode is 0.5 mm and of the outer electrodes of the symmetric einzel lens studied, 1 mm. The centre of the outer electrodes is 4 mm from the symmetry plane. There proves to be an optimum voltage ratio, for which C_s vanishes, for each value of the radius of curvature of the foil. Since it is usually not possible to choose the radius, which is determined by the electrical and mechanical forces acting on the foil in any given case, these results allow us to estimate the sensitivity of the device when used for aberration correction. In 1980, Scherzer described a spherically corrected foil-lens design that he believed beneficial for phase-contrast electron microscopy: 'Phase-contrast images should be possible with a limit of resolution far below 1 Å'. The idea dated back to 1933, when Ernst Brüche had suggested (in a conversation with Scherzer) that images could be formed with 'lighthouse lenses' (*Leuchtturm-Linsen*), in which the thickness distribution of the lens is chosen astutely (cf. Scherzer, 1948). Thon and Willasch, unaware of Brüche's suggestion, created a phase plate with such a thickness variation (1970); see Section 66.5.3 and Edgcombe (2017) for related endeavours. Scherzer gives a complete analysis of the optics of his design (Fig. 41.29) and of its contrast-transfer properties.

During much the same period, Maruse, Ichihashi and others in the University of Nagoya were also studying spherical correction by means of thin conducting foils. In their first paper (Maruse et al., 1970a,b), they suggest that the undesirable effects of scattering in the foil could be avoided by using the specimen itself or the supporting grid as the corrector, and they present measurements of C_s for a hemispherical foil and for a plane foil close to a small aperture, in conjunction with a magnetic lens. Much more detailed results, indicating that the spherical aberration of the magnetic lens can be successfully compensated over a wide angle, were presented by Ichihashi and Maruse (1971). The further theoretical studies of Ichihashi and Maruse (1973) have been extended by Hibino and Maruse (1976), who

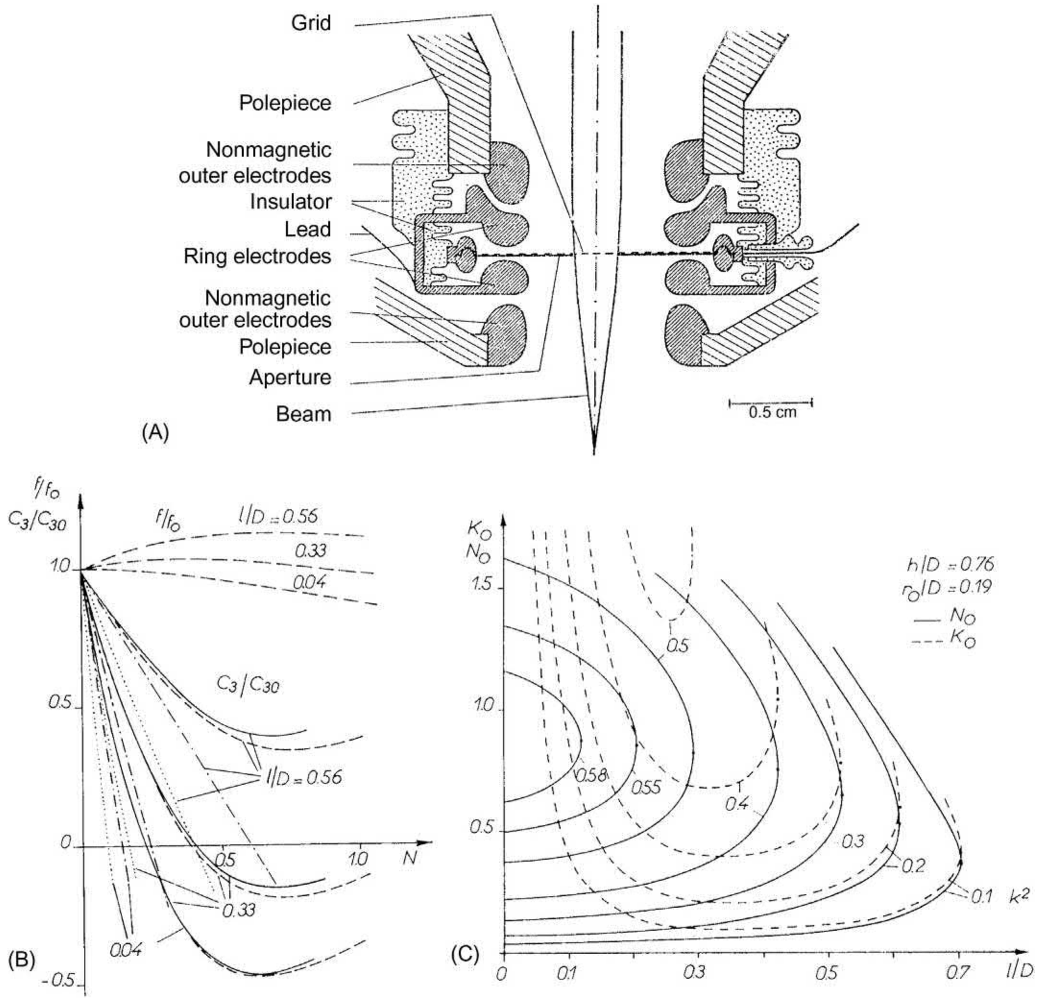

Figure 41.27

(A) A corrector grid located between the polepieces of a magnetic lens. (B) The focal length and spherical aberration coefficient of the lens (A) as functions of the grid voltage NU, where U denotes the accelerating voltage. The curves are normalized with respect to the value at $N = 0$ and correspond to three different geometries. (C) Variation of the correction voltage N_0U and the voltage on the ring electrodes K_0U with ring width l for various values of magnetic lens excitation k^2; l denotes the width of the ring electrodes and D their bore radius, r_0 the distance of the field-free point on the foil from the axis and h the half-width of the magnetic field. *After Typke (1972a), Courtesy Wissenschafliche Verlagsgesellschaft.*

discuss in detail the configuration of Fig. 41.30. They found that the third- and fifth-order spherical aberrations were not corrected at the same foil potential with the result that compensation of the third-order aberration of the magnetic lens slightly increased its fifth-order aberration. The latter is, however, negligible up to angles of 25 mrad. Furthermore,

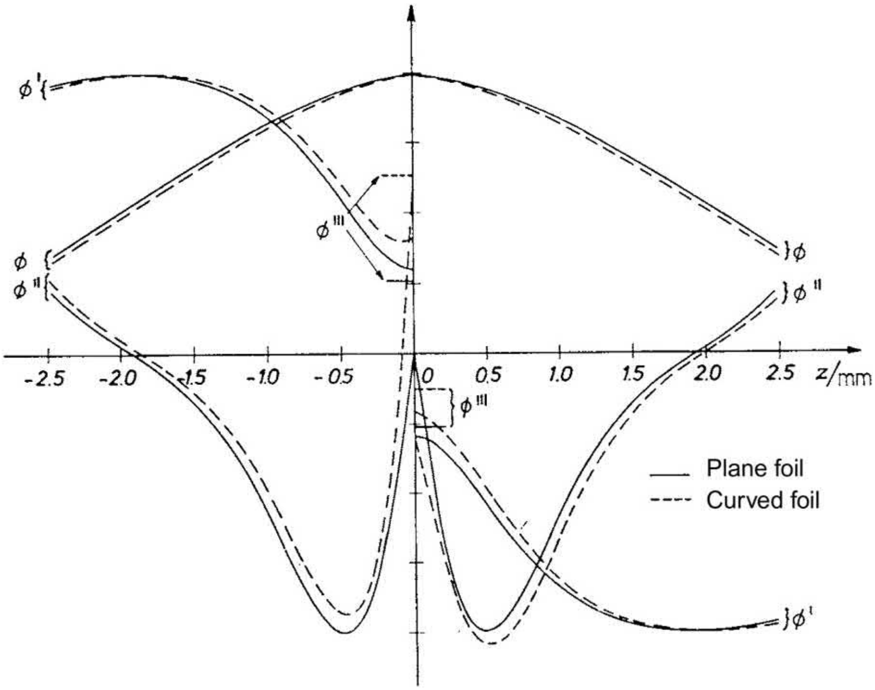

Figure 41.28
Correction of spherical and chromatic aberration by means of charged foils. Distribution of potential ϕ and its derivatives close to the foil. *After Typke (1972a), Courtesy Wissenschafliche Verlagsgesellschaft.*

the residual fifth-order spherical aberration varies with the geometry, and the authors believed that it should be possible to find a configuration for which the angle can be appreciably increased. Conversely, the chromatic aberration is slightly worse with the foil corrector in action. The simultaneous correction of third- and fifth-order spherical aberration is shown by Hibino et al. (1977), who contemplated using a foil corrector in a 400 kV STEM.

Subsequent developments may be traced in the papers of Hibino et al. (1978, 1981), Hanai et al. (1982, 1984, 1994, 1995, 1998), Kuzuya et al. (1982, 1984), Hanai and Hibino (1984) and Hibino and Hanai (1986), in which the emphasis is on the reduction of the probe-size in scanning instruments. Fig. 41.31 shows the arrangement of foil lens and objective employed by Hanai et al. (1984) in a STEM with encouraging results. Scattering in the foil was studied simultaneously by Sugiyama et al. (1984). Kato and Sekine (1995, 1996) have examined the properties of spherical meshes instead of plane grids and found that, depending on the geometry, negative spherical aberration can be obtained. Correction of a four-electrode lens was simulated. In their second paper, the adverse effect of the holes in the mesh is calculated. Their approach was reconsidered by Matsuda et al. (2005), who showed that an ellipsoidal mesh performs better than a spherical shape.

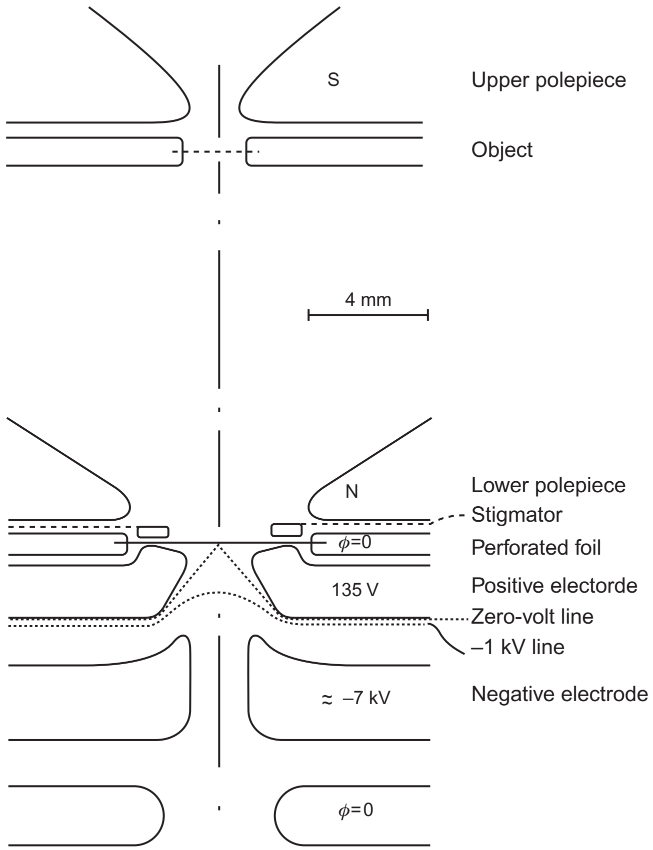

Figure 41.29
The foil-lens corrector designed by Scherzer. *After Scherzer (1980), Courtesy Wissenschaftliche Verlagsgesellschaft.*

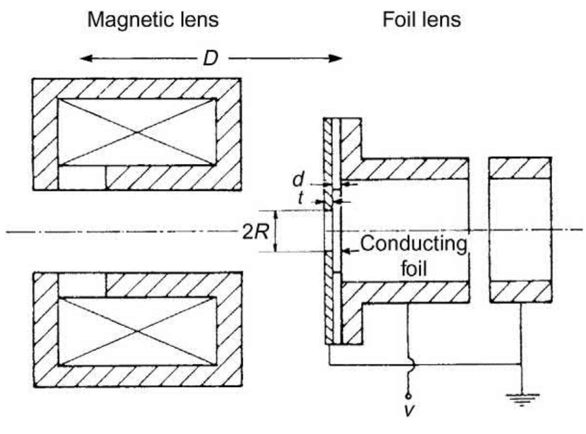

Figure 41.30
The foil-lens corrector studied by Hibino and Maruse. In their experiments, $R = 0.25$ mm and $t = 0.1$ mm. *After Hibino and Maruse (1976), Courtesy Japanese Electron Microscopy Society.*

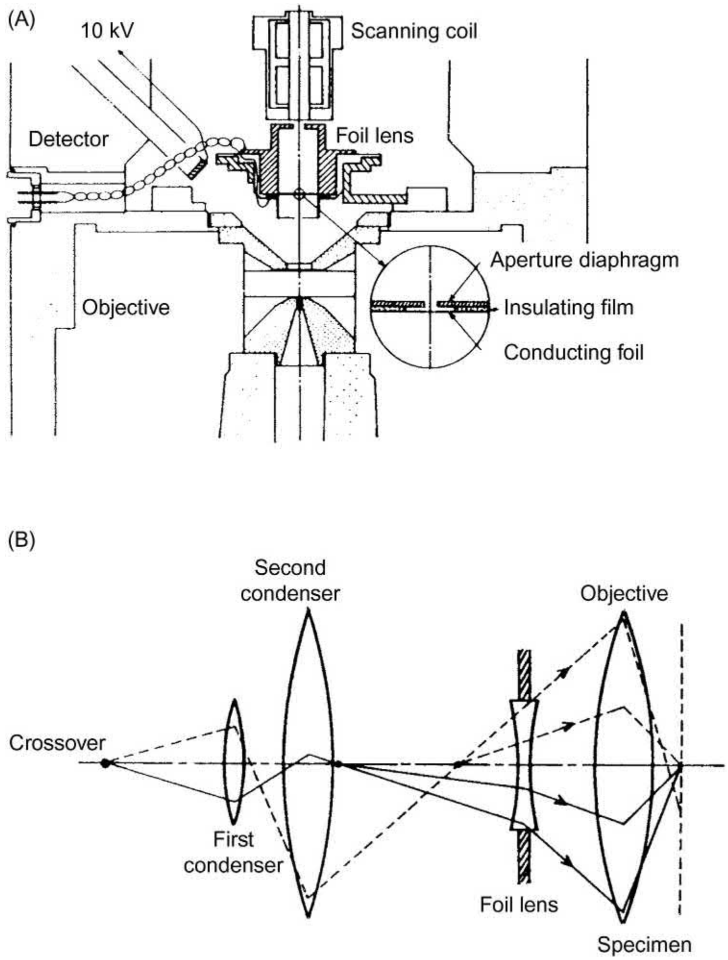

Figure 41.31
The arrangement used by Hanai et al. to reduce probe-size with the aid of a foil. (A) Cross-section and (B) ray diagram. *After Hanai et al. (1984), Courtesy Japanese Electron Microscopy Society.*

The use of aspherical meshes had already been considered by van Gorkum (1983) and van Gorkum and Beirens (1986), who explored mesh or foil shapes based on the zero-order Bessel function J_0. An experimental lens incorporating such a foil was constructed and performed as predicted.

The properties of a double-foil corrector, first examined long ago by Gianola (1950a,b), have been estimated by Thomson and Jacobsen (1971) and Thomson (1973), who planned to use such a corrector in a high-resolution Auger electron microscope (King et al., 1978). For further information on double-foil structures, see Meisburger and Jacobsen (1982).

For their studies on electrostatic and magnetic lenses containing charged foils, Munro and Wittels (1977) derived a convenient unified expression for the aberration coefficients of round lenses; these have already been mentioned in Section 35.4. Wittels (1975) and Wittels and Jacobsen (1975, 1976) had tested an einzel lens, the outer electrodes of which were closed with electron-transparent foils consisting of carbon films about 12 nm thick; the measurements were not very accurate but they did show that the sign of the spherical aberration coefficient could be reversed. Many properties of foil lenses have been studied theoretically by van der Merwe (1978a–c, 1979a,b, 1981a,b).

A very different way of using thin foils for correction has been investigated by van Aken (2005; van Aken et al., 2002a,b, 2004, 2010). Here, the unexpected finding of Seah and Dench (1979) that the mean free path of electrons in metals increases at very low energies is exploited. The corrector consists of a thin metal foil sandwiched between two plane electrodes, the role of which is to retard the electrons to an extremely low energy in front of the foil and then to accelerate them after they have passed through it; the system is shown schematically in Fig. 41.32. If the foil is sufficiently thin, the electrons pass through ballistically. The optics of the device is described in detail in the papers cited. The authors point out that it is prudent to use the primitive form of C_s (24.46) in calculations, before any partial integration has been performed.

The treatment of discontinuities is studied by Dodin (1983).

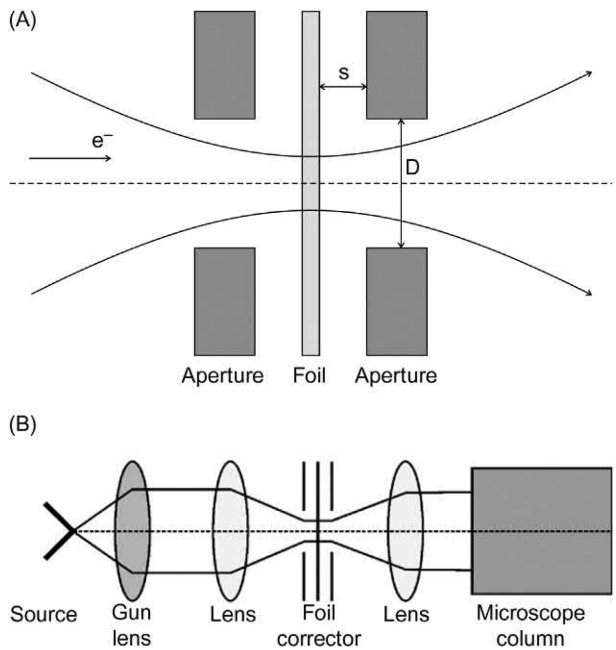

Figure 41.32
The van Aken foil corrector. (A), Basic design. (B) The position of the corrector in a microscope.
After van Aken (2002a), Courtesy Elsevier.

41.4 Axial Conductors

The presence of conductors on the axis of a lens has the obvious drawback that the axial zone is excluded from the image-forming process and the beam must form a hollow cone. Gabor (1946) proposed a system subsequently studied in detail by Dungey and Hull (1947) that provided some measure of zonal correction. This contained three axial conductors. The suggestion was taken up by Wilska (1961) and Lenz and Wilska (1966, 1966/67) and by Kunath (1968, 1970, 1972, 1976, 1976/77). A simpler version with a single axial element, which could equally be used to carry current and hence produce a magnetic field, has also been considered (Dupouy et al., 1964; Marais, 1970; Communay and Marais, 1971). Lenses with one or more axial elements have been reconsidered, with high-energy ions in mind, by Krejcik et al. (1979, 1980a,b) and Krejcik (1980), cf. Liebl (1979) and Ovsyannikova and Pasovetz (1987). The optics of conical-beam systems was studied by Noven (1963, 1964, 1965). See also van der Merwe (1981c). An image-processing technique based on hollow-cone illumination may be found in the work of Kitade et al. (2008), Taya et al. (2008) and Takai et al. (2008).

In the early days of electron tomography, Hoppe (1972) described a three-dimensionally imaging electron microscope, which included a lens with an axial electrode. The optics of such a lens was studied in detail by Typke (1981) and Plies (1981). Such *core-lenses* were reconsidered by Nishi and Takaoka (2012a,b) and Takaoka et al. (2015) for situations in which large tilts are required. Khursheed and Ang have returned to Scherzer's suggestion that the presence of an axial electrode would make aberration correction possible (Khursheed and Ang, 2015, 2016a,b). Their design for a corrector for a probe-forming lens is shown in Fig. 41.33; Fig. 41.33A shows the general layout and Fig. 41.33B and C show possible designs for an electrostatic and a magnetic corrector. If both electrostatic and magnetic fields are included, chromatic aberration can also be corrected in principle. Khursheed and Ang point out that it will not be easy to create the necessary excitations in the chromatic corrector. A possible configuration is shown schematically in Fig. 41.34. The use of an annular beam for aberration correction has also been revived by Kawasaki et al. (2015, 2016a,b, 2017a,b) in their annular-circular-electrode (ACE) corrector. The device consists of two plane electrodes separated by a thin insulator. The first electrode has a circular opening while the second has an annular slit (Fig. 41.35). The latter acts as a diverging lens and the overall spherical aberration coefficient can be negative; any image will be formed by a cone beam. The dimensions of the device are shown in Fig 41.36A and details of its construction in Fig. 41.36B. The corrector has been tested in a Hitachi STEM, where it was attached to the regular aperture-holder. Annular dark field images of CeO_2 are very promising. See also Oguni et al. (2017), Yoshida et al. (2017) and Lee et al. (2017).

The parasitic aberrations arising from ellipticity of a ring electrode have been studied by Kasper (1968/69b).

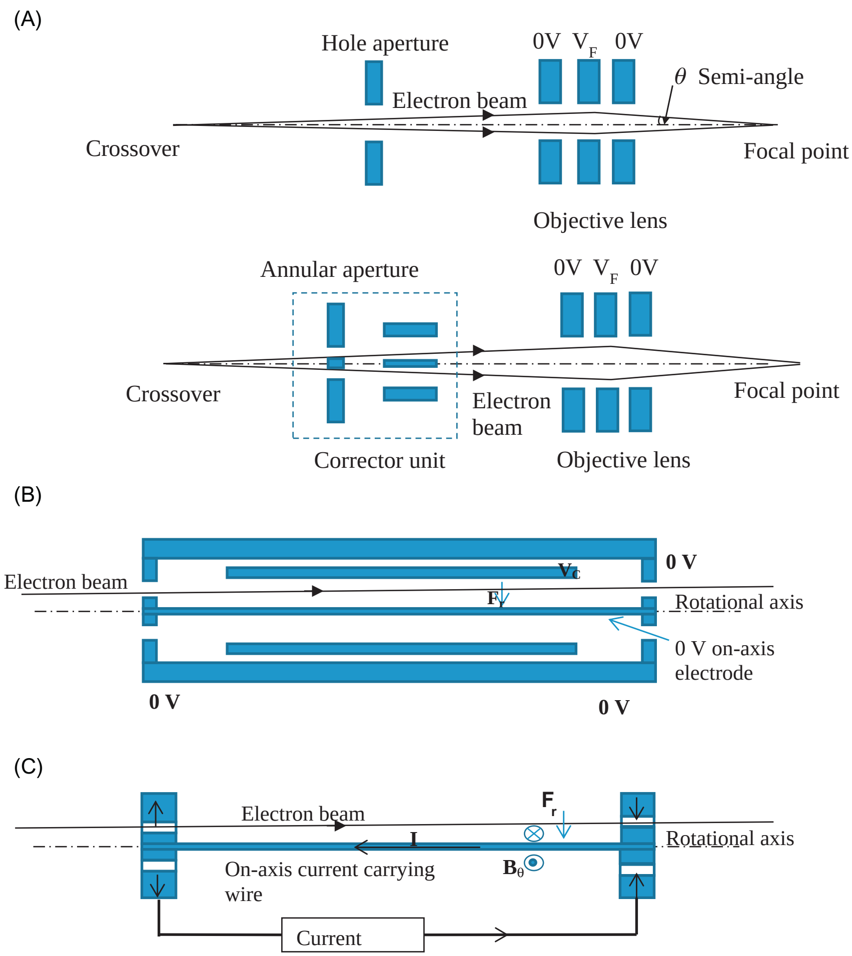

Figure 41.33
The Khursheed—Ang on-axis corrector. (A) The spherical aberration corrector and probe-forming lens. (B) Electrostatic version. (C) Magnetic version. *After Khursheed and Ang (2015), Courtesy Cambridge University Press.*

41.5 Mirrors

When the direction of motion of the electrons is reversed, as it is in an electron mirror, the angle of inclination of the beam to the optic axis rises to $\pi/2$ and Scherzer's theorem is no longer applicable. Since electron mirrors can be convergent or divergent, it should be possible to find combinations of lens and mirror for which the spherical aberration is cancelled and a number of low-energy-electron microscopes and photoelectron emission microscopes have indeed been corrected in this way. One early design was discussed by Zworykin et al. (1945) and again by Septier (1966) but this had the double disadvantage

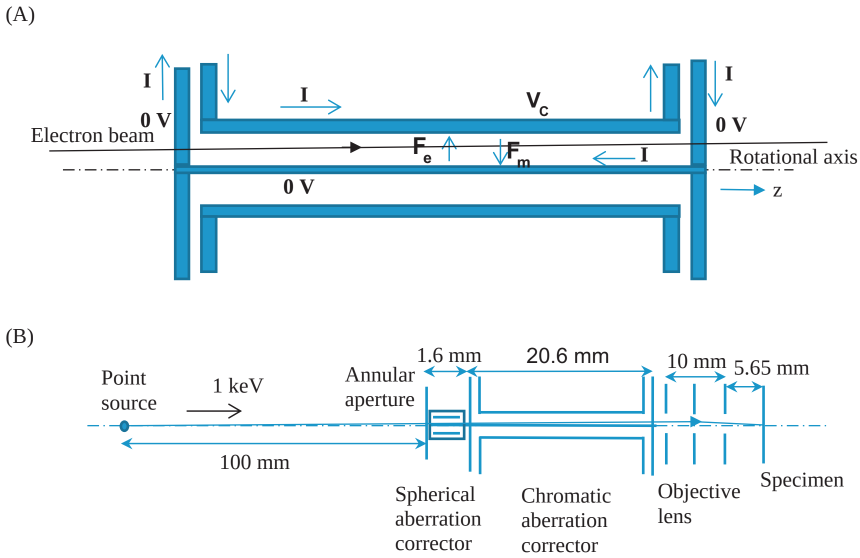

Figure 41.34
The Khursheed–Ang on-axis corrector. (A) Chromatic aberration corrector. (B) A practical design. *After Khursheed and Ang (2015), Courtesy Cambridge University Press.*

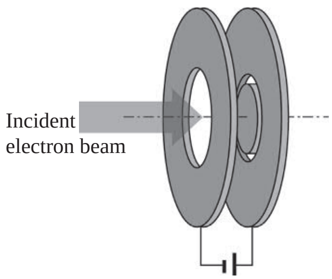

Figure 41.35
The two electrodes of the ACE corrector. *After Kawasaki et al. (2016a), Courtesy Wiley.*

that the object or target lay in a strong electric field and very little space was available to the beam. This idea was revived by Słowko (1973, 1975). A rather different arrangement (Fig. 41.37) uses the rotation within a magnetic lens to separate the incoming and outgoing parts of the beam (Kasper, 1968/69b; see also Hawkes, 1980). Neither system has been tested in practice.

Mirror studies have been revolutionized by the growing interest in LEEM and PEEM. The evolution of these is briefly described in Section 37.3 and at length by Bauer (2014); here we describe the optics of mirror correctors, and especially those designed for the SMART

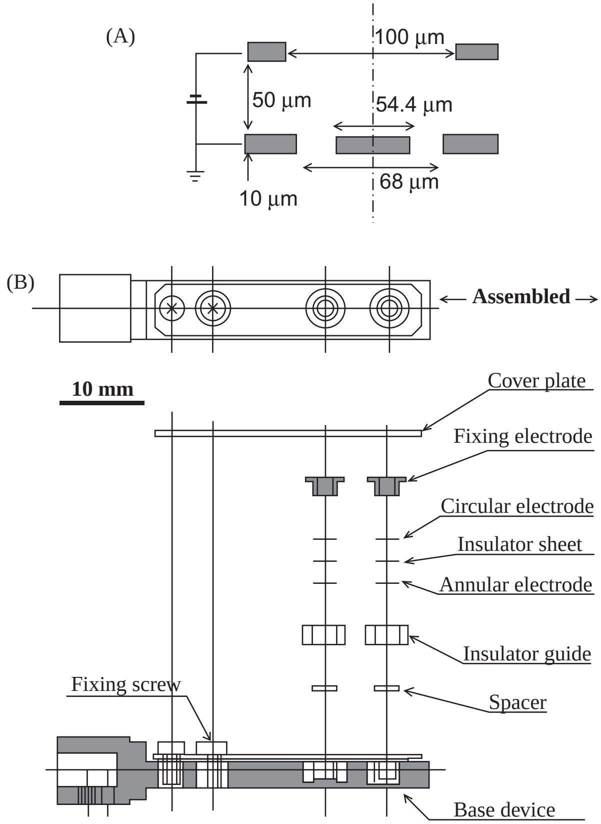

Figure 41.36
The ACE corrector. (A) Dimensions of the device. (B) Assembly of the different parts. *After Kawasaki et al. (2016a), Courtesy Wiley.*

instrument, PEEM-3, the MAD-LEEM of Mankos and Shadman (2013) and that designed by Tromp et al. (2010, 2013). Pioneering studies had been made by Rempfer and Mauck (1985, 1986, 1992), Rempfer (1990a) and Rempfer et al. (1997) and by Shao and Wu (1989, 1990a,b), who considered four-element mirrors (cf. Rempfer, 1990b). Tsuno et al. (2009) also describe a mirror corrector for a LEEM.

The central element of the SMART LEEM−PEEM is the magnetic beam separator shown in Fig. 41.38. Fig. 41.39A shows how it could be incorporated in a transmission electron microscope, where a tetrode mirror (Fig. 41.39B) provides the aberration correction. A mirror with fewer than four electrodes cannot provide the flexibility needed to vary the spherical and chromatic aberration coefficients and the focal length independently. In the complete SMART (Fig. 41.39C), electron and X-ray sources are present for LEEM or PEEM operation (Rose and Preikszas, 1992; Preikszas and Rose, 1994, 1995, 1997; Fink et al., 1997; Wichtendahl et al.,

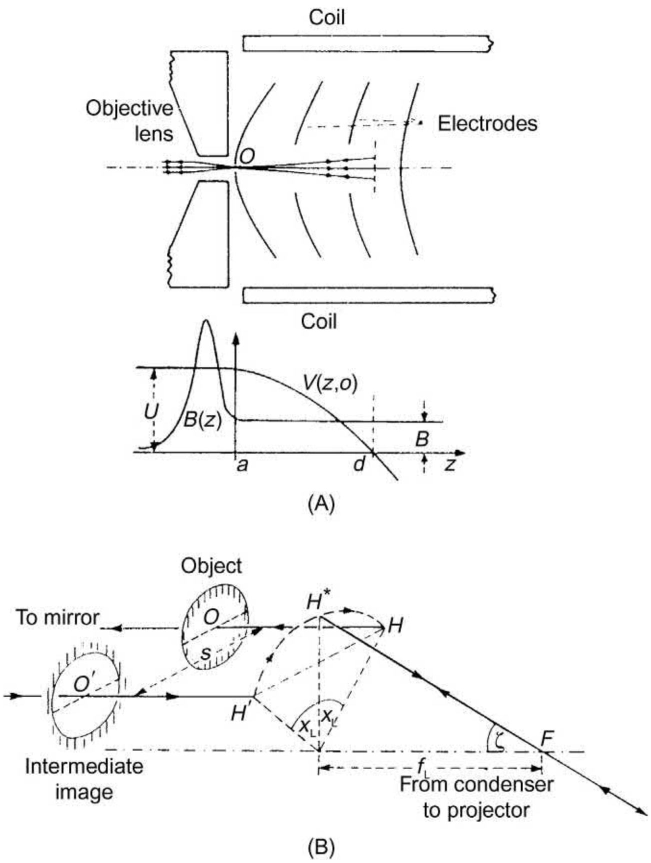

Figure 41.37
Correction of spherical aberration by combining an electron lens and a mirror. (A) Arrangement of electrodes and polepieces and the corresponding field and potential distributions. The object is placed at O ($r = 0$, $z = a$). (B) Separation of the incident beam from the returning beam. The rotation due to the coil twists the incident beam away from H^* to H, after which the beam traverses the object and is reflected by the mirror. An intermediate image is formed at O' and the returning beam is twisted from H' back to H^*, after which it retraces its original path and enters the projector system. *After Kasper (1968/69a), Courtesy Wissenschaftliche Verlagsgesellschaft.*

1998; Müller et al., 1999; Preikszas et al., 2000; Hartel et al., 2000, 2002; Schmidt et al., 2002, 2007; Rose et al., 2004; Bauer, 2008, 2018). This elegant configuration is too complex for routine instruments and simpler arrangements (Figs 41.40 and 41.41) have been described by Tromp et al. (2010, 2013) and Mankos (Mankos et al., 2012; Mankos and Shadman, 2013). At a LEEM−PEEM congress in 2006, Thomas Schmidt showed a schematic diagram of the unusual arrangement of the instrument built by Elmitec. This was reproduced by Bauer (2014) and is included here as Fig. 41.42. Another highly perfected design is PEEM-3 at the

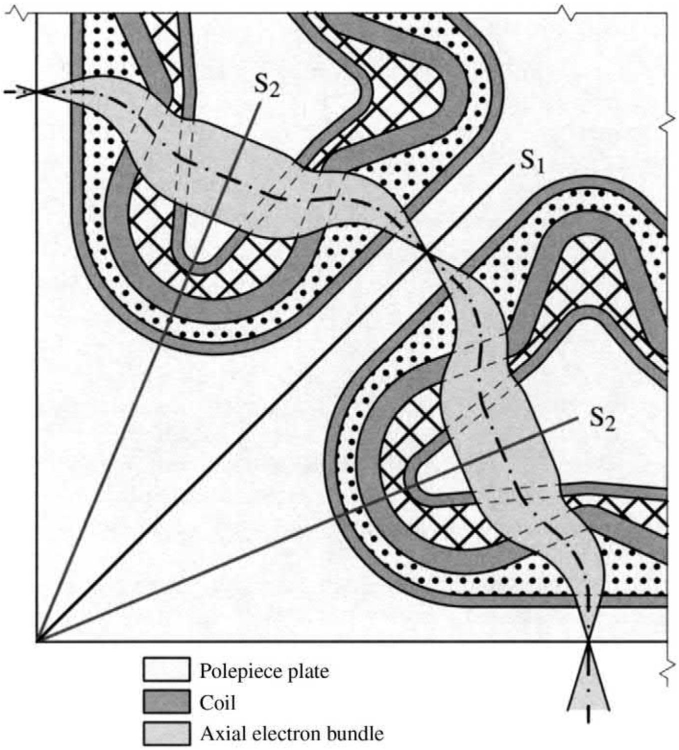

Figure 41.38
The SMART beam separator. *After Hartel et al. (2002), Courtesy Elsevier.*

Advanced Light Source in Berkely, CA (Fig. 41.43). Here too, correction is provided by a tetrode mirror. For a clear account of the optics, see Feng and Scholl (2008, 2018). The progress of the instrument can be followed in Wan et al. (2004, 2006), Wu et al. (2004), Feng et al. (2005) and Schmid et al. (2005). A new design that will permit ultrafast operation and the use of a spin-polarized beam is described by Wan et al. (2017); the many elements of the instrument can be seen in Fig. 41.44.

A novel design has been proposed by Dohi and Kruit (2017), the S-corrector, illustrated in Fig. 41.45. This is much more compact than the other instruments mentioned here. An alternative geometry is also included in Fig. 41.45. This compact design should be capable of correcting the objective aberrations of scanning electron microscopes.

Crewe has suggested that the properties of a uniform magnetic field and a mirror field could be combined to make an unusual type of corrected image-forming instrument, in which the beam traverses the specimen to which it returns free of spherical aberration after reflection at the mirror (Crewe, 1992; Crewe et al., 1995, 2000; Tsai, 2000).

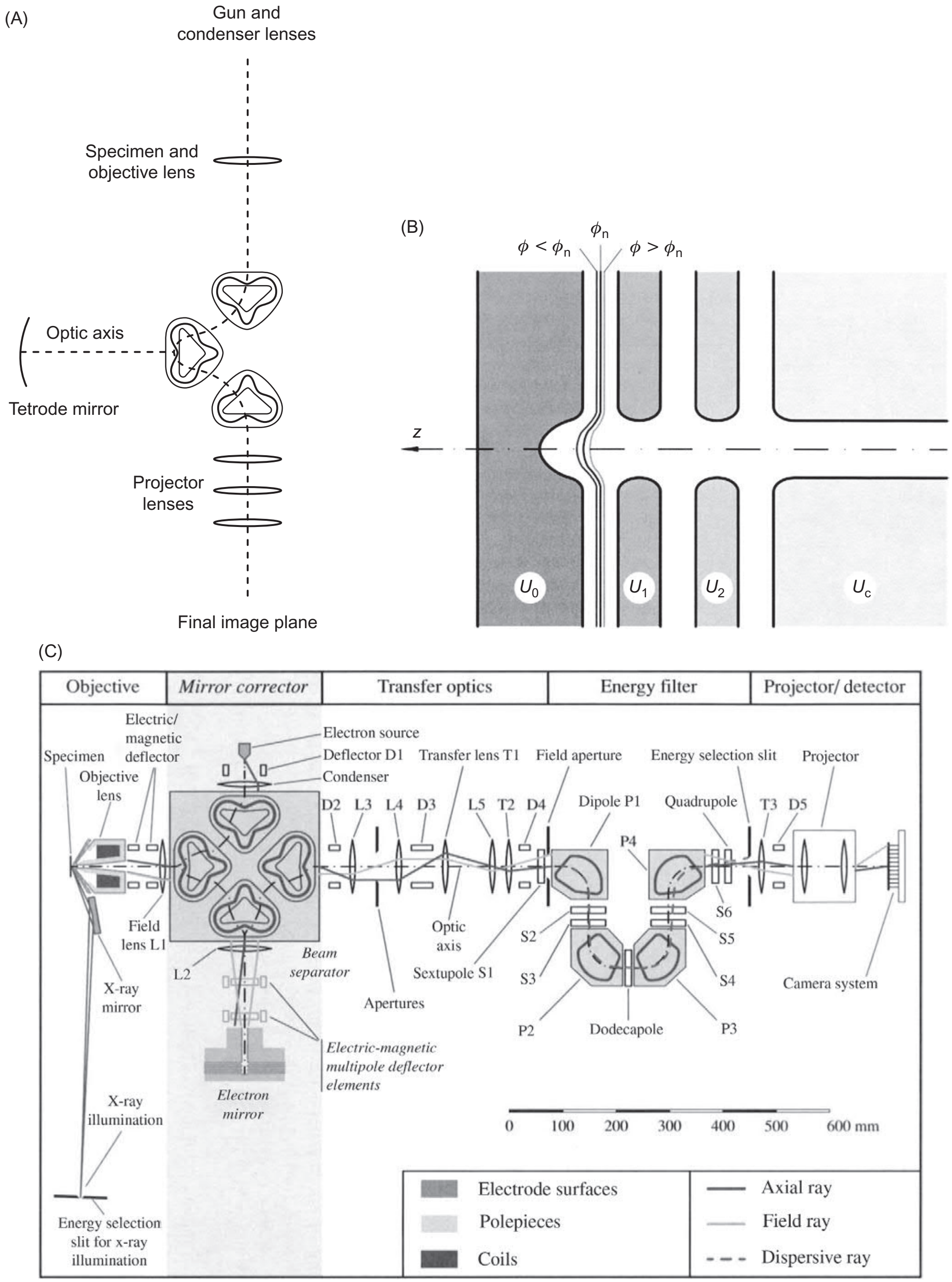

Figure 41.39

(A) Mirror as a corrector in a TEM. (B) Tetrode mirror. (C) The complete SMART. *After Hartel et al. (2002a), Courtesy Elsevier (B and C).*

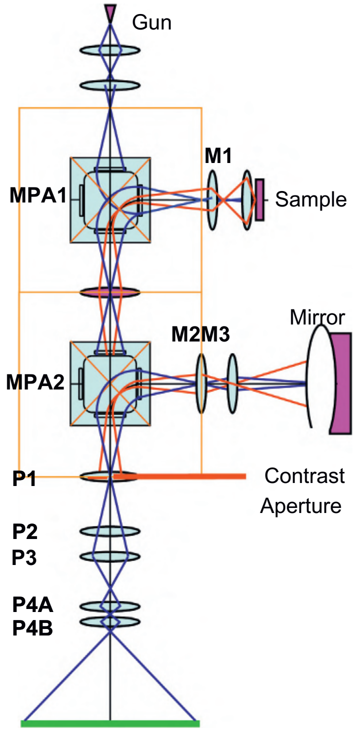

Figure 41.40
The IBM LEEM with spherical and chromatic correction. MPA: multiprism array; M and P are magnetic lenses. *After Tromp et al. (2010), Courtesy Elsevier.*

Finally, we mention a design by Yakushev and Aldiyarov (2014) in which a corrected (virtual) image is formed in a plane very close to the uncorrected image and extracted by means of a magnetic deflector.

41.6 High-Frequency Lenses

41.6.1 Spherical Correction

Interest in electron lenses with time-varying fields goes back to the 1930s and, in particular, to the work of Neßlinger (1939), who examined the behaviour of an einzel lens excited by connecting not a static voltage but a high-frequency supply to the central electrode.
A deflection system chopped the incident beam into pulses and Neßlinger showed, on the basis of a simple model, how the focal length of the lens would vary with the phase of the r.f. cycle when the electron pulse arrives and with the transit time. The focal length may be positive or negative and for a particular choice of transit time and entry phase, the lens will be achromatic for a narrow range of entry phases about the central value. It is therefore to

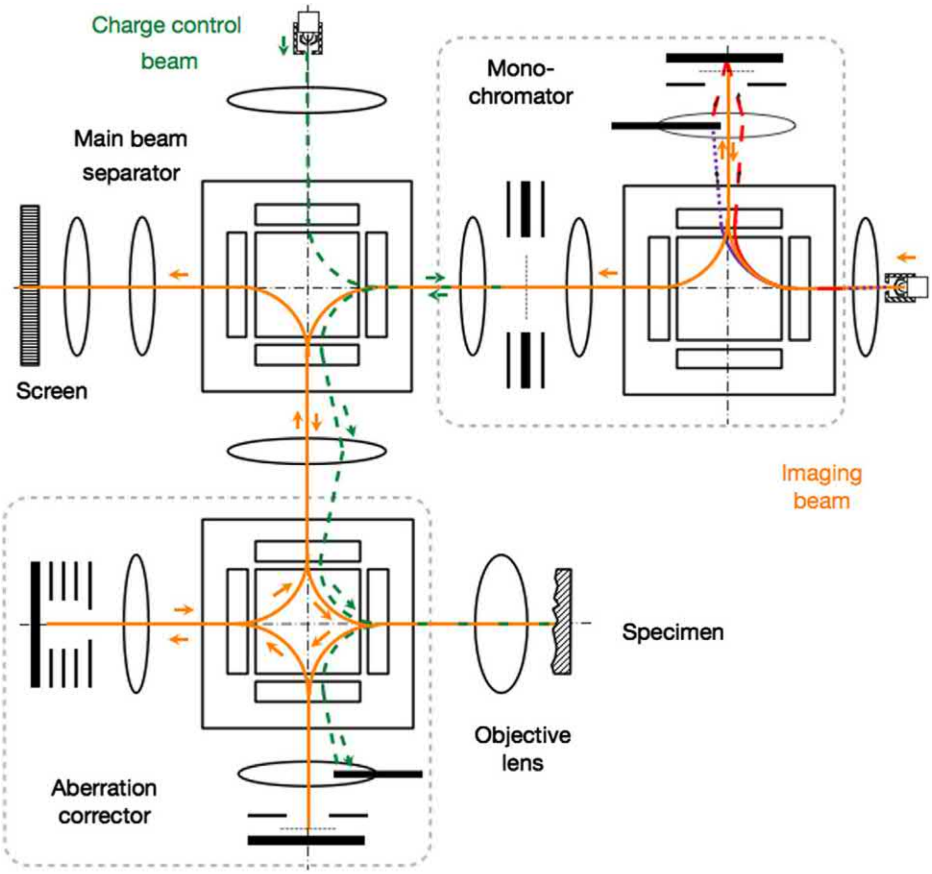

Figure 41.41
The monochromatic, aberration-corrected, dual-beam, low-energy-electron microscope (MAD-LEEM) of Mankos and Shadman. *After Mankos and Shadman (2013), Courtesy Elsevier.*

Neßlinger that we owe the important notion of the *phase condition*, the condition for which a high-frequency lens will be least sensitive to entry phase and hence provide the highest current in the sense that the pulses need not be excessively narrow. Later proposals involving high-frequency lenses that do not respect this condition are thus of little value; this is the case for the correctors described by Zworykin et al. (1945) and by Kompfner (1941), who consider a system in which an electron pulse sets out from a point on the axis; electrons that remain close to the axis arrive sooner than those that travel nearer the periphery so that if the lens strength is reduced, the effect of spherical aberration on the outer electrons can in principle be reduced. This simple picture may help to explain why the high-frequency lens came to be regarded as capable of correction but the true behaviour cannot be understood without considering both entry phase and transit time (or in other words, the part of the cycle traversed by the electron pulse). Fig. 41.46 shows Neßlinger's system and focal length curves.

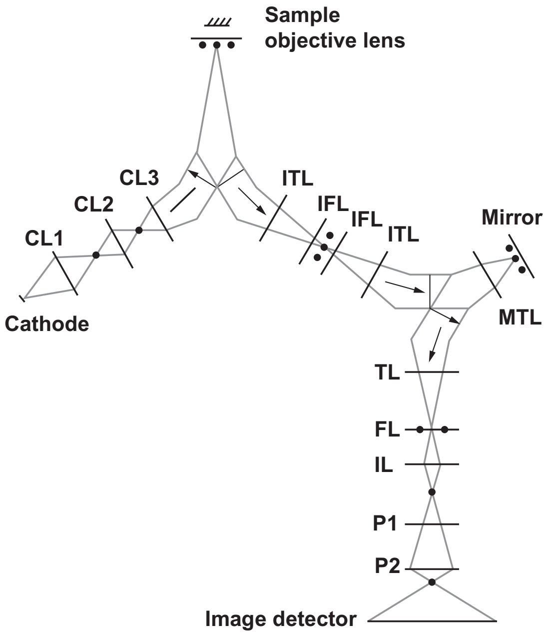

Figure 41.42
The layout of the Elmitec LEEM. IFL is a double-field lens. *Courtesy T. Schmidt.*

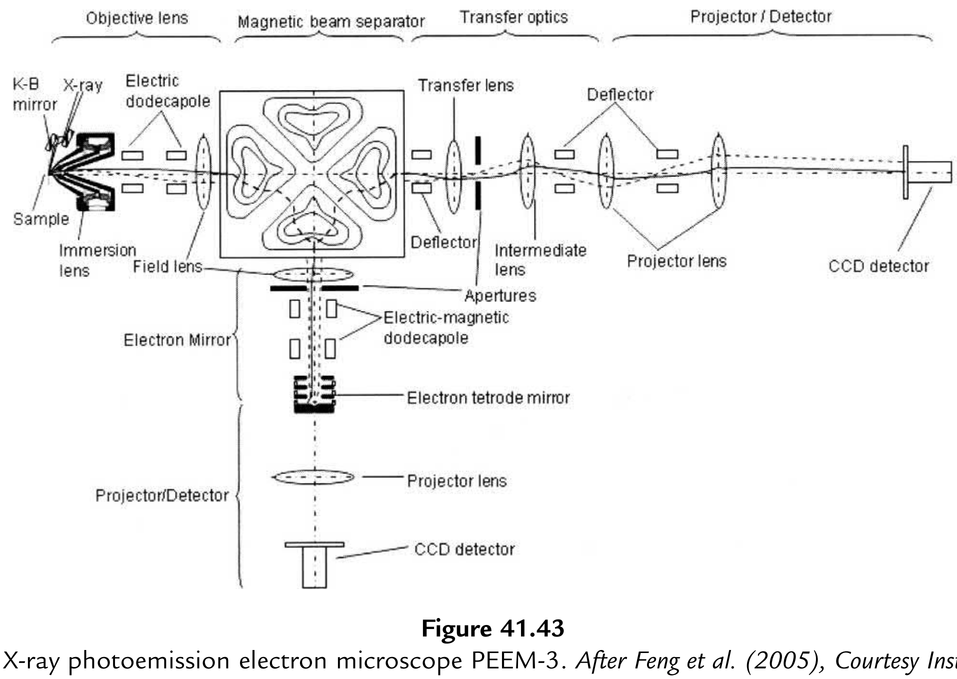

Figure 41.43
The X-ray photoemission electron microscope PEEM-3. *After Feng et al. (2005), Courtesy Institute of Physics Publishing.*

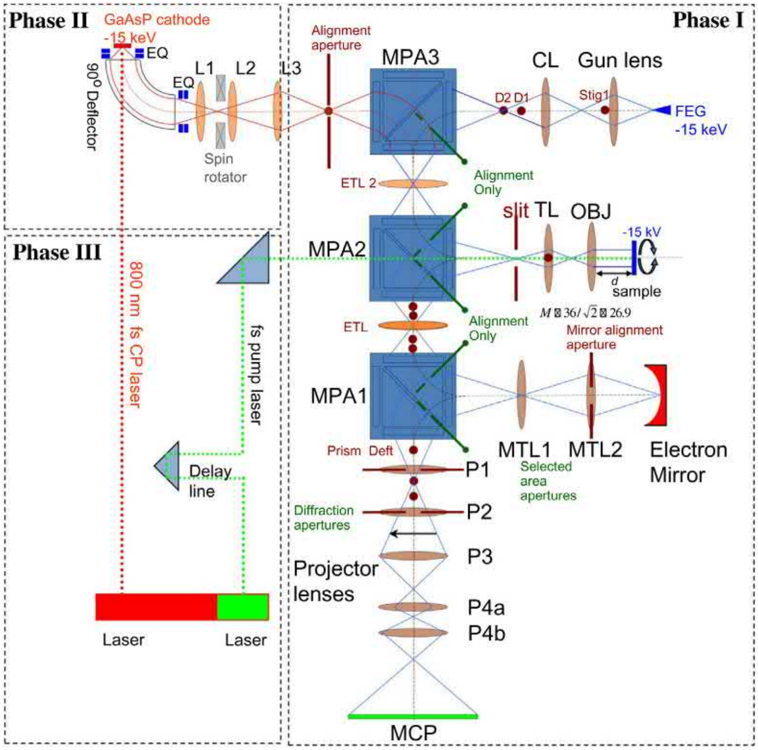

Figure 41.44

Layout of an aberration-corrected, ultrafast, spin-polarized LEEM. MPA: multiprism array; CL condenser lens; TL: transfer lens; MTL: magnetic transfer lens; OBJ: objective; ETL: electrostatic transfer lens. *After Wan et al. (2017), Courtesy Elsevier.*

The need to satisfy the phase condition in any attempt to defeat spherical aberration was clearly realized by Scherzer (1946, 1947), who discussed the design illustrated in Fig. 41.47. The working conditions that he estimated are indeed such that the condition is satisfied and there is no reason to believe that his lens would not behave as predicted (subject to some improvement in the shape of the cavity for operation in the gigahertz range.).

Several theoretical works followed, by Gabor (1950a), Sturrock (1955), Gallagher (1969) and Butler (1970). The work of Sturrock is particularly noteworthy in that a method of studying the theory of image formation in such systems is set out very fully. In Butler's paper, it seems that the phase condition is not respected. The proposal of Gallagher is to use a cavity excited in the TE mode (the other suggestions implicitly or explicitly use the TM mode); this would be attractive, since TE-mode cavity lenses can be much less sensitive to the entry phase than TM-mode cavities, were it not for the fact that the power required to achieve a short focal length is prohibitive.

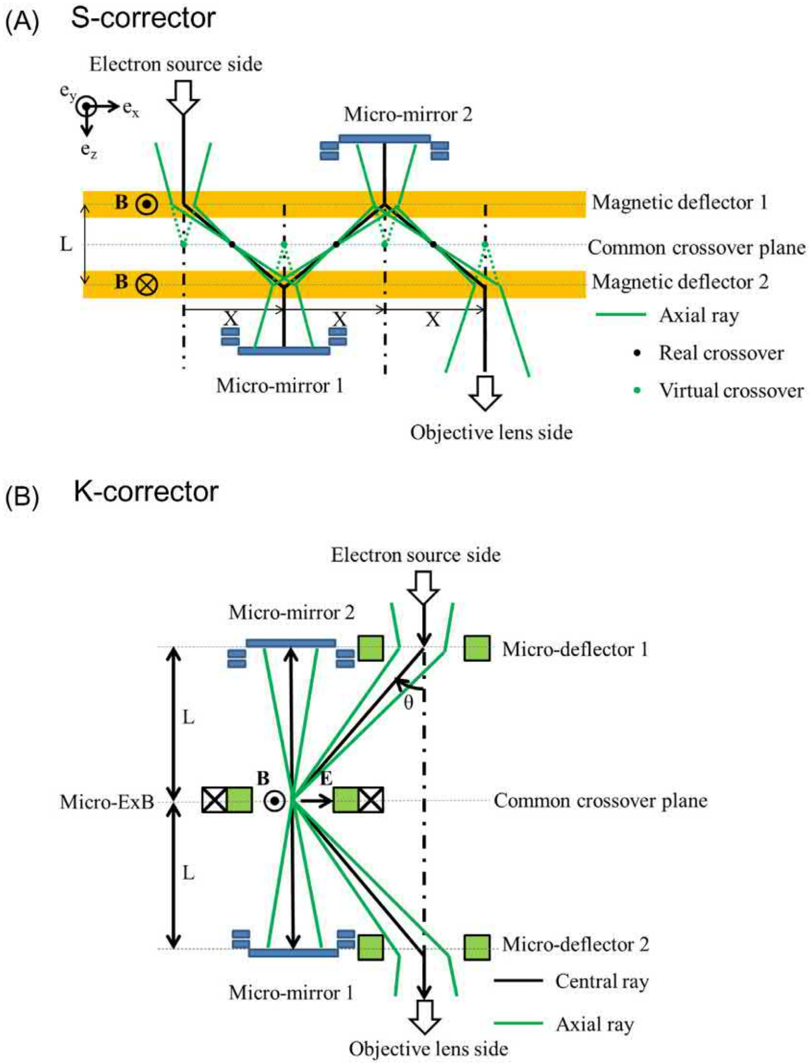

Figure 41.45

Novel corrector designs of Dohi and Kruit. (A) S-corrector. (B) K-corrector. *After Dohi and Kruit (2017). Courtesy the Japanese Society of Microscopy (A) and P. Kruit (B).*

During the 1970s, four distinct lines of research can be identified: a series of attempts by Vaidya and colleagues to correct the spherical aberration of a magnetic lens by means of a 'synklysmotron[2]', a combination of two cavities, one acting as a buncher, the other as a

[2] Synklysmotron is derived from a Greek word meaning 'washing together on a beach'. The name 'synklysmotron, therefore, stands for a process of washing the electron waves by means of electromagnetic waves, so as to clean them of aberrations' (Vaidya, 1972).

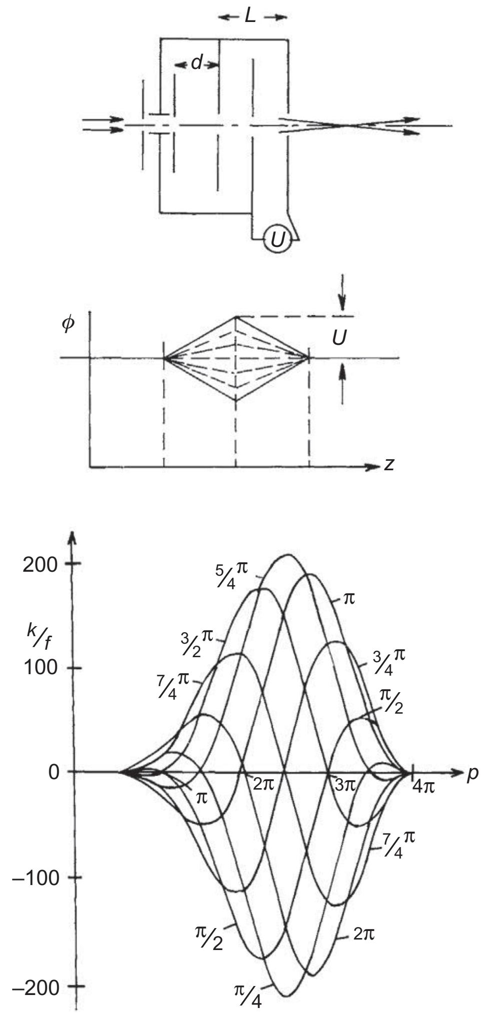

Figure 41.46
Neßlinger's system for the correction of chromatic aberration: Top, sketch of the system with the potential distribution; below, k/f against the transit angle $p = \omega L/v$, where $k = m\omega^2 L^3/eU$. *After Neßlinger (1939).*

corrector (Vaidya and Hawkes, 1970; Vaidya, 1972, 1975a,b; Garg and Vaidya, 1974; Vaidya and Garg, 1974; Pandey and Vaidya, 1975, 1977, 1978); derivation of formulae for many of the aberration coefficients by Matsuda and Ura (1974a,b) and Hawkes (1983a,b); a thorough study of the fields inside re-entrant cavities and of their paraxial properties by Oldfield (1971, 1973a,b, 1974, 1976); and a proposal for a high-voltage electron microscope incorporating high-frequency lenses and superconducting lenses (Dietrich et al., 1975; Passow, 1976a,b,c; Dietrich, 1976, 1978). The last proposal is a natural development

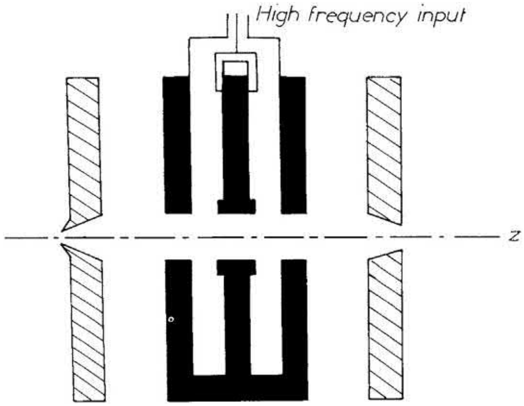

Figure 41.47
Scherzer's high-frequency einzel lens for elimination of spherical aberration. *After Scherzer (1947), Courtesy Wissenschaftliche Verlagsgesellschaft.*

of the experimental attempts of Watanabe et al. (1974) and Anazawa et al. (1975) to couple a pulsed field-emission gun to a linear accelerator for microscopy in the 5–10 MV range.

The progress made by Vaidya and colleagues in the design of synklysmotron lenses for various applications – electrostatic or magnetic objective and probe-forming lenses – culminated in a proposal for a corrected high-voltage system to be placed between the final condenser and the objective of a 5 MV microscope (Pandey and Vaidya, 1977). Oldfield (1973a) had pointed out that some of their earlier estimates may have been over-optimistic.

By far the most complete study of microwave cavities as electron lenses is that of Oldfield. This is based on full calculation of the field in the cavity by means of an iterated relaxation technique. The variation of the space and time cardinal elements is discussed at length and illustrated with numerous graphs and tables. These show clearly, in the frequency range considered (around 3 GHz), the conditions in which cavity lenses will be divergent and convergent and the sensitivity of the various characteristics to changes. A rotationally symmetric chopper capable of providing picosecond pulses was designed on the basis of this (Oldfield, 1976). The beam choppers then in use were criticized by Menzel and Kubalek (1978) on the grounds that each was only suitable for its own particular application. A more versatile system was proposed and its performance analysed; a much improved chopper was later described by Fehr et al. (1990). Fig. 41.48 shows how a microwave cavity could be used to correct a magnetic lens.

Finally, we turn to the very ambitious project described by Dietrich et al. (1975) and further discussed by Passow (1976a–c), Dietrich (1978) and Strojnik and Passow (1978a,b). The suggestion here is that the technology already developed in the field of particle accelerators

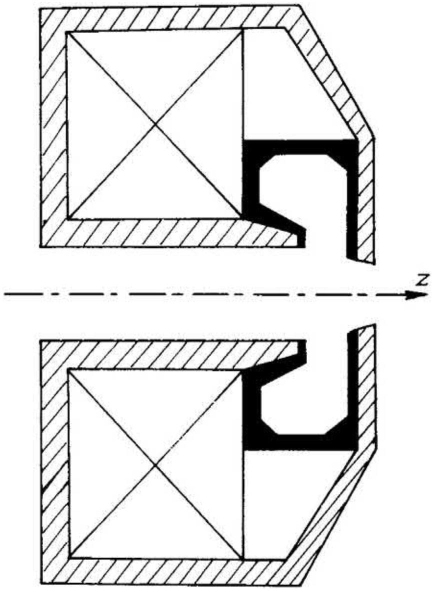

Figure 41.48
Oldfield's design incorporating a microwave cavity in the gap of a magnetic lens. *After Oldfield (1973a), Courtesy the author.*

(e.g. Hartwig and Passow, 1975) should be combined with work on superconducting lens design (Dietrich, 1976, 1978; Bonjour, 1976; Hawkes and Valdrè, 1977) to produce a very high-voltage pulsed-beam electron microscope. (The paper by Strojnik and Passow (1978a) considers what conventional lenses for such a microscope would be like.) This projected instrument (Fig. 41.49) is discussed briefly in the context of other new or avant-garde machines by Riecke (1977), Herrmann (1978) and Cosslett (1978). There has been no further work on this proposal; one reason for this may be that the restrictive relation between geometry, microwave frequency and accelerating voltage is undoubtedly a major inconvenience.

41.6.2 Chromatic Correction

The ideal corrector of chromatic aberration would redistribute the energies of the beam electrons in such a way as to reduce the range of energies present. A way of achieving this has been proposed by Schönhense and Spiecker (2002a,b, 2003), with LEEM and PEEM (Section 37.3) in mind. The trigger that provokes emission of electrons by the specimen is now pulsed. The electrons are accelerated and collimated as usual before entering a drift space, in which the faster electrons draw away from the 'field', like racehorses or Formula One cars. Beyond this drift space is a pulsed accelerator segment, which is switched on when the faster electrons have already passed; the slower electrons are speeded up and

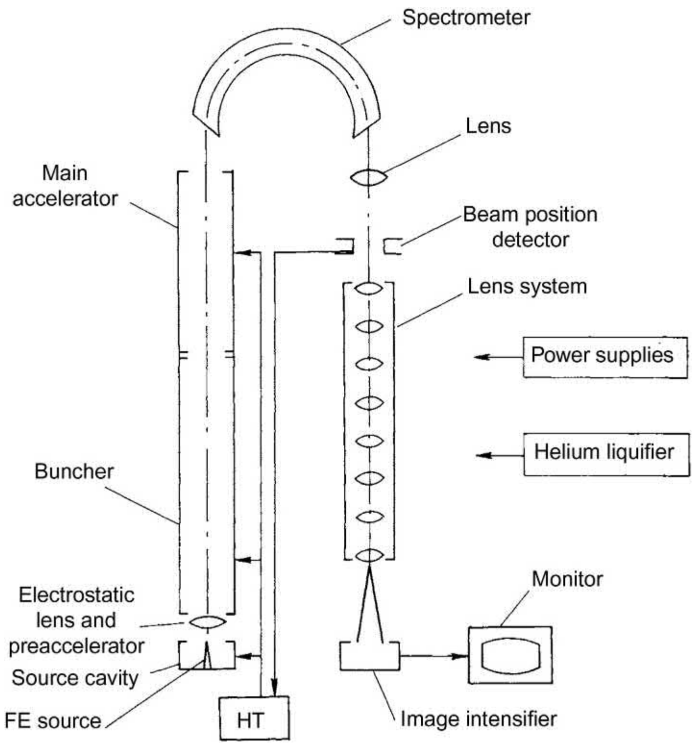

Figure 41.49
The ultrahigh-voltage microscope proposed by Dietrich et al., incorporating a microwave accelerator and superconducting lenses. *After Dietrich et al. (1975), Courtesy Wissenschaftliche Verlagsgesellschaft.*

acquire more energy than the faster ones. The beam energy has thus been redistributed and the chromatic aberration of the subsequent lens should generate a smaller spot than in the absence of the device. The principle is shown in Fig. 41.50. Schönhense and Spiecker suggest that a similar device could be used to correct the spherical aberration of an electrostatic lens. Here, a pulsed beam is again used and the lens strength is changed abruptly when the pulse reaches the centre of the lens. The field encountered by the electrons is thus discontinuous and Scherzer's theorem does not apply.

Khursheed (2005) has also suggested a means of achieving dynamic correction of chromatic aberration in low-voltage scanning electron microscopes, based on his design for a low-voltage time-of-flight electron emission microscope (Khursheed, 2002). Here again, the beam electron pulses traverse a drift space after being decelerated to a very low energy (typically 5–20 eV); on emerging, they are accelerated but while in the drift space, they will have become dispersed in space and time. The objective lens now consists of both polepieces and electrodes. The voltage on the latter is ramped in synchronism with the gun

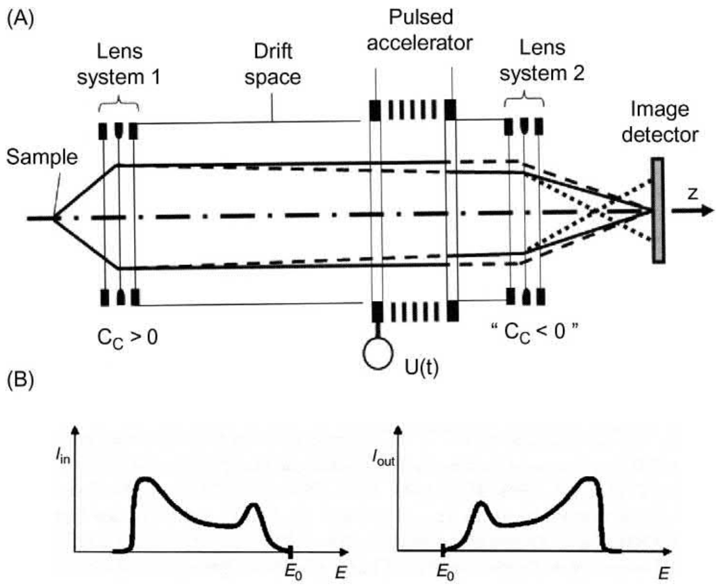

Figure 41.50
Inversion of the electron energy distribution as a means of overcoming chromatic aberration. (A) Cross-section of the device. (B) The electron energy distribution before and after passage through the corrector. *After Schönhense et al. (2002), Courtesy the American Institute of Physics.*

pulses so that electrons arriving at different times with different energies are all focused at the same plane. This could be achieved by means of a triangular waveform (Fig. 41.51). For many more details, see Khursheed (2005).

41.7 Other Aspects of Aberration Correction

Perhaps the most celebrated proposal for aberration correction is absent from the foregoing accounts, not because it has failed but because its explanation requires wave optics, which is the subject of Volume 3. The method in question is holography, which Gabor originally introduced (1948, 1949) as a means of eliminating the effect of spherical aberration from a micrograph recorded with an uncorrected microscope. This technique properly belongs with the various geometrical optics correction techniques already described, therefore. Although holography is no longer regarded as an aberration-correction technique, it is gratifying to note that Tonomura et al. (1979), Franke et al. (1987), Lichte (1991, 1993, 1995) and Fu et al. (1991) have shown that Gabor's original plan does work. Today electron holography is often performed on corrected microscopes.

Otherwise, there have been a number of suggestions for aberration correction that do not fit into the earlier sections. Proposals such as those of Kas'yankov (1950, 1952, 1955), Dutova and Kas'yankov (1963), Taganov and Kas'yankov (1964, 1965, 1967), Taganov (1966) and Gurbanov and Kas'yankov (1966, 1968) for minimizing various aberration coefficients have

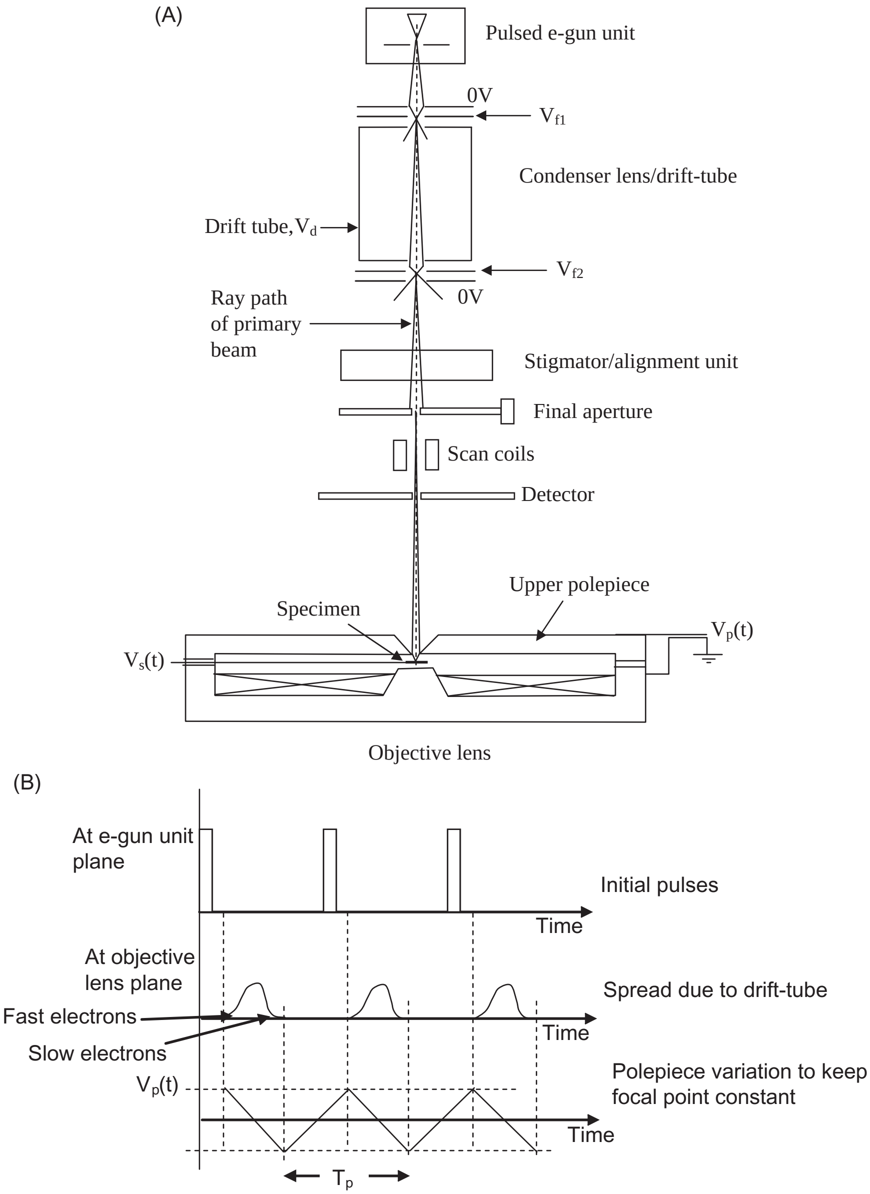

Figure 41.51

Dynamic aberration correction in a SEM. (A) Layout of the instrument. (B) Pulse shapes at the gun and at the objective lens. The bottom line shows the applied potential at the level of the upper polepiece. *After Khursheed (2005), Courtesy Elsevier.*

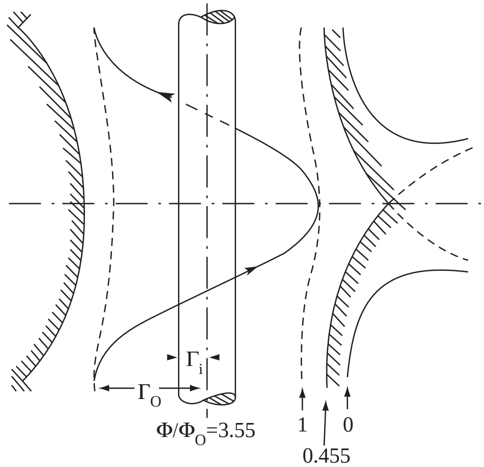

Figure 41.52
Electrode design for a helical lens. *After Gabor (1951), Courtesy Institute of Physics Publishing.*

lost much of their interest in the face of more powerful computer-aided design techniques such as that introduced by Moses (1971, 1973) and applied by him to various problems (Rose and Moses, 1973; Moses, 1974). The use of a compound lens consisting of a strong lens with the object beyond the focus and hence producing a virtual image followed by a weak lens to convert the latter into a real image (Marton, 1939; Marton and Bol, 1947) is no longer attractive now that condenser-objective and even second-zone lenses are in routine use.

An egregious system with negative chromatic aberration was devised by Gabor (1950b, 1951), who considered systems with helical optic axes. The necessary fields could be created by helical electrodes with the same pitch or even by coaxial cylinders. He showed that, subject to certain conditions, electrons perform a 'radial, simple harmonic oscillation' about the helical axis. For a suitable choice of the pitch of the helix, an electron beam will exhibit no lateral chromatic aberration at the sequence of image planes along the helix. An electrode design for a helical lens is shown in Fig. 41.52.

The needs of ion optics have led Dalglish (1981) and Dalglish et al. (1983a,b) to examine the behaviour of two pairs of rods, each forming a deflector (the so-called 'Caledonian quadruplet'); this is mentioned by McKee and Smith (1989).

41.8 Concluding Remarks

From this account of the many ways of correcting spherical and chromatic aberration in electron microscopes and related instruments, it is clear that correction of the coefficients of lowest order, C_s and C_c, is only a first step towards any real improvement in their resolution unless the uncorrected instrument is not operating at its highest performance. The other third-order aberrations, parasitic aberrations and higher-order aberrations must all be kept under control. This point has been recognized and addressed by the designers of modern sextupole and quadrupole−octopole correctors and mirror correctors but is not taken into account in the other approaches to aberration correction. It is therefore not likely that any of these will become real rivals of the types of corrector that have proved their worth in the past few years.

Other types of corrector, in particular those with curved optic axes, are examined in Chapter 52, Sector Fields and Their Applications.

We have not discussed here the stability of the correction process. This important aspect is considered by Schramm et al. (2012), Barthel and Thust (2013), Tromp and Schramm (2013) and Kisielowski et al. (2015).

Caustics and Their Uses

42.1 Introduction

Hitherto we have considered the aberrations in electron optical systems mainly as a geometric effect in the sense that we have focused our attention on the geometric shifts between real and ideal image coordinates. Another important branch of the electron optical imaging process is concerned with the intensity distribution in the vicinity of a recording plane. Surfaces exist over which the electron intensity is very high; these surfaces are characterized by the fact that neighbouring rays intersect one another on them. Such surfaces, known as caustics, are of great interest in practice, since their intersections with the recording plane are seen as lines of very high current density.

The intensity distributions in electron beams will be dealt with in some detail in Chapter 47, Brightness, but the theory of brightness outlined there is developed mainly with electron guns in mind. Here we shall make some simplifications, since the study of the influence of aberrations on the intensity distribution otherwise becomes too complicated.

42.2 The Concept of the Caustic

In the following account we shall essentially follow Glaser (1952). Caustics have also been studied by Kanaya and Kawakatsu (1960a, 1960b), Kanaya et al. (1959a, b. 1990), Lenz and Hahn (1953), Scheffels et al. (1953), Lenz (1956) and Tavabi et al. (2015). Kimoto et al. (2003) have used caustic figures for coma-free alignment.

Let us consider all trajectories that start from a fixed object point P_o with coordinates $\boldsymbol{r}_o(x_o, y_o, z_o)$. Each particular ray is then uniquely defined by a set of three additional parameters (α, β, U), where α and β are, for instance, initial slopes or coordinates of intersection with a given aperture plane, while U is a measure of the energy. Thus

$$x = x(\boldsymbol{r}_o, \alpha, \beta, U; z), \quad y = y(\boldsymbol{r}_o, \alpha, \beta, U; z) \tag{42.1}$$

For reasons of conciseness we shall omit parameters that are kept fixed; here these are the coordinates x_o, y_o, z_o and the energy U. We now consider two neighbouring rays, given by

Principles of Electron Optics: Applied Geometrical Optics.
DOI: http://dx.doi.org/10.1016/B978-0-12-813369-9.00042-7

$$x_1 = x(\alpha, \beta, z) \qquad y_1 = y(\alpha, \beta, z)$$
$$x_2 = x(\alpha + \Delta\alpha, \beta + \Delta\beta, z) \quad y_2 = y(\alpha + \Delta\alpha, \beta + \Delta\beta, z)$$

For very small increments $\Delta\alpha$ and $\Delta\beta$, x_2 and y_2 can be expanded as Taylor series, which are then truncated after the linear terms:

$$x_2 = x_1 + \frac{\partial x}{\partial \alpha}\Delta\alpha + \frac{\partial x}{\partial \beta}\Delta\beta$$

$$y_2 = y_1 + \frac{\partial y}{\partial \alpha}\Delta\alpha + \frac{\partial y}{\partial \beta}\Delta\beta$$

The condition for the two rays in question to intersect takes the form

$$\frac{\partial x}{\partial \alpha}\Delta\alpha + \frac{\partial x}{\partial \beta}\Delta\beta = 0$$
$$\frac{\partial y}{\partial \alpha}\Delta\alpha + \frac{\partial y}{\partial \beta}\Delta\beta = 0$$

This system of equations has nonzero solutions for $\Delta\alpha$ and $\Delta\beta$ only if the determinant of the coefficients vanishes:

$$D(\alpha, \beta; z) \coloneqq \frac{\partial x}{\partial \alpha}\frac{\partial y}{\partial \beta} - \frac{\partial x}{\partial \beta}\frac{\partial y}{\partial \alpha} = 0 \tag{42.2}$$

This is the essential condition for the existence of a caustic, since together with (42.1), (42.2) describes a surface in the three-dimensional space. A two-dimensional section through a caustic has already been seen in Fig. 5.5.

The mathematical representation of the caustic can take different forms. We can, for example, solve Eq. (42.2) for z, which gives a number n of different roots:

$$z = z_j(\alpha, \beta), \quad j = 1 \ldots n \tag{42.3a}$$

These can be introduced into (42.1) in order to determine

$$x = x_j(\alpha, \beta), \quad y = y_j(\alpha, \beta), \quad j = 1 \ldots n \tag{42.3b}$$

These relations now form a parametric representation of n different surfaces: these are the n different branches of the caustic. They may be separate, tangent to each other or intersect each other. In general, the whole caustic will thus have a very complicated structure: some typical examples will be presented below. The above representation is the most general, but is not always very convenient. In many practical cases there is a field-free image space behind the system in question. Both the recording plane $z = z_i$ and the plane $z = z_a$ of the exit pupil are then located in this space. We now identify the parameters $\alpha = x_a$ and $\beta = y_a$

with the Cartesian ray coordinates referring to the aperture plane $z = z_a$. The rays, being straight lines in field-free space, can be written

$$x = x_a + (z - z_a)\, p(x_a, y_a), \quad y = y_a + (z - z_a)\, q(x_a, y_a) \tag{42.4}$$

where p and q denote their slopes. With the abbreviations

$$\left.\begin{aligned} \sigma = \frac{1}{z - z_a}, \quad A_{11} &= \frac{\partial p}{\partial x_a}, \quad A_{12} = \frac{\partial p}{\partial y_a} \\ A_{21} &= \frac{\partial q}{\partial x_a}, \quad A_{22} = \frac{\partial q}{\partial y_a} \end{aligned}\right| \tag{42.5}$$

the caustic condition (42.4) can be put into the convenient form

$$\begin{vmatrix} \sigma + A_{11} & A_{12} \\ A_{21} & \sigma + A_{22} \end{vmatrix} = \sigma^2 + \sigma(A_{11} + A_{22}) + A_{11}A_{22} - A_{12}A_{21} = 0 \tag{42.6}$$

This can be interpreted in the following two ways.

i. We may prescribe reasonable values for x_a and y_a; Eq. (42.6) is then a quadratic equation for the reciprocal distance σ at which the particular ray is tangent to the caustic. There are no more than two such points.
ii. We may prescribe a fixed reference plane $z = \text{const} \neq z_a$ and hence $\sigma = (z - z_a)^{-1}$. Eq. (42.6) is then a condition from which the values of the coordinates x_a and y_a may be found. This may be considered as the equation of a curve in the (x_a, y_a)-plane, called the *basis-curve* (Glaser, 1952). It has the following concrete meaning: all rays that are tangent to the caustic in the reference plane (z) intersect the aperture plane along the basis-curve. A typical example is shown in Fig. 42.1.

For practical purposes, (42.6), having the form $f(x_a, y_a, \sigma) = 0$, is inconvenient. It is better to introduce an additional parameter τ and write the solution in the form

$$x_a = x_a(z, \tau), \quad y_a = y_a(z, \tau) \tag{42.7}$$

Introducing this into Eq. (42.4), we obtain the caustic equations in a hybrid Cartesian-parametric form $x = x(z, \tau)$, $y = y(z, \tau)$. Since the caustic consists of different branches, the same must, of course, hold for the basis-curves.

42.3 The Caustic of a Round Lens

We study first – as a comparatively simple example – the caustic of a round lens at high magnification M. For reasons of simplicity we assume that the corresponding object point is located on the optic axis and quite near to the focal point on the object side of the lens. Without loss of generality we may choose the image principal point as the origin of the

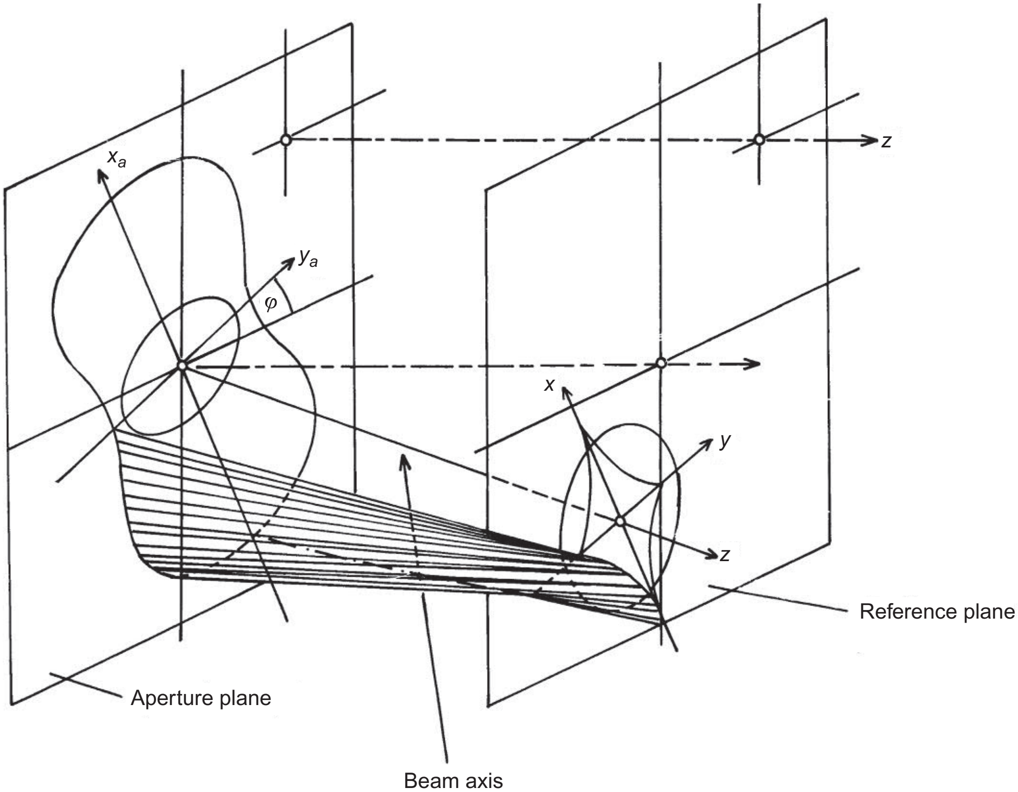

Figure 42.1
Basis-curves in the aperture plane and lines of intersection of the caustic with the corresponding reference plane. *After Glaser (1952), Courtesy Springer Verlag.*

axial scale and also as the centre of the aperture, so that $z_a = 0$. The asymptotic representation of a ray starting with an aperture angle α and passing through a lens with focal lengths f_o and f_i and spherical aberration coefficient C_s is then given by

$$r(z, \alpha) = \alpha\left(f_o + \frac{zf_o}{Mf_i} - \frac{\alpha^2 C_s z}{f_i}\right) + O\left(\alpha^5\right) \tag{42.8}$$

The reciprocal magnification M^{-1} may pass through zero and change sign, but $|M^{-1}|$ will be so small that we need not consider the variation of C_s with M.

The second parameter β is the azimuth φ round the optic axis; thus (42.1) takes the form

$$\begin{aligned} x(z, \alpha, \varphi) &= \left(f_o + zf_o/Mf_i - \alpha^2 C_s z/f_i\right)\alpha \cos\varphi \\ y(z, \alpha, \varphi) &= \left(f_o + zf_o/Mf_i - \alpha^2 C_s z/f_i\right)\alpha \sin\varphi \end{aligned} \tag{42.9}$$

The caustic condition (42.2) now becomes

$$\left(f_o + zf_o/Mf_i - 3\alpha^2 C_s z/f_i\right) r(z,\alpha) = 0$$

One possible root is $r(z,\ \alpha) = 0$ which yields the axial singularity of the caustic. The more interesting root results from the vanishing of the other factor:

$$z(\alpha) = \frac{f_o f_i}{3\alpha^2 C_s - f_o/M} \tag{42.10a}$$

Introducing this into (42.8), we obtain the radial caustic coordinate:

$$r(\alpha) = \frac{2\alpha^3 f_o C_s}{3\alpha^2 C_s - f_o/M} \tag{42.10b}$$

and with this the lateral coordinates

$$x(\alpha,\varphi) = r(\alpha)\cos\varphi, \quad y(\alpha,\varphi) = r(\alpha)\sin\varphi \tag{42.10c}$$

The caustic is clearly a rotationally symmetric surface, as it must be in the present example. It is hence sufficient to investigate an axial section through the caustic. A study of the basis-curves is not particularly illuminating here. It is clear that the basis-curve referring to a plane $z = \text{const}$ and located in the principal plane $z_a = 0$ must be a circle. Its radius is $r_B = \alpha f_o$, $\alpha = \alpha(z)$ being a solution of (42.10a) for α.

When discussing the geometric shape of the caustic, we have to distinguish between two essentially different cases, in one of which the caustic has an axial cusp while in the other the caustic has an off-axis waist. The first case arises when $3\alpha_M^2 C_s < f_o|M|^{-1}$, α_M being the maximum aperture angle. The denominator in Eq. (42.10a,b) can then never vanish. For the following discussion the sign of M is irrelevant, so that the same formulae are valid for real and virtual focusing alike.

The position of the cusp is obtained from Eq. (42.10a):

$$\alpha = 0, \quad z_s := z(0) = -Mf_i \tag{42.11}$$

In practice it is usually sufficient to study only the vicinity of this point; it is then permissible to carry out a power series expansion with respect to α and truncate this after the nontrivial terms of lowest order; we obtain

$$\begin{aligned} z(\alpha) &= -Mf_i - 3\alpha^2 M^2 C_s f_i/f_o + O\left(\alpha^4\right) \\ r(\alpha) &= 2MC_s\alpha^3 + O\left(\alpha^5\right) \end{aligned} \tag{42.12}$$

It is now easy to eliminate the parameter α, giving

$$r(z) = \frac{2C_s}{M^2}\left\{\frac{f_0(z_s - z)}{3f_iC_s}\right\}^{3/2}, \quad (z \le z_s) \tag{42.13}$$

This is the familiar Neile parabola for the spherical aberration, which is shown in Fig. 42.2. Since $|\alpha| \le \alpha_M$, the caustic occupies only a finite part of this curve.

The caustic with a waist will be obtained if the denominator of Eq. (42.10) has a zero. The caustic then extends to infinity in the positive and negative directions. One part of it has an axial cusp, as in the former case, and corresponds to pure virtual focusing. The other part may form a waist, as shown in Fig. 42.3. The position of the waist is found by writing $dr/d\alpha = 0$ in (42.10b); for $M > 0$, we find

$$\alpha_w = \sqrt{\frac{f_o}{MC_s}}, \quad z_w = \frac{1}{2}Mf_i, \quad r_w = f_o\alpha_w \tag{42.14}$$

The curvature of the waist is given by

$$\left(\frac{d^2r}{dz^2}\right)_w = \frac{r_w}{3z_w^2} > 0 \tag{42.15}$$

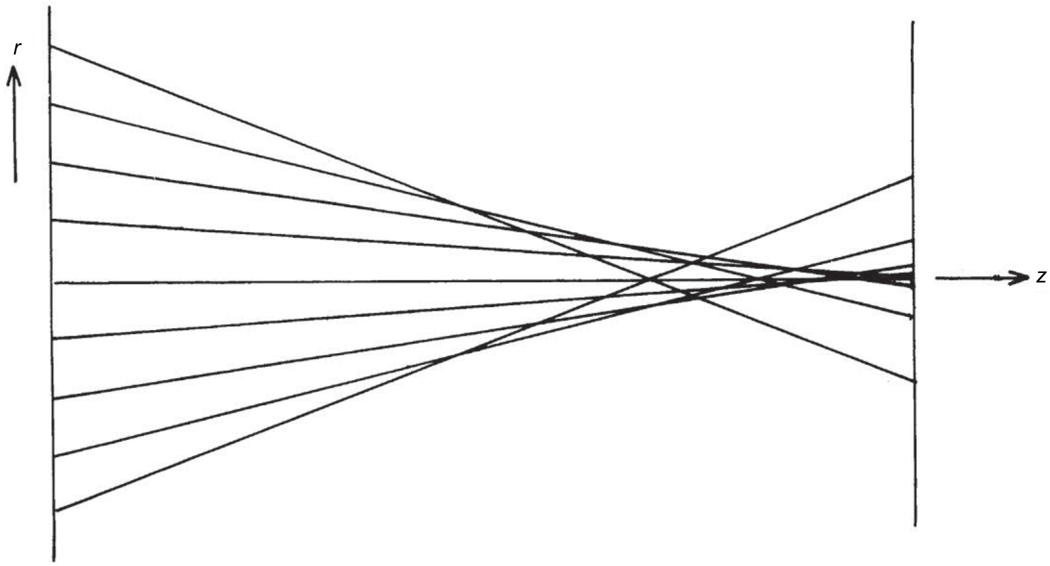

Figure 42.2
Caustic for a round lens. In this example, the caustic consists of a real branch terminating in a cusp and a virtual branch with a waist.

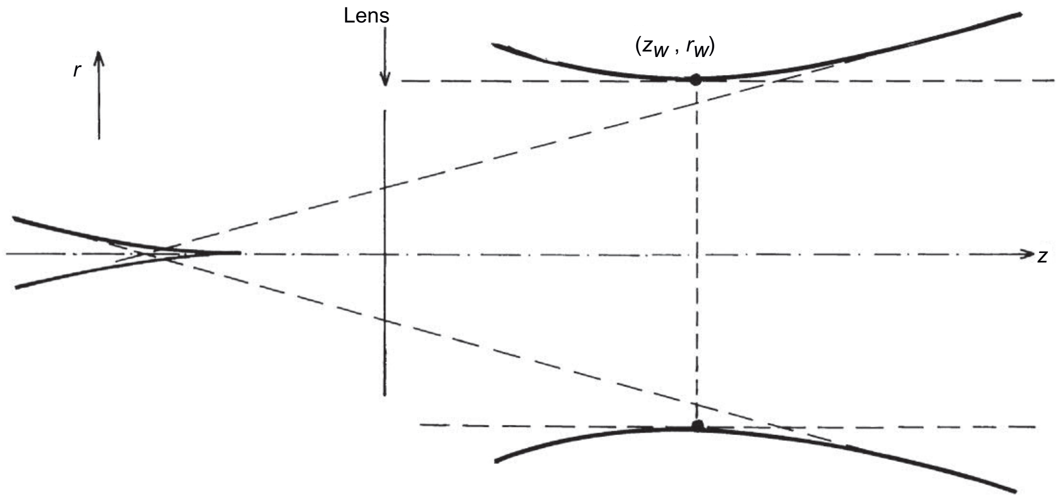

Figure 42.3
Caustic for a round lens. In this example, the caustic consists of a real branch terminating in a cusp and a virtual branch with a waist.

A structure like that shown in Fig. 42.3 occurs in all devices in which the electron beam is as nearly as possible parallel.

42.4 The Caustic of an Astigmatic Lens

This question has been investigated in great detail by Glaser (1952). The astigmatism may be caused by imperfections of the rotational symmetry or by skew propagation of the beam through the lens.

For a *fixed* off-axis object point the coma can always be eliminated by means of a suitably placed off-axis circular aperture and the distortion by a lateral shift of the image coordinates. It is then favourable to introduce a curved and deflected beam axis passing through the given object point, the centre of the aperture, and through the image point shifted by distortion. Relative to this beam axis, the remaining aberrations can be considered as those of an *isoplanatic* approximation. This approximation, dealt with in detail in Chapter 31, Parasitic Aberrations, will be made here so that the lateral coordinates are now measured relative to the beam axis.

In the isoplanatic case we consider the defocus, the axial chromatic aberration, the two-fold astigmatism and the spherical aberration. For simplicity we shall assume that the space between the aperture and the reference or recording plane is field-free, so that it is permissible to deal with ray-asymptotes.

Without loss of generality we again identify the centre of the aperture with the origin of the coordinate system. Furthermore, by a suitable rotation round the beam axis (here the z-axis), the transverse coordinate axes can be oriented parallel to the symmetry directions of the astigmatism. Let s be the distance between the aperture plane and the Gaussian image plane; the asymptotic ray equations are then

$$\begin{aligned} x &= x_a\left(1-\frac{z}{s}\right)+\left(\Delta z_i + C_c'\frac{\Delta U}{U} - C_A'\right)\frac{x_a z}{s^2} - \frac{C_s'}{s^4} z\left(x_a^2+y_a^2\right)x_a \\ y &= y_a\left(1-\frac{z}{s}\right)+\left(\Delta z_i + C_c'\frac{\Delta U}{U} + C_A'\right)\frac{y_a z}{s^2} - \frac{C_s'}{s^4} z\left(x_a^2+y_a^2\right)y_a \end{aligned} \tag{42.16}$$

Here x_a and y_a again denote the ray coordinates in the aperture plane, so that $\gamma = (x_a^2+y_a^2)^{1/2}/s$ is the slope of the aberration-free ray in the image space. The positive coefficients C_c', C_A' and C_s' of the axial chromatic aberration, astigmatism and spherical aberration, respectively, refer to the image side; their meaning is clear from the formula for the angle γ; Δz_i denotes the defocus and $\Delta U/U$ a specified relative energy variation.

The explicit appearance of many constants in Eq. (42.16) renders the formulae unwieldy. Following Glaser, we cast them into a concise form by introducing suitable reduced coordinates. We write

$$\xi_a + \mathrm{i}\eta_a =: \rho_a \mathrm{e}^{\mathrm{i}\psi} = (x_a + \mathrm{i}y_a)s^{-1}\sqrt{C_s'/C_a'} \tag{42.17a}$$

$$\xi + \mathrm{i}\eta = -(x+\mathrm{i}y)\sqrt{C_s'/C_a'^3} \tag{42.17b}$$

for the transverse coordinates and

$$\zeta = \left(z - z_i'\right)/C_a' \tag{42.17c}$$

for the axial coordinate with

$$z_t' \coloneqq s + \Delta z_i + C_c'\Delta U/U \tag{42.17d}$$

These have now to be substituted into Eq. (42.16). Moreover, the simplifications arising from $|C_a'\,\zeta| \ll s$ and from $|z_i' - s| \ll s$ are always justified in practice. After some elementary calculation, we obtain the normalized equations

$$\begin{aligned} \xi &= \rho_a\left(\zeta + \rho_a^2 + 1\right)\cos\psi \\ \eta &= \rho_a\left(\zeta + \rho_a^2 - 1\right)\sin\psi \end{aligned} \tag{42.18}$$

This is the reduced representation of a two-parameter manifold of straight lines $\xi = \xi(\zeta)$, $\eta = \eta(\zeta)$, the parameters being ρ_a and ψ. The caustic condition is again the vanishing of the determinant:

$$D' := \frac{\partial(\xi, \eta)}{\partial(\xi_a, \eta_a)} \equiv \frac{1}{\rho_a} \frac{\partial(\xi, \eta)}{\partial(\rho_a, \psi)} \tag{42.19}$$

which leads to

$$D' \equiv 3\rho_a^4 + 2\rho_a^2(2\zeta - \cos 2\psi) + \zeta^2 - 1 = 0 \tag{42.20}$$

This is a quadratic equation for ρ_a^2 as a function of ζ and ψ, its two roots being given by

$$\rho_{1,2}^2 = \frac{1}{3}\left[(\cos 2\psi - 2\zeta) \pm \left\{(\cos 2\psi - 2\zeta)^2 + 3\left(1 - \zeta^2\right)\right\}^{1/2}\right] \tag{42.21}$$

Since ρ_a and ψ have been introduced as the reduced polar ray coordinates in the aperture plane, Eq. (42.21) is a representation of the *basis-curves* referring to the aperture plane and to the recording plane $\zeta = \text{const}$. For $\zeta > 1$ there are no real solutions of (42.21), for $-1 \leq \zeta \leq 1$ exactly one and for $\zeta < -1$ two separate solutions. Fig. 42.4 shows some basis-curves, already published by Glaser.

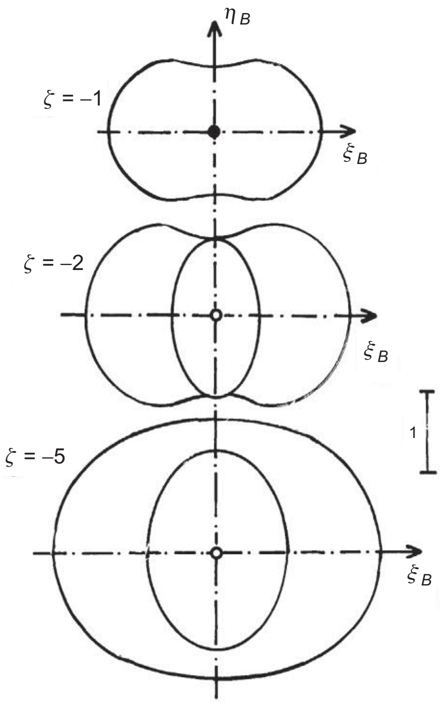

Figure 42.4
Basis-curves in various cross-sections through the caustic. *After Glaser (1952), Courtesy Springer Verlag.*

The equations for the caustic itself are obtained by introducing Eq. (42.21) for ρ_a into (42.18). The two possible solutions represent the two different surfaces of the caustic, which have a fairly complicated structure. Simple equations are obtained for the two axial sections through the caustic with $\psi = 0$ and $\psi = \pi/2$, respectively. For $\psi = 0$, $\eta = 0$, we find

$$\begin{aligned} &\rho_1^2 = 1 - \zeta, &&\rho_2^2 = -(1+\zeta)/3 \\ &\xi_1 = \pm 2\sqrt{1-\zeta}, &&\zeta_2 = \pm 2\left(\frac{-1-\zeta}{3}\right)^{3/2} \end{aligned} \tag{42.22a}$$

and in the other case, $\psi = \pi/2$, $\xi = 0$, we have

$$\begin{aligned} &\rho_1^2 = (1-\zeta)/3, &&\rho_2^2 = -1-\zeta \\ &\eta_1 = \pm 2\left(\frac{1-\zeta}{3}\right)^{3/2} &&\eta_2 = \pm 2\sqrt{-1-\zeta} \end{aligned} \tag{42.22b}$$

These curves are shown in Fig. 42.5 (in Glaser's original publications the coordinates ξ and η were accidentally interchanged in this figure).

Still more important are the cross-sections $\zeta = \text{const}$ through the caustic, since these can be observed experimentally; such curves are shown in Fig. 42.6 (again the labelling of the axes has been corrected). Curves as sharp as these are not observed in practice for various reasons, which will be discussed later.

In the *paraxial* approximation, the plane $\zeta = +1$ corresponding to $z = z_i' + C_a'$ contains a line focus in the x-direction, while the plane $\zeta = -1$ corresponding to $z = z_i' - C_a'$ contains a line focus in the y-direction; the circle of least confusion is characterized by $\zeta = 0$, $z = z_i'$ and by its radius $r = C_a'\gamma$. Owing to the spherical aberration, this circle is not a cross-section through the caustic.

42.5 Intensity Considerations

The caustic is a surface of very high electron intensity. We now examine the intensity distribution in the neighbourhood of the caustic, a question also analysed by Glaser (1952). The following account does not go into much detail as this is a subject to which we shall return in Chapter 47, Brightness.

We set out from a differential or incremental expression for the current density I, which we write

$$dI = K d\Omega_0 dA_0 dU = dJ_z dA \tag{42.23}$$

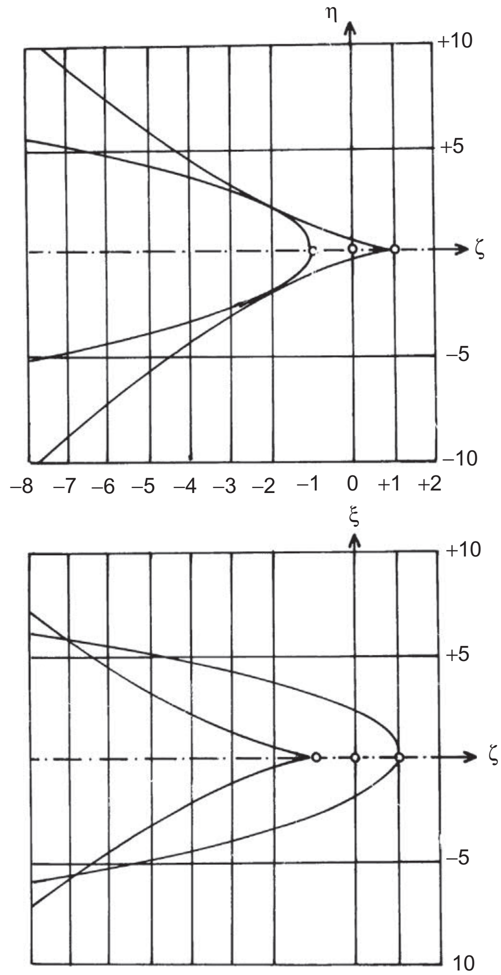

Figure 42.5
Meridional and sagittal sections through the caustic. *After Glaser (1952), Courtesy Springer Verlag.*

$d\Omega_o$ being an element of solid angle and dA_o an element of area, both in the object plane, while the element of area dA refers to the recording plane; dJ_z is then the element of current density in the latter. The factor K is usually a slowly varying function of the position (x_o, y_o) and the slope coordinates; in the following discussion, this factor K and the element dA_o are of little importance.

Between the element of area $dA = dxdy$ in the recording plane and the (very small) initial slopes α_o and β_o in the object plane the following relation holds:

$$dA = dxdy = \frac{\partial(x, y)}{\partial(\alpha_o, \beta_o)} d\alpha_o d\beta_o \equiv D d\Omega_o \tag{42.24}$$

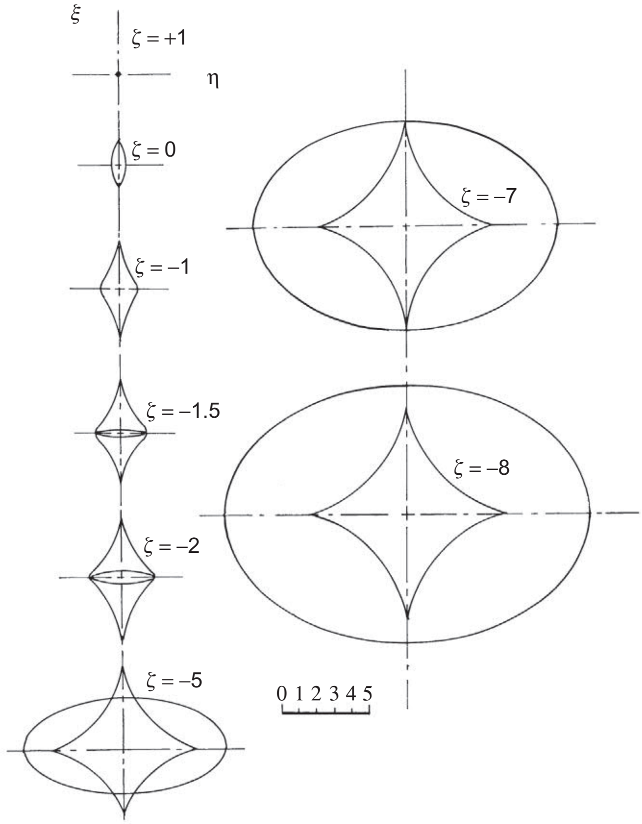

Figure 42.6
Cross-sections through the caustic. *After Glaser (1952), Courtesy Springer Verlag.*

where $d\Omega_o = d\alpha_o d\beta_o$, and D is the corresponding Jacobian. This is identical with (42.2) if we identify α with α_o and β with β_o. Introducing (42.24) into (42.23) we obtain:

$$J_z(x, y) = \int\int K D^{-1} dA_o dU \tag{42.25}$$

which is essentially the same as Glaser's formula. The integrand becomes singular at the caustic, but the double integration over this singularity gives a finite result. Physically, this is understandable in terms of the blurring of the caustic by chromatic aberration and of the convolution over a finite object domain. Nevertheless Eq. (42.25) is not without problems, since the singularity that arises when $D^{-1} \to \infty$ reveals the breakdown of the classical mechanical description of the electron beam. In the more correct wave-mechanical approximation, this singularity disappears. Even for the artificial situation of a point source emitting monochromatic electrons, the caustic is a surface of very high, but finite, current density. The subsequent considerations are therefore only approximately valid.

We now attempt to evaluate (42.25) for the model treated in the last section. Since the aberrations will be small, it is sufficient to employ the paraxial relations between (α_o, β_o) and (x_a, y_a) in the calculation of D, so that

$$\alpha_o + \mathrm{i}\beta_o = -Mn(x_a + \mathrm{i}y_a)/s$$

M being the lateral magnification and $n = f_i/f_o$ the refractive index of the image space relative to the object. The Jacobian in Eq. (42.25) then transforms according to

$$D \equiv \frac{\partial(x, y)}{\partial(\alpha_o \beta_o)} = \left(\frac{s}{Mn}\right)^2 \frac{\partial(x, y)}{\partial(x_a, y_a)}$$

Using the linear transforms (42.17a,b) together with (42.19) (but with $D' \neq 0$), we obtain

$$D = \left(\frac{C'_A}{Mn}\right)^2 \frac{\partial(\xi, \eta)}{\partial(\xi_a, \eta_a)} \equiv \left(\frac{C'_A}{Mn}\right)^2 D'$$

Introducing this into (42.26) we arrive at the relation

$$J_z(x, y) = \left(\frac{Mn}{C'_A}\right)^2 \int\int \frac{K}{D'} dA_o dU$$

Since D' depends on the parameter U via the reduced coordinate ζ (42.21), it is convenient to express dU in terms of $d\zeta$; from Eq. (42.17c,d) we find

$$dU = U dz'_i / C'_c = -U\left(C'_A / C'_c\right) d\zeta$$

It is also convenient to refer the aberration coefficients C'_A and C'_c to the *object* side: $C'_A = C_A M^2 n$, $C'_c = C_c M^2 n$. The refractive index thus cancels out and we obtain

$$J_z(x, y) = -\frac{U}{M^2 C_A C_c} \int\int \frac{K}{D'} d\zeta dA_o \qquad (42.26)$$

with the expression (42.20) for D', if $D' \neq 0$.

In this expression the only rapidly varying factor is the determinant D' in the denominator. The lines of constant value of J_z, which are known as lines of equidensity or isophotes, are hence simply the lines $D' = \text{const}$. Such lines were first determined by Grümm (1952) and are reproduced in Glaser (1952). Some of these line distributions are shown in Fig. 42.7. In such cross-sections through the caustic, there may be overlapping domains. In these cases the intensities, originating from different branches and referring to the same reference point, are simply to be added before determining the lines of equidensity.

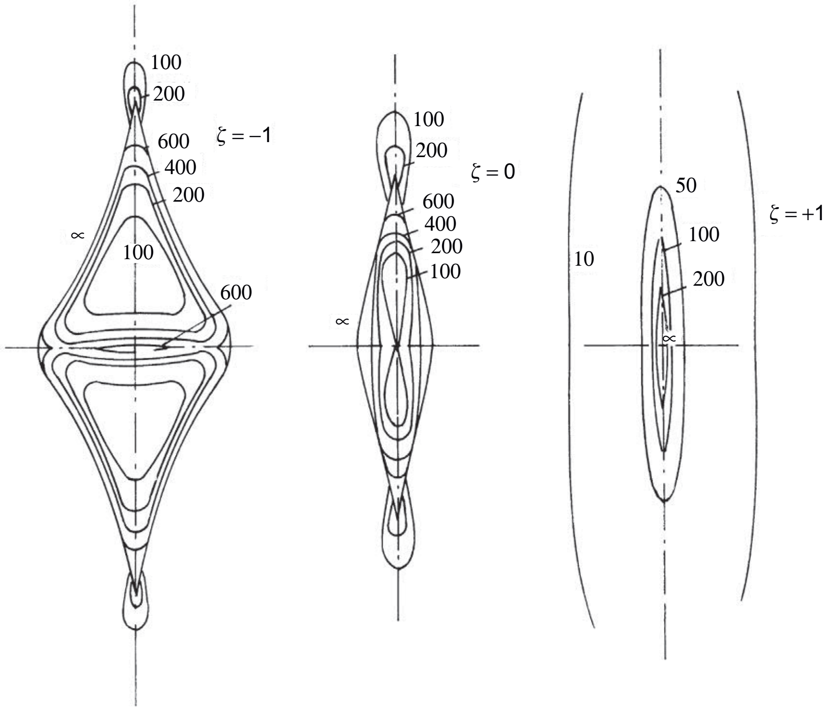

Figure 42.7
Equidensity lines in different recording planes. Left: $\zeta = -1$ (second caustic tip); centre: $\zeta = 0$ (plane of least confusion); right: $\zeta = 1$ (first caustic tip). *After Glaser (1952), Courtesy Springer Verlag.*

42.6 Higher Order Focusing Properties

In electron optics, paraxial focusing is usually dominant, since the various kinds of aberrations are so severe that the beam must be confined to the paraxial domain. There are, however, systems in which this is not the case. An example is provided by beta-ray spectrometers, in which the paraxial domain is blocked off by a shield and the particles must pass through an *annular* aperture with a fairly large inner radius. The object and its image still lie in the vicinity of the axis of rotational symmetry. A schematic representation of such arrangements is shown in Fig. 42.8.

Since the familiar concepts of focusing and aberrations are inadequate in such cases, Lenz (1957) developed a more general theory, which is outlined below. This theory gave rise to more detailed theoretical and experimental investigations, the object of which was to find new types of electron optical systems with superior focusing properties. These investigations are dealt with in the next section. Despite all this effort, such annular systems remained impractical, since no solution emerged to the problems caused by deviation from rotational

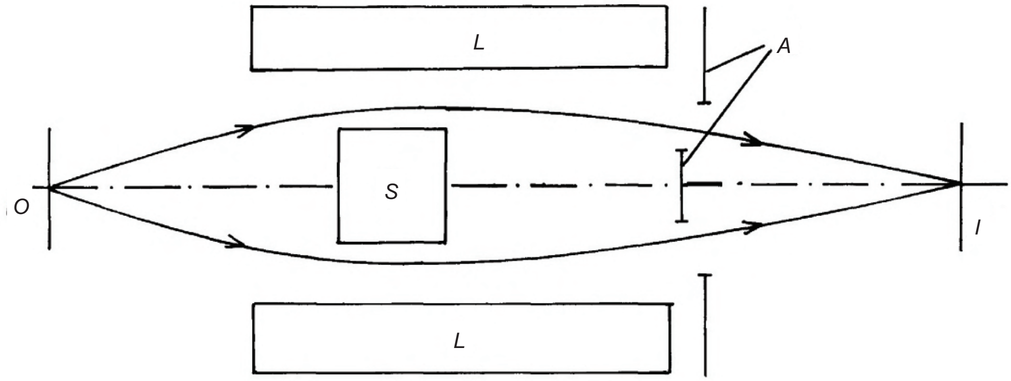

Figure 42.8
Schematic representation of an annular electron optical system with a double magnetic lens. *S*: shielding block; *O*: object; *A*: aperture; *I*: image.

symmetry, to which annular systems are very sensitive. For this reason, we shall outline the corresponding theory only briefly.

We again assume that the object point is situated on the axis at $z = z_o$. Since the aperture angles may become fairly large (about 20° and more), we now have to distinguish clearly between the aperture angle α_o and the corresponding slope $s := \tan \alpha_o = r'_{\mathrm{o}}$; the latter is more suitable as a ray parameter. Since the azimuth is of no importance in the present context, we write the ray equation in the form

$$r = r(z, s) \quad \text{with} \quad r(z_o, s) = 0 \tag{42.27}$$

It is convenient to allow r to take negative values, so that r' remains continuous at the axis. The caustic condition now simplifies to

$$\frac{\partial r(z, s)}{\partial s} = 0 \tag{42.28}$$

Together with Eq. (42.27) this provides a parametric representation $r = r(s)$, $z = z(s)$ of the rotationally symmetric caustic surface. The latter will generally have a very complicated structure; further examples are given below.

We now investigate the possible focusing properties of annular systems; for this, we introduce a power series expansion of (42.27) in terms of the *slope difference* $\Delta s = s - s_k$, s_k being some fixed value of s; $z = z_k$ is an arbitrary, but fixed, reference plane in image space. We have (with $r_k := r(z_k,\ s_k) = A_k^{(0)}$)

$$r(z_k, s) = \sum_{n=0}^{\infty} \frac{1}{n!} A_k^{(n)} (\Delta s)^n, \quad A_k^{(n)} := \left(\frac{\partial^n r(z_k, s)}{\partial s^n} \right) \Bigg|_{s_k} \tag{42.29}$$

In practice, this expansion can be truncated after the first nonvanishing term. Let this be the term in $(\Delta s)^{N+1}$; we then speak of N-th order focusing with respect to the slope s, and the remaining terms are a measure of the electron optical aberration.

The familiar *paraxial* focusing (subscript $k \to p$) is characterized by $N = 2$ and:

$$s_p = 0, \quad r_p = A_p^{(1)} = A_p^{(2)} = 0, \quad A_p^{(3)} = 6MC_s \tag{42.30}$$

$z = z_p$ here being the Gaussian image plane. Lenz (1957) has also introduced the following less familiar types of foci:

1. line focus ($k \to l$, $N = 1$)

$$r_l \neq 0, \quad A_l^{(1)} = 0, \quad A_l^{(2)} \neq 0; \tag{42.31}$$

2. cone focus ($k \to c$, $N = 1$)

$$r_c = 0, \quad A_c^{(1)} = 0, \quad A_c^{(2)} \neq 0; \tag{42.32}$$

3. blade focus ($k \to b$, $N = 2$)

$$r_b \neq 0, \quad A_b^{(1)} = A_b^{(2)} = 0, \quad A_b^{(3)} \neq 0; \tag{42.33}$$

4. cross focus ($k \to x$, $N = 1$)

$$r_x \neq 0, \quad A_{x_1}^{(1)} = A_{x_2}^{(1)} = 0, \quad A_{x_1}^{(2)} \neq 0 \neq A_{x_2}^{(2)}; \tag{42.34}$$

5. cone-edge focus ($k \to e$, $N = 2$)

$$r_e = 0, \quad A_e^{(1)} = A_e^{(2)} = 0, \quad A_e^{(3)} \neq 0; \tag{42.35}$$

The line focus is an ordinary circle on the caustic with no additional special properties. The cross focus is characterized by the fact that the line-focus conditions (42.31) are satisfied simultaneously for two different slopes $s_{x1} \neq s_{x2}$. Since (42.28) is satisfied for *all* different types of foci, all of them are located on the caustic, but at different positions. This is presented schematically in Figs 42.9 and 42.10, where the foci are marked by the corresponding subscripts. Fig. 42.9 also shows the caustic waist (subscript w) of Section 42.3. Noven (1965) was able to observe all these complicated structures in a simple symmetric double-lens system.

The cone-edge focus is of special theoretical interest, since it gives a very high intensity concentration. Provided that it is permissible to employ third-order aberration theory, the lateral aberration is given by

$$\Delta r = MC_s(s - s_e)^3 \tag{42.36}$$

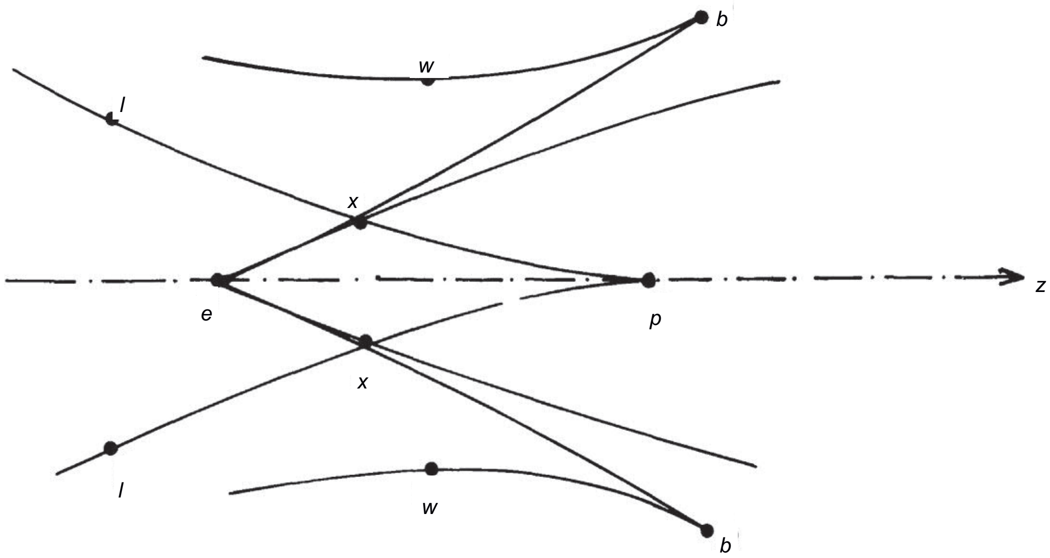

Figure 42.9
Meridional section through the kind of rotationally symmetric caustic that may occur in an annular system. The letters indicate the different types of focus described in the text; *w* denotes waist. *After Noven (1964), Courtesy the author.*

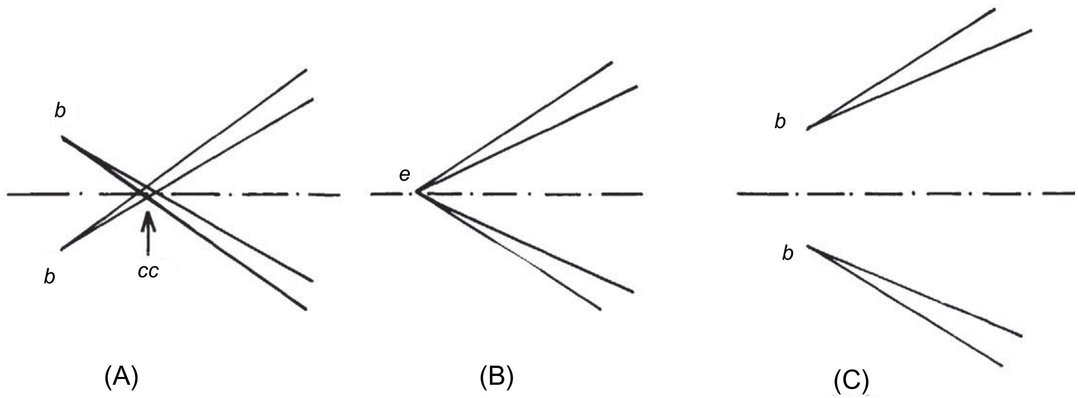

Figure 42.10
The cone-edge focus *e* (B) as a degenerate case of a pure blade focus *b* (C) and a double-cone focus *cc* (A). *After Noven (1964), Courtesy the author.*

The cone-edge focus is superior to the ordinary paraxial focus in that, for the same semi-aperture angle $\alpha = \mathrm{Max}|s - s_e| \ll 1$, the solid angle subtended is increased from $\pi\alpha^2$ to $2\pi\alpha s_e$, where $s_e \gg \alpha$. The cone-edge focus is therefore suitable for devices in which a high intensity concentration in one small spot is required. For imaging, the cone-edge focus is, however, less suitable, as the off-axis aberrations are invariably larger than in conventional lens systems.

A still higher intensity concentration should be obtained with a suitable cross focus. Fig. 42.10 shows the cone-edge focus as a degenerate case between cone foci and blade foci. In the case of four intersecting caustic branches (Fig. 42.10A and B), a circle of least confusion can be defined as the cross focus, shown in Fig. 42.11. The ring radii of the annular aperture can be chosen in such a way that the rays with greatest slopes intersect this circle on the opposite side. This is quite analogous to the definition of the optimal defocus in conventional lens systems. Theoretically, a very small focus with extremely high intensity concentration can be achieved in this way, but there are difficulties in practice, as will become obvious later.

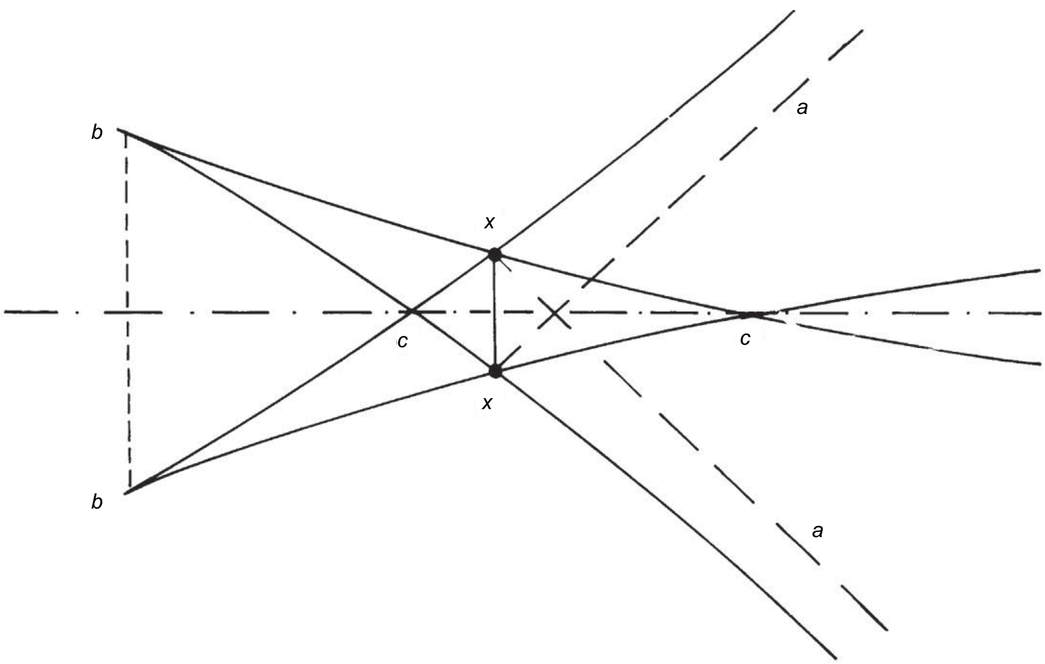

Figure 42.11
Enlargement of the double-cone focus of Fig. 42.10A, showing the circle of least confusion *xx*; the rays labelled *a* are those of greatest slope. *After Noven (1964), Courtesy the author.*

42.7 Applications of Annular Systems

Annular systems are electron optical devices with an axial stop and a ring-shaped aperture, as sketched in Fig. 42.8. A first successful device of this type was a beta-spectrometer built by Slätis and Siegbahn (1949), see Fig. 42.12. This arrangement motivated Lenz's early investigations. Lenz (1957) showed that, as a result of the symmetry properties of the spectrometer (Fig. 42.13), a caustic waist is formed in the vicinity of the symmetry plane, and this is already sufficient for the formation of a cone-edge focus in the vicinity of the counter (recording plane). Lenz also showed that third-order aberration theory is clearly insufficient for the calculation of such a focus; nevertheless, in later investigations on annular systems, aberrations of fifth order have mostly been ignored for simplicity.

Later, Noven (1965) investigated experimentally the caustics in symmetric double lenses, both electrostatic (Fig. 42.14A) and magnetic (Fig. 42.14B). He observed all the different types of foci shown in Figs 42.9 and 42.10, but he also found that such systems are extremely sensitive to deviations from rotational symmetry caused by imperfect machining, misalignments and vibrations. This is not at all surprising, since the electrons travel long distances far from the axis, where such perturbations are often much stronger than in the paraxial domain.

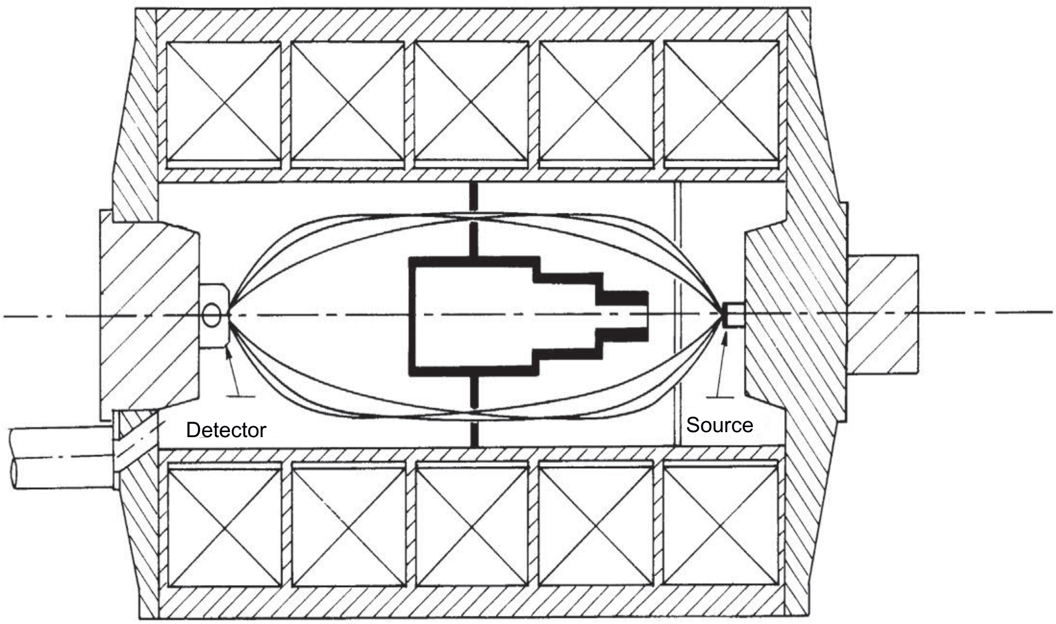

Figure 42.12
General appearance of a spectrometer of the Siegbahn—Slätis type, operating on the focal separation principle.

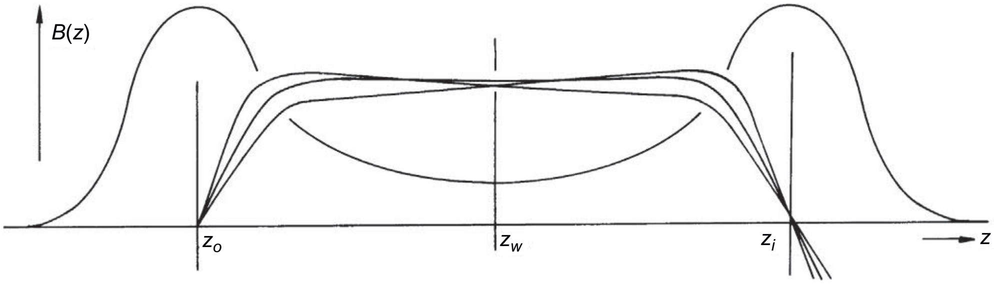

Figure 42.13
The caustic waist at $z = z_w$ and the cone-edge focus at $z = z_i$ in a symmetric double-lens system.

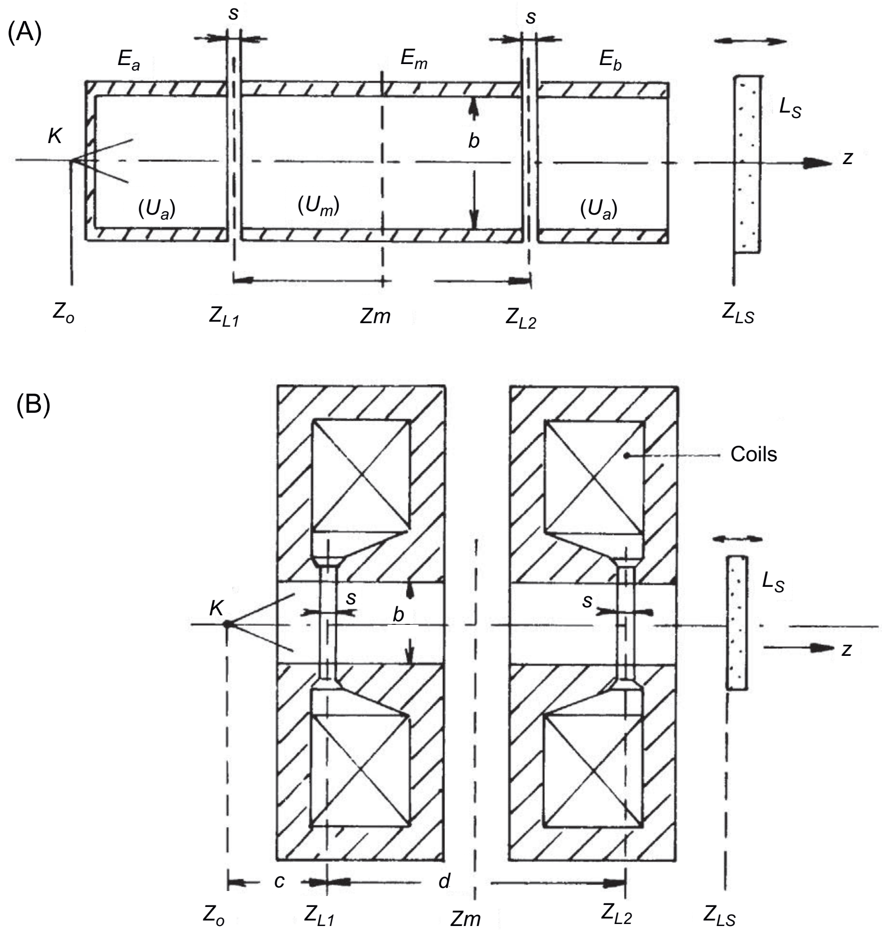

Figure 42.14
Symmetric double-lens systems. (A) Electrostatic and (B) magnetic arrangements.

Another interesting proposal was an annular electron microscope (Lenz and Wilska, 1966, 1966/67). Fig. 42.15 shows schematically a device in which a condenser lens and a magnetic objective, both equipped with an annular electrostatic lens, are combined in one symmetric system. A partial compensation of the spherical aberration should be possible with the central electrodes of the electrostatic lenses positively biased, since the latter then produce a converging force that decreases with increasing distance from the optic axis. This, together with the stronger than linearly increasing focusing by the magnetic lenses, can exert a nearly linear converging effect on the beam. In spite of this possibility, such a system has not been built, mainly because of constructional difficulties and the anticipated very high sensitivity to misalignments. Moreover, it is doubtful whether such annular microscopes can give a better resolution than conventional ones, since the chromatic aberrations and diffraction at the annular apertures may well become serious.

The problem of a suitable stigmator for annular systems was investigated theoretically by Kasper (1968/69), who came to the conclusion that such a stigmator should have the shape shown in Figs 42.16A and B. The central electrode, which must have a varying diameter, is surrounded by two rings of outer electrodes. Theoretically, all astigmatisms of twofold and threefold symmetry can be compensated, as in conventional lens systems, but in practice

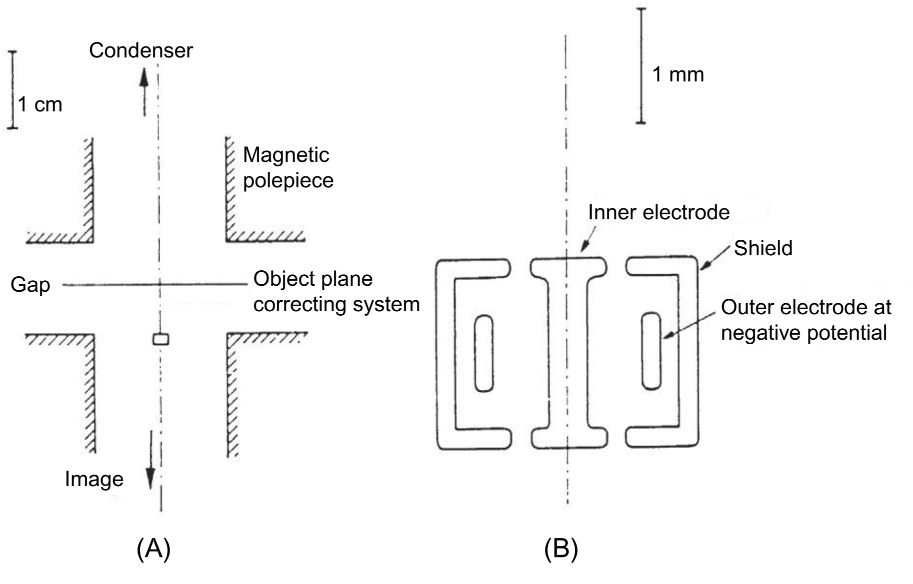

Figure 42.15
A magnetic condenser-objective lens with an electrostatic corrector. (A) Complete system and (B) electrostatic correction device. *After Lenz and Wilska (1966/67), Courtesy Wissenschaftliche Verlagsgesellschaft.*

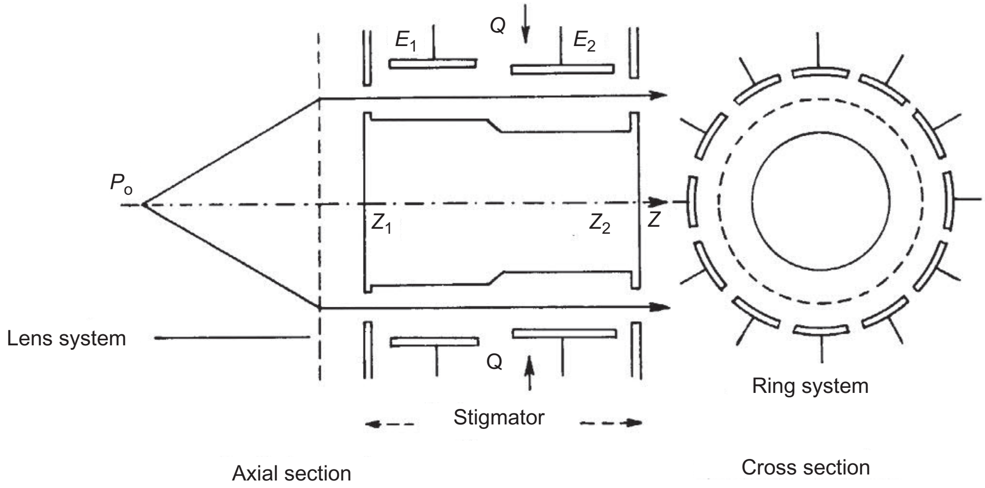

Figure 42.16
Electrostatic 24-pole stigmator for the correction of annular systems. The cross-section corresponds to the plane indicated by QQ. E_1 and E_2 denote the sector-shaped ring electrodes.

the appropriate adjustment of such a stigmator in conditions demanding long-term stability would be highly complicated.

Systems of two and three magnetic round lenses without a central core have been investigated by Kunath (1976/77). He found that at least three such lenses are necessary to achieve a dispersion-free cone-edge focus. In principle, a resolution of 0.1 nm is possible, but some of the off-axis aberrations, which cannot be corrected, will be so large that the useful image field becomes too small for practical purposes.

The computer-aided reconstruction of a three-dimensional object requires a set of images corresponding to very different directions of the illumination incident on the object. Usually the direction of the incident beam is kept fixed and the object is tilted mechanically (Fig. 42.17A). Since this is a very slow procedure with a limited accuracy, Hoppe (1972) suggested keeping the object fixed and tilting the beam electronically (Fig. 42.17B). The beam then has to pass in sequence through the openings in a tubular lens. The latter can be considered as a system of minilenses with different curved optic axes. Such systems have been investigated theoretically by Plies and Typke (1978), Typke (1981) and Plies (1981). The structure of such a system and the shape of the trajectories passing through it is shown in Fig. 42.18. Theoretically, a dispersion-free cone-edge focus with a resolution of 1.4 nm is possible. The problems that arise with such devices are practical ones: sufficiently accurate machining and alignment and adequate compensation of the various forms of astigmatism.

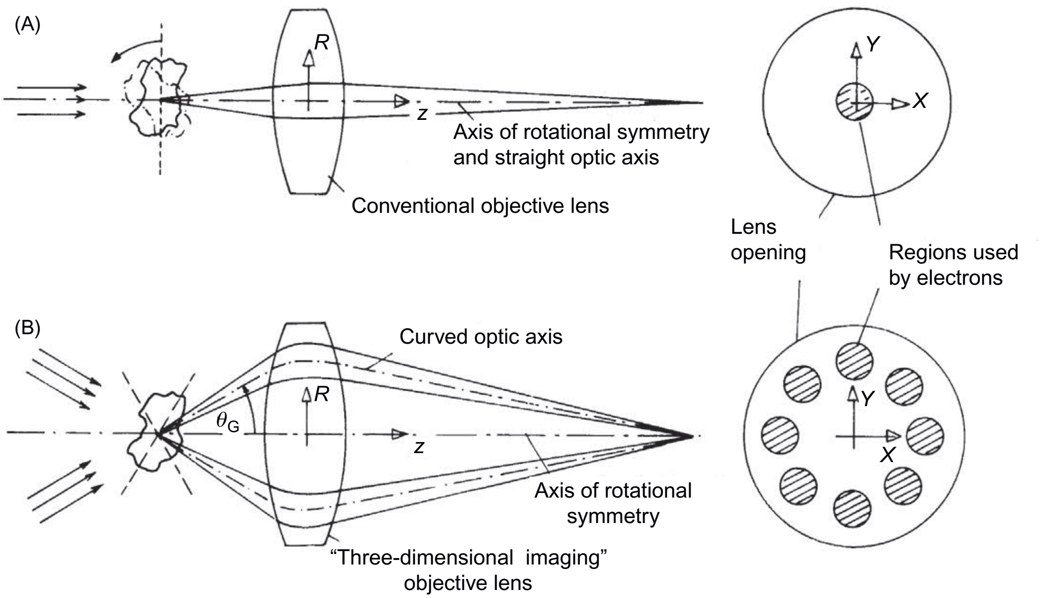

Figure 42.17
The two-dimensional projections needed for three-dimensional image reconstruction can be obtained by (A) mechanical tilting of the object or (B) electron optical tilting of the illuminating and imaging rays. On the right, the lens regions occupied by electrons are indicated for (A) conventional electron microscopy and (B) three-dimensional electron microscopy with 'ring-zone segment imaging'. *After Plies (1981), Courtesy Elsevier.*

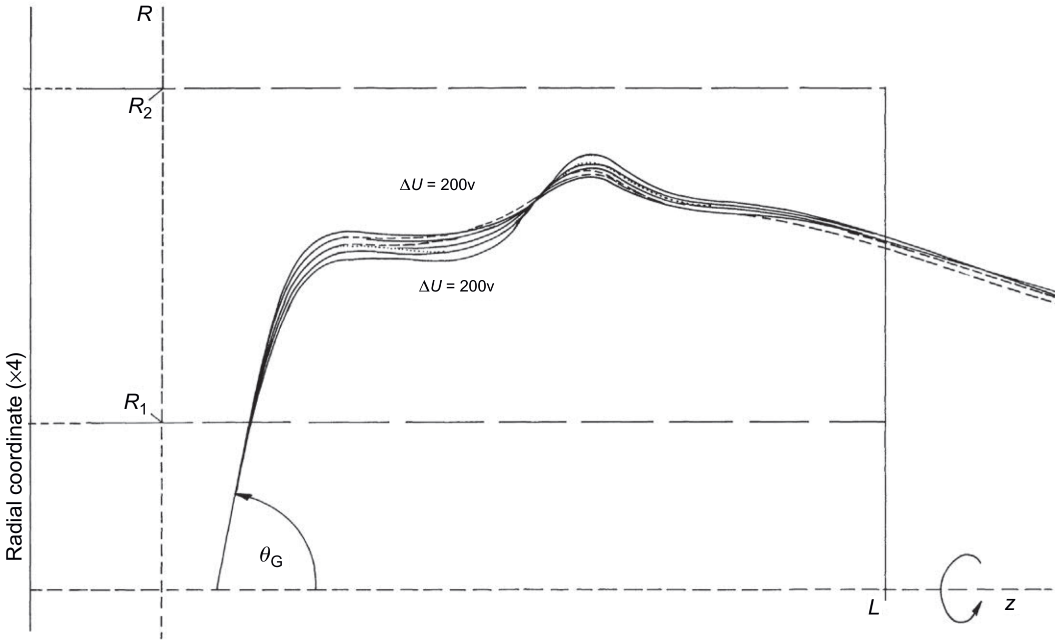

Figure 42.18
Trajectories and aberrations in an electrostatic multitubular core-lens, which gives dispersion-free cone-edge focusing. *After Plies (1981), Courtesy Elsevier.*

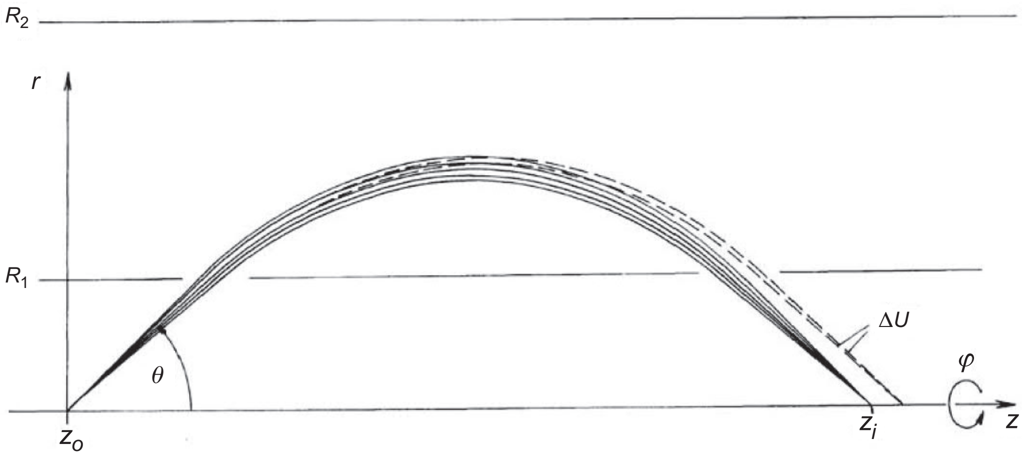

Figure 42.19
Cone-edge focusing in the cylindrical mirror analyser. The figure shows two pencils of rays, one corresponding to the nominal energy, the other departing from the latter by $e\Delta U$. *After Plies (1981), Courtesy Elsevier.*

A simple device with a cone-edge focus is the cylindrical mirror analyser (Fig. 42.19). This is none other than an annular round lens formed by the radial electrostatic field between two coaxial cylinders. The beam passes through two round gaps in the inner electrode which produce weak fringe fields. These have only a very small influence on the focus; this effect is negligible since here the resolution requirements are far less stringent than in annular systems designed as objective lenses.

In conclusion, we observe that so severe are the practical problems that the more sophisticated types of annular systems have not yet found widespread application. The role of annular systems in connection with aberration correction has been mentioned in Section 41.4.

PART IX

Electron Guns

CHAPTER 43

General Features of Electron Guns

The study of electron sources is a major and important task in electron optics. Electron sources in the widest sense are all devices in which electrons are released from material surfaces or gas phases by some physical emission process. The complexity of this whole subject is, however, so great that we have to confine it reasonably.

One purpose of producing electron emission is the *imaging* of the emitting surface, which is itself the object of the investigation. This is achieved in emission microscopes of all kinds and in image converters. In the design of such devices the reduction of image aberrations is the most important task. This is so different from the problems dealt with in the present chapter that we have excluded this topic here. We have mentioned emission microscopes and image converters in Chapter 37, Electron Mirrors, Low-energy-electron Microscopes and Photoemission Electron Microscopes, Cathode Lenses and Field-Emission Microscopy.

Another important function of electron sources is to provide the intense, well-focused electron beam needed in devices such as electron microscopes, interferometers and older oscillographs and television tubes. Here it is not the imaging of the cathode surface that is required but maximum intensity and stability of the emission. Electron sources designed for this purpose are called *electron guns.* The investigation of these requires several new concepts, which do not fit into the familiar physics of focusing and aberrations; these concepts form the main theme of the present Part. In this Chapter, we shall give only a short introductory survey in order to acquaint the nonspecialist with the problems and terminology; more details will be found in the subsequent chapters.

In electron guns, virtually every possible process for releasing electrons from material surfaces or from gas phases can be employed. In fact, the first successful electron sources relied on gas discharge. Induni (1947, 1955) designed these guns in such a manner that their operation was stable and easily controllable. They were also considered by Möllenstedt and Düker (1953). Nowadays guns of this type have been abandoned, mainly because the energy spectrum of the electrons emitted is too broad for practical purposes. The photoelectric effect can be employed to release electrons from cold cathodes, but this process has the disadvantage that the efficiency is very low. This effect is therefore of importance only in special conditions; the main devices that rely on the photoelectric effect

Principles of Electron Optics: Applied Geometrical Optics.
DOI: http://dx.doi.org/10.1016/B978-0-12-813369-9.00043-9

are image converters and photoemission electron microscopes (PEEM), described briefly in Chapter 37. Another application is ultrafast electron microscopy and diffraction, in which extremely short pulses of electrons are created by bombarding the emitter with short bursts of photons from a laser or synchrotron. In this way, dynamic processes in the specimen can be followed; this too was mentioned in Chapter 37.

Here, we shall concentrate on *thermionic emission*, *Schottky emission* and *cold field electron emission*. In thermionic emission, the electrons are liberated by heating; in Schottky emission, this is increased by a moderate electric field; and in cold field emission, the emitter is not heated, the electrons are extracted by a strong electric field. A detailed knowledge of these processes is necessary to understand the technical properties of electron guns and we summarize the corresponding theories in Chapter 44, Theory of Electron Emission. The subsequent chapters are devoted to specific aspects and modes of operation of electron guns. In the following sections, we briefly introduce the various types of guns.

43.1 Thermionic Electron Guns

Thermionic guns are the simplest type and are still in widespread use though they have been superseded in microscopes designed for high resolution by Schottky or cold field-emission guns. In thermionic emission, electrons are released from materials by heating. In tungsten cathodes, for example, at $T = 2600$ K a considerable fraction of the conduction electrons gain so much kinetic energy that they can surmount the potential barrier at the cathode surface. This still occurs if the local electric field vanishes or even repels the electrons; an electric field is only necessary to accelerate the electrons already emitted. So long as this is essentially confined to the space between the cathode and the closest positive electrode, we shall call this acceleration the 'extraction' process.

The simplest arrangement consists of the cathode and a second electrode in front of it, the anode. This anode must always be at a positive potential with respect to the cathode and must have a small opening through which the extracted electron beam passes. Such a device is, however, very impractical, since many of the emitted electrons hit the anode and heat it strongly. Moreover, for a constant acceleration voltage, the emission current can be altered only by a corresponding alteration of the cathode temperature, and this acts only very slowly. For all these reasons Wehnelt (1903) introduced a third electrode, held at a negative potential with respect to the cathode (see also Wehnelt and Jentsch, 1909). This electrode, frequently called the grid, the control electrode or simply the wehnelt, is situated between the cathode and the anode; it prevents the electron beam from striking the anode and also has a strong focusing effect on the beam.

The essential structure of such an electrode system, a triode gun (Fig. 43.1B), and the shape of the electron beam emitted are presented in a simplified and exaggerated manner in

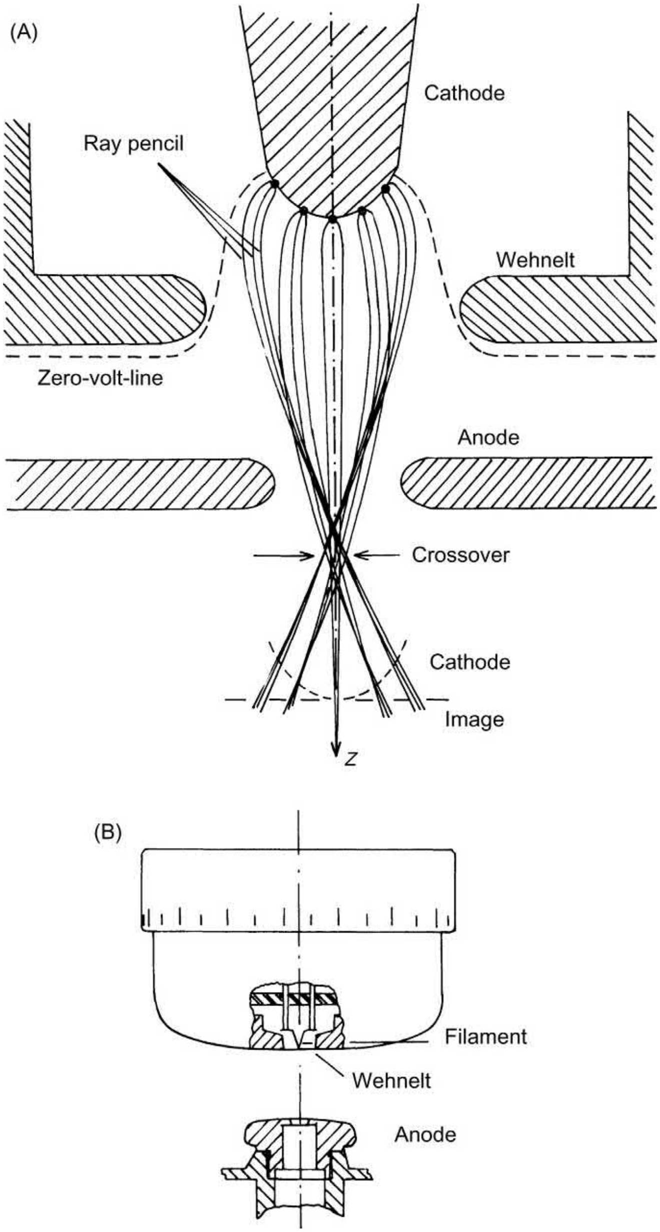

Figure 43.1
Thermionic triode electron gun. (A) Terminology and typical trajectories. The width of the pencils of rays and the magnitude of the aberrations are considerably exaggerated. (B) A more realistic view. *Courtesy of Philips, Eindhoven.*

Fig. 43.1A. In reality, the asymptotic slopes relative to the optic axis are so small that they cannot be depicted to scale. The emission area at the cathode surface is essentially confined by the equipotential at cathode potential, the zero-volt line in the axial section. The strong influence of the wehnelt on the electron beam is due to the intimate dependence of the shape of this line on the wehnelt potential. Raising this potential enlarges the emission area, while a reduction of the potential drop diminishes it. At a certain value of the wehnelt potential, the *cutoff potential*, the emission area vanishes completely and the emission is then suppressed. The effect of varying the wehnelt potential is shown in Fig. 43.2. It is clear that the beam intensity can be altered quite easily without changing the anode potential or the cathode temperature.

This triode configuration has, however, a serious drawback. Since the electrons are travelling very slowly in the vicinity of the zero-volt surface, they are strongly bent there. This causes large aberrations, which are indicated in Fig. 43.1 and will be studied in more detail in later sections. Moreover, the weak electric field cannot remove the electrons quickly enough from the vicinity of the cathode surface, with the result that a dense cloud of negative space charge builds up and reduces the electron emission. This drawback is an inevitable consequence of the lateral confinement of the emission domain by an equipotential surface and is therefore common to all such thermionic guns, regardless of their particular geometry. The determination of the space-charge distribution and of the corresponding electric potential is a highly sophisticated task, even with the powerful computers now available. Nevertheless, this task is of great importance and will be dealt with in considerable detail in Chapter 46, Space Charge Effects.

A wide variety of designs has been used, differing in the choice of cathode material, the method of heating and the shape of the electrodes. It would be wearisome to describe them all; we mention briefly only some familiar forms. For easy adjustment and simplicity of construction, the cathode is almost always heated electrically. In electron microscopes and similar instruments, the cathode is usually a fine tungsten tip, welded on a hairpin-shaped tungsten filament. The latter conducts the heating current; its temperature is about 2600 K. For historical reasons, this design is known as a pointed filament, to distinguish it from the unadorned hairpin that was used in the distant past. Another shape was a flat pointed blade, which was known as a 'lancet cathode' (Fig. 43.3A and B). In old television tubes and cathode-ray tubes, the cathode had a plane front surface and the emitting material was then a layer of an alkali-earth carbonate, prepared by a special processing technique; the temperature was substantially lower, about 1500 K. Today, however, LCD flat-screen displays have largely supplanted the older types of tube.

A later development is the lanthanum hexaboride (LaB_6) cathode, first built by Broers (1967) (see Fig. 43.3C and D), though the idea of using boride emitters goes back to Lafferty (1951). The emitter is here a small rod of LaB_6 with a very fine tip and was

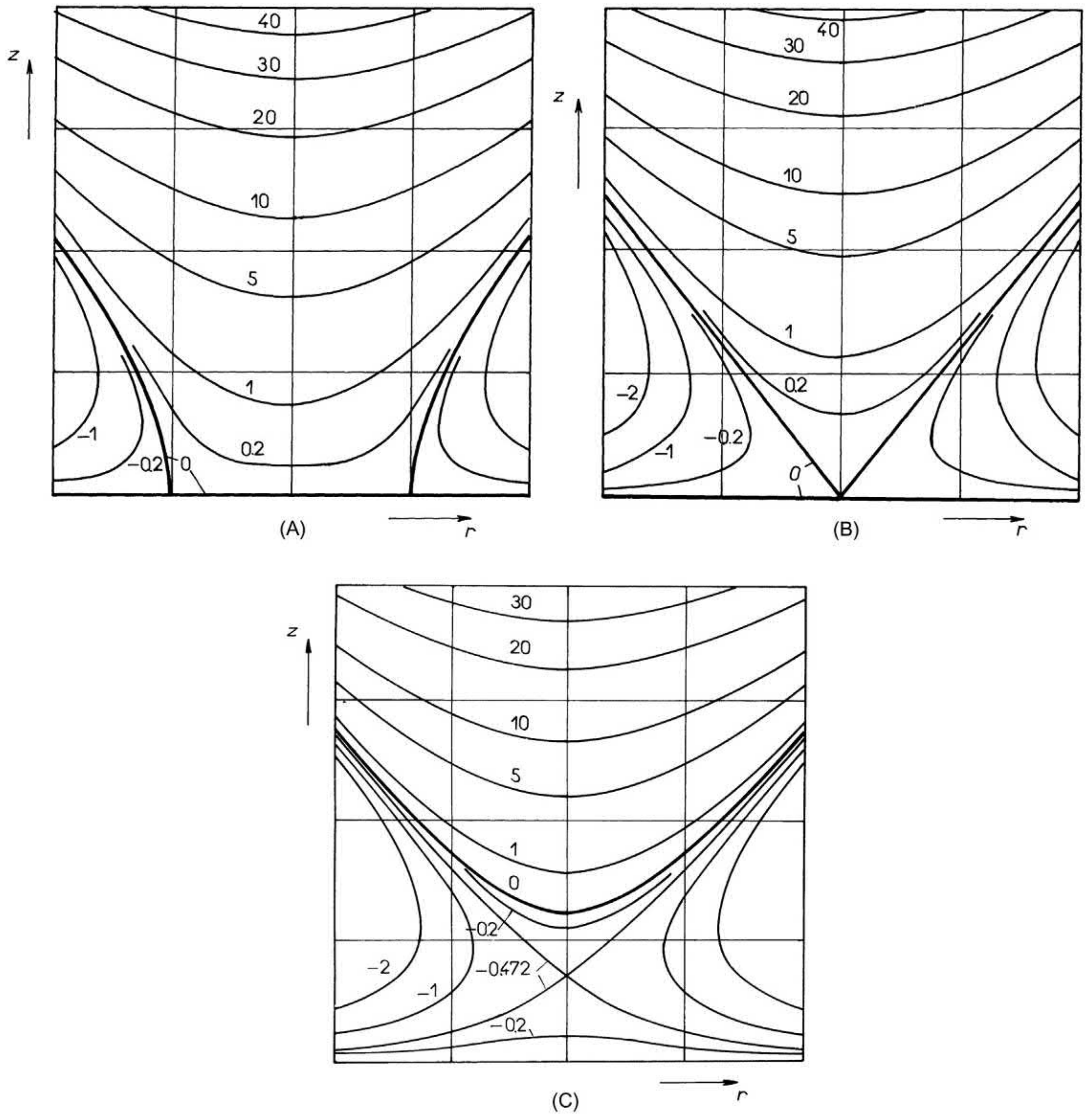

Figure 43.2
Equipotentials in the vicinity of a plane cathode for different values of the wehnelt potential and in the absence of space charge. (A) Emission mode. (B) Saddle-point at the centre of the cathode. (C) Emission suppressed, a negative potential minimum forms a barrier in front of the cathode. *After Kamke (1956), Courtesy Springer Verlag.*

originally heated indirectly by a small coil. The advantage is that the emission is much higher as a result of the low work function (see Chapter 44, Theory of Electron Emission). A technological problem, which was not easy to overcome, was the suppression of chemical reactions between the LaB_6 rod and the cathode support. Since the early design of Broers

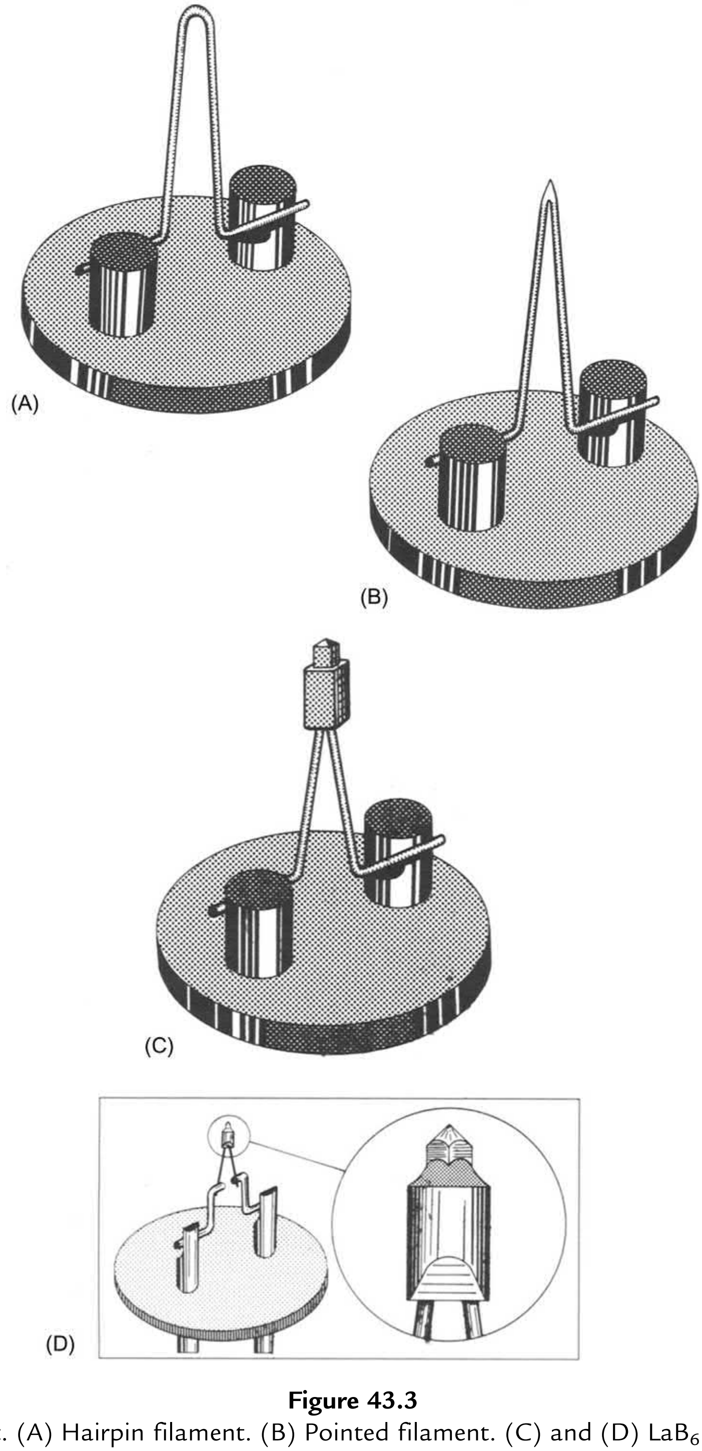

Figure 43.3
Types of filament. (A) Hairpin filament. (B) Pointed filament. (C) and (D) LaB_6 emitters. *Courtesy of Balzers Union AG.*

appeared, many other solutions have been published. The properties of the various forms of LaB_6 guns have been reviewed by Hohn (1985). Cerium hexaboride is also in use and the properties of gadolinium hexaboride have been investigated by Saito et al. (2014). LaB_6 cathodes are now available commercially in many shapes and on different supports. These can be found illustrated with their properties on the manufacturers' websites.

In addition to these thermionic emitters that are in widespread use and available commercially, a number of other materials have been investigated, for instance carbon emitters with a glassy structure (Lea, 1973; Heinrich et al., 1977, 1978; Essig and Geiger, 1981; Speidel et al., 1984). These are, however, operated in a transition regime between thermionic and field electron emission.

43.2 Schottky Emission Guns

The electrons are extracted from a Schottky emission source by the combined effect of heating and a moderate electric field. The gun typically consists of three elements: the emitter itself, a suppressor electrode which effectively screens the shank of the cathode and the extraction electrode. The suppressor, like the wehnelt of a triode gun, is held at a negative potential relative to the cathode and the extraction electrode is of course at a high positive potential. The cathode takes the form of a single-crystal tungsten wire, of the order of 1 mm in length and 125 μm in diameter; one end is etched down to a facet about 1 μm in diameter. A reservoir of zirconium oxide is attached to the wire and the elements reach the {100} planes of the heated tungsten wire and reduce the work function of the {100} plane that forms the emissive facet. Dokania and Kruit (2009) have argued that a Schottky gun can be operated without a suppressor electrode. The potential at the extraction electrode can then be reduced while the electrons emitted by the shank do not seriously degrade the properties of the gun.

An extremely detailed account of Schottky sources is to be found in Bronsgeest (2014); See also Swanson and Schwind (2009) and the earlier publications of Bronsgeest, Kruit and others (Bronsgeest and Kruit, 2006, 2008, 2009; Bronsgeest et al., 2007) as well as Kim et al. (1995, 1997a, b), Kawasaki et al. (2009), Yada and Saito (2014) and Emura et al. (2014).

43.3 Cold Field Electron Emission Guns

In cold field electron emission (CFE) guns (Fig. 43.4), the electrons escape from the cathode by penetrating through the narrow potential barrier in front of the cathode surface by means of a quantum mechanical tunnelling effect. This requires a very high local electric field strength $F \sim 10^8\ \mathrm{Vcm}^{-1}$ (to prevent confusion, it is usual in the literature on electron guns to denote the field strength by F and the particle energy by E, and we shall

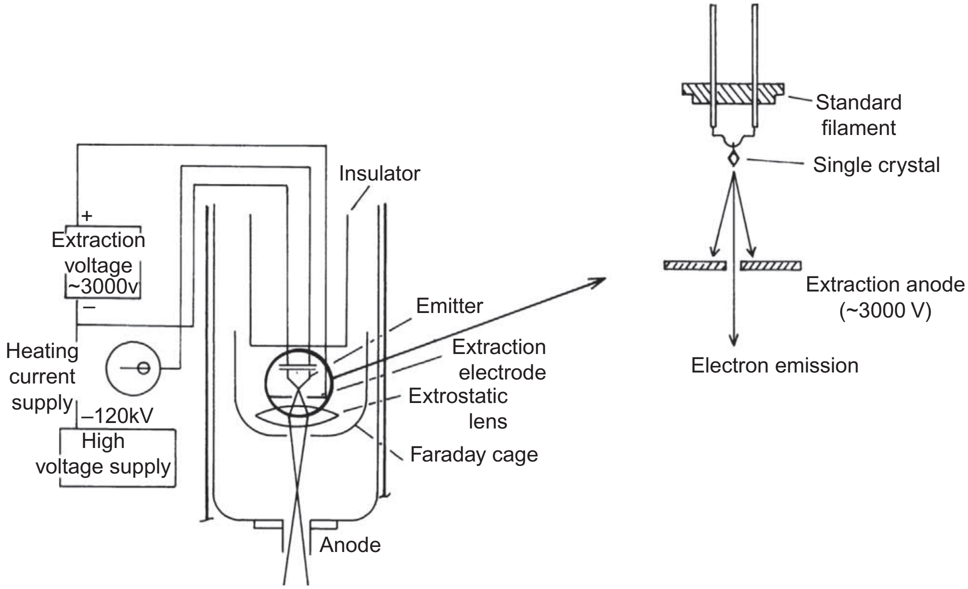

Figure 43.4
General appearance of a field-emission gun: this design has been used in Philips electron microscopes. *Courtesy of Philips, Eindhoven.*

follow this common practice). In order to achieve a high field strength, the cathode takes the form of a very small tip on a slim shank, the radius of curvature at the apex usually being about 100 nm or less.

With increasing distance from the apex, the field strength decreases so rapidly that the emission is strong only in the vicinity of the apex. There is hence no need to confine this area artificially, and this makes the design of CFE guns comparatively simple despite the complicated theory of the tunnelling process. The next electrode downstream is always *positive* relative to the cathode. Its aperture is so narrow that any further electrodes have no influence on the high extraction field in the vicinity of the cathode; the electron probe current passing through this aperture is hence determined by the potential of this electrode alone. The terminology of CFE guns is not yet standard; this electrode is often called the first anode, which implies that others will follow, or the extraction anode. In this volume we call any electrode that is designed to adjust the electron probe *current* passing through its aperture, by appropriate variation of its potential (regardless of the polarity), the *wehnelt*. In this sense, the first anode of a CFE gun is the wehnelt, and we reserve the term *anode* for the next electrode, which determines the asymptotic kinetic energy of the electrons. The terminology is then the same as for thermionic triode guns. If there is more than one electrode after the wehnelt, as is often the case, we shall speak of intermediate electrodes.

As already mentioned, the influence of the anode on the extraction process can be neglected. We can thus deal with the *diode* formed by the cathode and the wehnelt separately. We shall see that this device forms a virtual point source. The latter is then focused by the subsequent electrodes and lenses. All this is presented schematically in Fig. 43.5A and B. The diode approximation, an extreme but still valid simplification, is dealt with in Chapter 45, Pointed Cathodes without Space Charge, while the focusing is treated in Chapter 50, Complete Electron Guns. The reason for this separation is that the electron optical properties of the diode approximation have some general significance, while those of the focusing parts depend essentially on details of the design. For instance, the diode approximation also holds for thermionic guns with LaB_6 cathode and positive wehnelt and for the hybrid emission gun designed by Kang et al. (1983), described in Section 50.3.

The assumption that a CFE electron gun can be usefully separated into a diode, producing a virtual crossover at V (Fig. 43.5), and a focusing lens, generated by the electric field between the wehnelt and the anode, is quite common. It is already implicit in the very early successful designs of Butler (1966), Crewe et al. (1968) and Munro (1973). In Chapter 50, Complete Electron Guns, we shall give a detailed justification of this simplification.

In comparison with thermionic sources, CFE guns have several advantages and also some disadvantages. Their main advantage is the fact that the lateral extension of the virtual source at V (Fig. 43.5) is extremely small, so that the maximum current density in the focus can be

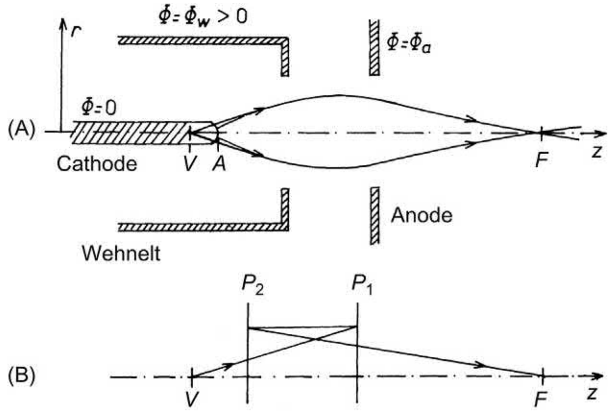

Figure 43.5
Field-emission triode electron gun. (A) Axial section through the system. In the diode formed by the cathode and the wehnelt, the rays are bent in such a way that they appear to have emerged from a virtual point source V; they form a real crossover at F. (B) Corresponding optical ray construction using the principal planes P_1 and P_2.

very high if the anode lens has very low aberrations. The brightness of field-emission guns is high; this concept is analysed in Chapter 47, Brightness. The main disadvantage of such guns is the fact that the total probe current in the crossover is too small for many important purposes, electron beam lithography in particular. This was predicted by Cosslett and Haine (1954), long before Crewe et al. (1968) built the first scanning electron microscope with a CFE source, but for these instruments the requirement of high brightness is far more important than that of high probe current. A second drawback of field-emission guns is that the vacuum pressure must be exceedingly low: for stable operation, a vacuum better than 10^{-7} Pa is necessary, but this technological problem has now been solved. We recall that thermionic guns operate satisfactorily at about 10^{-3} Pa.

There is an extensive literature concerning the technological features of electron guns, especially the preparation and stable operation of cathodes. For reasons of space we have had to exclude all these topics, important though they are; the general purpose of this chapter is to explore the underlying principles. The volume edited by Hawkes (2009) contains a wealth of information on the subject.

For very small ('nanoscopic') field emitting surfaces, Kyritsakis and Xanthakis (2015) have derived a generalized form of the theory that takes the shape of the tip into account. We return to this in Chapter 44, Theory of Electron Emission.

43.4 Beam Transport Systems

The study of electron guns is not confined to the physical processes in the vicinity of the cathode, but also includes the behaviour of the electron beam further away from the emitter. Since the specific differences between the emission processes are then no longer important, general concepts governing beam formation can be introduced. In particular these are the concepts of *brightness* and *emittance*, which are analysed in Chapters 47 and 48 respectively. These concepts permit us to establish general rules for the spatial intensity distribution in the beam. Although this is a quite general concern in electron optics, the concepts of brightness and emittance are mostly applied to guns and beam transport systems.

An important physical phenomenon that appears in intense electron beams, mainly in the vicinity of foci, is the *Boersch effect.* This effect, which is dealt with in Chapter 46, Space Charge Effects, is an anomalous broadening of the energy distribution and of any crossovers due to (statistical) Coulomb interactions between pairs of electrons.

The optics of electron guns requires a different approach from that we have employed for lenses. The theories proposed by Fujita and Shimoyama and by Rose are the subjects of Chapter 49, Gun Optics.

In Chapter 50, Complete Electron Guns, we give some guidelines for the design of guns and transport systems. Since the optimum shape of a system is essentially determined by the particular purpose to which it is to be put, the discussion remains general in order to avoid too wide a diversification. We also examine multibeam devices and the extremely small emitters based on carbon nanotubes.

CHAPTER 44

Theory of Electron Emission

In this Part we shall deal mainly with the emission of electrons from clean metallic surfaces. Emission from dirty surfaces and from semiconductors is not discussed, since the processes involved are rather numerous and all cannot be treated within the framework of this volume. Emission from carbon nanotubes is briefly considered in Chapter 50, Complete Electron Guns.

44.1 General Relations

The theory of electron emission from metallic surfaces is based on two main assumptions: that the Sommerfeld–Bethe (1933) model represents the electronic states in the metal and that the Fermi–Dirac distribution describes all thermionic functions.

In the Sommerfeld–Bethe model, the metal is regarded as a box with a constant inner potential V, lower than that of the adjacent vacuum domains. At the surface, the potential rises sharply, thus forming a steep wall as shown in Fig. 44.1. In the metal, the electrons of the conduction band are assumed to form a free gas, their charges being neutralized by those of the atomic cores. The quantum mechanical motion of each conduction electron is described by a standing wave with nodes at the surfaces. Beginning with the ground state, all the quantum mechanical one-particle states are filled up according to the Pauli exclusion principle. At zero absolute temperature this process is complete at the Fermi level, having an energy ζ_0 with respect to the ground state (the lower edge of the conduction band). If the temperature T is nonzero, the upper edge is replaced by a smooth curve determined by the Fermi–Dirac statistics; the corresponding thermal distribution is then given by

$$f(E,T) = \left\{1 + \exp\left(\frac{E-\zeta}{kT}\right)\right\}^{-1} \tag{44.1}$$

E being the constant energy of the corresponding one-particle motion and k Boltzmann's constant. The Fermi level ζ, defined by $f(\zeta, T) = 1/2$, depends on the bias of the energy scale and is slightly temperature-dependent. This dependence on T can be neglected, so that

$$\zeta = \zeta_0 - V_0 \tag{44.2}$$

V_0 being a free constant for the origin of the energy scale.

Principles of Electron Optics: Applied Geometrical Optics.
DOI: http://dx.doi.org/10.1016/B978-0-12-813369-9.00044-0

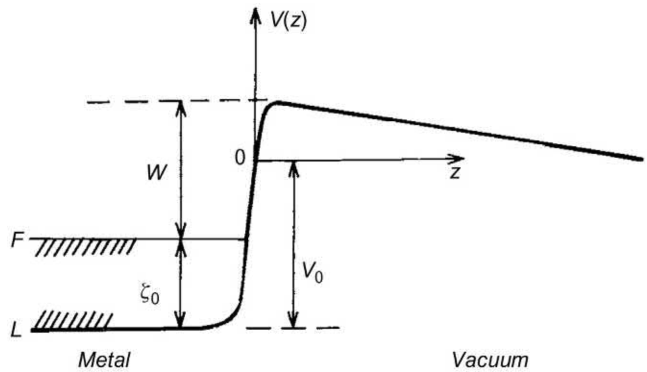

Figure 44.1
Electronic potential variation $V(z)$ in the vicinity of a cathode surface. L: lower edge of the conduction band; ζ_0: Fermi energy; W: work function (uncorrected). The negative slope of $V(z)$ in the vacuum zone is due to a weak electric field. The choice of the origin and hence of the constant V_0 is arbitrary.

All the quantities of interest concerning the emission of electrons can be calculated by appropriate integrations over the particle density $\rho^*(\boldsymbol{r}^*)$ in the one-particle phase space. We shall mark quantities referring to the phase space by asterisks, whenever this is necessary. Thus the six-dimensional space vector $\boldsymbol{r}^*$ is defined by

$$\boldsymbol{r}^* := (\boldsymbol{r}, \boldsymbol{p}) = \left(x, y, z, p_x, p_y, p_z\right) \tag{44.3}$$

$\boldsymbol{p}$ being the canonical momentum. The phase density $\rho^*(\boldsymbol{r}^*)$ is then given by

$$\rho^*(\boldsymbol{r}^*) = \frac{2}{h^3} f(E, T) D(r^*) \tag{44.4}$$

h being Planck's constant and D a transmission factor. The latter is defined as the ratio of the wave-mechanical intensity after passing the potential barrier and the incident intensity. Thus we have $D = 1$ for the free-electron gas in the metal and $D < 1$ as a result of energy restrictions and tunnel effects in the emission process. Detailed formulae for the transmission factor will be given below. In order to perform practical calculations, the conservation law

$$E = H(\boldsymbol{r}^*) = \frac{1}{2m}\left\{\boldsymbol{p} + e\boldsymbol{A}(\boldsymbol{r})\right\}^2 + V(\boldsymbol{r}) \tag{44.5}$$

for the Hamiltonian H is introduced into Eq. (44.4). In the vast majority of cases, magnetic fields are not relevant in this context, hence $\boldsymbol{A} = 0$; $\boldsymbol{p} = m\boldsymbol{v}$ is then simply the kinetic momentum. There are also guns in which the electrostatic field is enclosed in a magnetic field (see for example Troyon and Laberrigue, 1977; Troyon, 1980a,b, 1984a,b, 1989a,b;

Shimoyama et al., 1982, 1983; Ura and Takaoka, 1986; Takaoka et al., 1989; Delong et al., 1988, 1989; Saito and Uno, 1995; Saito et al., 1995; Kawasaki et al., 2000; Tamura et al., 2008; and Kasuya et al., 2014a,b, 2016). The papers of Knell and Plies (1999), Jin et al. (2002), Yonezawa et al. (2002), Khursheed and Karuppiah (2002) and Zhao et al. (2012) are also relevant here.

From Eqs (44.4) and (44.5), the three-dimensional distribution $F(\boldsymbol{r})$ associated with any classical observable $\boldsymbol{F}^*(\boldsymbol{r}, \boldsymbol{p})$ can be obtained by integration:

$$F(\boldsymbol{r}) = \iiint F^*(\boldsymbol{r},\boldsymbol{p})\rho^*(\boldsymbol{r},\boldsymbol{p})d^3p \tag{44.6}$$

Practical examples are the expectation values of the electron charge density ρ with $F^* = -e$:

$$\rho(\boldsymbol{r}) = -\frac{2e}{h^3}\iiint f(E,T)D(\boldsymbol{r}^*)d^3p \tag{44.7}$$

and of the electric current density $\boldsymbol{j}$; with $\boldsymbol{F}^* = e\boldsymbol{v} = e\boldsymbol{p}/m$ we find

$$j(\boldsymbol{r}) = \frac{2e}{mh^3}\iiint \boldsymbol{p}f(E,T)D(\boldsymbol{r}^*)d^3p \tag{44.8}$$

In Eq. (44.8) the sign of $\boldsymbol{j}$ has been chosen in such a way that this vector has the same direction as the mean particle motion (not opposite to it), since $e > 0$. This is customary in the literature.

44.2 Transmission Through a Plane Barrier

The surfaces of cathodes are generally curved, but the penetration of the potential wall occurs in such a short zone that the curvature is considered negligible in a first approximation. We therefore replace the real cathode surface by its local tangential plane. The atomic structure of the metal is neglected in order to simplify the theory. Without loss of generality we can choose a local Cartesian coordinate system (x, y, z) in such a way that $z = 0$ is the surface and $z > 0$ the vacuum half-space. Consequently the potential is a function $V(z)$, independent of x and y. With the assumption $\boldsymbol{A}(\boldsymbol{r}) = 0$ we find the following three conservation laws:

$$\frac{1}{2m}\left(p_x^2 + p_y^2\right) =: U_t = \text{const} \tag{44.9a}$$

$$\frac{1}{2m}p_z^2 + V(z) =: U_n = \text{const} \tag{44.9b}$$

$$U_t + U_n = E = \text{const} \tag{44.9c}$$

the constants U_t, U_n and E being the tangential, normal and total energy, respectively. Owing to the assumptions made above, the motions in the three Cartesian directions are independent of each other, the potential barrier acting only on the normal (z) component. As will be shown later, $D(\boldsymbol{r}^*)$ is then only a function of U_n, $D(U_n)$, a fact which strongly simplifies the calculations. Owing to the symmetries of the problem, the current density (44.8) has only one nonzero component, $j_z(z)$.

In order to evaluate Eq. (44.8), we introduce cylindrical coordinates in the momentum space. From Eq. (44.9a), we thus have

$$p_x = \sqrt{2mU_t}\cos\varphi, \quad p_y = \sqrt{2mU_t}\sin\varphi$$
$$dp_x dp_y = mdU_t d\varphi$$

The integration over φ is trivial. By introducing the differential $dp_z = mp_z^{-1}\, dU_n$, obtained from (44.9b) for a fixed value of z, the integral (44.8) can be expressed in terms of U_t and U_n. From Eqs (44.1 and 44.8), we have

$$j_z = \frac{4\pi me}{h^3}\int\int \frac{D(U_n)}{1+\exp\dfrac{U_T+U_n-\zeta}{kT}}dU_T dU_n$$

$$= \frac{4\pi me}{h^3}\int\int \frac{D(U_n)\exp\left(-U_T/kT\right)}{\exp\left(-U_T/kT\right)+\exp\dfrac{U_n-\zeta}{kT}}dU_T dU_n$$

$$= -\frac{4\pi mekT}{h^3}\int D(U_n)\ln\left\{\exp(-U_n/kT)+\exp\frac{U_n-\zeta}{kT}\right\}dU_n$$

$$= -\frac{4\pi mekT}{h^3}\int D(U_n)\left\{\ln\exp\frac{U_n-\zeta}{kt}-\ln\left(1+\exp\frac{U_n-\zeta}{kt}\right)\right\}dU_n$$

and so

$$j_z = \frac{4\pi mekT}{h^3}\int_{-\infty}^{\infty} D(U_n)\ln\left\{1+\exp\left(\frac{\zeta-U_n}{kT}\right)\right\}dU_n \tag{44.10}$$

With the assumptions introduced above, this formula is *exactly* valid in the sense that no further simplifications were needed to derive it. The remaining integration, will, however, be very complicated. In the general case, Eq. (44.10) can be evaluated only numerically (Dolan and Dyke, 1954; El-Kareh et al., 1977).

44.3 Thermionic Electron Emission

The evaluation of expectation values is quite easy in the case of purely thermionic electron emission. In a first approximation, the external electric field in front of the cathode is so weak that its influence on the potential barrier can be neglected. It is then reasonable to replace the true potential $V(z)$ by a step function:

$$V(z) = \begin{cases} -V_0 := -(\zeta_0 + W) & \text{for} \quad z < 0 \\ 0 & \text{for} \quad z \geq 0 \end{cases}$$

W here being the *work function*, a material property of the cathode. The particular choice of the energy and potential scale is shown in Fig. 44.2; it implies that $V_0 = \zeta + W$ in Eq. (44.2).

Since only electrons with $U_n \geq 0$ can be emitted, we have the transmission factor

$$D(U_n) = \begin{cases} 0 & \text{for} \quad U_n < 0 \\ 1 & \text{for} \quad U_n \geq 0 \end{cases}$$

Since both E and kT are then very small in comparison with W and ζ_0, we may simplify Eq. (44.1) by neglecting the unit term in the denominator:

$$f(E, T) = \exp\left(-\frac{E + W}{kT}\right)$$

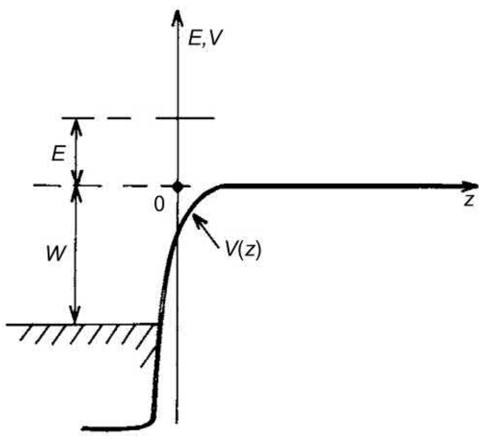

Figure 44.2
Potential barrier and choice of the origin *O* in the case of thermionic emission. The potential drop associated with the weak electric field has been omitted here.

and consequently

$$\rho^*(\boldsymbol{r}^*) = 2h^{-3}\exp\left(-\frac{E+W}{kT}\right) \quad \begin{cases} z > 0 \\ E \geq 0 \end{cases} \tag{44.11}$$

The evaluation of Eq. (44.8) or (44.10) now results in the well-known Richardson[1]–Dushman equation for the *saturation* current density:

$$j_s = A(kT)^2\exp\left(-\frac{W}{kT}\right) \tag{44.12a}$$

with the constant

$$A = 4\pi meh^{-3} \tag{44.12b}$$

Later studies that take quantum effects and the band structure of the emitter into account show that this expression for A is an upper limit.

As well as the total current density, the energy and angular distributions of this quantity are of practical interest. In order to calculate these distributions, it is necessary to introduce polar coordinates in the momentum space by writing

$$\left.\begin{aligned} p_z &= \sqrt{2mE}\cos\gamma \\ p_x &= \sqrt{2mE}\sin\gamma\cos\varphi \\ p_y &= \sqrt{2mE}\sin\gamma\sin\varphi \end{aligned}\right\} \tag{44.13a}$$

so that γ is clearly the emission angle relative to the outward-directed surface normal. The volume element in momentum space is then given by

$$d^3p = p^2dpd\Omega = m\sqrt{2mE}\sin\gamma\, dEd\gamma d\varphi \tag{44.13b}$$

$d\Omega = \sin\gamma\, d\gamma d\varphi$ being the element of solid angle. The current density element can now be easily expressed in polar coordinates:

$$\begin{aligned} d^3j &= \frac{ep\cos\gamma}{m}\rho^* d^3p \\ &= \frac{4me}{h^3}E\exp\left(-\frac{E+W}{kT}\right)\sin\gamma\cos\gamma\, dEd\gamma d\varphi \end{aligned}$$

[1] O.W. Richardson was awarded the Nobel Prize (Physics) in 1928 for his work on electron emission.

It is convenient to introduce the function

$$S(E,T) = \frac{1}{\pi} AE \exp\left(-\frac{E+W}{kT}\right) \tag{44.14a}$$

which will be called the *spectral radiance* of the cathode. Finally we obtain

$$d^3 j = S(E,T)\cos\gamma\, dE\, d\Omega \tag{44.14b}$$

The *total energy distribution* is now found by integration over all allowed emission angles ($0 \leq \varphi \leq 2\pi$, $0 \leq \gamma \leq \pi/2$), the result being

$$dj = AE\exp\left(-\frac{E+W}{kT}\right)dE \tag{44.15}$$

Integration over E gives Eq. (44.12), as it must. It is helpful to introduce a normalized distribution function by setting

$$\begin{aligned} g(E)\, dE &:= j_s^{-1}\, dj \\ g(E) &= \frac{E}{(kT)^2}\exp\left(-\frac{E}{kT}\right) \end{aligned} \tag{44.16}$$

This can be used for the calculation of statistical expectation values from

$$< f > := \int_0^\infty f(E)g(E)dE$$

In this way we obtain the mean energy $< E > = 2kT$ and the standard deviation

$$\Delta E = \left(< E^2 > - < E >^2\right)^{1/2} = kT\sqrt{2}$$

An important quantity, which cannot be expressed as an expectation value, is the most probable energy $E_m = kT$, corresponding to the maximum of the distribution. The function $g(E)$ is shown in Fig. 44.3. Its most important feature is its long tail of high-energy electrons, which is undesirable in most practical applications.

The angular emission distribution is obtained by integration of Eq. (44.14b) over all positive energies E, but with fixed angle, the result being

$$\tilde{B}(\gamma) := \frac{dj}{d\Omega} = \frac{1}{\pi} j_s \cos\gamma \tag{44.17}$$

This is *Lambert's law*, which is quite similar to the corresponding law for the thermal emission of light (Born and Wolf, 1959, Eq. 4.8.8).

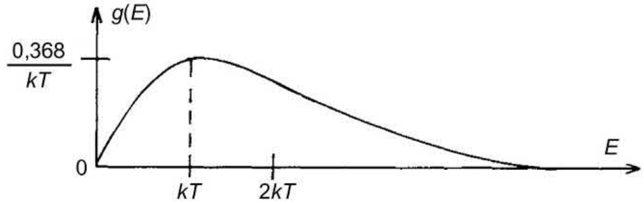

Figure 44.3
Energy spectrum of thermionic emission. The function has been normalized so that the area under the curve is unity.

The cosine law (44.17) refers to the angular emission distribution immediately after the emission of electrons. However, this cannot be observed experimentally because the electron beam is rapidly rendered parallel by the applied electric field. From this point of view it is more favourable to introduce the *transverse momentum distribution,* since p_x and p_y are conserved in all one-dimensional potential fields $V(z)$. Writing the differential current-density distribution in Cartesian momentum coordinates and recalling that $p \cos\gamma = p_z$ and $2mE = p_x^2 + p_y^2 + p_z^2$, we have

$$\begin{aligned} d^3 j &= \frac{2e}{mh^3} p_z \exp\left(-\frac{W}{kT}\right) \exp\left(-\frac{E}{kT}\right) \\ &= \frac{2e}{mh^3} \exp\left(-\frac{W}{kT}\right) \exp\left(-\frac{p_x^2 + p_y^2}{2mkT}\right) p_z \exp\left(-\frac{p_z^2}{2mkT}\right) \end{aligned}$$

Integrating over p_z gives

$$d^2 j = \frac{2ekT}{h^3} \exp\left(-\frac{W}{kT}\right) \exp\left(-\frac{p_x^2 + p_y^2}{2mkT}\right)$$

or

$$d^2 j = \frac{j_s}{2\pi mkT} \exp\left(-\frac{p_x^2 + p_y^2}{2mkT}\right) dp_x\, dp_y \tag{44.18a}$$

This distribution is rotationally symmetric and *Gaussian*, the average transverse energy being given by

$$< U_t > = \frac{1}{2m} < p_x^2 + p_y^2 > = kT \tag{44.18b}$$

This result is of importance for the physics of thermionic guns with pointed cathodes, as will become obvious in Chapter 45, Pointed Cathodes without Space Charge.

44.4 The Tunnel Effect

We now investigate the influence of strong electric fields on the emission process. First, the form of the potential wall will be considered in more detail.

Inside the metal ($z < 0$) we still assume that $V(z) = \text{const}$, although this is a very crude simplification, but taking into account the crystalline structure of the metal would complicate the theory considerably. In the vacuum half-space, $z > 0$, we assume that a homogeneous electric field, of field strength $|\boldsymbol{E}| =: F$, is applied. In addition we consider the potential of image charges. An electron at a distance $z > 0$ from the surface is associated with an image charge of opposite sign in the mirror-symmetric position. This gives rise to a Coulomb potential $V_c = -e^2/16\pi\varepsilon_0 z$. The complete representation of the potential is then

$$V(z) = \begin{cases} 0 & \text{for } z < 0 \\ W - eF_Z - e^2/16\pi\varepsilon_0 z & \text{for } z > 0 \end{cases} \tag{44.19}$$

which implies that $V_0 \approx \zeta_0$, $\zeta \approx 0$ in Eq. (44.2). This function V is shown in Fig. 44.4. At $z = 0$, the formula is clearly wrong, but the potential at this point has no influence on the tunnel effect described below. In any case, Eq. (44.19) is a very crude representation of the potential. The most important effect of the image charge on the potential barrier is that the maximum is lowered, the latter being given by

$$\begin{aligned} z_m &= \sqrt{e/16\pi\varepsilon_0 F}, \quad \delta W = \sqrt{e^3 F/4\pi\varepsilon_0} \\ V_m &:= V(z_m) = W - \delta W \end{aligned} \tag{44.20}$$

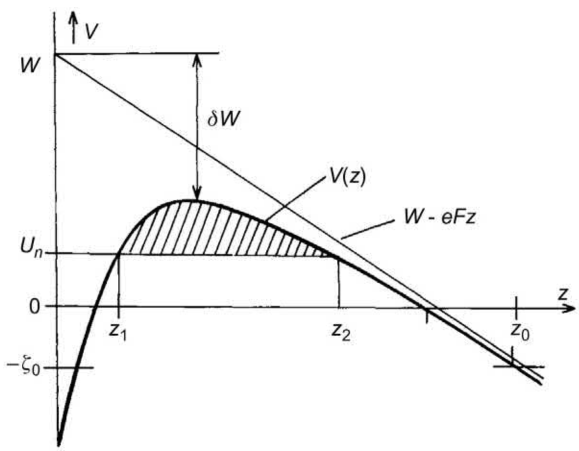

Figure 44.4
Potential barrier in the case of field emission. The origin O is set at the Fermi level. The hatched area indicates the potential barrier for a given normal energy U_n. The plane $z = z_0$ at which $V(z_0) = -\zeta_0$ is a favourable reference plane for the start of classical trajectories.

The quantum mechanical tunnelling probability at a given normal energy U_n is essentially governed by the part of the barrier for which $V(z) \geq U_n$. The corresponding z-interval is given by $z_1 \leq z \leq z_2$ with $V(z_{1,2}) = U_n$. This is shown in Fig. 44.4. In the Wentzel–Kramers–Brillouin (WKB) approximation, the transmission factor $D(U_n)$ is given by

$$D(U_n) = \frac{1}{1 + e^G} \tag{44.21}$$

with the familiar Gamow exponent

$$G(U_n) = \frac{2}{\hbar} \int_{z_1}^{z_2} \sqrt{2m(V(z) - U_n)}dz \tag{44.22}$$

It often happens that $G(U_n) \gg 1$ and the approximation $D = e^{-G}$ is then valid. For the potential (44.19), the integration in (44.22) can be carried out analytically and results in an expression containing elliptic integrals. It is convenient to define two dimensionless variables y and κ by

$$y := \frac{\delta W}{W - U_n}, \quad \kappa = \sqrt{\frac{1 - y}{1 + y}} \tag{44.23a}$$

with values between 0 and 1. Furthermore, we introduce a so-called 'correction' function

$$\upsilon(y) := \sqrt{1 + y}\,\{E(\kappa) - yK(\kappa)\} \tag{44.23b}$$

$K(\kappa)$ and $E(\kappa)$ being the complete elliptic integrals of first and second kind, respectively. The transmission factor is then given by

$$D(U_n) = \exp\left\{ -\frac{4}{3e\hbar F}\left\{2m(W - U_n)^3\right\}^{1/2}\upsilon(y)\right\} \tag{44.24}$$

The function $\upsilon(y)$ describes the contribution of the image-charge potential; $\upsilon(y) = 1$ would correspond to an unsmoothed triangular potential barrier of height $W - U_n$. Since $\upsilon(y) \leq 1$, the image charge *increases* $D(U_n)$ by lowering the potential barrier.

Although (44.24) is the correct result of the integration, it is too complicated for further calculations. The exponent in (44.24) is therefore expanded as a Taylor series in the vicinity of the Fermi level, where the electron emission is strongest. With the assumption $|U_n| \ll W$, this Taylor series can be truncated after the linear term, and we thus obtain

$$D(U_n) = D_0 \exp\left(U_n/d\right) \tag{44.25}$$

with $D_0 \coloneqq D(0)$ obtained by setting $U_n = 0$ in (44.23), (44.24) and with

$$d \coloneqq \frac{e\hbar F}{2t(y)}(2mW)^{-1/2} \eqqcolon \frac{1}{2}eF\lambdabar \tag{44.26}$$

The function $t(y)$ is defined by

$$t(y) \coloneqq \upsilon - \frac{2}{3}y\upsilon' = \sqrt{1+y}\left\{E(\kappa) - \frac{y}{1+y}K(\kappa)\right\} \tag{44.27}$$

It varies only slowly, remaining close to unity.

The quantity d, given by Eq. (44.26), is an energy and plays a similar role in the physics of field emission to the thermal energy in thermionic emission. This will be obvious later and will prove to be very useful. The representation $d = eF\lambdabar/2$ makes it clear that this quantity d can be interpreted as an acceleration energy gained over a distance $\lambdabar/2$. Apart from the unimportant factor $t^{-1} \sim 1$, the quantity $\lambdabar = \lambda/2\pi$ is a reduced de Broglie wavelength corresponding to a momentum $(2mW)^{1/2}$. The functions $\upsilon(y)$ and $t(y)$ have been tabulated by Good and Müller (1956). Eupper (1980) found that the simple approximation

$$\upsilon(y) = 1 - y^{1.69}, \quad t(y) = 1 + 0.1107y^{1.33} \tag{44.28}$$

is sufficiently accurate for all practical purposes, so that it is no longer necessary to use these tables.

When the emissive surface is extremely small, the expression for the current density expression can be improved by modifying Eq. (44.19) thus (Kyritsakis and Xanthakis, 2015):

$$V(z) = W - eFz - \frac{B}{z(1+z/2R)} + \frac{eF}{R}z^2 \tag{44.29a}$$

in which

$$B = e^2/16\pi\varepsilon_0 \approx 0.36 \text{ eV.nm} \tag{44.29b}$$

and R is the radius of the inscribed circle at the apex of the tip, which need not be spherical elsewhere; F is the local electric field at the apex. The Gamow exponent is then

$$G = g\int_{z_1}^{z_2}\left(W - eFz - \frac{B}{z(1+z/2R)} + \frac{eF}{R}z^2\right)^{1/2} dz \tag{44.30a}$$

which can be transformed into

$$G = g\frac{W^{3/2}}{eF}\int_{\zeta_1}^{\zeta_2}\left(1 - \zeta - \frac{y^2}{4(\zeta + x\zeta^2/2)} + x\zeta\right)^{1/2} d\zeta \eqqcolon \frac{2g}{3}\frac{W^{3/2}}{eF}\,\Xi(x,y) \tag{44.30b}$$

by setting

$$\zeta = eFz/W, \quad x = W/eFR, \quad y = 2(BF)^{1/2}/W \text{ and } g = (8m)^{1/2}/\hbar \tag{44.31}$$

To a linear approximation,

$$\Xi(x,y) = \int_{\zeta_1}^{\zeta_2} \left(1-\zeta-y^2/4\zeta\right)^{1/2} d\zeta + x\int_{\zeta_1}^{\zeta_2} \frac{\zeta^2+y^2/8}{2(1-\zeta-y^2/4\zeta)^{1/2}}d\zeta \tag{44.32}$$

in which ζ_1 and ζ_2 are the roots of $1-\zeta-y^2/4\zeta$. We can now calculate the current density, j:

$$j = \frac{aF^2}{W\left\{t(y)+W\psi(y)/eFR\right\}^2}\exp\left[-b\frac{W^{3/2}}{F}\left\{\upsilon(y)+\frac{W}{eFR}\omega(y)\right\}\right] \tag{44.33}$$

in which

$$\begin{aligned} t(y) &= \upsilon(y) - \frac{2}{3}y\frac{d\upsilon}{dy} \approx 1 + \frac{y^2}{9} - \frac{y^2\ln y}{11} \\ \psi(y) &= \frac{5}{3}\omega(y) - \frac{2}{3}y\frac{d\omega}{dy} \approx \frac{4}{3} - \frac{y^2}{500} - \frac{y^2\ln y}{15} \end{aligned} \tag{44.34}$$

and

$$\begin{aligned} &\upsilon(y) = \frac{3}{2}\int_{\zeta_1}^{\zeta_2}(1-\zeta-y^2/4\zeta)^{1/2}d\zeta \quad \omega(y) = \frac{3}{4}\int_{\zeta_1}^{\zeta_2}\frac{\zeta^2+y^2/8}{(1-\zeta-y^2/4\zeta)^{1/2}}d\zeta \\ &a = e^3/8h \quad b = 8\pi(2m)^{1/2}/3e \end{aligned} \tag{44.35}$$

The functions $t(y)$ and $\upsilon(y)$ are the same as those in the traditional form of the theory (44.23b, 44.27) while the terms in $\omega(y)$ and $\psi(y)$ represent the corrections required for very sharp tips.

44.5 Field Electron Emission

Field electron emission is the physical process that enables electrons to escape from a metal by the quantum mechanical tunnel effect treated above. Pure field emission is obtained at $T = 0$, and is hence an idealization. The more realistic emission process occurring at finite temperatures is called cold field emission, to distinguish it from Schottky emission in which the cathode is deliberately heated; the terms thermal-field (TF) emission and temperature-and-field emission have also been used.

The expression (44.25) for the transmission factor is simple enough for it to be possible to perform the necessary integrations. Very little error is introduced by extending the lower limit of integration from $U_n = -\zeta_0$ to $U_n = -\infty$. Evaluation of Eq. (44.10) then yields the emission current density:

$$j_T = j_F \frac{\pi p}{\sin \pi p} = \frac{j_F}{\operatorname{sinc} \pi p}, \quad \operatorname{sinc} x := \frac{\sin x}{x} \tag{44.36}$$

with

$$j_F = Ad^2 \exp\left(-b\frac{W}{d}\right) \tag{44.37}$$

$$p := kT/d \leq 0.7 \tag{44.38a}$$

$$b := \frac{2\upsilon(y_0)}{3t(y_0)} \approx 0.6, \quad y_0 = \frac{\delta W}{W} \tag{44.38b}$$

and $A = 4\pi meh^{-3}$ as in (44.12b). Eq. (44.37) is the celebrated Fowler–Nordheim equation (Fowler and Nordheim, 1928; Nordheim, 1928) for pure field emission. Eq. (44.36) is named after Murphy and Good (1956) and after Young (1959; see also Young and Müller, 1959). Obviously this equation breaks down as $p \to 1$, so that the restriction imposed in (44.38a) must be respected. For larger values of p no satisfactory simple theory is known. Comprehensive theoretical investigations in the region between TF emission and thermionic emission have been made by Christov (1966). The structure of the Fowler–Nordheim equation is obviously similar to that of the Richardson–Dushman equation (44.12) if d is replaced by kT. This correspondence will be more evident later.

Once again we are interested in formulae for the distribution of energy, emission angle and transverse momentum. Unlike the corresponding considerations in Section 44.3, a problem is now created by the fact that the real cathode surface must not be used as a reference plane. In front of the cathode is the potential barrier in which the longitudinal momentum p_z of the tunnelling electron is imaginary. We need, however, a *classical* description of the particle motion, if we are not to leave the framework of geometric electron optics. Following Kasper (1981), we choose the reference plane $z = \text{const} = z_0$ such that $V(z_0) = -\zeta_0$, as shown in Fig. 44.4. This plane is in practice at a distance $z_0 = (W + \zeta_0)/eF$ from the true cathode surface. This distance is at once large enough for the classical description of the electrons to be applicable and short enough for the effects of curvature to be still very small for $F \geq 10^7$ V/cm. One objection to this very simple choice is that the Fermi energy ζ_0 can hardly be measured, but this does not matter, since we shall see that ζ_0 cancels out from the final formulae.

It is convenient to introduce a polar representation of the momenta, but this differs from (44.13a,b) in that the total energy E must now be replaced by the kinetic energy $E - V$, since the potential does not vanish. Using $U_t = (E - V)\sin^2\gamma$ and $U_n = E\cos^2\gamma + V\sin^2\gamma$, we can derive a spectral radiance S analogous to (44.14a) and (44.14b). We can even do this for any plane $z = $ const beyond the barrier, provided that $V = V(z)$ remains valid. With $\zeta = 0$ the result is

$$S = S(E, T, z, \gamma) = \frac{4me}{h^3}\frac{E - V(z)}{1 + \exp(E/kT)}\exp\left(\frac{E\cos^2\gamma + V\sin^2\gamma - bW}{d}\right) \tag{44.39a}$$

The inequalities $|E| \ll W$, $d \ll W$, $\gamma \ll 1$ and the particular choice $V = -\zeta_0$ bring some simplification; we then obtain

$$S = \frac{A\zeta_0}{\pi}\frac{1}{1 + \exp(E/pd)}\exp\left(\frac{-bW - \zeta_0\sin^2\gamma + E}{d}\right) \tag{44.39b}$$

where (44.12a) and (44.38) have been used. Note that the origin of E is different from that adopted in Section 44.3! Integration of $S\cos\gamma$ over all permitted emission angles yields the total energy distribution $G(E)$ with $dj = G(E)dE$:

$$G(E) \coloneqq j_T g(E) = \frac{Ad}{1 + \exp(E/pd)}\exp\left(\frac{E - bW}{d}\right) \tag{44.40}$$

The function $g(E)$ is again the normalized statistical distribution function. As mentioned above, the Fermi energy ζ_0 has disappeared in the integration.

Total energy distribution curves are shown in Fig. 44.5. They have an asymmetric form, the tails for $E \to \infty$ extending very far for higher values of $p = kT/d$. With the distribution function $g(E)$ of (44.40), the following expectation values can be derived:

$$< E > = \pi pd\cot\pi p = d\left(1 - \frac{\pi^2 p^2}{3} - \frac{\pi^4 p^4}{45} + \ldots\right) \tag{44.41}$$

$$\Delta E = d\frac{\pi p}{\sin\pi p} = d\left(1 + \frac{\pi^2 p^2}{6} + \frac{7\pi^4 p^4}{360} + \ldots\right) \tag{44.42}$$

Recalling (44.36), we conclude that (Kasper, 1981)

$$\frac{\Delta E}{d} = \frac{j_T}{j_0} \tag{44.43}$$

which means that the width of the energy spectrum increases with temperature in the same way as the total current density. This relation shows why it is impossible to build a field

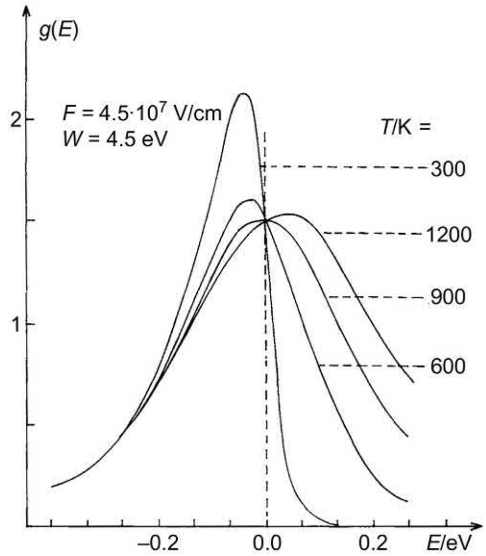

Figure 44.5
Total energy distribution curves for thermal-field (TF) electron emission at various temperatures T; $E = 0$ corresponds to the Fermi level. The vertical scale is in arbitrary units.

emission gun with high current density and low energy width ΔE. This is impossible even if no external heat is supplied to the cathode, since the intense emission process itself heats the cathode (Nottingham effect). The maximum of the total energy distribution curve is located at

$$E_m = kT\{\ln p - \ln(1-p)\}$$

This value is negative for $p < 1/2$ and positive for $p > 1/2$. This formula may be helpful in determining the origin of the energy scale, which cannot be measured directly.

By integration of (44.39), an angular emission distribution analogous to (44.17) can be derived (Kern, 1978a,b; Kasper, 1982). In any reference plane $z = \text{const}$, this is given by

$$\tilde{B}(\gamma) = -\frac{j_T}{\pi d} V(z)\cos\gamma \exp\left\{\frac{V(z)\sin^2\gamma}{d}\right\} \tag{44.44}$$

if $-V(z) \gg d$. The formula then satisfies $\int \tilde{B}(\gamma)\, d\Omega = j_T$ for $\gamma \leq \pi/2$, as it should do. Eq. (44.44) describes mathematically the strong parallelizing effect of the extraction field on the electron beam: a significant contribution to the total current density is obtained only for $\gamma^2 \leq d/|V(z)|$. This last quantity is already very small at the starting plane $z = z_0$, since $\zeta_0 = 10$ eV, $d = 0.1$ eV are typical values.

The transverse momentum distribution can be calculated as in (44.18a,b). The integrations are straightforward and result in

$$d^2j = \frac{j_T}{2\pi md}\exp\left(-\frac{p_x^2+p_y^2}{2md}\right)dp_x dp_y \tag{44.45a}$$

and

$$< U_t > \; = \frac{1}{2m} < p_x^2 + p_y^2 > \; = d \tag{44.45b}$$

The analogy with (44.18a,b) for $kT \leftrightarrow d$ is quite obvious. The fact that emission mechanisms as different as those treated here both have Gaussian transverse momentum distributions may be considered as a justification of the heuristic assumption that beam profiles are Gaussian, which is frequently made in theoretical studies.

In the foregoing derivations, we have followed the traditional route to (44.25) with the usual definitions of $\upsilon(y)$ and $t(y)$ in terms of the parameter y. In the past decade, however, Forbes and others have re-examined the Fowler–Nordheim formula and shown convincingly that it is preferable to reformulate it in terms of the variable $s = y^2$; we write

$$\overline{\upsilon}(s) \coloneqq \upsilon(y) \tag{44.46}$$

This has several advantages, both mathematical and physical. In their major paper, Forbes and Deane (2007) have shown that $\overline{\upsilon}$ satisfies the differential equation

$$s(1-s)\frac{d^2\overline{\upsilon}}{ds^2} = \frac{3}{16}\overline{\upsilon} \tag{44.47a}$$

with

$$\overline{\upsilon}(0) = 1 \quad \text{and} \quad \lim_{s\to 0}\left(\frac{d\overline{\upsilon}}{ds} - \frac{3}{16}\ln s\right) = -\frac{9}{8}\ln 2 \tag{44.47b}$$

Eq. (44.47a) is a special case of the differential equation satisfied by the hypergeometric function (Whittaker and Watson, 1927, Section 14.2). From an examination of the solutions of this equation, set out in full by Forbes and Deane, it emerges that a good approximation to the particular solution $\overline{\upsilon}(s)$ is

$$\begin{aligned} \overline{\upsilon}(s) &= 1 - \alpha s + \beta s \ln s \\ \alpha &= \frac{3}{16}(6\ln 2 + 1), \quad \beta = \frac{3}{16} \end{aligned} \tag{44.48}$$

This expression, in the form $\overline{\upsilon}(s) = 1 - s + \frac{1}{6}s\ln s$ had already been found by Forbes (2006); the numerical factors are very close: $\alpha = 0.9673$ and $\beta = 0.1875$ $(1/6 = 0.1667)$. For very extensive discussion of this and comparison with other approximate expressions for $\overline{\upsilon}(s)$ or $\upsilon(y)$, see Forbes and Deane (2007, 2010). It is interesting that the approximations found by Eupper (1980),

$$\begin{aligned} \upsilon(y) &= 1 - y^{1.69} \quad \text{or} \quad \overline{\upsilon}(s) = 1 - s^{0.845} \\ t(y) &= 1 - 0.1107y^{1.33} \quad \text{or} \quad \bar{t}(s) = 1 - 0.1107s^{0.665} \end{aligned} \tag{44.49}$$

are close runners-up to (44.48), as shown by Forbes and Deane (2010).

This short account is no more than an introduction to recent work in this area. For further information, see Deane and Forbes (2008), Edgcombe (2005), Edgcombe and Valdrè (2001), Edgcombe and de Jonge (2006, 2007), Forbes (1999a,b,c, 2004, 2006, 2008a,b,c, 2009, 2010), Forbes and Deane (2010), Forbes and Jensen (2001), Forbes et al. (2015), Jensen (1999, 2001, 2012), Jensen and Ganguly (1993), Jensen et al. (2017) and Kolosko et al. (2016).

44.6 Schottky Emission

The theory of Section 44.3 is extremely simplified. In practice, the influence of the field strength F on thermionic emission cannot be neglected. Here we assume that, apart from the image-charge term, the electric field is homogeneous for $z > 0$, which implies that space charge effects are still excluded from the discussion; the latter will be dealt with in Chapter 46.

One very simple improvement consists in replacing W by

$$W_F := W - \delta W \tag{44.50}$$

in the Richardson–Dushman equation, δW being given by (44.20). The result is enhanced emission, which is known as the Schottky effect. This is, however, not quite satisfactory. It is still essential to take into account the tunnelling process. The necessary approximations are justified in the following manner: since the field strength is comparatively weak (about 100 V/cm), the potential barrier is broad and flat, so that tunnelling occurs essentially at energies near the maximum of $V(z)$. In the vicinity of this maximum, given by Eq. (44.20), the function $V(z)$ is approximated by a parabola $V = V_m - \alpha(z - z_m)^2$; the integration in (44.22) can then be carried out, the result being

$$G(U_n) = (V_m - U_n)/c \tag{44.51}$$

with

$$c = \frac{\hbar}{\pi\sqrt{m}}(4\pi\varepsilon_0 eF^3)^{1/4} = \frac{\hbar eF}{\pi\sqrt{m\delta W}} \tag{44.52}$$

It is now necessary to use Eq. (44.21) in its exact form. The formula remains valid when $U_n > V_m$, though (44.22) does not hold then. In fact

$$D(U_n) = \left\{1 + \exp\left(\frac{V_m - U_n}{c}\right)\right\}^{-1} \tag{44.53}$$

gives the correct results, $D(V_m) = 1/2$, $D(\infty) = 1$. Since the electron emission is most probable in the vicinity of the maximum, and since $W_F \gg kT$, we may simplify the Fermi function by writing

$$f(E, T) = \exp\left(-\frac{W_F + E}{kT}\right) \tag{44.54}$$

the origin of the energy scale being chosen here at the maximum V_m. The subsequent calculations are now very similar to those of Section 44.5; we shall give only some important results. The total current density is

$$j_s = A(kT)^2 \exp\left(-\frac{W_F}{kT}\right)\frac{\pi q}{\sin \pi q} \tag{44.55}$$

with the dimensionless parameter

$$q = \frac{c}{kT} \leq 0.7 \tag{44.56}$$

The transverse momentum distribution still satisfies (44.18a,b). The total energy distribution is broadened and the formula

$$\Delta E = \sqrt{2}kT\frac{\pi q}{\sin \pi q} \tag{44.57}$$

is approximately valid, the last term expressing the broadening caused by the weak tunnel effect. Comparing these formulae with those for field emission, it is seen that there is an exchange-symmetry $kT \leftrightarrow d$, $q \leftrightarrow p$.

As mentioned earlier, a very complete account of Schottky emitters has been prepared by Bronsgeest (2015).

44.7 Concluding Remarks

In the preceding sections we have outlined the theory of electron emission in its most simplified version. This gives us some understanding of the physical processes that take place in electron emission. The formulae obtained are useful for the preliminary design of electron guns. We emphasize that numerous details have had to be omitted for reasons of space. The reader will find a fuller discussion in the relevant literature of surface science, e.g. Swanson and Bell (1973) for earlier work and Swanson and Schwind (2009). The reliable operation of an electron gun depends on a great many technological details, for which no exact theory exists and which often cannot be fully investigated by experiments. Thus a successful electron gun design requires much practical experience as well as a knowledge of the underlying theory.

CHAPTER 45

Pointed Cathodes Without Space Charge

In many electron gun designs, especially those with field electron emission, the cathode is treated as a point source emitting electrons with an energy that corresponds to the acceleration voltage of the wehnelt (extraction anode). The gun is then simply regarded as a lens system focusing this electron beam. Such designs have, for instance, been made by Butler (1966), Munro (1972) and Riddle (1978). This model can be very useful if it is applied correctly. In order to understand its justification and its limitations, we study it in some detail. We have generalized to some extent a presentation given by Kasper (1981), which is otherwise followed closely. The term 'pointed cathodes' now includes a new family of field emitters, the carbon nanotips. These are so small that they need to be studied separately. We give an introduction to these emitters in Section 50.7.

45.1 The Spherical Cathode

A pointed cathode usually consists of a fine needle welded on a thicker supporting shank. This device is not exactly axisymmetric but we shall nevertheless treat it as though it were for reasons of simplicity. The wehnelt electrode (see Fig. 43.3) is *positive* with respect to the cathode. This has the consequence that the field strength never vanishes at the cathode surface. The importance of this restriction has already been pointed out in Chapter 43, General Features of Electron Guns.

The electric field strength F is strongest in the vicinity of the apex of the needle, and thus the electron emission is mainly confined to this domain. It is clear that the shape of the needle, especially close to the apex, is of great importance for the operation of the gun. Unfortunately this shape is rarely known exactly. For want of any more exact information, therefore, we assume that the vicinity of the apex is spherical with a radius of curvature R_s. This is a most reasonable assumption under the circumstances. An attempt to model the evolution of the tip shape has been made by Iiyoshi (2011).

The notation used below is shown in Fig. 45.1. In the purely spherical field, the law of conservation of angular momentum gives

$$L = mR_s \upsilon_t = mR_s \upsilon_0 \sin \gamma = m\upsilon_\infty b$$

Principles of Electron Optics: Applied Geometrical Optics.
DOI: http://dx.doi.org/10.1016/B978-0-12-813369-9.00045-2

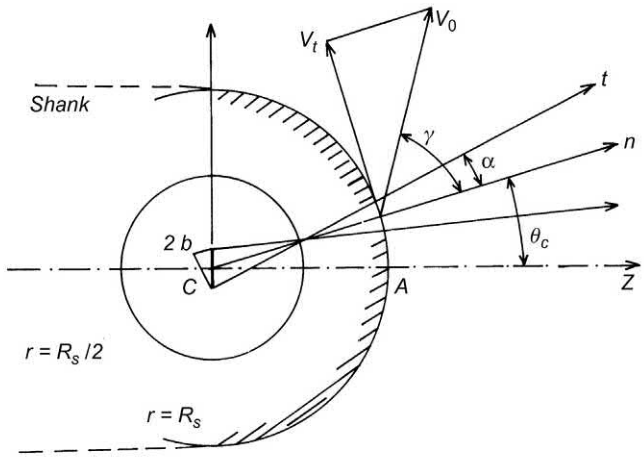

Figure 45.1
Notation employed in connection with the spherical cathode model; t is an arbitrary meridional trajectory while n is the corresponding normal trajectory (for which $\upsilon_t = 0$).

b here denoting both the minor semiaxis of the hyperbolic electron trajectory and the distance of its asymptote from the centre of force, the 'impact parameter'. The asymptotic velocity υ_∞ in the accelerating Coulomb field is obtained from the conservation of energy:

$$\frac{m\upsilon_\infty^2}{2} = \frac{m\upsilon_0^2}{2} + eF_sR_s$$

The latter term is just the work done by the Coulomb field of field strength F_s at the cathode surface. Usually, we can make the approximations $m\upsilon_0^2/2 \ll eF_sR_s$ and $\alpha \ll 1$ (see Fig. 45.1). Eliminating υ_∞, we find

$$b = \upsilon_t\sqrt{\frac{mR_s}{2eF_s}} = \frac{R_s}{2}\alpha \tag{45.1}$$

The last term of this relation arises from the fact that — with the approximations made above — the asymptote of each trajectory intersects the surface normal at approximately $R = R_s/2$, as is shown in Fig. 45.1. The relation Eq. (45.1) is well known and frequently encountered in the literature.

A consequence of the intersection of the asymptotes on a sphere of radius $R_s/2$ is that an aberration figure is described in the vicinity of the centre C, as seen in Fig. 45.1. We are not interested in one particular aberration radius b but in its mean square value $<b^2>^{1/2}$. We therefore replace υ_t in Eq. (45.1) by $<\upsilon_t^2>^{1/2}$. Since $U_t = m\upsilon_t^2/2$ is the tangential energy, introduced in Section 44.2, we may conclude from Eq. (45.1) that

$$\rho_0 := \sqrt{<b^2>} = \sqrt{\frac{<U_t>R_s}{eF_s}}$$

Thus for thermionic cathodes, $<U_t> = kT$ gives

$$\rho_0^{(T)} = \sqrt{\frac{kTR_s}{eF_s}} \tag{45.2}$$

while for field-emission cathodes, for which $<U_t> = d$,

$$\rho_0^{(F)} = \sqrt{\frac{dR_s}{eF_s}} = \sqrt{R_s\lambda\!\!\!^{-}/2} \tag{45.3}$$

$\lambda\!\!\!^{-}$ being defined by Eq. (44.26). Since $\lambda\!\!\!^{-}$ is almost independent of the field strength F_s, the same holds for $\rho_0^{(F)}$, so that it is impossible to decrease $\rho_0^{(F)}$ by increasing the field strength.

45.2 The Diode Approximation

Although the main body of the needle and its support do not contribute to the emission of electrons, the field between them and the wehnelt electrode acts on the electron beam farther away from the tip. In order to simplify the discussion, we shall neglect any deviations of the cathode support from rotational symmetry. This is clearly wrong in the vicinity of this support, but the error is very small in the region occupied by the electron beam. Until 1983, this was only an assumption, which seemed to be confirmed by experimental observations, but in 1985, Eupper made a full calculation of the field in an electron gun with a hairpin as the cathode support. The electron beam emitted by such a gun does indeed have very little astigmatism, so that our assumption is justified.

The combination of the cathode and the (positive) wehnelt is called a *diode*. Beyond the wehnelt, there is assumed to be an asymptotically field-free space at wehnelt potential Φ_W relative to the cathode. The entire electric field in the diode can be regarded as the superposition of a spherical field and the field of a weak round lens. The reasons why this lens is weak are as follows.

i. In the vicinity of the apex all deviations from the spherical symmetry of the field are, in fact, very small. This is immediately obvious from an inspection of accurate plots of equipotentials (Fig. 45.2).
ii. At larger distances from the cathode tip, the electric field is not at all spherical. In this region, however, the electrons have gained so much kinetic energy that the curvatures of the trajectories are very small.

The focusing effect caused by the total diode field is shown in Figs 45.3 and 45.4. Trajectories starting perpendicular to the tip surface are bent in such a way that their

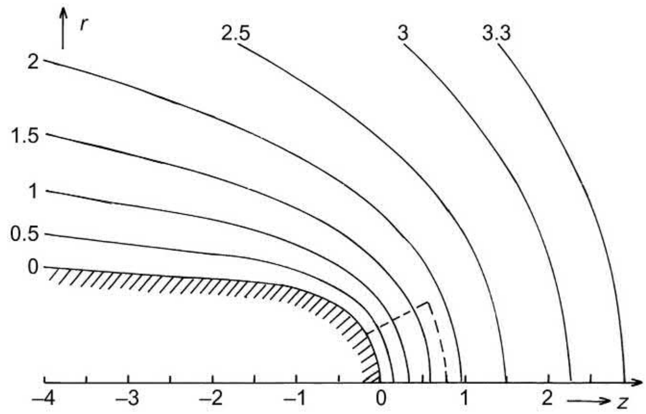

Figure 45.2
Equipotentials in the vicinity of a hemispherical cathode. In the marked zone near the apex, the field is practically spherical.

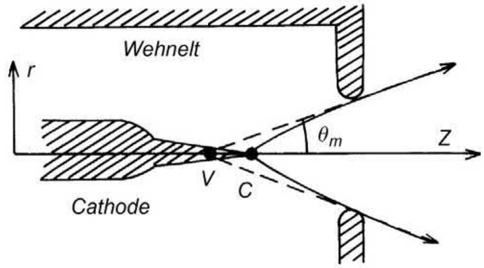

Figure 45.3
Diode model with real source at C and virtual source at V; θ_m is the maximum aperture angle.

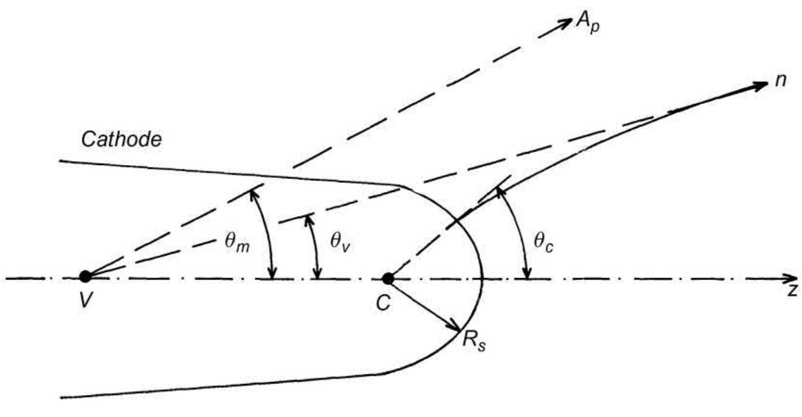

Figure 45.4
Notation associated with an arbitrary normal trajectory n in the vicinity of the cathode in the diode model.

asymptotes intersect in a very small zone around a virtual source point V. That the aberrations of this virtual focusing must be very small first became evident in E.W. Müller's field-emission microscopes (Müller, 1937, 1951), which form excellent stereographic projections of the emitting surfaces.

In order to understand this, we introduce a refractive index and an angular magnification M_A. Since the electrons, starting with negligible initial velocity υ_0, gain kinetic energy eF_sR_s in the purely spherical field, a momentum $p_1 = (2meF_sR_s)^{1/2}$ is associated with this partial field. In the field-free space outside the diode they have a kinetic energy $e\Phi_W$ and hence a momentum $p_2 = (2me\Phi_W)^{1/2}$. The refractive index n is conventionally defined as p_2/p_1 and we write

$$n := \frac{p_2}{p_1} = \sqrt{\frac{\Phi_W}{F_sR_s}} =: \sqrt{\mu} \tag{45.4}$$

Since the solution of the appropriate Dirichlet problem in the diode domain tells us that Φ_W is exactly proportional to F_s, the quantity μ is a purely geometric shape factor of the device.

Fig. 45.4 shows schematically a normal ray n, by which we mean a ray that leaves the cathode in the direction of the local surface normal, its initial tangent hence intersecting the optic axis at C. The focusing effect of the electric field can be understood as some kind of stereographic projection of the cathode surface, the projection centre shifting from C to V. In the paraxial approximation $|\theta_C| \ll 1$, there must hence be a simple proportionality of the type $\theta_V = M_A\theta_C$, M_A being the constant angular magnification. We now generalize this to include larger angles.

It can be shown that for a distortion-free projection, the sine condition $\sin\theta_V/\sin\theta_C = \text{const} = M_A$ must hold (see Section 15.4). From the exact numerical trajectory calculations carried out by Kern (1978a,b) and Eupper (1980), it has been found that

$$M_A = \theta_C^{-1}\tan\theta_V = \text{const} \tag{45.5}$$

with a value of M_A slightly larger than 0.5. This is, indeed, practically compatible with the sine condition if $M_A = 3^{-1/2} = 0.577$, as can be verified by expanding all the trigonometric functions as power series. The terms of first and third order are then compatible. This is better than in Gaussian dioptrics, where there is compatibility only in the first-order terms. In this way we can understand why, in this particular case, Eq. (45.5) is the appropriate definition of the angular magnification.

Since the tip radius R_s is much smaller than the geometrical dimensions of the diode lens, it is reasonable to assume that M_A is unaffected by small shifts of the order of R_s, and we thus have the same value of M_A for the virtual imaging of all the cathode surface, at least in the neighbourhood of the apex. Combining Eqs (45.4) and (45.5), we can introduce the lateral magnification M_L by means of the relation $M_L M_A \mu^{1/2} = 1$, which remains valid at least for small values of θ_C; thus we find

$$M_L = \frac{1}{M_A\sqrt{\mu}} \approx \sqrt{\frac{3}{\mu}} \tag{45.6}$$

This enables us to find an approximate expression for the aberration radius ρ_V associated with the diode lens:

$$\rho_V = M_L\rho_0 \approx \sqrt{\frac{3R_s}{eF_s\mu} < U_t >} = R_s\sqrt{\frac{3 < U_t >}{e\Phi_W}}$$

In this relation, the form-factor μ has finally cancelled out. For *thermionic* diodes, $< U > = kT$ leads to

$$\rho_V^{(T)} = R_s\sqrt{\frac{3kT}{e\Phi_w}} \tag{45.7}$$

while for *field-emission* diodes, $< U > = d$ and $d = eF_s ƛ/2$ (44.26) lead to

$$\rho_V^{(F)} = \sqrt{\frac{3R_s d}{eF_s\mu}} = R_s\sqrt{\frac{3F_s ƛ}{2\Phi_w}} = \sqrt{\frac{3R_s ƛ}{2\mu}} \tag{45.8}$$

The consequences for thermionic guns and field-emission guns are different. From Eq. (45.7) it is obvious that the aberration radius of a thermionic gun with positive wehnelt (essentially a gun with a LaB_6 cathode) can be decreased slightly by increasing the wehnelt potential Φ_W, and one should do this, within the limits of what is technically feasible. From the last form of Eq. (45.8) it is obvious that in field-emission guns $\rho_V^{(F)}$ is practically independent of the field strength F_{ss} and consequently of the potential Φ_W. Since the form-factor μ is always between 2.5 and 5, the radius $\rho_V^{(F)}$ does not differ much from $\rho_0^{(F)}$ and is hence essentially determined by R_s and by the work function W, since $ƛ = \hbar(2mW)^{-1/2}$.

Practical evaluation shows that ρ_V is always much smaller than R_s. We can thus derive approximate formulae for the asymptotic emission angles of arbitrary electron trajectories. Since $\rho_V \ll R_s$, we now make the simplifying assumption that *all* asymptotes intersect at the virtual source point V, as shown in Fig. 45.4. This implies that in the spherical field close to the tip, all the trajectories are bent in such a way that they seem to have emerged from the centre C. This clearly contradicts the construction shown in Fig. 45.1 but the error incurred is negligible.

For the angles shown in Fig. 45.4, we can draw the following conclusions from Eq. (45.5):

$$\tan\theta_V = M_A\theta_C, \quad \tan(\theta_V + \beta) = M_A(\theta_C + \alpha)$$

Since $|\alpha| \ll 1$, $|\beta| \ll 1$, while θ_V and θ_C may be large, we have then

$$\beta = M_A\alpha(1+M_A^2\theta_C^2)^{-1} = M_A\alpha\cos^2\theta_V$$

We may calculate α from Eq. (45.1). Introducing the form-factor μ from Eq. (45.4), we obtain

$$\alpha = \upsilon_t\sqrt{\frac{2m\mu}{e\Phi_W}} \tag{45.9a}$$

and thus

$$\beta = \frac{M_A}{1+\theta_C^2 M_A^2}\upsilon_t\sqrt{\frac{2m\mu}{e\Phi_W}} \tag{45.9b}$$

Recalling that $m < \upsilon_t^2 > /2 = < U_t >$, we can easily find an expression for the mean square value of β:

$$< \beta^2 > = \frac{4M_A^2\mu < U_t >}{(1+\theta_C^2 M_A^2)^2 e\Phi_W} \tag{45.10}$$

with $< U_t > = kT$ or $< U_t > = d$ as appropriate. It is usually true that $M_A^2\theta_C^2 \ll 1$ so that $< \beta^2 >$ is practically independent of θ_C. Since the distribution of tangential velocities υ_t is Gaussian, as has been explained in Chapter 44, the same conclusion now holds for the distribution of the angles β. These results will be very useful in Chapter 47, Brightness.

If we know the exact location of the virtual source V and if we assume that the curvatures of the trajectories in the vicinity of the aperture of the wehnelt can be neglected, these formulae enable us to determine whether a trajectory will pass through the aperture or not. Since this can be done without explicit numerical ray-tracing, the foregoing formulae, Eq. (45.5) especially, are very useful for the calculation of probe currents.

Finally we must emphasize that these arguments are clearly only an approximation to reality, though a fairly good one. Of course, the asymptotes do not intersect exactly in a point V, not even those corresponding to normal trajectories, as has been assumed in Fig. 45.4. Furthermore, aberrations are introduced by the diode lens but there is as yet no rigorous theory of these. Fortunately they are small.

45.3 Field Calculation in Electron Sources with Pointed Cathodes

This subject can be very troublesome for three different reasons. The first is the aggregation of space charge in the path of the electron beam, which has an influence on the potential distribution. This complication is dealt with in Chapter 46, Space Charge Effects.
The second reason is that the true shape of the tip is often unknown. The very strong

electric field in field-emission sources may deform the tip, often in an unpredictable manner. As long as this deformation remains unknown, a field calculation that attempts to take it into account makes little sense; here, therefore, we assume that the shape of the cathode is well known. Even then, problems arise for the third reason. The differences between the geometric dimensions of the various parts of electron sources are so large that conventional field computation techniques, such as the methods of finite differences and finite elements, may break down, at least in their elementary forms. We recall that Khursheed has introduced a form of the finite-element procedure adapted to this situation (Chapter 12 of Volume 1).

Numerous attempts have been made to overcome these difficulties, so many that it is not possible to comment on all the corresponding publications. Instead, we shall concentrate on a few typical examples.

45.3.1 Analytic Field Models

One method of field calculation is based on the use of an appropriate analytic field model. The earliest is the sphere-on-orthogonal-cone (SOC) model, which was used by Dyke et al. as long ago as 1953. The basic idea is as follows. A rotationally symmetric solution of Laplace's equation in spherical coordinates R, ϑ, φ

$$\frac{\partial}{\partial R}\left(R^2\frac{\partial\Phi}{\partial R}\right)+\frac{1}{\sin\vartheta}\frac{\partial}{\partial\vartheta}\left(\sin\vartheta\frac{\partial\Phi}{\partial\vartheta}\right)=0$$

is obtained by separation of variables. The particular solution that satisfies the boundary condition $\Phi=0$ over the sphere $R=a$ takes the general form

$$\Phi(R,\vartheta)=\sum_{j=1}^{\infty}A_j\left\{\left(\frac{R}{a}\right)^{\nu_j}-\left(\frac{a}{R}\right)^{1+\nu_j}\right\}P_{\nu_j}(\cos\vartheta) \tag{45.11}$$

The powers and subscripts ν_j, which are in general not integers, are determined by the additional boundary conditions

$$\Phi(R,\pi-\alpha)=0\ \text{ for }\ R\geq a,\quad P_{\nu_j}(-\cos\vartheta)=0$$

on a cone of given semiaperture angle α, see Fig. 45.5. The calculation of these numbers ν_j and the corresponding Legendre functions P_{ν_j} is highly complicated. The coefficients A_j are determined by the boundary conditions at the other electrodes. For a long time, this problem remained unsolved. Wiesner (1970; see Wiesner and Everhardt, 1973, 1974), for instance, considered only the first term in Eq. (45.11), for which $j=1$. In this way he could describe the field in the vicinity of the cathode quite well but the asymptotic behaviour of the potential was wrong; at least in the bore of the wehnelt this gave a totally wrong field.

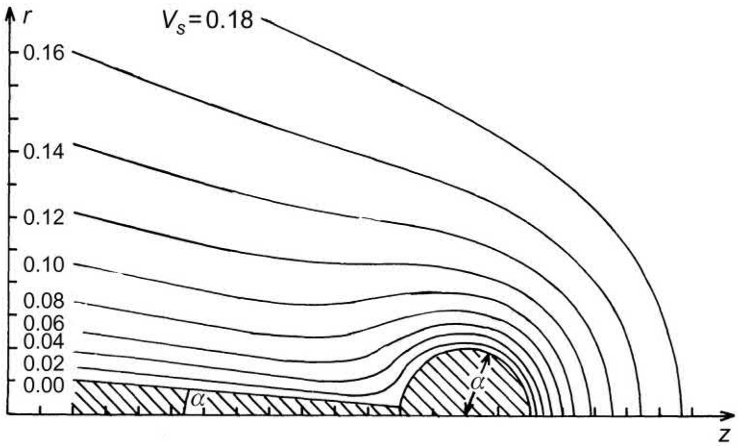

Figure 45.5
Equipotentials in the neighbourhood of a SOC structure. *After Kern (1978a), Courtesy the author.*

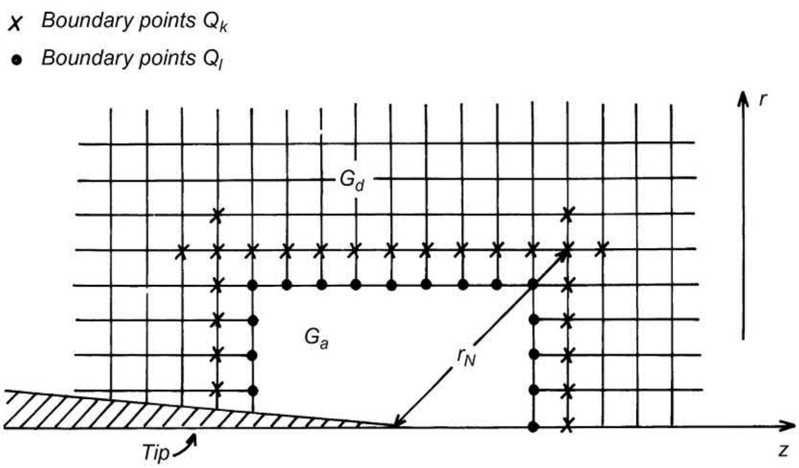

Figure 45.6
The regions G_a in which an analytic solution is employed and G_d in which the solution is obtained by means of the finite-difference method. *After Kern (1978a), Courtesy the author.*

The first convincing solution was given by Kern (1978a,b); it is demonstrated in Fig. 45.6. The SOC solution (45.11) with initially unknown coefficients A_j is confined to the vicinity of the tip, essentially the domain G_a in Fig. 45.6 and the boundary points Q_k ($k = 1, \ldots k$) marked by crosses. The series (45.11) is truncated after k terms so that the coefficients are determined uniquely by the boundary values of the potential at the points Q_k. In the domain G_d (Fig. 45.6), the finite-difference method (FDM) was used. The necessary boundary values at the points Q_l, marked by dots, were calculated from Eq. (45.11). The whole system of equations was then solved iteratively. Analytic differentiation of (45.11) and the application of numerical differentiation and interpolation techniques in the square-shaped mesh grid then gave accurate values of the field throughout the domain $G_a \cup G_d$. By solving the Lorentz trajectory equation in the form (3.12) numerically, Kern was able to confirm Eq. (45.2).

In order to avoid the complicated evaluation of Eq. (45.11) and the application of the FDM, Kasper (1979) proposed a simpler analytic field model. In the vicinity of the cathode tip, the potential is modelled by a uniform line-charge distribution of density q for $\vartheta = \pi$ and a point charge $Q_s = -q\lambda a$ at the origin:

$$\Phi_C(R, \vartheta) = q\left\{ \ln\left(\frac{R}{a}\right) + 2\ln\left(\cos\frac{\vartheta}{2}\right) + \lambda\left(1 - \frac{a}{R}\right)\right\} \tag{45.12}$$

λ and a being free parameters, which can be fitted to the form of the cathode in the vicinity of the apex. Eq. (45.12) satisfies $\Phi_C(a, 0) = 0$ at the apex. If $\lambda \approx 2$ is chosen and the length a is then related to the radius of curvature at the apex R_s by $a = R_s(\lambda + 0.5)/(\lambda + 1)$, a fairly good representation of the shape of the cathode tip is obtained. In order to fit the model to given boundary conditions at the surfaces of the wehnelt and any other electrodes, other line charges for $z < -s$ (s is a free parameter) and a uniform charge distribution on a screening cylindrical tube are introduced. The model was then combined with the boundary-element method (BEM), which provided the appropriate charge distribution on the wehnelt and the anodes.

This method works fairly well while remaining comparatively simple. A detailed treatment is to be found in Kasper (1982). The main objection to this model is that the shape of the cathode shank far from the tip is oversimplified, since this part was regarded as unimportant. Furthermore, in the vicinity of the apex, the cathode is assumed to be hemispherical (as in the SOC model). In some modern developments, appreciable deviations from hemispherical shapes are of interest. It is therefore necessary to consider more flexible models. A suitable expansion of the potential field is given by

$$\Phi_C(R, \vartheta) = \sum_{\nu=0}^{N} A_\nu \left(\frac{a}{R}\right)^{\nu+1} P_\nu(\cos\vartheta) + \int_{-L}^{0} q(z)\left(z^2 + 2zR\cos\vartheta + R^2\right)^{-1/2} dz \tag{45.13}$$

This is the superposition of an ordinary multipole expansion (ν is an integer) and of the potential of a line-charge distribution with density $q(z)$ on the optic axis. This continuous distribution has to be made discrete, for instance by using piecewise linear functions joined together continuously. The integration can then be carried out analytically, as has been outlined in Section 10.4. The expansion (45.13) is then combined with the BEM. The many degrees of freedom in this model can be used to adjust the potential at an appropriate number of control points on the cathode surface.

45.3.2 Rigorous Methods

We still assume that the cathode is rotationally symmetric, although this may often be too strong a simplification. For the computation of axisymmetric fields, the FDM, the BEM and the FEM can all be used. The FDM in cylindrical coordinates is not adequate. In order to adjust the grid to the very large differences between the dimensions of different parts of the gun, one has to alter the mesh-length so often while approaching the cathode that the method breaks down. Hauke (1977) tried to overcome this difficulty by using a discretization in prolate spheroidal coordinates, the centre of curvature of the tip being one of the foci. This was plausible only for thermionic cathodes ($R_s \approx 50\ \mu$m). Kang et al. (1981, 1983) introduced a spherical grid with exponentially increasing mesh-length in the radial direction. In this grid, they applied five-point formulae with a good measure of success. If the necessary local refinements of the grid are chosen suitably, a high accuracy is possible. Since this type of grid is a special case of those considered in Section 11.4, still higher accuracy can be achieved by the use of appropriate nine-point formulae, wherever this is possible. In any case, the laborious consideration of irregular mesh points in the vicinity of boundaries cannot be avoided.

In principle, arbitrary curved boundaries, even with extreme differences in the geometric dimensions, can be treated successfully by means of the BEM. High accuracy can be achieved, at least with the method outlined in Section 10.2.3. The main problem with the BEM is that, although the surface charge distribution may be known exactly, it is a major task to set up procedures for the accurate and very fast computation of the field strength in the vicinity of the singularities.

This difficulty can be overcome in different ways. Ozaki et al. (1981) obtained good results with a suitable parametric transform, devised by Uchikawa et al. (1981). Their findings will be discussed in the next section. Another possibility is to introduce a charged surface located inside the cathode, as is shown in Fig. 10.7. It is then necessary to apply the spline technique outlined in Section 10.2.3 to the charge distribution on this surface. This results in very smooth and accurate fields; the necessary numerical integrations create no problems.

For truly three-dimensional configurations like those shown in Figs 10.18 and 10.19, the BEM in the version introduced by Eupper (1985) seems to be suitable. The software from MEBS and SPOC offers routines for calculating gun properties.

We can safely assert that, even neglecting space charge effects, the accurate computation of electric fields in electron sources is a complicated task. The situation becomes even worse if space charge is considered, as we shall see in Chapter 46.

45.4 Simple Models

The diode approximation, outlined in Section 45.2, already gives us a very good description of the asymptotic properties of the electron beam in the space beyond the wehnelt. Essentially, two pieces of information are still missing: the axial position of the virtual source and the value of the correction parameter μ. The former can be estimated reasonably: the virtual source is located at a distance equal to a few times the radius of curvature R_s behind the centre of curvature C. Even if this estimate in terms of R_s is 100% wrong, this is not serious, since $R_s \sim 10^{-4}$ mm is much smaller than the distance from the wehnelt. A reasonable estimate for μ is not easy to guess but can be found with the aid of a model, as we shall now see.

45.4.1 A Diode-Field Model

A simple field model for the approximation of fields in diode configurations has been proposed by Kasper (1982). This is sketched in Fig. 45.7. The essential singularities of the

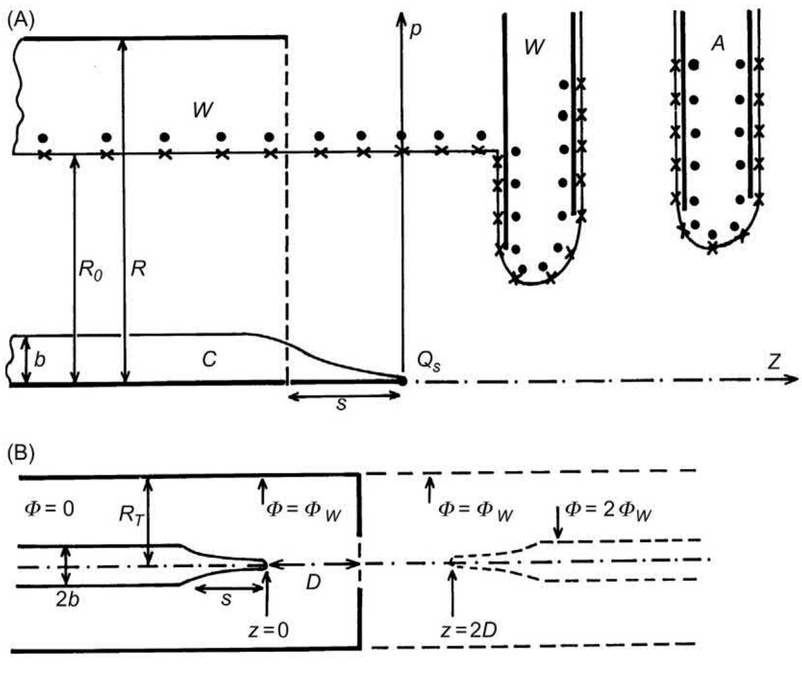

Figure 45.7
Computer simulation of a field-emission structure. (A) Half-axial section through a triode with cathode (C), wehnelt (W) and anode (A). The heavy lines and dots indicate the assumed singularities of the field. (B) Approximate simulation of the field in the left-hand part by means of a mirror-symmetry operation.

field are chosen to be a point charge Q_s located at the origin of the coordinate system, an axial line charge with the (one-dimensional) density $-q<0$ for $-s \le z \le 0$, an unbounded axial line charge with density $-q' < -q$ for $z < -s$, a coaxial screening tube with radius R_T and the opposite line-charge density $+q$ for $z < s$. This configuration has a net charge $Q = Q_s - qs$ and produces the potential Φ_C described by Eq. (45.12) in the vicinity of the apex. A good approximation for the potential at larger distances is given by

$$\begin{aligned}\Phi_C(z,r) = qF(z,r) + (q'-q)F(z+s,r) - q'F(z+s,R_T) \\ + Q_s(z^2+r^2)^{-1/2} + O(r^2)\end{aligned} \tag{45.14a}$$

with

$$F(z,r) := \ln\left\{\left(z+\sqrt{z^2+r^2}\right)/R_T\right\} \tag{45.14b}$$

It is now necessary to assume that the radius of the aperture in the wehnelt is negligible; this is reasonable, since this aperture is always so small that it has practically no influence on the field near the apex. The plane front of the wehnelt, located at $z = D \gg R_s$ and at potential Φ_W, is then easily simulated by mirror operations (see Fig. 45.7):

$$\Phi(z,r) = \Phi_C(z,r) + \Phi_W - \Phi_C(2D-z,r) \tag{45.14c}$$

All the parameters of the model are now determined uniquely: Q_s is related linearly to q, as is outlined in Section 45.3.1, q' is determined by the wehnelt potential and the asymptotic radii b and R_T in Fig. 45.7:

$$q' = \frac{0.5\Phi_W}{\ln(R_T/b)}$$

We thus have a linear condition $qg + q'g' = \Phi_W$ with the factors

$$g := \lambda + \ln\left\{\frac{2Ds}{(2D+s)a}\right\} \tag{45.15a}$$

$$g' := \ln\left[\frac{1+(1+R^2/s^2)^{1/2}}{1+\left\{1+R^2/(2D+s)^2\right\}^{1/2}}\right] \tag{45.15b}$$

the quantities a and λ being those of Kasper's model in Section 45.3.1. Hence

$$q = \frac{\Phi_W}{g}\left\{1 - \frac{g'}{2\ln(R/b)}\right\}$$

and the field strength at the apex becomes $F_s = q(1+\lambda)/a$. Finally the correction parameter μ, introduced in Eq. (45.4), is found to be

$$\mu = \frac{g(\lambda + 1/2)}{(1+\lambda)^2}\left\{1 - \frac{g'}{2\ln(R_T/b)}\right\}^{-1} \tag{45.15c}$$

with $\lambda \approx 2$. A comparison with the results of exact numerical calculations for the same configuration, but with a realistic aperture in the wehnelt, shows that the error is always less than 1%. For practical purposes, therefore, this model is accurate enough if it is possible to fit its free parameters adequately to the real geometric configuration. This may be laborious, but does not require a large computer program. For more information we refer to Kasper's (1982) publication.

The problem of the influence of the cathode shank and of other electrodes on the field strength F_s at the apex has been investigated in detail by a Japanese group (Ozaki et al., 1981), who performed a rigorous field computation based on the boundary-element method. They concluded that the shape of the shank does have a significant influence on the familiar parameter $\beta_s := F_s/\Phi_W$, which is related to μ by $\beta_s = (R_s\mu)^{-1}$. A small difference between the real and the assumed form of the shank close to the tip can cause an error of a few per cent. On the other hand, remote parts of the electrodes have no significant influence on the value of β_s.

From these findings it is clear that really accurate results can be expected only if the cathode geometry is known accurately; in practice, however, this is often not possible so that estimates based on simple models may still be useful.

45.4.2 Thermionic Triode Guns

In the preceding sections we have dealt with diode guns with pointed cathodes and positive wehnelt potentials relative to the cathode. The model outlined in Section 45.2 is fairly accurate, since it can be shown experimentally and theoretically that the inherent errors are slight. The situation becomes worse if the potential difference between wehnelt and cathode is negative, as is commonly the case in thermionic triode guns, since the purpose of the wehnelt is to confine the beam. The departure of the electric field from spherical symmetry is then large even in the vicinity of the cathode tip. In spite of this difficulty, Lauer (1968, 1982) has developed an elementary model for such guns.

The basic ideas behind this model are illustrated in Figs 45.8A and B. The cathode surface is again assumed to be spherical and the corresponding Coulomb field is extended to the front plane $z = z_W$ of the wehnelt. The accelerating field between the wehnelt and the anode is assumed to be homogeneous. The resulting axial potential distribution $\phi(z)$ is shown in Fig. 45.8A. Here, U_C is the potential at the cathode surface, U_A that at the anode, while U_W^0 is the axial potential at the centre of the wehnelt. This latter potential is always more positive than that of the wehnelt surface. At $z = z_W$ and $z = z_A$, the assumed axial potential

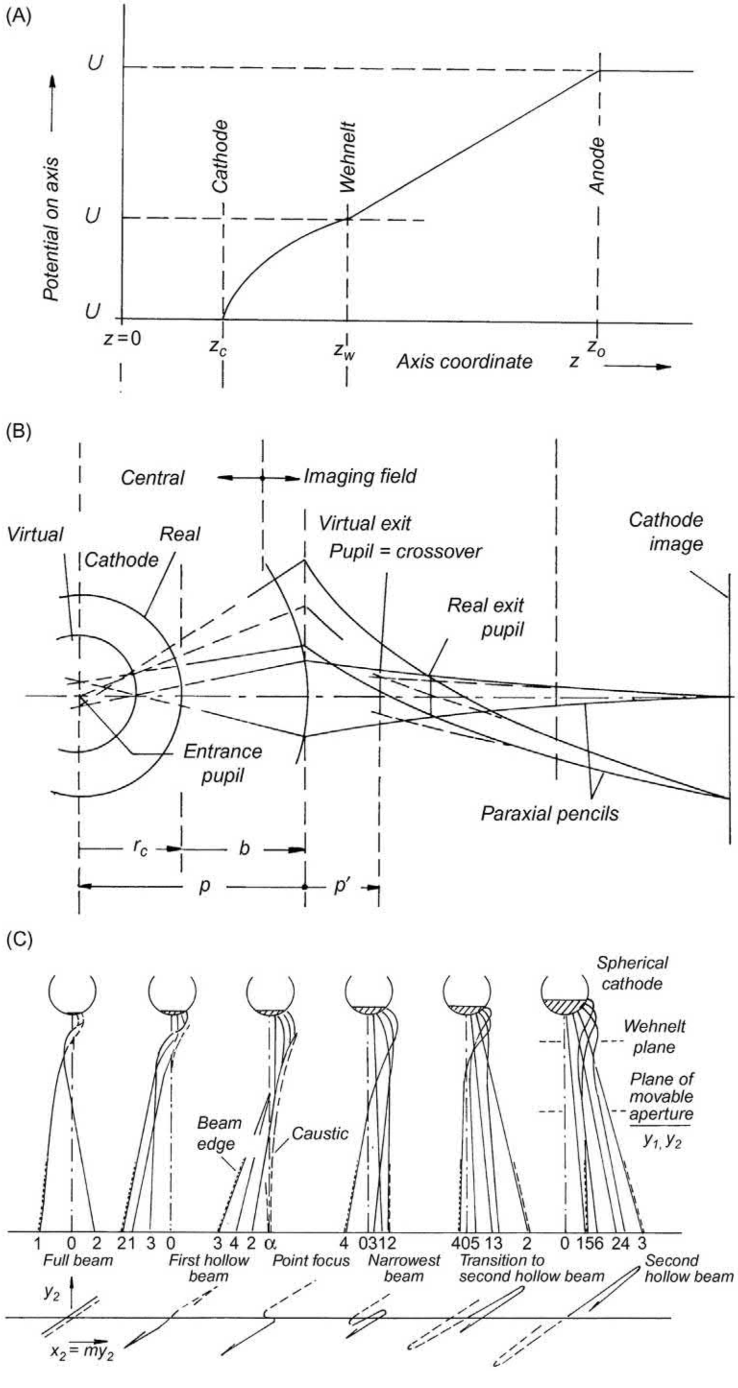

Figure 45.8

Paraxial model of electron gun. (A) Electrostatic potential on the optic axis. (B) Trajectories. Note that the entrance pupil of the pencils of rays is situated at the centre of the cathode. (C) Ray patterns (above) and shadow curves (below) for different operating conditions. The wehnelt voltage is progressively more positive from left (close to cutoff) to right (second hollow beam mode). The heavy dashed curve represents the caustic surface and the dotted line, the beam edge. Only the shaded zone of the filament contributes electrons to the beam. *After Lauer (1968) (A and B) and Hanszen and Lauer (1969b) (C), Courtesy Verlag der Zeitschrift für Naturforschung.*

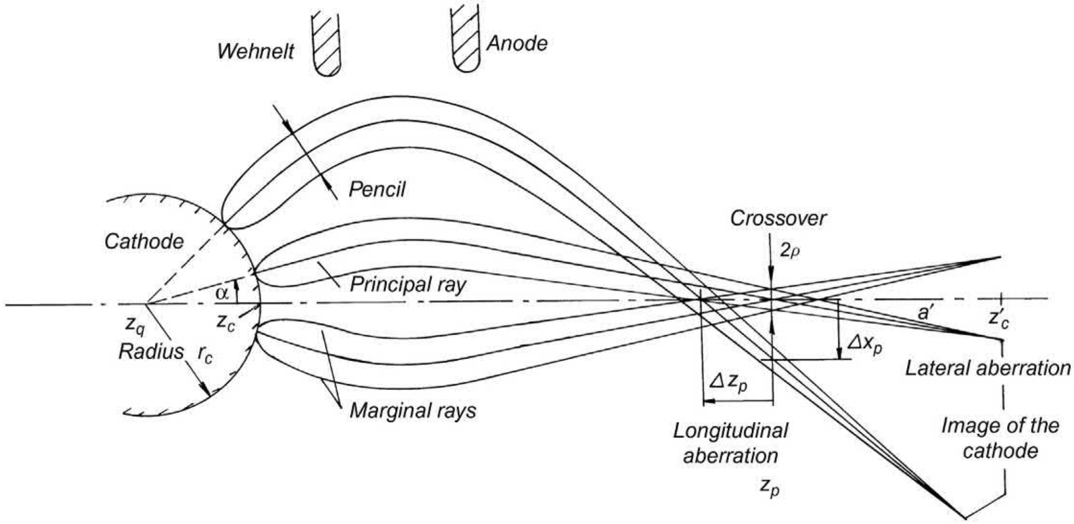

Figure 45.9
The aberrations of electron guns. Only for very small values of α will pencils of rays in the neighbourhood of the axis pass exactly through the crossover. For larger values of α, the pencils miss the latter altogether and suffer from an α-dependent transverse aberration (Δx_p) and longitudinal aberration (Δz_p). *After Lauer (1973), Courtesy Verlag der Zeitschrift für Naturforschung.*

$\phi(z)$ is not smooth. These unrealistic discontinuities of the field strength can be corrected by appropriate weak-lens approximations.

Lauer's model for the triode gun is now essentially a *paraxial* one. In the Coulomb field in front of the cathode, the electron motion satisfies the relations derived in Section 45.1. At the wehnelt, the electrons are focused by a thin, weak lens; in the homogeneous field beyond this lens, the trajectories are parabolae, which are then continued as their exit tangents after the anode. This is all depicted schematically in Fig. 45.8A and B.

Lauer considered only a single common kinetic energy $W_C = e(U_C - U_0) \approx kT$ at the cathode surface. In his notation (see Figs 45.8B and 45.9) he arrived at the following results: the axial position p' of the virtual (asymptotic) crossover and its radius ρ are given by:

$$
\begin{aligned}
p' = &-(z_A - z_W)\frac{(U_A - U_0)^{1/2} - (U_W^0 - U_0)^{1/2}}{(U_A - U_0)^{1/2} + (U_W^0 - U_0)^{1/2}} \\
&+ p\left\{1 + \frac{p}{4(z_A - z_W)}\frac{(U_A - U_W^0)}{(U_W^0 - U_0)}\right\}^{-1}\left(\frac{U_A - U_0}{U_W^0 - U_0}\right)^{1/2}
\end{aligned}
\tag{45.16}
$$

$$\rho = r_c \frac{(U_c - U_0)}{(U_W^0 - U_C)} \left\{ 1 + \frac{p}{4(z_A - z_W)} \frac{(U_A - U_W^0)}{(U_W^0 - U_0)} \right\}^{-1} \tag{45.17}$$

Here $p = -(r_C + b)$ is negative in the situation shown in Fig. 45.9.

From these equations it can be concluded that, in the paraxial approximation, the triode gun acts like a thick immersion lens. Its action becomes telescopic if the expression in parentheses is made zero by the appropriate choice of $U_W^{(0)}$. For smaller values of $U_W^{(0)}$ than the critical one, the triode lens has a converging effect on the beam, and for larger values of $U_W^{(0)}$, a diverging action. Experimentally, the potential $U_W^{(0)}$ cannot be determined directly. In order to obtain working relations, Lauer therefore proposed the approximation $U_W^{(0)} = U_C + U_W - U_{\mathrm{cutoff}}$, in which U_W is now the potential of the wehnelt surface and U_{cutoff} the largest value of U_W for which the emission current vanishes.

The results obtained with this model are in fairly good agreement with the corresponding experimental ones, as far as the paraxial properties are concerned. Lauer also investigated aberrations, but the model can now give only qualitative answers. The most important aberration is plausibly conjectured to be spherical aberration, which is shown qualitatively in Fig. 45.1. An exact determination requires extensive numerical calculations. Experimental methods for the determination of gun aberrations are discussed in Chapter 48, Emittance, and more information about gun optics is to be found in Chapter 49, Gun Optics.

CHAPTER 46

Space Charge Effects

Strictly speaking, space charge effects ought to be considered in all electron optical devices, since the electron beam contributes to the sources of the electric field and thus modifies the field itself. The electric potential should be the appropriate solution of the corresponding Poisson equation.

The reason why space charge effects are usually disregarded is the enormous complication they would cause, as will rapidly become obvious. Fortunately, in very many cases, the local intensity of the electron beam is so low that the neglect of space charge causes very little error. The situation is, however, quite different in many kinds of thermionic electron guns and in transport systems for high current beams; the same is true of multibeam sources and pulsed cathodes for ultrafast electron microscopy. In the first part of this chapter, only collective space charge effects are considered. In the second part, we examine the Boersch effect.

One new problem, then, is that Poisson's equation must be solved instead of Laplace's equation but this is only the least of the difficulties since standard procedures are available for this. The major problem is the fact that, prior to the rigorous self-consistent calculation, the space charge distribution $\rho(\boldsymbol{r})$ is unknown and has to be determined from the motion of electrons in an initially unknown electric field. There are only very few exact analytic solutions of this problem. One of them will be outlined in some detail, since it is the basis of a successful computational technique.

46.1 The Spherical Diode

We now consider a thermionic electron emitter with a spherical cathode of radius r_0 at zero electric potential. It is surrounded by a concentric spherical anode with radius r_A at a potential $\Phi_A > 0$. The cathode temperature T may be high enough for strong thermionic emission but the electric field strength in the vicinity of the cathode surface must be sufficiently low for the Schottky effect to be negligible. This problem has been studied by Porter et al. (1972) and later, Weyßer (1983) used the solution to obtain a local approximation for the charge density $\rho(\boldsymbol{r})$ in a realistic electron gun; this will be explained later. Clearly a device with perfect spherical symmetry is quite unrealistic but we can learn

Principles of Electron Optics: Applied Geometrical Optics.
DOI: http://dx.doi.org/10.1016/B978-0-12-813369-9.00046-4

much from the structure of the solution. The following account is based on a later contribution by Kasper (1985).

For reasons of convenience, we shall denote the distance from the origin by r instead of R. There is no danger of confusion, since in this section no other coordinates are used. In later applications to realistic electron guns, this variable r is not always a radial coordinate but may be the distance from the local centre of curvature of the cathode. The notation will then be adjusted accordingly.

We recapitulate the expressions for the Fermi function f and the transmission factor D, which are here given by

$$f = \exp\left(-\frac{W+E}{kT}\right), \quad D = \begin{cases} 1 & \text{for } p_{r0} \geq 0 \\ 0 & \text{for } p_{r0} < 0 \end{cases} \tag{46.1}$$

p_{r0} being the radial component of the momentum at the cathode surface. Outside the cathode the radial component p_r may become negative, which means that the electrons are reflected towards the cathode.

In a perfectly spherical field the angular momentum $\boldsymbol{L}$ is conserved and so is its magnitude L. We can therefore write the Hamiltonian in the form

$$E = H = \frac{p_r^2 + L^2 r^{-2}}{2m} - e\Phi(r) = \text{const} \tag{46.2}$$

It is convenient to use p_r and L as variables of integration in Eqs (44.7) and (44.8), while the integration over the third coordinate, an azimuth, merely gives a factor 2π. We thus obtain

$$d^3p \to 2\pi r^{-2} L dL dp_r$$

A further simplification is achieved by introducing

$$p_r =: \sqrt{2mkT}u, \quad L =: r_0\sqrt{2mkT}\sqrt{q}, \quad w := u^2$$

Then, after some elementary calculations, the integral representations

$$\rho(r) = -j_0 M\sqrt{\frac{2m}{kT}}\int\int \exp\left(-u^2 - Mq + \frac{e\Phi}{kT}\right) du dq \tag{46.3}$$

$$j(r) = j_0 M\int\int \exp\left(-w - Mq + \frac{e\Phi}{kT}\right) dw dq \tag{46.4}$$

are obtained, j_0 being the Richardson–Dushman current density at the cathode surface and $M := (r_0/r)^2$ the divergence factor.

The integrations over u and w can be carried out analytically, but the limits of integration depend on $q \propto L^2$ in a complicated manner. In order to establish these functions, it is convenient to introduce the effective radial potential:

$$P(r, L) := -e\Phi(r) + \frac{L^2}{2m}\left(\frac{1}{r^2} - \frac{1}{r_0^2}\right) = -e\Phi - kT(1 - M)q$$

The radial starting energy U_0 is then related to this function by

$$U_0 := p_{r0}^2/2m = kTu^2 + P(r, L) \tag{46.5}$$

A schematic graph of the effective potential is shown in Fig. 46.1. Here it is assumed that the electric potential $\Phi(r)$ has a (negative) minimum in front of the cathode. Depending on the value of L, the effective potential as a function of r may have a maximum at r_2 and may have a zero at r_1 with $r_0 < r_1 < r_2$. If no such zero at r_1 exists, we set $r_1 = r_0$. If no *positive* local maximum exists, we set $r_2 = 0$. For every value of L, we have now to distinguish between three different cases.

i. The domain $r > r_2(L)$ can only be reached by those electrons with starting energy U_0 higher than the maximum of the potential barrier P. Introducing $U_0 \geq P(r_2, L)$ into Eq. (46.5), we find

$$\begin{aligned} u_2^2 &= \frac{1}{kT}\{P(r_2, L) - P(r, L)\} \\ &= \frac{e}{kT}\{\Phi(r) - \Phi(r_2)\} + q\{M(r_2) - M(r)\} \end{aligned} \tag{46.6}$$

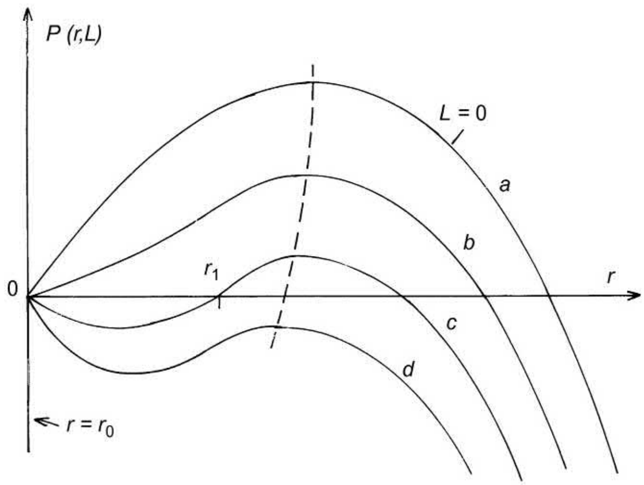

Figure 46.1
Qualitative representation of the function $P(r, L)$ for four fixed values of the angular momentum L, increasing from curve a to curve d. The broken line indicates the maxima, $r_2 = r_2(L)$.

as the square of the lower limit of integration, the upper being at infinity. These electrons can have only positive values of p_r and hence contribute once to the space charge integrals. In this way we obtain

$$Q_1(r, L) := \frac{2}{\sqrt{\pi}} \int_{u_2}^{\infty} \exp(-u^2) du = 1 - \operatorname{erf}(u_2)$$

erf(x) being the Gaussian error function. In the degenerate case $r_2 = r_0$, there is no reflecting potential barrier so that all electrons emitted can reach the anode.

ii. The domain $r_1(L) < r < r_2(L)$ can be reached by all electrons that cross the barrier and all those reflected from it. The latter group contributes twice to the space charge, once before the reflection and a second time after it. This corresponds to the interval $-u_2 \leq u < \infty$, hence

$$Q_2(r, L) := \frac{2}{\sqrt{\pi}} \int_{-u_2}^{\infty} \exp(-u^2)\, du = 1 + \operatorname{erf}(u_2)$$

iii. In the domain $r_0 < r < r_1(L)$ the situation is similar to that of case (ii), but $P(r, L)$ now becomes negative. Since both u^2 and W_0 must remain non-negative in Eq. (46.5), the interval for the reflected electrons must be confined to $u_1 \leq u \leq u_2$ with

$$u_1 = \left\{ \frac{1}{kT} \left| P(r, L) \right| \right\}^{1/2} < u_2$$

The corresponding integral is then given by

$$Q_3(r, L) = 1 + \operatorname{erf}(u_2) - 2\operatorname{erf}(u_1)$$

The degenerate case $r_1 = r_0$ means that $P(r, L) \geq 0$, so that case (iii) then does not occur.

Altogether we have

$$Q(r, L) = \begin{cases} 1 - \operatorname{erf}(u_2), & r \geq r_2 \\ 1 + \operatorname{erf}(u_2), & r_1 \leq r \leq r_2 \\ 1 + \operatorname{erf}(u_2) - 2\operatorname{erf}(u_1), & r_0 \leq r \leq r_1 \end{cases} \tag{46.7}$$

At the abscissae $r = r_1$ and r_2, this function remains continuous. Introducing Eq. (46.7) into (46.3), we obtain the integral representation

$$\rho(r) = -j_0 M \sqrt{\frac{\pi m}{2kT}} \exp\left(\frac{e\Phi}{kT}\right) \int_0^{\infty} e^{-Mq} Q(r, L(q)) dq \tag{46.8}$$

This integration could be carried out numerically if $\Phi(r)$ were known, but unfortunately this is not the case. In fact, $\Phi(r)$ is the solution of Poisson's equation

$$\nabla^2 \Phi = \Phi''(r) + \frac{2}{r}\Phi'(r) = -\frac{1}{\varepsilon_0}\rho(r) \tag{46.9}$$

satisfying the boundary conditions $\Phi(r_0) = 0$, $\Phi(r_A) = \Phi_A$. Starting with the solution of Laplace's equation, this problem can be solved iteratively by solving Eqs (46.8) and (46.9) alternately. The special techniques required cannot be described here. Some results, showing the essential physical features, are presented in Figs 46.2 and 46.3. With increasing temperature, a negative minimum of the electric potential develops and becomes deeper. This reduces the anode current, as we shall see below.

46.2 Asymptotic Properties and Generalizations

The model outlined above shows us the typical effect of space charge: in a weak field, the electrons emitted can accumulate in front of the cathode. This cloud of negative charge reduces the electric potential which, when a negative minimum is formed, partly repels the emitted electrons. Qualitatively, this happens in front of any sufficiently strongly heated cathode, regardless of whether its shape is spherical or not. It is therefore desirable to avoid

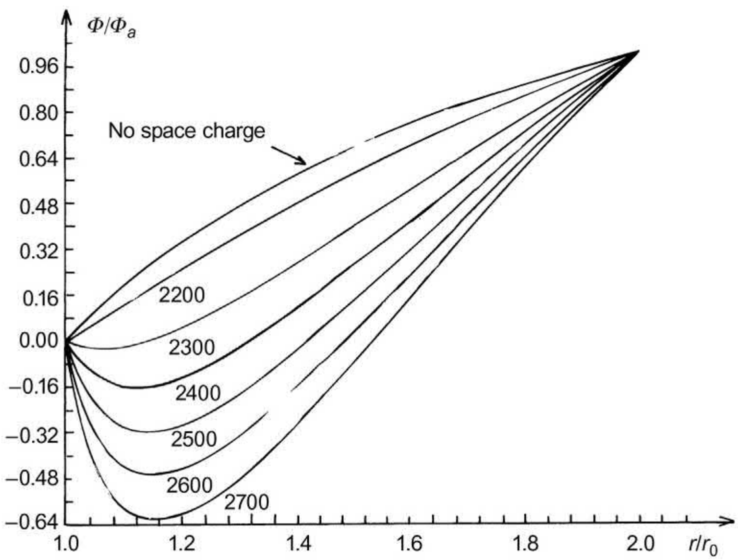

Figure 46.2
The potential $\Phi(r)$ in a spherical diode at different cathode temperatures (in kelvins); the radius r_0 is 0.2 mm. *After Weyβer (1983a), Courtesy the author.*

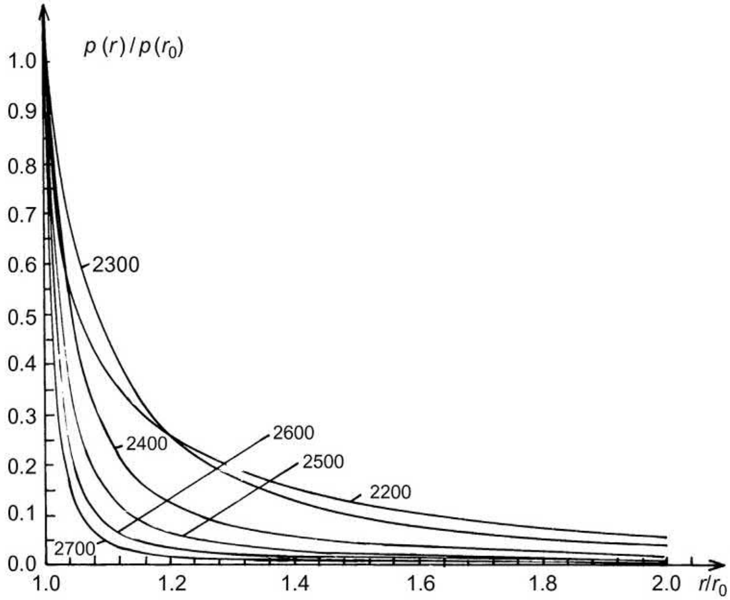

Figure 46.3
Normalized space charge distributions corresponding to Fig. 46.2. *After Weyβer (1983a), Courtesy the author.*

the assumption that the device is spherical. For this purpose, we study the asymptotic character of the solution, which will suggest how the generalizations are to be made.

We first evaluate the integral expression (46.4) for the current density. This is only of practical interest in the domain $r > r_2$ beyond the potential barrier. The integration over the variable w is now elementary and gives a factor $\exp\left(-u_2^2\right)$. Substituting this in Eq. (46.4) and using (46.6), we obtain

$$j(r) = j_0 M(r) \int_0^\infty \exp\left\{\frac{e\Phi(r_2)}{kT} - M(r_2)q\right\} dq$$

Since r_2 is a very slowly varying function of $q \propto L^2$, we can replace it by a suitable mean value r_m, which is very close to the coordinate of the potential minimum. The integration is then elementary. Recalling the general definition $M(r) = (r_0/r)^2$ of the divergence factor and writing $M_m = (r_0/r_m)^2$, we obtain the final result in vector form:

$$\boldsymbol{j}(\boldsymbol{r}) = j_0 \frac{M(\boldsymbol{r})}{M_m} \exp\left(\frac{e\Phi_m}{kT}\right) \boldsymbol{t}(\boldsymbol{r}) \quad (r \geq r_m) \tag{46.10}$$

$\boldsymbol{t}(\boldsymbol{r})$ being the local tangent vector (here in the radial direction) and $\Phi_m = \Phi(\boldsymbol{r}_m)$ the value of the potential minimum. For a planar diode this is exactly true. Evidently (46.10) satisfies the continuity equation $\nabla \boldsymbol{j} = 0$, as it should do. Since $\Phi_m \leq 0$, the exponential factor expresses a *decrease* of the emission current; this factor is the ratio of the asymptotic current to the Richardson–Dushman current.

In order to gain further insight, we determine the energy flux densities. The flux density of the *total* kinetic energy is defined by

$$S(r) = \frac{2}{h^3} \exp\left(-\frac{W}{kT}\right) \iiint \upsilon_r \frac{|\boldsymbol{p}|^2}{2m} \exp\left(-\frac{E}{kT}\right) d^3p$$

$\upsilon_r = p_r/m$ being the radial velocity. Introducing the same substitutions and simplifications as have been made for the current density integral, we obtain a very simple result, in vector form given by

$$\boldsymbol{S}(\boldsymbol{r}) = \frac{1}{e}\boldsymbol{j}(\boldsymbol{r})\left\{e(\Phi(\boldsymbol{r}) - \Phi_m) + 2kT\right\} \tag{46.11a}$$

Furthermore, we can determine the transverse contribution to this quantity, which in the present case is the angular component:

$$\begin{aligned} S_\perp &\coloneqq \frac{2}{h^3} \exp\left(-\frac{W}{kT}\right) \iiint \upsilon_r \frac{L^2}{2mr^2} \exp\left(-\frac{E}{kT}\right) d^3p \\ &= \frac{1}{e} j(r) kT \left(\frac{r_0}{r}\right)^2 \equiv \frac{jkTM(r)}{e} \end{aligned} \tag{46.11b}$$

The associated energy term is hence

$$< E_{\mathrm{kin}\perp} > = kTM(r) \tag{46.11c}$$

This result tells us that the transverse part of the kinetic energy decreases very rapidly during the acceleration of the electron beam, a fact which is of great importance in connection with the Boersch effect (see Section 46.4).

In the case of a weakly curved cathode ($r_m - r_0 \ll r_0$) it is even possible to simplify the formula (46.8) for the space charge density. In the vicinity of the cathode, the divergence factors M in Eq. (46.6) are so small that the centrifugal terms cause only very small perturbations. For large values of q, the exponential terms in Eq. (46.8) attenuate the integrand very considerably. Thus in the domain of interest, u_2 is very close to u_m, the latter referring to the potential minimum. The approximation $\operatorname{erfc}(u_2) = \operatorname{erfc}(u_m) \exp\left(u_m^2 - u_2^2\right)$ can then be made, $\operatorname{erfc}(u) = 1 - \operatorname{erf}(u)$ denoting the complementary error function. In Eq. (46.6) we can write $r_2 \approx r_m$, $u_m^2 = e\{\Phi(r) - \Phi_m\}/kT$ and $u_2^2 = u_m^2 + q(M_m - M)$.

Substituting all this into Eq. (46.7) for $r \geq r_m$ and then into Eq. (46.8), we obtain – constant factors apart – an elementary integral over q, which gives a factor $M_m^{-1} = r_m^2/r_0^2$. The case $r \leq r_m$ can be treated analogously. The results can be cast into a very convenient form; with

$$s := r - r_0, \quad s_m := r_m - r_0, \quad r = r(s) = r_0\left(1 + s/r_0\right) \tag{46.12a}$$

$\boldsymbol{r}(s)$ describes a radially directed ray, whereupon

$$\rho(\boldsymbol{r}) = -j(\boldsymbol{r})\sqrt{\frac{\pi m}{2kT}}\exp(w)\left\{(1-\sigma)\frac{M_m}{M(\boldsymbol{r})} + \sigma \operatorname{erfc}\sqrt{w}\right\} \tag{46.12b}$$

with

$$\sigma := \operatorname{sign}(s - s_m) = \pm 1 \tag{46.12c}$$

and

$$w := e\left\{\Phi(r) - \Phi_m\right\}/kT \tag{46.12d}$$

gives the space charge density along it. This is Langmuir's (1923) formula, originally derived for the planar diode, but here modified by a divergence factor M_m/M. In the limit of vanishing curvatures $r_0^{-1} \to 0$, $r_m^{-1} \to 0$, and with $M \to 1$, we do indeed obtain the well-known formula for the planar diode. The omission of the divergence factor is the reason why so many attempts to approximate a weakly curved cathode locally by a planar diode have been unsuccessful; this factor causes a rapid decrease of the space charge density far from the cathode surface.

In order to find a still more general formula, we investigate the asymptotic behaviour of Eq. (46.12b). For $w \geq 1$ the complementary error function is very accurately approximated by

$$\operatorname{erfc}\sqrt{w} = \pi^{-1/2}\exp(-w)\left\{1 + w - 0.4672(1+w)^{-0.85}\right\}^{-1/2}$$

Recalling Eq. (46.12d), we can now write (46.12b) in the familiar form

$$\rho(\boldsymbol{r}) = -j(\boldsymbol{r})/\upsilon_l(\boldsymbol{r}) \tag{46.13a}$$

with an average longitudinal velocity

$$\upsilon_l(r) = \left[\frac{2kT}{m}\left\{1 + w - 0.4672(1+w)^{-0.85}\right\}\right]^{1/2}, \quad (w \geq 1) \tag{46.13b}$$

Asymptotically, for $w \gg 1$, this corresponds to a kinetic energy

$$\tilde{E}_{\text{kin}} = e\left\{\Phi(\boldsymbol{r}) - \Phi_m\right\} + kT \tag{46.14a}$$

This result does *not* conflict with Eq. (46.11c); it simply means that since the distributions of the scalar densities and the flux densities are different, the corresponding mean energies may also be different. Eq. (46.14a) will prove to be important in the theory of brightness (Chapter 47). The complete formula (46.13b) can be rewritten in the form

$$\upsilon_l = \sqrt{\frac{2}{m}\tilde{E}_{\text{kin}}}\cos\gamma \tag{46.14b}$$

with an angle given by

$$\gamma = \arcsin\left(0.4672kT/\tilde{E}_{\text{kin}}\right)^{0.925} \tag{46.14c}$$

From these relations, we can see that the electron beam has a local mean angular spread γ which decreases rapidly with increasing kinetic energy.

Although the formulae given above have been derived from the statistics for spherical diodes, it is reasonable to generalize them to include any device with a weakly but arbitrarily curved cathode surface. This can easily be done subject to certain conditions; the general idea is illustrated in Fig. 46.4. We consider a bundle of electron trajectories leaving the cathode surface normally with a given velocity υ_0 specified below. These rays define a beamlet with a beam axis. The latter can be identified with one of these orthogonal trajectories, of which the one starting at the centroid of the corresponding element of area on the cathode surface is the most suitable. Instead of Eq. (46.12a), we now identify the parameter s with the arc-length along this beam axis, and Eq. (46.12b–d) with $\boldsymbol{r} = \boldsymbol{r}(s)$ then describe the space charge density along it. The necessary divergence factor $M(\boldsymbol{r})$ is obtained from the increase of cross-sectional area A of the beamlet: $M(\boldsymbol{r}) = A(\boldsymbol{r}_0)/A(\boldsymbol{r})$, as shown in Fig. 46.4. Since the electron that travels along the beam axis must have the asymptotic kinetic energy $\tilde{E}_{\text{kin}}$ given by Eq. (46.14a), its starting velocity must satisfy

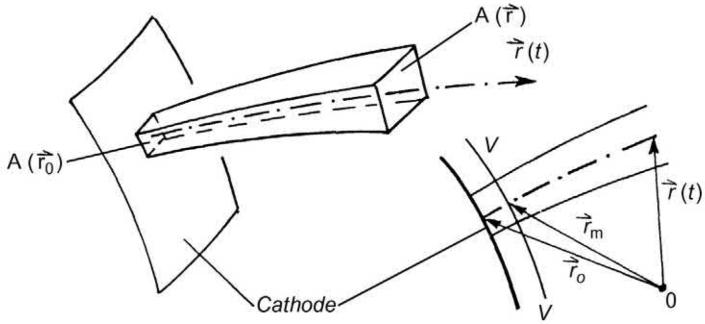

Figure 46.4
A beamlet in the neighbourhood of a reference trajectory $\boldsymbol{r}(t)$ that leaves the cathode surface orthogonally; V denotes the virtual cathode and $\boldsymbol{r}_m$ the position of the local minimum.

$$v_0 = \sqrt{2(kT - e\Phi_m)/m} \tag{46.15}$$

with $\Phi(\boldsymbol{r}_0) = 0$.

It is now obvious that most of the relations derived above, especially Eqs (46.10), (46.11), (46.12b−d), (46.13) and (46.14) remain valid, at least approximately. A minor complication arises from the fact that the distance s_m of the local potential minimum from the cathode surface and the quantity Φ_m depend on the position ($\boldsymbol{r}_o$) of the selected element of area on the cathode, but for numerical calculations this does not cause any serious problem. The surface $\Phi(\boldsymbol{r}) = \Phi_m(\boldsymbol{r})$ obtained by joining together all the surface elements with a local potential minimum is called the *virtual cathode*. This is the surface beyond which none of the electrons is repelled towards the real cathode.

A more serious problem is the fact that the beamlets may intersect one other, contrary to our tacit assumption of nonintersecting laminar flow. If there are such intersections, the local element of area $A(\boldsymbol{r})$ vanishes and hence the divergence factor M becomes singular. The solution of this problem is deferred to the next section.

In practical calculations, the formulae (46.12b−d) for $\rho(\boldsymbol{r})$ in the vicinity of the cathode and (46.13), (46.14) for $\rho(\boldsymbol{r})$ at greater distances are now to be combined with

$$\nabla^2\Phi(\boldsymbol{r}) = -\rho(\boldsymbol{r})/\varepsilon_0 \tag{46.16}$$

and thanks to the introduction of the divergence factor M, the continuity condition $\nabla \boldsymbol{j} = 0$ is satisfied approximately. In this way the field calculation strategy is clearly specified.

A dramatic and often used simplification is obtained if the thermal velocity distribution is completely neglected. For $T = 0$ we obtain $\Phi_m = 0$, $\gamma = 0$, $v_l = v = (2e\Phi/m)^{1/2}$. Poisson's equation then collapses to

$$\nabla^2\Phi(\boldsymbol{r}) = \frac{1}{\varepsilon_0} j(\boldsymbol{r}) \sqrt{\frac{m}{2e\Phi(\boldsymbol{r})}} \tag{46.17}$$

In the case of a planar diode, the solution of (46.17) is known as the Langmuir−Child law:

$$\phi(z) = \left(\frac{9}{4}\frac{j}{\varepsilon_0}\sqrt{\frac{m}{2e}}\right)^{2/3} z^{4/3} \tag{46.18}$$

More generally, the solutions of (46.17) are used in the design of Pierce systems (see Section 50.5).

In this section, we have derived a self-consistent approximation for space charge distributions, simple enough to be useful for practical applications.

46.3 Determination of the Space Charge

Here we shall confine the discussion to triode guns with negative wehnelt potential relative to the cathode. Diodes with positive wehnelt potential have been investigated by Kang et al. (1983) and by Hasker (1983) among others. In triodes, the negative wehnelt potential is used to confine the emission area on the cathode surface. The shape and the location of the zero-volt equipotential depend sensitively on the ratio of the wehnelt potential to the anode potential. Figs 46.5 and 46.6 show the immediate neighbourhood of the cathode. The electron emission is essentially confined to the region of the surface for which $\Phi \geq 0$. At the surface, the field strength distribution is almost parabolic; in the vicinity of the zero-volt line the field strength becomes very weak, so that there the influence of space charge will be very strong. Fig. 46.7 shows some electron trajectories starting in the direction of the surface normal. In the vicinity of the apex, these trajectories form a divergent beam which can be roughly described as emerging from a virtual source point. This part of the total electron beam forms a fairly small crossover, as shown in Fig. 43.2. The trajectories that start in the vicinity of the zero-volt equipotential are, however, strongly bent there, where they form a caustic. These rays suffer from very large aberrations and form a diffuse ring in the plane of the crossover: a *hollow beam* thus surrounds the paraxial beam. This well-known effect depends sensitively on the choice of the crossover plane, the wehnelt potential and the cathode temperature.

One of the most exhaustive theoretical and experimental studies of triode guns is that pursued for several years by Lauer, already mentioned in Section 42.4. His review article of 1982 describes the experiments and the interpretation of their results in terms of his model in great detail, and we refer the reader to it for a full account. We just mention here that space charge cannot be observed directly but only its influence on emittance diagrams; we return to the latter in Chapter 48, Emittance.

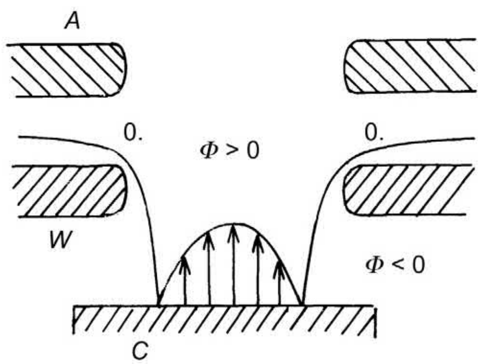

Figure 46.5
Zero-volt line and distribution of surface field strength in a triode with a flat cathode.

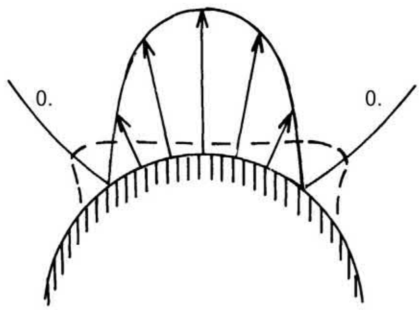

Figure 46.6
Zero-volt line and surface field strength in a triode with hemispherical cathode. The wehnelt and the anode are not shown. The dashed line gives an approximate idea of the extent of the space charge cloud.

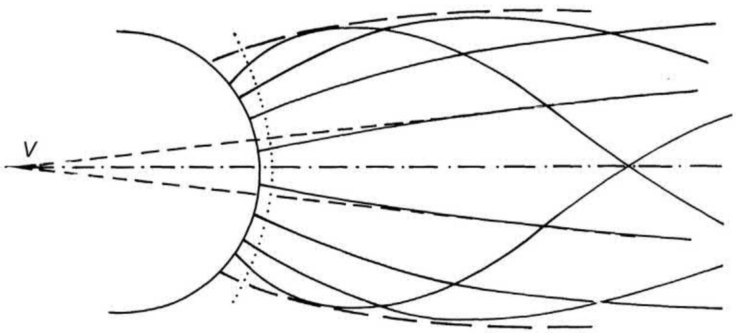

Figure 46.7
Schematic representation of electron trajectories close to a hemispherical cathode. The inner trajectories appear to have come from a small virtual source V while the outer ones form a caustic (dashed line). The dotted line represents the 'virtual cathode', the surface over which the potential has a local minimum, $\phi = \phi_m$.

It has sometimes been argued that space charge is 'visible' in direct images of the cathode surface, since the central part is imaged sharply while the marginal parts appear blurred. The conclusion that this blurring must be a space charge effect is not at all convincing, since geometric and chromatic aberrations can also cause blurring. Thus the only way of determining space charge distributions is to undertake the appropriate numerical calculation.

Theoretical investigations of triodes with negative wehnelt potential and space charge have been carried out in Tübingen. It has proved possible to achieve fairly good agreement with Lauer's measured emittance diagrams. There are essentially two different ways of performing the calculations, the counting method and the semianalytic method.

The *counting method*, combined with a Monte Carlo procedure, has been used by Hauke (1977). The cathode surface was dissected into discrete emission areas Δa_i. The half-space of emission directions relative to the local surface normal was dissected into rotationally symmetric elements of solid angle $\Delta \Omega_j = 2\pi \sin \gamma_j \, \Delta\gamma_j$. The emission energy E was discretized in intervals ΔE_k. Finally the space in front of the cathode was divided into a set of discrete volume elements ΔV_l. The space charge density at an arbitrary point r outside the cathode is then given by

$$\rho(\boldsymbol{r}) = \sum_{\Delta E, \Delta \Omega, \Delta a} \frac{\partial^2 j}{\partial E \partial \Omega} \frac{\Delta E \, \Delta \Omega \, \Delta a \, \Delta \tau(\boldsymbol{r})}{\Delta V(\boldsymbol{r})} \tag{46.19}$$

in which we have dropped all subscripts. The expression $\partial^2 j/\partial E \partial \Omega = S \cos \gamma$ is the spectral surface brightness, given by Eqs (44.14a) and (44.14b) for a thermionic gun. The quantity $\Delta V(\boldsymbol{r})$ is the volume of the cell that contains the point $\boldsymbol{r}$, and $\Delta \tau(\boldsymbol{r})$ is the time spent by a particular electron trajectory (with the appropriate initial conditions) in this cell.

In order to keep statistical fluctuations sufficiently small, a very large number of trajectories have to be traced. Even so, it is necessary to smooth the space charge distribution obtained. Since the points $\boldsymbol{r}$ can be chosen as the nodes of a suitable curvilinear grid, the combination of this method with the finite-difference method for the calculation of the potential is easy. Even today, the whole procedure is exceedingly time-consuming.

In order to speed up the calculation, Weyßer (1983a,b) developed a *semianalytic method* on the basis of diode models. In front of the cathode, laminar electron flow was assumed; in the vicinity of a hemispherical cathode, this flow is practically radial. In order to apply the diode models, Weyßer traced a number of 'reference' trajectories, starting in the direction of the surface normal with a given velocity v_0. The space in front of the cathode was now dissected into a set of ring-shaped volume elements bounded by the mantle surfaces through the reference rays and by a set of conical surfaces orthogonal to these. In each such volume element the laminar electron flow was approximated by that in a locally fitted spherical (or planar) diode element. The necessary divergence factor was determined from the distances and angles between neighbouring reference rays. Weyßer also developed an analytic method of solving Poisson's equation, which could be combined with the boundary-element technique. It was found that a considerable amount of computation time could be saved in this way. Some results of these investigations are shown in the equipotential plots in Figs 46.8 and 46.9. The most interesting new result is the skew angle of intersection of the zero-volt line with the cathode surface. The influence of the potential barrier on the size of the emitting area can be interpreted as a confinement by an 'iris aperture'.

The main drawback of Weyßer's method is that intersections of normal trajectories, as shown in Fig. 46.7, have to be neglected. This drawback can be removed and the method

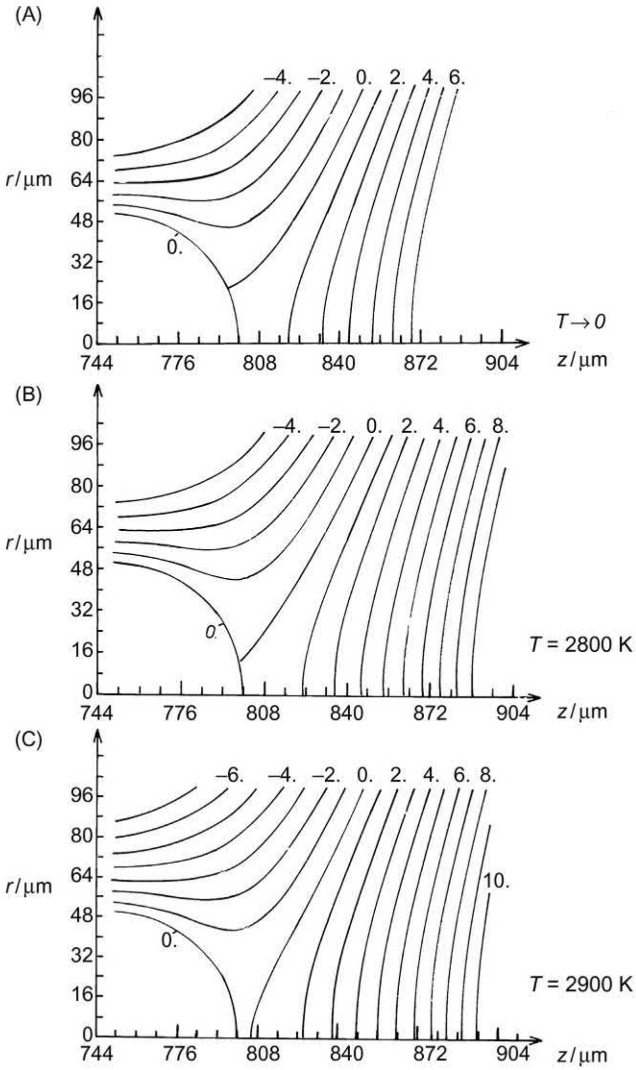

Figure 46.8

Equipotentials in the vicinity of a hemispherical cathode at different temperatures. (A) $T \to 0$; (B) $T = 2800$ K; (C) $T = 2900$ K. The electrode potentials are unaltered. *After Weyßer (1983a), Courtesy the author.*

can thus be improved considerably by making use of the approach described in the previous section (Kumar and Kasper, 1985) and illustrated in Fig. 46.4. Since the relation (46.12b) is essentially nonlinear, it is inevitably necessary to set up an iterative procedure. In the first loop we assume that space charge is absent and hence that we have to solve Laplace's equation with $\Phi_m = 0$, $s_m = 0$; in later loops we solve Poisson's equation with the newest available values for the position and the depth of the potential minimum.

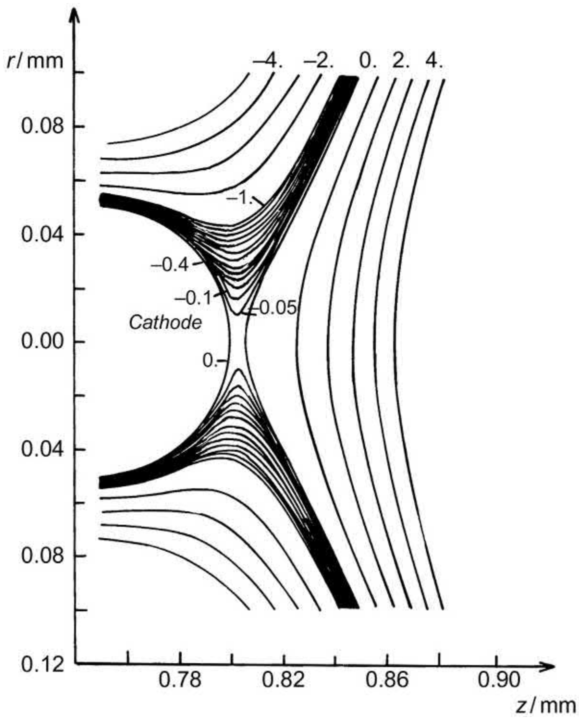

Figure 46.9
More detailed version of Fig. 46.8C. The potential barrier created by the space charge confines the emitting area like an iris aperture. *After Weyßer (1983a), Courtesy the author.*

In the electric field thus obtained, we have to trace normal trajectories with a starting velocity given by (46.15). As already explained, these solutions define the curved axes of electron bundles. A very suitable form of the ray equation is Eq. (3.12) in its nonrelativistic form and with vanishing magnetic terms. This can be cast in the compact form

$$\ddot{\boldsymbol{r}}(\tau) = \boldsymbol{F}(\boldsymbol{r}) \tag{46.20}$$

where, disregarding a constant normalization factor, $\boldsymbol{F}(\boldsymbol{r})$ is the electric field strength. For a perturbed ray we then have, in the linear approximation

$$\ddot{\boldsymbol{r}} + \delta\ddot{\boldsymbol{r}} = \boldsymbol{F}(\boldsymbol{r} + \delta\boldsymbol{r}) = \boldsymbol{F}(\boldsymbol{r}) + (\delta\boldsymbol{r}\cdot\nabla)\boldsymbol{F}$$

After subtracting Eq. (46.20), we see that

$$\delta\ddot{\boldsymbol{r}} = (\delta\boldsymbol{r}\cdot\nabla)\boldsymbol{F}(\boldsymbol{r}) \tag{46.21}$$

This can be solved at the same time as (46.20). At the cathode surface the initial vectors $\delta\boldsymbol{r}_0$ and $\delta\,\dot{\boldsymbol{r}}_0$ must satisfy

$$\delta\boldsymbol{r}_0 = \lambda_0\boldsymbol{t}_0, \quad \dot{\boldsymbol{r}}_0 = |\dot{\boldsymbol{r}}_0|\delta\boldsymbol{r}_0\, R_0^{-1} \tag{46.22}$$

for a small transverse shift λ_0, $|\dot{\boldsymbol{r}}_0|$ being the initial velocity in the τ-scale and R_0 the radius of local meridional curvature; $\boldsymbol{t}_0$ denotes the unit vector of the meridional surface tangent. After some elementary manipulations, the divergence factor is obtained correctly as

$$\begin{aligned} M &= \left|r_0\lambda_0 r^{-1}\lambda^{-1}\right| \quad &&\text{off the axis} \\ M &= \lambda_0^2\lambda^{-2} &&\text{on the axis} \end{aligned} \tag{46.23}$$

r_0 and r being radial cylindrical coordinates and λ_0, λ the perturbation components perpendicular to the unperturbed ray. For λ we find

$$\lambda = \frac{\dot{z}\delta r - \dot{r}\delta z}{\sqrt{\dot{z}^2 + \dot{r}^2}} \tag{46.24}$$

If the sign of λ is retained, the overlapping of electron bundles can be detected. This takes place for the first time if $\lambda\lambda_0 < 0$. At the caustic, where λ vanishes, some reasonable upper bound for M is to be adopted.

In this way, the charge density $\rho(\boldsymbol{r})$ along a set of normal trajectories can be determined and the overlapping branches can be separated. It is now necessary to calculate the values ρ_{ik} of $\rho(\boldsymbol{r})$ at the nodes of a two-dimensional grid, preferably a spherical one with exponentially increasing mesh-length (see Section 11.4). This is to be done by interpolation, which must be carried out for each branch *separately*, respecting the sign of λ. A correct though very cumbersome method is to determine the point of intersection of the rays and the grid lines. The values of ρ at these points are stored and interpolations along the grid lines can then be carried out.

A slightly less accurate but very simple method is based on bilinear interpolation. In the $u-v$ coordinate plane, the grid must be square-shaped, the grid lines being $u = \mu h$, $v = \nu h$ (μ, ν integers). If a trajectory point has the general coordinates (u, v), we define weight factors

$$\begin{aligned} g_{\mu\nu} &= \left(1 - \left|\frac{u}{h} - \mu\right|\right)\left(1 - \left|\frac{v}{h} - \nu\right|\right) \begin{cases} |u/h - \mu| \le 1 \\ |v/h - \nu| \le 1 \end{cases} \\ g_{\mu\nu} &= 0 \quad \text{otherwise} \end{aligned} \tag{46.25a}$$

This implies that only the four corners of the cell containing the point (u, v) have nonzero weights. The procedure is then as follows. As the trajectory calculation proceeds, the weights $g_{\mu\nu}$ and the contributions $\rho_{\mu\nu} = g_{\mu\nu}\rho(u, v)$ are computed and summed for every point on the trajectory. If we encounter two overlapping domains, the sums must be formed and stored separately according to the sign of λ. We thus have to calculate and store

$$G_{\mu\nu}^{(\pm)} = \sum_l g_{\mu\nu}(l), \quad \rho_{\mu\nu}^{(\pm)} = \sum_l \Delta\rho_{\mu\nu}(l) \tag{46.25b}$$

the label l indicating the successive trajectory points. Finally we obtain the required grid values from

$$\rho_{\mu\nu} = \rho_{\mu\nu}^{(+)}/G_{\mu\nu}^{(+)} + \rho_{\mu\nu}^{(-)}/G_{\mu\nu}^{(-)} \tag{46.26}$$

in which the accumulation of space charge due to the overlapping of electron bundles is taken into account approximately.

This is all to be carried out for each pair (μ, ν) of subscripts. The procedure can be made very fast and memory saving. Since we now know the values of ρ at the nodes of a grid, we can apply a combination of the finite-difference method and the boundary-element method, as explained in Chapter 10 of Volume 1.

Since the space charge distribution varies rapidly in the neighbourhood of the cathode surface, it is necessary to choose very fine meshes in this most important domain. The mesh size in the direction perpendicular to the cathode surface must be very small there. This should then increase steeply but smoothly with increasing distance from the cathode surface. The latter is often curved and the mesh system must then also be curved, to fit this surface. The problem is now to find a suitable curvilinear orthogonal coordinate system (u, v) in which the line $u = 0$ represents the cathode surface and the lines $u = ih$, $(i = 1, 2, 3, \ldots)$ are at rapidly increasing distances from it, when measured in the (z, r) plane. It is always possible to choose the transformation of scales such that the (u, v) grid remains square-shaped, and for easy application of the FDM this is also advisable. In the (z, r) plane we then have a curvilinear orthogonal mesh system, which is not necessarily conformal. Nevertheless, the five-point discretization explained in Chapter 11 is now easily applicable. Alternatively, special nine-point discretizations can be employed in order to improve the accuracy of the field calculation (Kumar and Kasper, 1985).

It has not been possible to include many important technical details here for reasons of space. Although the correct determination of space charge is a difficult task, there is no intrinsic obstacle that renders it impossible, as the work of Killes (1985, 1988) demonstrates. Among the many other papers on Coulomb interactions, we draw attention to Rouse et al. (1995, 2011), Stickel (1995), Radlička (2006), Radlička and Lencová (2008), Marianowski et al. (2011), Verduin et al. (2011) and Zelinka et al. (2015) and, as always in this context, to the monumental work of Jansen (1990).

46.4 The Boersch Effect

46.4.1 Introduction

In his investigations on the energy distributions in beams emitted from thermionic electron guns, Boersch (1954) found results that could not be brought into agreement with theory; he observed the following effects:

a. In comparison with the Maxwell distribution, there is an anomalous broadening of the energy distribution.
b. The energy distribution tends to become symmetric about its maximum.
c. The mean energy is shifted.
d. These effects become more pronounced with increasing beam current.

The anomalous broadening of the energy distribution is called the energetic Boersch effect. Since 1954, this effect has been studied frequently and is now well confirmed experimentally. Extensive lists of references are given by Hanszen and Lauer (1969a,b), Anderson and Mol (1970), Ohno (1974) and Lauer (1982). In theoretical studies, the energetic Boersch effect is assumed to be caused by residual stochastic Coulomb interactions in the electron beam after subtraction of the mean Coulomb interaction, caused by the space charge distribution. Major contributions to this theory have been made by Loeffler (1969), Zimmermann (1969, 1970), Crewe (1978), Knauer (1979a,b, 1981), Rose und Spehr (1980, 1983), van Leeuwen and Jansen (1983), Wiedenhausen et al. (1985), Tang (1983, 1987, 1991, 1996), Jansen (1990), Shimoyama et al. (1993), Read and Bowring (2002, 2003, 2004a–d) and Kruit and Jansen (2009). The work of Jansen is particularly useful as it contains a balanced appraisal of earlier studies.

The shift of the mean energy can be explained by the classical theory of emission, as will be explained in the next section. This is clearly to be distinguished from the anomalous effects.

In electron lithography, high probe currents and very small probe diameters are required. Attempts to satisfy these requirements have revealed another anomalous effect, the *spatial* Boersch effect. This is manifested as an anomalous broadening of the probe diameter due to stochastic Coulomb interactions. Again, the mean broadening due to space charge (Section 47.4) must be distinguished from this. Several authors have tried to study the spatial Boersch effect by means of Monte Carlo methods (e.g. Loeffler and Hudgin, 1970, Groves et al., 1979, Kang et al., 1983). Unfortunately, different situations have been simulated so that no reasonable comparison is possible. Soon after, Rose and Spehr (1983) developed an analytical theory based on thermodynamic considerations; we shall mainly follow this presentation, which also gives a good survey of earlier research into the Boersch effect.

46.4.2 The Shift of the Mean Energy

Here we concentrate our attention on those effects that can be explained satisfactorily and are hence not to be regarded as anomalous. We have seen that the influence of space charge can be modelled by replacing the true cathode by a 'virtual' cathode, which coincides with the surface of the potential minimum $\Phi(\boldsymbol{r}) = \Phi_m(\boldsymbol{r}) < 0$ in front of the former. If no such minimum exists, we set $\Phi_m = 0$, and the virtual cathode then coincides with the real one.

The potential barrier filters out all electrons with a starting energy $E_0 < |e\Phi_m|$, while the kinetic energy of all the transmitted electrons is simply $E_{\mathrm{kin}} = E_0 + e\Phi(r)$, with a Maxwell distribution for E_0. We can thus treat the virtual cathode as though it were the real one, provided that the origin of the energy scale is shifted to the value $|e\Phi_m|$ in the original scale and that the Richardson current density j_0 is replaced by $j_C := j_0 \exp(e\Phi_m/kT)$. In the shifted energy scale, the normal energy $\tilde{U}_n$, the transverse energy $\tilde{U}_t$ and the total energy $\tilde{E}$ have the following expectation values and variances with respect to the virtual cathode:

$$< \tilde{U}_n > = < \tilde{U}_t > = \frac{1}{2} < \tilde{E} > = kT \tag{46.27a}$$

$$\mathrm{var}\ \tilde{U}_n = \mathrm{var}\ \tilde{U}_t = \frac{1}{2} \mathrm{var}\ \tilde{E} = (kT)^2 \tag{46.27b}$$

This is not at all surprising and $< \tilde{E} > = 2kT$ is in accordance with (46.11b). A new aspect is that the temperature T, the work function W and the minimum potential Φ_m are no longer constant but functions of the surface coordinates. A consequence of this is that j_C and the expressions given in (46.27a,b) depend on these coordinates. More seriously, the energy distribution shifts with the variations of $W(\boldsymbol{r}) + e|\Phi_m(\boldsymbol{r})|$, since the Fermi level is the only well-defined one. Since the spectra originating from different cathode surface elements are superimposed in the crossover, the resulting spectrum can be altered considerably, as has been observed by Speidel and Gaukler (1968).

A numerical calculation of this effect by the Monte Carlo method has been performed by Hauke (1977). A typical example of the results is presented in Fig. 46.10. The spectrum in the crossover is, in fact, considerably altered but we cannot accept Hauke's conclusion that the shift effect is alone sufficient to explain the experimentally observed spectra. For simplicity, we shall disregard the shift effect in the following sections and deal exclusively with stochastic effects.

46.4.3 Thermodynamic Considerations

The Boersch effects can be understood quite easily in a qualitative manner by applying thermodynamic reasoning to the propagation of electron beams. This is valid in the vicinity

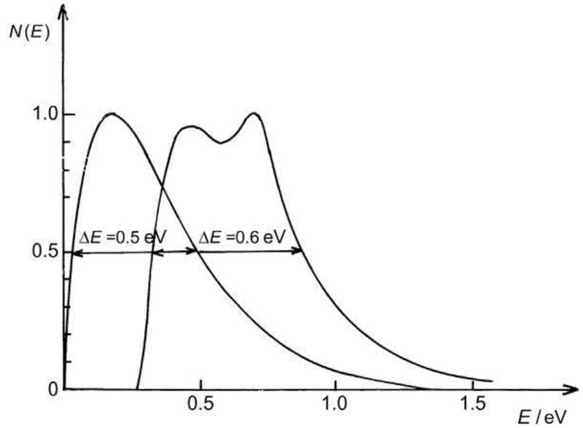

Figure 46.10
Energy distribution for an electron gun with a plane cathode (TELGUN) at $T = 2200$ K. Left: energy distribution at the cathode surface; right: at the crossover.

of the cathode as well as in domains distant from the latter. Although the following discussion is based on that of Rose and Spehr (1983), we have tried to generalize the theory and have harmonized the notation with that employed here wherever necessary.

Locally we have to distinguish between three mutually orthogonal directions in space: (i) the *longitudinal* direction (subscript 1 or ||), given by the tangent of a trajectory starting from some point on the cathode normal to the surface with energy $E_0 = 2kT + |e\Phi_m|$, (ii) the *transverse* meridional direction (subscript 2 or t) normal to direction 1 and outward from the optic axis, and (iii) the *azimuthal* direction (subscript 3 or a) orthogonal to the others and positively oriented. Sometimes it is not necessary to distinguish between transverse meridional and azimuthal quantities; we then use the subscript $\perp$. In the literature only two degrees of freedom are commonly distinguished (|| and $\perp$), but this may be too strong a simplification.

Although the propagation of electron beams bears little resemblance to a system in thermodynamic equilibrium, it can still be advantageous to introduce local beam temperatures thus:

$$kT_i = \frac{1}{m}\left\langle (p_i - <p_i>)^2 \right\rangle = \frac{1}{m}\left(<p_i^2> - <p_i>^2 \right) \quad \text{for} \quad i = 1, 2, 3 \tag{46.28}$$

Here p_i denote the corresponding components of the kinetic momentum $m\boldsymbol{v} = \boldsymbol{p}$ and the averaging is to be carried out with the (Gaussian) distribution for scalar densities.

46.4.3.1 Transverse temperatures

For the transverse modes $i = 2, 3$ we have $< p_i > = 0$, whereupon Eq. (46.28) simplifies to

$$\frac{1}{2}kT_i = \frac{1}{2m} < p_i^2 > =: < E_i > \quad (i = 2, 3) \tag{46.29}$$

This even holds relativistically provided that m is the relativistic mass, but for conciseness we shall henceforward adopt the *nonrelativistic* approximation. At the cathode surface ($\Phi = 0$) we obtain $T_2 = T_3 = T_C$, T_C denoting the cathode temperature. This is not surprising, since the transverse components of the momentum remain unaltered by the passage through the potential wall. For field emission cathodes the Gaussian distribution (44.36a) leads to $T_2 = T_3 = d/k$, d being given by (44.26).

Outside the cathode, the beam temperatures are rapidly lowered by the acceleration process. This is most easily understood for spherical diodes. Owing to the conservation of angular momentum, the transverse momenta must decrease as R^{-1}, R denoting the distance from the centre of curvature; thus $T_2 = T_3 = T_\perp$ with (see also 46.11c)

$$R^2 T_\perp = \text{const}_\perp \tag{46.30}$$

This is even approximately true for the diodes with pointed cathodes treated in Chapter 45. Then R denotes the distance from the virtual source point V.

In an essentially aspheric but still axisymmetric device, T_3 must be distinguished from T_2. From the conservation of axial angular momentum, we obtain

$$r^2 T_a = \text{const}_a \tag{46.31a}$$

$r = |R \sin \vartheta|$ denoting the distance from the optic axis. For the meridional component p_t, the Lagrange–Helmholtz relation tells us that $p_t\lambda = \text{const}$, λ being a measure of the meridional divergence, introduced in Section 46.3.

Hence

$$\lambda^2 T_t = \text{const}_t \tag{46.31b}$$

It is sometimes helpful to introduce a mean transverse temperature $T_\perp := (T_a T_t)^{1/2} \sim (T_a + T_t)/2$. From Eq. (46.23), we find

$$MT_\perp = T_{\perp,C} = \text{const} \tag{46.31c}$$

M being the divergence factor introduced in the previous sections. These relations apply to thermionic guns as well as field emission guns; they are quite generally valid. A practical consequence is that at every focus or crossover, these temperatures can become very high, whereas in the apertures of diaphragms they are usually very low, since M is inversely proportional to the cross-section of the beam. We notice that when $T_t \neq T_a$, the transverse motions are not in equilibrium.

46.4.3.2 The longitudinal temperature

For the normal component, the situation is more complicated than in the other cases, since $< p_{||} > \neq 0$. For reasons of space, we discuss only two simple special cases, the vicinity of the cathode surface and the asymptotic domain.

In the absence of space charge, at the surface of a thermionic cathode we find

$$T_{||,C} = T_C\left(1 - \frac{2}{\pi}\right) = 0.43T_C \tag{46.32}$$

This result shows very clearly that $T_{||}$ is discontinuous at the surface. The reason for this lies in the fact that outside the cathode material, the electrons are not in an equilibrium state, since only an outward-directed flux is allowed. For field emission guns the situation is still more complicated and has not yet been investigated. In both cases, we have $T_{||,C} \neq T_{\perp,C}$.

The acceleration of the electron beam leads to a very rapid decrease in the longitudinal temperature. Asymptotically, the following approximations are justified:

$$p_{||} = \sqrt{2m_0 e\Phi_T} + \Delta p_{||} = < p_{||} > + \Delta p_{||} \tag{46.33a}$$

with an acceleration potential

$$\Phi_T = \Phi - \Phi_m + 2kT_C/e \tag{46.33b}$$

corresponding to the mean energy given by Eq. (46.11b). With $|\Delta p_{||}| \ll < p_{||} >$ and $< \Delta p_{||} > = 0$ we obtain from (46.28)

$$kT_{||} = \frac{1}{m} < \Delta p_{||}^2 > \tag{46.34}$$

A more physically meaningful relation is found by introducing the energy difference

$$\Delta E = \frac{1}{2m}\left(p^2 - < p^2 >\right) \approx \frac{1}{m} < p_{||} > \Delta p_{||} + O\left(\Delta p^2\right) \tag{46.35}$$

Asymptotically, the contributions of the transverse motions, containing only quadratic terms, can be neglected. We now form the corresponding standard deviation

$$\delta E =: \sqrt{< \Delta E^2 >} = \frac{1}{m} < p_{||} > \sqrt{< \Delta p_{||}^2 >} \tag{46.36}$$

Recalling the definition of $T_{||}$ and $< p_{||} >$, we find the important relation

$$\delta E = < p_{||} > \sqrt{kT_{||}/m} = \sqrt{2e\Phi_T kT_{||}} \tag{46.37}$$

The quantities ΔE and δE remain *constant* during the acceleration because the potential terms cancel out from all the energy differences and so $T_{||}$ decreases as $< p_{||} >^{-2}$. This result essentially confirms those found by Rose and Spehr, although our derivation is different. In the immediate vicinity of the cathode, Eq. (46.37) does not hold, since the approximation in (46.35) is then unjustified. Despite all the simplifications, the correct order of magnitude is nevertheless obtained with $\Phi_T \approx 2kT_C/e$. Our derivation does not involve an adiabatic expansion and no special distribution is assumed; moreover, it reveals the underlying physics more clearly.

46.4.3.3 The thermodynamic limit

We can now understand the energetic Boersch effect qualitatively, indeed, we can even derive a simple formula for the energy spread in thermodynamic equilibrium. The contents of Eqs (46.31) and (46.37) are schematically presented in Fig. 46.11, which also shows their connection with the shape of the beam. In front of the cathode, T_t and T_a decrease rapidly with increasing z, have local minima in the plane of maximum beam cross-section, have very high and practically equal maxima in the crossover and then decrease afresh. The difference between T_a and T_t is only noteworthy in the vicinity of their minima: $T_{t,\min} = 0$ whereas $T_{a,\min}$ does not vanish.

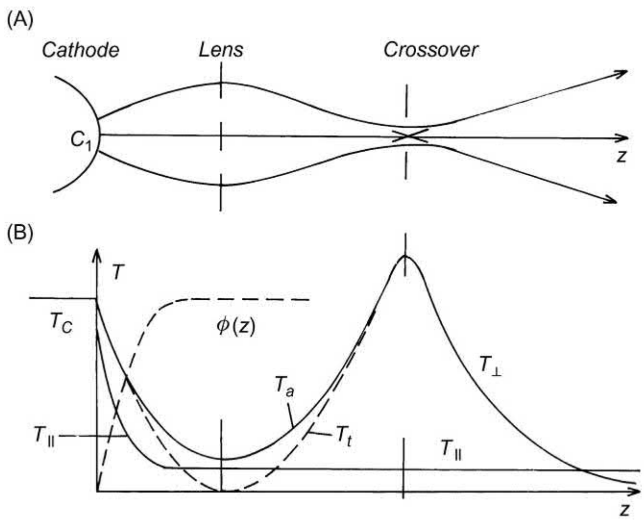

Figure 46.11

(A) Schematic representation of an electron beam. (B) Corresponding beam temperatures and the axial potential ϕ as functions of z. Close to and beyond the crossover, $T_a = T_t = T_\perp$.

The longitudinal temperature has quite a different behaviour. Since $T_{||}$ is essentially determined by the acceleration potential, it decreases rapidly with increasing Φ, faster than T_t and T_a. At the end of the acceleration process, where $\Phi = \text{const}$, $T_{||}$ also remains constant at a very low value. This all happens without any Boersch effect: interactions have not been considered.

The Boersch effect can now be understood as a thermodynamic relaxation process in which the system tends towards the equilibrium state by reducing the differences between the temperatures. The reason for this relaxation is to be found in the stochastic elastic Coulomb interactions between the electrons, which are usually not considered in electron optics. As is obvious from Fig. 46.11, the energetic Boersch effect is strongest in the vicinity of the cathode and of the crossover. In almost all practical cases, the flight time of the electrons in the domains of close encounter is too short for thermodynamic equilibrium to be reached, but the corresponding value δE_{therm} of the energy spread, given below, may be very useful for the estimation of an upper limit.

At equilibrium, the electron beam has a mean temperature $\overline{T} = (T_t + T_a + T_{||})/3 \approx (2T_\perp + T_{||})/3$. At a focus, the value of $T_{||}$ without relaxation is negligibly small and so $\overline{T} \approx 2T_\perp/3$. Introducing this into Eq. (46.37) in place of $T_{||}$, we find

$$\delta E_{\text{therm}} = <p_{||}> \sqrt{\frac{2}{3m}kT_\perp} = \frac{1}{m} <p_{||}> \sqrt{\frac{1}{3} <p_\perp^2>}$$

using the interaction-free value of $T_\perp$. If the angular intensity distribution in the beam is isotropic within a cone of a small semiaperture angle α_0, we have $<p_\perp^2> \approx \alpha_0^2 <p_{||}>^2 /2$ and

$$\delta E_{\text{therm}} = \frac{\alpha_0 <p_{||}>^2}{m\sqrt{6}} = \sqrt{\frac{2}{3}}\alpha_0 e\Phi \tag{46.38}$$

since $\Phi_T = \Phi$ is a good approximation far from the cathode. It is a surprising fact that δE_{therm} depends neither on the beam current nor on the diameter of the focus. In reality this upper limit may be too pessimistic by one or two orders of magnitude, since the beam is always far from thermodynamic equilibrium.

46.4.3.4 The beam entropy

In order to understand the spatial Boersch effect and the influence of the Boersch effects on the brightness, it is advantageous to introduce a *beam entropy*. This has been done by Rose and Spehr (1983) but we shall not follow their argument as it is easily generalized.

The z-coordinate along the optic axis, or more generally the arc-length along a particular trajectory defining the local axis of a narrow beamlet, is not treated as a dynamic variable, but as a parameter, like the time in everyday thermodynamics. The definition of the entropy then refers to the four-dimensional phase space of the *transverse* motions. In the case of paraxial beams, the latter is the phase space dealt with in Section 48.1.

We now dissect the phase space into a large number of hyperemittance volume elements

$$\Delta E_i^* = p_i^2 \Delta a_i \, \Delta \Omega_i = 2m_0 e \hat{\Phi}_i \Delta a_i \, \Delta \Omega_i \tag{46.39}$$

with elements of surface Δa_i and of solid angle $\Delta \Omega_i$. These hyperemittance elements are invariants of the undisturbed motions. For each, we define occupation probabilities (relativistically if necessary) by

$$P_i^{\perp} := \frac{R_i \Delta E_i^*}{2m_0 e I} = \frac{B_i \Delta a_i \Delta \Omega_i}{I} = \frac{\Delta I_i}{I} \tag{46.40}$$

R_i being the local normalized brightness, $B_i = R_i \hat{\Phi}_i$ the ordinary brightness and I the total current. From the definition of the brightness it is obvious that ΔI_i is the current flowing in the element considered and is hence an invariant of the undisturbed motion. We impose the self-evident condition $\Sigma P_i^{\perp} = 1$. The definition of the transverse entropy is now straightforward:

$$S_{\perp} := -k \sum_i P_i^{\perp} \ln \; P_i^{\perp} \tag{46.41}$$

The invariance of this expression for the undisturbed motion, that is to say without Boersch effects, has a simple physical meaning: the acceleration of the electron beam may be regarded as an adiabatic process. In fact, (46.31a,b) can be recognized as the adiabatic equations of one-dimensional gases, as can (46.37).

Another interesting aspect of this definition of the entropy is the requirement that the latter tends towards its maximum value. As constraints, we have $\Sigma P_i^{\perp} = 1$ and the constancy of the hyperemittances ΔE_i^*. The entropy $S^{\perp}$ then reaches a maximum for *uniform* normalized brightness R. The natural cell volume is $\Delta E^* = h^2/2$ (h being Planck's constant), since two electrons with opposite spins can be located in each element of volume h^2. The entropy can then be put into the form

$$S_{\perp} = -k \; \ln\left(\frac{R}{R_I}\right) = -k \; \ln\left(\frac{B}{B_I}\right) \tag{46.42a}$$

with the normalization constant

$$B_I = \hat{\Phi} R_I = 2I/\lambda^2 \tag{46.42b}$$

$\lambda := h/p$ being the corresponding de Broglie wavelength. Except for the normalization constant, this result agrees with that of Rose and Spehr. Our results in the next chapter, Eq. (47.12) and (47.13), can now be seen in a new light: the constancy of these expressions means that the emission process maximizes the beam entropy, the beam current I being unaltered.

It is now obvious without further calculations that the average brightness must be reduced by the Boersch effects. Close to the cathode, the beam uniformly fills a finite volume E_C^* in the four-dimensional phase space, the brightness $B = \overline{B}_C$ having the theoretical value, while the cells outside E_C^* are empty. Any scattering process, regardless of its nature, will certainly force a part of the beam to occupy empty cells, hence E_C^* increases to E^* say. Since B/I must always be normalized over the whole phase space, the averaging over the volume $E^*(>E_C^*)$ must result in a *smaller* value. As far as we know, this has not yet been investigated quantitatively for realistic configurations.

The spatial Boersch effect can be understood as a special aspect of the broadening of the brightness distribution. The square of the beam radius r_m may reasonably be defined by

$$r_m^2 = 2 < r^2 > = 2\sum_i P_i^{\perp} r_i^2 \tag{46.43a}$$

Using Eq. (46.40) and replacing the summation by an appropriate integration, we obtain

$$r_m^2 = 2I^{-1} \iiiint \left(x^2 + y^2\right) B(x, y;\; x', y';\; z) dxdydx'dy' \tag{46.43b}$$

Hence r_m can be evaluated if the alteration of B caused by scattering is known.

The entropy $S_\perp$ is not the total entropy since the spectrum of the electrons in the beam was not considered in its entirety. This is most obvious if (47.8) is introduced into (46.42a): (47.8) is just one of the many integral expressions which can be formed by integration over E. The more detailed exploitation of the information contained in the energy spectrum gives rise to an additional term $S_{||}$, since this information is essentially $-S_{||}/k$. Let

$$P_i^{||} = G(E_i)\Delta E \tag{46.44}$$

be the probability that the energy E lies in the range $E_i \leq E \leq E_i + \Delta E_i$. The condition $\Sigma P_i^{||} = 1$ must of course be imposed and

$$S_{||} = -k\sum_i P_i^{||} \ln P_i^{||} \tag{46.45}$$

is then the associated contribution to the entropy. The variable E is here not the kinetic energy but the *total* particle energy; this is an invariant of the corresponding motion, as long as no inelastic scattering occurs. Hence, in the absence of the Boersch effect, $S_{||}$ is also an invariant, the corresponding adiabatic law being Eq. (46.37).

In conclusion, we may state that the spatial Boersch effect essentially increases $S_\perp$, while the energetic Boersch effect increases $S_{||}$. Of course, the sum $S = S_\perp + S_{||}$ must increase in either case. We can go no further without making special calculations.

46.4.4 Analytical Calculations

The energetic Boersch effect has frequently been studied in the past decades. Unfortunately the present state of the theory is not quite satisfactory in every respect. The reason for this is that, owing to the enormous complexity of the problem, many simplifying assumptions have to be made, some of which are not really justified. Even neglecting this weakness, the necessary calculations are still very tedious and only comprehensible if presented in great detail. Both for reasons of space and because they are still imperfect, we do not feel justified in giving a comprehensive account of the existing theories: the reader is referred to the various publications. The present section is confined to some basic ideas and some essential results.

The most highly perfected theories of the Boersch effect at present seem to be those of Rose and Spehr (1980, 1983) and Jansen (1990). Like other authors, Rose and Spehr first studied the energy transfer between two colliding particles in their centre-of-mass frame of reference in the absence of any external forces. One of these two particles is chosen as the reference particle and the change in its energy is determined in the laboratory frame. This is a straightforward procedure, which results in

$$\Delta E = \frac{p^2}{m_0} \delta \sin 2\tilde{\theta} \sin \tilde{\psi} \tag{46.46}$$

2δ being the angle between the asymptotes before the collision, $2\tilde{\theta}$ the angle of deflection in the centre-of-mass frame and $\tilde{\psi}$ the angle between the angular momentum vector and the optic axis. The quantity p is the kinetic momentum in the laboratory frame before the collision; for reasons of simplicity this momentum is assumed to be the same for both particles. Since $\delta \leq 2\alpha_0$, α_0 being the semiaperture of the beam, the maximum energy transfer is given by

$$\Delta E_{\max} = \frac{p^2}{m_0} \alpha_0 \tag{46.47}$$

even relativistically. Rose and Spehr normalized with respect to this constant; the thermodynamic limit (46.38) is just 41% of this value.

The main problem now is to perform the necessary averaging over the angles δ, $\tilde{\theta}$ and $\tilde{\psi}$, which is only possible with certain simplifications. The forms and the validity of the different simplifying assumptions are a source of controversy in the literature. Knauer (1979a,b) assumed that many weak interactions are experienced by a reference electron and that the velocity distributions of the transverse motions of the colliding partners are Gaussian. With these assumptions and others, he derived the relation

$$\frac{d}{dl}\langle \Delta E^2 \rangle = \frac{2\pi^{3/2}e^3}{(4\pi\varepsilon_0)^2}\left(\frac{m}{kT_C}\right)^{1/2} j \ln \Lambda_t \tag{46.48a}$$

with

$$\Lambda_t = \frac{4\pi\varepsilon_0 kT_C}{e^2}\left(\frac{e}{j}\right)^{1/3}\left(\frac{2e\Phi}{m}\right)^{1/6} \tag{46.48b}$$

for the derivative of the mean square energy spread $<\Delta E^2> = (\delta E)^2$ with respect to the arc-length l along the beam, j being the current density. This formula can be applied to diverging, parallel and converging round beams.

Knauer's method has been criticized by Rose and Spehr (1980, 1983) who pointed out some discrepancies. Their main argument is that, owing to the many simplifications, the range of validity of Knauer's theory does *not* exceed that of the single-scattering approximation. In contrast to Knauer, Rose and Spehr assumed that at crossovers and foci – at low beam currents – *large-angle* single-scattering processes are the most important for the energetic Boersch effect. For this reason, they named their theory the 'closest encounter approach'. This theory is highly sophisticated. Unfortunately, in the general case, it does not lead to compact simple formulae and we therefore refer to the corresponding publications. Some of the numerical results are presented in Fig. 46.12. The variable κ is defined by $\kappa := I(I_0\alpha_0^2)^{-1}$, I being the beam current, α_0 the semiaperture angle and $I_0 = 3.4\times 10^4\beta^3(1-\beta^2)^{-3/2}$ A with $\beta = v/c$; λ is a parameter characterizing the astigmatism, defined as the ratio of the diameter of the circle of least confusion to the impact parameter at 90° deflection in the centre-of-mass frame. The value $\lambda = 0$ represents the stigmatic focus. As a consequence of the single-scattering approximation, the results can be valid only for small values of κ, $\kappa \le 10^{-2}$, the true limit being unknown. In the very simple case of a stigmatic focus, Rose and Spehr obtained the relation

$$\langle \Delta E^2 \rangle = 48\beta\left(1-\beta^2\right)^{-1/2} I \quad \left[(\mathrm{keV})^2/\mathrm{A}\right] \tag{46.49}$$

which, unlike the earlier results of Crewe (1978) and Loeffler (1969), does not depend on the aperture. Among other proposals for the reduction of the energetic Boersch effect, Rose and Spehr came to the conclusion that astigmatic foci should be employed instead of stigmatic ones, whenever this is technically possible.

Rose and Spehr (1983) have also developed an analytical treatment of the spatial Boersch effect. Their starting point is the transverse entropy $S_\perp$. In the special case of constant

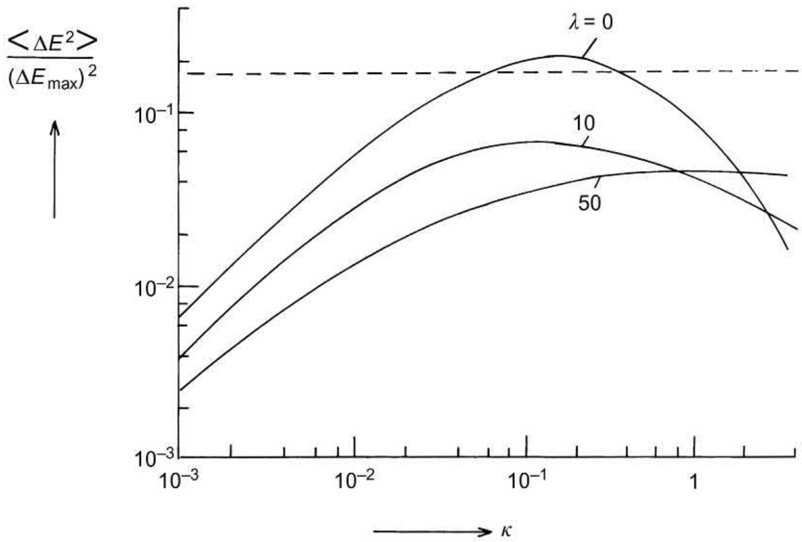

Figure 46.12

Mean quadratic energy broadening as a function of the normalized current $\kappa = I/I_0\alpha_0^2$ for three values of the astigmatism parameter λ. A muffin-tin distribution is assumed for the transmitted current density in the aperture plane. The dashed line indicates the thermodynamic limit. *After Rose and Spehr (1980), Courtesy Wissenschaftliche Verlagsgesellschaft.*

brightness $B = I/A_c\Omega_c$, A_c being the local cross-section of the beam (denoted here by subscript c) and Ω_c its solid angle, Eq. (46.42a) can be rewritten

$$S_\perp = k \ln\left(\frac{A_c}{A_d}\right) \quad \text{with} \quad A_d = \frac{\lambda^2}{2\Omega_c} \tag{46.50}$$

The quantity A_d can be interpreted as the area of the diffraction disc corresponding to an aperture of area A_c. Rose and Spehr suggested that the increase dA_c can be treated as though it were due to a heat transfer dQ to the transverse motion:

$$dS_\perp = dQ/T_\perp = k\, dA_c/A_c$$

This heat transfer stems mainly from parts of the beam that are far from the focus and is caused by many weak Coulomb deflections in those domains. The formula obtained is fairly complicated. The main result is that the probe diameter $d_c = 2(A_c/\pi)^{1/2}$ increases as the square root of the beam current I and is proportional to the distance l between focus and diaphragm.

The most important result for practical applications to emerge from the more recent theories (Rose and Spehr, 1983; van Leeuwen and Jansen, 1983) is that the spatial Boersch effect causes the radius of a small electron probe to increase linearly with the working distance between the probe and the principal plane of the final lens. Consequently, in electron lithography devices, this working distance should be made as small as possible subject to any technical constraints. The energetic Boersch effect, being proportional to the square root of the beam current in practice, gives rise to increased chromatic aberrations; the consequent undesirable beam spreading can be reduced only by designing electron optical systems with very low aberration coefficients.

The various theories have been compared in the light of dimensional analysis by Puretz (1986). In spite of the importance of the Boersch effects in practical optics, and despite the many experimental and theoretical investigations that have been devoted to them, our present knowledge about their origin and behaviour is still incomplete. The fullest study to date is contained in the work of Jansen already mentioned (Jansen, 1990; Kruit and Jansen, 2009). The discussion in Plies (1994) is also clear and scholarly.

Brightness

The concept of *brightness* in electron optics is very similar to the corresponding notion in light optics. The brightness of an electron beam will prove to be a property that is invariant with respect to the focusing action of lenses, provided that the latter have no net effect on the accelerating voltage of the beam.

In the last 50 years there have been many experimental and theoretical investigations of the brightness properties of electron beams, and although the aims and formulations often appear quite different at first sight, the ideas are basically equivalent. Langmuir (1937) investigated the brightness of thermionic electron guns and soon after, von Borries and Ruska (1939) introduced an average brightness[1] $\overline{B}$, defined as the emission current ΔI per element of area Δa normal to the beam and per element of solid angle $\Delta\Omega$, so that

$$\overline{B} = \Delta I/\Delta a\Delta\Omega \tag{47.1a}$$

This definition is widely and understandably adopted by experimentalists. Nevertheless, such a definition of $\overline{B}$ depends on the particular choice of Δa and $\Delta\Omega$, and Lenz (1957) therefore replaced it by its appropriate mathematical limit, in Cartesian coordinates given by

$$B(x, y, z, x', y') = \lim_{\Delta a \to 0} \lim_{\Delta\Omega \to 0} \left(\frac{\Delta I}{\Delta a \Delta\Omega} \right) \tag{47.1b}$$

Here Δa is the element of area $\Delta x \Delta y$ in the vicinity of the point (x, y, z); this element is thus located in the appropriate coordinate plane $z = \text{const.}$ $\Delta\Omega = \Delta x' \Delta y'$ is the element of solid angle in the vicinity of the direction given by the two components of gradient (x', y'); this implies that $x'^2 + y'^2 \ll 1$. Lenz called this quantity B the *brightness function*. Later Kasper and Lenz (1966) generalized this definition to include beams with an arbitrary curved optic axis. Although (47.1b) is a more satisfactory definition than that of $\overline{B}$, it still leaves something to be desired. The first reason is that Eq. (47.1b) is essentially a *paraxial* definition; this prevents it from being employed in the vicinity of cathode surfaces and, furthermore, we shall not know whether any invariance properties that it may possess are affected by aberrations. The second reason is that the presence of the limit-operation in

[1] This quantity was originally called the *Richtstrahlwert* and this term has been widely used, not only in German texts.

Principles of Electron Optics: Applied Geometrical Optics.
DOI: http://dx.doi.org/10.1016/B978-0-12-813369-9.00047-6

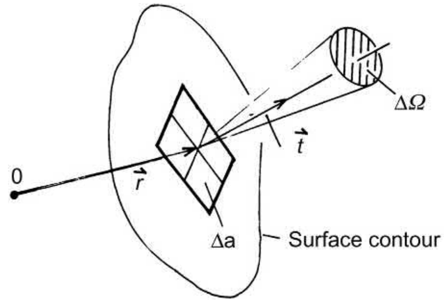

Figure 47.1
Elements of area and solid angle employed in the definition of brightness. Δa is an element of surface; $\Delta\Omega$ is an element of solid angle, the axis of which coincides with the unit vector $\boldsymbol{t}$ normal to the surface.

Eq. (47.1b) makes it impossible to measure the brightness function directly; the latter can only be obtained by numerical evaluation of sets of experimental data. Such numerical data processing is, however, inevitable in order to overcome the arbitrariness in the choice of the elements Δa and $\Delta\Omega$.

In order to escape the restriction of paraxiality, we introduce the definition

$$B(\boldsymbol{r},\boldsymbol{t}) = \lim_{\Delta a \to 0} \lim_{\Delta\Omega \to 0} \left(\frac{\Delta I}{\Delta a \Delta\Omega} \right) \tag{47.2}$$

which is very similar to Eq. (47.1b), but here $\boldsymbol{t}$ is a unit vector in an *arbitrary* given direction, $\Delta\Omega$ is an element of solid angle in the vicinity of this direction and Δa a surface element *normal* to it. This is illustrated in Fig. 47.1. The vector $\boldsymbol{t}$ will usually be the local tangent vector of an electron trajectory passing through the point $\boldsymbol{r}$. We shall find that the definition (47.2) has many interesting and useful properties. Whenever it is necessary to distinguish between the different definitions, we shall refer to (47.2) as the *generalized brightness function*.

For a useful discussion of the definitions of brightness and their use in practice, see Eades (1994).

With the growing interest in very small emitters, of which carbon nanotubes are the most common, the notion of brightness needs to be reconsidered. Indeed, in some situations it ceases to be a meaningful measure of the beam quality (Kruit et al., 2006). We comment briefly on this situation in Section 50.7.

47.1 Application of Liouville's Theorem

When particle interactions are negligible, the propagation of electron beams can be treated very conveniently in a six-dimensional phase space. In this connection, we shall need the definitions and relations given in Section 44.1 More generally, the Hamiltonian (44.5) will be replaced by the relativistic expression (4.28) with $Q = -e$, since we are also interested in the brightness of electron beams outside the electron gun.

We first complete the definitions (44.3) and (44.4) by introducing the phase velocity:

$$\boldsymbol{v}^* := \frac{d}{dt}\boldsymbol{r}^* = \left(\dot{x}, \dot{y}, \dot{z}, \dot{p}_x, \dot{p}_y, \dot{p}_z\right) \tag{47.3}$$

and a phase current density:

$$\boldsymbol{j}^* := \rho^* \boldsymbol{v}^* \tag{47.4}$$

The canonical equations $\dot{\boldsymbol{r}} = \partial H/\partial \boldsymbol{p}$, $\dot{\boldsymbol{p}} = -\partial H/\partial \boldsymbol{r}$(4.29, 4.30) can be rewritten in six-dimensional form as

$$\nabla^* \boldsymbol{v}^* = 0 \tag{47.5}$$

which means that the six-dimensional velocity field is source-free; here ∇^* denotes the six-dimensional nabla-operator (div).

Since no particles are created or destroyed, the continuity equation

$$\frac{\partial \rho^*}{\partial t} + \nabla^* \boldsymbol{j}^* = 0 \tag{46.6}$$

must be satisfied. In the stationary case, the first term vanishes. Carrying out the necessary differentiation and using Eq. (47.4), we obtain

$$\frac{d\rho^*}{dt} = \boldsymbol{v}^* \cdot \nabla^* \rho^*(\boldsymbol{r}^*(t)) = 0$$

which can be integrated to give

$$\rho^*(\boldsymbol{r}^*(t)) = \text{const} \tag{47.7}$$

This is *Liouville's theorem*, which states that along each particle trajectory the phase density ρ^* is constant with respect to time and hence determined uniquely by the initial conditions. Thus this theorem enables us to find relations between properties at different positions on a trajectory and, in particular, to establish any invariance properties.

In order to find an expression for the generalized brightness $B(\boldsymbol{r}, \boldsymbol{t})$, we start from Eq. (44.8) in differential form:

$$d^3\boldsymbol{j} = e\boldsymbol{v}\rho^*(\boldsymbol{r}^*)d^3\boldsymbol{p}$$

$\boldsymbol{p} = \boldsymbol{g} - e\boldsymbol{A}$ being the *canonical* momentum. The latter is rather inconvenient as a variable of integration. At each *fixed* three-dimensional position $\boldsymbol{r}$ we have $d^3\boldsymbol{p} = d^3\boldsymbol{g} = g^2 dg d\Omega$, $d\Omega$

being the element of solid angle in momentum space, which corresponds to the element of solid angle of trajectory directions. Using $\boldsymbol{\upsilon} dg = \upsilon \boldsymbol{t} dg = \boldsymbol{t} dE$, we obtain

$$d^3\boldsymbol{j} = e\rho^*(\boldsymbol{r}^*)g^2 dE d\Omega \boldsymbol{t}$$

Integration over all energies E results in

$$d^2\boldsymbol{j} = e\boldsymbol{t}\left(\int_{-\infty}^{\infty} \rho^*(\boldsymbol{r}^*)g^2(\boldsymbol{r}, E)dE\right)d\Omega$$

From the definition (47.2), it is obvious that $d^2\boldsymbol{j} = \boldsymbol{t}Bd\Omega$, since $\boldsymbol{t}\lim(\Delta I/\Delta a) = \boldsymbol{j}$. Hence we finally obtain the integral representation

$$B(\boldsymbol{r}, \boldsymbol{t}) = e\int_{-\infty}^{\infty} \rho^*(\boldsymbol{r}^*)g^2(\boldsymbol{r}, E)dE \tag{47.8}$$

which is always valid. One factor, g^2, the square of the kinetic momentum, is easily evaluated at any position $\boldsymbol{r}$ in space (see Eq. 2.13) with $\boldsymbol{Q} = -e$ and $E_0 \to E$); the other factor ρ^* is most easily evaluated at the cathode surface.

47.2 The Maximum Brightness

We come now to the practical evaluation of (47.8). This is most straightforward for *thermionic guns*, since for these ρ^* depends only on E. In the factor $g^2(\boldsymbol{r}, E)$ we may neglect the very small quadratic term in E and so, with $\varepsilon := e/2m_0c^2$ as usual, we have

$$g^2(\boldsymbol{r}, E) = 2m_0E\{1 + 2\varepsilon\Phi(\boldsymbol{r})\} + 2m_0e\Phi(\boldsymbol{r})\{1 + \varepsilon\Phi(\boldsymbol{r})\}$$

We recall that the expression $\hat{\Phi} = \Phi(1 + \varepsilon\Phi)$ is the relativistic accelerating potential. In (47.8) the integrals $\int \rho^* dE$ and $\int E\rho^*(E)\, dE$ remain to be evaluated. With (44.11) this is straightforward:

$$\int_0^{\infty} \rho^*(E)dE = \frac{2kT}{h^3}\exp\left(-\frac{W}{kT}\right)$$

$$\int_0^{\infty} E\rho^*(E)dE = \frac{2k^2T^2}{h^3}\exp\left(-\frac{W}{kT}\right)$$

Introducing all these expressions into (47.8) and using (44.12a,b), we can put the result into a very concise form:

$$B(\boldsymbol{r}, \boldsymbol{t}) = \frac{ej_s}{\pi kT}\hat{\Phi}_T(\boldsymbol{r}) \tag{47.9a}$$

with

$$\Phi_T := \Phi + \frac{kT}{e}, \quad \hat{\Phi}_T = \Phi_T(1 + \varepsilon\Phi_T) \tag{47.9b}$$

The dependence of B on the direction $\boldsymbol{t}$ has cancelled out in the integration. This is a characteristic property of thermionic emission and in particular a consequence of Eq. (44.11) in which $\boldsymbol{t}$ does not appear. Thermionic emission is just characterized by a transmission factor $D = 1$ for all electrons with sufficient energy, regardless of the direction $\boldsymbol{t}$. This property of the brightness is again discussed at the end of Section 47.3.

At the cathode surface with $\Phi = 0$ and $kT \ll m_0c^2$, Eq. (47.9a) simplifies to $B = j_s/\pi$. This is the *maximum* value $\tilde{B}(0)$ of the angular distribution function $\tilde{B}(\gamma)$ in (44.17). Far from the cathode, we can neglect the term kT/e in (47.9b), so that $\hat{\Phi}_T \approx \hat{\Phi}$. We then obtain the familiar result that the brightness B is proportional to the common accelerating potential $\hat{\Phi}(\boldsymbol{r})$.

Eqs (47.9a) and (47.9b) can be generalized in two ways:

i. In the case of *Schottky emission*, the expression (44.42) for j_s is to be introduced. Furthermore, expression (47.9b) for Φ_T is to be replaced by $\Phi_T := \Phi + (kT + \delta W)/e$, since the potential barrier is lowered by $\delta W/e$.
ii. In the case of emission limited by *space charge*, the accelerating potential is to be replaced by

$$\Phi_T = \frac{1}{e}\tilde{E}_{\mathrm{kin}} = \Phi - \Phi_m + \frac{kT}{e}, \quad \hat{\Phi}_T = \Phi_T(1 + \varepsilon\Phi_T) \tag{47.10a}$$

and the saturation current density j_s is to be replaced by the reduced value at the minimum of the potential barrier ($r = r_m$). The latter implies that the factor $\exp(e\Phi_m/kT)$ must be introduced so that now

$$B = \frac{ej_s}{\pi kT}\exp\left(\frac{e\Phi_m}{kT}\right)\hat{\Phi}_T(\boldsymbol{r}) \tag{47.10b}$$

This formula is not widely known, though it is obvious that it is more correct than Eq. (47.9a).

The expression for the brightness of *field emission* guns is slightly more complicated, since the phase density ρ^* in (47.8) is not a function of E alone. The full calculation requires a knowledge of the transformation between the emission angle γ and the corresponding inclination at the point $\boldsymbol{r}$ of reference; this is generally very complicated. The expression for the *maximum* brightness, however, is fairly simple. From Eq. (44.35), this maximum is given in the vicinity of the cathode by

$$\tilde{B}(0) = -\frac{j_T}{\pi d}V(\boldsymbol{r}) = B_{\max} \tag{47.11a}$$

Farther away from the cathode we must replace the accelerating energy $e\Phi$ by the appropriate relativistic expression $e\hat{\Phi}$, giving

$$B_{\max}(\boldsymbol{r}) = \frac{ej_T}{\pi d}\hat{\Phi}(\boldsymbol{r}) \tag{47.11b}$$

This expression resembles Eq. (47.9a): we have only to make the exchanges $j_s \leftrightarrow j_T$, $kT \leftrightarrow d$, a symmetry that has already been noticed in Chapter 44, Theory of Electron Emission.

Substitution of common values of the physical quantities into these formulae shows that in thermionic systems $B \sim 10^2$ A cm^{-2} sr^{-1}, in systems with strong Schottky emission (LaB_6 cathodes) $B \sim 10^4$ A cm^{-2} sr^{-1} and in good field-emission systems values up to 10^9 A cm^{-2} sr^{-1} can be reached. The brightness can of course apparently be increased indefinitely by increasing the voltage Φ, but in most practical cases $\Phi \sim 300$ kV is an upper limit; the higher brightness is noticeable in high-voltage microscopes operating in the megavolt range.

The dependence of the brightness on the choice of the accelerating potential led Fink and Schumacher (1975) and Schumacher (1976) to introduce a 'normalized' or reduced brightness

$$R := B/\hat{\Phi}$$

If we neglect the term kT/e in (47.9b), we obtain the simple formula

$$R_T = \frac{ej_s}{\pi kT} \tag{47.12}$$

for thermionic guns. From Eq. (47.11) it is obvious that

$$R_F = \frac{ej_T}{\pi d} \tag{47.13}$$

is the maximum normalized brightness of field-emission guns. These formulae express physical properties of the emitting surfaces alone. Since $R_F \gg R_T$, it seems obvious that field-emission guns are preferable and in practice, cold field-emission guns or Schottky guns are found in most modern electron microscopes, including scanning electron microscopes. The benefits of high brightness override the need for a very high vacuum, the instability of the emission when the pressure is not quite low enough and the disadvantage of low total emission current as well as some purely technological problems.

Before we go over to the next topic, we emphasize that the maximum normalized brightness R_T (or R_F) is the only truly invariant property of an electron emission source. It does not depend on focusing properties or lens aberrations, but its value is reduced by the Boersch effect (Section 46.4). The measurement of values lower than the theoretical limit, in cases where the Boersch effect can be neglected, is clearly a consequence of the averaging in the determination of $\overline{B}$, see Eq. (44.1a).

47.3 The Influence of Apertures

In the derivation of (47.8) and its special cases, we have tacitly assumed that all electrons with trajectories running from the cathode surface to the point $\boldsymbol{r}$ of reference will reach this point. Actually this is *not* the case, since some of these trajectories will be intercepted at any aperture stops placed across the beam to reduce aberrations. For thermionic electron guns, this question was first investigated by Langmuir (1937). Analogous considerations are, of course, necessary for field-emission guns, but they will be more complicated, since (44.30) is far more complicated than (44.14a). We therefore first present a simplified derivation and then try to generalize the result.

The physical situation is sketched in Fig. 47.2. We consider an emitting surface element in the vicinity of the apex. If we neglect aberrations, this surface element will be imaged as a magnified (or demagnified) element in the corresponding conjugate plane $z = z_i$, $M_L = |\Delta y_i / \Delta y_o|$ being the lateral magnification. From Abbe's sine condition we obtain a relation between the transverse components of the momenta:

$$q \;\coloneqq p_0 \sin\gamma = p_i M_L \sin\beta \tag{47.14a}$$

We now assume that $M_L^2 \sin^2\beta \ll 1$, which is justified for $M \leq 10$, $\beta \leq 10^{-2}$. The aperture stop shown in Fig. 47.2 then confines the transmission of transverse momenta q, but does not affect the longitudinal component. For larger values of $M_L^2 \sin^2\beta$ this is not true, but such cases are of little interest. With $\beta \leq \theta$ we obtain the upper limit:

$$q \leq q_m = p_i M_L \sin\theta \approx p_i M_L \theta \tag{47.14b}$$

We now return to the transverse distributions (44.18a,b) and (44.36a,b). Both are rotationally symmetric Gaussian distributions. With $q^2 = p_x^2 + p_y^2$ we can put them into a common form:

$$dj = \frac{j_0}{m_0 \tau} \exp\left(-\frac{q^2}{2 m_0 \tau}\right) q\, dq \tag{47.15a}$$

with j_0 being given by Eq. (44.42) or by (44.27) and

$$\tau = \begin{cases} kT & \text{for thermionic guns} \\ d & \text{for field emission guns} \end{cases} \tag{47.15b}$$

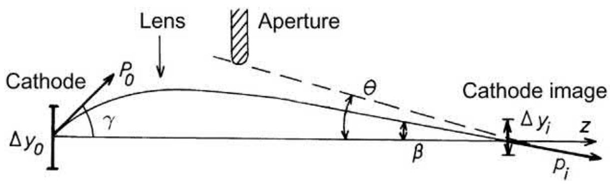

Figure 47.2
Imaging of an element of the cathode surface with the associated notation.

An additional factor M_L^{-2} arises from the magnification; the current density in the image element is thus given by

$$j_i = \frac{j_0}{m_0 \tau\, M_L^2} \int_0^{q_m} \exp\left(-\frac{q^2}{2m_0\tau}\right) q\, dq = \frac{j_0}{M_L^2}\left\{1 - \exp\left(-\frac{q_m^2}{2m_0\tau}\right)\right\}$$

q_m being given by Eq. (47.14b). With $p_i^2 = 2m_0 e\hat{\phi}_i$, we obtain the relativistically correct formula:

$$j_i = j_0 M_L^{-2}\left\{1 - \exp\left(-\frac{e\hat{\phi}_i}{\tau}\, M_L^2 \sin^2\theta\right)\right\} \tag{47.16}$$

A still more exact formula, which contains (47.16) and Langmuir's formula as special cases, is

$$j_i = j_0 M_L^{-2}\left[1 - \left(1 - M_L^2 \sin^2\theta\right)\exp\left\{-\frac{e\hat{\phi}_i M_L^2 \sin^2\theta}{\tau\left(1 - M_L^2\sin^2\theta\right)}\right\}\right] \tag{47.17}$$

An analogous formula can be derived for line foci:

$$j_i = j_0 M_L^{-1}\left[\operatorname{erf}\left(\frac{\lambda^2\kappa}{1-\lambda^2}\right)^{1/2} + \lambda\, \exp(\kappa)\left\{1 - \operatorname{erf}\left(\frac{\kappa}{1-\lambda^2}\right)^{1/2}\right\}\right]$$

with $\lambda := M_L \sin\theta$, $\kappa := e\hat{\phi}_i/\tau$.

We now examine the implications of Eq. (47.17) for two extreme cases.

i. *Large apertures*: the absolute value of the exponent is a large number and the whole exponential term can therefore be neglected. The simplified relation $j_i = j_0 M_L^{-2}$ expresses the obvious diminution of the intensity due to magnified imaging. This result is to be expected if the aperture transmits *all* the electrons emitted from the surface element on the cathode.
ii. *Narrow apertures*: if $M_L^2\theta^2 \ll 1$ but $e\hat{\phi}_i \gg \tau$, Eq. (47.16) should be used. In the extreme case in which the exponent is a small quantity even though $e\hat{\phi}_i \gg \tau$, we may expand the exponential function as a power series and terminate the latter after the linear term. This gives

$$j_i = j_0\left(1 + e\hat{\phi}_i/\tau\right)\sin^2\theta \;\approx\; e\hat{\phi}_i \tau^{-1} j_0 \theta^2$$

iii. With the aid of (47.9a) and (47.11), we can put the result into the more convenient form

$$j_i = \pi B_i \sin^2\theta$$

B_i being the axial brightness in the image plane. This result is in agreement with that obtained in the simpler case of a *uniformly* illuminated aperture.

Recalling that the brightness was originally introduced as a distribution of current density in a given direction per unit solid angle, we can find the expression for the brightness corresponding to (47.17). If we replace the (maximum) semiaperture angle θ by the variable β, Eq. (47.17) gives the fraction of the current density incident inside a cone of semiangle β. The brightness is then obtained by differentiation:

$$\begin{aligned} B_i^*(\beta) &:= \frac{1}{\cos\beta}\frac{dj_i(\beta)}{d\Omega_\beta} = \frac{1}{2\pi\cos\beta\sin\beta}\frac{dj_i(\beta)}{d\beta} \\ &= \frac{j_0}{\pi}\left(1 + \frac{e\hat{\phi}_i}{\tau\left(1 - M_L^2\sin^2\beta\right)}\right)\exp\left(-\frac{e\hat{\phi}_i M_L^2\sin^2\beta}{\tau\left(1 - M_L^2\sin^2\beta\right)}\right) \end{aligned} \tag{47.18}$$

In many practical cases $M_L^2\beta^2 \ll 1$ and we then obtain the simpler formula

$$B_i^*(\beta) = B_{i,\max}\exp\left(-e\hat{\phi}_i M_L^2\beta^2\tau^{-1}\right) \tag{47.19}$$

from which we see that the angular distribution of the incident intensity is *Gaussian*. Without explicit proof, we mention that the same conclusion also holds for the *virtual* imaging treated in Section 45.2. This is clearly true since in both cases only Abbe's sine condition has been used. We recall that the diode model furnished the relation $M_L = 1/M_A\sqrt{\mu}$, M_A and μ being defined in Section 45.2.

The conclusions reached so far in this section hold only for a single emitting cathode spot, for reasons of simplicity assumed to be at the apex; for this reason we have introduced the notation $B_i^*(\beta)$ instead of $B_i(\beta)$. Eq. (47.19) is useful if the emission from the cathode surface is so non-uniform that small single spots can be clearly distinguished. In reality, the brightness $B(\boldsymbol{r}, \boldsymbol{t})$ at a fixed point $\boldsymbol{r}$ and in a fixed direction $\boldsymbol{t}$ results from the contributions of *many* surface elements. Note that in Eq. (47.8) an integration is made over all energies E! This implies that electrons with different initial conditions at the cathode surface can reach the same final configuration $(\boldsymbol{r}, \boldsymbol{t})$ and thus contribute to the integral. From Eq. (47.9a) we notice that the resultant brightness is independent of the direction $\boldsymbol{t}$. This is a fundamental consequence of Lambert's law (44.17). The corresponding law is well known in light optics (where it is found to be a consequence of the definition of the photometric brightness and of the assumption that the emitting surface is plane and the radiation isotropic: see Born and Wolf, Section 4.8.1).

For thermionic sources the relation between Eqs (47.19) and (47.9a) is quite simple. Since $\tau \equiv kT \ll e\hat{\phi}_i$ the maximum value $B_{i,\max} = j_0(1 + e\hat{\phi}_i/\tau)/\pi$ in Eq. (47.19) is in practice identical with Eq. (47.9a) at $\boldsymbol{r} = \boldsymbol{r}_i$. The superposition is hence of such a kind that the *maximum* value (47.9a) is obtained everywhere on the equipotential $\Phi(\boldsymbol{r}) = \text{const}$. For field-emission sources a similar conclusion can be drawn (Kasper, 1982), but this is only approximately valid since field emission does not obey Lambert's law.

47.4 Lenz's Brightness Theory

A brightness theory that is very useful for the mathematical investigation of electron beams, even at large distances from the cathode, was developed by Lenz (1957) and later generalized by Kasper and Lenz (1966). Although it can be very helpful, it has not found widespread application, probably because experimentalists cannot measure the brightness *function* directly. This difficulty will be dealt with later. We first present here the theory for paraxial relativistic motion in rotationally symmetric electrostatic fields including the influence of space charge. We then explain how the theory can be generalized to arbitrary paraxial systems, in which the optic axis may be curved. See also Section 48.3, where the emittance is related to brightness.

47.4.1 Rotationally Symmetric Electrostatic Fields

The paraxial ray equation is given by

$$u'' + \frac{\gamma}{2}\frac{\phi'}{\hat{\phi}}u' + \frac{\gamma}{4\hat{\phi}}\left\{\phi'' + \frac{1}{\varepsilon_0}\rho_0(z)\right\}u = 0 \tag{47.20}$$

where $u(z) = x(z) + iy(z)$, $\phi(z)$ is the axial potential and $\rho_0(z)$ the axial space charge density. It is convenient to work in terms of the reduced brightness, R:

$$B(\boldsymbol{r}, \boldsymbol{t}) = R(x, y; x', y'; z)\,\hat{\Phi}(\boldsymbol{r}) \tag{47.21}$$

From Eq. (47.8) and Liouville's theorem together with the conservation of energy, we conclude that R must be constant along each trajectory, this constant value depending on the initial conditions; hence we have exactly

$$\frac{dR}{dz} = \frac{\partial R}{\partial x}x' + \frac{\partial R}{\partial y}y' + \frac{\partial R}{\partial x'}x'' + \frac{\partial R}{\partial y'}y'' + \frac{\partial R}{\partial z} = 0$$

Eliminating the derivatives of second order by means of (47.20), we obtain in the paraxial approximation

$$\begin{aligned}&\frac{\partial R}{\partial x}x' + \frac{\partial R}{\partial y}y' - \frac{\gamma}{2}\frac{\phi'}{\hat{\phi}}\left(\frac{\partial R}{\partial x'}x' + \frac{\partial R}{\partial y'}y'\right)\\ &\quad - \frac{\gamma}{4\hat{\phi}}\left(\phi'' + \frac{\rho_0(z)}{\varepsilon_0}\right)\left(\frac{\partial R}{\partial x'}x + \frac{\partial R}{\partial y'}y\right) + \frac{\partial R}{\partial z} = 0\end{aligned} \tag{47.22}$$

A solution of this homogeneous linear partial differential equation is an exponential function with a quadratic exponent. Since we are seeking a rotationally symmetric solution, we substitute an expression of the form

$$R = R_0 \exp\left[-\sqrt{\frac{\hat{\phi}(z)}{\hat{\phi}_0}}\left\{a(z)\left(x^2+y^2\right)+2b(z)(xx'+yy')+c(z)\left(x'^2+y'^2\right)\right\}\right] \tag{47.23}$$

into Eq. (47.22), R_0 and $\hat{\phi}_0$ being free constants and $a(z)$, $b(z)$, $c(z)$ functions to be determined. By treating $x^2 + y^2$, $2(xx' + yy')$ and $x'^2 + y'^2$ as linearly independent functions of z and noting that $\hat{\phi}'/\hat{\phi} = \gamma\phi'/\hat{\phi}$, we obtain three ordinary coupled differential equations for a, b and c:

$$a' + \frac{\gamma}{2}\frac{\phi'}{\hat{\phi}}a - \frac{\gamma}{2\hat{\phi}}\left(\phi'' + \frac{\rho_0}{\varepsilon_0}\right)b = 0 \tag{47.24a}$$

$$b' + a - \frac{\gamma}{4\hat{\phi}}\left(\phi'' + \frac{\rho_0}{\varepsilon_0}\right)c = 0 \tag{47.24b}$$

$$c' - \frac{\gamma}{2}\frac{\phi'}{\hat{\phi}}c + 2b = 0 \tag{47.24c}$$

One constant of integration is given by the discriminant:

$$\Delta := a(z)c(z) - b^2(z) = \text{const} > 0 \tag{47.25}$$

The solutions of (47.24a–c) are uniquely determined by the initial values a_0, b_0, c_0 in a starting plane $z = z_0$; there, of course, $\Delta = a_0c_0 - b_0^2$. The system (47.24) is only linear in the absence of space charge, as we shall see below.

The practical value of the theory lies in the fact that, once the reduced brightness $R(x, y; x', y'; z)$ has been calculated, it can be used to determine expectation values. In this connection, it is sufficient to make the approximation $\hat{\Phi}(\boldsymbol{r}) \approx \hat{\phi}(z)$ in Eq. (47.21).

The most important expectation value is the local current density:

$$j(\boldsymbol{r}) := \hat{\phi}(z)\int_{-\infty}^{\infty}\int_{-\infty}^{\infty} R(x, y; x', y'; z)\, dx'dy'$$

for which we obtain the Gaussian distribution:

$$j(\boldsymbol{r}) = \frac{\pi R_0\sqrt{\hat{\phi}_0\hat{\phi}(z)}}{c(z)}\exp\left\{-\sqrt{\frac{\hat{\phi}(z)}{\hat{\phi}_0}}\frac{\Delta}{c(z)}\left(x^2+y^2\right)\right\} \tag{47.26}$$

A further integration yields the total beam current:

$$I = \int_{-\infty}^{\infty} \int_{-\infty}^{\infty} j(\boldsymbol{r})\, dxdy = \frac{\pi^2 R_0 \hat{\phi}_0}{\Delta} = \text{const} \tag{47.27}$$

which is conserved as it must be. Eq. (47.26) also enables us to determine the space charge density. In the paraxial approximation we have

$$j = j_z, \quad v = v_z = \frac{1}{\gamma}\sqrt{\frac{2e}{m_0}\hat{\phi}(z)}, \quad \rho = -\frac{j_z}{v_z} = -\frac{j}{v}$$

where as usual $\gamma = m/m_0 = 1 + 2\varepsilon\phi$.

From Eq. (47.26) we then obtain

$$\rho(\boldsymbol{r}) = \rho_0(z)\exp\left\{-\sqrt{\frac{\hat{\phi}(z)}{\hat{\phi}_0}}\;\frac{\Delta}{c(z)}\left(x^2 + y^2\right)\right\} \tag{47.28a}$$

with the axial space charge density:

$$\rho_0(z) = -\frac{\pi R_0 \gamma}{c(z)}\sqrt{\frac{m_0\hat{\phi}_0}{2e}} = -\frac{\gamma I \Delta}{\pi c(z)}\sqrt{\frac{m_0}{2e\hat{\phi}_0}} \tag{47.28b}$$

Introducing this into Eq. (47.24), we see that this system of differential equations is *nonlinear*.

Another distribution function of interest is that describing the directions in the beam:

$$F(x', y', z) := \frac{\hat{\phi}(z)}{I}\int_{-\infty}^{\infty}\int_{-\infty}^{\infty} R(x, y; x', y'; z)\, dxdy \tag{47.29a}$$

It is normalized so that $\int\int F dx'dy' = 1$ and hence F may be interpreted as the directional probability density. Evaluation of (47.29a) results in the Gaussian distribution:

$$F(x', y', z) = \frac{\Delta}{\pi a(z)}\sqrt{\frac{\hat{\phi}(z)}{\hat{\phi}_0}}\exp\left\{-\sqrt{\frac{\hat{\phi}(z)}{\hat{\phi}_0}}\;\frac{\Delta}{a(z)}\left(x'^2 + y'^2\right)\right\} \tag{47.29b}$$

This result is in accordance with Eq. (47.19), since $\beta^2 = x'^2 + y'^2$. This may help to attach a physical meaning to the somewhat abstract form of (47.23).

A very interesting feature of this theory is that it shows us how to analyse the focusing of an extended electron beam. The narrowest cross-section, the *crossover*, lies in the plane

$z = z_c$, in which the radial width of (47.26) has its minimum. This means that $c/\hat{\phi}^{1/2}$ must pass through a minimum which implies that $c'/c = \hat{\phi}'/2\hat{\phi}$. Introducing this into Eq. (47.24c) we find that $b(z_c) = 0$. Since the term in $b(z)$ causes the coupling between x, y and x', y' in Eq. (47.23), $b(z_c) = 0$ means that in the plane of the crossover the brightness function separates into a product

$$B(x, y, x', y', z_c) = j(x, y, z_c)F(x', y', z_c) \tag{47.30}$$

Furthermore, the crossover can be defined as the 'optimum' case of an uncertainty relation. Let $r_0(z)$ and $s_0(z)$ be those widths, for which the distributions (47.26) and (47.29a), respectively, have decreased to e^{-1} of their axial values; we then have

$$\sqrt{\hat{\phi}/\hat{\phi}_0}r_0 s_0 = \frac{1}{\Delta}\sqrt{ac} \equiv \frac{1}{\Delta}\sqrt{\Delta + b^2} \geq \frac{1}{\sqrt{\Delta}} \tag{47.31}$$

and so $b(z_c) = 0$ is the only case in which the equality holds.

Still another interesting aspect of Lenz's theory is its application to electron beams with *high perveance*. For reasons of simplicity we assume that there is no external electric field. Since the space-charge field is mainly in the radial direction, $\phi(z) = \text{const} = \phi_0$ is a good approximation. Introducing (47.28a) into (47.24), we notice that the dimensionless constant

$$P := \frac{I\gamma^2}{2\pi\varepsilon_0}\sqrt{\frac{m_0}{2e\hat{\phi}_0^3}} \tag{47.32}$$

appears in the theory. The perveance is usually defined to be $I\hat{\phi}_0^{-3/2}$, but since the latter always appears in the above combination, we shall refer to P as the perveance. This expression is of great importance in equipment using high-intensity beams, since it is a qualitative measure of the influence of space charge on the focusing of the beam; with high perveance, the focus is broadened by the Coulomb forces acting in the beam. Equations (47.24) now take the form

$$a' = -Pb\Delta/c, \quad b' = -a - P\Delta/2, \quad c' = -2b$$

These can be reduced to a quadrature formula. We assume that the initial values are a_0, b_0, c_0 at $z = z_0$. We see that

$$a' = \frac{1}{2}P\Delta\frac{c'}{c} \rightarrow a = a_0 + \frac{1}{2}P\Delta\ln\left(\frac{c}{c_0}\right)$$

Since Eq. (47.25) is still valid, the next step is

$$b^2 = b_0^2 + ac - a_0c_0 = b_0^2 + a_0(c - c_0) + \frac{1}{2}P\Delta\ln\left(\frac{c}{c_0}\right)$$

Introducing this into $c' = -2b$, we obtain a differential equation for $c(z)$, which can be formally solved after some rearrangement. In order to bring out the physical meaning of the solution, we introduce the distribution widths of (47.26) and (47.29a), respectively:

$$r_0(z) = \sqrt{\frac{c(z)}{\Delta}}, \quad s_0(z) = \sqrt{\frac{a(z)}{\Delta}} \tag{47.33}$$

There is no loss of generality if the plane $z = z_0$ is chosen to coincide with a crossover. We then have $\Delta = a_0 c_0$, $b_0 = 0$, and the initial values of r_0 and s_0 are

$$r_0(z_0) =: \rho_0 = \frac{1}{\sqrt{a_0}}, \quad s_0(z_0) =: \sigma_0 = \frac{1}{\sqrt{c_0}}$$

Introducing the dimensionless variable of integration $u = c(z)/c_0$ with $1 \le u \le r_0^2(z)/\rho_0^2$, we finally obtain

$$z - z_0 = \pm \frac{\rho_0}{2\sigma_0} \int_1^{(r_0/\rho_0)^2} \frac{du}{\sqrt{u - 1 + \frac{1}{2} P \sigma_0^{-2} u \ln u}} \tag{47.34}$$

The inverse function is the required beam profile $r_0 = r_0(z)$. This is *symmetric* about the crossover plane: $r_0(z_0 + \zeta) = r_0(z_0 - \zeta)$ for all values of ζ.

We now discuss two limiting special cases, which illustrate the meaning of Eq. (47.34).

i. *Vanishing perveance P*: the integration and inversion are now elementary and result in

$$r_0(z) = \sqrt{\rho_0^2 + \sigma_0^2 (z - z_0)^2}, \quad s_0(z) = \sigma_0 = \text{const}$$

The profile of a beam free of space charge is hyperbolic and the angular distribution in it is independent of z.

ii. *Extremely high perveance P*: we are justified in retaining only the logarithmic term in the denominator of (47.34); with $u =: \exp(2y^2)$, we obtain the representation

$$z - z_0 = \pm \frac{2\rho_0}{\sqrt{P}} \int_0^{\sqrt{\ln(r_0/\rho_0)}} \exp(y^2) dy$$

This integral is not elementary. A good approximation for small values of $|z - z_0|$ is

$$z - z_0 = \pm 2.09\, \rho_0 P^{-1/2} \sqrt{\frac{r_0}{\rho_0} - 1}, \quad \frac{r_0}{\rho_0} \le 2$$

This leads to a quadratic beam profile in the vicinity of the crossover:

$$r_0(z) = \rho_0 + 0.229\, P \rho_0^{-1} (z - z_0)^2 \quad (r_0 \le 2\rho_0)$$

and P is then proportional to the curvature r_0'' of the beam waist.

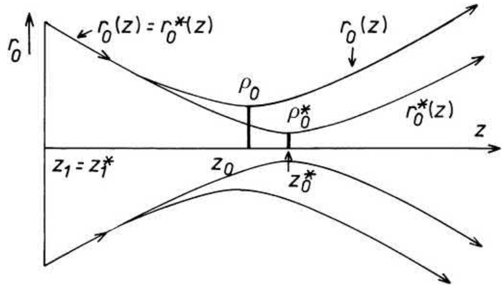

Figure 47.3
Electron beam profiles in axial section. Two beams are shown with different perveances but with identical initial conditions in the plane $z = z_1$. Quantities labelled with an asterisk refer to the beam with vanishing perveance.

Fig. 47.3 shows the width-function $r_0(z)$ for two electron beams with the same initial conditions in a plane $z = z_1$ but different perveances. With increasing perveance, the crossover increases in size and shifts towards the starting plane $z = z_1$. These results are essentially the same as those obtained by Watson (1927), but in Lenz's theory Watson's unrealistic assumption that the boundary of the beam is sharp has been removed.

47.4.2 The Generalized Theory

In the preceding section, the theory was presented in such a way that experimental results could be compared with its previsions. The theory has in fact been generalized by Kasper and Lenz (1966) for arbitrary paraxial systems, even those with curved optic axes.
A theory of such generality can, of course, lead only to very formal results. Furthermore, the formalism is still paraxial; a brightness theory including aberrations is unknown to the authors.

Since the brightness is of most interest close to the curved axis of a system consisting of an electron gun and deflecting elements, we denote the arc-length along this axis by z.
A straight optic axis is then a special case. The coordinates normal to the optic axis are denoted by x and y as usual. The construction of such a coordinate system is explained in Chapter 51, General Curvilinear Systems. If a magnetic field, rotationally symmetric about the axis, is present, the resulting Larmor rotation is denoted by $\theta(z)$. For such a magnetic field to be present, there must be a straight section of the axis before the beam reaches any deflecting elements.

Since linear deflection terms cannot appear on the axis, the paraxial functional takes the general form

$$M^{(2)} = P(z)\left\{1 + \frac{x'^2 + y'^2}{2}\right\} + \frac{1}{2}\left\{F_{2,0}(z)x^2 + 2F_{1,1}(z)xy + F_{0,2}(z)y^2\right\} - eB(z)\frac{xy' - x'y}{2} \tag{47.35}$$

$P(z)$ denoting the kinetic momentum $g = mv$ on the axis. A factor h, appearing in the line-element of the curved coordinate system (Eq. 51.4), contributes only to terms of third and higher orders and can hence be ignored here.

The canonical momenta ξ and η are given by

$$\begin{aligned} \xi &= \frac{\partial M^{(2)}}{\partial x'} = P(z)x' + \frac{1}{2}eB(z)y \\ \eta &= \frac{\partial M^{(2)}}{\partial y'} = P(z)y' - \frac{1}{2}eB(z)x \end{aligned} \tag{47.36}$$

The trajectory equations are then of the form

$$\begin{aligned} \xi' &= \frac{\partial M^{(2)}}{\partial x} = Q_1(z)x + Q_2(z)y - \theta'\eta \\ \eta' &= \frac{\partial M^{(2)}}{\partial y} = Q_2(z)x + Q_3(z)y + \theta'\xi \end{aligned} \tag{47.37}$$

with the new coefficients

$$\begin{aligned} &\theta'(z) = eB(z)/2P(z) \\ &Q_1(z) = F_{2,0}(z) - P(z)\theta'^2(z) \quad Q_2 = F_{1,1}(z) \quad Q_3(z) = F_{0,2}(z) - P(z)\theta'^2(z) \end{aligned} \tag{47.38}$$

These coefficients correspond to a focusing effect superimposed on an axial astigmatism. Any space charge term is included with equal weight in Q_1 and Q_3.

The general solution of this set of differential equations is a linear combination of four linearly independent partial solutions. It is now convenient to introduce the four-dimensional phase space and the vector $\boldsymbol{v}$ and its associate $\tilde{\boldsymbol{v}}$:

$$\boldsymbol{v} = (x, y, \xi, \eta)^T, \quad \tilde{\boldsymbol{v}} = (\xi, \eta, -x, -y)^T \tag{47.39}$$

where T denotes transpose as usual and hence $\boldsymbol{v}$ and $\tilde{\boldsymbol{v}}$ are column vectors. For any pair of solutions, the commutator

$$[\boldsymbol{v}_m, \boldsymbol{v}_n] = \xi_m x_n - \xi_n x_m + \eta_m y_n - \eta_n y_m = (\tilde{\boldsymbol{v}}_m, \boldsymbol{v}_n) \tag{47.40}$$

is constant; the last term is just the scalar product of the two vectors, $\tilde{\boldsymbol{v}}_m \cdot \boldsymbol{v}_n$. These commutators, invariant with respect to rotation about the z-axis, are generalizations of the familiar Wronskian determinant.

The differential equations (47.36) and (47.37) can be expressed compactly in terms of these vectors. It can easily be seen that

$$\boldsymbol{v}'(z) = \boldsymbol{C}(z)\boldsymbol{v}(z) \quad \tilde{\boldsymbol{v}}'(z) = -\boldsymbol{C}(z)\tilde{\boldsymbol{v}}(z) \tag{47.41}$$

in which

$$\boldsymbol{C}(z) = \begin{pmatrix} 0 & -\theta' & P^{-1} & 0 \\ \theta' & 0 & 0 & P^{-1} \\ Q_1 & Q_2 & 0 & -\theta' \\ Q_2 & Q_3 & \theta' & 0 \end{pmatrix} \tag{47.42}$$

Since all the diagonal elements are zero, the motion in phase space is source-free:

$$\operatorname{div} \boldsymbol{v}' = \frac{\partial x'}{\partial x} + \frac{\partial y'}{\partial y} + \frac{\partial \xi'}{\partial \xi} + \frac{\partial \eta'}{\partial \eta} = \operatorname{Trace}(\boldsymbol{C}) = 0 \tag{47.43}$$

It is convenient to combine the four fundamental solutions $\boldsymbol{v}_1, \ldots, \boldsymbol{v}_4$ into a matrix of rank 4:

$$\boldsymbol{W}(z) = (\boldsymbol{v}_1, \boldsymbol{v}_2, \boldsymbol{v}_3, \boldsymbol{v}_4) = \begin{pmatrix} x_1 & x_2 & x_3 & x_4 \\ y_1 & y_2 & y_3 & y_4 \\ \xi_1 & \xi_2 & \xi_3 & \xi_4 \\ \eta_1 & \eta_2 & \eta_3 & \eta_4 \end{pmatrix} \tag{47.44}$$

The four differential equations then assume the matrix form $\boldsymbol{W}' = \boldsymbol{CW}$. For the initial conditions, a very favourable choice is to set $\boldsymbol{W}_{i,k=}\delta_{i,k}$ in the starting plane, $z = z_0$; $\boldsymbol{W}(z_0)$ is then the unit matrix. A general solution with initial vector $\boldsymbol{v}_0$ is given by

$$\boldsymbol{v}(z) = \boldsymbol{W}(z)\boldsymbol{v}_0$$

Other favourable consequences of this choice are that $\det \boldsymbol{W}(z) = 1$ and there are six fundamental commutators:

$$\begin{aligned} &[\boldsymbol{v}_1, \boldsymbol{v}_2] = 0, \quad [\boldsymbol{v}_1, \ \boldsymbol{v}_3] = -1, \quad [\boldsymbol{v}_1, \ \boldsymbol{v}_4] = 0 \\ &[\boldsymbol{v}_2, \boldsymbol{v}_3] = 0, \quad [\boldsymbol{v}_2, \ \boldsymbol{v}_4] = -1, \quad [\boldsymbol{v}_3, \ \boldsymbol{v}_4] = 0 \end{aligned} \tag{47.45}$$

Some consequences of the ray equations can be derived as a generalization of Eq. (47.20). We now return to the derivation of the brightness and in particular, to the *reduced* brightness

$$R(x, y, \xi, \eta, z) \coloneqq B(x, y, \xi, \eta, z)/\hat{\Phi}(\boldsymbol{r}) \tag{47.46a}$$

in which $\hat{\Phi}(\boldsymbol{r}) = P^2(z)/2m_0e$ is the relativistic accelerating voltage. This definition is similar to Eq. (47.21) but here the canonical momenta have been introduced. Liouville's theorem takes the form

$$\frac{dR}{dz} = \frac{\partial R}{\partial z} + x'\frac{\partial R}{\partial x} + y'\frac{\partial R}{\partial y} + \xi'\frac{\partial R}{\partial \xi} + \eta'\frac{\partial R}{\partial \eta} = 0 \tag{47.46b}$$

from which we conclude that $R = R_0 = \text{const}$ along each trajectory. Just as for Eq. (47.23), we now try to solve (47.46b) in terms of an exponential function

$$R(\boldsymbol{v}, z) = R_0 \exp\left(-\sum_{i=1}^{4}\sum_{k=1}^{4} A_{i,k}(z)\, \tilde{\boldsymbol{v}}_i \tilde{\boldsymbol{v}}_k \right) \tag{47.47}$$

The coefficients $A_{i,k}$ satisfy the differential equations

$$A'_{i,k} = \sum_{n=1}^{4} \left\{ \boldsymbol{C}_{in}(z) A_{n,k}(z) + \boldsymbol{C}_{kn}(z) A_{n,i}(z) \right\} \tag{47.48}$$

and are uniquely determined by their initial values $A_{i,k}(z_0)$. The quadratic form in the exponent must be strictly negative so that the function R can be normalized and the norm must be equal to the total current, I:

$$\int_{-\infty}^{\infty}\int_{-\infty}^{\infty}\int_{-\infty}^{\infty}\int_{-\infty}^{\infty} R(\boldsymbol{v}, z)\, dx dy d\xi d\eta = I \tag{47.49}$$

The current density in the axial direction then becomes

$$j(x, y, z) = \int_{-\infty}^{\infty}\int_{-\infty}^{\infty} R(\boldsymbol{v}, z)\, d\xi d\eta \tag{47.50}$$

and the normalized distribution of momenta is

$$F(\xi, \eta) = \iint R(\boldsymbol{v}, z)\, dx dy \tag{47.51}$$

In the absence of an axial magnetic field ($B(z) = 0$), this is essentially the distribution of directions in the beam. So far, quite general relations have been derived. More specific results require specialization. The most important case, rotational symmetry, has already been dealt with in detail in Section 47.4. We now investigate two other cases: orthogonal systems and conjugate planes.

Orthogonal systems. These are systems in which motion in the x-direction is independent of that in the y-direction. This is possible even with a curved optic axis but not with a general one: the axis must lie entirely in a plane, the $x-z$ plane say, so that the torsion vanishes. Moreover, axial magnetic fields must be excluded as they cause torsion. Finally, the coefficient $Q_2(z)$ must vanish since it causes coupling between the motion in the x- and y-directions.

With these assumptions, the matrices $\boldsymbol{W}$ and $\boldsymbol{A}$ simplify to

$$\boldsymbol{W}(z) = \begin{pmatrix} x_1 & 0 & x_3 & 0 \\ 0 & y_2 & 0 & y_4 \\ \xi_1 & 0 & \xi_3 & 0 \\ 0 & \eta_2 & 0 & \eta_4 \end{pmatrix} \quad \boldsymbol{A}(z) = \begin{pmatrix} A_{11} & 0 & A_{13} & 0 \\ 0 & A_{22} & 0 & A_{24} \\ A_{31} & 0 & A_{33} & 0 \\ 0 & A_{42} & 0 & A_{44} \end{pmatrix} \tag{47.52}$$

and the brightness function then separates into a product of the form

$$R(\boldsymbol{v}, z) = R_0 \ \exp\{-E_x(x, \xi)\}\exp\{-E_y(y, \eta)\} \tag{47.53}$$

in which E_x and E_y are positive quadratic polynomials in their arguments.

Conjugate planes. These are now defined as planes $z_c = \text{const}$ in which $R(\boldsymbol{v}, z)$ separates into a product of functions, the arguments of one of which are only coordinates and those of the other are only momenta. For this condition, it is not necessary to assume orthogonality, it can be satisfied in more general cases. The normalization can be chosen in such a way that this product becomes

$$R(\boldsymbol{v}, z_c) = j(x, y, z_c)F(\xi, \eta, z_c) \tag{47.54}$$

A necessary and sufficient condition for this separation is that the coefficients causing coupling between coordinates and momenta vanish at z_c:

$$A_{13} = A_{14} = A_{23} = A_{24} = 0 \quad z = z_c \tag{47.55}$$

One such plane is the surface of a thermionic cathode, as explained in Section 47.4. The separation assumed in Eq. (47.54) means that the distribution of momenta in such a plane is the same for all points (x, y, z_c). It can be shown that another such plane is close to a plane in which the crossover is smallest and this is almost the same as the usual meaning of the imaging of conjugate planes. One such case is seen in Eq. (47.30) and the following equations. In the general case, however, the crossovers will be elliptic and astigmatic.

A possible way of determining the brightness function including the effect of aberrations is *numerical ray tracing*. According to Liouville's theorem, R is constant along each trajectory and it is therefore possible to launch a set of trajectories with the appropriate initial conditions, including the correct brightness $R(\boldsymbol{v}_0, z_0)$. In this way, the brightness at the end-point has the same value. The drawback of this approach is that it furnishes a large volume of data but outside the mathematical context (rather like the use of differential algebra in aberration studies in Section 34.8).

47.5 Measurement of the Brightness

The techniques for measuring the brightness all reduce to the measurement of beam currents. By a suitable arrangement of lenses, apertures and detectors, *finite* areas Δa and solid angles $\Delta\Omega$ are defined and the corresponding current ΔI is measured. The quantity $\Delta I \Delta a^{-1}\ \Delta\Omega^{-1}$ is a reliable measure of the average brightness $\overline{B}$ only if all apertures are illuminated *uniformly*, a requirement that is difficult to satisfy in practice.

Detailed investigations on this problem have been made by Lauer (see Lauer, 1982), who employed two different techniques, the two-aperture method and the lens method.

i. *Two-aperture method*: two coaxial apertures are brought into the path of the beam. The first, closer to the cathode, confines the element of solid angle $\Delta\Omega$ subtended at the centre of the second aperture. The second aperture defines the area Δa. This method works satisfactorily only if the diameter of the crossover is appreciably larger than the region corresponding to the area Δa. Since the crossovers of modern field-emission guns are too small to satisfy this requirement, this method is then not suitable.
ii. *Lens method*: this is shown in Fig. 47.4. The first aperture is now located in the principal plane of a lens. This lens produces a magnified image of the crossover in the plane of the second aperture. By a suitable choice of the magnification, it can be ensured that the area Δa is always uniformly illuminated. The aperture angle

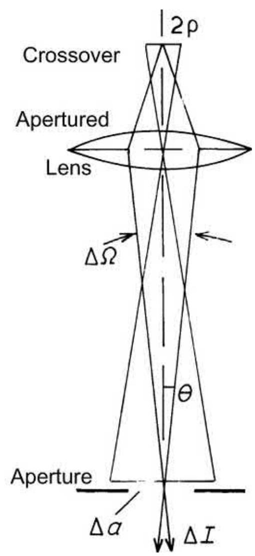

Figure 47.4
Lens method for the measurement of brightness. The lens images the crossover into the aperture plane. The aperture in the lens defines the solid angle subtended. (For simplicity, a thin lens is shown.)

$\theta = (\Delta\Omega/\pi)^{1/2}$ is, however, limited by the requirement that the spherical aberration disc referred back to the object must be appreciably smaller than the crossover. Hence a very good lens is needed.

Lauer has also investigated the systematic errors of the measurement. For thermionic guns, he derived (47.17) and (47.19) in the special case $M_L = 1$. Of decisive importance is the fact that the angular distribution in the beam is *Gaussian*. This knowledge can be used to eliminate the systematic errors of the measurement. In this context, Lenz's theory is very helpful.

Since the area Δa is located in an image plane $z = z_0$ of the crossover, (47.30) holds; the brightness is then given by

$$B = B_0(z_0)\exp\left(-\frac{x^2+y^2}{\rho_0^2}\right)\exp\left(-\frac{x'^2+y'^2}{\sigma_0^2}\right) \tag{47.56}$$

If the semiaperture angle behind the lens is θ, we have $x'^2 + y'^2 \leq \theta^2$; furthermore we have $x^2 + y^2 \leq \rho_a^2$, ρ_a being the radius of the second aperture. The measured part of the beam current is then

$$\Delta I = \int\limits_{x^2+y^2\leq\rho_a^2}\ \int\limits_{x'^2+y'^2\leq\theta^2} B\,dxdydx'dy'$$

With Eq. (47.56) this integration is elementary; introducing polar coordinates, we find

$$\Delta I = \pi^2 B_0\sigma_0^2\rho_0^2\left\{1-\exp\left(-\frac{\rho_a^2}{\rho_0^2}\right)\right\}\left\{1-\exp\left(-\frac{\theta^2}{\sigma_0^2}\right)\right\} \tag{47.57}$$

The average brightness is then given by

$$\begin{aligned}\overline{B} &= B_0\frac{1-\exp\left(-\rho_a^2/\rho_0^2\right)}{\rho_a^2/\rho_0^2}\ \frac{1-\exp\left(-\theta^2/\sigma_0^2\right)}{\theta^2/\sigma_0^2}\\ &= B_0\left(1-\frac{\rho_a^2}{2\rho_0^2}\right)\left(1-\frac{\theta^2}{2\sigma_0^2}\right) + \text{higher order terms}\end{aligned} \tag{47.58}$$

The axial brightness B_0 and the constants ρ_0 and σ_0 can be determined from the results of three (or more) independent measurements with different choices of ρ_a and θ.

The results of truly reliable measurements of the brightness are often in disagreement with the theoretical predictions. Disappointing though this may be, we should not be surprised. We must bear in mind that the theory, in spite of its complexity, contains all too many simplifying assumptions, which are never satisfied in practice. The cathode surface is rarely clean and never smooth. Even its macroscopic shape is often not known accurately. Moreover, the semiclassical theory of electron emission is an oversimplification. There are thus unjustified assumptions in the reasoning and the brightness is very sensitive to these. The great merit of the theory is that it enables us to understand the dependence of the brightness on the various geometrical and electrical parameters. Even though the absolute values may not be predicted accurately, the qualitative behaviour and trends are correct.

A comprehensive analysis of various concepts related to the brightness and the associated measurement techniques is given by Lejeune and Aubert (1980); these topics are dealt with in the next chapter, where more recent references will be found.

47.6 Coulomb Interactions and Brightness

In a series of papers and dissertations, Kruit, Cook, Verduin and colleagues have examined the effect of Coulomb interactions in the beam emitted by sources of various kinds on the virtual source size and hence on the brightness (Bi et al., 1997, 1998; Fransen et al., 1999; van Veen et al., 2001; Bronsgeest et al., 2007; Cook et al., 2009, 2010, 2011; Verduin et al., 2011; Cook, 2013; Cook and Kruit, 2016; Verduin, 2017). Here we concentrate on two of these studies. In the case of field-emission guns, Verduin et al. (2011) demonstrate by simulation of two gun models that the effect of Coulomb interactions, though complicated, can be understood in physical terms. The authors plot curves showing the dependence of mean reduced brightness on extraction voltage and on the electric field at the tip (radius 10 nm in their model). The maximum brightness and beam energy spread are also plotted against tip radius. The former is a U-shaped curve, suggesting that there is not much difference between the behaviour of sources with tip radii of 1 μm and 1 nm. In their second model, emission from a small thin protrusion is studied and the interplay between protrusion length and electric field is analysed. It is clear that brightness is governed by Coulomb interactions and that these depend on the time spent by the beam electrons in the gun zone.

Cook and Kruit (2016) have considered the role of Coulomb interactions in ultrafast electron microscopy (Section 37.5). They show that for a gun in which a laser provokes emission from a sharp tip immersed in a strong electric field (1 V/nm or more), Coulomb interactions can indeed adversely affect the energy spread and the brightness.

47.7 Aberrations in the Theory of Brightness

The theory of Lenz (Section 47.4) is essentially paraxial. This limitation is clearly unsatisfactory, as it implies that the intensity distribution in any beam cross-section is Gaussian. Thus a hollow-cone distribution appearing near a crossover cannot be described by this theory. We now generalize it to include the primary geometric aberrations. In this account, only rotationally symmetric electrostatic fields are considered; the inclusion of magnetic fields is straightforward.

The theory is developed on the basis of three rotational invariants

$$\begin{aligned} Q_1(z) &= x^2(z) + y^2(z) \\ Q_2(z) &= 2\{x(z)x'(z) + y(z)y'(z)\} \\ Q_3(z) &= x'^2(z) + y'^2(z) \end{aligned} \tag{47.59}$$

and their derivatives

$$Q_1'(z) = Q_2 \quad Q_2' = 2Q_3 + Q_4 \quad Q_3' = Q_5 \tag{47.60}$$

with

$$Q_4 = 2(xx'' + yy'') \quad Q_5 = 2(x'x'' + y'y'') \tag{47.61}$$

In Lenz's theory, only the linear terms are retained when substituting for x'' and y''; here we retain terms of third order, corresponding to aberrations. With $u := x + \mathrm{i}y$ the trajectory equation can be written

$$u''(z) + p(z)u'(z) + q(z)u(z) + S(z,u,u')u'(z) + T(z,u,u')u(z) = 0 \tag{47.62}$$

The coefficients, all real, are defined by

$$V(z) = \left(\frac{\hat{\phi}}{\hat{\phi}_0}\right)^{1/2} \tag{47.63a}$$

$$p(z) = \frac{V'(z)}{V(z)} = \frac{\gamma\phi'(z)}{2\hat{\phi}(z)} \tag{47.63b}$$

$$q(z) = \gamma\frac{\phi''(z) + \varepsilon_0\rho(z)}{4\hat{\phi}(z)} \tag{47.63c}$$

The terms Su' and Tu result from the third-order perturbation calculus:

$$S(z,u,u') = \sum_{n=1}^{3} S_n(z)Q_n \quad T(z,u,u') = \sum_{n=1}^{3} T_n(z)Q_n \tag{47.64}$$

The functions S_n and T_n can be extracted from Chapter 24. We introduce

$$p_T := p + S \quad q_T := q + T \tag{47.65a}$$

so that

$$x'' = -p_T x' - q_T x \quad y'' = -p_T y' - q_T y \tag{47.65b}$$

On substituting these expressions into Eq. (47.61) and then into Eqs (47.59) and (47.60), we find

$$\begin{aligned} Q_1' &= Q_2 \\ Q_2' &= 2Q_3 - p_T Q_2 - 2q_T Q_1 \\ Q_3' &= -q_T Q_2 - 2p_T Q_3 \end{aligned} \tag{47.66}$$

We have thus found a set of functions Q_n, the derivatives of which are combinations of the functions themselves. These are suitable for use in the theory of brightness. The general form of Lenz's condition for the constancy of the reduced brightness $R(z, u, u')$ is

$$\frac{dR}{dz} = \frac{\partial R}{\partial z} + x'\frac{\partial R}{\partial x} + y'\frac{\partial R}{\partial y} + x''\frac{\partial R}{\partial x'} + y''\frac{\partial R}{\partial y'} = 0$$

and with Eqs (47.65), this gives

$$\frac{\partial R}{\partial z} + x'\frac{\partial R}{\partial x} + y'\frac{\partial R}{\partial y} - (p_T x' + q_T x)\frac{\partial R}{\partial x'} - (p_T y' + q_T y)\frac{\partial R}{\partial y'} = 0 \tag{47.67}$$

We seek a solution of the form

$$R = R_0 \exp\left[-V(z)\left\{a(z)Q_1 + b(z)Q_2 + c(z)Q_3 + W(z, u.u')\right\}\right] \tag{47.68}$$

in which the last term is of fourth order and contains the aberrations. We find

$$-\frac{1}{RV}\frac{dR}{dz} = p(aQ_1 + bQ_2 + cQ_3) + a'Q_1 + b'Q_2 + c'Q_3 + aQ_1' + bQ_2' + cQ_3' + pW + \frac{dW}{dz}$$

After eliminating the Q_n' and reorganizing, we find

$$\begin{aligned} &Q_1\left\{a' + pa - 2(q+T)b\right\} + Q_2\left\{a + b' - Sb - (q+T)c\right\} \\ &+ Q_3(c' - pc + 2b - 2Sc) + \frac{dW}{dz} + pW = 0 \end{aligned} \tag{47.69}$$

Since the functions Q_n are considered to be linearly independent, quadratic terms cannot be compensated by those of higher order. Eq. (47.69) must therefore be satisfied for the second-order and fourth-order terms separately. For the second order, we recover the set of homogeneous linear equations found by Lenz:

$$a' = -pa + 2qb, \quad b' = -a + qc, \quad c' = -2b + pc \tag{47.70}$$

It is easy to confirm that the discriminant $\Delta = ac - b^2$ is a constant. After subtraction of (47.70) from (47.69), the remaining terms

$$-2bTQ_1 - (Sb + Tc)Q_2 - 2ScQ_3 + \frac{dW}{dz} + pW = 0 \tag{47.71}$$

contain all the aberration terms of fourth order. This equation can be solved in terms of products of the rotational invariants, which it is convenient to combine as a six-dimensional vector $\boldsymbol{F}$ with components F_n:

$$\boldsymbol{F} = (Q_1^2,\ Q_1Q_2,\ Q_2^2,\ Q_1Q_3,\ Q_2Q_3,\ Q_3^2) \tag{47.72}$$

The individual components are to be regarded as linearly independent. Although their derivatives are based on Eq. (47.66), we can adopt the approximation $p_T = p,\ \ q_T = q$ since the terms that have been omitted would generate sixth-order aberrations. The derivatives are now again linear combinations of the functions themselves. We represent them in matrix−vector form, $\boldsymbol{F}' = \boldsymbol{DF}$, in which

$$\boldsymbol{D} = \begin{pmatrix} 0 & 2 & 0 & 0 & 0 & 0 \\ -2q & -p & 1 & 2 & 0 & 0 \\ 0 & -4q & -2p & 0 & 4 & 0 \\ 0 & -q & 0 & -2p & 1 & 0 \\ 0 & 0 & -q & -2q & -3p & 2 \\ 0 & 0 & 0 & 0 & -2q & -4p \end{pmatrix} \tag{47.73}$$

The function $W(z, u, u')$ is now best expanded in terms of the components F_n, the coefficients of which form a vector $\boldsymbol{w}(z)$:

$$W = \boldsymbol{wF} = \sum w_n(z)F_n(z, u, u') \tag{47.74}$$

On differentiating with respect to z, we find

$$\frac{dW}{dz} + pW = (\boldsymbol{w}' + p\boldsymbol{w})\boldsymbol{F} + (\boldsymbol{D}^T\boldsymbol{w})\boldsymbol{F} \tag{47.75}$$

The transposed matrix $\boldsymbol{D}^{\boldsymbol{T}}$ is obtained by reordering the double products in $\boldsymbol{F}$. It only remains to reorganize the term G,

$$G := 2bTQ_1 + (Sb + Tc)Q_2 + 2TcQ_3 =: \boldsymbol{gF} \tag{47.76}$$

For this, Eqs (47.64) for S and T are substituted in Eq. (47.76), which leads to products of Q-functions, which are the components of $\boldsymbol{F}$. From this, the elements of the coefficient vector $\boldsymbol{g}$ can be extracted straightforwardly, yielding

$$\begin{aligned} &g_1 = 2bT_1, \quad g_2 = 2bT_2 + bS_1 + cT_1, \quad g_3 = bS_2 + cT_2, \\ &g_4 = 2bT_3 + 2cS_1, \quad g_5 = bS_3 + cT_3 + 2cS_2, \quad g_6 = 2cS_3 \end{aligned} \tag{47.77}$$

Bringing all this together, we obtain the scalar product

$$(\mathbf{w}' + p\boldsymbol{w} + D^T w - \boldsymbol{g})\boldsymbol{F} = 0$$

equivalent to Eq. (47.71). The components of $\boldsymbol{F}$ are linearly independent and the expression in parentheses must therefore vanish:

$$w' = -pw - \boldsymbol{D}^{\boldsymbol{T}}\boldsymbol{w} + g \tag{47.78a}$$

or explicitly,

$$w_n'(z) = -p(z)w_n(z) - \sum_{m=1}^{6} D_{m,n}(z)w_m(z) + g_n(z), \quad n = 1\cdots 6 \tag{47.78b}$$

This is an inhomogeneous linear system of differential equations. It is solved as follows. First, a starting plane $z = z_o$ and reasonable initial values of $a(z_o) =: a_{\mathrm{o}}$, b_{o} and c_{o} in this plane are chosen. Eqs (47.70) are then solved up to some 'image plane', $z = z_i$, and the results stored. Now, an initial vector $\mathbf{w}_o = \mathbf{w}(z_o)$ is chosen. In each step of the integration of Eq. (47.78), the vector $\boldsymbol{g}(z)$ is determined and substituted into Eq. (47.78). The integration then proceeds step by step until the terminal value at $z = z_i$ is attained. Alternatively, the whole system of differential equations can be solved simultaneously in a single stride from z_o to z_i. The resulting vector $\boldsymbol{w}$ then enables us to determine the perturbation W in Eq. (47.74). The required reduced brightness is then given by Eq. (47.68).

The effort required for this method is comparable with that needed to trace four electron trajectories. But the latter provide only local information whereas the information coded in the function R permits us to determine the intensity distribution in the whole beam at any position. This new method (Kasper, 2017, unpublished) merits more extensive study.

Emittance

In Chapter 47, Brightness, we have introduced the brightness B as a function of position ($\boldsymbol{r}$) and direction ($\boldsymbol{t}$). In Section 47.4, we showed in particular that the concept of brightness is very useful for describing the intensity distribution in an electron beam. One might conjecture that the brightness is only one of a family of functions that are useful in connection with beams. Another is the emittance, which is the subject of the present chapter.

48.1 Trace Space and Hyperemittance

The six-dimensional phase space considered in Sections 44.1 and 47.1 is inconvenient for practical purposes, since canonical momenta are not observable quantities and kinetic momenta are extremely difficult to measure directly. Unlike the latter, directions, characterized by *slope* coordinates $x' := dx/dz$, $y' := dy/dz$, can be determined easily by bringing appropriate arrangements of diaphragms into the beam. It is thus advantageous to introduce a four-dimensional *trace space* with the corresponding position vector $\boldsymbol{q} := (x, y; x', y')$. These four variables refer to the intersection of an arbitrary electron trajectory with a given plane $z = \text{const}$. Different values of z may be considered, but z is then treated as a mere parameter, not as a variable of the trace space.

We now seek a four-dimensional equivalent of the six-dimensional form of Liouville's theorem. This is exactly possible in the four-dimensional phase-subspace built up by x, y and p_x, p_y. We recall that Liouville's theorem is a consequence of Hamilton's canonical equations and it is therefore logical to look for a four-dimensional form of the latter. This is easily found even for systems with curved optic axes, but we shall not do this here, since this axis will usually be straight.

A suitable *Lagrangian* is already given by Eq. (4.35); in trace notation

$$M(z, \boldsymbol{q}) = \sqrt{1 + x'^2 + y'^2}\, g(\boldsymbol{r}) + Q\left(x'A_x + y'A_y + A_z\right) \tag{48.1}$$

$g(\boldsymbol{r})$ being the magnitude of the kinetic momentum and Q the charge of the particle. As in Eq. (3.16), we write

$$\rho := \sqrt{1 + x'^2 + y'^2} \tag{48.2}$$

Principles of Electron Optics: Applied Geometrical Optics.
DOI: http://dx.doi.org/10.1016/B978-0-12-813369-9.00048-8

It is not necessary to assume $x'^2 + y'^2 \ll 1$ in this expression. The canonical momentum is given by

$$p_x = \frac{\partial M}{\partial x'} = \frac{gx'}{\rho} + QA_x \tag{48.3a}$$

$$p_y = \frac{\partial M}{\partial y'} = \frac{gy'}{\rho} + QA_y \tag{48.3b}$$

$$p_z = \frac{g}{\rho} + QA_z \tag{48.3c}$$

Though Eq. (48.3c) is valid, it cannot be derived from the four-dimensional Lagrange formalism. The equations of motion are (4.36) but these are not needed here. The Hamiltonian, to be found, is given by a Legendre transform:

$$K\left(z, x, y, p_x, p_y\right) := M(z, x, y, x', y') - x'\, p_x - y'\, p_y \tag{48.4}$$

On eliminating x' and y' from Eq. (48.4) by means of (48.3a,b), we obtain

$$K = QA_z + \left\{ g^2 - (p_x - QA_x)^2 - \left(p_y - QA_y\right)^2 \right\}^{1/2} \tag{48.5}$$

It can be shown that the square root term is equal to g/ρ and hence K and p_z are the same. It can be proved quite generally that the solutions of the canonical equations

$$x' = -\frac{\partial K}{\partial p_x}, \quad y' = -\frac{\partial K}{\partial p_y}, \quad p_x' = \frac{\partial K}{\partial x}, \quad p_y' = \frac{\partial K}{\partial y} \tag{48.6}$$

are identical with those of the corresponding Lagrange equations. Using these equations we can also prove that the four-dimensional divergence of $\boldsymbol{q}' := (x', y', p_x', p_y')$ vanishes:

$$\nabla_4 \cdot \boldsymbol{q}' \equiv \frac{\partial x'}{\partial x} + \frac{\partial y'}{\partial y} + \frac{\partial p_x'}{\partial p_x} + \frac{\partial p_y'}{\partial p_y} = 0 \tag{48.7}$$

in which the role of the time has now been taken over by the parameter z. This is the four-dimensional form of Liouville's theorem.

In order to interpret this in physical terms, we consider an arbitrary but closed domain $\tilde{D}$ in the (x, y, p_x, p_y)-space, the corresponding hypersurface being formed by four-dimensional trajectory positions. The enclosed volume is then defined by

$$E^*\left(\tilde{D}\right) := \iiiint_{\tilde{D}} dx dy dp_x dp_y \tag{48.8a}$$

and is known as the *hyperemittance* of $\tilde{D}$. Eq. (48.7) now tells us that $E^*(\tilde{D})$ is *invariant* with respect to z: if the reference plane ($z = \text{const}$) is shifted and during this shift the surface of $\tilde{D}$ is always formed by the same trajectories, then $E^*(\tilde{D})$ does not vary.

In this form the invariance theorem is not particularly helpful; to improve matters, we eliminate p_x and p_y by means of Eqs (48.3a,b) and (48.2). The corresponding Jacobian takes the form

$$\frac{\partial(p_x, p_y)}{\partial(x', y')} = \frac{1}{\rho^4} g^2(r)$$

and from Eq. (48.8a) we now obtain

$$E^*(D) = \iiiint_D g^2(r)\rho^{-4} dx dy dx' dy' \tag{48.8b}$$

D being the corresponding domain in the trace space. Although this expression is still exactly valid, it remains too complicated for practical applications. We therefore proceed to the *paraxial approximation* $x'^2 + y'^2 \ll 1$ and $g^2(\boldsymbol{r}) = 2m_0 e\hat{\phi}(z)$, $\hat{\phi}(z)$ being the relativistic axial potential. We finally obtain, with $d^4q = dxdydx'dy'$

$$E^*(D) = 2m_0 e\hat{\phi}(z) \iiiint_D d^4q \tag{48.8c}$$

Often even the constant factor $2m_0e$ is omitted.

The hyperemittance $E^*(D)$ is only one of many integral invariants. Another is the fraction of the beam current flowing through D. In the paraxial approximation we have

$$I(D) = \iiiint_D B d^4q = \hat{\phi}(z) \iiiint_D R(z, q)\ d^4q \tag{48.9}$$

This is a generalization of Eq. (47.27) for arbitrary domains.

48.2 Two-Dimensional Emittances

In very many cases of practical interest, the devices in question have two planes of symmetry, which intersect each other orthogonally along the straight optic axis. There is no loss of generality in choosing these to be the coordinate planes $x = 0$ and $y = 0$. In the paraxial approximation the motions $x = x(z)$ and $y = y(z)$ are decoupled. It is then natural to introduce two-dimensional emittances:

$$\varepsilon_x := \frac{1}{\pi}\iint_{D_x} dx dx', \quad \varepsilon_y := \frac{1}{\pi}\iint_{D_y} dy dy' \tag{48.10}$$

Apart from the factor π^{-1} in the definition, these are the areas of the domains D_x and D_y obtained by projecting D onto the corresponding subspaces. Lejeune and Aubert (1980) mention other definitions, which differ from Eq. (48.10) by various normalization factors; these will not be listed here but it is important to realize that many slightly different definitions of ε_x and ε_y are to be found in the literature and the definition should always be checked.

48.2.1 General Emittance Ellipses

For simplicity the domains D_x and D_y are assumed to be tilted ellipses, each with uniform brightness distribution; one such ellipse is shown in Fig. 48.1. This assumption is justified whenever a paraxial approximation suffices. Owing to the linearity of the equations of motion, the projections of the general six-dimensional motion onto the corresponding two-dimensional phase-subspaces are then ellipses. This is analogous to the familiar case of the harmonic oscillator. Since the arguments are exactly similar for both ellipses D_x and D_y, we shall deal with only one of them, namely D_x. The contour of D_x can be represented by a general quadratic form

$$a(z)x^2 + 2b(z)xx' + c(z)x'^2 = d(z), \quad ac > b^2 \quad ad > 0 \tag{48.11}$$

With suitable scaling, the functions $a(z)$, $b(z)$, $c(z)$ and $d(z)$ are the Twiss parameters. For reasons that will be obvious later, it is not favourable to assume the normalization $d \equiv 1$, though this is permissible. The angle θ of tilt is given by $\tan 2\theta = 2b/(a - c)$. The semiaxes μ_1, μ_2 of the ellipse are obtained by diagonalization of the quadratic form and are given by

$$\mu_{1,2}^{-2} = \frac{1}{2d}\left(a + c \mp \sqrt{(a-c)^2 + 4b^2}\right)$$

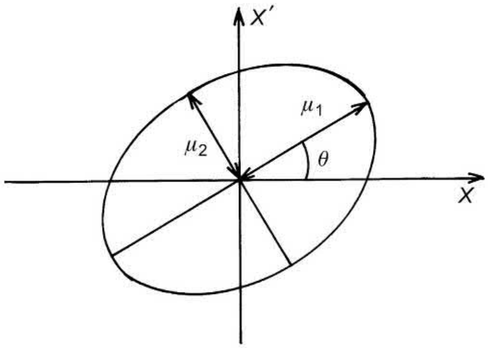

Figure 48.1
An emittance ellipse and the associated notation.

The emittance ε_x is then given by

$$\varepsilon_x = \mu_1 \mu_2 = d\left(ac - b^2\right)^{-1/2} \tag{48.12}$$

In the two-dimensional (x, x') trace subspace, the motion from a starting plane at z_o to the reference plane at z is given by a '*transfer*', represented by a linear transform

$$x = Ax_o + Bx'_o, \quad x' = Cx_o + Dx'_o \tag{48.13a}$$

the coefficients A, B, C and D being functions of z_o and z. The quadratic form (48.11) is form-invariant with respect to this transform, its coefficients in the starting plane being denoted by a_o, b_o, c_o and d_o. It is well-known from the Lagrange–Helmholtz relation that the transfer determinant satisfies

$$AD - BC = \sqrt{\hat{\phi}_o / \hat{\phi}(z)} \tag{48.13b}$$

and hence

$$\varepsilon_x = \frac{d}{\sqrt{ac - b^2}} = \sqrt{\frac{\hat{\phi}_o}{\hat{\phi}}} \frac{d_o}{\sqrt{a_o c_o - b_o^2}} = \varepsilon_{x,o} \sqrt{\frac{\hat{\phi}_o}{\hat{\phi}(z)}} \tag{48.14}$$

This means that acceleration of the electron beam decreases the emittance, mainly by parallelizing the rays.

An interesting simple transformation is *drift*, which means the propagation of rays through a field-free domain. A drift over an axial distance L is characterized by

$$x = x_o + Lx'_o, \quad x' = x'_o \tag{48.15}$$

and so $A = D = 1$, $B = L$, $C = 0$. The emittance ellipse is then sheared, see Fig. 48.2. The coefficients in Eq. (48.11) are now given by

$$a = a_o, \quad b = b_o - La_o, \quad c = c_o - 2Lb_o + a_o L^2, \quad d = d_o$$

By an appropriate choice of the length L, the tilt of the ellipse can be eliminated: $b = 0$ when $L = b_o a_o^{-1}$, and hence

$$L = \frac{b_o}{a_o}, \quad a = a_o, \quad c = c_o - \frac{b_o^2}{a_o}, \quad d = d_o \tag{48.16}$$

This minimizes the major semiaxis, but leaves the area of the ellipse, and thus the emittance, invariant. In connection with electron guns, this particular drift-length is of great importance since the plane $z = z_o + L$ is then that of a waist or narrowest cross-section.

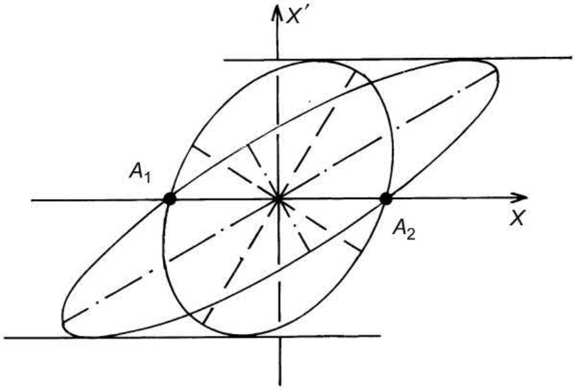

Figure 48.2
Shearing of the emittance ellipse in a drift space; A_1 and A_2 are fixed points.

Another important transfer is *focusing* in the x-direction: when the planes considered are conjugate, x must be independent of x'_o and the transfer matrix specializes to

$$\begin{pmatrix} A & B \\ C & D \end{pmatrix} = \begin{pmatrix} M_L & 0 \\ -f_i^{-1} & M_A \end{pmatrix} \tag{48.17}$$

M_L and M_A being the lateral and angular magnification, respectively, and f_i the focal length on the image side. $M_L M_A = \left(\hat{\phi}_0/\hat{\phi}_i\right)^{1/2}$ according to Eq. (48.13a) is again the Lagrange−Helmholtz relation. The requirement that the ellipse be untilted, $b \equiv 0$, $\theta = 0$, imposes a condition on the focal length:

$$\frac{1}{f_o} = \sqrt{\frac{\hat{\phi}_i}{\hat{\phi}_o}}\frac{1}{f_i} = -\frac{b_o}{M_L c_o} \tag{48.18}$$

f_o being the focal length on the object side. The length of the semiaxes of the ellipse may alter, but only in accordance with Eq. (48.14).

48.2.2 Acceptance and Matching

The acceptance domain of a transport system is the largest region in phase space within which all particles injected into the system can pass through it without striking the walls or apertures. If the motions in the x- and y-directions are uncoupled, the acceptance domain is the product of two independent two-dimensional subdomains in the (x, x') plane and the (y, y') plane. We again consider the (x, x') acceptance domain in a given reference plane $z = \text{const}$. Generally, this will *not* be elliptical in shape. In order to simplify the discussion,

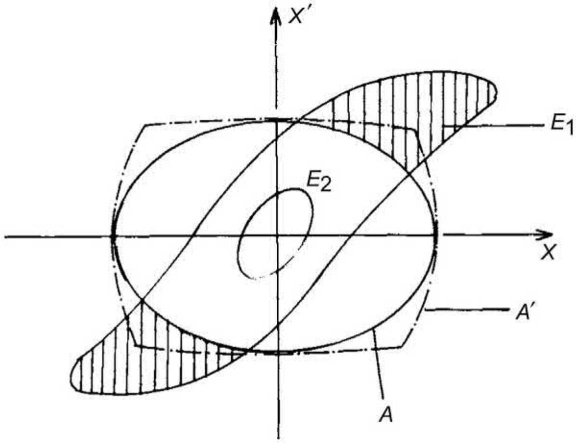

Figure 48.3
Various domains of acceptance and emittance. A': the acceptance domain of a system; A: the acceptance ellipse that fits inside A'; E_1: emittance domain too large, the particles outside A (hatched area) will be lost; E_2: unnecessarily small emittance domain. For a matched beam, the emittance domain coincides with the ellipse A.

we construct the largest ellipse that is contained entirely inside this domain, as demonstrated in Fig. 48.3, and call it the *acceptance ellipse*.

A beam is clearly transmitted without interruption if the emittance domain is entirely located inside the acceptance ellipse. Particles with trace-positions outside the acceptance ellipse will be lost, as indicated in Fig. 48.3. On the other hand, an uneconomic situation arises if the emittance diagram covers only a very small part of the acceptance diagram, since this means that the dimensions of some of the optical elements are unnecessarily large. The optimum situation occurs when the emittance diagram practically fills the acceptance diagram in each plane of reference. The beam is then *matched* to the system.

This matching is achieved by the appropriate arrangement of focusing elements and drift spaces; this is an optimization problem, which cannot be considered here. The matching is most important in the design of particle sources for accelerators in nuclear and elementary particle physics, which takes us beyond the scope of this volume. The reader who requires further details is referred to the corresponding literature. An extensive list of earlier references is given by Lejeune and Aubert (1980) and a modern treatment is given by Berz et al. (2015) where references to several other texts on accelerator physics can be found.

48.3 Brightness and Emittance

Emittance and related concepts can be incorporated in Lenz's theory of brightness (Section 47.4) without difficulty, since in both theories quadratic forms appear.

It is no problem to generalize Lenz's theory to astigmatic beams with independent motions $x = x_1(z)$, $y = x_2(z)$. We use the notations (x, y) and (x_1, x_2) and hence (x', y') and (x_1', x_2') interchangeably. With the assumption that the motion is independent in the x and y planes, the brightness separates into a product

$$B(\boldsymbol{r},\boldsymbol{t}) = R_o\hat{\phi}(z)\prod_{j=1}^{2}\beta_j\left(x_j, x_j', z\right) \tag{48.19}$$

We now choose a particular model for the factors β_j. By selecting exponentials, the arguments of which are quadratic forms in x_j and x_j', we obtain a representation of a 'Gaussian' beam with variable elliptic cross-section. The edges of the beam are not sharp but fall off smoothly in both position and angle. We write

$$\begin{gathered}\beta_j\left(x_j, x_j', z\right) = \exp\left\{-\sqrt{\frac{\hat{\phi}}{\hat{\phi}_o}}\left(a_j x_j^2 + 2b_j x_j x_j' + c_j x_j'^2\right)\right\}\\ a_j > 0, \quad a_j c_j > b_j^2 \quad \text{for} \quad j = 1, 2\end{gathered} \tag{48.20}$$

all the coefficients in these expressions being functions of z. The coefficients satisfy sets of ordinary differential equations which are similar to Eq. (47.24) (Kasper and Lenz, 1966); these will not be given here – their derivation is straightforward. Of course, $a_1 = a_2$, $b_1 = b_2$, $c_1 = c_2$ describes the round beam as a special case, as it must.

Since the reduced brightness R is an invariant of the motion, the same must be true of β_1 and β_2. We introduce new quantities η_j and d_j by:

$$\beta_j =: \exp\left(-\eta_j\right) =: \exp\left(-\sqrt{\frac{\hat{\phi}(z)}{\hat{\phi}_o}}d_j(z)\right) \quad j = 1, 2 \tag{48.21}$$

From Eqs (48.20) and (48.21) we then obtain two quadratic forms:

$$a_j x_j^2 + 2b_j x_j x_j' + c_j x_j'^2 = d_j, \quad j = 1, 2 \tag{48.22}$$

The fact that these have exactly the same structure as Eq. (48.11) shows that the Gaussian beam model adopted for β_j (48.20) corresponds to the use of ellipses to represent the emittance in the paraxial approximation. The initial conditions for the electron motion in the beam can always be chosen such that the coefficients in Eqs (48.11) and (48.20) become the same. We may therefore use (48.14) to define the two emittances:

$$\varepsilon_j = \frac{d_j(z)}{\sqrt{a_j c_j - b_j^2}} = \frac{\eta_j}{\sqrt{a_j c_j - b_j^2}}\sqrt{\frac{\hat{\phi}_o}{\hat{\phi}(z)}}, \quad j = 1, 2 \tag{48.23}$$

As the generalization of Eq. (47.25), we now have two constant discriminants $\Delta_j = a_j c_j - b_j^2$ $(j = 1,2)$, hence $d_j = d_j(z) \propto \hat{\phi}^{-1/2}$. This explains why we did not use the normalization $d_j \equiv 1$ in Eq. (48.22). From Eq. (48.23) we see that the hyperemittance $E^* \propto \varepsilon_1 \varepsilon_2 \hat{\phi}(z)$ is constant, as it should be. It is now a straightforward task to calculate the fraction of the particle beam that flows through the four-dimensional product volume $D = D_x D_y$ of the two emittance ellipses given by (48.22). By using the product separation (48.19), transforming to the principal axes of D_x and D_y, and then applying affine transformations to unit circles, we can evaluate Eq. (48.9) by elementary methods. The final result is

$$I(D) = R_0 \hat{\phi}_0 \prod_{j=1}^{2} \frac{\pi}{\sqrt{\Delta_j}} \left\{ 1 - \exp\left(-\eta_j \right) \right\} \tag{48.24}$$

With $\Delta_1 = \Delta_2 = \Delta$ and $\eta_1 = \eta_2 = \infty$ we again obtain Eq. (47.27), as we should.

The advantage of this theory is twofold. The first is that unrealistic sharp beam surfaces have been removed and replaced by more realistic Gaussian distributions. The second is that differential equations for the coefficients a_j, b_j and c_j in the quadratic form can be derived directly; in the case of a round beam we have Eq. (47.24). This makes the matching easier, since it is not necessary to compute trajectories and then determine a_j, b_j and c_j afterwards from the results. Instead, the coefficients can be determined *directly*. In practice it is necessary to accept reasonable tolerance limits for the loss of intensity during the transport of the beam, $\eta_j = 2$, $\exp(-\eta_j) = 2\%$, or $\eta_j = 2.5$, $\exp(-\eta_j) = 0.2\%$, for example, and to perform the matching with these.

48.4 Emittance Diagrams

A comprehensive review of the numerous and highly sophisticated methods for the measurement of brightness and emittance is given by Lejeune and Aubert (1980). Rather than repeat this review, we confine this account to one particular method, which has played a major role in the investigation of electron guns. This is the variable-shadow method, introduced by Hanszen (1964) and elaborated by Hanszen and Lauer (1967), for the determination of emittance diagrams (see also Lauer's review, 1982). In order to clarify the meaning and the significance of emittance diagrams, we consider first a planar motion $y = y(z)$ as a simple example. The complete graph of this motion, schematically presented in Fig. 48.4A, gives a clear idea of it. On the other hand, the corresponding emittance diagram shown in Fig. 48.4B is the *trace-space representation* with respect to a given and fixed reference plane $z = z_1$. For a single particle, this is simply a point (y'_1, y_1) in the (y', y) trace plane and thus contains less information about the motion. For the example chosen, this is clearly disadvantageous. The situation is different if we choose a reference plane $z = z_1$ in *field-free space*. The data (y'_1, y_1) are then sufficient to determine the whole asymptote $y(z) = y_1 + y'_1(z - z_1)$. The advantage of the emittance diagram becomes obvious in the

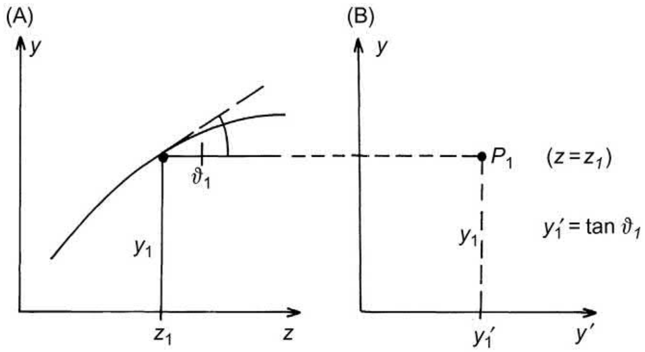

Figure 48.4
(A) Conventional representation of motion in the (y, z) plane and (B) trace-space representation referred to a particular axial coordinate $z = z_1$.

example shown in Fig. 48.5. In the conventional representation of focusing by a lens with spherical aberration (Fig. 48.5, left), only a *finite* number of rays can be shown, whereas the corresponding emittance diagram (Fig. 48.5, right) of the entire continuous electron bundle consists of a single curve, which contains all the relevant information. In fact, if we represent this curve analytically by

$$y = C_1 y' + C_3 y'^3 \approx C_1 \beta + C_3 \beta^3 \qquad \left(\beta^2 \approx y'^2 \ll 1\right)$$

we can determine the Gaussian image plane, which is located at $z_G = z_1 - C_1$, and the coefficient $C_s = C_3$ of spherical aberration.

The emittance diagram expresses very clearly the overlapping of electron bundles caused by aberrations. An example is given in Fig. 48.6A and B. While the conventional graph in the (y, z) plane is rather confusing on a first inspection, the corresponding emittance diagram shows clearly (at least in the vicinity of the reference plane) that the part that bends backward from the maximum belongs to the overlapping rays.

The experimental set-up for the determination of emittance diagrams with the shadow method is shown in Fig. 48.7. A very small aperture at a distance p^* from the virtual source moves meridionally in the y-direction through the electron beam. A fine slit, parallel to the direction of motion, collimates the beam in the x-direction. At a distance s^* from the aperture, the recording plate moves in synchronism in the x-direction at a fixed multiple m of the aperture speed. The spatial coordinate of the shadow curve, here denoted y_2, is recorded directly. The corresponding slope y' is given by $y' = (y_2 - y_1)/s^*$; since $y_1 = x_2/m$, we have $y' = (y_2 - x_2/m)/s^*$, x_2 being the actual shift of the recording plate. At the same time the distance $p^* = x_2/my'$ can be determined. The emittance diagram can now be constructed in two equivalent ways: (a) referred to the plane of the diaphragm, as a graph

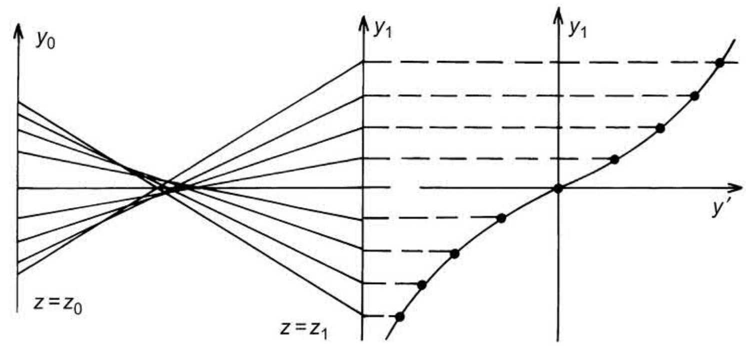

Figure 48.5
Left: Conventional representation of an electron beam with spherical aberration.
Right: Corresponding trace-space representation in the plane $z = z_1$.
In field-free regions, $y' = (y_1 - y_0)/(z_1 - z_0)$.

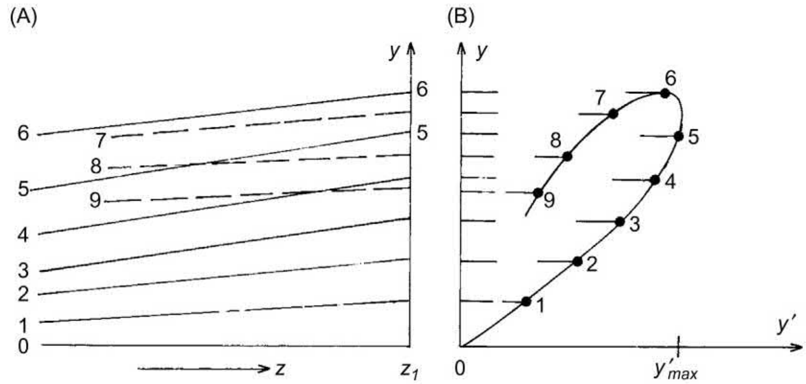

Figure 48.6
Conventional representation (A) and trace-space curve (B) of an overlapping electron bundle.
Ray 6 has the largest off-axis distance while ray 5 has the greatest slope.

of y_1 versus y'; and (b) referred to the plane of the recording plate, as a graph of y_2 versus y'. These graphs are related to each other by a shearing. Since the (virtual or real) crossover of the gun has a finite size and is not a point, as has been assumed in Fig. 48.7, the shadow curve and hence the (y_2, y') diagram have a finite width $\Delta y_2 = 2\rho p^*/s^*$ in the y_2 direction, ρ being the effective radius of the crossover.

Similar curves can also be obtained theoretically. By means of the methods outlined in Chapters 45 and 46, the fields in electron guns can be calculated. Electron trajectories can

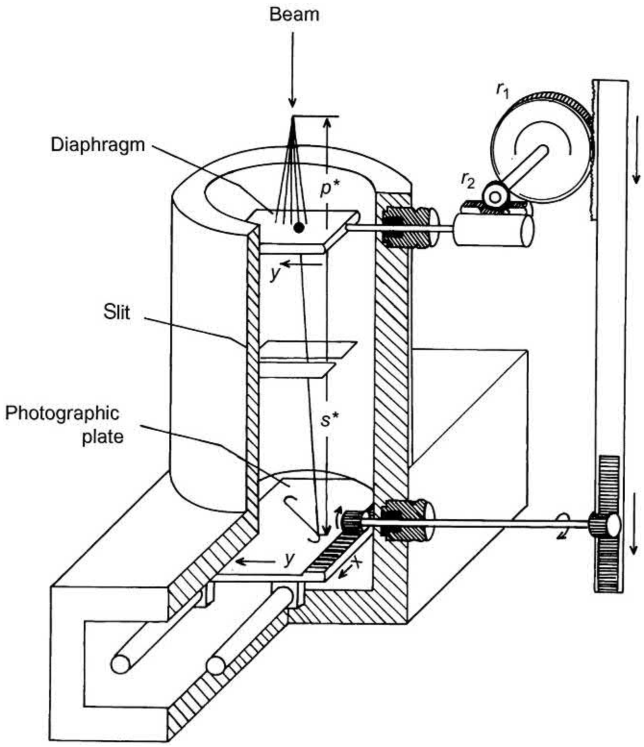

Figure 48.7
Experimental arrangement for determining emittance diagrams (shadow method). *After Hanszen (1964c), Courtesy Verlag der Zeitschrift für Naturforschung.*

be traced very accurately through these fields. For a large number of meridional trajectories with different starting conditions at the cathode surface, the radial coordinate $r(z_1)$ and the corresponding slope r' (z_1) in a given reference plane are determined and plotted in an (r', r) diagram. A pattern can be imposed on this cluster of trace points by connecting points belonging to the same starting point or to the same energy. Typical examples of such graphs are presented in Fig. 48.8. The outer contours agree fairly well with those determined from shadow curves measured for the same configuration. Typical examples of this agreement are presented by Lauer (1982) and Weyßer (1983a). Emittance diagrams are most informative if a shearing operation is performed in such a way that, in its central part, the middle line of the diagram is close to the r'-axis, as in Fig. 48.9. The corresponding reference plane then contains the crossover, and the central breadth of the diagram now gives the diameter of the central crossover spot. If there are outer branches in the diagram, these indicate the existence of a hollow beam. Fig. 48.9 also demonstrates that the trace domain should then be confined by a suitable arrangement of diaphragms in order to obtain a beam with low aberrations. This makes it necessary to cut off a major part of the

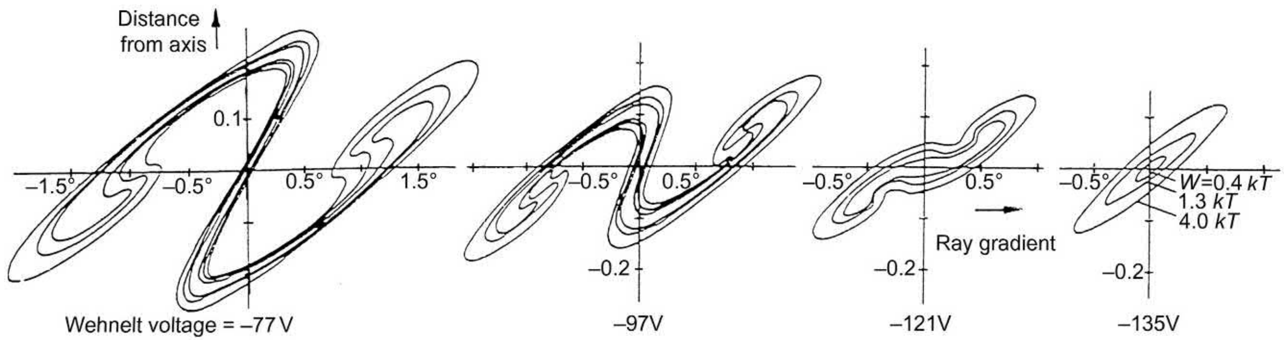

Figure 48.8

Emittance diagrams calculated for various values of the emission energy: $W/kT = 0.4$, 1.3 and 4.0 (weak space charge, cathode temperature 2600 K). *After Lauer (1982), Courtesy Elsevier.*

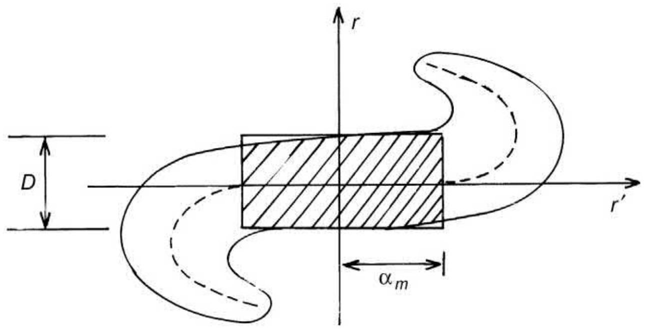

Figure 48.9
Emittance diagram at a crossover of diameter D; the hatched area is useful as an acceptance domain. The beam aperture is $2\alpha_m$.

beam current, so that an emittance diagram with a pronounced S-shape is undesirable in every respect.

Aberration coefficients can, we recall, be determined from emittance diagrams and Hanszen and Lauer (1969) have attempted this. The problem that arises is that the exit asymptotes of the electron trajectories must be traced back to the corresponding starting points at the cathode surface, which requires the use of a suitable lens model for the electric field in the gun. Following Hanszen and Lauer, the measured emittance diagrams can be represented in the parametric form

$$r = C_1\alpha + C_3\alpha^3 + C_5\alpha^5, \quad r' = D_1\alpha + D_3\alpha^3 + D_5\alpha^5$$

the line-width being neglected. Here α is the angle of inclination with respect to the optic axis referred back to the starting point. At least qualitatively, some useful insights can be obtained with this model.

Quite generally, as the wehnelt potential in a thermionic electron gun is raised, the emission area at the cathode increases, and those trajectories that start close to its margin suffer from strong aberrations, as they are bent strongly in the electric field near the cathode. This leads to multiple overlapping in parts of the beam. The details are discussed in the review article by Lauer (1982), to which the reader is referred. The occurrence of strong aberrations in conventional thermionic guns confirms our conjecture in Chapter 46, that the blurring of the cathode image in its marginal zone is not necessarily a pure space charge effect, although space charge may be important. Our understanding of aberrations in thermionic electron guns, though incomplete, has been advanced by the studies of Fujita and Shimoyama and Rose presented in Chapter 49.

Gun Optics

The nature of the field distribution inside an electron gun is such that the familiar paraxial equations and aberration theory that characterize lenses cannot be used. In the preceding chapters, we have encountered some attempts to use the familiar concepts in the context of electron guns. A modification of the usual approach introduced by Fujita and colleagues makes it possible to establish a useful theory of gun optics. In Section 49.1, we present this theory in some detail as it represents a real advance in gun studies. Another approach to gun optics, based on the modified temporal theory used to study mirrors (Sections 18.2 and 28.1), has been made by Rose (2012). We summarize this in Section 49.2.

49.1 The Fujita–Shimoyama Theory

The important parameters are illustrated in Fig. 49.1. At the cathode, ξ_x and ξ_y measure distance from the apex of the cathode – they are thus position coordinates. The gradient coordinates are $u_x = \sin\alpha_x$ and $u_y = \sin\alpha_y$, where α_x and α_y are the angles between the ray in question and the normal to the surface. The aim of the theory is to establish the mapping between ξ and u at the cathode and the corresponding variables at the crossover plane, η_c and $\upsilon = \sin\beta$ (and similarly for the y-coordinates). This mapping is represented by the canonical mapping transform (CMT) diagram, in which $\upsilon = \sin\beta$ is plotted as a function of η_{c} for several values of $u = \sin\alpha$. Fig. 49.2 shows a typical CMT diagram, corresponding to a simple model of a triode gun (Fig. 49.3); the values of u range from -1 to 1.

Fujita et al. (2010a) set out from

$$\Delta S^I = \left(\boldsymbol{p}_2^I \cdot \Delta\boldsymbol{x}_2 - \boldsymbol{x}_2^I \cdot \Delta\boldsymbol{p}_2\right) - \left(\boldsymbol{p}_1^I \cdot \Delta\boldsymbol{x}_1 - \boldsymbol{x}_1^I \cdot \Delta\boldsymbol{p}_1\right)$$

(22.23) but no longer require that $\boldsymbol{x}_1^I$ and $\boldsymbol{p}_1^I$ vanish. In a first step, they assume that the cathode is plane ($z = z_1$); the curvature of real cathodes is considered in a second step. They find

$$\begin{pmatrix} \dfrac{\partial S^I}{\partial x_1'} \\[2ex] \dfrac{\partial S^I}{\partial x_1} \end{pmatrix} = \left(2em\hat{\phi}_2\right)^{1/2} \begin{pmatrix} -h_2' & h_2 \\ -g_2' & g_2 \end{pmatrix} \begin{pmatrix} x_2^I \\ \upsilon_x^I \end{pmatrix} - \left(2em\hat{\phi}_1\right)^{1/2} \begin{pmatrix} -x_1^I \\ u_x^I \end{pmatrix} \tag{49.1}$$

Principles of Electron Optics: Applied Geometrical Optics.
DOI: http://dx.doi.org/10.1016/B978-0-12-813369-9.00049-X

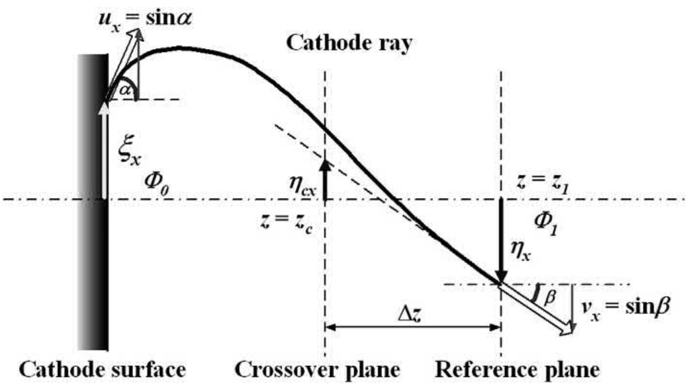

Figure 49.1
The variables employed in the canonical mapping transformation. *After Fujita et al. (2010a), Courtesy the authors and Oxford University Press.*

and

$$p^I_{1x} =: \left(2me\hat{\phi}_1\right)u^I_x, \quad p^I_{2x} =: \left(2me\hat{\phi}_2\right)\upsilon^I_x \tag{49.2}$$

From this, we obtain

$$\begin{pmatrix} x^I_2 \\ \upsilon^I_x \end{pmatrix} = \begin{pmatrix} g_2 & h_2 \\ g'_2 & h'_2 \end{pmatrix} \left\{ \begin{pmatrix} x^I_1 \\ u^I_x \end{pmatrix} + \frac{1}{\left(2me\hat{\phi}_1\right)} \begin{pmatrix} -\dfrac{\partial S^I}{\partial x'_1} \\ \dfrac{\partial S^I}{\partial x_1} \end{pmatrix} \right\} \tag{49.3}$$

In a plane $z = z_2$, therefore, we have

$$\begin{aligned} \eta_x &=: x^{(P)}_2 + x^I_2 = x_1 g(z_2) + x'_1 h(z_2) + x^I_2 \\ p_{2x} &= (2me\hat{\phi}_2)^{1/2}\upsilon_x =: p^{(P)}_{2x} + p^I_{2x} = (2me\hat{\phi}_2)^{1/2}\{x_1 g'(z_2) + x'_1 h'(z_2) + \upsilon^I_x\} \end{aligned} \tag{49.4}$$

or

$$\begin{pmatrix} \eta_x \\ \upsilon_x \end{pmatrix} = \begin{pmatrix} g_2 & h_2 \\ g'_2 & h'_2 \end{pmatrix} \left\{ \begin{pmatrix} \xi_x := x_1 + x^I_1 \\ u_x := x'_1 + u^I_x \end{pmatrix} + \frac{1}{(2me\hat{\phi}_1)^{1/2}} \begin{pmatrix} -\partial S^I/\partial x'_1 \\ \partial S^I/\partial x_1 \end{pmatrix} \right\} \tag{49.5}$$

(The index (P) denotes 'paraxial'.) Fujita et al. argue that

$$(2me\phi_1)^{1/2}u_x = p_{1x} \tag{49.6}$$

and in the absence of a magnetic field,

$$u_x = \sin\alpha \tag{49.7}$$

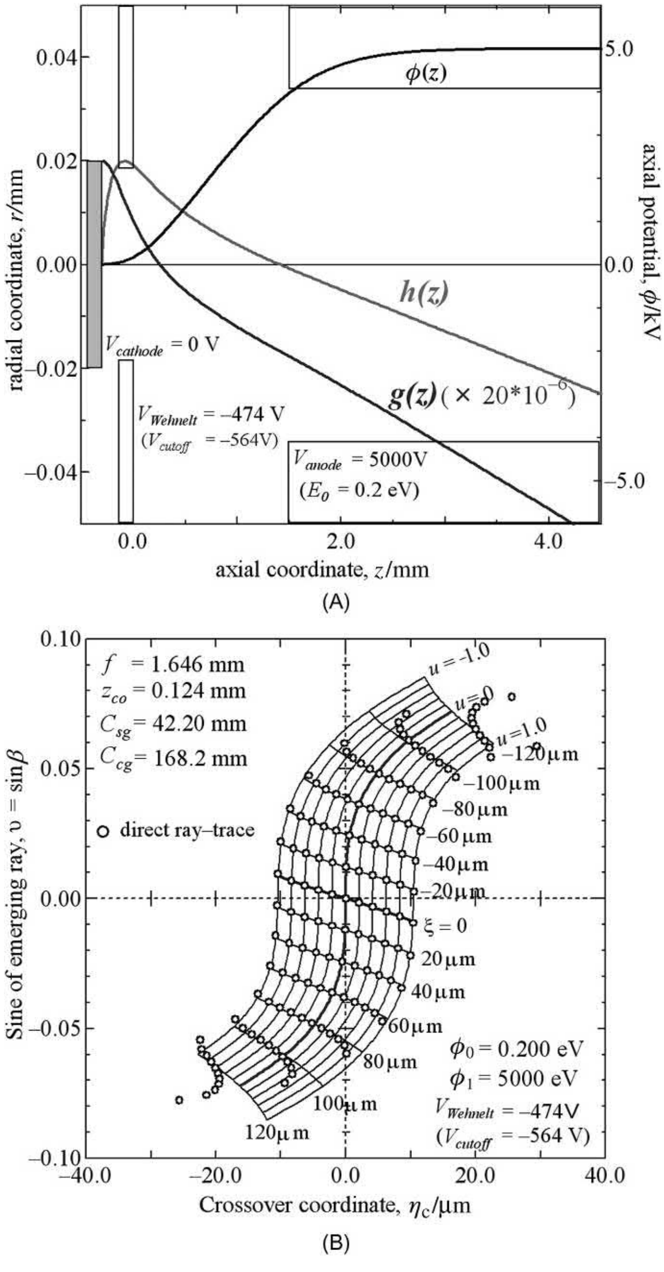

Figure 49.2

(A) The axial potential distribution and the fundamental paraxial trajectories for the model gun of Fig. 49.3; a real crossover is seen just in front of the wehnelt. (B) CMT diagram calculated by the generalized paraxial trajectory method in the third-order polynomial approximation. The small circles are the result of direct ray tracing, which should ideally coincide with the grid intersections. *After Fujita et al. (2010a), Courtesy the authors and Oxford University Press.*

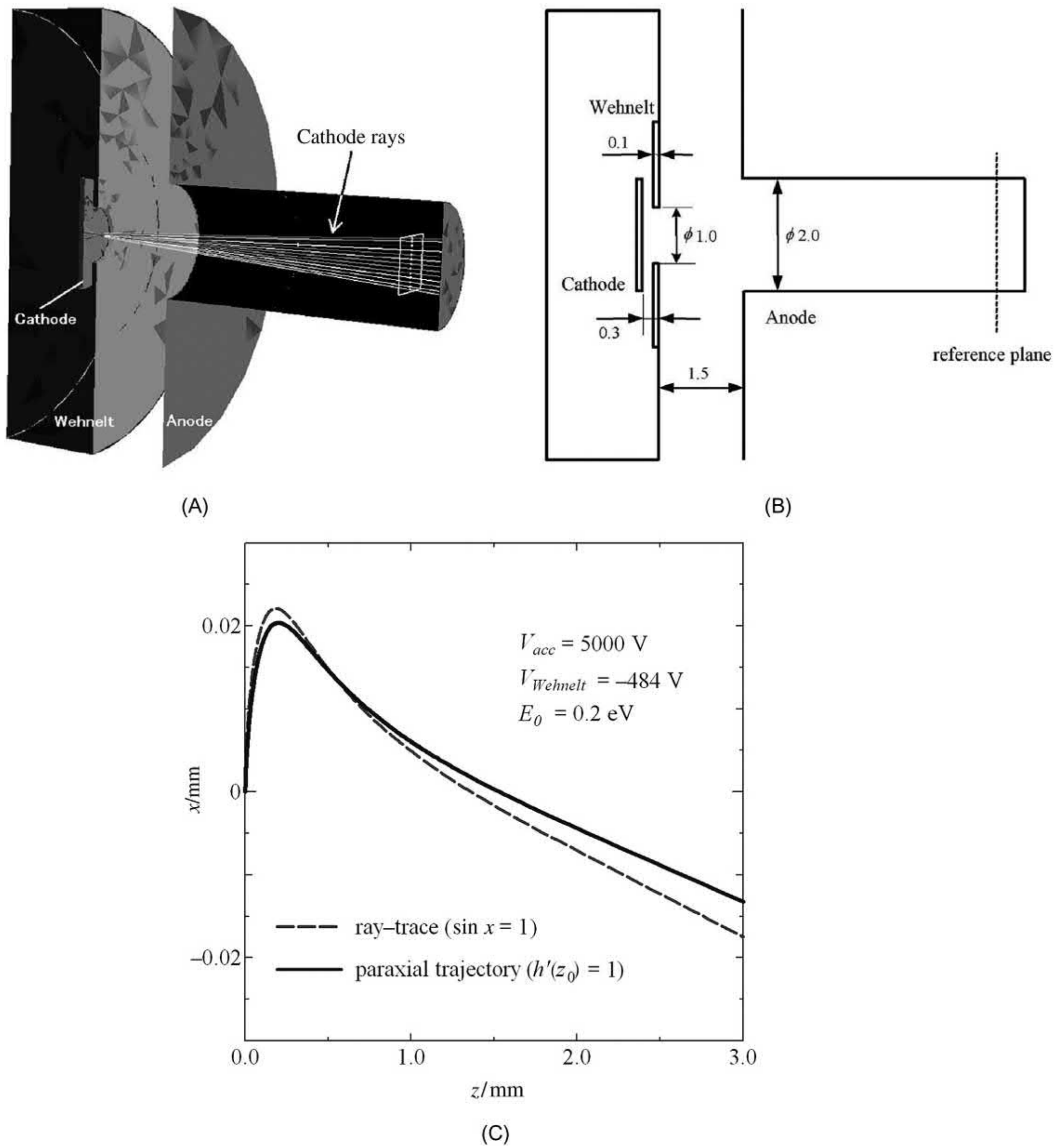

Figure 49.3

(A, B) The simplified triode gun model on which Fig. 49.2 is based and (C) comparison of fundamental rays. *After Fujita et al. (2008), Courtesy the authors and Elsevier.*

where α is defined in Fig. 49.1. How are (ξ_x, u_x) related to (x_1, x_1')? We can certainly choose $x_1 = \xi_x, y_1 = \xi_y$. For the gradients, the authors justify selecting $x_1' = u_x, y_1' = u_y$. With $\xi = \xi_x + \mathrm{i}\xi_y$, $u = u_x + \mathrm{i}u_y$, $\eta = \eta_x + \mathrm{i}\eta_y$, $v = v_x + \mathrm{i}v_y$ and $r = x + \mathrm{i}y$, Eq. (49.5) becomes

$$\begin{pmatrix} \eta \\ v \end{pmatrix} = \begin{pmatrix} g_2 & h_2 \\ g_2' & h_2' \end{pmatrix} \left\{ \begin{pmatrix} \xi \\ u \end{pmatrix} + \frac{2}{(2me\hat{\phi}_1)^{1/2}} \begin{pmatrix} -\partial S^I/\partial r_1'^* \\ \partial S^I/\partial r_1^* \end{pmatrix} \right\} \tag{49.8}$$

The geometrical aberrations are obtained by identifying S^I with $M^{(4)}$ (24.1). (Fujita et al. use $(2me)^{1/2}M^{(4)}$). We can now write

$$(2me)^{1/2}M^{(4)} = \sum_{k=1}^{10} C_k^I(r_1, r_1^*, r_1', r_1'^*) S_k^I\{g(z), h(z), \theta(z)\} \tag{49.9}$$

The appropriate quantities to be inserted in this expression are listed in Table 49.1.

The chromatic aberrations may be calculated in the same way (26.3):

$$(2me)^{1/2}M^{(c)} = \sum_{k=1}^{10} C_k^C(r_1, r_1^*, r_1', r_1'^*) S_k^C\left[\{g(z), h(z), \theta(z)\}\Delta\phi + B_k^C\{g(z), h(z), \theta(z)\}\Delta(NI)/NI\right] \tag{49.10}$$

Table 49.1: Components of the geometrical perturbation characteristic function

k	$C_k^I(r_0, r_0^*, r'_0, r_0'^*)$	r^4	$r^2(x'^2+y'^2)$	$(x'^2+y'^2)^2$	$r^2(xy'-x'y)$
1	$r_0{}^2 r_0^{*2}$	g^4	$g^2(g'^2+\theta'^2g^2)$	$(g'^2+\theta'^2g^2)^2$	$\theta' g^4$
2	$r_0 r_0^*(r_0 r_0'^* + r_0^* r'_0)$	$2g^3h$	$g^2(g'h'+\theta'^2gh) + gh(g'^2+\theta'^2g^2)$	$2(g'^2+\theta'^2g^2) \times (g'h'+\theta'^2gh)$	$2\theta' g^3 h$
3	$\mathrm{i}r_0 r_0^*(r_0 r_0'^* - r_0^* r'_0)$	–	$\theta' g^2(gh'-g'h)$	$2\theta'(g'^2+\theta'^2g^2) \times (gh'-g'h)$	$\frac{1}{2}g^2(gh'-g'h)$
4	$r_0 r_0^* r'_0 r_0'^*$	$2g^2h^2$	$g^2(h'^2+\theta'^2h^2) + h^2(g'^2+\theta'^2g^2)$	$2(g'^2+\theta'^2g^2) \times (h'^2+\theta'^2h^2)$	$2\theta' g^2h^2$
5	$(r_0 r_0'^* + r_0^* r'_0)^2$	g^2h^2	$gh(g'h'+\theta'^2gh)$	$(g'h'+\theta'^2gh)^2$	$\theta' g^2h^2$
6	$(r_0 r_0'^* - r_0^* r'_0)^2$	–	–	$-\theta'^2(gh'-g'h)^2$	–
7	$\mathrm{i}(r_0{}^2 r_0'^{*2} - r_0^{*2} r'_0 2)$	–	$\theta' gh(gh'-g'h)$	$2\theta'(g'h'+\theta'^2gh) \times (gh'-g'h)$	$\frac{1}{2}gh(gh'-g'h)$
8	$r'_0 r_0'^*(r_0 r_0'^* + r_0^* r'_0)$	$2gh^3$	$gh(h'^2+\theta'^2h^2) + h^2(g'h'+\theta'^2gh)$	$2(g'h'+\theta'^2gh) \times (h'^2+\theta'^2h^2)$	$2\theta' gh^3$
9	$\mathrm{i}r'_0 r_0'^*(r_0 r_0'^* - r_0^* r'_0)$	–	$\theta' h^2(gh'-g'h)$	$2\theta'(h'^2+\theta'^2h^2) \times (gh'-g'h)$	$\frac{1}{2}h^2(gh'-g'h)$
10	$r_0'{}^2 r_0'^{*2}$	h^4	$h^2(h'^2+\theta'^2h^2)$	$(h'^2+\theta'^2h^2)^2$	$\theta' h^4$

Each element of the geometrical perturbation characteristic function is shown. The second column gives the polynomial forms of the trajectory parameters and the remaining columns show the quantities to be substituted for the terms in the integral of Eq. (49.9).

see Table 49.2. In all, therefore,

$$\begin{pmatrix} \eta \\ \upsilon \end{pmatrix} = \begin{pmatrix} g_2 & h_2 \\ g_2' & h_2' \end{pmatrix} \left\{ \begin{pmatrix} \xi \\ u \end{pmatrix} + \frac{2}{(2me\hat{\phi}_1)^{1/2}} \begin{pmatrix} -\partial M^{(4)}/\partial r_1'^{*} \\ \partial M^{(4)}/\partial r_1^{*} \end{pmatrix} + \frac{2}{(2me\hat{\phi}_1)^{1/2}} \begin{pmatrix} -\partial M^{(c)}/\partial r_1'^{*} \\ \partial M^{(c)}/\partial r_1^{*} \end{pmatrix} \right\} \tag{49.11}$$

In the crossover plane, $z = z_k$, that is, the plane in which $g(z_k) = 0$, the geometric aberrations are given by

$$\begin{aligned} \eta_k(\xi, u) &= f\left(\hat{\phi}_1/\hat{\phi}_2\right)^{1/2} u + \sum_{i+j+k+l=3} a_{ijkl}\xi^i \xi^{*j} u^k u^{*l} \\ \upsilon_k(\xi, u) &= -\xi/f + mu + \sum_{i+j+k+l=3} b_{ijkl}\xi^i \xi^{*j} u^k u^{*l} \end{aligned} \tag{49.12}$$

The position of the crossover and hence the focal length can be defined in two ways. The *real* crossover lies in the plane $z = \zeta_k$ in which $g(z) = 0$, as stated above. The corresponding focal length is given by

$$f = -1/g'(\zeta_k) \tag{49.13a}$$

Alternatively, we may consider the *asymptotic* crossover, as seen from the image space of the gun. If $G(z)$ denotes the asymptote to $g(z)$, the asymptotic crossover will lie in the plane for which $G(z) = 0$, $z = \zeta_k'$ The asymptotic focal length $\tilde{f}$ will be given by

$$\tilde{f} = -1/G'(\zeta_k') \tag{49.13b}$$

We have met a similar distinction in connection with objective lenses (Section 17.1). The theory may be continued using either definition. In Eq. (49.12), ξ and u are the values at the cathode. When no magnetic field is present, the x and y components can be treated separately. The size of the crossover (the width of the diagram at $\upsilon = 0$) is given very accurately by this method, which justifies the use of sin α. Fujita et al. offer a theoretical justification for this choice, not reproduced here.

Table 49.2: Components of the chromatic perturbation characteristic function

k	$C_k^C(r_0, \bar{r}_0, r_0', \bar{r}_0')$	r^2	$x'^2 + y'^2$	$xy' - x'y$
1	$r_0 r_0^*$	g^2	$g'^2 + \theta'^2 g^2$	$\theta' g^2$
2	$r_0 r_0'^* + r_0^* r_0'$	gh	$g'h' + \theta'^2 gh$	$\theta' gh$
3	$r_0' r_0'^*$	h^2	$h'^2 + \theta'^2 h^2$	$\theta' h^2$
4	$\mathrm{i}\left(r_0 r_0'^* - r_0^* r_0'\right)$	–	$\theta\left(gh' - g'h\right)$	$\frac{1}{2}\left(gh' - g'h\right)$

Each element of the chromatic perturbation characteristic function is shown. The second column gives the polynomial forms of the trajectory parameters and the third to fifth columns shows the quantities to be substituted for the terms in the integral Eq. (49.10).

We now list the most useful results of this theory. Formulae for the spherical and chromatic aberration coefficients are given by Fujita et al. (Eqs 27c and 27d), not reproduced here, in fixed (not rotating) coordinates. In the linear approximation,

$$\eta_x = f\left(\phi_1/\phi_2\right)^{1/2} u_x \quad \upsilon_x(\xi_x, u_x) = -\xi_x/f + u_x/M$$

where M represents magnification. The focal length can also be written as

$$\frac{1}{f} = -\frac{\partial \sin \beta}{\partial \xi_x} \tag{49.13c}$$

In practice, the focal length is independent of the initial electron energy and this enables us to estimate the crossover diameter (d_k) and the current density (j_k):

$$d_k = 2f\left(kT/e\phi_2\right)^{1/2} \quad j_k = f^2 j_1$$

in which j_1 is the current density at the cathode. The crossover diameter is the full-width at 1/e of the maximum current density.

In a later paper, Fujita et al. (2010b) generalize their analysis in order to accommodate the curved cathodes of cold field emitters. First, they redefine $g(z)$ and $h(z)$:

$$\begin{aligned} &g(z_1) = 1 \quad g'(z_1) = 1/\rho \\ &h(z_1) = 0 \quad h'(z_1) = 1 \end{aligned} \tag{49.14}$$

The paraxial expression for the ray characterized by ξ_x and $u_x = \sin \alpha$ at the cathode is

$$x(z) = \xi_x g(z) + u_x h(z) \tag{49.15}$$

The effect of replacing a plane cathode by a curved cathode (here assumed to be spherical with radius ρ) is included by calculating corrected expressions for ξ_x and ξ_y. A ray that sets out along the normal to the cathode surface at ξ_x, ξ_y will intersect the plane that is tangent to the cathode at its apex at a point

$$x_1 = \xi_x + \Delta x_1, \quad \Delta x_1 = \frac{\xi_x^3}{3\rho^2} \tag{49.16}$$

For a ray that sets out at an angle α to the normal,

$$\Delta x_1 = \frac{\xi_x^2 u_x}{2\rho} \tag{49.17}$$

In all, therefore,

$$\Delta x_1 = \frac{\xi_x^2}{6\rho^2}\left(2\xi_x + 3u_x\rho\right) \tag{49.18a}$$

Similar arguments lead to

$$\Delta u_x = \frac{1}{2\rho^3}\left(\frac{F_1\rho}{2\phi_1} - \frac{1}{3}\right) - \frac{\xi_x u_x}{2\rho^2}\left(\xi_x + u_x\rho\right) \tag{49.18b}$$

in which F_1 is the electric field at the cathode surface. The geometric aberrations are then obtained by incorporating this correction in Eq. (49.8). For the chromatic aberrations, the quantity $\xi_x \Delta\phi/2\rho\phi_1$ must be added to u_x.

A program named G-Optk that simulates electron gun performance on the basis of this theory has been written by the authors. Several examples of calculations are included in the papers cited. See also Fujita and Shimoyama (2005a,b, 2006) and for an updated version of the program, Nagasao et al. (2011).

Note. The use of sin α in the gradient variable was introduced by Takaoka and Ura (1987, 1990), inspired by the work of Kel'man et al. on cathode lenses (1973). Although the present theory again uses sin α, the reasoning is quite different.

49.2 Rose's Theory

The method used by Preikszas and Rose to study electron mirrors has been adapted by Rose to explore the optics of field-emission guns (Rose, 2012). The cathode is assumed to be a surface with rotational symmetry with its apex at $z = \zeta_0$. Then with the notation of Section 18.2 the longitudinal distance $h(\tau)$ at the cathode is given by

$$\begin{aligned} h_0(\tau_0) &= h(w_0, w_0^*) = z_0 - \zeta_0 = \sum_{m=1}^{\infty} h_0^{(2m)} \\ h_0^{(2m)} &= \frac{1}{2}\Gamma_{2m}(w_0 w_0^*)^{2m} \end{aligned} \tag{49.19}$$

in which the terms Γ_{2m} measure the curvature of the tip. For a pointed tip, the radius of curvature at the apex, $-1/\Gamma_2$, is negative; higher order terms, Γ_{2m}, represent departures of the tip shape from the basic parabolic form.

Here, a slightly different time scale is used from that used in Chapter 18 of Volume 1 (defined by 3.9):

$$d\tilde{\tau} = \left(\frac{e\phi_0'^2}{2m\phi_A}\right)^{1/2} dt \tag{49.20}$$

in which ϕ_A is the anode potential. For an electron that emerges from the cathode with a small energy $\hat{\varepsilon}$, and initial velocity v_0, $\hat{\varepsilon} = mv_0^2/2$, conservation of energy requires that

$$\dot{w}\dot{w}^* + \left(\dot{\zeta}+\dot{h}\right)^2 = 4\frac{\phi_A\phi}{\phi_0'^2} + 2\frac{mv_0^2\phi_A}{e\phi_0'^2} \tag{49.21a}$$

or for the reference electron,

$$\dot{\zeta} = 2\frac{\left(\phi\phi_A\right)^{1/2}}{\phi_0'} \tag{49.21b}$$

With the new definition of the time, the paraxial equations take the form

$$\ddot{u} + \left(\frac{\phi_A\phi'' + \eta^2B^2\phi_A}{\phi_0'^2}\right)u = 0 \tag{49.22a}$$

$$\ddot{h} - 2\frac{\phi_A\phi''}{\phi_0'^2}h = 0 \tag{49.22b}$$

In order to prevent any confusion with the notation of Chapters 18 and 28, we denote the solutions of (49.22b) by h_α and h_γ; we shall see that h_α and h_γ are of the same nature as the rays $h(z)$ and $g(z)$ of round lenses. We have

$$h_\gamma\dot{h}_\alpha - \dot{h}_\gamma h_\alpha = 1 \tag{49.23}$$

and set

$$h_\alpha(\zeta_0) = \dot{h}_\gamma(\zeta_0) = 0 \quad \dot{h}_\alpha(\zeta_0) = h_\gamma(\zeta_0) = 1 \tag{49.24}$$

with the result that

$$h_\alpha(\tilde{\tau}) = \left(\frac{\phi}{\phi_A}\right)^{1/2} = \frac{\phi_0'}{2\phi_A}\dot{\zeta} \quad h_\gamma(\tilde{\tau}) = \frac{1}{2}\left(\phi\phi_A\right)^{1/2}\int_{\tilde{\tau}_\gamma}^{\tilde{\tau}}\frac{d\tilde{\tau}}{\phi} \tag{49.25}$$

The lower limit of integration is chosen in such a way that $\dot{h}_\gamma(\tilde{\tau}_0) = 0$. We write

$$v_{0z} = v_0\cos\theta_0 \quad v_{0w} := v_{0x} + \mathrm{i}v_{0y} = v_0\mathrm{e}^{\mathrm{i}\theta_0}\sin\theta_0$$

and obtain

$$\dot{w}(\tilde{\tau}_0) = \lambda\mathrm{e}^{\mathrm{i}\theta_0}\sin\theta_0 \quad \dot{h}_0(\tilde{\tau}_0) = \lambda\cos\theta_0 \tag{49.26}$$

with

$$\lambda = \frac{v_0\phi_A^{1/2}}{\eta\phi_0'}$$

We denote the solutions of (49.22a) by $\tilde{p}(\tilde{\tau})$ and $\tilde{q}(\tilde{\tau})$, the tilde is a reminder that the initial conditions are not the same as in Section 18.2:

$$\begin{aligned}\tilde{p}(\tilde{\tau}_0) = \dot{\tilde{q}}(\tilde{\tau}_0) = 1 \\ \dot{\tilde{p}}(\tilde{\tau}_0) = \tilde{q}(\tilde{\tau}_0) = 0\end{aligned} \tag{49.27}$$

With

$$\dot{u}_0 = \dot{w}_0 + \mathrm{i}\dot{\chi}_0 u_0 \quad \dot{\chi}_0 = \frac{\eta B_0 \phi_A^{1/2}}{\phi_0'} \tag{49.28a}$$

the paraxial solution adopts the familiar form

$$u(\tilde{\tau}) = \tilde{p}(\tilde{\tau})u_0 + \tilde{q}(\tilde{\tau})\dot{u}_0 \tag{49.28b}$$

The Gaussian image of the cathode tip is formed in the plane in which $\tilde{q}(\tilde{\tau})$ vanishes; at the crossover (ζ_k), $\tilde{p}(\zeta_k) = 0$. The radius of the crossover is thus

$$r_k = \tilde{q}(\zeta_k)\frac{\phi_A^{1/2}}{\phi_0'}\left(\frac{\upsilon_{0,\max}^2}{\eta^2} + \eta^2 B_0^2 r_0^2\right)^{1/2} \tag{49.29}$$

where r_0 denotes the radius of the area of emission, $u_{0,\max}$. We see that the crossover is smallest when there is no magnetic field at the tip.

Rose examines two classes of aberrations: the second-rank aberrations in the image and crossover planes and the spherical aberration at the crossover. We shall not reproduce the derivation of these aberration coefficients, given in full by Rose; here we simply list the results.

For the second-rank aberrations, Rose finds

$$\begin{aligned}\hat{u}^{(2)}(z) &= -w_\gamma \frac{\phi_0'}{2\phi_A}\dot{h}_0\dot{w}_0 + w_\alpha \frac{\phi_0''}{\phi_0'}\dot{h}_0 w_0 \\ &= -w_\gamma \frac{\upsilon_0^2}{4\eta^2\phi_0'}\mathrm{e}^{\mathrm{i}\theta}\sin 2\theta_0 + w_\alpha\left(\frac{\phi_A}{\eta}\right)^{1/2}\frac{\phi_0''}{\phi_0'^2}w_0\upsilon_0\cos\theta_0\end{aligned} \tag{49.30}$$

The first term is purely chromatic, depending on the velocity but not on the position coordinate. The second term is a mixture of υ_0 and w_0. The first term gives the familiar chromatic aberration at the image plane conjugate to the cathode tip:

$$\frac{w^{(2)}(\zeta_i)}{w_\gamma(\zeta_i)} = -C_c\left(\frac{1}{2}\mathrm{e}^{\mathrm{i}\theta_0}\sin 2\theta_0\right)\frac{\upsilon_0^2}{4\eta^2\phi_A} \quad \text{with} \quad C_c = \frac{2\phi_A}{\phi_0'} \tag{49.31}$$

Since ϕ_A cancels out from this expression, the only way of diminishing the chromatic aberration is by making ϕ_0', the electric field at the cathode, as high as possible.

The mixed term vanishes in this image plane. It does however generate a second-rank aberration at the crossover plane (ζ_k), where the first term vanishes.

For the spherical aberration at the crossover plane, Rose finds

$$\hat{w}^{(3)}(\zeta_k) = \tilde{C}_s w_0^2 w_0^* w_{\alpha k}$$

$$\tilde{C}_s = \frac{1}{4} w_{\gamma k}'^3 \int_{\zeta_\gamma}^{\zeta_k} \left(\frac{\phi_k}{\phi}\right)^{1/2} d\zeta + \frac{1}{16\phi_0'} \int_{\zeta_0}^{\zeta_k} \left(\frac{\phi_A}{\phi}\right)^{1/2} \left\{\phi^{(4)} - 4\phi''' \left(\frac{\phi''}{\phi_0'} + \frac{\phi_0'}{\phi_A} \frac{\dot{w}_\gamma^2}{w_\gamma^2}\right)\right\} w_\gamma^4 d\zeta \tag{49.32}$$

At first sight, this appears to be a distortion and not a spherical aberration; this is, however, normal because the cathode tip plane is not conjugate to the crossover; the aberrations there are analogous to those in the diffraction plane (the plane conjugate to the source) of a transmission electron microscope.

49.3 Matching the Paraxial Approximation to a Cathode Surface

There are two ways of determining electron trajectories starting from cathode surfaces, the parametric method (Section 49.2) using a time-like curve parameter, and the Cartesian method (Section 49.1). While the former is unproblematic, as all the variables remain confined, the presence of singularities gives rise to difficulties in the second. Despite this, the latter is frequently used since the paraxial approximation and the standard perturbation theory can be employed. Lenz's theory of brightness (Section 47.4) suffers from the same problem.

The difficulty arises from the fact that, near the cathode, the accelerating potential and hence the kinetic energy of the electrons vanish and the slopes of trajectories in the Cartesian representation may become steep. There is no question of a physical singularity, since the trajectories are well-behaved parabolic arcs; the problem arises from the choice of the axial coordinate z as curve parameter. This implies that the slope r' may become singular as $z^{-1/2}$ close to the point of emission. This contradicts the basic assumption that, close to the optic axis, the slopes and curvatures of trajectories are small enough for the linearization to be well justified. Moreover, the aberrations must be small corrections, as the perturbation calculus might otherwise diverge. We now explain how this difficulty can be overcome.

The planar cathode. In this case, the appropriate initial condition can be determined exactly. This model also indicates a way of treating more realistic cases. Without loss of generality, the plane cathode is taken to be the surface $z = 0$, all motion takes place in the half-space $z \geq 0$. Close to this surface (and especially near the apex when we come to consider curved cathodes), it is sufficient to consider *a homogeneous* electrostatic field F. The potential is then

$$\Phi(\boldsymbol{r}) = 0 \quad (z \leq 0) \quad \Phi(\boldsymbol{r}) = Fz \quad (z \geq 0)$$

At the cathode surface, the electron may have a kinetic energy, $E = e\Phi_0$, and the total acceleration potential is then $\Phi(\boldsymbol{r}) = \Phi_0 + Fz$. Since $\Phi''(0, z) = 0$, the nonrelativistic trajectory equation for the radial coordinate $r(z)$ simplifies to

$$\frac{d}{dz}\left(\sqrt{\frac{\Phi_0 + Fz}{1 + r'^2}}r'(z)\right) = 0 \tag{49.33}$$

and similarly for $x'(z)$ and $y'(z)$. Since x and y are not present in these equations, the trivial solutions are arbitrary constants, $x = x_0$, $y = y_0$. From Eq. (49.33) it is obvious that the operand of the differential must be a constant, c. Hence

$$(\Phi_0 + Fz)r'^2 = c^2(1 + r'^2)$$

from which we find

$$r'(z) = \frac{c}{\sqrt{\Phi_0 + Fz - c^2}} \qquad (c^2 \leq \Phi_0)$$

$$r(z) = \frac{2c}{F}\sqrt{\Phi_0 + Fz - c^2} + \text{const}$$

The constant is chosen in such way that $r(0) = 0$ is the origin of the coordinate system. We set

$$c =: \sqrt{\Phi_0}\sin\alpha$$

The meaning of the angle α will become clear later. It is also convenient to introduce the length $L = \Phi_0/F$, the distance in the z-direction in which the electron acquires the energy $e\Phi_0$ by acceleration in the field. The solutions can then be written very concisely as

$$r'(z) = \frac{\sin\alpha}{\sqrt{z/L + \cos^2\alpha}} \tag{49.34a}$$

$$r(z) = \frac{2z\sin\alpha}{\sqrt{z/L + \cos^2\alpha} + \cos\alpha} \tag{49.34b}$$

This solution satisfies the initial conditions $r(0) = 0, \;\; r'(0) = \tan\alpha$. The argument α is thus the angle of inclination with respect to the optic axis at the point of emission and $-\pi/2 < \alpha < \pi/2$. The general solutions are

$$\begin{aligned} x(z) &= x_0 + r(z)\cos\varphi, \quad & x'(z) &= r'\cos\varphi \\ y(z) &= y_0 + r(z)\sin\varphi, \quad & y'(z) &= r'\sin\varphi \end{aligned} \tag{49.35}$$

φ being the azimuth at the starting point. The problem of matching paraxial relations to the cathode surface can now be solved in the following way. If the paraxial theory requires a solution $g(0) = 1$, $g'(0) = 0$, then this is simply the constant $g = 1$ up to the matching point. The second fundamental ray, with initial conditions $h(0) = 0$, $h'(0) = 1$ is given by $r(z)$ in Eq. (49.34b) with $\alpha = \pi/4$. Again, this is valid only up to the matching point.

The homogeneous electric field has only a finite extent in the z-direction. The abscissa of the matching point, z_m, should be chosen far enough from the cathode for the slope $h'(z_m)$ to have become small enough for paraxial calculations but close enough to be outside the inhomogeneous field domain. At the junction, the values of the functions and their derivatives must remain continuous. In the interval $0 \leq z \leq z_m$ no perturbation calculus is needed because the results given above are exactly valid.

Formally, large emission angles do not present any problem, as is evident from the expressions given above. However, the paraxial approximation also requires that linear combinations of the fundamental solutions should be possible solutions. Here, however, this is allowable only for small angles, $|\alpha| \ll 1$, while there is no such restriction for the coordinates x and y. The results are invariant under transverse shifts, as they must be.

Spherical cathode surfaces. This approach can be generalized to the important case of the spherical cathode. We shall find that the relations derived above are again useful here. Fig. 49.4 shows the upper half of a spherical cathode with the corresponding notation.

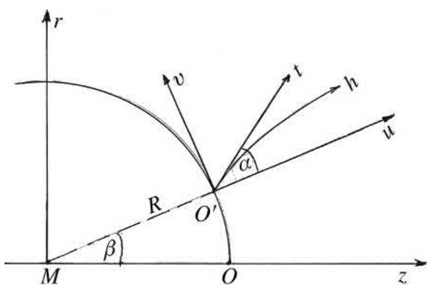

Figure 49.4
Upper half of a meridional section through spherical cathode with radius R and coordinates (u, v) adapted to a surface point O' from which a trajectory h sets out at an angle α relative to the surface normal.

A hyperbolic trajectory may set out from a surface point O′; the tangent ***t*** is inclined at an angle α (positive or negative) relative to the surface normal. It is advantageous to introduce new coordinates, (u, υ) as shown.

The potential of the cathode is set at 0 V and the electron energy is again $E = e\Phi_0$; the trajectory is thus completely defined. We now assume that the field immediately in front of the cathode is a Coulomb field; deviations from this are neglected. The trajectory is then part of a hyperbola and its second focal point is located at the centre of the sphere, M.

The subsequent calculations are elementary but tedious. We therefore consider the special case $\alpha = \pi/2$. The tangent ***t*** then coincides with the tangent to the surface and the point O′ is the vertex of the hyperbola. We adopt the standard notation for a hyperbola: semiaxes a and $p = b^2/a$, eccentricity $\varepsilon := e/a > 1$. The hyperbola with vertex O′ is then given by the familiar formula

$$\upsilon = \sqrt{2pu + (bu/a)^2} \tag{49.36a}$$

Close to the vertex, we can assume that the field is locally homogeneous with strength F. To a first approximation, we can use Eq. (49.34a) with $\alpha = \pi/2$ giving

$$\upsilon = \frac{2u}{\sqrt{u/L}} = \sqrt{4Lu} \tag{49.36b}$$

The coefficients of these two representations must agree and hence

$$L = \Phi_0 F = p/2 = b^2/2a \tag{49.36c}$$

This is the important connection between the mechanical and geometrical parameters. The second condition is that the back focal point must coincide with the midpoint M, which implies

$$a + e = a(1 + \varepsilon) = a + \sqrt{a^2 + 2aL} = R$$

All the parameters have now been determined and we find

$$a = \frac{R^2}{2(R + L)}, \quad b^2 = 2pa = 4La, \quad \varepsilon = 1 + \frac{p}{R} \tag{49.37}$$

It is now favourable to rewrite Eq. (49.36a) as

$$\upsilon(u) = 2\sqrt{Lu(1 + ku)} \tag{49.38}$$

with

$$k := \frac{1}{2a} = \frac{R + L}{R^2} \tag{49.39a}$$

When the emission energy is very small, for which $L \ll R$, this simplifies to the familiar case, $a = R/2$, $k = 1/R$.

In the case of skew rays, the ray vertex is shifted into the interior of the sphere. On the surface, the radial part of the kinetic energy is $T = e\Phi_0 \cos^2 \alpha$. In the field F, this gives rise to a shift $d = L \cos^2 \alpha$. The effective radius of the cathode is then $R' = R - d$. The calculations given above are now repeated with R' instead of R, giving

$$k = \frac{1}{2a} = \frac{R + L \sin^2\alpha}{(R - L\cos^2\alpha)^2} \quad L < R \tag{49.39b}$$

which is obviously a generalization of Eq. (49.39a). For skew rays, the field is again homogeneous close to the point O′ and so (49.34b) must be approximately valid for the variables u and v. It is sufficient to incorporate the factor $1 + ku$, where k is given by Eq. (49.39b). Hence

$$\begin{aligned} v(u) &= 2L \sin\alpha \left\{ \sqrt{u(1 + ku)/L + \cos^2\alpha} - \cos\alpha \right\} \\ v'(u) &= \frac{L \sin\alpha\,(1 + 2ku)}{\sqrt{u(1 + ku)/L + \cos^2\alpha}} \end{aligned} \tag{49.40}$$

This is exactly valid for $\alpha = \pi/2$ and fairly accurate for smaller angles. Considering the simplicity and general applicability of these formulae, they are useful in practice.

For $u = 0$, these equations lead to $v = 0$ and $v' = \tan\alpha$, as they should. Moreover, for $\alpha = 0$, we obtain $v(u) = 0$ for all u; these are the trivial radial solutions. A further generalization is obvious; in a spherical configuration there is no preferred direction. A plane containing the optic axis is usually chosen, which is determined by the technical arrangement but this is not really necessary. We may select any plane containing the midpoint M. This implies that Eqs (49.40) remain applicable for arbitrary sagittal rays, provided that the coordinate system is chosen appropriately.

There remains the matching of the coordinates u and v to the cylindrical coordinates z and r. This is a simple rotation through an angle β, as shown in Fig. 49.4, given by

$$z + \mathrm{i}r = (R + u + \mathrm{i}v)\exp(\mathrm{i}\beta)$$

It is obvious that as $1/R$ tends to 0, β also tends to 0 and thus $\beta R = \text{const}$; the planar field is a limiting case, as it should be.

The distance u from the cathode surface at which the matching is satisfactory depends on the strength of the non-spherical field and is hence a matter of experience.

Another interesting case is the concave cathode. The reasoning is then quite analogous with the important difference that the trajectories are now elliptic arcs and the constant $k = (L - R)/R^2$ becomes negative, since $L < R$ for ellipses.

A further extension of the method concerns domains near the cathode surface that are not perfectly spherical. The coordinates must then be adapted to the local surface normal and tangent and R will be the local radius of curvature. The domain of validity of this approximation may be rather limited but still large enough to avoid the use of a perturbation calculus with divergent terms. The space is then no longer isotropic and the formulae will be valid only in meridional planes containing the optic axis.

An alternative approach is the theory of Fujita et al. (2010), summarized in Section 49.1. There, the Cartesian representation of ray tracing is employed and, in the case of a convex cathode, this requires the introduction of a 'connecting space', without which not all domains occupied by electron rays can be reached. Fujita et al. developed a method of mapping the cathode surface onto a plane.

In the theory of brightness (Chapter 47), the presence of large slopes x'_o, y'_o does not create any difficulty since the Gaussian distributions always confine the corresponding functions to small values. The continuation of the value of R into the paraxial region is ensured by Liouville's theorem. In this way, therefore, the limitation on Lenz's theory close to the cathode is overcome.

The main drawback of the foregoing calculations is that they do not provide a complete theory of paraxial properties and aberrations in closed form but only some data, however important, that relate the cathode space to the rest of the instrument. For computing purposes, however, this is sufficient.

CHAPTER 50

Complete Electron Guns

In the previous chapters of this Part we have dealt with different aspects of the physics of electron sources but we have not yet considered an entire electron gun. In the operation of electron guns, three functions must be clearly distinguished: (a) the extraction of the beam from the cathode and the provision of the desired emission current I to the system beyond the gun; (b) the acceleration of the beam to a given kinetic energy $E_{\mathrm{kin}} = e\Phi_a$; and (c) the focusing of the beam in a probe or virtual source plane. Very often these three functions are coupled but devices in which they are practically independent are clearly advantageous, since such guns can be adjusted very easily.

In the past decades a great many different electron gun designs have been published. It would serve no useful purpose to describe them all and the list would never be complete. Moreover, a successful design is one that is well adapted to the purpose of the device: a field-emission gun designed for an electron interferometer is not a suitable source for an electron lithography machine and vice versa. Great care is needed even when comparing guns of a similar type, as Barth (1988) has shown. We make no attempt to give a complete review, therefore, but instead, we try to bring out the principles underlying gun design and draw attention to various ideas which may be helpful in the development of new designs.

50.1 Justification of the Point Source Model

In Chapter 45, Pointed Cathodes Without Space Charge, we studied the details of a diode system, consisting of a cathode and an extraction electrode, the (positive) wehnelt. We found that such a system forms a virtual point source with very low aberrations. In almost all theoretical and experimental investigations on field-emission guns (an exception is the work of Kang et al., 1983), the whole system has been more or less tacitly split into a point source in a locally field-free space and a subsequent lens system for acceleration and focusing, for want of any more detailed information about the interaction between the two parts. The lens system is then treated by means of the familiar theory of focusing and aberrations. Experiment has long since shown that this simplification gives a good approximation but it was not until 1978 that Kern could demonstrate its validity by comparison with guns calculated as a single entity. The understanding thus provided of the decoupling into two successive lens systems may also be very helpful in other design problems.

Principles of Electron Optics: Applied Geometrical Optics.
DOI: http://dx.doi.org/10.1016/B978-0-12-813369-9.00050-6

The basic ideas of the approximation, expressed qualitatively in Kasper (1982), are presented schematically in Figs 50.1A–C and 50.2. Fig. 50.1 illustrates the procedure. In the first step (Fig. 50.1B), the space beyond the wehnelt is assumed to be field-free and at wehnelt potential. The asymptotes concur at the point V and the associated kinetic energy is $e\Phi_w$. In the second step (Fig. 50.1C), the cathode is ignored and the space *in front* of the wehnelt is assumed to be field-free and at potential Φ_w. The electrons leaving the point source at V are then assumed to set out with energy $e\Phi_w$, so that the rays are straight until they reach the first fringe field. Note that the aperture of the wehnelt electrode appears in both figures (B) and (C); in reality this aperture is very small. Fig. 50.2 illustrates more clearly the idea underlying this approximation. In both steps there is a strong field ($\boldsymbol{E}_{1,2}$) on one side of the diaphragm, a comparatively weak fringe field domain ($S_{1,2}$) in the vicinity of the bore and an asymptotically field-free space on the other side. In each domain, the real electric field is the sum of the individual contributions. The approximation that consists in tracing the trajectories through the cathode field, determining their virtual intersection at V and then tracing the electrons through the wehnelt field treats the strong fields correctly and the weak fringe fields approximately. Indeed, the trajectory passing through the aperture is bent by *both* fringe field contributions, though not simultaneously, as it should be, but in two separate steps. The error remains small if two conditions are satisfied: (i) the diaphragm separating the two zones must be thin and the aperture small, so that the fringe fields are confined to a very small spatial domain; (ii) the electrons must be fast enough for their trajectories to be bent only weakly as they pass through the fringe fields.

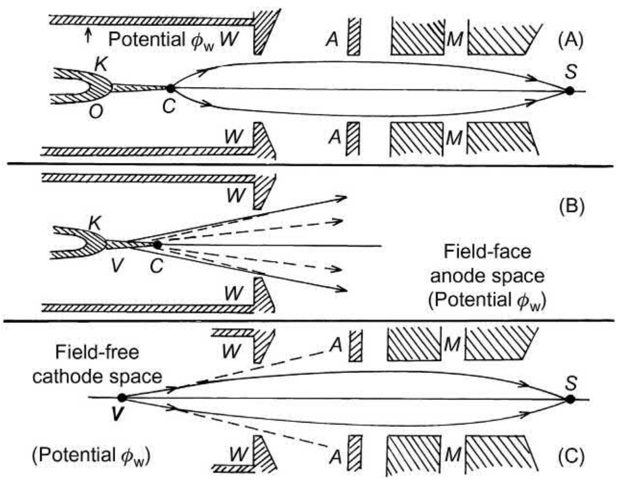

Figure 50.1

Division of a complete electron gun in subsections. (A) Complete gun; (B) 'extraction' system with field-free anode space. (C) Acceleration and focusing system with field-free cathode space. K: cathode with tip at C; V: virtual source; W: wehnelt; A: anode; M: magnetic lens; S: crossover.

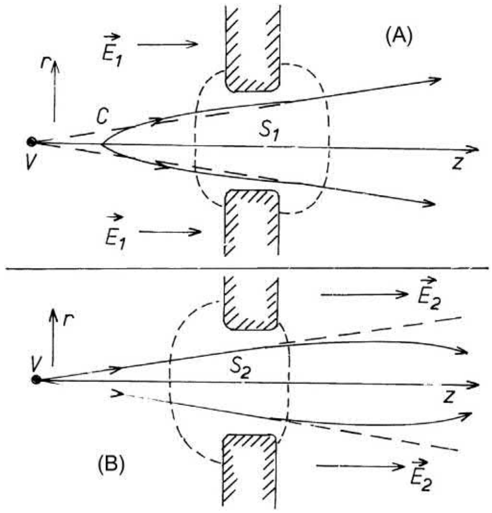

Figure 50.2
Schematic representation of the separation method. (A) Strong electric field ($\boldsymbol{E}_1$) on the left-hand side of a diaphragm, weak fringing field in the region S_1 and asymptotically field-free space on the right-hand side. The asymptotes of trajectories starting at C intersect at V. (B) Reverse situation, with the strong electric field ($\boldsymbol{E}_2$) now on the right-hand side. Note that it is not the trajectories themselves but their asymptotes that are used to specify the entrance conditions.

In the common designs of field-emission electron (FEE) guns, these conditions are satisfied, since the aperture is made very small in order to reduce aberrations in the subsequent part of the gun. Theoretical and experimental tests have been made by Kern et al. (1978/9). Some typical results of these investigations are shown in Fig. 50.3. These demonstrate that the errors are indeed small.

A consequence of these findings is that in all comparable cases, where the appropriate conditions are met, a complex system can be safely split up into simpler subsystems. These can then be treated by tracing the exit asymptotes from each part and treating them as the entrance asymptotes for the next part. By following this strategy, the design of complex systems can be facilitated considerably.

50.2 The Lens System in Field-Emission Devices

We now disregard the cathode and assume that a point source V emits electrons of energy $e\Phi_w$ into field-free space. This source may have a finite but very small radius given by Eq. (45.7) or (45.8). The electron beam supplied by this source is then accelerated and focused by a compound system of electrostatic and magnetic lenses. Numerous field-emission structures have been designed in this way, too many for all to be listed here.

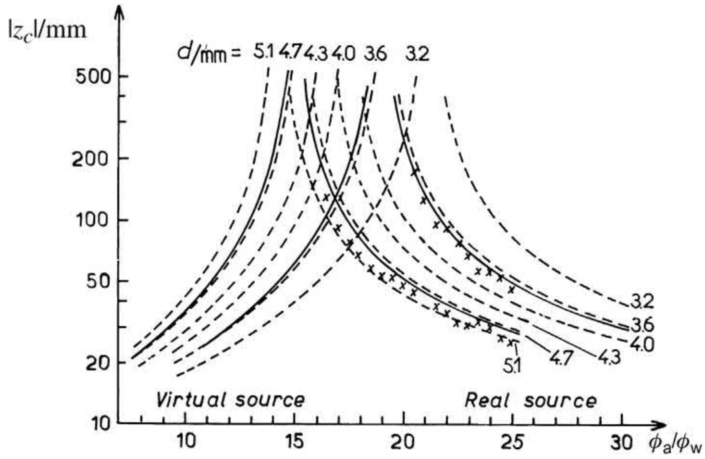

Figure 50.3
Measured and calculated positions of the crossover as a function of the voltage ratio Φ_a/Φ_w, and of the coordinate d of the apex. Broken lines: acceleration subsystem; full lines: total system for $d = 4.7$ mm; crosses: measured values also for $d = 4.7$ mm.

Once the shapes of the lenses and the excitation currents and voltages have been specified, the cardinal elements and aberration coefficients of the lens system are determined. Investigations of this kind have been published by Butler (1966), Munro (1973), Kern et al. (1978/79), Roques et al. (1983a,1983b) and Denizart et al. (1981) among others. These differ from studies of ordinary lens systems, intended for use as objectives or projector lenses, in that the following facts must be considered.

a. There is necessarily one electrostatic acceleration lens in the compound system, since the energy $e\Phi_w \approx 1$ keV is usually too small to be the final kinetic energy. The electrostatic lens field between the wehnelt and the anode may cause large aberrations.
b. The virtual source radius ρ_v is extremely small, often $\rho_v \sim 1$ nm, and hence considerable care must be taken to prevent the aberration disc of the lens system from greatly exceeding the magnified image of the virtual source. This often entails searching for a suitable (optimum) magnification.
c. The brightness of field-emission guns is very high (about 10^8 A cm^{-2} sr^{-1} or more), but the total probe current is rather low, about 1 μA. This is too low for some purposes so that thermionic or Schottky guns may be more suitable.

These particular difficulties with cold field-emission guns were studied long ago, by Cosslett and Haine (1954) and by Veneklasen (1972), for example. Usually the plane $z = z_c$ of the crossover, the voltages Φ_w and Φ_a, and the maximum acceptable crossover radius ρ_c are prescribed; the aperture angle θ_m of the beam supplied by the diode and the magnification M of the lens system can generally be varied for the purposes of optimization. Commonly the radii of the different contributions to the aberration disc are squared and summed up leading to the condition

$$\rho^2 = M^2 \left\{ \rho_v^2 + C_0^2 \theta_m^2 + \left(C_C \frac{\Delta\Phi}{\Phi_\omega} \theta_m \right)^2 + \left(\frac{1}{4} C_s \theta_m^3 \right)^2 + \left(\frac{0.61 \lambda_w}{\theta_m} \right)^2 \right\} \le \rho_c^2 \tag{50.1}$$

The five contributions come from first the virtual source, then any small but unavoidable defocus ($C_0 \approx R_s$), then the chromatic and the spherical aberration and finally the diffraction disc. Although this procedure is not rigorously correct, it is fairly reliable and quite simple. The correct expression for the size of the probe size is given by Barth and Kruit (1996):

$$d_p^2 = \left[\left\{ d_s^{1.3} + \left(\left(d_d^4 + d_{C_s}^4 \right)^{1/4} \right)^{1.3} \right\}^{1/1.3} \right]^2 + d_{C_c}^2$$

in which d_p is the diameter of the spot that contains 50% of the current (FW_{50}) and d_s, d_d, d_{C_s} and d_{C_c} are the FW_{50} values for the source image, the diffraction disc, the spherical aberration disc and the chromatic aberration disc, respectively; Kruit (2016) observes that the correct expression for an aberration-corrected instrument had not yet been derived. The coefficients C_c and C_s depend on M so that Eq. (50.1) is in reality a very complicated relation. The task is now to maximize θ_m by varying M and some of the lens parameters subject to the constraint $\rho = \rho_c$ at $z = z_c$ (it makes little sense to look for solutions $\rho < \rho_c$ if the size ρ_c is acceptable). This problem is necessarily solved by computer. Since the beam current increases as θ_m^2, the solution found will also correspond to maximum beam current.

An important point when estimating the performance of a field-emission gun is the effect of Coulomb interactions on the virtual source size and hence on the brightness (cf. Chapters 46 and 47). Simulations by Verduin et al. (2011) using two field-emission gun models show that the effect of Coulomb interactions is complicated but can be understood in physical terms as mentioned in Section 47.6. They plot curves showing the dependence of mean brightness on extractor voltage for a given geometry and the electric field at the tip (radius 10 nm in their simulation).

Rather than discuss all the many proposals to be found in the literature, we concentrate on a few special ones which seem to be advantageous. Figs 50.4A and 50.4B show the electrostatic and magnetic equipotentials, respectively, of a compound system, in which the wehnelt electrode is simultaneously one pole of a magnetic lens (Eupper, 1980). The bore of the magnetic lens is narrowed by a piece of non-magnetic material in order to obtain a reasonable aperture. The electrostatic field between the cathode and the wehnelt produces only a virtual projection of the cathode surface with very low aberrations (see Chapter 45).

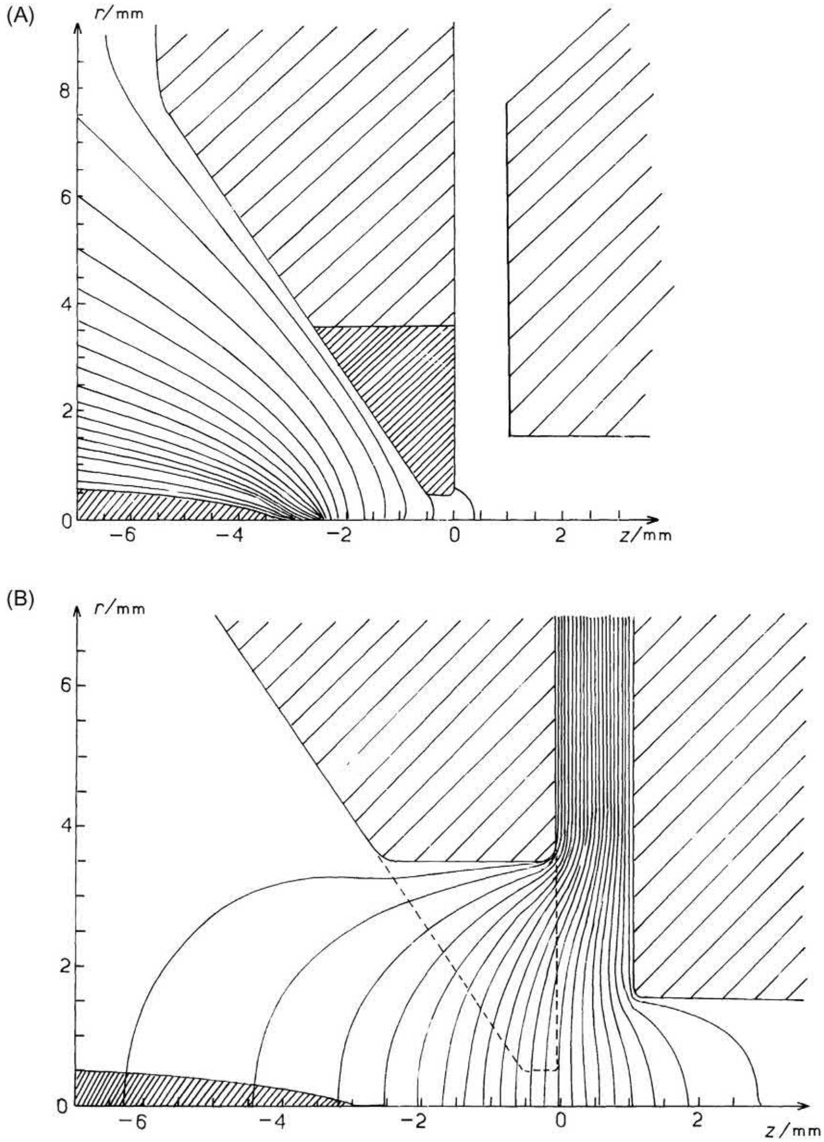

Figure 50.4
An electron gun with both magnetic and electrostatic fields. (A) Electrostatic field and (B) magnetic field in the cathode space.

If the necessary focusing of the beam is performed with magnetic lenses instead of electrostatic ones, the aberrations can be kept small. Such systems have thus the attraction that the properties of the beam are not deteriorated right at the beginning; $C_s \approx 5$ mm and $C_c \approx 2$ mm are realistic values for the aberration coefficients of the compound system. This was by no means the first attempt to incorporate magnetic focusing in a field-emission gun as we saw in Section 44.1. The attractions of a type of unconventional lens introduced by Mulvey (see Chapter 36, Magnetic Lenses) were recognized by Cleaver (1978/79, 1979) and such combinations have been investigated by Troyon and Laberrigue (1977) and Troyon (1980a,b, 1984a,b).

As Veneklasen (1972) and Veneklasen and Siegel (1972b) pointed out, the aberrations in the necessary electrostatic accelerator lens can be kept small if the beam is focused onto the entrance nodal point of this lens and hence emerges asymptotically undeflected from the corresponding exit nodal point. This is shown schematically in Figs 50.5A and B. The reason for the very low aberrations lies in the fact that in the region in which the electric field is strong, the beam remains essentially paraxial. Veneklasen and Siegel also pointed out that the positions of the nodal points are relatively insensitive to changes of the ratio $\kappa := \Phi_a/\Phi_w$. This means that the effect of the focusing lenses and that of the accelerator are clearly separated. The field just in front of the cathode and an accelerator of this type are the only really necessary *electric* fields in the whole device.

The general ideas of Veneklasen and Siegel and their main experimental findings have been confirmed theoretically by numerical ray-tracing through the exact fields in such electron guns (Eupper, 1980; Kasper, 1982).

The brightness of field-emission and Schottky-emission sources when a probe with a high beam current (I) is required has been examined carefully by Fujita and Shimoyama (2005b).

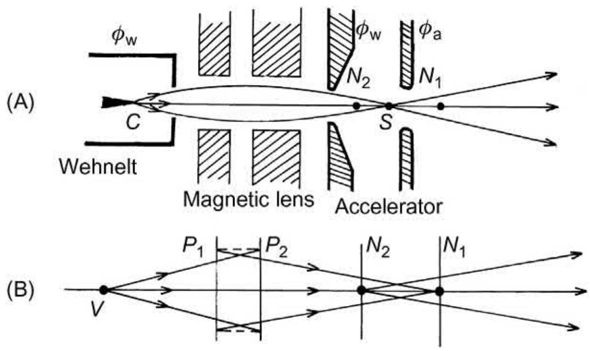

Figure 50.5

(A) Schematic representation of an electron gun with cathode apex at C, wehnelt electrode, magnetic round lens and accelerating lens. The electrostatic potential is zero at the cathode and $\Phi_w > 0$ at the wehnelt, through the magnetic lens and at the first electrode of the accelerating lens; at the second electrode and beyond it, $\Phi_a > \Phi_w$. The system forms a real crossover at S. (B) The corresponding construction using ray-asymptotes. The entrance asymptotes emerge from the virtual point source V; P_1 and P_2 denote the principal planes of the magnetic lens and N_1, N_2 the nodal planes of the accelerating lens.

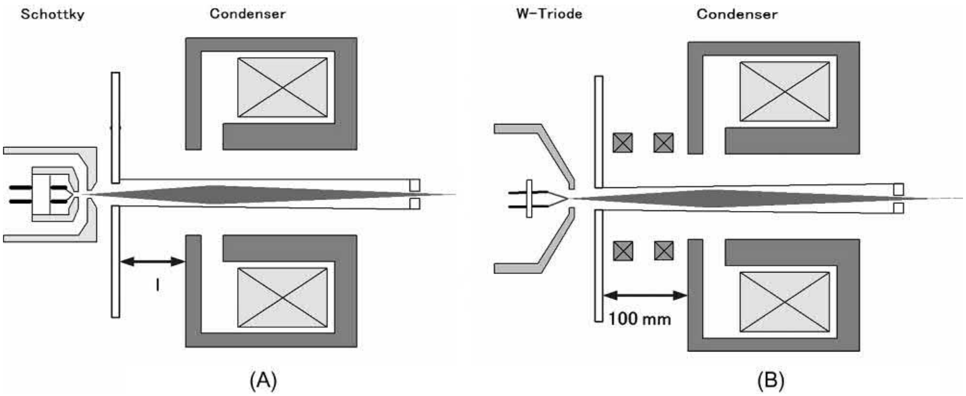

Figure 50.6
Gun models on which the calculation of brightness reduction is based. (A) Schottky emitter. (B) Thermionic emitter. *After Fujita and Shimoyama, (2005b), Courtesy by the authors and the Japanese Society of Microscopy.*

Table 50.1: Comparison of electron gun parameters

Gun Type	Focal Length/mm	Spherical Aberration/mm			Chromatic Aberration/mm			Current Density/ A cm^{-2}
		Emitter	Lens	Total	Emitter	Lens	Total	
Schottky emitter								
$l = 100$mm	-2.07×10^{-3}	0.037	2040	2040	0.098	24.3	24.4	10,000
$l = 50$mm	-2.07×10^{-3}	0.037	376	376	0.098	13.5	13.6	10,000
$l = 0$ mm	-2.07×10^{-3}	0.037	7.21	7.24	0.098	3.13	3.23	10,000
W-triode	2.17	10.2×10^3	7.04×10^3	17.2×10^3	8.15×10^3	112	8.26×10^3	3.0

Gun Type	Crossover Size/nm	Angular Current Intensity/mA sr^{-1}	Axial Brightness/A m^{-2} sr V
Schottky emitter	24.7	0.43	2.05×10^8
W-triode	17.3×10^3	140	3.98×10^4

The gun aberrations lead to a fall in brightness below the low-current value. As a result, the probe size at first remains constant, then enters a brightness-limited region in which the probe size increases as $I^{3/8}$; finally, it enters an angular-current-limited region, in which the probe size increases rapidly as $I^{3/2}$. In their analysis, Fujita and Shimoyama show that the important parameter is the electron gun focal length introduced in Chapter 49, Gun Optics. They examine two sets of gun models, one with a Schottky emitter, the other with a tungsten emitter (Fig. 50.6), the characteristics of which are summarized in Table 50.1. For the configuration illustrated in Fig 50.7, the resulting reduction in apparent brightness is shown as a function of beam current in Fig. 50.8.

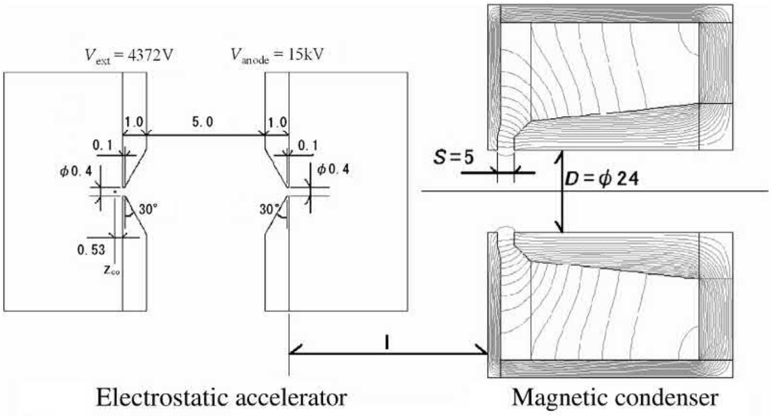

Figure 50.7

Left. Electrostatic accelerator lens model. The regions to the left of the extractor (wehnelt) and to the right of the anode are assumed to be field-free. *Right.* Magnetic condenser lens model, at a distance l from the electrostatic unit. Bore 24 mm and gap 5 mm. *After Fujita and Shimoyama, (2005b), Courtesy by the authors and the Japanese Society of Microscopy.*

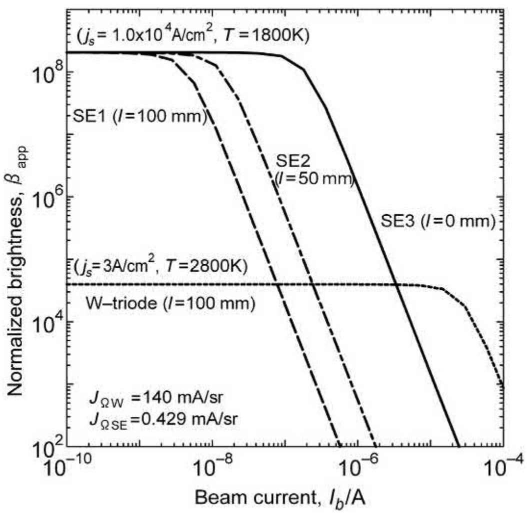

Figure 50.8

Reduction of apparent brightness β_{app} in A/mm^2 sr V as a function of beam current for three values of the separation l. The angular current density is denoted J_Ω. *After Fujita and Shimoyama, (2005b), Courtesy of the authors and the Japanese Society of Microscopy.*

50.3 Hybrid Emission

Field-emission guns have for many years been operated with some degree of cathode heating, thereby combining thermionic and field emission. A very successful design for such a hybrid source was developed by Kang et al. (1983), who investigated it in great detail, both theoretically and experimentally. The basic shape of this gun is

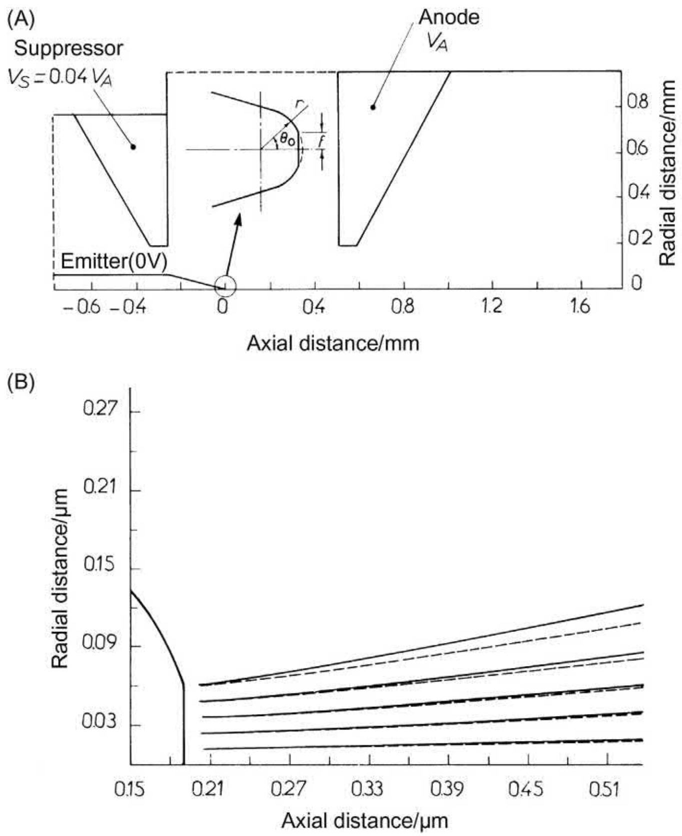

Figure 50.9

(A) Electrode configuration studied by Kang et al. (1983). The insert shows an expanded view of the emitter, apex radius r, for the round and faceted cases. (B) Calculated trajectories near the faceted emitter including (solid lines) and neglecting (dashed lines) space charge. The emitter is Zr/W, $T = 1800$ K, $\Phi = 2.6$ eV, $r = 0.2$ μm, $f/r = 0.3$, axial current density $J_0 = 0.082$ A/μm^2, axial field factor $\beta_0 = 0.04$ μm^{-1}. *After Kang et al. (1983), Courtesy Wissenschaftliche Verlagsgesellschaft.*

shown in Fig. 50.9. The emitter is a fine needle of zirconiated tungsten at the tip of an almost conical shank. The wehnelt (first anode) has a potential $V_A \approx 7.5$ kV relative to the cathode; a suppressor electrode, held at 0.04 V_A, strongly reduces the thermionic emission from the shank. By a field build-up process, the cathode assumes a faceted shape with a (100) crystal plane as its frontal surface. The corresponding work function is only 2.6 eV so that at a temperature of 1800 K, Schottky emission is already making an appreciable contribution to the local current density. In the transition range between field and Schottky emission, the current density is obtained by numerical integration of Eq. (44.10) using (44.21). At the edge of the frontal facet, strong field emission occurs; this increases the local current density and a hollow beam is created, see Fig. 50.10.

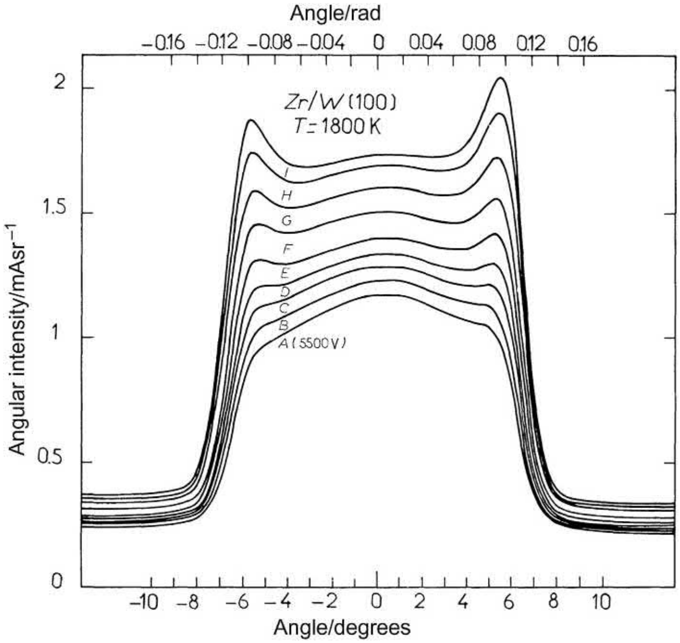

Figure 50.10
Angular intensity distribution for a faceted Zr/W emitter with $r = 1.5 \pm 0.5$ μm and $\beta \approx 590$ cm^{-1}; the full solid angle of the current probe is 3.1 mrad. The anode voltage increases in 100 V steps from curve *A* (5500 V) to *I* (6300 V). *After Kang et al. (1983), Courtesy Wissenschaftliche Verlagsgesellschaft.*

The presence of the frontal facet narrows the emission distribution pattern, see Fig. 50.11; in comparison with the rounded cathode, the angular aperture is roughly halved. The beam compression causes an increase in the space charge density in front of the cathode. Kang et al. (1981, 1983) therefore determined the space charge distribution by solving Poisson's equation using the finite-difference method with radially increasing mesh size (SCWIM) followed by ray-tracing. They found that the charge is concentrated in the vicinity of the cathode, the radial extent being about one cathode radius. At the cathode surface the field strength F is lowered but never becomes repulsive, so that no potential minimum develops in front of the real cathode. Kang et al. also found that the planar diode model is inapplicable, but this is not surprising since the divergence factor in Eq. (46.12b) was not considered.

On tracing back 'cold' electrons, that is, those leaving the cathode surface with zero velocity, the electron bundle is found to be subject to spherical aberration with an aberration coefficient $C_3 \approx 0.5$ mm. This is very low, and thus the faceted cathode structure does not cause a significant increase of the aberrations. This spherical aberration is, of course, to be superimposed on any others, essentially the chromatic aberration.

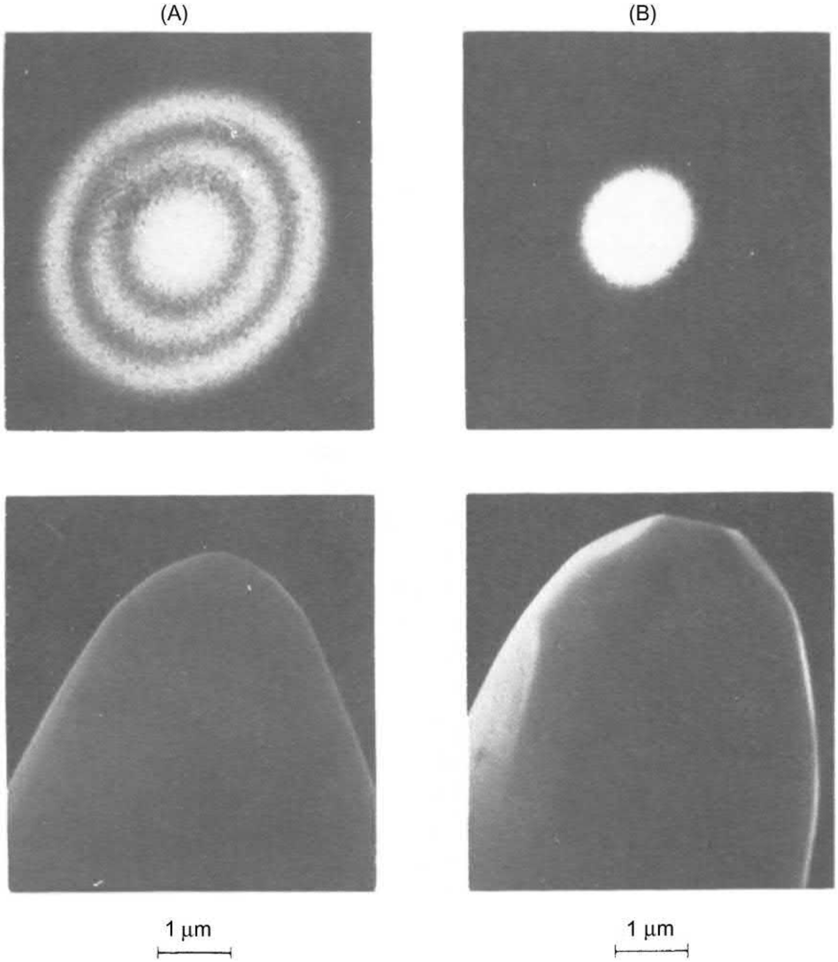

Figure 50.11
Emission distribution patterns (above) and SEM micrographs (below) for a Zr/W emitter. (A) Thermally annealed end-form and (B) field-built-up end-form. *After Kang et al. (1983), Courtesy Wissenschaftliche Verlagsgesellschaft.*

Summarizing, we see that intense electron emission with an average emission current density of 0.04 A cm^{-2} at the cathode and an axial angular intensity of about 1.7×10^{-3} A sr^{-1} can be achieved. This seems to be an excellent design. Since the aberrations are very low, the separation into a point source domain and a subsequent lens system, as outlined in the previous section, is still justified.

50.4 Conventional Thermionic Guns

All guns in which the wehnelt electrode is positive with respect to the cathode and hence not used for confining the area of emission are excluded from the following discussion.

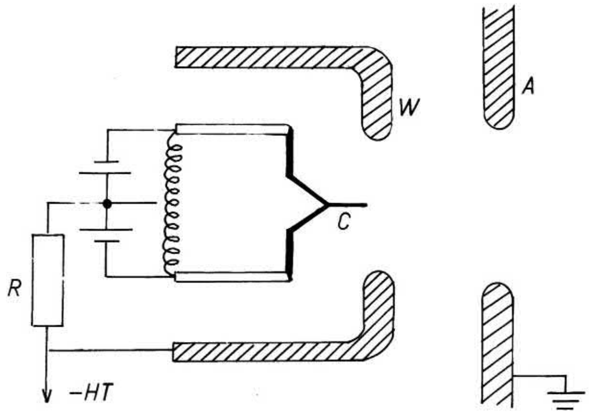

Figure 50.12
Conventional thermionic triode gun with automatic bias ('autobias'), the anode being earthed. (The shapes are highly simplified.)

All such guns, for instance those with laser-heated cathodes (Le Poole, 1981; Lau, 1981; van der Mast, 1983; van der Mast et al., 1974), LaB_6 cathodes (Elinson and Kudintseva, 1962; Kudintseva et al., 1967; Broers, 1967, 1969) or hybrid Schottky and field emission (Kang et al., 1983), behave essentially like field-emission guns, see Section 46.3.

Conventional thermionic electron guns with a pointed cathode welded on a hairpin-shaped carrier with direct electric heating (see Fig. 50.12) are quite simple devices, which can be operated straightforwardly. They are in widespread use, usually equipped with an automatic bias circuit for stabilization (Fig. 50.12). In this case the negative wehnelt potential relative to the cathode is generated by the voltage drop created along a resistor R of a few MΩ, when an emission current flows through the device. Since an increase in this current causes a corresponding increase in the voltage drop, this acts as a stabilizing feedback loop. However, according to our general statements in Sections 43.2 and 46.3, it is clear that we cannot expect the very highest electron optical performance from such guns.

Since the electric field of the anode penetrates through the aperture in the wehnelt up to the cathode, the separation method outlined in Section 50.1 cannot be employed and this makes the analysis of conventional guns surprisingly complicated. Lauer's (1982) model of a thermionic gun (see Sections 45.4.2 and 47.5) is necessarily oversimplified in many respects, since the true properties of thermionic guns can only be obtained at the price of very tedious numerical calculations. We recommend it, however, for it provides an understanding of the behaviour of such guns without these long calculations.

Depending on the shapes of the electrodes and on the distance between the apex of the cathode and the front plane of the wehnelt, the gun may behave in very different ways; we are led to distinguish between *short-focus* guns and *telefocus* guns, as presented

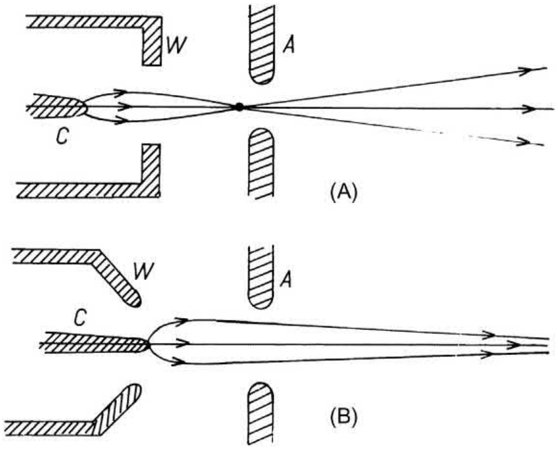

Figure 50.13
(A) Short-focus and (B) telefocus guns.

schematically in Figs 50.13A and B. Quite generally, in short-focus guns, the cathode is separated by a small gap from the wehnelt opening, so that the wehnelt exerts a strong screening effect on the field generated by the anode. In telefocus guns, on the other hand, the wehnelt usually has a conical shape and the cathode tip protrudes into the bore; the screening effect is thus much weaker.

In short-focus guns, the size of the emission area – roughly confined by the line of vanishing field strength on the cathode surface – and hence the emission current are more sensitive to small variations of the wehnelt potential. The complicated dependence of the gun performance on the many electrical and geometrical parameters was studied by Haine and Einstein (1951, 1952) and Haine et al. (1958), see Haine and Linder (1967). It is easier to adjust the intensity than in telefocus guns but the formation of a first crossover after a short distance implies strong bending of the trajectories and hence high aberrations. More seriously, each unnecessary crossover contributes to an avoidable increase of the energetic Boersch effect, as we have seen earlier. From this point of view, the telefocus guns are clearly superior.

Since the early designs of telefocus guns appeared (Bricka and Bruck, 1948; Steigerwald, 1949; Braucks, 1958, 1959) many different forms have been explored, and there is an extensive literature on this topic. Further information is to be found in all the major books on instrumental electron optics (e.g. Grivet, 1972; Klemperer and Barnett, 1971) and in the proceedings of many of the conferences on charged particle optics.

Today conventional thermionic guns have lost some of their earlier pre-eminence, since they are inferior to guns with field emission, with hybrid emission or with LaB_6 cathodes, so far as virtual spot size, brightness (only 10^2 A cm^{-2} sr^{-1}) and mean energy spread (about 2 eV) are concerned. Conversely they are clearly superior to cold field-emission guns in one respect: their total emission current can reach 50 μA and more. Moreover, their vacuum requirements are modest and their emission is stable. Altogether, the choice of the most suitable gun for a given purpose can be made only after careful consideration of all the particular requirements and constraints.

50.5 Pierce Guns

In many fields of application, in plasma physics and high-energy physics in particular, extremely intense electron beams are required. The aim of gun design is then not the production of a narrow crossover but the formation of a parallel or only slightly divergent beam. The radially outward directed forces in the beam caused by the space charge must be balanced by external electrostatic or magnetic forces. This can be achieved by shaping the electrodes or polepieces suitably. The first design of this kind was made by Pierce (1949), after whom such guns are named.

Usually, the thermal motion is neglected in the numerical treatment of such systems since it would contribute only a minor correction: hence Eq. (46.17) is to be solved in combination with the continuity equation. Unfortunately, there are very few exact analytic solutions of this problem, one of them being that given by Pierce (1949).

The configuration in question is presented in Fig. 50.14. A broad electron beam is emitted by a flat cathode and we wish it to propagate as a parallel laminar flow with sharp planar or cylindrical surfaces. The problem is to find the appropriate shape of the electrodes in the vacuum domain outside the beam. For simplicity, we consider a two-dimensional configuration independent of the Cartesian coordinate x, though this is an unrealistic

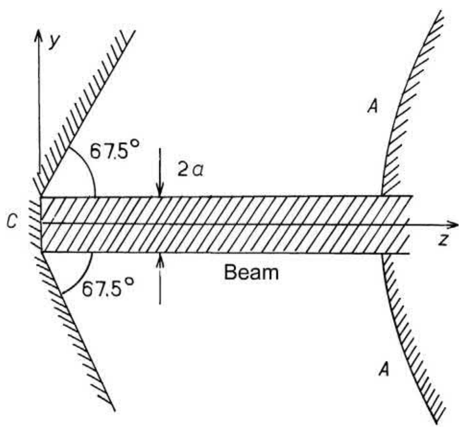

Figure 50.14
Planar Pierce systems.

assumption. Furthermore, we confine our consideration to the upper half-plane $y \geq 0$ of the configuration, since the lower half is symmetric.

Inside the beam, for $y \leq a$, with the above assumptions, we find $j = \text{const}$ and the Langmuir–Child solution (46.18), $\phi(z) \propto z^{4/3}$. At the beam surface the potential must be continuous and so Eq. (46.18) also gives us the boundary values for the solution of Laplace's equation in the vacuum domain. We now have to find a reasonably simple electrode configuration that is consistent with this requirement. An appropriate solution of $\nabla^2 \Phi = 0$ is given by a fractional power law in plane polar coordinates:

$$\Phi(z, y) = C\Re\left\{z + \mathrm{i}(y - a)\right\}^{4/3} = Cr^{4/3}\cos\left(4\varphi/3\right) \tag{50.2}$$

with the relations

$$z = r\cos\varphi, \quad y = a + r\sin\varphi, \quad 0 \leq \varphi < \pi/2$$

and the constant C is given by

$$C = \left(\frac{9}{4}\frac{j}{\varepsilon_0}\sqrt{\frac{m}{2e}}\right)^{2/3} = \left(\frac{9}{8}\frac{j}{\varepsilon_0 \eta}\right)^{2/3}$$

Obviously, this solution satisfies Eq. (46.17) for $y = a$. The equipotential $\Phi = 0$ is given by $\varphi_c = 3\pi/8 = 67.5°$; the cathode must therefore be prolonged by plates, inclined at this angle, as shown in Fig. 50.14. The surface of the anode coincides with the equipotential:

$$\Phi = Cr^{4/3}\sin\left(4\varphi/3\right) = \Phi_a = \text{const}$$

This solution is the prototype of all advanced solutions for Pierce guns. More sophisticated solutions for systems with round beams are possible in cylindrical and spherical coordinates. The zero-volt electrode, which is a continuation of the cathode, will then generally be curved in the meridional section too, but as in the foregoing solution, the angle at the edge of the cathode must be 67.5°. A design with a spherically curved cathode is shown in Fig. 50.15. It is impossible to obtain a beam that converges to a point focus; such a solution can be realized only approximately in domains with fairly large beam diameter. As soon as the diameter becomes very small, we cannot improve on a parallel beam, obtained by compensating the outward directed forces of the space charge.

The design of such systems is highly complicated and requires extensive numerical computation. Many designs of Pierce guns are reviewed by Brewer (1967) and very full accounts are to be found in Kirstein et al. (1967), Sushkov and Molokovskii (1972), and Nagy and Szilágyi (1974). A suitable computer program package has been developed by Herrmannsfeldt (1979) at SLAC (Stanford Linear Accelerator Center), based upon a finite-difference method for the solution of Poisson's equation; for more details we refer to the

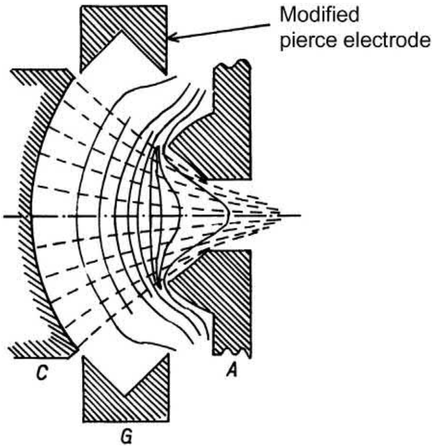

Figure 50.15
Pierce system with spherically curved cathode.

proceedings of the conferences on charged particle optics listed at the end of the book and, in particular, to Herrmannsfeldt (1981, 1987).

50.6 Multi-electron-beam Systems

For many years, electron beam lithography was limited by the low throughput of instruments designed to generate patterns at high resolution (Chapter 40, Deflection Systems). Among the ways of accelerating the process, we have already mentioned the SCALPEL[1] and PREVAIL[2] projects. Here we consider the use of multibeam arrangements, first suggested by O'Keeffe and Handy (1967). Over the years, four configurations have been examined: (i) Multiaxis systems (Fig. 50.16A), in which several separate miniature columns form an array (Chang et al., 1992); (ii) multisource, single-column systems (Fig. 50.16B); here, many beams are generated either by an array of sources or by laser-beams directed onto a photocathode (Schneider et al., 1996). (iii) Single-source, single-column systems (Fig. 50.16C), in which the beam from a single source is split into many subbeams before entering the column (Newman et al., 1983; Yasuda et al., 1993). (iv) Single-source, multiple-column systems (Fig. 50.16D), in which the beam from a single source is again split into subbeams as in (iii) but now, each subbeam travels along its own column (Kruit, 2007; Slot et al., 2008; references to other devices operating in this mode are cited separately below).

[1] SCattering with Angular Limitation Projection Electron-beam Lithography.
[2] Projection Reduction Exposure with Variable-axis Immersion Lenses.

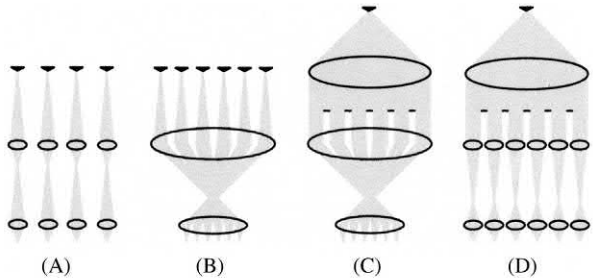

Figure 50.16

Multiple-beam configurations. (A) Multiple-axis system. (B) Multiple source, single column. (C) Single source, single column. (D) Single source, multiple column. *After Zhang (2008), Courtesy Yanxia Zhang.*

Each of these configurations has a large literature, in which the optics and constraints on the performance are examined in depth. This is reviewed in great detail by Zhang (2008). Here, we can consider them only very briefly.

Despite many efforts, the multisource, multiaxis systems have never proved entirely satisfactory. Even the digitally addressable field emitter array (DAFEA) of Baylor et al. (2002), in which the electrons are emitted by carbon nanofibres, was frustrated by the need for stable emission and a long lifetime. The same problem arises with arrangement (ii). The need for an array of sources is avoided in the single-source, single-column and single-source, multiple-column devices (iii and iv). In the first case, the device consists of a source, such as an LaB_6 emitter, a collimator lens, an aperture array and finally a beam-blanker array with individual control of the members of the array. A simplified version of the rather complicated arrangement of Muraki and Gotoh (2000) was proposed by van Bruggen et al. (2005, 2006b) and van Someren et al. (2006), who used a Schottky emitter; at the blanker plane, an aperture array and a microlens array were also introduced. However, it was not possible to reduce the aberrations of the collimator lens to an acceptable level. This brings us to the single-source, multiple-column configuration (Fig. 50.16D), in which Coulomb interactions are avoided by keeping the beams separate. This is employed in the Dutch MAPPER instrument, intended for maskless lithography with a much higher throughput than the rival arrangements. The electron beam originates in a Schottky source and is directed, as in (iii), onto an array of apertures followed by an array of beam blankers. Beyond this plane, each beam now has its own optics (diaphragm, deflector and projector lens), independent of the other beams. In this way, off-axis aberrations of the projector lens are negligible and there are no crossovers. This is the 'shower-beam concept' of van der Mast et al. (1985). Further aspects of the system are discussed by Zhang and Kruit (2007) and Zhang et al. (2008). Further developments can be followed in a series of publications in *Proc. SPIE*, of which we list only Wieland et al. (2009, 2010a,b), van den Berg et al. (2011), Belledent et al. (2013) and Lattard et al. (2017).

A high-throughput multibeam mask writer, developed by IMS Nanotechnology (now in collaboration with JEOL) is described by Klein and Platzgummer (2016). their column provides $512 \times 512 = 262{,}144$ programmable beams, each 20 nm in size. The current density can be varied up to 1 A/cm^2 with a total beam current of 1 μA. On emerging from the electron gun, the electrons are rendered parallel by the condenser lens and travel towards two electrostatic lenses enclosing a programmable aperture plate, which they traverse at relatively low energy (5 keV). They are then accelerated to 50 keV and the beam is demagnified by 200× before they reach the target. Multipoles and a magnetic lens are included for minor adjustments. The evolution of the project can be followed in the following publications: Platzgummer (2010), Platzgummer et al. (2012a,b), Klein et al. (2012a,b) Klein and Platzgummer (2016).

In another project, each of the beams of a multibeam device can be given a different shape. This is the multishaped-beam (MSB) instrument described by Slododowski et al. (2009, 2010a,b, 2011), Gramms et al. (2010) and Weidenmueller et al. (2010) at Vistec Electron Beam GmbH. In this structure (Fig. 50.17), not only is the beam provided by the gun divided into subbeams ($8 \times 8 = 64$ or $16 \times 16 = 256$) but the shape of each of these can be

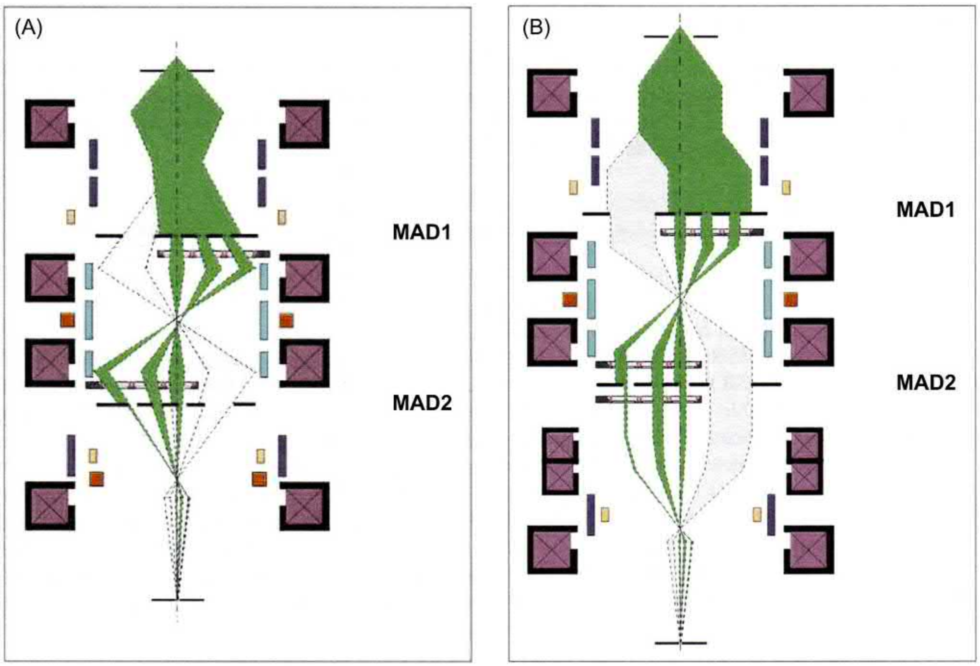

Figure 50.17
Paths of the beams in a multishaped-beam instrument. (A) Original design. (B) Improved design in which the beams are incident normal to the aperture diaphragms MAD1 and MAD2. *After Slodowski et al. (2011), Courtesy the authors and the Society of Photo-Optical Instrumentation Engineers.*

chosen separately. In the original version (Fig. 50.17A), the subbeams traversed the aperture diaphragms at oblique angles; in the improved version (Fig. 50.17B), the illumination is 'telecentric': the subbeams are travelling parallel to the optic axis when they arrive at the aperture diaphragms. The future of multibeam devices is discussed by Lee et al. (2016).

Progress on the development of a massively parallel electron-beam direct-writing system is charted by Kojima et al. (2014, 2016, 2017a,b). Yet another design is described by Du et al. (2016).

Multiple beams are not only of interest for lithography. In scanning electron microscopy, the high throughput of a multibeam instrument would be extremely beneficial: Ren and Kruit (2016) suggest that an experiment that would otherwise require 400 days could be accomplished in one or two days without sacrificing the quality of the image. Multibeam scanning electron microscopy has been attempted by Mohammadi-Gheidari and Kruit (2011), Mohammadi-Gheidari et al. (2010), Enyama et al. (2014, 2016), Iida et al. (2014), Keller et al. (2014), Eberle et al. (2015) and Kemen et al. (2015). Ren et al. (2014), Ren and Kruit (2016) and Zuidema et al. (2016) describe transmission imaging in the Delft multibeam scanning electron microscope (196 beams), which is an attractive mode for biological specimens.

Various aspects of these multicolumn devices have been treated by Spindt et al. (1976, 1983), Forman (1983), Chang et al. (1995, 2001), MacDonald et al. (1995), Munro (1999), Muray et al. (2000, 2006, 2014) and Thiel et al. (2014). Van Bruggen et al. (2004, 2005, 2006a) have considered including a foil aberration corrector in a multibeam instrument.

A magnetic lens modified to produce multiple beams has been built by Takizawa et al. (2011); this is described in Section 36.6.8.

50.7 Carbon Nanotube Emitters

The very small dimensions and mechanical strength of carbon nanotubes make them attractive candidates for field-emission cathodes. When the end of the tube is closed and the emissive surface is clean, the emission proves to be stable. Procedures for capping the tube and cleaning the cap are described by de Jonge (2009, 2010) and by Heeres et al. (2011). The work function is found to be 5.1 eV (Groening et al., 2000; de Jonge, 2004). and the current density obeys the Fowler–Nordheim equation (44.28), suitably modified to allow for the very small radius R of the emitting cap, assumed to be hemispherical. The total current I will be given by $I = 2\pi R^2 J$ (Edgcombe and de Jonge, 2007). The energy spread ΔE (FWHM) of the beam emitted is given to a reasonable approximation in the range $100 < T < 1000$ K by

$$\Delta E \approx 3.1 \times 10^{-4} T + 0.72d$$

where T denotes temperature and d is given by (44.26). De Jonge suggested that the reduced brightness is given to an acceptable approximation by

$$B_r \approx 0.04J(F,\ \phi)$$

where F is the field at the tip. For an improved understanding of the emission optics, it is necessary to know where the electrons are emitted. This question is studied by Heeres et al. (2012), who also summarize earlier findings on the emission sites. A field-emission microscope (see Section 37.4) was used to record the emission patterns from closed multiwalled carbon nanotubes, the tips of which were imaged in a transmission electron microscope. They found that electrons are emitted from localized sites about 1.6 nm in diameter and separated by a few nanometres.

There has been much work on these emitters, from which we have a much clearer picture of their properties and potential uses (Rinzler et al., 1995; Saito, 2010; Lin et al., 2014, 2015; Houdellier et al., 2012, 2015; Mamishin et al., 2017). An important point was raised by Kruit et al. (2006), who examined the concept of brightness and the useful beam current attainable for carbon nanotube sources. They point out that for such small sources, the spread of the electron wavefunction may be larger than the geometrical size of the tip – in the language of coherence, the source then behaves as though it were (spatially) coherent. The usual theory that describes probe size and probe current is no longer applicable and the effect of the aberrations of the electron gun becomes appreciable, which is not the case for other guns. A revised theory is proposed by Kruit et al., who comment that the notion of mean brightness loses its relevance in these extreme conditions.

A recent proposal by Jensen et al. (2017) for modelling such emitters lists related calculations.

50.8 Further Reading

Throughout Part IX we have been concerned mainly with the theoretical aspects of electron guns. The enormous complexity of this subject is such that there could be no question of presenting final solutions here; instead we have attempted to point out the basic principles and ideas. We are conscious of the fact that this account is very incomplete, as all the extensive technological knowledge and practical experience that have been accumulated over the years have been excluded. Important though this material is, it is far too vast to be covered in this volume; moreover, the techniques are developing so rapidly that any review rapidly becomes dated.

PART X

Systems with a Curved Optic Axis

General Curvilinear Systems

The feature of particle optics that distinguishes it from particle dynamics in general is the family behaviour of trajectories that remain in the vicinity of some plane or skew curve in space, which we call the optic axis. In the simplest case, this axis is a straight line but there are many devices, spectrometers with magnetic deflecting prisms for example, and some monochromators in which it is a plane curve, often a circular arc. Optic axes in the form of a skew curve are rare but cannot be excluded completely.

It is clearly advantageous to match the choice of coordinates to the optic axis. Numerous attempts to establish and study the equations of electron optics in the most general case of an arbitrary skew axis have been made but, as we might expect, the equations rapidly become unmanageable and it is possible to draw only very general conclusions. The analogous situation in which light propagates through a medium with an arbitrarily variable refractive index was studied in some detail by the mathematical ophthalmologist Allvar Gullstrand, who established the various categories of first-order behaviour (e.g., Gullstrand, 1900, 1906, 1915, 1924), and later by Constantin Carathéodory (1937), who used mathematical tools more familiar to the reader of today. In electron optics, the paraxial equations for a general system were first explored briefly by Cotte (1938), most of whose work was concerned with systems in which the axis is a plane curve. In 1941 and 1943, the nature of the paraxial imagery to be expected from the various types of systems − general, orthogonal and rotationally symmetric − was discussed by MacColl. Meanwhile, Grinberg (1942, 1943) published his 'General theory of the focusing action of electrostatic and magnetostatic fields', using the trajectory method; this work was subsequently re-examined and completed by numerous Russian authors, in particular by Strashkevich and Pilat (1951, 1952) and Strashkevich and Gluzman (1954), who attempted to extend Grinberg's work to include primary aberrations in their calculation of the second-order aberrations (cf. Section 51.6). Some points in Grinberg's work were criticized by Kas'yankov, who devoted an entire book to systems with curved axes (1956), and a lively polemic ensued. A very full study of the aberration question was made at about the same period by Vandakurov. On these matters, see Tsukkerman (1954), Kas'yankov (1956, 1957, 1958a,b), Grinberg (1957a,b) and Vandakurov (1955, 1957), and the textbooks of Strashkevich (1959) and Kel'man and Yavor (1959, 1968).

Returning to the 1940s, the paraxial properties of systems with curved axes were analysed afresh by Wendt (1942/3), many of whose findings are reproduced by Hutter (1948); Wendt

Principles of Electron Optics: Applied Geometrical Optics.
DOI: http://dx.doi.org/10.1016/B978-0-12-813369-9.00051-8

gives the expression for the third-order terms in the expansion of the refractive index but does not exploit it. Note that the vector drerivatives are not correct in Wendt's article and hence in that of Hutter, as pointed out by Tsukkerman (1954). Both paraxial properties and primary aberrations were analysed by Marschall (1944), in connection with mass-spectrograph design.

The Russian work on very general systems was all based on the trajectory method and Vandakurov justified this by his claim, which we do not believe well founded, that this method is less laborious than that of characteristic functions. The optics of systems with curved axes has been investigated in considerable detail by the method of characteristic functions by Sturrock (1952), who expands the function M (4.35) as a series of polynomials in suitable off-axis coordinates of increasing order and is thus able to derive the primary and secondary geometric aberrations and chromatic aberrations by differentiation. Sturrock gives explicit expressions for $M^{(2)}$ and $M^{(3)}$ and the corresponding quantities from which the chromatic aberrations may be derived. The condition that the optic axis must be a possible ray is expressed by requiring that $M^{(1)}$ vanish identically; $M^{(2)}$ then yields the paraxial trajectory equations, also given explicitly by Sturrock and in the Russian papers. The term $M^{(3)}$ then yields the primary (second-order) aberration coefficients. Sturrock considers in more detail systems for which the paraxial equations separate; these are usually known as orthogonal systems. The whole question of electron motion in the general case has been re-examined by Zhou (1984) and Zhou et al. (1987, 1988a,b).

In all these studies, an appropriate curvilinear coordinate system is needed, essentially based on the tangent to the optic axis at some point and on the normal and binormal at this point. Such coordinates are employed by Glaser (1956) and later used by Kasper (1965), Plies and Rose (1971) and Plies and Typke (1978), among others; we now describe such a system in detail.

51.1 Introduction of a Curvilinear Coordinate System

We denote conventional Cartesian coordinates by (X, Y, Z) and shall be led to introduce more suitable coordinates (x, y, z) as described below. The first step is illustrated in Fig. 51.1; the optic axis is defined in *parametric* form:

$$\boldsymbol{r}_0(z) = X_0(z)\boldsymbol{i}_x + Y_0(z)\boldsymbol{i}_y + Z_0(z)\boldsymbol{i}_z \tag{51.1}$$

z being chosen as the *arc-length* along the optic axis. Differentiation with respect to z (denoted by primes) thus gives the *tangential* unit vector $\boldsymbol{t}_o$:

$$\boldsymbol{t}_0 = \boldsymbol{r}_0'(z) \tag{51.2a}$$

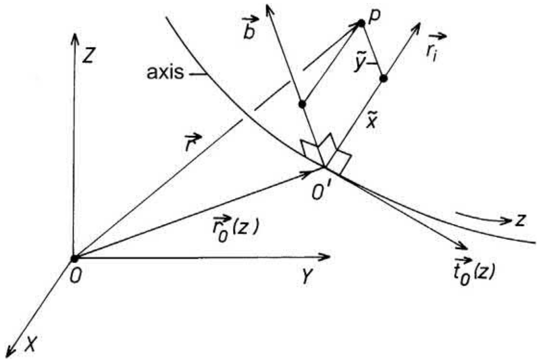

Figure 51.1
Introduction of a coordinate system adapted to a curved optic axis.

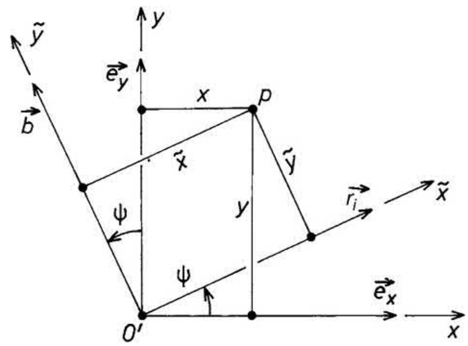

Figure 51.2
Local rotation of the coordinate system in a plane $z = \text{const}$ normal to the tangent $\boldsymbol{t}_0$ to the axis.

Further differentiation yields the curvature $\kappa(z)$ and the unit vector along the *principal normal*, $\boldsymbol{n}(z)$:

$$\kappa = \left|\boldsymbol{r}_0''\right| \quad n = \kappa^{-1}\boldsymbol{r}_0'' \tag{51.2b}$$

The unit vector along the *binormal*, $\boldsymbol{b}$, is defined by

$$\boldsymbol{b} = \boldsymbol{t}_0 \times \boldsymbol{n} = \kappa^{-1}\boldsymbol{r}_0' \times \boldsymbol{r}_0'' \tag{51.2c}$$

An arbitrary position vector $\boldsymbol{r}$ could be written $\boldsymbol{r} = \boldsymbol{r}_o(z) + \tilde{x}\boldsymbol{n}(z) + \tilde{y}\boldsymbol{b}(z)$, as shown in Fig. 51.1; $\tilde{x}$ and $\tilde{y}$ would then be Cartesian coordinates in the plane defined by the point $\boldsymbol{r}_o$ and the vectors $\boldsymbol{n}$ and $\boldsymbol{b}$. With such a representation, the metric element ds is not orthogonal and to avoid this inconvenience, we *twist* the system about the optic axis. The local rotation about the tangent vector $\boldsymbol{t}_0$ is shown in Fig. 51.2, where $\boldsymbol{t}_o$ is perpendicular to the plane of the diagram. It is convenient to introduce a complex transverse coordinate u:

$$u = x + \mathrm{i}y := (\tilde{x} + \mathrm{i}\tilde{y})\exp\{\mathrm{i}\psi(z)\} \tag{51.3a}$$

An elementary calculation in differential geometry shows that this twist angle ψ must be

$$\psi(z) = \int \tau(z)\, dz \tag{51.3b}$$

in order to obtain orthogonality, $\tau(z) = -\boldsymbol{n} \cdot d\boldsymbol{b}/dz$ being the *torsion* of the optic axis. When $d\boldsymbol{b}/dz = 0$, $\boldsymbol{b}$ is constant and is the normal to a plane surface. The line element is given by

$$ds^2 = dx^2 + dy^2 + h^2(x, y, z)dz^2 \tag{51.4}$$

with

$$\begin{aligned} h(x, y, z) &= 1 - \kappa\, \boldsymbol{n} \cdot (\boldsymbol{r} - \boldsymbol{r}_0) \\ &\equiv 1 - \kappa_1 x - \kappa_2 y \end{aligned} \tag{51.5a}$$

and

$$\kappa_1 := \kappa \cos\psi \quad \kappa_2 := \kappa \sin\psi \tag{51.5b}$$

The quantities κ_1 and κ_2 are the components of the curvature vector $\boldsymbol{\kappa} = \kappa\boldsymbol{n}$ in the local system (x, y).

In very many practical cases, the optic axis remains entirely in a plane of symmetry. The torsion τ then vanishes and hence ψ is constant. With no loss of generality, we can set $\psi = 0$ or $\psi = \pi$ and $Y_0(z) = 0$, whereupon Y and y become identical. Eqs (51.5b) simplify to $\kappa_1 = \pm\kappa = \pm R^{-1}$ and $\kappa_2 = 0$ so that

$$h = 1 \mp \kappa/R \tag{51.6}$$

R being the local radius of curvature. In Chapter 52, Sector Fields and Their Applications, we shall adopt this particular simplification.

51.2 Series Expansion of the Potentials and Fields

The general form of the trajectory equations tells us nothing about the optical properties of a system. Rather, we must derive paraxial and higher order approximations from which we can draw conclusions about the behaviour of families of rays. The potentials and fields must hence be expanded in power series, as in Chapter 7 of Volume 1, but since the number of terms is very large, we shall deal mainly with the paraxial approximation. The tensor form of the Laplace equation, $g^{ij}\Phi_{i,j} = 0$ where g^{ij} is the metric tensor and $\Phi_{i,j}$ is the second covariant derivative,

$$\Phi_{i,j} = \frac{\partial \Phi_i}{\partial x^j} - \left\{ \begin{matrix} t \\ ij \end{matrix} \right\} \Phi_t$$

here collapses to the simpler form

$$\nabla^2 \Phi \equiv h^{-1}\left\{\frac{\partial}{\partial x}\left(h\frac{\partial \Phi}{\partial x}\right)+\frac{\partial}{\partial y}\left(h\frac{\partial \Phi}{\partial y}\right)+\frac{\partial}{\partial z}\left(\frac{1}{h}\frac{\partial \Phi}{\partial z}\right)\right\}=0 \tag{51.7}$$

using the metric Eq. (51.4). A possible solution is found by introducing a general series expansion

$$\Phi(x,y,z)=\sum_{m=0}^{\infty}\sum_{n=0}^{\infty}a_{m,n}(z)x^m y^n \tag{51.8}$$

into Eq. (51.7). This yields infinite sequences of recurrence relations. Up to the second order we obtain

$$\begin{aligned}\Phi(x,y,z)&=\phi(z)-xE_1(z)-yE_2(z)\\&\quad-\frac{\alpha(z)}{2}\left(x^2+y^2\right)+\frac{f_1(z)}{2}\left(x^2-y^2\right)+f_2(z)xy\end{aligned} \tag{51.9}$$

Apart from $\alpha(z)$ all the coefficients on the right-hand side can be chosen independently, each having a concrete physical meaning: $\phi(z)$ is the axial potential, E_1 and E_2 are the transverse components of the axial field strength $\boldsymbol{E}_0$, and f_1 and f_2 are the coefficients characterizing quadrupole fields. The coefficient $\alpha(z)$ of the 'rotationally symmetric' term must satisfy

$$\alpha(z)=\frac{1}{2}\left(\phi''+\kappa_1E_1+\kappa_2E_2\right)=\frac{1}{2}\left(\phi''+\boldsymbol{\kappa}\cdot\boldsymbol{E}_0\right) \tag{51.10}$$

As well as the vector notation, a complex representation is often convenient and we therefore introduce

$$\tilde{E}_0 := E_1+\mathrm{i}E_2,\quad \tilde{\kappa}:=\kappa_1+\mathrm{i}\kappa_2,\quad \tilde{f}:=f_1+\mathrm{i}f_2 \tag{51.11}$$

the tilde acting as a reminder that these quantities are complex. Eqs (51.9) and (51.10) then take the form

$$\Phi=\phi-\Re\left(\tilde{E}_0u^*\right)-\frac{1}{2}\alpha uu^*+\frac{1}{2}\Re\left(\tilde{f}u^{*2}\right) \tag{51.12}$$

$$\alpha=\frac{1}{2}\phi''+\frac{1}{2}\Re\left(\tilde{E}_0\tilde{\kappa}^*\right) \tag{51.13}$$

When the series expansion Eq. (51.8) is extended to higher order, we find that the coefficients involve linear combinations of multipole terms of all lower orders. In contrast to the case of systems with straight optic axes, the presence of the curvatures κ_1 and κ_2

generates linear relations between the multipole coefficients of different orders; a simple example of this is Eq. (51.10).

It is almost invariably permissible to assume that the domain occupied by the particle beam does not encircle any external electric currents, which means that we are at liberty to calculate the magnetic flux $\boldsymbol{B}$ from a scalar potential χ or a vector potential $\boldsymbol{A}$ at will.

The explicit representation of $\boldsymbol{B} = -\mu_0 \nabla\chi = \nabla \times \boldsymbol{A}$ takes the form

$$B_x = -\mu_0 \frac{\partial\chi}{\partial x} = h^{-1}\left\{\frac{\partial}{\partial y}(hA_z) - \frac{\partial A_y}{\partial z}\right\} \tag{51.14a}$$

$$B_y = -\mu_0 \frac{\partial\chi}{\partial y} = h^{-1}\left\{-\frac{\partial}{\partial x}(hA_z) + \frac{\partial A_x}{\partial z}\right\} \tag{51.14b}$$

$$B_z = -\mu_0 h^{-1} \frac{\partial\chi}{\partial z} = \frac{\partial A_y}{\partial x} - \frac{\partial A_x}{\partial y} \tag{51.14c}$$

The series expansion for χ is quite similar to Eq. (51.12) and is hence not given here. The vector potential is not unique and any particular definition is associated with additional constraints. It is convenient to assume that

$$\operatorname{div}\ A = h^{-1}\left\{\frac{\partial}{\partial x}(hA_x) + \frac{\partial}{\partial y}\left(hA_y\right) + \frac{\partial A_z}{\partial z}\right\} \equiv 0 \tag{51.15}$$

We may equally prescribe the longitudinal component $B(z)$ and the transverse components $B_1(z)$, $B_2(z)$ on the optic axis and the magnetic quadrupole strengths $g_1(z)$ and $g_2(z)$. By analogy with Eq. (51.11) we define complex coefficients

$$\tilde{B}_0 = B_1 + \mathrm{i}B_2, \quad \tilde{g} = g_1 + \mathrm{i}g_2 \tag{51.16}$$

which will be useful later. The vector potential itself is better expressed in real form:

$$\begin{aligned}
A_x &= -\frac{1}{2}By\left(1 + \kappa_1 x + \frac{\kappa_2}{2}y\right) - B_1' xy + \ldots \\
A_y &= \frac{1}{2}Bx\left(1 + \frac{\kappa_1}{2}x + \kappa_2 y\right) + B_2' xy + \ldots \\
hA_z &= -B_2 x + B_1 y - g_1 xy + \frac{1}{2}g_2\left(x^2 - y^2\right) \\
&\quad + \frac{1}{2}\left\{\kappa_1 B_2 x^2 + (\kappa_2 B_2 - \kappa_1 B_1)xy - \kappa_2 B_1 y^2\right\} + \ldots
\end{aligned} \tag{51.17}$$

This particular choice satisfies $\boldsymbol{A} = 0$ on the optic axis and, furthermore, div $\boldsymbol{A} = 0$ up to the linear terms. The linear approximation to the magnetic field obtained by differentiation is found to be

$$B_z = B(z)\ \ (1 + \kappa_1 x + \kappa_2 y) + B_1' x + B_2' y + \ldots \tag{51.18a}$$

$$B_x + \mathrm{i}B_y = \tilde{B}_0(z) + \beta(z)u - \tilde{g}(z)u^* + \ldots \tag{51.18b}$$

with

$$\beta(z) = \frac{1}{2}(-B' + \kappa_1 B_1 + \kappa_2 B_2) = -\frac{1}{2}B' + \frac{1}{2}\Re\left(\tilde{B}_0\tilde{\kappa}^*\right) \tag{51.19}$$

This last definition is closely analogous to Eq. (51.13). Generally speaking the analogy between electric and magnetic quantities is reflected in the following exchanges:

$$\begin{array}{llll} E_i \leftrightarrow B_i, & \tilde{E}_0 \leftrightarrow \tilde{B}_0, & \Phi \leftrightarrow \mu_0\chi, & \phi' \leftrightarrow -B \\ \alpha \leftrightarrow \beta, & f_i \leftrightarrow g_i, & \tilde{f} \leftrightarrow \tilde{g} & \end{array}$$

Apart from minor changes in the notation of the quadrupole terms, the formulae given in Chapter 7 are special cases of those presented here if $\kappa_1 = \kappa_2 = 0$ and if higher order terms are neglected.

51.3 Variational Principle and Trajectory Equations

The appropriate variational principle is again the time-independent form of Hamilton's principle (4.33). We can cast this into a form quite similar to Eqs (4.33a), (4.34) and (4.35) if x, y and z are understood to be the coordinates introduced in the previous section. The presence of the factor h^2 in Eq. (51.4) slightly modifies our earlier expression for the tangent to a trajectory: instead of (3.15) and (3.16), we now have

$$\boldsymbol{r}' \equiv \rho\mathbf{t} = x'\boldsymbol{i}_x + y'\boldsymbol{i}_y + h\boldsymbol{i}_z \tag{51.20}$$

$$\rho := \left|\boldsymbol{r}'\right| = \sqrt{h^2 + x'^2 + y'^2} \tag{51.21}$$

Furthermore, we must allow for the fact that, owing to the curvature of the optic axis, the unit vectors $\boldsymbol{i}_x$, $\boldsymbol{i}_y$ and $\boldsymbol{i}_z \equiv \boldsymbol{t}_0$ of the coordinate system depend on z. In view of Eqs (51.20) and (51.21), the variational principle now takes the form

$$\overline{S} = \int_{z_0}^{z_1} \overline{M}(x, y, z, x', y')\, dz = \text{extr.} \tag{51.22}$$

with the Lagrangian

$$\overline{M} = g(\mathbf{r})\sqrt{h^2 + x'^2 + y'^2} + Q\left(x'A_x + y'A_y + hA_z\right) \tag{51.23}$$

The corresponding Euler equations again have the standard form (4.36). It is not advisable to evaluate them because the longitudinal component of the magnetic field causes a complicated coupling between these differential equations. This coupling is better eliminated in the Lagrangian itself. We shall keep the presentation quite general, since the results obtained are more frequently applied in ion optics than in electron optics; we adopt the notation of Chapter 2. On the optic axis itself, the *kinetic* momentum is given by

$$g_a(z) = \left[2m_0\{W - Q\phi(z)\}\left(1 + \frac{W - Q\phi(z)}{2m_0c^2}\right)\right]^{1/2} =: \sqrt{2m_0|Q|\hat{\phi}(z)} \tag{51.24}$$

in which the acceleration potential $\hat{\phi}$ is defined to be a non-negative quantity; g_a and $\hat{\phi}$ are related to the total energy W, which is of great importance in the physics of energy spectrometers, but we shall not introduce this dependence explicitly until we need it. The velocity on the optic axis is given by

$$v_a(z) = g_a(z)/m_0\gamma(z) \tag{51.25}$$

with the relativistic mass-ratio

$$\gamma(z) = \left(\frac{m}{m_0}\right)_{x=y=0} = 1 + \frac{W - Q\phi(z)}{m_0c^2} \tag{51.26}$$

The next stage of the calculation is quite elementary but very lengthy and we therefore describe it without reproducing the detailed mathematics. As the first step we have to introduce Eqs (51.4) and (2.13) together with (51.9) and (51.17) into (51.23) and then carry out the ensuing series expansions. In the paraxial approximation, we truncate this expansion after the terms of second order. The final result has the general structure

$$\begin{aligned}\overline{M} = g_a(z)\left(1 + \frac{1}{2}\left(x'^2 + y'^2\right)\right) + \frac{1}{2}QB(z)(xy' - x'y)\\ + a_1x + a_2y + b_{11}x^2 + 2b_{12}xy + b_{22}y^2\end{aligned}$$

The axial flux density $B(z)$ causes a coupling, as is obvious from the corresponding term in $\overline{M}$. We can eliminate this by twisting the coordinate system round the optic axis. The appropriate new coordinate will be

$$\overline{x} + i\overline{y} := (x + iy)\exp\{i\theta(z)\} \tag{51.27}$$

with the additional twist angle

$$\theta(z) = \int \frac{QB(z)}{2g_a(z)}dz \tag{51.28}$$

which is quite familiar from the physics of round magnetic lenses. In terms of these new coordinates, the Lagrangian takes the form

$$\begin{aligned}\overline{M} = g_a(z)\left(1 + \frac{1}{2}\overline{x}'^2 + \frac{1}{2}\overline{y}'^2\right) + \varepsilon_1(z)\overline{x} + \varepsilon_2(z)\overline{y} \\ + \frac{1}{2}c_{11}(z)\overline{x}^2 + c_{12}(z)\overline{x}\,\overline{y} + \frac{1}{2}c_{22}(z)\overline{y}^2 + \cdots\end{aligned} \tag{51.29}$$

The paraxial trajectory equations, the corresponding Euler equations, are now

$$\begin{aligned}\frac{d}{dz}(g_a\overline{x}') = \varepsilon_1 + c_{11}\overline{x} + c_{12}\overline{y} \\ \frac{d}{dz}(g_a\overline{y}') = \varepsilon_2 + c_{12}\overline{x} + c_{22}\overline{y}\end{aligned} \tag{51.30}$$

This linear system of ordinary differential equations is self-adjoint and in general inhomogeneous. The presence of nonvanishing deflection coefficients $\varepsilon_1(z)$, $\varepsilon_2(z)$, defined in complex form by

$$\tilde{\varepsilon} := \varepsilon_1 + \mathrm{i}\varepsilon_2 = \mathrm{e}^{\mathrm{i}\theta}\left\{-\tilde{\kappa}g_a + Q\left(\tilde{E}_0/\upsilon_\alpha + \mathrm{i}\tilde{B}_0\right)\right\} \tag{51.31}$$

means that the optic axis is *not* a possible trajectory. When $\tilde{\kappa} \neq 0$, the condition $\tilde{\varepsilon} \equiv 0$, necessary for the optic axis to be a possible trajectory, can only be satisfied for one well-specified energy W_0, so that dispersion is unavoidable with a polychromatic beam.

The linear homogeneous terms on the right-hand side of Eq. (51.30) describe focusing effects and axial astigmatism. The coefficients will not be given here explicitly, for they are lengthy expressions and the theory is rarely needed in so general a form. The reader interested in these is referred to the specialized literature (e.g., Sturrock, 1952; Glaser, 1956; Strashkevich, 1959). In the homogeneous case ($\tilde{\varepsilon} \equiv 0$), one integration constant of Eq. (51.30) is easily found. For any two linearly independent pairs of solutions, $(\overline{x}_j, \overline{y}_j)$ and $(\overline{x}_k, \overline{y}_k)$, the quantity

$$C_{jk} = g_0(z)\left(\overline{x}_j\overline{x}'_k - \overline{x}_k\overline{x}'_j + \overline{y}_j\overline{y}'_k - \overline{y}_k\overline{y}'_j\right) \tag{51.32}$$

is a constant of motion (Kasper, 1965), as can be easily verified by differentiation, recalling (51.30). Furthermore, an elementary calculation shows that this constant C_{jk} is also invariant with respect to the coordinate rotation (51.27), so that the bars may be omitted in (51.32). This is a generalization of the Lagrange–Helmholtz relation.

Apart from such basic observations, it is difficult to extract practical results from so general a form of the theory. Some further classification of systems is possible according to the behaviour of the line foci corresponding to a point object on the axis as this object is moved from one end of the axis to the other; the three types of behaviour are discussed in the work of Gullstrand and Carathéodory already cited. Concrete evaluation of the paraxial theory is highly dependent on the individual circumstances and the theory of aberrations is extremely tedious. A rare case in which these can reasonably be studied is a system with a helical axis, proposed by Gabor (1951) and analysed by Sturrock (1952). In the remainder of this chapter, therefore, we confine the discussion to realistic systems with a number of simplifying characteristics.

51.4 Simplifying Symmetries

Adjustment is easier and the aberration terms are fewer in number if some symmetry conditions are imposed on the configuration. As already mentioned briefly, we assume that the optic axis lies in the plane $Y = 0$; we assume too that there are other permitted trajectories that remain in this plane. These assumptions impose strong symmetry conditions on the fields. For any trajectory satisfying $y(z) \equiv 0$, $Y \equiv 0$, the electromagnetic force must remain in the symmetry plane, which requires that E_Y, B_X and B_Z disappear in this plane. The electrostatic potential Φ must hence be an even function of Y and the magnetic scalar potential χ an odd one. It is advantageous to derive Taylor series expansions with respect to Y. If the two-dimensional Laplacian is denoted by

$$\nabla_2^2 \equiv \Delta_2 := \frac{\partial^2}{\partial X^2} + \frac{\partial^2}{\partial Z^2} \tag{51.33}$$

and Δ_2^n denotes repeated application of Δ_2, these series expansions take the form

$$\begin{aligned}\Phi(r) &= \sum_{n=0}^{\infty} \frac{(-1)^n}{(2n)!} \Delta_2^n \Phi_S(X, Z) Y^{2n} \\ &= \Phi_S(X, Z) - \frac{Y^2}{2} \Delta_2 \Phi_S + \frac{Y^4}{24} \Delta_2^2 \Phi_S \mp \cdots \end{aligned} \tag{51.34}$$

$$\begin{aligned}-\mu_0 \chi(r) &= \sum_{n=0}^{\infty} \frac{(-1)^n}{(2n+1)!} \Delta_2^n B_S(X, Z) Y^{2n+1} \\ &= Y B_S(X, Z) - \frac{Y^3}{6} \Delta_2 B_S + \frac{Y^5}{120} \Delta_2^2 B_S \mp \cdots \end{aligned} \tag{51.35}$$

as can be verified easily by performing the appropriate differentiations. The coefficient functions Φ_S and B_S have a concrete physical meaning: Φ_S is the electrostatic potential in the symmetry plane while B_S is the magnetic flux density in this plane.

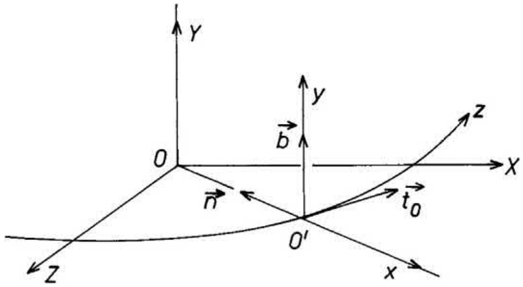

Figure 51.3
Choice of curvilinear coordinate system (x, y, z) when the optic axis lies in a plane. The vector $\boldsymbol{n}$ is always directed towards the local centre of curvature while the x-axis points in the opposite direction. It is sometimes necessary to change the orientation so that $y \to -y$ in order to arrange that $y = Y$

The curvilinear coordinate system (x, y, z) can always be orientated in such a way that the coordinates y and Y are identical. Depending on the orientation of the principal normal $\boldsymbol{n}$, this requires that $\psi = 0$ or $\psi = \pi$. For conciseness we shall confine the following considerations to the case $\psi = \pi$, $h = 1 + \kappa x$, which means that the positive x-axis has the outward direction, as shown in Fig. 51.3. This corresponds to the usual choice in applications to devices with a circular optic axis.

Since $y \equiv Y$, Eqs (51.34) and (51.35) are already the series expansions with respect to y. Calculation of the power series expansion with respect to x is facilitated by the fact that $h = 1 + \kappa(z)x$ does not depend on y and so

$$\nabla_2^2 = \Delta_2 = h^{-1}\left\{\frac{\partial}{\partial x}\left(h\frac{\partial}{\partial x}\right) + \frac{\partial}{\partial z}\left(\frac{1}{h}\frac{\partial}{\partial z}\right)\right\} \tag{51.36}$$

In order to apply this to Eqs (51.34) and (51.35), we have to expand Φ_S and B_S as power series with respect to x. For reasons of space, we shall terminate these after the third order in x:

$$\Phi_S = \phi(z) + xF_0(z) + \frac{x^2}{2}F_1(z) + \frac{x^3}{6}F_2(z) \tag{51.37}$$

On evaluating the expression $\Delta_2\Phi_S$ and introducing this into Eq. (51.34), we obtain

$$\begin{aligned}\Phi(\boldsymbol{r}) = \phi(z) + xF_0(z) + \frac{x^2}{2}F_1(z) + \frac{x^3}{6}F_2(z)\\ -\frac{y^2}{2}(F_1 + \kappa F_0 + \phi'')\\ -\frac{xy^2}{2}\left(F_2 + \kappa F_1 - \kappa^2 F_0 - 2\kappa\phi'' - \kappa'\phi' + F_0''\right)\end{aligned} \tag{51.38}$$

The notation for the coefficients differs slightly from that in Eq. (51.9), in that $F_0 = -E_1$, $F_1 = f_1 - \alpha$; the notation of (51.38) reveals the structure better.

The expression for the scalar magnetic potential up to third order is quite simple. With a power series expansion for B_S of the form

$$B_S(x,z) = G_0(z) + xG_1(z) + \frac{x^2}{2}G_2(z) \tag{51.39}$$

we obtain $\Delta_2 B_S = G_2 + \kappa G_1 + G_0''$ and hence

$$-\mu_0 \chi = y\left(G_0 + xG_1 + \frac{x^2}{2}G_2\right) - \frac{y^3}{6}\left(G_0'' + \kappa G_1 + G_2\right) \tag{51.40}$$

This gives the flux density components

$$B_x = y(G_1 + xG_2) \tag{51.41a}$$

$$B_y = G_0 + xG_1 + \frac{x^2}{2}G_2 - \frac{y^2}{2}\left(G_0'' + \kappa G_1 + G_2\right) \tag{51.41b}$$

$$B_z = y\left(G_0' + xG_1' - \kappa x G_0'\right) \pm \ldots \tag{51.41c}$$

In order to evaluate Eqs (51.22) and (51.23) in the third-order approximation, we must find a vector potential that yields the field (51.41). The symmetry properties of the field require that A_y be an odd function of y, while A_x and A_z must be even functions. The following considerations lead to a very simple gauge.

The Euler equations resulting from Eq. (51.23) will be simplest if as many low-order terms as possible are eliminated from A_x and A_y. The condition div $\boldsymbol{A} = 0$ may sometimes be convenient but not always and is certainly not really necessary. Instead, we now assume that $A_y \equiv 0$. The condition

$$B_x = \frac{\partial A_z}{\partial y} = y(G_1 + xG_2)$$

is then readily integrated to give

$$A_z = \frac{1}{2}y^2\left\{G_1(z) + xG_2(z)\right\} + a_z(x,z)$$

$a_z(x, z)$ being an arbitrary differentiable function. Similarly, the condition

$$B_z = -\frac{\partial A_x}{\partial y} = y\left(G_0' + xG_1' - \kappa x G_0'\right)$$

is integrated to give

$$A_x = -\frac{y^2}{2}\left(G_0' + xG_1' - \kappa x G_0'\right) + a_x(x, z)$$

The condition (51.14b) in conjunction with (51.41b) is still not sufficient to determine a_z and a_x uniquely; we are at liberty to choose $a_x \equiv 0$ and $a_z(0, z) = 0$. We then find

$$a_z = -xG_0 + \frac{x^2}{2}(\kappa G_0 - G_1) + \frac{x^3}{6}\left(-3\kappa^2 G_0 + 2\kappa G_1 - G_2\right)$$

It is convenient to calculate hA_z instead of A_z itself; bringing all this together, we obtain

$$A_x = -\frac{1}{2}y^2\left\{G_0' + x\left(G_1' - \kappa G_0'\right)\right\} \tag{51.42a}$$

$$A_y \equiv 0 \tag{51.42b}$$

$$\begin{aligned} hA_z = &-xG_0 - \frac{x^2}{2}(G_1 + \kappa G_0) - \frac{x^3}{6}(G_2 + \kappa G_1) \\ &+ \frac{y^2}{2}G_1 + \frac{xy^2}{2}(G_2 + \kappa G_1) \end{aligned} \tag{51.42c}$$

It is obvious that in the case of constant curvature κ and constant coefficients G_0, G_1, G_2, the component A_x vanishes and div $A = \partial A_z/\partial z$ is indeed equal to zero. Since the optic axis is then a circle with $z = R\varphi$, this means that the familiar circular vector potential is a special case of our particular gauge.

51.5 Trajectory Equations for Symmetric Configurations

Once the series expansions are known, we are in a position to evaluate the Lagrangian equation (51.23) in the third-order approximation; this is a straightforward procedure. The first step is to introduce Eq. (51.38) into the general expression for the kinetic momentum g:

$$g(\boldsymbol{r}) = \left[2m_0\left\{W - Q\Phi(\boldsymbol{r})\right\}\left(1 + \frac{W - Q\Phi(\boldsymbol{r})}{2m_0c^2}\right)\right]^{1/2} \tag{51.43}$$

the expression $g_a(z)$, given by Eq. (51.24), being its axial value. In order to facilitate the task of series expansion, we introduce the abbreviation $\Phi(\boldsymbol{r}) =: \phi(z) + \overline{\Phi}(\boldsymbol{r})$, the term $\overline{\Phi}$ containing all off-axis terms. Using Eq. (51.24) and (51.26), we obtain the exact formula

$$g^2 = g_a^2 - 2m_0\gamma Q\overline{\Phi} + Q^2\overline{\Phi}^2/c^2$$

The series expansion of $g(\boldsymbol{r})$ is now given by

$$g = g_a\left(1 - \gamma\zeta - \frac{\zeta^2}{2} - \gamma\frac{\zeta^3}{2}\right) + O\left(\zeta^4\right) \tag{51.44a}$$

in which ζ is the dimensionless quantity:

$$\zeta \coloneqq m_0 Q\overline{\Phi}/g_a^2 \tag{51.44b}$$

In this series expansion, the particular structure of the off-axis term $\overline{\Phi}$ has not been exploited and so (51.44a,b) are quite generally valid. The next task is to introduce Eq. (51.38) into (51.44a), after which we collect up the terms of different orders, truncating the series after the third-order terms. We shall not reproduce this in full, merely listing the final results.

For the square root term in Eq. (51.23), the approximation

$$\sqrt{h^2 + x'^2 + y'^2} \approx 1 + \kappa x + \frac{1}{2}\left(x'^2 + y'^2\right)(1 - \kappa x)$$

is sufficient. Bringing all the various series expansions together and organizing the terms by order, we finally obtain

$$\begin{aligned}\overline{M} &= g_a(z) + \frac{1}{2}(g_a + c_1 x)\left(x'^2 + y'^2\right) - \frac{c_2}{2}y^2 x' \\ &- a_1 x - \frac{a_2}{2}x^2 - \frac{a_3}{6}x^3 + \frac{b_2}{2}y^2 + \frac{b_3}{2}xy^2\end{aligned} \tag{51.45}$$

with the coefficients

$$\begin{aligned}&\mu_1(z) \coloneqq m_0\gamma Q g_{\mathrm{a}}^{-1}, \quad \mu_2(z) \coloneqq m_0^2 Q^2 g_a^{-3} \\ &c_1(z) = -\kappa g_a - \mu_1 F_0, \quad c_2(z) = QG_0' \\ &a_1(z) = -\kappa g_a + \mu_1 F_0 + QG_0 \\ &a_2(z) = \mu_1(F_1 + 2\kappa F_0) + \mu_2 F_0^2 + Q(G_1 + \kappa G_0) \\ &a_3(z) = \mu_1(F_2 + 3\kappa F_1) + 3\mu_2 F_0\left(F_1 + \kappa F_0 + \frac{\mu_1}{g_a}F_0^2\right) + Q(G_2 + \kappa G_1) \\ &b_2(z) = \mu_1(F_1 + \kappa F_0 + \phi'') + QG_1 \\ &b_3(z) = \mu_1\left(F_2 + 2\kappa F_1 + F_0'' - \kappa\phi'' - \kappa'\phi'\right) \\ &\qquad + \mu_2 F_0(F_1 + \kappa F_0 + \phi'') + Q(G_2 + \kappa G_1)\end{aligned} \tag{51.46}$$

The canonical momenta arising from Eq. (51.45) are given by

$$p_x = \frac{\partial \overline{M}}{\partial x'} = (g_a + c_1 x)x' - \frac{c_2}{2}y^2 \tag{51.47a}$$

$$p_y = \frac{\partial \overline{M}}{\partial y'} = (g_a + c_1 x)y' \tag{51.47b}$$

The corresponding Euler equations are then

$$p_x' = \frac{\partial \overline{M}}{\partial x} = \frac{c_1}{2}\left(x'^2 + y'^2\right) - a_1 - a_2 x - \frac{a_3}{2}x^2 + \frac{b_3}{2}y^2 \tag{51.48a}$$

$$p_y' = \frac{\partial \overline{M}}{\partial y} = -c_2 y x' + b_2 y + b_3 xy \tag{51.48b}$$

On examining the second-order terms, we see that these equations are coupled in such a manner that Eq. (51.48a) contains only terms in y^2 and y'^2, while Eq. (51.48b) is linear in y and y'. The assumed mirror symmetries of the fields are consequently satisfied by these equations, as of course they must be. This means that if $(x(z), y(z))$ is a permitted solution of (51.48a,b), so too is $(x(z), -y(z))$.

51.6 Aberration Theory

The coupled system of trajectory equations derived above can be solved by means of the standard perturbation techniques, and from their solutions the aberrations can then be determined. Unlike systems with straight optic axes, dispersion effects here play so important a role that they must be considered from the very beginning. For conciseness, we shall deal mainly with magnetic systems and discuss electric systems only very briefly in Section 53.2.

51.6.1 Magnetic Systems

We assume here that, for some fixed nominal value g_0 of the kinetic momentum, the optic axis is a possible trajectory. This assumption can always be satisfied, since along each trajectory g is constant. (In Section 52.6 the optic axis will be the extended fringing field (EFF)-axis.) Setting $g_a = g_0$, $x \equiv 0$ and $y \equiv 0$ in Eqs (51.47) and (51.48), we find the necessary condition $a_1(z, g_0) \equiv 0$. In view of this, we now have to expand (51.45) and (51.46) in terms of deviations δ from the nominal value of g_0:

$$g_a := g_0(1 + \delta) \tag{51.49}$$

This relative deviation δ is a small quantity, $|\delta| \ll 1$, and hence the series expansion of $\overline{M}$ can be terminated after the third-order terms in x, x', y, y' and δ.

With vanishing electric terms, g_a appears explicitly only in the coefficients c_1 and a_1; expansion of c_1 with respect to δ is unnecessary, while evaluation of a_1 gives

$$a_1 = -\kappa g_0 \delta \quad \text{with} \quad \kappa g_0 = QG_0 \tag{51.50}$$

It is convenient to introduce new field coefficients:

$$q_i = QG_i(z)/g_0 \quad \text{for} \quad i = 0, 1, 2; \quad q_0(z) = \kappa(z) \tag{51.51}$$

We can then normalize the Lagrangian and put it into the simple ordered form

$$N := g_0^{-1}\left(\overline{M} - g_a\right) =: N^{(2)} + N^{(3)} \tag{51.52}$$

where the paraxial term $N^{(2)}$ is given by

$$N^{(2)} = \frac{1}{2}\left(x'^2 + y'^2\right) - \frac{q_1}{2}\left(x^2 - y^2\right) - \frac{\kappa}{2}x^2 + \kappa x \delta \tag{51.53a}$$

and the perturbation term $N^{(3)}$ by

$$N^{(3)} = -\frac{\kappa'}{2}x'y^2 + \frac{1}{2}(\delta - \kappa x)\left(x'^2 + y'^2\right) - \frac{1}{6}(q_2 + \kappa q_1)\left(x^3 - 3xy^2\right) \tag{51.53b}$$

The paraxial ray equations now take the form

$$x'' + \left(q_1 + \kappa^2\right)x = \kappa\delta \tag{51.54a}$$

$$y'' - q_1(z)y = 0 \tag{51.54b}$$

In a given object plane $z = z_o$ we may prescribe initial values x_o, x'_o and y_o, y'_o. The corresponding solutions are then

$$x(z) = x_o s_1(z) + x'_o s_2(z) + \delta\, s_5(z) \tag{51.55a}$$

$$y(z) = y_o s_3(z) + y'_o s_4(z) \tag{51.55b}$$

in which s_1 and s_2 are solutions of (51.54a) with $\delta = 0$, s_3 and s_4 are solutions of (51.54b) and s_5 is a solution of (51.54a) with $\delta = 1$. The initial conditions are

$$\left.\begin{aligned} s_1 = s_3 = s'_2 = s'_4 = 1 \\ s'_1 = s'_3 = s_2 = s_4 = s_5 = s'_5 = 0 \end{aligned}\right\} \quad \text{at} \quad z = z_o \tag{51.56}$$

The paraxial solutions (51.55) and their derivatives are now introduced into the perturbation eikonal, defined as the integral over $N^{(3)}$ from z_o to the image coordinate z_i. This is then a function of the initial conditions:

$$L^{(3)}\left(x_o, x'_o; y_o, y'_o; \delta\right) = \int_{z_o}^{z_i} N^{(3)}(x, x'; y, y'; z)dz \tag{51.57}$$

The ordering with respect to the initial coordinates results in:

$$\begin{aligned} -L^{(3)} = {} & \frac{1}{6}\left(A_{11}x_o^3 + 3A_{12}x_o^2 x'_o + 3A_{21}{x'_o}^2 x_o + A_{22}{x'_o}^3\right) \\ & + \frac{x_o}{2}\left(B_{1,33}y_o^2 + 2B_{1,34}y_o y'_o + B_{1,44}{y'_o}^2\right) \\ & + \frac{x'_o}{2}\left(B_{2,33}y_o^2 + 2B_{2,34}y_o y'_o + B_{2,44}{y'_o}^2\right) \\ & + \frac{\delta}{2}\left(C_{1,11}x_o^2 + 2C_{1,12}x_o x'_o + C_{1,22}{x'_o}^2\right) \\ & + \frac{\delta}{2}\left(D_{33}y_o^2 + 2D_{34}y_o y'_o + D_{44}{y'_o}^2\right) \\ & + \frac{\delta^2}{2}\left(C_{2,15}x_o + C_{2,25}x'_o\right) + \frac{1}{6}\delta^3 C_{3,55} \end{aligned} \tag{51.58}$$

The numbering of the coefficients adopted here is easily understood if the initial coordinates (x_o, x'_o, y_o, y'_o, δ) are regarded as being numbered from one to five. The coefficients can be expressed very concisely by introducing the wholly symmetric auxiliary quantities $E_{k,mn}$ and $F_{k,mn}$ defined by

$$E_{k,mn} := \int_{z_o}^{z_i} (q_2 + \kappa\, q_1)s_k s_m s_n \, dz \tag{51.59a}$$

$$F_{k,mn} := \int_{z_o}^{z_i} \kappa\left(s'_k s'_m s_n + s'_k s_m s'_n + s_k s'_m s'_n\right)dz \tag{51.59b}$$

For the appropriate values of the subscripts k, m and n, we then have

$$A_{mn} = E_{m,mn} + F_{m,mn} \tag{51.60a}$$

$$B_{k,mn} = -E_{k,mn} + \int_{z_0}^{z_i} \left(\kappa s_k s'_m s'_n + \kappa' s'_k s_m s_n\right)dz \tag{51.60b}$$

$$C_{k,mn} = E_{k,mn} + F_{k,mn} - k \int_{z_0}^{z_i} s'_m s'_n \, dz \tag{51.60c}$$

$$D_{mn} = -E_{5,mn} + \int_{z_0}^{z_i} \left(\kappa s_5 s'_m s'_n + \kappa' s'_5 s_m s_n - s'_m s'_n \right) dz \tag{51.60d}$$

Notice that these coefficients are symmetric with respect to the subscripts m and n. It is not essential to use different letters, A, B, C and D, since the coefficients can already be distinguished by the values of their suffixes, but this notation brings out the meaning very clearly: the sets A and C refer to the x-direction only, while the sets B and D involve the motion in the y-direction; the sets A and B refer to dispersionless contributions, while C and D denote dispersions. The first suffix k in Eq. (51.60c) is the order of the corresponding dispersion term.

We now examine the special case in which there is stigmatic imaging in first order. This requires that $s_j(z_i) = 0$ for $j = 2, 4$.

The lateral geometric aberrations, referred back to the object plane, are simply given by

$$\Delta x_o = \frac{\partial}{\partial x'_o} L^{(3)}, \quad \Delta y_o = \frac{\partial}{\partial y'_o} L^{(3)} \tag{51.61}$$

since the corresponding Wronskians are equal to unity. So far as Eq. (51.61) is concerned, all terms in (51.58) that are independent of x'_o and y'_o are irrelevant; they could have been omitted but we have preferred to retain them since the complete form of (51.58) reveals the even symmetry with respect to y_o and y'_o more clearly.

We defer discussion of the possible types of aberrations to Chapter 52, where sector fields are investigated. For further discussion of the general case, see Vandakurov (1957), Rose and Plies (1973), Rose (1978a) and especially Plies and Typke (1978) and the very complete study of Plies (2002), which we now examine.

51.6.2 Compound Systems

51.6.2.1 Aberrations of second rank

A very thorough study of the optics of combined electrostatic and magnetic systems was made by Plies and Typke (1978), who even included the terms with which parasitic aberration coefficients could be derived. This was subsequently improved and completed by Plies (2002), who not only examined the third-rank aberrations but also indicated the best

Table 51.1: Potential expansions used by Plies and Typke

$$\Phi = \Re\breve{\phi}$$

$$\breve{\phi} = \phi_0 + \phi_1 w^* + \phi_2 w^{*2} + \frac{1}{4}\left(\phi_1\Gamma^* - \phi_0''\right)ww^* + \phi_3 w^{*3}$$

$$+\frac{1}{8}\left\{2\phi_2\Gamma^* - \phi_1'' + \frac{3}{2}\Re\left(\phi_1\Gamma^*\right)\Gamma - \frac{5}{2}\phi_0''\Gamma - \phi_0'\Gamma'\right\}ww^{*2} + \phi_4 w^{*4}$$

$$+\frac{1}{4}\left\{\phi_3\Gamma^* - \frac{1}{3}\phi_2'' + \frac{5}{12}\phi_2\Gamma\Gamma^* - \frac{3}{8}\phi_1''\Gamma - \frac{1}{6}\phi_1'\Gamma' + \frac{5}{16}\Re\left(\phi_1\Gamma^*\right)\Gamma^2 - \frac{11}{16}\phi_0''\Gamma^2 - \frac{13}{24}\phi_0'\Gamma'\Gamma\right\}ww^{*3}$$

$$+\frac{1}{32}\left(3\phi_2\Gamma^{*2} - 3\phi_1''\Gamma^* - 2\phi_1'\Gamma'^* - \frac{1}{2}\phi_1\Gamma''^* + \frac{9}{4}\phi_1\Gamma\Gamma^{*2} + \frac{1}{2}\phi'''' - \frac{19}{4}\phi_0''\Gamma\Gamma^* - \frac{7}{2}\phi_0'\Gamma'^*\Gamma\right)w^2w^{*2}$$

$$\phi_0 = \phi_0^* = \phi_{0c}(z) := \phi, \quad \phi_n = \phi_n(z) = \phi_{nc}(z) + \mathrm{i}\phi_{ns}(z) \ \text{ for } \ n \geq 1$$

For the scalar magnetic potential, it is only necessary to replace ϕ_n *by* Ψ_n in the expansion for Φ and $B = B(z) = -\Psi'_o(z)$. In the case described here, based on Plies (2002), the curvature is given by

$$\kappa = \frac{\Lambda\phi_{1c}}{2\hat{\phi}} - \hat{\eta}\Psi_{1s} = \Gamma = \Gamma^*$$

way of calculating the corresponding coefficients in practice. We now give an account of this work, which complements the analysis in the preceding sections. Although Plies requires that the curved part of the axis remains in a plane, he retains the rotationally symmetric terms in the magnetic flux and only requires that this round magnetic lens field and the deflection fields nowhere overlap. This is useful in practice as the various energy analysers in which the axis is curved will be used in conjunction with magnetic lenses.

The reader who wishes to pursue this further and perhaps include the formulae in a computer program will find it necessary to consult the 1978 article, since the very long expressions for the terms in the eikonal expansion given there are not reproduced here. We have therefore preferred to retain the notation used by Plies and Typke for the field and potential expansions — this can easily be translated into the notation used consistently above and elsewhere in these volumes with the aid of Table 51.1. We do however give all the material needed to evaluate the second-rank aberrations and the present account is therefore self-contained. Otherwise, the Plies–Typke notation has been replaced by our standard conventions. In particular, note that η denotes $(e/2m_0)^{1/2}$ as usual and not $(e/2m_0\hat{\phi}_0)^{1/2}$. However, in the present context it is certainly convenient to absorb $\hat{\phi}_0^{1/2}$ into η and we therefore write

$$\hat{\eta} := (e/2m_0\hat{\phi}_0)^{1/2} = \eta/\hat{\phi}_0^{1/2} \tag{51.62}$$

(To prevent confusion with the remainder of these books, we continue to use ϕ where Plies–Typke use Φ. The suffix 'G' (Gegenstand = object) is replaced by 'o' and 'B' (Bild = image) by 'i'.) We follow Plies and Typke in writing

$$\Lambda := 1 + 2\varepsilon\phi \tag{51.63}$$

The Gaussian trajectory equations now take the general form

$$\begin{aligned} &x'' + \frac{\Lambda}{2}\frac{\phi'}{\hat{\phi}}x' + \hat{\eta}By' + \left(-\Lambda\frac{\phi_{2c}}{\hat{\phi}} + \frac{3\Lambda^2+2}{8}\frac{\phi_{1c}^2}{\hat{\phi}^2} + \frac{\Lambda}{4}\frac{\phi''}{\hat{\phi}} - \frac{5\Lambda}{4}\frac{\phi_{1c}}{\hat{\phi}}\hat{\eta}\Psi_{1s} + 2\hat{\eta}\Psi_{2s} + \hat{\eta}^2\Psi_{1s}^2\right)x \\ &\quad + \frac{\hat{\eta}B'y}{2} = \left(-\frac{\Lambda^2+1}{2}\frac{\phi_{1c}}{\hat{\phi}} + \Lambda\hat{\eta}\Psi_{1s}\right)\frac{\phi_o}{2\hat{\phi}}\delta \end{aligned} \tag{51.64}$$

$$y'' + \frac{\Lambda}{2}\frac{\phi'}{\hat{\phi}}y' - \hat{\eta}Bx' + \left(\Lambda\frac{\phi_{2c}}{\hat{\phi}} - \frac{\Lambda^2}{8}\frac{\phi_{1c}^2}{\hat{\phi}^2} + \frac{\Lambda}{4}\frac{\phi''}{\hat{\phi}} + \frac{\Lambda}{4}\frac{\phi_{1c}}{\hat{\phi}}\hat{\eta}\Psi_{1s} - 2\hat{\eta}\Psi_{2s}\right)y - \frac{\hat{\eta}}{2}B'x = 0$$

As in the preceding section, δ is a measure of the chromatic variation: $\delta = \Delta\phi/\phi_o$. In regions in which the deflector fields (ϕ_{1c}, Ψ_{1s}) are present, B must vanish. Conversely, when $B \neq 0$, the functions ϕ_{1c} and Ψ_{1s} must be zero and Eq. (51.64) collapse to the familiar equations

$$\begin{aligned} &x'' + \frac{\Lambda}{2}\frac{\phi'}{\hat{\phi}}x' + \hat{\eta}By' + \left(-\Lambda\frac{\phi_{2c}}{\hat{\phi}} + \frac{\Lambda}{4}\frac{\phi''}{\hat{\phi}} + 2\hat{\eta}\Psi_{2s}\right)x + \frac{\hat{\eta}}{2}B'y = 0 \\ &y'' + \frac{\Lambda}{2}\frac{\phi'}{\hat{\phi}}y' - \hat{\eta}Bx' + \left(\Lambda\frac{\phi_{2c}}{\hat{\phi}} + \frac{\Lambda}{4}\frac{\phi''}{\hat{\phi}} - 2\hat{\eta}\Psi_{2s}\right)y - \frac{\hat{\eta}}{2}B'x = 0 \end{aligned} \tag{51.65}$$

Introduction of the rotating coordinate system for this case

$$\theta = \frac{1}{2}\int_{z_o}^{z}\hat{\eta}B\,d\zeta \tag{51.66}$$

converts these to

$$u'' + \frac{\Lambda}{2}\frac{\phi'}{\hat{\phi}}u' + \frac{1}{4}\left(\Lambda\frac{\phi''}{\hat{\phi}} + \hat{\eta}^2B^2\right)u - \left(\Lambda\frac{\phi_{2c}}{\hat{\phi}} - 2\hat{\eta}\Psi_{2s}\right)\mathrm{e}^{-2\mathrm{i}\theta}u^* = 0 \tag{51.67}$$

Plies notes that the Picht transformation can be used to eliminate the second term if desired.

As we saw in Section 51.6.1, the paraxial solutions for $B = 0$ are expressed in terms of five fundamental solutions, $s_1,\ldots s_5$; there we imposed the initial conditions (51.56):

$$\left.\begin{aligned} s_1 = s_3 = s_2' = s_4' = 1 \\ s_1' = s_3' = s_2 = s_4 = s_5 = s_5' = 0 \end{aligned}\right\} \quad \text{at} \quad z = z_o$$

Now, however, we define the fundamental solutions in terms of their values at $z = z_o$ and an aperture plane, $z = z_a$:

$$\begin{aligned} s_x(z_o) = s_y(z_o) = 1 \qquad & s_x(z_a) = s_y(z_a) = 0 \\ t_x(z_o) = t_y(z_o) = 0 \qquad & t_x'(z_o) = t_y'(z_o) = 1 \end{aligned} \tag{51.68}$$

$$\begin{aligned} s_\delta(z) \equiv s_5(z) &= t_x(z)\int_{z_a}^{z} r s_x d\zeta - s_x(z)\int_{z_o}^{z} r t_x d\zeta \\ r(z) &= \left\{-\frac{1}{4}\left(\Lambda^2+1\right)\frac{\phi_{1c}}{\hat{\phi}} + \frac{1}{2}\Lambda\hat{\eta}\Psi_{1s}\right\}\frac{\phi_o}{\left(\hat{\phi}\hat{\phi}_o\right)^{1/2}} \end{aligned} \tag{51.69}$$

The s- and t-rays correspond to the following rays in Plies (2002):

$$s_x \leftrightarrow x_\gamma \quad s_y \leftrightarrow y_\delta \quad t_x \leftrightarrow x_\alpha \quad t_y \leftrightarrow y_\beta \quad s_\delta \leftrightarrow x_\varepsilon \tag{51.70}$$

We shall see that in dispersive devices, there are four key planes: the object plane, the aperture plane (usually conjugate to the source and hence in a diffraction plane), the image plane (conjugate to the object plane) and the energy-selection plane (conjugate to the aperture plane). These are illustrated in Fig. 51.4.

The Gaussian or 'paraxial' trajectory is therefore of the form

$$w(z) = x_o' t_x(z) + x_o s_x(z) + \delta s_5(z) + \mathrm{i}\left\{y_o' t_y(z) + y_o s_y(z)\right\} \tag{51.71}$$

The dispersion ray s_δ tells us the effect of energy spread in the image plane, $z = z_i$ and in the energy-selection plane $z = z_s$, conjugate to the source. The coefficients are obtained by choosing the upper limits of the integrals in Eq. (51.69) appropriately. In the image plane,

$$s_\delta(z_i) = -s_x(z_i)\int_{z_o}^{z_i} t_x r dz \tag{51.72a}$$

and in the energy-selection plane,

$$s_\delta(z_s) = t_x(z_s)\int_{z_a}^{z_s} s_x r dz \tag{51.72b}$$

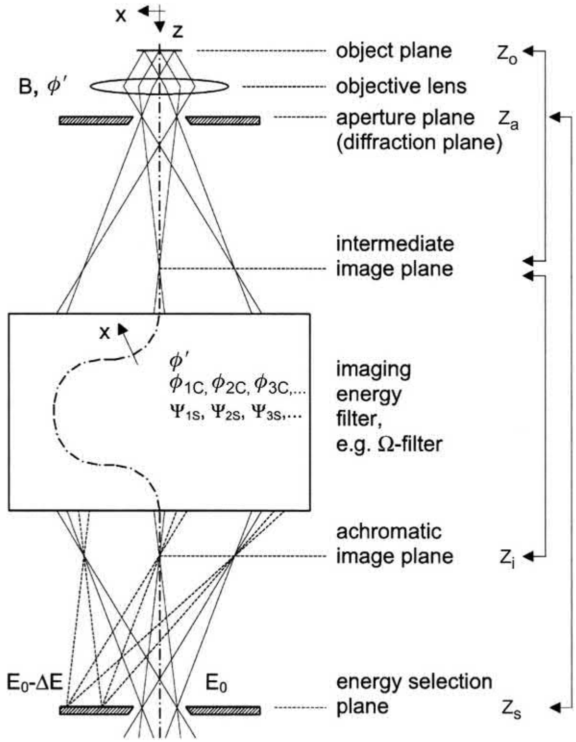

Figure 51.4

Ray diagram and the important planes in an in-column imaging filter. The object plane $z = z_o$ is conjugate to the image plane, $z = z_i$; the aperture or diffraction plane $z = z_a$ is conjugate to the energy-selection plane, $z = z_s$.

The second-rank aberrations are of three kinds: terms quadratic in position and gradient, a single term quadratic in δ and mixed terms (linear in δ and one other coordinate). Here again, the aberrations are of interest in the image plane and the selection plane. The aberration coefficients are obtained in the usual way by differentiating the associated eikonal function,

$$\Delta w^{(2)} = \left\{ \left(t_x \frac{\partial}{\partial x_o} - s_x \frac{\partial}{\partial x'_o} \right) + \mathrm{i} \left(t_y \frac{\partial}{\partial y_o} - s_y \frac{\partial}{\partial y'_o} \right) \right\} W_v^{(2)}(z) \tag{51.73}$$

The function $W_v^{(2)}(z)$ is given explicitly in Plies and Typke (1978, see Eqs 47, 48 and 55). This yields

$$\begin{aligned} \Delta x^{(2)}(z) &= x_o'^2 x_{\alpha\alpha} + y_o'^2 x_{\beta\beta} + x_o x'_o x_{\alpha x} + y_o y'_o x_{\beta y} + x_o^2 x_{xx} + y_o^2 x_{yy} \\ &\quad + x'_o \delta x_{\alpha\delta} + x_o \delta x_{x\delta} + \delta^2 x_{\delta\delta} \\ \Delta y^{(2)}(z) &= x'_o y'_o y_{\alpha\beta} + x'_o y_o y_{\alpha y} + x_{oo} y'_o y_{\beta x} + x_o y_o y_{xy} + y'_o \delta y_{\beta\delta} + y_o \delta y_{y\delta} \end{aligned} \tag{51.74}$$

in which the *second-rank fundamental rays* are as follows;

Axial rays

$$\begin{aligned} x_{\alpha\alpha} &= -s_x A_{\alpha\alpha\alpha} + t_x A_{\alpha\alpha x} \\ x_{\beta\beta} &= \frac{1}{2}\left(-s_x B_{\alpha\beta\beta} + t_x B_{x\beta\beta}\right) \\ y_{\alpha\beta} &= -s_y B_{\alpha\beta\beta} + t_y B_{\alpha\beta y} \end{aligned} \tag{51.75a}$$

Mixed rays

$$\begin{aligned} x_{\alpha x} &= 2(-s_x A_{\alpha\alpha x} + t_x A_{\alpha xx}) \\ x_{\beta y} &= -s_x B_{\alpha\beta y} + t_x B_{x\beta y} \\ y_{\alpha y} &= -s_y B_{\alpha\beta y} + t_y B_{\alpha yy} \\ y_{\beta x} &= -s_y B_{x\beta\beta} + t_y B_{x\beta y} \end{aligned} \tag{51.75b}$$

Field rays

$$\begin{aligned} x_{xx} &= -s_x A_{\alpha xx} + t_x A_{xxx} \\ x_{yy} &= \frac{1}{2}\left(-s_x B_{\alpha yy} + t_x B_{xyy}\right) \\ y_{xy} &= -s_y B_{x\beta y} + t_y B_{xyy} \end{aligned} \tag{51.75c}$$

Axial chromatic rays

$$\begin{aligned} x_{\alpha\delta} &= -s_x C_{\alpha\alpha\delta} + t_x C_{\alpha x\delta} \\ y_{\beta\delta} &= -s_y C_{\beta\beta\delta} + t_y C_{\beta y\delta} \end{aligned} \tag{51.75d}$$

Field chromatic rays

$$\begin{aligned} x_{x\delta} &= -s_x C_{\alpha x\delta} + t_x C_{xx\delta} \\ y_{y\delta} &= -s_y C_{\beta y\delta} + t_y C_{yy\delta} \end{aligned} \tag{51.75e}$$

Dispersion ray

$$x_{\delta\delta} = -s_x C_{\alpha\delta\delta} + t_x C_{x\delta\delta} \tag{51.75f}$$

From these very general expressions, much simpler formulae can be derived for the most important special cases. In a stigmatic image plane $z = z_i$, we put $t_x(z_i) = t_y(z_i) = 0$; the integrals run from z_o to z_i. Thanks to the use of the eikonal, two relations among the aberration coefficients emerge: the coefficient of β^2 in $\Delta x^{(2)}(z_i)$ is half the coefficient of $\alpha\beta$ in $\Delta y^{(2)}(z_i)$ and the coefficient of βy in $\Delta x^{(2)}(z_i)$ is the same as the coefficient of

αy in $\Delta y^{(2)}(z_i)$. For practical purposes, note that the magnifications in the x- and y-directions are different. In the selection plane, $z = z_s$, $s_x(z_s) = 0$; the integrals now run from z_a to z_s.

The coefficients A, B and C are now listed in compact form. The suffices may take the following values

$$\begin{aligned} &\lambda,\ \mu \to \alpha,\ x \text{ or } \delta \\ &\pi,\ \rho \to \alpha \text{ or } x \\ &\sigma,\ \tau \to \beta \text{ or } y \end{aligned} \tag{51.76}$$

and we use the mapping between x_α, ... and s_x, given in Eq. (51.70).

$$\begin{aligned} A_{\lambda\mu\pi} = {} & \left[\left(\frac{\hat{\phi}}{\hat{\phi}_0}\right)^{1/2}\left\{(3g_1+g_2)\left(\frac{x'_\lambda}{x_\lambda}+\frac{x'_\mu}{x_\mu}+\frac{x'_\pi}{x_\pi}\right)+3g_3\right\}x_\lambda x_\mu x_\pi\right]_{z_\nu}^{z} \\ & + \int_{z_\nu}^{z}\left(\frac{\hat{\phi}}{\hat{\phi}_0}\right)^{1/2}\left\{(g_5+g_6)\left(\frac{x'_\lambda x'_\mu}{x_\lambda x_\mu}+\frac{x'_\lambda x'_\pi}{x_\lambda x_\pi}+\frac{x'_\mu x'_\pi}{x_\mu x_\pi}\right)+(3g_7+g_8)\left(\frac{x'_\lambda}{x_\lambda}+\frac{x'_\mu}{x_\mu}+\frac{x'_\pi}{x_\pi}\right)+3(g_9+g_{10})\right\} \\ & \times x_\lambda x_\mu x_\pi d\zeta \end{aligned}$$

$$\begin{aligned} B_{\lambda\sigma\tau} = {} & 2\left[\left(\frac{\hat{\phi}}{\hat{\phi}_0}\right)^{1/2}\left\{g_1\left(\frac{x'_\lambda}{x_\lambda}+\frac{y'_\sigma}{y_\sigma}+\frac{y'_\tau}{y_\tau}\right)+g_2\left(3\frac{x'_\lambda}{x_\lambda}-\frac{y'_\sigma}{y_\sigma}-\frac{y'_\tau}{y_\tau}\right)+g_3\right\}x_\lambda y_\sigma y_\tau\right]_{z_\nu}^{z} \\ & +2\int_{z_\nu}^{z}\left(\frac{\hat{\phi}}{\hat{\phi}_0}\right)^{1/2}(G-3g_9+g_{10})x_\lambda y_\sigma y_\tau d\zeta \end{aligned} \tag{51.77}$$

$$G = g_5\left(\frac{x'_\lambda y'_\sigma}{x_\lambda y_\sigma}+\frac{x'_\lambda y'_\tau}{x_\lambda y_\tau}-\frac{y'_\sigma y'_\tau}{y_\sigma y_\tau}\right)+g_6\frac{y'_\sigma y'_\tau}{y_\sigma y_\tau}+g_7\left(\frac{x'_\lambda}{x_\lambda}+\frac{y'_\sigma}{y_\sigma}+\frac{y'_\tau}{y_\tau}\right)+g_8\left(3\frac{x'_\lambda}{x_\lambda}-\frac{y'_\sigma}{y_\sigma}-\frac{y'_\tau}{y_\tau}\right)$$

$$\begin{aligned} C_{\pi\pi\Delta} = {} & 2A_{\Delta\pi\rho}+2\left[\left(\frac{\hat{\phi}}{\hat{\phi}_0}\right)^{1/2} g_4 x_\pi x_\rho\right]_{z_\nu}^{z} \\ & +2\int_{z_\nu}^{z}\left(\frac{\hat{\phi}}{\hat{\phi}_0}\right)^{1/2}\left\{g_{11}\frac{x'_\pi x'_\rho}{x_\pi x_\rho}+\frac{1}{2}g_{12}\left(\frac{x'_\pi}{x_\pi}+\frac{x'_\rho}{x_\rho}\right)+g_{13}+g_{14}\right\}x_\pi x_\rho d\zeta \end{aligned}$$

$$C_{\pi\Delta\Delta} = A_{\Delta\Delta\pi} + 2\left[\left(\frac{\hat{\phi}}{\hat{\phi}_0}\right)^{1/2} g_4 x_\pi x_\Delta\right]_{z_\nu}^{z} + \int_{z_\nu}^{z}\left(\frac{\hat{\phi}}{\hat{\phi}_0}\right)^{1/2} g_{15} x_\pi d\zeta$$
$$+ 2\int_{z_\nu}^{z}\left(\frac{\hat{\phi}}{\hat{\phi}_0}\right)^{1/2}\left\{g_{11}\frac{x'_\pi x'_\Delta}{x_\pi x_\Delta} + \frac{1}{2}g_{12}\left(\frac{x'_\pi}{x_\pi} + \frac{x'_\Delta}{x_\Delta}\right) + g_{13} + g_{14}\right\} x_\pi x_\Delta d\zeta$$

$$C_{\sigma\tau\Delta} = B_{\Delta\sigma\tau} + 2\left[\left(\frac{\hat{\phi}}{\hat{\phi}_0}\right)^{1/2} g_4 y_\sigma y_\tau\right]_{z_\nu}^{z}$$
$$+ 2\int_{z_\nu}^{z}\left(\frac{\hat{\phi}}{\hat{\phi}_0}\right)^{1/2}\left\{g_{11}\frac{y'_\sigma y'_\tau}{y_\sigma y_\tau} + \frac{1}{2}g_{12}\left(\frac{y'_\sigma}{y_\sigma} + \frac{y'_\tau}{y_\tau}\right) - g_{13} + g_{14}\right\} y_\sigma y_\tau d\zeta$$

The potential functions $g_1, \ldots, g_{15}$ are as follows:

$$\begin{aligned}
g_1 &= \frac{\Lambda}{16}\frac{\phi_{1c}}{\hat{\phi}} \quad g_2 = -\frac{\hat{\eta}}{8}\Psi_{1s} \\
g_3 &= -\frac{\Lambda}{16}\frac{\phi'_{1c}}{\hat{\phi}} - \frac{\Delta^2+1}{32}\frac{\phi_{1c}\phi'}{\hat{\phi}^2} + \frac{\Lambda}{16}\frac{\phi'}{\hat{\phi}}\hat{\eta}\Psi_{1s} \quad g_4 = \frac{\phi'\phi_o}{16\hat{\phi}^2} \\
g_5 &= -\frac{\Lambda}{8}\frac{\phi_{1c}}{\hat{\phi}} + \frac{\hat{\eta}\Psi_{1s}}{4} \quad g_6 = \frac{\Lambda}{4}\frac{\phi_{1c}}{\hat{\phi}} - \frac{\hat{\eta}\Psi_{1s}}{2} \\
g_7 &= \frac{\Lambda^2+1}{16}\frac{\phi_{1c}\phi'}{\hat{\phi}^2} - \frac{\Lambda}{16}\frac{\phi'}{\hat{\phi}}\hat{\eta}\Psi_{1s} \quad g_8 = -\frac{\Lambda}{16}\frac{\phi'}{\hat{\phi}}\hat{\eta}\Psi_{1s} \\
g_9 &= \frac{\Lambda}{2}\frac{\phi_{3c}}{\hat{\phi}} - \frac{3\Lambda^2+2}{16}\frac{\phi_{2c}\phi_{1c}}{\hat{\phi}^2} + \frac{\Lambda\left(2\Lambda^2+5\right)}{128}\frac{\phi_{1c}^3}{\hat{\phi}^3} \\
&\quad + \hat{\eta}\left(-\Psi_{3s} + \frac{\Lambda}{8}\frac{\phi_{2c}}{\hat{\phi}}\Psi_{1s} + \frac{7\Lambda}{24}\frac{\phi_{1c}}{\hat{\phi}}\Psi_{2s} - \frac{\Lambda^2+1}{24}\frac{\phi_{1c}^2}{\hat{\phi}^2}\Psi_{1s}\right) \\
&\quad - \hat{\eta}^2\left(\frac{1}{12}\Psi_{2s} + \frac{\Lambda}{16}\frac{\phi_{1c}}{\hat{\phi}}\Psi_{1s}\right)\Psi_{1s} + \frac{1}{16}\hat{\eta}^3\Psi_{1s}^3
\end{aligned} \tag{51.78}$$

$$
\begin{aligned}
g_{10} = & -\frac{3\Lambda^2+2}{16}\frac{\phi_{2c}\phi_{1c}}{\hat{\phi}^2} + \frac{\Lambda\left(6\Lambda^2+13\right)}{128}\frac{\phi_{1c}^3}{\hat{\phi}^3} + \frac{2\Lambda^2+3}{32}\frac{\phi_{1c}\phi''}{\hat{\phi}^2} - \frac{\Lambda}{16}\frac{\phi_{1c}\phi'^2}{\hat{\phi}^3} \\
& + \hat{\eta}\left\{\frac{3\Lambda}{8}\frac{\phi_{2c}}{\hat{\phi}}\Psi_{1s} + \frac{3\Lambda}{8}\frac{\phi_{1c}}{\hat{\phi}}\Psi_{2s} - \frac{5(3\Lambda^2+1)}{64}\frac{\phi_{1c}^2}{\hat{\phi}^2}\Psi_{1s} - \frac{\Lambda}{16}\frac{\phi''}{\hat{\phi}}\Psi_{1s} + \frac{1}{32}\frac{\phi'^2}{\hat{\phi}^2}\Psi_{1s}\right\} \\
& - \frac{3\hat{\eta}^2}{8}\left(2\Psi_{2s}\Psi_{1s} - \Lambda\frac{\phi_{1c}}{\hat{\phi}}\Psi_{1s}^2\right) - \frac{3}{16}\hat{\eta}^3\Psi_{1s}^3 \\
g_{11} = & \frac{\Lambda}{4}\frac{\phi_o}{\hat{\phi}} \qquad g_{12} = -\frac{1}{8}\frac{\phi'\phi_o}{\hat{\phi}^2} \\
g_{13} = & \left\{-\frac{1}{4}\frac{\phi_{2c}}{\hat{\phi}} + \frac{\Lambda\left(\Lambda^2+11\right)}{64}\frac{\phi_{1c}^2}{\hat{\phi}^2} - \frac{3}{32}\frac{\phi_{1c}}{\hat{\phi}}\hat{\eta}\Psi_{1s} - \frac{\Lambda}{16}\hat{\eta}^2\Psi_{1s}^2\right\}\frac{\phi_o}{\hat{\phi}} \\
g_{14} = & \left\{\frac{\Lambda\left(\Lambda^2+5\right)}{32}\frac{\phi_{1c}^2}{\hat{\phi}^2} + \frac{3\Lambda}{32}\frac{\phi'^2}{\hat{\phi}^2} - \frac{\Lambda^2+1}{8}\frac{\phi_{1c}}{\hat{\phi}}\hat{\eta}\Psi_{1s} + \frac{\Lambda}{8}\hat{\eta}^2\Psi_{1s}^2\right\} \\
g_{15} = & \left(\frac{\Lambda}{4}\frac{\phi_{1c}}{\hat{\phi}} - \frac{1}{8}\hat{\eta}\Psi_{1s}\right)\frac{\phi_o^2}{\hat{\phi}^2}
\end{aligned}
$$

51.6.2.2 Third-rank aberrations

Second-order perturbation theory, as presented in Chapter 22 of Volume 1, is needed to establish third-rank aberration coefficients. For curved-axis systems, this is a complicated and very laborious task, even using computer algebra, and Plies (2002) proposes a simpler approach with which useful information about the magnitudes of the coefficients can be obtained with a reasonable expenditure of effort. Here we present in qualitative language the main steps in his argument, mathematical details of which are given in the article cited.

The starting point is an expression for $w(z)$ up to third-order terms in which only single derivatives of a suitable eikonal function appear (whereas multiple derivatives occur in the general form of the perturbation calculus). It is assumed that the potentials have been calculated by one of the methods described in Part II and that the second-rank fundamental rays (51.75) have also been calculated and stored. For the next stage of the calculation, the derivatives of the terms in the eikonal function denoted by F, F_{1g}, F_{2g} and F_{11c} (Eqs 9−14 of Plies and Typke, 1978) are required. Explicit formulae for these are given by Plies (Eq. 45ff). All the information needed to evaluate the integrals occurring in the second-rank trajectories, for a chosen set of values of α, β, x_o, y_o and δ, is thus available. The third-rank aberrations for the chosen conditions can now be evaluated in the image plane and the selection plane (and indeed in any other plane though it seems unlikely that such information would be wanted).

The foregoing calculation is designed to provide information for bundles of rays of immediate practical interest: axial rays ($x_o = y_o = 0$) for example, or field rays ($\alpha = \beta = \delta = 0$). In order to calculate the other aberrations, Plies notes that the trajectory equation can be recast in the form

$$\begin{aligned} w'' + h_z\Gamma + \operatorname{Re}\left(\Gamma' w^* + 2\Gamma w'^*\right)\frac{w'}{h_z} &= \frac{1+2\varepsilon\Phi}{2\hat{\Phi}}\left(h_z^2 + w'w'^*\right)\left(-E_w + \frac{w'}{h_z}E_z\right) \\ &+ \mathrm{i}\eta\hat{\Phi}^{-1/2}\left(h_z^2 + w'w'^*\right)^{1/2}\left(-h_zB_w + w'B_z - \frac{w'w'^*}{2h_z}B_w + \frac{w'^2}{2h_z}B_w^*\right) \end{aligned} \tag{51.79}$$

which lends itself well to numerical evaluation. We note in passing that the accuracy is better when the coordinates (x, y, z) are used instead of the primitive coordinates (X, Y, Z), as pointed out by Kasper (1987). When the torsion $\tau = 0$, so that $\Gamma = \kappa$ and $h_z = 1 - \kappa z$, Eq. (51.79) becomes

$$\begin{aligned} & x'' + \kappa(1-\kappa x) + (\kappa' x + 2\kappa x')\frac{x'}{1-\kappa x} \\ &\quad = \frac{1+2\varepsilon\Phi}{2\hat{\Phi}}\left(1 - 2\kappa x + \kappa^2x^2 + x'^2 + y'^2\right)\left(-E_x + \frac{x'}{1-\kappa x}E_z\right) \\ &\quad + \frac{\eta}{\hat{\Phi}^{1/2}}\left(1-2\kappa x+\kappa^2x^2+x'^2+y'^2\right)^{1/2}\left\{(1-\kappa x)B_y - y'B_z + \frac{x'}{1-\kappa x}\left(x'B_y - y'B_x\right)\right\} \\ \\ & y'' + (\kappa' x + 2\kappa x')\frac{y'}{1-\kappa x} \\ &\quad = \frac{1+2\varepsilon\Phi}{2\hat{\Phi}}\left(1 - 2\kappa x + \kappa^2x^2 + x'^2 + y'^2\right)\left(-E_y + \frac{y'}{1-\kappa x}E_z\right) \\ &\quad + \frac{\eta}{\hat{\Phi}^{1/2}}\left(1-2\kappa x+\kappa^2x^2+x'^2+y'^2\right)^{1/2}\left\{-(1-\kappa x)B_x + x'B_z + \frac{y'}{1-\kappa x}\left(-y'B_x + x'B_y\right)\right\} \end{aligned} \tag{51.80}$$

The fact that the optic axis is a ray implies that

$$\kappa = \frac{\Lambda}{2\hat{\phi}}\phi_{1c} - \hat{\eta}\Psi_{1s} \ \text{ and } \ \frac{\Lambda}{2\hat{\phi}}\phi_{1s} = -\hat{\eta}\Psi_{1c} \tag{51.81}$$

Numerical integration of Eq. (51.80) for a range of values of α, β, x_o, y_o and δ yields a set of values of $x(z)$ and $y(z)$ correct up to third rank from which the aberrations in the image and selection planes (or elsewhere) can be deduced.

CHAPTER 52

Sector Fields and Their Applications

52.1 Introduction

Magnetic and electrostatic sector fields, and indeed combinations of both, are used as dispersive elements. By this we mean that particles setting out from the same object point and in the same direction but with different values of momentum or energy or different masses will intersect some given recording plane at different points. In a well-designed device, the different families of particles will be widely separated, and to achieve this, we must arrange that all particles starting from a common object point in different directions but having the same momentum, energy and mass are focused in the recording plane; the latter is then known as the image plane. Focusing is indispensable in the symmetry plane at least, as illustrated in Fig. 52.1; in the general case, a line focus will then be formed in the y-direction perpendicular to the symmetry plane. A device that behaves in this way is said to provide single focusing.

It often happens that it is not sufficient to create a large dispersion and radial focusing: in addition, an image of the object is required, with the particles separated according to their different energies. An example of such a device is the combination of magnetic prism and electrostatic mirror introduced by Castaing and Henry (1962, 1964); see Fig. 18.1 and the full account in Metherell (1971). The necessary focusing in the axial direction, perpendicular to the plane of the diagram, is achieved by tilting the sector boundaries with respect to the optic axis. A device with this property is said to provide *double focusing*.[1] The resolution of focusing prisms will clearly be superior if the particles are focused not only in a first-order (linear) approximation but to the next higher order: in other words, it is advantageous to correct the primary (second order) aberrations. Various ways of achieving such correction are known, involving shaping the sector boundaries, exploiting the symmetry properties, or adding multipole correction elements at the ends of the sector.

A word is necessary here about the nomenclature associated with prism optics. The properties of magnetic and electrostatic sector fields have been studied for widely different

[1] This is not the only meaning of the term 'double focusing'. It is the usual meaning in particle spectroscopy and in ion momentum analysis, but in the mass spectrometer literature, a double focusing device is one in which a single image is formed of particles with one of the masses present in the beam, irrespective of angle and velocity at the source (to the usual approximation).

Principles of Electron Optics: Applied Geometrical Optics.
DOI: http://dx.doi.org/10.1016/B978-0-12-813369-9.00052-X

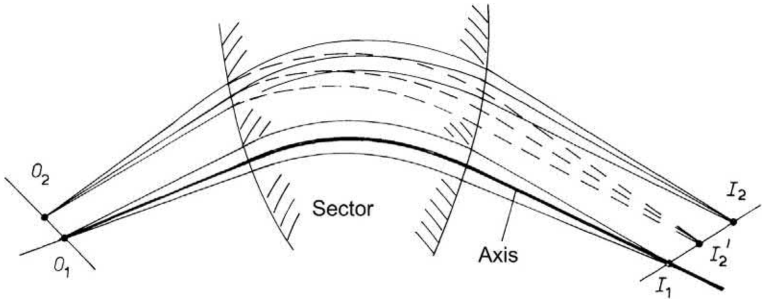

Figure 52.1
Focusing in the symmetry plane of a magnetic prism. The figure shows pencils of rays from two object points O_1 and O_2. For the latter, the effect of dispersion is also shown (broken lines), the dispersed particles having a momentum below the nominal value.

purposes and with very different energy ranges in mind. There is thus much duplication in the literature and a distinction that must be drawn with care in one situation may be irrelevant in another. Moreover, the vocabulary that is commonly used among the high-energy physics community is not obviously appropriate when discussing energy analysis for electron microscopy. In particular, the *radial* and *axial* directions, as we have defined them above, are often called the *horizontal* and *vertical* directions in the accelerator literature (e.g., Enge, 1967), though with the wide availability of large, standard, particle optics codes, there is a trend away from this terminology (e.g., Brown, 1968; Brown and Servranckx, 1985). We attempt to remain neutral, since the results are applicable to ion optics and electron optics and over a wide energy range.

52.2 Magnetic Devices with a Circular Optic Axis

We now consider magnetic fields that exhibit rotational symmetry about an axis $x = -R$, at least over a sector. At the ends of the sector, the fringing fields may well have a rather complex structure and, for the present, we neglect these fields. Fig. 52.2A shows a meridional section through a magnet with tapered poles and Fig. 52.2B, the corresponding axial or horizontal section. Since the system has rotational symmetry, all the coefficients in Eq. (51.46) are independent of the azimuth $\theta = z/R$; they must hence be constant and $c_2 \equiv 0$. The field component expansions of Eq. (51.41) are now

$$\begin{aligned} B_x &= y(G_1 + xG_2) \\ B_y &= G_0 + xG_1 + \frac{1}{2}x^2G_2 - \frac{1}{2}y^2(\kappa G_1 + G_2) \\ B_z &= 0 \end{aligned} \tag{52.1}$$

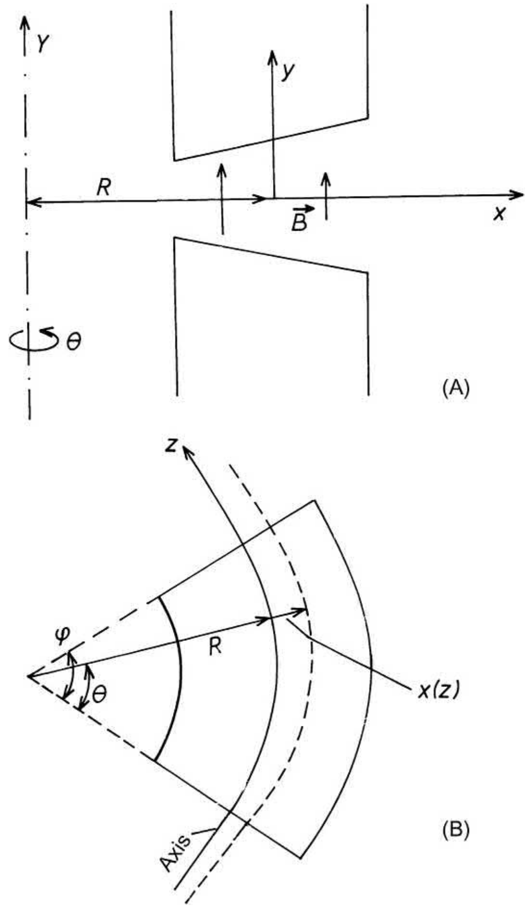

Figure 52.2
Sector magnet with tapered poles. (A) Meridional section: the arrows indicate the magnetic field, which decreases in the outward direction. (B) Symmetry plane, $Y = 0$: the deflection corresponds to a negatively charged particle.

A fairly suitable and widely used field model is given by

$$B_y(x, 0, 0) = B_0(1 + \kappa x)^{-n} \tag{52.2}$$

where $0 \leq n < 1$; B_0 denotes the constant magnetic field strength along the optic axis. For this field, we see that

$$G_0(z) = B_0, G_1 = -n\kappa B_0 \text{ and } G_2 = n(1+n)\kappa^2 B_0 \tag{52.3}$$

The equilibrium condition (51.50), $\kappa g_0 = QG_0$, takes the familiar form

$$B_0 = g_0/RQ = mv_0/RQ \tag{52.4}$$

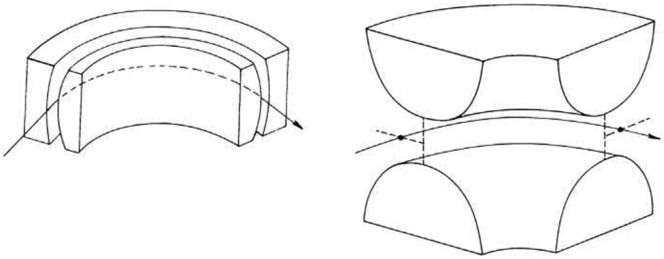

Figure 52.3
Toroidal electrodes (left) and magnetic polepieces (right). Note that the optic axis passes midway between the electrodes but does not necessarily lie in the cylindrical surface in which the poles are closest.

m being the mass corresponding to g_0. Certain values of the parameter n are associated with particular poleface shapes. The simplest case is the homogeneous field created between plane parallel faces, for which $n = 0$; the other two shapes that are amenable to exact analysis, toroidal and conical poles (Fig. 52.3), cannot be matched to Eq. (52.2) exactly but the conical field is quite well modelled by values of n close to unity for appropriate values of the cone angle (α). More generally, we find

$$G_1 = -G_0/R_m \quad G_2 = 2/R_m^2 \tag{52.5}$$

for the conical field

$$\frac{B_y}{G_0} = \frac{1}{1 + x/R_m} \tag{52.6}$$

where R_m is the gap between the polepieces at the optic axis multiplied by cot α. For the case of toroidal poles, for which

$$\frac{B_y}{G_0} = \frac{d}{d + R_m - \sqrt{R_m^2 - x^2}} \tag{52.7}$$

where d is the gap between the polepieces at their closest point and R_m is the radius of the circular section of each torus, we find

$$G_1 = 0 \quad G_2 = -1/2dR_m \tag{52.8}$$

Returning to the model (52.2), the coefficients introduced in Sections 51.5 and 51.6 take the particular values

$$\begin{aligned}
&a_1(z, g_0) = c_2 = 0, \ \ c_1 = -\kappa g_0 \\
&a_2(z, g_0) = (1-n)\kappa^2 g_0, \ \ b_2 = -n\kappa^2 g_0 \\
&a_3(z, g_0) = b_3 = \kappa^3 n^2 g_0 \\
&q_0 = \kappa, \quad q_1 = -n\kappa^2, \quad q_2 + \kappa q_1 = n^2\kappa^3
\end{aligned} \tag{52.9}$$

The paraxial ray equations simplify to

$$x'' + \kappa^2(1-n)x = \kappa\delta \tag{52.10a}$$

$$y'' + \kappa^2 n y = 0 \tag{52.10b}$$

The corresponding *homogeneous* equations, which we examine first, are known as the Kerst–Serber equations (Kerst and Serber, 1941). From these, it is obvious that oscillatory solutions are obtained only for $0 < n < 1$ and that the frequencies of oscillation are equal for $n = 1/2$. The Kerst–Serber equations are of importance for questions of stability in circular particle accelerators, where particles revolve very many times around the axis of the device before being deflected towards the target. We note in passing that Courant et al. (1952) pointed out that the amplitudes of the oscillations in the x and y directions can be very markedly reduced by arranging that $G_1(z)$ is a periodic function of z; the resulting guiding field is said to provide 'strong focusing' or focusing by alternating gradients and is very important in accelerator optics.

In many spectrometers and spectrographs, the magnet polefaces are plane-parallel, since the introduction of more complex surfaces such as cones or tori is often not really necessary and renders the machining much more complicated. In the following sections, therefore, we explore the case of the *homogeneous* magnetic field, for which $n = 0$ in Eq. (52.2), in more detail than the inhomogeneous situation. The ray equations then simply describe a flat helix in a curvilinear coordinate system. In this simple special case, it is often easier to use the Cartesian representation of the helix directly, especially in the calculation of aberrations.

The general case, in which G_1 and G_2 in Eq. (52.1) may have any form, will be examined in Section 53.3, in which we present a unified theory of ion optical focusing and deflecting elements.

52.3 Radial (Horizontal) Focusing for a Particular Model Field

We again adopt the field model of (52.2) and first consider the motion in the symmetry plane; the coordinate system adopted is shown in Fig. 52.4. (The notation is different from that employed in the widely used account of Enge, 1967.) The angles α and β characterizing the tilt of the endplanes of the magnet are taken to be positive in the orientation shown in Fig. 52.4. Our task now is to establish the linear relations between (x_o, x'_o) and (x_i, x'_i).

The case of a perpendicular entrance plane corresponds to $\alpha = 0$ and we have

$$x_1 = x_o + L_1 x'_o, \quad x'_1 = x'_o \tag{52.11}$$

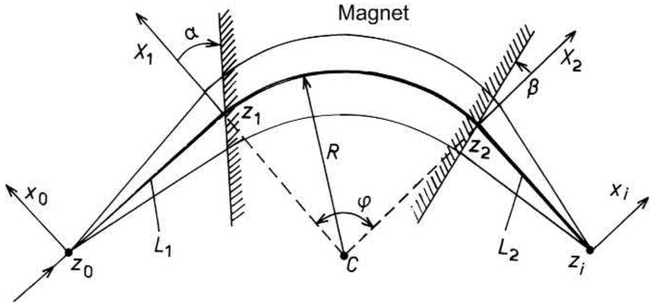

Figure 52.4
Focusing in the symmetry plane of a magnetic prism (radial focusing) and associated notation. For clarity, only one focused pencil is shown. The angles α and β will be positive in this situation.

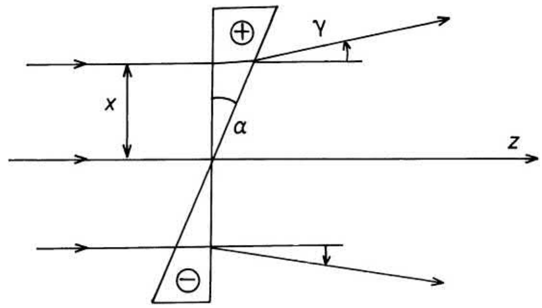

Figure 52.5
Deflection by a short magnetic prism; tan $\gamma = x$ tan α/R. The signs indicate the direction of B_y for a negatively charged particle.

Any tilt of the entrance plane ($\alpha \neq 0$) has the same effect as a deflecting prism, as shown in Fig. 52.5. Since the path-length through such a prism at a distance $|x_1|$ from the optic axis is approximately equal to $|x_1 \tan \alpha|$ and since $|x_1| \ll R$, a weak deflection $\delta x' = (x_1/R) \tan \alpha$ is produced. When the face is tilted, therefore, the effective entrance coordinates are given by

$$\bar{x}_1 \approx x_1 = x_o + L_1 x'_o, \quad \bar{x}'_1 = x'_o + \kappa x_1 \tan \alpha \tag{52.12}$$

These are now the initial conditions for the solution of (52.10a). The solution and its derivative are thus

$$\begin{aligned} x(z) &= \bar{x}_1 \cos \lambda(z - z_1) + \lambda^{-1} \bar{x}'_1 \sin \lambda(z - z_1) \\ x'(z) &= -\lambda \bar{x}_1 \sin \lambda(z - z_1) + \bar{x}'_1 \cos \lambda(z - z_1) \end{aligned}$$

in which $\lambda := \kappa(1 - n)^{1/2}$. In a fixed exit plane, $z = z_2 = z_1 + R\varphi$, φ being the deflection angle, we find the exit values

$$\bar{x}_2 = \bar{x}_1 \cos \varphi_x + R\varepsilon_x^{-1} \bar{x}'_1 \sin \varphi_x \tag{52.13a}$$

$$\bar{x}_2' = -\varepsilon_x R^{-1}\bar{x}_1 \sin\varphi_x + \bar{x}_1' \cos\varphi_x \tag{52.13b}$$

in which

$$\varepsilon_x = \lambda R = (1-n)^{1/2}, \quad \varphi_x = \varepsilon_x\varphi = (1-n)^{1/2}\varphi \tag{52.14}$$

These refer to a perpendicular exit plane; as with Eq. (52.12), any tilt (β) of this plane causes an additional deflection, now given by

$$x_2 = \bar{x}_2, \quad x_2' = \bar{x}_2' + \kappa x_2 \tan\beta \tag{52.15}$$

The coordinates in the image plane are then finally

$$x_i = x_2 + L_2 x_2', \quad x_i' = x_2' \tag{52.16}$$

The relation between (x_o, x_o') and (x_i, x_i') is represented most concisely in terms of transfer matrices. From the steps (52.11) to (52.16) we can extract the corresponding matrices. The result is represented best in dimensionless form:

$$\begin{pmatrix} \kappa x_i \\ x_i' \end{pmatrix} = T^x \begin{pmatrix} \kappa x_o \\ x_o' \end{pmatrix} \tag{52.17}$$

$$\begin{aligned} T^x = &\begin{pmatrix} 1 & \kappa L_2 \\ 0 & 1 \end{pmatrix} \begin{pmatrix} 1 & 0 \\ \tan\beta & 1 \end{pmatrix} \\ &\times \begin{pmatrix} \cos\varphi_x & \varepsilon_x{}^{-1}\sin\varphi_x \\ -\varepsilon_x \sin\varphi_x & \cos\varphi_x \end{pmatrix} \begin{pmatrix} 1 & 0 \\ \tan\alpha & 1 \end{pmatrix} \begin{pmatrix} 1 & \kappa L_1 \\ 0 & 1 \end{pmatrix} \end{aligned} \tag{52.18}$$

The explicit forms of the elements of this matrix product are not given here.

The condition for single focusing is now the disappearance of the matrix element T_{12}^x. For the important special case of a homogeneous magnetic field within the sector, $n = 0$, $\varepsilon_x = 1$, this takes the comparatively simple form

$$\sin\varphi + \kappa L_1 \frac{\cos(\varphi-\alpha)}{\cos\alpha} + \kappa L_2 \frac{\cos(\varphi-\beta)}{\cos\beta} - \kappa^2 L_1 L_2 \frac{\sin(\varphi-\alpha-\beta)}{\cos\alpha\cos\beta} = 0 \tag{52.19}$$

In the ultimate special case $\alpha = \beta = 0$ this simplifies further to Barber's rule (Barber, 1929–34):

$$L_1 = R\tan\varepsilon_1, \quad L_2 = R\tan\varepsilon_2 \text{ and hence } \varphi + \varepsilon_1 + \varepsilon_2 = \pi \tag{52.20}$$

This implies that the object point P_o, the edge of the sector and the focus position P_i are located on a straight line, as is shown in Fig. 52.6A. A similar rule has been devised by Judd (1950) for the case in which $0 < n < 1$; as shown in Fig. 52.6B, the edge of the sector and the points P_o^* and P_i^* are collinear when the sector angle is taken to be

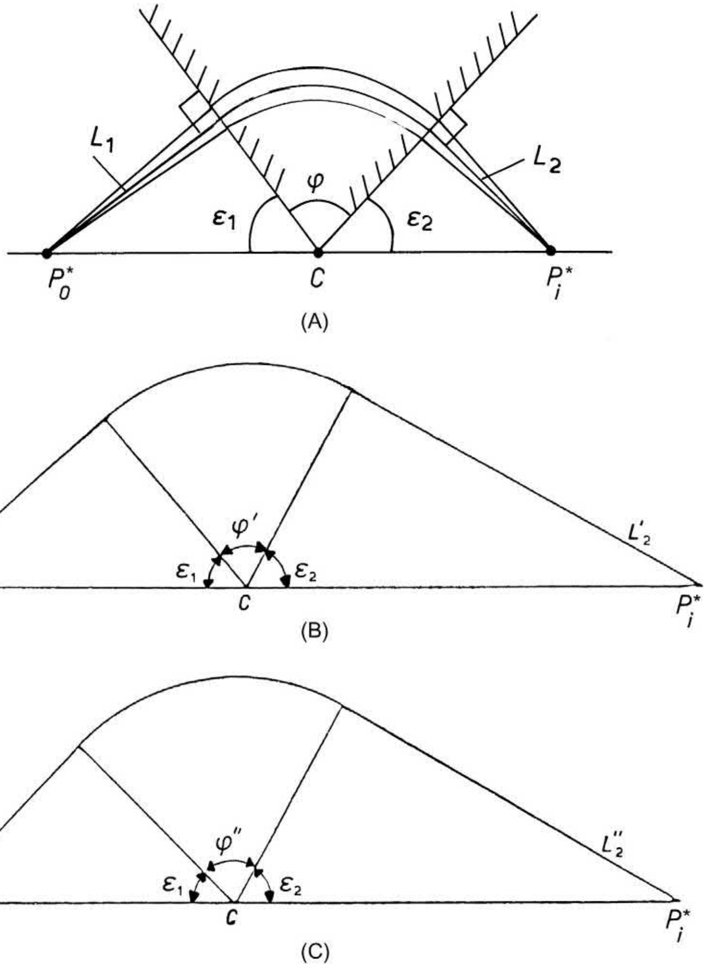

Figure 52.6

(A) Barber's rule. For normal incidence, the point source P_o, the edge C and the focus P_i lie on a straight line. There is no axial focusing! (B)–(C) Judd's rule. When $1 > n > 0$, a similar diagram relates scaled object and image distances, $L' := (1-n)^{1/2}L$, and the scaled deflection angle $\varphi' := (1-n)^{1/2}\varphi$, in the radial direction. The same is true in the axial direction for $L'' := n^{1/2}L$, $\varphi'' := n^{1/2}\varphi$.

$(1-n)^{1/2}\varphi$ and the distances to P_o^* and P_i^* to be $(1-n)^{1/2}L_1$ and $(1-n)^{1/2}L_2$. In the axial direction, $n^{1/2}$ replaces $(1-n)^{1/2}$ in the above construction.

52.4 The Linear Dispersion

We now have to consider the same transfer chain for a kinetic momentum g deviating from the nominal value of g_0. The deviation is best written in the dimensionless form

$$\delta := \frac{\Delta g}{g_0} = \frac{\Delta R}{R} \tag{52.21}$$

already introduced Eq. (51.49). In the linear approximation we can neglect all terms involving the products $x\delta$, $x'\delta$, which may be regarded as of second rank. Eqs (52.11), (52.12), (52.15) and (52.16) are thus unaltered. The only new aspect is the appearance of an inhomogeneous term in the Kerst−Serber equation:

$$x'' + \kappa^2 \varepsilon_x^2 x = \kappa\delta \tag{52.22}$$

The solution Eq. (52.13a,b) must now be replaced by inhomogeneous relations, therefore; in matrix notation, these have the form

$$\begin{pmatrix} \kappa\bar{x}_2 \\ \bar{x}_2' \end{pmatrix} = \begin{pmatrix} \cos\varphi_x & \varepsilon_x^{-1}\sin\varphi_x \\ -\varepsilon_x \sin\varphi_x & \cos\varphi_x \end{pmatrix} \begin{pmatrix} \kappa\bar{x}_1 \\ \bar{x}_1' \end{pmatrix} + \delta \begin{pmatrix} \varepsilon_x^{-2}(1-\cos\varphi_x) \\ \varepsilon_x^{-1}\sin\varphi_x \end{pmatrix}$$

The transfer matrices can be extended to rank 3 (e.g., Enge, 1967), so that only a single matrix-vector product appears on the right-hand side but we prefer the more compact (and less sparse) rank 2 form. After including the remaining transfer matrices, we finally obtain

$$\begin{pmatrix} \kappa x_i \\ x_i' \end{pmatrix} = T^x \begin{pmatrix} \kappa x_o \\ x_o' \end{pmatrix} + \delta \begin{pmatrix} D_l \\ D_a \end{pmatrix} \tag{52.23}$$

in which D_l denotes the linear dispersion and D_a the angular dispersion. These dispersions, which are given by the matrix product

$$\begin{pmatrix} D_l \\ D_a \end{pmatrix} = \begin{pmatrix} 1 & \kappa L_2 \\ 0 & 1 \end{pmatrix} \begin{pmatrix} 1 & 0 \\ \tan\beta & 1 \end{pmatrix} \begin{pmatrix} \varepsilon_x^{-2}(1-\cos\varphi_x) \\ \varepsilon_x^{-1}\sin\varphi_x \end{pmatrix} \tag{52.24}$$

refer to relative variations $\delta = \Delta g/g_0$ of the kinetic momentum. Sometimes it is not these but variations of the total energy W_0, of the charge Q or of the mass m_0 that are of interest. The corresponding relations are obtained by evaluating (51.43) for constant electric potential Φ. Differentiation of (51.43) with respect to W gives

$$\Delta g = v\Delta W, \quad v = \frac{g}{m} \tag{52.25}$$

v being the velocity and m the relativistic mass of the particle. The energy dispersion is then given by

$$\Delta x_i = RD_l m^{-1} \Delta W \tag{52.26}$$

Another quantity of interest for spectrometers is the resolving power. This is defined as the reciprocal relative momentum variation $g_0/\Delta g =: \delta_m^{-1}$, necessary to separate the images of an entrance slit with given width Δx_o. From

$$\Delta x_i = RD_l\delta_m = M_x\Delta x_o$$

$M_x = T_{11}^x$ being the radial magnification, we obtain

$$\frac{1}{\delta_m} = \frac{RD_l}{M_x\Delta x_o} \tag{52.27}$$

for a single sector magnet. A formula given by Wollnik (1971, 1980) shows that the resolving power is proportional to the area covered by the projection of the particle beam on the symmetry plane within the sector.

52.5 The Axial (Vertical) Focusing

In the previous sections, we have tacitly assumed that the field boundaries are sharp. In reality there are smooth fringing fields in the vicinity of the endplanes. Whereas these furnish only minor contributions to the radial focusing, which will be dealt with later (Section 52.6), they essentially determine the axial focusing. Fortunately, a complete knowledge of the fringing field distribution is not necessary, as will soon become obvious.

We now set out from Eq. (51.54b). Since we intend to apply Eq. (51.41) directly, it is convenient to return to the original coefficients. With $b_2 = QG_2$ and Eq. (52.3), we have

$$y'' = Qg_0^{-1}G_1(z)y(z) = \kappa B_0^{-1}G_1(z)y(z)$$

Since the fringing field is very short and $y(z)$ is a slowly varying function, we may replace $y(z)$ by its entrance value y_1. On integrating with respect to z, we find that the ray-gradient alters by an amount

$$\Delta y_1' = \kappa B_0^{-1}y_1\int G_1\,dz \tag{52.28}$$

From Eq. (51.41b), we see that $G_1 = \partial B_y/\partial x$ for $x = y = 0$. If the front-plane is inclined at an angle α to the optic axis (see Fig. 52.5), the local fringing field can depend only on the variable $\sigma \coloneqq (z - z_1)\cos\alpha - x\sin\alpha$ normal to the boundary. Hence

$$\frac{\partial B_y}{\partial x} = -\frac{\partial B_y}{\partial\sigma}\sin\alpha = -\frac{\partial B_y}{\partial z}\tan\alpha$$

Integrating now over the whole fringing field region from the field-free space outside into the domain of the unperturbed deflection field $B_y = B_0$, we find

$$\int G_1 dz = -\tan\alpha \int \frac{\partial B_y}{\partial z} dz = -B_0 \tan\alpha$$

Substituting this into Eq. (52.28), we finally obtain

$$\Delta y_1' = -\kappa y_1 \tan\alpha \tag{52.29}$$

Combining this with $\Delta x'_1 = \kappa x_1 \tan\alpha$, we see that the fringing field of a pole boundary, tilted through an angle α, acts like a short quadrupole lens of focal length $f = \pm R \cot\alpha$.

The transfer relations for the axial focusing are thus seen to be quite analogous to Eqs (52.17) and (52.18):

$$\begin{pmatrix} \kappa y_i \\ y_i' \end{pmatrix} = T^y \begin{pmatrix} \kappa y_o \\ y_o' \end{pmatrix} \tag{52.30}$$

with

$$\begin{aligned} T^y &= \begin{pmatrix} 1 & \kappa L_2 \\ 0 & 1 \end{pmatrix} \begin{pmatrix} 1 & 0 \\ -\tan\beta_y & 1 \end{pmatrix} \\ &\times \begin{pmatrix} \cos\varphi_y & \varepsilon_y^{-1}\sin\varphi_y \\ -\varepsilon_y \sin\varphi_y & \cos\varphi_y \end{pmatrix} \begin{pmatrix} 1 & 0 \\ -\tan\alpha_y & 1 \end{pmatrix} \begin{pmatrix} 1 & \kappa L_1 \\ 0 & 1 \end{pmatrix} \end{aligned} \tag{52.31}$$

and

$$\varepsilon_y = \sqrt{n}, \quad \varphi_y = \varepsilon_y \varphi, \quad \alpha_y \approx \alpha, \quad \beta_y \approx \beta \tag{52.32}$$

The differences $\alpha_y - \alpha$, $\beta_y - \beta$ are small corrections, which will be dealt with later.

When the field inside the sector is homogeneous ($n = 0$), we have $\varepsilon_y = 0$, $\varphi_y = 0$ and $\lim\,(\varepsilon_y^{-1} \sin\varphi_y) = \varphi$. The matrix involving φ_y and α_y then degenerates to

$$\begin{pmatrix} 1 & \kappa L \\ 0 & 1 \end{pmatrix} \text{ with } L = R\varphi$$

which indicates that, so far as the axial motion is concerned, the sector acts as a drift space of length L. The condition for axial focusing, $T_{12}^y = 0$, now takes the comparatively simple form

$$\begin{aligned} &L + L_1 + L_2 - \kappa L_1(L_2 + L)\tan\alpha_y - \kappa L_2(L_1 + L)\tan\beta_y \\ &\quad + \kappa^2 L L_1 L_2 \tan\alpha_y \tan\beta_y = 0 \end{aligned} \tag{52.33}$$

This equation and (52.19) are therefore the conditions for double or stigmatic focusing in first order when the field is homogeneous ($n = 0$).

52.6 Fringing Field Effects

The theory presented in the preceding sections is incomplete in two respects: we have not yet considered aberrations and we have neglected the effect of fringing fields on the radial focusing. In this section we consider the latter in a simple way. References to more sophisticated treatments are to be found in the Notes and References for Part X.

Fig. 52.7 shows an axial section through a sector magnet in a direction normal to the exit surface and the corresponding field component $B_y(s)$, s being a coordinate in this normal direction. Exact analysis of such a field requires extensive numerical calculation and so, in order to simplify the design procedures, certain approximations are commonly adopted.

In the 'sharp cutoff fringing field' approximation (SCOFF), the smooth curve $B_y(s)$ is replaced by a step function of equal area (see Fig. 52.7). We normalize all the variables as follows:

$$s := \left\{(z - z_a)\cos\beta + x\sin\beta\right\}D^{-1} \tag{52.34}$$

where D is the gap-width in the magnet, and

$$h(s) := B_0^{-1}B_y(s) \tag{52.35}$$

$$h_0(s) := \begin{cases} 1 & \text{for } s < 0 \\ 0 & \text{for } s > 0 \end{cases} \tag{52.36}$$

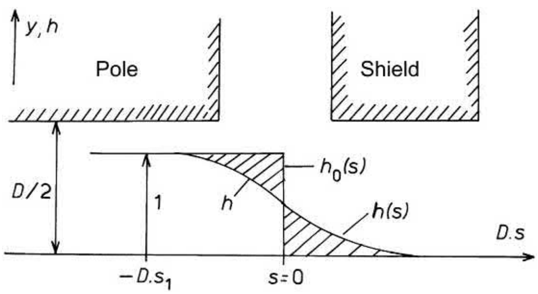

Figure 52.7
Axial section through the exit zone of a magnet fitted with a shield plate (only the upper half, $y \geq 0$, of the symmetric arrangement is shown). The SCOFF approximation is denoted by $h_0(s)$ while $h(s)$ is the normalized field strength B_y/B_0; the hatched areas must be equal.

The condition of equal areas,

$$\int_{-s_1}^{\infty} h(s)ds = \int_{-s_1}^{\infty} h_0(s)ds = s_1 \quad \text{for} \quad s_1 \gg 1$$

defines the position of the jump at $s = 0$ or, in other words, defines the virtual field boundary. In a real design, it is not the physical boundary of the prism that is used in the first-order approximation but the *virtual* field boundary, which intersects the axis at $z = z_2$. The virtual field boundary on the entrance side is defined in a similar manner; the approximation is represented schematically in Fig. 52.8.

A more refined treatment is provided by the 'extended fringing field' approximation (EFF), in which the variation of the reduced field function $h(s)$ is considered more closely. In the symmetry plane, the optic axis must deviate from that assumed in the SCOFF approximation since near the exit plane inside the sector, the EFF (52.35) already starts to decrease. The condition that the integrals be equal implies that the asymptotic direction of the optic axis cannot alter and the latter must therefore be shifted, as shown in Fig. 52.8. According to Enge (1967), the entrance and exit shifts are given by

$$\Delta x_1 = \kappa D^2 \frac{I_1}{\cos^2\alpha}, \quad \Delta x_2 = \kappa D^2 \frac{I_1}{\cos^2\beta} \tag{52.37}$$

with

$$I_1 := \int_{-s_1}^{\infty} \left[\int_{-s_1}^{s} \{h_0(s') - h(s')\} ds' \right] ds \tag{52.38}$$

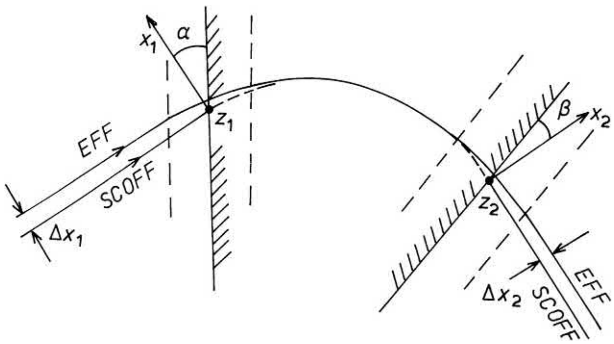

Figure 52.8
Difference between the SCOFF and the EFF approximations. The field boundaries are the *virtual* ones ($s = 0$). The origins of the coordinates x_1 and x_2 are situated on the SCOFF axis. The broken lines indicate roughly the extent of the fringing field zone.

In the fringing field domain, the angle of inclination $\tilde{\beta}$ between the optic axis and the boundary normal is a function of s. This in turn influences the axial focusing, the force causing which is proportional to $h'(s)$ tan $\tilde{\beta}$ (s). In the fringing field, where the derivative $h'(s)$ is greatest, $\tilde{\beta}(s)$ has not yet reached its asymptotic value β and the effective angle β_y is hence smaller than β (Enge, 1967):

$$\tan \beta_y = \tan \beta - \frac{DI_2(1 + \sin^2\beta)}{R \cos^3\beta} \tag{52.39}$$

$$\tan \alpha_y = \tan \alpha - \frac{DI_2(1 + \sin^2\alpha)}{R \cos^3\alpha} \tag{52.40}$$

with

$$I_2 := \int_{-\infty}^{\infty} h(s)\{h_0(s) - h(s)\}ds \tag{52.41}$$

These expressions are to be introduced into Eqs (52.31) and (52.33). These effects should not be regarded as aberrations but merely as corrections to the oversimplified SCOFF approximation.

There have been several more sophisticated attempts to include the effects of fringing fields (Hoffstätter and Berz, 1995; Müller et al., 1996; Huber and Plies, 1999). Hartmann et al. (1990) have used differential algebra (Section 34.8) to obtain numerical values of the many coefficients. The most complete theoretical study of motion through the fringing field of a homogeneous bending magnet is that of Hartmann and Wollnik (1994). We cannot give all the details of their lengthy calculations but we do reproduce the matrix elements for the entrance fringing field (from which those for the exit fringing field can be written down immediately). Note that this article supersedes those of Matsuda and Wollnik (1970a,b) and Sakurai et al. (1989). Hartmann and Wollnik define

$$a := p_x/p_0 \quad b := p_y/p_0 \quad L := v_0(t - t_0) \quad P := (p - p_0)/p_0$$
$$t = \tan\varepsilon \quad c := 1/R \quad c_0 := \cos\varepsilon \quad h = 1/\rho_0$$

(Fig. 52.9A) and find

First-order elements:

$$(x, x) = 1 - chI_{1a}\frac{t}{c_0}(2 + 3t^2)$$

$$(x, a) = -2h\frac{t}{c_0^2}I_{1a}$$

$$(x, P) = \frac{h}{c_0^2}$$

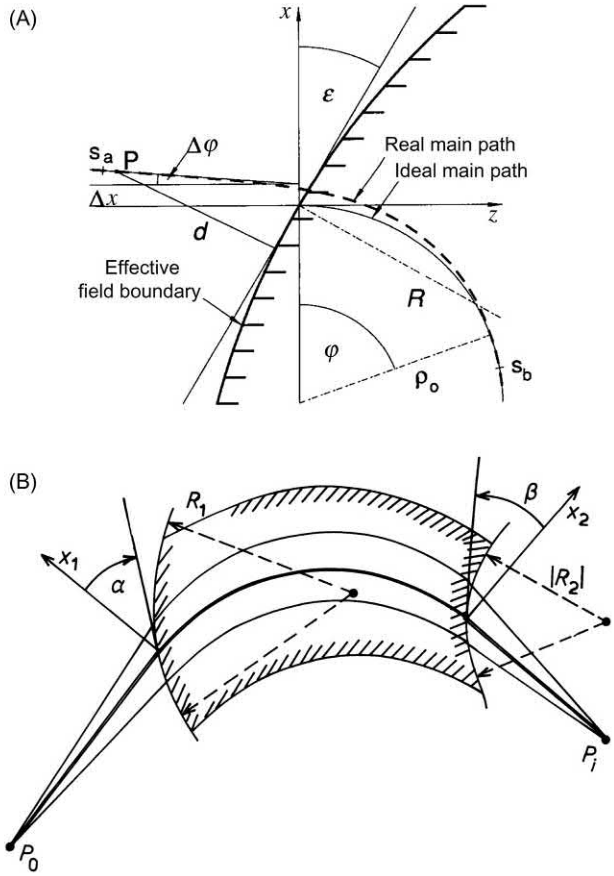

Figure 52.9

(A) Trajectory of the reference particle in a fringing field. The ideal and real paths coincide inside the magnet. The fringing field shifts the real path a distance Δx and tilts it through an angle $\Delta\varphi$. (B) Sector magnet with cylindrically curved virtual entrance and exit boundaries. Convex surfaces correspond to positive curvature and concave surfaces to negative curvature, so that in this example, $R_1 > 0$, $R_2 < 0$. *After Hartmann and Wollnik (1994), Courtesy Elsevier.*

$$(a, x) = th + chI_{1a}\frac{t}{c_0}(2 + 3t^2)\left(\frac{c}{c_0} - ht\right)$$

$$(a, a) = 1 - 2h^2\frac{t^2}{c_0^2}I_{1a} + chI_{1a}\frac{t}{c_0}(2 + 3t^2)$$

$$(a, P) = \frac{ht}{c_0}I_{1a}\left(\frac{h}{c_0} - ct\right)$$

$$(y, y) = 1 - h^2 I_{1b}\frac{1 + 2t^2}{c_0^2} + chtI_{1a}\frac{2 + 3t^2}{c_0}$$

$$(y, b) = 2h\frac{t}{c_0^2}I_{1a}$$

$$(b, y) = -th - h^2\frac{1+2t^2}{c_0}\left(I_{4a} - \frac{ht}{c_0}I_{1b}\right) + h^3 I_9\frac{t}{c_0^2}(7+10t^2) - chI_{1a}\frac{t}{c_0}(2+3t^2)\left(th + \frac{c}{c_0}\right)$$
$$+ ch^2 I_{1b}\frac{t^2}{c_0}(5+6t^2)$$

$$(b, b) = 1 - 2h^2 I_{1a}\frac{t^2}{c_0^2} + h^2 I_{1b}\frac{1+2t^2}{c_0^2} - chtI_{1a}\frac{2+3t^2}{c_0}$$

$$(L, x) = -ch\frac{t^2}{c_0}I_{1a}$$

$$(L, a) = -hI_{1a}\frac{1}{c_0^2}$$

Second-order elements:

$$(x,xx) = -\frac{1}{2}ht^2$$

$$(x,yy) = \frac{h}{2c_0^2} + h^2 tI_{4a}\frac{5+6t^2}{2c_0}$$

$$(a,xx) = \frac{ch}{2c_0^3}$$

$$(a,xa) = ht^2$$

$$(a,yy) = \frac{1}{2}h^2 t(1+2t^2) - \frac{ch}{2c_0^3} + h^3 I_{4a}\frac{t^2}{2c_0}(7+10t^2) - h^2 cI_{4a}\frac{t}{2c_0^2}(5+6t^2)$$

$$(a,yb) = -ht^2 - h^2 I_{4a}t\frac{1+2t^2}{c_0}$$

$$(y,xy) = t^2 h + h^2 tI_{4a}\frac{1+2t^2}{c_0}$$

$$(b,xy) = -\frac{ch}{c_0^3} - ch^2 tI_{4a}(5+11t^2+6t^4)$$

$$(b,xb) = -t^2 h - h^2 tI_{4a}\frac{1+2t^2}{c_0}$$

$$(b,ay) = -\frac{h}{c_0^2} - h^2 tI_{4a}\frac{5+6t^2}{c_0}$$

$$(b,yp) = h^2 I_{4a}\frac{1+2t^2}{c_0}$$

$$(L,yy) = \frac{h^2 I_{4a}}{2c_0}(1+2t^2)$$

Third-order elements:

$$(x,\ xxx) = -\frac{cht}{2c_0^3}$$

$$(x,\ xxa) = -ht^3$$

$$(x,\ xyy) = -\frac{1}{2}h^2t^2(1+2t^2) + \frac{3hct}{2c_0^3}$$

$$(x,\ xyb) = ht(1+2t^2)$$

$$(x,\ xxP) = \frac{1}{2}ht^2$$

$$(x,\ ayy) = \frac{ht}{c_0^2}$$

$$(x,\ yyP) = -\frac{h}{2c_0^2}$$

$$(a,\ xxx) = \frac{c^2ht}{2c_0^4}$$

$$(a,\ xxa) = \frac{3cht}{2c_0^3}$$

$$(a,\ xaa) = ht^3$$

$$(a,\ xaP) = -ht^2$$

$$(a,\ xyy) = h^2c\frac{1+6t^2}{2c_0^3} - \frac{3hc^2t}{2c_0^4}$$

$$(a,\ xyb) = h^2t^2(1+2t^2) - 3ht\frac{c}{c_0^3}$$

$$(a,\ xbb) = -t^3h$$

$$(a,\ ayy) = \frac{1}{2}h^2t^2(5+6t^2) - 3ht\frac{c}{2c_0^3}$$

$$(a,\ ayb) = -ht(1+2t^2)$$

$$(a,\ yyP) = -\frac{1}{2}h^2t(1+2t^2)$$

$$(a,\ ybP) = ht^2$$

$$(y,\ xxy) = \frac{3cht}{2c_0^3}$$

$$(y,\ xxb) = ht^3$$

$$(y,\ xay) = ht(1+2t^2)$$

$$(y,\ xyP) = -\,ht^2$$

$$(y,\ yyy) = h^2\frac{1+6t^2}{6c_0^2} + 2h^2I_6\frac{1+2t^2}{3c_0^2} - \frac{cht}{2c_0^3}$$

$$(y,\ yyb) = -\,\frac{th}{c_0^2}$$

$$(b,\ xxy) = -\,ht\frac{3c^2}{2c_0^4}$$

$$(b,\ xxb) = -\,ht\frac{3c}{2c_0^3}$$

$$(b,\ xay) = -\,3ht\frac{c}{c_0^3}$$

$$(b,\ xab) = -\,ht(1+2t^2)$$

$$(b,\ aay) = -\,\frac{ht}{c_0^2}$$

$$(b,\ xbP) = ht^2$$

$$(b,\ ayP) = \frac{h}{c_0^2}$$

$$(b,\ yyy) = -\,2h^2\frac{1+2t^2}{3c_0^2}(I_5c_0 + htI_6) + \frac{2}{9}h^3t(1+t^2)(2+3t^2) + 2h^3tI_{10}\frac{9+14t^2}{3c_0^2}$$
$$-\,h^2c\frac{1+6t^2}{6c_0^3} - 2h^2ct^2I_6\frac{5+6t^2}{3c_0} + ht\frac{c^2}{2c_0^4}$$

$$(b,\ yyb) = ht\frac{2c}{3c_0^3} - h^2\frac{1+2t^2}{2c_0^2}(1+4I_6)$$

$$(b,\ ybb) = \frac{ht}{c_0^2}$$

$$(L,\ xxx) = -\,\frac{1}{6}h^2t^3$$

$$(L,\ xxa) = -\,\frac{1}{2}ht^2$$

$$(L,\ xyy) = -\,\frac{1}{2}h^2t^3$$

$$(L,\ xyb) = ht^2$$

$$(L,\ ayy) = \frac{h}{2c_0^2}$$

The quantities $I_{1a} \ldots I_{10}$ denote various integrals of $h(s)$, for which Hartmann and Wollnik give the following approximate values:

$$I_{1a} \sim G_0^2, \quad I_{1b} \sim G_0^2, \quad I_{4a} \sim G_0, \quad I_5 \sim 1/G_0, \quad I_6 \sim 1, \quad I_9 \sim G_0^2, \quad I_{10} \sim 1$$

52.7 Aberration Theory: The Homogeneous Magnetic Field (n = 0)

It is convenient to treat the aberrations of sector fields thoroughly in the general case of electrostatic and magnetic fields and we defer this to Section 53.3. Here we concentrate on the conceptually simpler case of the homogeneous magnetic sector field, from which it is possible to gain much insight into the nature and correction of the various primary (second order) aberrations. In particular, we can show how the aberrations depend on the shape of the sector boundaries. Although curving these boundaries introduces additional terms in the expressions for the aberration coefficients, the effort is worthwhile since the most important second-order aberrations can be corrected by a suitable choice of the endface curvatures. It is usual and in most cases sufficient to assume that these endfaces are cylindrical, with radii R_1 and R_2 on the entrance and exit sides respectively, as shown in Fig. 52.9B. It will prove convenient to introduce the dimensionless curvature parameters C_1 and C_2:

$$C_1 := R/R_1 \cos^3\alpha \quad C_2 = R/R_2 \cos^3\beta \tag{52.42}$$

We shall not reproduce here the full derivation of the resulting coefficients; for additional details see Brown et al. (1964), Brown (1965) and Enge (1967). The results are listed in Tables 52.1 and 52.2, in which a certain amount of novel notation is employed:

i. The weighted partial derivatives of any differentiable function $f(u, v)$ are denoted by

$$(f|u^m v^n) := \frac{1}{m!n!}\left(\frac{\partial^{m+n} f}{\partial u^m \partial v^n}\right)_{u=v=0} \tag{52.43}$$

Table 52.1: Nonzero Transfer Coefficients of First Order for a Uniform-Field Magnetic Sector

$(u\|u) = \cos(\varphi - \alpha)\sec\alpha$
$(u\|u') = \sin\varphi$
$(u\|\delta) = 1 - \cos\varphi$
$(u'\|u) = -\sin(\varphi - \alpha - \beta)\sec\alpha\sec\beta$
$(u'\|u') = \cos(\varphi - \beta)\sec\beta$
$(u'\|\delta) = \sin\varphi + (1 - \cos\varphi)\tan\beta$
$(v\|v) = 1 - \varphi\tan\alpha_y$
$(v\|v') = \varphi$
$(v'\|v) = -\tan\alpha_y - \tan\beta_y + \varphi\tan\alpha_y\tan\beta_y$
$(v'\|v') = 1 - \varphi\tan\beta_y$

Table 52.2: Focusing Coefficients of Second Order

$$(u|u^2) = \{(u'|u)\sin(\varphi - \alpha + \beta)\sec\alpha\sec\beta + C_1\sin\varphi\}/2$$

$$(u|uu') = (u|u)\tan\alpha + \sin(\varphi - \alpha)\sec\alpha\sec^2\beta\cos\varphi + \tan\alpha\tan^2\beta$$

$$(u|u\delta) = 1 + (u|u)(\tan^2\beta - \sec^2\beta\cos\varphi)$$

$$(u|u'^2) = \{\cos\varphi - (u'|u')\cos(\varphi + \beta)\sec\beta\}/2$$

$$(u|u'\delta) = (u|\delta)\sec^2\beta\sin\varphi$$

$$(u|\delta^2) = \{(u|\delta)^2\tan^2\beta - \sin^2\varphi\}/2$$

$$(u'|u^2) = \left\{-(u'|u)^2\tan\beta + C_1(u'|u') + C_2(u|u)^2\right\}/2$$

$$(u'|uu') = (u'|u)(\tan\alpha - (u'|u')\tan\beta) + C_2(u|u)\sin\varphi$$

$$(u'|u\delta) = -(u'|u)(\sec^2\beta + \sin(\varphi - \beta)\sec\beta\tan\beta) + C_2(u|u)(u|\delta)$$

$$(u'|u'^2) = \left\{-\sin(\varphi - \beta)\sec\beta - (u'|u')^2\tan\beta + C_2\sin^2\varphi\right\}/2$$

$$(u'|u'\delta) = -(u'|u')(u'|\delta)\tan\beta + C_2(u|\delta)\sin\varphi$$

$$(u'|\delta^2) = \{-(u'|\delta)(2 + (u'|\delta)\tan\beta) + C_2(u|\delta)^2\}/2$$

$$(u|v^2) = \{(u|u)\sec^2\alpha + \sin\varphi\tan^3\alpha - (u|\delta)\tan^2\alpha - (v|v)^2\sec^2\beta - C_1\sin\varphi\}/2$$

$$(u|vv') = (u|\delta)\tan\alpha - (u|u')\tan^2\alpha - (v|v)(v|v')\sec^2\beta$$

$$(u|v'^2) = -\left\{(u|\delta) + (v|v')^2\sec^2\beta\right\}/2$$

$$(u'|v^2) = \{(u'|u)\sec^2\alpha + (u'|u')\tan^3\alpha - (u'|\delta)\tan^2\alpha + 2(v|v)(v'|v)\tan^2\beta + (v|v)^2\tan^3\beta - C_1(u'|u') - C_2(v|v)^2\}/2$$

$$(u'|vv') = (u'|\delta)\tan\alpha - (u'|u')\tan^2\alpha + \{(v|v')(v'|v) + (v|v)(v'|v')\}\tan^2\beta + (v|v)(v|v')\tan^3\beta - C_2(v|v)(v|v')$$

$$(u'|v'^2) = \left\{(v|v')^2\tan^3\beta + 2(v|v')(v|v')\tan^2\beta - (u'|\delta) - C_2(v|v')^2\right\}/2$$

$$(v|uv) = (u'|u)\tan\alpha + (u|u)(v'|v)\tan\beta - C_1\varphi$$

$$(v|uv') = (v|v)\tan\alpha + (u|u)(v'|v')\tan\beta - (u'|u)$$

$$(v|u'v) = -\varphi\sec^2\alpha - \{1 - (u'|u')\}\tan\alpha + (u|u')(v'|v)\tan\beta$$

$$(v|u'v') = 1 - (u'|u') + (u|u')(v'|v')\tan\beta$$

$$(v|v\delta) = (u'|\delta)\tan\alpha + (u|\delta)(v'|v)\tan\beta$$

$$(v|v'\delta) = \varphi - (u'|\delta) + (u|\delta)(v'|v')\tan\beta$$

$$(v'|uv) = (u'|u)\{(v|v)\sec^2\beta - \tan\alpha\tan\beta\} - C_1(v'|v') - C_2(u|u)(v|v)$$

$$(v'|uv') = (u'|u)(\varphi\sec^2\beta + \tan\beta) + (v'|v)\tan\alpha - C_2\varphi(u|u)$$

$$(v'|u'v) = (u'|u')(v|v)\sec^2\beta - (v'|v')\sec^2\alpha + \{1 - (u'|u')\}\tan\alpha\tan\beta - C_2(v|v)\sin\varphi$$

$$(v'|u'v') = (u'|u')(\varphi\sec^2\beta + \tan\beta) - \tan\beta - C_2\varphi\sin\varphi$$

$$(v'|v\delta) = (u'|\delta)\{(v|v)\sec^2\beta - \tan\alpha\tan\beta\} - (v'|v) - C_2(v|v)(u|\delta)$$

$$(v'|v'\delta) = (u'|\delta)(\varphi\sec^2\beta + \tan\beta) - C_2\varphi(u|\delta)$$

After Enge (1967)

The Taylor series expansion of $f(u, \upsilon)$ thus takes the simple form

$$f(u,\upsilon) = f(0,0) + (f|u)u + (f|\upsilon)\upsilon + (f|u^2)u^2 + (f|u\upsilon)u\upsilon + (f|\upsilon^2)\upsilon^2 \\ + \text{third and higher order terms} \tag{52.44}$$

ii. In Tables 52.1 and 52.2, only the transfer through the field is considered, not that from the object plane to the entrance plane $z = z_1$ and from the exit plane $z = z_2$ to the image plane. In our notation x_2, y_2, x_2', y_2' are expressed as functions of x_1, y_1, x_1', y_1' and δ.

iii. The results are given in *dimensionless* form, all distances and coordinates being normalized with respect to the radius R:

$$u = x/R, \quad \upsilon = y/R, \quad \zeta = z/R \tag{52.45}$$

The slopes are then invariant; for instance $x' \equiv dx/dz = u' = du/d\zeta$. (Note that these quantities u and υ are the same as those denoted by y and z respectively in Enge (1967).)

iv. The coefficients $(a|b)$ tabulated relate the contribution associated with the second element b to the first element a. For example

$$u_2 = (u|u)u_1 + (u|u')u_1' + (u|\delta)\delta \\ + (u|u^2)u_1^2 + (u|uu')u_1u_1' + (u|u'^2)u_1'^2 + \ldots$$

and similarly for υ_2, u'_2 and υ'_2.

The coefficients listed in Table 52.1 are to be introduced into the expressions collected in Table 52.2. It is immediately clear that the number of nonzero coefficients is already quite large and so there is little incentive to go beyond the second-order aberrations for this model field.

52.8 Optimization Procedures

So numerous are the possible aberrations of magnetic prisms that some means of designing such devices with as few aberrations as possible is clearly most desirable. Many ways of achieving this end are to be found in the literature, which depend very intimately on the purpose of the instrument. We must refer the reader to the specialized literature, therefore, and here we simply discuss the single prism, which is of interest in the electron microscope energy range, and the use of symmetries for certain more complex situations. Many references from the mass spectrometry literature are listed in the bibliography of this Part. The book of Livingood (1969) remains an excellent introduction and the later texts of Kel'man et al. (1979, 1985), Afanas'ev and Yavor (1978), Wollnik (1987a) and Carey (1987b) describe many practical devices, as does the text of Berz et al. (2015).

52.8.1 Single Deflection Prisms

For a single magnetic prism, optimization procedures have been published by Parker et al. (1978) and Shuman (1980). These authors recognize that it is unlikely that all the aberrations can be cancelled and they therefore attempt to identify and correct only the more important, subject to certain instrumental assumptions: (i) The area of the specimen to be imaged is very small; the isoplanatic approximation is adequate and only the aberrations that affect the axial region ($x_o \approx 0$, $y_o \approx 0$) need be investigated. (ii) The resolution is more important in the radial (x) direction than in the axial (y) direction. Second-order radial focusing is therefore necessary whereas first-order axial focusing is sufficient.

With these assumptions, the surviving terms in the series expansion for the coordinate x_i are as follows:

$$\kappa x_i = A_1 x'_o + D_1\delta + A_2 x'^2_o + B_2 y'^2_o + D_2\delta^2 + E_2 x'_o\delta \tag{52.46}$$

The conditions to be satisfied are here $A_1 = A_2 = B_2 = E_2 = 0$ with Eq. (52.33) for the axial focusing. The coefficients in Eq. (52.46) may be expressed as linear combinations of Enge's focusing coefficients; for instance

$$A_1 = (u|u') + \kappa L_1(u|u') + \kappa L_2(u'|u') + \kappa^2 L_1 L_2(u'|u)$$

which is identical with the left-hand side of Eq. (52.19). Similar expressions may be derived for A_2, B_2 and E_2.

Inspection of Table 52.2 shows that all the coefficients depend linearly on the curvatures C_1 and C_2; this certainly simplifies the subsequent optimization. We now proceed as follows.

i. The radius R, the deflection angle φ and the object distance L_1 are chosen in accordance with the experimental requirements and kept fixed during the calculations.
ii. Some initial estimate is adopted for $\alpha > 0$, after which Eqs (52.19) and (52.33) are solved for L_2 and β, taking (52.39) and (52.40) into account. Usually, $\beta > 0$ gives a high dispersion.
iii. The coefficients in

$$\begin{aligned} A_2 &= A_{20} + A_{21}C_1 + A_{22}C_2 \\ B_2 &= B_{20} + B_{21}C_1 + B_{22}C_2 \\ E_2 &= E_{20} \qquad\qquad\; + E_{22}C_2 \end{aligned}$$

can now be determined after which C_1 and C_2 are calculated by setting $A_2 = B_2 = 0$.
iv. The second and third steps are repeated with different values of α until a value is found for which E_2 vanishes. Usually, there is one solution for which $C_1 > 0$ and $C_2 < 0$.

The remaining shortcomings are of different kinds. First, there are the uncorrected aberrations of second order, especially those affecting the axial focusing and those arising from the lateral extent of the source. A second class consists of the numerous aberrations of third and higher order. Finally, there still remain some aberrations of first order; at first sight, this may seem surprising but we emphasize that the theory of fringing fields, outlined in Section 52.6, is an approximation.

The remaining aberrations can best be determined by tracing Lorentz trajectories through the exact magnetic field, computed by solving the appropriate boundary-value problem. Strictly speaking, the latter is fully three-dimensional but, for well-shielded magnets, sufficiently broad in the x-direction, a two-dimensional approximation is accurate enough if the fringing fields are assumed to be rotationally symmetric about the axis of local cylindrical curvature. Such calculations have, for example, been made by Killes (1983). Fig. 52.10 shows aberration discs computed in this way. These demonstrate that the axial focusing is indeed less perfect than the radial focusing. They also reveal that the results of the optimization routine outlined above are not quite optimal, as a small shift of the image plane considerably reduces the radial aberrations. In practice, this is not serious for it is

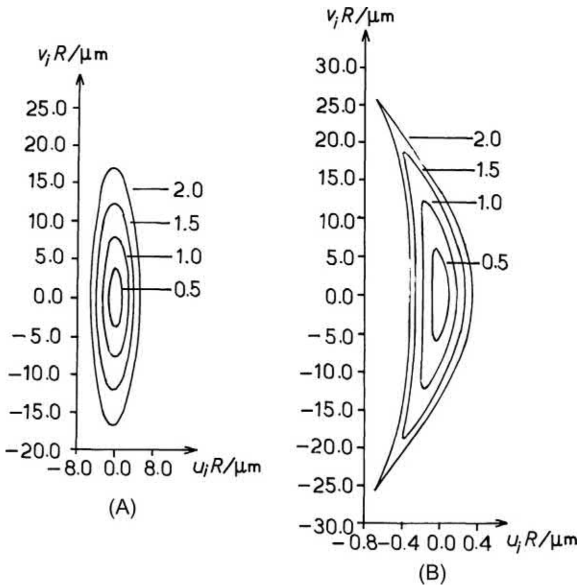

Figure 52.10
Typical examples of aberration figures in the image plane of a single-sector spectrometer for four different values of the aperture angle at the object point. (A) Image plane obtained from the optimization routine. (B) Defocusing of $\Delta z = 2.1$ mm at $R = 25$ cm and $L_2 = 72$ cm. Note the different scales in the radial and axial directions.

always necessary to include a multipole lens system outside the sector magnet to correct aberrations caused by imperfect machining and other sources of parasitic errors.

52.8.2 Use of Symmetries

Procedures that exploit symmetries are of interest in multicomponent systems. In the accelerator literature, attention is concentrated on the chromatic aberrations whereas it is the geometric aberrations that are of more interest at lower energies for energy filters and analysers: see the survey by Brown and Servranckx (1985) and the papers of Rose and colleagues (Rose and Plies, 1973, 1974; Rose, 1978; Rose and Pejas, 1979), especially those of Lanio (1986) and Lanio et al. (1986). A typical situation is shown in Fig. 52.11. Here, the configuration has an additional plane of symmetry and external multipole elements, which are adjusted in such a way that the paraxial rays are either positively or negatively mirror-symmetric with respect to this second symmetry plane. All the integrals for the aberration coefficients (51.60) then cancel out and hence such an arrangement is free of second-order aberrations. For more details we refer to the papers listed above, where the

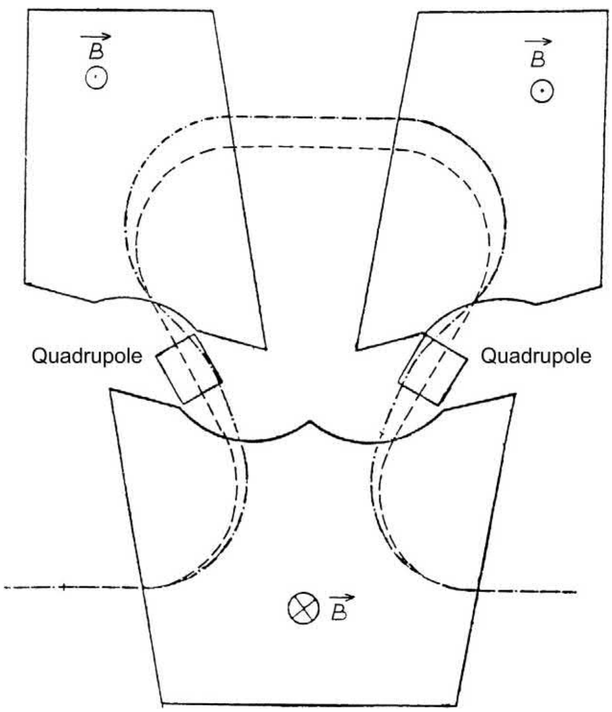

Figure 52.11
A magnetic, imaging energy filter free of second-order aberration. The boundaries are those of the effective fields in the SCOFF approximation.

necessary multipole correction systems are also dealt with extensively, and to Section 52.9 as well as to the relevant papers mentioned in the Notes and References for Part X. A paper by Zeitler (1990) is relevant here, since the Lanio design is re-examined using matrix methods and relations between the many coefficients are exploited. Symmetry is an important feature of time-of-flight and multipassage mass spectrometers; see for example Campana (1987a,b), Matsuo et al. (1987), Wollnik et al. (1987a,b) and Berger and Baril (1987). The history of time-of-flight mass analysers is traced by Wollnik (2013) and many references to these devices, in which there has been a resurgence of interest, are included in Chapter 53, Unified Theories of Ion Optical Systems.

52.9 Energy Analysers and Monochromators

52.9.1 Introduction

With the exception of Wien filters, electron energy analysers have curved axes and, as we shall see, numerous combinations of magnetic prisms or occasionally electrostatic prisms have been investigated.

For the highest microscope resolution, chromatic aberration must be combated; two approaches are current: limitation of the energy spread of the illuminating beam by means of a monochromator and incorporation of a chromatic-aberration corrector in the column, in conjunction with the corrector of geometric aberrations. We examine the optics of some monochromators here but for detailed studies of these highly perfected devices the reader must return to the original publications. Methods of designing energy analysers are described by Gurov et al. (2015).

52.9.2 In-column Energy Analysers

Introduction. The first imaging analyser to be incorporated in the column of an electron microscope was the prism—mirror combination of Castaing and Henry (1962), described at length by Henry (1964) and reviewed by Metherell (1971), already mentioned in Sections 18.1 and 37.3. An analyser of this type was installed in a Siemens 1A microscope by Henkelman and Ottensmeyer (1974a, Ottensmeyer, 1984); the mirror is described in (Henkelman and Ottensmeyer, 1974b). For the intermediate-voltage and high-voltage microscopes that came into operation in the 1960s, it was not reasonable to use a mirror and designs in which a magnetic field replaced the latter were proposed (Rose, 1974). These were the early members of the family of Ω-filters, so called from their resemblance to this Greek letter. Thus Zanchi et al. (1975, 1977a,b; Sevely et al., 1977) adapted a three-prism Ω-filter to the 1-MeV electron microscope in Toulouse. At JEOL, Oikawa et al. (1986) added such a filter to a 200 kV instrument (JEM-200CX). A B-type Ω-filter has been installed in one of the new generation of high-voltage microscopes by Omoto et al. (2008) at Kyushu University.

Wien filters have also been incorporated in the microscope column. Their optics is presented in Chapter 38, The Wien Filter. For convenience, we indicate sources of information about their use in practice in this section, even though the axis is not curved. An example of a very sophisticated design is the multipole Wien filter incorporated in an X-ray photoemission electron microscope by Marx et al. (1997).

Nomenclature. Before describing the various geometries that have been studied, we make a short digression to introduce the vocabulary of the subject. As shown schematically in Fig. 52.12, there are several devices with the basic Ω structure and two α configurations. In all of these, there is mechanical symmetry about a midplane. In Ω-filters, the polarity of the magnets in the second half is the reverse of that in the first half and the sum of the deflection angles is zero. In the α-filters, the polarity is not reversed and the sum of the deflection angles is 2π.

The four Ω devices shown in Fig. 52.12 differ in the symmetry behaviour of the ray $t_y(z)$, in the symmetries present and in the shape of the poles ($t_y(z)$ is the same as $y_\beta(z)$ in the notation employed by Scherzer and used consistently in the publications of the Darmstadt school, Tsuno and others). In the A-type filter, the axial ray $t_y(z)$ is antisymmetric about the midplane (Lanio, 1986) while in the B-type, it is symmetric (Tsuno et al., 1998). The 'symmetric' Ω design introduces an important new symmetry property: the device is mechanically symmetric not only about the midplane but also about the 120° planes shown. In the mandoline[2] filter, the most highly perfected member of the family, the magnetic fields are no longer homogeneous, as explained below. Kujawa and Krahl (1988) compare the A- and B-type Ω-filters.

The A- and B-type α-filters again differ in the behaviour of the axial ray $t_y(z)$; for the B-type α-filter, see Taya et al. (1996).

By enclosing an Ω-filter between deflecting magnets, we obtain the family of W-filters. These are still in-column devices but the column is now turned through 180° by the filter, thus reducing its overall height and increasing its mechanical stability. The original version was incorporated in the SESAM instrument (Koch et al., 2006). A variant was considered by Tsuno.

This does not exhaust the configurations of possible interest. Tsuno has investigated an S-filter and an ∞-filter.; here again, the sum of the deflection angles is different, as in the

[2] The filter is so named because of its resemblance to the musical instrument and also because the word forms an acronym: Magnetic Aberration-free Noticeably Dispersive Omega-Like INhomogeneous Energy. But the usual spelling of the musical instrument is 'mandolin'; 'mandoline' is the kitchen utensil.

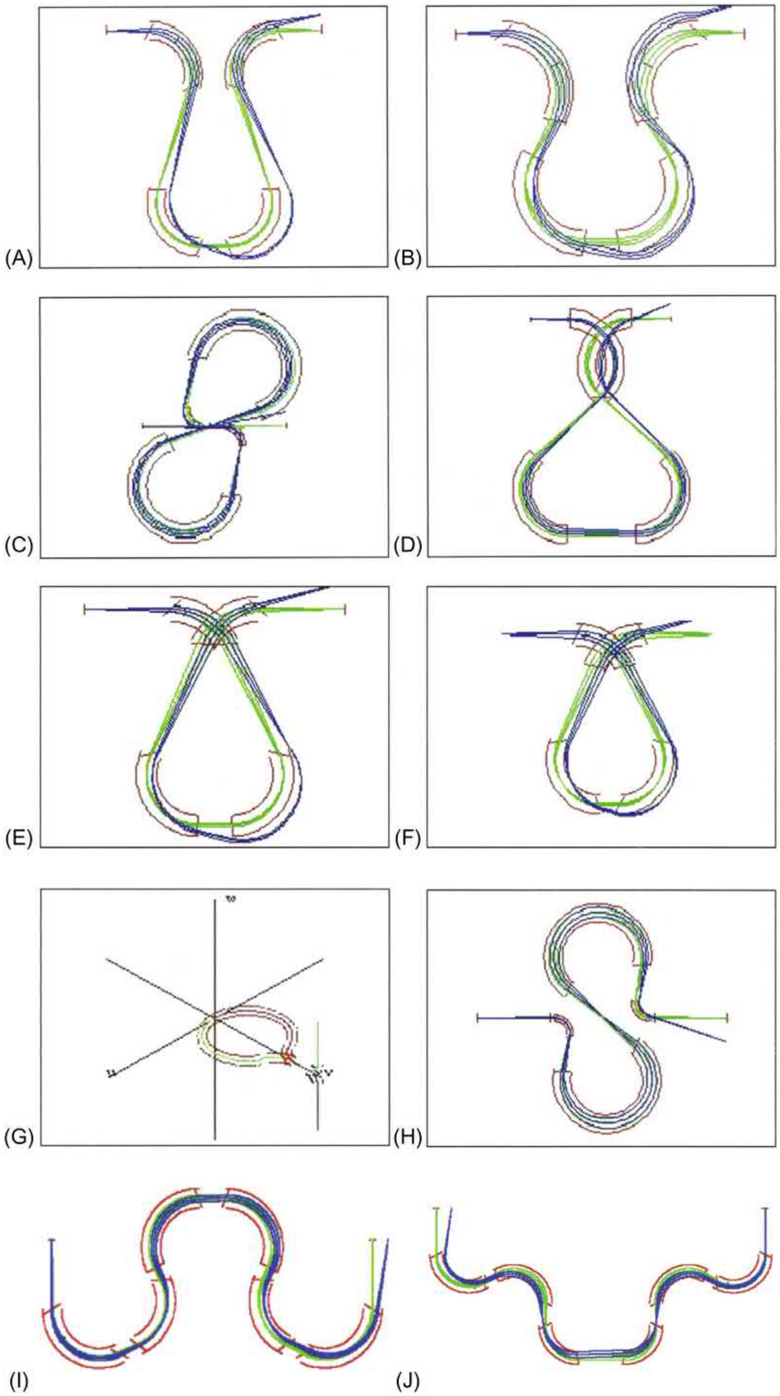

Figure 52.12
The optic axis and fundamental rays in imaging filters. (A) Ω-filter, A-type. (B) Ω-filter, B-type. (C) Infinity (∞) filter. (D) Mandoline filter. (E) α-filter, A-type. (F) α-filter, B-type. (G) Φ-filter. (H) S-filter. (I) Twin-column W-filter. (J) Variant of the W-filter (Courtesy Dr Katsushige Tsuno).

case of the Ω- and α-filters. Unlike the latter, magnets are now present on both sides of the optic axis. A last design is the Φ-filter, proposed by Souche and Jouffrey (1998), which is different from all the others in that the dispersion magnet is situated in a plane perpendicualr to the axis of the microscope column, which is thus hardly any longer than in its unmodified state.

This diversity can be understood by considering the points of importance in filter design (Tsuno, 2001):

i. Symmetry or antisymmetry of the dispersion ray about the midplane.
ii. Relative magnet polarity.
iii. Homogeneity of the magnetic fields: parallel pole faces (homogeneous) or conical pole faces (inhomogeneous).
iv. Symmetry or antisymmetry of the axial rays $t_x(z)$ and $t_y(z)$ about the midplane.
v. Direction of dispersion.

Altering one or more of these choices generates a new filter.

52.9.3 Details of the Various Filters

We now give a little more information about each of these filters.

Ω-filters. The optics of the first Ω-filters was investigated in depth in the papers by Zanchi et al. (1977a,b). The next important contribution was made by Lanio (1986), who looked for the best design of Ω and α devices with as few magnets as possible. His designs are illustrated in Fig. 52.13, where the fundamental rays are also shown. However, the aberrations of these models are still too large for high-resolution work. An improved but more complicated filter was designed by Rose and Pejas (1979); this consisted of four magnets with curved pole faces and included three sextupoles, which provided further correction. The curved pole faces created multipole fields, which could be used for aberration correction. However, the presence of the curved faces generated uncontrollable parasitic aberrations and the curved surfaces had to be replaced by flat surfaces. Seven sextupoles were now needed to compensate for the absence of the fields associated with the curved faces (Lanio et al., 1986).

The final stage in the evolution of filters of the Ω type is the mandoline filter (Uhlemann and Rose, 1994), shown schematically in Fig. 52.14. Here, the inner magnets are no longer homogeneous, the polepieces being conical or 'tapered'. The resulting dispersion is higher than that of any earlier filter and about twice that of the best post-column filters. The optics of the mandoline filter is presented in great detail by Uhlemann and Rose and in Rose's book (2012, Section 13.2.2), and is not reproduced here.

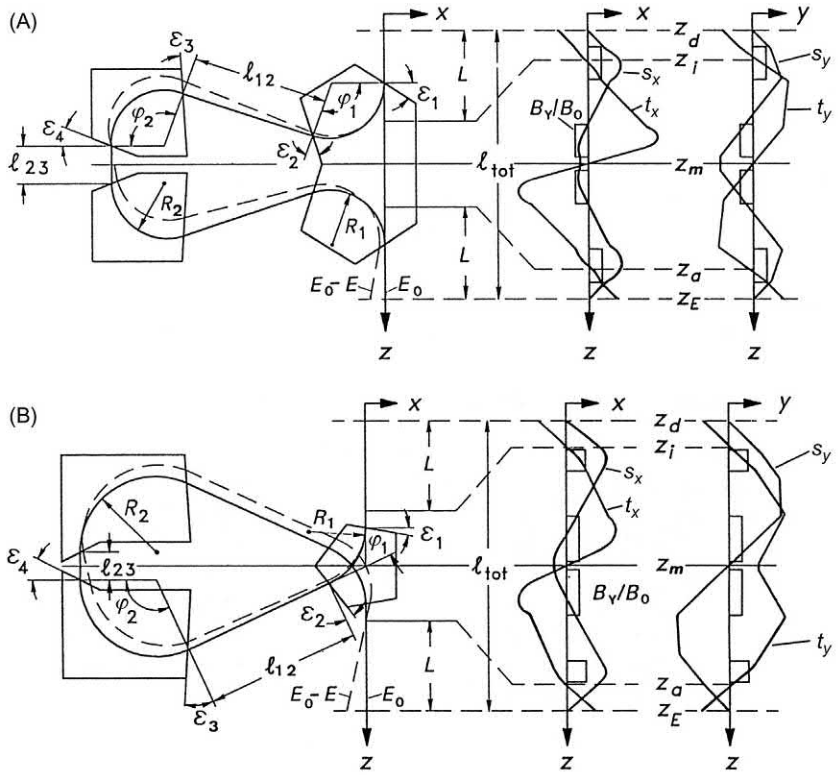

Figure 52.13
Positions of the magnets and fundamental trajectories (relative to a straightened optic axis) in (A) an Ω-filter and (B) an α-filter. *After Rose and Krahl (1995), Courtesy Springer Verlag.*

W-filters. Every new element lengthens the column of an electron microscope, which is not only inconvenient but also affects its mechanical stability adversely. These problems can be alleviated by use of a twin-column design. One column contains the source and its monochromator if present, condenser lenses, the specimen chamber, the objective lens and the aberration corrector. The second column, parallel and of course adjacent to the first, contains the projector lenses and detector. The two columns are connected by the energy filter consisting of an Ω-type device enclosed between sector magnets designed to guide the beam from the first column into the filter and subsequently direct it up into the second column. It is desirable to arrange that the (astigmatic) images of the object and diffraction planes lie in the midplane of the Ω-element. For this,

$$s'_x(z_m) = s_y(z_m) = t_x(z_m) = t'_y(z_m) = 0$$

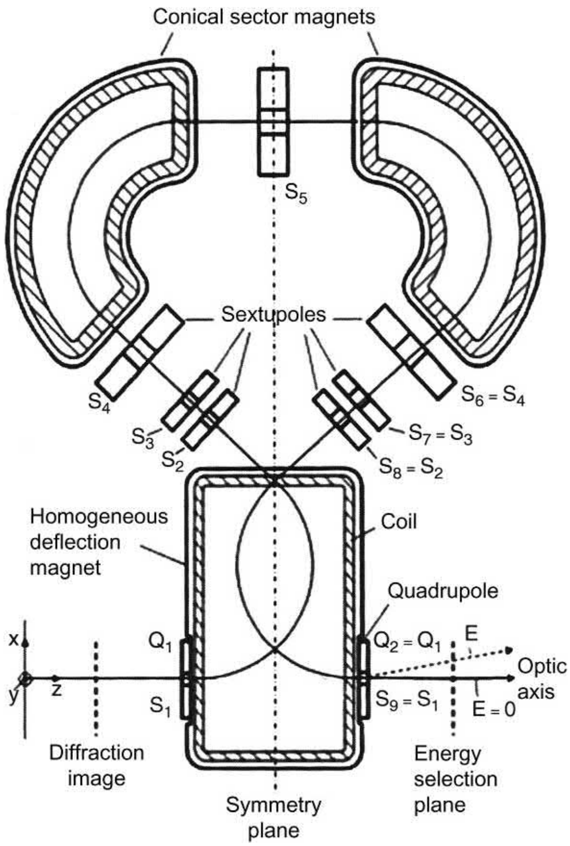

Figure 52.14
Details of the Mandoline filter *After Rose (2012), Courtesy of Springer Verlag.*

Two of these four conditions can be satisfied by suitable choice of the lengths a and $2g$ shown in Fig. 52.15: the other two are satisfied by choosing the cone-angle (θ) of the pole-faces correctly. This angle is frequently expressed in terms of the *field index* ν,

$$\nu := \left(\frac{2R}{D}\tan\theta\right)^{1/2}$$

where D is the distance between the pole faces at the optic axis, of radius R. The angle θ measures the tilt of each pole face relative to the x-coordinate. Sextupoles are inserted between the bending magnets to cancel any remaining second-order geometrical aberrations.

An alternative form of the W-filter (Fig. 52.12J) has been studied by Tsuno (2004), who describes its optical properties and compares its performance with those of a B-type Ω-filter and the S-filter.

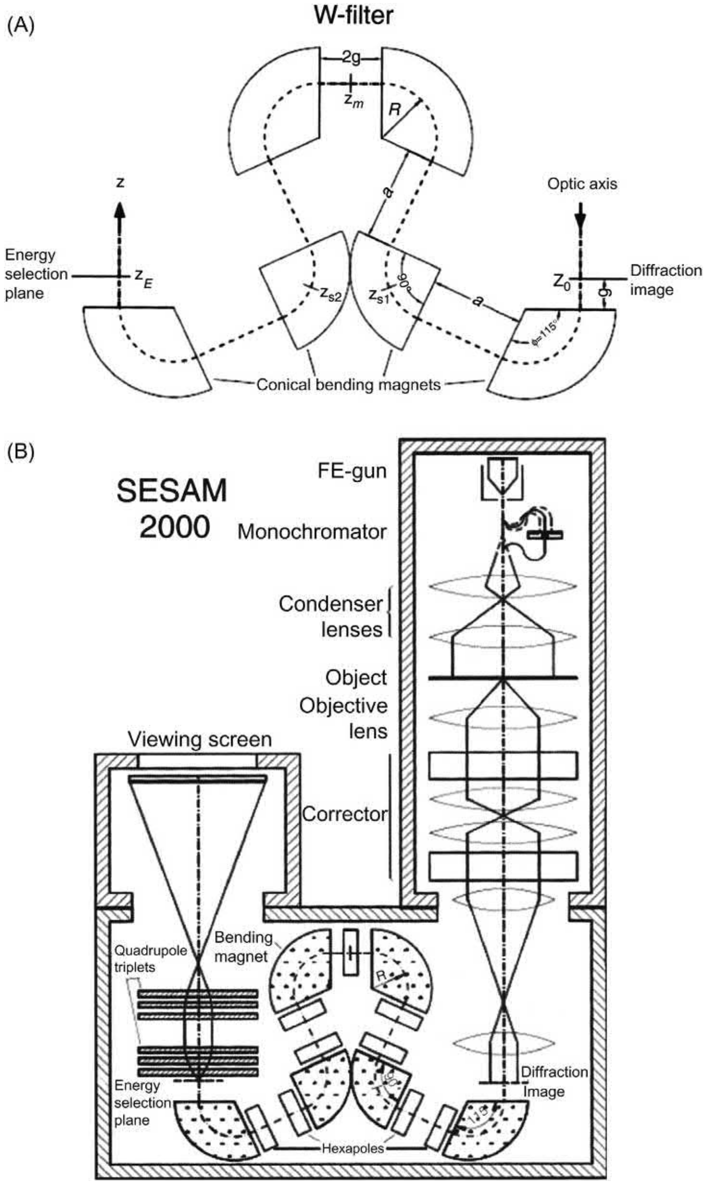

Figure 52.15

The W-filter. (A) Arrangement of the conical bending magnets. (B) The filter incorporated in an analytical transmission electron microscope (SESAM). *After Rose (2012), Courtesy of Springer Verlag.*

S- and ∞*-filters*. These two designs are unusual in that the space through which the beam travels extends on both sides of the column. This has the advantage of distributing the weight of the filter evenly. In both cases, four magnets are required and the two central magnets must have opposite polarity. If the first two magnets have the same polarity (and

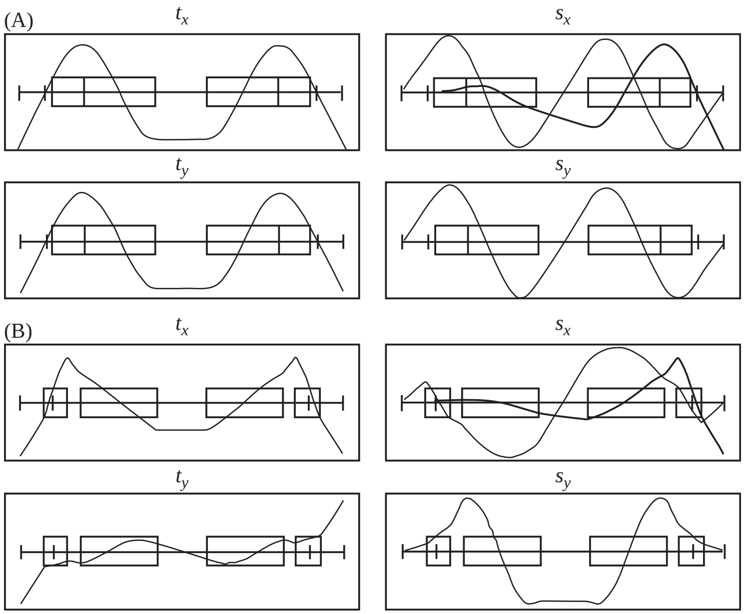

Figure 52.16

Fundamental rays in the S-filter. (A) A-type. (B) B-type. Two dispersion rays are also shown. *After Tsuno (2001), Courtesy Society of Photo-optical Instrumentation Engineers.*

thus the opposite of that of the last two magnets, NNSS say, we have the ∞ configuration. When the polarity of the first two magnets is not the same (NSNS), we have the S-filter. In each case, there is an A-type and a B-type. In the former, the rays t_x and t_y intersect the axis n times, where n is even – typically $n = 4$. In the B-type, if t_x intersects the axis n times, then t_y intersects it $n - 1$ times. Fig. 52.16 shows the fundamental rays for an A-type S-filter (52.16a) and for a B-type ∞-filter (52.16b). It is not practical to use homogeneous fields and the poles are therefore tilted. For a particular choice of tilt angle, the fundamental rays are the same: $t_x(z) = t_y(z)$ and likewise for s_x and s_y; this is known as the *round-lens focus condition* (shown in Fig. 52.16A) but it does not provide the highest dispersion. We refer to Tsuno (2001), where many examples are illustrated and the corresponding dispersion is given. Some possible arrangements are shown in Fig. 52.17.

52.9.4 The Möllenstedt and Ichinokawa Analysers

A large dispersion can be obtained by allowing the beam to enter an electrostatic lens not along the optic axis but through a slit placed at a certain distance from the latter. In the original model (Möllenstedt, 1949), a round lens was used but it is preferable to use a cylindrical lens (Chapter 20 of Volume 1). The optics of such a device is presented in full detail by Metherell (1971), with many early references. The mode of operation can be understood from Fig. 52.18.

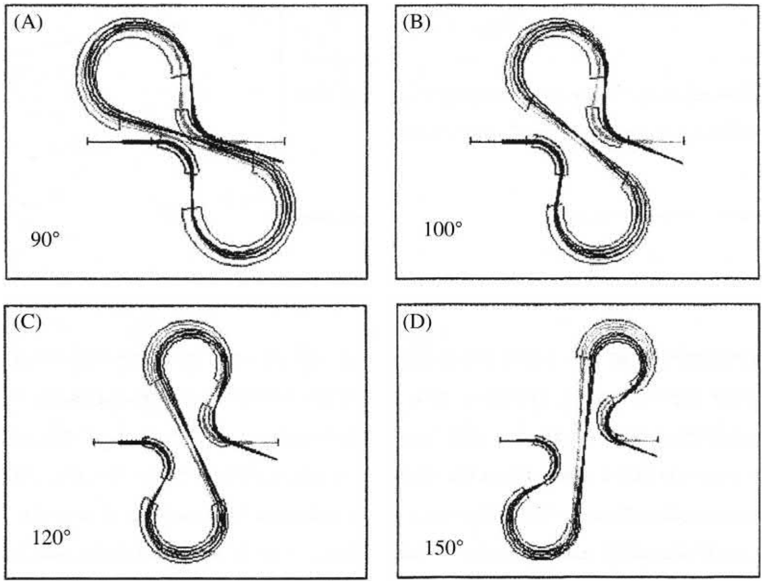

Figure 52.17
Several S-filter configurations for different bending angles. (A) Dispersion at slit plane (D_s) = 4.17 μm/eV, dispersion at the midplane (D_m) = 0.901 μm/eV. (B) D_s = 4.509 μm/eV, D_m = 0.838 μm/eV. (C) D_s = 4.271 μm/eV, D_m = 1.301 μm/eV. (D) D_s = 4.693 μm/eV, D_m = 1.968 μm/eV. *After Tsuno (2001), Courtesy Society of Photo-optical Instrumentation Engineers.*

A magnetic version for use at higher voltages was proposed by Ichinokawa (1965, 1968; Ichinokawa and Kamiya, 1966) and a cylindrical magnetic analyser of this type was installed in the Cambridge 750 kV electron microscope (Considine and Smith, 1968; Considine, 1969). Two pairs of polepieces are staggered relative to one another (Fig. 52.19) and the ray paths resemble those in the electrostatic version, modified of course by the rotation.

52.9.5 Postcolumn Spectrometers

These consist of a magnetic prism, together with multipoles to improve the imaging quality. Here, we mention some of the stages through which these devices have passed and indicate the improvements that have been made to their optics. A very complete account is available in Egerton (2011) and a useful survey is to be found in Krivanek et al. (2013). Darlington (1980) recapitulates the optics of these prisms lucidly.

The first attempt to correct the second-order aberrations of the basic prism (Brown, 1965, 1968; Enge, 1967; Livingood, 1969; Liebl, 2008) was made by Crewe et al. (1971), who needed an improved spectrometer for the first STEM. Several related papers followed (Crewe, 1977; Parker et al., 1978; Shuman, 1980; Tang, 1982a–c; Isaacson and Scheinfein; 1983). The performance of Krivanek's uncorrected spectrometer (1979) was greatly

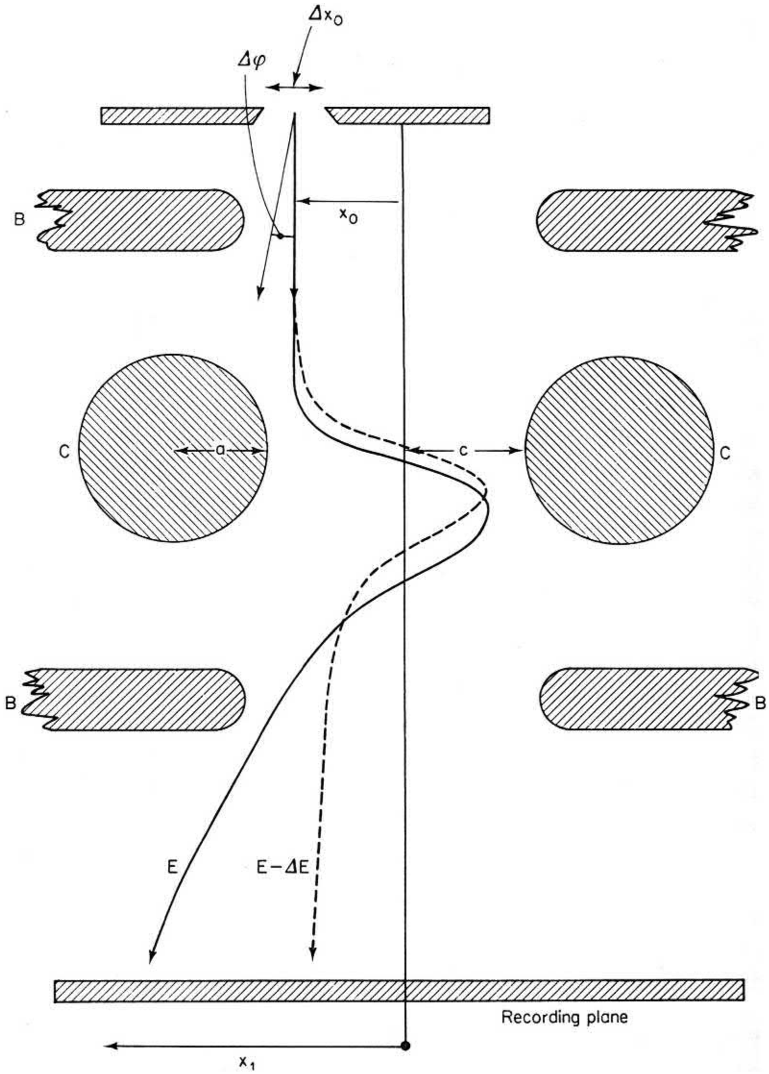

Figure 52.18
The Möllenstedt analyser *After Metherell (1971), Courtesy Elsevier.*

improved by the addition of correcting elements (Krivanek and Swann, 1981). These efforts culminated in the highly perfected GIF [Gatan Imaging Filter] 'Quantum' of Gubbens et al. (2010), illustrated in Fig. 52.20. See also Pearce-Percy et al. (1976) and Krahl et al. (1978).

52.9.6 Monochromators

Monochromators installed immediately after the electron gun may resemble Ω-filters or exploit the properties of Wien filters (Tsuno, 2011; Kimoto, 2014). In the first case, they are usually electrostatic. A first Ω-type design was described by Plies (1978; Huber et al.,

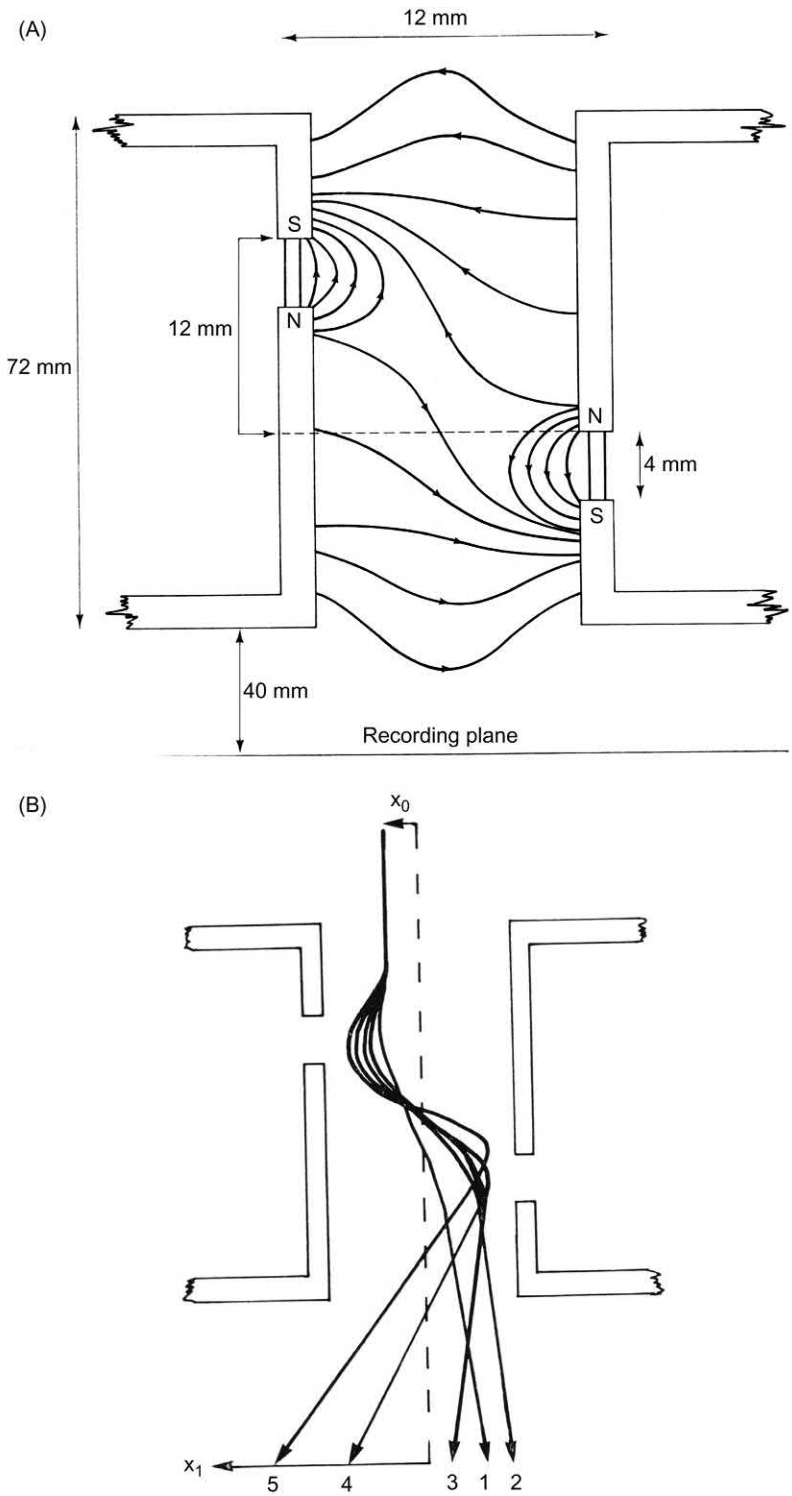

Figure 52.19
The Ichinokawa analyser. (A) Field lines in a practical model. (B) Rays traversing the analyser for increasing values of the analyser current. *After Metherell (1971), Courtesy Elsevier.*

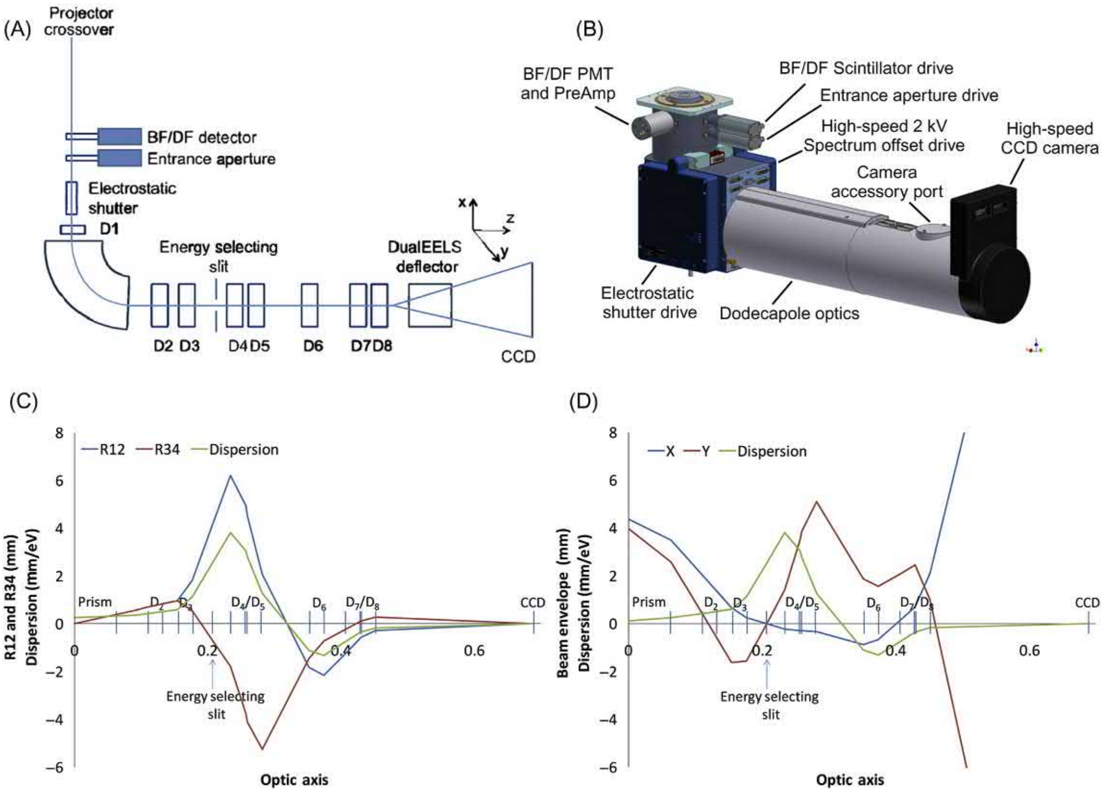

Figure 52.20
The Gatan Imaging Filter [GIF] Quantum. (A) The different elements of the device (D denotes dodecapole). (B) General appearance of the filter. (C) Axial rays starting from the image plane of the microscope. (D) The beam envelope and energy dispersion. Distances along the optic axis are in metres. *After Gubbens et al. (2010), Courtesy Elsevier.*

2004; Bärtle and Plies, 2008) and later by Rose (1999) and studied in detail by Kahl (1999; Kahl and Rose, 1998a,b, 2000). Fig. 52.21 shows the disposition of the electrodes. Many technical details of the model adopted by Zeiss for the SESAM instrument (a Zeiss Libra 200 MC) are given by Essers et al. (2010). The SALVE monochromator is discussed by Mohn et al. (2017).

For the Nion UltraSTEM, a highly perfected α-type design was adopted (Krivanek et al., 2012, 2013; Hawkes and Krivanek, 2018). Fig. 52.22A shows the site of the device in the Nion microscope and Fig. 52.22B indicates the numerous elements of which it is composed: three magnetic prisms (one of which is traversed twice), 16 multipoles and the slit in the midplane. The multipoles are capable of generating quadrupole, sextupole and octopole fields and weak dipole fields when required. The central prism turns the beam through 75° in each passage; it creates a uniform magnetic field and hence has a focusing effect only in

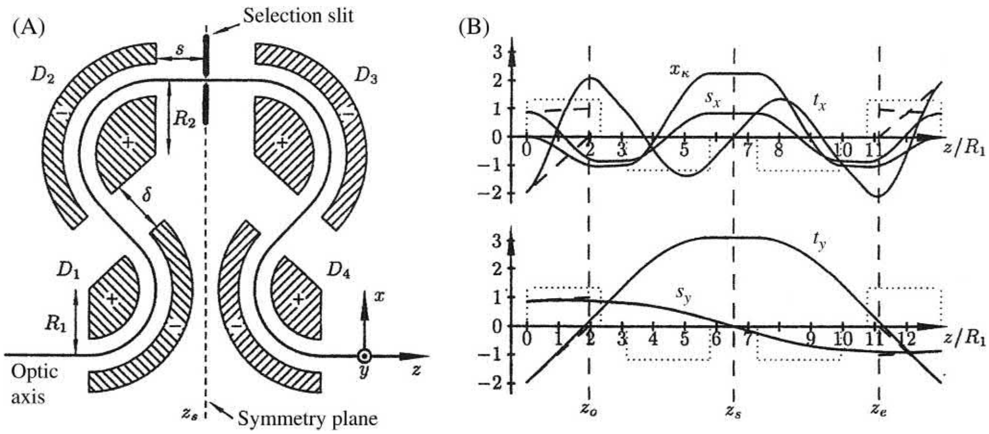

Figure 52.21

An Ω-shaped monochromator (A), section through the device. (B) Fundamental rays relative to the straightened optic axis. *After Kahl and Rose (1998), Courtesy Springer Verlag.*

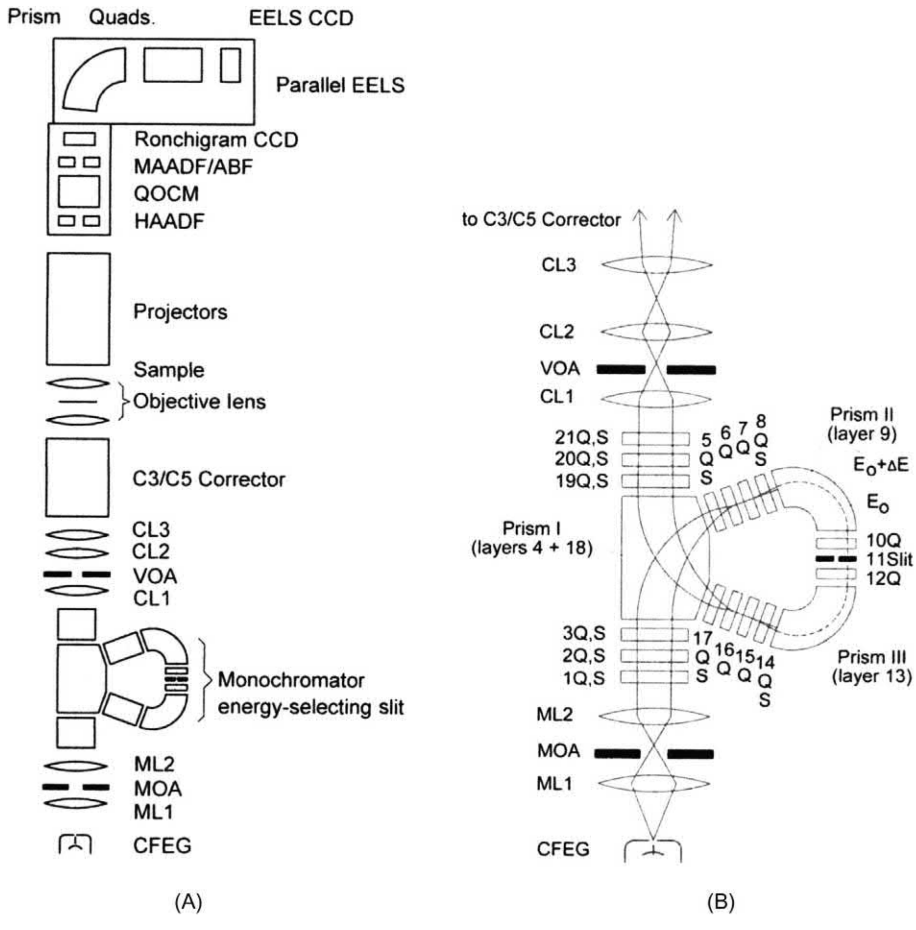

Figure 52.22

The Nion monochromator. (A) The column of the Nion UltraSTEM showing the position of the monochromator. (B) Cross-section of the monochromator. *After Krivanek et al. (2013), Courtesy Oxford University Press.*

the dispersion plane. The other two prisms turn the beam though 105° and focus it in both directions. The optics is described in full detail in Krivanek (2013) and discussed by Dellby et al. (2014). For information about the sophisticated energy-loss spectrometer developed by Nion, see Lovejoy et al. (2017).

The second group of monochromators employs Wien filters. The dispersion of these filters is rather low but can be augmented by reducing the energy of the beam before it enters the filter and increasing it again when it emerges. A Wien filter enclosed between a retarding lens and an accelerating lens was first tested by Legler (1963) and by Boersch et al. (1964) who used two such filters, one as a monochromator, the other as an energy analyser. Essig et al. (1986) describe an improved model (see also Essig, 1981). The optics of Wien filter monochromators was reconsidered in depth by Rose (1987b), who concluded that the necessary conditions could best be satisfied by means of a mixed, electrostatic–magnetic octopole (Fig. 52.23). The inner surfaces of the combined electrode–polepieces are circular arcs and all subtend the same angle at the axis. Rose explains how the excitations should be chosen to produce the desired optical properties. Like all Wien filters, the fringing fields are a source of errors but Rose argues that these can be kept acceptably small. A dodecapole Wien filter is described in detail by Marx et al. (1997), for use in a high-resolution X-PEEM.

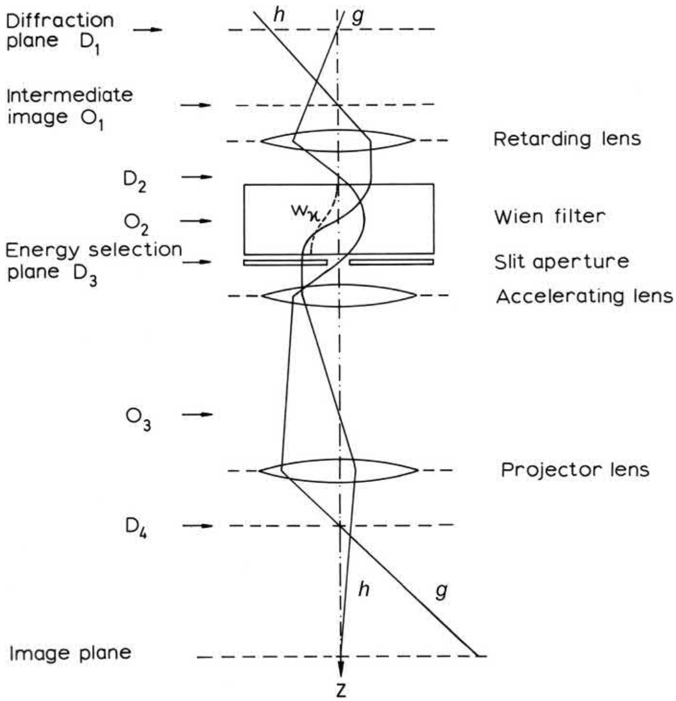

Figure 52.23
A retarding Wien filter incorporated into a TEM column w_k is the dispersion ray. *After Rose (1987), Courtesy Wissenschaftliche Verlagsgesellschaft.*

Several other Wien filter monochromators have been developed. Tiemeijer (1999) discussed the possible operating modes of a Wien filter placed just after a field-emission gun. In later papers, Tiemeijer et al. (2012a,b) analyse very carefully the relation between the action of such a monochromator and the resolution of the host microscope as this monochromator was to be installed in the TEAM 0.5 electron microscope; the results obtained are presented in the second paper (Fig. 52.24). Later improvements to the monochromator employed in FEI Themis electron microscopes are mentioned by Freitag and Tiemeijer (2017).

Mook and Kruit have described a *fringe-field monochromator*, so called because the filter is so short (4 mm) that its effect is largely due to its fringing fields (Mook, 2000; Mook and Kruit, 1997, 1988, 1999a–c, 2000a,b). It is placed just after the gun (a Schottky emitter in their first model, a cold field-emission gun in an improved version; Mook et al., 1999a,b; Mook and Batson, 1999). The fields are created by means of eight (later reduced to six) stainless steel electrodes inside two Ni–Fe poles (Fig. 52.25).

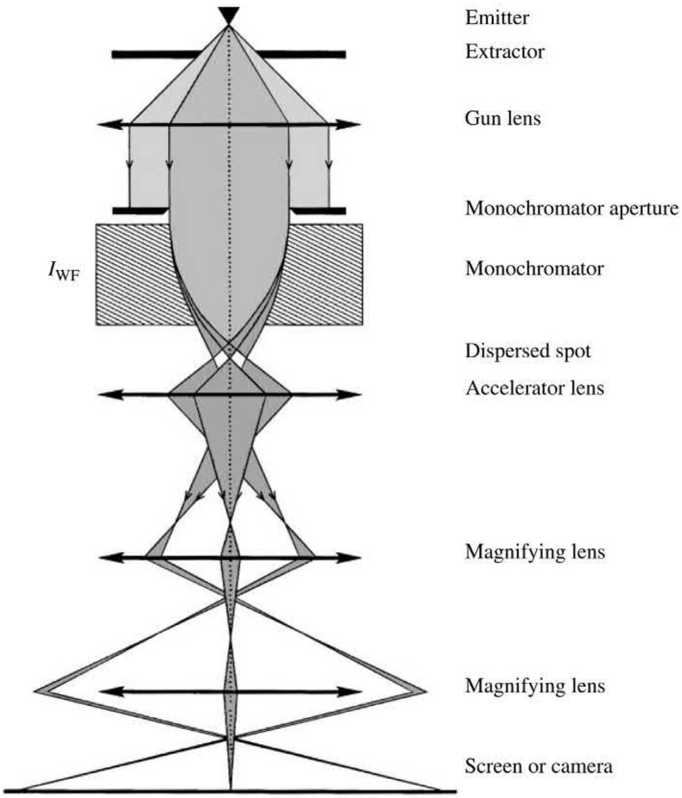

Figure 52.24
Optics of a Wien monochromator. *After Tiemeijer (1999), Courtesy Elsevier.*

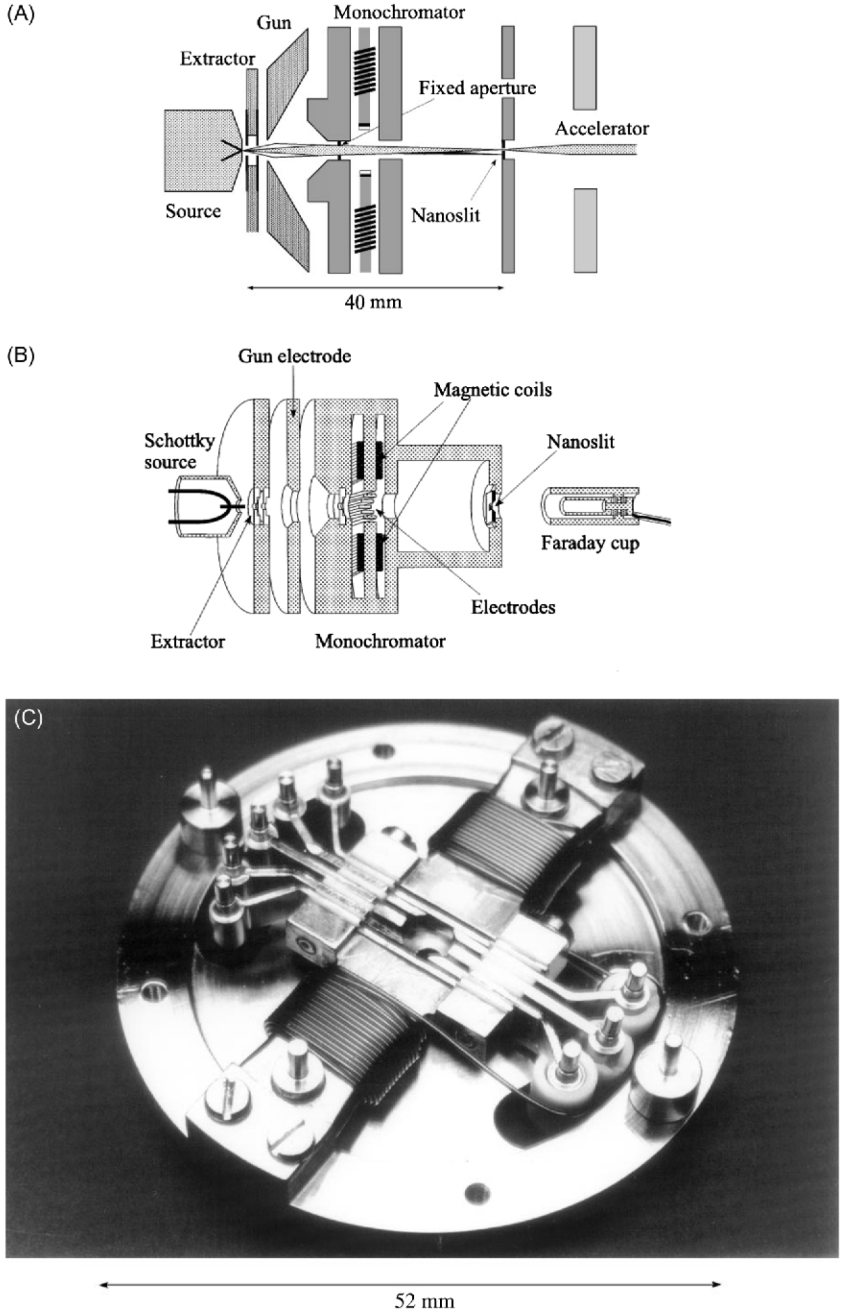

Figure 52.25

The fringing-field monochromator. (A) The optics of the monochromator with a field-emission gun. (B) Details of the environment of the monochromator. (C) View of the device. The coils provide a dipole field and the electrodes create an electric field perpendicular to the magnetic field. *After Mook and Kruit (2000), Courtesy of Elsevier.*

By placing two Wien filters symmetrically about the selection slit, the overall dispersion can be cancelled. This arrangement is employed by Mukai et al. (2014a,b) in a double aberration-corrected JEOL microscope which includes an Ω-type analyser.

Ogawa et al. (2015a,b, 2016) describe a monochromator in which offset slits are used to produce the filtering effect.

An original design is described by Mankos et al. (2016) in which an electron mirror is combined with a magnetic prism sequence and a knife-edge (Fig. 52.26). Some of the electrons with energy less than the nominal energy are intercepted when they arrive at the knife-edge while a part of those with energy greater than the nominal value are intercepted on their return journey after reflection at the mirror. Fig. 52.27 shows the mirror and typical

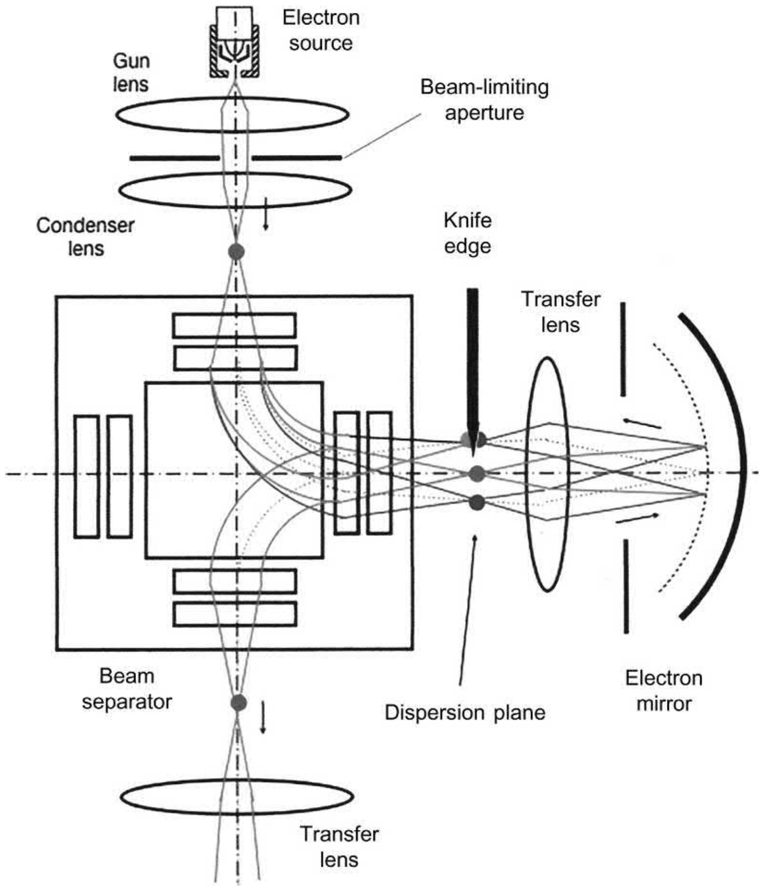

Figure 52.26
Monochromator based on an electron mirror and a knife-edge. *After Mankos et al. (2016), Courtesy the authors and the American Vacuum Society.*

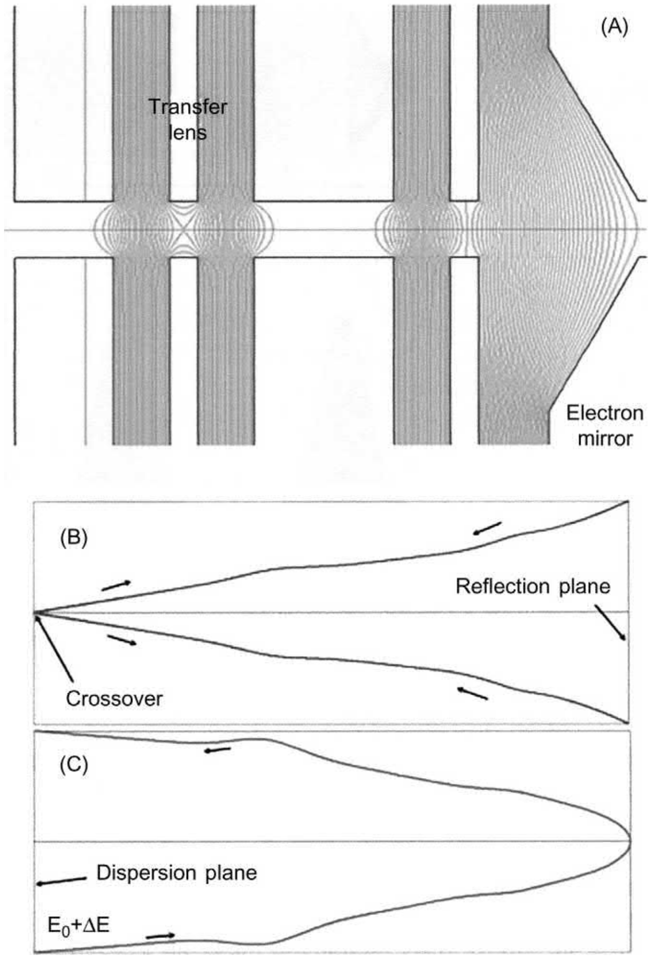

Figure 52.27
(A) Equipotentials in the mirror region of Fig. 51.26. (B). Reflection of axial rays, which retrace their path. (C) Reflection of a field ray with energy greater than the nominal value. *After Mankos et al. (2016), Courtesy the authors and the American Vacuum Society.*

axial and field rays. First tests showed that the energy spread of the beam from a Schottky emitter could be reduced from about 0.7 eV to 0.18 eV for an exit beam current better than 1 nA and to 0.1 eV for a current of 50 pA.

CHAPTER 53

Unified Theories of Ion Optical Systems

53.1 Introduction

The properties of the numerous types of optical element employed in ion optics have been studied in considerable detail over the years; expressions for the focusing properties and aberrations, including the effects of fringing fields, are available for electrostatic and magnetic sector fields, quadrupoles, sextupoles and higher order multipoles. Since these elements are frequently used in combination, computer programs have been developed for performing the necessary matrix multiplications and the subsequent search for optimum configurations. Such programs are complicated by the fact that although each of the individual members may be well understood, an effort of interpretation is still needed on the part of the user owing to the different formalism associated with the different elements. In an attempt to overcome this difficulty, unified theories, in which the various optical elements are regarded as special cases of an all-purpose element represented by very general transfer matrices, have been developed.

We present one such theory (Nakabushi et al., 1983b, 1983/84) in Section 53.3. First, however, we say a few words about electrostatic prisms to avoid including distracting explanations in Section 53.3.

53.2 Electrostatic Prisms

The literature of electrostatic prisms is nearly as voluminous as that devoted to magnetic sector fields but we discuss the former only briefly here, for various reasons. First, the general methods of study and the optical properties are not very different from those encountered in Chapter 52, Sector Fields and Their Applications; it therefore seems more sensible to regard electrostatic prisms as just one of the special cases included in the unified theory presented in Section 53.3. Furthermore, electrostatic prisms are not so commonly used as their magnetic counterparts for energy analysis, owing to the high voltages required except with low particle energies; they are, on the other hand, routinely used in mass spectrometer design.

Electrostatic prisms are capacitors with curved plates; a typical example is illustrated in Fig. 53.1. The plates may be cylindrical, spherical or toroidal and the optical properties are of course different in each case. Within the field region, the optic axis coincides with an

Principles of Electron Optics: Applied Geometrical Optics.
DOI: http://dx.doi.org/10.1016/B978-0-12-813369-9.00053-1

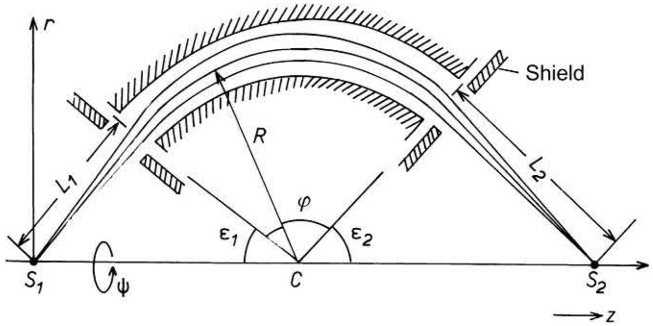

Figure 53.1
Axial section through an electron deflection prism with a focused pencil. If the capacitor is spherical, the arrangement is rotationally symmetric about the z-axis.

effectively circular trajectory along which the potential has a constant value ϕ. The three-dimensional potential is described by an expansion of the form

$$\Phi = \phi + F_0\left\{x + \frac{y^2}{2\rho} - \frac{x^2}{2}\left(\frac{1}{\rho} + \frac{1}{R}\right) + \frac{1}{6}x^3\left(\frac{1+\rho'}{\rho^2} + \frac{2}{R^2} + \frac{2}{R\rho}\right)\cdots\right\} \tag{53.1}$$

in which R denotes the radius of curvature of the optic axis and ρ that of the curve in which the equipotential surface $\Phi = \phi$ intersects a plane $z = \text{const}$ (perpendicular to the optic axis); $\rho' = (d\rho/dx)_{x=0}$. On comparing Eq. (53.1) with (51.38), we see that

$$F_1 = -\left(R^{-1} + \rho^{-1}\right)F_0$$

If a particle has the nominal energy W_0, the condition $a_1 = 0$ in Eq. (51.46) yields the following expressions for a_2 and b_2:

$$a_2 = \frac{g_0}{R}\left(\frac{2}{R} - \frac{1}{\rho}\right), \quad b_2 = -\frac{g_0}{R\rho}$$

The paraxial ray equations then take the form

$$x'' + \left(\frac{2}{R^2} - \frac{1}{\rho R}\right)x = 0, \quad y'' + \frac{1}{\rho R}y = 0 \tag{53.2}$$

These are not valid in the fringing field domain where a SCOFF approximation can be made. There are two interesting special cases of Eq. (53.2), the cylindrical capacitor and the spherical capacitor.

The cylindrical capacitor is characterized by $\rho \to \infty$. Eqs (53.2) then simplify to

$$x'' + 2R^{-2}x = 0, \quad y'' = 0 \tag{53.3}$$

There is hence no axial focusing, while in the radial direction, focusing occurs at an angle $\Delta\varphi = \Delta z/R = \pi/\sqrt{2} = 127.3°$. The strong astigmatism, which must be corrected outside the prism, is a disadvantage of this device.

The spherical capacitor is characterized by $\rho = R$ and $\rho' = 1$. Setting $\kappa := 1/R$, we have

$$x'' + \kappa^2 x = 0, \quad y'' + \kappa^2 y = 0 \tag{53.4}$$

It is obvious that there is stigmatic focusing for any deflection angle φ. The focusing properties are illustrated in Fig. 53.1. The point source S_1, the centre C of the spherical capacitor plates and the image point S_2 form a straight axis which can be considered as though it were the axis of rotational symmetry of a round lens. In fact, the spherical prism can be considered as an azimuthal sector of a round lens.

Such devices do of course have aberrations, like any other spectrometer. The main geometric aberration is the spherical aberration of the corresponding round lens while the dispersion is essentially the axial chromatic aberration of this lens. An elementary calculation gives

$$\Delta r = \left\{R(1 - \cos\varphi) + L_2 \sin\varphi\right\} \frac{\Delta U}{U \sin\varepsilon_2} \tag{53.5}$$

(see Fig. 53.1), in which U is the voltage equivalent of the kinetic energy of the particle and ΔU the deviation from its nominal value.

The analysis of electrostatic prisms passes through exactly the same stages as that of magnetic prisms. First, the linear focusing properties of the pure sector field are established by solution of linear ray equations, the boundary conditions being those appropriate to the SCOFF approximation already described in the magnetic case. It is again convenient to introduce dimensionless coordinates u, v, ζ as in Eq. (52.45), R being as usual the radius of curvature of the optic axis. Including the dispersion term, Eq. (53.2) then take the form

$$u'' + (2 - c)u = \delta \qquad v'' + cv = 0 \tag{53.6}$$

where primes now denote derivatives with respect to ζ and

$$c := R/\rho \tag{53.7}$$

Integration of Eq. (53.6) between the ideal field boundaries $\zeta = \zeta_{1,2}$ yields expressions that can be cast into the form of transfer relations:

$$\begin{aligned}
\begin{pmatrix} u_2 \\ u_2' \end{pmatrix} &= \begin{pmatrix} \cos\varphi_x & \varepsilon_x^{-1}\sin\varphi_x \\ -\varepsilon_x \sin\varphi_x & \cos\varphi_x \end{pmatrix} \begin{pmatrix} u_1 \\ u_1' \end{pmatrix} + \delta \begin{pmatrix} \varepsilon_x^{-2}(1 - \cos\varphi_x) \\ \varepsilon_x^{-1}\sin\varphi_x \end{pmatrix} \\
\begin{pmatrix} v_2 \\ v_2' \end{pmatrix} &= \begin{pmatrix} \cos\varphi_y & \varepsilon_y^{-1}\sin\varphi_y \\ -\varepsilon_y \sin\varphi_y & \cos\varphi_y \end{pmatrix} \begin{pmatrix} v_1 \\ v_1' \end{pmatrix}
\end{aligned} \tag{53.8a}$$

with the abbreviations

$$\varepsilon_x = \sqrt{2-c}, \quad \varepsilon_y = c^{1/2}, \quad \varphi_x = \varepsilon_x \varphi, \quad \varphi_y = \varepsilon_y \varphi \tag{53.8b}$$

These are analogous to the corresponding relations for magnetic prisms.

In the next stage, fringing field effects are examined. Unlike the case of their magnetic counterparts, electrostatic prisms are usually designed in such a way that the angles α and β of incidence and emergence (see Fig. 52.4) are zero since obliquity causes large aberrations. The fringing fields therefore leave the paraxial transfer matrices unaltered but affect higher order terms (see Wollnik (1967a) for an extremely detailed analysis of these effects). It is therefore only necessary to multiply the matrices (53.8a) by those representing the object and image drift spaces; the resulting matrix products are not given here − their formulation is straightforward.

The final stage is the determination of the possible aberrations. This is a very lengthy task, since the number of permitted aberrations is large and the formulae for the individual coefficients are voluminous. Space does not permit us to give these in full and we therefore refer the reader to the comprehensive investigations of Wollnik, Matsuda and others, full references to which are to be found in the Notes and References for Part X.

It is customary to incorporate all the aberrations into the transfer matrices, which hence become huge. The advantage of doing this is that complex systems consisting of a sequence of simpler subsystems can be treated by matrix multiplication. Owing to the fact that there are so many aberrations and that the fringing field effects can be incorporated only very crudely, this procedure is not always satisfactory. An alternative approach, which may be simpler and should certainly be more accurate, is the numerical determination of aberrations from computed exact Lorentz trajectories, as outlined in Chapter 34 in Volume 1. The methods presented in Sections 34.5 and 34.8 are especially well suited to situations in which the optic axis is curved. The axis is then the only trajectory that must be calculated by solving the Lorentz equation in its full form. Other trajectories can be determined from the incremental form, which gives higher accuracy. There is then in principle no need for a transfer-matrix formalism: in the progressive study of complex systems, the initial coordinates and velocities of the particles at the entrance to each particular subsystem are simply the final values found by tracing through the preceding parts. In view of the considerable progress in techniques for computing fields and trajectories, this method is now in widespread use. Even when the matrix formalism is preferred for the insight it gives into the relative importance of the contributions of individual subsystems and into the effect of modifying or replacing the latter, more accurate values of the matrix elements can be obtained by these exact ray-tracing techniques than by a SCOFF approximation modified by appropriate fringing field matrices.

53.3 A Unified Version of the Theory

The range of optical elements employed in spectrometers and beam-transport systems is wide: electrostatic and magnetic prisms with a range of field configurations, electrostatic and magnetic quadrupoles, sextupoles and higher order multipoles. Electrostatic and magnetic dipole fields may be superposed to form a 'crossed-field' analyser, a special case of which is the Wien filter (Chapter 38). Each of these elements has a voluminous literature devoted to the needs of ion optics in particular, which differs from the electron optical analysis in that it is usually adequate to study transfer by a very simple 'ideal' field, terminated by fringing fields. The latter are invariably regarded as thin lenses and expressions of general applicability can hence be derived to represent their effect.

It would clearly be very attractive, for the purposes of computer-aided design in particular, to unify all these separate efforts, that is, to derive a single set of transfer matrices capable of representing all these various components. A unified theory of this kind has been developed by Nakabushi et al. (1983b, 1983/84); it is not quite as general as we might desire, since only the first-order approximation is considered in the axial direction and the second-order approximation in the radial direction, but this is nevertheless sufficient to explore many situations of practical interest. We therefore reproduce the main formulae here. In the Notes and References for this Part, we list the principal publications in which more detailed investigations of individual components are to be found.

We set out from the field and potential expansions of Chapter 51, General Curvilinear Systems, into which we introduce a convenient scaling. For magnetic fields, we write Eq. (51.41)

$$\begin{aligned}
B_x &= y(G_1 + xG_2) =: B_0 y(g_1 + xg_2)\\
B_y &= G_0 + xG_1 + \frac{1}{2}x^2 G_2 - \frac{1}{2}y^2\left(G_0'' + \kappa G_1 + G_2\right)\\
&=: B_0\left\{g_0 + xg_1 + \frac{1}{2}x^2 g_2 - \frac{1}{2}y^2\left(g_0'' + \kappa g_1 + g_2\right)\right\}\\
B_z &= y\left(G_0' + xG_1' - \kappa x G_0'\right)\\
&= B_0 y\left(g_0' + xg_1' - \kappa x g_0'\right)\\
A_x &= -\frac{1}{2}B_0 y^2\left\{g_0' + x\left(g_1' - \kappa g_0'\right)\right\}\\
A_y &= 0\\
hA_z &= B_0\left\{-xg_0 - \frac{1}{2}x^2(g_1 + \kappa g_0) - \frac{1}{6}x^3(g_2 + \kappa g_1) + \frac{1}{2}y^2 g_1 + \frac{1}{2}xy^2(g_2 + \kappa g_1)\right\}
\end{aligned} \tag{53.9a}$$

(and as usual $h = 1 + \kappa x$). The electrostatic potential is given by

$$\begin{aligned}
\Phi &= \phi + xF_0 + \frac{1}{2}x^2F_1 + \frac{1}{6}x^3F_2 \\
&\quad - \frac{1}{2}y^2(F_1 + \kappa F_0 + \phi'') \\
&\quad - \frac{1}{2}xy^2\left(F_2 + \kappa F_1 - \kappa^2F_0 - 2\kappa\phi'' - \kappa'\phi' + F_0''\right) \\
&=: \phi + E_0\Big\{xf_0 + \frac{1}{2}x^2f_1 + \frac{1}{6}x^3f_2 \\
&\qquad - \frac{1}{2}y^2\left(f_1 + \kappa f_0 + \phi''/E_0\right) \\
&\qquad - \frac{1}{2}xy^2\left(f_2 + \kappa f_1 - \kappa^2 f_0 + f_0'' - 2\kappa\phi''/E_0 - \kappa'\phi'/E_0\right)
\end{aligned} \tag{53.9b}$$

Since the theory is designed to be applicable to beams of particles with different energies, masses and charges, we set the origin of potential at the optic axis within the element in question. Thus ϕ is constant and equal to zero in Eq. (53.9b). All particle properties are measured relative to those of a nominal particle having kinetic energy Q_0U_0, charge Q_0 and rest-mass $m_0^{(0)}$. We must now add a suffix to ε and γ:

$$\varepsilon_0 := Q_0/2m_0^{(0)}c^2 \quad \gamma_0 = 1 + 2\varepsilon_0U_0 = 1 + Q_0U_0/m_0^{(0)}c^2 \tag{53.10a}$$

and we introduce fractional mass and energy deviations as follows:

$$\begin{aligned}
\frac{m_0}{Q} &=: \frac{m_0^{(0)}}{Q_0}(1 + p) \\
U &=: U_0(1 + q)
\end{aligned} \tag{53.10b}$$

All these definitions and expressions are now used to expand the refractive index $\overline{M}$ (51.23), scaled so that $M^{(0)} = 1$. We find

$$\begin{aligned}
M^{(1)} &= (\kappa - g_0H_m + f_0H_e)x \\
M^{(2)} &= -\frac{1}{2}\left\{(g_1 + \kappa g_0)H_m - (f_1 + 2\kappa f_0)H_e + \kappa^2H_e^2/\gamma^2\right\}x^2 \\
&\quad + \frac{1}{2}\left\{g_1H_m - (f_1 + \kappa f_0)H_e\right\}y^2 \\
&\quad + \frac{1}{2}\left(x'^2 + y'^2\right)
\end{aligned}$$

$$M^{(3)} = -\frac{1}{3}\left\{\left(\frac{1}{2}g_2 + \kappa g_1\right)H_m - \frac{1}{2}(f_2 + 3\kappa f_1)H_e + \frac{3}{2\gamma^2}(f_1 + \kappa f_0)\, f_0 H_e^2 - \frac{3}{2\gamma^2}\, f_0^3 H_e^3\right\}x^3$$
$$+ \frac{1}{2}\left\{(g_2 + \kappa_0 g_1)H_m - (f_2 + 2\kappa f_1)H_e + (f_1 + \kappa f_0)\, f_0 H_e^2/\gamma^2\right\}xy^2$$
$$+ \frac{1}{2}(f_0 H_e - \kappa)x\left(x'^2 + y'^2\right) \tag{53.11}$$

in which

$$H_m = \eta B_0/\hat{U}^{1/2}$$
$$H_e = -\frac{\gamma E_0}{2\hat{U}} \tag{53.12}$$

and as usual $\hat{U} = U(1 + \varepsilon U)$. For the nominal particle, we write

$$h_m := H_m\left(U = U_0, Q = Q_0, m_0 = m_0^{(0)}\right) = \eta_0 B_0/\hat{U}_0^{1/2}$$
$$h_e := H_e\left(U = U_0, Q = Q_0, m_0 = m_0^{(0)}\right) = -\gamma_0 E_0/2\hat{U}_0 \tag{53.13}$$

and find that $H_m = h_m(1 + \ldots)$, $H_e = h_e(1 + \ldots)$, the series containing terms in γ_0, p and q; these series are given explicitly by Nakabushi *et al*.

This formalism is general enough to include all the devices mentioned earlier: Table 53.1 shows how the parameters should be set to obtain a particular structure.

We are now in a position to write down and solve the paraxial and second-order equations. The latter will be considered only in the radial direction, however. The condition that the optic axis must be a trajectory gives

$$\kappa = g_0 h_m - f_0 h_e \tag{53.14}$$

The equations of motion take the form

$$x'' + k_x x = x^{(2)}$$
$$y'' + k_y y = 0 \tag{53.15}$$

(neglecting aberrations in the axial direction), where

$$k_x = h_1 + \kappa(\kappa - f_0 h_e) + h_e^2 f_0^2/\gamma_0^2$$
$$k_y = -h_1 + \kappa h_e f_0 \tag{53.16}$$

Table 53.1: The values of the parameters κ, h_e, . . . g_2 for a wide range of devices (Fig. 53.2)

	κ	h_e	f_0	f_1	f_2	h_m	g_0	g_1	g_2
Electrostatic sector									
Cylindrical	κ	κ	-1	κ	$-2\kappa^2$	0	0	0	0
Spherical	κ	κ	-1	2κ	$-6\kappa^2$	0	0	0	0
Toroidal	κ	κ	-1	(53.1)		0	0	0	0
Magnetic sector									
Homogeneous	κ	0	0	0	0	κ	1	0	0
Conical	κ	0	0	0	0	κ	1	(52.5)	
Toroidal	κ	0	0	0	0	κ	1	(52.7)	
Electric									
Quadrupole	0	$\times$	0	$\times$	0	0	0	0	0
sextupole	0	$\times$	0	0	$\times$	0	0	0	0
Multipole	0	$\times$	0	$\times$	$\times$	0	0	0	0
Magnetic									
Quadrupole	0	0	0	0	0	$\times$	0	$\times$	0
sextupole	0	0	0	0	0	$\times$	0	0	$\times$
Multipole	0	0	0	0	0	$\times$	0	$\times$	$\times$
Achromatic quadrupole	0	$\times$	0	$\times$	0	$\times$	0	$\times$	0
Wien filter									
Homogeneous	0	$-h_m$	-1	0	0	$-h_e$	1	0	0
Inhomogeneous	0	$-h_m$	-1	$1/r_e$	$-2/r_e^2$	$-h_e$	1	$-1/r_m$	$2/r_m^2$
Crossed-field analyser									
	κ	κ	-1	(53.1)		κ	1	(52.7)	

In some cases, the values are to be found in the equations indicated and for multipoles, we simply show which coefficients are nonzero ($\times$); the explicit expressions may be extracted from the potential expansions or trajectory equations. For the inhomogeneous Wien filter, we introduce separate electrostatic and magnetic radii, r_e and r_m, analogous to the radius R appearing in Eq. (53.1), see Fig. 53.2. For the crossed-field analyser we have $h_e + h_m = \kappa$.

with

$$h_1 = h_m g_i - h_e f_1 \tag{53.17}$$

The inhomogeneous term in the equation for $x(z)$ has the form

$$\begin{aligned} x^{(2)} = {} & C_p p + C_q q + D_{xx} x^2 + D_{xp} xp + D_{xq} xq \\ & + D_{x'x'} x'^2 + D_{pp} p^2 + D_{pq} pq + D_{qq} q^2 + D_{yy} y^2 + D_{y'y'} y'^2 \end{aligned} \tag{53.18}$$

in which

$$C_p = \frac{\gamma_0 \kappa + f_0 h_e}{\gamma_0 (1 + \gamma_0)}, \quad C_q = \frac{\gamma_0^2 \kappa - f_0 h_e}{\gamma_0 (1 + \gamma_0)}$$

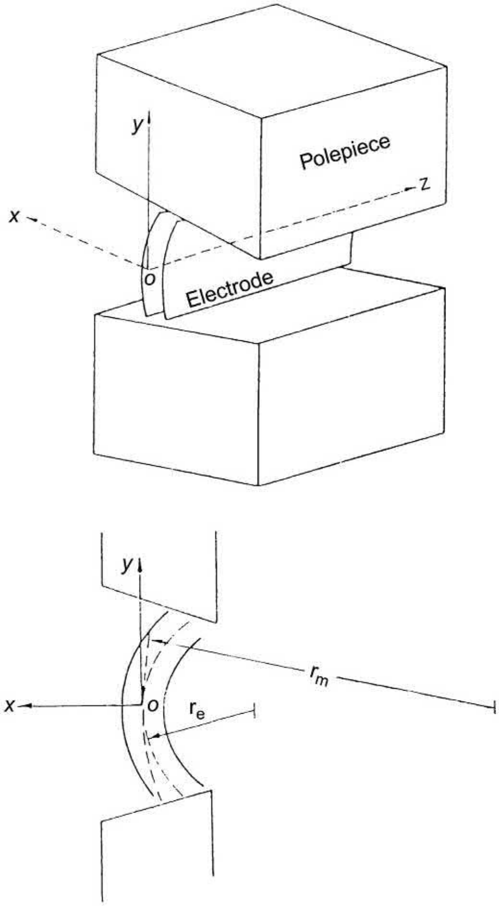

Figure 53.2
Wien filter with inhomogeneous fields; the lower diagram shows the notation.

$$D_{xx} = -h_2 - \frac{1}{2}\kappa(2h_1 - f_1 h_e) - \frac{3h_e^2 f_0}{2\gamma_0^2}\left(f_1 + \kappa f_0 - h_e f_0^2\right) - (\kappa - f_0 h_e)k_x$$

$$D_{xp} = 3\kappa C_p + \frac{1}{1+\gamma_0}\left\{h_1 + \frac{h_e f_1}{\gamma_0} + \left(1 - \frac{3}{\gamma_0} + \frac{2}{\gamma_0^2}\right)h_e^2 f_0^2 - h_m^2 g_0^2\right\}$$

$$D_{xq} = 3\kappa C_q + \frac{\gamma_0}{1+\gamma_0}\left\{h_1 - \frac{h_e f_1}{\gamma_0^2} + \left(1 + \frac{5}{\gamma_0^2}\right)h_e^2 f_0^2 - h_m^2 g_0^2\right\}$$

$$D_{x'x'} = \frac{1}{2}(\kappa - h_e f_0) = -D_{y'y'}$$

$$\begin{aligned}
D_{pp} &= \frac{1}{2\gamma_0(1+\gamma_0)^2}\{4(\gamma_0-1)h_e f_0 - 3\gamma_0 h_m g_0\}\\
D_{pq} &= \frac{1}{\gamma_0(1+\gamma_0)^2}\left\{2(\gamma_0-1)^2 h_e f_0 - \gamma_0(2\gamma_0-1)h_m g_0\right\}\\
D_{qq} &= \frac{1}{2(1+\gamma_0)^2}\{2(\gamma_0^2+3)h_e f_0 - (2\gamma_0^2+1)h_m g_0\}\\
D_{yy} &= h_2 + \frac{1}{2}\kappa(h_1 - h_e f_1) + \frac{h_e^2 f_0}{2\gamma_0^2}(f_1+\kappa f_0)
\end{aligned} \tag{53.19}$$

We have already defined the quadrupole term h_1 (53.16); the undefined term h_2 characterizes any sextupole contribution,

$$h_2 := \frac{1}{2}(h_m g_2 - h_e f_2) \tag{53.20}$$

The solutions of (53.14) consist of paraxial terms $x^{(p)}$, $y^{(p)}$, and in the radial direction, aberrations; as usual, we write the coefficients in the form $(x \mid \cdot)$, the second term characterizing the aberration in question (e.g. $(x \mid x^2)x_o^2$). We find

$$\begin{aligned}
x^{(p)} &= Cx_o + Sx'_o + \frac{1-C}{k_x}(C_p p + C_q q)\\
x'^{(p)} &= -k_x S x_o + Cx'_o + S(C_p p + C_q q)\\
y^{(p)} &= C_y y_o + S_y y'_o\\
y'^{(p)} &= -k_y S_y y_o + C_y y'_o
\end{aligned} \tag{53.21}$$

The functions C, C_y, S and S_y are defined in Table 53.2.

The aberration coefficients are linear combinations of the functions

Table 53.2: Definitions of the functions appearing in Eq. (53.21)

k_x, k_y	Positive	Negative	Small
S	$\sin(\sqrt{k_x}z)/\sqrt{k_x}$	$\sinh(\sqrt{-k_x}z)/\sqrt{-k_x}$	$z(1-k_xz^2/6+k_x^2z^4/120)$
C	$\cos(\sqrt{k_x}z)$	$\cosh(\sqrt{-k_x}z)$	$1-k_xz^2/2+k_x^2z^4/24$
S_y	$\sin(\sqrt{k_y}z)/\sqrt{k_y}$	$\sinh(\sqrt{-k_y}z)/\sqrt{-k_y}$	$z\left(1-k_yz^2/6+k_y^2z^4/120\right)$
C_y	$\cos(\sqrt{k_y}z)$	$\cosh(\sqrt{-k_y}z)$	$1-k_yz^2/2+k_y^2z^4/24$

D_{ab} defined above (53.18). We find

$$\begin{pmatrix} x|x^2 \\ x|xx' \\ x|xp \\ x|xq \\ x|x'^2 \\ x|x'p \\ x|x'q \\ x|p^2 \\ x|pq \\ x|q^2 \end{pmatrix} = T_1^x \begin{pmatrix} D_{xx} \\ D_{x'x'} \\ D_{xp} \\ D_{xq} \\ D_{pp} \\ D_{pq} \\ D_{qq} \\ 1 \end{pmatrix} \tag{53.22}$$

$$\begin{pmatrix} x|y^2 \\ x|yy' \\ x|y'^2 \end{pmatrix} = T_2^x \begin{pmatrix} D_{yy} \\ D_{y'y'} \end{pmatrix}$$

where

$$T_1^x = \begin{pmatrix} x^2|x^2 & x'^2|x^2 & 0 & 0 & 0 & 0 & 0 & 0 \\ x^2|xx' & x'^2|xx' & 0 & 0 & 0 & 0 & 0 & \kappa S \\ x^2|xp & x'^2|xp & x\,|\,x & 0 & 0 & 0 & 0 & 0 \\ x^2|xq & x'^2|xq & 0 & x|x & 0 & 0 & 0 & 0 \\ x^2|x'^2 & x'^2|x'^2 & 0 & 0 & 0 & 0 & 0 & 0 \\ x^2|x'p & x'^2|x'p & x|x' & 0 & 0 & 0 & 0 & 0 \\ x^2|x'q & x'^2|x'q & 0 & x|x' & 0 & 0 & 0 & 0 \\ x^2|p^2 & x'^2|p^2 & x|p & 0 & 1|1 & 0 & 0 & 0 \\ x^2|pq & x'^2|pq & x|q & x|p & 0 & 1|1 & 0 & 0 \\ x^2|q^2 & x'^2|q^2 & 0 & x|q & 0 & 0 & 1|1 & 0 \end{pmatrix} \tag{53.23a}$$

and

$$T_2^x = \begin{pmatrix} y^2|yy' & y'^2|yy' \\ y^2|y'^2 & y'^2|y'^2 \end{pmatrix} \tag{53.23b}$$

The elements of the matrices T_1^x and T_2^x are listed in Table 53.3 in two forms, one general, the other to be used when k_x, k_y are very small. Similar formulae for the gradient aberrations are given by Nakabushi et al. (1983) but are not reproduced here.

A theory that disregards fringing fields is clearly inadequate. Nakabushi et al. remedy this in a second paper (1983/84), in which it is shown that the effects due to these fields can be

Table 53.3: Elements of the matrices defined in Eqs (53.23a) and (53.23b)

	Normal Expression	Expression for Small k_x and k_y
$1\|1$	$(1/k_x)(1-C)$	$\frac{1}{2}z^2\left(1-\frac{1}{12}k_xz^2+\frac{1}{360}k_x^2z^4\right)$
$x\|x$	$\frac{1}{2}zS$	$\frac{1}{2}z^2\left(1-\frac{1}{6}k_xz^2+\frac{1}{120}k_x^2z^4\right)$
$x\|x'$	$(1/2k_x)(S-zC)$	$\frac{1}{6}z^3\left(1-\frac{1}{10}k_xz^2+\frac{1}{280}k_x^2z^4\right)$
$x\|p$	$(C_p/k_x^2)\left(1-C-\frac{1}{2}zk_xS\right)$	$\frac{1}{24}C_pz^4\left(1-\frac{1}{15}k_xz^2+\frac{1}{560}k_x^2z^4\right)$
$x\|q$	$(C_q/k_x^2)\left(1-C-\frac{1}{2}zk_xS\right)$	$\frac{1}{24}C_qz^4\left(1-\frac{1}{15}k_xz^2+\frac{1}{560}k_x^2z^4\right)$
$x^2\|x^2$	$(1/3k_x)(1-C+k_xS^2)$	$\frac{1}{2}z^2\left(1-\frac{1}{4}k_xz^2+\frac{1}{360}k_x^2z^4\right)$
$x^2\|xx'$	$(2/3k_x)S(1-C)$	$\frac{1}{3}z^3\left(1-\frac{1}{4}k_xz^2+\frac{1}{40}k_x^2z^4\right)$
$x^2\|xp$	$(C_p/k_x^2)\left\{zk_xS-\frac{1}{3}(1-C+k_xS^2)\right\}$	$\frac{1}{12}C_pz^4\left(1-\frac{1}{15}k_xz^2+\frac{1}{560}k_x^2z^4\right)$
$x^2\|xq$	$(C_q/k_x^2)\left\{zk_xS-\frac{1}{3}(1-C+k_xS^2)\right\}$	$\frac{1}{12}C_qz^4\left(1-\frac{1}{15}k_xz^2+\frac{1}{560}k_x^2z^4\right)$
$x^2\|x'^2$	$(1/3k_x^2)\{2(1-C)-k_xS^2\}$	$\frac{1}{12}z^4\left(1-\frac{1}{6}k_xz^2+\frac{1}{80}k_x^2z^4\right)$
$x^2\|x'p$	$(C_p/3k_x^2)(S-3zC+2SC)$	$\frac{1}{20}C_pz^5\left(1-\frac{1}{7}k_xz^2+\frac{1}{112}k_x^2z^4\right)$
$x^2\|x'q$	$(C_q/3k_x^2)(S-3zC+2SC)$	$\frac{1}{20}C_qz^5\left(1-\frac{1}{7}k_xz^2+\frac{1}{112}k_x^2z^4\right)$
$x^2\|p^2$	$(C_p{}^2/3k_x^3)\{4(1-C)-3zk_xS+k_xS^2\}$	$\frac{1}{120}C_p{}^2z^6\left(1-\frac{1}{28}k_xz^2+\frac{1}{560}k_x{}^2z^4\right)$
$x^2\|pq$	$(2C_pC_q/3k_x^3)\{4(1-C)-3zk_xS+k_xS^2\}$	$\frac{1}{60}C_pC_qz^6\left(1-\frac{1}{28}k_xz^2+\frac{1}{560}k_x^2z^4\right)$
$x^2\|q^2$	$(C_q{}^2/3k_x^3)\{4(1-C)-3zk_xS+k_xS^2\}$	$\frac{1}{120}C_q^2z^6\left(1-\frac{1}{28}k_xz^2+\frac{1}{560}k_x^2z^4\right)$

$y^2\|y^2$	$\begin{cases} \{1/(k_x-4k_y)\}[\{1-(2k_y/k_x)\}(1-C)-k_yS_y^2] \\ (1/4k_x)\{2(1-C)+zk_xS\} \text{ if } k_x \;=\; 4k_y \end{cases}$	$\begin{cases} \frac{1}{2}z^2\left\{1-\frac{1}{12}(k_x+2k_y)z^2+\frac{1}{360}(k_x^2+2k_xk_y+8k_y^2)z^4\right\} \\ \{1/(k_x-4k_y)\}\left\{(k_x-2k_y)(z^2/2)\left(1-\frac{1}{12}k_xz^2 + \frac{1}{360}k_x^2z^4\right)\;-k_yS_y^2\right\} \\ \text{if } k_x\approx 0,\; k_y \not\approx 0 \end{cases}$
$y^2\|yy'$	$\begin{cases} \{2/(k_x-4k_y)\}(S_yC_y-S) \\ (1/k_x)(S-zC) \text{ if } k_x=4k_y \end{cases}$	$\begin{cases} \frac{1}{3}z^3\left\{1-\frac{1}{20}(k_x+4k_y)z^2+\frac{1}{840}(k_x^2+4k_xk_y+16k_y^2)z^4\right\} \\ \{2/(k_x-4k_y)\}\left\{S_yC_y-z(1-\frac{1}{6}k_xz^2+\frac{1}{120}k_x^2k^4)\right\} \\ \text{if } k_x\approx 0, k_y \not\approx 0 \end{cases}$
$y^2\|y'^2$	$\begin{cases} \{1/(k_x-4k_y)\}\{S_y{}^2-(2/k_x)(1-C)\} \\ (1/k_x{}^2)\{2(1-C)-zk_xS\} \text{ if } k_x=4k_y \end{cases}$	$\begin{cases} \frac{1}{12}z^4\left\{1-\frac{1}{30}(k_x+4k_y)z^2+\frac{1}{1680}(k_x^2+4k_xk_y + 16k_y{}^2)z^4\right\} \\ \{1/(k_x-4k_y)\}\left\{S_y^2-z^2\left(1-\frac{1}{12}k_xz^2+\frac{1}{360}k_x^2z^4\right)\right\} \\ \text{if } k_x\approx 0, k_y \not\approx 0 \end{cases}$
	$\begin{aligned} (x'^2\|x^2) &= k_x^2(x^2\|x'^2) \\ (x'^2\|xx') &= -\,k_x(x^2\|xx') \\ (x'^2\|xp) &= -\,2k_xC_p(x^2\|x'^2) \\ (x'^2\|xq) &= -\,2k_xC_q(x^2\|x'^2) \\ (x'^2\|x'^2) &= (x^2\|x^2) \\ (x'^2\|x'p) &= C_p(x^2\|xx') \\ (x'^2\|x'q) &= C_q(x^2\|xx') \\ (x'^2\|p^2) &= C_p^2(x^2\|x'^2) \\ (x'^2\|pq) &= 2C_pC_q(x^2\|x'^2) \\ (x'^2\|q^2) &= C_q^2(x^2\|x'^2) \\ (y'^2\|y^2) &= k_y^2(y^2\|y'^2) \\ (y'^2\|yy') &= -\,k_y(y^2\|yy') \\ (y'^2\|y'^2) &= (y^2\|y^2) \end{aligned}$	

incorporated by pre- and postmultiplying the ideal transfer matrices given above by suitable fringing field matrices. Full details of the derivation are given in the paper cited; here we simply list the resulting matrix elements. The nonzero elements of the *radial transfer matrix* are as follows:

$$
\begin{aligned}
(x|x) &= 1\\
\left(x|x^2\right) &= -\frac{1}{2}\left(h_e f_0 + h_m g_0 t^2\right)\\
\left(x|y^2\right) &= h_m g_0/2c^2\\
(x'|x) &= h_m g_0 t - h_e(f_1 + \kappa f_0)z_e - \left(1+\gamma_0^2\right)h_e^2 f_0^2(IE_1 - z_e)/\gamma_0^2\\
&\quad - h_e f_0 h_m g_0\left\{\left(t^2-1\right)(IC_1 - jz_e) + t^2 z_e\right\}\\
(x'|x') &= 1\\
(x'|p) &= -\frac{1-\gamma_0}{\gamma_0\left(1+\gamma_0\right)}h_e f_0 z_e\\
(x'|q) &= \frac{1+\gamma_0^2}{\gamma_0\left(1+\gamma_0\right)}h_e f_0 z_e\\
\left(x'|x^2\right) &= h_e f_0/2R_e + h_m\left(g_1 t + g_0/2R_m c^3\right)\\
&\quad - h_e h_m f_0 g_0 t\left(t^2-3\right)(IC_0 + j - 1)/2\\
(x'|xx') &= h_m g_0 t^2\\
(x'|xp) &= -h_m g_0 t/\left(1+\gamma_0\right)\\
(x'|xq) &= -\gamma_0 h_m g_0 t/\left(1+\gamma_0\right) = \gamma_0(x'|xp)\\
\left(x'|y^2\right) &= -h_e f_0/2R_e - h_m\left(g_1 t + g_0/2R_m c^3\right) + h_m^2 g_0^2 t\left(1+2t^2\right)/2\\
&\quad + h_e h_m f_0 g_0 t\left(1+t^2\right)(IC_0 + j - 1)/2\\
(x'|yy') &= -h_m g_0 t^2 = -(x'|xx')
\end{aligned}
\tag{53.24a}
$$

In the axial direction,

$$
\begin{aligned}
(y|y) &= 1\\
(y|xy) &= h_m g_0 t^2\\
(y'|y) &= -h_m g_0 t + h_e(f_1 + \kappa f_0)z_e - h_m^2 g_0^2\left(1+2t^2\right)IM_1\\
&\quad + h_e h_m f_0 g_0\left\{IC_1 + (1-j)z_e\right\}/c^2\\
(y'|y') &= 1\\
(y'|xy) &= -h_e f_0/R_e - h_m\left(2g_1 t + g_0/R_m c^3\right)\\
&\quad - h_e h_m f_0 g_0 t\left\{t^2 - (IC_0 + j)/c^2\right\}
\end{aligned}
$$

$$
\begin{aligned}
(y'|x'y) &= -\,h_m g_0/c^2 \\
(y'|yp) &= h_m g_0 t/\big(1+\gamma_0\big) \\
(y'|yq) &= \gamma_0 h_m h_0 t/\big(1+\gamma_0\big) = \gamma_0\big(y'|yp\big) \\
(y'|xy') &= \kappa - h_m g_0/c^2
\end{aligned}
\tag{53.24b}
$$

In these matrix elements, R_e and R_m are the radii of curvature of the endfaces in the radial plane for the electric and magnetic cases; any tilt of the normal to the magnetic endface relative to the z-axis is characterized by an angle α (or β for an exit face), as in Section 52.6 and

$$
c := \cos\alpha, \quad t := \tan\alpha \tag{53.25}
$$

The electric and magnetic endfaces may be different and we write

$$
\begin{aligned}
\frac{1}{B_0}\int^{z_b} B(z)dz &= z_b \\
\frac{1}{E_0}\int^{z_b} E(z)dz &= z_b - z_e
\end{aligned}
\tag{53.26}
$$

where the integrals run from field-free space to a point z_b in the uniform field inside the component; the functions $B(z)$ and $E(z)$ are those that replace the constants B_0 and E_0 in the fringing region. Finally, $j = 1$ if $z_e \geq 0$ and $j = 0$ if $z_e < 0$ and the quantities preceded by I denote the following integrals:

$$
\begin{aligned}
IE_1 &= \frac{1}{E_0^2}\int_{z_a}^{z_b} E^2 dz - (z_b - z_e) \\
IM_1 &= \frac{1}{B_0^2}\int_{z_a}^{z_b} B^2 dz - z_b \\
IC_0 &= \frac{1}{E_0 B_0}\int_{z_a}^{z_b} BE' dz - j \\
IC_1 &= \frac{1}{E_0 B_0}\int_{z_a}^{z_b} BE dz - z_b + j z_e
\end{aligned}
\tag{53.27}
$$

In its present form, this unified theory is still of rather limited application, since primary aberrations are included only in the radial direction and secondary aberrations are not considered. Once it has been extended to include primary aberrations in the axial direction and secondary aberrations in the radial direction, it should be of great help to designers, and it is for this reason that we have presented it in some detail. We must, however, stress that it represents only part of a larger activity in ion optics, designed to generalize the theory and facilitate further development despite the complexity of the formulae to be manipulated. A first large step forward was the ‘truncated power series algebra’ of Berz (1987), with which differential equations for the elements of the transfer matrices could be derived, and the special-purpose algebra language HAMILTON of Berz and Wollnik (1987), with which the heavy algebra involved in calculating aberration coefficients could be performed by computer. These have been superseded by the extensive work of Berz and colleagues based on differential algebra (see Berz et al, 2015 and the many references listed in Chapter 34).

53.4 The Literature of Ion Optics

It has been possible to give only a very superficial idea of the optics of magnetic and electrostatic prisms and of the various multipoles that commonly accompany deflecting magnets or condensers. We have attempted to compensate for this by providing lists of references that are representative of the various families. In many ambiguous cases, spectrometers that incorporate both electrostatic and magnetic prisms for example, we have not always duplicated the references but rather included them in whichever list seemed more appropriate. These lists are situated at the head of the Notes and References for Part X.

Despite their length, the lists of references for the two types of prisms are very far from complete and hardly any papers on instrumental design in general or on the results obtained are included; nevertheless, we believe that they give a reasonably faithful coverage of the optics of these devices and hope that few major contributions have been overlooked. Crossed-field devices, of which the Wien filter is the classic example, are grouped separately as are quadrupoles, sextupoles and higher order multipoles. General theoretical papers share a subsection with computer programs. Finally, we have listed some general papers and review articles concerning energy analysers and descriptions of specific designs; the Möllenstedt analyser and its magnetic counterpart, the Ichinokawa analyser are included here as are further references to the Castaing−Henry device, its all-magnetic analogues, the Ω and α imaging filters, and the one all-electrostatic Ω structure. This Part now includes a section on energy analysers and monochromators (52.9) where other references to these devices are to be found.

Notes and References

Part VII, Chapter 35

The following papers deal with two-electrode lenses: Kirkpatrick and Beckerley (1936), Gundert (1937, 1939), Klemperer and Wright (1939), Goddard (1946), Archard (1957), Hamish and Oldenburg (1964), Read (1969a, 1971), Read et al. (1971), Kuyatt et al. (1972, 1973a,b, 1974), Natali et al. (1972a,b), Galejs and Kuyatt (1973), DiChio et al. (1974a,b, 1975), Cook and Heddle (1976), Bonjour (1979a), Saito and Sovers (1979), Kodama (1982) and Barton and Allison (1988). Additional information about einzel lenses is to be found in Ramberg (1942), Tani et al. (1950), Rang and Weitsch (1956), Aberth et al. (1974), Marghitu et al. (1982), Rempfer (1982, 1985), Kurihara (1985a) and Dunham et al. (1994). On immersion lenses, see Ramberg (1942), Bas and Preuss (1963), Heddle (1969), Wardly (1972), Orloff and Swanson (1979a,b), Kurihara (1985b), Lei (1987), the exchange of papers between Renau and Heddle (1986, 1987) and Hawkes (1987) and Lenc (1995). Accelerating structures are discussed by Gyarmati and Koltay (1967), Szilágyi (1981), Joy (1990) and Tamura (2016) and in connection with the LinacTEM project, by Nagatani et al. (2015, 2016, 2017). On grid lenses, see Bernard (1951a−c, 1952, 1953) and on foil lenses see Verster (1963) and Meisburger and Jacobsen (1982). Cylindrical lenses are considered in Afanas'yev et al. (1975) and in the earlier work of Laudet (1955, 1956) and Grümm (1956c). Various theoretical points concerning potential calculations are raised by Berger (1981), Berger et al. (1979, 1980), Boers (1973) and van der Merwe (1979), while Bedford (1934) reconsiders the papers of Davisson and Calbick (1931, 1932), Bonshtedt (1955) discusses potential models for which analytical solutions are available, van Gorkum and Spanjer (1986) and Burghard et al. (1987) compare certain magnetic and electrostatic lenses, Kuyatt et al. (1971) and Lewis et al. (1986) examine the aberration polynomials, Read (1970b, 1983) discusses design theory and Yan et al. (1984) calculate the aberration coefficients of particular geometries. An early paper by von Ardenne (1939) is also concerned with electrostatic lenses and Spangenburg (1948) and Spangenburg and Field (1943, 1944) published very useful sets of design curves. The use of electrostatic lenses as velocity filters is proposed by Möllenstedt (1949) and Möllenstedt and Heise (1949), see also Stenzel (1971) and Part X. The calculation of the electrode shapes that create a given axial potential was analysed by Berz (1950) and other proposals are made by Vecheslavov and Kononov (1970) and Upadhyay (1967, 1972a,b). The papers by Jiang and Kruit (1996), Kawanami and Ishitani (1999) and Read (1978, 1979) are of general interest.

Electrostatic microscopes are described by Brüche (1932) and Brüche and Johannson (1932, cf. Brüche and Recknagel, 1941) [these are emission microscopes], Mahl (1939a,b, 1940a,b, 1942), Bachman and Ramo (1943), Grivet (1946), Bruck and Grivet (1946a,b, 1947), Fleming et al. (1948), Grivet and Regenstreif (1950), Rang and Schluge (1951), Recknagel (1952), Wegmann (1952), Schluge (1954), Guyenot (1955), Hahn (1955), Mahl et al. (1956), Gribi et al. (1958, 1959), Schulze (1960, 1992), Wilska (1960, 1962, 1964a, b, 1970), Fickler and Guyenot (1963), and Rempfer et al. (1972); for details of many of these instruments with historic photographs, see Agar (1996) and the articles by Fukami et al. (1996), Ura (1996) and Yada (1996). Overall column design is the subject of the papers by Mayer and Gaukler (1987), Aihara et al. (1988, 1989), Oku et al. (1988), Meisburger et al. (1992), Chalupka et al. (1994) and Gierak et al. (2006).

***

W. H. Aberth, R. Schnitzer and F. C. Engessser (1974). Construction of an einzel lens capable of high voltage operation. *Rev. Sci. Instrum.* **45**, 1289–1290.

A. Adams and F. H. Read (1972a). Electrostatic cylinder lenses.II: Three element einzel lenses. *J. Phys. E: Sci. Instrum.* **5**, 150–155.

A. Adams and F. H. Read (1972b). Electrostatic cylinder lenses.III: Three element asymmetric voltage lenses. *J. Phys. E: Sci. Instrum.* **5**, 156–160.

V. P. Afanas'ev, Yu. O. Glukhoi and S. Ya Yavor (1975). Two-dimensional three-electrode einzel lenses. I. Focusing properties. II. Aberration properties. *Zh. Tekh. Fiz.* **45**. 1526–1528 & 1973–1976. *Sov. Phys. Tech. Phys*. **20**, 969–970 & 1240–1242.

A. Agar (1996). The story of European commercial electron microscopes. *Adv. Imaging Electron Phys.* **96**, 415–584.

A. K. Ahmad (1998). Computerized design of a unipotential lens with small relativistic spherical and chromatic aberration. *J. Coll. Education, Al-Mustansiriya Univ*. **3**, 1–16.

A. K. Ahmad (1999). Electrostatic polynomial lens. *J. Saddam Univ*. **3** (1), 65–75.

A. K. Ahmad (2010). CAD of a three-electrode electrostatic immersion lens using the spline model. *J. Al-Nahrain Univ. (Sci.)* **12** (4), 82–87.

A. K. Ahmad and S. M. Juma (1999). Computer-aided-design of two-electrode electrostatic lenses under space-charge effect. *J. Saddam Univ*. **3** (1), 47–56.

A. K. Ahmad, S. M. Juma and S. K. Yaseen (1998). Effect of space charge on the design of low aberration einzel lens. *J. Saddam Univ*. **2** (1), 73–81.

A. K. Ahmad, S. M. Juma and S. K. Yaseen (1999). Computation of the design of three-electrode electrostatic lenses for zero and infinite magnification. *J. Coll. Education, Al-Mustansiriya Univ*. **3**, 65–72.

A. K. Ahmad, S. M. Juma and A. A. Al-Tabbakh (2002). Computer aided design of an electrostatic FIB system. *Indian J. Phys. B* **76** (6), 711–714.

A. K. Ahmad, F. A. Ali and S. M. Juma (2007). Computer-aided-design of an electrostatic lenses column by using a combined dynamic programming procedure and artifical intelligence technique. *i-Manager's J. Future Eng. Technol.* **2** (2), 87–93.

A. K. Ahmad, K. K. Ajeel and B. H. Hamad (2010). Design of an electrostatic immersion lens using the charge density method. *J. Al-Nahrain Univ. (Sci.)* **13** (1), 60–68.

R. Aihara, M. Obata, H. Sawaragi and M. H. Shearer (1988). Stabilization of an electrostatic lens for a focused ion beam system. *J. Vac. Sci. Technol. B* **6**, 958–961.

R. Aihara, H. Kasahara, H. Sawaragi, M. H. Shearer and W. B. Thompson (1989). Optical system for a low-energy focused ion beam. *J. Vac. Sci. Technol. B* **7**, 79–82.

M. A. Al-Khashab and A. A. Ahmad (2012). The influence of electrode angle on the minimization of the aberration coefficients of the two electrodes electrostatic immersion lens. *Jordan J. Phys.* **5** (2), 67–75.

M. A. Al-Khashab and A. E. Al-Abdullah (2012). The confront electrodes faces curvature effect on the electron gun performance. *Rafidain J. Sci.* **23** (2), 138–147.

M. A. Al-Khashab and A. E. Al-Abdullah (2013a). The effect of bore diameter in two electrodes electrostatic immersion lens design. *Rafidain J. Sci.* **24** (2), 82–91.

M. A. Al-Khashab and A. I. M. Al-Abdullah (2013b). Effect of electrode bore angle on the two-electrode electrostatic immersion lens design. *Jordan J. Phys.* **6** (1), 1–5.

M. A. Al-Khashab and M. T. Al-Shamma (2009a). The effect of multi-electrodes on the optical performance of electrostatic immersion lenses. *Dirasat (Pure Sci.)* **36** (2), 171–182.

M. A. Al-Khashab and M. T. Al-Shamma (2009b). Minimizing the aberration of the unipotential electrostatic lens of multi-electrodes. *Dirasat (Pure Sci.)* **36** (2), 183–193.

F. A. Al-Mudarris, S. M. Juma and A. K. Ahmad (2006). Design of a multi-electrode immersion lens for ion-optical ystems. *Iraqi J. Appl. Phys.* **2** (1–2), 27–30.

M. L. Aleksandrov, L. N. Gall', G. V. Lebedev and V. A. Pavlenko (1977). Cylindrical electrostatic lenses. *Zh. Tekh. Fiz.* **47**, 241–243. *Sov. Phys. Tech. Phys*. **22**, 139–140.

T. Ambe, H. Tanaka, H. Teguri, I. Honjo and A. Ito (2002). Miniature electrostatic colum for a compact scanning electron microscope. *Microelectron. Eng.* **61–62**, 317–321.
B. Aničin, I. Terzić, J. Vukanić and V. Babović (1976). Symmetrical three-tube unipotential lens. I: determination of potential distribution. *J. Phys. E: Sci. Instrum.* **9**, 837–839.
G. D. Archard (1954). Potential distribution of symmetrical cylindrical electron lenses. *Br. J. Appl. Phys.* **5**. 179–181 & 395.
G. D. Archard (1956). Focal properties and chromatic and spherical aberrations of the three-electrode electron lens. *Br. J. Appl. Phys.* **7**, 330–332.
G. D. Archard (1957). Properties of two-aperture electron lenses. *Br. J. Appl. Phys.* **8**, 127–130.
J. R. Ashley (1971). Hybrid computer-aided synthesis of thick electrostatic electron lenses. In *Rec. 11th Symp. Electron, Ion & Laser Beam Technology* (R. F. M. Thornley, Ed.), 157–166 (San Francisco Press, San Francisco).
J. R. Ashley (1972). Hybrid computer aided design of thick electrostatic electron lenses. *Proc. IEEE* **60**, 115–119.
C. H. Bachman and S. Ramo (1943). Electrostatic electron microscopy. I, II and III. *J. Appl. Phys.* **14**. 8–18, 69–76, 155–160.
L. A. Baranova and S. Ya. Yavor (1984). Electrostatic lenses. *Zh. Tekh. Fiz.* **54**, 1417–1453. *Sov. Phys. Tech. Phys*. **29**, 827–848.
L. A. Baranova and S. Ya. Yavor (1986). *Elektrostaticheskie Elektronnye Linzy* (Nauka, Moscow).
L. A. Baranova and S. Ya. Yavor (1989). The optics of round and multipole electrostatic lenses. *Adv. Electron. Electron Phys.* **76**, 1–207.
L. A. Baranova, G. N. D'yakova and S. Ya. Yavor (1989a). Focusing of hollow conical beams of charged particles. *Zh. Tekh. Fiz.* **59** (6), 95–98. *Sov. Phys. Tech. Phys*. **34**, 642–644.
L. A. Baranova, N. S. Ul'yanova and S. Ya. Yavor (1989b). Chromatic aberration of electrostatic axially symmetric lenses consisting of circular cylinders. *Zh. Tekh. Fiz.* **59** (12), 68–72. *Sov. Phys. Tech. Phys*. **34**, 1409–1411.
L. A. Baranova, M. I. Yavor and S. Ya. Yavor (1990). Conical lenses with a longitudinal field for focusing hollow beams. II. *Zh. Tekh. Fiz.* **60** (8), 16–22. *Sov. Phys. Tech. Phys*. **35**, 882–885.
J. E. Barth, J. B. Le Poole and K. J. P. Stigter (1974). Low aberration electrostatic probe lens for low voltage. ICEM-8, Canberra. **1**, 138–139.
R. A. Barton and W. Allison (1988). End effects in electrostatic cylinder lenses: the focal properties of systems containing an equipotential aperture plate. *J. Phys. E: Sci. Instrum.* **21**, 291–296.
E. B. Bas (1960). 1.5 Mill. Volt Elektronenbeschleuniger für Elektronenmikroskopie. EUREM-2, Delft. **1**, 126–130.
E. B. Bas and L. Preuss (1963). Bemerkungen zur relativistischen Elektronenoptik einer Immersionslinse. *Z. Angew. Math. Phys.* **14**, 84–90.
E. B. Bas, L. Preuss and W. Schneider (1959). Über die relativistische Elektronenoptik elektrostatischer Beschleuniger. *Z. Angew. Math. Phys.* **10**, 533–544.
L. H. Bedford (1934). A note on Davisson's electron-lens formula. *Proc. Phys. Soc. (Lond.)* **46**, 882–888.
E. P. Benis and T. J. M. Zouros (2008). The hemispherical deflector analyser revisited. II. Electron-optical properties. *J. Electron Spectrosc. Relat. Phenom.* **163**, 28–39.
C. Berger (1981). Electrostatique de systèmes cylindriques de révolution où le potentiel sur certaines parties de la frontière est un polynôme du second degré de la cote suivant l'axe. *Can. J. Phys.* **59**, 202–206.
C. Berger and M. Baril (1982). Studies of three-cylinder electrostatic mirrors and lenses. *J. Appl. Phys.* **53**, 3950–3956.
C. Berger, M. Lambinet and M. Baril (1979). Electrostatique des systèmes à symétrie de révolution à rayon constant. *J. Microsc. Spectrosc. Electron* **4**, 333–340.
C. Berger, M. Lambinet and M. Baril (1980). Expressions diverses du potentiel électrostatique et de ses dérivées pour des systèmes à symétrie de révolution composés de cylindres de même rayon et à charge d'espace nulle. *Rev. Phys. Appl.* **15**, 61–66.
M. Bernard (1951a). Le potentiel axial des lentilles à grille. *C. R. Acad. Sci. Paris* **233**, 298–299.

M. Bernard (1951b). Eléments gaussiens des lentilles à grilles. *C. R. Acad. Sci. Paris* **233**, 1354–1356.
M. Bernard (1951c). Etude théorique des lentilles à grille à l'aide d'une représentation approchée du potentiel. *National Bureau of Standards Circular* **527**, 213–221 [Published 1954].
M. Bernard (1952). Aberration de sphéricité des lentilles à grille. *C. R. Acad. Sci. Paris* **235**, 1115–1117.
M.-Y. Bernard (1953). Focalisation des particules de grande énergie par des lentilles à grille. I. La convergence des lentilles à grille. II. Défauts des lentilles. *J. Phys. Radium* **14**. 381–394 & 451–458.
M. T. Bernius, K. F. Man and A. Chutjian (1988). An electrostatically and magnetically confined electron gun lens system. *Rev. Sci. Instrum.* **59**, 2418–2423.
S. Bertram (1942). Calculation of axially symmetric fields. *J. Appl. Phys.* **13**, 496–502.
F. Berz (1950). Note on potentials derived from axial values in electron optics. *Philos. Mag.* **41**, 209–220.
M. Berz, K. Makino and W. Wan (2015). *An Introduction to Beam Physics* (CRC Press, Boca Raton).
R. D. Birkhoff, J. D. Allen, V. E. Anderson, H. H. Hubbell, R. S. Becker, T. L. Ferrell and D. P. Spears (1980). The ultimate electron lens – deflection of low-energy electrons by the image potential in a pinhole. *Optik* **55**, 157–164.
B. V. Bobykin, V. S. Zhdanov, A. A. Zernov, S. K. Lyubov, V. I. Malka and Yu. A. Nevinnyi (1976). Cardinal elements of three-electrode axisymmetric lenses. *Zh. Tekh. Fiz.* **46**, 1348–1353. *Sov. Phys. Tech. Phys*. **21**, 766–769.
A. J. H. Boerboom (1959). Numerical calculation of the potential distribution in ion slit lens systems. I. Three narrow slits. *Z. Naturforsch.* **14a**, 809–816.
A. J. H. Boerboom (1960a). Numerical calculation of the potential distribution in ion slit lens systems. II. Three broad slits. *Z. Naturforsch.* **15a**, 244–252.
A. J. H. Boerboom (1960b). Numerical calculation of the potential distribution in ion slit lens systems. III. Arbitrary number of slits. *Z. Naturforsch.* **15a**, 253–259.
A. J. H. Boerboom (1960c). A modified ion slit lens for virtual variation of slit widths. *Z. Naturforsch.* **15a**, 350–355.
A. J. H. Boerboom and H.-n. Chen (1984). Calculation of the parameters for the Schwarz–Christoffel transformation of ion slit lens sytems. *Int. J. Mass Spectrom. Ion Processes* **61**, 1–13.
J. E. Boers (1973). Digital computer simulation of charged particle beams and electrostatic lenses. *J. Vac. Sci. Technol.* **10**, 1120–1123.
L. Boesten (1988). Modified operation of the seven-element electrostatic Chutjian–Kuyatt lens system. *Rev. Sci. Instrum.* **59**, 233–237.
P. Bonjour (1979a). A simple accurate expression of the potential in electrostatic lenses. Part I: Two cylinder lenses. *Rev. Phys. Appl.* **14**, 533–540.
P. Bonjour (1979b). A simple accurate expression of the potential in electrostatic lenses. Part II: Triple cylinder lenses. *Rev. Phys. Appl.* **14**, 715–728.
B. E. Bonshtedt (1955). Method of calculation of a broad class of magnetic and electrostatic fields, for which solutions of the fundamental equations of electron optics can be expressed in terms of well-known functions. *Zh. Tekh. Fiz.* **25**, 541–543.
M. Born and E. Wolf (1959). *Principles of Optics* (Pergamon, London & New York; 7th edn, 2002, corrected printing, Cambridge University Press, Cambridge).
G. Bosi (1969). An approximate calculation of the axial potential in electrostatic lenses. *Nucl. Instrum. Meth.* **70**, 317–319.
G. Bosi (1974). Analytic field forms in axially symmetric systems. *Nucl. Instrum. Meth.* **119**, 613–614.
E. Brüche (1932). Elektronenmikroskop. *Naturwissenschaften* **20**, 49.
E. Brüche and H. Johannson (1932). Elektronenoptik und Elektronenmikroskop. *Naturwissenschaften* **20**, 353–358.
E. Brüche and A. Recknagel (1941). *Elektronengeräte. Prinzipien und Systematik* (Springer, Berllin).
H. Bruck and P. Grivet (1946a). Le microscope électronique. Application au microscope électrostatique de la Compagnie Générale de Télégraphie sans Fil. *Onde Electrique* **26**, 217–227.
H. Bruck and P. Grivet (1946b). Le microscope électronique électrostatique. *Ann. Radioél.* **1**, 293–310.

H. Bruck and P. Grivet (1947). Perfectionnements apportés aux microscopes électrostatiques. *Ann. Radioél.* **2**, 244–248.

H. Bruck and L. Romani (1944). Sur les propriétés de quelques lentilles électrostatiques indépendantes. *Cahiers Phys.* **24**, 15–28.

J. N. H. Brunt and F. H. Read (1975). Aberrations in electrostatic lenses. *J. Phys. E: Sci. Instrum.* **8**, 1015–1020.

C.-D. Bubeck, A. Fleischmann, G. Knell, R. Y. Lutsch, E. Plies and D. Winkler (1999). Miniature electron lens for generation of a low-voltage high current electron probe. *Nucl. Instrum. Meth. Phys. Res. A* **427**, 104–108.

F. Burstert, D. Winkler and B. Lischke (1996). Novel high brightness miniature electron gun for high current e-beam applications. *Microelectron. Eng.* **31**, 95–100.

L. Cartan (1937). Sur une nouvelle méthode de focalisation des faisceaux d'ions positifs rapides. Applications à la spectrométrie de masse. *J. Phys. (Paris)* **8**, 111–120.

A. Chalupka, G. Stengl, H. Buschbeck, G. Lammer, H. Vonach, R. Fischer, E. Hammel, H. Löschner, R. Nowak, P. Wolf, W. Finkelstein, R. W. Hill, I. L. Berry, L. R. Harriott, J. Melngailis, J. N. Randall, J. C. Wolfe, H. Stroh, H. Wollnik, A. A. Mondelli, J. J. Petillo and K. Leung (1994). Novel electrostatic column for ion projection lithography. *J. Vac. Sci. Technol. B* **12**, 3513–3517.

T. H. P. Chang, D. P. Kern and L. P. Muray (1990). Microminiaturization of electron optical systems. *J. Vac. Sci. Technol. B* **8**, 1698–1705.

P. Chanson (1946). Caractéristiques optiques des lentilles électrostatiques. In *L'Optique Electronique* (L. de Broglie, Ed.), 85–104 (Editions de la Revue d'Optique, Paris).

P. Chanson (1947). Les élements optiques des lentilles électrostatiques et le microscope à protons. *Ann. Phys. (Paris)* **2**, 333–413.

P. Chanson, A. Ertaud and C. Magnan (1945). Détermination des éléments du premier ordre des lentilles électrostatiques symétriques. *C. R. Acad. Sci. Paris* **221**, 233–235.

Y. C. Chou, M. J. Robrecht and B. P. Tonner (1987). Theoretical modeling and experimental testing of a multimode optical system and energy analyzer for electron spectroscopy. *Rev. Sci. Instrum.* **58**, 1164–1172.

A. Chutjian (1979). Geometries and focal properties of two electron-lens systems useful in low-energy electron or ion scattering. *Rev. Sci. Instrum.* **50**, 347–355.

D. Ćirić, I. Terzić and J. Vukanić (1976a). Symmetrical three-tube unipotential lens II. First-order focal properties. *J. Phys. E: Sci. Instrum.* **9**, 839–841.

D. Ćirić, I. Terzić and J. Vukanić (1976b). Plane symmetrical unipotential lens. II: first-order focal properties. *J. Phys. E: Sci. Instrum.* **9**, 844–846.

R. A. Colman and G. J. F. Legge (1994). An investigation of the optics of a 5-element electrostatic lens for use with a high brightness ion source. *Nucl. Instrum. Meth. Phys. Res. B* **84**, 515–520.

R. D. Cook and D. W. O. Heddle (1976). The simple accurate calculation of cylinder lens potentials and focal properties. *J. Phys. E: Sci. Instrum.* **9**, 279–282.

A. V. Crewe (1991a). The three element electrostatic lens. *Optik* **90**, 151–157.

A. V. Crewe (1991b). An algebraic approach to the symmetrical einzel lens. *Optik* **88**, 118–125.

D. A. Crewe, D. C. Perng, S. E. Shoaf and A. D. Feinerman (1992). A micromachined electrostatic electron source. *J. Vac. Sci. Technol. B* **10**, 2754–2758.

D. A. Crewe, M. M. Ruffin and A. D. Feinerman (1996). Initial tests of a micromachined SEM. *J. Vac. Sci. Technol. B* **14**, 3808–3812.

J. D. Cross, F. H. Read and E. A. Riddle (1967). Electron optical systems with fixed image positions for beams of variable energy. *J. Sci. Instrum.* **44**, 993–996.

C. J. Davisson and C. J. Calbick (1931). Electron lenses. *Phys. Rev.* **38**, 585.

C. J. Davisson and C. J. Calbick (1932). Electron lenses [corrigenda]. *Phys. Rev.* **42**, 580.

G. V. Der-Shvarts and S. A. Belen'kii (1962). A study of the aberrations of electrostatic lens filters. *Radiotekh. Elektron.* **7**, 126–132. *Radio Eng. Electron.* **7**, 112–117.

G. V. Der-Shvarts and I. S. Makarova (1966). Study of the spherical aberration of axisymmetric einzel lenses. *Radiotekh. Elektron.* **11**, 1802–1806. *Radio Eng. Electron. Phys*. **11**, 1581–1585.

G. V. Der-Shvarts and I. S. Makarova (1969). Axially symmetric einzel lenses with small third-order spherical aberration. *Radiotekh. Elektron.* **14**, 378–380. *Radio Eng. Electron. Phys*. **14**, 330–332.

G. V. Der-Shvarts and I. S. Makarova (1971). Field aberrations of electrostatic, axially symmetric einzel lenses. *Radiotekh. Elektron.* **16**, 2289–2294. *Radio Eng. Electron. Phys*. **16**, 2098–2102.

D. DiChio, S. V. Natali and C. E. Kuyatt (1974a). Focal properties of the two-tube electrostatic lens for large and near-unity voltage ratios. *Rev. Sci. Instrum.* **45**, 559–565.

D. DiChio, S. V. Natali, C. E. Kuyatt and A. Galejs (1974b). Use of matrices to represent electron lenses. Matrices for the two-tube electrostatic lens. *Rev. Sci. Instrum.* **45**, 566–569.

D. DiChio, S. V. Natali and C. E. Kuyatt (1975). A new form for the third-order asymptotic aberration coefficients of electrostatic lenses; application to the two-tube electrostatic lens. *Rev. Sci. Instrum.* **46**, 71–76.

D. Dunham, D. M. Desloge, G. F. Rempfer, W. P. Skoczylas and B. P. Tonner (1994). Evaluation of aberration coefficients of practical electrostatic lenses for X-ray absorption micro-spectroscopy and imaging. *Nucl. Instrum. Meth. Phys. Res. A* **347**, 441–445.

E. Durand (1961). *Solutions Numériques des Equations Algébriques* Vol. II. (Masson, Paris).

E. Durand (1966). *Electrostatique* Vol. 2. (Masson, Paris).

J. Edmunson, J. A. Gaskin, G. A. Jerman, R. P. Harvey, I. J. Doloboff, E. L. Neidholdt, and J. E. Edmunson (2016). A miniaturized variable pressure scanning electron microscope (MVP–SEM) for in-situ Mars surface sample analysis. 47th Lunar and Planetary Science Conference, No. 2301.

J. Edmunson, J. A. Gaskin, I. J. Doloboff and J. E. Edmunson (2017). Unveiling the mysteries of Mars with a miniaturized variable pressure scanning electron microcope (MVP–SEM). Lunar and Planetary Science XLVIII, No. 2811.

P. Ehinger (1954a). Calcul du potentiel axial des lentilles électroniques constituées par deux cylindres coaxiaux de diamètres différents. *C. R. Acad. Sci. Paris* **238**, 879–881.

P. Ehinger (1954b). Calcul du potentiel axial dans une lentille électrostatique à trois électrodes. *C. R. Acad. Sci. Paris* **238**, 1306–1308.

P. Ehinger and M. Bernard (1954). Théorie de la lentille électrostatique indépendante à électrode centrale épaisse. *Cahiers Phys.* **50**, 8–16.

A. B. El-Kareh (1969). Design and analysis of symmetrical and asymmetrical electrostatic immersion lenses using a digital computer. In *Rec. 10th Symp. Electron, Ion & Laser Beam Technol.* (L. Marton, Ed.), 393–406 (San Francisco Press, San Francisco).

A. B. El-Kareh and J. C. J. El-Kareh (1970). *Electron Beams, Lenses and Optics* (Academic Press, New York & London).

A. B. El-Kareh and M. A. Sturans (1971a). Analysis of the 3-tube symmetrical electrostatic unipotential lens. *J. Appl. Phys.* **42**, 1870–1876.

A. B. El-Kareh and M. A. Sturans (1971b). Analysis of the 3-tube asymmetrical electrostatic unipotential lens. *J. Appl. Phys.* **42**, 4902–4907.

A. B. El-Kareh and M. A. Sturans (1972). Analysis of a range of symmetrical three-aperture electrostatic lenses. *IEEE Trans. Electron Dev.* **19**, 1075–1084.

M. Escher, M. Merkel and G. Schönhense (2002). Optimisation of an electrostatic tetrode objective for XPEEM. *Recent Trends* **8**, 95–96.

C. W. F. Everitt and K.-J. Hanszen (1956). Zur experimentellen Bestimmung der Brennweiten und Hauptebenen von asymmetrischen Elektronen-Einzellinsen. *Optik* **13**, 385–398.

A. D. Feinerman and D. A. Crewe (1997). Miniature electron optics. *Adv. Imaging Electron Phys.* **102**, 187–234.

A. D. Feinerman and D. A. Crewe (2002). Three-dimensional fabrication of miniature electron optics. *Adv. Imaging Electron Phys.* **121**, 91–142.

A. D. Feinerman, D. A. Crewe, D. C. Perng, S. E. Shoaf and A. V. Crewe (1992). Sub-centimeter micromachined electron microscope. *J. Vac. Sci. Technol. A* **10**, 611–616.
A. D. Feinerman, D. A. Crewe and A. V. Crewe (1994a). Microfabrication of arrays of scanning electron microscopes. *J. Vac. Sci. Technol. B* **12**, 3182–3186.
A. D. Feinerman, D. A. Crewe, D. C. Perng, C. A. Spindt, P. R. Schwoebel and A. V. Crewe (1994b). Miniature electron microscopes for lithography. *Proc. SPIE* **2194**, 262–273.
J. Feng, H. Padmore, D. H. Wei, S. Anders, Y. Wu, A. Scholl and D. Robin (2002). Modeling the acceleration field and objective lens for an aberration corrected photoemission electron microscope. *Rev. Sci. Instrum.* **73**, 1514–1517.
C. Fert (1952). Trajectoires électroniques paraxiales dans les lentilles électrostatiques. *J. Phys. Radium* **13**, 83A–90A.
W. Fickler and E. Guyenot (1963). Über die neue elektronenoptische Anlage EF. *Jenaer Jahrbuch* (Part II), 345–375.
M. Fink and J. Kessler (1963). Experimente zur Elektronenoptik elektrostatischer Beschleuniger. *Z. Phys.* **174**, 197–205.
M. Fink and E. Kisker (1980). A method for rapid calculations of electron trajectories in multi-element electrostatic cylinder lenses. *Rev. Sci. Instrum.* **51**, 918–920.
F. Firestein and J. Vine (1963). Properties of two-cylinder electron lenses. *Br. J. Appl. Phys.* **14**, 449–455.
J. P. S. Fitzgerald, R. C. Word and R. Könenkamp (2012a). Simultaneous and adaptive correction of spherical and chromatic aberration using an electron mirror and lens combination. *Ultramicroscopy* **115**, 35–40.
J. P. S. Fitzgerald, R. C. Word and R. Könenkamp (2012b). Aberrations in asymmetrical electron lenses. *Ultramicroscopy* **119**, 40–44.
G. Fleming, R. Rempfer, E. Asherman and P. Nolan (1948). Recent electronmicrographs obtained with a new electrostatic electron microscope. *J. Appl. Phys.* **19**, 125.
D. L. Fraser, W. J. Meyers and T. G. Elser (1971). A computer analysis of the spherical aberration of three electrostatic immersion lenses. In *Rec, 11th Symp. Electron, Ion and Laser Beam Technology* (R. F. M. Thornley, Ed.), 209–228 (San Francisco Press, San Francisco).
T. C. Fry (1932). Two problems in potential theory. *Am. Math. Monthly* **39**, 199–209.
A. Fukami, K. Adachi and K. Asakura (1996). Development of electron microscopes at Tokyo Imperial University. *Adv. Imaging Electron Phys.* **96**, 251–256.
A. Galejs and C. E. Kuyatt (1973). Representation of focal properties of the equal-diameter two-tube electrostatic lens for computer calculations. *J. Vac. Sci. Technol.* **10**, 1114–1117.
A. Galejs and P. H. Rose (1967). Optics of electrostatic accelerator tubes. In *Focusing of Charged Particles* (A. Septier, Ed.), **2**, 297–326 (Academic Press, New York & London).
R. Gans (1937). Strahlengang in elektronenoptischen Systemen. *Z. Tech. Phys.* **18**, 41–48.
J. G. Gaskin, G. A. Jerman, B. D. Ramsey, C. K. Ferguson, T. O. Abbott, S. O'Brien, D. C. Joy, K. G. Thaisen, L. A. Taylor, A. R. Sampson, E. A. Rhodes, E. H. Darlington, B. J. Bussey, R. P. Harvey and P. D. Spudis (2009). Miniature scanning electron microscope for in-situ planetary studies: electron gun development. 40th Lunar and Planetary Science Confeence, The Woodlands (TX). No. 2318.
J. Gaskin, T. Abbott, S. Medley, K. Patty, D. Gregory, K. Thaisen, B. Ramsey, G. Jerman, A. Sampson, R. Harvey and L. Taylor (2010). Miniaturized scanning electron microscope for in-situ planetary studies. Earth and Space 2010: Engineering, Science, Construction, and Operations in Challenging Environments, 1246–1257.
J. A. Gaskin, G. Jerman, D. Gregory and A. Sampson (2012). Miniature variable pressure scanning electron microscope for in-situ imaging and chemical analysis. IEEE Aerospace Conference, Big Sky (MT).
J. Gierak, A. Madouri, A. L. Biance, E. Bourhis, G. Patriarche, C. Ulysse, D. Lucot, X. Lafosse, L. Auvray and L. Bruchhaus (2007). Sub-5 nm FIB direct patterning of nanodevices. *Microelectron. Eng.* **84**, 779–783.
G. H. Gillespie and T. A. Brown (1997). Optics elements for modeling electrostatic lenses and accelerator components. I. Einzel lenses. In *Proc. Particle Accelerator Conference, Vancouver* (M. Comyn, M. K. Craddock, M. Reiser and J. Thomson, Eds), **3**, 2559–2561 (IEEE, Piscataway, NJ).

G. H. Gillespie and T. A. Brown (1999). Optics elements for modeling electrostatic lenses and accelerator components. II. Accelerator columns. *Nucl. Instrum. Meth. Phys. Res. A* **427**, 315–320.

W. Glaser (1948). Maxwell's 'fish eye' as an ideal electron lens. *Nature* **162**, 455–456.

W. Glaser (1952). *Grundlagen der Elektronenoptik* (Springer, Vienna).

A. Glaser and W. Henneberg (1935). Die Potentialverteilung in Schlitzblende und Lochblende. *Z. Tech. Phys.* **8**, 222–230.

W. Glaser and H. Robl (1951). Strenge Berechnung typischer elektrostatischer Elektronenlinsen. *Z. Angew. Math. Phys.* **2**, 444–469.

W. Glaser and P. Schiske (1954). Strenge Durchrechnung einer typischen elektrostatischen Einzellinse. *Optik* **11**, 422–443 & 445–467.

W. Glaser and P. Schiske (1955). Die Bildfehler dritter Ordnung einer typischen elektrostatischen Einzellinse. *Optik* **12**, 233–245.

U. Glatzel and F. Lenz (1988). Optimization of electrostatic immersion lenses. *Optik* **79**, 15–18.

L. G. Glikman and M. S. Nurmanov (1976). Approximate equations for the cardinal elements of multi-electrode immersion tubular lenses. *Zh. Tekh. Fiz.* **46**, 1582–1585. *Sov. Phys. Tech. Phys.* **21**, 911–913.

L. G. Glikman and E. M. Yakushev (1967). Field of a three-electrode cylindrical electrostatic lens. *Zh. Tekh. Fiz.* **37**, 2097–2099. *Sov. Phys. Tech. Phys.* **12**, 1544–1545.

L. G. Glikman, V. M. Kel'man and E. M. Yakushev (1967a). On the impossibility of constructing a divergent cylindrical electrostatic lens. *Zh. Tekh. Fiz.* **37**, 13–16. *Sov. Phys. Tech. Phys.* **12**, 9–11.

L. G. Glikman, V. M. Kel'man and E. M. Yakushev (1967b). Electron optical parameters of two-electrode cylindrical immersion lenses. *Zh. Tekh. Fiz.* **37**, 1028–1034. *Sov. Phys. Tech. Phys.* **12**, 740–744.

L. G. Glikman, V. M. Kel'man and E. M. Yakushev (1967c). Telescopic systems of cylindrical lenses. *Zh. Tekh. Fiz.* **37**, 1720–1725. *Sov. Phys. Tech. Phys.* **12**, 1261–1264.

L. G. Glikman, V. M. Kel'man and M. S. Nurmanov (1973a). Multi-electrode tubular electrostatic immersion lenses. *Zh. Tekh. Fiz.* **43**, 1358–1363. *Sov. Phys. Tech. Phys.* **18**, 864–867.

L. G. Glikman, V. M. Kel'man and M. S. Nurmanov (1973b). Multi-electrode tubular lenses with constant potential difference between electrodes. *Zh. Tekh. Fiz.* **43**, 2278–2280. *Sov. Phys. Tech. Phys.* **18**, 1441–1442.

L. G. Glikman, V. M. Kel'man and M. S. Nurmanov (1974). Symmetric multi-electrode tubular electrostatic lenses. *Zh. Tekh. Fiz.* **44**, 1084–1087. *Sov. Phys. Tech. Phys.* **19**, 680–682.

R. Gobrecht (1941). Experimentelle Untersuchungen über den Öffnungsfehler elektrostatischer Linsen. *Arch. Elektrotech.* **35**, 672–686.

R. Gobrecht (1942). Die Bildfeldwölbung bei elektrostatischen Linsen. *Arch. Elektrotech.* **36**, 484–492.

L. S. Goddard (1946). Optical characteristics of a two-cylinder electrostatic lens. *Proc. Cambridge Philos. Soc.* **42**, 106–126.

F. Gray (1939). Electrostatic electron-optics. *Bell Syst. Tech. J.* **18**, 1–31.

M. Gribi, M. Thürkauf, W. Villiger and L. Wegmann (1958). Ein 70 kV-Elektronenmikroskop mit kalter Kathode und elektrostatischem Objektiv. ICEM-4, Berlin. **1**, 174.

M. Gribi, M. Thürkauf, W. Villiger and L. Wegmann (1959). Ein 70 kV-Elektronenmikroskop mit kalter Kathode und elektrostatischer Linse. *Optik* **16**, 65–86.

G. A. Grinberg (1953). On some classes of static, axially symmetric, electric and magnetic fields, for which the basic equations of electron optics admit of solutions in terms of known functions. *Zh. Tekh. Fiz.* **23**, 1904–1914.

P. Grivet (1946). Réalisation industrielle d'un microscope électronique électrostatique. In *L'Optique Electronique* (L. de Broglie, Ed.), 129–160 (Editions de la Revue d'Optique, Paris).

P. Grivet (1950). Electron lenses. *Adv. Electron.* **2**, 47–100.

P. Grivet (1951). Lentilles électroniques. *National Bureau of Standards Circular* **527**, 167–196 [Published 1954].

P. Grivet and M. Bernard (1951). Eléments gaussiens dans la lentille électrostatique formée de deux cylindres coaxiaux de même diamètre. *C. R. Acad. Sci. Paris* **233**, 788–790.

P. Grivet and M. Bernard (1952a). Etude théorique de la lentille formée de deux cylindres coaxiaux de même diamètre à l'aide d'une représentation approchée du potentiel axial. *National Bureau of Standards Circular* **527**, 205–211 [Published 1954].

P. Grivet and M. Bernard (1952b). Théorie de la lentille électrostatique constituée par deux cylindres coaxiaux. *Ann. Radioel.* **6**, 3–9.

P. Grivet and E. Regenstreif (1950). Sur un nouveau microscope électrostatique à trois lentilles agrandissantes. ICEM-2, Paris. **1**, 230–236.

H. Grümm (1956a). Ebene elektrostatische Felder, die eine strenge Berechnung der Elektronenbahnen zulassen. *Ann. Phys. (Leipzig)* **17** (452), 269–274.

H. Grümm (1956b). Rotationssymmetrische elektrostatische Felder, die eine strenge Berechnung der Elektronenbahnen zulassen. *Ann. Phys. (Leipzig)* **17** (452), 275–280.

H. Grümm and H. Kremser (1956). Beispiele streng berechenbarer Ionen- und Elektronenbahnen im ebenen elektrostatischen Feld. *Optik* **13**, 295–306.

H. Grümm and H. Spurny (1957). Beispiele streng berechenbarer Ionen- und Elektronenbahnen im ebenen elektrostatischen Feld. *Acta Phys. Austr.* **11**, 193–220.

R. Guckenberger and H. Heil (1972). Design and computer evaluation of the aperture lens, the electric lens with the shortest focal length and the lowest aperture defect. EUREM-5, Manchester. 112–113.

E. Gundert (1937). Nachweis der Abbildungsfehler von Elektronenlinsen nach der Fadenstrahlmethode. *Phys. Z.* **38**, 462–467.

E. Gundert (1939). Der Öffnungsfehler von elektrostatischen Rohrlinsen. *Z. Phys.* **112**, 689–690.

E. Gundert (1941). Der Öffnungsfehler elektrostatischer Elektronenlinsen. *Telefunken-Röhre* **19–20**, 61–98.

E. Guyenot (1955). Über die Entwicklung eines fünfstufigen elektrostatischen Elektronenmikroskops. *Jenaer Jahrbuch (*Part I*)*, 28–34.

B. Gyarmati and E. Koltay (1967). Lens characteristics for electrode systems used in acceleration tubes. *Atom. Közlemények* **9**, 319–331.

E. Hahn (1955). Die elektronenoptische Elemente des ELMI D2. *Jenaer Jahrbuch (*Part I*)*, 35–53.

B. H. Hamad, A. K. Ahmad and S. M. Juma (2005). Some optical properties of an electrostatic immersion lens using the charge density method. *Iraqi J. Appl. Phys.* **1** (3), 21–27.

H. Hamisch and K. Oldenburg (1964). Experimentelle Untersuchung von Immersionslinsen im Bereich großer Potentialverhältnisse (f_1/f_2 = 10 bis 2000). EUREM-3, Prague. **1**, 41–42.

T. Hanai, M. Hibino and S. Maruse (1982). Improvement of an electron probe profile using the foil lens. *J. Electron Microsc.* **31**, 360–367.

K.-J. Hanszen (1958a). Vergleichende Betrachtungen über den Öffnungsfehler symmetrischer und asymmetrischer Elektronen-Einzellinsen auf Grund von Vermessungen der Austrittsstrahltangenten. *Z. Naturforsch.* **13a**, 409–414.

K.-J. Hanszen (1958b). Zur Systematik asymmetrischer Elektronen-Einzellinsen. *Optik* **15**, 304–317.

K.-J. Hanszen (1964). Ein abgewandeltes Schattenverfahren zur genaueren Bestimmung der geometrisch-optischen Daten von Elektronenstrahl-Erzeugern und Elektronenlinsen. *Z. Naturforsch.* **19a**, 896–905.

K.-J. Hanszen and R. Lauer (1965). Der Einfluß der Pupillenlage auf den chromatischen Fehler der Vergrößerung von elektrostatischen und magnetischen Elektronenlinsen. *Optik* **23**, 478–494.

K.-J. Hanszen and R. Lauer (1967). Electrostatic lenses. In *Focusing of Charged Particles* (A. Septier, Ed.), **1**, 251–307 (Academic Press, New York & London).

E. Harting and F. H. Read (1976). *Electrostatic Lenses* (Elsevier, Amsterdam, Oxford & New York).

P. W. Hawkes (1987). Comment on "Geometric aberrations in electrostatic lenses, II" by A. Renau and D.W.O. Heddle: the thin-lens approximation for the geometric aberration coefficients of accelerating lenses. *J. Phys. E: Sci. Instrum.* **20**, 234–235.

P. W. Hawkes and B. Lencová (2002). Studies on the asymptotic cardinal elements and aberration coefficients of symmetric unipotential electrostatic lenses. *Optik* **113**, 78–82.

D. W. O. Heddle (1969). The design of three-element electrostatic electron lenses. *J. Phys. E: Sci. Instrum.* **2**, 1046–1050.

D. W. O. Heddle (1971). An afocal electrostatic lens. *J. Phys. E: Sci. Instrum.* **4**, 981−983.
D. W. O. Heddle (1991). *Electrostatic Lens Systems* (Adam Hilger, Bristol; 2nd edn, 2000, Institute of Physics Publishing, Bristol & Philadelphia).
D. W. O. Heddle (1999). Accurate calculation of cylindrical lens potentials usung the nine-point relaxation and Bessel expansion methods. *J. Phys. D: Appl. Phys.* **32**, 1447−1454.
D. W. O. Heddle and M. V. Kurepa (1970). The focal properties of three-element electrostatic electron lenses. *J. Phys. E: Sci. Instrum.* **3**, 552−554.
D. W. O. Heddle and N. Papadovassilakis (1984). The magnification behaviour of a five-element electrostatic lens. *J. Phys. E: Sci. Instrum.* **17**, 599−605.
D. W. O. Heddle, N. Papadovassilakis and A. M. Yateem (1982). Measurements of the magnification behaviour of some three-element electrostatic lenses. *J. Phys. E: Sci. Instrum.* **15**, 1210−1213.
K. Heinemann and G. Möllenstedt (1967). Elektronemikroskopie mit langsamen Elektronen mittels Zwischenverzögerer. *Optik* **26**, 11−21.
F. Heise (1949). Bestimmung von Verzeichnung und Öffnungsfehler elektrostatischer Linsen aus Hauptflächen und Brennpunkt-Hilfsflächen. *Optik* **5**, 479−489.
F. Heise and O. Rang (1949). Experimentelle Untersuchungen an elektrostatischen Elektronenlinsen. *Optik* **5**, 201−216.
T. Hibi, S. Takahashi and K. Takahashi (1967). Experimental study on electrostatic cylindrical lens. *J. Electron Microsc.* **16**, 225−231.
M. Hibino and S. Maruse (1976). Correction of the spherical aberration of a magnetic lens with a foil lens. *J. Electron Microsc.* **25**, 229−236.
M. Hibino, S. Sugiyama, T. Hanai and S. Maruse (1978). Characteristics of the foil lens for the correction of the spherical aberration of the strongly excited magnetic lens. *J. Electron Microsc.* **27**, 259−265.
R. Hill and K. C. A. Smith (1980). An interactive computer system for magnetic lens analysis. EUREM-7, The Hague. **1**, 60−61.
R. Hill and K. C. A. Smith (1981). Applications of the Cambridge interactive lens analysis system: CIELAS. EMAG, Cambridge. 71−74.
H. Hoch, E. Kasper and D. Kern (1976). Der Öffnungsfehler 3. Ordnung und der axiale Farbfehler von rotationssymmetrischen Elektronenlinsen mit gekrümmter geladener transparenter Folie. *Optik* **46**, 463−473.
J. Hoeft (1959). Eine Erweiterung des Anwendungsbereiches der Brennweitenformel für die Lochblendenlinse. *Z. Angew. Phys.* **11**, 380−382.
L. S. Horden, B. B. Boyer and R. F. W. Pease (1995). Retarding field optics with field-free sample. *Proc. SPIE* **2522**, 44−53.
P. Hubert (1949). Lentille électronique corrigée de l'aberration de sphéricité. *C. R. Acad. Sci. Paris* **228**, 233−235.
S. Humphries (1986). *Principles of Charged Particle Acceleration* (Wiley−Interscience, New York & Chichester).
R. G. E. Hutter (1945). Rigorous treatment of the electrostatic immersion lens whose axial potential distribution is given by: $\phi(z) = \phi_0\,\mathrm{e}^{K\,\arctan\,z}$. *J. Appl. Phys.* **16**, 678−699.
T. Ichinokawa, T. Ohyama and M. Komuro (1973). Simple electron monochromator of three-diaphragm einzel lens. *Jpn. J. Appl. Phys.* **12**, 163−166.
R. E. Imhof and F. H. Read (1968). A three-aperture electron optical lens for producing an image of variable energy but fixed position. *J. Phys. E: Sci. Instrum.* **1**, 859−860.
G. Induni (1945a). Das Schweizerische Übermikroskop. *Neue Zürcher Zeitung* **357**, 28.
G. Induni (1945b). Das Schweizerische Übermikroskop. *Vierteljahresschr. Naturforsch. Ges. Zürich* **90**, 181−195.
R. S. Ingarden (1957). On the geometrically absolute optical representation in the electron microscope. *Trav. Soc. Sci. Lett. Wroclaw, Ser. B* **No. 45**. 60 pp.

N. Isik (2016). Determination of electron optical properties for aperture zoom lenses using an artificial neural network. *Microsc. Microanal.* **22**, 458–462.

L. Jacob and M. B. O'Sullivan (1973). Some computerised trajectories and focal properties of asymmetrical electron lenses. *Proc. R. Irish Acad.* **73A**, 47–62.

B. K. Jasim, A. K. Ahmad and A.-J. M. Abdal-Ghffur (2001). Design of unipotential lens operated under space charge effect and low aberration. *J. Coll. Educ., Al-Mustansiriya Univ.* **1** (3), 153–164.

B. K. Jasim, A. K. Ahmad and A.-J. M. Abdal-Ghffur (2010). Design of unipotential electrostatic lenses operated under zero magnification. *J. Al-Nahrain Univ. (Sci.)* **13** (3), 21–26.

X. R. Jiang and P. Kruit (1996). Comparison between different imaging modes in focussed ion beam instruments. *Microelectron. Eng.* **30**, 249–252.

H. Johannson and O. Scherzer (1933). Über die elektrische Elektronensammellinse. *Z. Phys.* **80**, 183–192.

T. Joy (1990). Electrostatic accelerator tubes – recent progress and future directions. *Nucl. Instrum. Meth. Phys. Res. A* **287**, 48–63.

S. M. Juma, A. K. Ahmad and L. M. W. Qaseer (2000). An electrostatic lens system design for telescopic mode of operation. *J. Coll. Educ., Al-Mustansiriya Univ.* **5**, 1–12.

S. M. Juma, F. A. Al-Mudarris and A. K. Ahmad (2002). A hyperbolic potential field model for designing an einzel lens of low aberrations. *Iraqi J. Phys.* **1** (1), 61–68.

E. Kamke (1977). *Differentialgleichungen, Lösungsmethoden und Lösungen.* I. *Gewohnliche Diffferentialgleichungen*, 9th edn (Teubner, Stuttgart).

K. Kanaya and N. Baba (1977). Rigorous treatment of bipotential lens whose axial potential distribution is given by $\Phi(\mu) = V \exp(K_0 \arccos \mu)$. *Optik* **47**, 239–269.

K. Kanaya and N. Baba (1978). General theory of three-electrode lenses based on the axial potential model $\Phi(z/a) = \Phi(0)\exp[K_0 \tan^{-1}(z/a)^m]$. *J. Phys. E: Sci. Instrum.* **11**, 265–275.

K. Kanaya, H. Yamazaki, T. Taoka, H. Fujita, M. Iwanaga and S. Shibata (1965). Focusing properties of acceleration tube for high voltage electron microscope. *J. Electron Microsc.* **14**, 196–202.

K. Kanaya, H. Kawakatsu, H. Yamazaki and S. Shibata (1966). Electron-optical properties of three-electrode electron lenses. *J. Sci. Instrum.* **43**, 416–429.

K. Kanaya, H. Kawakatsu and T. Miya (1972). Optical properties of bipotential electron lenses. *J. Electron Microsc.* **21**, 261–270.

Y. Kawanami and T. Ishitani (1999). Generalization of electrostatic lens characteristics using the Picht ray trajectories. *J. Vac. Sci. Technol. B* **17**, 1400–1405.

D. P. Kern and T. H. P. Chang (1994). Miniaturized electron optics: basics and applications. ICEM-13, Paris. **1**, 149–152.

J. Kessler (1961). Zur Elektronenoptik elektrostatischer Beschleuniger im relativistischen Bereich. *Z. Naturforsch.* **16a**, 1138–1146.

A. Khursheed (2001). Recent developments in scanning electron microscope design. *Adv. Imaging Electron Phys.* **115**, 197–285.

P. Kirkpatrick and J. G. Beckerley (1936). Ion optics of equal coaxial cylinders. *Rev. Sci. Instrum.* **7**, 24–26.

T. Kishi, H. Yokota and K. Katayama (1987a). Multiple slit lens for focusing–deflection of charged particles. *Jpn. J. Appl. Phys.* **26**, 1394.

T. Kishi, H. Yokota and K. Katayama (1987b). A proposal for a new energy analyser. In *Proc. Second Japan–China Joint Symposium on Mass Spectrometry* (H. Matsuda and X.-t. Liang, Eds), 145–148 (Bando Press, Osaka).

E. Kisker (1982). Simple method for accurate ray-tracing in electrostatic lenses. *Rev. Sci. Instrum.* **53**, 114–116.

O. Klemperer and W. D. Wright (1939). The investigation of electron lenses. *Proc. Phys. Soc. (Lond.)* **51**, 296–317.

M. Knoll and E. Ruska (1932). Beitrag zur geometrischen Elektronenoptik, I, II. *Ann. Physik (Leipzig)* **12** (404). 607–640 & 641–661.

E. S. Kochanov (1963). Determination of trajectories in the plane three-electrode lens. *Zh. Tekh. Fiz.* **33**, 1301–1310. *Sov. Phys. Tech. Phys.* **8**, 969–975.

M. Kodama (1982). An improvement to the variational method for boundary value problems and its application to two-cylinder electrostatic lenses. *J. Phys. D: Appl. Phys.* **15**, 1657–1666.

E. Koltay and S. Czeglédy (1965). Lens characteristics for electrode systems used in accelerator tubes. *Nucl. Instrum. Meth.* **37**, 179–180.

H. Koops, E. Munro, J. Rouse, J. Kretz, M. Rudolph, M. Weber and G. Dahm (1995). Miniature low voltage beam systems producable by combined lithographies. *Nucl. Instrum. Meth. Phys. Res. A* **363**, 1–10.

M. V. Kurepa, M. D. Tasić and J. M. Kurepa (1974). A four element energy scanning electron lens system with fixed image position and magnification. *J. Phys. E: Sci. Instrum.* **7**, 940–944.

K. Kurihara (1985a). Low-aberration einzel lens for a focused-ion-beam system. *Jpn. J. Appl. Phys.* **24**, 225–230.

K. Kurihara (1985b). A focused ion beam system for submicron lithography. *J. Vac. Sci. Technol. B* **3**, 41–44.

C. E. Kuyatt, S. V. Natali and D. DiChio (1971). Third-order aberration coefficients of electron lenses. In *Rec. 11th Symp. Electron, Ion and Laser Beam Technology* (R. F. M. Thornley, Ed.), 177–181 (San Francisco Press, San Francisco).

C. E. Kuyatt, S. V. Natali and D. DiChio (1972). Accurate calculation of properties of the two-tube electrostatic lens. III. Aberration coefficients. *Rev. Sci. Instrum.* **43**, 84–87.

C. E. Kuyatt, D. DiChio and S. V. Natali (1973a). Focal properties of the two-tube electrostatic lens for large voltage ratios. *J. Vac. Sci. Technol.* **10**, 1118–1119.

C. E. Kuyatt, D. DiChio and S. V. Natali (1973b). Third-order aberration coefficients of electron lenses. II. *J. Vac. Sci. Technol.* **10**, 1124–1126.

C. E. Kuyatt, D. DiChio and S. V. Natali (1974). Third-order asymptotic aberration coefficients of electron lenses. III. Formulas and results for the two-tube electrostatic lens. *Rev. Sci. Instrum.* **45**, 1275–1280.

M. Kuzuya, T. Hanai, M. Hibino and S. Maruse (1982). Numerical evaluations of characteristics of the foil lens in correcting the spherical aberration of the objective lens of a conventional transmission elelctron microscope. *J. Electron Microsc.* **31**, 18–26.

J. Laplume (1947). Les lentilles électrostatiques en mécanique relativiste. *Cahiers Phys.* **29–30**, 55–66.

P. M. Lapostolle and A. Septier, Eds (1970). *Linear Accelerators* (North-Holland, Amsterdam).

M. Laudet (1953). Potentiel et champ d'une lentille électrostatique cylindrique à trois fentes. *Cahiers Phys.* **41**, 73–80.

M. Laudet (1955). Optique électronique des systèmes cylindriques présentant un plan de symétrie. I. L'approximation du premier ordre. II. Les aberrations. *J. Phys. Radium* **16**, 118–124 & 908–916.

M. Laudet (1956). Contribution à l'étude du calcul numérique des champs et des trajectoires en optique électronique des systèmes cylindriques. *Ann. Fac. Sci. Toulouse* **20**, 111–230.

J. D. Lawson (1977). *The Physics of Charged-Particle Beams* (Clarendon Press, Oxford). 2nd edn, 1988.

N. N. Lebedev and I. P. Skal'skaya (1960). Electrostatic field of an electron lens consisting of two coaxial cylinders. *Zh. Tekh. Fiz.* **30**, 472–479. *Sov. Phys. Tech. Phys.* **5**, 443–450.

H.-n. Lei (1987). Etude d'un canon à émission de champ pour son utilsation en micro-analyse Auger. Dissertation, Lyon.

B. Lencová (1997). Electrostatic lenses. In *Handbook of Charged Particle Optics* (J. Orloff, Ed.), 177–221 (CRC Press, Boca Raton). 2nd edn, 2009, 161–208.

F. Lenz (1956). Zur Berechnung von rotationssymmetrischen Potentialfeldern in Elektronenlinsen. *Ann. Phys. (Leipzig)* **19** (454), 82–88.

G. N. Lewis, H. Paik, J. Mioduszewski and B. M. Siegel (1986). A hydrogen field ion source with focusing optics. *J. Vac. Sci. Technol. B* **4**, 116–119.

G. Liebmann (1949). Measured properties of strong "unipotential" electron lenses. *Proc. Phys. Soc. (Lond.) B* **62**, 213–228.

W. Lippert and W. Pohlit (1952). Zur Kenntnis der elektronenoptischen Eigenschaften elektrostatischer Linsen. *Optik* **9**, 456–462.

W. Lippert and W. Pohlit (1953). Zur Kenntnis der elektronenoptischen Eigenschaften elektrostatischer Linsen. II. *Optik* **10**, 447–454.

W. Lippert and W. Pohlit (1954). Zur Kenntnis der elektronenoptischen Eigenschaften elektrostatischer Linsen. III. *Optik* **11**, 181–186.

J. S. Loyd (2015). Miniature electron microscope beam column optics. Dissertation, Alabama in Huntsville.

J. S. Loyd and D. A. Gregory (2016). Precision enhancement in boundary element methods with application to electron optics. *Microscopy* **65**, 325–336.

J. S. Loyd, D. A. Gregory and J. A. Gaskin (2017). Field modeling and ray-tracing of a miniature scanning electron microscope beam column. *Microscopy* **66**, 245–253.

R. K. Luneberg (1964). *Mathematical Theory of Optics* (University of California, Berkeley).

M. M. MacNaughton (1952). The focal properties and spherical aberration constants of aperture electron lenses. *Proc. Phys. Soc. (Lond.) B* **65**, 590–596.

H. Mahl (1939a). Optique électronique appliquée. Le microscope électronique et ses applications. *Rev. Gén. Electricité* **45**, 241–248.

H. Mahl (1939b). Über das elektrostatische Elektronen-Mikroskop hoher Auflösung. *Z. Tech. Phys.* **20**, 316–317.

H. Mahl (1940a). Über das elektrostatische Elektronen-Übermikroskop und einige Anwendungen in der Kolloidchemie. *Kolloid-Z.* **91** (2), 105–117.

H. Mahl (1940b). Das elektrostatische Elektronen-Übermikroskop. *Jahrb. AEG-Forsch.* **7**, 43–56.

H. Mahl (1942). Ein Versuch zur Emissionsmikroskopie mit elektrostatischer Linse. *Z. Tech. Phys.* **23** (4), 117–119.

H. Mahl (1947). Über ein neues elektrostatisches Klein-Elektronenmikroskop. *Optik* **2**, 190–195.

H. Mahl and A. Recknagel (1944). Über den Öffnungsfehler von elektrostatischen Elektronenlinsen. *Z. Phys.* **122**, 660–679.

H. Mahl, H. Volkmann and W. Weitsch (1956). Über ein neues elektrostatisches Gebrauchs-Elektronenmikroskop. EUREM-1, Stockholm. 34–37.

S. Marghitu, C. Oproiu and R. Cramariuc (1982). Studiul modificării formei fasciculului de electroni în cîmpul lentilenor unipotenţiale. *Stud. Cerc. Fiz.* **34**, 972–981.

G. Martínez and M. Sancho (1983). Four-cylinder electrostatic lens I: Potential distribution and focal properties. *J. Phys. E: Sci. Instrum.* **16**, 625–630.

G. Martínez, M. Sancho and F. H. Read (1983). Four-cylinder electrostatic lens, II. Energy scanning at constant image position and magnification. *J. Phys. E: Sci. Instrum.* **16**, 631–635.

H. P. Mayer and K.-H. Gaukler (1987). Berechnungen elektrostatischer Abbildungssysteme für Flüssigmetall-Feldionenquellen. *Optik* **77**, 129–134.

W. D. Meisburger and E. H. Jacobsen (1982). Electrostatic lens of very low spherical aberration. *Optik* **62**, 359–366.

W. D. Meisburger, A. D. Brodie and A. A. Desai (1992). Low-voltage electron-optical system for the high-speed inspection of integrated circuits. *J. Vac. Sci. Technol. B* **10**, 2804–2808.

C. Mileikowsky and R. T. Paul (1952). A 1.5 MV accelerator for heavy particles with analyzing magnet for use in nuclear research. *Ark. Fys.* **4**, 287–298.

G. Möllenstedt (1949). Die elektrostatische Linse als hochauflösender Geschwindigkeitsanalysator. *Optik* **5**, 499–517.

G. Möllenstedt (1955). 100 keVolt-Elektronen im elektrostatischen Elektronenmikroskop (Zwischenbeschleuniger). *Optik* **12**, 441–466.

G. Möllenstedt and F. Heise (1949). Die elektrostatische Linse als hochauflösender Geschwindigkeits-Analysator. *Phys. Blätt.* **2**, 80–83.

M. Morikawa (1962a). Weak lens formulas for accelerating tubes. *Nucl. Instrum. Meth.* **15**, 282–287.

M. Morikawa (1962b). Electron optics in accelerating tubes. *J. Appl. Phys.* **33**, 87–90.

M. Morikawa (1963a). Approximate formulas for coaxial two-cylinder lenses. *J. Appl. Phys.* **34**. 211–217 & 1836.

M. Morikawa (1963b). Polynomial approximation to focal constants of equi-diameter two-cylinder lenses. *J. Appl. Phys.* **34**, 1657–1660.

M. Morikawa (1963c). Calculation of axially symmetric electrostatic fields for two coaxial equidiameter cylinders. *J. Appl. Phys.* **34**, 3179–3181.

C. Morita, T. Ohye and H. Shimoyama (1995). Optimization of the operating conditions of the accelerating tube for the high voltage electron microscope equipped with the field emission gun. *Nucl. Instrum. Meth. Phys. Res. A* **363**, 291–294.

I. Müllerová, L. Frank and E. Weimer (1998). Variable mode retarding field element for low energy SEM. *Recent Trends* **6**, 51–52.

W. Mühlfriedel and E. Hellmuth (2004). *Carl Zeiss in Jena, 1945–1990* (Böhlau, Köln, Weimar & Wien). Vol. III of *Carl Zeiss*, *Die Geschichte eines Unternehmens*.

T. Mulvey and M. J. Wallington (1973). Electron lenses. *Rep. Prog. Phys.* **36**, 347–421.

E. Munro and N. D. Wittels (1977). Calculation of the optical properties of electron lenses with electron-transparent foils. *Optik* **47**, 25–38.

L. P. Muray, C. S. Silver and J. P. Spallas (2006). Sub-100-nm lithography with miniature electron beam columns. *J. Vac. Sci. Technol. B* **24**, 2945–2950.

L. P. Muray, J. Spallas and D. Meisburger (2014). On the limits of miniature electron column technology. *Proc. SPIE* **9236**, 92360C.

Y. Nagatani, Y. Arai, T. Sannomiya, T. Shirai, R. Aihara, G. Iijima and K. Nagayama (2015). Development of the 500kV LinacTEM. *Kenbikyo* **50**, 160–163.

Y. Nagatani, Y. Arai, T. Sannomiya, T. Shirai, R. Aihara, G. Iijima and K. Nagayama (2016). Development of the 500kV LinacTEM. *Kenbikyo* **51** (Suppl. 1), 34.

Y. Nagatani, Y. Arai, T. Sannomiya, T. Shirai, R. Aihara, G. Iijima and K. Nagayama (2017). Nanometre-resolution by the 500 kV LinacTEM. *Kenbikyo* **52** (Suppl. 1), 22.

S. V. Natali, D. DiChio and C. E. Kuyatt (1972a). Accurate calculation of properties of the two-tube electrostatic lens. I. Improved digital methods for the precise calculation of electric fields and trajectories. *J. Res. Natl Bur. Stand.* **76A**, 27–35.

S. V. Natali, D. DiChio, E. Uva and C. E. Kuyatt (1972b). Accurate calculation of properties of the two-tube electrostatic lens. II. First-order focal properties and *P-Q* curves. *Rev. Sci. Instrum.* **43**, 80–83.

S. Nomura (1998). Electrostatic accel–decel lens with the advantage of reduced chromatic aberration. *J. Vac. Sci. Technol. B* **16**, 104–108.

S. Nomura (1999). Tandem accel lens advantageous in producing a small spot focused ion beam. *J. Vac. Sci. Technol. B* **16**, 82–85.

T. Ohye, C. Morita and H. Shimoyama (1993). Computer simulation of electron optical characteristics of accelerating tube for high voltage electron microscope. *Proc. SPIE* **2014**, 36–44.

K. Oku, M. Maruyama and M. Fukushima (1988). Electrostatic focusing and electrostatic deflection systems with reduced aperture aberrations. *J. Vac. Sci. Technol. B* **6**, 1999–2002.

F. Ollendorff (1955). *Elektronik des Einzelelektrons* (Springer, Vienna). This is Part I of Vol. II, "Innere Elektronik" of *Technische Elektrodynamik* by F. Ollendorff.

J. Orloff and L. W. Swanson (1979a). An asymmetric electrostatic lens for field-emission microprobe applications. *J. Appl. Phys.* **50**, 2494–2501.

J. Orloff and L. W. Swanson (1979b). A study of some electrostatic gun lenses for field emission. *Scanning Electron Microsc.* Pt. I, 39–44.

H. G. Parks (1971). Analytic solution of the axial potential for a three-element electrostatic lens. In *Rec. 11th Symp. Electron, Ion & Laser Beam Technology* (R. F. M. Thornley, Ed.), 229–238 (San Francisco Press, San Francisco).

D. C. Perng, D. A. Crewe and A. D. Feinerman (1992). Micromachined thermionic emitters. *J. Micromech. Microeng.* **2**, 25–30.

E. G. Ramberg (1942). Variation of the axial aberrations of electron lenses with lens strength. *J. Appl. Phys.* **13**, 582–594.

C. Ramsauer (1941). *Zehn Jahre Elektronenmikroskopie, ein Selbstbericht des AEG Forschungs-Instituts* (Springer, Berlin).

O. Rang (1948). Ein verzeichnungsfreies kurzbrennweitiges elektrostatisches Projektiv. *Optik* **4**, 251–257.
O. Rang and H. Schluge (1951). Aufbau des AEG–Zeiss Elektronenmikroskops EM8. *AEG-Mitteilungen* Nos. 7/8, 3–9.
O. Rang and W. Weitsch (1956). Ein regelbares elektrostatisches Vierelektroden-Projektiv. *Optik* **13**, 201–208.
F. H. Read (1969a). Accurate calculations of double-aperture electrostatic immersion lenses. *J. Phys. E: Sci. Instrum.* **2**, 165–169.
F. H. Read (1969b). Calculated properties of electrostatic einzel lenses of three apertures. *J. Phys. E: Sci. Instrum.* **2**, 679–684.
F. H. Read (1970a). Asymmetric electrostatic lenses of three apertures. *J. Phys. E: Sci. Instrum.* **3**, 127–131.
F. H. Read (1970b). A collocation method for solving Laplace's equation. *J. Comput. Phys.* **6**, 527–532.
F. H. Read (1971). 'Zero-gap' electrostatic aperture lenses. *J. Phys. E: Sci. Instrum.* **4**, 562–566.
F. H. Read (1978). Electrostatic lenses. In *Low-Energy Ion Beams*, Salford (K. G. Stephens, I. H. Wilson and J. L. Moruzzi, Eds), 249–256. IoP Conference Series, Vol. 38.
F. H. Read (1979). Electrostatic lenses. *Radiat. Effects* **44**, 129–136.
F. H. Read (1983). A 'movable' electrostatic lens. *J. Phys. E: Sci. Instrum.* **16**, 636–642.
F. H. Read (2015). Optimization of the shapes of electrodes of electrostatic lenses. *Microsc. Microanal.* **21** (Suppl. 4), 276–279.
F. H. Read, A. Adams and J. R. Soto-Montiel (1971). Electrostatic cylinder lenses I: Two element lenses. *J. Phys. E: Sci. Instrum.* **4**, 625–632.
A. Recknagel (1952). Über ein elektrostatisches Elektronenmikroskop. *Wiss. Z. Technischen Hochschule Dresden* **2**, 515–522.
E. Regenstreif (1949). Sur la théorie de la lentille électrostatique indépendante à trois diaphragmes. *C. R. Acad. Sci. Paris* **229**, 1311–1313.
E. Regenstreif (1950a). Expression simple de la distance focale et de l'aberration chromatique pour une famille étendue de lentilles électrostatiques. *C. R. Acad. Sci. Paris* **230**, 630–632.
E. Regenstreif (1950b). Rayons principaux pour une famille de lentilles et de miroirs électrostatiques. *C. R. Acad. Sci. Paris* **230**, 1262–1264.
E. Regenstreif (1950c). La lentille électrostatique indépendante en régime transgaussien. *C. R. Acad. Sci. Paris* **230**, 1650–1652.
E. Regenstreif (1951). Théorie de la lentille électrostatique à trois électrodes. *Ann. Radioel.* **6**, 51–83 & 114–155.
G. Rempfer (1982). Some design considerations in electrostatic electron optics. ICEM-10, Hamburg. **1**, 285–286.
G. Rempfer (1985). Unipotential electrostatic lenses: paraxial properties and aberrations of focal length and focal point. *J. Appl. Phys.* **57**, 2385–2401.
G. F. Rempfer (1999). The relationship of lens aberrations to image aberrations in electron optics. *Optik* **110**, 17–24.
G. F. Rempfer, R. Connell, L. Mercer and I. Louisette (1972). An electrostatic transmission electron microscope. *Am. Lab.* **4** (4), 39–46.
A. Renau and D. W. O. Heddle (1986a). Geometric aberrations in electrostatic lenses: I. A simple and accurate computer model. *J. Phys. E: Sci. Instrum.* **19**, 284–288.
A. Renau and D. W. O. Heddle (1986b). Geometric aberrations in electrostatic lenses: II. Aberration coefficients and their interrelations. *J. Phys. E: Sci. Instrum.* **19**, 288–295.
A. Renau and D. W. O. Heddle (1987). Reply to comment on "Geometric aberrations in electrostatic lenses: II". *J. Phys. E: Sci. Instrum.* **20**, 235–236.
G. H. N. Riddle (1978). Electrostatic einzel lenses with reduced spherical aberration for use in field-emission guns. *J. Vac. Sci. Technol.* **15**, 857–860.
C. Rochow, T. Ohnweiler and E. Plies (2008). A miniaturized electron optical column with an electrostatic–permanent magnet objective lens. *Recent Trends* **11**, 97–98.
R. Rüdenberg (1948). Electron lenses of hyperbolic field structure. *J. Franklin Inst.* **246**, 311–339 & 377–408.

E. Ruska and M. Knoll (1931). Die magnetische Sammelspule für schnelle Elektronenstrahlen. *Z. Tech. Phys.* **12**, 389–400 & 448.

R. Saini, Z. Jandric, K. Tsui, T. Udeshi and D. Tuggle (2005). Manufacturable MEMS microcolumn. *Microelectron. Eng.* **78–79**, 62–72.

R. Saini, Z. Jandric, J. Gammell, S. A. M. Mentink and D. Tuggle (2006). Manufacturable MEMS miniSEMs. *Microelectron. Eng.* **83**, 1376–1381.

T. Saito and O. J. Sovers (1977). Numerical calculations of focal and aberration properties of unipotential electron lenses. *J. Appl. Phys.* **48**, 2306–2311.

T. Saito and O. J. Sovers (1979). Spherical aberration coefficients of double-cylinder electrostatic lenses over wide magnification ranges. *J. Appl. Phys.* **50**, 3050–3056.

T. Saito, S. Kubota and S. Miyoka (1973). Digital computer studies of electron lenses for cathode-ray tubes. *J. Appl. Phys.* **44**, 4505–4510.

T. Saito, M. Kikuchi and O. J. Sovers (1979). Design of complex electron lenses consisting of two double cylinders. *J. Appl. Phys.* **50**, 6123–6128.

T. Sakae, Y. Tsumura, Y. Matsumoto, K. Ishibashi and A. Katase (1990). Characteristics of a seven-element electrostatic lens system studied by an exact beam-tracing method. *Rev. Sci. Instrum.* **61**, 61–65.

M. Scheinfein and A. Galantai (1986). Multiobjective optimization techniques for design of electrostatic charged particle lenses. *Optik* **74**, 154–164.

P. Schiske (1953). An electrostatic single lens permitting rigorous calculation. *Nature* **171**, 443.

H. Schluge (1954). Das AEG–Zeiss Elektronenmikroskop. *Zeiss Werkzeitschr*, 104–112.

S. Schubert, R. Y. Lutsch, M. Rauscher, D. Winkler and E. Plies (2002). Design and simulation of a miniaturised electrostatic column for high probe current. *Recent Trends* **8**, 27–28.

D. Schulze (1960). Elektronenmikroskop Elmi D2 aus Jena in der Festkörperphysik. *Jenauer Rundschau* **5**, 131–134.

D. Schulze (1992). Elektronenmikroskope aus dem Osten. *Elektronenmikroskopie* **6**, 32–40.

R. Seeliger (1948). Ein neues Verfahren zur Bestimmung des Öffnungsfehlers von Elektronenlinsen. *Optik* **4**, 258–262.

A. Sellidj and J. L. Erskine (1990). A tandem four-element lens system for surface electron spectroscopy. *Rev. Sci. Instrum.* **61**, 49–56.

A. Septier (1960). Aberration sphérique de quelques lentilles électrostatiques à symétrie de révolution pour des faisceaux de grande ouverture. *CERN Report 60-39*.

A. Septier and M. Ruytoor (1959a). Aberration sphérique de lentilles électrostatiques de révolution pour des faisceaux de grande ouverture. Méthodes de mesure. *C. R. Acad. Sci. Paris* **249**, 2175–2177.

A. Septier and M. Ruytoor (1959b). Aberration sphérique de lentilles électrostatiques de révolution aux grandes ouvertures. Lentilles hyperboliques symétriques et lentilles dissymétriques. *C. R. Acad. Sci. Paris* **249**, 2746–2748.

J. R. Shah and L. Jacob (1951). Investigation of field distribution in symmetrical electron lens. *J. Appl. Phys.* **22**, 1236–1241.

K. Shimizu (1983). Determination of the optimum electrode shape of electrostatic einzel lenses. *Jpn. J. Appl. Phys.* **22**, 1623–1626.

K. Shimizu and H. Kawakatsu (1974). Design charts of electrostatic three-aperture lenses. *J. Phys. E: Sci. Instrum.* **7**, 472–476.

H. Shimoyama (1982). The axial field distributions which give analytical solutions of the paraxial ray equation. *J. Electron Microsc.* **31**, 127–136.

I. Sinno, A. Sanz-Velasco, S. Kang, H. Jansen, E. Olsson, P. Enoksson and K. Svensson (2010). Fabrication of nanoscale electrostatic lenses. *J. Micromech. Microeng.* **20**, 095031.

O. Sise (2014). Electrostatic afocal-zoom lens design using computer optimization technique. *J. Electron Spectrosc. Relat. Phenom.* **197**, 7–12.

O. Sise (2015). Imaging properties and aberration analysis of electrostatic afocal–zoom lenses using computer optimization. *Microsc. Microanal.* **21** (Suppl. 4), 72–77.

O. Sise, M. Ulu and M. Dogan (2005). Multi-element cylindrical electrostatic lens systems for focusing and controlling charged particles. *Nucl. Instrum. Meth. Phys. Res. A* **554**, 114–131.

O. Sise, M. Ulu and M. Dogan (2007a). Aberration coefficients of multi-element cylindrical electrostatic lens systems for charged particle beam applications. *Nucl. Instrum. Meth. Phys. Res. A* **573**, 329–339.

O. Sise, M. Ulu and M. Dogan (2007b). Characterization and modeling of multi-element electrostatic lens systems. *Rad. Phys. Chem.* **76**, 593–598.

O. Sise, N. Okumus, M. Ulu and M. Dogan (2009). Computer simulation of electrostatic aperture lens systems for electron spectroscopy. *J. Electron Spectrosc. Relat. Phenom.* **175**, 76–86.

G. Slodzian and A. Figueras (1978). Remarques sur les aberrations des lentilles électrostatiques unipotentielles accélératrices. *J. Phys. Lett.* **39**, L90–L93.

V. V. Sorokina and P. V. Timofeev (1948). The field shape for electrostatic lenses. *Zh. Tekh. Fiz.* **18**, 509–516.

J. P. Spallas, C. S. Silver, L. Muray, T. Wells and M. El-Gomati (2006). A manufacturable miniature electron beam column. *Microelectron. Eng.* **83**, 984–989.

J. P. Spallas, D. Meisburger and L. Muray (2016). Ultralow voltage imaging using a miniature electron beam column. *J. Vac. Sci. Technol. B* **34**. 06KB02, 6 pp.

K. R. Spangenburg (1948). Electrostatic electron optics. In *Vacuum Tubes* (K. R. Spangenburg, Ed.), 328–393 (McGraw–Hill, New York, Toronto & London).

K. Spangenburg and L. M. Field (1943). Some simplified methods of determining the optical characteristics of electron lenses. *Elec. Commun.* **20**, 305–313.

K. Spangenburg and L. M. Field (1944). The measured characteristics of some electrostatic electron lenses. *Elec. Commun.* **21**, 194–204.

W. Stenzel (1971). Die elektrostatische Linse als Energiefilter. *Optik* **32**, 352–374.

H. Stolz (1978). Elektronenmikroskopie mit einem elektrostatischen Zwischenverzögerer. Teil I. *Optik* **52**, 369–383.

H. Stolz (1979). Elektronenmikroskopie mit einem elektrostatischen Zwischenverzögerer. Teil II. *Optik* **53**, 35–45.

R. R. A. Syms, L. Michelutti and M. M. Ahmad (2003). Two-dimensional microfabricated electrostatic einzel lens. *Sens. Actuat. A* **107**, 285–295.

J. Szép and M. Szilágyi (1987). Statistical error analysis of electrode construction for electrostatic spline lenses. *J. Appl. Phys.* **62**, 3539–3542.

M. Szilágyi (1977). A new approach to electron optical optimization. *Optik* **48**, 215–224.

M. Szilágyi (1978a). A dynamic programming search for electrostatic immersion lenses with minimum spherical aberration. *Optik* **50**, 35–51.

M. Szilágyi (1978b). A solution to the problem of the ideal quadrupole lens. *Optik* **50**, 121–128.

M. Szilágyi (1981). A novel approach to beam optics design for particle accelerators. *Part. Accel.* **11**, 213–217.

M. Szilágyi (1983). Improvement of electrostatic lenses for ion beam lithography. *J. Vac. Sci. Technol. B* **1**, 1137–1140.

M. Szilágyi (1984a). Reconstruction of electrodes and pole pieces from optimized axial field distributions of electron and ion optical systems. *Appl. Phys. Lett.* **45**, 499–501.

M. Szilágyi (1984b). Synthesis of electron lenses. In *Electron Optical Systems for Microscopy, Microanalysis and Microlithography* (J. J. Hren, F. A. Lenz, E. Munro and P. B. Sewell, Eds), 75–84 (Scanning Electron Microscopy, AMF O'Hare).

M. Szilágyi (1985). Electron optical synthesis and optimization. *Proc. IEEE* **73**, 412–418.

M. Szilágyi (1986). Electrostatic lenses with very small spherical aberration. *Appl. Phys. Lett.* **49**, 767–769.

M. Szilágyi (1987a). Electrostatic spline lenses. *J. Vac. Sci. Technol. A* **5**, 273–278.

M. Szilágyi (1987b). Synthesis of electron optical systems with very low aberrations. In *Proc. Int. Symposium on Electron Optics, ISEOB* (J.-y. Ximen, Ed.), 238–240 (Institute of Electronics, Academia Sinica, Beijing).

M. Szilágyi and J. Szép (1988). Optimum design of electrostatic lenses. *J. Vac. Sci. Technol. B* **6**, 953–957.

M. Szilágyi, S. J. Yakowitz and M. O. Duff (1984). Procedure for electron and ion lens optimization. *Appl. Phys. Lett.* **44**, 7–9.
M. Tamura (2016). Aberration characteristics of accelerating tube for high voltage electron microscope. *Kenbikyo* **51** (Suppl. 1), 64.
T.-t. Tang (1991). Tube wall electrode electron optical systems. *Optik* **88**, 96–102.
Y. Tani, A. Yamashita, H. Kamogawa and S. Wakaki (1950). Calculation of electric field and focal length of electrostatic electron lens. ICEM-2, Paris. **1**, 201–206.
T. Taoka, H. Fujita, K. Kanaya, M. Iwanaga and N. Iwasa (1967). Functional features of a 500 kV electron microscope. *J. Sci. Instrum.* **44**, 747–754.
K. G. Thaisen, L. A. Taylor, J. A. Gaskin, G. Jerman and B. D. Ramsey (2009). An ESEM/SEM study of lunar soil and the potential for a miniaturized version on the moon. 40th Lunar and Planetary Science Conference, No. 1697.
U. Timm (1955). Zur Berechnung elektrostatischer Linsen. *Z. Naturforsch.* **10a**, 593–602, and Berichtigung *ibid*. **11a** (1956) 176.
C. Trager-Cowan, S. M. Kay and D. W. O. Heddle (1990a). Multiple-element electrostatic lenses: I. The five-element lens. *Meas. Sci. Technol.* **1**, 738–746.
C. Trager-Cowan, R. B. Miller, S. M. Kay and D. W. O. Heddle (1990b). Multiple-element electrostatic lenses: II. A multiple disc lens. *Meas. Sci. Technol.* **1**, 747–750.
T. Tsumagari, J. Murakami, H. Ohiwa and T. Noda (1986). Aberrations of electrostatic systems with machining error. *J. Vac. Sci. Technol. B* **4**, 140–142.
T. Tsumagari, H. Ohiwa and T. Noda (1988). Design of a low-aberration lens for focused ion beams. *J. Vac. Sci. Technol. B* **6**, 949–952.
D. Typke (1968). Der Öffnungsfehler von rotationssymmetrischen Elektronenlinsen mit Raumladung. *Optik* **28**, 488–494.
M. Ulu, O. Sise and M. Dogan (2007). Optimizing the performance of an electron gun design followed by lenses and apertures. *Rad. Phys. Chem.* **76**, 636–641.
C. S. Upadhyay (1972a). Synthesis of electrostatic electron optical systems. *J. Inst. Telecommun. Eng.* **18**, 74–78.
C. S. Upadhyay (1972b). Design of wide aperture electrostatic electron optical systems. *J. Inst. Telecommun. Eng.* **18**, 142–144.
K. Ura (1994). Magnification dependence of aberration coefficients in electrostatic bipotential lens. *J. Electron Microsc.* **43**, 406–407.
K. Ura (1996). Early electron microscopes at Osaka University. *Adv. Imaging Electron Phys.* **96**, 263–269.
K. Ura (1998). Normalization of optical parameters for electrostatic lenses. ICEM-14, Cancún. **1**, 107–108.
K. Ura (1999). Unified representation of optical properties for electrostatic lenses. *J. Electron Microsc.* **48**, 99–103.
J. P. van der Merwe (1978a). A Fourier–Bessel solution of an einzel-type electrostatic field with rotational symmetry. *J. Appl. Phys.* **49**, 4335–4340.
J. P. van der Merwe (1978b). Electron optical properties of some Fourier–Bessel electrostatic fields with rotational symmetry. I. Basis fields. II. An analytical study of weak fields. III. Computed properties of synthesized fields. *Publications Univ. Zululand, Ser. 3,* Nos, 23–25.
J. P. van der Merwe (1979a). Fourier–Bessel series solution for potential and intensity field of open electron optical systems with rotational symmetry, in terms of I_0 Bessel functions. *J. Appl. Phys.* **50**, 2506–2511.
J. P. van der Merwe (1979b). The inverse interior Dirichlet problem. *J. Appl. Phys.* **50**, 5120–5126.
J. P. van der Merwe (1979c). Fourier–Bessel series solution of an exterior Dirichlet boundary-value problem with rotational symmetry. *J. Appl. Phys.* **50**, 5609–5614.
A. A. van Gorkum and T. G. Spanjer (1986). A generalized comparison of spherical aberration of magnetic and electrostatic electron lenses. *Optik* **72**, 134–136.
K. J. van Oostrum (1985). CAD in light optics and electron optics. *Philips Tech. Rev.* **42**, 69–84.

G. K. Varakin (1974). Characteristics of a three-element electrostatic immersion lens. *Prib. Tekh. Eksp.* (1), 211–212. *Instrum. Exp. Tech.* **17**, 242–243.
V. V. Vecheslavov and V. I. Kononov (1970). Determination of electrode profiles for axially symmetric electrostatic lenses. *Radiotekh. Elektron.* **15**, 880–883. *Radio Eng. Electron. Phys.* **15**, 758–760.
J. L. Verster (1963). On the uses of gauzes in electron optics. *Philips Res. Rep.* **18**, 465–608.
P. S. Vijayakumar and M. Szilágyi (1987). Chromatic aberration of symmetric two-cylinder electrostatic lenses. *Rev. Sci. Instrum.* **58**, 953–957.
J. Vine (1960). Numerical investigation of a range of unipotential electron lenses. *Br. J. Apl. Phys.* **11**, 408–411.
M. von Ardenne (1939). Über eine elektrostatische Hochspannungslinse kurzer Brennweite. *Naturwiss* **27**, 614–615.
J. Vukanić, I. Terzić, B. Aničin and D. Ćirić (1976). Plane symmetrical unipotential lens I: Determination of potential distribution. *J. Phys. E: Sci. Instrum.* **9**, 842–843.
M. J. Wallington (1970). An improved iteration method for calculating the axial potential distribution in slit-aperture electrostatic lenses. *J. Phys. E: Sci. Instrum* **3**, 599–604.
M. J. Wallington (1971). The focal properties of electron bombardment ion sources for mass spectrometers. *J. Phys. E: Sci. Instrum.* **4**, 1–8.
C. C. Wang (1945). Electromagnetic field inside a cylinder with a gap. *J. Appl. Phys.* **16**, 351–366.
B. Wannberg and A. Sköllermo (1977). Computer optimization of retarding lens systems for ESCA spectrometers. *J. Electron Spectrosc. Relat. Phenom.* **10**, 45–78.
G. A. Wardly (1972). Dependence of spherical and chromatic aberration upon magnification in an immersion lens. *J. Appl. Phys.* **43**, 2632–2635.
L. Wegmann (1952). Eine neues schweizerisches Elektronenmikroskop. *Neue Zürcher Zeitung* (No. 1562).
G. Wendt (1951). Zur Dioptrik elektrostatischer Elektronenlinsen. *Z. Angew. Phys.* **3**, 219–225.
D. Werner (1971). Zur Elektronenoptik einer elektrostatischen Rohr-Einzellinse. *Optik* **32**, 320–337.
E. T. Whittaker and G. N. Watson (1927). *A Course of Modern Analysis*, 4th edn (Cambridge University Press, Cambridge).
H. Wiedemann (2015). *Particle Accelerator Physics*, 4th edn (Springer, Berlin).
A. P. Wilska (1960). Low voltage electron microscope. EUREM-2, Delft. **1**, 105–109.
A. P. Wilska (1962). A new low voltage electron microscope. ICEM-5, Philadelphia. **1**, D-6.
A. P. Wilska (1964a). Low-voltage electron microscope: a 6 kV instrument. *J. R. Microsc. Soc.* **83**, 207–211.
A. P. Wilska (1964b). Some basic features of a new low-voltage electron microscope. EUREM-3, Prague. **A**, 29–30.
A. P. Wilska (1970). Low voltage electron microscope with energy filtering and amplitude contrast. ICEM-7, Grenoble. **1**, 149–150.
A. P. Wilska, K.-J. Hanszen and R. Lauer (1970). A high-efficiency 5-electrode filter lens for low voltage electron microscopy. ICEM-7, Grenoble. **2**, 29–30.
D. Winkler, C.-D. Bubeck, A. Fleischmann, G. Knell, Y. Lutsch and E. Plies (1998). Experimental evaluation of a miniature electrostatic thin-foil electron optical column for high current and low-voltage operation. *J. Vac. Sci. Technol. B* **16**, 3181–3184.
K. Yada (1996). History of electron microscopes at Tohoku University. *Adv. Imaging Electron Phys.* **96**, 245–249.
H. Yamazaki (1973). Practical analysis of symmetric einzel lenses. *Optik* **38**, 9–20.
H. Yamazaki (1977). The dependence of the aberration constants of an einzel lens on the magnification. *Optik* **48**, 357–370 & Erratum *ibid.* **49** (1977) 373.
H. Yamazaki (1979). An analytical formula of axial potential of symmetric einzel lenses with the thick central electrode. *Optik* **54**, 343–346.
J.-w. Yan, W.-x. Chen and Q. Zhu (1984). The calculation of third-order aberrations of electrostatic lenses by non-paraxial electron trajectories [in Chinese]. *Acta Electron. Sin.* **12**, 47–53.

S. K. Yaseen Al-Ani, A. K. Ahmad and I. A. Mohammed (2002). Design of four-electrode einzel electrostatic lens for electron gun. *J. Coll. Educ. Women, Baghdad Univ.* **13** (4), 783−789. [In Arabic].

S. K. Yassin, A. K. Ahmad and B. H. Hussein (2012). Computer aided design of an electron optical transport and focusing system. *J. Coll. Educ., Al-Mustansiriya Univ.* **3**, 336−343.

S. Ya. Yavor and L. A. Baranova (1990). Optics of conical electrostatic analysing and focusing systems. *Nucl. Instrum. Meth. Phys. Res. A* **298**, 421−425.

M. I. Yavor, H. Weick and H. Wollnik (1999). Fringing-field effects in acceleration columns. *Nucl. Instrum. Meth. Phys. Res. A* **427**, 79−85.

H. Yokota and T. Kishi (1970). Hyperbolic two-dimensional electrostatic lens taking account of aperture effects. *J. Inst. Elec. Eng. Japan* **90**, 2587−2594. *Elec. Eng. Japan* **90**(6), 265−272.

H. Yokota and T. Kishi (1987). Analytic potential expression of a three-plane parallel-electrode system with special apertures. *IEEE Trans Electron Dev.* **34**, 486−489.

H. Yokota and K. Nagami (1978). Modified hyperbolic electrostatic lens. *Trans. Inst. Elec. Eng. Japan* **98-A**, 489−493. *Elec. Eng. Japan* **98**, No. 9/10, 117.

H. Yokota and K. Nagami (1987). Optical properties of a symmetrical slit electron lens. *J. Phys. E: Sci. Instrum.* **20**, 444−447.

H. Yokota, T. Kishi and K. Nagami (1975). Aberrations of hyperbolic two-dimensional electrostatic lens with apertures. *Trans. Inst. Elec. Eng. Japan* **95-C**, 171−178.

T. J. M. Zouros, A. Kanellakopoulos, I. Madesis, A. Dimitriou, M. Fernández-Martín, G. Martínez and T. J. Mertzimekis (2015). The optimization of a 4-element input lens on a hemispherical deflector analyzer using SIMION. *Microsc. Microanal.* **21** (Suppl. 4), 148−153.

Part VII, Chapter 36

For early measurements of lens properties and comparison with theory, see Dosse (1941b), who gives references to related work. The spherical aberration of saturated objectives is discussed by Kunath et al. (1966) and measurements of probe-lens aberrations are given by Hanai et al. (1986). Objective or probe-lens design is considered by Honda et al. (1982), Sparrow et al. (1982), Yanaka (1986), Strojnik (1975, 1984), Greschner et al. (1976) and by Craven and Buggy (1981) and Craven and Scott (1985) who use the Munro programs to calculate the properties of a VG STEM; Koops (1969, 1972) and Koops et al. (1968/69) analyse lens combinations for use in microlithography, see also the reviews by Koops (1980) and Munro (1980a,b) and the study of a four-lens demagnifying system by Lenz (1988). Many aspects of magnetic lens design are examined by Alamir (1992, 1995a,b, 2000, 2001, 2002, 2003, 2004; El-Shahat et al., 2014) and see Ahmad et al. (2014) and Kadhem (2014). Cryo-lenses are the subject of papers by Lefranc et al. (1984), Iwatsuki et al. (1986) and Uchida and Heide (1986). Huang and Lei (1981) and Huang and Cheng (1982) describe a lens design with several coils, with which the axial field distribution can be shaped at will, which recalls the proposal by Glaser (1941d) for choosing the winding density to generate particular axial fields. On coil design, see Podbrdský (1988). Li et al. (1986) and Xie (1986) are concerned with field calculation. A gun incorporating a single-polepiece lens is described by Newman et al. (1987). On triple-polepiece lenses, see Anderson et al. (1975) for a condenser-objective design and Kubozoe et al. (1977) for a permanent-magnet projector. Some high current density designs are considered by Lund (1967) and Parker et al. (1976). Grümm (1956) pointed out that the analysis in Tretner's earlier papers was not suitable for antisymmetric fields, such as $B(z) = B_0 z(1 + z^2/a^2)^{-2}$, for which $B' \neq 0$, $B = 0$ at $z = 0$. An extreme lens design matched to an energy filter is analysed by Richardson and Muray (1988). For completeness, we mention an earlier paper by Glaser (1940b) dealing in general terms with the chromatic aberration and a patent protecting his lens with vanishing spherical aberration (Glaser, 1959). Many of the themes of this chapter are surveyed in Hawkes (1980a) and an extremely full bibliography with titles forms an appendix to Hawkes (1982). See also Lencová and Lenc (1989, 1990) and especially the long surveys by Tsuno (1997, 2009).

***

N. S. Abd-Hujazie (2006). Design of a compound lens (magnetic−electrostatic) for low voltage scanning electron microscope. Dissertation, Mosul, Iraq.

P. Adamec, A. Delong and B. Lencová (1995). Miniature magnetic electron lenses with permanent magnets. *J. Microsc. (Oxford)* **179**, 129−132.

J.-P. Adriaanse (1994). High-T_c superconductors and magnetic electron lenses. *Adv. Opt. Electron Microsc.* **14**, 1−120.

J.-P. Adriaanse, W. C. Heerens, K. D. van der Mast and P. van Zuylen (1991a). A thin film superconducting lens element for electron optics. *Supercond. Sci. Technol.* **4**, 495−498.

J.-P. Adriaanse, K. D. van der Mast and P. van Zuylen (1991b). First step towards application of high-temperature superconductors for planar magnetic lenses. *J. Vac. Sci. Technol. B* **9**, 2866−2869.

A. K. Ahmad, F. A. Ali, A. A. Al-Tabbakh and S. M. Juma (2014). Computer-aided-design of a magnetic lens using combined dynamic programming and artifical intelligence techniques. *Iraqi J. Appl. Phys.* **10** (1), 33−37.

A. S. A. Alamir (1992). Iron-free objective lenses. *J. Phys. D: Appl. Phys.* **25**, 1039−1041.

A. S. A. Alamir (1995a). Studies on condenser−objective lenses. *J. Microsc. (Oxford)* **179**, 137−142.

A. S. A. Alamir (1995b). A study on scaling symmetrical condenser−objective lenses. *J. Phys. III* **5**, 641−645.

A. S. A. Alamir (2000). High voltage and high current density objective lenses. *Chin. J. Phys. (Taiwan)* **38**, 139−145.

A. S. A. Alamir (2001). Magnetic electron lenses performance. *Optik* **112**, 507−510.

A. S. A. Alamir (2002). Iron-free objective lenses. II. *Eur. Phys. J. (Appl. Phys.)* **17**, 243−245.

A. S. A. Alamir (2003a). A study on the effect of current density on magnetic lenses. *Optik* **114**, 85−88.

A. S. A. Alamir (2003b). On the rotation-free and distortion-free systems. *Optik* **114**, 509−513.

A. S. A. Alamir (2003c). Spiral distortion of magnetic lenses with field of the form $B(z) \propto z^{-n}$, $n = 2, 3, 4$. *Optik* **114**, 525−528.

A. S. A. Alamir (2004). Ultimate performance of objective magnetic lens. *Ultramicroscopy* **101**, 241−246.

W. J. Al-Jubori [Kadhem] (2001). Inverse design of asymmetrical magnetic lenses in the absence of magnetic saturation. Dissertation, Al-Mustansiryah University, Baghdad.

M. A. Al-Khashab (1983). The electron optical limits of performance of single-polepiece magnetic electron lenses. Dissertation, Aston in Birmingham.

M. A. Al-Khashab (2001). New development of electron projector lenses. *Eng. Technol.* **20**, 591−601.

M. A. Al-Khashab and I. K. Abbas (1991). Optimized polepiece shape for single polepiece magnetic electron lenses. *Model. Simul. Control* **35** (3), 1−9.

M. A. Al-Khashab and A. A. Ahmad (2002). Strongly-excited projector lens in high-voltage electron microscope. *Dirasat (Pure Sci.)* **29** (1), 1−11.

M. A. Al-Khashab and A. A. H. Ahmad (2004). Some approaches to the projector lens polepiece geometry and their effect on magnetic flux lines. *Dirasat (Pure Sci.)* **31** (1), 22−29.

M. A. Al-Khashab and A. A. H. Ahmad (2005). Designing a double lens of optimized polepiece angle. *Dirasat (Pure Sci.)* **32** (2), 182−187.

M. A. Al-Khashab and A. E. Al-Abdullah (2006). The effect of the snout shape geometry of the polepiece on objective lens parameters. *Dirasat (Pure Sci.)* **33** (1), 28−34.

M. A. Al-Khashab and Al-Obaidy (2000). The theoretial limits of polepiece angle of the magnetic objective lenses. *J. Educ. Sci.* **40**, 81−99.

M. A. Al-Khashab and R. Y. Al-Salih (2013). New design of objective lens geometry for low voltage SEM. *Jordan J. Phys.* **6** (2), 87−94.

M. A. Al-Khashab and N. S. Hujazie (2010). Design of the objective magnetic and electrostatic lenses for low beam energies. *Dirasat (Pure Sci.)* **37** (2), 85−95.

M. A. Al-Khashab and N. S. Hujazie (2011). The electron optical performance of the Gemini lens design for low voltage scanning electron microscope. *Dirasat (Pure Sci.)* **38** (1), 52−59.

H. N. Al-Obaidi (1995). Determination of the design of magnetic electron lenses operated under preassigned magnification conditions. Dissertation, Baghdad.

K. Anderson, K. A. Brookes and D.C. Fibow (1975). The double-field condenser objective lens. EMSA, Las Vegas, **33**, 136–137.

N. Baba and K. Kanaya (1979). General theory of the magnetic einzel lens based on the axial field distribution model $H(z) = H_0C(|z/a|^{m-1})/(1 + |z/a|^{2m})$. *J. Phys. E: Sci. Instrum.* **12**, 525–537.

J. M. Baldwin, R. Henderson, E. S. Beckman and F. Zemlin (1988). Images of purple membrane at 2.8 Å resolution obtained by cryo-electron microscopy. *J. Mol. Biol.* **202**, 585–591.

J.-L. Balladore and R. Murillo (1977). Nouveau type de lentille magnétique pour microscope électronique. *J. Microsc. Spectrosc. Electron* **2**, 211–222.

J.-L. Balladore, R. Murillo, J. Trinquier and B. Jouffrey (1977). New type of magnetic lens for electron microscopy. HVEM-5, Kyoto. 41–44.

J.-L. Balladore, R. Murillo, P. W. Hawkes, J. Trinquier and B. Jouffrey (1981). Magnetic electron lenses for high voltage microscopes. *Nucl. Instrum. Meth.* **187**, 209–215.

J.-L. Balladore, R. Murillo and J. Trinquier (1984). Various attempts to reduce the dimensions of magnetic electron lenses used for high voltage microscopes. In *Electron Optical Systems for Microscopy, Microanalysis and Microlithography* (J. J. Hren, F. A. Lenz, E. Munro and P. B. Sewell, Eds), 29–35 (Scanning Electron Microscopy, AMF O'Hare).

R. Bassett and T. Mulvey (1969a). Iron-free lenses for electron probe-forming systems. In *Proc. Fifth Int. Cong. X-ray Optics and Microanalysis, Tübingen 1968* (G. Möllenstedt and K.-H. Gaukler, Eds), 224–230 (Springer, Berlin).

R. Bassett and T. Mulvey (1969b). Flat helical electron-optical lenses. *Z. Angew. Phys.* **27**, 142–145.

M. Bauer (1968). Pole piece saturation in magnetic electron lenses. *J. Phys. E: Sci. Instrum.* **1**, 1081–1089.

S. Beck, E. Plies and B. Schiebel (1995). Low-voltage probe forming columns for electrons. *Nucl. Instrum. Meth. Phys. Res. A* **363**, 31–42.

H. Becker and A. Wallraff (1940). Bildfehleruntersuchungen an einer bilddrehungsfreien magnetischen Linse. *Arch. Elektrotech.* **34**, 115–120.

S. Bertram (1940). Determination of the axial potential distribution in axially symmetric electrostatic fields. *Proc. Inst. Radio. Eng.* **28**, 418–420.

C. S. Biddlecombe and C. W. Trowbridge (1984). CAE of electromagnetic devices. *Computer-Aided Eng. J.* **1**, 84–90.

H. Boersch, O. Bostanjoglo and K. Grohmann (1966). Supraleitender Hohlzylinder als magnetische Linse. *Z. Angew. Phys.* **20**, 193–194.

P. Bonjour (1969). Eléments cardinaux et coefficients d'aberration de lentilles supraconductrices à pôles d'holmium. *C. R. Acad. Sci. Paris B* **268**, 23–26.

P. Bonjour (1974). Une lentille magnétique supraconductrice à pôles d'holmium pour microscopie à très haute tension. *J. Microsc. (Paris)* **20**, 219–239.

P. Bonjour (1975a). New shapes for magnetic superconducting lenses for high voltage microscopy. *IEEE Trans. Magn.* **11**, 1470–1471.

P. Bonjour (1975b). Proposed designs for superconducting lenses for high voltage electron microscopes. *J. Phys. E: Sci. Instrum.* **8**, 761–763.

P. Bonjour (1975c). High field superconducting electron lenses with holmium polepieces. *J. Phys. E: Sci. Instrum.* **8**, 764–768.

P. Bonjour (1976). Superconducting lenses: present trends and design. EUREM-6, Jerusalem. **1**, 73–78.

P. Bonjour and A. Septier (1967a). Lentilles magnétiques supraconductrices à pièces polaires en métaux des terres rares. *C. R. Acad. Sci. Paris B* **264**, 747–750.

P. Bonjour and A. Septier (1967b). Caractéristiques optiques d'une lentille supraconductrice à pôles de dysprosium. *C. R. Acad. Sci. Paris B* **265**, 1392–1395.

P. Bonjour and A. Septier (1968). Eléments cardinaux et coefficients d'aberration des lentilles supraconductrices à pôles en metal de terres rares. EUREM-4, Rome. **1**, 189–190.

B. Bormans and P. Hagemann (1986). The twin lens system – a high resolution objective lens at 300 kV. EMSA, Albuquerque, **44**, 610–613.

K. A. Brookes, T. Mulvey and M. J. Wallington (1968). Magnetic electron lenses of minimum spherical and chromatic aberration. EUREM-4, Rome. **1**, 165–166.

S. Chandran and B. Biswas (2015). A double pole-gap design for low spherical aberration in thin solenoids. *Nucl. Instrum. Methods Phys. Res. A* **798**, 121–126.

J. N. Chapman and J. P. Jakubovics (1981). Observation of magnetic domain structures in thin foils at low temperatures by transmission electron microscopy. *Phys. Stat. Sol. (a)* **67**, K1–K3.

W.-x Chen (1988). How does polepiece saturation affect the spherical and chromatic aberration coefficient of the magnetic lenses? *J. Chin. Electron Microsc. Soc.* **7**, 55–66.

J. Chmelík, L. Veneklasen and G. Marx (1989). Comparing cathode lens configurations for low energy electron microscopy. *Optik* **83**, 155–160.

S. Christofides and T. Mulvey (1980). A high flux density single polepiece objective lens. EUREM-7, The Hague. **1**, 70–71.

J. R. A. Cleaver (1978). Some optical characteristics of the saturated symmetrical condenser–objective lens. *Optik* **49**, 413–431.

J. R. A. Cleaver (1978). Field emission electron gun systems incorporating single-pole magnetic lenses. *Optik* **52**, 293–303.

J. R. A. Cleaver (1979). The single-pole magnetic lens as a condenser for use with field-emission electron guns. EMAG, Brighton. 55–58.

J. R. A. Cleaver (1980). The choice of polepiece shape and lens operating mode for magnetic objective lenses with saturated polepieces. *Optik* **57**, 9–34.

J. R. A. Cleaver (1981). The off-axis aberrations of magnetic objective lenses with saturated polepieces. *Optik* **58**, 409–432.

C. J. Cooke and P. Duncumb (1969). Performance analysis of a combined electron microscope and electron probe microanalyser "EMMA". In *Proc. Fifth Int. Cong. X-ray Optics and Microanalysis, Tübingen 1968* (G. Möllenstedt and K.-H. Gaukler, Eds), 245–247 (Springer, Berlin).

E. Coufalová and A. Delong (2000). Low voltage electron microscope. II. Applications. EUREM-12, Brno. **3**, I183–I184.

E. Coufalová, M. Mynář, P. Štěpán, M. Drštička and I.M. Sintorn (2014). Low voltage mini TEM. ICM-18, Prague. IT-1-P-2685.

E. Coufalová, M. Mynář, P. Štěpán, M. Drštička and V. Kolařík (2015). Low voltage TEM from 10 kV to 25 kV. MCM-12, Eger. 278–280.

E. Coufalová, E. Pavlova, M. Šlouf, P. Štěpán, M. Dřstička, V. Kolařík, et al. (2017). Comparison of LVEM5, LVEM25 and standard TEM. MC-2017, Lausanne, 501–502.

A. J. Craven and T. W. Buggy (1981). Design considerations and performance of an analytical STEM. *Ultramicroscopy* **7**, 27–37.

A. J. Craven and C. P. Scott (1985). The effect of systematic variation of the data in the Munro programs on the predicted optical properties of a high excitation STEM objective lens. EMAG, Newcastle-upon-Tyne. 105–108.

A. V. Crewe (1976). Design trends in the STEM. EUREM-6, Jerusalem. **1**, 65–66.

A. V. Crewe (2001). On the peculiarities of monopole and multipole focusing. *Optik* **112**, 181–183.

A. V. Crewe (2004). Electron focusing in magnetic fields of the form z^n. *Optik* **115**, 31–35.

A. V. Crewe and D. Kielpinski (1996). Magnetic dipole lenses. EUREM-11, Dublin. **1**, 357–358.

M. L. De (1962). On an analytical expression for the axial field of electromagnetic lenses. *Philos. Mag.* **7**, 1065–1067.

M. L. De and D. K. Saha (1954). Distortion in electron lens. *Indian J. Phys.* **28**, 263–268.

A. Delong (1992). Low voltage TEM. EUREM-10, Granada. **1**, 79–81.

A. Delong (1993). Instruments development. MCEM, Parma. *Microsc. Elettron.* **14** (2), Suppl., 341–344.

A. Delong (1994). Low voltage TEM – possibilities and limitations. ICEM-13, Paris. **1**, 237–238.

A. Delong, V. Kolařík and D. Martin (1998). Low voltage transmission electron microscope LVEM-5. ICEM-14, Cancún. **1**, 463–464.

A. Delong, K. Hladil, V. Kolařík and P. Pavelka (2000). Low voltage electron microscope. I. Design. EUREM-12, Brno. **3**, I197–I198.

A. Delong, E. Coufalová and P. Štěpán (2002). Low voltage STEM. ICEM-15, Durban. **1**, 107–108.

G. V. Der-Shvarts (1970). Approximate analytical expresions for calculating the spherical aberration constant of axially symmetric magnetic lenses with yokes. *Elektrofiz. Elektrokhim. Met. Obrabot. Vyp.* **4**, 7–10.

G. V. Der-Shvarts (1971). Calculation of the spherical aberration of axially symmetric magnetic lenses. *Radiotekh. Elektron.* **16**, 1305–1306. *Radio Eng. Electron. Phys.* **16**, 1240–1241.

G. V. Der-Shvarts and I. S. Makarova (1967). Calculation of the spherical aberration of axisymmetric magnetic lenses. *Radiotekh. Elektron.* **12**, 168–171. *Radio Eng. Electron. Phys.* **12**, 161–163.

G. V. Der-Shvarts and I. S. Makarova (1972). Third-order field aberrations of axially symmetrical magnetic lenses. *Izv. Akad. Nauk SSSR. (Ser. Fiz.)* **36**, 1304–1311. *Bull. Acad. Sci. USSR* (*Phys. Ser.*) **36**, 1164–1170.

G. V. Der-Shvarts and I. S. Makarova (1973). Simple formulae for an approximate calculation of the third-order aberration coefficients of thin, axially symmetric, one-slit magnetic lenses. *Radiotekh. Elektron.* **18**, 2374–2378. *Radio Eng. Electron. Phys.* **18**, 1722–1725.

G. V. Der-Shvarts and I. S. Makarova (1976). On the calculation of the spherical aberration of axisymmetric magnetic lenses. *Radiotekh. Elektron.* **11**, 89–93. *Radio Eng. Electron. Phys.* **11**, 27–75.

G. V. Der-Shvarts and V. P. Rachkov (1965). Some electron optical properties of double-gap lenses. *Radiotekh. Elektron.* **10**, 922–928. *Radio Eng. Electron. Phys.* **10**, 783–789.

I. Dietrich (1976). *Superconducting Electron-Optic Devices* (Plenum, New York & London).

I. Dietrich (1978). Superconducting lenses. ICEM-9, Toronto. **3**, 173–184.

I. Dietrich, H. Pfisterer and R. Weyl (1969). Eine supraleitende Linse für das Elektronenmikroskop. *Z. Angew. Phys.* **28**, 35–39.

I. Dietrich, R. Weyl and H. Zerbst (1970). Electronoptical testing on the rotational symmetry of a superconducting lens. ICEM-7, Grenoble. **2**, 101–102.

I. Dietrich, A. Koller and G. Lefranc (1972a). Feldverteilung in eisenfreien supraleitenden Linsen. *Optik* **35**, 468–478.

I. Dietrich, R. Weyl and H. Zerbst (1972b). An electron optical 400 kV-system for testing a superconducting lens. EUREM-5, Manchester. 120–121.

I. Dietrich, G. Lefranc, R. Weyl and H. Zerbst (1973). Supraleitendes Abbildungssystem hoher Auflösung für die Elektronenmikroskopie. *Optik* **38**, 449–453.

I. Dietrich, F. Fox, R. Weyl and H. Zerbst (1974). A high-voltage superconducting lens. HVEM-3, Oxford. 103–107.

I. Dietrich, E. Knapek, R. Weyl and H. Zerbst (1975). Superconducting lenses in electron microscopy. *Cryogenics* **15**, 691–699.

I. Dietrich, F. Fox, E. Knapek, G. Lefranc, K. Nachtrieb, R. Weyl, and H. Zerbst (1976). High resolution imaging with a superconducting electron microscope lens system with helium cooled specimen stage. EUREM-6, Jerusalem. **1**, 405–407.

I. Dietrich, F. Fox, E. Knapek, G. Lefranc, K. Nachtrieb, R. Weyl and H. Zerbst (1977). Improvements in electron microscopy by application of superconductivity. *Ultramicroscopy* **2**, 241–249.

I. Dietrich, G. Lefranc, K. H. Müller and A. Stemmer (1980). Testing of a superconducting lens system for commercial microscopes. EUREM-7, The Hague. **1**, 84–85.

A. L. Dodin and M. B. Nesvizhskii (1980). Magnetic lenses with discontinuous fields. *Zh.Tekh. Fiz.* **50**, 38–41. *Sov. Phys. Tech. Phys.* **25**, 19–21.

J. Dosse (1941a). Strenge Berechnung magnetischer Linsen mit unsymmetrischer Feldform nach $H = \frac{H_0}{1+(z/a)^2}$. *Z. Phys.* **117**, 316–321.

J. Dosse (1941b). Über optische Kenngrößen starker Elektronenlinsen. *Z. Phys.* **117**, 722–753.

J. Dosse (1941c). Ergänzung zur Arbeit "Über optische Kenngrößen starker Elektronenlinsen". *Z. Phys.* **118**, 375–383.

J. Dugas, P. Durandeau and C. Fert (1961). Lentilles électroniques magnétiques symétriques et dissymétriques. *Rev. Opt.* **40**, 277–305.

P. Durandeau (1956a). Construction des lentilles électroniques magnétiques. *J. Phys. Radium* **17**, 18A–25A.

P. Durandeau (1956b). Lentilles électroniques magnétiques: expressions simples et générales du champ sur l'axe et des caractéristiques électrooptiques. *J. Phys. Radium* **17**, 33S–35S.
P. Durandeau (1957). Etude sur les lentilles électroniques magnétiques. *Ann. Fac. Sci. Univ. Toulouse* **21**, 1–88.
P. Durandeau and C. Fert (1957). Lentilles électroniques magnétiques. *Rev. Opt.* **36**, 205–234.
H. H. El-Kamali and T. Mulvey (1977). Improved viewing arrangements in the TEM. EMAG, Glasgow. 33–34.
H. H. El-Kamali and T. Mulvey (1979). A double lens system for the correction of spiral distortion. EMAG, Brighton. 63–64.
H. H. El-Kamali and T. Mulvey (1980). A wide-angle TEM projection system. EUREM-7, The Hague. **1**, 74–75.
S. S. El-Shahat, G. S. Hassan and A. S. A. Al Amir (2014). The effect of the lens size on performance of the single pole magnetic lens. *J. Sci. Res. Phys. Math. Sci.* **1** (5), 8–21.
H. Fernández-Morán (1965). Electron microscopy with high-field superconducting solenoid lenses. *Proc. Natl. Acad. Sci. U.S.A.* **53**, 445–451.
C. Fert and P. Durandeau (1967). Magnetic electron lenses. In *Focusing of Charged Particles* (A. Septier, Ed.), **1**, 309–352 (Academic Press, New York & London).
L. A. Fontijn, A. B. Bok and J. G. Kornet (1969). The TPD electron probe X-ray micro analyzer. In *Proc. Fifth Int. Cong. X-ray Optics and Microanalysis, Tübingen 1968* (G. Möllenstedt and K.-H. Gaukler, Eds), 261–268 (Springer, Berlin).
J. C. Francken (1967). Analogical methods for resolving Laplace's and Poisson's equations. In *Focusing of Charged Particles* (A. Septier, Ed.), **1**, 45–162 (Academic Press, New York & London).
J. C. Francken (1972). On the design of a condensor–objective lens for a low-voltage electron microscope. EUREM-5, Manchester. 124–125.
J. C. Francken and A. Heeres (1973). Telescopic condenser–objective lenses for electrons. *Optik* **37**, 483–500.
L. Frank (2016). Scanning electron microscopy with a retarded primary beam. In *Modern Electron Microscopy in Physical and Life Sciences* (M. Janeček and R. Král, Eds), 49–78 (InTech, London and Rijeka).
J. Frank, W. Chiu and R. Henderson (1993). Flopping polypeptide chains and SULEIKA's subtle imperfections: analysis of variations in the electron micrograph of a purple membrane crystal. *Ultramicroscopy* **49**, 387–396.
J. Frosien and E. Plies (1987). High performance electron optical column for testing ICs with submicrometer design rules. *Microelectron. Eng.* **7**, 163–172.
J. Frosien, E. Plies and K. Anger (1989). Compound magnetic and electrostatic lenses for low-voltage applications. *J. Vac. Sci. Technol. B* **7**, 1874–1877.
D. Génotel, C. Séverin and A. Laberrigue (1967a). Lentilles magnétiques à enroulements supraconducteurs en microscopie électronique. *J. Microsc. (Paris)* **6**, 933–944.
D. Génotel, A. Laberrigue, P. Levinson and C. Séverin (1967b). Caractéristiques optiques de lentilles magnétiques supraconductrices à très grand champ. *C. R. Acad. Sci. Paris* **265**, 226–229.
D. Génotel, G. Balossier, C. Séverin, M. Girard, J.-C. Homo and A. Laberrigue (1971). Microscope supraconducteur 400 kV. *C. R. Acad. Sci. Paris* **272**, 1461–1464.
U. F. Gianola (1952). Investigation of magnetic lenses having the axial field $H(0,z) = \gamma/z^n$. *Proc. Phys. Soc. (Lond.) B* **65**, 597–603.
W. Glaser (1940a). Über ein von sphärischer Aberration freies Magnetfeld. *Z. Phys.* **116**, 19–33.
W. Glaser (1940b). Die Farbabweichung bei Elektronenlinsen. *Z. Phys.* **116**, 56–67.
W. Glaser (1940c). Über den Öffnungsfehler der Elektronenlinsen. Bemerkungen zu vorstehender Erwiderung. *Z. Phys.* **116**, 734–735. This refers to Rebsch (1940).
W. Glaser (1941a). Strenge Berechnung magnetischer Linsen der Feldform $H = \frac{H_0}{1+(z/a)^2}$. *Z. Phys.* **117**, 285–315.
W. Glaser (1941b). Über die zu einem vorgegebenen Magnetfeld gehörende Windungsdichte einer Kreispule. *Z. Phys.* **118**, 264–268.
W. Glaser (1952). *Grundlagen der Elektronenoptik* (Springer, Vienna).
W. Glaser (1956a). Zum Öffnungsfehler magnetischer Elektronenlinsen. *Optik* **13**, 7–12 & 478.
W. Glaser (1956b). Elektronen- und Ionenoptik. *Handbuch der Physik* **33**, 123–395.
W. Glaser (1959). Imaging apparatus. US Patent 2,906,879.

W. Glaser and W. Lammel (1943). Strenge Berechnung der elektronenoptischen Aberrationskurven eines typischen Magnetfeldes. *Arch. Elektrotech.* **37**, 347–356.

W. Glaser and F. Lenz (1951). Berechnung der elektronenoptischen Abbildung durch drei typische, starke Magnetlinsen und ihr Zusammenhang mit der gewöhnlichen Linsengleichung. *Ann. Phys. (Leipzig)* **9** (444), 19–28.

J. Gratsiatos (1937). Die Bildfehler der schwachen magnetischen Elektronenlinsen. *Z. Phys.* **107**, 382–386.

F. Gray (1939). Electrostatic electron-optics. *Bell Syst. Tech. J.* **18**, 1–31.

J. Greschner, D. Kern and R. Speidel (1976). Ein Elektronenstrahl-Mikroschreiber hoher Sondenstromdichte und großer Bildpunktzahl. *Optik* **45**, 269–279.

P. Grivet (1951). Un nouveau modèle mathématique de lentille électronique. *C. R. Acad. Sci. Paris* **233**, 921–923.

P. Grivet (1952a). Eléments cardinaux d'un nouveau modèle de lentille électronique. *C. R. Acad. Sci. Paris* **234**, 73–75.

P. Grivet (1952b). Un nouveau modèle mathématique de lentille électronique. *J. Phys. Radium* **13**, 1A–9A.

P. Grivet (1972). *Electron Optics* (Pergamon, Oxford).

H. Grümm (1956). Zur Frage der unteren Grenze des Öffnungsfehlers bei magnetischen Elektronenlinsen. *Optik* **13**, 92–93.

C.-x. Gu and N.-q. Chen (1984). The optimization design of an electron-optical system [in Chinese]. *Acta Electron. Sin.* **12**, 41–47.

C.-x. Gu and L.-y. Shan (1984). Constrained optimization design of an electron optical system. In *Electron Optical Systems for Microscopy, Microanalysis and Microlithography* (J. J. Hren, F. A. Lenz, E. Munro and P. B. Sewell, Eds), 91–96 (Scanning Electron Microscopy, AMF O'Hare).

E. Hahn (1965a). Theorie der elektrisch-magnetischen Linsen bei Zugrundelegung einer natürlichen Maßbestimmung der Achsenabszisse. *Jenaer Jahrbuch*, 107–145.

E. Hahn (1965b). Feldfunktionen und Kardinalelemente der Magnetlinsen vom Typus des Glaserschen Glockenfeldes und des Stufenfeldes. *Exp. Tech. Phys.* **13**, 375–392.

T. Hanai, M. Hibino and S. Maruse (1986). A shadow image method for measurements of axial geometrical aberrations of a probe-forming lens. ICEM-11, Kyoto. **1**, 307–308.

H. Hänsel (1964). Über eine magnetische Feldverteilung mit exakt lösbarer Paraxialgleichung. *Optik* **21**, 273–280.

T. Haraguchi, T. Sakazaki, S. Hamaguchi and H. Yasuda (2002). Development of electromagnetic lenses for multielectron beam lithography system. *J. Vac. Sci. Technol. B* **20**, 2726–2729.

D. F. Hardy (1973). Superconducting electron lenses. *Adv. Opt. Electron Microsc.* **5**, 201–237.

P. W. Hawkes (1968a). The dependence of the spherical aberration coefficient of an electron optical objective lens on object position and magnification. *J. Phys. D: Appl. Phys.* **1**, 131–133.

P. W. Hawkes (1968b). The relation between the spherical aberration and distortion coefficients of electron probe-forming and projector lenses. *J. Phys. D: Appl. Phys.* **1**, 1549–1558.

P. W. Hawkes (1970). Can objective spherical aberration be expressed as a polynomial of fourth degree in reciprocal magnification? A study of the Grivet–Lenz model. *J. Microsc. (Paris)* **9**, 435–454.

P. W. Hawkes (1973). Computer-aided design of electron lens combinations. In *Image Processing and Computer-Aided Design in Electron Optics* (P. W. Hawkes, Ed.), 230–248 (Academic Press, London & New York).

P. W. Hawkes (1974). A note on the structure of the aberration coefficients of bell-shaped fields. ICEM-8, Canberra. **1**, 156–157.

P. W. Hawkes (1980a). Methods of computing optical properties and combating aberrations for low-intensity beams. In *Applied Charged Particle Optics* (A. Septier, Ed.), 45–157 (Academic Press, New York & London). *Adv. Electron. Electron Phys.* Suppl. 13A.

P. W. Hawkes (1980b). Some approximate magnetic lens aberration formulae: a commentary. *Optik* **56**, 293–320.

P. W. Hawkes, Ed. (1982). *Magnetic Electron Lenses* (Springer, Berlin & New York).

P. W. Hawkes (2002). On the optical properties of magnetic lenses with fields of the form $B(z) \propto z^{-n}$, $n = 2, 3, 4$. *Optik* **113**, 273–275.
P. W. Hawkes (2004). Electron focusing in magnetic fields of the form z^n by A.V. Crewe, a footnote. *Optik* **115**, 528.
P. W. Hawkes and U. Valdrè (1977). Superconductivity and electron microscopy. *J. Phys. E: Sci. Instrum.* **10**, 309–328.
K. Heinemann (1971). In-situ measurement of objective lens data of a high-resolution electron microscope. *Optik* **34**, 113–128.
R. Henderson, J. M. Baldwin, K. H. Downing, J. Lepault and F. Zemlin (1986). Structure of purple membrane from *Halobacterium halobium*: recording, measurement and evaluation of electron micrographs at 3.5 Å resolution. *Ultramicroscopy* **19**, 147–178.
R. Henderson, J. M. Baldwin, T. A. Ceska, F. Zemlin, E. Beckmann and K. H. Downing (1990). Model for the structure of bacteriorhodopsin based on high-resolution electron cryo-microscopy. *J. Mol. Biol.* **213**, 899–929.
M. B. Heritage (1971). Third-order aberrations of magnetic electron lenses. In *Rec. 11th Symp. Electron, Ion and Laser Beam Technology* (R. F. M. Thornley, Ed.), 219–228 (San Francisco Press, San Francisco).
M. B. Heritage (1973). The computation of the third-order aberration coefficients of electron lenses. In *Image Processing and Computer-Aided Design in Electron Optics* (P. W. Hawkes, Ed.), 324–338 (Academic Press, London & New York).
M. B. Hesse (1950). The calculation of magnetic lens fields by relaxation methods. *Proc. Phys. Soc. (Lond.)* **B63**, 386–401.
R. Hill and K. C. A. Smith (1980). An interactive computer system for magnetic lens analysis. EUREM-7, The Hague. **1**, 60–61.
R. Hill and K. C. A. Smith (1982). The single-pole lens as a scanning electron microscope objective. *Scanning Electron Microsc.* Pt. II, 465–471.
J. Hillier (1946). A study of distortion in electron microscope projection lenses. *J. Appl. Phys.* **17**, 411–419.
K. Hladil and A. Delong (1994). Multifunctional electrostatic octupole systems in the miniature low voltage transmission and scanning electron microscope. ICEM-13, Paris. **1**, 245–246.
J. Hodkinson and K. Tahir (1995). Saturated electron lens design using a second-order finite element method. *Proc. SPIE* **2522**, 264–269.
T. Honda, K. Tsuno and H. Watanabe (1982). Magnetic field distribution and optical properties of objective lens with 1.3 Å resolution in high voltage electron microscope. ICEM-10, Hamburg. **1**, 307–308.
R. Hooke and T. A. Jeeves (1961). "Direct search" solution of numerical and statistical problems. *J. Assoc. Comput. Machin.* **8**, 212–229.
W. Hoppe and R. Hegerl (1980). Three-dimensional structure determination by electron microscopy (nonperiodic specimens). In *Computer Processing of Electron Microscope Images* (P. W. Hawkes, Ed.), 127–185 (Springer, Berlin & New York).
W. Hoppe and D. Typke (1979). Three-dimensional reconstruction of aperiodic objects in electron microscopy. *Adv. Struct. Res. Diffr. Meth.* **7**, 137–190.
L. Y. Huang and S. C. Cheng (1982). A low aberration probe forming lens with large free space around the specimen. ICEM-10, Hamburg. **1**, 293–294.
L. Y. Huang and H. N. Lei (1981). Proposal for a new low aberration probe forming lens. *Scanning Electron Microsc.* Pt. I, 21–28.
R. G. E. Hutter (1945). The class of electron lenses which satisfy Newton's image relation. *J. Appl. Phys.* **16**, 670–678.
K. Ito, T. Ito, K. Kanaya and N. Morito (1950). Calculations on the magnetic lens. ICEM-2, Paris. **1**, 207–212.
M. Iwatsuki, H. Kihara, K. Nakanishi and Y. Harada (1986). Cryo electron microscope with superconducting lens. ICEM-11, Kyoto. **1**, 251–254.
O. Jandeleit and F. Lenz (1959). Berechnung der Bildfehlerkoeffizienten magnetischer Elektronenlinsen in Abhängigkeit von der Polschuhgeometrie und den Betriebsdaten. *Optik* **16**, 87–107.

J. Jiruše, M. Havelka and F. Lopour (2014). Novel field emission SEM column with beam deceleration technology. *Ultramicroscopy* **146**, 27–32.

J. Jiruše, M. Havelka and J. Polster (2016). Ultra-high resolution SEM for materials analysis. EMC-16, Lyon **1**, 404–405.

J. Jiruše, M. Havelka and J. Polster (2017). A new SEM column combining ultra-high resolution and flexible scanning. *Microsc. Microanal.* **23** (Suppl. 1), 38–39.

S. M. Juma (1986). Design parameters of an unconventional probe-forming lens. *J. Phys. E: Sci. Instrum.* **19**, 457–462.

S. M. Juma and A. A. Al-Shwaikh (1979). Single-polepiece objective and projector lenses for the electron microscope. EMAG, Brighton. 61–62.

S. M. Juma and A. D. Faisal (1981). Properties of the axial flux density distribution of magnetic electron lenses with a single cylindrical pole-piece. *J. Phys. E: Sci. Instrum.* **14**, 1389–1393.

S. M. Juma and T. Mulvey (1974). New rotation-free magnetic electron lenses. ICEM-8, Canberra. **1**, 134–135.

S. M. Juma and T. Mulvey (1975). A new experimental electron microscope with a rotation-free projector system. EMAG, Bristol. 45–48.

S. M. Juma and T. Mulvey (1978). Miniature rotation-free magnetic electron lenses for the electron microscope. *J. Phys. E: Sci. Instrum.* **11**, 759–764.

S. M. Juma and T. Mulvey (1979). The axial field distribution of single-polepiece lenses. EMAG, Brighton. 59–60.

S. M. Juma and T. Mulvey (1980). Some electron optical properties of single-polepiece projector lenses. EUREM-7, The Hague. **1**, 78–79.

S. M. Juma and A. A. Yahya (1984). Characteristics of the axial magnetic field of asymmetrical electron lenses. *J. Phys. E: Sci. Instrum.* **17**, 398–404.

S. M. Juma, I. S. Al-Nakeshli and M. A. A. Khaliq (1983a). Pole design in single pole piece projector electron lenses. *J. Phys. E: Sci. Instrum.* **16**, 171–176.

S. M. Juma, M. A. A. Khaliq and F. H. Antar (1983b). Some properties of single pole piece objective electron lenses. *J. Phys. E: Sci. Instrum.* **16**, 1063–1068.

W. J. Kadhem (2014). Reconstructed polepieces to the objective magnetic lens depending on some geometrical and physical parameters. *Adv. Phys. Theor. Appl* **31**, 43–52.

W. J. Kadhem (2015). Obtaining doublet magnetic lenses by synthesis technique. *Optik* **126**, 4066–4071.

W. J. Kadhem and H. N. Al-Obaidi (2013). An inverse design approach for magnetic lenses operated under infinite magnification condition. *Optik* **124**, 3523–3526.

W. Kamminga (1976). Properties of magnetic objective lenses with highly saturated pole pieces. *Optik* **45**, 39–54.

W. Kamminga, J. L. Verster and J. C. Francken (1968). Design considerations for magnetic objective lenses with unsaturated pole pieces. *Optik* **28**, 442–461.

K. Kanaya (1949a). Aberrations of compound magnetic lenses with pole pieces of double gaps [in Japanese]. *Bull. Electrotech. Lab.* **13**, 453–458.

K. Kanaya (1949b). Theory of aberrations for an axisymmetrical magnetic type electron microscope. *Res. Electrotech. Lab*. No. 495, 35 pp.

K. Kanaya (1951a). Spherical and chromatic aberrations in magnetic lenses for electron microscopes [in Japanese]. *Bull. Electrotech. Lab.* **15**, 86–91.

K. Kanaya (1951b). Distortion in magnetic lenses for electron microscopes [in Japanese]. *Bull. Electrotech. Lab.* **15**, 91–94.

K. Kanaya (1951c). Curvature of field and astigmatism in magnetic lenses for electron microscopes [in Japanese]. *Bull. Electrotech. Lab.* **15**, 193–198.

K. Kanaya (1951d). Coma in magnetic lenses for electron microscopes [in Japanese]. *Bull. Electrotech. Lab.* **15**, 199–202.

K. Kanaya (1954). On the field aberrations in the electron microscope [in Japanese, abstract in English]. *Denshikenbikyo* **3**, 167–170.

K. Kanaya (1955). Electron optic theory on the design of magnetic lenses for electron microscopes. *Res. Electrotech. Lab*. No. 548, 70 pp.
K. Kanaya, N. Baba and S. Ono (1976). Rigorous treatment of magnetic lens whose axial field distribution is given by $H(z/a) = H_0(1-\mu^2)^{(2m-1)/2}$. *Optik* **46**, 125–148.
M. Kato and K. Tsuno (1990). Optimization of electron lens shape giving minimum spherical aberration coefficient. *IEEE Trans. Magn.* **26**, 1023–1026.
A. Khursheed (2000). Magnetic axial field measurements on a high resolution miniature scanning electron microscope. *Rev. Sci. Instrum.* **71**, 1712–1715.
A. Khursheed, J. T. L. Thong, J. C. Phang and I. P. Ong (1997). Miniature scanning electron microscope design based upon the use of permanent magnets. *Proc. SPIE* **3155**, 175–184.
A. Khursheed, J. C. Phang and J. T. L. Thong (1998). A portable scanning electron microscope column design based on the use of permanent magnets. *Scanning* **20**, 87–91.
H. Kimura (1956). A new electron microscope excited with permanent magnets. APEM-1, Tokyo. 108–113.
H. Kimura (1959a). Permanent magnet lens systems of electron microscope. Part II, Various methods of changing the focal length and performances. *Denshikenbikyo* **8** (1), 36–43.
H. Kimura (1959b). Double-gap lens and its characteristics. *Denshikenbikyo* **8** (2–3), 2–3.
H. Kimura (1962). Electron lens system excited by permanent magnet. *J. Electron Microsc.* **11**, 10–17.
H. Kimura and Y. Idei (1957). Permanent magnet lens systems of electron microscope. Part I. Various lens systems and its characteristics. *Denshikenbikyo* **5** (2), 7–14.
H. Kimura and S. Katagiri (1959). An electron lens system excited by permanent magnets with a new astigmatism compensator. *Optik* **16**, 50–55.
H. Kimura and Y. Kikuchi (1958). Permanent magnetic lens systems and their characteristics. ICEM-4, Berlin. **1**, 53–57.
H. Kimura and Y. Kikuchi (1959). Permanent magnet lens systems and their characteristics. *J. Electron Microsc.* **7**, 1–14.
N. Kitamura, M. P. Schulhof and B. M. Siegel (1966). Superconducting lens for electron microscopy. *Appl. Phys. Lett.* **9**, 377–380.
O. Klemperer and M. E. Barnett (1971). *Electron Optics* (Cambridge University Press, Cambridge).
E. Knapek (1975). Modellversuche zur elektromagnetischen Justierung der supraleitenden Abschirmlinse. *Optik* **41**, 506–514.
E. Knapek (1976). Objektfreie Prüfung supraleitender Abschirmlinsen mit zwei verschiedenen teleskopischen Strahlengängen. *Optik* **46**, 97–106.
Y. Kohno, S. Morishita and N. Shibata (2017a). Development of Lorentz objective lens for high resolution imaging. *Kenbikyo* **52** (Suppl. 1), 24.
Y. Kohno, S. Morishita and N. Shibata (2017b). Development of magnetic field free lens for atomic resolution imaging. MC-2017, Lausanne, 505-506.
Y. Kohno, S. Morishita and N. Shibata (2017c). New STEM/TEM objective lens for atomic resolution Lorentz imaging. *Microsc. Microanal.* **23** (Suppl. 1), 456–457.
H. Koops (1969). Verwendung der Kondensor-Objektiv-Einfeldlinse zur elektronenoptischen Mikrominiaturisation. *Optik* **29**, 119–121.
H. Koops (1972). Elektronenoptische Verkleinerung durch Kombination einer langbrennweitigen Feldlinse mit einer starken kurzbrennweitigen Magnetlinse. *Optik* **36**, 93–110.
H. Koops (1980). Electron beam projection techniques. In *Fine Line Lithography* (R. Newman, Ed.), 233–335 (North-Holland, Amsterdam, New York & Oxford).
H. Koops, G. Möllenstedt and R. Speidel (1968). Zur elektronenoptischen Mikrominiaturisation von Schablonen. *Optik* **28**, 518–531.
L. Kordas (1982). A charge simulation method for the calculation of the single-polepiece lens field distribution. ICEM-10, Hamburg. **1**, 337–338.
P. Kruit and M. Lenc (1992). Optical properties of the magnetic monopole field applied to electron microscopy and spectroscopy. *J. Appl. Phys.* **72**, 4505–4513.

M. Kubozoe, H. Sato, S. Kasai and S. Ozasa (1977). An electron microscope for high quality low magnification with a wide field. EMSA, Boston. **35**, 88–89.

W. Kunath and W. D. Riecke (1965). Zur Bestimmung der Öffnungsfehlerkoeffizienten magnetischer Objektivlinsen. *Optik* **23**, 322–342.

W. Kunath, W. D. Riecke and E. Ruska (1966). Spherical aberration of saturated strong objective lenses. ICEM-6, Kyoto. **1**, 139–140.

D. Kynaston and T. Mulvey (1962). Distortion-free operation of the electron microscope. ICEM-5, Philadelphia. **1**, D-2.

D. Kynaston and T. Mulvey (1963). The correction of distortion in the electron microscope. *Br. J. Appl. Phys.* **14**, 199–206.

A. Laberrigue and P. Levinson (1964). Utilisation des propriétés des fils supraconducteurs en microscopie électronique. *C. R. Acad. Sci. Paris* **259**, 530–532.

A. Laberrigue and C. Séverin (1967). Caractéristiques optiques de lentilles magnétiques sans fer à enroulements supraconducteurs en microscopie électronique. *J. Microsc. (Paris)* **6**, 123–133.

A. Laberrigue, P. Levinson, G. Beriot and P. Bonhomme (1967). Objectifs supraconducteurs utilisés en microscopie électronique. Premiers résultats. *Ann. Univ. ARERS* **5**, 50–54.

A. Laberrigue, P. Levinson and J.-C. Homo (1971). Microscope électronique 400 kV à lentilles supraconductrices. 1. Description générale du cryostat et du montage. *Rev. Phys. Appl.* **6**, 453–458.

A. Laberrigue, D. Génotel, M. Girard, C. Séverin, G. Balossier and J.-C. Homo (1973). A 400 kV superconducting electron microscope: performance, viability, and possibilities in the 3 MV range. HVEM-3, Oxford. 108–113.

A. Laberrigue, G. Balossier, D. Génotel, J.-C. Homo and C. Séverin (1976). Un nouveau cryotat pour le microscope électronique supraconducteur 400 kV. *Rev. Phys. Appl.* **11**, 685–687.

E. Lambrakis, F. Z. Marai and T. Mulvey (1977). Correction of spiral distortion in the transmission electron microscope. EMAG, Glasgow. 35–38.

J. B. Le Poole (1964). Miniature lens. EUREM-3, Prague. Appendix, 6.

G. Lefranc and K.-H. Müller (1981). Asymmetric superconducting shielding lens for TEM and STEM. EMAG, Cambridge. 91–94.

G. Lefranc and K. Nachtrieb (1979). A superconducting lens system for electron microscopes with beam voltages up to 500 kV. EMAG, Brighton. 31–34.

G. Lefranc, K.-H. Müller and I. Dietrich (1981). A superconducting lens system operated in the fixed-beam and the scanning mode. *Ultramicroscopy* **6**, 81–84.

G. Lefranc, E. Knapek and I. Dietrich (1982). Superconducting lens design. *Ultramicroscopy* **10**, 111–123.

G. Lefranc, H. Anzinger, E. Knapek and I. Dietrich (1984). Some data of a superconducting lens with iron circuit. EMSA, Detroit. **42**, 626–627.

M. Lenc (1992). Immersion objective lenses in electron optics. Dissertation, Delft.

M. Lenc and B. Lencová (1984). Saturated single polepiece objective lenses. EUREM-8, Budapest. **1**, 27–28.

B. Lencová (1980). Numerical computation of electron lenses by the finite element method. *Comput. Phys. Commun.* **20**, 127–132.

B. Lencová (2015). Influence of saturation of magnetic lens material on fields of deflectors and parasitic fields. *Microsc. Microanal.* **21** (Suppl. 4), 188–193.

B. Lencová and M. Lenc (1982). Infinite elements for the computation of open lens structures. ICEM-10, Hamburg. **1**, 317–318.

B. Lencová and M. Lenc (1984). The computation of open electron lenses by coupled finite element and boundary integral methods. *Optik* **68**, 37–60.

B. Lencová and M. Lenc (1986). A finite element method for the computation of magnetic electron lenses. *Scanning Electron Microsc.* Pt. III, 897–915.

B. Lencová and M. Lenc (1989). Paraxial trajectory computation in magnetic electron lenses. *Optik* **82**, 64–68.

B. Lencová and M. Lenc (1990). Computation of multi-lens focusing systems. *Nucl. Instrum. Meth. Phys. Res. A* **298**, 45–55.

F. Lenz (1950a). Berechnung der Feldverteilung längs der Achse magnetischer Elektronenlinsen aus Polschuhabmessungen und Durchflutung. *Optik* **7**, 243–253.

F. Lenz (1950b). Annäherung von rotationssymmetrischen Potentialfeldern mit zylindrischen Äquipotentialflächen durch eine analytische Funktion. *Ann. Phys. (Leipzig)* **8** (443), 124–128.

F. Lenz (1950c). Berechnung optischer Kenngrößen magnetischer Elektronenlinsen vom erweiterten Glockenfeldtyp. *Z. Angew. Phys.* **2**, 337–340.

F. Lenz (1950d). Berechnung optischer Kenngrößen magnetischer Elektronenlinsen aus Polschuhabmessungen und Betriebsdaten. *Z. Angew. Phys.* **2**, 448–453.

F. Lenz (1951). Berechnung der elektronenoptischen Kenngrößen eines speziellen magnetischen Linsenfeldes ohne numerische Bahnintegrationen. *Ann. Phys. (Leipzig)* **9** (444), 245–258.

F. Lenz (1952). Ein einfaches Verfahren zur Bestimmung der Feldform magnetischer Elektronenlinsen. *Optik* **9**, 3–18.

F. Lenz (1956a). Ein mathematisches Modellfeld für eine permanentmagnetische Einzellinse. *Z. Angew. Phys.* **8**, 492–496.

F. Lenz (1956b). Über asymptotische Bildfehler. EUREM-1, Stockholm. 48–51.

F. Lenz (1957). Über asymptotische Bildfehler. *Optik* **14**, 74–82.

F. Lenz (1982). Properties of electron lenses. In *Magnetic Electron Lenses* (P. W. Hawkes, Ed.), 119–161 (Springer, Berlin & New York).

F. Lenz (1988). Optimization of the imaging properties of an electron optical demagnifying system consisting of four magnetic lenses. *Optik* **78**, 135–140.

Z. Li, H. Zhou and G. Shen (1986). An integral equation method for the analysis of the iron-shielded magnetic lens. ICEM-11, Kyoto. **1**, 291–292.

G. Liebmann (1952). Magnetic electron microscope projector lenses. *Proc. Phys. Soc. (Lond.) B* **65**, 94–108.

G. Liebmann (1955a). The magnetic pinhole electron lens. *Proc. Phys. Soc. (Lond.) B* **68**, 682–685.

G. Liebmann (1955b). A unified representation of magnetic electron lens properties. *Proc. Phys. Soc. (Lond.) B* **68**, 737–745.

G. Liebmann and E. M. Grad (1950). Imaging properties of a series of magnetic electron lenses. ICEM-2, Paris. **1**, 138–147.

G. Liebmann and E. M. Grad (1951). Imaging properties of a series of magnetic electron lenses. *Proc. Phys. Soc. (Lond.)* **B64**, 956–971.

N. D. Lund (1967). High ampère-turn density coils for the reduction of magnetic lens size. EMSA, Chicago **25**, 228–229.

M. E. C. Maclachlan (1973). Procedure for designing electron microscope imaging systems. Dissertation, Cambridge.

F. Z. Marai and T. Mulvey (1974). Electron optical characteristics of single-pole magnetic lenses. ICEM-8, Canberra. **1**, 130–131.

F. Z. Marai and T. Mulvey (1975). Electron-optical characteristics of single-pole and related magnetic electron lenses. EMAG, Bristol. 43–44.

F. Z. Marai and T. Mulvey (1977). Scherzer's formula and the correction of spiral distortion in the electron microscope. *Ultramicroscopy* **2**, 187–192.

L. Marton and K. Bol (1947). Spherical aberration of compound magnetic lenses. *J. Appl. Phys.* **18**, 522–529.

H. Miyokawa, H. Kazumori, S. Nakagawa and C. Nielsen (1995). Ultra-high resolution semi-in-lens type FE-SEM, JSM-6320F with strong magnetic field lens with built-in secondary electron detector. *MSA, Kansas City.*, 484–485.

R. W. Moses (1970). Minimum aperture aberrations of quadrupole lens systems. *Rev. Sci. Instrum.* **41**, 729–740.

R. W. Moses (1971a). Minimum chromatic aberrations of magnetic quadrupole objective lenses. *Rev. Sci. Instrum.* **42**, 828–831.

R. W. Moses (1971b). Quadrupole–octopole aberration correctors with minimum fields. *Rev. Sci. Instrum.* **42**, 832–839.

R. W. Moses (1972). Minimum spherical aberration of coma-free magnetic round lenses. EUREM-5, Manchester. 86–87.

R. W. Moses (1973). Lens optimization by direct application of the calculus of variations. In *Image Processing and Computer-Aided Design in Electron Optics* (P. W. Hawkes, Ed.), 250–272 (Academic Press, London & New York).

R. W. Moses (1974). Aberration correction for high-voltage electron microscopy. *Proc. R. Soc. (Lond.) A* **339**, 483–512.

K. Müller (1956). Über magnetostatische Linsenanordnungen mit mechanischen Regelgliedern. EUREM-1, Stockholm. 17–20.

K. Müller (1957). Regelbare magnetostatische Linsensysteme für Elektronenmikroskope. *Z. Wiss. Mikrosk.* **63**, 303–328.

K. Müller and E. Ruska (1958). Ein Hilfselektronenmikroskop für Kurs- und Routinebetrieb. ICEM-4, Berlin. **1**, 184–187.

K. Müller and E. Ruska (1968). Über ein einfaches und leistungsfähiges permanentmagnetisches Durchstrahlungs-Elektronenmikroskop. *Mikroskopie* **23**, 197–219.

K. Müller, E. Ruska and H. Neff (1969). The Elmiskop 51, a transmission electron-miroscope with permanent magnet magnification system. EMSA, St Paul. **27**, 74–75.

I. Müllerová and M. Lenc (1992). Some approaches to low-voltage scanning electron microscopy. *Ultramicroscopy* **41**, 399–410.

T. Mulvey (1971). Developments in magnetic electron lenses for electron microscopes and probe-forming systems. EMAG, Cambridge. 78–83.

T. Mulvey (1972). Progress in electron optics. EUREM-5, Manchester. 64–69.

T. Mulvey (1974). Mini-lenses and the SEM. *Scanning Electron Microsc.* Pt. I, 43–49.

T. Mulvey (1976). Design trends in TEM, STEM and SEM. EUREM-6, Jerusalem. **1**, 59–64.

T. Mulvey (1978). Instrumentation for electron diffraction. In *Electron Diffraction 1927–1977* (P. J. Dobson, J. B. Pendry and C. J. Humphreys, Eds), 295–312 (Institute of Physics, Bristol).

T. Mulvey (1980). Electron guns and instrumentation. EUREM-7, The Hague. **1**, 46–53.

T. Mulvey (1982a). Unconventional lens design. In *Magnetic Electron Lenses* (P. W. Hawkes, Ed.), 359–412 (Springer, Berlin & New York).

T. Mulvey (1982b). Magnetic electron lenses. ICEM-10, Hamburg. **1**, 277–284.

T. Mulvey (1984). Magnetic electron lenses. II. In *Electron Optical Systems for Microscopy, Microanalysis and Microlithography* (J. J. Hren, F. A. Lenz, E. Munro and P. B. Sewell, Eds), 15–27 (Scanning Electron Microscopy, AMF O'Hare).

T. Mulvey (1986). Unconventional lens design and columns. ICEM-11, Kyoto. **1**, 239–242.

T. Mulvey and L. Jacob (1949). Distortion-free electrostatic lenses. *Nature* **163**, 525–526.

T. Mulvey and H. Nasr (1979). Limitations of the finite element method. EMAG, Brighton. 53–54.

T. Mulvey and H. Nasr (1981). An improved finite element method for calculating the magnetic field distribution in magnet electron lenses and electromagnets. *Nucl. Instrum. Meth.* **187**, 201–208.

T. Mulvey and C. D. Newman (1972). Versatile miniature electron lenses. EUREM-5, Manchester. 116–117.

T. Mulvey and C. D. Newman (1973). New electron-optical systems for SEM and STEM. In *Scanning Electron Microscopy, Systems and Applications* (W. C. Nixon, Ed.), 16–21 (Institute of Physics, London).

T. Mulvey and C. D. Newman (1974). New experimental lens designs for high voltage electron microscopy. HVEM-3, Oxford. 98–102.

T. Mulvey and K. Tahir (1990). Recent developments in electron-optical instrumentation and computer-aided design. *Ultramicroscopy* **33**, 1–13.

T. Mulvey and M. J. Wallington (1969). The focal properties and aberrations of magnetic electron lenses. *J. Phys. E: Sci. Instrum.* **2**, 466–472.

T. Mulvey and M. J. Wallington (1973). Electron lenses. *Rep. Prog. Phys.* **36**, 347–421.

E. Munro (1973). Computer-aided design of electron lenses by the finite-element method. In *Image Processing and Computer-Aided Design in Electron Optics* (P. W. Hawkes, Ed.), 284–323 (Academic Press, London & New York).

E. Munro (1974). Scanning electron microscope lens design. *Scanning Electron Microsc.* Pt. I, 35–42.
E. Munro (1975a). Design and optimization of magnetic lenses and deflection systems for electron beams. *J. Vac. Sci. Technol.* **12**, 1146–1150.
E. Munro (1975b). A set of computer programs for calculating the properties of electron lenses. *Report CUED/B-ELECTR/TR45*, Cambridge University Engineering Department.
E. Munro (1980a). Electron beam lithography. In *Applied Charged Particle Optics* (A. Septier, Ed.), 73–131. *Adv. Electron. Electron Phys.* Suppl. 13B.
E. Munro (1980b). Electron optics for microcircuit engineering. In *Microcircuit Engineering '79* (H. Ahmed and W. C. Nixon, Eds), 513–534 (Cambridge University Press, Cambridge).
R. Murillo (1978). Contribution à l'étude des lentilles magnétiques utilisées en microscopie électronique à très haute tension. Dissertation, Toulouse.
R. Murillo and J.-L. Balladore (1974). Etude des éléments cardinaux d'un objectif à pièces polaires saturées. *J. Microsc. (Paris)* **20**, 1–13.
R. Murillo, J.-L. Balladore, R. Fourmaux and C. Trémollières (1987a). Electron lenses with anisotropic magnetic circuit. Part 1. Why and how to reduce the volume of electron magnetic lenses. *J. Microsc. Spectrosc. Electron* **12**, 263–279.
R. Murillo, J.-L. Balladore, R. Fourmaux and C. Trémollières (1987b). Electron lenses with anisotropic magnetic circuit. Part 2. Realisation of new type of magnetic lens. *J. Microsc. Spectrosc. Electron* **12**, 281–298.
T. Nagatani, S. Saito, M. Sato and M. Yamada (1987). Development of an ultra high resolution scanning electron microscope by means of a field emission source and in-lens system. *Scanning Microsc.* **1**, 901–909.
H. Nakagawa, N. Nomura, T. Koizumi, N. Anazawa and K. Harafuji (1991). A novel high-resolution scanning electron microscope for the surface analysis of high-aspect-ratio three-dimensional structures. *Jpn. J. Appl. Phys.* **30**, 2112–2117.
H. A. I. Nasr (1982). Microcomputer-aided design in electron optics. ICEM-10, Hamburg. **1**, 313–314.
H. Nasr, W. Chen and T. Mulvey (1981). Improved programs for calculating optical properties of electron lenses. EMAG, Cambridge. 75–78.
J. A. Nelder and R. Mead (1965). A simplex method for function minimization. *Comput. J.* **7**, 308–313. Corrigenda *ibid*. **8** (1965) 27.
T. H. Newman, K. E. Williams and R. F. W. Pease (1987). High resolution patterning system with a single bore objective lens. *J. Vac. Sci. Technol. B* **5**, 88–91.
M. T. Otten (1989). The CM30-SuperTWIN: a dedicated ultra-high resolution transmission electron microscope. *MRS Proc.* **139**, 251–258.
M. T. Otten, H. G. Bakker and M. J. C. de Jong (1991). The CM20-UltraTWIN: a new analytical ultra-high resolution microscope. EMAG, Bristol. 527–530.
S. Ozasa, S. Katagiri, H. Kimura and B. Tadano (1966). Superconducting electron lens. ICEM-6, Kyoto. **1**, 149–150.
N. W. Parker, M. Utlaut and A. V. Crewe (1976). Evaporative cooling of high current density mini-lenses. EMSA. **34**, 536–537.
S. J. Pennycook and P. D. Nellist, Eds (2011). *Scanning Transmission Electron Microscopy Imaging and Analysis* (Springer, New York).
G. N. Plass (1942). Electrostatic electron lenses with a minimum of spherical aberration. *J. Appl. Phys.* **13**. 49–55 & 524.
E. Plies (1981). Calculation of electrostatic multi-tubular core-lenses for a 3D imaging electron microscope: three-dimensionally imaging electron microscopes (Part IV). *Nucl. Instrum. Meth.* **187**, 227–235.
E. Plies (1994). Electron optics of low-voltage electron beam testing and inspection. Part I: Simulation tools. *Adv. Opt. Electron Microsc.* **13**, 123–242. Reprinted in *Adv. Imaging Electron Phys*. **205** (2018).
E. Plies and D. Typke (1978). Dreidimensional abbildende Elektronenmikroskope. II. Theorie elektronenoptischer Systeme mit gekrümmter Achse. *Z. Naturforsch.* **33a**, 1361–1377.

E. Plies and M. Schweizer (1987). Calculation of fields and secondary electron trajectories in a new in-lens spectrometer for electron beam testing. *Siemens Forsch. Entwickl.-Ber.* **16**, 30–36.

E. Plies (1994). Electron optics of low-voltage electron beam testing and inspection. Part 1: Simulation tools. *Adv. Opt. Electron Microsc.* **13**, 123–242.

J. Podbrdský (1980). The optical system of the analytical electron microscope with mini-lenses. EUREM-7, The Hague. **1**, 66–67.

J. Podbrdský (1982). The use of the diffraction mini-lens in the optical system of a transmission electron microscope. ICEM-10, Hamburg. **1**, 303–304.

J. Podbrdský (1988). Excitation coils of improved design for magnetic electron lenses. *J. Phys. E: Sci. Instrum.* **21**, 296–302.

D. Preikszas and H. Rose (1995). Procedures for minimizing the aberrations of electromagnetic compound lenses. *Optik* **100**, 179–187.

E. G. Ramberg (1942). Variation of the axial aberrations of electron lenses with lens strength. *J. Appl. Phys.* **13**, 582–594.

R. Rebsch (1938). Das theoretische Aulösungsvermögen des Elektronenmikroskops. *Ann. Phys. (Leipzig)* **31** (423), 551–560.

R. Rebsch (1940). Über den Öffnungsfehler der Elektronenlinsen. *Z. Phys.* **116**, 729–733.

R. Rebsch and W. Schneider (1937). Der Öffnungsfehler schwacher Elektronenlinsen. *Z. Phys.* **107**, 138–143.

A. Recknagel (1941). Über die sphärische Aberration bei elektronenoptischer Abbildung. *Z. Phys.* **117**, 67–73.

J. H. Reisner (1951). Permanent magnet lenses. *J. Appl. Phys.* **22**, 561–565.

J. H. Reisner and E. G. Dornfeld (1950). A small electron microscope. *J. Appl. Phys.* **21**, 1131–1139.

J. H. Reisner and S. M. Zollers (1951). Permanent-magnet electron microscope. *Electronics* **24**, 86–91.

N. Richardson and A. Muray (1988). An improved magnetic-collimating secondary electron energy filter for very large scale integrated diagnostics. *J. Vac. Sci. Technol.* **B6**, 417–421.

W. D. Riecke (1982). Practical lens design. In *Magnetic Electron Lenses* (P. W. Hawkes, Ed.), 163–357 (Springer, Berlin & New York).

W. D. Riecke and E. Ruska (1966). A 100 kV transmission electron microscope with single-field condenser objective. ICEM-6, Kyoto. **1**, 19–20.

H. Riedl (1937). Die Bildfehler 3. Ordnung der kurzen schwachen rein elektrischen Elektronen-Einzellinsen. *Z. Phys.* **107**, 210–216.

H. Rose and R. W. Moses (1973). Minimaler Öffnungsfehler magnetischer Rund- und Zylinderlinsen bei feldfreiem Objektraum. *Optik* **37**, 316–336.

E. Ruska (1951). Experiments with adjustable magnetostatic electron lenses. *National Bureau of Standards Circular* **527**, 389–409 [Published 1954].

E. Ruska (1952). Untersuchungen über regelbare magnetostatische Elektronenlinsen. *Z. Wiss. Mikrosk.* **61**, 152–171.

M. Sato, H. Todokoro and K. Kageyama (1993). Snorkel type conical objective lens with $\boldsymbol{E}$ cross $\boldsymbol{B}$ field for detecting secondary electrons. *Proc. SPIE* **2014**, 17–23.

O. Scherzer (1936a). Die schwache elektrische Einzellinse geringster sphärischer Aberration. *Z. Phys.* **101**, 23–26.

O. Scherzer (1936b). Über einige Fehler von Elektronenlinsen. *Z. Phys.* **101**, 593–603.

O. Scherzer (1941). Die unteren Grenzen der Brennweite und des chromatischen Fehlers von magnetischen Elektronenlinsen. *Z. Phys.* **118**, 461–466.

P. Schiske (1956). Die untere Grenze des Farbfehlers magnetischer Linsen bei vorgeschriebene Maximalfeldstärke. *Optik* **13**, 502–505.

P. Schiske (1977). Partial fraction expansion of electron optical cardinal elements. *Ultramicroscopy* **2**, 193–198.

A. Septier (1972). Superconducting lenses. EUREM-5, Manchester. 104–109.

C. Séverin, D. Génotel, M. Girard and A. Laberrigue (1971). Microscope électronique 400 kV à lentilles supraconductrices. 2. Caractéristiques électrooptiques et fonctionnement. *Rev. Phys. Appl.* **6**, 459–465.

Z. Shao and P. S. D. Lin (1989). High-resolution low-voltage elecron optical system for very large specimens. *Rev. Sci. Instrum* **60**, 3434–3441.

H. Shimoyama, K. Nimura, M. Suzuki and S. Maruse (1982). A magnetic-field-superposed electron gun with a point cathode. ICEM-10, Hamburg. **1**, 359–360.

H. Shimoyama, K. Nimura, M. Suzuki and S. Maruse (1983). Magnetic-field-superposed electron gun with a point cathode. *J. Electron Microsc.* **32**, 99–104.

K. Shirota, A. Yonezawa, K. Shibatomi and T. Yanaka (1976). Ferro-magnetic material observation lens system for CTEM with a eucentric goniometer. *J. Electron Microsc.* **25**, 303–304.

K. Siegbahn (1946). A magnetic lens of special field form for β- and γ-ray investigations; designs and applications. *Philos. Mag.* **37**, 162–184.

B. M. Siegel, N. Kitamura, R. A. Kropfli and M. P. Schulhof (1966). High resolution objective lenses using superconducting materials. ICEM-6, Kyoto. **1**, 151–152.

I.-M. Sintorn, G. Kylborg, R. Nordström, M. Uppström, J. Fulin, J. Åkesson, P. Štěpán, V. Kolařík, M. Drštička, and E. Coufalová (2014). A desk-top low voltage TEM for high quality imaging of biological specimen. XV International Conference on Electron Microscopy, EM2014, Kraków. 261–262.

T. G. Sparrow, T. Tang and U. Valdrè (1982). Multipurpose objective lens and specimen stages for a high voltage TEM/STEM. ICEM-10, Hamburg. **1**, 305–306.

G. Stabenow (1935). Eine magnetische Elektronenlinse ohne Bilddrehung. *Z. Phys.* **96**, 634–642.

P. D. Štěpán and A. Delong (2000). Low voltage electron microscope. III. Present and future possibilities. EUREM-12, Brno. **3**, I195–I196.

A. T. Stokes (1980). Computational analysis of a field emission gun system incorporating a single-pole lens. EUREM-7, The Hague. **1**, 58–59.

A. Strojnik (1984). High current electron microscope lenses. *Optik* **67**, 95–100.

M. Strojnik (1975). Field distribution of strongly excited magnetic lenses. EMSA, Las Vegas. **33**, 140–141.

P. A. Sturrock (1951). Propriétés optiques des champs magnétiques de révolution de la forme $H = H_0/[1-(z/a^2)]$ [*sic*] et $H = H_0/[(z/a)^2-1]$. *C. R. Acad. Sci. Paris* **233**, 401–403.

Y. Sugiura and S. Suzuki (1943). On the magnetic lens of minimum spherical aberration. *Proc. Imp. Acad. Japan* **9**, 293–302.

S. Suzuki, K. Akashi and H. Tochigi (1968). Objective lens properties of very high excitation. EMSA, New Orleans. **26**, 320–321.

S. Suzuki, A. Ishikawa, H. Kawamoto and S. Yamazaki (1982). The magnetic electron lens of minimum spherical aberration and its application for SEM. ICEM-10, Hamburg. **1**, 295–296.

N. Svartholm (1942). Berechnung magnetischer Linsen mit gegebener Feldform. *Ark. Mat. Astron. Fys. B* **28** (No.16). 8 pp.

P. Sytar and A. Zavodny (2017). A novel ultra-high resolution SEM column with a combined magnetic–elecrostatic lens and flexible scanning. MC-2017, Lausanne, 503–504.

M. Szilágyi (1969). Electron motion in a stationary axially symmetric magnetic field varying linearly along the axis. *Periodica Polytech. Elec. Eng.* **13**, 221–233.

M. Szilágyi (1970). A new magnetic lens model. ICEM-7, Grenoble. **2**, 61–62.

M. Szilágyi (1977a). A new approach to electron optical optimization. *Optik* **48**, 215–224.

M. Szilágyi (1977b). A dynamic programming search for magnetic field distributions with minimum spherical aberration. *Optik* **49**, 223–246.

M. Szilágyi (1978a). A dynamic programming search for electrostatic immersion lenses with minimum spherical aberration. *Optik* **50**, 35–51.

M. Szilágyi (1978b). A solution to the problem of the ideal quadrupole lens. *Optik* **50**, 121–128.

M. Szilágyi (1978c). Reduction of aberrations by new optimization techniques. ICEM-9, Toronto. **1**, 30–31.

M. Szilágyi (1984a). Procedure for electron and ion lens optimization. *Appl. Phys. Lett.* **44**, 7–9.

M. Szilágyi (1984b). Reconstruction of electrodes and pole pieces from optimized axial field distributions of electron and ion optical systems. *Appl. Phys. Lett.* **45**, 499–501.

M. Szilágyi (1984c). Synthesis of electron lenses. In *Electron Optical Systems for Microscopy, Microanalysis and Microlithography* (J. J. Hren, F. A. Lenz, E. Munro and P. B. Sewell, Eds), 75–84 (Scanning Electron Microscopy, AMF O'Hare).

M. Takizawa, H. Komami, M. Kurokawa and A. Yamada (2011). Position accuracy evaluation of multi-column e-beam exposure system. *Proc. SPIE* **7970**. 7970-0B, 8 pp.

T.-t. Tang and J.-p. Song (1990). Side pole-gap magnetic electron lenses. *Optik* **84**, 108–112.

J. H. Taylor and K. C. A. Smith (1986). The application of the the complex optimization technique to the design of magnetic electron lenses. ICEM-11, Kyoto. **1**, 297–298.

M. N. Thompson (1983). Design of the EM240 and its applications. *Electron Opt. Rep.* **30** (1EM), 1–23.

H. Tochigi, H. Uchida, S. Shirai, K. Akashi, D. J. Evins and J. Bonnici (1969). A new high resolution transmission electron microscope with second-zone objective lens. EMSA, St Paul. **27**, 176–177.

W. Tretner (1950). Die untere Grenze des Öffnungsfehlers magnetischer Elektronenobjektive. *Optik* **7**, 242.

W. Tretner (1954). Die untere Grenze des Öffnungsfehlers bei magnetischen Elektronenlinsen. *Optik* **11**, 312–326. Errata: *Optik* **12** (1955) 293–294.

W. Tretner (1956). Zur unteren Grenze des Öffnungsfehlers magnetischer Elektronenlinsen. *Optik* **13**, 516–519.

W. Tretner (1959). Existenzbereiche rotationssymmetrischer Elektronenlinsen. *Optik* **16**, 155–184.

M. Troyon (1980a). A magnetic field emission electron probe forming system. EUREM-7, The Hague. **1**, 56–57.

M. Troyon (1980b). High current efficiency field emission gun system incorporating a preaccelerator magnetic lens. Its use in CTEM. *Optik* **57**, 401–409.

M. Troyon and A. Laberrigue (1977). A field emission gun with high beam current capability. *J. Microsc. Spectrosc. Electron* **2**, 7–11.

K. Tsuno (1984). Computer simulation of aberrations in a transmission electron microscope with a triple polepiece projector lens. *J. Phys. E: Sci. Instrum.* **17**, 1038–1045.

K. Tsuno (1993). Resolution limit of a transmission electron microscope with an uncorrected conventional magnetic objective lens. *Ultramicroscopy* **50**, 245–253.

K. Tsuno (1997). Magnetic lenses for electron microscopy. In *Handbook of Charged Particle Optics* (J. Orloff, Ed.), 143–175; 2nd edn, 2009, 129–159 (CRC Press, Boca Raton).

K. Tsuno (1999). Optical design of electron microscope lenses and energy filters. *J. Electron Microsc.* **48**, 801–820.

K. Tsuno and Y. Harada (1981a). Minimisation of radial and spiral distortion in electron microscopy through the use of a triple pole-piece lens. *J. Phys. E: Sci. Instrum.* **14**, 313–320.

K. Tsuno and Y. Harada (1981b). Elimination of spiral distortion in electron microscopy using an asymmetrical triple pole-piece lens. *J. Phys. E: Sci. Instrum.* **14**, 955–960.

K. Tsuno and Y. Harada (1981c). Calculation of field distribution and optical properties of saturated asymmetrical objective lenses. EMAG, Cambridge. 95–98.

K. Tsuno and Y. Harada (1982). Image distortion free conditions in a transmission electron microsope with a triple polepiece projector lens. ICEM-10, Hamburg. **1**, 301–302.

K. Tsuno and Y. Harada (1983a). Design procedure for a high resolution electron microscope objective lens. *J. Electron Microsc.* **32**, 289–298.

K. Tsuno and Y. Harada (1983b). New objective lenses for the lattice imaging electron microscopy and the application to Sm–Co permanent magnets. *Trans. Jpn. Inst. Met.* **24**, 473–478.

K. Tsuno and T. Honda (1983). Magnetic field distribution and optical properties of asymmetrical objective lenses for an atomic resolution high voltage microscope. *Optik* **64**, 367–378.

K. Tsuno and M. Inoue (1984). Double gap objective lens for observing magnetic domains by means of differential phase contrast electron microscopy. *Optik* **67**, 363–376.

K. Tsuno, N. Handa and S. Matsumoto (1995). Immersion lenses for low voltage SEM and LEEM. *Proc. SPIE* **2522**, 243–252.

K. Tsuno and D. A. Jefferson (1997). Design of an objective lens with a minimum chromatic aberration coefficient. EMAG, Cambridge. 73–76.

K. Tsuno and D. A. Jefferson (1998). Design of an objective lens pole piece for a transmission electron microscope with a resolution less than 0.1 nm at 200 kV. *Ultramicroscopy* **72**, 31–39.

K. Tsuno and K. C. A. Smith (1985). Computation of lens shape with minimum spherical aberration coefficient in TEM. EMAG, Newcastle-upon-Tyne. 121–124.

K. Tsuno and K. C. A. Smith (1986). Optimization of objective lens shape for high resolution electron microscopes. ICEM-11, Kyoto. **1**, 295–296.

K. Tsuno and K. C. A. Smith (1987). Optimization of objective lens shape for high resolution electron microscope. In *Proc. Int. Symposium on Electron Optics, ISEOB* (J.-y. Ximen, Ed.), 252–254 (Institute of Electronics, Academia Sinica, Beijing).

K. Tsuno and T. Taoka (1982). Magnetic-field-free objective lens system around a specimen for observing fine structure of ferromagnetic materials. ICEM-10, Hamburg. **1**, 289–290.

K. Tsuno and T. Taoka (1983). Magnetic-field-free objective lens around a specimen for observing fine structure of ferromagnetic materials in a transmission electron microscope. *Jpn. J. Appl. Phys.* **22**, 1041–1047.

K. Tsuno, N. Handa, S. Matsumoto and A. Mogami (1996). Optical properties of immersion objective lenses and collimation of secondary electrons in low voltage SEM. *Proc. SPIE* **2858**, 46–57.

D. Typke (1981). Image aberrations of axially symmetric imaging systems with off-axial rays: Three-dimensionally imaging electron microscopes (Part III). *Nucl. Instrum. Meth.* **187**, 217–226.

D. Typke, W. Hoppe, W. Seßler and M. Burger (1976). Conception of a 3-D imaging electron microscope. EUREM-6, Jerusalem. **1**, 334–335.

D. Typke, M. Burger, N. Lemke and G. Lefranc (1980). Determination of the shielding geometry of a superconducting two-lens-system with off-axial ray paths for 3D imaging. EUREM-7, The Hague. **1**, 82–83.

Y. Uchida and H. G. Heide (1986). Objective lens for cryo microscopy and its application. ICEM-11, Kyoto. **1**, 247–250.

U. Valdrè (1975). The user's view of the electron microscope specimen section. In *Electron Microscopy in Materials Science* (U. Valdrè and E. Ruedl, Eds), 113–134 (CEE, Luxembourg).

K. van der Mast, C. J. Rakels and J. B. Le Poole (1980). A high quality multipurpose objective lens. EUREM-7, The Hague. **1**, 72–73.

M. van Ments and J. B. Le Poole (1947). Numerical computation of the constants of magnetic electron lenses. *Appl. Sci. Res.* **B1**, 3–17.

J. A. Venables and G. D. Archer (1980). On the design of F.E.G–S.E.M. columns. EUREM-7, The Hague. **1**, 54–55.

B. von Borries (1949). Ein magnetostatisches Objektiv–Projektiv–System für das Elektronenmikroskop. *Kolloid-Z.* **114**, 164–167.

B. von Borries (1952). Ein magnetostatisches Gebrauchs-Elektronenmikroskop für 60 kV Strahlspannung. *Z. Wiss. Mikrosk.* **60**, 329–358.

B. von Borries and G. Langner (1956). Sur les lentilles électroniques à aimant permanent. In *Les Techniques Récentes en Microscopie Electronique et Corpusculaire*. 285–295 (CNRS, Paris).

B. von Borries and F. A. Lenz (1956). Vorausberechnung magnetostatischer elektronenoptischer Abbildungssysteme. *Optik* **13**, 264–276.

B. von Borries, E. Ruska, J. Krumm and H. O. Müller (1940). Übermikroskopische Abbildung mittels magnetostatischer Linsen. *Naturwissenschaften* **28**, 350–351.

B. von Borries, F. A. Lenz and G. Opfer (1953). Über die Remanenz in Weicheisenkreisen magnetischer Elektronenlinsen. *Optik* **10**, 132–136.

B. von Borries, I. Johann, J. Huppertz, G. Langner, F. Lenz and W. Scheffels (1956a). Die Entwicklung regelbarer permanentmagnetischer Elektronenlinsen hoher Brechkraft und eines mit ihnen ausgerüsteten Elektronenmikroskopes neuer Bauart. *Forschungsberichte des Wirtschafts- und Verkehrsministeriums Nordrhein–Westfalen* Nr 156. 88 pp.

B. von Borries, G. Langner and W. Scheffels (1956b). Imaging elements operating with permanent magnets. EUREM-1, Stockholm. 14–17.

L. Wegmann (1953). Ein verzeichnungsarmes elektromagnetisches Doppelprojektivs für Elektronenmikroskope. *Helv. Phys. Acta* **26**, 448–449.

L. Wegmann (1954). Ein verzeichnungsarmes elektromagnetisches Doppelprojektivs für Elektronenmikroskope. *Optik* **11**, 153–170.

R. Weyl, I. Dietrich and H. Zerbst (1972). Die supraleitende Abschirmlinse. *Optik* **35**, 280–286.

J. Worster (1975). Aberrations at multiple foci in magnetic electron lenses. *J. Phys. D: Appl. Phys.* **8**, L29–L30.

S. K. Xie (1986). A set of simple calculating method for calculated the total flux and flux density in the lens. ICEM-11, Kyoto. **1**, 293–294.

J.-y Ximen, P. S. D. Lin, J. B. Pawley and M. Schippert (1993). Electron optical design of a high-resolution low-voltage scanning electron microscope with field emission gun. *Rev. Sci. Instrum.* **64**, 2905–2910.

K. Yada (1986). Effect of concave-lens action of a mini static lens on the spherical aberration coefficient of a magnetic lens. ICEM-11, Kyoto. **1**, 305–306.

K. Yada and H. Kawakatsu (1976). Magnetic electron lens with small bores. *J. Electron Microsc.* **25**, 1–9.

K. Yada and C. Kimura (1982). Pinhole objective lens for analytical TEM. ICEM-10, Hamburg. **1**, 291–292.

A. Yamada, H. Yasuda and M. Yamabe (2008). Electron beams in individual column cells of multicolumn cell systems. *J. Vac. Sci. Technol. B* **26**, 2025–2031.

A. Yamada, Y. Oae, T. Okawa, M. Yakizawa and M. Yamabe (2010). Evaluation of throughput improvement by MCC and CP in multicolumn e-beam exposure system. *Proc. SPIE* **7637**, 7637–0C.

T. Yanaka (1986). Strongly-excited CTEM/STEM objective lens. ICEM-11, Kyoto. **1**, 23–246.

T. Yanaka and M. Watanabe (1966). Aberration coefficients of extremely asymmetrical objective lenses. ICEM-6, Kyoto. **1**, 141–142.

H. Yasuda, T. Haraguchi and A. Yamada (2004). A proposal of MCC (multi-column cell with lotus root lens) system to use as a mask-making e-beam tool. *Proc. SPIE* **5567**, 911–921.

H. Yasuda, A. Yamada and M. Yamabe (2008). Multi column cell (MCC) e-beam exposure system for mask writing. *Proc. SPIE* **7028**, 7028-0B, 9 pp.

H. Yasuda, A. Yamada and M. Yamabe (2009). Present status of multi column cell exposure system for mask writing. *Proc. SPIE* **7379**, 7379-18, 7 pp.

Y. W. Yau, R. F. W. Pease, A. A. Iranmanesh and K. J. Polasko (1981). Generation and applications of finely focused beams of low-energy electrons. *J. Vac. Sci. Technol.* **19**, 1048–1052.

H. C. Yin and T. Mulvey (1987). Saturated magnetic objective lenses with super-conducting windings. In *Proc. Int. Symposium on Electron Optics, ISEOB* (J.-y. Ximen, Ed.), 293–294 (Institute of Electronics, Academia Sinica, Beijing).

S. F. Zelev (1982). Dependence of the maximum magnetic induction and half-width of the field of electron-microscope lenses on the shape and material of the polepieces. *Opt.-Mekh. Prom.* **49** (9), 20–22. *Sov. J. Opt. Technol*. **49**, 557–559.

F. Zemlin (1991). Recent developments in electron crystallography of protein crystals. *Curr. Opinion Struct. Biol.* **1**, 1023–1029.

F. Zemlin (1992). Desired features of a cryoelectron microscope for the electron crystallography of biological material. *Ultramicroscopy* **46**, 25–32.

F. Zemlin, E. Beckmann and K. D. van der Mast (1996). A 200 kV electron microscope with Schottky field emitter and a helium-cooled superconducting objective lens. *Ultramicroscopy* **63**, 227–238.

F. Zemlin, E. Beckmann, K.-P. Charlé, M. Schatz and R. Schlögl (1999). Solid nitrogen: electron microscopy and beam damage quantification at 4 K. *Ultramicroscopy* **80**, 153–161.

Part VII, Chapters 37–40

Most of the supplementary references for mirrors (Chapter 37) are concerned with mirror microscope design though a few are devoted to mirror properties alone. See Henneberg and Recknagel (1935), Recknagel (1936, 1937), Spivak et al. (1955, 1959a,b, 1960, 1961, 1962, 1963, 1978, 1983), Spivak and Lyubchenko (1959), Mayer (1961, 1962), Igras (1961), Premanand (1962), Brand and Schwartze (1963), Barnett and Nixon (1964, 1966, 1967, 1967/68), Schwartze (1964, 1965), Igras and Warminski (1965), Heydenreich (1966), Artamonov and Komolov (1966, 1970c), Artamonov et al. (1966), Artamonov (1968), Oman (1969), Kel'man et al (1972a,b), Luk'yanov et al (1973), which contains 187 references, Henkelman and Ottensmeyer (1974), Witzani and Hörl (1981) and Hamarat et al. (1984). Filter lenses are the subject of papers by Schiekel (1952), Beaufils (1959), Hahn (1961), Der-Shvarts and Belen'kii (1962), Wilska (1970) and Lenz (1973). A highly original proposal for using an electrostatic mirror as a data storage device is made by Kasper and Wilska (1967).

Cathode lenses, frequently referred to as immersion objectives, have a vast literature, of which the following references are only a modest sample, biased towards the theory of these devices: Brüche and Johannson (1932a), Behne (1936a–c), Mecklenburg (1942), Jenkins (1942/43), Einstein and Jacob (1948), Duchesne (1949, 1953), Jacob (1950), Ashworth (1951), Müller (1951), Clarke and Jacob (1953), Dolan and Dyke (1954), Drechsler and Pankow (1954), Möllenstedt and Keller (1954), Bas (1956), Bonshtedt et al. (1956), Good and Müller (1956), Vorob'ev (1956, 1959), Rozenfel'd (1959), Gobrecht (1961), Kas'yankov (1961), Rozenfel'd and Zaitsev (1961), Aeschlimann and Bas (1962), Brand and Schwartze (1963), Düker (1964, 1968), Vlasov et al. (1964), Kulikov (1966, 1971, 1972, 1973, 1975), Der-Shvarts and Kulikov (1968), Heinemann (1968), Heinemann and Lenz (1968), Müller and Tsong (1969), Bowkett and Smith (1970), Vlasov and Shapiro (1971, 1974), Berger and Babout (1972), Shapiro (1972), Tsyganenko et al. (1972), Berger and Bernard (1974), Schwarzer (1975/76a,b, 1979), Monastyrskii and Kulikov (1976, 1978), Ignat'ev et al. (1979), Liebl (1979), Ivanov et al. (1983), Nesvizhskii (1984, 1985, 1986), Il'ín et al. (1984, 1987), Monastyrskii (1986), Monastyrskii and Korneeva (1986) and Kolesnikov and Monastyrskii (1988).

Low-energy-electron microscopes and photoemission electron microscopes (LEEM and PEEM) are also included in Chapter 37. Recent review articles on these instruments are mentioned there and we refer to those for additional literature. The same is true of Wien filters (Chapter 38).

In addition to the cited references in Chapter 39, we mention the book of Baranova and Yavor (1986b, 1989) and the papers by Lobb (1970), Afanas'ev (1985), Nevinnyi et al. (1985), Baranova and Yavor (1986a), Ovsyannikova (1986), Petrov and Khersonskaya (1986), Okayama (1988), Gaafer (2014) and, on parasitic aberrations, Martin and Goloskie (1988) and Baranova and Read (2001). In a series of papers, Preston (1968, 1969, 1970, 1972) analyses in great detail the field distribution in electrostatic quadrupoles in which the pairs of opposite poles are at different distances from the axis, thereby creating round, quadrupole and octopole components.

Finally, we draw attention to the following papers on deflection systems or on calculation of fields in such systems or again on yoke design: Amboss (1975, 1976), Sheppard and Ahmed (1976), Karetskaya and Fedulina (1977), Ohiwa (1977, 1978), Speidel et al. (1979/80), de Chambost (1980), Hosokawa (1980), Munro (1980b), Pearce-Percy and Spicer (1980), Li (1981), Owen (1981), Li and Ximen (1982), Chen et al. (1983), Goto et al. (1983), Hosokawa and Morita (1983), Idesawa et al. (1983), Hanssum (1983, 1984, 1985, 1986), Pfeiffer and Sturans (1984), Evdokimov (1985), Paik and Siegel (1985), Strong (1985), Zhukov and Abraamyants (1986a,b), Alles et al. (1987), Baranova et al. (1987c, 1988), Zhou et al. (1988) and Jiang (1988). Deflection systems were studied in great detail by K. Kanaya and colleagues in the 1960s. See Kanaya (1962), Kanaya and Kawakatsu (1961a,b, 1962), Kanaya et al. (1961, 1963, 1964) amd Kawakatsu and Kanaya (1961); cf. Ito et al. (1954). Variable-axis lenses are mentioned by Schmid and Rose (1998), Spehr (1998), Zhao and Khursheed (1999a–c) and Zhao et al. (2012a,b). Ren et al. (2002) describe a rotating deflection field that matches the rotation of the electron beam.

***

R. Aeschlimann and E. B. Bas (1962). Ein Universal-Emissions-Elektronenmikroskop. ICEM-5, Philadelphia. **1**, D9.

V. P. Afanas'ev (1982). Biplanar electrostatic lenses. *Zh. Tekh. Fiz.* **52**, 945–949. *Sov. Phys. Tech. Phys.* **27**, 604–606.

V. P. Afanas'ev (1985). Production of multipole electrostatic fields by means of biplanar lenses. *Zh. Tekh. Fiz.* **55** (405–408). *Sov. Phys. Tech. Phys.* **30**, 239–241.

V. P. Afanas'ev and A. D. Sadykin (1982). Experimental investigation of a symmetric single-section biplanar lens. I. Focusing properties. II. Aberration properties. *Zh. Tekh. Fiz.* **52**, 1213–1215 & 1226–1228. *Sov. Phys. Tech. Phys.* **27**, 735–736 & 737–738.

V. P. Afanas'ev and A. D. Sadykin (1983). Experimental study of the properties of a first-order doublet of biplanar lenses. *Zh. Tekh. Fiz.* **53**, 585–587. *Sov. Phys. Tech. Phys.* **28**, 368–369.

V. P. Afanas'ev and A. D. Sadykin (1984). Experimental study of a biplanar lens with independently controlled focusing and aberration properties. *Zh. Tekh. Fiz.* **54**, 2394–2396. *Sov. Phys. Tech. Phys.* **29**, 1413–1414.

V. P. Afanas'ev, N. P. Gritsyuk, R. A. Lachashvili and S. Ya. Yavor (1979). Electron-optical characteristics of crossed lenses. *Zh. Tekh. Fiz.* **49**, 1498–1501. *Sov. Phys. Tech. Phys.* **24**, 833–835.

V. P. Afanas'ev, L. A. Baranova, I. A. Petrov and S. Ya. Yavor (1980). Crossed lenses. *Optik* **56**, 261–282.

V. P. Afanas'ev, L. A. Baranova and S. Ya. Yavor (1981). Crossed lenses. *Izv. Akad. Nauk Kaz SSR (Ser. Fiz. Mat.)* (No. 6), 1–14.

V. P. Afanas'ev, L. P. Ivanova and A. D. Sadykin (1982). Rectangular model for calculating the focusing properties of biplanar electrostatic lenses. *Zh. Tekh. Fiz.* **52**, 1240–1241. *Sov. Phys. Tech. Phys.* **27**, 756.

D. S. Alles, C. J. Biddick, J. M. Bruning, J. T. Clemens, R. J. Collier, E. A. Gere, L. R. Harriott, F. Leone, R. Liu, T. J. Mulrooney, R. J. Nielsen, N. Paras, R. M. Richman, C. M. Rose, D. P. Rosenfeld, D. E. A. Smith and M. G. R. Thomson (1987). EBES4: a new electron-beam exposure system. *J. Vac. Sci. Technol. B* **5**, 47–52.

K. Amboss (1975). Design of fast deflection coils for an electron-beam microfabrication system. *J. Vac. Sci. Technol.* **12**, 1152–1155.

K. Amboss (1976). Electron optics for microbeam fabrication. *Scanning Electron Microsc.* **1**, 699–714.

W. H. J. Andersen (1967). Optimum adjustment and correction of the Wien filter. *Br. J. Appl. Phys.* **18**, 1573–1579.

W. H. J. Andersen and J. B. Le Poole (1970). A double wienfilter as a high resolution, high transmission electron energy analyser. *J. Phys. E: Sci. Instrum.* **3**, 121–126.

Yu. A. Andreev, L. G. Glikman and Z. D. Iskakova (1975a). Astigmatic two-electrode tubular lenses. *Zh. Tekh. Fiz.* **45**, 1604–1614. *Sov. Phys. Tech. Phys.* **20**, 1024–1028.

Yu. A. Andreev, L. G. Glikman and Z. D. Iskakova (1975b). Spherical aberration of a two-electrode astigmatic tubular lens. *Zh. Tekh. Fiz.* **45**, 2043–2050. *Sov. Phys. Tech. Phys.* **20**, 1289–1292.

P. Antony-Spies and P. Junior (1967). Verzeichnungsfreie elektronenoptische Abbildungen mit Systemen aus drei Vierpollinsen. *Z. Angew. Phys.* **22**, 490–492.

M. R. Armstrong, K. Boyden, N. D. Browning, G. H. Campbell, J. D. Colvin, W. J. DeHope, A. M. Frank, D. J. Gibson, F. Hartemann, J. S. Kim, W. E. King, T. B. LaGrange, B. J. Pyke, B. W. Reed, R. M. Shuttlesworth, B. C. Stuart and B. R. Torralva (2007). Practical considerations for high spatial and temporal resolution dynamic transmission electron microscopy. *Ultramicroscopy* **107**, 356–367.

O. M. Artamonov (1968). A simple electron mirror microscope. EUREM-4, Rome. **1**, 99–100.

O. M. Artamonov and G. N. Brodskii (1969). Electron-optical parameters of a two-electrode cylindrical mirror. I. *Zh. Tekh. Fiz.* **39**, 1126–1128. *Sov. Phys. Tech. Phys.* **14**, 846–847; for Part II, see Brodskii and Gall' (1970).

O. M. Artamonov and S. A. Komolov (1966). On the reflection of potential relief in an electron mirror. *Radiotekh. Elektron.* **11**, 2186–2190. *Radio Eng. Electron. Phys.* **11**, 1927–1932.

O. M. Artamonov and S. A. Komolov (1970a). Some properties of the beam reflected in an electron mirror. *Radiotekh. Elektron.* **15**, 220–222. *Radio Eng. Electron. Phys.* **15** (1), 192–194.

O. M. Artamonov and S. A. Komolov (1970b). Principal parameters of a mirror electron microscope with spherical electrodes. *Izv. Akad. Nauk SSSR (Ser. Fiz.)* **34**, 1548–1553. *Bull. Acad. Sci. USSR (Phys. Ser.)* **34**, 1373–1377.

O. M. Artamonov and S. A. Komolov (1970c). Die wesentlichen Characteristiken des Elektronenspiegels mit sphärischen Elektroden. ICEM-7, Grenoble. **1**, 193–194.

O. M. Artamonov, N. B. Gerasimova and S. A. Komolov (1966). Experimental study of an electron-optical mirror. *Opt-.Mekh. Prom.* **33** (12), 17–20. *Sov. J. Opt. Technol*. **33**, 603–606.

L. A. Artsimovich (1944). Electron-optical properties of emission systems. *Izv. Akad. Nauk SSSR (Ser. Fiz.)* **8**, 313–329.

F. Ashworth (1951). Field emission microscopy. *Adv. Electron.* **3**, 1–42.

A. P. Banford (1966). *The Transport of Charged Particle Beams* (Spon, London).

L. A. Baranova (2000). The fifth order aperture aberration of electrostatic quadrupole lens systems. *Proc. SPIE* **4187**, 14–23.

L. A. Baranova and F. H. Read (1994). Electrostatic electron-optical crossed lens with controlled astigmatism. *Rev. Sci. Instrum.* **65**, 1993–1997.

L. A. Baranova and F. H. Read (1998). Reduction of the chromatic and aperture aberrations of the stigmatic quadrupole lens triplet. *Optik* **109**, 15–21.

L. A. Baranova and F. H. Read (1999). Minimisation of the aberrations of electrostatic lens systems composed of quadrupole and octupole lenses. *Int. J. Mass Spectrom.* **189**, 19–26.

L. A. Baranova and F. H. Read (2001). Aberrations caused by mechanical misalignments in electrostatic quadrupole lens sysems. *Optik* **112**, 131–138.

L. A. Baranova and S. Ya. Yavor (1984a). Electrostatic lenses. *Zh. Tekh. Fiz.* **54**, 1417–1453. *Sov. Phys. Tech. Phys*. **29**, 827–848.

L. A. Baranova and S. Ya. Yavor (1984b). Radial conical electron-optical systems. *Zh. Tekh. Fiz.* **54**, 1999–2003. *Sov. Phys. Tech. Phys*. **29**, 1173–1175.

L. A. Baranova and S. Ya. Yavor (1986a). An approximate method for calculating the properties of post-acceleration systems in electron-beam devices. *Zh. Tekh. Fiz.* **56**, 986–988. *Sov. Phys. Tech. Phys*. **31**, 603–604.

L. A. Baranova and S. Ya. Yavor (1986b). *Elektrostaticheskie Elektronnye Linzy* (Nauka, Moscow).

L. A. Baranova and S. Ya. Yavor (1989). The optics of round and multipole electrostatic lenses. *Adv. Electron. Electron Phys.* **76**, 1–207.

L. A. Baranova and S. Ya. Yavor (1997). Deflection systems with energy focusing. *Zh. Tekh. Fiz.* **67** (1), 128–129. *Tech. Phys.* **42**, 113–114.

L. A. Baranova, T. Ya. Fishkova and S. Ya. Yavor (1968). Some types of electrostatic quadrupole lenses. *Radiotekh. Elektron.* **13**, 2108–2110. *Radio Eng. Electron. Phys*. **13**, 1854–1856.

L. A. Baranova, L. P. Ovsyannikova and S. Ya. Yavor (1972). Asymmetric quadrupole lenses. *Zh. Tekh. Fiz.* **42**, 210–213. *Sov. Phys. Tech. Phys*. **17**, 170–172.

L. A. Baranova, I. A. Petrov and S. Ya. Yavor (1978a). A new type of corrector of spherical aberration. *Zh. Tekh. Fiz.* **48**, 2588–2590. *Sov. Phys. Tech. Phys*. **23**, 1481–1483.

L. A. Baranova, I. A. Petrov and S. Ya. Yavor (1978b). Crossed lenses for electron-microscopic devices. ICEM-9, Toronto. **1**, 28–29.

L. A. Baranova, A. D. Sadykin, V. M. Mukhin and S. Ya. Yavor (1982). Effect of electrode shape on the electron-optical properties of crossed lenses. *Zh. Tekh. Fiz.* **52**, 246–250. *Sov. Phys. Tech. Phys*. **27**, 161–163.

L. A. Baranova, S. G. Narylkov and S. Ya. Yavor (1984). A wedge-shaped radial lens. *Zh. Tekh. Fiz.* **54**, 2245–2248. *Sov. Phys. Tech. Phys*. **29**, 1314–1316.

L. A. Baranova, S. G. Narylkov and S. Ya. Yavor (1985a). Fields of conical electron-optical systems. *Zh. Tekh. Fiz.* **55**, 804–807. *Sov. Phys. Tech. Phys*. 3**0,** 481–483.

L. A. Baranova, S. G. Narylkov and S. Ya. Yavor (1985b). Field calculations for radial wedge lenses. *Zh. Tekh. Fiz.* **55**, 2209–2211. *Sov. Phys. Tech. Phys*. **30**, 1303–1304.

L. A. Baranova, S. G. Narylkov and S. Ya. Yavor (1986a). Studies of the optics of a conical radial lens. *Zh. Tekh. Fiz.* **56**, 2075–2079. *Sov. Phys. Tech. Phys*. **31**, 1246–1249.

L. A. Baranova, S. G. Narylkov and S. Ya. Yavor (1986b). Achromatic radial wedge systems. *Zh. Tekh. Fiz.* **56**, 2279–2282. *Sov. Phys. Tech. Phys*. **31**, 1366–1369.

L. A. Baranova, A. D. Sadykin and S. Ya. Yavor (1986c). Multi-electrode wedge lenses. *Radiotekh. Elektron.* **31**, 365–369. *Sov. J. Commun. Technol. Electron*. **31** (2), 135–139.

L. A. Baranova, S. G. Narylkov and S. Ya. Yavor (1986d). Linearization of the fields of radial and quadrupole lenses. *Radiotekh. Elektron.* **31**, 778–782. *Sov. J. Commun. Technol. Electron*. **31** (8), 169–174.

L. A. Baranova, S. G. Narylkov and S. Ya. Yavor (1987a). Solution in closed form of the Dirichlet problem for conical electrodes. *Zh. Tekh. Fiz.* **57**, 156–158. *Sov. Phys. Tech. Phys*. **32**, 91–92.

L. A. Baranova, R. A. Bublyaev and S. Ya. Yavor (1987b). Approximate method of calculating the paraxial optics of crossed lenses. *Zh. Tekh. Fiz.* **57**, 430–433. *Sov. Phys. Tech. Phys*. **32**, 261–262.

L. A. Baranova, S. G. Narylkov and S. Ya. Yavor (1987c). A study of cylindrical and conical deflectors. *Zh. Tekh. Fiz.* **57**, 1872–1876. *Sov. Phys. Tech. Phys*. **32**, 1126–1128.

L. A. Baranova, N. P. Zanadvorov, Yu. A. Flegontov and S. Ya. Yavor (1988). Edge effects in conical multielectrode deflecting systems. *Radiotekh. Elektron* **33**, 2607–2613. *Sov. J. Commun. Technol. Electron*. **33** (12), 90–95.

L. A. Baranova, N. P. Zanadvorov, Yu. A. Flegontov and S. Ya. Yavor (1989). Conical multielectrode deflecting systems. *Radiotekh. Elektron.* **34**, 2607–2613. *Sov. J. Commun. Technol. Electron*. **34**, 90–96.

L. A. Baranova, V. I. Stankevich, Yu. A. Flegontov and S. Ya. Yavor (1990). Effective lengths of deflection systems employing cylindrical electrodes. *Radiotekh. Elektron.* **35**, 1307–1312. *Sov. J. Commun. Technol. Electron*. **35** (6), 87–91.

L. A. Baranova, R. A. Bublyaev and S. Ya. Yavor (1993). Chromatic aberration of a crossed einzel lens. *Zh. Tekh. Fiz.* **63**, 119–121. *Tech. Phys*. **38**, 1096–1097.

L. A. Baranova, S. Ya. Yavor and F. H. Read (1996). Crossed aperture lenses for the correction of chromatic and aperture aberrations. *Rev. Sci. Instrum.* **67**, 756–760.

M. E. Barnett and W. C. Nixon (1964). Image formation in an electron mirror microscope using magnetic lenses. EUREM-3, Prague. **A**, 37–38.

M. E. Barnett and W. C. Nixon (1966). Image contrast in mirror electron microscopy. ICEM-6, Kyoto. **1**, 231–232.

M. E. Barnett and W. C. Nixon (1967). A mirror electron microscope using magnetic lenses. *J. Sci. Instrum.* **44**, 893–898.

M. E. Barnett and W. C. Nixon (1967). Electrical contrast in mirror electron microscopy. *Optik* **26**, 310–325.

G. Bartz and G. Weissenberg (1957). Abbildung von p–n–Übergängen in Halbleitern mit dem Auflichtelektronenmikroskop. *Naturwissenschaften* **44**, 229.

G. Bartz, G. Weissenberg and D. Wiskott (1954). Ein Auflichtelektronenmikroskop. ICEM-3, London. 395–404.

E. B. Bas (1956). Bolzenkathode als Objekt im Elektronenemissionsmikroskop. EUREM-1, Stockholm. 37–41.

E. Bauer (2008). LEEM and SPLEEM. In *Science of Microscopy* (P. W. Hawkes and J. C. H. Spence, Eds), **1**, 605–656 (Springer, New York).

E. Bauer (2012). LEEM and UHV-PEEM: a retrospective. *Ultramicroscopy* **119**, 18–23.

E. Bauer (2014). *Surface Microscopy with Low Energy Electrons* (Springer, New York).

E. Bauer (2018). LEEM, SPLEEM aand SPELEM. In *Handbook of Microscopy* (P. W. Hawkes and J. C. H. Spence, Eds), (Springer, Cham), forthcoming.

R. Beaufils (1959). Réalisation d'un filtre électrostatique de vitesses. Utilisation en microdiffraction électronique. *C. R. Acad. Sci. Paris* **248**, 3145–3147.

R. Behne (1936a). Die Eigenschaften des Immersionsobjektivs für die Abbildung mit schnellen Elektronen. *Ann. Phys. (Leipzig)* **26** (418), 372–384.

R. Behne (1936b). Folienabbildung mit dem Immersionsobjektiv. *Ann. Phys. (Leipzig)* **26** (418), 385–397.

R. Behne (1936c). Beitrag zur Kenntnis der elektronenoptischen Immersionslinse. II. *Z. Phys.* **101**, 521–526; for Part I, see Hess (1934).

C. Berger and M. Babout (1972). Méthode de calcul du potentiel en tout point de l'axe de l'objectif de Johannson. *C. R. Acad. Sci. Paris B* **275**, 333–336.

C. Berger and R. Bernard (1974). Méthode de calcul du champ élecrostatique de l'objectif de Johannson. *J. Microsc. (Paris)* **20**, 113–122.

H. Bethge and J. Heydenreich (1971). Ein Elektronenspiegel-Mikroskop mit Umlenkfeld und seine Einsatzmöglichkeiten. *Exp. Tech. Phys.* **19**, 375–382.

H. Bethge and J. Heydenreich (1982). Emissions-Elektronenmikroskopie, Spiegel-Elektronenmikroskopie. In *Elektronenmikroskopie in der Festkörperphysik* (H. Bethge and J. Heydenreich, Eds), 186–203 (Springer, Berlin & New York).

H. Bethge and J. Heydenreich (1987). Special methods for direct imaging of surfaces: emission electron microscopy, reflection electron microscopy and mirror electron microscopy. In *Electron Microscopy in Solid State Physics* (H. Bethge and J. Heydenreich, Eds), 219–235 (Elsevier, Amsterdam, Oxford & New York). Translation after revision of Bethge & Heydenreich (1982).

H. Bethge, J. Hellgardt and J. Heydenreich (1960). Zum Aufbau einfacher Anordnungen für Untersuchungen mit dem Elektronenspiegel. *Exp. Tech. Phys.* **8**, 49–61.

S. B. Bimurzaev and E. M. Yakushev (2004). Methods of parametrization of exact electron trajectory equations. Proc. *SPIE* **5398**, 51–58.

W. Bischof, M. Höfert, H. R. Wilde, B. Raith, B. Gonsior and K. Enderer (1982). Trace element analysis of biological samples using a proton microprobe. *Nucl. Instrum. Meth.* **197**, 201–207.

A. M. Blackburn (2008). Electrostatic micro-lens within an AFM cantilever for LEEM. *Phys. Procedia* **1**, 537–543.

H. Boersch (1947). Über die Kontraste von Atomen im Elektronenmikroskop. *Z. Naturforsch.* **2a**, 615–633.

H. Boersch (1948). Über die Beseitigung der inkohärenten Streuung in elektronen-mikroskopischen Abbildungen und Elektronenbeugungsdiagrammen durch Elektronenfilter. *Naturwissenschaften* **35**, 26.

H. Boersch (1949). Ein Elektronenfilter für Elektronenmikroskopie und Elektronenbeugung. *Optik* **5**, 436–450.

H. Boersch (1953). Gegenfeldfilter für Elektronenbeugung und Elektronenmikroskopie. *Z. Phys.* **134**, 156–164.

H. Boersch and H. Miessner (1962). Ein hochempfindlicher Gegenfeld-Energieanalysator für Elektronen. *Z. Phys.* **168**, 298–304.

H. Boersch and S. Schweda (1962). Eine inverse Gegenfeldmethode zur Energieanalyse von Elektronen- und Ionen-Strahlen. *Z. Phys.* **167**, 1–10.

A. B. Bok (1968). A mirror electron microscope. Dissertation, Delft.

A. B. Bok (1978). Mirror electron microscopy, theory and applications. In *Diffraction and Imaging Techniques in Material Science* (S. Amelinckx, R. Gevers and J. Van Landuyt, Eds), 2nd edn, 761–788 (North Holland, Amsterdam, New York & Oxford).

A. B. Bok, J. Kramer and J. B. Le Poole (1964). A mirror-microscope with quadrupoles. EUREM-3, Prague. **A**, 445–446.

A. B. Bok, J. B. Le Poole, J. Roos, H. de Lang, H. Bethge, J. Heydenreich and M. E. Barnett (1971). Mirror electron microscopy. *Adv. Opt. Electron Microsc.* **4**, 161–261. Reprinted in *Adv. Imaging Electron Phys.* **203** (2017) 99–192.

B. E. Bonshtedt (1964). Calculation of cathode lens aberrations. *Radiotekh. Elektron.* **9**, 844–850. *Radio Eng. Electron. Phys*. **9**, 686–692.

B. E. Bonshtedt, T. G. Dmitrieva and I. I. Tsukkerman (1956). Calculation of the resolving power of an electron optical transformer with homogeneous fields. *Zh. Tekh. Fiz.* **26**, 1966–1968. *Sov. Phys. Tech. Phys*. **1**, 1897–1899.

R. Bormann, S. Strauch, S. Schäfer and C. Ropers (2015). An ultrafast electron microscope gun driven by two-photon photoemission from a nanotip cathode. *J. Appl. Phys.* **118**, 173105.

G. Bosi (1974). Quadrupole fields in circular concave electrodes and poles. *Rev. Sci. Instrum.* **45**, 1260–1262.

O. Bostanjoglo (1989). Electron microscopy of fast processes. *Adv. Electron. Electron Phys.* **76**, 209–279.

O. Bostanjoglo (1999). High-speed electron microscopy. *Adv. Imaging Electron Phys.* **110**, 21–61.
O. Bostanjoglo (2002). High-speed electron microscopy. *Adv. Imaging Electron Phys.* **121**, 1–51.
O. Bostanjoglo, R. Elschner, Z. Mao, T. Nink and M. Weingärtner (2000). Nanosecond electron microscopes. *Ultramicroscopy* **81**, 141–147.
K. M. Bowkett and D. A. Smith (1970). *Field Ion Microscopy* (North Holland, Amsterdam).
K. Brack (1962). Über eine Anordnung zur Filterung von Elektroneninterferenzen. *Z. Naturforsch.* **17a**, 1066–1070.
U. Brand and W. Schwartze (1963). Modellversuche zur Bildentstehung im Elektronenspiegel–Oberflächenmikroskop. *Exp. Tech. Phys.* **11**, 18–25.
G. N. Brodskii and L. N. Gall' (1970). Electron-optical parameters of a two-electrode cylindrical mirror. II. *Zh. Tekh. Fiz.* **40**, 2015–2017. *Sov. Phys. Tech. Phys*. **15**, 1570–1571; for Part I, see Artamonov and Brodskii (1969).
G. N. Brodskii and S. Ya. Yavor (1970). Electron optical properties of a two-potential two-dimensional lens. *Zh. Tekh. Fiz.* **40**, 1310–1313. *Sov. Phys. Tech. Phys*. **15**, 1011–1012.
G. N. Brodskii and S. Ya. Yavor (1971). Spherical aberration of a two-potential lens with a curved focusing region. *Zh. Tekh. Fiz.* **41**, 460–463. *Sov. Phys. Tech. Phys*. **16**, 356–358.
N. D. Browning, M. A. Bonds, G. H. Campbell, J. E. Evans, T. LaGrange, K. L. Jungjohann, D. J. Masiel, J. McKeown, S. Mehraeen, B. W. Reed and M. Santala (2012a). Recent developments in dynamic transmission electron microscopy. *Curr. Opin. Solid State Mater. Sci.* **16**, 23–30.
N. D. Browning, G. H. Campbell, J. E. Evans, T. B. LaGrange, K. L. Jungjohann, J. S. Kim, D. J. Masiel and B. W. Reed (2012b). Dynamic transmission electron microscopy. In *Handbook of Nanoscopy* (G. Van Tendeloo, D. Van Dyck and S. J. Pennycook, Eds), Vol. 1, 309–343 (Wiley–VCH, Weinheim).
E. Brüche (1932). Elektronenmikroskop. *Naturwissenschaften* **20**, 49.
E. Brüche and H. Johannson (1932a). Elektronenoptik und Elektronenmikroskop. *Naturwissenschaften* **20**, 353–358.
E. Brüche and H. Johannson (1932b). Einige neue Kathodenuntersuchungen mit dem elektrischen Elektronenmikroskop. *Phys. Z.* **33**, 898–899.
K. Bücker, M. Picher, O. Crégut, T. LaGrange, B. Reed, S.T. Park, D. Masiel and F. Banhart (2016a). Ultrafast transmission electron microscopy reveals electron dynamics and trajectories in a thermionic gun setup. EMC-16, Lyon. **1**, 445–446.
K. Bücker, M. Picher, O. Crégut, T. LaGrange, B. W. Reed, S. T. Park and D. J. Masiel (2016b). Electron beam dynamics in an ultrafast transmission electron microscope with wehnelt electrode. *Ultramicroscopy* **171**, 8–18.
G. H. Campbell, J. T. McKeown and M. K. Santala (2018). High-speed electron microscopy. In *Handbook of Microscopy* (P. W. Hawkes and J. C. H. Spence, Eds), (Springer, Cham). forthcoming.
R. Castaing and L. Henry (1962). Filtrage magnétique des vitesses en microscopie électronique. *C. R. Acad. Sci. Paris* **255**, 76–78.
R. Castaing and L. Henry (1963). Filtrage magnétique des vitesses en microscopie électronique. *J. Microsc. (Paris)* **2**, 5–6.
R. Castaing and L. Henry (1964). Filtrage magnétique des vitesses en microscopie électronique. *J. Microsc. (Paris)* **3**, 133–152.
D. Cesar, J. Maxson, P. Musumeci, Y. Sun, J. Harrison, P. Frigola, F. H. O'Shea, H. To, D. Alesini and R. K. Li (2016). Demonstration of single-shot picosecond time-resolved MeV electron imaging using a compact permanent magnet quadrupole based lens. *Phys. Rev. Lett.* **117** (024801). 5 pp.
Z.-w. Chen, P.-y. Qiu and J.-k. Wang (1983). The optical properties of "swinging objective lens" in a combined magnetic lens and deflection system with superimposed field. *Optik* **64**, 341–347.
M. Cheng and T.-t. Tang (2000a). Study on wide beam curved optical axes focusing for magnetic immersed lenses without crossovers. *Optik* **11**, 509–513.
M. Cheng and T.-t. Tang (2000b). Demagnifying immersion magnetic lenses used for projection electron beam lithography without crossovers. *J. Vac. Sci. Technol. B* **18**, 3132–3136.
M. Cheng and T.-t. Tang (2001). Curvilinear-axis focusing and aberration theory of wide electron beams for combined immersion magnetic–electrostatic lens systems. *Optik* **112**, 259–267.

H. C. Chu and E. Munro (1982a). Numerical analysis of electron beam lithography systems. Part III: Calculation of the optical properties of electron focusing systems and dual-channel deflection systems with combined magnetic and electrostatic fields. *Optik* **61**, 121−145.

H. C. Chu and E. Munro (1982b). Numerical analysis of electron beam lithography systems. Part IV: Computerized optimization of the electron optical performance of electron beam lithography systems using the damped least squares method. *Optik* **61**, 213−236.

W. W. H. Clarke and L. Jacob (1953). Some characteristics of a low voltage immersion objective. *Proc. Phys. Soc. (Lond.) B* **66**, 284−295.

B. Cook and P. Kruit (2016). Coulomb interactions in sharp tip pulsed photo field emitters. *Appl. Phys. Lett.* **109**, 151901.

J. A. Cookson (1979). The production and use of a nuclear microprobe at MeV energies. *Nucl. Instrum. Meth.* **165**, 477−508.

J. A. Cookson, A. T. G. Ferguson and F. D. Pilling (1972). Proton microbeams, their production and use. *J. Radioanal. Chem.* **12**, 39−52.

A. V. Crewe and I. Gorodezky (2006). Flat electron beams. *Optik* **117**, 15−20.

A. V. Crewe, D. N. Eggenberger, L. M. Welter and J. Wall (1967). Experiments with quadrupole lenses in a scanning microscope. *J. Appl. Phys.* **38**, 4257−4266.

Z. Cui (2017). *Nanofabrication, Principles, Capabilities and Limits* (Springer, Switzerland). Chapter 3: Nanofabrication by electron beams.

T. D. Daumenov, A. A. Sapargaliev and E. M. Yakushev (1978). New method for determining the point characteristic function for charged particles in an electron-optical system with a straight optic axis. *Zh. Tekh. Fiz.* **48**, 2447−2454. *Sov. Phys. Tech. Phys*. **23**, 1400−1404.

E. de Chambost (1980). Optimization parameters of combined magnetic lenses and deflection system for electron beam microlithography. In *Microcircuit Engineering* (H. Ahmed and W. C. Nixon, Eds), 547−562 (Cambridge University Press, Cambridge).

J. M. H. Deltrap (1964). Correction of spherical aberration with combined quadrupole−octupole units. EUREM-3, Prague. **A**, 45−46.

G. V. Der-Shvarts and S. A. Belen'kii (1962). A study of the aberrations of electrostatic lens-filters. *Radiotekh. Elektron.* **7**, 126−132. *Radio Eng. Electron*. **7**, 112−117.

G. V. Der-Shvarts and Yu. V. Kulikov (1968). Third-order aberrations of cathode lenses with imperfect axial symmetry. *Radiotekh. Elektron.* **13**, 2223−2227. *Radio Eng. Electron. Phys*. **13**, 1945−1949.

R. S. Dhaliwal, W. A. Enichen, S. D. Golladay, M. S. Gordon, R. A. Kendall, J. E. Lieberman, H. C. Pfeiffer, D. J. Pinckney, C. F. Robinson, J. D. Rockrohr, W. Stickel and E. V. Tressler (2001). PREVAIL − electron projection technology approach for next-generation lithography. *IBM J. Res. Dev*. **45**, 615−638.

D. Dhuicq (1961). Recherche de systèmes de lentilles quadrupolaires stigmatiques au 1er ordre. Dissertation, Paris.

E. A. Dobisz, Z. Z. Bandic and M. C. Peckerar (2018). Electron beam nanolithography. In *Microlithography: Science and Technology* (K. Suzuki and B. W. Smith, Eds), 3rd edn). (CRC Press, Boca Raton). forthcoming.

A. L. Dodin and M. B. Nesvizhskii (1981). Accuracy of expansions in deriving the geometric aberration coefficients of cathode systems. *Zh. Tekh. Fiz.* **51**, 897−901. *Sov. Phys. Tech. Phys*. **26**, 539−541.

W. W. Dolan and W. P. Dyke (1954). Temperature-and-field emission of electrons from metals. *Phys. Rev*. **95**, 327−332.

M. Drechsler (1978). Erwin Müller and the early development of field emission microscopy. *Surf. Sci.* **70**, 1−18.

M. Drechsler and G. Pankow (1954). Ionen-Feldemissionsmikroskopie. ICEM-3, London. 405−411.

E. M. Dubinina, G. V. Spivak and I. A. Pryamkova (1959). On obtaining images with pulsed operation of a high-resolution emission microscope. *Izv. Akad. Nauk SSSR (Ser. Fiz.)* **23**, 762−764. *Bull. Acad. Sci. USSR (Phys. Ser.)* **23**, 756−758.

M. Duchesne (1949). Sur le calcul dans un objectif à immersion à symétrie axiale du potential le long de l'axe et de ses dérivées. *C. R. Acad. Sci. Paris* **228**, 1407−1408.

M. Duchesne (1953). Un récepteur de lumière à très haute sensibilité: le télescope électronique. Etude et amélioration. *Bull. Astron. (Paris)* **17** (No. 1). 88 pp.

H. Düker (1964). Emissions-Elektronenmikroskopie. *Acta Phys. Austr.* **18**, 232–251.

H. Düker and A. Illenberger (1962). A new immersion objective lens for the emission electron microscope. ICEM-5, Philadelphia. **1**, D-5.

H. Dušek (1959). Über die elektronenoptische Abbildung durch Orthogonalsysteme unter Verwendung eines neuen Modellfeldes mit streng angebbaren Paraxialbahnen. *Optik* **16**, 419–445.

W. P. Dyke and W. W. Dolan (1956). Field emission. *Adv. Electron. Electron Phys.* **8**, 89–185.

A. D. Dymnikov, T. Ya. Fishkova and S. Ya. Yavor (1965a). Using a rectangular model to obtain analytical expressions for spherical aberration of electromagnetic quadrupole lenses. *Phys. Lett.* **15**, 132–134.

A. D. Dymnikov, T. Ya. Fishkova and S. Ya. Yavor (1965b). Spherical aberration of a combined quadrupole lens with rectangular field distribution. *Dokl. Akad. Nauk SSSR* **162**, 1265–1268. *Sov. Phys. Dokl*. **10**, 547–550.

A. D. Dymnikov, T. Ya. Fishkova and S. Ya. Yavor (1965c). Spherical aberration of a combined quadrupole lens with bell-shaped field distribution. *Zh. Tekh. Fiz.* **35**, 1068–1076. *Sov. Phys. Tech. Phys*. **10**, 822–827.

A. D. Dymnikov, T. Ya. Fishkova and S. Ya. Yavor (1965d). Spherical aberration of compound quadrupole lenses and systems. *Nucl. Instrum. Meth.* **37**, 268–275.

R. F. Egerton (2015). Outrun radiation damage with electrons? *Adv. Struct. Chem. Imaging* **1**, 5–15.

W. Egle, D. Kurz and A. Rilk (1984). The EM 902, a new analytical TEM for ESI and EELS. *Zeiss Information MEM* No. 3, 4–12.

P. A. Einstein and L. Jacob (1948). On some focal properties of an electron optical immersion objective. *Philos. Mag.* **39**, 20–31.

A. B. El-Kareh and E. Grorud (1975). The analysis of the mirror area of an electrostatic electron mirror microscope. *Optik* **41**, 488–505.

W. Engel, R. Degenhardt, A. M. Bradshaw, R. Schlögl, H. J. Freund, H. Kuhlenbeck, R. Wichtendahl, E. Bauer, G. Lilienkamp, T. Schmidt, H. Rose, R. Spehr, D. Preikszas, P. Hartel, E. Umbach, R. Fink, M. Weiß, H. Petersen, M. Jung and G. Benner (1996). Design of a new photoemission spectro-microscope for BESSY II. *Recent Trends* **5**, 61–62.

V. N. Evdokimov (1985). Calculation of the field of multipole electrostatic deflection devices. *Radiotekh. Elektron.* **30**, 136–138. *Sov. J. Commun. Technol*. **30** (4), 70–73.

A. Fallahi, M. Fakhari, A. Yahaghi, M. Arrieta and F. Kärtner (2016). Short electron bunch generation using single-cycle ultrafast electron guns. *Phys. Rev. Accel. Beams* **19** (081302). 5 pp.

J. Fehr, W. Reiners, L. J. Balk, E. Kubalek, D. Köther and I. Wolff (1990). A 100-femtosecond electron beam blanking system. *Microelectron. Eng.* **12**, 221–226.

A. Feist, R. Bormann, J. Schauss, J. G. Gatzmann, N. Rubiano da Silva, S. Strauch, S. Schäfer and C. Ropers (2014). Ultrafast transmission electron microscopy with nanoscopic electron sources. IMC-18, Prague. IT-8-P-6048.

A. Feist, K. E. Echternkamp, J. Schauss, S. V. Yalunin, S. Schäfer and C. Ropers (2015). Quantum coherent optical phase modulation in an ultrafast transmission electron microscope. *Nature* **521**, 200–203.

A. Feist, N. Rubiano da Silva, W.-x. Liang, C. Ropers and S. Schäfer (2016). Spatio-temporal probing of lattice dynamics in graphite by ultrafast TEM. EMC-16, Lyon. **1**, 330–331.

A. Feist, N. Bach, N. Rubiano da Silva, T. Danz, M. Möller, K. E. Priebe, T. Domröse, J. G. Gatzmann, S. Rost, J. Schauss, S. Strauch, R. Bormann, M. Sivis, S. Schäfer and C. Ropers (2017). Ultrafast transmission electron microscopy using a laser-driven field emitter: femtosecond resolution with a high coherence electron beam. *Ultramicroscopy* **176**, 63–73.

J. Feng and A. Scholl (2008). Photoemission electron microscopy (PEEM). In *Science of Microscopy* (P. W. Hawkes and J. C. H. Spence, Eds), **1**, 657–695 (Springer, New York).

J. Feng and A. Scholl (2018). Photoemission electron microscopy (PEEM); In *Handbook of Microscopy* (P. W. Hawkes and J. C. H. Spence, Eds), (Springer, Cham); forthcoming.

J. Feng, A. A. Macdowell, R. Duarte, A. Doran, E. Forest, N. Kelez, M. Marcus, D. Munson, H. Padmore, K. Petermann, S. Raoux, D. Robin, A. Scholl, R. Schlueter, P. Schmid, J. Stohr, W. Wan, D. H. Wei and Y. Wu (2004). An aberration corrected photoemission electron microscope at the Advanced Light Source. In *Proc. Synchrotron Radiation Instrumentation*, San Francisco. *AIP Conference Proceedings*, **705**, 1070−1073.

J. Feng, E. Forest, A. A. Macdowell, M. Marcus, H. Padmore, S. Raoux, D. Robin, A. Scholl, R. Schlueter, P. Schmid, J. Stöhr, W. Wan, D. H. Wei and Y. K. Wu (2005). An X-ray photoemission electron microscope using an electron mirror aberration corrector for the study of complex materials. *J. Phys.: Condens. Matter* **17**, S1339−S1350.

C. Fert and R. Simon (1956). Amélioration du pouvoir de résolution du microscope électronique à émission. *C. R. Acad. Sci. Paris* **243**, 1300−1303.

C. Fert and R. Simon (1957). Pouvoir séparateur d'un microscope à émission en présence d'un diaphragme, et spectre de vitesses des électrons transmis. *C. R. Acad. Sci. Paris* **244**, 1177−1179.

R. Fink, M. R. Weiss, E. Umbach, D. Preikszas, H. Rose, R. Spehr, P. Hartel, W. Engel, R. Degenhardt, R. Wichtendahl, H. Kuhlenbeck, W. Erlebach, K. Ihmann, R. Schlögl, H. J. Freund, A. M. Bradshaw, G. Lilienkamp, T. Schmidt, E. Bauer and G. Benner (1997). SMART: a planned ultrahigh-resolution spectromicroscope for BESSY II. *J. Electron Spectrosc. Relat. Phenom.* **84**, 231−250.

T. Ya. Fishkova, L. A. Baranova and S. Ya. Yavor (1968). Coefficients of spherical aberration of a stigmatic doublet of quadrupole lenses (rectangular model). *Zh. Tekh. Fiz.* **38**, 694−703. *Sov. Phys. Tech. Phys*. **13**, 520−525.

T. Ya. Fishkova, E. V. Shpak and N. A. Tsaplina (1984). Axisymmetric quadrupole immersion system. *Zh. Tekh. Fiz.* **54**, 1179−1182. *Sov. Phys. Tech. Phys*. **29**, 671−673.

G. Forst (1966). Energiefilterung von gestreuten Ionen. *Z. Angew. Phys.* **20**, 265−267.

G. Forst and B. Wende (1964). Zur Bildentstehung im Elektronenspiegelmikroskop. *Z. Angew. Phys.* **17**, 479−481.

A. Foster (1968). Correction of aperture aberrations in magnetic lens spectrometers. Dissertation, London.

M. S. Foster, J. C. Campuzano, R. F. Willis and J. C. Dupuy (2011). A mirror electron microscope for surface analysis. *J. Microsc. (Oxford)* **140**, 395−403.

L. Frank, I. Müllerová and M. M. El Gomati (2000). A novel in-lens detector for electrostatic LEEM mini-column. *Ultramicroscopy* **81**, 99−110.

L. Frank, M. Hovorka, I. Konvalina, S. Mikmeková and I. Müllerová (2011). Very low energy scanning electron microscopy. *Nucl. Instrum. Meth. Phys. Res. A* **645**, 46−54.

N. Franzen (1984). Computer programs for analyzing certain classes of 3-D electrostatic fields with two planes of symmetry. In *Electron Optical Systems for Microscopy, Microanalysis and Microlithography* (J. J. Hren, F. A. Lenz, E. Munro and P. B. Sewell, Eds), 115−126 (Scanning Electron Microscopy, AMF O'Hare).

H. Fujioka and K. Ura (1983). Electron beam blanking systems. *Scanning* **5**, 3−13.

F. N. Gaafer (2014). Minimization of the spherical aberration coefficient of [systems] composed of quadrupole and octupole lenses using the rectangular field distribution model. *Al-Qadisiyha J. Pure Sci.* **19** (3), 155−167.

J. Gardez (1959). Construction d'un microscope à émission fonctionnant en impulsions à très haute tension. *C. R. Acad. Sci. Paris* **249**, 2034−2036.

J. R. Garrood and W. C. Nixon (1968). Scanning mirror electron microscopy. EUREM-4, Rome. **1**, 95−96.

F. Gaydou (1961). Beitrag zur Theorie des Immersionsobjektivs. Dissertation, Zürich.

J. W. Gibson and R. E. Thomas (1985). Computer controlled techniques for high emission density mapping of thermionic cathodes. *Appl. Surf. Sci.* **24**, 518−537.

W. Glaser (1955). Investigations of 4-pole lenses; an electron microscope corrected with respect to spherical aberration. *Farrand Optical Co. Internal Reports.*

L. G. Glikman and Z. D. Iskakova (1976). Spherical aberration of a two-electrode astigmatic tubular lens for an arbitrary object position. I, II. *Zh. Tekh. Fiz.* **46**, 1171−1181 & 1182−1191. *Sov. Phys. Tech. Phys*. **21**, 666−671 & 672−677.

L. G. Glikman and Z. D. Iskakova (1982). Electrostatic einzel astigmatic tubular lenses. *Zh. Tekh. Fiz.* **52**, 1874–1877. *Sov. Phys. Tech. Phys*. **27**, 1150–1152.
L. G. Glikman and L. M. Sekunova (1981). Electrostatic box lens with four planes of symmetry. *Zh. Tekh. Fiz.* **51**, 1804–1808. *Sov. Phys. Tech. Phys*. **26**, 1046–1048.
L. G. Glikman, S. P. Karetskaya, V. M. Kel'man and E. M. Yakushev (1971). Electron-optical parameters of three-electrode transaxial cylindrical lenses. *Zh. Tekh. Fiz.* **41**, 330–335. *Sov. Phys. Tech. Phys*. **16**, 247–251.
L. G. Glikman, V. M. Kel'man and L. V. Fedulina (1973a). Wedge-shaped electrostatic prism. *Zh. Tekh. Fiz.* **43**, 1793–1798. *Sov. Phys. Tech. Phys*. **18**, 1139–1141.
L. G. Glikman, V. M. Kel'man and L. V. Fedulina (1973b). Geometrical aberrations of a wedge-shaped electrostatic prism. *Zh. Tekh. Fiz.* **43**, 2017–2022. *Sov. Phys. Tech. Phys*. **18**, 1273–1276.
L. G. Glikman, V. M. Kel'man, O. V. Pavlichkova and I. F. Spivak-Lavrov (1976a). Geometrical angular aberrations of three-electrode and five-electrode wedge-shaped electrostatic prisms. I. II. *Zh. Tekh. Fiz.* **46**, 1810–1820 & 1821–1825. *Sov. Phys. Tech. Phys*. **21**, 1055–1059 & 1060–1062.
L. G. Glikman, V. M. Kel'man, O. V. Pavlichkova and I. F. Spivak-Lavrov (1976b). Telescopic and dispersion conditions for three-electrode and five-electrode wedge-shaped electrostatic prisms. *Zh. Tekh. Fiz.* **46**, 1978–1981. *Sov. Phys. Tech. Phys*. **21**, 1153–1155.
L. G. Glikman, V. M. Kel'man, O. V. Pavlichkova and A. A. Sapargaliev (1977a). Wedge-shaped prism with combined electric and magnetic fields. *Zh. Tekh. Fiz.* **47**, 1361–1371. *Sov. Phys. Tech. Phys*. **22**, 782–787.
L. G. Glikman, O. V. Pavlichkova and I. F. Spivak-Lavrov (1977b). Cone-shaped prisms with combined electric and magnetic fields. *Zh. Tekh. Fiz.* **47**, 1372–1379. *Sov. Phys. Tech. Phys*. **22**, 788–792.
R. Gobrecht (1961). Der Öffnungsfehler elektrischer Immersionslinsen in Beschleunigungs- und Verzögungsschaltung. *Exp. Tech. Phys.* **9**, 184–196.
R. Godehardt (1995). Mirror electron microscopy. *Adv. Imaging Electron Phys.* **94**, 81–150.
R. Gomer (1961). *Field Emission and Field Ionization* (Harvard University Press, Cambridge MA).
R. Gomer (1994). Field emission, field ionization, and field desorption. *Surf. Sci.* **299/300**, 129–152.
R. H. Good and E. W. Müller (1956). Field emission. *Handbuch der Physik* **21**, 176–231.
E. Goto and T. Soma (1977). MOL (moving objective lens). Formulation of deflective aberration free system. *Optik* **48**, 255–270.
E. Goto, T. Soma, M. Idesawa, T. Sasaki, T. Goto, S. Konno, T. Someya, K. Tanaka and S. Miyauchi (1983). In-lens deflection system with nonequisectored-type multipole electrostatic deflectors. *J. Vac. Sci. Technol. B* **1**. 1289–1282.
J. Greer, A. Korkin and J. Labanowski, Eds (2003). *Nano and Giga Challenges in Microelectronics* (Elsevier, Amsterdam).
O. H. Griffith, P. A. Habliston and G. B. Birrell (1991). Bibliography on emission microscopy, mirror electron microscopy, low-energy electron microscopy and related techniques: 1985–1991. *Ultramicroscopy* **36**, 262–274.
G. W. Grime and F. Watt (1984). *Beam Optics of Quadrupole Probe-Forming Systems* (Hilger, Bristol).
N. P. Gritsyuk and R. A. Lachashvili (1979). An immersion crossed lens. *Zh. Tekh. Fiz.* **49**, 2467–2468. *Sov. Phys. Tech. Phys*. **24**, 1389–1390.
P. Grivet (1965). *Electron Optics* (Pergamon, Oxford & New York).
P. Grivet and A. Septier (1958). Les lentilles quadrupolaires magnétiques. CERN Report 58-25.
P. Grivet and A. Septier (1960). Les lentilles quadrupolaires magnétiques, I & II. *Nucl. Instrum. Meth.* **6**, 126–156 & 243–275.
K. Grzelakowski (2012). A novel imaging energy filter for cathode lens electron microscopy. *Ultramicroscopy* **116**, 95–105.
K. Grzelakowski and R. M. Tromp (2013). Temporal and lateral electron pulse compression by a compact spherical electrostatic capacitor. *Ultramicroscopy* **130**, 36–43.
M. Gulde, S. Schweda, G. Storeck, M. Maiti, H.-k. Yu, A. M. Wodtke, S. Schäfer and C. Ropers (2014). Ultrafast low-energy electron diffraction in transmission resolves polymer/graphene superstructure dynamics. *Science* **345**, 200–204.

E. Hahn (1958a). Zur numerischen Durchrechnung von elektrostatischen Immersionsobjektiven. *Optik* **15**, 500–516.

E. Hahn (1958b). Berechnung der Kardinalelemente und Bildfehler bis zur 3. Ordnung des elektrostatischen Immersionsobjektives. *Jenaer Jahrbuch* Pt. I, 184–202.

E. Hahn (1959). Numerische Untersuchungen an einem typischen elektrostatischen Immersionsobjektiv. *Optik* **16**, 513–521.

E. Hahn (1961). Zur Theorie des elektrostatischen Geschwindigkeitsfilters. *Jenaer Jahrbuch* Pt. II, 325–399.

R. T. Hamarat, J. Witzani and E. M. Hörl (1984). Electron optical characteristics of a concave electrostatic electron mirror for a scanning electron microscope. *Scanning* **6**, 75–79.

H. Hanssum (1983). Exact solution of the Poisson equation for a DC current on a saddle-shaped Helmholtz coil. *J. Phys. A: Math. Gen.* **16**, 3385–3392.

H. Hanssum (1984). The magnetic field of saddle-shaped coils: I. Symmetry of the magnetic field around the coil centre. *J. Phys. D: Appl. Phys.* **17**, 1–18.

H. Hanssum (1985). The magnetic field of saddle-shaped coils: II. Transverse components. *J. Phys. D: Appl. Phys.* **18**, 1971–1978.

H. Hanssum (1986). The magnetic field of saddle-shaped coils: III. Improving the uniformity of $|\boldsymbol{B}|$ in a large volume. *J. Phys. D: Appl. Phys.* **19**, 493–501.

D. F. Hardy (1967). Combined magnetic and electrostatic quadrupole electron lenses. Dissertation, Cambridge.

P. Hartel, D. Preikszas, R. Spehr and H. Rose (1998). Test of a beam separator for a corrected PEEM/LEEM. *Recent Trends* **6**, 24–25.

P. Hartel, D. Preikszas, R. Spehr and H. Rose (2000). Performance of the mirror corrector for an ultrahigh-resolution spectromicroscope. EUREM-12, Brno. **3**, I.153–I.154.

P. Hartel, D. Preikszas, R. Spehr, H. Müller and H. Rose (2002). Mirror corrector for low-voltage electron microscopes. *Adv. Imaging Electron Phys.* **120**, 41–133.

W. A. M. Hartl (1964). Monochromatic fast electrons produced by a filter lens. *Phys. Lett.* **13**, 133–134.

W. A. M. Hartl (1966). Die Filterlinse als Monochromator für schnelle Elektronen. *Z. Phys.* **191**, 487–502.

P. W. Hawkes (1966). *Quadrupole Optics* (Springer, Berlin & New York).

P. W. Hawkes (1967a). Asymptotic quadrupole aberrations: the bell-shaped model. I. *Optik* **25**, 439–449.

P. W. Hawkes (1967b). Asymptotic quadrupole aberrations: the bell-shaped model. III. *Optik* **26**, 497–506.

P. W. Hawkes (1970). Quadrupoles in Electron Lens Design. *Adv. Electron. Electron Phys.* Suppl. 7.

P. W. Hawkes (1980). Methods of computing optical properties and combating aberrations in low intensity beams. In *Applied Charged Particle Optics* (A. Septier, Ed.), 45–157 (Academic Press, New York & London). ; *Adv. Electron. Electron Phys*. Suppl. 13A.

P. W. Hawkes (2012). Examples of electrostatic electron optics: the Farrand and Elektros microscopes and electron mirrors. *Ultramicroscopy* **119**, 9–17.

P. W. Hawkes and E. L. Cham (1967a). Asymptotic quadrupole aberrations: the bell-shaped model. IV. *Optik* **26**, 507–552.

P. W. Hawkes and D. F. Hardy (1967b). Asymptotic quadrupole aberrations: the bell-shaped model. II. *Optik* **25**, 450–458.

K. Heinemann (1968). Grenzauflösung der Emissionsmikroskopie mit einer Drei-Elektroden-Kathodenlinse für ionenausgelöste Elektronen. *Optik* **27**, 369–376.

K. Heinemann and F. Lenz (1968). Berechnungen zur Grenzauflösung einer 3-Elektroden-Kathodenlinse für ionenausgelöste Elektronen. *Optik* **27**, 454–465.

K. Heinemann and G. Möllenstedt (1967). Elektronenmikroskopie mit langsamen Elektronen mittels Zwischenverzögerer. *Optik* **26**, 11–21.

R. M. Henkelman and F. P. Ottensmeyer (1974). An electrostatic mirror. *J. Phys. E: Sci. Instrum.* **7**, 176–178.

W. Henneberg and A. Recknagel (1935). Zusammenhänge zwischen Elektronenlinse, Elektronenspiegel und Steuerung. *Z. Tech. Phys.* **16**, 621–623.

E. Hess (1934). Beitrag zur Kenntnis der elektronenoptischen Immersionslinse. I. *Z. Phys.* **92**, 274–282, for Part II, see Behne (1936c).

J. Heydenreich (1966). Some remarks on the image formation in the diverging electron mirror microscope. ICEM-6, Kyoto. **1**, 233–234.

M. Horáček, I. Vlček and M. Zobać (2008). Wien filter electron optical characteristics determining using shadow projection method. *Recent Trends* **11**, 47–48.

T. Hosokawa (1980). Systematic elimination of third order aberrations in electron beam scanning systems. *Optik* **56**, 21–30.

T. Hosokawa and H. Morita (1983). Electron beam optical system with large field coverage for submicron lithography. *J. Vac. Sci. Technol. B* **1**, 1293–1297.

T. Hosokawa, H. Fujioka and K. Ura (1978a). Generation and measurement of subpicosecond electron beam pulses. *Rev. Sci. Instrum.* **49**, 624–628.

T. Hosokawa, H. Fujioka and K. Ura (1978b). Gigahertz stroboscopy with the scanning electron microscope. *Rev. Sci. Instrum.* **49**, 1293–1299.

G. Hottenroth (1936). Über Elektronenspiegel. *Z. Phys.* **103**, 460–462.

G. Hottenroth (1937). Untersuchungen über Elektronenspiegel. *Ann. Phys. (Leipzig)* **30** (422), 689–712.

F. Houdellier, G. M. Caruso, P. Abeilhou and A. Arbouet (2016). Design and realization of an ultrafast cold field emission source operating under high voltage. EMC-16, Lyon. **1**, 316–317.

E.-L. Huguenin (1954). Un essai de microscopie électronique à photoémission. *C. R. Acad. Sci. Paris* **239**, 404–406.

E.-L. Huguenin (1957). Sur le microscope électronique à photoémission. *Ann. Phys. (Paris)* **2**, 214–266.

S. Humphries (1986). *Principles of Charged Particle Acceleration* (Wiley–Interscience, New York).

J. W. Hurd (1987). Derivation of the first-order transformation matrix for a simple Wien filter and comparison to results of numerical integration. *Nucl. Instrum. Meth. Phys. Res. A* **258**, 542–547.

A. T. Ibrayev (2015). Theory of cathode lens with multipole components of electrostatic field and space charge. *Microsc. Microanal.* **21** (Suppl. 4), 270–275.

A. T. Ibraev and A. A. Sapargaliev (1981). A transaxial electrostatic cathode lens. *Zh. Tekh. Fiz.* **51**, 22–30. *Sov. Phys. Tech. Phys.* **26**, 11–15.

M. Idesawa, T. Soma, E. Goto and T. Sasaki (1983). Numerical considerations on multipole-type electrostatic deflectors. *J. Vac. Sci. Technol. B* **1**, 1322–1326.

A. N. Ignat'ev, B. E. Dashevskii, V. Ya. Ivanov and Yu. V. Kulikov (1979). Cathode lens having a quasi-spherical field. *Opt.-Mekh. Prom.* **46** (11), 41–43. *Sov. J. Opt. Technol*. **46**, 675–676.

E. Igras (1961). Mapping of the electric structure of semiconductor surfaces by the method of the electron mirror. *Bull. Acad. Polon. Sci. (Sér. Sci. Math. Astron. Phys.)* **9**, 403–407.

E. Igras and T. Warminski (1965). Electron mirror observations of semiconductor surfaces at low temperatures. *Phys. Stat. Sol. (b)* **9**, 79–85.

V. P. Il'in, V. A. Kateshov, Yu. V. Kulikov and M. A. Monastyrskii (1984). Optimization of cathode lenses in the EFIR applications software. *Avtometriya* No. 5, 93–101. *Autom. Monit. Meas*. No. 5, 92–100.

V. P. Il'in, V. A. Kateshov, Yu. V. Kulikov and M. A. Monastyrskii (1987). *Chislennye Metody Optimizatsii Emissionnykh Elektronno-Opticheskikh Sistem* (Nauka, Novosibirsk).

D. Ioanoviciu (1973). Ion optics of a Wien filter with inhomogeneous fields. *Int. J. Mass Spectrom. Ion Phys.* **11**, 169–184.

D. Ioanoviciu, K. Tsuno and G. Martínez (2004). Third order aberration theory of double Wien filters. *Rev. Sci. Instrum.* **75**, 4434–4441.

Z. D. Iskakova (1978). Triplets made up of two-electrode astigmatic tubular lenses with small spherical aberration in one direction. *Zh. Tekh. Fiz.* **48**, 1537–1539. *Sov. Phys. Tech. Phys*. **23**, 870–872.

K. Ito, T. Ito and M. Watanabe (1954). An improved reflection type electron microscope. *J. Electronmicrosc* **2**, 10–14.

V. Ya. Ivanov, A. N. Ignat'ev, Yu. V. Kulikov, S. V. Kolesnikov and A. M. Mechetin (1983). Image defocusing in the presence of small defects in axisymmetric cathode lenses. *Opt.-Mekh. Prom.* **50** (3), 7–8. *Sov. J. Opt. Technol*. **50**, 139–141.

L. Jacob (1950). Some crossover properties in the electron immersion objective. *J. Appl. Phys.* **21**, 966–970.

R. O. Jenkins (1942). Field emission of electrons. *Rep. Prog. Phys.* **9**, 177–197.

X.-r Jiang (1988). Simple calculation formulas for field and aberrations of resistance box yokes. *J. Vac. Sci. Technol. B* **6**, 422–425.

H. Johannson (1933). Über das Immersionsobjektiv der geometrischen Elektronenoptik. *Ann. Phys. (Leipzig)* **18** (410), 385–413.

H. Johannson (1934). Über das Immersionsobjektiv der geometrischen Elektronenoptik. II. *Ann. Phys. (Leipzig)* **21** (413), 274–284.

S. M. Juma, F. A. Jalil and I. L. Mohammad (2007). Computations on the optical properties of the electrostatic symmetric quadrupole triplet lens. *J. Al-Nahrain Univ.* **10** (1), 73–77.

P. Junior and P. Antony-Spies (1967). Möglichkeiten stigmatischer Abbildungen mit Vierpollinsen. *Z. Angew. Phys.* **22**, 420–425.

K. Kanaya (1962). An anastigmatic alinement system by double magnetic deflectors with stigmator in the electron beam instruments. *Bull. Electrotech. Lab* **26**, 161–172.

K. Kanaya and H. Kawakatsu (1961a). Double electro-static deflection of electron beams without aberrations. *Bull. Electrotech. Lab* **25**, 241–252.

K. Kanaya and H. Kawakatsu (1961b). Deflection system with eight-pole stigmator used in correcting astigmatism. *J. Electronmicrosc* **10**, 218–221.

K. Kanaya and H. Kawakatsu (1962). An anastigmatic deflection system consisting of eight poles for use with electron beam instruments. *Bull. Electrotech. Lab* **26**, 241–250.

K. Kanaya, H. Kawakatsu, I. Okazaki and T. Takizawa (1963). Magnetic deflection of electron beams and caustic patterns. *Bull. Electrotech. Lab* **27**, 401–417.

K. Kanaya, H. Kawakatsu, I. Okazaki and T. Takizawa (1964). A star pattern of deflected beam caused by coma aberration. *J. Electronmicrosc* **13**, 80–86.

K. Kanaya, H. Kawakatsu and K. Tanaka (1961). Electron-optical design of deflection system free from aberrations by means of stigmator. *Bull. Electrotech. Lab* **25**, 481–494.

S. P. Karetskaya and L. V. Fedulina (1977). Focusing properties of a transaxial electrostatic lens for a curved charged particle beam. *Zh. Tekh. Fiz.* **47**, 1141–1149. *Sov. Phys. Tech. Phys*. **22**, 656–660.

S. P. Karetskaya, V. M. Kel'man and E. M. Yakushev (1970). A transaxial electrostatic lens. *Zh. Tekh. Fiz.* **40**, 2563–2567. *Sov. Phys. Tech. Phys*. **15**, 2010–2013.

S. P. Karetskaya, V. M. Kel'man and E. M. Yakushev (1971). Aberrations of transaxial electrostatic lenses. *Zh. Tekh. Fiz.* **41**, 325–329. *Sov. Phys. Tech. Phys*. **16**, 244–246.

P. P. Kas'yankov (1953). On the calculation of electron lenses with given focusing properties in the paraxial region. *Zh. Tekh. Fiz.* **23**, 531–540.

P. P. Kas'yankov (1961). Calculation of cathode lens aberrations. *Opt. Spektrosk.* **11**, 765–767. *Opt. Spectrosc*. **11**, 413–414.

E. Kasper and A. P. Wilska (1967). An electron optical filter projection system with image intensification through storage. *Optik* **26**, 247–253.

M. Kato and K. Tsuno (1990). Numerical analysis of trajectories and aberrations of a Wien filter including the effect of fringing fields. *Nucl. Instrum. Meth. Phys. Res. A* **298**, 296–320.

H. Kawakatsu and K. Kanaya (1961). Electro-static deflection system used in electron beam apparatus. *J. Electronmicrosc* **10**, 119–124.

V. M. Kel'man, L. V. Fedulina and E. M. Yakushev (1971). Combined cylindrical electron mirrors. I. *Zh. Tekh. Fiz.* **41**, 2016–2022. *Sov. Phys. Tech. Phys*. **16**, 1598–1602.

V. M. Kel'man, L. V. Fedulina and E. M. Yakushev (1972a). Theory of compound cylindrical electron mirrors. II. *Zh. Tekh. Fiz.* **42**, 297–302. *Sov. Phys. Tech. Phys*. **17**, 238–241.

V. M. Kel'man, L. M. Sekunova and E. M. Yakushev (1972b). A new method for the design of axially symmetric electron mirrors. *Zh. Tekh. Fiz.* **42**, 2279–2287. *Sov. Phys. Tech. Phys*. **17**, 1786–1791.

V. M. Kel'man, L. M. Sekunova and E. M. Yakushev (1973a). Theory of axisymmetric electron mirrors. I. Trajectory equations. *Zh. Tekh. Fiz.* **43**, 1799–1806. *Sov. Phys. Tech. Phys*. **18**, 1142–1146.

V. M. Kel'man, L. M. Sekunova and E. M. Yakushev (1973b). Theory of axisymmetric electron mirrors. II. Electron-optical properties. *Zh. Tekh. Fiz.* **43**, 1807–1817. *Sov. Phys. Tech. Phys.* **18**, 1147–1152.

V. M. Kel'man, L. M. Sekunova and E. M. Yakushev (1973c). The transaxial elecron mirror. I. *Zh. Tekh. Fiz.* **43**, 2238–2245. *Sov. Phys. Tech. Phys.* **18**, 1418–1421.

V. M. Kel'man, L. M. Sekunova and E. M. Yakushev (1973d). The transaxial electron mirror. II. Aberrations. *Zh. Tekh. Fiz.* **43**, 2463–2471. *Sov. Phys. Tech. Phys.* **18**, 1552–1556.

V. M. Kel'man, A. A. Sapargaliev and E. M. Yakushev (1974). The theory of cathode lenses. III, IV. *Zh. Tekh. Fiz.* **44**, 928–937 & 938–943. *Sov. Phys. Tech. Phys.* **19**, 592–596 & 597–599.

D. P. Kern and T. H. P. Chang (1994). Miniaturized electron optics: basics and applications. ICEM-13, Paris. **1**, 149–152.

D. P. Kern, M. A. Sturans, H. C. Pfeiffer and W. Stickel (1985). Computer analysis of VAIL. In *Microcircuit Engineering 84* (A. Heuberger and H. Beneking, Eds), 185–194 (Academic Press, London & Orlando).

J. Kessler and H. Lindner (1964). Erfahrungen mit der Fünf-Elektroden-Filterlinse. *Z. Angew. Phys.* **18**, 7–9.

A. Khursheed (2002). A low voltage time of flight electron emission microscope. *Optik* **113**, 505–509.

W. E. King, M. R. Armstrong, O. Bostanjoglo and B. W. Reed (2008). High-speed electron microscopy. In *Science of Microscopy* (P. W. Hawkes and J. C. H. Spence, Eds), **1**, 406–444 (Springer, New York).

H. Kleinschmidt and O. Bostanjoglo (2000). Nanosecond mirror electron microscope. EMC-12, Brno. **4**, S77–S78.

O. Klemperer (1953). *Electron Optics* (Cambridge University Press, Cambridge).

M. Knoll and E. Ruska (1932). Beitrag zur geometrischen Elektronenoptik. I & II. *Ann. Phys. (Leipzig)* **12** (404), 607–640 & 641–661.

M. Knoll, F. G. Houtermans and W. Schulze (1932). Untersuchung der Emissionsverteilung an Glühkathoden mit dem magnetischen Elektronenmikroskop. *Z. Phys.* **78**, 340–362.

S. V. Kolesnikov and M. A. Monastyrskii (1988). General theory of spatial and temporal aberrations in cathode lenses with slightly imperfect axial symmetry. *Zh. Tekh. Fiz.* **58**, 3–10 & 11–19. *Sov. Phys. Tech. Phys.* **33**, 1–5 & 6–11.

E. Koltay, I. Kish, L. A. Baranova and S. Ya. Yavor (1972). The effective lengths of dipole, quadrupole and octopole electron-optical elements with concave electrodes. *Radiotekh. Elektron.* **17**, 1906–1910. *Radio Eng. Electron. Phys.* **17**, 1518–1521.

R. Könenkamp, T. Jones, J. Elstner, R. C. Word, G. Rempfer, T. Dixon, L. Almaraz and W. Skoczylas (2008). Image properties in an aberration-corrected photoemission electron microscope. *Phys. Procedia* **1**, 505–511.

R. Könenkamp, R. C. Word, G. F. Rempfer, T. Dixon, L. Almarez and T. Jones (2010). 5.4 nm spatial resolution in biological photoemission electron microscopy. *Ultramicroscopy* **110**, 899–902.

I. Konvalina and I. Müllerová (2011). Properties of the cathode lens combined with a focusing magnetic/immersion-magnetic lens. *Nucl. Instrum. Meth. Phys. Res. A* **645**, 55–59.

I. Konvalina, M. Hovorka and I. Müllerová (2010). Electron optical properties of the cathode lens combined with a focusing magnetic/immersion-magnetic lens. *Recent Trends* **12**, 21–22.

H. W. P. Koops (1980). Electron beam projection techniques. In *Materials Processing, Theory and Practice* (F. F. Wang, Ed.), **1**, 233–336 (North Holland, Amsterdam).

H. W. P. Koops (1989). Capacity of electron beam reducing image projection systems with dynamically compensated field aberrations. *Microelectron. Eng.* **9**, 217–220.

Yu. V. Kulikov (1966). On the calculation of the image current density in cathode lenses. *Radiotekh. Elektron.* **11**, 2196–2199. *Radio Eng. Electron. Phys.* **11**, 1936–1938.

Yu. V. Kulikov (1971). Geometrical optics of a five-electrode immersion objective. *Radiotekh. Elektron.* **16**, 654–655. *Radio Eng. Electron. Phys.* **16**, 715–717.

Yu. V. Kulikov (1972). The problem of evaluating the image quality of cathode electron-optical systems. *Radiotekh. Elektron.* **17**, 373–375. *Radio Eng. Electron. Phys.* **17**, 286–288. *Radio Eng. Electron. Phys.* **18** (11), 286–288.

Yu. V. Kulikov (1973). Some problems of cathode lenses with image transfer. *Radiotekh. Elektron.* **18**, 2379–2383. *Radio Eng. Electron. Phys.* **18** (11), 286–288.

Yu. V. Kulikov (1975). Evaluation of the image quality of cathode electron-optical systems with third-order aberrations taken into account. *Radiotekh. Elektron.* **20**, 1249–1254. *Radio Eng. Electron. Phys.* **20** (6), 93.

Yu. V. Kulikov, M. A. Monastyrskii and K. I. Feygin (1978). Theory of third-order aberrations of cathode lenses. Aberrations of cathode lenses with combined electric and magnetic fields. *Radiotekh. Elektron.* **23**, 167–174. *Radio Eng. Electron. Phys.* **23** (1), 120.

M. Kuwahara, F. Ichihashi, S. Kusunoki, Y. Takeda, K. Saitoh, T. Ujihara, H. Asano, T. Nakanishi and N. Tanaka (2011a). Development of spin-polarized pulsed TEM. EMAG, Birmingham. 012004, 4 pp.

M. Kuwahara, Y. Takeda, K. Saitoh, T. Ujihara, H. Asano, T. Nakanishi and N. Tanaka (2011b). Development of spin-polarized transmission electron microscopy. *J. Phys. Conf. Ser.* **298**. 012006, 6 pp.

M. Kuwahara, S. Kusunoki, X.-g. Jin, T. Nakanishi, Y. Takeda, K. Saitoh and K. Tanaka (2012). 30-kV spin-polarized transmission electron microscope with GaAs–GaAsP strained superlattice cathode. *Appl. Phys. Lett.* **101**, 033102.

M. Kuwahara, Y. Nambo, S. Kusunoki, X.-g. Jin, K. Saitoh, H. Asano, T. Ujihara, Y. Takeda, T. Nakanishi and N. Tanaka (2013). Phase-locking of oscillating images using laser-induced spin-polarized pulse TEM. *Microscopy* **62**, 607–614.

M. Kuwahara, S. Kusunoki, Y. Nambo, K. Saitoh, X.-g. Jin, T. Ujihara, H. Asano, Y. Takeda and N. Tanaka (2014). Coherence of a spin-polarized electron beam emitted from a semiconductor photocathode in a transmission electron microscope. *Appl. Phys. Lett.* **105**, 193101.

M. Kuwahara, K. Sameshima, K. Aoki, H. Asano, T. Ujihara, K. Saitoh and K. Tanaka (2015). Coherences of spin-polarized and pulsed electron beam extracted from a semiconductor cathode in TEM. *Microscopy* **64** (Suppl. 1), i17.

M. Kuwahara, K. Aoki, H. Suzuki, H. Asano, T. Ujihara, K. Saitoh, and N. Tanaka (2016a). Coherence of a pulsed electron beam extracted from a semiconductor photocathode in transmission electron microscope. EMC-16, Lyon. **1**, 318–319.

M. Kuwahara, Y. Nambo, K. Aoki, K. Sameshima, X.-g Jin, T. Ujihara, H. Asano, T. Nakanishi and N. Tanaka (2016b). The Boersch effect in a picosecond pulsed electron beam emitted from a semiconductor. *Appl. Phys. Lett.* **109**, 013108.

T. LaGrange, G. H. Campbell, B. W. Reed, M. Taheri, J. B. Pesavento, J. S. Kim and N. D. Browning (2008). Nanosecond time-resolved investigations using the in situ [*sic*] of dynamic transmission electron microscope (DTEM). *Ultramicroscopy* **108**, 1441–1449.

T. LaGrange, B. W. Reed, W. E. King, J. S. Kim and G. H. Campbell (2012a). Dynamic transmission electron microscopy. In *In-situ Electron Microscopy* (G. Dehm, J. M. Howe and J. Zweck, Eds), 71–97 (Wiley–VCH, Weinheim).

T. LaGrange, B. W. Reed, M. K. Santala, J. T. McKeown, A. Kulovits, J. M. K. Wiezorek, L. Nikolova, F. Rosei, B. J. Siwick and G. H. Campbell (2012b). Approaches for ultrafast imaging of transient materials processes in the transmission electron microscope. *Micron* **43**, 1108–1120.

J. D. Lawson (1977). *The Physics of Charged-Particle Beams* (Clarendon Press, Oxford); 2nd edn, 1988.

J. B. Le Poole (1964). Scanning microscope using quadrupole lenses. EUREM-3, Prague. Appendix, 443–444.

J. B. Le Poole, J. E. Barth and W. F. Rosenbrand (1972). Crossed slits magnetic pseudo-quadrupoles. EUREM-5, Manchester. 80.

Y. M. Lee, Y. J. Kim, Y.-j Kim and O.-h. Kwon (2017a). Ultrafast electron microscopy integrated with a direct electron detection camera. *Struct. Dyn* **4**, 044023, 8 pp.

Z.-b. Lee, U. Kaiser and H. Rose (2017b). Advantages of nonstandard imaging methods in TEM and STEM. MC-2017, Lausanne, 509–510.

G. E. Lee-Whiting (1970). Third-order aberrations of a magnetic quadrupole lens. *Nucl. Instrum. Meth.* **83**, 232–244.

M. Lenc and I. Müllerová (1992a). Electron optical properties of a cathode lens. *Ultramicroscopy* **41**, 411–417.

M. Lenc and I. Müllerová (1992b). Optical properties and axial aberration coefficients of the cathode lens in combination with a focusing lens. *Ultramicroscopy* **45**, 159–162.

F. Lenz (1973). Computer-aided design of electron optical systems. In *Image Processing and Computer-Aided Design in Electron Optics* (P. W. Hawkes, Ed.), 274–282 (Academic Press, London & New York).

F. Lenz (1979). Third-order distortion of axisymmetric electrostatic post-deflection lenses. *Proc. Soc. Inform. Display* **20**, 65–70.

H. J. Levinson (2010). *Principles of Lithography*, 3rd ed. (SPIE Press, Bellingham).

Y. Li (1981). The relativistic aberration theory of a combined electric–magnetic focusing–deflection system. *Acta Phys. Sin.* **30**, 1155–1164.

R. K. Li and P. Musumeci (2014). Single-shot MeV transmission electron microscopy with picosecond temporal resolution. *Phys. Rev. Appl.* **2**. 024003, 15 pp.

Y. Li and J.-y. Ximen (1982). On the relativistic aberration theory of a combined focusing–deflection system with multi-stage deflectors. *Optik* **61**, 315–332.

J. A. Liddle, S. D. Berger, C. J. Biddick, M. I. Blakey, K. J. Bolan, S. W. Bowler, K. Brady, R. M. Camarda, W. F. Connelly, A. H. Crorken, J. Custy, R. C. Farrow, J. A. Felker, L. A. Fetter, R. Freeman, L. R. Harriott, L. Hopkins, H. A. Huggins, C. S. Knurek, J. S. Kraus, D. A. Mixon, M. M. Mkrtchyan, A. E. Novembre, M. L. Peabody, W. A. Simpson, R. G. Tarascon, H. H. Wade, W. K. Waskiewicz, G. P. Watson, J. K. Williams and D. L. Windt (1995). The SCattering with Angular Limitation in Projection Electron-beam Lithography (SCALPEL) system. *Jpn. J. Appl. Phys.* **34**, 6663–6671.

H. Liebl (1979). A new emission lens. *Optik* **53**, 69–72.

C. Lienau, M. Raschke and C. Ropers (2015). Ultrafast nano-focusing for imaging and spectroscopy with electrons and light. In *Attosecond Nanophysics. From Basic Science to Applications* (P. Hommelhoff and M. F. Kling, Eds), 281–323 (Wiley–VCH, Weinheim).

W. Lippert (1955a). Über einige Eigenschaften von elektrostatischen Einzellinsen, deren Achsenpotential fast das Kathodepotential erreicht. *Optik* **12**, 173–180.

W. Lippert (1955b). Zur Wirkungsweise des Möllenstedtschen Geschwindigkeitsanalysators. *Optik* **12**, 467–475.

X. D. Liu and T.-t. Tang (1995). Aberration analysis of Wien filters and design of an electron energy-selective imaging system. *Nucl. Instrum. Meth. Phys. Res. A* **363**, 254–260.

D. E. Lobb (1970). The effect on charged particle trajectories of higher multipolarity components in a magnetic quadrupole field. *Nucl. Instrum. Meth.* **86**, 177–187.

K. Lucas, S. Postnikov, C. Henderson and S. Hector (2003). Lithography: concepts, challenges and prospects. In *Nano and Giga Challenges in Microelectronics* (J. Greer, A. Korkin and J. Labanowski, Eds), 69–128 (Elsevier, Amsterdam).

A. E. Luk'yanov, G. V. Spivak, N. N. Sedov and V. I. Petrov (1968). Geometrical optics of an electron mirror microscope with a two-electrode immersion objective. *Izv. Akad. Nauk SSSR (Ser. Fiz.)* **32**, 987–995. *Bull. Acad. Sci. USSR (Phys. Ser.)* **32**, 915–923.

A. E. Luk'yanov, G. V. Spivak and R. S. Gvosdover (1973). Mirror electron microscopy. *Usp. Fiz. Nauk* **110**, 623–668. *Sov. Phys. Usp.* **16**, 529–552.

A. E. Luk'yanov, E. I. Rau and G. V. Spivak (1974). A scanning electron microscope operating in the mirror and low-voltage modes. *Izv. Akad. Nauk SSSR (Ser. Fiz.)* **38**, 1406–1408. *Bull. Acad. Sci. USSR (Phys. Ser.)* **38** (7), 40–42.

A.A. Macdowell, J. Feng, A. DeMello, A. Doran, R. Duarte, E. Forest, N. Kelez, M. A. Marcus, T. Miller, H. Padmore, S. Raoux, D. Robin, A. Scholl, R. Schlueter, P. Schmid, J. Stöhr, W. Wan, D. H. Wei and Y. Wu (2007). Progress on PEEM3 – an aberration corrected X-ray photoemission electron microscope at the ALS. In *Proc. Synchrotron Radiation Instrumentation*, Daegu. *AIP Conference Proceedings*, 879, 1341–1344.

H. Mahl and A. Pendzich (1943). Das Elektronen-Spiegelmikroskop, ein neues Übermikroskop. *Z. Tech. Phys.* **24**, 38–52.

M. Mankos (2011). Electron optics for dual-beam low energy electron microscopy. *Nucl. Instrum. Meth. Phys. Res. A* **645**, 35–40.

M. Mankos and T. H. P. Chang (2000). Advances in high-throughput multiple electron-beam lithography. EUREM-12, Brno. **3**, 433–434.

M. Mankos and K. Shadman (2013). A monochromatic, aberration-corrected, dual-beam low energy electron microscope. *Ultramicroscopy* **130**, 13–28.

M. Mankos, K. Y. Lee, L. Muray, J. Spallas, Y. Hsu, C. Steble, W. DeVore, E. Bullock and T. H. P. Chang (2000). Optimization of microcolumn electron optics for high-current applications. *J. Vac. Sci. Technol. B* **18**, 3057–3060.

M. Mankos, D. Adler, L. Veneklasen and E. Munro (2007). Electron optics for high throughput low energy electron microscopy. *Surf. Sci.* **601**, 4733–4741.

M. Mankos, D. Adler, L. Veneklasen and E. Munro (2008). Electron optics for low energy electron microscopy. *Phys. Procedia* **1**, 485–504.

M. Mankos, V. Spasov and E. Munro (2010). Principles of dual-beam low-energy electron microscopy. *Adv. Imaging Electron Phys.* **161**, 1–53.

M. Mankos, K. Shadman, A. T. N'Diaye, A. K. Schmid, H. J. Persson and R. W. Davis (2012). Progress towards an aberration-corrected low energy electron microscope for DNA sequencing and surface analysis. *J. Vac. Sci. Technol. B* **30**, 06F02.

M. Mankos, K. Shadman and V. Kolarík (2016). Novel electron monochromator for high resolution imaging and spectroscopy. *J. Vac. Sci. Technol. B* **34**. 06KP01, 11 pp.

M. Mankos, K. Shadman and B. J. Siwick (2017). A novel electron mirror pulse compressor. *Ultramicroscopy*. in press.

S. Manz, A. Casandruc, D.-f. Zhang, Y.-p. Zhong, R. A. Loch, A. Marx, T. Hasegawa, L. C. Liu, S. Bayesteh, H. Delsim-Hashemi, M. Hoffmann, M. Felber, M. Hachmann, F. Mayet, J. Hirscht, S. Keskin, M. Hada, S. W. Epp, K. Flöttmann and R. J. D. Miller (2015). Mapping atomic motions with ultrabright electrons: towards fundamental limits in space–time resolution. *Faraday Discuss.* **177**, 467–491.

S. Manz, S. Keskin, S. Besztejan, B. Zeitler, S. Azim, G. Kassier, R. Buecker, D. Venegas-Rojas, S. Riekeberg, D.-f. Zhang, A. Casandruc, R. A. Loch, Y.-p. Zhong, H. Delsim-Hashemi, S. W. Epp, K. Floettmann, H. K. Trieu, A. Rentmeister and R. J. D. Miller (2016). Dynamic-transmission electron microscopy at the relativistic electron gun for atomic exploration (REGAE) for live cell imaging. EMC-16, Lyon. **1**, 354–355.

F. W. Martin and R. Goloskie (1988). Simultaneous compensation of 2nd-order parasitic aberrations in both principal sections of an achromatic quadrupole lens doublet. *Nucl. Instrum. Meth. Phys. Res. B* **30**, 242–247.

G. Martínez and K. Tsuno (2002). BEM simulation of Wien filters. *Ultramicroscopy* **93**, 253–261.

G. Martínez and K. Tsuno (2004a). Design of Wien filters with high resolution. *Ultramicroscopy* **100**, 105–114.

G. Martínez and K. Tsuno (2004b). 2nd order aberration corrected Wien filter. EMC-13, Antwerp. **1**, 63–64.

G. Martínez and K. Tsuno (2008). The use of multipole fields for aberration correction in $\pi/2$ Wien filters. *Phys. Procedia* **1**, 193–198.

L. Mayer (1955). On electron mirror microscopy. *J. Appl. Phys.* **26**, 1228–1230.

L. Mayer (1957a). Stereo-micrographs of conductivity. *J. Appl. Phys.* **28**, 259–262.

L. Mayer (1957b). Electron mirror microscopy of magnetic domains. *J. Appl. Phys.* **28**, 975–983.

L. Mayer (1959a). Electron mirror microscopy of magnetic stray fields on grain boundaries. *J. Appl. Phys.* **30**, 1101–1104.

L. Mayer (1959b). Domain pattern movements in silicon–iron observed by electron mirror microscopy. *J. Appl. Phys.* **30**, 252S–253S.

L. Mayer (1961). Electron mirror microscopy. In *The Encyclopedia of Microscopy* (G. L. Clark, Ed.), 316–325 (Reinhold, New York; Chapman & Hall, London).

L. Mayer (1962). Magnetic contrast in electron mirror microscopy. ICEM-5, Philadelphia. **1**, II-2.

L. Mayer, R. Rickett and H. Stenemann (1962). Design features of a new electron mirror microscope. ICEM-5, Philadelphia. **1**, D-10.

M. A. McCord and M. J. Rooks (1997). Electron beam lithography. In *SPIE Handbook of Microlithography, Micromachining and Microfabrication* (P. Rai-Choudhury, Ed.), **1**, 139–250 (SPIE Press, Bellingham).
W. Meckelburg (1942). Über das elektrostatische Emissions-Übermikroskop. *Z. Phys.* **120**, 21–30.
S. A. M. Mentink, T. Steffen, P. C. Tiemeijer and M. P. C. M. Krijn (1999). Simplified aberration corrector for low-voltage SEM. EMAG, Sheffield. 83–96.
A. J. F. Metherell (1971). Energy analysing and energy selecting electron microscopes. *Adv. Opt. Electron Microsc.* **4**, 263–360. Reprinted in *Adv. Imaging Electron Phys.* **204** (2017) 147–230.
V. I. Milyutin (1949). Emission electron microscopy. *Usp. Fiz. Nauk* **38**, 377–409.
G. Möllenstedt (1955). 100-keV Elektronen im elektrostatischen Elektronenmikroskop (Zwischenbeschleuniger). *Optik* **12**, 441–466.
G. Möllenstedt and H. Düker (1953). Emissionsmikroskopische Oberflächenabbildung mit Elektronen, die durch schrägen Ionenbeschuß ausgelöst wurden. *Optik* **10**, 192–205.
G. Möllenstedt and H. Gruner (1968). Monochromatisierung von Elektronenstrahlen und Verbesserung von Emissionsbildern mittels eines Elektronenspiegels. *Optik* **27**, 602–604.
G. Möllenstedt and M. Keller (1954). Direkte Übermikroskopische Sichtbarmachung von Oberflächen mittels ionenausgelöster Elektronen. ICEM-3, London. 390–395.
G. Möllenstedt and F. Lenz (1963). Electron emission microscopy. *Adv. Electron. Electron Phys.* **18**, 251–329.
G. Möllenstedt and O. Rang (1951). Die elektrostatische Linse als hochauflösender Geschwindigkeitsfilter. *Z. Angew. Phys.* **3**, 187–189.
G. Möllenstedt and R. Speidel (1960). Elektronenoptischer Mikroschreiber unter elektronenmikroskopischer Arbeitskontrolle (Informations-Speichrung auf kleinstem Raum). *Phys. Blätt.* **16**, 192–198.
M. A. Monastyrskii (1978a). Asymptotic solutions of the paraxial equation of electron optics [for cathode lenses]. *Zh. Tekh. Fiz.* **48**, 1117–1122. *Sov. Phys. Tech. Phys.* **23**, 624–627.
M. A. Monastyrskii (1978b). Influence functions in the optimization of a cathode electron-optical system. *Zh. Tekh. Fiz.* **48**, 2228–2234. *Sov. Phys. Tech. Phys.* **23**, 1275–1278.
M. A. Monastyrskii (1980). Jump in Green's functions for cathode lenses with a non-smooth electrostatic potential distribution. *Zh. Tekh. Fiz.* **50**, 1939–1947. *Sov. Phys. Tech. Phys.* **25**, 1129–1133.
M. A. Monastyrskii (1986). Pontryagin's maximum principle in the design of cathode lenses. I. *Zh. Tekh. Fiz.* **56**, 625–633. *Sov. Phys. Tech. Phys.* **31**, 379–383.
M. A. Monastyrskii and M. V. Korneeva (1986). Pontryagin's maximum principle in the design of cathode lenses. II. *Zh. Tekh. Fiz.* **56**, 634–643. *Sov. Phys. Tech. Phys.* **31**, 384–389.
M. A. Monastyrskii and Yu. V. Kulikov (1976). Chromatic aberrations of cathode lenses. *Radiotekh. Elektron.* **21**, 2251–2254. *Radio Eng. Electron. Phys.* **21** (10), 148–150.
M. A. Monastyrskii and Yu. V. Kulikov (1978). Theory of the aberrations of cathode lenses. Chromatic aberrations. *Radiotekh. Elektron.* **23**, 644–647. *Radio Eng. Electron. Phys.* **23** (3), 137–140.
H. M. Montagu-Pollock (1972). Field emission/field-ion microscopy as a tool for thin film and surface studies. *Thin Solid Films* **14**, 193–209.
E. W. Müller (1936a). Versuche zur Theorie der Elektronenemission unter der Einwirkung hoher Feldstärken. *Z. Tech. Phys.* **17**, 412–416.
E. W. Müller (1936b). Versuche zur Theorie der Elektronenemission unter der Einwirkung hoher Feldstärken. *Phys. Z.* **37**, 838–842.
E. W. Müller (1937a). Beobachtungen über die Feldemission und die Kathodenzerstäubung an thoriertem Wolfram. *Z. Phys.* **106**, 132–140.
E. W. Müller (1937b). Elektronenmikroskopische Beobachtungen von Feldkathoden. *Z. Phys.* **106**, 541–550.
E. W. Müller (1951). Das Feldionenmikroskop. *Z. Phys.* **131**, 136–142.
E. W. Müller (1953). Feldemission. *Ergeb. Exakt Naturwiss* **27**, 290–360.
E. W. Müller (1960). Field ionization and field ion microscopy. *Adv. Electron. Electron Phys* **13**, 83–179.
E. W. Müller (1975). The atom-probe field ion microscope. In *Methods of Surface Analysis* (A. W. Czanderna, Ed.), 329–378 (Elsevier, Amsterdam).
E. W. Müller (1976). The imaging process in field ion microscopy from the FEM to the atom-probe. *Crit. Rev. Solid State Sci.* **6**, 85–109.

E. W. Müller (1978a). Surface studies by field emission. In *Diffraction and Imaging Techniques in Material Science* (S. Amelinckx, R. Gevers and J. Van Landuyt, Eds), 791−810 (North Holland, Amsterdam, New York & Oxford).

E. W. Müller (1978b). Developments in field ion microscopy. In *Diffraction and Imaging Techniques in Material Science* (S. Amelinckx, R. Gevers and J. Van Landuyt, Eds), 811−847 (North Holland, Amsterdam, New York & Oxford).

E. W. Müller and T. T. Tsong (1969). *Field-Ion Microscopy, Principles and Applications* (Elsevier, New York & Amsterdam).

E. W. Müller and T. T. Tsong (1974). Field ion microsopy, field ionization and field evaporation. *Prog. Surf. Sci.* **4**, 1−139.

H. Müller, D. Preikszas and H. Rose (1996). Precise design of a corrected beam separator for a high-resolution PEEM−LEEM. EUREM-11, Dublin. **1**, 469−470.

I. Müllerová and L. Frank (2003). Scanning low-energy electron microscopy. *Adv. Imaging Electron Phys.* **128**, 309−443.

I. Müllerová and M. Lenc (1992). Some approaches to low-voltage scanning electron microscopy. *Ultramicroscopy* **41**, 399−410.

I. Müllerová, L. Frank and E. Weimer (1998). Variable mode retarding field element for low energy SEM. *Recent Trends* **6**, 51−52.

I. Müllerová, K. Matsuda, P. Hrnčiřík and L. Frank (2007). Enhancement of SEM to scanning LEEM. *Surf. Sci.* **601**, 4768−4773.

I. Müllerová, E. Mikmeková, I. Konvalina and L. Frank (2013). Low energy scanning transmission electron microscope. *Microsc. Microanal.* **19** (Suppl. 2), 1236−1237.

E. Munro (1980a). Electron optics for microcircuit engineering. In *Microcircuit Engineering* (H. Ahmed and W. C. Nixon, Eds), 513−534 (Cambridge University Press, Cambridge).

E. Munro (1980b). Electron beam lithography. In *Applied Charged Particle Optics* (A. Septier, Ed.), **B**, 73−131 (Academic Press, New York & London). *Adv. Electron. Electron Phys*. Suppl. 13B.

E. Munro and H. C. Chu (1982a). Numerical analysis of electron beam lithography systems. Part I: Computation of fields in magnetic deflectors. *Optik* **60**, 371−390.

E. Munro and H. C. Chu (1982b). Numerical analysis of electron beam lithography systems. Part II: Computation of fields in electrostatic deflectors. *Optik* **61**, 1−16.

P. Musumeci and C. Li (2018). High energy time resolved electron diffraction. In *Handbook of Microscopy* (P. W. Hawkes and J. C. H. Spence, Eds), (Springer, Cham). forthcoming.

P. Musumeci, D. Cesar and J. Maxson (2017). Double-shot MeV electron diffraction and microscopy. *Struct. Dyn* **4**, 044025, 7 pp.

L. M. Myers (1939). *Electron Optics* (Chapman & Hall, London).

M. B. Nesvizhskii (1984). Chromatic aberrations of cathode systems containing deflection elements. *Radiotekh. Elektron.* **29**, 972−979. *Radio Eng. Electron. Phys*. **29** (5), 150−157.

M. B. Nesvizhskii (1985). Expansion of the aberration coefficients of cathode electron-optical systems. *Radiotekh. Elektron.* **30**, 1814−1820. *Sov. J. Commum. Technol. Electron*. **31** (1), 142−148.

M. B. Nesvizhskii (1986). Aberration coefficients of complicated electron optical cathode systems. *Radiotekh. Elektron.* **31**, 162−168. *Sov. J. Commum. Technol. Electron*. **31** (5), 153−160.

Yu. A. Nevinnyi, L. M. Sekunova and E. M. Yakushev (1985). Systems of transaxial lenses for electrostatic prism spectrometers with improved focusing. *Zh. Tekh. Fiz.* **55**, 1713−1718. *Sov. Phys. Tech. Phys*. **30**, 1001−1004.

F. H. Nicoll (1938). The focusing properties of the electrostatic field between two cylinders. *Proc. Phys. Soc. (Lond.)* **50**, 888−898.

H. Ohiwa (1977). The design of deflection coils. *J. Phys. D: Appl. Phys.* **10**, 1437−1449.

H. Ohiwa (1978). Design of electron-beam scanning systems using the moving objective lens. *J. Vac. Sci. Technol.* **15**, 849−852.

H. Ohiwa, E. Goto and A. Ono (1971). Elimination of third-order aberrations in electron-beam scanning systems. *Trans. Inst. Elecron. Commun. Eng. Japan* **54-B**, 730–737. *Electron. Commun. Japan* **54-B** (12), 44–51.

T. Okano, K. Utagawa and G. Tominaga (1976). Topographic representation of emission intensity by the scanning-type field emission microscope. *Jpn. J. Appl. Phys.* **15**, 2035–2036.

S. Okayama (1988). Electron-beam lithography system using a quadrupole triplet. *J. Vac. Sci. Technol.* **B6**, 199–203.

R. M. Oman (1969). Electron mirror microscopy. *Adv. Electron. Electron Phys.* **26**, 217–250.

R. Orthuber (1948). Über die Anwendung des Elektronenspiegels zum Abbilden der Potentialverteilung auf metallischen und Halbleiter-Oberflächen. *Z. Angew. Phys.* **1**, 79–89.

C. Oshima, R. Souda, M. Aono and Y. Ishizawa (1983). On the field emission microscope with a base pressure of 10^{-10} Pa [in Japanese]. *J. Vac. Sci. Japan* **26**, 726–730.

M. Osterberg and A. Khursheed (2008). A chromatic and spherical aberration corrected PEEM. *Recent Trends* **11**, 89–90.

F. P. Ottensmeyer (1984). Energy selecting electron microscopy. In *Electron Optical Systems for Microscopy, Microanalysis and Microlithography* (J. J. Hren, F. A. Lenz, E. Munro and P. B. Sewell, Eds), 245–251 (Scanning Electron Microscopy, AMF O'Hare).

K. Oura, V. G. Lifshits, A. Saranin, A. Zotov and M. Katyama, Eds (2003). *Surface Science, an Introduction* (Springer, Berlin).

L. P. Ovsyannikova (1968). Dependence of the geometrical aberration coefficients of oblique beams in a quadrupole lens on the value of its excitation. *Radiotekh. Elektron.* **13**, 1489–1493. *Radio Eng. Electron. Phys.* **13**, 1292–1295.

L. P. Ovsyannikova (1986). Field calculations for electron-optical systems with a variable aperture. *Zh. Tekh. Fiz.* **56**, 604–607. *Sov. Phys. Tech. Phys.* **31**, 366–368.

L. P. Ovsyannikova and E. V. Shpak (1982). Frequency-contrast characteristics of crossed lenses. *Zh. Tekh. Fiz.* **52**, 143–144. *Sov. Phys. Tech. Phys.* **27**, 97.

L. P. Ovsyannikova and S. Ya. Yavor (1967). Analytical expressions for the third-order aberration coefficients of quadrupole lenses (rectangular model). *Radiotekh. Elektron.* **12**, 489–493. *Radio Eng. Electron. Phys.* **12**, 449–453.

L. P. Ovsyannikova, B. A. Utochkin, T. Ya. Fishkova and S. Ya. Yavor (1972). The use of quadrupole lenses for simultaneous beam focusing and deflection in oscilloscope tubes. *Radiotekh. Elektron.* **17**, 1062–1066. *Radio Eng. Electron. Phys.* **17**, 825–828.

L. P. Ovsyannikova, T. Ya. Fishkova and I. A. Petrov (2001). Achromatic deflectors with combined electrodes and poles. *Zh. Tekh. Fiz.* **71** (12), 62–65. *Tech. Phys.* **46**, 1549–1552.

G. Owen (1981). Automatic measurement and correction of deflection astigmatism and defocusing in the Hewlett–Packard 605 electron beam lithography system. *J. Vac. Sci. Technol.* **19**, 1064–1068.

H. Paik and B. M. Siegel (1985). Pre-lens deflection electrostatic optical system free of deflection aberration to third order. *Optik* **70**, 152–159.

N. Paras (1961). Etude d'un dispositif de filtrage des images électroniques. Diplôme d'Etudes Supérieures, Paris–Orsay.

H. T. Pearce-Percy and D. F. Spicer (1980). Integration of trajectory equations for deflection and focusing systems avoiding paraxial type approximations. In *Microcircuit Engineering* (H. Ahmed and W. C. Nixon, Eds), 535–545 (Cambridge University Press, Cambridge).

I. A. Petrov (1976). Study of the first-order electron-optical properties of a single crossed lens. *Zh. Tekh. Fiz.* **46**, 1085–1089. *Sov. Phys. Tech. Phys.* **21**, 640–642.

I. A. Petrov (1977). Study of the electron-optical properties of a system of two crossed lenses. *Zh. Tekh. Fiz.* **47**, 1380–1384. *Sov. Phys. Tech. Phys.* **22**, 792–795.

I. A. Petrov and R. S. Khersonskaya (1986). A new type of aberration corrector. *Zh. Tekh. Fiz.* **56**, 217–220. *Sov. Phys. Tech. Phys.* **31**, 131–133.

I. A. Petrov and E. V. Shpak (1975). A quadrupole−octopole lens system with an axisymmetric component. *Zh. Tekh. Fiz.* **45**, 191−195. *Sov. Phys. Tech. Phys*. **20**, 125−127.
I. A. Petrov and S. Ya. Yavor (1975). A crossed electrostatic lens with negative spherical aberration. *Pis'ma Zh. Tekh. Fiz.* **1**, 651−654. *Sov. Tech. Phys. Lett*. **1**, 289−290.
I. A. Petrov and S. Ya. Yavor (1986). Spherical aberration of a single crossed lens. *Zh. Tekh. Fiz.* **46**, 1710−1712. *Sov. Phys. Tech. Phys*. **21**, 985−986.
I. A. Petrov, E. V. Shpak and S. Ya. Yavor (1972). A new astigmatic lens. *Izv. Akad. Nauk SSSR (Ser. Fiz.)* **36**, 1922−1923. *Bull. Acad. Sci. USSR (Phys. Ser.)* **36**, 1699−1701.
I. A. Petrov, E. V. Shpak and S. Ya. Yavor (1974). A quadrupole−octopole lens system with an axisymmetric component. *Izv. Akad. Nauk SSSR (Ser. Fiz.)* **38**, 1502−1504. *Bull. Acad. Sci. USSR (Phys. Ser.)* **38** (7), 133−135.
I. A. Petrov, L. A. Baranova and S. Ya. Yavor (1978). Stigmatic operation of a six-electrode doublet of crossed lenses. *Zh. Tekh. Fiz.* **48**, 408−410. *Sov. Phys. Tech. Phys*. **23**, 242−244.
A. A. Petruk, K. Pichugin and G. Sciaini (2017). Shaped cathodes for the production of ultra-short multi-electron pulses. *Struct. Dyn.* **4**, 044005, 8 pp.
H. C. Pfeiffer (1978). Variable spot shaping for electron-beam lithography. *J. Vac. Sci. Technol.* **15**, 887−890.
H. C. Pfeiffer (1979). Recent advances in electron-beam lithography for the high-volume production of VLSI devices. *IEEE Trans. Electron Dev*. **26**, 663−664.
H. C. Pfeiffer (1983). Exposure concepts of electron beam lithography systems. In *Microcircuit Engineering 83* (H. Ahmed, J. R. A. Cleaver and G. A. C. Jones, Eds), 3−14 (Academic Press, London & New York).
H. C. Pfeiffer (1995). Projection exposure with variable axis immersion lenses, a high-throughput electron beam approach to "suboptical" lithography. *Jpn. J. Appl. Phys.* **34**, 6658−6662.
H. C. Pfeiffer (2000). PREVAIL − proof-of-concept system and results. *Microelectron. Eng*. **53**, 61−66.
H. C. Pfeiffer and G. O. Langner (1981). Advanced deflection concept for large area, high resolution e-beam lithography. *J. Vac. Sci. Technol.* **19**, 1058−1063.
H. C. Pfeiffer and W. Stickel (1995). PREVAIL − an e-beam stepper with variable axis immersion lenses. *Microelectron. Eng*. **27**, 143−146.
H. C. Pfeiffer and M. A. Sturans (1984). Electron beam deflection without off-axis aberrations. In *Electron Optical Systems for Microscopy, Microanalysis and Microlithography* (J. J. Hren, F. A. Lenz, E. Munro and P. B. Sewell, Eds), 109−114 (Scanning Electron Microscopy, AMF O'Hare).
H. C. Pfeiffer, G. O. Langner and M. A. Sturans (1981). Variable axis lens for electron beams. *Appl. Phys. Lett.* **39**, 775−776.
L. Piazza, P. Musumeci, O. J. Luiten and F. Carbone (2014). A proposal for fs-electron microscopy experiments on high-energy excitations in solids. *Micron* **63**, 40−46.
J. Picht (1939). Bemerkungen zu einigen Fragen der Elektronenoptik (Elektronenlinse mit Zwischennetz, Elektronenspiegel, Immersionslinse). *Ann. Phys. (Leipzig)* **36** (428), 249−264.
E. Plies and J. Bärtle (2003). Proposal of a novel highly symmetric Wien filter monochromator. *Microsc. Microanal.* **9** (Suppl. 3), 28−29.
E. Plies and D. Typke (1978). Dreidimensional abbildende Elektronenmikroskope. II. Theorie elektronenoptischer Systeme mit gekrümmter Achse. *Z. Naturforsch.* **33a**, 1361−1377.
E. Plies, K. Marianowski and T. Ohnweiler (2011). The Wien filter: history, fundamentals and modern applications. *Nucl. Instrum. Meth. Phys. Res. A* **645**, 7−11.
V. Premanand (1962). Réalisation d'un microscope électrostatique à miroir. Dissertation, Paris.
H. E. R. Preston (1968). The search for mechanical simplicity in a quadrupole multiplet corrected for third order spherical aberration. EUREM-4, Rome. **1**, 179−180.
H. E. R. Preston (1969). An analytic solution for the potential distribution within an asymmetrically excited electrostatic quadrupole lens. *Proc. Roy. Soc. (Lond.)* **A313**, 217−238.
H. E. R. Preston (1970). Aberration correction in an electrostatic quadrupole multiplet employing asymmetric excitation and variable geometry. ICEM-7, Grenoble. **2**, 41−42.

H. E. R. Preston (1972). Potential distribution calculations in electrostatic quadrupole multiplets. EUREM-5, Manchester. 82–83.

I. N. Prilezhaeva, V. V. Lifshits and G. V. Spivak (1955). On the electron-optical study of non-stationary emission from an oxide cathode in vacuum and in a gas. *Zh. Tekh. Fiz.* **25**, 97–107.

A. Recknagel (1936). Zur Theorie des Elektronenspiegels. *Z. Tech. Phys.* **17**, 643–645.

A. Recknagel (1937). Zur Theorie des Elektronenspiegels. *Z. Phys.* **104**, 381–394.

A. Recknagel (1941). Theorie des elektrischen Elektronenmikroskops für Selbststrahler. *Z. Phys.* **117**, 689–708.

A. Recknagel (1943). Das Auflösungsvermögen des Elektronenmikroskops für Selbststrahler. *Z. Phys.* **120**, 331–362.

B. W. Reed, T. LaGrange, R. M. Shuttlesworth, D. J. Gibson, G. H. Campbell and N. D. Browning (2010). Solving the accelerator–condenser coupling problem in a nanosecond dynamic transmission electron microscope. *Rev. Sci. Instrum.* **81**, 053706.

E. Regenstreif (1951). Théorie de la lentille électrostatique à trois électrodes. *Ann. Radioél.* **6**, 51–83 and 114–155.

E. Reisman (1957). The imaging properties of crossed magnetic quadripoles. Dissertation, Cornell.

G. Rempfer and M. S. Mauck (1992). Correction of chromatic aberration with an electron mirror. *Optik* **92**, 3–8.

Y. Ren, T.-t. Tang, Y.-f. Kang and X.-l. Guo (2007). The aberration theory of a combined electron focusing–deflection system with a rotating deflection field following the rotation of the electrons. *Optik* **118**, 569–574.

C. Ropers, D. R. Solli, C. P. Schulz, C. Lienau and T. Elsaesser (2007). Localized multiphoton emission of femtosecond electron pulses from metal nanotips. *Phys. Rev. Lett.* **98**, 043907, 4 pp.

H. Rose (1987). The retarding Wien filter as a high-performance imaging filter. *Optik* **77**, 26–34.

H. Rose (1990). Inhomogeneous Wien filter as a corrector compensating for the chromatic and spherical aberration of low-voltage electron microscopes. *Optik* **84**, 91–107.

H. Rose and D. Preikszas (1992). Outline of a versatile corrected LEEM. *Optik* **92**, 31–44.

H. Rose and D. Preikszas (1995). Time-dependent perturbation formalism for calculating the aberrations of systems with large ray gradients. *Nucl. Instrum. Meth. Phys. Res. A* **363**, 301–315.

H. Rose, D. Preikszas and H. Müller (1996). Outline of a corrected PEEM–LEEM. *Recent Trends* **5**, 35–38.

A. M. Rozenfel'd (1959). On the effect of the thickness of the focusing electrode on the optical properties of an electrostatic immersion objective. *Zh. Tekh. Fiz.* **29**, 584–588. *Sov. Phys. Tech. Phys.* **4**, 521–524.

A. M. Rozenfel'd and P. V. Zaitsev (1961). A magnetic objective lens for an emission electron microscope. *Izv. Akad. Nauk SSSR (Ser. Fiz.)* **25**, 713–716. *Bull. Acad. Sci. USSR (Phys. Ser.)* **25**, 726–729.

T. Sakurai, M. Toyoda, H. Hayashibara and T. Matsuo (1995). Third-order trajectory calculations of Wien filters. *Int. J. Mass Spectrom. Ion Processes* **146/147**, 217–222.

F. A. Savchenko (1938). Experimental determination of the optical properties of electron lenses. *Fiz. Zap. Akad. Nauk Ukr. RSR* **7**, 147–157.

F. Savchenko (1939). The dependence of certain optical parameters on the electric and geometric parameters of an electric immersion lens. *Zh. Tekh. Fiz.* **9**, 2211–2219.

M. R. Scheinfein (1989). Second order transfer matrices for inhomogeneous field Wien filters including spin-procession. *Optik* **82**, 99–113.

M. Ya. Schelev, M. A. Monastyrskiy, N. S. Vorobiev, S. V. Garnov and D. E. Greenfield (2013). Aspects of streak image tube photography. *Adv. Imaging Electron Phys* **180**.

W. Scherle (1983). Berechnung von magnetischen Ablenksystemen. Dissertation, Tübingen.

O. Scherzer (1965). Vorschläge zur Terminologie unrunder Elektronenlinsen. *Optik* **22**, 314–318.

M. Schiekel (1952). Elektronenoptische Geschwindigkeitsfilter. *Optik* **9**, 145–153.

P. Schiske (1966). Ein Modellfeld für eine Elektronenlinse mit rotationssymmetrischem Feld, das von einem Quadrupolfeld überlagert ist und eine geschlossene Darstellung der paraxialen Elektronenbahnen erlaubt. *Optik* **24**, 521–528.

P. Schmid and H. Rose (1998). Outline of a variable-axis lens with arbitrary shift of the axis in one directon. *Recent Trends* **6**, 64.

W. Schwartze (1964). "Feldkontrast" im Emissionsmikroskop und Elektronenspiegel. EUREM-3, Prague. **A**, 15–16.

W. Schwartze (1965). Fokussierte Abbildung mit dem Elektronenspiegel–Oberflächenmikroskop. *Naturwissenschaften* **52**, 448–449.

W. Schwartze (1966). Ein Elektronenspiegel–Oberflächenmikroskop. *Exp. Tech. Phys.* **14**, 293–300.

W. Schwartze (1967). Elektronen-Oberflächenmikroskopie mit fokussierter Abbildung. *Optik* **25**, 260–272.

R. A. Schwarzer (1975). Der Einfluß von Loch- und Ringblenden auf die Energieverteilung der Elektronen im Emissions-Elektronenmikroskop. *Optik* **44**, 61–78.

R. A. Schwarzer (1975). Die Verbesserung des Bildkontrastes im Emissions-Elektronenmikroskop durch eine ringförmige Aperturblende. *Optik* **44**, 121–131.

R. A. Schwarzer (1979). Physical aspects of emission electron microscopy. *Beiträge zur Elektronenmikroskopischen Direktabbildung von Oberflächen* **12** (2), 3–38.

N. N. Sedov (1968). Solution of the inverse problem of microfield contrast in electron microscopy. *Izv. Akad. Nauk SSSR (Ser. Fiz.)* **32**, 1175–1184.

N. N. Sedov (1970a). Théorie quantitative des systèmes en microscopie électronique à balayage, à miroir et à émission. *J. Microsc. (Paris)* **9**, 1–26.

N. N. Sedov (1970b). Image formation in emission and mirror electron-optical systems. *Izv. Akad. Nauk SSSR (Ser. Fiz.)* **34**, 1529–1534. *Bull. Acad. Sci. USSR (Phys. Ser.)* **34**, 1356–1361.

N. N. Sedov, G. V. Spivak, V. G. Dyukov and A. N. Nevzorov (1968). Contrast of microfield images in an emission electron microscope and calculation of the imaged microfields from the contrast. *Izv. Akad. Nauk SSSR (Ser. Fiz.)* **32**, 978–986. *Bull. Acad. Sci. USSR (Phys. Ser.)* **32**, 906–914.

A. Septier (1952a). Sur le pouvoir séparateur de l'objectif électrostatique à immersion. *C. R. Acad. Sci. Paris* **235**, 609–611.

A. Septier (1952b). Objectif à immersion électrostatique à haut pouvoir séparateur d'un type nouveau. *C. R. Acad. Sci. Paris* **235**, 652–654.

A. Septier (1952c). Calcul de la répartition du potentiel $\Phi(z)$ sur l'axe d'un objectif électrostatique à immersion à électrodes épaisses. *C. R. Acad. Sci. Paris* **235**, 1203–1206.

A. Septier (1952d). Etude expérimentale de l'objectif électrostatique à immersion à électrodes planes: courbes de focalisation et distance focale. *C. R. Acad. Sci. Paris* **235**, 1621–1623.

A. Septier (1953a). Etude expérimentale de l'objectif à immersion électrostatique à électrodes planes: champ extracteur E_0 dans les conditions de focalisation. Aberrations géométriques en dehors de l'axe. *C. R. Acad. Sci. Paris* **236**, 58–60.

A. Septier (1953b). Sur l'obtention d'images électroniques de surfaces bombardées par des ions. *C. R. Acad. Sci. Paris* **237**, 231–233.

A. Septier (1954a). Quelques types d'objectifs électrostatiques à immersion à fort grandissement. *Ann. Radioél.* **9**, 374–410.

A. Septier (1954b). Le pouvoir séparateur théorique de l'objectif à immersion électrostatique. *J. Phys. Radium* **15**, 573–581.

A. Septier (1961). Strong-focusing lenses. *Adv. Electron. Electron Phys.* **14**, 85–205.

A. Septier (1966). The struggle to overcome spherical aberration in electron optics. *Adv. Opt. Electron Microsc.* **1**, 204–274. reprinted in *Adv. Imaging Electron Phys*. **202** (2017) 75–147.

Yu. A. Shapiro (1972). Stabilization of the accelerating potential in electromagnetic cathode lenses. *Opt.-Mekh. Prom.* **39** (1), 13–15. *Sov. J. Opt. Technol*. **39**, 11–13.

C. J. R. Sheppard and H. Ahmed (1976). The analysis of scan coils for scanning electron diffraction. *Optik* **44**, 139–151.

C.-s. Shern (1989). Properties of the cathode lens in a MEM–LEED apparatus. *Chin. J. Phys.* **27**, 58–71.

C.-s. Shern and W. N. Unertl (1987). A simple mirror electron microscope–low-energy electron diffraction apparatus for surface studies. *J. Vac. Sci. Technol. A* **5**, 1266–1270.

D. Shorokhov and A. H. Zewail (2016). Perspective: 4D ultrafast electron microscopy – evolutions and revolutions. *J. Chem. Phys.*. **144**, 080901, 14 pp.
K. R. Siefermann and A. Neff (2018). Time-resolved photoemission electron microscopy. *Encyclopedia of Interfacial Chemistry*, *Surface Science and Electrochemistry* (K. Wandelt, Ed.), forthcoming (Elsevier, Amsterdam). Available (2017) in *Reference Module in Chemistry, Molecular Sciences and Chemical Engineering* (www.elsevier.com), 10 pp.
J. A. Simpson (1961). Design of retarding field energy analyzers. *Rev. Sci. Instrum.* **32**, 1283–1293.
J. A. Simpson and L. Marton (1961). Improved electron filter lens. *Rev. Sci. Instrum.* **32**, 802–803.
W. Skoczylas, G. F. Rempfer and O. H. Griffith (1991). A proposed modular imaging system for photoelectron and electron probe microscopy with aberration correction, and for mirror microscopy and low-energy electron microscopy. *Ultramicroscopy* **36**, 252–261.
W. Skoczylas, G. F. Rempfer and O. H. Griffith (1994). Electron optical benches for in-line and branched systems. A new bench designed for mirror-based aberration correction and low energy electron microscopy. *Rev. Sci. Instrum.* **65**, 3183–3193.
N. A. Smirnov, M. A. Monastyrskii and Yu. V. Kulikov (1979). Electron optics of cathode lenses with spherically symmetric combined fields. *Zh. Tekh. Fiz.* **49**, 2590–2595. *Sov. Phys. Tech. Phys*. **24**, 1462–1465.
D. L. Smith (1970). Focusing properties of electric and magnetic quadrupole lenses. *Nucl. Instrum. Meth.* **79**, 144–164.
M. R. Smith and E. Munro (1986). A unified aberration theory for electrostatic round lenses, multipole lenses and deflectors. *Optik* **74**, 7–16.
E.-A. Soa (1959). Systematische Untersuchungen an elektrostatischen Immersionsobjektiven. *Jenaer Jahrbuch* Part I, 115–153.
T. Someya and M. Watanabe (1968a). Development of electron mirror microscope. EUREM-4, Rome. **1**, 97–98.
T. Someya and M. Watanabe (1968b). Development of electron mirror microscope. EMSA, New Orleans. **26**, 300–301.
R. Spehr (1998). Variable axis lens with an extremely large scanning area in one direction. *Recent Trends* **6**, 75–76.
R. Speidel, G. Kilger and E. Kasper (1979). Optical properties of combined magnetic lenses and deflection systems. *Optik* **54**, 433–438.
J. C. H. Spence (2017). Outrunning damage; electrons vs x-rays – timescales and mechanisms. *Struct. Dyn* **4**, 044027, 12 pp.
J. C. H. Spence, G. Subramanian and P. Musumeci (2015). Hollow cone illumination for fast TEM, and outrunning damage with electrons. *J. Phys. B: At. Mol. Opt. Phys.* **48** (214003). 6 pp.
A. J. Speth, A. D. Wilson, A. Kern and T. H. P. Chang (1975). Electron-beam lithography using vector-scan techniques. *J. Vac. Sci. Technol.* **12**, 1235–1239.
G. V. Spivak and E. M. Dubinina (1953). On the resolving power of an immersion electron objective. *Dokl. Akad. Nauk SSSR* **88**, 673–675.
G. V. Spivak and V. I. Lyubchenko (1959). Resolving power of an immersion objective in the presence of electric and magnetic microfields at the cathode. *Izv. Akad. Nauk SSSR (Ser. Fiz.)* **23**, 697–705. *Bull. Acad. Sci. USSR (Phys. Ser.)* **23**, 691–700.
G. V. Spivak, I. N. Prilezhaeva and V. K. Azovtsev (1955). Magnetic contrast in the electron mirror and observation of ferromagnetic domains. *Dokl. Akad. Nauk SSSR* **105**, 965–967.
G. V. Spivak, I. A. Pryamkova and E. Igras (1959a). Observation of ferromagnetic and piezoelectric domains by means of an electron mirror. *Izv. Akad. Nauk SSSR (Ser. Fiz.)* **23**, 729–733. *Bull. Acad. Sci. USSR (Phys. Ser.)* **23**, 723–728.
G. V. Spivak, E. Igras, I. A. Pryamkova and I. S. Zheludev (1959b). Observation of the domain structure of barium titanate with the aid of an electron mirror. *Kristallografiya* **4**, 123–125.
G. V. Spivak, I. A. Pryamkova and V. N. Lepeshinskaya (1960). *Dokl. Akad. Nauk SSSR* **130**, 751–754.

G. V. Spivak, I. A. Pryamkova, D. V. Fetisov, A. N. Kabanov, L. V. Lazareva and A. I. Shilina (1961). Mirror electron microscope for studying the structure of surfaces. *Izv. Akad. Nauk SSSR (Ser. Fiz.)* **25**, 683–690. *Bull. Acad. Sci. USSR (Phys. Ser.)* **25**, 698–705.

G. V. Spivak, G. V. Saparin and N. A. Pereverzev (1962). Potential distribution in a p-n junction as observed by electron optical scanning. *Izv. Akad. Nauk SSSR (Ser. Fiz.)* **26**, 1339–1342. *Bull. Acad. Sci. USSR (Phys. Ser.)* **26**, 1362–1365.

G. V. Spivak, R. D. Ivanov, O. P. Pavlyuchenko and N. N. Sedov (1963). Mechanism of contrast formation in mirror, emission and scanning electron-optical systems. *Izv. Akad. Nauk SSSR (Ser. Fiz.)* **27**, 1139–1146. *Bull. Acad. Sci. USSR (Phys. Ser.)* **27**, 1120–1127.

G. V. Spivak, V. P. Ivannikov, A. E. Luk'yanov and E. I. Rau (1978). Development of scanning mirror electron microscopy for quantitative evaluation of electric microfields. *J. Microsc. Spectrosc. Electron* **3**, 89–100.

G. V. Spivak, E. I. Rau and A. Yu. Sasov (1983). Colour-coded display of information in scanning electron microscopy. *Usp. Fiz. Nauk* **139**, 165–168. *Sov. Phys. Usp.* **26**, 84–86.

W. Steckelmacher (1973). Energy analysers for charged particle beams. *J. Phys. E: Sci. Instrum.* **6**, 1061–1071.

K. G. Steffen (1965). *High Energy Beam Optics* (Wiley–Interscience, New York & London).

T. Steffen, P. C. Tiemeijer, M. P. C. M. Krijn and S. A. M. Mentink (2000). Correction of chromatic and spherical aberration using a Wien filter. EMC-12, Brno. **3**, I.151–I.152.

W. Stenzel (1971). Die elektrostatische Linse als Energiefilter. *Optik* **32**, 352–374.

H. Stolz (1978). Elektronenmikroskopie mit einem elektrostatischen Zwischenverzögerer. I. *Optik* **52**, 369–383.

H. Stolz (1978). Elektronenmikroskopie mit einem elektrostatischen Zwischenverzögerer. II. *Optik* **53**, 35–45.

H. Stolz and G. Möllenstedt (1971). Beitrag zur Niedervolt-Elektronenmikroskopie. *Optik* **33**, 35–46.

G. Storeck, S. Vogelgesang, M. Sivis, S. Schäfer and C. Ropers (2017). Nanotip-based photoelectron microgun for ultrafast LEED. *Struct. Dyn.* **4**, 044024, 7 pp.

A. M. Strashkevich (1959). *Elektronnaya Optika Elektrostaticheskikh Polei ne Obladayushchikh Osevoi Simmetriei* (Gos. Izd. Fiz.-Mat. Lit., Moscow).

A. M. Strashkevich (1962). Principal electron-optical properties of transaxial electrostatic systems. *Zh. Tekh. Fiz.* **32**, 1142–1152. *Sov. Phys. Tech. Phys.* **7**, 841–847.

A. M. Strashkevich (1966). *Elektronnaya Optika Elektrostaticheskikh Sistem* (Energiya, Moscow & Leningrad).

D. K. Strong (1985). A clamshell deflection yoke. *Proc. Soc. Inform. Display* **26**, 41–45.

M. A. Sturans and H. C. Pfeiffer (1983). Variable axis immersion lens (VAIL). In *Microcircut Engineering 83* (H. Ahmed, J. R. A. Cleaver and G. A. C. Jones, Eds), 107–116 (Academic Press, London & New York).

N. G. Sushkin (1941). Study of an oxide cathode with the aid of an electron microscope. *Fiz. Zap. Akad. Nauk Ukr. RSR* **9**, 152–156.

K. Suzuki (2018). Electron beam lithography system. In *Microlithography: Science and Technology* (K. Suzuki and B. W. Smith, Eds), 3rd edn. (CRC Press, Boca Raton), forthcoming.

M. Szilágyi, E. V. Shpak and S. Ya. Yavor (1968). Measurement of the field of an electrostatic quadrupole lens with concave electrodes using a resistance network. *Radiotekh. Elektron.* **13**, 185–187. *Radio Eng. Electron. Phys.* **13**, 159–160.

M. Szilágyi, F. Blaschta, K. Kando, L. P. Ovsyannikova and S. Ya. Yavor (1973). Analytical expressions for all third-order aberration coefficients of quadrupole lenses. Bell-shaped model. *Optik* **38**, 416–424.

M. Szilágyi, F. Blaschta, L. P. Ovsyannikova and S. Ya. Yavor (1974). A comparison of the real quadrupole aberrations for a bell-shaped model with those for a rectangular model. *Optik* **39**, 351–358.

T.-t. Tang (1986a). Asymptotic aberrations of combined electrostatic focusing-deflection systems. *Optik* **74**, 43–47.

T.-t. Tang (1986b). Aberration analysis of a crossed-field analyzer. *Optik* **74**, 51–56.

P. Tanguy (1965a). Sur des expressions simplifiées pour les distances focales d'une lentille quadripolaire courte. *C. R. Acad. Sci. Paris* **261**, 1811–1813.

P. Tanguy (1965b). Sur les aberrations géométriques des lentilles quadripolaires courtes. *C. R. Acad. Sci. Paris* **261**, 1945–1947.

P. Tanguy and S. Joly (1967). Sur le nombre de coefficients indépendants nécessaires pour décrire les aberrations géométriques des lentilles quadripolaires. *C. R. Acad. Sci. Paris* **265**, 532–535.

D. N. Tennant and A. R. Bleier (2011). Electron beam lithography of nanostructures. In *Comprehensive Nanoscience and Technology* (D. L. Andrews, G. D. Scholes and G. P. Wiederrecht, Eds), **4**, 36–62 (Elsevier, Amsterdam).
M. G. R. Thomson (1975). Aberrations and tolerances in a double-deflection electron-beam scanning system. *J. Vac. Sci. Technol.* **12**, 1156–1159.
M. G. R. Thomson (1996). The electrostatic moving objective lens and optimized deflection systems for microcolumns. *J. Vac. Sci. Technol. B* **14**, 3802–3807.
J. T. L. Thong, Ed. (1993). *Electron Beam Testing Technology* (Plenum, New York).
J. T. L. Thong and W. C. Nixon (1990). An electron-optical phase-shifting element for high-speed electron beam testing. *Meas. Sci. Technol.* **1**, 337–344.
J. T. L. Thong, S. C. J. Garth, B. C. Breton and W. C. Nixon (1987). Ultra high speed electron beam testing system. *Microelectron. Eng.* **6**, 683–688.
R. M. Tromp (2011). Measuring and correcting aberrations of a cathode objective lens. *Ultramicroscopy* **111**, 273–281.
R. M. Tromp (2013). Characterization of the cathode objective lens by real-space microspot low energy electron diffraction. *Ultramicroscopy* **130**, 2–6.
R. M. Tromp (2015a). Catadioptric aberration correction in cathode lens microscopy. *Ultramicroscopy* **151**, 191–198.
R. M. Tromp (2015b). An adjustable electron achromat for cathode lens microscopy. *Ultramicroscopy* **159**, 497–502.
R. M. Tromp, J. B. Hannon, A. W. Ellis, W. Wan, A. Berghaus and O. Schaff (2010). A new aberration-corrrected, energy-filtered LEEM/PEEM instrument. I. Principles and design. *Ultramicroscopy* **110**, 852–861.
R. M. Tromp, W. Wan and S. M. Schramm (2012). Aberrations of the cathode objective lens up to fifth order. *Ultramicroscopy* **119**, 33–39.
R. M. Tromp, J. B. Hannon, W. Wan, A. Berghaus and O. Schaff (2013). A new aberration-corrrected, energy-filtered LEEM/PEEM instrument. II. Operation and results. *Ultramicroscopy* **127**, 25–39.
K. Tsuno (1991). Aberration analysis of a Wien filter for electrons. *Optik* **89**, 31–40.
K. Tsuno (1992). Electron optical analysis of a high-resolution electron energy loss spectrometer with a retarding Wien filter. *Rev. Sci. Instrum.* **63**, 4112–4121.
K. Tsuno (1993). Electron optical analysis of a retarding Wien filter for electron spectroscopic imaging. *Rev. Sci. Instrum.* **64**, 659–666.
K. Tsuno and D. Ioanoviciu (2013). The Wien filter. *Adv. Imaging Electron Phys.* **176**.
K. Tsuno and J. Rouse (1996). Simulation of electron trajectories of Wien filters for high-resolution EELS installed in TEM. *J. Electron Microsc.* **45**, 417–427.
K. Tsuno, M. Terauchi and M. Tanaka (1988). Electron trajectory calculation of a stigmatic-focus Wien filter for electron energy loss spectroscopy. I. *Optik* **78**, 71–77.
K. Tsuno, M. Terauchi and M. Tanaka (1989a). Electron trajectory calculation of a stigmatic-focus Wien filter for electron energy loss spectroscopy. II. *Optik* **80**, 149–154.
K. Tsuno, M. Terauchi and M. Tanaka (1989b). Electron trajectory calculation of a stigmatic-focus Wien filter for electron energy loss spectroscopy. III. *Optik* **83**, 77–84.
K. Tsuno, M. Terauchi and M. Tanaka (1989c). Design and performance of a retarding Wien filter installed in a TEM for EELS. EMAG–MICRO, London. **1**, 71–74.
K. Tsuno, N. Handa and S. Matsumoto (1995). Immersion lenses for low voltage SEM and LEEM. *Proc. SPIE* **2522**, 243–252.
K. Tsuno, N. Handa, S. Matsumoto and A. Mogami (1996). Optical properties of immersion objective lenses and collimation of secondary electrons in low voltage SEM. *Proc. SPIE* **2858**, 46–57.
K. Tsuno, D. Ioanoviciu and G. Martínez (2003). Aberration corrected Wien filter as a monochromator of high spatial and high energy resolution electron microscopes. *Microsc. Microanal.* **9** (Suppl. 2), 944–945.

K. Tsuno, D. Ioanoviciu and G. Martínez (2005). Third-order aberration theory of Wien filters for monochromators and aberration correctors. *J. Microsc. (Oxford)* **217** (Suppl. 2), 205−215.

K. Tsuno, T. Yasue and T. Koshikawa (2009). Design of a mirror aberration corrector and a beam separator for LEEM. *Appl. Surf. Sci.* **256**, 1035−1041.

V. V. Tsyganenko, R. A. Lachashvili and I. A. Bobrovskii (1972). Estimation of the paraxial resolving power of cathode lenses. *Opt-.Mekh. Prom.* **39** (12), 12−16. *Sov. J. Opt. Technol*. **39**, 733−737.

P. J. Turner, B. J. Regan and M. J. Southon (1972). Surface microscopy and analysis with the atom-probe field-ion microscope. *Vacuum* **22**, 443−446.

Y. Uchikawa and S. Maruse (1969). Theory of chromatic aberrations of the cathode lens. *J. Electron Microsc.* **18**, 118−127.

M. Ueda and K. Nagami (1975). Three types of stigmatic image formations by a quadrupole triplet. *Optik* **43**, 319−335.

M. Ueda, K. Nagami and H. Kuroda (1969). Focusing characteristics of electrostatic symmetrical quadrupole triplet lens [in Japanese]. *Oyo Butsuri* **38**, 1037−1046.

M. Ueda, K. Nagami and H. Kuroda (1970). Focusing characteristics of electrostatic symmetrical quadrupole triplet lens. *Bull. Univ. Osaka Prefect. A* **19**, 119−132.

M. Ueda, K. Nagami and H. Kuroda (1971). Focusing characteristics of a three element quadrupole lens system for demagnifying stigmatic images. *Oyo Butsuri* **40**, 756−757.

M. Ueda, K. Nagami and H. Kuroda (1973a). Stigmatic demagnified image formation by three elements electrostatic quadrupole lenses. *Optik* **37**, 528−541.

M. Ueda, M.-T. Noda, K. Nagami and H. Kuroda (1973b). Calculations of fringing fields of a quadrupole doublet. *IEEE Trans. Electron Dev.* **20**, 662−663.

M. Ueda, M.-T. Noda, K. Nagami and H. Kuroda (1974). Considerations on fringing fields of quadrupole lenses. *Optik* **39**, 375−385.

W. N. Unertl and C.-s. Shern (1991). Mirror electron microscope−low energy electron diffraction for studies of surface ordering and melting. In *Advances in Surface and Thin Film Diffraction* (T. C. Huang, P. I. Cohen and D. J. Eaglesham, Eds), 261−272 (Materials Research Society, Pittsburgh); MRS Proceedings **208**.

K. Ura (1991). New normalization in optical properties of the electrostatic quadrupole lens. *J. Electron Microsc.* **40**, 374−377.

K. Ura (2016). Tilting and moving-object lens for a 3D electron microscope. *Microscopy* **65**, 460−464.

K. Ura and H. Fujioka (1989). Electron beam testing. *Adv. Electron. Electron Phys.* **73**, 233−317.

T. van Oudheusden, E. F. de Jong, S. B. van der Geer, W. P. E. M. Op ‘t Root, O. J. Luiten and B. J. Siwick (2007). Electron source concept for single-shot sub-100 fs electron diffraction in the 100 keV range. *J. Appl. Phys.* **102**, 093501, 8 pp.

T. van Oudheusden, P. L. E. M. Pasmans, S. B. van der Geer, M. J. de Loos, M. J. van der Wiel and O. J. Luiten (2010). Compression of subrelativistic space-charge-dominated electron bunches for single-shot femtosecond electron diffraction. *Phys. Rev. Lett.* **105**, 264801, 4 pp.

V. S. Vavilov (1952). An electron-optical method for investigating electromagnetic fields and its application to the study of the internal photoeffect. *Zh. Tekh. Fiz.* **22**, 1644−1657.

V. N. Vertsner and Yu. V. Chentsov (1963). A mirror scanning electron microscope. *Prib. Tekhn. Eksp* (5), 180−182. *Instrum. Exp. Tech.* **6**, 956−958.

V. N. Vertsner and Yu. F. Shchetnev (1967). Low-voltage electron microscopy. *Opt.-Mekh. Prom.* **34** (7), 20−25. *Sov. J. Opt. Technol.* **34**, 430−434.

V. N. Vertsner, L. A. Garbarets, M. I. Govorukha, V. N. Keys, G. D. Kisel’, V.M. Krygin, and Yu. V. Chentsov (1969). Low-voltage scanning electron microscopy. *Opt.-Mekh. Prom*. **36** (1), 66–68. *Sov. J. Opt. Technol*. **36**, 71−73

R. Viswanathan, A. D. Wilson, J. Lafuente, H. Voelker and A. Kern (1984). Electron beam pattern writer for X-ray masks. *Proc. SPIE* **448**, 130−138.

A. G. Vlasov and Yu. A. Shapiro (1971). Some methods of calculating the resolving power of electron-optical systems. *Avtometriya* No. 6, 20−23.

A. G. Vlasov and Yu. A. Shapiro (1974). *Metody Rascheta Emissionnykh Elektronno-opticheskikh Sistem* (Mashinostroenie, Leningrad).

A. G. Vlasov, I. M. Minkov, B. I. Orlov, I. S. Reidman and Yu. A. Shapiro (1964). Calculation of the resolving power of electron-optical systems by the trajectory method. *Opt.-Mekh. Prom.* **31** (2), 25–27.

H.-U. von Gersch, D. Grambole, F. Herrmann and H.-J. Thomas (1982). Protonenmikrosonde am Rossendorfer Tandemgenerator. *Exp. Tech. Phys.* **30**, 227–234.

Yu. V. Vorob'ev (1956). Diffusion pattern in electrostatic immersion lenses. *Zh. Tekh. Fiz.* **26**, 2269–2280. *Sov. Phys. Tech. Phys*. **1**, 2200–2211.

Yu. V. Vorob'ev (1959). Aberrations of cathode electron lenses with violation of the axial symmetry of the field. *Zh. Tekh. Fiz.* **29**, 589–596. *Sov. Phys. Tech. Phys*. **4**, 525–531.

W. Wan, J. Feng, H. A. Padmore and D. S. Robin (2004). Simulation of a mirror corrector for PEEM3. *Nucl. Instrum. Meth. Phys. Res. A* **519**, 222–229.

W. Wan, L. Yu, L. Zhu, X.-d. Yang, Z. Wei, J. Z. Liu, J. Feng, K. Kunze, O. Schaff, R. M. Tromp and W.-x Tang (2017). Design and commissioning of an aberration-corrected ultrafast spin-polarized low energy electron microscope with multiple electron sources. *Ultramicroscopy* **174**, 89–96.

W. K. Waskiewicz, C. J. Biddick, M. I. Blakey, K. J. Brady, R. M. Camarda, W. F. Connelly, A. H. Crorken, J. P. Custy, R. DeMarco, R. C. Farrow, J. A. Felker, L. A. Fetter, R. R. Freeman, L. R. Harriott, L. C. Hopkins, H. A. Huggins, R. J. Kasica, C. S. Knurek, J. S. Kraus, J. A. Liddle, M. M. Mkrtchyan, A. E. Novembre, M. L. Peabody, L. Rutberg, H. H. Wade, P. G. Watson, K. S. Werder, D. L. Windt, R. G. Tarascon-Auriol, S. D. Berger and S. W. Bowler (1997). SCALPEL proof-of-concept system: preliminary lithography results. *Proc. SPIE* **3048**, 255–263.

F. Watt and G. W. Grime, Eds (1987). *Principles and Applications of High-Energy Ion Microbeams* (Hilger, Bristol).

F. Watt, G. W. Grime, G. D. Blower and J. Takacs (1981). A coupled triplet configuration of the Oxford microprobe. *IEEE Trans. Nucl. Sci.* **28**, 1413–1416.

F. Watt, G. W. Grime, G. D. Blower, J. Takacs and D. J. T. Vaux (1982). The Oxford 1 μm proton microprobe. *Nucl. Instrum. Meth.* **197**, 65–77.

S. P. Weathersby, G. Brown, M. Centurion, T. F. Chase, R. Coffee, J. Corbett, J. P. Eichner, J. C. Frisch, A. R. Fry, M. Gühr, N. Hartmann, C. Hast, R. Hettel, R. K. Jobe, E. N. Jongewaard, J. R. Lewandowski, R. K. Li, A. M. Lindenberg, I. Makasyuk, J. E. May, D. McCormick, M. N. Nguyen, A. H. Reid, X. Shen, K. Sokolowski-Tinten, T. Vecchione, S. L. Vetter, J. Wu, J. Yang, H. A. Dürr and X. J. Wang (2015). Mega-electron-volt ultrafast electron diffraction at SLAC National Accelerator Laboratory. *Rev. Sci. Instrum.* **86**. 073702, 7 pp.

R. Wichtendahl, R. Fink, H. Kuhlenbeck, D. Preikszas, H. Rose, R. Spehr, P. Hartel, W. Engel, R. Schlögl, H. J. Freund, A. M. Bradshaw, G. Lilienkamp, T. Schmidt, E. Bauer, G. Benner and E. Umbach (1998). SMART: an aberration-corrected XPEEM/LEEM with energy filter. *Surf. Rev. Lett.* **5**, 1249–1256.

W. Wien (1897). Die elektrostatischen Eigenschaften der Kathodenstrahlen. *Verhandlungen der Deutschen Physikalischen Gesellschaft* **16**, 165–172.

W. Wien (1898). Untersuchungen über die elektrische Entladung in verdünnten Gasen. *Ann. Phys. (Leipzig)* **301**, 440–452.

J. Williams, F. Zhou, T. Sun, Z. Tao, K. Chang, K. Makino, M. Berz, P. M. Duxbury and C.-y. Ruan (2017). Active control of bright electron beams with RF optics for femtosecond microscopy. *Struct. Dyn*. **4**, 044035, 20 pp.

A. P. Wilska (1970). Low voltage electron microscope with energy filtering and amplitude contrast. ICEM-7, Grenoble. **1**, 149–150.

D. Wiskott (1956). Zur Theorie des Auflichtelektronenmikroskops. *Optik* **13**. 463–478 & 481–493.

J. Witzani and E. M. Hörl (1976). An electron mirror attachment for a scanning electron microscope. EUREM-6, Jerusalem. **1**, 325–327.

J. Witzani and E. M. Hörl (1981). Scanning electron mirror microscopy. *Scanning* **4**, 53–61.

H. Wollnik (1987). *Optics of Charged Particles* (Academic Press, Orlando & London).

C.-d. Wu (1956). Influence of the velocity distribution of photoelectrons on the quality of the image in emission electron-optical systems. I. [in Russian]. *Acta Phys. Sin.* **12**, 419−438.
C.-d. Wu (1957a). Influence of the velocity distribution of photoelectrons on the quality of the image in emission electron-optical systems. II. [in Russian]. *Acta Phys. Sin.* **13**, 78−89.
C.-d. Wu (1957b). Influence of the velocity distribution of photoelectrons on the quality of the image in emission electron-optical systems. *Sci. Sin.* **6**, 381−397. English translation of Wu (1956 and 1957a).
Y. K. Wu, D. S. Robin, E. Forest, R. Schlueter, S. Anders, J. Feng, H. Padmore and D. H. Wei (2004). Design and analysis of beam separator magnets for third generation aberration corrected PEEMs. *Nucl. Instrum. Meth. Phys. Res. A* **519**, 230−241.
J.-y. Ximen (1957). On the electron-optical properties and aberration theory of combined immersion objectives. *Acta Phys. Sin.* **13**, 339−355.
J.-y. Ximen (1981). On the linear transformations of Gaussian trajectory parameters and their influence upon electron optical aberrations. *Acta Phys. Sin.* **30**, 472−477.
J.-y. Ximen, L.-w. Zhou and K.-c. Ai (1983). Variational theory of aberrations in cathode lenses. *Optik* **66**, 19−34, also *Acta Phys. Sin*. **32** (1983) 1536−1546.
S. N. Yachmenev (1986a). Image aberration of a projector, taking into account the effect of the collimating portion of the illumination system. *Radiotekh. Elektron.* **31**, 140−143. *Radio Eng. Electron. Phys*. **31** (1), 132−136.
S. N. Yachmenev (1986b). A method of calculating aberrations in a projection system with electrostatic lenses. *Radiotekh. Elektron.* **31**, 144−149. *Radio Eng. Electron. Phys*. **31** (1), 136−142.
S. N. Yachmenev (1986c). Chromatic aberrations of a projector with electrostatic lenses. *Radiotekh. Elektron.* **31**, 150−155. *Radio Eng. Electron. Phys*. **31** (1), 142−147.
E. M. Yakushev (2013). Theory and computation of electron mirrors: the central particle method. *Adv. Imaging Electron Phys.* **178**, 147−247.
E. M. Yakushev and L. M. Sekunova (1986). Theory of electron mirrors and cathode lenses. *Adv. Electron. Electron Phys.* **68**, 337−416.
J.-f. Yang, Y. Yoshida and K. Tanimura (2017a). Ultrafast electron microscopy using femtosecond electron pulses. *Kenbikyo* **52** (Suppl. 1), 21.
J.-f. Yang, Y. Yoshida and K. Tanimura (2017b). A relativistic-energy femtosecond-pulse electron microscopy. APMC-11, Phuket. 164 (paper number O10303).
S.Ya. Yavor (1968). Fokusirovka Zaryazhennykh Chastits Kvadrupol'nymi Linzami (Atomizdat, Moscow).
S. Ya. Yavor (1970). Calculation of crossed electron-optical lenses. *Zh. Tekh. Fiz.* **40**, 2257−2260. *Sov. Phys. Tech. Phys*. **15**, 1763−1765.
S. Ya. Yavor (1984). Radial lenses. *Pis'ma Zh. Tekh. Fiz.* **10**, 183−186. *Sov. Tech. Phys. Lett*. **10**, 76−77.
A. H. Zewail (2010). Four-dimensional electron microscopy. *Science* **328**, 187−193.
A. H. Zewail and J. M. Thomas (2010). *4D Electron Microscopy* (Imperial College Press, London).
Y. Zhao and A. Khursheed (1999a). Variable axis lens of mixed electrostatic and magnetic fields and its application in electron-beam lithography systems. *J. Vac. Sci. Technol. B* **17**, 2795−2798.
Y. Zhao and A. Khursheed (1999b). Comparative study on magnetic variable axis lenses using electrostatic and magnetic in-lens deflectors. *Proc. SPIE* **3777**, 107−114.
Y. Zhao and A. Khursheed (1999c). General condition for moving objective lens (MOL) with combined electrostatic and magnetic fields. *Optik* **110**, 563−568.
J.-y. Zhao, T.-t. Tang, Y.-f. Kang and D. Zhang (2012a). Study on combined immersion electrostatic−magnetic focusing lenses without crossovers. *Optik* **123**, 1271−1278.
J.-y. Zhao, T.-t. Tang, Y.-f. Kang and W.-j. Sun (2012b). Study on rotation-free combined immersion magneto−electrostatic lenses. *Optik* **123**, 1233−1235.
L.-w. Zhou (1984). Optics of wide electron beam focusing. In *Electron Optical Systems for Microscopy, Microanalysis and Microlithography* (J. J. Hren, F. A. Lenz, E. Munro and P. B. Sewell, Eds), 45−62 (Scanning Electron Microscopy, AMF O'Hare).

L.-w. Zhou (1985). A generalized theory of wide electron beam focusing. *Adv. Electron. Electron Phys.* **64B**, 575–589.
L.-w. Zhou, K.-c. Ai and S.-c. Pan (1983). On aberration theory of the combined electromagnetic focusing cathode lenses. *Acta Phys. Sin.* **32**, 376–392.
L.-w. Zhou, B. Qiu and G. Ni (1988). An inverse design of magnetic focusing coil for electrostatic and magnetic imaging. *Optik* **78**, 54–58.
V. A. Zhukov and A. B. Abraamyants (1986a). Synthesis of magnetic objectives for scanning electron-optical systems. *Zh. Tekh. Fiz.* **56**, 1962–1966. *Sov. Phys. Tech. Phys.* **31**, 1172–1174.
V. A. Zhukov and A. B. Abraamyants (1986b). Predeflection aberrations in magnetic objectives with a swinging axis. *Radiotekh. Elektron.* **31**, 981–988. *Sov. J. Commum. Technol. Electron.* **31** (90), 142–149.
N. K. Zolina and Yu. A. Flegontov (1978). Calculation of the properties of the electron image in cathode electrostatic lenses. *Zh. Tekh. Fiz.* **48**, 2479–2489. *Sov. Phys. Tech. Phys.* **23**, 1417–1423.
N. K. Zolina and Yu. A. Flegontov (1982). Design of electrostatic lenses with a concave electrode. *Zh. Tekh. Fiz.* **52**, 1938–1945. *Sov. Phys. Tech. Phys.* **27**, 1190–1195.
N. K. Zolina and Yu. A. Shapiro (1972). Calculation of image parameters of cathode lenses. *Opt.-Mekh. Prom.* **39** (2), 12–14. *Sov. J. Opt. Technol.* **39**, 69–71.
V. K. Zworykin (1933). On electron optics. *J. Franklin Inst.* **215**, 535–555.

Part VIII, Chapters 41 and 42

The papers of Baranova and Read (1999) and Baranova et al. (1991, 1995, 2002, 2004, 2008) are concerned with multipole correctors. Smith and Munro (1987), Munro et al. (2001) and Rose (1996) consider aberration correction in general. The accounts of the history of the STEM by Pennycook (2011) and Tanaka (2015a,b) are of interest here.

***

H. Akima and T. Yoshida (2014). Measurement of large low-order aberrations by using a series of through focus Ronchigrams. *Microscopy* **63**, 325–332.
N. Anazawa, R. Aihara and S. Ohta (1975). Stabilization of pulsed-field emission. *J. Phys. E: Sci. Instrum.* **8**, 971–976.
G. D. Archard (1954a). Requirements contributing to the design of devices used in correcting electron lenses. *Br. J. Appl. Phys.* **5**, 294–299.
G. D. Archard (1954b). Electron optical properties of electrode systems of four- and eight-fold symmetry. ICEM-3, London. 97–105.
G. D. Archard (1955a). Two new simplified systems for the correction of spherical aberration in electron lenses. *Proc. Phys. Soc. (Lond.) B* **68**, 156–164.
G. D. Archard (1955b). A possible chromatic corrrection system for electron lenses. *Proc. Phys. Soc. (Lond) B* **68**, 817–829.
G. D. Archard (1958). An unconventional electron lens. *Proc. Phys. Soc. (Lond.) B* **72**, 135–137.
G. D. Archard (1960). Proposed system for magnetic electron probe. In *Proc. 2nd Int. Conf. X-ray Microscopy and X-ray Microanalysis* (A. Engström, V. E. Cosslett and H. Pattee, Eds), 337–343 (Elsevier, Amsterdam, London & New York).
G. D. Archard, T. Mulvey and D. P. R. Petrie (1960). Experiments with correction of spherical aberration. EUREM-2, Delft. **1**, 51–54.
E. A. Ash (1955). Use of space charge in electron optics. *J. Appl. Phys.* **26**, 327–330.
E. A. Ash and D. Gabor (1955). Experimental investigations on electron interaction. *Proc. R. Soc. (Lond.) A* **228**, 477–490.
L. A. Baranova and F. H. Read (1999). Minimisation of the aberrations of electrostatic lens systems composed of quadrupole and octupole lenses. *Int. J. Mass Spectrom.* **189**, 19–26.

L. A. Baranova and S. Ya. Yavor (1984). Electrostatic lenses. *Zh. Tekh. Fiz.* **54**, 1417–1453. *Sov. Phys. Tech. Phys*. **29**, 827–848.

L. A. Baranova and S. Ya. Yavor (1986). *Elektrostaticheskie Elektronnye Linzy* (Nauka, Moscow).

L. A. Baranova and S. Ya. Yavor (1989). The optics of round and multipole electrostatic lenses. *Adv. Electron. Electron Phys.* **76**, 1–207.

L. A. Baranova, N. S. Ul'yanova and S. Ya. Yavor (1991). Correction of chromatic aberration in systems of electrostatic lenses containing quadrupoles. *Zh. Tekh. Fiz* **61** (7), 157–159. *Sov. Phys. Tech. Phys*. **36**, 813–815.

L. A. Baranova, S. Ya. Yavor and E. Munro (1995). Electrostatic lens with corrected chromatic and spherical aberrations. *Proc. SPIE* **2522**, 260–263.

L. A. Baranova, F. H. Read and D. Cubric (2002). Computer simulation of an electrostatic aberration corrector for a low-voltage scanning electron microscope. *Recent Trends* **8**, 74.

L. A. Baranova, F. H. Read and D. Cubric (2004). Computational simulation of an electrostatic aberration corrector for a low-voltage scanning electron microscope. *Nucl. Instrum. Meth. Phys. Res. A* **519**, 42–48.

L. A. Baranova, F. H. Read and D. Cubric (2008). Computer simulations of hexapole aberration correctors. *Phys. Procedia* **1**, 185–191.

J. E. Barth (1967). Electrostatic correction of the spherical aberration of electron lenses. Dissertation, University of Arizona.

J. Barthel and A. Thust (2013). On the optical stability of high-resolution transmission electron microscopes. *Ultramicroscopy* **134**, 6–17.

B. Bastian, K. Spengler and D. Typke (1971). Ein elektrisch-magnetisches Oktopol-Element zur sphärischen und chromatischen Korrektur von Elektronenlinsen. *Optik* **33**, 591–596.

P. E. Batson (2003a). Aberration correction results in the IBM STEM instrument. *Ultramicroscopy* **96**, 239–249.

P. E. Batson (2003b). Experience with the IBM sub-Angstrom STEM. *Microsc. Microanal.* **9** (Suppl. 2), 136–137.

P. E. Batson (2008). First results using the Nion third-order scanning transmission eletcron microscope corrector. *Adv. Imaging Electron Phys.* **153**, 163–194.

P. E. Batson, N. Dellby and O. L. Krivanek (2002). Sub-ångström resolution using aberration-corrected electron optics. *Nature* **418**, 617–620.

E. Bauer (2007). LEEM and SPLEEM. In *Science of Microscopy* (P. W. Hawkes and J. C. H. Spence, Eds), **1**, 605–656 (Springer, New York).

E. Bauer (2014). *Surface Microscopy with Low Energy Electrons* (Springer, New York).

E. Bauer (2018). LEEM, SPLEEM and SPELEM. In *Handbook of Microscopy* (P. W. Hawkes and A. J. Spence, Eds), (Springer, Cham), forthcoming.

V. Beck (1977). Experiments with a quadrupole octopole corrector in a STEM. EMSA, Boston. **35**, 90–91.

V. D. Beck (1979). A hexapole spherical aberration corrector. *Optik* **53**, 241–255.

V. D. Beck (2011). Chicago aberration correction work. *Microsc. Microanal.* **17** (Suppl. 2), 1246–1247.

V. D. Beck and A. V. Crewe (1974). A quadrupole octupole corrector for a 100 keV STEM. EMSA, St Louis. **32**, 426–427.

V. D. Beck and A. V. Crewe (1976). Progress in aberration correction in the STEM. EMSA, Miami Beach. **34**, 578–579.

H. Becker and A. Wallraff (1938). Über die sphärische Aberration magnetischer Linsen. *Arch. Elektrotech.* **32**, 664–675.

M. Bernard (1952). Aberration de sphéricité des lentilles à grilles. *C. R. Acad. Sci. Paris* **235**, 1115–1117.

M.-Y. Bernard (1953). Focalisation des particules de grande énergie par des lentilles à grille. I. La convergence des lentilles à grille. II. Défauts des lentilles. *J. Phys. Radium* **14**, 381–394 & 451–458.

W. Bernhard (1980). Erprobung eines sphärisch und chromatisch korrigierten Elektronenmikroskopes. *Optik* **57**, 73–94.

W. Bernhard and H. Koops (1977). Kompensation der Farbabhängigkeit der Vergrößerung und der Farbabhängigkeit der Bilddrehung eines Elektronenmikroskops. *Optik* **47**, 55–64.

S. B. Bimurzaev and E. M. Yakushev (2011). Electromagnetic mirror objective with removable spherical aberration. *Nucl. Instrum. Meth. Phys. Res. A* **645**, 33–34.

S. B. Bimurzaev, N. U. Aldiyarov and E. M. Yakushev (2017). The objective lens of the electron microscope with correction of spherical and axial chromatic aberrations. *Microscopy* **66**, 356–365.

J. H. Boerboom (1972). Ion optics of the electric hexapole. *Int. J. Mass Spectrom. Ion Phys.* **8**, 475–492.

H. Boersch (1947). Über die Kontraste von Atomen im Elektronenmikroskop. *Z. Naturforsch.* **2a**, 615–633.

P. Bonjour (1976). Superconducting lenses: present trends and design. EUREM-6, Jerusalem. **1**, 73–78.

J. Burfoot (1953). Correction of electrostatic lenses by departure from rotational symmetry. *Proc. Phys. Soc. (Lond.) B* **66**, 775–792.

J.W. Butler (1970). New results in high-frequency electron optics. ICEM-7, Grenoble. **2**, 49–50.

L. C. Chao, J. Orloff and L. Wang (1997). Spherical aberration corrector using space charge. *J. Vac. Sci. Technol. B* **15**, 2732–2736.

L. Clark, A. Béché, G. Guzzinati, A. Lubk, M. Mazilu, R. Van Boxem and J. Verbeeck (2013). Exploiting lens aberrations to create electron-vortex beams. *Phys. Rev. Lett.* **111**. 064801, 5 pp.

P. Communay and B. Marais (1971). Utilisation d'un dispositif corrigeant partiellement l'aberration sphérique d'un objectif magnétique de microscope électronique. *J. Microsc. (Paris)* **11**, 473–482.

V. E. Cosslett (1978). Introduction and state of the art [The Instrument Today and Tomorrow]. ICEM-9, Toronto. **3**, 163–172.

J. M. Cowley (1979a). Adjustment of a STEM instrument by use of shadow images. *Ultramicroscopy* **4**, 413–418.

J. M. Cowley (1979b). Coherent interference in convergent-beam electron diffraction and shadow imaging. *Ultramicroscopy* **4**, 435–450.

J. M. Cowley (1980). Interference effects in a STEM instrument. *Micron* **11**, 229–233.

A. V. Crewe (1978). Is there a future for the STEM? ICEM-9, Toronto. **3**, 197–204.

A. V. Crewe (1980). Studies on sextupole correctors. *Optik* **57**, 313–327.

A. V. Crewe (1982). A system for the correction of axial aperture aberrations in electron lenses. *Optik* **60**, 271–281.

A. V. Crewe (1984). The sextupole corrector. 1. Algebraic calculations. *Optik* **69**, 24–29.

A. V. Crewe (1992). Electron motion in tuned fields. I. The algebra. II. Some applications. *Ultramicroscopy* **41**, 269–277 & 279–285.

A. V. Crewe (2009). The work of Albert Victor Crewe on the scanning transmission electron microscope and related topics. *Adv. Imaging Electron Phys.* **159**, 1–61.

A. V. Crewe and D. Kopf (1980a). A sextupole system for the correction of spherical aberration. *Optik* **55**, 1–10.

A. V. Crewe and D. Kopf (1980b). Limitations of sextupole correctors. *Optik* **56**, 391–399.

A. V. Crewe, J. Wall and L. M. Welter (1968). A high-resolution scanning transmission electron microscope. *J. Appl. Phys.* **39**, 5861–5868.

A. V. Crewe, S. Ruan, F. Tsai and P. Korda (1995). The first test on a magnetically focused mirror corrector. EMAG, Birmingham. 301–304.

A. V. Crewe, S. Ruan, P. Korda and F. C. Tsai (2000). Studies of a magnetically focused electrostatic mirror. I. Experimental test of the first order properties. *J. Microsc. (Oxford)* **197**, 110–117; for Part II, see Tsai (2000).

U. Dahmen, R. Erni, V. Radmilovic, C. Kisielowski, M.-D. Rossell and P. Denes (2009). Background, status and future of the Transmission Electron Aberration-corrected Microscope project. *Philos. Trans. R. Soc. (Lond.) A* **367**, 3795–3808.

R. L. Dalglish (1981). Corrected electrostatic lens systems for ion beams. *Nucl. Instrum. Meth.* **191**, 191–198.

R. L. Dalglish, A. M. Smith and S. Hughes (1983a). Geometric aberration correction in ion lenses – the Caledonian quadruplet. *Nucl. Instrum. Meth.* **215**, 9–15.

R. L. Dalglish, T. Winchester and A. M. Smith (1983b). A new concept for improved ion and electron lenses – aberration corrected systems of planar electrostatic deflection elements. *Nucl. Instrum. Meth.* **218**, 7–10.

R. Danev and K. Nagayama (2001). Transmission electron microscope with Zernike phase plate. *Ultramicroscopy* **88**, 243–252.

R. Danev and K. Nagayama (2011). Optimizing the phase shift and the cut-on periodicity of phase plates for TEM. *Ultramicroscopy* **111**, 1305–1315.

R. Danev, R. M. Glaeser and K. Nagayama (2009). Practical factors affecting the performance of a thin-film phase plate for transmission electron microscopy. *Ultramicroscopy* **109**, 312–325.

N. H. Dekkers (1969). Correction of spherical aberration. Dissertation, Delft.

N. H. Dekkers and J. B. Le Poole (1968). Correction of spherical aberration. EUREM-4, Rome. **1**, 167–168.

N. Dellby, O. L. Krivanek, P. D. Nellist, P. E. Batson and A. R. Lupini (2001). Progress in aberration-corrected scanning transmission electron microscopy. *J. Electron Microsc.* **50**, 177–185.

N. Dellby, O. L. Krivanek and M. F. Murfitt (2008). Optimized quadrupole–octupole C_3/C_5 aberration corrector for STEM. *Phys. Procedia* **1**, 179–183.

N. Dellby, N. J. Bacon, P. Hrncirik, M. F. Murfitt, G. S. Skone, Z. S. Szilagyi and O. L. Krivanek (2011). Dedicated STEM for 200 to 40keV operation. *Eur. Phys. J.: Appl. Phys.* **54**. 33505, 11 pp.

J. M. H. Deltrap (1964a). Correction of spherical aberration with combined quadrupole–octupole units. EUREM-3, Prague. **A**, 45–46.

J. M. H. Deltrap (1964b). Correction of spherical aberration of electron lenses. Dissertation, Cambridge.

J. M. H. Deltrap and V. E. Cosslett (1962). Measurement of aperture aberrations of magnetic quadrupoles. ICEM-5, Philadelphia. **1**, KK-8.

D. Dhuicq (1968a). Condition de corrrection des aberrations géométriques: application aux aberrations d'ouverture du 3e ordre des systèmes quadrupolaires stigmatiques. *C. R. Acad. Sci. Paris B* **266**, 906–908.

D. Dhuicq (1968b). Calcul des potentiels octopolaires permettant la correction des aberrations d'ouverture d'un système formé de lentilles quadrupolaires équivalent à un objectif à symétrie de révolution. *J. Microsc. (Paris)* **7**, 297–313.

D. Dhuicq and P. A. Möller (1970). Etude d'un objectif formé de lentilles quadrupolaires et octopolaires: aberration d'ouverture du 5e ordre, correction simultanée de l'aberration d'ouverture du 3e ordre et de la distorsion. ICEM-7, Grenoble. **2**, 45–46.

D. Dhuicq and A. Septier (1966a). Vers la réalisation d'un objectif formé de quatre lentilles quadrupolaires et corrigé des aberrations d'ouverture. 1. Etude à l'approximation de Gauss. *C. R. Acad. Sci. Paris B* **263**, 280–283.

D. Dhuicq and A. Septier (1966b). Vers la réalisation d'un objectif formé de quatre lentilles quadrupolaires et corrigé des aberrations d'ouverture. 2. Correction des aberrations d'ouverture. *C. R. Acad. Sci. Paris B* **263**, 364–367.

D. Dhuicq and A. Septier (1968). Correction des aberrations d'ouverture d'un objectif formé de lentilles quadrupolaires. EUREM-4, Rome. **1**, 177–178.

I. Dietrich (1976). *Superconducting Electron-Optic Devices* (Plenum, New York & London).

I. Dietrich (1978). Superconducting lenses. ICEM-9, Toronto. **3**, 173–184.

I. Dietrich, K.-F. Herrmann and C. Passow (1975). A proposal for a high voltage electron microscope with superconducting microwave linear accelerator and superconducting lenses. *Optik* **42**, 439–462.

L. Dodin (1983). Electrostatic electron-optical systems with discontinuous fields. *Zh. Tekh. Fiz.* **53**, 1759–1763. *Sov. Phys. Tech. Phys*. **28**, 1083–1085.

H. Dohi and P. Kruit (2017). Suggestion of aberration corrected SEM using double micro-mirror. *Kenbikyo* **52** (Suppl. 1), 145.

A. J. Dragt and E. Forest (1986). Lie algebraic theory of charged-particle optics and electron microscopes. *Adv. Electron. Electron Phys.* **67**, 65–120.

M. Dries, K. Schultheiss, B. Gamm, A. Rosenauer, R. R. Schröder and D. Gerthsen (2011). Object-wave reconstruction by carbon film-based Zernike- and Hilbert-phase plate microscopy: a theoretical study not restricted to weak-phase objects. *Ultramicroscopy* **111**, 159–168.

M. Dries, S. Hettler, T. Schulze, W. Send, E. Müller, R. Schneider, D. Gerthsen, Y.-s. Luo and K. Samwer (2016). Thin-film phase plates for transmission electron microscopy fabricated from metallic glasses. *Microsc. Microanal.* **22**, 95–963.

J. W. Dungey and C. R. Hull (1947). Coaxial electron lenses. *Proc. Phys. Soc. (Lond.) B* **59**, 828–843.

G. Dupouy, F. Perrier and J. Trinquier (1964). Contribution à la correction de l'aberration chromatique du microscope électronique magnétique. *J. Microsc. (Paris)* **3**, 115–132.

K. P. Dutova and P. P. Kas'yankov (1963). Calculation of electron-optical systems corrected for astigmatism. *Izv. Akad. Nauk SSSR (Ser. Fiz.)* **27**, 1127–1130. *Bull. Acad. Sci. USSR (Phys. Ser.)* 27, 1108–1111.

D. Dymnikov and S. Ya. Yavor (1963). Four quadrupoles as the analogue of an axially symmetric system. *Zh. Tekh. Fiz.* **33**, 851–858. *Sov. Phys. Tech. Phys.* **8**, 639–643.

D. Dymnikov, T. Ya. Fishkova and S. Ya. Yavor (1963). System of four quadrupole lenses analogous to an axially symmetric lens. *Izv. Akad. Nauk SSSR (Ser. Fiz.)* **27**, 1131–1134. *Bull. Acad. Sci. USSR (Phys. Ser.)* **27**, 1112–1115.

D. Dymnikov, T. Ya. Fishkova and S. Ya. Yavor (1964a). System of revolution composed of four quadrupole lenses. EUREM-3, Prague. **A**, 43–44.

D. Dymnikov, T. Ya. Fishkova and S. Ya. Yavor (1964b). Electron-optical properties of a pseudo-axially symmetric quadrupole system. *Radiotekh. Elektron.* **9**, 1828–1831. *Radio Eng. Electron. Phys*. **9**, 1515–1518.

D. Dymnikov, T. Ya. Fishkova and S. Ya. Yavor (1965a). Using a rectangular model to obtain analytical expressions for spherical aberration of electromagnetic quadrupole lenses. *Phys. Lett.* **15**, 132–134.

D. Dymnikov, T. Ya. Fishkova and S. Ya. Yavor (1965b). The influence of the geometrical parameters on the optical characteristics of a system of four quadrupole lenses analogous to an axisymmetric lens. *Zh. Tekh. Fiz.* **35**, 431–440. *Sov. Phys. Tech. Phys*. **10**, 340–346.

D. Dymnikov, T. Ya. Fishkova and S. Ya. Yavor (1965c). Spherical aberration of a combined quadrupole lens with rectangular field distributiions. *Dokl. Akad. Nauk SSSR* **162**, 1265–1268. *Sov. Phys. Dokl*. **10**, 547–550.

D. Dymnikov, T. Ya. Fishkova and S. Ya. Yavor (1965d). Spherical aberration of a combined quadrupole lens with bell-shaped field distributions. *Zh. Tekh. Fiz.* **35**, 1068–1076. *Sov. Phys. Tech. Phys*. **10**, 822–827.

J. Edgcombe (2012). The positioning of thin-film magnetic rings as phase plates for transmission electron microscopy. EMC-15, Manchester. **2**, 489–490.

J. Edgcombe (2017a). Phase plates for transmission electron microscopy. *Adv. Imaging Electron Phys.* **200**, 61–102.

C. J. Edgcombe (2017b). Imaging with straight-edge phase plates in the TEM. *Ultramicroscopy* **182**, 124–130.

J. Edgcombe and J. C. Loudon (2012). Use of Aharonov–Bohm effect and chirality control in magnetic phase plates for transmission microscopy. EMAG 2011, Birmingham. *J. Phys. Conf. Ser*. **371**, 012006, 4 pp.

C. J. Edgcombe, A. Ionescu, J. C. Loudon, A. M. Blackburn, H. Kurebayashi and C. H. W. Barnes (2012). Characterisation of ferromagnetic rings for Zernike phase plates using the Aharonov–Bohm effect. *Ultramicroscopy* **120**, 75–85.

N. Erdman and D. C. Bell (2013). SEM instrumentation developments for low kV imaging amd microanalysis. In *Low Voltage Electron Microscopy: Principles and Applications* (D. C. Bell and N. Erdman, Eds), 31–55 (Wiley, Chichester and Royal Microscopical Society, Oxford).

R. Erni (2015). *Aberration-Corrected Imaging in Transmission Electron Microscopy. An Introduction.* 2nd edn (Imperial College Press, London; 1st edn 2010).

J. Fehr, W. Reiners, L. J. Balk, E. Kubalek, D. Köther and I. Wolff (1990). A 100-femtosecond electron beam blanking system. *Microelectron. Eng*. **12**, 221–226.

J. Feng and A. Scholl (2008). Photoemission electron microscopy (PEEM). In *Science of Microscopy* (P. W. Hawkes and J. C. H. Spence, Eds), **1**, 657–695 (Springer, New York).

J. Feng and A. Scholl (2018). Photoemission electron microscopy (PEEM. In *Handbook of Microscopy* (P. W. Hawkes and J. C. H. Spence, Eds), (Springer, Cham), forthcoming.

J. Feng, E. Forest, A. A. Macdowell, M. Marcus, H. Padmore, S. Raoux, D. Robin, A. Scholl, R. Schlueter, P. Schmid, J. Stöhr, W. Wan, D. H. Wei and Y. Wu (2005). An X-ray photoemission electron microscope using an electron mirror aberration corrector for the study of complex materials. *J. Phys.: Condens. Matter* **17**, S1339–S1350.

G. Fey (1980). Elektrische Versorgung eines elektronenoptischen Korrektivs. *Optik* **55**, 55–65.

R. Fink, M. R. Weiss, E. Umbach, D. Preikszas, H. Rose, R. Spehr, P. Hartel, W. Engel, R. Degenhardt, R. Wichtendahl, H. Kuhlenbeck, W. Erlebach, K. Ihmann, R. Schlögl, H.-J. Freund, A. M. Bradshaw, G. Lilienkamp, T. Schmidt, E. Bauer and G. Benner (1997). SMART: a planned ultrahigh-resolution spectromicroscope for BESSY II. *J. Electron Spectrosc. Relat. Phenom.* **84**, 231–250.

F. J. Franke, K.-H. Herrmann and H. Lichte (1987). Numerical reconstruction of the electron object wave from an electron hologram including the correction of aberrations. *Scanning Microsc.* Suppl. 2, 59–67.

Q. Fu, H. Lichte and E. Völkl (1991). Correction of aberrations of an electron microscope by means of holography. *Phys. Rev. Lett.* **67**, 2319–2322.

D. Gabor (1945a). Stationary electron swarms in electromagnetic fields. *Proc. R. Soc. (Lond.) A* **183**, 436–453.

D. Gabor (1945b). Dynamics of electron beams. Applications of Hamiltonian dynamics to electronic problems. *Proc. Inst. Radio. Eng* **33**, 792–805.

D. Gabor (1946). A zonally corrected electron lens. *Nature* **158**, 198.

D. Gabor (1947). A space-charge lens for the focusing of ion beams. *Nature* **160**, 89–90.

D. Gabor (1948). A new microscope principle. *Nature* **161**, 777–778.

D. Gabor (1949). Microscopy by reconstructed wave-fronts. *Proc. R. Soc. (Lond.) A* **197**, 454–487.

D. Gabor (1950a). Electron optics at high frequencies and at relativistic velocities. *Rev. Opt.* **29**, 209–231.

D. Gabor (1950b). Electron optical systems with curved axes. ICEM-2, Paris. **1**, 57–62.

D. Gabor (1951). Electron-optical systems with helical axis. *Proc. Phys. Soc. (Lond.) B* **64**, 244–255.

W. J. Gallagher (1969). Lenses for high energy electron beams. *IEEE Trans. Nucl. Sci.* **16**, 277–278.

B. Gamm, M. Dries, K. Schultheiss, H. Blank, A. Rosenauer, R. R. Schröder and D. Gerthsen (2010). Object wave reconstruction by phase-plate transmission electron microscopy. *Ultramicroscopy* **110**, 807–814.

R. K. Garg (1982). A simple and practical approach to correct spherical aberration in existing electron probe microscopes. *Ultramicroscopy* **7**, 411–413.

R. K. Garg and N. C. Vaidya (1974). Computer design and electron optics of synklysmotron lenses. ICEM-8, Canberra. **1**, 154–155.

U. F. Gianola (1950a). Reduction of the spherical aberration of magnetic electron lenses. *Proc. Phys. Soc. (Lond.) B* **63**, 703–708.

U. F. Gianola (1950b). The correction of the spherical aberration of electron lenses using a correcting foil element. *Proc. Phys. Soc. (Lond.) B* **63**, 1037–1039.

W. Glaser (1952). *Grundlagen der Elektronenoptik* (Springer, Vienna).

H. Grümm (1952). Zur Frage der geometrisch-optischen Intensitätsverteilung im Bildraum von Elektronenlinsen. *Optik* **9**, 281–311. Berichtigung *ibid*. 528.

G. Gurbanov and P. P. Kas'yankov (1966). On the problem of calculating electron-optical systems corrected for astigmatism. *Izv. Akad. Nauk SSSR (Ser. Fiz.)* **30**, 735–738. *Bull. Acad. Sci. USSR (Phys. Ser.)* **30**, 762–765.

G. Gurbanov and P. P. Kas'yankov (1968). Calculation of electron-optical systems with minimum third-order aberration coefficients. *Opt.-Mekh. Prom.* **35** (3), 27–29. *Sov. J. Opt. Technol.* **35**, 171–173.

G. Guzzinati, L. Clark, A. Béché, R. Juchtmans, R. Van Boxem, M. Mazilu and J. Verbeeck (2015). Prospects for versatile phase manipulation in the TEM: Beyond aberration correction. *Ultramicroscopy* **151**, 85–93.

M. Haider (1996). Correctors for electron microscopes: tools or toys for scientists? EUREM-11, Dublin. **1**, 350–351.

M. Haider (2000). Towards sub-Ångstrom point resolution by correction of spherical aberration. EUREM-12, Brno. **3**, I.145–I.148.

M. Haider and S. Uhlemann (1998). A computer controlled C_s-corrected 200 keV TEM. ICEM-14, Cancun. **1**, 265–266.

M. Haider and S. Uhlemann (2014). Instrumental developments for high resolution EM approaching its physical limitations. Abstracts XV International Conference on Electron Microscopy, Kraków. 4–5.

M. Haider and J. Zach (1998). Resolution improvement of electron microscopes by means of correctors to compensate for axial aberrations. ICEM-14, Cancun. **1**, 53–54.

M. Haider, W. Bernhardt and H. Rose (1982). Design and test of an electric and magnetic dodecapole lens. *Optik* **63**, 9–23.

M. Haider, G. Braunshausen and E. Schwan (1994). State of the development of a C_s corrected high resolution 200 kV TEM. ICEM-13, Paris. **1**, 195–196.

M. Haider, G. Braunshausen and E. Schwan (1995). Correction of the spherical aberration of a 200 kV TEM by means of a hexapole corrector. *Optik* **99**, 167–179.

M. Haider, H. Rose, S. Uhlemann, B. Kabius and K. Urban (1998a). Towards 0.1 nm resolution with the first spherically corrected transmission electron microscope. *J. Electron Microsc.* **47**, 395–405.

M. Haider, H. Rose, S. Uhlemann, E. Schwan, B. Kabius and K. Urban (1998b). A spherical-aberration-corrected 200 kV transmission electron microscope. *Ultramicroscopy* **75**, 53–60.

M. Haider, S. Uhlemann, E. Schwan, H. Rose, B. Kabius and K. Urban (1998c). Electron microscopy image enhanced. *Nature* **392**, 768–769.

M. Haider, P. Hartel, U. Loebau, R. Hoeschen, H. Müller, S. Uhlemann, F. Kahl and F. Zach [sic] (2008a). Progress on the development of a C_c/C_s corrector for TEAM. *Microsc. Microanal.* **14** (Suppl. 2), 800–801.

M. Haider, H. Müller and S. Uhlemann (2008b). Present and future hexapole aberration correctors for high resolution electron microscopy. *Adv. Imaging Electron Phys.* **153**, 43–120.

M. Haider, H. Müller, S. Uhlemann, J. Zach, U. Loebau and R. Hoeschen (2008c). Prerequisites for a C_c/C_s-corrected ultrahigh-resolution TEM. *Ultramicroscopy* **108**, 167–178.

M. Haider, P. Hartel, H. Müller, S. Uhlemann and J. Zach (2009). Current and future aberration correctors for the improvement of resolution in electron microscopy. *Philos. Trans. R. Soc. (Lond.) A* **367**, 3665–3682.

T. Hanai and M. Hibino (1984). Effect of the spherical aberration on electron probe size. *J. Electron Microsc.* **33**, 116–122.

T. Hanai, M. Hibino and S. Maruse (1982). Improvement of an electron probe profile using the foil lens. *J. Electron Microsc.* **31**, 360–367.

T. Hanai, M. Hibino and S. Maruse (1984). Reduction of the probe diameter through the correction of spherical aberration by the foil lens. *J. Electron Microsc.* **33**, 329–334.

T. Hanai, M. Hibino and S. Maruse (1994). Effect of the three-fold astigmatism on the performance of the foil lens used for correction of the spherical aberration of a probe-forming lens. *Optik* **97**, 86–90.

T. Hanai, S. Arai and M. Hibino (1995). Increase of current density of the electron probe by correction of the spherical aberration with a side-entry type foil lens. *J. Electron Microsc.* **44**, 301–306.

T. Hanai, H. Yoshida and M. Hibino (1998). Characteristics and effectiveness of a foil lens for correction of spherical aberration in scanning transmission electron microscopy. *J. Electron Microsc.* **47**, 185–192.

D. F. Hardy (1967). Combined magnetic and electrostatic quadrupole electron lenses. Dissertation, Cambridge.

P. Hartel, D. Preikszas, R. Spehr and H. Rose (2000). Performance of the mirror corrector for an ultrahigh-resolution spectromicroscope. EUREM-12, Brno. **3**, I.153–I.154.

P. Hartel, D. Preikszas, R. Spehr, H. Müller and H. Rose (2002). Mirror corrector for low-voltage electron microscopes. *Adv. Imaging Electron Phys.* **120**, 41–133.

W. R. Hartwig and C. Passow (1975). RF superconducting devices. In *Applied Superconductivity* (V. L. Newhouse, Ed.), 541–639 (Academic Press, New York & London).

G. Haufe (1958). Korrektur des Öffnungsfehlers bei elektrostatischen Linsen durch Raumladung. *Optik* **15**, 521–537.

P. W. Hawkes (1964). The paraxial chromatic aberrations of quadrupole systems. EUREM-3, Prague. **A**, 5–6.

P. W. Hawkes (1965a). The geometrical aberrations of general electron optical systems. *Philos. Trans. R. Soc. (Lond.)* **A257**, 479–552.

P. W. Hawkes (1965b). The paraxial chromatic aberrations of rectilinear orthogonal systems. *Optik* **22**, 543−551.
P. W. Hawkes (1966). *Quadrupole Optics* (Springer, Berlin & New York).
P. W. Hawkes (1970). Quadrupoles in electron lens design. *Adv. Electron. Electron Phys.* Suppl. 7.
P. W. Hawkes (1980). Methods of computing optical properties and combating aberrations in low intensity beams. In *Applied Charged Particle Optics* (A. Septier, Ed.), **A**, 45−157 (Academic Press, New York & London). *Adv. Electron. Electron Phys*. Suppl. 13A.
P. W. Hawkes (1983a). Computer-aided calculation of the aberration coefficients of microwave cavity lenses. I. Primary (second-order) aberrations. *Optik* **63**, 129−156.
P. W. Hawkes (1983b). Computer-aided calculation of the aberration coefficients of microwave cavity lenses. II. Secondary (third-order) aberrations. *Optik* **65**, 227−251.
P. W. Hawkes (2009a). Aberration correction past and present. *Philos. Trans. R. Soc. (Lond.) A* **367**, 3637−3664.
P. W. Hawkes (2009b). Can the Nomura lens be free of spherical aberration? *J. Microsc. (Oxford)* **234**, 325.
P. W. Hawkes (2015). The correction of electron lens aberrations. *Ultramicroscopy* **156**, A1−A64.
P. W. Hawkes and O. L. Krivanek (2018). Aberration correctors, monochromators, spectrometers. In *Handbook of Microscopy* (P. W. Hawkes and J. C. H. Spence, Eds), (Springer, Cham). forthcoming.
P. W. Hawkes and U. Valdrè (1977). Superconductivity and electron microscopy. *J. Phys. E: Sci. Instrum.* **10**, 309−328.
H. Hely (1982a). Technologische Voraussetzungen für die Verbesserung der Korrektur von Elektronenlinsen. *Optik* **60**, 307−326.
H. Hely (1982b). Messungen an einem verbesserten korrigierten Elektronenmikroskop. *Optik* **60**, 353−370.
K.-H. Herrmann (1978). The present state of instrumentation in high-resolution electron microscopy. *J. Phys. E: Sci. Instrum.* **11**, 1076−1091.
M. Hibino and T. Hanai (1986). Foil lens-correction of spherical aberration. ICEM-11, Kyoto. **1**, 255−258.
M. Hibino and S. Maruse (1976). Correction of the spherical aberration of a magnetic lens with a foil lens. *J. Electron Microsc.* **25**, 229−236.
M. Hibino, S. Sugiyama, T. Hanai and S. Maruse (1977). Correction of the spherical aberration of a magnetic lens using a foil lens. HVEM-5, Kyoto. 49−52.
M. Hibino, S. Sugiyama, T. Hanai and S. Maruse (1978). Characteristics of the foil lens for the correction of the spherical aberration of the strongly excited magnetic lens. *J. Electron Microsc.* **27**, 259−265.
M. Hibino, M. Kuzuya and S. Maruse (1981). Correction of the spherical aberration of the objective lens in a conventional transmission electron microscope by means of a foil lens. *Jpn. J. Appl. Phys.* **20**, 781−782.
K. Hirose, T. Nakano and T. Kawasaki (2011). Automatic aberration-correction system for scanning electron microscopy. *Microelectron. Eng.* **88**, 2559−2562.
H. Hoch, E. Kasper and D. Kern (1976). Der Öffnungsfehler 3. Ordnung und der axiale Farbfehler von rotationssymmetrischen Elektronenlinsen mit gekrümmter geladener transparenter Folie. *Optik* **46**, 463−473.
W. Hoppe (1972). Dreidimensional abbildende Elektronenmikroskope. I. Prinzip der Geräte. *Z. Naturforsch.* **27a**, 919−929.
S. Hoque, H. Ito, R. Nishi, A. Takaoka and E. Munro (2016). Spherical aberration correction with threefold symmetric line currents. *Ultramicroscopy* **161**, 74−82.
S. Hoque, H. Ito, R. Nishi and A. Takaoka (2017a). A novel *N*-SYLC model for correcting higher order geometrical aberrations. *Kenbikyo* **52** (Suppl. 1), 145.
S. Hoque, H. Ito, A. Takaoka and R. Nishi (2017b). A novel method for higher order aberration correction in electron microscopes. *Microsc. Microanal.* **23** (Suppl. 1), 472−473.
S. Hoque, H. Ito, A. Takaoka and R. Nishi (2017c). Axial geometrical aberration correction up to 5th order with N-SYLC. *Ultramicroscopy* **182**, 68−80.

F. Hosokawa, T. Sannomiya, H. Sawada, T. Kaneyama, Y. Kondo, M. Hori, S. Yuasa, M. Kawazoe, Y. Nakamichi, T. Tanishiro, N. Yamamoto and K. Takayanagi (2006). Design and development of C_s correctors for 300 kV TEM and STEM. IMC-16, Sapporo. **2**, 582.

F. Hosokawa, H. Sawada, Y. Kondo, K. Takayanagi and K. Suenaga (2013). Development of C_s and C_c correctors for transmission electron microscopy. *Microscopy* **62**, 23–41.

M. Ichihashi and S. Maruse (1971). Correction of spherical aberration by means of a thin conducting foil. *J. Electron Microsc.* **20**, 167–171.

M. Ichihashi and S. Maruse (1973). Optical properties of the foil lens for the correction of the spherical aberration. *J. Electron Microsc.* **22**, 321–328.

K. Ishizuka (1994). Coma-free alignment of a high-resolution electron microscope with three-fold astigmatism. *Ultramicroscopy* **55**, 407–418.

R. Janzen (2010). Electrostatic hexapole corrector for reduction of spherical aberration within miniaturised columns. *Recent Trends* **12**, 17–18.

R. Janzen (2011). Concept for electrostatic correctors for reduction of aberrations within miniaturized columns. MC-2011, Kiel. **1**, IM1.P104.

R. Janzen, S. Burkhardt, P. Fehlner, T. Späth and M. Haider (2013). The SPANOCH method: a key to establish aberration correction in miniaturized (multi)column systems? MC-2013, Regensburg. **1**, 107–108.

U. Kaiser, A. Chuvilin, J. Meyer and J. Biskupek (2009). Microscopy at the bottom. MC-2009, Graz. **3**, 1–6.

U. Kaiser, J. Biskupek, J. C. Meyer, J. Leschner, L. Lechner, H. Rose, M. Stöger-Pollach, A. N. Khlobystov, P. Hartel, H. Müller, M. Haider, S. Eyhusen and G. Benner (2011). Transmission electron microscopy at 20 kV for imaging and spectroscopy. *Ultramicroscopy* **111**, 1239–1246.

K. Kanaya and H. Kawakatsu (1960a). Method of measuring spherical and astigmatic aberrations by shadow electron microscope images. *J. Electronmicrosc* **8**, 1–3.

K. Kanaya and H. Kawakatsu (1960b). Caustic properties due to second and third order astigmatisms in the electron microscope. *J. Electron Microsc.* **9**, 71–73.

K. Kanaya and H. Kawakatsu (1960c). Caustic properties combined with second and third order astigmatisms in the electron lens. *Bull. Electrotech. Lab.* **24**, 721–732.

K. Kanaya, H. Kawakatsu and A. Kato (1959a). Third order caustic due to large misalignment in the electron microscope. *Bull. Electrotech. Lab.* **23**, 431–440.

K. Kanaya, H. Kawakatsu and A. Kato (1959b). Theoretical considerations for shadow electron microscope images. *Bull. Electrotech. Lab.* **23**, 801–816.

P. P. Kas'yankov (1950). Conditions for the correction of the aberrations of astigmatism and field curvature in electron lenses. *Zh. Tekh. Fiz.* **20**, 1426–1434.

P. P. Kas'yankov (1952). Calculation of an electron lens for given conditions on the aberrations of third order. *Zh. Tekh. Fiz.* **22**, 80–83.

P. P. Kas'yankov (1955). On electron lenses, the spherical aberration of which can be made as small as desired. *Zh. Tekh. Fiz.* **25**, 1639–1648.

E. Kasper (1968). Die Korrektur des Öffnungs- und Farbfehlers im Elektronenmikroskop durch Verwendung eines Elektronenspiegels mit überlagertem Magnetfeld. *Optik* **28**, 54–64.

E. Kasper (1968).). Die Korrektur von Bildfehlern, die in elektronenoptischen Systemen mit Ringblende durch Störung der Rotationssymmetrie verursacht werden. *Optik* **28**, 407–416.

M. Kato and T. Sekine (1995). Spherical aberration correction of electrostatic lenses using spherical meshes. *J. Vac. Sci. Technol. A* **13**, 2255–2260.

M. Kato and T. Sekine (1996). Evaluation of the dispersive nature of meshes used for the spherical aberration correction of electrostatic lenses. *J. Vac. Sci. Technol. A* **14**, 453–461.

T. Kawasaki, T. Nakano and K. Hirose (2009). Developing an aberration-corrected Schottky emission SEM and method for measuring aberration. *Microelectron. Eng.* **86**, 1017–1020.

T. Kawasaki, T. Mizuno, T. Ishida, M. Tomita, Y. Takai, Y. Ogawa, D. Kanamori, T. Ikuta, T. Matsutani, T. Kodama and T. Tanji (2015). Development of spherical-aberration-corrector with annular and circular electrodes. In *10th Internat. Symp. on Atomic Level Characterization for New Materials and Devices*, Matsue, Japan. 27p-P-58.

T. Kawasaki, T. Ishida, Y. Takai, Y. Ogawa, M. Tomita, T. Matsutani, T. Kodama and T. Ikuta (2016a). Development of electrostatic spherical aberration corrector using annular and circular electrodes. *Surf. Interface Anal.* **48**, 1160−1165.

T. Kawasaki, T. Ishida, M. Tomita, T. Kodama, T. Matsutani and T. Ikuta (2016b). Development of a new electrostatic C_s-corrector consisted of annular and circular electrodes. EMC-16, Lyon. **1**, 430−432.

T. Kawasaki, R. Yoshida, T. Kato, T. Nomaguchi, T. Agemura, T. Kodama, T. Kodama, M. Tomita and T. Ikuta (2017a). Development of C_s/C_c corrector using electrostatic field. *Kenbikyo* **52** (Suppl. 1), 22.

T. Kawasaki, R. Yoshida, T. Kato, T. Nomaguchi, T. Agemura, T. Kodama, M. Tomita and T. Ikuta (2017b). Development of compact C_s/C_c corrector with annular and circular electrodes. *Microsc. Microanal.* **23** (Suppl. 1), 466−467.

H. Kazumori, K. Honda, M. Matsuya and M. Date (2004a). Field emission SEM with a spherical and chromatic corrector. APEM-8, Kanazawa. 52−53.

H. Kazumori, K. Honda, M. Matsuya, M. Date and C. Nielsen (2004b). Field emission SEM with a spherical and chromatic corrector. *Microsc. Microanal.* **10** (Suppl. 2), 1370−1371.

V. M. Kel'man and S. Ya. Yavor (1961). Achromatic quadrupole electron lenses. *Zh. Tekh. Fiz.* **31**, 1439−1442. *Sov. Phys. Tech. Phys*. **6**, 1052−1054.

A. Khursheed (2002). A low voltage time of flight electron emission microscope. *Optik* **113**, 505−509.

A. Khursheed (2005). A method of dynamic chromatic aberration correction in low-voltage scanning electron microscopes. *Ultramicroscopy* **103**, 255−260.

A. Khursheed and W. K. Ang (2015). On-axis electrode aberration correctors for scanning electron/ion microscopes. *Microsc. Microanal.* **21** (Suppl. 4), 106−111.

A. Khursheed and W. K. Ang (2016a). Annular focused electron beam aberration corrector. *Recent Trends* **15**, 20−21.

A. Khursheed and W. K. Ang (2016b). Annular focused electron/ion beams for combining high spatial resolution with high probe current. *Microsc. Microanal.* **22**, 948−954.

K. Kimoto and K. Ishizuka (2017). Rapid measurement of low-order aberrations using Fourier transforms of crystalline Ronchigrams. *Ultramicroscopy* **180**, 59−65.

J. G. King, J. W. Coleman and E. H. Jacobsen (1978). A high-resolution Auger electron microscope using foil lenses. *Ann. N. Y. Acad. Sci.* **306**, 75−84.

C. Kisielowski, B. Freitag, M. Bischoff, H. v. Lin, S. Lazar, G. Krippels, P. Tiemeijer, M. v. d. Stam, S. v. Harrach, M. Stekelenburg, M. Haider, S. Uhlemann, H. Müller, P. Hartel, B. Kabius, D. Miller, I. Petrov, E. A. Olson, T. Donchev, E. A. Kenik, A. R. Lupini, J. Bentley, S. J. Pennycook, I. M. Anderson, A. M. Minor, A. K. Schmid, T. Duden, V. Radmilovic, Q. M. Ramasse, M. Watanabe, R. Erni, E. A. Stach, P. Denes and U. Dahmen (2008). Detection of single atoms and buried defects in three dimensions by aberration-corrected electron microscope with 0.5-Å information limit. *Microsc. Microanal.* **14**, 469−477.

C. Kisielowski, P. Specht, S. M. Gygax, B. Barton, H. A. Calderon, J. H. Kang and R. Cieslinski (2015). Instrumental requirements for the detection of electron beam-induced object excitations at the single atom level in high-resolution transmission electron microscopy. *Micron* **68**, 186−193.

K. Kitada, H. Yoshimori, T. Ikuta, Y. Kimura and Y. Takai (2008). Aberration-free imaging by dynamic hollow-cone illumination in transmission electron microscopy. APMC-9, Jeju, 35−36.

R. Kompfner (1941). On a method of correcting the spherical error of electron lenses, especially those employed with electron microscopes. *Philos. Mag.* **32**, 410−416.

H. Koops (1978a). Aberration correction in electron microscopy. ICEM-9, Toronto. **3**, 185−196.

H. Koops (1978b). Erprobung eines chromatisch korrigierten elektronenmikroskopischen Objektives. *Optik* **52**, 1−18.

H. Koops, G. Kuck and O. Scherzer (1977). Erprobung eines elektronenoptischen Achromators. *Optik* **48**, 225−236.

A. J. Koster and A. F. de Jonge (1991). Measurement of the spherical aberration coefficient of transmission electron microscopes by beam-tilt-induced image displacements. *Ultramicroscopy* **38**, 235−240.

A. J. Koster and W. J. de Ruijter (1992). Practical autoalignment of transmission electron microscopes. *Ultramicroscopy* **40**, 89−107.

P. Krejcik (1980). The focusing of GeV particles with electrostatic coaxial lenses. *Nucl. Instrum. Meth.* **171**, 233–236.

P. Krejcik, R. L. Dalglish and J. C. Kelly (1979). An electrostatic coaxial probe forming lens suitable for high-energy ion beams. *J. Phys. D: Appl. Phys.* **12**, 161–167.

P. Krejcik, J. C. Kelly and R. L. Dalglish (1980a). A new electrostatic ion microprobe system. *Nucl. Instrum. Meth.* **168**, 247–249.

P. Krejcik, B. V. King and J. C. Kelly (1980b). An analysis of some solution techniques for electrostatic coaxial lenses. *Optik* **55**, 385–393.

O. L. Krivanek, N. Dellby and L. M. Brown (1996). Spherical aberration corrector for a dedicated STEM. EUREM-11, Dublin. **1**, I352–I353.

O. L. Krivanek, N. Dellby, A. J. Spence, R. A. Camps and L. M. Brown (1997a). Aberration correction in the STEM. EMAG, Cambridge. 35–39.

O. L. Krivanek, N. Dellby, A. J. Spence, R. A. Camps and L. M. Brown (1997b). On-line aberration measurement and correction in STEM. *Microsc. Microanal.* **3** (Suppl. 2), 1171–1172.

O. L. Krivanek, N. Dellby, A. J. Spence and L. M. Brown (1998). Spherical aberration correction in dedicated STEM. ICEM-14, Cancun. **1**, 55–56.

O. L. Krivanek, N. Dellby and A. R. Lupini (1999a). Towards sub-Å electron beams. *Ultramicroscopy* **78**, 1–11.

O. L. Krivanek, N. Dellby and A. R. Lupini (1999b). STEM without spherical aberration. *Microsc. Microanal.* **5** (Suppl. 2), 670–671.

O. L. Krivanek, N. Dellby and A. R. Lupini (2000). Advances in C_s-corrected STEM. EUREM-12, Brno. **3**, I149–I150.

O. L. Krivanek, G. J. Corbin, N. Dellby, B. F. Elston, R. J. Keyse, M. F. Murfitt, C. S. Own, Z. S. Szilagyi and J. W. Woodruff (2008a). An electron microscope for the aberration-corrected era. *Ultramicroscopy* **108**, 179–195.

O. L. Krivanek, N. Dellby, R. J. Keyse, M. Murfitt, C. Own and Z. Szilagyi (2008b). Advances in aberration-corrected scanning transmission electron microscopy and electron spectroscopy. *Adv. Imaging Electron Phys.* **153**, 121–160.

O. L. Krivanek, J. P. Ursin, N. C. Bacon, G. J. Corbin, N. Dellby, P. Hrncirik, M. F. Murfitt, C. S. Own and Z. S. Szilagyi (2009a). High-energy-resolution monochromator for aberration-corrected scanning transmission electron microscopy/electron energy-loss spectroscaopy. *Philos. Trans. R. Soc. (Lond.) A* **367**, 3683–3697.

O. L. Krivanek, N. Dellby and M. F. Murfitt (2009b). Aberration correction in electron microscopy.. In *Handbook of Charged Particle Optics* (J. Orloff, Ed.), 601–640 (CRC Press, Boca Raton).

O. L. Krivanek, T. C. Lovejoy and N. Dellby (2015). Aberration-corrected STEM for atomic-resolution imaging and analysis. *J. Microsc. (Oxford)* **259**, 165–172.

G. Kuck (1979). Erprobung eines elektronenoptischen Korrektivs für Farb- und Öffnungsfehler. Dissertation, Darmstadt.

W. Kunath (1968). Zonal correction of spherical aberration by magnetic fields of rotational symmetry. EUREM-4, Rome. **1**, 175–176.

W. Kunath (1970). Über die Zonenkorrektur von Objektivlinsen. ICEM-7, Grenoble. **2**, 21–22.

W. Kunath (1972). Correction of a ring shaped objective lens with the aid of two round lenses. EUREM-5, Manchester. 70–71.

W. Kunath (1976). Probe forming by hollow cone beams. EUREM-6, Jerusalem. **1**, 340–341.

W. Kunath (1976/77). Hochauflösende elektronenoptische Abbildung durch Hohlstrahlbündel in rotationssymmetrischen Dreilinsensystemen. Dissertation, Tübingen.

M. Kuzuya, T. Hanai, M. Hibino and S. Maruse (1982). Numerical evaluations of characteristics of the foil lens in correcting the spherical aberration of the objective lens of a conventional transmission electron microscope. *J. Electron Microsc.* **31**, 18–26.

M. Kuzuya, M. Hibino and S. Maruse (1984). Correction of the spherical aberration of the CTEM objective lens using a foil lens. *Ultramicroscopy* **15**, 233−237.

Z.-b. Lee, U. Kaiser and H. Rose (2017). Advantages of nonstandard imaging methods in TEM and STEM. MC-2017, Lausanne, 509−510.

J. B. Le Poole (1972). Space charge correction of spherical aberration. EUREM-5, Manchester. 130−131.

M. Lentzen, A. Thust and K. Urban (2004). The error of aberration measurements in HRTEM using Zemlin tableaux. *Microsc. Microanal.* **10** (Suppl. 2), 980−981.

F. Lenz (1954). Die Kaustikfläche bei dreizähliger Unsymmetrie. ICEM-3, London. 83−85.

F. Lenz (1956). The geometry of distorted projections of caustic cross-sections. ACEM-1, Tokyo. 105−107.

F. Lenz (1957). Theoretischen Untersuchungen über die Ausbreitung von Elektronenstrahlbündeln in rotationssymmetrischen elektrischen und magnetischen Felder. Habilitationsschrift, Aachen.

F. Lenz (1960). The caustic surface in electron optical systems of fourfold axial symmetry. EUREM-2, Delft. **1**, 41−43.

F. Lenz and M. Hahn (1953). Die Untersuchung der Unsymmetrie magnetischer Polschuhlinsen im schwach unterteleskopischen Strahlengang. *Optik* **10**, 15−27.

F. Lenz and A. P. Wilska (1966). Correction of spherical aberration in a system a with a ring-shaped aperture. ICEM-6, Kyoto. **1**, 145−146.

F. Lenz and A. P. Wilska (1966). Electron optical systems with annular apertures and with corrected spherical aberration. *Optik* **24**, 383−396.

H. Lichte (1991). Electron image plane off-axis holography of atomic structures. *Adv. Opt. Electron Microsc.* **12**, 25−91.

H. Lichte (1993). Parameters for high-resolution electron holography. *Ultramicroscopy* **51**, 15−20.

H. Lichte (1995). Electron holography: state and experimental steps towards 0.1 nm with the CM-30-Special Tübingen. In *Electron Holography* (A. Tonomura, L. F. Allard, G. Pozzi, D. C. Joy and Y. A. Ono, Eds), 11−31 (North-Holland, Amsterdam).

H. Liebl (1979). An electrostatic radial field doublet lens. *Optik* **53**, 333−338.

J. A. Lin and J. M. Cowley (1986). Calibration of the operating parameters for an HB5 STEM instrument. *Ultramicroscopy* **19**, 31−42.

M. Linck, B. McMorran, J. Pierce and P. Ercius (2014). Aberration-corrected STEM by means of diffraction gratings. *Microsc. Microanal.* **20** (Suppl. 3), 946−947.

M. Linck, P. Hartel, S. Uhlemann, F. Kahl, H. Müller, J. Zach, J. Biskupek, M. Niestadt, U. Kaiser and M. Haider (2016a). Status of the SALVE-microscope: C_c-correction for atomic-resolution TEM imaging at 20 kV. EMC-16, Lyon. **1**, 314−315.

M. Linck, P. Hartel, S. Uhlemann, F. Kahl, H. Müller, J. Zach, M. Haider, M. Niestadt, M. Bischoff, J. Biskupek, Z. Lee, T. Lehnert, F. Börrnert, H. Rose and U. Kaiser (2016b). Chromatic aberration correction for atomic resolution TEM imaging from 20 to 80 kV. *Phys. Rev. Lett.* **117**, 076101, 5 pp.

M. Linck, P. A. Ercius, J. S. Pierce and B. J. McMorran (2017). Aberration corrected STEM by means of diffraction gratings. *Ultramicroscopy* **182**, 36−43.

A. R. Lupini (2001). Aberration correction in STEM. Dissertation, Cambridge.

R. Lupini (2011). The electron Ronchigram. In *Scanning Transmission Electron Microscopy, Imaging and Analysis* (S. J. Pennycook and P. D. Nellist, Eds), 117−161 (Springer, New York).

R. Lupini, O. L. Krivanek, N. Dellby, P. D. Nellist and S. J. Pennycook (2001). Developments in C_s-corrected STEM. EMAG, Dundee. 31−34.

A. R. Lupini, M. Chi and S. Jesse (2016). Rapid aberration measurement with pixelated detectors. *J. Microsc. (Oxford)* **263**, 43−50.

D. Maas, S. Henstra, M. Krijn and S. Mentink (2001). Electrostatic aberration correction in low voltage SEM. *Proc. SPIE* **4510**, 205−217.

H. Mahl and A. Recknagel (1944). Über den Öffnungsfehler von elektrostatischen Elektronenlinsen. *Z. Physik* **122**, 660−679.

M. Mankos and K. Shadman (2013). A monochromatic, aberration-corrected, dual-beam low energy electron microscope. *Ultramicroscopy* **130**, 13–28.

M. Mankos, K. Shadman, A. T. N'Diaye, A. K. Schmid, H. J. Persson and R. W. Davis (2012). Progress towards an aberration-corrected low energy electron microscope for DNA sequencing and surface analysis. *J. Vac. Sci. Technol. B* **30**, 06F02.

B. Marais (1970). Etude d'un dispositif corrigeant partiellement l'aberration de sphéricité des lentilles électroniques. *J. Microsc. (Paris)* **9**, 683–690.

M. Marko and H. Rose (2010). The contributions of Otto Scherzer (1909–1982) to the development of the electron microscope. *Microsc. Microanal.* **16**, 366–374.

L. Marton (1939). Field measurements and possible correction of aberrations for magnetic electron lenses. *Phys. Rev.* **55**, 672.

L. Marton and K. Bol (1947). Spherical aberration of compound magnetic lenses. *J. Appl. Phys.* **18**, 522–529.

S. Maruse, S. Hiratake and M. Ichihashi (1970a). Korrektur vom Öffnungsfehler der Elektronenlinse. *Jpn. J. Appl. Phys.* **9**, 1549–1550.

S. Maruse, M. Ichihashi and S. Hiratake (1970b). Korrektur des Öffnungsfehlers mittels einer durchstrahlten Folie. ICEM-7, Grenoble. **2**, 1–2.

H. Matsuda, H. Daimon, M. Kato and M. Kudo (2005). Approach for simultaneous measurement of two-dimensional angular distribution of charged particles: spherical aberration correction using an ellipsoidal mesh. *Phys. Rev. E* **71**. 066503, 8 pp.

J.-I. Matsuda and K. Ura (1974a). The aberration theory of the electron trajectory in the R-F fields. Part 1. The second-order aberration. Part 2. The third-order aberration. *Optik* **40**, 179–192 & 284–295.

J.-I. Matsuda and K. Ura (1974b). The imaging properties of electron trajectories in RF fields. *Trans. Inst. Commun. Eng.* **57B**, 273–280. *Electron Commun. Japan*, **57B** (5), 67–73.

T. Matsuo, J.-I. Matsuda, H. Nakabushi, Y. Fujita and A. J. H. Boerboom (1982). Third-order ion optics of an electrostatic multipole lens. *Int. J. Mass Spectrom. Ion Phys.* **42**, 217–241.

J. S. C. McKee and G. R. Smith (1989). Proton microprobes and their applications. *Adv. Electron. Electron Phys.* **73**, 93–132.

R. Meinel and D. Janssen (1985). Spherical and chromatic aberration of a homogeneous spherical space charge lens. *Optik* **70**, 178–180.

W. D. Meisburger and E. H. Jacobsen (1982). Electrostatic lens of very low spherical aberration. *Optik* **62**, 359–366.

S. A. M. Mentink, T. Steffen, P. C. Tiemeijer and M. P. C. M. Krijn (1999). Simplified aberration corrector for low-voltage SEM. EMAG, Sheffield. 83–86.

S. A. M. Mentink, M. J. van der Zande, C. Kok and T. L. van Rooy (2003). Development of a C_s corrector for a Tecnai 20 FEG STEM/TEM. EMAG, Oxford. 165–168.

E. Menzel and E. Kubalek (1978). Elektronenstrahlaustastsysteme. *Beiträge zur Elektronenmikroskopische Direktabbildung von Oberflächen* **11**, 47–66.

R. Meyer, A. I. Kirkland and W. O. Saxton (2002). A new method for the determination of the wave aberration function for high resolution TEM. I. Measurement of the symmetric aberrations. *Ultramicroscopy* **92**, 89–109.

R. Meyer, A. I. Kirkland and W. O. Saxton (2004). A new method for the determination of the wave aberration function for high resolution TEM. II. Measurement of the antisymmetric aberrations. *Ultramicroscopy* **99**, 115–123.

H. Minoda, T. Tamai, H. Iijima, F. Hosokawa and Y. Kondo (2015). Phase-contrast scanning transmission electron microscopy. *Microscopy* **64**, 181–187.

H. Minoda, T. Tamai, Y. Ohmori and H. Iijima (2017). Contrast enhancement of nanomaterials using phase plate STEM. *Ultramicroscopy* **182**, 163–168.

K. Mitsuishi, M. Takeguchi, Y. Kondo, F. Hosokawa, K. Okamoto, T. Sannomiya, M. Hori, T. Iwama, M. Kawazoe and K. Furuya (2006). Ultrahigh-vacuum third-order spherical aberration (C_s) corrector for a scanning transmission electron microscope. *Microsc. Microanal.* **12**, 456–460.

G. Möllenstedt (1954). Elektronenmikroskopische Bilder mit einem nach O. Scherzer sphärisch korrigierten Objektiv. ICEM-3, London. 694–697.

G. Möllenstedt (1956). Elektronenmikroskopische Bilder mit einem nach O. Scherzer sphärisch korrigierten Objektiv. *Optik* **13**, 209–215.

S. Morishita, M. Mukai, Y. Kohno, T. Sasaki, Y.-c. Lin, K. Suenaga and H. Sawada (2017a). Aberration-corrected transmission electron microscopy with monochromatic low-energy electrons in Triple C project. *Kenbikyo* **52** (Suppl. 1), 53.

S. Morishita, Y. Kohno, F. Hosokawa, K. Suenaga and H. Sawada (2017b). Evaluation of residual aberrations in higher-order geometrical aberration correctors. *Microscopy*, in press.

R. W. Moses (1971). Quadrupole–octopole aberration correctors with minimum fields. *Rev. Sci. Instrum.* **42**, 832–839.

R. W. Moses (1973). Lens optimization by direct application of the calculus of variations. In *Image Processing and Computer-Aided Design in Electron Optics* (P. W. Hawkes, Ed.), 250–272 (Academic Press, London & New York).

R. W. Moses (1974). Aberration correction for high-voltage electron microscopy. *Proc. R. Soc. (Lond.) A* **339**, 483–512.

H. Müller, D. Preikszas and H. Rose (1999). A beam separator with small aberrations. *J. Electron Microsc.* **48**, 191–204.

H. Müller, S. Uhlemann, P. Hartel and M. Haider (2008). Aberration-corrected optics: from an idea to a device. *Phys. Procedia* **1**, 167–178.

H. Müller, M. Haider, P. Hartel, S. Uhlemann and J. Zach (2010). Improved aberration correctors for the conventional and the scanning transmission electron microscope. *Recent Trends* **12**, 39–40.

H. Müller, I. Maßmann, S. Uhlemann, P. Hartel, J. Zach and M. Haider (2011). Aplanatic imaging systems for the transmission electron microscope. *Nucl. Instrum. Meth. Phys. Res. A* **645**, 20–27.

H. Müller, I. Maßmann, S. Uhlemann, P. Hartel, J. Zach and M. Haider (2012). Practical aspects of an aplanatic transmission electron microscope. *Recent Trends* **13**, 47–48.

H. Müller, M. Linck, P. Hartel, F. Kahl, J. Zach, S. Uhlemann, J. Biskupek, F. Börrnert, Z. Lee, M. Mohn, U. Kaiser and M. Haider (2016). Correction of the chromatic and spherical aberration in low-voltage transmission electron microcopy. *Recent Trends* **15**, 38–39.

E. Munro and N. D. Wittels (1977). Calculation of the optical properties of electron lenses with electron-transparent foils. *Optik* **47**, 25–38.

E. Munro, X. Zhu, J. Rouse and H. Liu (2001). Aberration correction for charged particle lithography. *Proc. SPIE* **4510**, 218–224.

K. Nagayama (2005). Phase contrast enhancement with phase plates in electron microscopy. *Adv. Imaging Electron Phys.* **138**, 69–146.

S. Nakagawa (1977). A method for measuring the spherical and chromatic aberration coefficients of an objective lens. *Scanning Electron Microsc* Pt 1, 33–40.

T. Nakano, K. Hirose and T. Kawasaki (2011). C_{3c} measurement and dispersion reduction for beam-tilt optics of aberration-corrected SEM. *Nucl. Instrum. Meth. Phys. Res. A* **645**, 28–32.

D. Nellist, N. Dellby, O. L. Krivanek, M. F. Murfitt, Z. Szilagyi, A. R. Lupini, and S. J. Pennycook (2003). Towards sub-0.5 angstrom beams through aberration corrected STEM. EMAG, Oxford. 159–164.

D. Nellist, M. F. Chisholm, N. Dellby, O. L. Krivanek, M. F. Murfitt, Z. S. Szilagyi, A. R. Lupini, A. Borisevich, W. H. Sides and S. J. Pennycook (2004). Direct sub-Angstrom imaging of a crystal lattice. *Science* **305**, 1741–1742.

A. Neßlinger (1939). Über Achromasie von Elektronenlinsen. *Jahrb. AEG-Forsch.* **6**, 83–85.

R. Nishi and A. Takaoka (2012a). Stigmatic condition for electrostatic core-lens by using diagram of axis intercept. *Optik* **123**, 1492–1496.

R. Nishi and A. Takaoka (2012b). Addition of energy dispersion characteristics to the diagram of axis intercept for aberration analysis of core-lens. *Optik* **123**, 1691–1693.

R. Nishi, H. Ito and S. Hoque (2014). Wire corrector for aberration corrected electron optics. IMC-18, Prague. IT-1-P-2984.

R. Nishi, S. Hoque, H. Ito and A. Takaoka (2017). Higher order aberration analysis and optimization of *N*-SYLC spherical aberration corrector by differential algebra method. *Kenbikyo* **52** (Suppl. 1), 23.
S. Nomura (2008). Design of apochromatic TEM composed of usual round lenses. EMC-14, Aachen. **1**, 41–42.
H. Noven (1963). Realisierung eines elektronenoptischen Fokussierungssystems mit Kegelschneidenfokus. *Naturwissenschaften* **50**, 469–470.
H. Noven (1964). Elektronenoptische Fokussierungssysteme mit Kegelschneidenfokus. Dissertation, Tübingen.
H. Noven (1965). Elektronenoptische Fokussierungssysteme mit Kegelschneidenfokus. *Z. Angew. Phys.* **18**, 329–341.
H. Oguni, T. Kodama, T. Kawasaki and T. Ikuta (2017). Optical properties of an electrostatic correcting system. *Kenbikyo* **52** (Suppl. 1), 154.
S. Okayama and H. Kawakatsu (1982). A new correction lens. *J. Phys. E: Sci. Instrum.* **15**, 580–586.
L. C. Oldfield (1971). Focal properties of cylindrically symmetric microwave cavities. EMAG, Cambridge. 94–96.
L. C. Oldfield (1973a). Microwave cavities as electron lenses. Dissertation, Cambridge.
L. C. Oldfield (1973b). Computer design of high frequency electron-optical systems. In *Image Processing and Computer-Aided Design in Electron Optics* (P. W. Hawkes, Ed.), 370–399 (Academic Press, London & New York).
L. C. Oldfield (1974). The use of microwave cavities as electron lenses. ICEM-8, Canberra. **1**, 152–153.
L. C. Oldfield (1976). A rotationally symmetric electron beam chopper for picosecond pulses. *J. Phys. E: Sci. Instrum.* **9**, 455–463.
J. Orloff (1997). Spherical aberration correction of a focused ion beam with space charge. *Proc. SPIE* **3155**, 216–220.
L. P. Ovsyannikova and S. V. Pasovets (1987). First-order focusing properties of coaxial lenses. *Zh. Tekh. Fiz.* **57**, 2351–2354. *Sov. Phys. Tech. Phys*. **32**, 1422–1424.
K. Pandey and N. C. Vaidya (1975). Possible use of the synklysmotron lenses in high voltage electron microscopy. HVEM-4, Toulouse. 51–54.
K. Pandey and N. C. Vaidya (1977). Use of synklysmotron lenses in high voltage electron microscopy. HVEM-5, Kyoto. 53–56.
K. Pandey and N. C. Vaidya (1978). On improving the resolving power of high voltage electron microscopes. *Bull. Electron Microsc. Soc. India* **2** (2), 1–2.
N. W. Parker, S. D. Golladay and A. V. Crewe (1976a). Third-order aberration correction in the SEM and STEM. EMSA, Miami Beach. **34**, 464–465.
N. W. Parker, S. D. Golladay and A. V. Crewe (1976b). A theoretical analysis of third-order aberration correction in the SEM and STEM. *Scanning Electron Microsc.* Pt. I. 37–44 & 777.
C. Passow (1976a). Prospects for achieving a high beam quality and resolution in a high voltage microwave microscope with microwave correction lenses. *Optik* **44**, 427–445.
C. Passow (1976b). On prospects of high voltage microwave microscopes. *Optik* **46**, 501–504.
C. Passow (1976c). Calculations of the energy spread of an electron beam generated by a high voltage microwave illumination system. EUREM-6, Jerusalem. **1**, 375–376.
W. Pejas (1978). Magnetische Abschirmung eines korrigierten Elektronenmikroskops. *Optik* **50**, 61–72.
S. J. Pennycook (2011). A scan through the history of STEM. In *Scanning Transmission Electron Microscopy* (S. J. Pennycook and P. D. Nellist, Eds), 1–90 (Springer, New York).
J. M. Perry-Houts, B. Barton, A. K. Schmid, N. Andresen and C. Kisielowski (2012). Novel long-lived electrostatic work function phase plates for TEM. *Microsc. Microanal.* **18** (Suppl. 2), 476–477.
G. Pfefferkorn (1979). Some historical remarks on emission electron microscopy. *Beiträge zur Elektronenmikroskopischen Direktabbildung von Oberflächen* **12** (2), 1–2.
G. Pfefferkorn and K. Schur (1979). Bibliography of emission electron microscopy (EEM) especially of photo EEM. *Beiträge zur Elektronenmikroskopischen Direktabbildung von Oberflächen* **12** (2), 205–234.
E. Plies (1973). Korrektur der Öffnungsfehler elektronenoptischer Systeme mit krummer Achse und durchgehend astigmatismusfreien Gaußschen Bahnen. *Optik* **38**, 502–518.

E. Plies (1974). Korrektur der Öffnungsfehler elektronenoptischer Systeme mit krummer Achse und durchgehend astigmatismusfreien Gaußschen Bahnen. II. *Optik* **40**, 141–160.

E. Plies (1981). Calculation of electrostatic multitubular core-lenses for a 3D imaging electron microscope: three-dimensionally imaging electron microscopes (Part IV). *Nucl. Instrum. Meth.* **187**, 227–235.

E. Plies and D. Typke (1978). Dreidimensional abbildende Elektronenmikroskope. II. Theorie elektronenoptischer Systeme mit gekrümmter Achse. *Z. Naturforsch.* **33a**, 1361–1377.

W. Pöhner (1976). Ein in dritter und fünfter Ordnung sphärisch korrigierter elektronenoptischer Aplanat. *Optik* **45**, 443–454.

W. Pöhner (1977). Ein sphärisch korrigierter elektronenoptischer Apochromat. *Optik* **47**, 283–297.

D. Preikszas and H. Rose (1994). Corrected low-energy electron microscope for multi-mode operation. ICEM-13, Paris. **1**, 197–198.

D. Preikszas and H. Rose (1995). Procedures for minimizing the aberrations of electromagnetic compound lenses. *Optik* **100**, 179–187.

D. Preikszas and H. Rose (1997). Correction properties of electron mirrors. *J. Electron Microsc.* **46**, 1–9.

D. Preikszas, P. Hartel, R. Spehr and H. Rose (2000). SMART electron optics. EUREM-12, Brno. **3**, I.181–I.184.

Q. M. Ramasse and A. L. Bleloch (2005). Diagnosis of aberrations from crystalline samples in scanning transmission electron microscopy. *Ultramicroscopy* **106**, 37–56.

F. H. Read, N. J. Bowring, P. D. Bullivant and R. R. A. Ward (1999). Short- and long-range penetration of fields and potentials through meshes, grids and gauzes. *Nucl. Instrum. Meth. Phys. Res. A* **427**, 363–367.

M. Reichenbach and H. Rose (1968). Entwurf eines korrigierten magnetischen Objektivs. *Optik* **28**, 475–487.

G. F. Rempfer (1985). Unipotential electrostatic lenses: paraxial properties and aberrations of focal length and focal point. *J. Appl. Phys.* **57**, 2385–2401.

G. F. Rempfer (1990a). A theoretical study of the hyperbolic electron mirror as a correcting element for spherical and chromatic aberration in electron optics. *J. Appl. Phys.* **67**, 6027–6040.

G. F. Rempfer (1990b). Comment on "A study on hyperbolic mirrors as correctors". *Optik* **86**, 73–74.

G. F. Rempfer and M. S. Mauck (1985). Aberration-correcting properties of the hyperbolic electron mirror. EMSA, Louisville. **43**, 132–133.

G. F. Rempfer and M. S. Mauck (1986). An experimental study of the hyperbolic electron mirror. EMSA, Albuquerque. **43**, 886–887.

G. F. Rempfer and M. S. Mauck (1992). Correction of chromatic aberration with an electron mirror. *Optik* **92**, 3–8.

G. F. Rempfer, D. M. Desloge, W. P. Skoczylas and O. H. Griffith (1997). Simultaneous correction of spherical and chromatic aberrations with an electron mirror: an electron optical achromat. *Microsc. Microanal.* **3**, 14–27.

W. D. Riecke (1977). Instrumentation in HVEM. HVEM-5, Kyoto. 73–78.

V. Ronchi (1964). Forty years of history of a grating interferometer. *Appl. Opt.* **3**, 437–451.

H. Rose (1970). Berechnung eines elektronenoptischen Apochromaten. *Optik* **32**, 144–164.

H. Rose (1971a). Abbildungseigenschaften sphärisch korrigierter elektronenoptischer Achromate. *Optik* **33**, 1–24.

H. Rose (1971b). Elektronenoptische Aplanate. *Optik* **34**, 285–311.

H. Rose (1981). Correction of aperture aberrations in magnetic systems with threefold symmetry. *Nucl. Instrum. Meth.* **187**, 187–199.

H. Rose (1983). Otto Scherzer gestorben. *Optik* **63**, 185–188.

H. Rose (1990). Outline of a spherically corrected semi-aplanatic medium-voltage transmission electron microscope. *Optik* **85**, 19–24.

H. Rose (1996). Prospects for improving the resolution by correction of aberrations. *Recent Trends* **5**, 21–23.

H. Rose (2003). Outline of an ultracorrector compensating for all primary and chromatic geometrical aberrations of charged-particle lenses. *Microsc. Microanal.* **9** (Suppl. 3), 32–33.

H. Rose (2004). Outline of an ultracorrector compensating for all primary and chromatic geometrical aberrations of charged-particle lenses. *Nucl. Instrum. Meth. Phys. Res. A* **519**, 12–27.

H. Rose (2008). Optics of high-performance electron microscopes. *Sci. Technol. Adv. Mater.* **9**, 014107, 30 pp.

H. Rose (2009a). *Geometrical Charged-Particle Optics* (Springer, Berlin).

H. Rose (2009b). Historical aspects of aberration correction. *J. Electron Microsc.* **58**, 77–85.

H. Rose (2009c). In memoriam of Otto Scherzer on the occasion of his hundredth birthday. MC-2009, Graz. **1**, 1–2.

H. Rose (2012). *Geometrical Charged-Particle Optics*, 2nd edn (Springer, Berlin).

H. Rose and U. Kaiser (2012). Prospects and first results of sub-angstroem low-voltage electron microscopy—the SALVE project. *Recent Trends* **13**, 65–66.

H. Rose and R. W. Moses (1973). Minimaler Öffnungsfehler magnetischer Rund- und Zylinderlinsen bei feldfreiem Objektraum. *Optik* **37**, 316–336.

H. Rose and E. Plies (1973). Correction of aberrations in electron optical systems with curved axes. In *Image Processing and Computer-Aided Design in Electron Optics* (P. W. Hawkes, Ed.), 344–369 (Academic Press, London & New York).

H. Rose and D. Preikszas (1992). Outline of a versatile corrected LEEM. *Optik* **92**, 31–44.

H. Rose, M. Haider and K. Urban (1998). Elektronenmikroskopie mit atomarer Auflösung. Ein Durchbruch bei der Korrektur von auflösungsbegrenzenden Linsenfehlern. *Phys. Blätt.* **54**, 411–416.

H. Rose, P. Hartel and D. Preikszas (2004). Outline of the mirror corrector for SMART and PEEM3. *Microsc. Microanal.* **10** (Suppl. 3), 28–29.

P. J. Rus (1965). Correctie van sferische aberratie met behulp van een gaaslens. Dissertation, Delft.

Y. Sakaki and S. Maruse (1954). Method of measuring spherical and astigmatic aberrations of an electron lens. *J. Electron Microsc.* **2**, 8–9.

T. Sannomiya, J. Junesch, F. Hosokawa, K. Nagayama, Y. Arai and Y. Kayama (2014). Multi-pore carbon phase plate for phase-contrast transmission electron microscopy. *Ultramicroscopy* **146**, 91–96.

T. Sasaki, S. Morishita, Y. Kohno, M. Mukai, K. Kimoto and K. Suenaga (2017). Performance of low-kV aberration-corrected STEM with delta-corrector and CFEG in ultrahigh vacuum environment. *Microsc. Microanal.* **23** (Suppl. 1), 468–469.

H. Sawada (2015a). Aberration correction in STEM. In *Scanning Transmission Electron Microscopy of Nanomaterials* (N. Tanaka, Ed.), 283–305 (Imperial College Press, London).

H. Sawada (2015b). Ronchigram and geometrical aberrations in STEM. In *Scanning Transmission Electron Microscopy of Nanomaterials* (N. Tanaka, Ed.), 461–485 (Imperial College Press, London).

H. Sawada, T. Sasaki, F. Hosokawa, S. Yuasa, M. Terao, M. Kawazoe, T. Nakamichi, T. Kaneyama, Y. Kondo, K. Kimoto and K. Suenaga (2009). Correction of higher order geometrical aberration by triple 3-fold astigmatism field. *J. Electron Microsc.* **58** (6), 341–347.

H. Sawada, T. Sasaki, F. Hosokawa, S. Yuasa, M. Terao, M. Kawazoe, T. Nakamichi, T. Kaneyama, Y. Kondo, K. Kimoto and K. Suenaga (2010). Higher-order aberration corrector for an image-forming system in a transmission electron microscope. *Ultramicroscopy* **110**, 958–961.

H. Sawada, F. Hosokawa, T. Sasaki, T. Kaneyama, Y. Kondo and K. Suenaga (2011). Aberration correctors developed under the triple C project. *Adv. Imaging Electron Phys.* **168**, 297–336.

H. Sawada, C. S. Allen, S. Wang, J. H. Warner and A. I. Kirkland (2017). Aberration measurement of the probe-forming system of an electron microscope using two-dimensional materials. *Ultramicroscopy* **182**, 195–204.

W. O. Saxton (1995a). Simple prescriptions for measuring three-fold astigmatism. *Ultramicroscopy* **58**, 239–243.

W. O. Saxton (1995b). Observation of lens aberrations for very high-resolution electron microscopy. I. Theory. *J. Microsc. (Oxford)* **179**, 201–213.

W. O. Saxton (2000). A new way of measuring microscope aberrations. *Ultramicroscopy* **81**, 41–45.

W. O. Saxton (2015). Observation of lens aberrations for high-resolution electron microscopy. II. Simple expressions for optimal estimates. *Ultramicroscopy* **151**, 168–177.

W. O. Saxton, G. Chand and A. I. Kirkland (1994). Accurate determination and compensation of lens aberrations in high resolution TEM. ICEM-13, Paris. **1**, 203–204.

W. Scheffels, M. Hahn and F. Lenz (1953). Eine Methode zur direkten Ausmessung der Kaustikflächen von Elektronenlinsen. *Optik* **10**, 455−458.

O. Scherzer (1936). Über einige Fehler von Elektronenlinsen. *Z. Phys.* **101**, 593−603.

O. Scherzer (1946). Zur Korrigierbarkeit von Elektronenlinsen. *Phys. Blätt.* **2**, 110.

O. Scherzer (1947). Sphärische und chromatische Korrektur von Elektronen-Linsen. *Optik* **2**, 114−132.

O. Scherzer (1948). Ein elektronenoptischer Apochromat. *Z. Naturforsch.* **3a**, 544−545.

O. Scherzer (1949). Sphäriche Korrektur mit Hilfe eines astigmatischen Zwischenbildes. *Optik* **5**, 497−498.

O. Scherzer (1950). Méthodes pour éliminer les aberrations sphérique et chromatique. ICEM-2, Paris. **1**, 191−195.

O. Scherzer (1978). Limitations for the resolving power of electron microscopes. ICEM-9, Toronto. **3**, 123−129.

O. Scherzer (1980). Eine sphärisch korrigierte Folien-Linse für die Phasenmikroskopie mit Elektronen. *Optik* **56**, 133−147.

O. Scherzer (1982). How not to correct an electron lens. *Ultramicroscopy* **9**, 385−386.

O. Scherzer and D. Typke (1967). Die Auflösungsgrenze eines in zwei Schnitten sphärisch korrigierten Objektivs. *Optik* **26**, 564−573.

P. Schmid, J. Feng, H. Padmore, D. Robin, H. Rose, R. Schlueter and W. Wan (2005). Correction and alignment strategies for the beam separator of the photoemission electron microscope 3 (PEEM3). *Rev. Sci. Instrum.* **76**, 023302, 14 pp.

T. Schmidt, U. Groh, R. Fink, E. Umbach, O. Schaff, W. Engel, R. Richter, H. Kuhlenbeck, R. Schlögl, H.-J. Freund, A. M. Bradshaw, D. Preikszas, P. Hartel, R. Spehr, H. Rose, G. Lilienkamp, E. Bauer and G. Benner (2002). XPEEM with energy-filtering: advantages and first results from the SMART project. *Surf. Rev. Lett.* **9**, 223−232.

T. Schmidt, H. Marchetto, U. Groh, P. L. Lévesque, F. C. Maier, T. Skála, H. Kuhlenbeck, P. Hartel, R. Spehr, D. Preikszas, G. Lilienkamp, E. Bauer, R. Fink, H. Rose, H.-J. Freund and E. Umbach (2007). SMART: spectro-microscopy with aberration correction for many relevant techniques. Presented at LEEM–PEEM V, Himeji; not included in the proceedings (*Surf. Sci*. **601**, 2007).

G. Schönhense and H. Spiecker (2002a). Chromatic and spherical aberration correction using time-dependent acceleration and lens fields. *Recent Trends* **8**, 71−73.

G. Schönhense and H. Spiecker (2002b). Correction of chromatic and spherical aberration in electron microscopy utilizing the time structure of of pulsed electron sources. *J. Vac. Sci. Technol. B* **20**, 2526−2534.

G. Schönhense and H. Spiecker (2003). Chromatic and spherical correction using time-dependent acceleration and lens fields. *Microsc. Microanal.* **9** (Suppl. 3), 34−35.

S. M. Schramm, S. J. van der Molen and R. M. Tromp (2012). Intrinsic stability of aberration-corrected electron microscopes. *Phys. Rev. Lett.* **109**, 163901, 5 pp.

K. Schultheiss, F. Pérez-Willard, B. Barton, D. Gerthsen and R. R. Schröder (2006). Fabrication of a Boersch phase plate for phase contrast imaging in a transmission electron microscope. *Rev. Sci. Instrum.* **77**, 033701, 4 pp.

K. Schultheiss, J. Zach, B. Gamm, M. Dries, N. Frindt, R. R. Schröder and D. Gerthsen (2010). New electrostatic phase plate for phase-contrast transmission electron microscopy and its application for wave-function reconstruction. *Microsc. Microanal.* **16**, 785−794.

R. A. Schwarzer (1979). Physical aspects of emission electron microscopy. *Beiträge zur Elektronenmikroskopischen Direktabbildung von Oberflächen* **12** (2), 3−38.

M. P. Seah and W. A. Dench (1979). Quantitative electron spectroscopy of surfaces: a standard data base for electron inelastic mean free paths in solids. *Surf. Interface Anal.* **1**, 2−11.

R. Seeliger (1948). Ein neues Verfahren zur Bestimmung des Öffnungsfehlers von Elektronenlinsen. *Optik* **4**, 258−262.

R. Seeliger (1949). Versuche zur sphärischen Korrektur von Elektronenlinsen mittels nichtrotationssymmetrischer Abbildungselemente. *Optik* **5**, 490−496.

R. Seeliger (1951). Die sphärische Korrektur von Elektronenlinsen mittels nichtrotationssymmetrischer Abbildungselemente. *Optik* **8**, 311–317.

R. Seeliger (1953). Über die Justierung sphärisch korrigierter elektronenoptischer Systeme. *Optik* **10**, 29–41.

O. I. Seman (1952). Aberrations of electron-optical systems with charged surfaces in the optically active part of the field. *Zh. Tekh. Fiz.* **22**, 1581–1591.

A. Septier (1957). La correction des aberrations d'ouverture d'un système de deux lentilles quadrupolaires magnétiques. *C. R. Acad. Sci. Paris* **245**, 2036–2039.

A. Septier (1958). Mesure et correction de l'aberration d'ouverture des lentilles quadrupolaires magnétiques. ICEM-4, Berlin. **1**, 57–61.

A. Septier (1963). Lentille quadrupolaire magnéto-électrique corrigée de l'aberration chromatique. Aberration d'ouverture de ce type de lentilles. *C. R. Acad. Sci. Paris* **256**, 2325–2328.

A. Septier (1966). The struggle to overcome spherical aberration in electron optics. *Adv. Opt. Electron Microsc.* **1**, 204–274; reprinted in *Adv. Imaging Electron Phys*. **202** (2017) 75–147.

A. Septier and J. van Acker (1960a). Mesure de l'aberration d'ouverture de lentilles quadrupolaires électrostatiques. *C. R. Acad. Sci. Paris* **251**, 346–348.

A. Septier and J. van Acker (1960b). Correction de l'aberration d'ouverture de lentilles quadrupolaires électrostatiques en fonctionnement astigmatique. *C. R. Acad. Sci. Paris* **251**, 1750–1752.

Z. Shao (1988a). Correction of spherical aberration in the transmission electron microscope. *Optik* **80**, 61–75.

Z. Shao (1988b). On the fifth order aberration in a sextupole corrected probe forming system. *Rev. Sci. Instrum.* **59**, 2429–2437.

Z. Shao and X.-d. Wu (1989). Adjustable four-electrode mirror as an aberration corrector. *Appl. Phys. Lett.* **55**, 2696–2697.

Z. Shao and X.-d. Wu (1990a). Properties of a four-electrode adjustable electron mirror as an aberration corrector. *Rev. Sci. Instrum.* **61**, 1230–1235.

Z. Shao and X.-d. Wu (1990b). A study on hyperbolic mirrors as correctors. *Optik* **84**, 51–54.

Z. Shao, V. Beck and A. V. Crewe (1988). A study of octupoles as correctors. *J. Appl. Phys.* **64**, 1646–1651.

R. Shiloh, R. Remez and A. Arie (2016). Prospects for electron beam aberration correction using sculpted phase masks. *Ultramicroscopy* **163**, 69–74.

H. Slätis and K. Siegbahn (1949). An intermediate image β-spectrometer of high transmission. *Ark. Fys.* **1**, 339–357.

W. Słówko (1973). Ograniczenia zakresu kompensacji aberracji sferycznej w dwusoczewkowym ukladzie odwzorowujacym. *Prace Nauk. Inst. Technol. Elektron. Politech. Wrocław* **10** (Pt. 1), 71–79.

W. Słówko (1975). On compensation of spherical aberration in electron lenses by using an electron mirror. *Opt. Appl.* **5** (2), 27–32.

M. R. Smith and E. Munro (1987). Computer aided design of multipole focusing and deflection sytems. In *Proc. Int. Symposium on Electron Optics Beijing, ISEOB* (J.-y. Ximen, Ed.), 227–230 (Institute of Electronics, Academia Sinica, Beijing).

A. Steinecker and W. Mader (2000). Measurement of lens aberrations by means of image displacements in beam-tilt series. *Ultramicroscopy* **81**, 149–161.

D. Stenkamp (1998). Detection and quantitative assessment of image aberrations from single HRTEM lattice images. *J. Microsc. (Oxford)* **190**, 194–203.

A. M. Strashkevich (1966). *Elektronnaya Optika Elektrostaticheskikh Sistem* (Energiya, Moscow).

A. Strojnik and C. Passow (1978a). A conventional lens for a 5 MV electron microscope. *Optik* **50**, 169–173.

A. Strojnik and C. Passow (1978b). Scanning system for a 5 MeV electron microscope. *Scanning Electron Microsc.* Pt. I, 319–324.

P. A. Sturrock (1955). *Static and Dynamic Electron Optics* (Cambridge University Press, Cambridge).

S. Sugiyama, M. Hibino and S. Maruse (1984). Transmission rate of electrons for carbon films used as the foil of the foil lens. *J. Electron Microsc.* **33**, 323–328.

I. N. Taganov (1966). Design of electron-optical systems with correction of third-order aberrations. *Radiotekh. Elektron.* **11**, 1329–1330. *Radio Eng. Electron. Phys*. **11**, 1160–1162.

I. N. Taganov and P. P. Kas'yankov (1964). On a direct method of calculating electromagnetic systems. *Opt.-Mekh. Prom.* **31** (11), 14–16.

I. N. Taganov and P. P. Kas'yankov (1965). On the calculation of electron-optical systems corrected for field curvature and anisotropic astigmatism. *Opt.-Mekh. Prom.* **32** (12), 21–23.

I. N. Taganov and P. P. Kas'yankov (1967). Use of the direct method for calculating electron optical systems with corrected third-order aberrations. In *Vychislitel'nye Sistemy: Chislennye Metody Rascheta Elektronno-opticheskikh Sistem* (G. I. Marchuk, Ed.), 11–22 (Nauka, Novosibirsk).

Y. Takai, M. Taya, Y. Kimura and T. Ikuta (2008). Aberration-free STEM imaging system incorporating parallel detection and processing techniques using a multi-detector array. APMC-9, Jeju, 37–38.

A. Takaoka, R. Nishi and H. Ito (2015). Low-aberration optics for large-angle beam with unit core lenses. *Optik* **126**, 1666–1671.

N. Tanaka (2015a). Historical survey of the development of STEM instruments. In *Scanning Transmission Electron Microscopy of Nanomaterials* (N. Tanaka, Ed.), 9–38 (Imperial College Press, London).

N. Tanaka (2015b). Recent topics and future prospects in STEM. In *Scanning Transmission Electron Microscopy of Nanomaterials* (N. Tanaka, Ed.), 425–440 (Imperial College Press, London).

T.-t. Tang, J. Orloff and L. Wang (1996a). Modeling and design of space charge lenses/aberration correctors for focused ion beam systems. *J. Vac. Sci. Technol. B* **14**, 80–84.

T.-t. Tang, J. Orloff and L. Wang (1996b). Monte-Carlo simulation on discrete space charge effects of space charge lenses. *Optik* **102**, 141–146.

A. H. Tavabi, M. Beleggia, V. Migunov, A. Savenko, O. Öktem, R. Dunin-Borkowski, et al. (2017). A new perspective for a tunable phase plate based on Ampère's law. MC-2017, Lausanne, 791–792.

S. Taya (1978). Second-order image aberration correction of double-focusing mass spectrometers by electrostatic hexapole lens. *Nucl. Instrum. Meth.* **152**, 407–414.

S. Taya and H. Matsuda (1971). Third order transfer matrices for the fringing fields of an electrostatic hexapole lens. *Mass Spectrosc.* **19**, 266–273.

S. Taya and H. Matsuda (1972). A third-order transfer matrix of an electrostatic hexapole lens. *Int. J. Mass Spectrom. Ion Phys.* **9**, 235–245.

M. Taya, T. Ikuta and Y. Takai (2008). Wave field restoration using focal-depth extension techniques under dynamic hollow-cone illumination. *Optik* **119**, 153–160.

M. G. R. Thomson (1966). Quadrupole lens aberrations. ICEM-6, Kyoto. **1**, 207–208.

M. G. R. Thomson (1967). The aberrations of quadrupole electron lenses. Dissertation, Cambridge.

M. G. R. Thomson (1972). The primary aberrations of a quadrupole corrector system. *Optik* **34**, 528–534.

M. G. R. Thomson (1973). A spherical-aberration corrector using electron-transparent foils. EMSA, New Orleans. **31**, 262–263.

M. G. R. Thomson and E. H. Jacobsen (1971). Quadrupole–octopole and foil lens corrector systems. EMSA, Houston. **29**, 16–17.

F. Thon and D. Willasch (1970). Hochauflösungs-Elektronenmikroskopie mit Spezialaperturblenden und Phasenplatten. ICEM-7, Grenoble. **1**, 3–4.

A. Tonomura, H. Matsuda and J. Endo (1979). Spherical-aberration correction of an electron lens by holography. *Jpn. J. Appl. Phys.* **18**, 1373–1377.

R. M. Tromp and S. M. Schramm (2013). Optimization and stability of the contrast transfer function in aberration-corrected electron microscopy. *Ultramicroscopy* **125**, 72–80.

R. M. Tromp, J. B. Hannon, A. W. Ellis, W. Wan, A. Berghaus and O. Schaff (2010). A new aberration-corrrected, energy-filtered LEEM/PEEM instrument. I. Principles and design. *Ultramicroscopy* **110**, 852–861.

R. M. Tromp, J. B. Hannon, W. Wan, A. Berghaus and O. Schaff (2013). A new aberration-corrrected, energy-filtered LEEM/PEEM instrument. II. Operation and results. *Ultramicroscopy* **127**, 25–39.

F. C. Tsai (2000). Studies of a magnetically focused electrostatic mirror. II. Aberration corrections. *J. Microsc. (Oxford)* **197**, 118–135; for Part I, see Crewe et al. (2000).

K. Tsuno, N. Handa, S. Matsumoto and A. Mogami (1996). Optical properties of immersion objective lenses and collimation of secondary electrons in low voltage SEM. *Proc. SPIE* **2858**, 46–57.

D. Typke (1968). Der Öffnungsfehler von rotationssymmetrischen Elektronenlinsen mit Raumladung. *Optik* **28**, 488–494.

D. Typke (1972a). Sphärische und chromatische Korrektur von Elektronenlinsen mit Hilfe von Influenzladungen, I. *Optik* **34**, 573–594.

D. Typke (1972b). Sphärische und chromatische Korrektur von Elektronenlinsen mit Hilfe von Influenzladungen, II. *Optik* **36**, 124–138; errata: *Optik* **44** (1976) 509.

D. Typke (1981). Image aberrations of axially symmetric imaging systems with off-axial rays: three-dimensionally imaging electron microscopes (Part III). *Nucl. Instrum. Meth.* **187**, 217–226.

D. Typke (2010). Zernike phase contrast electron microscopy with a spherically corrected foil lens. *Microsc. Microanal.* **16**, 441–444.

D. Typke and K. Dierksen (1995). Determination of image aberrations in high-resolution electron microscopy using diffractogram and cross-correlation methods. *Optik* **99**, 155–166.

S. Uhlemann and M. Haider (1998). Residual wave aberrations in the first spherical aberration corrected transmission electron microscope. *Ultramicroscopy* **72**, 109–119.

S. Uhlemann, M. Haider, E. Schwan and H. Rose (1996). Towards a resolution enhancement in the corrected TEM. EUREM-11, Dublin. **1**, 365–361.

S. Uno, K. Honda, N. Nakamura, M. Matsuya and J. Zach (2005). Aberration correction and its automatic control in scanning electron microscopes. *Optik* **16**, 438–448.

N. C. Vaidya (1972). Synklysmotron lenses—a new electron-optical correcting system. *Proc. IEEE* **60**, 245–247.

N. C. Vaidya (1975a). Correction of spherical aberration by a new system of high frequency lenses (synklysmotron lenses). *Optik* **42**, 129–134.

N. C. Vaidya (1975b). The design and properties of synklysmotron lenses. *J. Phys. D: Appl. Phys.* **8**, 368–373.

N. C. Vaidya and R. K. Garg (1974). Correction of spherical aberration in electron lenses by time-varying fields. ICEM-8, Canberra. **1**, 150–151.

N. C. Vaidya and P. W. Hawkes (1970). Correction of spherical aberration by means of microwave lenses. ICEM-7, Grenoble. **2**, 19–20.

R. H. van Aken (2005). Low-energy electron beams through ultra-thin foils, applications for electron microscopy. Dissertation, Delft.

R. H. van Aken, C. W. Hagen, J. E. Barth and P. Kruit (2002a). Low-energy foil aberration corrector. *Ultramicroscopy* **93**, 321–330.

R. H. van Aken, C. W. Hagen, J. E. Barth and P. Kruit (2002b). Concept for a low energy foil corrector. ICEM-15, Durban. **1**, 1101–1102.

R. H. van Aken, M. Lenc and J. E. Barth (2004). Aberration integrals for the low-voltage foil corrector. *Nucl. Instrum. Meth. Phys. Res. A* **519**, 205–215; erratum, *ibid*. **527** (2004) 660.

R. H. van Aken, D. J. Maas, C. W. Hagen, J. E. Barth and P. Kruit (2010). Design of an aberration corrected low-voltage SEM. *Ultramicroscopy* **110**, 1411–1419.

M. J. van Bruggen, B. van Someren and P. Kruit (2006a). Use of a "foil corrector" in a multibeam source: correction of off-axis macrolens aberrations. *Recent Trends* **10**, 69–70.

M. J. van Bruggen, B. van Someren and P. Kruit (2006b). Aberration model of a multibeam scanning microscope for electron beam-induced deposition. *Scanning* **28**, 42–47.

P. van der Merwe (1978a). Electron optical properties of some Fourier–Bessel electrostatic fields with rotational symmetry. I. Basis fields. *University of Zululand Publ., Ser. III* **23**. 23 pp.

J. P. van der Merwe (1978b). Electron optical properties of some Fourier–Bessel electrostatic fields with rotational symmetry. II. An analytical study of weak fields. *University of Zululand Publ., Ser. III* **24**. 20 pp.

J. P. van der Merwe (1978c). Electron optical properties of some Fourier–Bessel electrostatic fields with rotational symmetry. III. Computed properties of synthesized fields. *University of Zululand Publ., Ser. III* **25**. 32 pp.

J. P. van der Merwe (1979a). The optimization of electron optical systems. *University of Zululand Publ., Ser. III* **29**. 53 pp.

J. P. van der Merwe (1979b). Electron optical properties of one-foil lenses, as related to charges induced on the foils. *S. Afr. J. Phys.* **2**, 117–124.

J. P. van der Merwe (1981a). The chromatic and spherical aberration of round electron optical lenses with spatially periodic electrostatic fields: cone-edge and cone focusing. *J. Appl. Phys.* **52**, 589–592.

J. P. van der Merwe (1981b). The minimization of the spherical aberration of symmetrical electrostatic round two-foil lenss. *J. Appl. Phys.* **52**, 1179–1183.

J. P. van der Merwe (1981c). Cone-edge focusing by single round electrostatic lenses with a bell-shaped axial potential distribution. *S. Afr. J. Phys.* **4**, 69–72.

A. A. van Gorkum (1983). Correction of spherical aberration in charged particle lenses using aspherical foils. *J. Vac. Sci. Technol. B* **1**, 1312–1315.

A. A. van Gorkum and L. C. M. Beirens (1986). Experiments on eliminating spherical aberration in electron guns using aspherical mesh lenses. *J. Vac. Sci. Technol. A* **4**, 2297–2306.

J. Verbeeck, H. Tian and A. Béché (2012). A new way of producing electron vortex probes for STEM. *Ultramicroscopy* **113**, 83–87.

J. L. Verster (1963). On the use of gauzes in electron optics. *Philips Res. Rep.* **18**, 465–605.

W. Wan, J. Feng, H. A. Padmore and D. S. Robin (2004). Simulation of a mirror corrector for PEEM. *Nucl. Instrum. Meth. Phys. Res. A* **519**, 222–229.

W. Wan, J. Feng and H. A. Padmore (2006). A new separator design for aberration-corrected photoemission electron microscopes. *Nucl. Instrum. Meth. Phys. Res. A* **564**, 537–543.

L. Wang, J. Orloff, D. Book and T.-t. Tang (1995a). A new method for calculating the axial potential due to space charge in electrostatic optics. *J. Phys. D: Appl. Phys.* **28**, 1791–1801.

L. Wang, J. Orloff and T.-t. Tang (1995b). Study of space-charge devices for focused ion beam systems. *J. Vac. Sci. Technol. B* **13**, 2414–2418.

L. Wang, T.-t. Tang and J. Orloff (1995c). Calculation of aberrations of a space charge lens and its possible applications. *Proc. SPIE* **2522**, 363–374.

I. R. M. Wardell and P. E. Bovey (2009). A history of Vacuum Generators' 100-kV scanning transmission electron microscope. *Adv. Imaging Electron Phys.* **159**, 221–285.

H. Watanabe, T. Taoka, S. Ohta, N. Anazawa and S. Kato (1974). Electron diffraction instrument using the high energy beam of LINAC. *J. Phys. E: Sci. Instrum.* **7**, 412.

C. Weißbäcker and H. Rose (2000). Electrostatic correction of the chromatic and the spherical aberration of charged particle lenses. EUREM-12, Brno. **3**, I.157–I.158.

C. Weißbäcker and H. Rose (2001). Electrostatic correction of the chromatic and the spherical aberration of charged-particle lenses. I. *J. Electron Microsc.* **50**, 383–390.

C. Weißbäcker and H. Rose (2002). Electrostatic correction of the chromatic and the spherical aberration of charged-particle lenses. II. *J. Electron Microsc.* **51**, 45–51.

R. Wichtendahl, R. Fink, H. Kuhlenbeck, D. Preikszas, H. Rose, R. Spehr, P. Hartel, W. Engel, R. Schlögl, H.-J. Freund, A. M. Bradshaw, G. Lilienkamp, T. Schmidt, E. Bauer, G. Benner and E. Umbach (1998). SMART: an aberration-corrected XPEEM/LEEM with energy filter. *Surf. Rev. Lett.* **5**, 1249–1256.

L. Williams, F. H. Read and N. J. Bowring (1995). Defocussing of charged particle beams transmitted through meshes. *Nucl. Instrum. Meth. Phys. Res. A* **363**, 120–123.

A. P. Wilska (1961). A method of reducing spherical aberration in electronic lenses. *Norelco Reporter* **8**, 115.

N. D. Wittels (1975). Unipotential lens with electron-transparent electrodes. *J. Vac. Sci. Technol.* **12**, 1165–1168.

N. D. Wittels and E. H. Jacobsen (1975). The unipotential foil lens. EMSA, Las Vegas. **33**, 142–143.

N. D. Wittels and E. H. Jacobsen (1976). Bessel–Fourier series solutions of cylindrically symmetric electrostatic lens potentials. *J. Appl. Phys.* **47**, 2716–2723.

Y. K. Wu, D. S. Robin, E. Forest, R. Schleuter, S. Anders, J. Feng, H. Padmore and D. H. Wei (2004). Design and analysis of beam separator magnets for third generation aberration compensated PEEMs. *Nucl. Instrum. Meth. Phys. Res. A* **519**, 230–241.

J.-y. Ximen (1988). Theory of electron beam optics in a combined magnetic round lens and sextupole system. *Optik* **78**, 95–100.

J.-y. Ximen and A. V. Crewe (1985). Correction of spherical and coma aberrations with a sextupole–round lens–sextupole system. *Optik* **69**, 141–146.

J.-y. Ximen, Z. Shao and A. V. Crewe (1985). The wave electron optical properties of a magnetic round lens corrected with sextupoles. *Optik* **70**, 37–42.

M. Yakushev and N. U. Aldiyarov (2014). Electron mirror as a corrector of electron microscope objective aberrations. *Zh. Tekh. Fiz.* **84** (6), 126–131. *Tech. Phys.* **59**, 911–916.
F.-d. Yao (1957a). Determination of the aberrations of rotationally symmetric electron-optical systems in the presence of space charge with relativistic correction [in Russian]. *Acta Sci. Nat. Univ. Pekin.* **3** (2), 211–216.
F.-d. Yao (1957b). The aberration of axially symmetrical electron-optical system in presence of space charges [in Chinese]. *Acta Phys. Sin.* **13**, 207–216.
F.-d. Yao (1958). The aberration of axially symmetrical electron-optical system in presence of space charges. *Sci. Sin.* **7**, 31–44. English translation of *Acta Phys. Sin.* above.
S. Ya. Yavor (1968). *Fokusirovka Zaryazhennykh Chastits Kvadrupol'nymi Linzami* (Atomizdat, Moscow).
R. Yoshida, T. Kawasaki, T. Kato, T. Nomaguchi, S. Motomura, K. Nishinaka and T. Agemura (2017). Simulated estimation of electrostatic field type C_s corrector for SEM. *Kenbikyo* **52** (Suppl. 1), 217.
J. Zach (1989a). Design of a high-resolution low-voltage scanning electron microscope. *Optik* **83**, 30–40.
J. Zach (1989b). Entwurf und Berechnung eines hochauflösenden Niederspannungs-Rasterelektronenmikroskops. Dissertation, Darmstadt.
J. Zach (2009). Chromatic correction: a revolution in electron microscopy? *Philos. Trans. R. Soc. A* **367**, 3699–3707.
J. Zach and M. Haider (1994). Correction of spherical and chromatic aberrations in a LVSEM. ICEM-13, Paris. **1**, 199–200.
J. Zach and M. Haider (1995a). Aberration correction in a low voltage SEM by a multipole corrector. *Nucl. Instrum. Meth. Phys. Res. A* **363**, 316–325.
J. Zach and M. Haider (1995b). Correction of spherical and chromatic aberration in a low voltage SEM. *Optik* **93**, 112–118.
J. Zach and H. Rose (1987). Entwurf einer korrigierten Elektronensonde für die Niederspannungs-Rasterelektronenmikroskopie. *Optik* **77** (Suppl. 3), 63.
X. Zhu, E. Munro, H. Liu and J. Rouse (1999). Aberration compensation in charged particle projection lithography. *Nucl. Instrum. Meth. Phys. Res. A* **427**, 292–298.
V. K. Zworykin, G. A. Morton, E. G. Ramberg, J. Hillier and A. W. Vance (1945). *Electron Optics and the Electron Microscope* (Wiley, New York and Chapman & Hall, London).

Part IX, Chapters 43–50

The following lists of references provide some guidance, certainly incomplete, to the abundant literature. Even, here, we concentrate on papers dealing with gun properties and largely exclude those dealing with gun technology. Pierce guns are not covered. Papers cited in the text are not repeated in these lists with the result that the latter are not very different from those in the first edition.

General References

The following publications are of a general nature in the sense that they discuss gun properties without special reference to a particular type, or are review articles, or compare several types of gun, or deal with methods of calculation that can be applied to any gun: Al-Khashab and Al-Abdullah (2012), Alyamovskii (1966), Amboss (1964), Büchsel et al. (1982), Fink and Schumacher (1974), Hamza (1966), Hamza and Kino (1967), Hardy (1974), Herrmann (1957, 1958), Kamigaito (1964, 1965), Killes (1985, 1988), Miskovsky and Cutler (1984), Miskovsky et al. (1984), Moss (1968), Mulvey (1980, 1984), Ohshita et al. (1973), Orloff (1984a,b), Schumacher (1982), Strojnik and Scholl (1975), Taranenko (1964), Troyon (1984b), Uchikawa et al. (1977, 1978), Wiesner (1973), Wiesner and Everhart (1969, 1970), Wolter et al. (1970) and Zaima et al. (1984). Wilska (1970) describes a gun suitable for (spatially) incoherent beam formation. Stoelinga et al. (1983) have designed a gun with a strongly heated tungsten cathode that advances mechanically as it 'burns down'.

Brightness is discussed by Worster (1969b) and Davey (1971).

A special gun structure for the measurement of work functions is proposed by Klauser and Bas (1979).

Thermionic Emission

The literature of thermionic guns is vast. The following list is reasonably representative but the reader who wishes to retrace their development in detail must go to the references cited in these publications and follow up the clues thus unearthed: Andersen and Mol (1968, 1970), André (1967), Barber and Sander (1959), Bas (1954), Bas and Gaydou (1959), Bas et al. (1967), Bradley (1961), Buchanan and Jacob (1960), Castaing (1960), Davey (1973), Dedieu et al. (1970), Delâge amd Sewell (1984), Dolby and Swift (1960), Dosse (1940), Drechsler et al. (1958), Ehrenberg and Spear (1951), Einstein and Jacob (1948), Ellis (1947), Essig (1985, 1986), Everhart (1967), Hanszen (1962, 1964a,b,c), Hanszen and Lauer (1967, 1968), Hasker (1966, 1972), Hibi (1954, 1956, 1962), Hibi and Takahashi (1959), Hibi and Yada (1964), Hibi et al. (1962), Hillier and Baker (1945, 1946), Hillier and Ellis (1949), Hoffmann (1972), Holl (1968/69, 1969), Ichinokawa and Maeda (1978), Iiyoshi et al. (1986), Jacob (1948, 1950a,b), Johansen (1973), Kamminga (1973), Kamminga and Francken (1971), Klemperer and Klinger (1951), Klemperer and Mayo (1948), Komoda (1960), Kudintseva et al. (1966), Lauer (1973, 1974, 1975, 1976), Lauer and Hanszen (1966, 1974), Law (1937), Linn and Pöschl (1968), Maloff and Epstein (1934), Maruse (1960), Ohno (1971, 1972, 1974, 1975), Ohshita et al. (1977), Ohye and Uchikawa (1980, 1986), Ozaki et al. (1982), Passow (1976), Pilod and Sonier (1961, 1968), Ploke (1951, 1952), Pugh and West (1977), Rauh and Kern (1978), Reusse (1939), Reusse and Ripper (1940), Sakaki and Maruse (1958), Sakaki and Möllenstedt (1956), Sakaki et al. (1956), Sewell (1980), Shimoyama et al. (1966, 1970, 1972, 1974, 1982), Someya et al. (1966), Spear (1951), Speidel (1965/66), Sugata (1950), Sugata and Kischi (1950), Swift and Nixon (1960, 1962), Tochigi et al. (1962), Troyon and Zinzindohué (1986), Uchikawa et al. (1977, 1978, 1983), van den Broek (1986a,b),Vasin and Nevrovskii (1979), von Borries (1948), Winkler (1988), Wolter et al. (1970), Woolf and Joy (1971), Worobjew and Shukov (1972), Worster (1970) and Yamazaki (1969).

Schottky Emission, Lanthanum Hexaboride Cathodes

Much of the literature related to LaB_6 as a cathode material is concerned with the problems of producing suitable crystals, of heating the point and of choosing the appropriate vacuum. The following papers are, for the most part, concerned more with the optical properties of guns with LaB_6 cathodes: Ahmed (1971, 1972, 1973), Ahmed and Broers (1972), Ahmed and Munro (1973), Ahmed and Nixon (1973), Ahmed et al. (1972), Batson et al. (1976), Boussoukaya and Septier (1976), Broers (1970), Ferris et al. (1975), Frosien et al. (1985), Futamoto et al. (1980), Gibson and Verhoeven (1975), Hohn (1982), Kang (1987), Kanitkar et al. (1976), Kato et al. (1983), Khairnar et al. (1985), Kim et al. (1997a,b), Leung et al. (1986), Loeffler (1970a,b), Nakagawa and Yanaka (1975), Nakasuji and Wada (1980), Noack et al. (1980), Parol' et al. (1984), Roslyakov et al. (1974), Sewell and Delâge (1984), Takaoka and Ura (1986), Takigawa et al. (1980, 1982), Tsukamoto et al. (1982), Vogel (1970), Vogt (1972), Watari and Yada (1986), Windsor (1969), Wolter and Sanders (1970), Yamabe et al. (1984), Yamazaki et al. (1984), Yonezawa et al. (1977) and Zaima et al. (1980).

Field Emission

Despite its length, the following list is confined to papers concerned with field electron emission sources, although a few do consider field ion emission as well: Adachi (1985), Batson (1987), Bottoms and Haydon (1977), Brock et al. (1992), Broers (1968), Brünger (1968, 1969), Burghard et al. (1987), Cleaver (1975a, b), Cleaver and Smith (1972, 1973), Davydova et al. (1979), Delong (1982), Denizart et al. (1981), Dyke and Dolan (1956), Eggenberger et al. (1968), El Gomati and Prutton (1985), El Gomati et al. (1985), Elinson (1958), Engel and Sauer (1980), Engel et al. (1974), Garg et al. (1984), Gaukler et al. (1975), Hadley et al. (1985), Hübner (1983), Hübner and Röhm (1988), Ichinokawa et al. (1982), Isakozawa et al. (2016), Kanitkar et al. (1976), Katsuda et al. (1986), Kern (1978b), Kuo and Siegel (1976), Kurihara (1985), Kuroda and Suzuki (1972a,b, 1974a,b, 1975), Kuroda et al. (1974a,b), Kurz (1979), Martin et al. (1960), Matsuda et al. (1981), Mayer and Gaukler (1986), Menadue (1974), Morita et al. (1996), Mubanga-N et al. (1986), Mundt (1973), Munro (1972), Ohiwa et al. (1981), Orloff (1986), Orloff and Swanson (1979a,b, 1982), Orloff et al. (1985), Pitaval et al. (1973), Plomp (1972), Plomp et al. (1968), Röhm (1986a,b), Samoto et al. (1985), Scheinfein (1986), Shimoyama et al. (1972a,b), Smith and Cumming

(1978), Someya et al. (1972a,b), Speidel and Benner (1982, 1986), Speidel and Brauchle (1982, 1987), Speidel and Hirschner (1988), Speidel and Kurz (1977), Speidel and Vorster (1975), Speidel et al. (1979, 1985), Stokes (1980), Swanson (1984), Swanson and Crouser (1969), Swanson and Tuggle (1981), Takaoka and Ura (1984, 1985), Takaoka et al. (1986a,b), Tonomura and Komoda (1970), Trolan and Dyke (1958), Troyon (1976, 1986), Troyon and Jiang (1984), Troyon et al. (1972, 1973, 1976), Ura and Takaoka (1982, 1986), van der Mast (1981, 1983), van Oostrom (1962), Vanselow (1973), Venables and Archer (1980), Veneklasen (1973), Veneklasen and Siegel (1970), Worsham et al. (1972), Worster (1969a–d), Yamamoto and Miyokawa (1998), Yonezawa et al. (1979), Zaima et al. (1978), Zinzindohué (1986), Zinzindohué and Troyon (1986).

Field emission from extremely sharp tips is considered by Bleloch et al. (1992), Elswijk et al. (1995), Binh and Garcia (1992), Binh et al. (1996), James et al. (1997), Kim et al. (1995, 1997a,b), Knápek et al. (2015), Murata et al. (2001), Shimoyama et al. (2001), Qian et al. (1993), Read and Bowring, (2004), Scheinfein and Spence (1993), Spallas et al. (2006) and Zhang et al. (2016).

Ion guns are not included in these lists, although some of the above publications devote some space to them. An electrode structure intended for an ion source but of wider interest is described by Cleaver and Ahmed (1981).

Emission From Carbon Fibres and Other Unconventional Materials

A number of older studies were concerned with emission from carbon: Adler et al. (1985), Baker et al. (1972, 1974), English et al. (1973), Ishizawa et al. (1986), Khatapova and Romanova (1982), Khatapova et al. (1985a,b), Latham and Salim (1987), Osipov (1984), Prohaska and Fisher (1982), Yada (1982a,b, 1986) and Yada and Shimoyama (1985). Recent publications on carbon nanotube and similar emitters are cited in Section 50.7.

Emission from silicon is studied by von Gorkom and Hoeberechts (1984, 1986a,b) and Lin et al. (2015). The 'shower-beam concept', introduced by van der Mast et al. (1985), for microlithographic purposes, depends on arrays of such emitters. Such arrays had been developed earlier by Spindt et al. (1976, 1983) and Forman (1983).

***

H. Adachi (1985). Approach to a stable field emission electron source. *Scanning Electron Microsc.* Pt II, 473–487.

R. J. Adler, G. F. Kiuttu, B. E. Simpkins, D. J. Sullivan and D. E. Voss (1985). Improved electron emission by use of a cloth fiber cathode. *Rev. Sci. Instrum.* **56**, 766–767.

H. Ahmed (1971). The use of lanthanum hexaboride and composite boride cathodes in electron optical instruments. EMAG, Cambridge. 30–33.

H. Ahmed (1972). A high-brightness boride emitter electron gun. EUREM-5, Manchester. 10–11.

H. Ahmed (1973). Some characteristics of boride emitters. EMAG, Newcastle-upon-Tyne. 32–34.

H. Ahmed and A. N. Broers (1972). Lanthanum hexaboride electron emitter. *J. Appl. Phys.* **43**, 2185–2192.

H. Ahmed and E. Munro (1973). Optimization of the performance of high-brightness electron guns. *J. Vac. Sci. Technol.* **10**, 972–974.

H. Ahmed and W. C. Nixon (1973). 100 kV boride-emitter electron gun system for conventional and scanning transmission microscopy. EMSA, New Orleans. **31**, 300–301.

H. Ahmed, W. Blair and R. Lane (1972). A low-power heater for the LaB_6 rod cathode. *Rev. Sci. Instrum.* **43**, 1048–1049.

M. A. Al-Khashab and A. E. Al-Abdullah (2012). The confront electrodes faces curvature effect on the electron gun performance. *Rafidain J. Sci.* **23** (2), 138–147.

A. V. Alyamovskii (1966). *Elektronnye Puchki i Elektronnye Pushki* (Sovetskoe Radio, Moscow).

K. Amboss (1964). Verification and use of Herrmann's optical theory of thermal velocity effects in electron beams in the low perveance regime. *IEEE Trans. Electron Dev.* **11**, 479–485.

W. H. J. Andersen and A. Mol (1968). Combined measurements of brightness and energy distribution of electrons emitted from a triode gun. EUREM-4, Rome. **1**, 339–340.

W. H. J. Andersen and A. Mol (1970). Simultaneous measurements of the brightness and the energy distribution of electrons emitted from a triode gun. *J. Phys. D: Appl. Phys.* **3**, 965−979.

B. André (1967). Sur l'apparition de répartitions non gaussiennes de la densité électronique dans une section droite de faisceaux d'électrons issus d'un canon expérimental à trois eelectrodes. *C. R. Acad. Sci. Paris B* **264**, 18−21.

F. S. Baker, A. R. Osborn and J. Williams (1972). Field emission from carbon fibres: a new electron source. *Nature* **239**, 96−97.

F. S. Baker, A. R. Osborn and J. Williams (1974). The carbon-fibre emitter. *J. Phys. D: Appl. Phys.* **7**, 2105−2115.

M. R. Barber and K. F. Sander (1959). The calculation of electrostatic electron-gun performance. *J. Electron. Control* **7**, 465−481.

J. E. Barth (1988). Realistic comparison of gun lens designs. *Ultramicroscopy* **24**, 1−5.

J. E. Barth and P. Kruit (1996). Addition of different contributions to the charged particle probe size. *Optik* **103**, 101−109.

E. B. Bas (1954). Eine neue Feinstrahl-Elektronenkanone mit indirekt geheizter Wolfram-Bolzenkathode und Ionentrennung. ICEM-3, London. 621−628.

E. B. Bas and F. Gaydou (1959). Über eine Fernfokus-Elektronenkanone und ihre Anwendungen. *Z. Angew. Math. Phys.* **11**, 370−375.

E. B. Bas, G. Cremosnik, R. N. Thomas and H. B. Weidmer (1967). Numerisch-theoretisch und experimentelle Untersuchung einer Hochstrom-Fernfokus-Elektronenkanone vom Tetroden-Typus. *Z. Angew. Math. Phys.* **18**, 379−396.

P. E. Batson (1987). Low-workfunction field-emission source for high-resolution EELS. EMSA, Baltimore **45**, 132−133.

P. E. Batson, C. H. Chen and J. Silcox (1976). Use of LaB_6 for a high quality, small energy spread beam in an electron velocity spectrometer. EMSA, Miami Beach. **34**, 634−635.

L. R. Baylor, D. H. Lowndes, M. L. Simpson, C. E. Thomas, M. A. Guillorn, V. I. Merkulov, J. H. Whealton, E. D. Ellis, D. K. Hensley and A. V. Melechko (2002). Digital electrostatic electron-beam array lithography. *J. Vac. Sci. Technol. B* **20**, 2646−2650.

J. Belledent, G. Z. M. Berglund, P. L. Brandt, S. Bérard-Bergery, M. J. Wieland and L. Pain (2013). Matching of beams on the MAPPER MATRIX tool. *Proc. SPIE* **8680**, 8680−0J.

M. Berz, K. Makino and W. Wan (2015). *An Introduction to Beam Physics* (CRC Press, Boca Raton).

J. Bi, X. R. Jiang and P. Kruit (1997). Theoretical and experimental investigations on Coulomb interactions in a two-lens focussed ion beam instrument. *Microelectron. Eng.* **35**, 439−442.

J. Bi, P. W. H. de Jager, J. E. Barth and P. Kruit (1998). Influence of Coulomb interactions on current density distribution in a two-lens focused ion beam system. *Microelectron. Eng.* **41−42**, 249−252.

V. T. Binh and N. Garcia (1992). On the electron and metallic ion emission from nanotips fabricated by field-surface-melting technique: experiments on W and Au tips. *Ultramicroscopy* **42−44**, 80−90.

V. T. Binh, N. Garcia and S. T. Purcell (1996). Electron field emission from atom-sources: fabrication, properties, and applications of nanotips. *Adv. Imaging Electron Phys.* **95**, 63−153.

A. L. Bleloch, M. G. Walls and A. Howie (1992). Field emission from atomically-sharp tips in a STEM. EUREM-10, Granada. **1**, 643−644.

H. Boersch (1954). Experimentelle Bestimmung der Energieverteilung in thermisch ausgelösten Elektronenstrahlen. *Z. Phys.* **139**, 115−146.

H. Boersch and G. Born (1958). Messungen an Elektronenstrahlerzeugern. ICEM-4, Berlin. **1**, 35−39.

M. Born and E. Wolf (1959). *Principles of Optics* (Pergamon, Oxford & New York); 7th edn, Cambridge University Press, Cambridge 2002.

W. R. Bottoms and G. B. Haydon (1977). A stable field emission source. EMSA, Boston. **35**, 58−59.

M. Boussoukaya and A. Septier (1976). Canon à électrons à forte brillance utilisant une cathode en borure de lanthane. *Rev. Phys. Appl.* **11**, 603−607.

D. E. Bradley (1961). Simple methods for preparing pointed filaments for the electron microscope. *Nature* **189**, 298–300.
F. W. Braucks (1958). Untersuchungen an der Fernfokuskathode nach Steigerwald. *Optik* **15**, 242–260.
F. W. Braucks (1959). Verbesserung der von Steigerwald entwickelten Fernfokuskathode durch Einbau einer weiteren Elektrode. *Optik* **16**, 304–312.
G. R. Brewer (1967a). High-intensity electron guns. In *Focusing of Charged Particles* (A. Septier, Ed.), **2**, 23–72 (Academic Press, New York & London).
G. R. Brewer (1967b). Focusing of high-density electron beams. In *Focusing of Charged Particles* (A. Septier, Ed.), **2**, 73–121 (Academic Press, New York & London).
M. Bricka and H. Bruck (1948). Sur un nouveau canon électronique pour tubes à haute tension. *Ann. Radioél.* **3**, 339–343.
J. M. Brock, M. T. Otten and W. M. Coene (1992). High-resolution imaging with a coherent electron source: the field emission gun. *Micron Microsc. Acta* **23**, 149–150.
A. N. Broers (1967). Electron gun using long-life lanthanum hexaboride cathode. *J. Appl. Phys.* **38**. 1991–1992; Erratum *ibid*. 3040.
A. N. Broers (1968). High brightness electron gun using a field emission cathode. EMSA, New Orleans. **26**, 294–295.
A. N. Broers (1969). Some experimental and estimated characteristics of the lanthanum hexaboride rod cathode electron gun. *J. Phys. E: Sci. Instrum.* **2**, 273–276.
A. N. Broers (1970). The use of Shottky [sic] emission lanthanum hexaboride cathodes for high resolution scanning electron microscopy. ICEM-7, Grenoble. **1**, 239–240.
M. Bronsgeest (2014). *Physics of Schottky Electron Sources. Theory and Optimum Operation* (Pan Stanford, Singapore).
M. Bronsgeest and P. Kruit (2006). Temperature dependence of the work function of Zr/O/W(100) Schottky electron source in typical operating conditions and its effect on beam brightness. *J. Vac. Sci. Technol. B* **24**, 887–891.
M. Bronsgeest and P. Kruit (2008). Effect of the electric field on the form stability of a Schottky electron emitter: a step model. *J. Vac. Sci. Technol. B* **26**, 2073–2079.
M. Bronsgeest and P. Kruit (2009). Reversible shape changes of the end facet on Schottky electron emitters. *J. Vac. Sci. Technol. B* **27**, 2424–2531.
M. Bronsgeest, J. E. Barth, G. A. Schwind, L. W. Swanson and P. Kruit (2007). Extracting the Boersch effect contribution from experimental energy spread measurements for Schottky electron emitters. *J. Vac. Sci. Technol. B* **25**, 2049–2054.
W. Brünger (1968). Feldemissionskathode zur kohärenten Beleuchtung des Elektronen-Biprismas. *Naturwissenschaften* **55**, 295.
W. Brünger (1971). Ultrahochvakuum-Interferometer zur Messung von Kontaktpotentialdifferenzen mit feldemittierten Elektronen. Dissertation, Tübingen.
W. Brünger (1979). Eine neue LaB_6-Einkristall-Elektronenquelle und ihre Anwendung in der Elektronen- und Röntgenmikroskopie. Habilitationsschrift, Tübingen.
R. Buchanan and L. Jacob (1960). Beam profiles near the crossover in the electron gun. EUREM-2, Delft. **1**, 60–63.
M. Büchsel, H. Rose and R. Spehr (1982). Comparison of low-voltage high-current electron microprobes using different types of cathodes. ICEM-10, Hamburg. **1**, 353–354.
R. A. Burghard, L. W. Swanson and J. Orloff (1987). Performance comparison of electrostatic lenses for field emission ion and electron sources. *J. Vac. Sci. Technol. A* **5**, 364–371.
J. W. Butler (1966). Digital computer techniques in electron microscopy. ICEM-6, Kyoto. **1**, 191–192.
R. Castaing (1960). Electron probe microanalysis. *Adv. Electron. Electron Phys.* **13**, 317–386.
T. H. P. Chang, D. P. Kern and L. P. Muray (1992). Arrayed miniature electron beam columns for high throughput sub-100 nm lithography. *J. Vac. Sci. Technol. B* **10**, 2743–2748.

T. H. P. Chang, M. G. R. Thomson, M. L. Yu, R. Kratschmer, H. S. Kim, K. Y. Lee, S. A. Rishton and D. P. Kern (1995). Electron beam microcolumn technology and applications. *Proc. SPIE* **2522**, 4−12.

T. H. P. Chang, M. Mankos, K. Y. Lee and L. P. Muray (2001). Multiple electron-beam lithography. *Microelectron. Eng.* **57−58**, 117−135.

S. G. Christov (1966). General theory of electron emission from metals. *Phys. Stat. Sol.* **17**, 11−26.

J. R. A. Cleaver (1975a). Field emission guns for electron probe instruments. *Int. J. Electron.* **38**, 513−529.

J. R. A. Cleaver (1975b). Stabilization of the electron probe current in the scanning electron microscope with a field emission cathode. *Int. J. Electron.* **38**, 531−540.

J. R. A. Cleaver (1978). Field emission electron gun systems incorporating single-pole magnetic lenses. *Optik* **52**, 293−303.

J. R. A. Cleaver (1979). The single-pole magnetic lens as a condenser for use with field-emission electron guns. EMAG, Brighton. 55−58.

J. R. A. Cleaver and H. Ahmed (1981). A 100-kV ion probe microfabrication system with a tetrode gun. *J. Vac. Sci. Technol.* **19**, 1145−1148.

J. R. A. Cleaver and K. C. A. Smith (1972). An experimental field emission gun for the scanning electron microscope. EUREM-5, Manchester. 18−19.

J. R. A. Cleaver and K. C. A. Smith (1973). Optical characteristics of a field emission scanning microscope. EMAG, Newcastle-upon-Tyne. 6−11.

B. Cook (2013). Brightness limitations in sources for static and ultra-fast high resolution electron microscopy. Dissertation, Delft.

B. Cook and P. Kruit (2016). Coulomb interactions in sharp tip pulsed photo field emitters. *Appl. Phys. Lett.* **109**, 151901.

B. Cook, M. Bronsgeest, C. W. Hagen and P. Kruit (2009). Improving the energy spread and brightness of thermal-field (Schottky) emitters with PHAST—PHoto Assisted Schottky Tip. *Ultramicroscopy* **109**, 403−412.

B. Cook, T. Verduin, C. W. Hagen and P. Kruit (2010). Brightness limitations of cold field emitters caused by Coulomb interactions. *J. Vac. Sci. Technol. B* **28**, C6C74.

B. Cook, T. Verduin and P. Kruit (2011). Statistical Coulomb interactions in cold field emitters. International Vacuum Nanoelectronics Conference (IVNC), Wuppertal. 9−10.

V. E. Cosslett and M. E. Haine (1954). The tungsten point cathode as an electron source. ICEM-3, London. 639−644.

A. V. Crewe (1978). Collision broadening in electron beams. *Optik* **50**, 205−212.

A. V. Crewe, D. N. Eggenberger, J. Wall and L. M. Welter (1968). Electron gun using a field emission source. *Rev. Sci. Instrum.* **39**, 576−583.

J. P. Davey (1971). The brightness relation in electron optics. *Optik* **33**, 580−590.

J. P. Davey (1973). Grid control mechanisms in the hairpin filament electron gun. *Optik* **38**, 123−137.

E. I. Davydova, A. D. Karpenko and V. A. Shishkin (1979). Stability of the field emission of fine-tip cathodes passivated by transition-metal films. *Zh. Tekh. Fiz.* **49**, 2344−2348. *Sov. Phys. Tech. Phys.* **24**, 1307−1309.

J. H. B. Deane and R. G. Forbes (2008). The formal derivation of an exact series expansion for the principal Schottky−Nordheim barrier function υ, using the Gauss hypergeometric differential equation. *J. Phys. A: Math. Theor.* **41**, 395301, 9 pp.

E. de Chambost (1982). Transverse Coulombian aberrations in electron lithography probes. *Optik* **62**, 189−198.

E. de Chambost and C. Hennion (1980). Energy broadening in an electron gun. Theoretical model and experimental results. *Optik* **55**, 357−370.

P. Dedieu, J. Huret and A. Séguéla (1970). Source d'électrons à 3 MV de très haute stabilité pour le grand microscope électronique du CNRS de Toulouse. ICEM-7, Grenoble. **2**, 69−70.

N. de Jonge (2004). The brightness of carbon nanotube electron emitters. *J. Appl. Phys.* **95**, 673−681.

N. de Jonge (2009). Carbon nanotube electron sources for electron microscopes. *Adv. Imaging Electron Phys.* **156**, 203−233.

N. de Jonge (2010). The optical performance of carbon nanotube field emitters. In *Carbon Nanotube and Related Field Emitters* (Y. Saito, Ed.), 67–80 (Wiley–VCH, Weinheim).

N. de Jonge and J. M. Bonard (2004). Carbon nanotube electron sources and applications. *Philos. Trans. R. Soc. (Lond.) A* **362**, 2239–2266.

A. Delâge and P. B. Sewell (1984). Study of space charge limitation of thermionic cathodes in triode guns. In *Electron Optical Systems for Microscopy, Microanalysis and Microlithography* (J. J. Hren, F. A. Lenz, E. Munro and P. B. Sewell, Eds), 171–178 (Scanning Electron Microscopy, AMF O'Hare).

A. Delong (1982). A field-emission cathode in electron-optical instruments. ICEM-10, Hamburg. **1**, 343–350.

A. Delong, J. Chmelík, V. Kolařik, J. Komůrka, B. Lencová and J. Očadlík (1988). New design of FE gun with magnetic lens. EUREM-9, York. **1**, 103–104.

A. Delong, J. Chmelík, V. Kolařik and J. Očadlík (1989). A new design of field emission electron gun with a magnetic lens. *Optik* **81**, 103–108.

M. Denizart, S. Roques, F. Sonier, B. Jouffrey and J. Trinquier (1981). Triode and tetrode guns for field emission electron microscopes. *Ultramicroscopy* **7**, 65–80.

W. Dietrich (1958). Bestätigung der anomalen Energiebreiten in Elektronenstrahlen mit dem elektrostatischen Analysator. *Z. Phys.* **152**, 306–313.

R. W. Ditchfield and M. J. Whelan (1977). Energy broadening of the electron beam in the electron microscope. *Optik* **48**, 163–172.

A. K. Dokania and P. Kruit (2009). Concept and operation of Schottky emitter without suppressor electrode. *J. Vac. Sci. Technol. B* **27**, 2426–2431.

A. K. Dokania, J. F. M. Velthuis, Y. Zhang and P. Kruit (2007). Thermal model of a miniaturized Schottky emitter for parallel electron beam lithography. *J. Vac. Sci. Technol. B* **25**, 504–507.

W. W. Dolan and W. P. Dyke (1954). Temperature-and-field emission of electrons from metals. *Phys. Rev.* **95**, 327–332.

R. M. Dolby and D. W. Swift (1960). The bias network and electron gun current stability. EUREM-2, Delft. **1**, 114–118.

J. Dosse (1940). Theoretische und experimentelle Untersuchungen über Elektronenstrahler. *Z. Phys.* **115**, 530–556.

M. Drechsler, V. E. Cosslett and W. C. Nixon (1958). The point cathode as an electron source. ICEM-4, Berlin. **1**, 13–20.

X.-d. Du, Y. Wen, L. Traverso, A. Datta, C. Chen, X.-f. Xu and L. Pan (2016). Design and fabrication of electrostatic microcolumn in multiple electron-beam lithography. *Proc. SPIE* **9777**, 9777-1D.

W. P. Dyke and W. W. Dolan (1956). Field emission. *Adv. Electron. Electron Phys.* **8**, 89–185.

W. P. Dyke, J. K. Trolan, W. W. Dolan and G. Barnes (1953). The field emitter: fabrication, electron microscopy, and electric field calculations. *J. Appl. Phys.* **24**, 570–576.

J. A. Eades (1994). On optimum illumination for channeling experiments. *Scanning* **16**, 97–100.

A. L. Eberle, S. Mikula, R. Schalek, J. Lichtman, M. L. Knothe Tate and D. Zeidler (2015). High-resolution high-throughput imaging with a multibeam scanning electron microscope. *J. Microsc. (Oxford)* **259**, 114–120.

C. J. Edgcombe (2005). Development of Fowler–Nordheim theory for a spherical field emitter. *Phys. Rev. B* **72**, 045420, 7 pp; Erratum *ibid*. 089901.

C. J. Edgcombe and N. de Jonge (2006). Properties of a field emitter deduced from curvature of its Fowler–Nordheim plot. *J. Vac. Sci. Technol. B* **24**, 869–873.

C. J. Edgcombe and N. de Jonge (2007). Deduction of work function of carbon nanotube field emitter by use of curved-surface theory. *J. Phys. D: Appl. Phys.* **40**, 4123–4128.

C. J. Edgcombe and U. Valdrè (1998). Experimental and computational study of field emission from carbon nano-tips grown on W minispheres. ICEM-14, Cancún. **1**, 69–70.

C. J. Edgcombe and U. Valdrè (2001). Fowler–Nordheim theory for a spherical emitting surface. EMAG, Dundee. 155–158.

D. N. Eggenberger, R. K. Hart and A. C. Libal (1968). A field emission high voltage electron gun. EMSA, New Orleans. **26**, 330–331.

W. Ehrenberg and W. E. Spear (1951). An electrostatic focusing system and its application to a fine focus X-ray tube. *Proc. Phys. Soc. (Lond.) B* **64**, 67–75.

P. A. Einstein and L. Jacob (1948). On some focal properties of an electron optical immersion objective. *Philos. Mag.* **39**, 20–31.

M. M. El Gomati and M. Prutton (1985). A miniature variable energy electron probe for nanometric analysis. EMAG, Newcastle-upon-Tyne. 133–136.

M. M. El Gomati, M. Prutton and R. Browning (1985). An all-electrostatic, small beam diameter, high probe current field emission electron probe. *J. Phys. E: Sci. Instrum.* **18**, 32–38.

A. B. El-Kareh and M. A. Smither (1979). Analysis of the energy broadening in an electron-beam system. *J. Appl. Phys.* **50**, 5596–5602.

A. B. El-Kareh, J. C. Wolfe and J. E. Wolfe (1977). Contribution to the general analysis of field emission. *J. Appl. Phys.* **48**, 4749–4753.

M. I. Elinson (1958). Zur Frage der Stabilität der Feldelektronenemission. ICEM-4, Berlin. **1**, 25–28.

M. I. Elinson and G. A. Kudintseva (1962). Field-emission cathodes based on metal-like refractory compounds. *Radiotekh. Elektron.* **7**, 1511–1515. *Radio Eng. Electron. Phys.* **7**, 1417–1423.

S. G. Ellis (1947). The optics of three-electrode electron guns. *J. Appl. Phys.* **18**, 879–890.

H. B. Elswijk, T. van Rooy and C. Schiller (1995). Energy broadening by Coulomb interactions of an electron beam emitted from a point source. *J. Vac. Sci. Technol. B* **13**, 1037–1043.

Y. Emura, H. Murata, E. Rokuta, H. Shimoyama, H. Yasuda and T. Haraguchi (2014). Determination of geometrical form factor of emitter from Schottky plot. IMC-18, Prague. IT-1-P-6004.

W. Engel and H. Sauer (1980). A field emission electron gun with a three-electrode accelerating lens. *Ultramicroscopy* **5**, 262.

W. Engel, W. Kunath and S. Krause (1974). Properties of three electrode accelerating lenses for field emission electron guns. ICEM-8, Canberra. **1**, 118–119.

T. H. English, C. Lea and M. T. Lilburne (1973). The carbon field emitter as an electron gun source. EMAG, Newcastle-upon-Tyne. 12–14.

M. Enyama, M. Sakakibara, S. Tanimoto and H. Ohta (2014). Optical system for a multi-beam scanning electron microscope. *J. Vac. Sci. Technol. B* **32**, 051801.

M. Enyama, M. Sakakibara, S. Tanimoto and H. Ohta (2016). Optical sysem for a multiple-beam scanning electron microscope. *J. Vac. Sci. Technol. B* **32**, 051801.

M. Essig (1981). Hochaufgelöste Elektronenspektroskopie der infraroten Gitterschwingungen in kleinen würfelförmigen MgO-Kristallen und Messung der Energieverteilung der aus Kohlefaserspitzen thermofeldemittierten Elektronen. Dissertation, Kaiserslautern.

M. Essig (1985). A test stand for the development of imaging triode guns. *Microelectron. Eng.* **3**, 113–115.

M. Essig (1986). Illumination tuning by imaging triode guns. ICEM-11, Kyoto. **1**, 279–280.

M. Essig and J. Geiger (1981). Broadening of the energy distribution of thermal-field emitted electrons from carbon fibres. *Appl. Phys.* **25**, 115–118.

M. Eupper (1980). Numerische Berechnung elektronenoptischer Eigenschaften von Strahlerzeugern mit Spitzenkathode. Diplomarbeit, Tübingen.

M. Eupper (1982). Eine methode zur Lösung des Dirichlet-Problems in drei Dimensionen und seine Anwendung auf einen neuartigen Elektronenstrahlerzeuger. *Optik* **62**, 299–307.

M. Eupper (1985). Eine verbesserte Integralgleichungsmethode zur numerischen Lösung dreidimensionaler Dirichletprobleme und ihre Anwendung in der Elektronenoptik. Dissertation, Tübingen.

T. E. Everhart (1967). Simplified analysis of point-cathode electron sources. *J. Appl. Phys.* **38**, 4944–4957.

S. D. Ferris, D. C. Joy, H. J. Leamy and C. K. Crawford (1975). A directly heated LaB_6 electron source. *Scanning Electron Microsc.*, 11–18.

J. H. Fink and B. W. Schumacher (1974). The anatomy of a thermionic electron beam. *Optik* **39**, 543–557.

J. H. Fink and B. W. Schumacher (1975). Characterization of charged particle beam sources. *Nucl. Instrum. Meth.* **130**, 353–358.
R. G. Forbes (1999a). Refining the application of Fowler–Nordheim theory. *Ultramicroscopy* **79**, 11–23.
R. G. Forbes (1999b). Field emission: new theory for the derivation of emission area from a Fowler–Nordheim plot. *J. Vac. Sci. Technol. B* **17**, 526–533.
R. G. Forbes (1999c). Use of a spreadsheet for Fowler–Nordheim equation calculations. *J. Vac. Sci. Technol. B* **17**, 534–541.
R. G. Forbes (2004). Use of energy–space diagrams in free-electron models of field electron emission. *Surf. Interface Anal.* **36**, 395–401.
R. G. Forbes (2006). Simple good approximations for the special elliptic functions in standard Fowler–Nordheim tunneling theory for a Schottky–Nordheim barrier. *Appl. Phys. Lett.* **89**, 113122, 3 pp.
R. G. Forbes (2008a). Call for experimental test of a revised mathematical form for empirical field emission current–voltage characteristics. *Appl. Phys. Lett.* **92**, 193105, 3 pp.
R. G. Forbes (2008b). On the need for a tunneling pre-factor in Fowler–Nordheim tunneling theory. *J. Appl. Phys.* **103**, 114911.
R. G. Forbes (2008c). Physics of generalized Fowler–Nordheim-type equations. *J. Vac. Sci. Technol. B* **26**, 788–793.
R. G. Forbes (2010). Thin-slab model for the field electron emission. *J. Vac. Sci. Technol. B* **28**, C2A43.
R. G. Forbes and J. H. B. Deane (2007). Reformulation of the standard theory of Fowler–Nordheim tunnelling and cold field electron emission. *Proc. R. Soc. (Lond.) A* **463**, 2907–2927; Errata. *ibid.* **464** (2008) 3378.
R. G. Forbes and J. H. B. Deane (2010). Comparison of approximations for the principal Schottky–Nordheim barrier function $\upsilon(f)$ and comments on Fowler–Nordheim plots. *J. Vac. Sci. Technol. B* **28**, C2A33–C2A42.
R. G. Forbes and J. H. B. Deane (2011). Transmission coefficients for the exact triangular barrier: an exact general analytical theory that can replace Fowler and Nordheim's 1928 theory. *Proc. R. Soc. (Lond.) A* **467**, 2927–2947.
R. G. Forbes and K. L. Jensen (2001). New results in the theory of Fowler–Nordheim plots and the modelling of hemi-ellipsoidal emitters. *Ultramicroscopy* **89**, 17–22.
R. G. Forbes, J. H. B. Deane, A. Fischer and M. S. Mousa (2015). Fowler–Nordheim plot analysis: a progress report. *Jordan J. Phys.* **8**, 125–147.
R. Forman (1983). Evaluation of the emission capabilities of Spindt-type field emitting cathodes. *Appl. Surf. Sci.* **16**, 277–291.
R. H. Fowler and L. W. Nordheim (1928). Electron emission in intense electric fields. *Proc. R. Soc. (Lond.) A* **119**, 173–181.
M. J. Fransen, T. L. van Rooy, P. C. Tiemeijer, M. H. F. Overwijk, J. S. Faber and P. Kruit (1999). On the electron-optical properties of the ZrO/W Schottky electron emitter. *Adv. Imaging Electron Phys.* **111**, 91–166.
W. Franzen and J. H. Porter (1975). Energy spectrum of electrons emitted by a hot cathode. *Adv. Electron. Electron Phys.* **39**, 73–119.
W. Franzen, R. Gupta, J. H. Porter and R. S. Wenstrup (1973). Nonanomalous distribution of electrons emitted by a thermionic cathode. *J. Appl. Phys.* **44**, 145–151.
J. Frosien, B. Lischke and R. Kerner (1985). Emission properties of LaB_6-cathodes for e-beam systems. In *Microcircuit Engineering 84* (A. Heuberger and H. Beneking, Eds), 125–130 (Academic Press, London & Orlando).
S. Fujita and H. Shimoyama (2005a). Theory of cathode trajectory characterization by canonical mapping transformation. *J. Electron Microsc.* **54**, 331–343.
S. Fujita and H. Shimoyama (2005b). A new evaluation method of electron optical performance of high beam current probe forming systems. *J. Electron Microsc.* **54**, 413–427.
S. Fujita and H. Shimoyama (2006). Gun lens theory for nonparaxial trajectories by canonical mapping transformation: characterization of general skewed rays inside electron guns by electron gun focal length. *J. Vac. Sci. Technol. B* **24**, 1891–1901.

S. Fujita, M. Takebe and H. Shimoyama (2008). Lens theory of non-paraxial rays for electron gun characterization. *Phys. Procedia* **1**, 18–33.

S. Fujita, M. Takebe, W. Ushio and H. Shimoyama (2010a). Generalization of the paraxial trajectory method for the analysis of non-paraxial rays: simulation program G-optk for electron gun characterization. *J. Electron Microsc.* **59**, 3–15.

S. Fujita, M. Takebe and T. Ohye (2010b). Characterization of curved cathode guns by the generalized trajectory method: upgrade of G-optk programme for applications to non-planar objects. *J. Electron Microsc.* **59**, 351–358.

Y. Furukawa (1986). Statistical treatment of anomalous energy spread in a charged particle beam. *J. Vac. Sci. Technol. A* **4**, 1908–1912.

M. Futamoto, M. Nakazawa, K. Usami, S. Hosoki and U. Kawabe (1980). Thermionic emission properties of a single-crystal LaB_6 cathode. *J. Appl. Phys.* **51**, 3869–3876.

R. K. Garg, A. Séguéla and B. Jouffrey (1984). Electron optics of a field emission electron source for a variable high voltage scanning transmission electron microscope. APEM-3, Singapore. 100–101.

K. H. Gaukler, R. Speidel and F. Vorster (1975). Energieverteilungen von Elektronen aus einer Feldemissionskathode. *Optik* **42**, 391–400.

E. D. Gibson and J. D. Verhoeven (1975). The preparation of single crystal LaB_6 cathodes for electron microscopes. *J. Phys. E: Sci. Instrum.* **8**, 1003–1004.

R. H. Good and E. W. Müller (1956). Field emission. *Handbuch der Physik* **21**, 176–231.

P. Grivet (1972). *Electron Optics*, 2nd edn (Pergamon, Oxford & New York).

O. Gröning, O. M. Küttel, C. Emmenegger, P. Gröning and L. Schlapbach (2000). Field emission properties of carbon nanotubes. *J. Vac. Sci. Technol. B* **18**, 665–678.

T. Groves (1981). Mutual repulsion effects in a high throughput e-beam lithography column. *J. Vac. Sci. Technol.* **19**, 1106–1110.

T. Groves, D. L. Hammond and H. Kuo (1979). Electron-beam broadening effects caused by discreteness of space charge. *J. Vac. Sci. Technol.* **16**, 1680–1685.

K. W. Hadley, P. J. Donders and M. J. G. Lee (1985). Influence of shank profile on laser heating of a field emitter. *J. Appl. Phys.* **57**, 2617–2625.

M. E. Haine and P. A. Einstein (1951). High-voltage electron guns. *National Bureau of Standards Circular* **527**, 319–328 [Published 1954].

M. E. Haine and P. A. Einstein (1952). Characteristics of the hot cathode electron microscope gun. *Br. J. Appl. Phys.* **3**, 40–46.

M. E. Haine and D. Linder (1967). High brightness electron guns. In *Focusing of Charged Particles* (A. Septier, Ed.), **1**, 233–250 (Academic Press, New York & London).

M. E. Haine, P. A. Einstein and P. H. Borcherds (1958). Resistance bias characteristic of the electron microscope gun. *Br. J. Appl. Phys.* **9**, 482–486.

V. Hamza (1966). Computer experiments on electron guns. *IEEE Trans. Electron Dev.* **13**, 551–554.

V. Hamza and G. S. Kino (1967). The accuracy of numerical solutions for electron gun design. *IEEE Trans. Electron Dev.* **14**, 195–200.

K.-J. Hanszen (1962). Beziehungen zwischen den geometrisch-optischen und den elektrischen Eigenschaften von Haarnadel- und Spitzenkathode. ICEM-5, Philadelphia. **1**, KK-11.

K.-J. Hanszen (1964a). Neue Ergebnisse über die geometrisch-optischen und die elektrischen Eigenschaften von Elektronenstrahlern. EUREM-3, Prague. **1**, 47–48.

K.-J. Hanszen (1964b). Über Fokussierungsmöglichkeiten mit rotationssymmetrischen Elektronenstrahl-Erzeugern. *Naturwissenschaften* **51**, 379–380.

K.-J. Hanszen (1964c). Ein abgewandeltes Schattenverfahren zur genaueren Bestimmung der geometrisch-optischen Daten von Elektronenstrahl-Erzeugern und Elektronenlinsen. *Z. Naturforsch.* **19a**, 896–905.

K.-J. Hanszen and R. Lauer (1967). Richtstrahlwertmessungen mit dem Zwei-Blendenverfahren an Elektronenstrahlern mit Kugelkathoden von 2μ50 bis 1,5 m [*sic*] Durchmesser. *Z. Naturforsch.* **22a**, 238–254.

K.-J. Hanszen and R. Lauer (1968). Der Einfluss des Strahlverlaufs im Beschleunigungsfeld einer Elektronenkanone auf die Energieverteilung im axialen Strahlenbündel. EUREM-4, Rome. **1**, 349–350.

K.-J. Hanszen and R. Lauer (1969a). Characteristische Kaustikverläufe in austretenden Strahlenbündeln von Elektronenkanonen. *Z. Naturforsch.* **24a**, 97–104.

K.-J. Hanszen and R. Lauer (1969b). Die Energieverteilung im Strahlenbündel einer Elektronenkanone mit einkristalliner Kugelkathode. *Z. Naturforsch.* **24a**, 214–225.

D. F. Hardy (1974). Spot sizes in probe-forming instruments with high coherence electron sources. ICEM-8, Canberra. **1**, 124–125.

J. Hasker (1966). The influence of initial velocities on the beam-current characteristic of electron guns. *Philips Res. Rep.* **21**, 122–150.

J. Hasker (1969a). A simple approximate method for calculating the space-charge-limited beam current of rotation-symmetrical electron guns. *Philips Res. Rep.* **24**, 249–262.

J. Hasker (1969b). Anomalous electron velocity distributions. *Philips Res. Rep.* **24**, 263–274.

J. Hasker (1972). Beam-current characteristic and cathode loading of electron guns with rotational symmetry: some important properties and method of calculation. *Philips Res. Rep.* **27**, 513–538.

J. Hasker (1983). Calculation of diode characteristics and proposed characterization of cathode emission capability. *Appl. Surf. Sci.* **16**, 220–237.

R. Hauke (1977). Theoretische Untersuchungen rotationssymmetrischer Elektronenstrahlerzeugungssysteme unter Berücktsichtigung von Raumladung. Dissertation, Tübingen.

P. W. Hawkes, Ed. (2009). Cold field emission and the scanning transmission electron microscope. *Adv. Imaging Electron Phys.* **159**.

E. C. Heeres, T. H. Oosterkamp and N. de Jonge (2011). Making carbon nanotube electron sources of defined lengths and with closed caps. *Nanotechnology* **22**, 235308, 6 pp.

E. C. Heeres, T. H. Oosterkamp and N. de Jonge (2012). Site of the localized electron emission sites on a closed multiwalled carbon nanotube. *Phys. Rev. Lett.* **108**, 036804, 5 pp.

H. Heinrich, M. Essig and J. Geiger (1977). Energy distribution of post-accelerated electrons field-emitted from carbon fibres. *Appl. Phys.* **12**, 197–202.

H. Heinrich, T. Haag and J. Geiger (1978). A metallic glass tip – a promising field electron emission source. *J. Phys. D: Appl. Phys.* **11**, 2439–2442.

G. Herrmann (1957). Transverse scaling of electron beams. *J. Appl. Phys.* **28**, 474–478.

G. Herrmann (1958). Optical theory of thermal velocity effects in cylindrical beams. *J. Appl. Phys.* **29**, 127–138.

W. B. Herrmannsfeldt (1979). Electron trajectory program. *SLAC Report* No. 226.

W. B. Herrmannsfeldt (1981). Numerical design of electron guns and space charge limited transport systems. *Nucl. Instrum. Meth.* **187**, 245–253.

W. B. Herrmannsfeldt (1987). Some applications of particle-in-cell codes to problems of high intensity beams. *Nucl. Instrum. Meth. Phys. Res. A* **258**, 583–588.

T. Hibi (1954). Pointed filament and its applications. ICEM-3, London. 636–638.

T. Hibi (1956). Pointed filament (I) Its production and its applications. *J. Electronmicrosc* **4**, 10–15.

T. Hibi (1962). Point cathode and resolution of electron microscope. ICEM-5, Philadelphia. **1**, KK-1.

T. Hibi and S. Takahashi (1959). Two-stage electronmicroscope using pointed filament. *J. Electronmicrosc* **7**, 15–18.

T. Hibi and K. Yada (1964). Point cathodes and resolution of electronmicroscope. II. The effect of the operating condition of the point cathode and that of stigmator. *J. Electron Microsc.* **13**, 94–100.

T. Hibi, K. Yada and S. Takahashi (1962). Point cathodes and resolution of electronmicroscope. *J. Electron Microsc.* **11**, 244–252.

J. Hillier and R. F. Baker (1945). A discussion of the illuminating system of the electron microscope. *J. Appl. Phys.* **16**, 469–483.

J. Hillier and R. F. Baker (1946). On the improvement of resolution in electron diffraction cameras. *J. Appl. Phys.* **17**, 12–22.

J. Hillier and S. G. Ellis (1949). The illuminating system of the electron microscope. *J. Appl. Phys.* **20**, 700–706.

H. Hoffmann (1972). Richtstrahlwerte und Kenngrößen von Elektronenstrahl-Erzeugersystemen bei 50–125 kV und 0,1–1 mA. *Optik* **36**, 494–509.

F. J. Hohn (1982). Improved high brightness electron source using LaB_6 single crystal material. ICEM-10, Hamburg. **1**, 363–364.

F. J. Hohn (1985). Development and use of high brightness lanthanum hexaboride electron guns. *Scanning Electron Microsc.*, 1327–1338.

P. Holl (1968). Ein Elektronen-Strahlerzeugungssystem hoher Stabilität fur Spitzen- und Haarnadelkathoden. *Optik* **28**, 76–78.

P. Holl (1969). Ein elektronenoptischer Mikroschreiber hoher Stabilität und seine Anwendung. *Optik* **30**, 116–137.

F. Houdellier, A. Masseboeuf, M. Monthioux and M. Hÿtch (2012). New carbon cone nanotip for use in a highly coherent cold field emission electron microscope. *Carbon* **50**, 2037–2044.

F. Houdellier, L. de Knoop, C. Gatel, A. Masseboeuf, S. Mamishin, Y. Taniguchi, M. Delmas, M. Monthioux, M. Hÿtch and E. Snoeck (2015). Development of TEM and SEM high brightness electron guns using cold-field emission from a carbon nanotip. *Ultramicroscopy* **151**, 107–115.

H. Hübner (1983). First results of a microwave field emission cathode. *Optik* **64**, 113–123.

H. Hübner and E. Röhm (1988). Die Erzeugung von Elektronenpulsen im Pikosekundenbereich mittels Hochfrequenz-Feldemission. *Optik* **78**, 173–182.

T. Ichinokawa and H. Maeda (1978). New type electron gun with electrostatic and electromagnetic lenses. ICEM-9, Toronto. **1**, 62–63.

T. Ichinokawa, M. Sekine, Z. S. Gur and A. Ishikawa (1982). Electron optical properties of low energy field emission gun in the energy range from 100 to 2000 eV. ICEM-10, Hamburg. **1**, 351–352.

S. Iida, R. Hirano, T. Amano, T. Terasawa, H. Watanabe and T. Murakami (2014). Analysis of image distortion on projection electron microscope image. IMC-18, Prague. IT-8-P-1428.

R. Iiyoshi (1998). Numerical analysis of pencil of rays in point cathode electron gun. ICEM-14, Cancún. **1**, 89–90.

R. Iiyoshi (2011). Modeling of tip evolution of point cathode for numerical calculation of electric field in electron gun. *Nucl. Instrum. Meth. Phys. Res. A* **645**, 316–320.

R. Iiyoshi and S. Maruse (1996). Tungsten-point-cathode electron gun using electron bombardment for cathode tip heating: cathode life and operating characteristics at cathode temperatures above 2,800 K. *J. Electron Microsc.* **45**, 128–134.

R. Iiyoshi, H. Takematsu and S. Maruse (1986). Point cathode electron gun using electron beam heating. ICEM-11, Kyoto. **1**, 235–238.

R. Iiyoshi, H. Takematsu and S. Maruse (1988). Point cathode electron gun using electron bombardment for cathode tip heating. *J. Electron Microsc.* **37**, 1–7.

G. Induni (1947). Sur une source d'électrons pour microscopes électroniques. *Helv. Phys. Acta* **20**, 463–467.

G. Induni (1955). La cathode froide et ses applications. In *Les Techniques Récentes en Microscopie Electronique et Corpusculaire.* 189–197 (Colloques du CNRS).

S. Isakozawa, I. Nagaoki, A. Watabe, Y. Nagakubo, N. Saito, H. Matsumoto, X. F. Zhang, Y. Taniguchi and N. Baba (2016). Design of a 300-kV gas environmental transmission electron microscope equipped with a cold field emission gun. *Microscopy* **65**, 353–362.

Y. Ishizawa, S. Aoki, C. Oshima and S. Otani (1986). Carbide field emission source. ICEM-11, Kyoto. **1**, 223–226.

L. Jacob (1948). The variation of beam angle wih modulation in electron optical immersion systems. *Philos. Mag.* **39**, 400–408.

L. Jacob (1950a). The field in an electron-optical immersion objective. *Proc. Phys. Soc. (Lond.) B* **63**, 75–83.

L. Jacob (1950b). Some crossover properties in the electron immersion objective. *J. Appl. Phys.* **21**, 966–970.

E. M. James, A. L. Bleloch and J. M. Rodenburg (1997). A novel ultra-sharp field emission source demonstrated in a STEM. EMAG, Cambridge. 65–68.

G. H. Jansen (1990). Coulomb interactions in particle beams. *Adv. Electron. Electron Phys,* Suppl. 21, 546 pp.
K. L. Jensen (1999). Exchange-correlation, dipole, and image charge potentials for electron sources: temperature and field variations of the barrier height. *J. Appl. Phys.* **85**, 2667–2680.
K. L. Jensen (2001). Theory of field emission. In *Vacuum Microelectronics* (W. Zhu, Ed.), 33–104 (Wiley, New York).
K. L. Jensen (2012). Electron emission physics. *Adv. Imaging Electron Phys.* **149**.
K. L. Jensen and A. K. Ganguly (1993). Numerical simulation of field emission from silicon. *J. Vac. Sci. Technol. B* **11**, 371–378.
K. L. Jensen, D. A. Shiffler, J. R. Harris, I. M. Rittersdorf and J. J. Petillo (2017). 2D/3D image charge for modeling field emission. *J. Vac. Sci. Technol. B* **35**, 02C101, 5 pp.
W.-q. Jin, L.-w. Zhou and G.-q. Ni (1995). On realizing any specified image rotation in the electrostatic and magnetic imaging. *Proc. SPIE* **2522**, 90–99.
B. V. Johansen (1973). A high performance Wehnelt grid for transmission electron microscopy. *Micron* **4**, 121–135.
O. Kamigaito (1964). Focussing, current density and brightness of electron beams from electron guns with various bias voltages—a study with oxide-cored cathode. *J. Electron Microsc.* **13**, 124–132.
O. Kamigaito (1965). Focussing of electron beam from biased electron gun. A study with oxide-cored cathode as well as tungsten hair-pin filament. *Jpn. J. Appl. Phys.* **4**, 604–612.
D. Kamke (1956). Elektronen- und Ionenquellen. *Handbuch der Physik* **33**, 1–122.
W. Kamminga (1973). Numerical calculation of the effective current density of the source for triode electron guns with spherical cathodes. In *Image Processing and Computer-Aided Design in Electron Optics* (P. W. Hawkes, Ed.), 400–415 (Academic Press, London & New York).
W. Kamminga and J. C. Francken (1971). Some properties of triode electron guns with spherical cathodes. *Optik* **33**, 375–398.
N. Kang (1987). Computations on the characteristics of LaB_6 cathode electron guns. In *Proc. Int. Symposium on Electron Optics* (J.-y. Ximen, Ed.), 110–114 (Institute of Electronics, Academia Sinica, Beijing).
N. K. Kang, J. Orloff, L. W. Swanson and D. Tuggle (1981). An improved method for numerical analysis of point electron and ion source optics. *J. Vac. Sci. Technol.* **19**, 1077–1081.
N. K. Kang, D. Tuggle and L. W. Swanson (1983). A numerical analysis of the electric field and trajectories with and without the effect of space charge for a field electron source. *Optik* **63**, 313–331.
P. L. Kanitkar, C. V. Dharmadhikari, D. S. Joag and V. N. Shukla (1976). Field emission studies of the lanthanum hexaboride/tungstem system. *J. Phys. D: Appl. Phys.* **9**, L165–L166.
E. Kasper (1979). On the numerical field calculation in field emission devices. *Optik* **54**, 135–147.
E. Kasper (1981). Numerical design of electron lenses. *Nucl. Instrum. Meth.* **187**, 175–180.
E. Kasper (1982). Field electron emission systems. *Adv. Opt. Electron Microsc.* **8**, 207–260.
E. Kasper (1985). A theory of space charges in thermionic electron guns. *Optik* **71**, 129–134.
E. Kasper and F. Lenz (1966). Theorie der Richtstrahlfunktion für beliebige paraxiale Korpuskularstrahlbündel. *Z. Angew. Phys.* **20**, 177–183.
K. Kasuya, T. Kawasaki, N. Moriya, M. Arai and T. Furutsu (2014a). Magnetic field superimposed cold field emission gun. *J. Vac. Sci. Technol. B* **32**, 031802.
K. Kasuya, T. Kawasaki, N. Moriya, M. Arai and T. Furutsu (2014b). Magnetic-field-superimposed cold field emission gun for 1.2 MV transmission electron microscope. IMC-18, Prague. IT-1-O-1664.
K. Kasuya, S. Katagiri and T. Ohshima (2016). High emission current of 1000 μA at 4×10^{-10} Pa from W < 310 > cold field emitter in electron gun. *J. Vac. Sci. Technol. B* **34**, 042202.
T. Kato, A. Shigetomi, Y. Watakabe, H. Hagiwara and H. Hiraoka (1983). Evaluation of single crystal LaB_6 cathodes. *J. Vac. Sci. Technol. B* **1**, 100–106.
C. Katsuta, A. Takaoka, K. Ura, T. Tomita and Y. Harada (1986). The characteristics of a magnetic-field-immersed pulse field emission gun. ICEM-11, Kyoto. **1**, 267–268.
T. Kawasaki, I. Matsui, T. Yoshida, T. Katsuta, S. Hayashi, T. Onai, T. Furutsu, K. Myochin, M. Numata, H. Mogaki, M. Gorai, T. Akashi, O. Kamimura, T. Matsuda, N. Osakabe, A. Tonomura and K. Kitazawa (2000). Development of a 1 MV field-emission transmission electron microscope. *J. Electron Microsc.* **49**, 711–718.

T. Kawasaki, T. Nakano and K. Hirose (2009). Developing an aberration-corrected Schottky emission SEM and method for measuring aberration. *Microelectron. Eng.* **86**, 1017–1020.
V. M. Kel'man, A. A. Sapargaliev and E. M. Yakushev (1973). The theory of cathode lenses. II. Electrostatic cathode lens with rotational field symmetry. *Zh. Tekh. Fiz.* **43**, 52–60. *Sov. Phys. Tech. Phys.* **18**, 33–37.
A. L. Keller, D. Zeidler and T. Kemen (2014). High throughput data acquisition with a multi-beam SEM. *Proc. SPIE* **9236**, 9236-0B, 6 pp.
T. Kemen, T. Garbowski and D. Zeidler (2015). Multi-beam SEM technology for ultra-high throughput. *Proc. SPIE* **9658**, 9658-07, 6 pp.
D. Kern (1978a). Theoretische Untersuchungen an rotationssymmetrischen Strahlerzeugungssystemen mit Feldemissionsquelle. Dissertation, Tübingen.
D. Kern (1978b). Theoretical investigations on rotationally symmetric guns with field-emission source. ICEM-9, Toronto. **1**, 54–55.
D. Kern, D. Kurz and R. Speidel (1978). Elektronenoptische Eigenschaften eines Strahlerzeugungssystems mit Feldemissionskathode. *Optik* **52**, 61–70.
R. S. Khairnar, P. W. Mahajan, D. S. Joag, A. S. Nigavekar and P. L. Kanitkar (1985). Processing and characterization of LaB_6-coated hairpin cathodes. *J. Vac. Sci. Technol. A* **3**, 398–402.
R. M. Khatapova and V. K. Romanova (1982). Emission stability of carbon field-emission cathodes in sealed instruments. *Zh. Tekh. Fiz.* **52**, 567–569. *Sov. Phys. Tech. Phys.* **27**, 369–370.
R. M. Khatapova, V. K. Romanova, L. L. Demskaya and V. A. Gushchin (1985a). Field-emission cathodes for Kwikscan scanning electron microscopes. *Prib. Tekh. Eksp.* (No. 3), 203–204. *Instrum. Exp. Tech.* **28**, 727–728.
R. M. Khatapova, L. L. Demskaya and V. K. Romanova (1985b). Technology for producing carbon field emitters. *Prib. Tekh. Eksp.* (No. 3), 205–207. *Instrum. Exp. Tech.* **28**, 729–731.
A. Khursheed and N. Karuppiah (2002). A high-resolution mixed field immersion lens attachment for conventional scanning electron microscopes. *Rev. Sci. Instrum.* **73**, 2906–2909.
P. Killes (1985). Solution of Dirichlet problems using a hybrid finite-differences and integral-equation method applied to electron guns. *Optik* **70**, 64–71.
P. Killes (1988). Neuartige Verfahren zur Berechnung rotationssymmetrischer Elektronenstrahlerzeugungssysteme unter Berücksichtigung der Raumladung. Dissertation, Tübingen.
D. H. Kim, M. L. Yu, E. Kratschmer, B. W. Hussey, M. G. R. Thomson and T. H. P. Chang (1995). Miniature Schottky electron source. *J. Vac. Sci. Technol. B* **13**, 2468–2472.
D. H. Kim, M. L. Yu, M. G. R. Thomson, E. Kratschmer and T. H. P. Chang (1997a). Performance of Zr/O/W Schottky emitters at reduced temperatures. *J. Vac. Sci. Technol. B* **15**, 2284–2288.
H. S. Kim, M. L. Yu, M. G. R. Thomson, E. Kratschmer and T. H. P. Chang (1997b). Energy distributions of Zr/O/W Schottky electron emission. *J. Appl. Phys.* **81**, 461–465.
P. T. Kirstein, G. S. Kino and W. E. Waters (1967). *Space-Charge Flow* (McGraw–Hill, New York & London).
S. J. Klauser and E. B. Bas (1979). A miniaturised electron gun for measurements of work function variations by the method of retarding potential in an axial magnetic field. *J. Phys. E: Sci. Instrum.* **12**, 841–844.
C. Klein and E. Platzgummer (2016). MBMW–101: world's 1st high-throughput multi-beam mask writer. *Proc. SPIE* **9985**, 9685-05, 7 pp.
C. Klein, H. Loeschner and E. Platzgummer (2012). 50-keV electron multibeam mask writer for the 11-nm HP mode: first results of the proof-of-concept electron multibeam mask exposure tool. *J. Micro/Nanolithogr. MEMS MOEMS* **11**, 031402, 7 pp.
O. Klemperer and M. E. Barnett (1971). *Electron Optics* (Cambridge University Press, Cambridge).
O. Klemperer and Y. Klinger (1951). On the spherical aberration of electron emission systems. *Proc. Phys. Soc. (Lond.) B* **64**, 231–233.
O. Klemperer and B. J. Mayo (1948). Electron optics and space charge in simple emission systems with circular symmetry. *J. Inst. Elec. Eng.* Part III **95**, 135–141.
A. Knápek, T. Radlička and S. Krátký (2015). Simulation and optimization of a carbon nanotube electron source. *Microsc. Microanal.* **21** (Suppl. 4), 60–65.

W. Knauer (1979a). Analysis of energy broadening in electron and ion beams. *Optik* **54**, 211–234.

W. Knauer (1979b). Boersch effect in electron-optical instruments. *J. Vac. Sci. Technol.* **16**, 1676–1679.

W. Knauer (1981). Energy broadening in field emitted electron and ion beams. *Optik* **59**, 335–354.

G. Knell and E. Plies (1999). Simulation of an improved magnetic–electrostatic detector objective lens for LVSEM. *Nucl. Instrum. Meth. Phys. Res. A* **427**, 99–103.

A. Kojima, N. Ikegami, T. Yoshida, H. Miyaguchi, M. Muroyama, H. Nishino, S. Yoshida, M. Sugata, H. Ohyi, N. Koshida and M. Esashi (2014). Massively parallel electron beam direct writing (MPEBDW) system based on micro-electro-mechanical system (MEMS)/nanocrystalline Si emitter array. *Proc. SPIE* **9049**, 9049–18.

A. Kojima, N. Ikegami, T. Yoshida, N. Ikegami, H. Miyaguchi, M. Muroyama, S. Yoshida, K. Totsu, N. Koshida and M. Esashi (2016). Development of a MEMS electrostatic condenser lens array for nc-Si surface electron emitters of the massive parallel electron beam direct-write system. *Proc. SPIE* **9777**, 9777–12.

Kojima, N. Ikegami, H. Miyaguchi, T. Yoshida, R. Suda, S. Yoshida, M. Muroyama, K. Totsu, M. Esashi and N. Koshida (2017). Simulation analysis of a miniaturized electron optics of the massively parallel electron-beam direct-write (MPEBDW) for multi-column system. *Proc. SPIE* **10144**, 10144-0L.

A. G. Kolosko, S. V. Filippov, P. A. Romanov, E. O. Popov and R. G. Forbes (2016). Real-time implementation of the "orthodoxy test" for conformity of current–voltage characteristics with classical field emission theory. *J. Vac. Sci. Technol. B* **34**, 041802, 7 pp.

T. Komoda (1960). Performances of the gun with a re-entrant shaped Wehnelt cylinder. *J. Electronmicrosc* **8**, 8–12.

P. Kruit (2007). The role of MEMS in maskless lithography. *Microelectron. Eng.* **84**, 1027–1032.

P. Kruit (2016). Electron sources. In *Transmission Electron Microscopy, Diffraction, Imaging and Spectroscopy* (C. B. Carter and D. B. Williams, Eds), 1–15 (Springer, Switzerland).

P. Kruit and G. H. Jansen (1997). Space charge and statistical Coulomb effects. In *Handbook of Charged Particle Optics* (J. Orloff, Ed.), 275–318 (CRC Press, Boca Raton; pp. 341–389 in 2nd edn, 2009).

P. Kruit, M. Bezuijen and J. E. Barth (2006). Source brightness and useful beam current of carbon nanotubes and other very small emitters. *J. Appl. Phys.* **99**, 024315, 7 pp.

G. A. Kudintseva, A. I. Mel'nikov, A. V. Morozov and B. P. Nikonov (1966). *Termoelektronnye Katody* (Energiya, Moscow).

G. A. Kudintseva, G. M. Kuznetsova and V. V. Nikulov (1967). Investigation of the emissive properties of emitters based on lanthanum hexaboride. *Radiotekh. Elektron.* **12**, 857–861. *Radio Eng. Electron. Phys.* **12**, 798–802.

L. Kumar and E. Kasper (1985). On the numerical design of electron guns. *Optik* **72**, 23–30.

H. P. Kuo and B. M. Siegel (1976). A field emission probe forming system with a magnetic pre-accelerator lens. EMSA, Miami Beach. **34**, 522–523.

K. Kurihara (1985). A focused ion beam system for submicron lithography. *J. Vac. Sci. Technol. B* **3**, 41–44.

K. Kuroda and T. Suzuki (1972a). Aperture effect of electrostatic lenses. *Jpn. J. Appl. Phys.* **11**, 1222–1223.

K. Kuroda and T. Suzuki (1972b). Electron trajectory and virtual source of field emission gun of SEM. *Jpn. J. Appl. Phys.* **11**, 1390–1391.

K. Kuroda and T. Suzuki (1974a). Analysis of accelerating lens system in field-emission scanning electron microscope. *J. Appl. Phys.* **45**, 1436–1441.

K. Kuroda and T. Suzuki (1974b). Three-anode accelerating lens system for field emission scanning electron microscope (II). *Appl. Phys. Lett.* **25**, 23–24.

K. Kuroda and T. Suzuki (1975). High currrent efficiency accelerating lens system of field emission scanning electron microscope. *J. Appl. Phys.* **46**, 454–456.

K. Kuroda, H. Ebisui and T. Suzuki (1974a). Three-anode accelerating lens system for the field emission scanning electron microscope. *J. Appl. Phys.* **45**, 2336–2442.

K. Kuroda, Y. Shingu and T. Suzuki (1974b). Effect of eccentricity of anodes in accelerating lens for field emission scanning electron microscope. *Jpn. J. Appl. Phys.* **13**, 2033–2036.

D. Kurz (1979). Untersuchungen an einem Elektronenstrahl-Erzeugungssystem mit Feldemissionskathode. Dissertation, Tübingen.
A. Kyritsakis and J. P. Xanthakis (2015). Derivation of a generalized Fowler–Nordheim equation for nanoscopic field-emitters. *Proc. R. Soc. (Lond.) A* **471**. 2014.0811.
J. M. Lafferty (1951). Boride cathodes. *J. Appl. Phys.* **22**, 299–308.
D. B. Langmuir (1923). The effect of space charge and initial velocities on the potential distribution and thermionic current between plane parallel electrodes. *Phys. Rev.* **21**, 419–435.
D. B. Langmuir (1937). Theoretical limitations of cathode-ray tubes. *Proc. Inst. Radio. Eng.* **25**, 977–991.
R. V. Latham and M. A. Salim (1987). A microfocus cathode ray tube using an externally stabilised carbon-fibre field-emitting source. *J. Phys. E: Sci. Instrum.* **20**, 181–188.
L. Lattard, I. Servin, J. Pradelles, Y. Blancquaert, G. Rademaker, L. Pain, G. de Boer, P. Brandt, M. Dansberg, R. J. A. Jager, J. J. M. Peijster, E. Slot, S. W. H. K. Steenbrink, N. Vergeer and M. J. Wieland (2017). Overlay performance assessment of MAPPER's FLX-1200. *Proc. SPIE* **10144**, 10144-0N.
B. Lau (1981). Untersuchungen an einer Elektronenquelle mit laserbeheizter Kathode. Dissertation, Tübingen.
R. Lauer (1968). Ein einfaches Modell für Elektronenkanonen mit gekrümmter Kathodenoberfläche. *Z. Naturforsch.* **23a**, 100–109.
R. Lauer (1973). Experimentelle Bestimmung der Öffnungsfehlerkonstante von Elektronenkanonen. *Z. Naturforsch.* **28a**, 1937–1945.
R. Lauer (1974). Vergleich zwischen gemessenen und berechneten Emittanz-Diagrammen von Elektronenkanonen. *Z. Naturforsch.* **29a**, 1291–1298.
R. Lauer (1975). Untersuchungen mit der Linsenmethode über den Raumladungseinfluß auf den Richtstrahlwert. *Z. Naturforsch.* **30a**, 1395–1402.
R. Lauer (1976). Emittanz-Diagramme und Bildfehler von Elektronenkanonen. *Z. Naturforsch.* **31a**, 1160–1167.
R. Lauer (1982). Characteristics of triode electron guns. *Adv. Opt. Electron Microsc.* **8**, 137–206.
R. Lauer and K.-J. Hanszen (1966). An electron-gun model for describing the general behaviour of the cross-over data in dependence of the cathode radius. ICEM-6, Kyoto. **1**, 129–130.
R. Lauer and K.-J. Hanszen (1974). Emittance properties of electron guns. ICEM-8, Canberra. **1**, 126–127.
R. R. Law (1937). High current electron gun for projection kinescopes. *Proc. Inst. Radio. Eng.* **25**, 954–976.
J. B. Le Poole (1981). Electron guns, state of the art. *Nucl. Instrum. Meth.* **187**, 241–244.
J. B. Le Poole, J. Kramer and K. D. van der Mast (1972). An electron gun with locally heated cathode. EUREM-5, Manchester. 8–9.
C. Lea (1973). Field emission from carbon fibres. *J. Phys. D: Appl. Phys.* **6**, 1105–1114.
S. H. Lee, B.-s Ahn, J. Choi, I. K. Shin, S. Tamamushi and C.-u. Jeon (2016). The technical consideration of multi-beam mask writer for production. *Proc. SPIE* **9985**, 9985-06, 8 pp.
C. Lejeune and J. Aubert (1980). Emittance and brightness: definitions and measurements. In *Applied Charged Particle Optics* (A. Septier, Ed.), **A**, 159–259 (Academic Press, New York & London). *Adv. Electron. Electron Phys*. Suppl. 13A.
F. Lenz (1957). Theoretischen Untersuchungen über die Ausbreitung von Elektronenstrahlbündeln in rotationssymmetrischen elektrischen und magnetischen Feldern. Habilitationsschrift, Aachen.
F. Lenz (1958). Der Boersch-Effekt und ein Ansatz zu seiner theoretischen Deutung. ICEM-4, Berlin. **1**, 39–40.
K. N. Leung, D. Moussa and S. B. Wilde (1986). Directly heated lanthanum hexaboride cathode. *Rev. Sci. Instrum.* **57**, 1274–1276.
C. Y. Lin, W. T. Chang, W. H. Hsu, W. C. Lai, Y. S. Chen and I. S. Hwang (2014). Design and characterization of a single-atom electron column. IMC-18, Prague. IT-1-P-2975.
W. R. Lin, Y. J. Chuang, C. H. Lee, F. G. Tseng and F. R. Chen (2015). Fabrication and characterization of silicon field emission tips for miniature field emission electron microscope. *Microscopy* **64** (Suppl. 1), i94.
H. J. Linn and K. Pöschl (1968). Numerische Berechnung von Elektronenkanonen. *Arch. Elektrischen Übertragung* **22**, 146–149.
K. H. Loeffler (1969). Energy-spread generation in electron-optical instruments. *Z. Angew. Phys.* **27**, 145–149.

K. H. Loeffler (1970a). A new cathode [LaB_6]. ICEM-7, Grenoble. **2**, 77–78.

K. H. Loeffler (1970b). Corrosion of lanthanum hexaboride emitters. ICEM-7, Grenoble. **2**, 381–382.

K. H. Loeffler and R. H. Hudgin (1970). Energy-spread generation and image deterioration by the stochastic interactions between beam electrons. ICEM-7, Grenoble. **2**, 67–68.

N. C. MacDonald, W. Hofmann, L.-y. Chen and J. H. Das (1995). Micro-machined electron gun arrays (MEGA). *Proc. SPIE* **2522**, 220–229.

I. G. Maloff and D. W. Epstein (1934). Theory of electron gun. *Proc. Inst. Radio. Eng.* **22**, 1386–1411.

S. Mamishin, Y. Kubo, R. Cours, M. Monthioux and F. Houdellier (2017). 200 keV cold field emission source using carbon cone nanotip: application to scanning transmission electron microscopy. *Ultramicroscopy* **182**, 303–307.

K. Marianowski, T. Ohnweiler and E. Plies (2011). Coulomb interactions in a low-voltage focussed ion beam system. *Nucl. Instrum. Meth. Phys. Res. A* **645**, 116–119.

E. E. Martin, J. K. Trolan and W. P. Dyke (1960). Stable, high density field emission cold cathode. *J. Appl. Phys.* **31**, 782–789.

S. Maruse (1960). Vergleichende Untersuchungen der Eigenschaften von Spitzenkathoden und Haarnadelkathoden in Strahlerzeugungssystemen mit negativer Wehneltblende. EUREM-2, Delft. **1**, 73–77.

J. Matsuda, T. Ohba, T. Yamashita and N. Morito (1981). Energy distributions of field emission electron beams emitted from superconducting cathodes [in Japanese]. *Oyo Butsuri* **50**, 502–505.

H. P. Mayer and K.-H. Gaukler (1986). Investigation of a liquid Ga ion source at low emission currents. *J. Phys.* **47** (C7), 365–370.

S. K. Medley, D. A. Gregory, A. R. Sampson and J. A. Gaskin (2010). Optimization of a cold field emission electron gun for a miniaturized scanning electron microscope. 41st Lunar and Planetary Science Conference, The Woodlands (TX). No. 2676.

J. F. Menadue (1974). A low noise field-emission electron gun. ICEM-8, Canberra. **1**, 108–109.

N. M. Miskovsky and P. H. Cutler (1984). Comment on the validity of first-order paraxial theory for electron and ion sources with needle-type or pointed geometry. *Appl. Phys. A* **33**, 43–45.

N. M. Miskovsky, P. H. Cutler and T. E. Feuchtwang (1984). Derivation of a modified paraxial formalism for two-dimensional trajectories in electron and ion sources of non-simple geometries. *Appl. Phys. A* **33**, 113–120.

A. Mohammadi-Gheidari and P. Kruit (2011). Electron optics of multi-beam scanning electron microscope. *Nucl. Instrum. Meth. Phys. Res. A* **645**, 60–67.

A. Mohammadi-Gheidari, C. W. Hagen and P. Kruit (2010). Multi-beam scanning electron microscope: experimental results. *J. Vac. Sci. Technol. B* **28**, C6G5.

G. Möllenstedt and H. Düker (1953). Das Energiespektrum hoher Auflösung von Kathodenstrahlen aus der Gasentladung. *Z. Naturforsch.* **8a**, 79–90.

C. Morita, T. Ohye and H. Shimoyama (1996). Optimization of operating conditions for the FE gun system of HVEM. *J. Electron Microsc.* **45**, 372–379.

H. Moss (1968). Narrow angle electron guns and cathode ray tubes. *Adv. Electron. Electron Phys.* Suppl. 3. 224 pp.

N. Mubanga, M. Tholomier and E. Vicario (1986). Bruit d'un canon à émission de champ. *J. Microsc. Spectrosc. Electron* **11**, 65–79.

E. W. Müller (1937). Versuche zur Theorie der Elektronenemission unter der Einwirkung hoher Feldstärken. *Phys. Z.* **37**, 838–842.

E. W. Müller (1951). Das Feldionenmikroskop. *Z. Phys.* **131**, 136–142.

T. Mulvey (1980). Electron guns and instrumentation. EUREM-7, The Hague. **1**, 46–53.

T. Mulvey (1984). Instrumentation, electron optics and X-ray spectroscopy. *J. Phys.* **45** (C2), 149–154.

B. Mundt (1973). Langzeitige Stromstabilität der Feldelektronenemission aus Wolframspitzen bei 2.10^{-7} Pa und unterschiedlicher Zusammensetzung des Restgases in Abhängigkeit von der Emitterheizung. *Optik* **38**, 351–367.

E. Munro (1972). Design of electrostatic lenses for field-emission electron guns. EUREM-5, Manchester. 22–23.

E. Munro (1973). Computer-aided design of electron lenses by the finite element method. In *Image Processing and Computer-Aided Design in Electron Optics* (P. W. Hawkes, Ed.), 284–323 (Academic Press, London & New York).

E. Munro (1999). Simulation of discrete Coulomb interactions in high-current projection and multi-beam columns. *Proc. SPIE* **3777**, 215–227.

M. Muraki and S. Gotoh (2000). New concept for high-throughput multielectron beam direct write system. *J. Vac. Sci. Technol. B* **18**, 3061–3066.

H. Murata, H. Shimoyama and T. Ohye (2001). Computer simulation of electric field analysis for vertically aligned carbon nanotubes. 1. Simulation method and computing model. *Proc. SPIE* **4510**, 156–162. Pt. 2 is Shimoyama et al. (2001).

L. P. Muray, J. Spallas, C. Stebler, K. Lee, M. Mankos, Y. Hsu, M. Gmur and T. H. P. Chang (2000). Advances in arrayed column lithography. *J. Vac. Sci. Technol. B* **8**, 3099–3104.

L. P. Muray, C. S. Silver and J. P. Spallas (2006). Sub-100-nm lithography with miniature electron beam columns. *J. Vac. Sci. Technol. B* **24**, 2945–2950.

L. P. Muray, J. Spallas and D. Meisburger (2014). On the limits of miniature electron column technology. *Proc. SPIE* **9236**, 9236-0C, 8 pp.

E. L. Murphy and R. H. Good (1956). Thermionic emission, field emission, and the transition region. *Phys. Rev.* **102**, 1464–1473.

K. Nagasao, M. Takebe, W. Ushio, S. Fujita, T. Ohye and H. Shimoyama (2011). Upgraded G-optk program for electron gun characterization. *Nucl. Instrum. Meth. Phys. Res. A* **645**, 321–338.

G. A. Nagy and M. Szilágyi (1974). *Introduction to the Theory of Space-Charge Optics.* (Macmillan, London and Akadémiai Kiado, Budapest); first published as *Bevezetés a Tértöltés-optika Elméletébe.*

S. Nakagawa and T. Yanaka (1975). A highly stable electron probe obtained with LaB_6 cathode electron gun. *Scanning Electron Microsc.*, 19–26.

M. Nakasuji and H. Wada (1980). Single crystal LaB_6 electron gun for variably shaped electron beam optics. *J. Vac. Sci. Technol.* **17**, 1367–1372.

T. H. Newman, R. F. W. Pease and W. DeVore (1983). Dot matrix electron beam lithography. *J. Vac. Sci. Technol. B* **1**, 999–1002.

T. H. Newman, K. E. Williams and R. F. W. Pease (1987). High resolution patterning system with a single bore objective lens. *J. Vac. Sci. Technol. B* **5**, 88–91.

M. A. Noack, E. D. Gibson and J. D. Verhoeven (1980). Brightness of LaB_6 cathodes. *J. Appl. Phys.* **51**, 5566–5567.

L. W. Nordheim (1928). The effect of image force on the emission and reflexion of electrons by metals. *Proc. R. Soc. (Lond.) A* **121**, 626–639.

H. Ohiwa, R. J. Blackwell and B. M. Siegel (1981). Design of an electrostatic ion optical system for microfabrication with 100 Å resolution. *J. Vac. Sci. Technol.* **19**, 1074–1076.

T. Ohno (1971). Measurements of the energy distribution in thermionically emitted electron beams [in Japanese]. *J. Electron Microsc.* **20**, 294–298.

T. Ohno (1972). Energy distribution of electrons from thermionic cathodes with a Wehnelt cylinder. *J. Phys. Soc. Japan* **32**, 1587–1594.

T. Ohno (1974). Effect of emitting area on the energy distribution of thermionic electrons. *J. Electron Microsc.* **23**, 1–7.

T. Ohno (1975). A computer study of the effect of biased Wehnelt cylinder on the energy distribution of electrons. *J. Electron Microsc.* **24**, 59–63.

A. Ohshita, H. Shimoyama and S. Maruse (1973). Field strength at the cathode tip of the point cathode electron gun. *J. Electron Microsc.* **22**, 135–140.

A. Ohshita, H. Shimoyama and S. Maruse (1977). Gun brightness at high electron emission densities. HVEM-5, Kyoto. 65–68.

T. Ohye and Y. Uchikawa (1980). Theoretical and experimental analyses of electron gun characteristics. ICEM-10, Hamburg. **1**, 361–362.

T. Ohye and Y. Uchikawa (1986). Dependence on electrode shapes of brightness characteristics of a thermionic cathode electron gun. ICEM-11, Kyoto. **1**, 281–282.

T. Ohye, H. Murata and H. Shimoyama (1998). An application of improved 3-D boundary charge method to field analysis for a misaligned field emission gun. ICEM-14, Cancún. **1**, 99–100.

T. W. O'Keeffe and R. M. Handy (1967). Resistless fabrication of integrated circuits. International Electron Devices Meeting (IEDM), Washington DC. **13**, 148.

J. Orloff (1984a). A comparison of lanthanum hexaboride, cold field emission and thermal field emission electron guns for low voltage scanning electron microscopy. In *Electron Optical Systems for Microscopy, Microanalysis and Microlithography* (J. J. Hren, F. A. Lenz, E. Munro and P. B. Sewell, Eds), 149–162 (Scanning Electron Microscopy, AMF O'Hare).

J. Orloff (1984b). A comparison of electron guns for high speed electron beam inspection. *Scanning Electron Microsc.*, 1585–1600.

J. Orloff (1986). Development of the ZrO/W thermal field cathode. ICEM-11, Kyoto. **1**, 211–214.

J. Orloff and L. W. Swanson (1979a). A study of some electrostatic gun lenses for field emission. *Scanning Electron Microsc*. Pt. I, 39–44 & 10.

J. Orloff and L. W. Swanson (1979b). An asymmetic electrostatic lens for field-emission microprobe applications. *J. Appl. Phys.* **50**, 2494–2501.

J. Orloff and L. W. Swanson (1982). Some considerations on the design of a field emission gun for a shaped spot lithography system. *Optik* **61**, 237–245.

J. Orloff, L. W. Swanson and J.-z. Li (1985). The prospects of field emission for e-beam inspection. *J. Vac. Sci. Technol. B* **3**, 224–226.

N. I. Osipov (1984). Autoemission cathodes made of carbon fibre for an electron microscope. *Prib. Tekh. Eksp.* No. 5, 199–201. *Instrum. Exp. Tech*. **27**, 1265–1266.

K. Ozaki, T. Ohye, N. Tamura and Y. Uchikawa (1981). Computation of field distribution on the emitter tip using the surface charge method. *J. Electron Microsc.* **30**, 281–291.

K. Ozaki, Y. Uchikawa and S. Maruse (1982). Dependence of brightness characteristics upon point cathode electron gun geometries. *J. Electron Microsc.* **31**, 137–143.

N. V. Parol', B. I. Lazanov, A. A. Golovchenko, N. A. Iofis, B. P. Kovalev and V. F. Zholobova (1984). Lanthanum hexaboride cathodes for electron-beam devices. *Prib. Tekh. Eksp.* No. 5, 146–148. *Instrum. Exp. Tech*. **27**, 1205–1208.

C. Passow (1976). Calculations of the energy spread of an electron beam generated by a high voltage microwave illumination system. EUREM-6, Jerusalem. **1**, 375–376.

H. C. Pfeiffer (1971). Experimental investigation of energy broadening in electron optical instruments. In *Proc. 11th Symposium on Electron, Ion and Photon Beam Technology* (R. F. M. Thornley, Ed.), 239–246 (San Francisco Press, San Francisco).

J. R. Pierce (1949). *Theory and Design of Electron Beams* (Van Nostrand, Princeton & London).

P. Pilod and F. Sonier (1961). Sources d'électrons à grande brillance. *C. R. Acad. Sci. Paris* **253**, 2338–2340.

P. Pilod and F. Sonier (1968). Etude d'un canon à électrons équipé d'une cathode à pointe. *J. Microsc. (Paris)* **7**, 313–322.

M. Pitaval, E. Vicario and G. Fontaine (1973). Field emission gun for SEM. EMAG, Newcastle-upon-Tyne. 60–62.

E. Platzgummer (2010). Maskless lithography and nanopatterning with electron and ion multi-beam projection. *Proc. SPIE* **7637**, 7637-02, 12 pp.

E. Platzgummer, C. Klein and H. Loeschner (2012a). Results of proof-of-concept 50 keV electron multi-beam mask exposure tool (eMET POC). *Proc. SPIE* **8441**, 8441-58, 6 pp.

E. Platzgummer, C. Klein and H. Loeschner (2012b). Printing results of proof-of-concept 50 keV electron multi-beam mask exposure tool (eMET POC). *Proc. SPIE* **8522**, 8522-52, 8 pp.

E. Plies (1994). Electron optics of low-voltage electron beam testing and inspection. Part I: Simulation tools. *Adv. Opt. Electron Microsc.* **13**, 123–242.

M. Ploke (1951). Elementare Theorie der Elektronenstrahlerzeugung mit Triodensystemen. I. Eigenschaften des statischen Feldes der gebräuchlichen Strahlsysteme. *Z. Angew. Phys.* **3**, 441–449.

M. Ploke (1952). Elementare Theorie der Elektronenstrahlerzeugung mit Triodensystemen. II. Stromstärke und Struktur des Elektronenbündels. *Z. Angew. Phys.* **4**, 1–12.

F. L. Plomp (1972). Field emission guns. EUREM-5, Manchester. 2–7.

F. L. Plomp, L. Veneklasen and B. M. Siegel (1968). Development of a field emission electron source for an electron microscope. EUREM-4, Rome. **1**, 141–142.

J. H. Porter, W. Franzen and R. S. Wenstrup (1972). A new analysis of space-charge-limited emission between concentric spheres and concentric cylinders. *J. Appl. Phys.* **43**, 344–354.

R. Prohaska and A. Fisher (1982). Field emission cathodes using commercial carbon fibers. *Rev. Sci. Instrum.* **53**, 1092–1093.

D. J. Pugh and P. D. West (1977). An electron source for a microfocus X-ray tube incorporating a single pole magnetic lens and novel focusing system. EMAG, Glasgow. 29–32.

J. Puretz (1986). Dimensional analysis and energy broadening in particle beams. *J. Phys. D: Appl. Phys.* **19**, L237–L240.

W. Qian, M. R. Scheinfein and J. C. H. Spence (1993). Brightness measurements of nanometer-sized field-emission-electron sources. *J. Appl. Phys.* **73**, 7041–7045.

T. Radlička (2006). Coulomb interaction in ion and electron beams. *Recent Trends* **10**, 61–62.

T. Radlička and B. Lencová (2008). Coulomb interactions in Ga LMIS. *Ultramicroscopy* **108**, 445–454.

H. Rauh and D. Kern (1978). Theoretische Untersuchngen an einem Elektronenstrahlerzeuger mit Spitzenkathode. *Z. Naturforsch.* **33a**, 910–913.

F. H. Read and N. J. Bowring (2002). Accurate calculation of Boersch energy spreading. *Recent Trends* **8**, 11–12.

F. H. Read and N. J. Bowring (2003). Accurate Mont Carlo calculation of Boersch energy and angle spreading. *Rev. Sci. Instrum.* **74**, 2280–2287.

F. H. Read and N. J. Bowring (2004a). Monte Carlo calculation of Boersch energy spreading. *Nucl. Instrum. Meth. Phys. Res. A* **519**, 196–204.

F. H. Read and N. J. Bowring (2004b). Field enhancement factors of random arrays of carbon nanotubes. *Nucl. Instrum. Meth. Phys. Res. A* **519**, 305–314.

F. H. Read and N. J. Bowring (2004c). Simulation of thermionic cathodes. *Nucl. Instrum. Meth. Phys. Res. A* **531**, 407–415.

F. H. Read and N. J. Bowring (2004d). Simulation of electron and ion sources. *Recent Trends* **9**, 61–64.

Y. Ren and P. Kruit (2016). Transmission electron imaging in the Delft multibeam scanning electron microscope 1. *J. Vac. Sci. Technol. B* **34**, 06KF02, 10 pp.

Y. Ren, C. W. Hagen and P. Kruit (2014). High throughput imaging in a multibeam SEM. IMC-18, Prague. IT-8-O-3019.

W. Reusse (1939). Messung der Ladungsverteilung in einem Elektronenstrahl. *Telegraphen- Fernsprech- Funk- und Fernseh-Technik* **28** (Mai), 184–187.

W. Reusse and N. Ripper (1940). Der Einfluß der Raumladung auf die Fokussierung von Kathodenstrahlen. *Telegraphen- Fernsprech- Funk- und Fernseh-Technik* **29** (3), 68–74.

G. H. N. Riddle (1978). Electrostatic einzel lenses with reduced spherical aberration for use in field-emission guns. *J. Vac. Sci. Technol.* **15**, 857–860.

A. G. Rinzler, J. H. Hafner, P. Nikolaev, P. Nordlander, D. T. Colbert, R. E. Smalley, L. Lou, S. G. Kim and D. Tománek (1995). Unraveling nanotubes: field emission from an atomic wire. *Science* **269**, 1550–1553.

E. Röhm (1986a). Berechnung zeitabhängiger elektromagnetischer Felder nach der Integralgleichungsmethode mit der Anwendung auf ein Hochfrequenz-Feldemissions-Elektronenstrahlerzeugungssystem. Dissertation, Tübingen.

E. Röhm (1986b). Berechnung zeitabhängiger Felder mittels der Integralgleichungsmethode und die Anwendung auf ein Hochfrequenzstrahlerzeugungssystem. *Optik* **74**, 99–113.

S. Roques, M. Denizart and F. Sonier (1983a). Tetrode field emission guns for electron microscopy. *Optik* **64**, 51–66.

S. Roques, M. Denizart and F. Sonier (1983b). Optical characteristics of the electron source given by a tetrode field emission gun. *Optik* **64**, 299–312.

H. Rose (2012). *Geometrical Charged-particle Optics*, 2nd edn. (Springer, Berlin; 1st edn, 2009).
H. Rose and R. Spehr (1980). On the theory of the Boersch effect. *Optik* **57**, 339–364.
H. Rose and R. Spehr (1983). Energy broadening in high-density electron and ion beams: the Boersch effect. In *Applied Charged Particle Optics* (A. Septier, Ed.), **C**, 475–530 (Academic Press, New York & London). *Adv. Electron. Electron Phys*. Suppl. 13C.
Yu. V. Roslyakov, L. Yu. Vol'fson and A. N. Kabanov (1974). Triode electron gun with lanthanum hexaboride rod cathodes. *Izv. Akad. Nauk SSSR (Ser. Fiz.)* **38**, 1496–1499. *Bull. Acad. Sci. USSR (Phys. Ser.)* **38** (7), 128–130.
J. Rouse, X. Zhu and E. Munro (1995). Solution of electron optics problems with space charge in 2D and 3D. *Proc. SPIE* **2522**, 375–386.
J. Rouse, X. Zhu, H. Liu and E. Munro (2011). Simulation of Coulomb interaction effects in electron sources. *Nucl. Instrum. Meth. Phys. Res. A* **645**, 310–315.
Y. Saito, Ed. (2010). *Carbon Nanotube and Related Field Emitters: Fundamentals and Applications* (Wiley, Chichester).
K. Saito and Y. Uno (1995). Accurate electron ray tracing for analysis of electron guns immersed in a magnetic-lens field. *Nucl. Instrum. Meth. Phys. Res. A* **363**, 48–53.
K. Saito, H. Morita, N. Shimazu and Y. Uno (1995). A new design for a field emission electron gun immersed in a magnetic-lens field. *Proc. SPIE* **2522**, 180–188.
Y. Saito, K. Yamagishi and K. Yada (2014). Thermal emission properties of GdB_6 cathode. IMC-18, Prague. IT-1-P-2410.
Y. Sakaki and S. Maruse (1958). Über die Arbeitsweise und die elektronenoptischen Eigenschaften der Spitzenkathode. ICEM-4, Berlin. **1**, 9–13.
Y. Sakaki and G. Möllenstedt (1956). Beitrag zur Verwendung von Spitzenkathoden in der Elektronenoptik. *Optik* **13**, 193–200.
Y. Sakaki, S. Maruse, K. Hara, N. Morito and T. Komoda (1956). Pointed filament for electron microscopy and X-ray microscopy. APEM-1, Tokyo. 143–146.
N. Samoto, R. Shimizu, H. Hashimoto, N. Tamura, K. Gamo and S. Namba (1985). A stable high-brightness electron gun with Zr/W-tip for nanometer lithography. I. Emission properties in Schottky- and thermal field-emission regions. *Jpn. J. Appl. Phys.* **24**, 766–771.
M. Scheinfein (1986). High performance two-electrode electron gun lenses: beyond the Butler gun. *Ultramicroscopy* **19**, 225–234.
M. R. Scheinfein, W. Qian and J. C. H. Spence (1993). Aberrations of emission cathodes: nanometer diameter field-emission electron sources. *J. Appl. Phys.* **73**, 2057–2068.
J. E. Schneider, A. W. Baum, G. I. Winograd, R. F. W. Pease, M. McCord, W. E. Spicer, K. A. Costello and V. W. Aebi (1996). Semiconductor on glass photocathodes as high-performance sources for parallel electron beam lithography. *J. Vac. Sci. Technol. B* **14**, 3782–3786.
W. Schottky (1923). Über kalte und warme Elektronenentladungen. *Z. Phys.* **14**, 63–106.
B. W. Schumacher (1976). Radiance and radiant energy density in light optics and electron optics – analogies, differences, and practical consequences. *Optik* **45**, 355–380.
B. W. Schumacher (1982). Characteristic numbers for particle beam sources. *Optik* **62**, 249–254.
U. Schwab and R. Speidel (1987). Der Boersch-Effekt in elektronenoptischen Anordnungen. *Optik* **77**, 141–147.
P. B. Sewell (1980). High brightness thermionic electron guns for electron microscopes. *Scanning Electron Microsc.* **Pt. I**, 11–24.
P. B. Sewell and A. Delâge (1984). Thermionic emission studies of micro-flat single crystal lanthanum hexaboride cathodes. In *Electron Optical Systems for Microscopy, Microanalysis and Microlithography* (J. J. Hren, F. A. Lenz, E. Munro and P. B. Sewell, Eds), 163–170 (Scanning Electron Microscopy, AMF O'Hare).
H. Shimoyama, A. Oshita and S. Maruse (1966). Bias characteristics of the hot cathode electron microscope gun. ICEM-6, Kyoto. **1**, 133–134.

H. Shimoyama, A. Oshita and S. Maruse (1970). The mean brightness of the electron gun. ICEM-7, Grenoble. **2**, 81–82.

H. Shimoyama, A. Ohshita, S. Maruse and Y. Minamikawa (1972a). An application of the LaB_6 cathode gun to the transmission electron microscope. *J. Electron Microsc.* **21**, 119–125.

H. Shimoyama, A. Oshita and S. Maruse (1972b). Relativistic considerations on electron optical brightness. *Jpn. J. Appl. Phys.* **11**, 150–157.

H. Shimoyama, A. Oshita and S. Maruse (1974). Electron optical brightness of T-F emission gun. ICEM-8, Canberra. **1**, 116–117.

H. Shimoyama, K. Nimura, M. Suzuki and S. Maruse (1982). A magnetic-field-superposed electron gun with a point cathode. ICEM-10, Hamburg. **1**, 359–360.

H. Shimoyama, K. Nimura, M. Suzuki and S. Maruse (1983). Magnetic-field-superposed electron gun with a point cathode. *J. Electron Microsc.* **32**, 99–104.

H. Shimoyama, Y. Shimazaki and A. Tanaka (1993). Computer simulation of energetic Boersch effect in the diode region of the field emission gun. *Proc. SPIE* **2014**, 99–103.

H. Shimoyama, H. Murata and T. Ohye (2001). Computer simulation of electric field analysis for vertically aligned carbon nanotubes. 2. Electric field on the nanotube apex. *Proc. SPIE* **4510**, 163–171. Pt. 1 is Murata et al. (2001).

M. Slodowski, H.-J. Doering, W. Dorl and I. A. Stolberg (2010a). Multi-shaped beam proof of lithography. *Proc. SPIE* **7637**, 7637-41, 8 pp.

M. Slodowski, H.-J. Döring, I. A. Stolberg and W. Dorl (2010b). Multi-shaped-beam (MSB): an evolutionary approach for high throughput e-beam lithography. *Proc. SPIE* **7823**. 7823-1J, 8 pp.

M. Slodowski, H.-J. Doering, W. Dorl and I. A. Stolberg (2011). Multi shaped beam: development status and update on lithography results. *Proc. SPIE* **7970**, 7970-0E, 8 pp.

E. Slot, M. J. Wieland, G. de Boer, P. Kruit, G. F. ten Berge, A. M. C. Houkes, R. Jager, T. van de Peut, J. J. M. Peijster, S. W. H. K. Steenbrink, T. F. Teepen, A. H. V. van Veen and B. J. Kampherbeek (2008). MAPPER: high throughput maskless lithography. *Proc. SPIE* **6921**, 6921-1P, 9 pp.

K. C. A. Smith and A. D. G. Cumming (1978). Noise and energy broadening in field emission systems. ICEM-9, Toronto. **1**, 56–57.

T. Someya, T. Goto and M. Watanabe (1966). Study on electron beam formation in a triode electron gun. ICEM-6, Kyoto. **1**, 135–136.

T. Someya, T. Goto, Y. Harada and M. Watanabe (1972a). Development of field emission electron gun for high resolution 100 kV electron microscope. EUREM-5, Manchester. 20–21.

T. Someya, T. Goto, Y. Harada and M. Watanabe (1972b). Development of field emission electron gun for high resolution 100 kV electron microscope. EMSA, Los Angeles. **30**, 430–431.

J. P. Spallas, C. S. Silver, L. Muray, T. Wells and M. El-Gomati (2006). A manufacturable miniature electron beam column. *Microelectron. Eng.* **83**, 984–989.

W. E. Spear (1951). Investigation of electron optical properties of an electrostatic focusing system. *Proc. Phys. Soc. (Lond.) B* **64**, 233–243.

R. Spehr (1984). Analytical treatment of electron probe broadening due to stochastic interaction within the beam. EUREM-8, Budapest. **1**, 53–54.

R. Spehr (1985). Broadening of charged particle microprobes by stochastic Coulomb interactions. *Optik* **70**, 109–114.

R. Spehr and H. Rose (1978). Studies on the Boersch effect in stigmatic and astigmatic focusing. EMSA, San Antonio. **37**, 570–571.

R. Speidel (1965). Elektronenoptischer Mikroschreiber mit magnetischer Strahlablenkung unter elektronenmikroskopischer Arbeitskontrolle. *Optik* **23**, 125–144.

R. Speidel and G. Benner (1982). Field emission system for high beam currents. ICEM-10, Hamburg. **1**, 357–358.

R. Speidel and G. Benner (1986). Elektronenstrahlschreiber mit Feldemissionskathode. *Optik* **73**, 138–145.

R. Speidel and P. Brauchle (1982). Low energy, high current field emission electron gun. ICEM-10, Hamburg. **1**, 355–356.

R. Speidel and P. Brauchle (1987). Elektronenstrahl-Meßgerät mit Feldemissionskathode. *Optik* **77**, 46–54.

R. Speidel and G. H. Gaukler (1968). Energieverteilung der Elektronen aus Spitzenkathoden. *Z. Phys.* **208**, 419–426.

R. Speidel and H. Hirscher (1988). Entwicklung und Untersuchung eines 100 kV-Elektronen-Feldemissions-Strahlers für die Rastermikroskopie. *Optik* **78**, 149–157.

R. Speidel and D. Kurz (1977). Richtstrahlwertmessungen an einem Strahlerzeugungssystem mit Feldemissionskathode. *Optik* **49**, 173–185.

R. Speidel and F. Vorster (1975). Ein Elektronenstrahlerzeugungssystem mit Feldemissionskathode. *Optik* **42**, 383–390.

R. Speidel, D. Kurz and G. H. Gaukler (1979). Energieverteilungen der Elektronen aus einem Strahlerzeugungssystem mit Feldemissionskathode. *Optik* **54**, 257–265.

R. Speidel, U. Behringer, P. Brauchle and W. Franz (1984). Elektronenfeldemission aus glasartigem Kohlenstoff. *Optik* **67**, 47–57.

R. Speidel, P. Brauchle, B. Kramer and U. Schwab (1985). Die Zr-O-W-Feldemissionskathode im Niedertemperaturbereich. *Optik* **71**, 167–172.

C. Spindt, I. Brodie, L. Humphrey and E. Westerberg (1976). Physical properties of thin-film field-emission cathodes with molybdenum cones. *J. Appl. Phys.* **47**, 5248–5263.

C. A. Spindt, C. E. Holland and R. D. Stowell (1983). Field emission cathode array development for high-current-density applications. *Appl. Surf. Sci.* **16**, 268–276.

K. H. Steigerwald (1949). Ein neuartiges Strahlerzeugungs-System für Elektronenmikroskope. *Optik* **5**, 469–478.

W. Stickel (1995). Coulomb interactions in particle beam systems. *Proc. SPIE* **2522**, 340–350.

F. A. Stoelinga, J. B. Le Poole and J. E. Barth (1983). A high brightness, high current electron source. In *Microcircuit Engineering 83* (H. Ahmed, J. R. A. Cleaver and G. A. C. Jones, Eds), 117–124 (Academic Press, London & New York).

A. T. Stokes (1980). Computational analysis of a field emission gun system incorporating a single-pole lens. EUREM-7, The Hague. **1**, 58–59.

A. Strojnik and J. W. Scholl (1975). Some problems in matching the electron source with the imaging system in high voltage electron microscopes. HVEM-4, Toulouse. 31–34.

E. Sugata (1950). The electron gun in the electron microscope. ICEM-2, Paris. **1**, 261–263.

E. Sugata and Y. Kischi (1950). A study of electron guns in the electron microscope [in Japanese]. *Oyo Buturi* [*Jpn. J. Appl. Phys.*] **19**, 81–86.

A. D. Sushkov and S. I. Molokovskii (1972). *Intensivnye Elektronnye i Ionnye Puchki* (Energiya, Leningrad).

L. W. Swanson (1984). Field emission source optics. In *Electron Optical Systems for Microscopy, Microanalysis and Microlithography* (J. J. Hren, F. A. Lenz, E. Munro and P. B. Sewell, Eds), 137–147 (Scanning Electron Microscopy, AMF O'Hare).

L. W. Swanson and A. E. Bell (1973). Recent advances in field electron microscopy of metals. *Adv. Electron. Electron Phys.* **32**, 193–309.

L. W. Swanson and L. C. Crouser (1969). Angular confinement of field electron and ion emission. *J. Appl. Phys.* **40**, 4741–4749.

L. W. Swanson and G. A. Schwind (2009). A review of the cold-field electron cathode. *Adv. Imaging Electron Phys.* **159**, 63–100.

L. W. Swanson and D. Tuggle (1981). Recent progress in thermal field electron source performance. *Appl. Surf. Sci.* **8**, 185–196.

D. W. Swift and W. C. Nixon (1960). The behaviour of a point cathode in a triode electron gun. EUREM-2, Delft. **1**, 69–72.

D. W. Swift and W. C. Nixon (1962). Characteristics of a point cathode triode electron gun. *Br. J. Appl. Phys.* **13**, 288–293.

A. Takaoka and K. Ura (1984). Paraxial rays and aberrations in field emission gun. *Optik* **68**, 107–119.

A. Takaoka and K. Ura (1985). Energy broadening in a pulsed field emission gun by the transit time effect. *J. Phys. D: Appl. Phys.* **18**, 1761–1772.

A. Takaoka and K. Ura (1986). Analysis of space-charge-limited LaB_6 electron gun. *Optik* **75**, 20–25.
A. Takaoka and K. Ura (1987). New calculation method for current density at an arbitrary cross section of electron beam. *J. Electron Microsc.* **36**, 275–282.
A. Takaoka and K. Ura (1990). Trajectory theory of cathode lens with weak surface electric field. *Optik* **84**, 176–182.
A. Takaoka, K. Sato and K. Ura (1986a). Measurement of Boersch effect in a TEM with a pulsed field emission gun. ICEM-11, Kyoto. **1**, 269–270.
A. Takaoka, M. Tsukii and K. Ura (1986b). Analysis of space-charge-limited LaB_6 electron gun. ICEM-11, Kyoto. **1**, 283–284.
A. Takaoka, K. Ura, T. Tomita and Y. Harada (1989). Improvement of beam characteristics by superimposing a magnetic field on a field emission gun. *J. Electron Microsc.* **38**, 83–94.
T. Takigawa, S. Yoshii, I. Sasaki, K. Motoyama and T. Meguro (1980). Emission characteristics for <100>, <110> and <111> LaB_6 cathodes. *Jpn. J. Appl. Phys.* **19**, L537–L540.
T. Takigawa, I. Sasaki, T. Meguro and K. Motoyama (1982). Emission characteristics of single-crystal LaB_6 electron gun. *J. Appl. Phys.* **53**, 5891–5897.
M. Takizawa, H. Komami, M. Kurokawa and A. Yamada (2011). Position accuracy evaluation of multi-column e-beam exposure system. *Proc. SPIE* **7970**, 7970-0B, 8 pp.
K. Tamura, T. Ikuta, R. Shimizu and M. Ichihashi (2008). Performance evaluation of the magnetic field immersion type field emission gun by boundary element method. *Phys. Procedia* **1**, 35–42.
T.-t. Tang (1983). Monte Carlo simulation of discrete space charge effects in electron beam lithography systems. *Optik* **64**, 237–249.
T.-t. Tang (1987). Statistical dynamics theory of the space charge effects in a charged particle beam. *Optik* **76**, 38–43.
T.-t. Tang (1991). Study on Boersch effect in a field emission gun. *Optik* **86**, 149–154.
T.-t. Tang (1996). Modeling and design of space charge lenses/aberration correctors for focused ion beam systems. *J. Vac. Sci. Technol. B* **14**, 80–84.
V. P. Taranenko (1964). *Elektronnye Pushki* (Tekhnika, Kiev).
B. Thiel, M. Lercel, B. Bunday and M. Malloy (2014). Assessing the viability of multi-electron beam wafer inspection for sub-20 nm defects. *Proc. SPIE* **9236**, 9236-0E.
H. Tochigi, K. Sonehara and I. Tanaoka (1962). An application of oxide-cored cathode to telefocal electron gun for electron microscope. ICEM-5, Philadelphia. **1**, KK-13.
A. Tonomura and T. Komoda (1970). Field emission electron gun for electron microscope. ICEM-7, Grenoble. **2**, 75–76.
J. K. Trolan and W. P. Dyke (1958). Recent progress in field emission at high current densities. ICEM-4, Berlin. **1**, 20–25.
M. Troyon (1976). Use of a field emission gun in transmission electron microscopy. Improvement of phase contrast transfer owing to its low energy spread. *Optik* **46**, 439–450.
M. Troyon (1980a). High current efficiency field emission gun system incorporating a preaccelerator magnetic lens. Its use in CTEM. *Optik* **57**, 401–419.
M. Troyon (1980b). A magnetic field emission probe forming system. EUREM-7, The Hague. **1**, 56–57.
M. Troyon (1984a). Canon à émission de champ à lentille magnétique préaccélératrice. *J. Microsc. Spectrosc. Electron* **9**, 127–129.
M. Troyon (1984b). A survey of illuminating systems and electron guns in E.M. EUREM-8, Budapest. **1**, 11–20.
M. Troyon (1986). Magnetic field superimposed field emission gun. ICEM-11, Kyoto. **1**, 231–234.
M. Troyon (1988). Energy spread of different electron beams. Part II: Field emission electron beams. *J. Microsc. Spectrosc. Electron* **13**, 49–64.
M. Troyon (1989a). New field emission gun with energy filtering effect. *J. Appl. Phys.* **66**, 1–4.
M. Troyon (1989b). Magnetic field emission gun with zirconiated emitter. *J. Electron Microsc. Tech.* **11**, 191–195.

M. Troyon and J.-y. Jiang (1984). Energy spread measurement in field electron microscopy. *J. Phys.* **45** (C2), 155–156.

M. Troyon and A. Laberrigue (1977). A field emission gun with high beam current capability. *J. Microsc. Spectrosc. Electron* **2**, 7–11.

M. Troyon and P. Zinzindohoué (1986). Energy spread of different thermoionic electron beams. ICEM-11, Kyoto. **1**, 273–274.

M. Troyon, N. Bonnet and F. Payen (1972). Propriétés optiques et aberrations d'un canon à émission de champ pour la microscopie électronique à 75 et 100 kV. *Rev. Phys. Appl.* **7**, 3–9.

M. Troyon, P. Gallion and A. Laberrigue (1976). In-line Fraunhofer holography: advantages of field emission gun. EUREM-6, Jerusalem. **1**, 344–345.

T. Tsukamoto, T. Gunji, K. Hojou and K. Kanaya (1982). The electron optical properties of a special cathode deposited with LaB_6 films made by ion beam sputter deposition for the high resolution scanning electron microscopy. ICEM-10, Hamburg. **1**, 365–366.

Y. Uchikawa, T. Ohye and S. Maruse (1977). A new method of electron gun design. HVEM-5, Kyoto. 69–72.

Y. Uchikawa, T. Ohye and S. Maruse (1978). Computer analysis of electron gun characteristics by surface charge method. ICEM-9, Toronto. **1**, 64–65.

Y. Uchikawa, K. Gotoh and T. Ohye (1981). Improved surface charge method. *Denki Gakkai Ronbunshi* **101A**, 263–270. *Elec. Eng. Japan* **101** (3), 8–13.

Y. Uchikawa, K. Ozaki and T. Ohye (1983). Electron optics of point cathode electron gun. *J. Electron Microsc.* **32**, 85–98.

K. Ura and A. Takaoka (1982). Paraxial rays and aberrations in field emission diode. ICEM-10, Hamburg. **1**, 309–310.

K. Ura and A. Takaoka (1986). Trajectory theory of field emission gun. *J. Electron Microsc.* **35**, 1–8.

K. Ura, H. Fujioka and T. Hosokawa (1978). Picosecond pulse stroboscopic scanning electron microscope. *J. Electron Microsc.* **27**, 247–252.

M. J. van Bruggen, B. van Someren and P. Kruit (2004). Electron microlenses and microlens arrays. *Recent Trends* **9**, 17–18.

M. J. van Bruggen, B. van Someren and P. Kruit (2005). Development of a multi-electron beam source for sub-10 nm electron beam induced deposition. *J. Vac. Sci. Technol. B* **23**, 2833–2839.

M. J. van Bruggen, B. van Someren and P. Kruit (2006a). Use of a 'foil corrector' in a multibeam source: correction of off-axis macrolens aberrations. *Recent Trends* **10**, 69–70.

M. J. van Bruggen, B. van Someren and P. Kruit (2006b). Aberration model of a multibeam scanning microscope for electron beam-induced deposition. *Scanning* **28**, 42–47.

C. van den Berg, G. de Boer, S. Boschker, E. A. Hakkennes, G. Holgate, M. Hoving, R. Jager, J. J. Koning, V. Kuiper, Y. Ma, I. L. van Mil, H. W. Mook, T. Ooms, T. van de Peut, S. Postma, M. Sanderse, P. Scheffers, E. Slot, A. Tudorie, A. M. C. Valkering, N. Venema, N. Vergeer, A. Weirsma, S. Woutersen, M. J. Wieland and B. J. Kampherbeek (2011). Scanning exposures with a MAPPER multibeam system. *Proc. SPIE* **7970**, 7970-0D, 9 pp.

M. H. L. M. van den Broek (1986a). Calculation of the radius of the emitting area and the current in triode electron guns. *J. Phys. D: Appl. Phys.* **19**, 1389–1399.

M. H. L. M. van den Broek (1986b). Experimental emittance diagrams of triode electron guns. *J. Phys. D: Appl. Phys.* **19**, 1401–1419.

K. van der Mast (1981). A field emission source for the EM400 transmission electron microscope. *Norelco Reporter* **28** (1), 1–10.

K. van der Mast (1983). Field emission, developments and possibilities. *J. Microsc. (Oxford)* **130**, 309–324.

K. van der Mast, J. E. Barth and J. B. Le Poole (1974). A continuously renewed laser heated tip in a T.F. emission gun. ICEM-8, Canberra. **1**, 120–12.

K. van der Mast, G. H. Jansen and J. E. Barth (1985). The shower-beam concept. *Microelectron. Eng.* **3**, 43–51.

G. G. P. van Gorkom and A. M. E. Hoeberechts (1984). An efficient silicon cold cathode for high current densities. I. Experimental data and main results. *Philips J. Res.* **39**, 51–60.

G. G. P. van Gorkom and A. M. E. Hoeberechts (1986a). An efficient silicon cold cathode for high current densities. II. Comparison with theory and discussion. *Philips J. Res.* **41**, 343–384.

G. G. P. van Gorkom and A. M. E. Hoeberechts (1986b). Performance of silicon cold cathodes. *J. Vac. Sci. Technol. B* **4**, 108–111.

J. M. J. van Leeuwen and G. H. Jansen (1983). Statistical limitations in electron beam lithography. I. Theory. *Optik* **65**, 179–207.

A. van Oostrom (1962). Field emission cathodes. *J. Appl. Phys.* **33**, 2917–2922.

B. van Someren, M. J. van Bruggen, Y. Zhang, C. Hagen and P. Kruit (2006). Multibeam electron source using MEMS electron optical components. *J. Phys. Conf. Ser.* **34**, 1092–1097.

A. H. V. van Veen, C. Hagen, J. E. Barth and P. Kruit (2001). Reduced brightness of the ZrO/W Schottky electron emitter. *J. Vac. Sci. Technol. B* **19**, 2038–2044.

R. Vanselow (1973). Field electron emission from an aluminum oxide covered tungsten {112} plane at tempertaures up to 1700°K. *Appl. Phys.* **2**, 229–235.

V. A. Vasin and V. A. Nevrovskii (1979). Electric field distribution in a diode with a pointed cathode. *Zh. Tekh. Fiz.* **49**, 110–116. *Sov. Phys. Tech. Phys.* **24**, 62–66.

J. A. Venables and G. D. Archer (1980). On the design of F.E.G.–S.E.M columns. EUREM-7, The Hague. **1**, 54–55.

L. H. Veneklasen (1972). Some general considerations concerning the optics of the field emission illumination system. *Optik* **36**, 410–433.

L. H. Veneklasen (1973). Generalizing the field emission illumination system. EMSA, New Orleans. **31**, 292–293.

L. H. Veneklasen and B. M. Siegel (1970). A field emission illuminating system for transmission microscopy. ICEM-7, Grenoble. **2**, 87–88.

L. H. Veneklasen and B. M. Siegel (1972a). Oxygen-processed field emission source. *J. Appl. Phys.* **43**, 1600–1604.

L. H. Veneklasen and B. M. Siegel (1972b). A field-emission illumination system using a new optical configuration. *J. Appl. Phys.* **43**, 4989–4996.

T. Verduin (2017). Quantum noise effects in e-beam lithography and metrology. Dissertation, Delft.

T. Verduin, B. Cook and P. Kruit (2011). Influence of gun design on Coulomb interactions in a field emission gun. *J. Vac. Sci. Technol. B* **29**, 06F605.

S. F. Vogel (1970). Pyrolytic graphite in the design of a compact inert heater of a lanthanum hexaboride cathode. *Rev. Sci. Instrum.* **41**, 585–587.

R. Vogt (1972). Richtstrahlwert und Energieverteilung der Elektronen aus einem Elektronenstrahlerzeuger mit LaB_6-Kathode. *Optik* **36**, 262–267.

B. von Borries (1948). Die energetischen Daten und Grenze der Übermikroskopie. *Optik* **3**, 321–377 & 389–412.

B. von Borries and E. Ruska (1939). Versuche, Rechnung und Ergebnisse zur Frage des Auflösungsvermögens beim Übermikroskops. *Z. Tech. Phys.* **20**, 225–235.

F. Watari and K. Yada (1986). Photoemission from LaB_6 cathode using an excimer laser. ICEM-11, Kyoto. **1**, 261–262.

E. E. Watson (1927). Dispersion of an electron beam. *Philos. Mag.* **3**, 849–853.

L. Wegmann and M. Gribi (1956). Richtstrahlwerte der kalten Kathode. EUREM-1, Stockholm. 41–42.

A. Wehnelt (1901). Strom- und Spannungsmessungen an Kathoden in Entladungsröhren. Dissertation, Erlangen–Nürnberg.

A. Wehnelt (1903). Uber Kathodenstrahlen an Glühenden Kathoden. *Verhandlungen der Deutschen Physikalischen Gesellschaft* **5** (14), 255–258.

A. Wehnelt and F. Jentzsch (1909). Über die Energie der Elektronenemission glühender Körper. *Ann. Phys. (Leipzig)* **28** (333), 537–552.

A. Weidenhausen, R. Spehr and H. Rose (1985). Stochastic ray deflections in focused charged particle beams. *Optik* **69**, 126–134.

U. Weidenmueller, H.-J. Doering, R. Jaritz, D. Melzer and A. Stoeckel (2010). Multi-shaped beam data preparation. *Proc. SPIE* **7545**, 7545-06, 8 pp.

R. Weyßer (1983a). Feldberechnung in rotationssymmetrischen Elektronenstrahlerzeugern mit Spitzenkathode unter Berücksichtigung von Raumladungen. Dissertation, Tübingen.

R. Weyßer (1983b). Feldberechnung in rotationssymmetrischen Elektronenstrahlerzeugern mit Spitzkathode und Raumladungen. *Optik* **64**, 143–156.

E. T. Whittaker and G. N. Watson (1927). *A Course of Modern Analysis*, 4th edn (Cambridge University Press, Cambridge).

M. J. Wieland, G. de Boer, G. F. ten Berge, R. Jager, T. van de Peut, J. J. M. Peijster, E. Slot, S. W. H. K. Steenbrink, T. F. Teepen, A. H. V. van Veen and B. J. Kampherbeek (2009). MAPPER: high-throughput maskless lithography. *Proc. SPIE* **7271**, 7271-0O, 8 pp.

M. J. Wieland, G. de Boer, G. F. ten Berge, M. van Kervinck, R. Jager, J. J. M. Peijster, E. Slot, S. W. H. K. Steenbrink, T. F. Teepen and B. J. Kampherbeek (2010). MAPPER: high-throughput maskless lithography. *Proc. SPIE* **7637**, 7637-0F, 10 pp.

J. C. Wiesner (1970). Point cathode electron sources. *University of California at Berkeley Report*, No. ERL-70-6,

J. C. Wiesner (1973). Characteristics and applications of pointed cathodes in scanning electron microscopes. *Scanning Electron Microsc.* Pt. I, 33–40.

J. C. Wiesner and T. E. Everhart (1969). Point cathode electron source. EMSA, St Paul. **27**, 174–175.

J. C. Wiesner and T. E. Everhart (1970). Electron guns using pointed cathodes. ICEM-7, Grenoble. **2**, 85–86.

J. C. Wiesner and T. E. Everhart (1973). Point-cathode electron sources – electron optics of the initial diode region. *J. Appl. Phys.* **44**, 2140–2148; Errata and addendum. *ibid.* **45** (1974) 2797–2798.

A. P. Wilska (1970). Electron gun for incoherent beams. ICEM-7, Grenoble. **2**, 83–84.

E. E. Windsor (1969). Construction and performance of practical field emitters from lanthanum hexaboride. *Proc. Inst. Elec. Eng.* **116**, 348–350.

O. Winkler (1988). Tungsten hairpin cathodes with longer lifetimes. *Optik* **78**, 111–116.

R. F. Wolter and K. Sanders (1970). Electron source for high-resolution video recording using directly heated lanthanum hexaboride emitter. EMSA, Houston. **28**, 356–357.

R. F. Wolter, R. M. Schneider, H. J. Roalson and S. J. Rostocki (1970). An electron gun for high-resolution image recording. ICEM-7, Grenoble. **2**, 79–80.

R. J. Woolf and D. C. Joy (1971). Quantitative assessment of pointed filaments as bright electron sources. EMAG, Cambridge. 34–37.

Ju. W. Worobjew [Yu. V. Vorob'ev] and W. A. Shukov [V. A. Zhukov] (1972). Theorie der Gestaltung der dünnsten Elektronenbündel. EUREM-5, Manchester. 26–27.

R. E. Worsham, J. E. Mann and E. G. Richardson (1972). A field emission gun. EMSA, Los Angeles. **30**, 426–427.

J. Worster (1969a). Focal properties and aberrations in the cathode region of a field emission electron gun. *Optik* **29**, 498–505.

J. Worster (1969b). The brightness of electron beams. *J. Phys. D: Appl. Phys.* **2**, 457–462.

J. Worster (1969c). The brightness of electron emission systems. *J. Phys. D: Appl. Phys.* **2**, 889–893.

J. Worster (1969d). Focal properties and spherical aberration of a field emission electron gun. *Int. J. Electron.* **27**, 49–58.

J. Worster (1970). Digital computer studies of electron guns for electron microscopes. *Int. J. Electron.* **28**, 117–128.

K. Yada (1982a). A new preparation method of refractory carbides and their thermionic emission properties. *J. Electron Microsc.* **31**, 349–359.

K. Yada (1982b). A new preparation method of carbide emitters and their characteristics. ICEM-10, Hamburg. **1**, 367–368.

K. Yada (1986). Researches of cathode materials for thermionic emission. ICEM-11, Kyoto. **1**, 227–230.

K. Yada and Y. Saito (2014). AC-voltage operated Schottky electron source. IMC-18, Prague. IT-1-P-2325.

K. Yada and H. Shimoyama (1985). Brightness characteristics of carbide emitters for electron microscopy. *J. Electron Microsc.* **34**, 147–155.
M. Yamabe, Y. Furukawa and T. Inagaki (1984). Electron emission from <100> LaB_6 cathodes with large cone angles and flat tips. *J. Vac. Sci. Technol. A* **2**, 1361–1364.
Y. Yamamoto and T. Miyokawa (1998). Emission characteristics of a conical field emission gun. *J. Vac. Sci. Technol. B* **16**, 2871–2875.
H. Yamazaki (1969). On the chromatic aberration constant of a pointed cathode gun. *Bull. Electrotech. Lab.* **33**, 1256–1258.
S. Yamazaki, H. Kawamoto, K. Saburi, H. Nakatsuka and R. Buchanan (1984). Improvement in scanning electron microscope gun brightness at low kV using an intermediate extraction electrode. *Scanning Electron Microsc.* Pt. I, 23–28.
H. Yasuda, S. Arai, J.-i Kai, Y. Ooae, T. Abe, Y. Takahashi, S. Hueki, S. Maruyama, S. Sago and K. Betsui (1993). Fast electron beam lithography system with 1024 beams individually controlled by blanking aperture array. *Jpn. J. Appl. Phys.* **32**, 6012–6017.
H. Yasuda, T. Haraguchi and A. Yamada (2004). A proposal of MCC (multi-column cell with lotus root lens) system to be used as a mask-making e-beam tool. *Proc. SPIE* **5567**, 911–921.
H. Yasuda, A. Yamada and M. Yamabe (2008). Multi-column cell (MCC) e-beam exposure system for mask writing. *Proc. SPIE* **7028**, 7028-oB, 9 pp.
H. Yasuda, A. Yamada and M. Yamabe (2009). Present status of multi-column cell exposure system for mask writing. *Proc. SPIE* **7379**, 7379-18, 7 pp.
A. Yonezawa, S. Nakagawa and M. Suzuki (1977). An application of high brightness LaB_6 cathode gun to JEM-100CX. EMSA, Boston. **35**, 62–63.
A. Yonezawa, S. Nakagawa and M. Suzuki (1979). An application of the LaB_6 cathode gun to the transmission electron microscope. *J. Electron Microsc.* **28**, 43–45.
A. Yonezawa, M. Maruo, T. Takeuchi, S. Morita, A. Noguchi, O. Takaoka, M. Sato and B. Wannberg (2002). Single pole-piece objective lens with electrostatic bipotential lens for SEM. *J. Electron Microsc.* **51**, 149–156.
R. D. Young (1959). Theoretical total-energy distribution of field-emitted electrons. *Phys. Rev.* **113**, 110–114.
R. D. Young and E. W. Müller (1959). Experimental measurement of the total-energy distribution of field-emitted electrons. *Phys. Rev.* **113**, 115–120.
S. Zaima, M. Sase, H. Adachi and Y. Shibata (1978). Measurements of energy spread of thermal field-emitted electron flow from tungsten. *J. Phys. D: Appl. Phys.* **11**, L179–L180.
S. Zaima, M. Sase, H. Adachi, Y. Shibata, C. Ohshima, T. Tanaka and S. Kawai (1980). Spread of total energy distribution of thermal field-emitted electrons from LaB_6 single crystal needles. *J. Phys. D: Appl. Phys.* **13**, L47–L49.
S. Zaima, H. Adachi and Y. Shibata (1984). Promising cathode materials for high brightness electron beams. *J. Vac. Sci. Technol. B* **2**, 73–78.
J. Zelinka, M. Oral and T. Radlička (2015). Simulation of space charge effects in electron optical system based on the calculation of current density. *Microsc. Microanal.* **21** (Suppl. 4), 246–251.
Y. Zhang (2008). A 100-electron-beam source from a high brightness Schottky emitter for fast patterning applications. Dissertation, Delft.
Y. Zhang and P. Kruit (2007). High brightness 100-electron-beam source for high-resolution applications. *J. Vac. Sci. Technol. B* **25**, 2239–2244.
Y. Zhang and P. Kruit (2008). Design of a high brightness multi-electron-beam source. *Phys. Procedia* **1**, 553–563.
Y. Zhang, C. T. H. Heerkens, M. J. van Bruggen and P. Kruit (2006). Integrated multi-electron-beam blanker array for sub-10-nm electron beam induced deposition. *J. Vac. Sci. Technol. B* **24**, 2857–2860.
Y. Zhang, J. E. Barth and P. Kruit (2008). Electron optics of microlenses with inclined beams. *J. Vac. Sci. Technol. B* **26**, 655–660.

H. Zhang, J. Tang, J. Yuan, Y. Yamauchi, T. T. Suzuki, N. Shinya, K. Nakajima and L.-c. Qin (2016). An ultrabright and monochromatic electron point source made of LaB_6 nanowire. *Nature Nanotechnol.* **11**, 273–279.

J.-y. Zhao, T.-t. Tang, Y.-f. Kang and W.-j. Sun (2012). Study on rotation-free combined immersion magneto-electrostatic lenses. *Optik* **123**, 1233–1235.

V. A. Zhukov and K. A. Kalabushev (1983). The Boersch effect and resolution in electron optical systems. *Zh. Tekh. Fiz.* **53**, 906–912. *Sov. Phys. Tech. Phys.* **28**, 578–582.

V. A. Zhukov and K. A. Kalabushev (1984). Magnitude of the Boersch effect in three-electrode electron guns. *Zh. Tekh. Fiz.* **54**, 2279–2283. *Sov. Phys. Tech. Phys.* **29**, 1339–1341.

B. Zimmermann (1969). Energy broadening in accelerated electron beams by Coulomb interactions. *In Rec. Tenth Symposium Electron, Ion and Laser Beam Technology* (L. Marton, Ed.), 297–304 (Gaithersburg).

B. Zimmermann (1970). Broadened energy distributions in electron beams. *Adv. Electron. Electron Phys.* **29**, 257–312.

P. Zinzindohoué (1986). Experimental investigation of energy broadening in thermal field emission electron beams. *Optik* **74**, 131–133.

P. Zinzindohoué and M. Troyon (1986). Energy spread of different field emission electron beams. ICEM-11, Kyoto. **1**, 271–272.

W. Zuidema, Y. Ren, J. Hoogenboom, C. W. Hagen and P. Kruit (2016). Transmission imaging of biological tissue with the Delft multi-beam SEM. EMC-16, Lyon. **1**, 394–395.

Part X, Chapters 51–53

Only a very small part of the relevant literature is cited in the text of Part X. The lists that follow give some guidance to the field but we stress again that these are strongly biased in favour of theoretical papers at the expense of publications on applications of these instruments.

Magnetic Prisms

For much additional information about the earlier literature, see Livingood (1969) and the books edited by Siegbahn (1955, 1965). The papers listed here are mostly concerned with theoretical aspects of linear image formation, aberrations and the effect of fringing fields in various types of prisms. Only a few descriptions of full spectrometer designs are included, most of which are celebrated historical papers. In some cases, such as the publications of the group formerly headed by the late V.M. Kel'man in the Institute of Nuclear Physics in Alma-Ata, few original papers are listed because full lists are available in recent books or review articles by the same authors.

The surviving references are as follows: Afanas'ev and Gol'dshtein (1968), Afanas'ev et al. (1963a,b), Alekseevskii et al. (1955), Amadori and Wollnik (1971), Aspelund (1975), Aucouturier and Leboutet (1970), Bainbridge (1949), Basargin (1966, 1967, 1968, 1969), Bastard and Lafoucrière (1958), Beiduk and Konopinski (1948), Boerboom (1958, 1964, 1970), Boerboom et al. (1959), Bosi (1967, 1970), Bounin (1967, 1971a, 1971b), Carey (1987a), Cartan (1937a,b, 1938), Coggeshall (1947), Cross (1951), Darlington (1980), Dempsey (1955), Ehrenberg and Jennings (1952), Enge (1963), Fedoseev (1968a,b, 1970a,b,c,d), Gall' and Sachenko (1980), Glikman (1984), Glikman et al. (1977a,b, 1985), Grümm (1953/54), Herzog (1950/51), Hintenberger (1948a,b, 1949, 1951), Hintenberger and König (1957, 1958), Hintenberger et al. (1955), Hu (1987), Ikegami (1958), Ioanoviciu (1970, 1973b), Ioanoviciu et al. (1972, 1973), Ismagulova and Rastorguev (1984), Jennings (1952), Johnson and Nier (1953), Judd and Bludman (1957), Kekk (1962), Kel'man and Rodnikova (1951), Kerwin (1949), Kerwin and Geoffrion (1949), Khurgin (1939), König and Hintenberger (1957, 1958), Korsunskii et al. (1944), Kosiara (1976), Krahl et al. (1981), Langenbeck (1987), Lee-Whiting (1966a,b), Lee-Whiting and Taylor (1957), Leithäuser (1904), Ludwig (1967), Malov (1985a,b), Malov and Trubacheev (1981), Malov et al. (1965a,b, 1975), Matsuda and Matsuo (1971), Matsuda and Wollnik (1970), Matsuo and Matsuda (1971), Musumeci (1950, 1952), Nakai (1975, 1977), Oikawa et al. (1986), Pavinskii (1954), Pearce-Percy (1976), Perez et al. (1975), Ploch and Walcher (1950), Richardson (1947), Rosenblum (1950), Rüdenauer (1970), Rüdenauer and Viehböck (1965, 1966), Sachenko (1980), Sachenko and Fridlyanskii (1980), Saulit (1954, 1956), Scheinfein and Isaacson (1984), Shanker (1987), Shull and Dennison (1947), Siegbahn and Svartholm (1946), Svartholm (1950), Syso(j)ev and Samsonov (1970a,b), Takeshita (1966a,b,c, 1967), Tasman and Boerboom (1959, 1960), Tasman et al. (1959, 1960), Tsoupas et al. (1987), Verster (1950), Voorhies (1955), Wachsmuth et al. (1959a,b), Walen (1957), Wollnik (1965, 1967a,b), Wollnik and Ewald (1965), Wooster (1927), Ximen and Shao (1985) and Yagi (1964, 1965, 1966). General relations between the primary aberration coefficients are derived by Meinel and Thiem (1986).

Electrostatic Prisms

The number of papers devoted principally to the paraxial optics and aberrations of electrostatic prisms appears to be smaller than that concerned with magnetic prisms from the list below but this is principally because we have somewhat arbitrarily excluded most of the vast number of papers that deal with reflecting structures. These are commonly referred to as mirrors but they are mirrors in which the angle of incidence is large and the electron or ion speed never becomes very small. The problems raised in Chapters 18 and 28 hence do not occur. Such mirrors are surveyed in the textbook of Afanas'ev and Yavor (1978) and the general optical properties are of course dictated by the overall symmetry, not by the particular electrode configuration. The remaining references are as follows:

Afanas'ev and Yavor (1972a,b,c, 1975b), Albrecht (1956), Arnow (1976), Boerboom (1960, 1976, 1987a), Bosi (1972, 1978), de Celles (1974), Chen and Boerboom (1982), Decreau et al. (1972, 1975), Ewald (1959a,b), Ewald and Liebl (1955, 1957), Ewald and Sauermann (1956), Ewald et al. (1959), Frank (1976), Glikman et al. (1973, 1976a,b, 1977a,b, 1978, 1985), Grümm (1953/54), Hafner et al. (1968), Herzog (1934, 1940), Hintenberger and König (1957, 1958), Hughes and Rojansky (1929), Ioanoviciu (1982), Johnson and Nier (1953), König and Hintenberger (1957, 1958), Kovalenko and Polenov (1974), Liebl (1958, 1976), Liebl and Ewald (1957a,b, 1959a,b), Liebl and Wachsmuth (1959), Matsuda (1961, 1971, 1974, 1975), Matsuda and Fujita (1975), Matsuo et al. (1972), Paolini and Theodoris (1967), Roy and Carette (1971), Sar-El (1966, 1967, 1968, 1971, 1972), Takeshita (1966a–c, 1967), Theodoris and Paolini (1968, 1969), Wollnik (1965, 1967a,c, 1968), Wollnik and Ewald (1965) and Young et al. (1987).

Crossed-Field Devices

The best-known of these devices is the filter introduced by Wien (1897) in which the particles that are intended to pass through remain in the vicinity of a straight optic axis. More generally, however, the axis may be curved, typically circular. The following list is limited to relatively recent studies of the optics of these configurations. We recall that Chapter 38, The Wien Filter, is devoted wholly to these filters.

Andersen (1967), Andersen and Le Poole (1970), Andersen and Kramer (1972), Batson (1985, 1986), Boersch et al. (1964), Collins (1973), Curtis and Silcox (1971), Holmlid (1975), Hurd (1987), Ioanoviciu (1973a, 1974), Ioanoviciu and Cuna (1974, 1977), Legler (1963), Nakabushi and Sakurai (1983), Nakabushi et al. (1983a), Pearce-Percy (1978), Rose (1987b), Seliger (1972), Solovyev and Tolstoguzov (1987), Tang (1986), Tsuno et al. (1988a,b, 1989), Ximen (1980) and Ximen and Chen (1982a,b). Wien filters are surveyed in depth by Tsuno and Ioanoviciu (2013).

Multipoles

In ion optics, quadrupoles, sextupoles and higher-order multipoles are used mainly as correcting elements; the corresponding fields may be produced by shaping the endfaces of prisms or by separate structures with numerous magnetic poles or electrodes. The publications on these elements frequently consider more than one family of multipoles and the following categories should therefore be regarded as only approximate. For quadrupoles, we refer to the bibliographies of Chapter 19, 29 and 39 and to Boerboom et al. (1976), Matsuda and Wollnik (1972), Matsuo et al. (1977) and Yagi (1964, 1965, 1966). Sextupoles are considered by Boerboom (1972), Taya and Matsuda (1971), Evseeva and Yukhvidin (1980) and Guignard and Hagel (1986). Other multipoles are analysed by Boerboom (1987b), Boerboom et al. (1985), Haider et al. (1982), Matsuo et al. (1982), Nakabushi and Matsuo (1982), Tang (1982c), White et al. (1987) and Wollnik (1972).

General Theory and Computer Programs

A number of rather general papers on the theory of systems with curved axes are more conveniently classified apart. We draw attention in particular to the series of papers by Geerk (1966, 1975, 1984, 1985, 1986); an early paper by Hutter (1945); surveys by Ioanoviciu (1988), Rose (1987a), Brown and Servranckx (1987) and Servranckx and Brown (1987); and general papers by Malov (1985a,b), Rose and Petri (1971), Ismagulova and Rastorguev (1984), Dormont (1959), Zhou (1984) and Zhou et al. (1987, 1988a,b). The paper by Penner (1961) was one of the earliest to use a matrix formalism in this context.

Numerous computer programs have been and continue to be developed for ion optics, some of which have already been cited. Of the earlier software, we mention TURTLE (see Carey, 1981, for earlier references), TRANSOPTR (Heighway and Hutcheon, 1981), the algebra program HAMILTON (Berz and Wollnik, 1987) to be used in conjunction with COSY 5.0 (Berz et al., 1987) and the GIOS–BEAMTRACE package (Wollnik et al., 1987b), MARYLIE and MICROLIE (Dragt, 1987), RAYTRACE (Kowalski and Enge, 1987) and the programs developed by Munro and colleagues (www.mebs.co.uk) and by Lencová (www.lencova.com). We recall that TRANSPORT, with which later programs are frequently compared, is described in Brown (1968). Programs that are still in use continue to be improved. Rather than give references that will soon be out of date, we refer the reader to to the appropriate websites, which are easily found.

Energy Analysers

Section 52.5 is devoted to energy analysers and monochromators and this list is hence quite short. It has not been possible to examine in detail the various types of electron energy analyser used at moderate energies (up to a few hundred kilovolts, say) or the numerous mass spectrometer designs. In this concluding section, therefore, we draw attention to general texts and review articles and also to some fundamental papers on energy analyser design.

For broad surveys and review articles see Afanas'ev and Yavor (1975a, 1978), Klemperer (1965), Leckey (1987), Matsuda (1983a,b, 1987), Matsuo and Wollnik (1975), Metherell (1971), Pearce-Percy (1978), Steckelmacher (1973), Sysoev and Samsonov (1972) and Wannberg et al. (1974). Time-of-flight mass spectrometers are covered by Matsuda et al. (1982), Matsuo (1984a,b), Matsuo et al. (1987), Sakurai et al. (1985), Trötscher et al. (1990), Trötscher (1993), Wollnik (1987b) and Wollnik et al. (1987a). For the history of mass spectrometry see Svec (1985) and Wollnik (2013). The revival of interest in time-of-flight mass analysers is reflected in the papers of Wollnik and Casares (2001), Ishida et al. (2004), Wolf et al. (2013), Ito et al. (2013), Makarov et al. (2014) and Schury et al. (2017), where many further references can be found.

The Castaing–Henry mirror-prism device is first described by Paras (1961) and is surveyed by Castaing et al. (1967) as well as in the articles cited elsewhere. A similar arrangement is used as an electron monochromator by Möllenstedt and Gruner (1968) and Gruner et al. (1971). The all-magnetic Ω design is discussed by Senoussi (1971), Senoussi et al. (1971), Rose and Plies (1974), Wollnik et al. (1976), Plies and Rose (1977), Zanchi et al. (1975, 1977a,b), Pearce-Percy et al. (1976) and Rose and Pejas (1979). A wholly electrostatic energy filter and monochromator with an Ω-shaped axis has been proposed by Plies (1978). A magnetic design in which the optic axis is α rather than Ω-shaped is examined by Perez et al. (1984).

A very different analyser was introduced by Möllenstedt (1949, 1952) and Möllenstedt and Heise (1949). Here, the particles enter a cylindrical or round lens far from the axis and follow sinuous trajectories that vary rapidly with energy (Möllenstedt and Dietrich, 1955; Gaukler, 1966; Aumüller, 1968). Later developments are fully described by Metherell (1971). See also Tian and Fink (1987). A magnetic analogue was later introduced by Ichinokawa and Kamiya (1966); a version of this was built for the Cambridge high-voltage microscope (Considine and Smith, 1968; Considine, 1969).

Most of the papers dealing with magnetic prism analysers have been listed in Section *Magnetic Prisms*; here we merely recall the early design of Wittry (1969) and the papers of Johnson (1979, 1980). Hemispherical analysers have been re-examined by Zouros and colleagues (Benis and Zouros, 2008; Benis et al., 1998; Martínez et al., 2016; Sise et al., 2010, 2016; Zouros, 2008; Zouros and Benis, 2002; Zouros et al., 2008).

The revival of interest in Bessel-box analysers (Allen et al., 1972, 1976) is demonstrated by Schiwiech et al. (2015) and Suri et al. (2017).

***

(1971). *Prismennye Beta-Spektrometry i ikh Primenenie* (Vilnius).

N. G. Afanas'ev (1960). Double-focusing magnetic spectrometer. *Izv. Akad. Nauk SSSR (Ser. Fiz.)* **24**, 1157–1164. *Bull. Acad. Sci. USSR (Phys. Ser.)* **24,** 1158–1164.

N. G. Afanas'ev and V. A. Gol'dshtein (1968). Aberrations of magnetic spectrometers with uniform field and double focusing for particles. *Prib. Tekh. Eksp.* **6**, 44–48.

V. P. Afanas'ev and S. Ya. Yavor (1972a). Combined focusing and deflecting fields in a cylindrical system with diaphragms and thick electrodes. *Zh. Tekh. Fiz* **42**, 320–327. *Sov. Phys. Tech. Phys*. **17**, 254–259.

V. P. Afanas'ev and S. Ya. Yavor (1972b). Approximate calculation of the field in a two-dimensional lens formed by two slotted coaxial cylinders. *Zh. Tekh. Fiz.* **42**, 1187–1195. *Sov. Phys. Tech. Phys.* **17**, 944–950.

V. P. Afanas'ev and S. Ya. Yavor (1972c). Cylindrical condenser with corrected spherical aberration. *Zh. Tekh. Fiz.* **42**, 2221–2228. *Sov. Phys. Tech. Phys*. **17**, 1746–1751.

V. P. Afanas'ev and S. Ya. Yavor (1975a). Electrostatic energy analysers. *Zh. Tekh. Fiz.* **45**, 1137–1170. *Sov. Phys. Tech. Phys*. **20**, 715–733.

V. P. Afanas'ev and S. Ya. Yavor (1975b). Determination of the instrument function of the electron spectrometer. *Pis'ma Zh. Tekh. Fiz.* **1**, 227–231. *Sov. Tech. Phys. Lett*. **1**, 109–110.

V. P. Afanas'ev and S. Ya. Yavor (1978). *Elektrostaticheskie Energoanalizatory dlya Puchkov Zaryazhennykh Chastits* (Nauka, Moscow).

G. Afanas'ev, A. V. Vysotskaya and V. A. Gol'dshtein (1963a). Calculation of a magnetic spectrometer with circular boundaries. *Prib. Tekh. Eksp.* **5**, 29–33.

N. G. Afanas'ev, A. V. Vysotskaya and V. A. Gol'dshtein (1963b). Aberrations of a magnetic spectrometer with circular boundaries. *Prib. Tekh. Eksp.* **5**, 34–39.

P. Albrecht (1956). Das Potential in doppelt gekrümmten Kondensatoren. *Z. Naturforsch.* **11a**, 156–163.

N. E. Alekseevski, G. P. Prudkovskii, G. I. Kosourov and S. I. Filimonov (1955). Utilization of a heterogeneous magnetic field to increase the resolving power of a mass spectrometer. *Dokl. Akad. Nauk SSSR* **100**, 229–232.

P. Allard and J.-D. Carette (1971). Spectromètres électrostatiques, Partie II. *Can. J. Phys.* **49**, 2132–2137. Part 1 is Y. Delage and J.-D. Carette, *ibid*. **49**, 2118–2131; Part 3 is D. Roy and J.-D. Carette, *ibid*. **49**, 2138–2159.

J. D. Allen, J. P. Wolfe and G. K. Schweitzer (1972). A new electron spectrometer design. *Int. J. Mass Spectrom. Ion Phys* **8**, 81–83.

J. D. Allen, J. D. Durham, G. K. Schweitzer and W. E. Deeds (1976). A new electron spectrometer design: II. *J. Electron Spectrosc. Related Phenom* **8**, 395–510.

R. Amadori and H. Wollnik (1971). Stigmatische Fokussierung mit homogenen magnetischen Sektorfeldern. *Int. J. Mass Spectrom. Ion Phys.* **6**, 347–360.

W. H. J. Andersen (1967). Optimum adjustment and correction of the Wien filter. *Br. J. Appl. Phys.* **18**, 1573–1579.

W. H. J. Andersen and J. Kramer (1972). A double-focusing Wien filter as a full-image energy analyser for the electron microscope. EUREM-5, Manchester. **1**, 146–147.

W. H. J. Andersen and J. B. Le Poole (1970). A double wienfilter as a high resolution, high transmission energy analyser. *J. Phys. E: Sci. Instrum.* **3**, 121–126.

M. Arnow (1976). Electrostatic cylindrical spectrometers. *J. Phys. E: Sci. Instrum.* **9**, 372–376.

O. Aspelund (1975). A fourth-order aberration theory for magnetic momentum-analysing systems. *Nucl. Instrum. Meth.* **128**, 73–92.

J. Aucouturier and H. Leboutet (1970). Systèmes déviateurs de faisceaux stigmatiques et achromatiques. *Nucl. Instrum. Meth.* **80**, 268–276.

W. Aumüller (1968). Ein schnell registrierender elekrostatischer Energieanalysator für Elektronen. *Optik* **27**, 577–581.

K. T. Bainbridge (1949). Fringing field corrections for magnetic sector lenses and prisms. *Phys. Rev.* **75**, 216.

N. F. Barber (1929–34). Note on the shape of an electron beam bent in a magnetic field. *Proc. Leeds Philos. Lit. Soc., Sci. Sect.* **2**, 427–434.

J. Bärtle and E. Plies (2008). Energy width reduction using an electrostatic Ω-monochromator. *Phys. Procedia* **1**, 479–483.

Yu. G. Basargin (1966). Second-order chromatic aberrations in a magnetic sector analyser with radially inhomogeneous field and curved boundaries. *Zh. Tekh. Fiz.* **36**, 1075–1083. *Sov. Phys. Tech. Phys.* **11**, 790–795.

Yu. G. Basargin (1967). Calculation of the second-order spherical aberrations in a magnetic sector analyser. *Zh. Tekh. Fiz.* **37**, 1360–1363. *Sov. Phys. Tech. Phys.* **12**, 989–991.

Yu. G. Basargin (1968). Influence of the vertical motion on the horizontal aberrations of second order in a magnet with inclined circular boundaries. *Zh. Tekh. Fiz.* **38**, 1400–1402. *Sov. Phys. Tech. Phys.* **13**, 1145–1147.

Yu. G. Basargin (1969). Some general properties of magneto-optical systems with a plane of symmetry. *Zh. Tekh. Fiz.* **39**, 241–248. *Sov. Phys. Tech. Phys.* **14**, 171–175.

C. Bastard and J. Lafoucrière (1958). Formation de l'image d'un point dans un spectrographe magnétique utilisant un champ en r^{-1}. *J. Phys. Radium* **19**, 674–676.

P. E. Batson (1985). A Wien filter energy loss spectrometer for the dedicated scanning transmission electron microscope. *Scanning Electron Microsc.*, 15–20.

P. E. Batson (1986). High-energy resolution electron spectrometer for 1-nm spatial analysis. *Rev. Sci. Instrum.* **57**, 43–48.

P. E. Batson, H. W. Mook and P. Kruit (2000). High brightness monochromator for STEM. In *Microbeam Analysis 2000*, Kailua-Kona, Hawaii. 213–214. Institute of Physics Conference Series No. 165.

F. M. Beiduk and E. J. Konopinski (1948). Focusing field for a 180° type spectrograph. *Rev. Sci. Instrum.* **19**, 594–598.

E. P. Benis and T. J. M. Zouros (2008). The hemispherical deflector analyser revisited. II. Electron-optical properties. *J. Electron Spectrosc. Relat. Phenom.* **163**, 28–39. Part I is Zouros and Benis (2002).

E. P. Benis, K. Zaharakis, M. M. Voultsidou, T. J. M. Zouros, M. Stöckli, P. Richard and S. Hagmann (1998). A new hemispherical analyser with 2-D PSD and focusing lens for use in 0° electron spectroscopy. *Nucl. Instrum. Meth. Phys. Res. B* **146**, 120–125.

C. Berger and M. Baril (1987). The electrostatic systems used for the multipassage magnetic mass spectrometers. *Nucl. Instrum. Meth. Phys. Res. A* **258**, 335–338.

M. Berz (1987). The method of power series tracking for the mathematical description of beam dynamics. *Nucl. Instrum. Meth. Phys. Res. A* **258**, 431–436.

M. Berz and H. Wollnik (1987). The program HAMILTON for the analytic solution of the equations of motion through fifth order. *Nucl. Instrum. Meth. Phys. Res. A* **258**, 364–373.

M. Berz, H. C. Hoffmann and H. Wollnik (1987). COSY 5.0 – the fifth order code for corpuscular optical systems. *Nucl. Instrum. Meth. Phys. Res. A* **258**, 402–406.

M. Berz, K. Makino and W. Wan (2015). *An Introduction to Beam Physics* (CRC Press, Boca Raton).

A. J. H. Boerboom (1958). Theory of the aberrations in the focusing properties of a magnetic field with one plane of symmetry. *Appl. Sci. Res. B* **7**, 52–62.

A. J. H. Boerboom (1960). The potential distribution in a toroidal condenser. *Z. Naturforsch.* **15a**, 347–350.

A. J. H. Boerboom (1964). Ion optics of fields with rotational symmetry and circular main orbit. *J. Appl. Phys.* **35**, 1691–1697.

A. J. H. Boerboom (1970). Ion optics. In *Recent Developments in Mass Spectroscopy* (K. Ogata and T. Hayakawa, Eds), 83–87 (University of Tokyo Press, Tokyo).

A. J. H. Boerboom (1972). Ion optics of the electric hexapole. *Int. J. Mass Spectrom. Ion Phys.* **8**, 475–492.

A. J. H. Boerboom (1976). Image aberrations in an imperfectly-shaped electrostatic analyser. *Int. J. Mass Spectrom. Ion Phys.* **22**, 259–271.

A. J. H. Boerboom (1987a). The influence of misadjustment of poles on the magnetic field and on its ion optical properies. *Nucl. Instrum. Meth. Phys. Res. A* **258**, 412–416.

A. J. H. Boerboom (1987b). Ion optics of multipoles. *Nucl. Instrum. Meth. Phys. Res. A* **258**, 426–430.

A. J. H. Boerboom (1990). How far the computer can be avoided in mass spectrometer design. *Int. J. Mass Spectrom. Ion Processes* **100**, 15–29.

A. J. H. Boerboom (1995). Ion optics of multipole devices. 2. Field calculations and contributions of higher harmonics. *Int. J. Mass Spectrom. Ion Processes* **146–147**, 131–138. Part I is Boerboom et al. (1985).

A. J. H. Boerboom, H. A. Tasman and H. Wachsmuth (1959). Shape of the magnetic field between conical pole faces. *Z. Naturforsch.* **14a**, 816–818.

A. J. H. Boerboom, H. Matsuda and T. Matsuo (1976). Ion orbits in quadrupole lenses. *Int. J. Mass Spectrom. Ion Phys.* **22**, 273–282.

A. J. H. Boerboom, D. B. Stauffer and F. W. McLafferty (1985). Ion optics of multipole devices. I. Theory of the dodecapole. *Int. J. Mass Spectrom. Ion Processes* **63**, 17–28. Part II is Boerboom (1995).

A. J. H. Boerboom, S. K. Boerboom and H. S. K. Boerboom (1989). A computer program for the analytical calculation of potential and electric field in ion slit lens systems. *Int. J. Mass Spectrom. Ion Processes* **93**, 283–301.

H. Boersch, J. Geiger and W. Stickel (1964). Das Auflösungsvermögen des elektrostatisch-magnetischen Energieanalysators für schnelle Elektronen. *Z. Phys.* **180**, 415–424.

G. Bosi (1967). Axially symmetric magnetic fields: an investigation about conically shaped pole faces, a general method to evaluate the scalar potential. *Nucl. Instrum. Meth.* **46**, 55–60.

G. Bosi (1970). The trajectories of charged particles in magnetic fringe fields. *J. Phys. D: Appl. Phys.* **3**, 1925–1930.

G. Bosi (1972). Fringing field of electrostatic analyzers. *Rev. Sci. Instrum.* **43**, 475–478.

G. Bosi (1978). Fringing field of cylindrical analyzers. *Nucl. Instrum. Meth.* **155**, 517–525.

P. Bounin (1967). Application of Fermat's principle to magnetic spectrometers. *Rev. Sci. Instrum.* **38**, 1305–1312.

P. Bounin (1971a). Exemples d'application du principe de Fermat aux spectromètres magnétiques. *Nucl. Instrum. Meth.* **94**, 73–76.

P. Bounin (1971b). Amélioration au troisième ordre des propriétés optiques des spectromètres magnétiques. *Nucl. Instrum. Meth.* **94**, 77–85.

K. L. Brown (1965). First- amd second-order magnetic optics of a circular-pole uniform-field magnet. I. *Rev. Sci. Instrum.* **36**, 271–274.

K. L. Brown (1968). A first- and second-order matrix theory for the design of beam transport systems and charged particle spectrometers. In *Advances in Particle Physics* (R. L. Cool and R. E. Marshak, Eds), **1**, 71–134 (Wiley–Interscience, New York & London). Distributed as SLAC Report No. 75 (1967) 105 pp.

K. L. Brown and R. V. Servranckx (1985a). Optics modules for circular accelerator design. *Nucl. Instrum. Meth. Phys. Res. A* **258**, 480–502.

K. L. Brown and R. V. Servranckx (1985b). First- and second-order charged particle optics. In *Physics of High Energy Accelerators* (M. Month, P. F. Dahl and M. Dienes, Eds), 62–138 (American Institute of Physics, New York). AIP Conf. Proc. No. 127.

K. L. Brown, R. Belbeoch and P. Bounin (1964). First- and second-order magnetic optics matrix equations for the midplane of uniform-field wedge magnets. *Rev. Sci. Instrum.* **35**, 481–485.

J. E. Campana (1987b). Time-of-flight mass spectrometry: a historical overview. *Instrum. Sci. Technol.* **16**, 1–14.

C. Carathéodory (1937). Geometrische Optik. *Ergebn. Math. Grenzgeb.* **4** (5). 104 pp.

D. C. Carey (1981). High energy charged particle optics computer programs. *Nucl. Instrum. Meth.* **187**, 97–102.

D. C. Carey (1987a). Two dogmas of charged particle optics. *Nucl. Instrum. Meth. Phys. Res.* **A258**, 417–420.

D. C. Carey (1987b). *The Optics of Charged Particle Beams* (Harwood, Chur & London).

L. Cartan (1937a). Sur une nouvelle méthode de focalisation des faisceaux d'ions positifs rapides. Application à la spectrographie de masse. *J. Phys. (Paris)* **8**, 111–120.

L. Cartan (1937b). Sur la focalisation des faisceaux de particules chargées par déviation circulaire en champ magnétique transversal. *J. Phys. (Paris)* **8**, 453–470.

L. Cartan (1938). L'optique des rayons positifs et ses applications à la spectrographie de masse. *Ann. Phys. (Paris)* **10**, 426–502.

R. Castaing and L. Henry (1962). Filtrage magnétique des vitesses en microscopie électronique. *C. R. Acad. Sci. Paris* **255**, 76–78.

R. Castaing and L. Henry (1964). Filtrage magnétique des vitesses en microscopie électronique. *J. Microsc. (Paris)* **3**, 133–152.

R. Castaing, J. F. Hennequin, L. Henry and G. Slodzian (1967). The magnetic prism as an optical system. In *Focusing of Charged Particles* (A. Septier, Ed.), **2**, 265–293 (Academic Press, New York & London).

H.-n. Chen and A. J. H. Boerboom (1982). A new electrostatic analyser for wide beams and its ion-optical properties. *Int. J. Mass Spectrom. Ion Phys.* **44**, 117–127.

K. H. Cheong, W. Han, A. Khursheed and K. Nelliyan (2015). A parallel radial mirror energy analyzer attachment for the scanning electron microscope. *Microsc. Microanal.* **21** (Suppl. 4), 142–147.

N. G. Coggeshall (1947). Fringing flux corrections for magnetic focusing devices. *J. Appl. Phys.* **18**, 855–861.

C. Colliex (1984). Electron energy loss spectroscopy in the electron microscope. *Adv. Opt. Electron Microsc.* **9**, 65–177.

R. E. Collins (1973). The design of double focusing Wien filters. *J. Vac. Sci. Technol.* **10**, 1106–1109.

K. T. Considine (1969). An energy analyser for high-voltage electron microscopy. Dissertation, Cambridge.

K. Considine and K. C. A. Smith (1968). An energy analyser for high voltage microscopy. EUREM-4, Rome. **1**, 329–330.

M. Cotte (1938). Recherches sur l'optique électronique. *Ann. Phys. (Paris)* **10**, 335–405. Errata, *Ann. Phys. (Paris)* **11** (1939) 351–352.

E. D. Courant, M. S. Livingston and H. S. Snyder (1952). The strong-focusing synchrotron – a new high energy accelerator. *Phys. Rev.* **88**, 1190–1196.

A. V. Crewe (1977). Post-specimen optics in the STEM. 1 General information. 2. A corrected spectrometer. *Optik* **47**. 299–311 & 371–380.

A. V. Crewe and F. Scaduto (1982). A gradient field spectrometer for STEM use. EMSA, Washington. **40**, 734–735.

A. V. Crewe, M. S. Isaacson and D. Johnson (1971). A high resolution electron spectrometer for use in transmission scanning electron microscopy. *Rev. Sci. Instrum.* **42**, 411–420.

W. G. Cross (1951). Two-directional focusing of charged particles with a sector-shaped uniform magnetic field. *Rev. Sci. Instrum.* **22**, 717–722.

D. Cubric, S. van Kranen, P. Kruit and S. Kumashiro (2004). On the performance of an energy filter for a high brightness electron gun. *Recent Trends* **9**, 19–20.

G. H. Curtis and J. Silcox (1971). A Wien filter for use as an energy analyzer with an electron microscope. *Rev. Sci. Instrum.* **42**, 630–637.

E. F. H. St. G. Darlington (1980). Evaluation of the properties of uniform field magnetic sector spectrometers. *Ultramicroscopy* **5**, 429–435.

M. de Celles (1974). Transfer matrix of the toroidal electrostatic mirror in a second-order approximation including the aberrations off the symmetry plane. *Nucl. Instrum. Meth.* **114**, 557–571.

P. Decreau, R. Prange and J. J. Berthelier (1972). Détermination des grandeurs caractéristiques des analyseurs électrostatiques toriques. Application à l'optimisation d'analyseurs utilisés en physique spatiale. *Rev. Phys. Appl.* **7**, 95–106.

P. Decreau, R. Prange and J. J. Berthelier (1975). Optimization of toroidal electrostatic analyzers for measurements of low energy particles in space. *Rev. Sci. Instrum.* **46**, 995–1007.

R. Degenhardt and W. Engel (1996). Calculation, analysis and evaluation of the transfer optics optimized for a corrected imaging energy filter. *Recent Trends* **5**, 31–34.

Y. Delage and J.-D. Carette (1971). Spectromètres électrostatiques, Partie I. *Can. J. Phys.* **49**, 218–2131. Part 2 is P. Allard and J.-D. Carette, *ibid*. **49**, 2132–2137; Part 3 is Roy and J.-D. Carette, *ibid*. **49**, 2138–2159.

N. Dellby, T.C. Lovejoy and L.O. Křivánek [sic] (2014). Tuning and operation of a sub-20 meV monochromator. IMC-18, Prague, IT-1-O-2914.

D. F. Dempsey (1955). Third-order aberration and focusing with sector-shaped magnetic fields. *Rev. Sci. Instrum.* **26**, 1141–1145.

H. Dormont (1959). Optique corpusculaire des pinceaux d'axe courbe. *Ann. Phys. (Paris)* **4**, 1341–1387.

A. J. Dragt (1987). Elementary and advanced Lie algebraic methods with applications to accelerator design, electron microscopes and light optics. *Nucl. Instrum. Meth. Phys. Res. A* **258**, 339–354.

R. F. Egerton (1996). *Electron Energy-Loss Spectrosopy in the Electron Microscope* (Plenum, New York); 2nd edn, 1996; 3rd edn, 2011, published by Springer, New York.

W. Ehrenberg and J. C. E. Jennings (1952). Measurements of the electron-optical properties of solenoid prisms. *Proc. Phys. Soc. (Lond.) B* **65**, 265–275.

H. A. Enge (1963). Achromatic magnetic mirror for ion beams. *Rev. Sci. Instrum.* **34**, 385–389.

H. A. Enge (1967). Deflecting magnets. In *Focusing of Charged Particles* (A. Septier, Ed.), **2**, 203–264 (Academic Press, New York & London).

E. Essers, G. Benner, T. Mandler, S. Meyer, D. Mittmann, M. Schnell and R. Höschen (2010). Energy resolution of an omega-type monochromator and imaging properties of the MANDOLINE filter. *Ultramicroscopy* **110**, 971–980.

M. Essig (1981). Hochaufgelöste Elektronenspektroskopie der infraroten Gitterschwingungen in kleinen würfelförmigen MgO-Kristallen und Messungen der Energieverteilung der aus Kohlefaserspitzen thermofeldemittierten Elektronen. Dissertation, Kaiserslauterten.

L. A. Evseeva and Ya. A. Yukhvidin (1980). Magnetic deflection angles and dispersion in the field of a hexapole magnet. *Zh. Tekh. Fiz.* **50**, 1460–1463. *Sov. Phys. Tech. Phys*. **25**, 846–848.

H. Ewald (1959a). Zur Bildfehlerkorrektur von doppelfokussierenden Massenspektrographen. *Z. Naturforsch.* **14a**, 198–199.

H. Ewald (1959b). Öffnungsfehlerfreie Kugelkondensatoren. *Z. Naturforsch.* **14a**, 680–681.

H. Ewald and H. Liebl (1955). Der Astigmatismus des Toroidkondensators. *Z. Naturforsch.* **10a**, 872–876.

H. Ewald and H. Liebl (1957). Die Bildfehler des Toroidkondensators. *Z. Naturforsch* **12a**, 28–33. Errata: *ibid*. **14a** (1959) 588.

H. Ewald and G. Sauermann (1956). Ein stigmatisch abbildender doppelfokussierender Massenspektrograph. *Z. Naturforsch.* **11a**, 173–174.

H. Ewald, H. Liebl and G. Sauermann (1959). Berechnung eines doppelfokussierenden stigmatisch abbildenden Massenspektrographen. *Z. Naturforsch.* **14a**, 129–137.

E. P. Fedoseev (1968a). Magnetic focusing prisms with r^{-1} field for focusing wide-angle beams of charged particles. *Zh. Tekh. Fiz.* **38**, 1320–1329. *Sov. Phys. Tech. Phys*. **13**, 1081–1087.

E. P. Fedoseev (1968b). Study of the image parameters of magnetic focusing prisms with r^{-1} fields. *Zh. Tekh. Fiz.* **38**, 1330–1335. *Sov. Phys. Tech. Phys*. **13**, 1088–1091.

E. P. Fedoseev (1968c). Ion-optical properties of magnetic prisms with r^{-1} field for focusing wide-angle beams of charged particles. *Kernenergie* **11**, 191–197.

E. P. Fedoseev (1970a). Three-sector focusing magnetic prisms with r^{-1} field. I. General considerations and methods [in Russian]. *Kernenergie* **13**, 127–132.

E. P. Fedoseev (1970b). Three-sector focusing magnetic prisms with r^{-1} field. II. Ion-optical properties. Focusing of double-wedge-shaped charged particle beams [in Russian]. *Kernenergie* **13**, 151–156.

E. P. Fedoseev (1970c). Three-sector focusing magnetic prisms with r^{-1} field. III. Focusing of charged particle beams with point source [in Russian]. *Kernenergie* **13**, 178–181.

E. P. Fedoseev (1970d). Three-sector focusing magnetic prisms with r^{-1} field. IV. Focusing of cylindrical charged particle beams [in Russian]. *Kernenergie* **13**, 228–231.

J. Fink (1989). Recent developments in energy-loss spectroscopy. *Adv. Electron. Electron Phys.* **75**, 121–232.

L. Frank (1976). Note on the design of the cylindrical mirror energy analyser. *J. Phys. E: Sci. Instrum.* **9**, 670–676.

B. Freitag and P. Tiemeijer (2017). Sub 30 meV energy resolution in the monochromated Themis transmission electron microscope. MC-2017, Lausanne, 467.

D. Gabor (1951). Electron-optical systems with helical axis. *Proc. Phys. Soc. (Lond.) B* **64**, 244–255.

R. N. Gall' and V. D. Sachenko (1980). On the possibility of compensating the aberrations of magnetic sector analysers. *Zh. Tekh. Fiz.* **50**, 824–830. *Sov. Phys. Tech. Phys*. **25**, 491–495.

K.-H. Gaukler (1966). Auflösunsgrenze des elektrostatischen Energie-Analysators und hochauflösende Elektronen-Spektrometrie. *Z. Phys.* **196**, 85–102.

J. Geerk (1966). Nouveaux spectromètres de masse à déviation de 360°. *C. R. Acad. Sci. Paris B* **262**, 479–482.

J. Geerk (1975). Ein Beitrag zur Grundlegung einer allgemeinen, ebenen Strahlenoptik und neue Erkenntnisse für die Konstruktion Massenspektrometrischer Instrumente. *Int. J. Mass Spectrom. Ion Phys.* **18**, 137–152.

J. Geerk (1984). Zur Grundlegung einer asymmetrischen ebenen Strahlenoptik mit Anwendungen auf Massenspektrometrische Instrumente. *Int. J. Mass Spectrom. Ion Processes* **61**, 157–190.

J. Geerk (1985). Das ionenoptische magnetische Sektorfeld als ein geradliniges Strahlensystem Linse–Prisma–Linse. *Int. J. Mass Spectrom. Ion Phys.* **65**, 237–251.

J. Geerk (1986). Eine Theorie der Abbildungen durch das ionenoptische magnetische Sektorfeld. *Nucl. Instrum. Meth. Phys. Res. A* **243**, 285–301.

W. Glaser (1956). Elektronen- und Ionenoptik. *Handbuch der Physik* **33**, 123–395.

L. G. Glikman (1984). Conical deflectors with combined electric and magnetic fields. *Zh. Tekh. Fiz.* **54**, 1986–1991. *Sov. Phys. Tech. Phys*. **29**, 1166–1169.

L. G. Glikman, V. M. Kel'man and L. V. Fedulina (1973a). A wedge-shaped electrostatic prism. *Zh. Tekh. Fiz.* **43**, 1793–1798. *Sov. Phys. Tech. Phys*. **18**, 1139–1141.

L. G. Glikman, V. M. Kel'man and L. V. Fedulina (1973b). Geometrical aberrations of a wedge-shaped electrostatic prism. *Zh. Tekh. Fiz.* **43**, 2017–2022. *Sov. Phys. Tech. Phys*. **18**, 1273–1276.

L. G. Glikman, V. M. Kel'man, O. V. Pavlichkova and I. F. Spivak-Lavrov (1976a). Geometric angular aberrations of three-electrode and five-electrode wedge-shaped electrostatic prisms. I, II. *Zh. Tekh. Fiz.* **46**, 1810–1820 & 1821–1825. *Sov. Phys. Tech. Phys*. **21**, 1055–1059 & 1060–1062.

L. G. Glikman, V. M. Kel'man, O. V. Pavlichkova and I. F. Spivak-Lavrov (1976b). Telescopic and dispersion conditions for three-electrode and five-electrode wedge-shaped electrostatic prisms. *Zh. Tekh. Fiz.* **46**, 1978–1981. *Sov. Phys. Tech. Phys*. **21**, 1153–1155.

L. G. Glikman, V. M. Kel'man, O. V. Pavlichkova and A. A. Sapargaliev (1977a). A wedge-shaped prism with combined electric and magnetic fields. *Zh. Tekh. Fiz.* **47**, 1361–1371. *Sov. Phys. Tech. Phys*. **22**, 782–7787.

L. G. Glikman, O. V. Pavlichkova and I. F. Spivak-Lavrov (1977b). Cone-shaped prisms with combined electric and magnetic fields. *Zh. Tekh. Fiz.* **47**, 1372–1379. *Sov. Phys. Tech. Phys*. **22**, 788–792.

L. G. Glikman, V. M. Kel'man and O. V. Pavlichkova (1985). Design formulae for wedge-shaped prisms with conical electric and magnetic fields. *Zh. Tekh. Fiz.* **55**, 181–185. *Sov. Phys. Tech. Phys*. **30**, 103–105.

G. A. Grinberg (1942). General theory of the focusing action of electrostatic and magnetostatic fields. I. Two-dimensional fields. II. Three-dimensional electrostatic fields [in English]. *Dokl. Akad. Nauk SSR* **37**, 172–178 & 261–268.

G. A. Grinberg (1943). General theory of the focusing action of electrostatic and magnetostatic fields. III. Three-dimensional (twisted) trajectories in the presence of both an electrostatic and a magnetic field [in English]. *Dokl. Akad. Nauk SSR* **38**, 78–81.

G. A. Grinberg (1957a). Remark on the paper by P.P. Kas'yankov [*Opt. Spektrosk.* **3**, 1957, 169]. *Opt. Spektrosk.* **3**, 673.

G. A. Grinberg (1957b). Concerning the criticism by P.P. Kas'yankov of my method of obtaining the principal electron-optical equations for pencils with curvilinear axis. *Zh. Tekh. Fiz.* **27**, 2425–2431. *Sov. Phys. Tech. Phys.* **2**, 2259–2265.

H. Grümm (1953). Zur Dioptrik des Elektronen- und Ionenbündels mit kreisförmiger Hauptbahn. *Acta Phys. Aust.* **8**, 119–140.

H. Gruner, K.-H. Gaukler and G. Möllenstedt (1971). Monochromatisierung von Elektronenstrahlen mittels Spiegelung und ihre Anwendung in der Emissions-Mikroskopie. *Optik* **33**, 255–269.

A. J. Gubbens, B. Kraus, O. L. Krivanek and P. E. Mooney (1995). An imaging filter for high voltage electron microscopy. *Ultramicroscopy* **59**, 255–265.

A. Gubbens, M. Barfels, C. Trevor, R. Twesten, P. Mooney, P. Thomas, N. Menon, B. Kraus, C.-y. Mao and B. McGinn (2010). The GIF Quantum, a next generation post-column imaging energy filter. *Ultramicroscopy* **110**, 962–970.

G. Guignard and J. Hagel (1986). Sextupole correction and dynamic aperture: numerical and analytical tools. *Part. Accel.* **18**, 129–165.

A. Gullstrand (1900). Allgemeine Theorie der monochromatischen Aberrationen und ihre nächsten Ergebnisse für die Ophthalmologie. *Nova Acta Reg. Soc. Sci. Upsaliensis* **20** (3). 204 pp.

A. Gullstrand (1906). Die reelle optische Abbildung. *K. Svensk. Vetenskapsakad. Hand.* **41** (3). 119 pp.

A. Gullstrand (1915). Das allgemeine optische Abbildungssystem. *K. Svensk. Vetenskapsakad. Hand.* **55** (1). 139 pp.

A. Gullstrand (1924). Optische Systemgesetze zweite und dritter Ordnung. *K. Svensk. Vetenskapsakad. Hand* **63** (13). 175 pp.

V. S. Gurov, A. O. Saulebekov and A. A. Trubitsyn (2015). Analytical, approximate-analytical and numerical methods in the design of energy analyzers. *Adv. Imaging Electron Phys.* **192**, 209 pp.

H. Hafner, J. A. Simpson and C. E. Kuyatt (1968). Comparison of the spherical deflector and the cylindrical mirror analyzers. *Rev. Sci. Instrum.* **39**, 33–35.

M. Haider, W. Bernhardt and H. Rose (1982). Design and test of an electric and magnetic dodecapole lens. *Optik* **63**, 9–23.

B. Hartmann and H. Wollnik (1994). Third-order particle motion through the fringing field of a homogeneous bending magnet. *Nucl. Instrum. Meth. Phys. Res. A* **344**, 278–285.

B. Hartmann, M. Berz and H. Wollnik (1990). The computation of aberrations of fringing fields of magnetic multipoles and sector magnets using differential algebra. *Nucl. Instrum. Meth. Phys. Res. A* **297**, 343–353.

E. A. Heighway and R. M. Hutcheon (1981). TRANSOPTR – a second order beam transport design code with optimization and constraints. *Nucl. Instrum. Meth.* **187**, 89–95.

R. M. Henkelman and F. P. Ottensmeyer (1974a). An energy filter for biological electron microscopy. *J. Microsc. (Oxford)* **102**, 79–94.

R. M. Henkelman and F. P. Ottensmeyer (1974b). An electrostatic mirror. *J. Phys. E: Sci. Instrum.* **7**, 176–178.

W. Henneberg (1934a). Feldkombinationen zur Geschwindigkeits- und Massenspektrographie. I. *Ann. Phys. (Leipzig)* **19** (411), 335–344.

W. Henneberg (1934b). Feldkombinationen zur Geschwindigkeits- und Massenspektrographie. II. *Ann. Phys. (Leipzig)* **20** (412), 1–12.

W. Henneberg (1934c). Feldkombinationen zur Geschwindigkeits- und Massenspektrographie. III. *Ann. Phys. (Leipzig)* **21** (413), 390–404.

L. Henry (1964). Filtrage magnétique des vitesses en microscopie électronique. Dissertation, Paris.

R. Herzog (1934). Ionen- und elektronenoptische Zylinderlinsen und Prismen. *Z. Phys.* **89**, 447–473.

R. Herzog (1940). Elektronenoptische Zylinderlinsenwirkung der Streufelder eines Kondensators. *Phys. Z.* **41**, 18–26.

R. F. K. Herzog (1950). Elekronenoptischer Abbildungseigenschaften von homogenen transversalen magnetischen Feldern. *Acta Phys. Austriaca* **4**, 506.

R. F. K. Herzog (1955). Einfluß magnetischer Streufelder auf die Lage und Güte der Bilder bei Massenspektrographen und Spektrometern. *Z. Naturforsch.* **10a**, 887–893.

H. Hintenberger (1948a). Über magnetische Zylinderlinsen mit korrigiertem Bildfehler. *Z. Naturforsch.* **3a**, 125–127.

H. Hintenberger (1948b). Richtungsfokussierung zweiter Ordnung geladener Teilchen in homogenen Magnetfeldern. *Z. Naturforsch.* **3a**, 669–670.

H. Hintenberger (1949). Improved magnetic focusing of charged particles. *Rev. Sci. Instrum.* **20**, 748–750.

H. Hintenberger (1951). Der Öffnungsfehler bei der ionenoptischen Abbildung eines Punktes mit Hilfe eines beliebig begrenzten homogenen Magnetfeldes. *Z. Naturforsch.* **6a**, 275–276.

H. Hintenberger and L. A. König (1957). Massenspektrometer mit Doppelfokussierung zweiter Ordnung. *Z. Naturforsch.* **12a**, 773–785.

H. Hintenberger and L. A. König (1958). Massenspektrographen mit Doppelfokussierung erster Ordnung für alle Massen, die geringe Bildfehler in einem grossen Massenbereich entlang der Photoplatte aufweisen. *Nucl. Instrum.* **3**, 250–259.

H. Hintenberger, H. Wende and L. A. König (1955). Massenspektrographen mit Doppelfokussierung zweiter Ordnung. *Z. Naturforsch.* **10a**, 605–612.

H. Q. Hoang and A. Khursheed (2011). A radial mirror analyzer for scanning electron/ion microscopes. *Nucl. Instrum. Meth. Phys. Res. A* **635**, 64–68.

H. Q. Hoang, J.-l. Wu and A. Khursheed (2006). Direct ray tracing of electrons through curved magnetic sector plates. *Recent Trends* **10**, 29–30.

G. H. Hoffstätter and M. Berz (1995). Accurate and fast computation of high order fringe-field maps via symplectic scaling. *Nucl. Instrum. Meth. Phys. Res. A* **363**, 124–127.

L. Holmlid (1975). Mass dispersion and mass resolution in crossed homogeneous electric and magnetic fields: the Wien velocity filter as a mass spectrometer. *Int. J. Mass Spectrom. Ion Phys.* **17**, 403–421.

N. Hu (1987). Ion optical properties of a magnet with tilted magnetic poles. In *Proc. Int. Symposium on Electron Optics, ISEOB* (J.-y. Ximen, Ed.), 83–84 (Institute of Electronics, Academia Sinica, Beijing).

A. Huber and E. Plies (1999). Numerical ray tracing of electrons in different 3D fringing fields of spherical deflectors. *Proc. SPIE* **3777**, 264–274.

A. Huber, J. Bärtle and E. Plies (2004). Initial experiences with an electrostatic Ω-monochromator for electrons. *Nucl. Instrum. Meth. Phys. Res. A* **519**, 320–324.

A. L. Hughes and V. Rojansky (1929). On the analysis of electronic velocities by electrostatic means. *Phys. Rev.* **34**, 284–290.

J. W. Hurd (1987). Derivation of the first-order transformation matrix for a simple Wien filter and comparison to results of numerical integration. *Nucl. Instrum. Meth. Phys. Res. A* **258**, 542–547.

R. G. E. Hutter (1945). The electron optics of mass spectrographs and velocity focusing devices. *Phys. Rev.* **67**, 248–253.

R. G. E. Hutter (1948). The deflection of beams of charged particles. *Adv. Electron* **1**, 167–218.

T. Ichinokawa (1965). A new electron-energy analyser of magnetic type. In *Int. Conf. on Electron Diffraction and the Nature of Defects in Crystals*, Melbourne. IM-14.

T. Ichinokawa (1968). Electron energy analysis by a cylindrical magnetic lens. *Jpn. J. Appl. Phys.* **7**, 799–813.

T. Ichinokawa and Y. Kamiya (1966). Electron energy analysis in a cylindrical magnetic lens. ICEM-6, Kyoto. **1**, 89–90.

H. Ikegami (1958). Second-order properties of double-focusing spectrometer with nonuniform magnetic field. *Rev. Sci. Instrum.* **29**, 943–948.

D. Ioanoviciu (1970). Ion-optical properties of magnetic prisms with axially symmetric r^{-1} fields and spiral main paths. *Int. J. Mass Spectrom. Ion Phys.* **5**, 29–47.

D. Ioanoviciu (1973a). Ion optics of a Wien filter with inhomogeneous fields. *Int. J. Mass Spectrom. Ion Phys.* **11**, 169–184.

D. Ioanoviciu (1973b). Transfer matrices of real r^{-1} prisms with a spiral main path. *Int. J. Mass Spectrom. Ion Phys.* **11**, 185–195.

D. Ioanoviciu (1974). Transfer matrices of real crossed electric and magnetic fields. *Int. J. Mass Spectrom. Ion Phys.* **15**, 89–103; Erratum: *ibid* **18** (1975) 301.

D. Ioanoviciu (1975). Transfer matrices of the magnetic wedge field sectors. *Int. J. Mass Spectrom. Ion Phys.* **18**, 289–301.

D. Ioanoviciu (1982). Ion optics of electric deflectors with a spiral main path. *Int. J. Mass Spectrom. Ion Phys.* **41**, 229–239.

D. Ioanoviciu (1988). Ion optics. *Adv. Electron. Electron Phys.* **73**, 1–92.

D. Ioanoviciu (1995). Oversimplified, compact double focusing mass spectrometer geometries. *Nucl. Instrum. Meth. Phys. Res. A* **363**, 406–410.

D. Ioanoviciu and C. Cuna (1974). Electrostatic deflector–Wien filter double focusing mass spectrometers. *Int. J. Mass Spectrom. Ion Phys.* **15**, 79–87.

D. Ioanoviciu and C. Cuna (1977). Resolution test of a Wien filter mass spectrometer with inhomogeneous fields. *Int. J. Mass Spectrom. Ion Phys.* **25**, 117–119.

D. Ioanoviciu and C. Cuna (1995). Compact Wien filter/magnetic sector double-focusing mass spectrometer. *Rapid Commun. Mass Spectrom.* **9**, 512–514.

D. Ioanoviciu, V. Mercea and C. Cuna (1972). Mass spectrometer with trochoidal ion beam. I. Theory. *Rev. Roum. Phys.* **17**, 1165–1175.

D. Ioanoviciu, V. Mercea, C. Cuna and P. Ardelean (1973). Mass spectrometer with trochoidal ion beam. II. Apparatus. *Rev. Roum. Phys.* **18**, 75–80.

M. S. Isaacson and M. Scheinfein (1983). A high performance electron energy loss spectrometer for use with a dedicated STEM. *J. Vac. Sci. Technol. B* **1**, 1338–1343.

M. S. Ismagulova and V. A. Rastorguev (1983). Matrix calculation of the aberrations of prism charged-particle energy analysers. *Zh. Tekh. Fiz.* **53**, 1568–1574. *Sov. Phys. Tech. Phys.* **28**, 964–967.

M. S. Ismagulova and V. A. Rastorguev (1984). Matrix method for designing sector magnet analysers with corrections for edge effects. *Zh. Tekh. Fiz.* **54**, 1605–1609. *Sov. Phys. Tech. Phys*. **29**, 938–940.

Y. Ito, P. Schury, M. Wada, S. Naimi, T. Sonoda, H. Mita, F. Arai, A. Takamine, K. Okada, A. Ozawa and H. Wollnik (2013). Single-reference high-precision mass measurement with a multireflection time-of-flight mass spectrograph. *Phys. Rev. C* **88**, 011306.

J. C. E. Jennings (1952). The virtual optics of the median plane of axially symmetric magnetic prisms. *Proc. Phys. Soc. (Lond.) B* **65**, 256–265.

X.-g. Jiang and F. P. Ottensmeyer (1993). Optimization of a prism–mirror–prism imaging energy filter for high resolution electron microanalysis. *Optik* **94**, 88–95.

D. E. Johnson (1979). Basic aspects of energy loss spectrometer systems. *Ultramicroscopy* **3**, 361–365.

D. E. Johnson (1980). Pre-spectrometer optics in a CTEM/STEM. *Ultramicroscopy* **5**, 163–174.

E. G. Johnson and A. O. Nier (1953). Angular aberrations in sector shaped electromagnetic lenses for focusing beams of charged particles. *Phys. Rev.* **91**, 10–17.

D. L. Judd (1950). Focusing properties of a generalized magnetic spectrometer. *Rev. Sci. Instrum.* **21**, 213–216.

D. L. Judd and S. A. Bludman (1957). Aberrations and fringing effects in a 180° double focussing magnetic spectrometer. *Nucl. Instrum.* **1**, 46–52.

F. Kahl (1999). Design eines Monochromators für Elektronenquellen. Dissertation, Darmstadt.

F. Kahl and H. Rose (1998a). Outline of an electron monochromator with small Boersch effect. *Recent Trends* **6**, 37–38.

F. Kahl and H. Rose (1998b). Outline of an electron monochromator with small Boersch effect. ICEM-14, Cancún. **1**, 71–72.

F. Kahl and H. Rose (2000). Design of a monochromator for electron sources. EUREM-12, Brno. I.459–I.460.

P. P. Kas'yankov (1956). *Teoriya Elektromagnitnykh Sistem s Krivolineinoi Os'yu* (Leningrad University Press, Leningrad).

P. P. Kas'yankov (1957). On the trajectory equations for an electron in electron-optical systems with a curvilinear axis. *Opt. Spektrosk.* **3**, 169–179.

P. P. Kas'yankov (1958a). On the condition for the existence of stigmatic imaging in electron optical systems with curvilinear axis. *Dokl. Akad. Nauk SSSR* **120**, 497–500. *Sov. Phys. Dokl.* **3**, 573–576.

P. P. Kas'yankov (1958b). On the letter of Corresponding Member of the Academy of Sciences, Prof. G.A. Grinberg. *Zh. Tekh. Fiz.* **28**, 915–918. *Sov. Phys. Tech. Phys*. **3**, 854–857.

E. Kasper (1965). Theoretische Untersuchungen über die Möglichkeit stigmatischer korpuskularoptischer Fokussierung durch beliebige stationäre räumlich begrenzte elektrisch-magnetische Felder. *Z. Angew. Phys.* **19**, 112–120.

E. Kasper (1987). Computer simulation of electron optical systems. *Nucl. Instrum. Meth. Phys. Res. A* **258**, 466–479.

M. Kato and K. Tsuno (1990). Numerical analysis of trajectories and aberrations of a Wien filter including the effect of fringing fields. *Nucl. Instrum. Meth. Phys. Res. A* **298**, 296–320.

K. Kekk (1962). Calculation of the characteristics of magnetic spectrometers. *Zh. Tekh. Fiz.* **32**, 859–866. *Sov. Phys. Tech. Phys*. **7**, 627–633.

V. M. Kel'man and I. V. Rodnikova (1951). Motion of charged particles in the magnetic field of a linear current and the electric field of a cylindrical capacitor. *Zh. Eksp. Teor. Fiz.* **21**, 1364–1369.

V. M. Kel'man and S. Ya. Yavor (1959). *Elektronnaya Optika* (*Izd. Akad. Nauk SSSR*, Moscow & Leningrad; 2nd edn, 1963; 3rd edn, 1968, *Izd. Nauka*, Leningrad).

V. M. Kel'man, S. P. Karetskaya, L. V. Fedulina and E. M. Yakushev (1979). *Elektronno-opticheskie Elementy Prismennykh Spektrometrov Zaryazhennykh Chastits* (Nauka, Alma-Ata).

V. M. Kel'man, I. V. Rodnikova and L. M. Sekunova (1985). *Staticheskie Mass-Spektrometry* (Nauka, Alma-Ata).

D. W. Kerst and R. Serber (1941). Electronic orbits in the induction accelerator. *Phys. Rev.* **60**, 53–58.

L. Kerwin (1949). Improved magnetic focusing of charged paricles. *Rev. Sci. Instrum.* **20**, 36–41.

L. Kerwin and C. Geoffrion (1949). Further improvements in magnetic focusing. *Rev. Sci. Instrum.* **20**, 381–384.

Ya. L. Khurgin (1939). On the vertical focusing of a beam of charged particles deflected in a magnetic field. *Zh. Eksp. Teor. Fiz.* **9**, 824–825.

A. Khursheed (2011). Second-order focusing parallel electron energy magnetic sector analyzer designs. *Nucl. Instrum. Meth. Phys. Res. A* **645**, 253–256.

A. Khursheed, K. Nelliyan and F. Chao (2011). First-order focusing parallel electron energy magnetic sector analyzer design. *Nucl. Instrum. Meth. Phys. Res. A* **645**, 248–252.

A. Khursheed, H. Q. Hoang and A. Srinivasan (2012). A wide-range parallel radial mirror analyzer for scanning electron/ion microscopes. *J. Electron Spectrosc. Relat. Phenom.* **184**, 525–532.

P. Killes (1983). Optimierung eines magnetischen Sektorfeldspektrometers. Dissertation, Tübingen.

K. Kimoto (2014). Practical aspects of monochromators developed for transmission electron microscopy. *Microscopy* **63**, 337–344.

K. Kimoto and T. Aoyama (1998). Proposal of a symmetric post-column energy filter. ICEM-14, Cancún. **1**, 91–92.

O. Klemperer (1965). Electron beam spectroscopy. *Rep. Prog. Phys.* **28**, 77–111.

C. T. Koch, W. Sigle, R. Höschen, M. Rühle, G. Essers, G. Benner and M. Matjevich (2006). SESAM: exploring the frontiers of electron microscopy. *Microsc. Microanal.* **12**, 506–514.

L. A. König (1955). Die Newtonsche Abbildungsgleichung des magnetischen Sektorfeldes bei Berücksichtigung des Streufeldes. *Z. Naturforsch.* **10a**, 652–654.

L. A. König and H. Hintenberger (1955). Über die Abbildungseigenschaften magnetischer Sektorfelder bei Berücksichtigung des Streufeldes. *Z. Naturforsch.* **10a**, 877–886.

L. A. König and H. Hintenberger (1957). Über die Abbildungsfehler von beliebig begrenzten homogenen magnetischen Sektorfeldern. *Z. Naturforsch.* **12a**, 377–384.

L. A. König and H. Hintenberger (1958). Massenspektrographen mit korrigierten Bildfehlern. *Nucl. Instrum.* **3**, 133–148.

M. I. Korsunskii, V. M. Kel'man and B. V. Petrov (1944). A β-spectrograph with non-uniform magnetic field. *Zh. Eksp. Teor. Fiz.* **14**, 394–401.

A. A. Kosiara (1976). Aberrations due to linear fringe fields in a magnetic spectrometer. *J. Appl. Phys.* **47**, 1048–1050.

V. G. Kovalenko and B. V. Polenov (1974). Electrostatic analyser for wide beams. *Zh. Tekh. Fiz.* **44**, 878–880. *Sov. Phys. Tech. Phys.* **19**, 561–562.

S. B. Kowalski and H. A. Enge (1987). The ion-optical program RAYTRACE. *Nucl. Instrum. Meth. Phys. Res. A* **258**, 407.

D. Krahl, K.-H. Herrmann and W. Kunath (1978a). Electron optical experiments with a magnetic imaging filter. ICEM-9, Toronto. **1**, 42–43.

D. Krahl, K.-H. Herrmann and E. Zeitler (1978b). Experiments with an imaging filter in a CTEM. EMSA, Atlanta, **39**, 366–367.

O. L. Krivanek (1979). Design of a compact, medium resolution electron energy-loss spectrometer. EMSA, San Antonio. **37**, 530–531.

O. L. Krivanek (1982). Recent results in EELS. ICEM-10, Hamburg. **1**, 167–172.
O. L. Krivanek and P. R. Swann (1981). An advanced electron energy-loss spectrometer. In *Quantitative Microanalysis with HIgh Spatial Resolution* (M. H. Jacobs, G. W. Lorimer and P. Doig, Eds), 136–140 (Metals Society, London).
O. L. Krivanek, A. J. Gubbens and N. Dellby (1991). Developments in EELS instrumentation for spectroscopy and imaging. *Microsc. Microanal. Microstruct.* **2**, 315–332.
O. L. Krivanek, A. J. Gubbens, N. Dellby and C. E. Meyer (1992). Design and first applications of a post-column imaging filter. *Microsc. Microanal. Microstruct.* **3**, 187–199.
O. L. Krivanek, S. L. Friedman, A. J. Gubbens and B. Kraus (1995). An imaging filter for biological applications. *Ultramicroscopy* **59**, 267–282.
O. L. Krivanek, J. P. Ursin, N. J. Bacon, G. J. Corbin, N. Dellby, P. Hrncirik, M. F. Murfitt, C. S. Own and Z. S. Szilagyi (2009). High-energy-resolution monochromator for aberration-corrected scanning transmission electron microscopy/electron energy-loss spectroscopy. *Philos. Trans. R. Soc. Lond. A* **367**, 3683–3697.
O. L. Krivanek, T. C. Lovejoy, Q. M. Ramasse and N. Dellby (2012a). Atom-by-atom imaging and spectroscopy by aberration-corrected STEM. EMC-15, Manchester. **2**, 407–408.
O. L. Krivanek, T. Lovejoy, N. Bacon, G. Corbin, M. Murfitt and N. Dellby (2012b). Advances in monochromators and aberration correctors. MC-2013, Regensburg **1**, 91–92.
O. L. Krivanek, T. C. Lovejoy, N. Dellby and R. W. Carpenter (2013). Monochromated STEM with a 30 meV-wide, atom-sized electron probe. *Microscopy* **62**, 3–21.
O. L. Krivanek, T. C. Lovejoy and N. Dellby (2015). Aberration-corrected STEM for atomic resolution and analysis. *J. Microsc. (Oxford)* **259**, 165–172.
S. Kujawa and D. Krahl (1998). Comparison between A-type and B-type imaging Ω-filters. ICEM-14, Cancún. **1**, 241–242.
B. Langenbeck (1987). On the ion optics of dipole magnets with parallel ends including stray field effects. *Nucl. Instrum. Meth. Phys. Res. A* **258**, 515–524.
S. Lanio (1986). High-resolution imaging magnetic energy filters with simple structure. *Optik* **73**, 99–107.
S. Lanio, H. Rose and D. Krahl (1986). Test and improved design of a corrected imaging magnetic energy filter. *Optik* **73**, 56–68.
R. C. G. Leckey (1987). Recent developments in electron energy analysers. *J. Electron Spectrosc. Relat. Phenom.* **43**, 183–214.
G. E. Lee-Whiting (1966a). Improved beta-spectometers. *Nucl. Instrum. Meth.* **43**, 182–193.
G. E. Lee-Whiting (1966b). Proposed electrostatic correction of the Chalk River $\pi\sqrt{2}$ β-beta-spectrometer. *Nucl. Instrum. Meth.* **43**, 194–198.
G. E. Lee-Whiting and E. A. Taylor (1957). Higher-order focusing in the $\pi\sqrt{2}$ β-spectrometer. *Can. J. Phys.* **35**, 1–15.
W. Legler (1963). Ein modifiziertes Wiensches Filter als Elektronenmonochromator. *Z. Phys.* **171**, 424–435.
G. E. Leithäuser (1904). Über den Geschwindigkeitsverlust, welchen die Kathodenstrahlen beim Durchgang durch dünne Metallschichten erleiden, und über die Ausmessung magnetischer Spektren. *Ann. Phys. (Leipzig)* **15** (320), 283–306.
H. Liebl (1958). Neigung und Krümmung der Richtungs- und Energiefokussierungskurven bei doppelfokussierenden Massenspektrographen. *Z. Naturforsch.* **13a**, 490–491.
H. Liebl (1976). A modified cylindrical condenser as electrostatic prism. *Int. J. Mass Spectrom. Ion Phys.* **22**, 203–207.
H. Liebl (2008). *Applied Charged Particle Optics* (Springer, Berlin).
H. Liebl and H. Ewald (1957a). Die Bildfehler doppelfokussierender Massenspektrographen. *Z. Naturforsch.* **12a**, 538–540.
H. Liebl and H. Ewald (1957b). Stigmatisch abbildende Massenspektrographen mit Doppelfokussierung praktisch von zweiter Ordnung. *Z. Naturforsch.* **12a**, 541–544; Errata: *ibid.* **14a** (1959) 588.

H. Liebl and H. Ewald (1959). Massenspektrographen mit Doppelfokussierung zweiter Ordnung. *Z. Naturforsch.* **14a**, 199–200.

H. Liebl and H. Ewald (1959). Stigmatisch abbildende bildfehlerfreie Massenspektrometer. *Z. Naturforsch.* **14a**, 842–843.

H. Liebl and H. Wachsmuth (1959). Einseitige Erdung des Ablenkkondensators in Massenspektrographen. *Z. Naturforsch.* **14a**, 846–847.

J. J. Livingood (1969). *The Optics of Dipole Magnets* (Academic Press, New York & London).

T. C. Lovejoy, N. J. Bacon, A. L. Bleloch, N. Dellby, M. V. Hoffman and O. L. Krivanek (2017). Ultra-high energy resolution EELS. *Microsc. Microanal.* **23** (Suppl. 1), 1552–1553.

R. Ludwig (1967). Die Ionenbahnen dritter Näherung in magnetischen Sektorfeldern einschließlich ihrer Streufelder. *Z. Naturforsch.* **22a**, 553–565.

L. A. MacColl (1941). Trajectories of mononenergetic electrons, in an arbitrary static electromagnetic field, in the neighborhood of a given trajectory. *J. Math. Phys.* **20**, 355–369.

L. A. MacColl (1943). The fundamental equations of electron motion (dynamics of high speed particles). *Bell Syst. Tech. J.* **22**, 153–177.

A. F. Malov (1968). Aberration and drift of an ion beam caused by a fringing field exhibiting transverse variation in magnetic prisms. *Zh. Tekh. Fiz.* **38**, 914–921. *Sov. Phys. Tech. Phys.* **13**, 688–693.

A. F. Malov (1985a). Trajectories of charged particle in the symmetry plane of an electromagetic field. *Zh. Tekh. Fiz.* **55**, 1426–1431. *Sov. Phys. Tech. Phys.* **30**, 822–824.

A. F. Malov (1985b). Equations of trajectories of charged particles in an electromagnetic field expressed in terms of a generalized orthogonal coordinate system. *Zh. Tekh. Fiz.* **55**, 1467–1469. *Sov. Phys. Tech. Phys.* **30**, 849.

A. F. Malov and G. M. Trubacheev (1981). Aberrationless variants of symmetric magnetic focusing prisms with a hyperbolic field. *Zh. Tekh. Fiz.* **51**, 1290–1292. *Sov. Phys. Tech. Phys.* **26**, 735–736.

A. F. Malov, V. A. Suzdarev and E. P. Fedoseev (1965a). Nonlinear study of spatial focusing in magnetic focusing prisms with r^{-1} fields. *Zh. Tekh. Fiz.* **35**, 914–926. *Sov. Phys. Tech. Phys.* **10**, 705–713.

A. F. Malov, V. A. Suzdarev and E. P. Fedoseev (1965b). Aberration and displacement of a beam by a fringing field without transverse variation in magnetic prisms. *Zh. Tekh. Fiz.* **35**, 1617–1620. *Sov. Phys. Tech. Phys.* **10**, 1249–1251.

A. F. Malov, A. I. Zaboev, V. A. Suzdalev and E. P. Fedoseev (1975). Ion-optical properties of an axisymmetric magnetic field varying as r^{-1} in the median plane. *Zh. Tekh. Fiz.* **45**, 2026–2032. *Sov. Phys. Tech. Phys.* **20**, 1280–1283.

M. Mankos, K. Shadman and V. Kolařik (2016). Novel electron monochromator for high resolution imaging and spectroscopy. *J. Vac. Sci. Technol. B* **34**. 06KP01, 11 pp.

H. Marschall (1944). Grundlegung der elektronenoptischen Theorie eines Massenspektrographen. *Phys. Z.* **45**, 1–37.

G. Martínez, M. Fernández-Martín, O. Sise, I. Madesis, A. Dimitriou, A. Laoutaris and T. J. M. Zouros (2016). Voltage optimization of a 4-element injection lens on a hemispherical spectrograph with virtual entry aperture. *Nucl. Instrum. Meth. Phys. Res. B* **369**, 92–94.

G. K. L. Marx, V. Gerheim and G. Schönhense (1997). Multipole Wien-filter for a high-resolution X-PEEM. *J. Electron Spectrosc. Relat. Phenom.* **84**, 251–261.

H. Matsuda (1961). Electrostatic analyzer with variable focal length. *Rev. Sci. Instrum.* **32**, 850–852.

H. Matsuda (1971). The influence of a toroidal electric fringing field on the trajectories of charged particles in a third order approximation. *Nucl. Instrum. Meth.* **91**, 637–647.

H. Matsuda (1974). Double focusing mass spectrometers of second order. *Int. J. Mass Spectrom. Ion Phys.* **14**, 219–233.

H. Matsuda (1975). Ion optics of parallel plane condensers. *Int. J. Mass Spectrom. Ion Phys.* **18**, 367–377.

H. Matsuda, Ed. (1983a). *Mass Spectrometry* (Asakura Shoten, Tokyo).

H. Matsuda (1983b). High-resolution high-sensitivity mass spectrometers. *Mass Spectrom. Rev.* **2**, 299–325.

H. Matsuda (1987). Improvement of mass spectrometers. *Nucl. Instrum. Meth. Phys. Res. A* **258**, 310–317.

H. Matsuda and Y. Fujita (1975). Potential distribution in a cylindrical condenser terminated by Matsuda plates. *Int. J. Mass Spectrom. Ion Phys.* **16**, 395–404.

H. Matsuda and T. Matsuo (1971). Influence of fringing fields on image aberrations of double-focusing mass spectrometers. *Int. J. Mass Spectrom. Ion Phys.* **6**, 385–392.

H. Matsuda and H. Wollnik (1970a). The influence of an inhomogeneous magnetic fringing field on the trajectories of charged particles in a third order approximation. *Nucl. Instrum. Meth.* **77**, 40–54.

H. Matsuda and H. Wollnik (1970b). Third order transfer matrices of the fringing field of an inhomogeneous magnet. *Nucl. Instrum. Meth.* **77**, 283–292.

H. Matsuda and H. Wollnik (1972). Third order transfer matrices for the fringing field of magnetic and electrostatic quadrupole lenses. *Nucl. Instrum. Meth.* **103**, 117–124.

H. Matsuda, T. Matsuo, D. Ioanoviciu, H. Wollnik and V. Rabbel (1982). Particle flight times through electrostatic and magnetic sector fields and quadrupoles to second order. *Int. J. Mass Spectrom. Ion Phys.* **42**, 157–168.

T. Matsuo (1984a). Computer-aided design of a new high-performance mass spectrometer. *Jpn. J. Appl. Phys.* **23**, 1518–1525.

T. Matsuo (1984b). Computer program TRIO-FIT for third order calculation of ion trajectory with help of automatic fitting function. *Mass Spectrosc.* **32**, 319–326.

T. Matsuo and H. Matsuda (1971). Third order calculation of the ion trajectories in an inhomogeneous magnetic sector field. *Int. J. Mass Spectrom. Ion Phys.* **6**, 361–383.

T. Matsuo and H. Wollnik (1975). The all electric adjustment of a double focusing mass spectrometer. *Int. J. Mass Spectrom. Ion Phys.* **18**, 205–214.

T. Matsuo, H. Matsuda and H. Wollnik (1972). Particle trajectories in a toroidal condenser calculated in a third order approximation. *Nucl. Instrum. Meth.* **103**, 515–532.

T. Matsuo, N. Takahashi, H. Matsuda and A. J. H. Boerboom (1977). Applications of quadrupole lenses to mass spectrometers. *Adv. Mass Spectrom.* **7**, 851–854.

T. Matsuo, H. Matsuda, H. Nakabushi, Y. Fujita and A. J. H. Boerboom (1982). Third-order ion optics of an electrostatic multipole lens. *Int. J. Mass Spectrom. Ion Phys.* **42**, 217–241.

T. Matsuo, T. Sakurai and H. Matsuda (1987). Ion optics of a new TOF mass spectrometer in the third order approximation. *Nucl. Instrum. Meth. Phys. Res. A* **258**, 327–330.

R. Meinel and S. Thiem (1986). A complete set of independent asymptotic aberration coefficients for deflection magnets. *Optik* **74**, 1–2.

A. J. F. Metherell (1971). Energy analysing and energy selecting electron microscopes. *Adv. Opt. Electron Microsc.* **4**, 263–360. Reprinted in *Adv. Imaging Electron Phys.* **204** (2017) 147–230.

M. Mohn, J. Biskupek and U. Kaiser (2017). Performance of SALVE III energy filter for low-voltage energy-filtered TEM. MC-2017, Lausanne, 545–546.

G. Möllenstedt (1949). Die elektrostatische Linse als hochauflösender Geschwindigkeitsanalysator. *Optik* **5**, 499–517.

G. Möllenstedt (1952). Über die chromatischen Verluste von Elektronen beim Durchtritt durch Materie. *Optik* **9**, 473–480.

G. Möllenstedt and W. Dietrich (1955). Verbesserung der Optik des hochauflösenden elektrostatischen Geschwindigkeits-Analysators. *Optik* **12**, 246–249.

G. Möllenstedt and H. Gruner (1968). Monochromatisierung von Elektronenstrahlen und Verbesserung von Emissionsbildern mittels eines Elektronenspiegels. *Optik* **27**, 602–604.

G. Möllenstedt and F. Heise (1949). Die elektrostatische Linse als hochauflösender Geschwindigkeits-Analysator. *Phys. Blätt.* **5**, 80–83.

H. W. Mook (2000). The fringe field monochromator. Energy filter for high brightness electron guns. Dissertation, Delft.

H. W. Mook and P. E. Batson (1999). Integration of a monochromator in the field emission STEM. *Microsc. Microanal.* **5** (Suppl. 2), 648–649.

H. W. Mook and P. Kruit (1997). Electrostatic in-line monochromator for Schottky field emission guns. EMAG, Cambridge. 81–84.

H. W. Mook and P. Kruit (1998). Fringe field monochromator for high brightness electron sources. ICEM-14, Cancún. **1**, 73–74.

H. W. Mook and P. Kruit (1999a). Optics and design of the fringe field monochromator for a Schottky field emission gun. *Nucl. Instrum. Meth. Phys. Res. A* **427**, 109–120.

H. W. Mook and P. Kruit (1999b). On the monochromatisation of high brightness electron sources for electron microscopy. *Ultramicroscopy* **78**, 43–51.

H. W. Mook and P. Kruit (1999c). Operation of the fringe-field monochromator in field emission STEM. EMAG, Sheffield. 223–226.

H. W. Mook and P. Kruit (2000a). Construction and characterization of the fringe field monochromator for a field emission gun. *Ultramicroscopy* **81**, 129–139.

H. W. Mook and P. Kruit (2000b). Optimization of the short field monochromator configuration for a high brightness electron source. *Optik* **111**, 339–346.

H. W. Mook, A. H. V. v. Veen and P. Kruit (1999a). Energy filtering of Schottky field emission gun using fringe field monochromator. *Microsc. Microanal.* **5** (Suppl. 2), 648–649.

H. W. Mook, P. E. Batson and P. Kruit (1999b). Operation of the fringe-field monochromator in field emission STEM. EMAG, Sheffield. 223–226.

H. W. Mook, P. E. Batson and P. Kruit (2000). Monochromator for high brightness electron guns. EUREM-12, Brno. **3**, 315–316.

M. Mukai, J. S. Kim, K. Omoto, H. Sawada, A. Kimura, A. Ikeda, J. Zhou, T. Kaneyama, N. P. Young, J. H. Warner, P. D. Nellist and A. I. Kirkland (2014). The development of a 200 kV monochromated field emission electron source. *Ultramicroscopy* **140**, 37–43.

M. Mukai, K. Omoto, T. Sasaki, Y. Kohno, S. Morishita, A. Kimura, A. Ikeda, K. Somehara, H. Sawada, K. Kimoto and K. Suenaga (2014). Design of a monochromator for aberration-corrected low-voltage (S)TEM. IMC-18, Prague. IT-1-P-2578.

H. Müller, D. Preikszas and H. Rose (1996). Semi-analytical fringing field calculation and design aspects of a magnetic beam separator. *Recent Trends* **5**, 57–58.

E. Munro (1987). Computer programs for the design and optimization of electron and ion beam lithgraphy systems. *Nucl. Instrum. Meth. Phys. Res. A* **258**, 443–461.

E. Munro, J. Rouse, H. Liu, L. Wang and X. Zhu (2006). Simulation software for designing electron and ion beam equipment. *Microelectron. Eng.* **83**, 994–1002.

L. Musumeci (1950). Dispersione e aberrazione nello spettrografo di massa a campo magnetico. *Nuovo Cim.* **7**, 351–363.

L. Musumeci (1952). Sull'aberrazioni negli spectrometri di massa a settore magnetico. *Nuovo Cim.* **9**, 429–435.

H. Nakabushi and T. Matsuo (1982). A third order transfer matrix of a magnetic multipole lens. *Nucl. Instrum. Meth.* **198**, 207–212.

H. Nakabushi and T. Sakurai (1983). Flight time of relativistically fast particles in crossed toroidal electric and inhomogeneous magnetic fields. *Int. J. Mass Spectrom. Ion Phys.* **50**, 275–286.

H. Nakabushi, T. Sakurai and H. Matsuda (1983a). Relativistic ion optics of crossed toroidal electric and inhomogeneous magnetic fields. *Int. J. Mass Spectrom. Ion Phys.* **49**, 89–101.

H. Nakabushi, T. Sakurai and H. Matsuda (1983b). Unified theory of ion optics. *Int. J. Mass Spectrom. Ion Phys.* **52**, 319–336.

H. Nakabushi, T. Sakurai and H. Matsuda (1983c). Unified theory of ion opics. II. The influences of fringing fields and boundary shapes of unified fields on particle trajectories. *Int. J. Mass Spectrom. Ion Phys.* **55**, 291–306.

A. Nakai (1975). Geometrical image aberrations for a sector type magnetic analyzer with fringing field in a third order approximation. I. *Mass Spectrosc.* **23**, 161–171.

A. Nakai (1977). Geometrical image aberrations for a sector type magnetic analyzer with fringing field in a third order approximation. II. *Mass Spectrosc.* **25**, 11–48.

T. Ogawa and B. Cho (2015). A new monochromator with multiple offset cylindrical lenses. *Nucl. Instrum. Meth. Phys. Res. A* **772**, 5–13.

T. Ogawa, B. Cho and S. J. Ahn (2015a). A novel monochromator with double cylindrical lenses. *Microsc. Microanal.* **21** (Suppl. 4), 112−117.
T. Ogawa, B. Cho and S. J. Ahn (2015b). Low-energy scanning electron microscope using a monochromator with double-offset cylindrical lenses. *J. Vac. Sci. Technol. B* **33**. 06FJ01, 11 pp.
T. Ogawa, G. W. Gang, L.-y. Park, J. H. Kim, S. J. Ahn and B. L. Cho (2016). Fabrication of nano-slits for a monochromator with double offset cylindrical lenses. *Recent Trends* **15**, 42−43.
T. Oikawa, N. Shibata, K. Nakanishi, Y. Kokubo and Y. Bando (1986). An EELS spectrometer with a double dispersion lens for a medium voltage TEM. *J. Electron Microsc.* **35**, 353−358.
K. Omoto, K. Tsuno, M. Ohsaki, S. Matsumura and Y. Tomokiyo (2008). Omega filter installed in the 1 MV microsope of Kyushu University. *Micron* **39**, 666−675.
F. P. Ottensmeyer (1984). Energy selecting electron microscopy. In *Electron Optical Systems for Microscopy, Microanalysis and Microlithography* (J. J. Hren, F. A. Lenz, E. Munro and P. B. Sewell, Eds), 245−251 (Scanning Electron Microscopy, AMF O'Hare).
F. R. Paolini and G. C. Theodoridis (1967). Charged particle transmision through spherical plate electrostatic analyzers. *Rev. Sci. Instrum.* **38**, 579−588.
N. Paras (1961). *Etude d'un dispositif de filtrage des images électroniques* (Diplôme d'Etudes Supérieures, Paris).
N. W. Parker, M. Utlaut and M. S. Isaacson (1978). Design of magnetic spectrometers with second-order aberrations corrected. I. Theory. *Optik* **51**, 333−351.
P. P. Pavinskii (1954). On the motion of electrons in magnetic spectrometers with non-uniform fields. *Izv. Akad. Nauk SSSR (Ser. Fiz.)* **18**, 175−191.
H. T. Pearce-Percy (1976). An energy analyser for a CTEM/STEM. *J. Phys. E: Sci. Instrum.* **9**, 135−138.
H. T. Pearce-Percy (1978). The design of spectrometers for energy loss spectroscopy. *Scanning Electron Microsc.* Pt. I, 41−51.
H. T. Pearce-Percy, D. Krahl and J. Jaeger (1976). A 4-magnet imaging spectrometer for a fixed-beam transmission microscope. EUREM-6, Jerusalem. **1**, 348−349.
S. Penner (1961). Calculations of properties of magnetic deflection systems. *Rev. Sci. Instrum.* **32**, 150−160; Errata: ibid. 1068−1069.
J.-P. Perez, G. Zanchi, J. Sevely and B. Jouffrey (1975). Discussion on a magnetic energy analyser used for very high voltage electron microscopy (1 MV and 3 MV). *Optik* **43**, 487−494.
J.-P. Perez, J. Sirven, A. Séguéla and J. C. Lacaze (1984). Etude, au premier ordre, d'un système dispersif, magnétique, symétrique, de type alpha. *J. Phys. (Paris)* **45** (C2), 171−174.
E. Plies (1978). Proposal for an electrostatic energy filter and a monochromator. ICEM-9, Toronto. **1**, 50−51.
E. Plies (2002). Simplified computation of third-rank image aberrations of electron-optical systems with curved axis. *Ultramicroscopy* **93**, 305−319.
E. Plies and H. Rose (1971). Über die axialen Bildfehler magnetischer Ablenksysteme mit krummer Achse. *Optik* **34**, 171−190.
E. Plies and H. Rose (1977). Bemerkungen zu "Ein in zweiter Näherung bildfehlerfreies Energiefilter für Elektronenmikroskope" [Wollnik et al., *Optik* **46** (1976) 255]. *Optik* **47**, 365−368.
E. Plies and D. Typke (1978). Dreidimensional abbildende Elektronenmikroskope. II. Theorie elektronenoptischer Systeme mit gekrümmter Achse. *Z. Naturforsch.* **33a**, 1361−1377; Errata: *ibid.* **35a** (1980) 566.
W. Ploch and W. Walcher (1950). Die Abbildungseigenschaften magnetischer Sektorfelder unter Berücksichtigung des Streufeldes. *Z. Phys.* **127**, 274−288.
H. O. W. Richardson (1947). Magnetic focusing between inclined plane pole-faces. *Proc. Phys. Soc. (Lond.)* **59**, 791−804.
H. Rose (1978). Aberration correction of homogeneous magnetic deflection systems. *Optik* **51**, 15−38.
H. Rose (1987a). Hamiltonian magnetic optics. *Nucl. Instrum. Meth. Phys. Res. A* **258**, 374−401.
H. Rose (1987b). The retarding Wien filter as a high-performance imaging filter. *Optik* **77**, 26−34.
H. Rose (1994). Correction of aberrations, a promising means for improving the spatial and energy resolution of energy-filtering electron microscopes. *Ultramicroscopy* **56**, 11−25.
H. Rose (1999). Prospects for realizing a sub-Å sub-eV resolution EFTEM. *Ultramicroscopy* **78**, 13−25.

H. Rose (2012). *Geometrical Charged-particle Optics* (Springer, Berlin; 1st edn, 2009).
H. Rose and D. Krahl (1995). Electron optics of imaging energy filters. In *Energy-Filtering Transmission Electron Microscopy* (L. Reimer, Ed.), 43–149 (Springer, Berlin).
H. Rose and W. Pejas (1979). Optimization of imaging magnetic energy filters free of second-order aberrations. *Optik* **54**, 235–250.
H. Rose and U. Petri (1971). Zur systematischen Berechnung elektronenoptischer Bildfehler. *Optik* **33**, 151–165.
H. Rose and E. Plies (1973). Correction of aberrations in electron optical systems with curved axes. In *Image Processing and Computer-Aided Design in Electron Optics* (P. W. Hawkes, Ed.), 344–369 (Academic Press, London & New York).
H. Rose and E. Plies (1974). Entwurf eines fehlerarmen magnetischen Energie-Analysators. *Optik* **40**, 336–341.
E. S. Rosenblum (1950). A sector-type double-focusing magnetic spectrometer. *Rev. Sci. Instrum.* **21**, 586–592.
D. Roy and J.-D. Carette (1971). Spectromètres électrostatiques, Partie III. *Can. J. Phys.* **49**, 2138–2159. Part 1 is Y. Delage and J.-D. Carette, *ibid*. **49**, 2118–2131; Part 2 is P. Allard and J.-D. Carette, *ibid*. **49**, 2132–2137.
F. G. Rüdenauer (1970). Focusing properties of magnetic sectors of the wedge type. I, II. *Int. J. Mass Spectrom. Ion Phys.* **4**, 181–194 & 195–201.
F. G. Rüdenauer and F. P. Viehböck (1965). On inhomogeneous magnetic fields for mass separators. *Nucl. Instrum. Meth.* **38**, 140–143.
F. G. Rüdenauer and F. P. Viehböck (1966). A numerical method for the calculation of image aberrations of inhomogeneous magnetic sector fields between conical pole faces. *Z. Naturforsch.* **21a**, 2–8.
V. D. Sachenko (1980). Magnetic analysers of a generalized symmetry. *Zh. Tekh. Fiz.* **50**, 461–464. *Sov. Phys. Tech. Phys*. **25**, 279–281.
V. D. Sachenko and G. V. Fridlyanskii (1980). High-resoluton mass spectrometer with correction for horizontal and vertical aberrations. *Zh. Tekh. Fiz.* **50**, 1974–1982. *Sov. Phys. Tech. Phys*. **25**, 1149–1153.
T. Sakurai, T. Matsuo and H. Matsuda (1985). Ion optics for time-of-flight mass spectrometers with multiple symmetry. *Int. J. Mass Spectrom. Ion Processes* **63**, 273–287.
T. Sakurai, T. Matsuo and H. Matsuda (1989). The vertical component of an ion trajectory in a homogeneous magnet to a third-order approximation. *Int. J. Mass Spectrom. Ion Proc.* **91**, 51–68.
H. Z. Sar-El (1966). More on the spherical condenser as an analyser. I. Nonrelativistic part. *Nucl. Instrum. Meth.* **42**, 71–76.
H. Z. Sar-El (1967). Cylindrical capacitor as an analyzer. I. Nonrelativistic part. *Rev. Sci. Instrum.* **38**, 1210–1216.
H. Z. Sar-El (1968). Cylindrical capacitor as an analyzer. II. Relativistic part. *Rev. Sci. Instrum.* **39**, 533–540.
H. Z. Sar-El (1971). Cylindrical mirror analyzer with surface entrance and exit slots. I. Nonrelativistic part. *Rev. Sci. Instrum.* **42**, 1601–1606.
H. Z. Sar-El (1972). Cylindrical mirror analyzer with surface entrance and exit slots. II. Relativistic part. *Rev. Sci. Instrum.* **43**, 259–263.
V. P. Saulit (1954). Concerning the focusing of a plane beam of charged particles in magnetic fields varying along one cartesian coordinate. *Izv. Akad. Nauk SSSR (Ser. Fiz.)* **18**, 233–242.
V. P. Saulit (1956). Some precisions on the article "Concerning the focusing of a plane beam of charged particles in magnetic fields varying along one cartesian coordinate". *Izv. Akad. Nauk SSSR (Ser. Fiz.)* **20**, 374–376.
M. Scheinfein and M. Isaacson (1984). Design and performance of second order corrected spectrometers for use with the scanning transmission electron microscope. *Scanning Electron Microsc.*, 1681–1696.
G. Schiwietz, M. Beye, D. Kühn and G. Xiao (2015). The retarding Bessel-box – an electron spectrometer designed for pump/probe experiments. *J. Electron Spectrosc. Related Phenom* **203**, 51–59.
P. Schury, M. Wada, Y. Ito, D. Kaji, F. Arai, M. MacCormick, I. Murray, H. Haba, S. Jeong, S. Kimura, H. Koura, H. Miyatake, K. Morimoto, K. Morita, A. Ozawa, M. Rosenbusch, M. Reponen, P.-A. Söderström, A. Takamine, T. Tanaka and H. Wollnik (2017). First online multireflection time-of-flight mass measurements of isobar chains produced by fusion–evaporation reactions: toward identification of super-heavy elements via mass spectroscopy. *Phys. Rev. C* **95**, 011305.

R. L. Seliger (1972). $\boldsymbol{E} \times \boldsymbol{B}$ mass-separator design. *J. Appl. Phys.* **43**, 2352–2357.

S. Senoussi (1971). Etude d'un dispositif de filtrage des vitesses purement magnétique adaptable à un microscope électronique à très haute tension. Thèse 3e Cycle, Paris–Orsay.

S. Senoussi, L. Henry and R. Castaing (1971). Etude d'un analyseur filtre de vitesses purement magnétique adaptable aux microscopes électroniques très haute tension. *J. Microsc. (Paris)* **11**, 19.

R. V. Servranckx and K. L. Brown (1987). Circular machine design techniques and tools. *Nucl. Instrum. Meth. Phys. Res. A* **258**, 525–535.

J. Sevely, J.-P. Perez and B. Jouffrey (1973). Réalisation d'un analyseur de pertes d'énerge des électrons à très haute tension (300 à 1200 kV). *C. R. Acad. Sci. Paris B* **276**, 515–518.

J. Sevely, G. Zanchi, J.-P. Perez and B. Jouffrey (1977). Optics of a magnetic energy filter for CTEM. EMAG, Glasgow. 45–48.

J. Sevely, J.-P. Perez, G. Zanchi, Y. Kihn and B. Jouffrey (1982). Electron energy loss spectroscopy from 1 MV to 3 MV. ICEM, Hamburg. **1**, 589–590.

O. Shanker (1987). Achromatic magnet. *Rev. Sci. Instrum.* **58**, 709.

F. B. Shull and D. M. Dennison (1947). The double focusing beta-ray spectrometer. *Phys. Rev.* **71**, 681–687; Errata: *Phys. Rev.* **72** (1947) 256.

H. Shuman (1980). Correction of the second-order aberrations of uniform field magnetic sectors. *Ultramicroscopy* **5**, 45–53.

K. Siegbahn, Ed. (1955). *Beta- and Gamma-Ray Spectroscopy* (North Holland, Amsterdam).

K. Siegbahn, Ed. (1965). *Alpha-, Beta- and Gamma-Ray Spectroscopy* (North Holland, Amsterdam).

K. Siegbahn and N. Svartholm (1946). Focusing of electrons in two dimensions by an inhomogeneous magnetic field. *Nature* **157**, 872–873.

O. Sise, T. J. M. Zouros, M. Ulu and M. Dogan (2008a). First-order focusing and energy resolution optimization of a biased paracentric hemispherical spectrograph. *Phys. Procedia* **1**, 467–472.

O. Sise, T. J. M. Zouros, M. Ulu and M. Dogan (2008b). Comparison of fringing field correction schemes for the 180° hemispherical detector analyzer. *Phys. Procedia* **1**, 473–477.

O. Sise, M. Ulu, M. Dogan and G. Martínez (2010). Fringing field optimization of hemispherical deflector analyzers using BEM and FDM. *J. Electron Spectrosc. Relat. Phenom.* **177**, 42–51.

O. Sise, G. Martínez, I. Madesis, A. Laoutaris, A. Dimitriou, M. Fernández-Martín and T. J. M. Zouros (2016). The voltage optimization of a four-element lens used on a hemispherical spectrograph with virtual entry for highest energy resolution. *J. Electron Spectrosc. Relat. Phenom.* **211**, 19–31.

A. V. Solov'ev and A. B. Tolstoguzov (1987). Ion-optical characteristics of a Wien filter with uniform orthogonal fields. *Zh. Tekh. Fiz.* **57**, 953–959. *Sov. Phys. Tech. Phys.* **32**, 580–583.

C. Souche and B. Jouffrey (1998). Proposal of a new energy filter for TEM: the Phi filter. ICEM-14, Cancún. **1**, 247–248.

W. Steckelmacher (1973). Energy analysers for charged particle beams. *J. Phys. E: Sci. Instrum.* **6**, 1061–1071.

A. M. Strashkevich (1959). *Elektronnaya Optika Elektrostaticheskikh Polei ne Obladayushchikh Osevoi Simmetriei* (Gos. Izd. Fiz.-Mat. Lit., Moscow).

A. M. Strashkevich and N. G. Gluzman (1954). Aberrations of relativistic electron beams. *Zh. Tekh. Fiz.* **24**, 2271–2284.

A. M. Strashkevich and I. M. Pilat (1951). The aberrations of corpuscular beams of arbitrary form in arbitrary electrostatic fields. *Izv. Akad. Nauk SSSR (Ser. Fiz.)* **15**, 448–466.

A. M. Strashkevich and I. M. Pilat (1952). Aberrations of beams with a curved axis in an arbitrary plane electrostatic field. *Uch. Zap. Chernovitskii Gos. Univ. (Ser. Fiz.-Mat. Nauk)* **4**, 113–122.

P. A. Sturrock (1952). The imaging properties of electron beams in arbitrary static electromagnetic fields. *Philos. Trans. R. Soc. (Lond.) A* **245**, 155–187.

A. Suri, A. Pratt, S. Tear, C. Walker and M. El-Gomati (2017). Characterization of a miniature electron energy analyzer for scanning electron microscopes. EMAG Manchester. *J. Phys. Conf.* **902**, 012017, 4 pp.

N. Svartholm (1950). The focusing properties of inhomogeneous magnetic sector fields. *Ark. Fys.* **2**, 115–118.

H. J. Svec (1985). Mass spectroscopy – ways and means. A historical prospectus. *Int. J. Mass Spectrom. Ion Processes* **66**, 3–29.

A. A. Sysojev and G. A. Samsonov (1970a). Calculation of sector-shaped mass spectrometric analysers with curvilinear boundaries. *Int. J. Mass Spectrom. Ion Phys.* **5**, 49–62.

A. A. Sysoev and G. A. Samsonov (1970b). Refraction of ion trajectories at mass-spectrometer boundaries. *Zh. Tekh. Fiz.* **40**, 1986–1993. *Sov. Phys. Tech. Phys.* **15**, 1548–1553.

A. A. Sysoev and G. A. Samsonov (1972). *Teoriya i Raschet Staticheskikh Mass-analizatorov* (Ordena Trudivogo Krasnogo Znameni Inzhenerno-Fizicheskii Institut, Moscow).

I. Takeshita (1966a). Matrix representation for calculation of the second-order aberration in ion optics. *Z. Naturforsch.* **21a**, 9–14.

I. Takeshita (1966b). Mattauch–Herzog type mass spectrograph with a two stage electrostatic field. *Z. Naturforsch.* **21a**, 14–25.

I. Takeshita (1966c). Mattauch–Herzog type mass spectrograph with two-stage electrostatic field. *Mass Spectrosc.* **14**, 59–71.

I. Takeshita (1967). Mattauch–Herzog type mass spectrograph with corrected β-dependent image defects for all masses. *Rev. Sci. Instrum.* **38**, 1361–1367.

T.-t. Tang (1982a). Design of an electron spectrometer for scanning transmission electron microscope (STEM). *Scanning Electron Microsc.* Pt. I, 39–50.

T.-t. Tang (1982b). Second and third order aperture aberrations of uniform magnetic field spectrometers. *Optik* **62**, 379–399.

T. T. Tang (1982c). Corrrection of aberrations in a magnetic spectrometer by electric multipole lenses. *Ultramicroscopy* **7**, 305–310.

T. T. Tang (1986). Aberration analysis of a crossed-field analyzer. *Optik* **74**, 51–56.

H. A. Tasman and A. J. H. Boerboom (1959). Calculation of the ion optical properties of inhomogeneous magnetic sector fields including the second order aberrations in the median plane. *Z. Naturforsch.* **14a**, 121–129; Errata *ibid*. **15a** (1960) 79.

H. A. Tasman and A. J. H. Boerboom (1960). Elimination of the radial second order angular aberrations in inhomogeneous field mass spectrometers by inclined plane boundaries. *Z. Naturforsch.* **15a**, 736–738.

H. A. Tasman, A. J. H. Boerboom and H. Wachsmuth (1959). Calculation of the ion optical properties of inhomogeneous magnetic sector fields. Part 3: Oblique incidence and exit at curved boundaries. *Z. Naturforsch.* **14a**, 822–827; Errata *ibid.* **15a** (1960) 79 & **17a** (1962) 362.

H. A. Tasman, A. J. H. Boerboom and H. Wachsmuth (1960). Calculation of the ion optical properties of inhomogeneous magnetic sector fields: note on the trajectories outside the median plane with oblique incidence, and on the second order angular aberration coefficient. *Z. Naturforsch.* **15a**, 78–79.

S. Taya and H. Matsuda (1971). Third order transfer matrices for the fringing fields of an electrostatic hexapole lens. *Mass Spectrosc.* **19**, 266–273.

S. Taya, Y. Taniguchi, E. Nakazawa and J. Usukura (1996). Development of γ-type energy filtering TEM. *J. Electron Microsc.* **45**, 307–313.

M. Terauchi, R. Kuzuo, F. Satoh, M. Tanaka, K. Tsuno and J. Ohyama (1991). Performance of a new high-resolution energy-loss spectroscopy microscope. *Microsc. Microanal. Microstruct.* **2**, 351–358.

G. C. Theodoridis and F. R. Paolini (1968). Charged particle transmission through cylindrical plate electrostatic analyzers. *Rev. Sci. Instrum.* **39**, 326–330.

G. C. Theodoridis and F. R. Paolini (1969). The angular response of spherical plate electrostatic analyzers. *Rev. Sci. Instrum.* **40**, 621–631.

R. Tian and M. Fink (1987). Higher-order caustics and spectra of a Moellenstedt electron energy analyzer. *Rev. Sci. Instrum.* **58**, 1450–1455.

P. C. Tiemeijer (1999). Operation modes of a TEM monochromator. EMAG, Sheffield. 191–194.

P. C. Tiemeijer, M. Bischoff, B. Freitag and C. Kisielowski (2012a). Using a monochromator to improve the resolution in TEM to below 0.5 Å. Part I: Creating highly coherent monochromated illumination. *Ultramicroscopy* **114**, 72–81.

P. C. Tiemeijer, M. Bischoff, B. Freitag and C. Kisielowski (2012b). Using a monochromator to improve the resolution in TEM to below 0.5 Å. Part II: Application to focal series reconstruction. *Ultramicroscopy* **118**, 35–43.

P. C. Tiemeijer, S. Lazar and A. Bright (2017). An improved gun monochromator with <30 meV energy resolution. *Kenbikyo* **52** (Suppl. 1), 10.

J. Trötscher, H. Irnich and H. Wollnik (1990). Transfer matrices of electrostatic lenses and ion mirrors both consisting of rotationally symmetric electrodes. *Nucl. Instrum. Meth. Phys. Res. A* **298**, 480–487.

N. Tsoupas, J. Colman, M. Levine, R. McKenzie-Wilson, T. Ward, P. Grand and H. A. Enge (1987). Effects of dipole magnet inhomogeneities on the beam ellipsoid. *Nucl. Instrum. Meth. Phys. Res. A* **258**, 421–425.

I. I. Tsukkerman (1954). On a theory of electron-optical systems with arbitrarily curved axis. *Zh. Tekh. Fiz.* **24**, 258–273.

K. Tsuno (1999a). Design of energy filters for electron microscopes. *Proc. SPIE* **3777**, 242–251.

K. Tsuno (1999b). Optical design of electron microscope lenses and energy filters. *J. Electron Microsc.* **48**, 801–820.

K. Tsuno (2001). "S filter", a compact, high dispersion in-column energy filter. *Proc. SPIE* **4510**, 71–79.

K. Tsuno (2004). Evaluation of in-column energy filters for analytical electron microscopes. *Nucl. Instrum. Meth. Phys. Res. A* **519**, 286–296.

K. Tsuno (2011). Monochromators in electron microscopy. *Nucl. Instrum. Meth. Phys. Res. A* **645**, 12–19.

K. Tsuno and D. Ioanoviciu (2013). The Wien filter. *Adv. Imaging Electron Phys.* **176**.

K. Tsuno and E. Munro (1997). Design of an omega filter for a 200 kV electron microscope. *Rev. Sci. Instrum.* **68**, 109–115.

K. Tsuno and J. Rouse (1996). Simulation of electron trajectories of Wien filters for high-resolution EELS installed in TEM. *J. Electron Microsc.* **45**, 417–427.

K. Tsuno, M. Terauchi and M. Tanaka (1988a). Electron trajectory calculations of a stigmatic-focus Wien filter for electron energy loss spectroscopy. I. *Optik* **78**, 71–77.

K. Tsuno, M. Terauchi and M. Tanaka (1988b). Electron trajectory calculations of a stigmatic-focus Wien filter for electron energy loss spectroscopy. II. *Optik* **80**, 149–154.

K. Tsuno, M. Terauchi and M. Tanaka (1989). Electron trajectory calculations of a stigmatic-focus Wien filter for electron energy loss spectroscopy. III. *Optik* **83**, 77–84.

K. Tsuno, T. Kaneyama, T. Honda, M. Terauchi and M. Tanaka (1997). Design and testing of Omega mode imaging energy filters at 200 kV. *J. Electron Microsc.* **46**, 357–368.

K. Tsuno, T. Kaneyama, T. Honda and Y. Ishida (1998). Non-isochromaticity of an omega filter in a 200 kV transmission electron microscope. *J. Electron Microsc.* **47**, 611–619.

K. Tsuno, T. Kaneyama, T. Honda, Y. Ishida, K. Tsuda, M. Terauchi and M. Tanaka (1998). Design of an omega filter for 200 kV TEM. ICEM-14, Cancún. **1**, 253–254.

K. Tsuno, T. Kaneyama, T. Honda and Y. Ishida (1999). Design of omega mode imaging energy filters. *Nucl. Instrum. Meth. Phys. Res. A* **427**, 187–196.

S. Uhlemann and H. Rose (1994a). The MANDOLINE filter – a new high-performance imaging filter. *Optik* **96**, 163–178.

S. Uhlemann and H. Rose (1994b). Comparison of the performance of existing and proposed imaging energy filters. ICEM-13, Paris. **1**, 163–164.

S. Uhlemann and H. Rose (1996). Acceptance of imaging energy filters. *Ultramicroscopy* **63**, 161–167.

Yu. V. Vandakurov (1955). The equations of electron optics for wide pencils with calculation of the chromatic aberration and their applications to the study of the motion of particles in axially symmetric fields. *Zh. Tekh. Fiz.* **25**, 1412–1425.

Yu. V. Vandakurov (1957). On the theory of the aberrations in electron-optical focusing systems with a curvilinear axis. *Zh. Tekh. Fiz.* **27**, 1850–1862. *Sov. Phys. Tech. Phys.* **2**, 1719–1733.

N. F. Verster (1950). Spherical aberration of a double focusing beta ray spectrometer. *Physica* **16**, 815–816.

H. G. Voorhies (1955). Second-order aberrations in sector shaped electromagnetic analyzers. *Rev. Sci. Instrum.* **26**, 716–717; Errata *ibid.* **27** (1956) 58.

H. Wachsmuth, A. J. H. Boerboom and H. A. Tasman (1959a). Calculation of the ion optical properties of inhomogeneous magnetic sector fields. Part 2: The second order aberrations outside the median plane. *Z. Naturforsch.* **14a**, 818–822.

H. Wachsmuth, H. Liebl and H. Ewald (1959b). Doppelfokussierende bildfehlerfreie Massenspektrometer mit besonders hoher Auflösung und Dispersion. *Z. Naturforsch.* **14a**, 844–846.

R. J. Walen (1957). Transformation d'une focalisation de premier ordre en focalisation de deuxième ordre en spectrographie magnétique à champ homogène. *Nucl. Instrum.* **1**, 242–250.

B. Wannberg, U. Gelius and K. Siegbahn (1974). Design principles in electron spectroscopy. *J. Phys. E: Sci. Instrum.* **7**, 149–159.

G. Wendt (1942). Zur Dioptrik elektronenoptischer Geräte mit beliebig gekrümmten Abbildungsachsen. *Z. Phys.* **120**, 720–740.

N. R. White, K. H. Purser and S. B. Kowalski (1987). The design of magnets with nondipole field components. *Nucl. Instrum. Meth. Phys. Res. A* **258**, 437–442.

W. Wien (1897). Die elektrostatischen Eigenschaften der Kathodenstrahlen. *Verhandlungen der Deutschen Physikalischen Gesellschaft Berlin* **16**, 165–172.

D. B. Wittry (1969). An electron spectrometer for use with the transmission electron microscope. *J. Phys. D: Appl. Phys.* **2**, 1757–1766.

H. Wollnik (1965). Second order approximation of the three-dimensional trajectories of charged particles in deflecting electrostatic and magnetic fields. *Nucl. Instrum. Meth.* **34**, 213–221.

H. Wollnik (1967a). Second order transfer matrices of real magnetic and electrostatic sector fields. *Nucl. Instrum. Meth.* **52**, 250–272.

H. Wollnik (1967b). The correction of image aberrations of second order for mass or energy separators consisting of one single magnetic sector field. *Nucl. Instrum. Meth.* **53**, 197–215.

H. Wollnik (1967c). Electrostatic prisms. In *Focusing of Charged Particles* (A. Septier, Ed.), **2**, 163–202 (Academic Press, New York & London).

H. Wollnik (1968). Image aberrations of second order of electrostatic sector fields. *Nucl. Instrum. Meth.* **59**, 277–282.

H. Wollnik (1971). A "Q-value" for particle spectrometers. *Nucl. Instrum. Meth.* **95**, 453–460.

H. Wollnik (1972). Multipole elements for the correction of image aberrations. *Nucl. Instrum. Meth.* **103**, 479–484.

H. Wollnik (1980). Mass spectrographs and isotope separators. In *Applied Charged Particle Optics* (A. Septier, Ed.), **B**, 133–172 (Academic Press, New York & London). *Adv. Electron. Electron Phys*. Suppl. 13B.

H. Wollnik (1987a). *Optics of Charged Particles* (Academic Press, Orlando & London).

H. Wollnik (1987b). Development of time-of-flight mass spectrometer systems. *Instrum. Sci. Technol.* **16**, 15–29.

H. Wollnik (1993). Higher-order aberrations in sector fields and quadrupole systems. *Proc. SPIE* **2014**, 156–164.

H. Wollnik (2013). History of mass measurements in time-of-flight mass analyzers. *Int. J. Mass Spectrom.* **349–350**, 38–46.

H. Wollnik and H. Ewald (1965). The influence of magnetic and electric fringing fields on the trajectories of charged particles. *Nucl. Instrum. Meth.* **36**, 93–104.

H. Wollnik, T. Matsuo and E. Kasseckert (1976). Ein in zweiter Näherung bildfehlerfreies Energiefilter für Elektronenmikroskope. *Optik* **46**, 255–270.

H. Wollnik, J. M. Wouters and D. J. Vieira (1987a). TOFI: an isochronous time-of-flight mass spectrometer. *Nucl. Instrum. Meth. Phys. Res. A* **258**, 331–334.

H. Wollnik, J. Brezina and M. Berz (1987b). GIOS–BEAMTRACE – a program package to determine optical properties of intense ion beams. *Nucl. Instrum. Meth. Phys. Res. A* **258**, 408–411.

W. A. Wooster (1927). The analysis of beams of moving charged particles by a magnetic field. *Proc. R. Soc. (Lond.) A* **114**, 729–744.

J.-y. Ximen (1980). First- and second-order trajectories and ion optical properties of crossed toroidal electric and inhomogeneous magnetic fields. *Adv. Mass Spectrom.* **8**, 1778–1785.

J.-y. Ximen and R.-s. Chen (1982a). Ion-optical theory for the third-order trajectory in crossed toroidal electric and inhomogeneous magnetic fields. I. Calculation of trajectory and matrix formalism. *Int. J. Mass Spectrom. Ion Phys.* **44**, 129–150.

J.-y. Ximen and R.-s. Chen (1982b). Ion-optical theory for the third-order trajectory in crossed toroidal electric and inhomogeneous magnetic fields. II. Transfer matrices, Liouville's theorem and transform matrices. *Int. J. Mass Spectrom. Ion Phys.* **44**, 153–165.

J.-y. Ximen and Z.-f. Shao (1985). A study of an inhomogeneous gradient magnetic field spectrometer with a curvilinear axis. *Optik* **71**, 73–79.

K. Yagi (1964). A new broad range spectrometer with a uniform-field sectorial magnet and a preceding quadrupole-magnet doublet. *Nucl. Instrum. Meth.* **31**, 173–188.

K. Yagi (1965). The third-order aberrations in a broad range spectrometer with a uniform-field sectorial magnet and a preceding quadrupole-magnet doublet. *Nucl. Instrum. Meth.* **34**, 146–154.

K. Yagi (1966). A method for calculations of the reduction of the resolution in a uniform-field magnetic analyzer system due to inhomogeneity of the magnetic field. *Nucl. Instrum. Meth.* **39**, 88–92.

D. T. Young, A. G. Ghielmetti, E. G. Shelley, J. A. Marshall, J. L. Burch and T. L. Booker (1987). Experimental tests of a toroidal electrostatic analyzer. *Rev. Sci. Instrum.* **58**, 501–508.

G. Zanchi, J.-P. Perez and J. Sevely (1975). Adaptation of a magnetic filtering device on a one megavolt electron microscope. *Optik* **43**, 495–501.

G. Zanchi, J. Sevely and B. Jouffrey (1977a). An energy filter for high voltage electron microscopy. *J. Microsc. Spectrosc. Electron.* **2**, 95–104.

G. Zanchi, J. Sevely and B. Jouffrey (1977b). Second order image aberration of a one megavolt magnetic filter. *Optik* **48**, 173–192.

E. Zeitler (1990). Analysis of an imaging magnetic energy filter. *Nucl. Instrum. Meth. Phys. Res. A* **298**, 234–246.

L.-w. Zhou (1984). Optics of wide electron beam focusing. In *Electron Optical Systems for Microscopy, Microanalysis and Microlithography* (J. J. Hren, F. A. Lenz, E. Munro and P. B. Sewell, Eds), 45–62 (Scanning Electron Microscopy, AMF O'Hare).

L. Zhou, G. Ni and B. Qiu (1987). Tensor analysis of electron motion in curvilinear coordinate systems. In *Proc. Int. Symposium on Electron Optics, ISEOB* (J.-y. Ximen, Ed.), 299–302 (Institute of Electronics, Academia Sinica, Beijing).

L. Zhou, G. Ni and B. Qiu (1988a). Tensor analysis of electron motion in curvilinear coordinate systems (I). *Optik* **79**, 53–66.

L. Zhou, G. Ni and B. Qiu (1988b). Tensor analysis of electron motion in curvilinear coordinate system (II). *Optik* **78**, 101–107.

T. J. M. Zouros and E. P. Benis (2002). The hemispherical deflector analyser revisited. I. Motion in the ideal $1/r$ potential, generalized entry conditions, Kepler orbits and spectrometer basic equations. *J. Electron Spectrosc. Relat. Phenom.* **125**, 221–248; Errata: *ibid*. **142** (2005) 175–176.

T. J. M. Zouros, F. M. Spiegelhalder and D. J. Manura (2008). Modelling SIMION's accuracy for hemispherical deflector analyzers using a spherical capacitor. *Phys. Procedia* **1**, 461–466.

Conference Proceedings

1. International Congresses on Electron Microscopy, later International Microscopy Congresses
2. European Regional Congresses on Electron Microscopy, later European Microscopy Congresses
3. Asia-Pacific Congresses on Electron Microscopy, later Asia–Pacific Microscopy Congresses
4. Charged Particle Optics Conferences
5. High-voltage Electron Microscopy Conferences
6. EMAG [Electron Microscopy and Analysis Group of the Institute of Physics] meetings
7. Multinational Congresses on (Electron) Microscopy (MCEM, MCM)
8. The Dreiländertagungen (Germany, Austria, Switzerland) and related meetings
9. Recent Trends in Charged Particle Optics and Surface Physics Instrumentation (Skalský Dvůr)
10. SPIE Proceedings
11. Soviet All-Union Conferences on Electron Microscopy

12. Problems of Theoretical and Applied Electron Optics [Problemyi Teoreticheskoi i Prikladnoi Elektronnoi Optiki]
13. Related Meetings

The following list gives full publishing details of the series of International and Regional conferences on Electron Microscopy. The South American (CIASEM) conferences are not listed as they contain little optics. For the reader's convenience, a few other meetings are included, in particular those on charged particle optics, the Multinational Conferences on Electron Optics (now Multinational Conferences on Microscopy), the Dreiländertagungen (now Microscopy Conferences) and the conferences organized by the Electron Microscopy and Analysis Group (EMAG) of the British Institute of Physics. In the lists of references, these are referred to by their acronyms and venue. The irregular, short-lived series of meetings on high-voltage electron microscopy is identified by the acronym HVEM.

The list does not include the proceedings of the annual meetings of the Electron Microscopy Society of America, which are identified in the reference lists by EMSA or MSA, venue and the meeting number until publication as a Supplement to Microscopy and Microanalysis was adopted. Proceedings were first issued for the 25th meeting (1967) and have been published ever since, at first in print and more recently on-line. For full details, see the lists published by Hawkes in *Advances in Imaging and Electron Physics*, Vol. 117 (2003) 203−379 and Vol. 190 (2015) 143−175.

Many other national electron microscopy societies publish proceedings of their major meetings but few contain much optics. A notable exception is the series of All-Union meetings held in Russia, the proceedings of which are mainly published in *Izv. Akad. Nauk (Ser. Fiz.)*, translated as *Bull. Acad. Sci. USSR (Phys. Ser.)*, though a few papers appear in *Radiotekhnika i Elektronika (Radio Engineering and Electronic Physics* and later *Soviet Journal of Communications Technology and Electronics)*. Brief details of these are given at the end of the main list. The other noteworthy exception is Japan; abstracts of Japanese national meetings were published regularly and rapidly in the *Journal of Electron Microscopy* and now appear in a supplement to *Kenbikyo*.

Details of other related meetings are to be found in the articles by Hawkes mentioned above, notably the International Congresses on X-ray Optics and Microscopy (ICXOM), the Low-energy Electron Microscopy and Photoemission Electron Microscopy (LEEM, PEEM) meetings and Frontiers of Aberration-corrected Electron Microscopy (PICO).

1. International Congresses on Electron Microscopy, later International Microscopy Congresses

ICEM-1, Delft, 1949: *Proceedings of the Conference on Electron Microscopy*, Delft, 4−8 July, 1949 (A. L. Houwink, J. B. Le Poole and W. A. Le Rütte, Eds) Hoogland, Delft, 1950.

ICEM-2, Paris, 1950: *Comptes Rendus du Premier Congrès International de Microscopie Electronique*, Paris, 14−22 September, 1950. Editions de la Revue d'Optique Théorique et Instrumentale, Paris, 1953. 2 Vols.

ICEM-3, London, 1954: *The Proceedings of the Third International Conference on Electron Microscopy,* London, 15−21 July 1954 (R. Ross, Ed.) Royal Microscopical Society, London, 1956.

ICEM-4, Berlin, 1958: *Vierter Internationaler Kongress für Elektronenmikroskopie*, Berlin, 10−17 September, 1958, *Verhandlungen* (W. Bargmann, G. Möllenstedt, H. Niehrs, D. Peters, E. Ruska and C. Wolpers, Eds) Springer, Berlin, 1960. 2 Vols; on-line via SpringerLink.

ICEM-5, Philadelphia, 1962: *Electron Microscopy. Fifth International Congress for Electron Microscopy*, Philadelphia, Pennsylvania, 29 August to 5 September, 1962 (S. S. Breese, Ed.) Academic Press, New York, 1962. 2 Vols.

ICEM-6, Kyoto, 1966: *Electron Microscopy 1966. Sixth International Congress for Electron Microscopy*, Kyoto, 28 August − 4 September 1966 (R. Uyeda, Ed.) Maruzen, Tokyo, 1966. 2 Vols.

ICEM-7, Grenoble, 1970: *Microscopie Electronique 1970. Résumés des Communications Présentées au Septième Congrès International*, Grenoble, 30 August − 5 September 1970 (P. Favard, Ed.) Société Française de Microscopie Electronique, Paris, 1970. 3 Vols.

ICEM-8, Canberra, 1974: *Electron Microscopy 1974. Abstacts of Papers Presented to the Eighth International Congress on Electron Microscopy*, Canberra, 25−31 August 1974 (J. V. Sanders and D. J. Goodchild, Eds) Australian Academy of Science, Canberra, 1974. 2 Vols.

ICEM-9, Toronto, 1978: *Electron Microscopy 1978. Papers Presented at the Ninth International Congress on Electron Microscopy*, Toronto, 1–9 August 1978 (J. M. Sturgess, Ed.) Microscopical Society of Canada, Toronto, 1978. 3 Vols.

ICEM-10, Hamburg, 1982: *Electron Microscopy, 1982. Papers Presented at the Tenth International Congress on Electron Microscopy*, Hamburg, 17–24 August 1982. Deutsche Gesellschaft für Elektronenmikroskopie, Frankfurt, 1982. 3 Vols.

ICEM-11, Kyoto, 1986: *Electron Microscopy 1986. Proceedings of the XIth International Congress on Electron Microscopy*, Kyoto, 31 August–7 September 1986 (T. Imura, S. Maruse and T. Suzuki, Eds.). Japanese Society of Electron Microscopy, Tokyo. 4 Vols; published as a supplement to *J. Electron Microsc*. **35** (1986).

ICEM-12, Seattle, 1990: *Electron Microscopy 1990. Proceedings of the XIIth International Congress for Electron Microscopy*, Seattle WA, 12–18 August 1990 (L. D. Peachey, and D. B. Williams, Eds). San Francisco Press, San Francisco. 4 Vols. See also *Ultramicroscopy* **36** (1991) Nos 1–3, 1–274.

ICEM-13, Paris, 1994: *Electron Microscopy 1994. Proceedings of the 13th International Congress on Electron Microscopy*, Paris, 17–22 July 1994 [B. Jouffrey, C. Colliex, J. P. Chevalier, F. Glas, P. W. Hawkes, D. Hernandez–Verdun, J. Schrevel and D. Thomas (Vol. 1), B. Jouffrey, C. Colliex, J. P. Chevalier, F. Glas and P. W. Hawkes (Vols 2A and 2B) and B. Jouffrey, C. Colliex, D. Hernandez–Verdun, J. Schrevel and D. Thomas (Vols 3A and 3B), Eds]. Editions de Physique, Les Ulis, 1994.

ICEM-14, Cancún, 1998: *Electron Microscopy 1998. Proceedings of the 14th International Congress on Electron Microscopy*, Cancún, 31 August–4 September 1998 [Memorias del 14to Congreso Internacional de Microscopía Electrónica celebrado en Cancún (México) del 31 de Agosto al 4 de Septiembre de 1998] (H. A. Calderón Benavides and M. J. Yacamán, Eds). Institute of Physics Publishing, Bristol and Philadelphia 1998. 4 Vols. See also *Micron* **31** (2000), No. 5.

ICEM-15, Durban, 2002: *Electron Microscopy 2002. Proceedings of the 15th International Congress on Electron Microscopy*, International Convention Centre, Durban, 1–6 September 2002 [R. Cross, P. Richards, M. Witcomb and J. Engelbrecht (Vol. 1, Physical, Materials and Earth Sciences), R. Cross, P. Richards, M. Witcomb and T. Sewell, (Vol. 2, Life Sciences) and R. Cross, P. Richards, M. Witcomb, J. Engelbrecht and T. Sewell (Vol. 3, Interdisciplinary), Eds]. Microscopy Society of Southern Africa, Onderstepoort 2002.

IMC-16, Sapporo, 2006: *Proceedings 16th International Microscopy Conference, "Microscopy for the 21st Century"*, Sapporo, 3–8 September 2006 (H. Ichinose and T. Sasaki, Eds). Vol. 1, Biological and Medical Science; Vol. 2, Instrumentation; Vol. 3, Materials Science. Publication Committee of IMC16, Sapporo 2006.

IMC-17, Rio de Janeiro, 2010: *Proceedings IMC17, The 17th IFSM International Microscopy Congress*, Rio de Janeiro, 19–24 September 2010 (G. Solórzano and W. de Souza, Eds). Sociedade Brasileira de Microscopia e Microanálise, Rio de Janeiro 2010.

IMC-18, Prague, 2014: Prague Convention Centre, 7–12 September 2014. Proceedings open-access at www.microscopy.cz/proceedings/all.html, edited by P. Hozak.

IMC-19, Sydney, 9–14 September 2018.

2. European Regional Congresses on Electron Microscopy, later European Microscopy Congresses

EUREM-1, Stockholm, 1956: *Electron Microscopy. Proceedings of the Stockholm Conference*, 17–20 September, 1956 (F. J. Sjöstrand and J. Rhodin, Eds) Almqvist and Wiksells, Stockholm, 1957.

EUREM-2, Delft, 1960: *The Proceedings of the European Regional Conference on Electron Microscopy*, Delft, 29 August – 3 September 1960 (A. L. Houwink and B. J. Spit, Eds) Nederlandse Vereniging voor Elektronenmicroscopie, Delft n.d. 2 Vols.

EUREM-3, Prague, 1964: *Electron Microscopy 1964. Proceedings of the Third European Regional Conference*, Prague, 26 August – 3 September 1964 (M. Titlbach, Ed.) Publishing House of the Czechoslovak Academy of Sciences, Prague, 1964. 2 Vols.

EUREM-4, Rome, 1968: *Electron Microscopy 1968. Pre-Congress Abstracts of Papers Presented at the Fourth Regional Conference*, Rome, 1–7 September 1968 (D. S. Bocciarelli, Ed.) Tipografia Poliglotta Vaticana, Rome, 1968. 2 Vols.

EUREM-5, Manchester, 1972: *Electron Microscopy 1972. Proceedings of the Fifth European Congress on Electron Microscopy*, Manchester, 5–12 September 1972 (Institute of Physics, London, 1972).

EUREM-6, Jerusalem, 1976: *Electron Microscopy 1976. Proceedings of the Sixth European Congress on Electron Microscopy*, Jerusalem, 14–20 September 1976 (D. G. Brandon (Vol. I) and Y. Ben-Shaul (Vol. II), Eds) Tal International, Jerusalem, 1976. 2 Vols.

EUREM-7, The Hague, 1980: *Electron Microscopy 1980. Proceedings of the Seventh European Congress on Electron Microscopy*, The Hague, 24–29 August 1980 (P. Brederoo and G. Boom (Vol. I), P. Brederoo and W. de Priester (Vol. II), P. Brederoo and V. E. Cosslett (Vol. III) and P. Brederoo and J. van Landuyt (Vol. IV), Eds). Vols. I and II contain the proceedings of the Seventh European Congress on Electron Microscopy, Vol. III those of the Ninth International Conference on X-Ray Optics and Microanalysis, and Vol. IV those of the Sixth International Conference on High Voltage Electron Microscopy. Seventh European Congress on Electron Microscopy Foundation, Leiden, 1980.

EUREM-8, Budapest, 1984: *Electron Microscopy 1984. Proceedings of the Eighth European Congress on Electron Microscopy*, Budapest 13–18 August 1984 (A. Csanády, P. Röhlich and D. Szabó, Eds) Programme Committee of the Eighth European Congress on Electron Microscopy, Budapest, 1984. 3 Vols.

EUREM-9, York, 1988: *Proceedings of the Ninth European Congress on Electron Microscopy*, York, 4–9 September, 1988 (P. J. Goodhew and H. G. Dickinson, Eds) Institute of Physics, Bristol and Philadelphia, 1988. Conference Series 93, 3 Vols.

EUREM-10, Granada, 1992: *Electron Microscopy 92. Proceedings of the 10th European Congress on Electron Microscopy*, Granada, 7-11 September 1992 [A. Ríos, J. M. Arias, L. Megías-Megías and A. López-Galindo (Vol. I), A. López-Galindo and M. I. Rodríguez-García (Vol. II) and L. Megías-Megías, M. I. Rodríguez-García, A. Ríos and J. M. Arias, (Vol. III), Eds]. Secretariado de Publicaciones de la Universidad de Granada, Granada. 3 Vols.

EUREM-11, Dublin, 1996: *Electron Microscopy 1996. Proceedings of the 11th European Conference on Electron Microscopy*, Dublin, 26–30 August 1996, distributed on CD-ROM [defective]. Subsequently published in book form by CESM, the Committee of European Societies of Microscopy, Brussels 1998. 3 Vols.

EUREM-12, Brno, 2000: *Electron Microscopy 2000. Proceedings of the 12th European Conference on Electron Microscopy*, Brno, 9–14 July 2000 (L. Frank and F. Čiampor, General Eds); Vol. I, Biological Sciences (S. Čech and R. Janisch, Eds); Vol. II, Physical Sciences (J. Gemperlová and I. Vávra, Eds); Vol. III, Instrumentation and Methodology (P. Tománek and R. Kolařík, Eds); Vol. IV, Supplement (L. Frank and F. Čiampor, Eds); Vols I–III also distributed on CD-ROM. Czechoslovak Society of Electron Microscopy, Brno 2000.

EMC-13, Antwerp, 2004: *Proceedings European Microscopy Congress*, Antwerp, 23–27 August 2004. (D. Schryvers, J.-P. Timmermans and E. Pirard, General Eds); Biological Sciences, (J.-P. Verbelen and E. Wisse, Eds); Materials Sciences, (G. van Tendeloo and C. van Haesendonck, Eds); Instrumentation and Methodology, (D. van Dyck and P. van Oostveldt, Eds). Belgian Society for Microscopy, Liège 2004.

EMC-14, Aachen, 2008: *Proceedings EMC 2008, 14th European Microscopy Congress*, Aachen, 1–5 September 2008. Volume 1, Instrumentation and Methods (M. Luysberg and K. Tillmann, Eds); Volume 2, Materials Science (S. Richter and A. Schwedt, Eds); Volume 3, Life Science (A. Aretz, B. Hermanns–Sachweh and J. Mayer, Eds). Springer, Berlin 2008.

EMC-15, Manchester, 2012: *Proceedings EMC2012, 15th European Microscopy Congress*, Manchester, 16–21 September 2012. Volume 1, Physical Sciences: Applications (D. J. Stokes and W. M. Rainforth, Eds); Volume 2, Physical Sciences: Tools and Techniques (D. J. Stokes and J. L. Hutchison, Eds); Volume 3, Life Sciences (D. J. Stokes, P. J. O'Toole and T. Wilson, Eds). Royal Microscopical Society, Oxford 2012.

EMC-16, Lyon, 2016: 28 August–2 September 2016. *European Microscopy Congress 2016*. Vol. 1: Instrumentation and Methods (O. Stéphan, M. Hÿtch, B. Satiat–Jeunemaître, C. Venien-Bryan, P. Bayle-Guillemaud and T. Epicier, Eds); Vols 2.1 and 2.2: Materials Science (O. Stéphan, M. Hÿtch and T. Epicier, Eds); Vol. 3: Life Sciences (B. Satiat-Jeunemaître, C. Venien-Bryan and T. Epicier, Eds). Wiley–VCH, Weinheim 2016.

EMC-17, Copenhagen, 23–28 August 2020.

3. Asia-Pacific Congresses on Electron Microscopy, later Asia–Pacific Microscopy Congresses

APEM-1, Tokyo, 1956: *Electron Microscopy. Proceedings of the First Regional Conference in Asia and Oceania*, Tokyo, 23–27 October 1956. Electrotechnical Laboratory, Tokyo, 1957.

APEM-2, Calcutta, 1965: *Proceedings of the Second Regional Conference on Electron Microscopy in Far East and Oceania*, Calcutta 2-6 February 1965. Electron Microscopy Society of India, Calcutta.

APEM-3, Singapore, 1984: *Conference Proceedings 3rd Asia Pacific Conference on Electron Microscopy*, Singapore, 29 August–3 September, 1984 (Chung Mui Fatt, Ed.) Applied Research Corporation, Singapore.

APEM-4, Bangkok, 1988: *Electron Microscopy 1988. Proceedings of the IVth Asia-Pacific Conference and Workshop on Electron Microscopy*, Bangkok, 26 July–4 August 1988 (V. Mangclaviraj, W. Banchorndhevakul and P. Ingkaninun, Eds.) Electron Microscopy Society of Thailand, Bangkok, 1988.

APEM-5, Beijing, 1992: *Electron Microscopy I and II. 5th Asia-Pacific Electron Microscopy Conference*, Beijing, 2–6 August 1992 (K. H. Kuo and Z. H. Zhai, Eds.). World Scientific, Singapore, River Edge NJ, London and Hong Kong, 1992. 2 Vols. See also *Ultramicroscopy* **48** (1993) No. 4, 367–490.

APEM-6, Hong Kong, 1996: *Proceedings of the 6th Asia–Pacific Conference on Electron Microscopy*, Hong Kong, 1–5 July, 1996 (D. Barber, P. Y. Chan, E. C. Chew, J. S. Dixon, and J. K. L. Lai, Eds). Chinetek Promotion, Kowloon, Hong Kong, 1996.

APEM-7, Singapore, 2000: *Proceedings of the 7th Asia–Pacific Conference on Electron Microscopy*, Singapore International Convention & Exhibition Centre, Suntec City, Singapore, 26–30 June 2000 (two volumes and CD-ROM, Y. T. Yong, C. Tang, M. Leong, C. Ng and P. Netto, Eds). 7th APEM Committee, Singapore 2000.

APEM-8, Kanazawa, 2004: *Proceedings 8th Asia–Pacific Conference on Electron Microscopy* (8APEM), Kanazawa, Ishikawa Prefecture, 7–11 June 2004. Full proceedings on CD-ROM, Japanese Society of Microscopy, Tokyo 2004.

APMC-9, Jeju, 2008: *Proceedings of the Ninth Asia–Pacific Microscopy Conference* (APMC9) Jeju, Korea, 2–7 November 2008. (H.-c. Lee, D. H. Kim, Y.-w. Kim, I. J. Rhyu and H.-t. Jeong, Eds). *Korean Journal of Microscopy* **38** (2008), No. 4, Supplement, on CD-ROM only.

APMC-10, Perth, 2012: *Proceedings of the Tenth Asia–Pacific Microscopy Conference* (APMC-10) Perth, Australia, 5–9 February 2012 (B. Griffin, L. Faraone and M. Martyniuk, Eds). Held in conjunction with the 2012 International Conference on Nanoscience and Nanotechnology (ICONN2012) and the 22nd Australian Conference on Microscopy and Microanalysis (ACMM22).

APMC-11, Phuket, 2016: *11th Asia-Pacific Microscopy Conference* (APMC-11) Phuket, Thailand, 23–27 May 2016. Held in conjunction with the 33rd Annual Conference of the Microscopy Society of Thailand (MST-33) and the 39th Annual Conference of the Anatomy Association of Thailand (AAT-39). Selected articles published in *Siriraj Medical Journal* **8**(3), Suppl. 1 (2016) and *Journal of the Microscopy Society of Thailand*.

APMC-12, Hyderabad, 2020.

4. Charged Particle Optics Conferences

CPO-1, Giessen, 1980: *Proceedings of the First Conference on Charged Particle Optics, Giessen*, 8–11 September, 1980 (H. Wollnik, Ed.) *Nucl. Instrum. Meth.* **187** (1981) 1–314.

CPO-2, Albuquerque, 1986: *Proceedings of the Second International Conference on Charged Particle Optics*, Albuquerque, 19–23 May, 1986 (S. O. Schriber and L. S. Taylor, Eds) *Nucl. Instrum. Meth. Phys. Res. A* **258** (1987) 289–598.

CPO-3, Toulouse, 1990: *Proceedings of the Third International Conference on Charged Particle Optics*, Toulouse, 24-27 April 1990 (P. W. Hawkes, Ed.) *Nucl. Instrum. Meth. Phys. Res. A* **298** (1990) 1–508.

CPO-4, Tsukuba, 1994: *Proceedings of the Fourth International Conference on Charged Particle Optics*, Tsukuba 3–6 October 1994 (K. Ura, M. Hibino, M. Komuro, M. Kurashige, S. Kurokawa, T. Matsuo, S. Okayama, H. Shimoyama and K. Tsuno, Eds) *Nucl. Instrum. Meth. Phys. Res. A* **363** (1995) 1–496.

CPO-5, Delft, 1998: *Proceedings of the Fifth International Conference on Charged Particle Optics*, Delft 14–17 April 1998 (P. Kruit and P. W. van Amersfoort, Eds). *Nucl. Instrum. Meth. Phys. Res. A* **427** (1999) 1–422.

CPO-6, College Park, 2002: *Proceedings of the Sixth International Conference on Charged Particle Optics*, Marriott Hotel, Greenbelt MD, 21–25 October 2002 (A. Dragt and J. Orloff, Eds). *Nucl. Instrum. Meth. Phys. Res. A* **519** (2004) 1–487.

CPO-7, Cambridge, 2006: *Charged Particle Optics. Proceedings of the Seventh International Conference on Charged Particle Optics*, Trinity College, Cambridge, 24–28 July 2006 (E. Munro and J. Rouse, Eds). *Physics Procedia* **1** (2008) 1–572.

CPO-8, Singapore, 2010: *Proceedings of the Eighth International Conference on Charged Particle Optics*, Suntec Convention Centre, Singapore 12–16 July 2010 (A. Khursheed, P. W. Hawkes and M. B. Osterberg, Eds). *Nucl. Instrum. Meth. Phys Res. A* **645** (2011) 1–354.

CPO-9, Brno, 2014: *Proceedings of the Ninth International Conference on Charged Particle Optics*, Brno 31 August–5 September, 2014 (L. Frank, P. W. Hawkes and T. Radlička, Eds). *Microsc. Microanal.* **21** (2015) Suppl. 4.

CPO-10, Key West (FL), 17–21 October 2018.

5. High-Voltage Electron Microscopy Conferences

HVEM Monroeville, 1969: *Current Developments in High Voltage Electron Microscopy (First National Conference)*, Monroeville, 17–19 June, 1969. Proceedings not published but *Micron* **1** (1969) 220–307 contains official reports of the meeting based on the session chairmen's notes.

HVEM Stockholm, 1971: *The Proceedings of the Second International Conference on High-Voltage Electron Microscopy*, Stockholm, 14–16 April, 1971; published as *Jernkontorets Annaler* **155** (1971) No. 8.

HVEM Oxford, 1973: *High Voltage Electron Microscopy. Proceedings of the Third International Conference*, Oxford, August, 1973 (P. R. Swann, C. J. Humphreys and M. J. Goringe, Eds) Academic Press, London and New York, 1974.

HVEM Toulouse, 1975: *Microscopie Electronique à Haute Tension. Textes des Communications Présentées au Congrès International*, Toulouse, 1–4 Septembre, 1975 (B. Jouffrey and P. Favard, Eds) SFME Paris, 1976.

HVEM The Hague, 1980 see EUREM-7, The Hague, 1980.

HVEM Berkeley, 1983: *Proceedings of the Seventh International Conference on High Voltage Electron Microscopy,* Berkeley, 16–19 August, 1983 (R. M. Fisher, R. Gronsky and K. H. Westmacott, Eds). Published as a Lawrence Berkeley Laboratory Report, LBL-16031, UC-25, CONF-830819.

6. EMAG [Electron Microscopy and Analysis Group of the Institute of Physics] Meetings

EMAG, 1971: *Electron Microscopy and Analysis. Proceedings of the 25th Anniversary Meeting of the Electron Microscopy and Analysis Group of the Institute of Physics*, Cambridge, 29 June–1 July, 1971 (W. C. Nixon, Ed.) Institute of Physics, London, 1971. Conference Series 10.

EMAG, 1973: *Scanning Electron Microscopy: Systems and Applications*, Newcastle-upon-Tyne, 3–5 July, 1973 (W. C. Nixon, Ed.) Institute of Physics, London, 1973. Conference Series 18.

EMAG, 1975: *Developments in Electron Microscopy and Analysis. Proceedings of EMAG 75*, Bristol, 8–11 September, 1975 (J. A. Venables, Ed.; Academic Press, London and New York, 1976).

EMAG, 1977: *Developments in Electron Microscopy and Analysis. Proceedings of EMAG 77*, Glasgow, 12–14 September, 1977 (D. L. Misell, Ed.) Institute of Physics, Bristol, 1977. Conference Series 36.

EMAG, 1979: *Electron Microscopy and Analysis, 1979. Proceedings of EMAG 79*, Brighton, 3–6 September, 1979 (T. Mulvey, Ed.) Institute of Physics, Bristol, 1980) Conference Series 52.

EMAG, 1981: *Electron Microscopy and Analysis, 1981. Proceedings of EMAG 81*, Cambridge, 7–10 September, 1981 (M. J. Goringe, Ed.) Institute of Physics, Bristol, 1982. Conference Series 61.

EMAG, 1983: *Electron Microscopy and Analysis, 1983. Proceedings of EMAG 83*, Guildford, 30 August–2 September, 1983 (P. Doig, Ed.) Institute of Physics, Bristol, 1984. Conference Series 68.

EMAG, 1985: *Electron Microscopy and Analysis, 1985. Proceedings of EMAG 85*. Newcastle-upon-Tyne, 2–5 September, 1985 (G. J. Tatlock, Ed.) Institute of Physics, Bristol, 1986. Conference Series 78.

EMAG, 1987: *Electron Microscopy and Analysis, 1987. Proceedings of EMAG 87*, Manchester, 8–9 September, 1987 (L. M. Brown, Ed.) Institute of Physics, Bristol and Philadelphia, 1987. Conference Series 90.

EMAG, 1989: *EMAG-MICRO 89. Proceedings of the Institute of Physics Electron Microscopy and Analysis Group and Royal Microscopical Society Conference*, London, 13-15 September 1989 (P. J. Goodhew and H. Y. Elder, Eds.) Institute of Physics, Bristol and New York, 1990. Conference Series 98, 2 Vols.

EMAG, 1991: *Electron Microscopy and Analysis 1991. Proceedings of EMAG 91*, Bristol, 10–13 September 1991 (F. J. Humphreys, Ed.) Institute of Physics, Bristol, Philadelphia and New York, 1991. Conference Series 119.

EMAG, 1993: *Electron Microscopy and Analysis 1993. Proceedings of EMAG 93*, Liverpool, 15–17 September 1993 (A. J. Craven, Ed.) Institute of Physics, Bristol, Philadelphia and New York, 1994. Conference Series 138.

EMAG, 1995: *Electron Microscopy and Analysis 1995. Proceedings of EMAG 95*. Birmingham, 12–15 September 1995 (D. Cherns, Ed.) Institute of Physics, Bristol, Philadelphia and New York, 1995. Conference Series 147.

EMAG, 1997: *Electron Microscopy and Analysis 1997. Proceedings of EMAG 97*, Cavendish Laboratory, Cambridge, 2–5 September 1997 (J. M. Rodenburg, Ed.); Institute of Physics, Bristol and Philadelphia, 1997. Conference Series 153.

EMAG, 1999: *Electron Microscopy and Analysis 1999. Proceedings of EMAG 99*, University of Sheffield, 25–27 August 1999 (C. J. Kiely, Ed.); Institute of Physics, Bristol and Philadelphia, 1999. Conference Series 161.

EMAG, 2001: *Electron Microscopy and Analysis 2001. Proceedings of the Institute of Physics Electron Microscopy and Analysis Group Conference*, University of Dundee, 5–7 September 2001 (M. Aindow and C. J. Kiely, Eds); Institute of Physics Publishing, Bristol and Philadelphia 2002) Conference Series 168.

EMAG, 2003: *Electron Microscopy and Analysis 2003. Proceedings of the Institute of Physics Electron Microscopy and Analysis Group Conference*, Examination Schools, University of Oxford, 3–5 September 2003 (S. McVitie and D. McComb, Eds); Institute of Physics Publishing, Bristol and Philadelphia 2004. Conference Series 179.

EMAG–NANO, 2005. University of Leeds, 31 August–2 September 2005 (P. D. Brown, R. Baker and B. Hamilton, Eds). *J. Phys. Conf.* **26** (2006).

EMAG, 2007: Caledonian University and University of Glasgow, 3–7 September 2007 (R. T. Baker, G. Möbus and P. D. Brown, Eds). *J. Phys.: Conf.* **126** (2008).

EMAG, 2009: University of Sheffield, 8–11 September 2009 (R. T. Baker, Ed.). *J. Phys.: Conf.* **241** (2010).

EMAG, 2011: University of Birmingham (R. T. Baker, P. D. Brown and Z. Li, Eds). *J. Phys.: Conf.* **371** (2012).

EMAG, 2013: University of York, 3–6 September 2013 (P. Nellist, Ed.). *J. Phys.: Conf.* **522** (2014).

EMAG, 2015: Manchester, 29 June–2 July 2015, joint with the Microscience Microscopy Conference (Royal Microscopical Society) (I. MacLaren, Ed.). *J. Phys.: Conf.* **644** (2015).

EMAG, 2016: Durham, 7–8 April 2016 (no publication).

EMAG 2017, Manchester, 3–6 July 2017, joint with the Microscience Microscopy Conference (Royal Microscopical Society). *J. Phys.: Conf.* **902** (2017).

7. Multinational Congresses on (Electron) Microscopy (MCEM, MCM)

The first of these meetings brought together the Italian, Hungarian, Czechoslovak and Slovenian Societies. For subsequent congresses, these were joined by the Austrian and Croatian societies.

MCEM-93. Multinational Congress on Electron Microscopy, Parma, 13–17 September 1993; *Proceedings* issued as Supplement to **14** (2) of *Microscopia Elettronica*.

MCEM-95. *Proceedings Multinational Conference on Electron Microscopy*, Stará Lesná (High Tatra Mountains), 16–20 October 1995. Slovak Academic Press, Bratislava 1995.

MCEM-97. *Proceedings Multinational Congress on Electron Microscopy*, Portorož (Slovenia), 5–8 October 1997. Part I, Microscopy Applications in the Life Sciences; Part II, Microscopy Applications in the Material Sciences; Part III, Microscopy Methods and Instrumentation. *J. Computer-assisted Microsc.* **8** (1996) No. 4 and 9 (1997) Nos 1 and 2.

MCEM-99. *Proceedings 4th Multinational Congress on Electron Microscopy*, Veszprém (Hungary), 5–8 September 1999 (K. Kovács, Ed.). University of Veszprem 1999.

MCEM-5. *Proceedings of the 5th Multinational Congress on Electron Microscopy*, Department of Biology, University of Lecce (Italy), 20–25 September 2001 (L. Dini and M. Catalano, Eds). Rinton Press, Princeton NJ 2001.

MCM-6. *Proceedings of the Sixth Multinational Congress on Electron Microscopy*, Pula (Croatia), 1–5 June 2003 (O. Milat and D. Ježek, Eds). Croatian Society for Electron Microscopy, Zagreb 2003.

MCM-7. *Proceedings of the 7th Multinational Congress on Microscopy*, Portorož, (Slovenia) 26–30 June 2005 (M. Čeh, G. Dražič and S. Fidler, Eds). Slovene Society for Microscopy and Department for Nanostructured Materials, Jožef Stefan Institute, Ljubljana 2005.

MCM-8. *Proceedings 8th Multinational Congress on Microscopy*, Prague (Czech Republic), 17–21 June 2007 (J. Nebesářova and P. Hozák, Eds). Czechoslovak Microscopy Society, Prague 2007.

MC 2009 incorporating MCM-9. Microscopy Conference, Graz, Austria 30 August–4 September 2009. *Proceedings First Joint Meeting of Dreiländertagung & Multinational Congress on Microscopy*. Volume 1, Instrumentation and Methodology (G. Kothleitner and M. Leisch, Eds); Volume 2, Life Sciences (M. A. Pabst and G. Zellnig, Eds); Volume 3, Materials Science (W. Grogger, F. Hofer and P. Pölt, Eds). Verlag der Technischen Universität, Graz 2009.

MCM-10. *Proceedings 10th Multinational Conference on Microscopy*, Urbino, 4–9 September 2011 (E. Falcieri, Ed.). Società Italiana di Scienze Microscopiche (SISM), 2011.

MC-2013, Regensburg, 25–30 August 2013. Joint Meeting of Dreiländertagung & Multinational Congress on Microscopy, together with the Serbian and Turkish Microscopy Societies. Proceedings can be downloaded from www.mc2013.de. urn:nbn:de:bvb:355-epub-287343 (R. Rachel, J. Schröder, R. Witzgall and J. Zweck, Eds).

MCM-12. Multinational Conference on Microscopy, Eger (Hungary) 23–29 August 2015. Webarchive.

MCM-13. Multinational Conference on Microscopy, Rovinj (Croatia), 24–29 September 2017. Abstracts at mcm2017.irb.hr/programme. Selected papers published in *Resolution and Discovery* (2017).

MCM-14, Multinational Conference on Microscopy, Belgrade (Serbia), 15–20 September 2019.

8. The Dreiländertagungen (Germany, Austria, Switzerland) and Related Meetings

These conferences are organized in turn by the Austrian, German and Swiss Microscopy societies; originally designed for German-speaking microscopists, they now tend to use English and attract a wider participation.

Dreiländertagung für Elektronenmikroskopie: Konstanz, 15–21 September 1985. *Optik* (1985) Supplement 1 or *Eur. J. Cell Biol.* (1985) Supplement 10. See also *Beiträge zur Elektronenmikroskopische Direktabbildung von Oberflächen* **18** (1985).

Dreiländertagung für Elektronenmikroskopie: Salzburg, 10–16 September 1989. *Optik* **83** (1989) Suppl. 4 or *Eur. J. Cell Biol.* **49** (1989) Suppl. 27.

Dreiländertagung für Elektronenmikroskopie: Zürich, 5–11 September 1993. *Optik* **94** (1993) Suppl. 5 or *Eur. J. Cell Biol.* **61** (1993) Suppl. 39.

Dreiländertagung für Elektronenmikroskopie: Regensburg, 7–12 September 1997. *Optik* **106** (1997) Suppl. 7 or *Eur. J. Cell Biol.* **74** (1997) Suppl. 45.

Dreiländertagung für Elektronenmikroskopie: Innsbruck, 9–14 September 2001. Abstracts book (168 pp.) not published as a Supplement to *Optik* or *Eur. J. Cell Biol.*

MC-2003, Dresden 7–12 September 2003. *Microsc. Microanal.* **9** (2003) Suppl. 3 (T. Gemming, M. Lehmann, H. Lichte and K. Wetzig, Eds).

Dreiländertagung für Elektronenmikroskopie: Microscopy Conference 2005. Paul Scherrer Institute, Davos, 25 August–2 September, 2005. *Paul-Scherrer-Institute Proceedings* **PSI 05–01**, 2005.

MC-2007, Saarbrücken, 2–7 September 2007. *Microsc. Microanal.* **13** (2007) Suppl. 3 (T. Gemming, U. Hartmann, P. Mestres and P. Walther, Eds).

Microscopy Conference (MC 2009), Graz, 30 August–4 September 2009. First Joint Meeting of Dreiländertagung & Multinational Congress on Microscopy. Volume 1, Instrumentation and Methodology (G. Kothleitner and M. Leisch, Eds); Volume 2, Life Sciences (M. A. Pabst and G. Zellnig, Eds); Volume 3, Materials Science (W. Grogger, F. Hofer and P. Pölt, Eds). Verlag der Technischen Universität, Graz 2009.

MC-2011, Kiel, 28 August−2 September 2011. Joint meeting of the German Society (DGE), the Nordic Microscopy Society (SCANDEM), and the Polish Microscopy Society (PTMi) with participation of microscopists from Estonia, Latvia, Lithuania and St Petersburg, Russia. Proceedings published in 3 volumes by the German Society for Electron Microscopy and also distributed as a USB key (W. Jäger, W. Kaysser, W. Benecke, W. Depmeier, S. Gorb, L. Kienle, M. Mulisch, D. Häußler and A. Lotnyk, Eds).

MC-2013, Regensburg, 25−30 August 2013. Joint Meeting of Dreiländertagung & Multinational Congress on Microscopy, together with the Serbian and Turkish Microscopy Societies. Proceedings can be downloaded from www.mc2013.de. urn:nbn:de:bvb:355-epub-287343 (R. Rachel, J. Schröder, R. Witzgall and J. Zweck, Eds).

MC-2015, Georg-August-Universität, Göttingen, 6−11 September 2015. Proceedings at www.mc2015.de.

MC-2017, Lausanne, 21−25 August 2017. Proceedings at epub.uni-regensburg.de/36143.

MC-2019, Berlin, 1−5 September 2019.

9. Recent Trends in Charged Particle Optics and Surface Physics Instrumentation (Skalský Dvůr)

1989: First Seminar, Brno, 4−6 September 1989 (no proceedings).

1990: Second Seminar, Brno, 27−29 September 1990 (no proceedings).

1992: Third Seminar, Skalský Dvůr (near Brno), 15−19 June 1992 (no proceedings).

1994: Fourth Seminar, Skalský Dvůr, 5−9 September 1994 (no proceedings).

1996: Fifth Seminar, Skalský Dvůr, 24−28 June 1996. (I. Müllerová and L. Frank, Eds). 92 pp.

1998: Sixth Seminar, Skalský Dvůr, 29 June−3 July 1998. (I. Müllerová and L. Frank, Eds). 84 pp. Published by the CSEM (Brno 1998).

2000: 7th Seminar, Skalský Dvůr, 15−19 July 2000. No proceedings book.

2002: 8th Seminar, Skalský Dvůr, 8−12 July 2002. (L. Frank, Ed.). 96 pp + Supplement, 6 pp. Published by the CSMS (Brno 2002).

2004: 9th Seminar, Skalský Dvůr, 12−16 July 2004. (I. Müllerová, Ed.). Published by the CSMS (Brno 2004).

2006: 10th Seminar, Skalský Dvůr, 22−26 May 2006. (I. Müllerová, Ed.). Published by the CSMS (Brno 2006).

2008: 11th Seminar, Skalský Dvůr, 14−18 July 2008. (F. Mika, Ed.). Published by the CSMS (Brno 2008).

2010: 12th Seminar, Skalský Dvůr, 31 May−4 June 2010. (F. Mika, Ed.). Published by the CSMS (Brno 2010).

2012: 13th Seminar, Skalský Dvůr, 25 −29 June 2012. (F. Mika, Ed.). Published by the CSMS (Brno 2012).

2014: 14th Seminar, incorporated in CPO-9, Brno, see Section 5.1.

2016: 15th Seminar, Skalský Dvůr, 29 May−3 June 2016. (F. Mika, Ed.). Published by the CSMS (Brno 2016).

10. SPIE Proceedings

1. Charged Particle Optics, San Diego CA, 15 July 1993 (W. B. Thompson, M. Sato and A. V. Crewe, Eds). *Proc SPIE* **2014** (1993).
2. Electron-beam Sources, *and Charged Particle Optics*, San Diego, 19−14 July 1995 (E. Munro and H. P. Freund, Eds). *Proc. SPIE* **2522** (1995).
3. Charged Particle *Optics II*, Denver CO, 5 August 1996 (E. Munro, Ed.). *Proc. SPIE* **2858** (1996).
4. Charged Particle *Optics III*, San Diego CA, 27−28 July 1997 (E. Munro, Ed.). *Proc. SPIE* **3155** (1997).
5. Charged Particle *Optics IV*, Denver CO, 22−23 July 1999 (E. Munro, Ed.). *Proc. SPIE* **3777** (1999).
6. Charged Particle Beam Optics Imaging, San Diego CA, 30 July 2001. In Charged Particle Detection, Diagnostics and Imaging (O. Delage, E. Munro and J. A. Rouse, Eds). *Proc. SPIE* **4510** (2001) 71−236.

11. Soviet All-Union Conferences on Electron Microscopy

The Proceedings of the Soviet All-Union conferences on electron microscopy are to be found in the volumes of *Izv. Akad. Nauk (Ser. Fiz.)* or *Bull. Acad. Sci. (Phys. Ser.)* indicated:

1. Moscow 15−19 December 1950; **15** (1951) Nos 3 and 4 (no English translation).
2. Moscow 9−13 May 1958; **23** (1959) Nos 4 and 6.
3. Leningrad 24−29 October 1960; **25** (1961) No. 6.
4. Sumy 12−14 March 1963; **27** (1963) No. 9.
5. Sumy 6−8 July 1965; **30** (1966) No. 5.
6. Novosibirsk 11−16 July 1967; **32** (1968) Nos 6 and 7.
7. Kiev 14−21 July 1969; **34** (1970) No. 7.

8. Moscow 15–20 November 1971; **36** (1972) Nos 6 and 9.
9. Tbilisi 28 October–2 November 1973; **38** (1974) No. 7.
10. Tashkent 5–8 October 1976; **41** (1977) Nos 5 and 11.
11. Tallin October 1979; **44** (1980) Nos 6 and 10.
12. Sumy 1982; **48** (1984), No. 2.
13. Sumy October 1987; **52** (1988) No. 7 and **53** (1989) No. 2.
14. Suzdal, October and November 1990; **55** (119) No. 8.
    From now on, the names of the journal and its English translation are *Izv. Ross. Akad. Nauk (Ser. Fiz.)* and *Bull. Russ. Acad. Sci. (Phys.)*.
15. Chernogolovka, May 1994; **59** (1995) No. 2.
16. Chernogolovka, December 1996; **61** (1997) No. 10.
17. Chernogolovka, June 1998; **63** (1999) No. 7.
18. Chernogolovka, 5–8 June 2000; **65** (2001) No. 9.
19. Chernogolovka, 27–31 May 2002; **67** (2003) No. 4.
20. Chernogolovka, 1 June 2004; **69** (2005) No. 4.
21. Chernogolovka, 5–10 June 2006; **71** (2007) No. 10.
22. Chernogolovka, 2008; **73** (2009) No. 4; also *Poverkhnost'* (2009), No. 10, *J. Surface Invest. X-Ray Synchrotron Neutron Techs* **3** (2009) No. 5.
23. Chernogolovka, 2010; **75** (2011) No. 9; also *Poverkhnost'* (2011), No. 10.
24. Chernogolovka, 2012; **77** (2013) No. 8.
25. Chernogolovka, 2014; **79** (2015) No. 11.
26. Chernogolovka, 2016; **81** (2017).

12. Problems of Theoretical and Applied Electron Optics [Problemyi Teoreticheskoi i Prikladnoi Elektronnoi Optiki][1]

1. Proceedings of the First All-Russia Seminar, Scientific Research Institute for Electron and Ion Optics, Moscow 1996. *Prikladnaya Fizika* (1996) No. 3.
2. Proceedings of the Second All-Russia Seminar, Scientific Research Institute for Electron and Ion Optics, Moscow, 25 April 1997. *Prikladnaya Fizika* (1997) No. 2–3.
3. Proceedings of the Third All-Russia Seminar, Scientific Research Institute for Electron and Ion Optics, Moscow, 31 March–2 April 1998. *Prikladnaya Fizika* (1998) Nos 2 and 3/4.
4. Proceedings of the Fourth All-Russia Seminar, Scientific Research Institute for Electron and Ion Optics, Moscow, 21–22 October 1999. *Prikladnaya Fizika* (2000) Nos 2 and 3; *Proc SPIE* **4187** (2000), edited by A. M. Filachev and I. S. Gaidoukova.
5. Proceedings of the Fifth All-Russia Seminar, Scientific Research Institute for Electron and Ion Optics, Moscow, 14–15 November 2001. *Prikladnaya Fizika* (2002) No. 3; *Proc SPIE* (2003) **5025**, edited by A. M. Filachev.
6. Proceedings of the Sixth All-Russia Seminar, Scientific Research Institute for Electron and Ion Optics, Moscow, 28–30 May 2003. *Prikladnaya Fizika* (2004) No. 1 and *Proc SPIE* **5398** (2004), edited by A. M. Filachev and I. S. Gaidoukova.
7. Proceedings of the Seventh All-Russia Seminar, Scientific Research Institute for Electron and Ion Optics, Moscow, 25–27 May 2005. *Prikladnaya Fizika* (2006) No. 3 and *Proc SPIE* **6278** (2004), edited by A. M. Filachev and I. S. Gaidoukova.
8. Proceedings of the Eighth All-Russia Seminar, Scientific Research Institute for Electron and Ion Optics, Moscow, 29–31 May 2007. *Prikladnaya Fizika* (2008) No. 2 and *Proc SPIE* **7121** (2008), edited by A. M. Filachev and I. S. Gaidoukova.
9. Proceedings of the Ninth All-Russia Seminar, Scientific Research Institute for Electron and Ion Optics, Moscow, 28–31 May 2009. *Prikladnaya Fizika* (2010) No. 3, pp. 31–115, edited by A. M. Filachev and I. S. Gaidoukova.

[1] For *Prikladnaya Fizika*, see applphys.vimi.ru

10. Proceedings of the Tenth All-Russia Seminar, Scientific Research Institute for Electron and Ion Optics, Moscow, 24–26 May 2011. *Prikladnaya Fizika* (2012) No. 2, edited by A. L. Dirochka and A. M. Filachev.
11. Proceedings of the Eleventh All-Russia Seminar, Scientific Research Institute for Electron and Ion Optics, Moscow, 28–30 May 2013. *Uspekhi Prikladnoi Fiziki* **1** (2013) No. 5, pp. 571–600.
12. Proceedings of the Twelfth All-Russia Seminar, Scientific Research Institute for Electron and Ion Optics, Moscow, 10 December 2015. *Uspekhi Prikladnoi Fiziki*. Papers are not collected in a single issue, see vol. 4, No. 1.

13. Related Meetings

Beijing, 1986: *Proceedings of the International Symposium on Electron Optics*, Beijing, 9–13 September, 1986 (J.-y. Ximen, Ed.) Institute of Electronics, Academia Sinica, 1987.

Gent, 1954: *Rapport Europees Congrès Toegepaste Electronenmicroscopie*, Gent, 7–10 April, 1954, edited and published by G. Vandermeersche (Uccle-Bruxelles, 1954).

Ocean City, 1984: *Electron Optical Systems for Microscopy, Microanalysis and Microlithography. Proceedings of the 3rd Pfefferkorn Conference*, Ocean City (MD), 9–14 April, 1984 (J. J. Hren, F. A. Lenz, E. Munro and P. B. Sewell, Eds) Scanning Electron Microscopy, AMF O'Hare, IL.

Toulouse, 1955: *Les Techniques Récentes en Microscopie Electronique et Corpusculaire*, Toulouse, 4–8 April, 1955 (C.N.R.S., Paris, 1956).

Washington, 1951: *Electron Physics. Proceedings of the NBS Semicentennial Symposium on Electron Physics*, Washington, 5–7 November, 1951. Issued as National Bureau of Standards Circular 527 (1954).

Corrigenda, Volume 1

p. 203, Fig. 12.10, caption. *After Kubo et al. (2017), Courtesy Elsevier*.

p. 698, Section 9, 2016, the correct dates are 29 May–3 June 2016.

Index

Note: Page numbers followed by "*f*" refer to figures.

F

G

N

O

P

Q

Principles of
Electron Optics

Volume Two: Applied Geometrical Optics

Peter Hawkes • Erwin Kasper

Fully revised and updated reference covering the role of electron optics in electron-optical instrument design

- Offers a fully revised and expanded new edition based on the latest research developments in electron optics
- Expands and applies the theory presented in Volume 1
- Covers every significant advance in electron optics since the subject originated
- Contains exceptionally complete and carefully selected references and notes

Principles of Electron Optics: Applied Geometrical Optics, Second Edition, provides an expanded exploration of the many optical elements that use the theory presented in Volume 1: electrostatic lenses, among which are miniature lenses; magnetic lenses, with coverage of permanent-magnet lenses and a selection of unusual designs; quadrupoles; cathode-lens-based instruments including the new ultrafast microscopes, low-energy-electron microscopes and photoemission electron microscopes; the use of electron mirrors in these devices for aberration correction is illustrated. A new chapter presents the theory of the Wien filter, which also appears in connection with monochromators. An extensively rewritten chapter on aberration correction is a major feature, in which the many sextupole, quadrupole and mirror correctors are studied at length as well as other ways of achieving correction, at least in principle. The book also includes a section on electron guns, describing recent theories and covering multicolumn systems and carbon nanotube emitters. Monochromators and energy analysers are examined in the section on curved-axis systems.

The book is intended for postgraduate students and teachers in physics and electron optics, as well as researchers and scientists in academia and industry working in the field of electron optics, electron and ion microscopy and nanolithography.

Peter Hawkes graduated from the University of Cambridge and subsequently obtained his PhD in the Electron Microscopy Section of the Cavendish Laboratory. He remained there for several years, working on electron optics and digital image processing before taking up a research position in the CNRS Laboratory of Electron Optics (now CEMES–CNRS) in Toulouse, France. He was the founder-president of the European Microscopy Society and is a Fellow of the Royal Microscopical Society, the Optical Society of America and the Microscopy Society of America and an honorary member of the French Microscopy Society. His interests also include the history of electron optics and electron microscopy.

Erwin Kasper studied physics at the Universities of Münster and Tübingen (Germany), where he obtained his PhD in 1965 and the habilitation to teach physics in 1969. After scientific spells in the University of Tucson, Arizona, United States (1966) and in Munich, Germany (1970), he resumed his research and teaching in the Institute of Applied Physics, University of Tübingen, Germany, where he was later appointed to a professorship. He lectured on general physics and especially on electron optics. The bulk of his research has been in theoretical electron optics and related numerical methods.

ELSEVIER

ACADEMIC PRESS
An imprint of Elsevier
elsevier.com/books-and-journals

ISBN 978-0-12-813369-9

9 780128 133699